

CONF-85113 -

Fourth International Radiopharmaceutical Dosimetry Symposium

Dosimetry
for
Ultrashort-lived Radionuclides
Radiolabeled Blood Cells
Monoclonal Antibodies
Positron Emitters
Microdosimetry
Children
Fetus

November 5-8, 1985
Oak Ridge, Tennessee



Oak Ridge Associated Universities

**CONF-851113--
(DE86010102)**

Distribution Category UC-48

CONF-851113--

DE86 010102

Fourth International Radiopharmaceutical Dosimetry Symposium

Proceedings of a Conference
Held at Oak Ridge, Tennessee

November 5-8, 1985

Edited and Compiled by

Audrey T. Schlafke-Stelson
Evelyn E. Watson

SPONSORS

Oak Ridge Associated Universities
U.S. Food and Drug Administration
U.S. Department of Energy

April 1986

This report was prepared under contract number DE-AC05-76OR00033 between the U.S. Department of Energy and Oak Ridge Associated Universities.

PREFACE

The Fourth International Symposium on Radiopharmaceutical Dosimetry was held November 5-8, 1985, in Oak Ridge, Tennessee. The major objective of the symposium was to discuss the impact of developments in nuclear medicine on absorbed dose calculational techniques. About 150 participants from nine countries attended the meeting which was cosponsored by Oak Ridge Associated Universities, the Department of Energy, and the Food and Drug Administration. Nuclear Pharmacy/Syncor, Medi-Physics, Mallinckrodt, Squibb Diagnostics, Du Pont NEN Medical Products, and Cadema Medical Products also provided funds to help pay for the travel of invited speakers from foreign countries.

Since 1980 when the third in this series of symposia was held, many changes have taken place in nuclear medicine. In 1985 radiolabeled monoclonal antibodies and blood elements, positron emitters, and ultrashort-lived radionuclides received considerable attention. Of particular interest was the question of whether "average organ" dose estimates adequately express the dose from radionuclides that emit low-energy electrons especially if the radioactive material is incorporated into the cells. During the discussion periods after the presentations, challenging questions were introduced, many of which were not answered but will give rise to new avenues of research.

This volume contains the written text prepared by each of the 52 speakers, the discussions after the presentations, a summary of the meeting, and the major points made during a panel discussion that addressed dosimetry needs from the viewpoints of government agencies, physicians, and industry.

The goal of the planning committee was to provide up-to-date information on absorbed dose and to generate ideas for research that will improve dose calculational techniques. Time will tell how well we accomplished this goal.

Symposium Planning Committee

Neil Abel
Rodney Bigler
Keith Eckerman
Don Hamilton
F. F. Knapp, Jr.

Carol Marcus
James Robertson
Audrey Schlafke-Stelson
Michael Stabin
Evelyn E. Watson

ACKNOWLEDGMENTS

Publication of a book such as this combines the efforts of a great many people. The editors wish to gratefully acknowledge all who have assisted in preparing and printing this proceedings. The authors without whom we would have no book deserve our special thanks for submitting their manuscripts in time for us to meet our publication deadline. The Center for Drugs and Biologics and the Center for Devices and Radiological Health of the Food and Drug Administration and the Human Health and Assessments Division of the Department of Energy provided the necessary funds. The Office of Information Services of the Oak Ridge Associated Universities advised the editors and helped coordinate the tasks associated with the printing and binding.

Finally, we particularly wish to express our thanks to Fanny Smith and Martha Kahl for their work in transcribing the discussions from definitely imperfect recording tapes, to Fanny for retyping manuscripts and sections of manuscripts that could not be printed as received, and to Michael Stabin who provided invaluable help to the editors by interpreting ambiguous comments in the discussions and suggesting ways of expressing them more clearly.

Audrey T. Schlafke-Stelson
Evelyn E. Watson

CONTENTS

PREFACE.....	iii
ACKNOWLEDGMENTS.....	iv
ABSTRACT.....	x

INTRODUCTORY PAPERS AND MICRODOSIMETRY - TUESDAY MORNING SESSION

Session Chairpersons: Evelyn E. Watson and Kandula S.R. Sastry

Ionizing Radiation: Benefits vs. Risks H. N. Wagner, Jr.....	1
Cellular vs. Organ Approaches to Dose Estimates S.J. Adelstein, A.I. Kassis, and K.S.R. Sastry.....	13
The Microdosimetry of Monoclonal Antibodies Labeled with Alpha Particles D. R. Fisher.....	26
Physical and Chemical Events that Follow the Passage of a Charged Particle in Liquid Water H.A. Wright, R.N. Hamm, J.E. Turner, J.L. Magee, and A. Chatterjee.....	37
Spermatogonial Cell Killing by Radiolabeled Methionine: A Comparative Study of the Effects of Se-75, S-35, and H-3 D. V. Rao, G. F. Govelitz, K.S.R. Sastry, and R.W. Howell.....	52
Traversal of Cells by Radiation and Absorbed Fraction Estimates for Electrons and Alpha Particles K.F. Eckerman, J.C. Ryman, A.C. Taner, and G.D. Kerr.....	67

KINETIC DATA ACQUISITION AND PEDIATRICS - TUESDAY AFTERNOON SESSION

Session Chairpersons: Neil M. Abel and Michael G. Stabin

SPECT Quantification of Regional Radionuclide Distributions R.J. Jaszcak, K.L. Greer, and R.E. Coleman.....	82
Quantitation of Radiopharmaceutical Distribution for Use in Dose Estimates with Positron Emission Tomography E.J. Hoffman.....	97
Maximizing Precision and Accuracy in Quantitative Aautoradiographic Determination of Radiopharmaceutical Distribution for Dosimetry Calculation J.L. Lear, K. Mido, J. Plotnick, and R. Muth.....	105
Acquisition of Biokinetic Data for Internal Dose Calculations for Some Novel Radiopharmaceuticals T. Smith, G.D. Zanelli, and J.C.W. Crawley.....	118

Quantitative Clinical Uptake Measurements Using Conjugate Counting K.A. Lathrop, R.D. Bartlett, C.-T. Chen, J.-S. Chou, P.F. Faulhaber, P.V. Harper, and V.J. Stark.....	135
Considerations Regarding Dosimetry in Children D.L. Gilday.....	148
Specific Absorbed Fractions and S-Factors for Calculating Absorbed Dose to Embryo and Fetus U. Elsasser, K. Henrichs, A. Kaul, A.R. Reddy, and H.D. Roedler.....	155
Radio pharmaceuticals in Breast Milk P.J. Mountford and A.J. Coakley.....	167
Radiation Exposure to Parents Nursing their Child During Treatment with ^{131}I -Meta-Iodobenzyl Guanidine for Neuroblastoma H.R. Marcuse, J. van der Steen, H.J.M. Maessen, C.A. Hoefnagel, and P.A. Vôute.....	181
POSITRON-EMITTING RADIONUCLIDES - WEDNESDAY MORNING SESSION	
Session Chairpersons: Carol Marcus and Fure F. Knapp, Jr.	
Medical Concerns in the Application of Ultrashort-lived Radionuclides H.W. Strauss, J. Gill, D.D. Miller, R. Callahan, and D. Elmaleh.....	186
Problems in Radiation Absorbed Dose Estimation From Positron Emitters G.F. Powell, P.V. Harper, C.S. Reft, C.-T. Chen, and K.A. Lathrop.....	194
Radiation Dose Estimates for Copper-64 Citrate in Man J.E. Crook, J.E. Carlton, M. Stabin, and E. Watson.....	212
N-13 Labeled Amino Acids: Biodistribution, Metabolism and Dosimetric Considerations K.C. Rosenspire and A.S. Gelbard.....	217
Dosimetry of D- and L-Enantiomers of C-11-Labeled Tryptophan and Valine L.C. Washburn, B.L. Byrd, T.T. Sun, J.E. Crook, K.F. Hubner, J.L. Coffey, and E.E. Watson.....	239
Considerations for Dosimetry Calculations with Neuroreceptor Binding Radioligands D.F. Wong, A.N. Bice, T. Beck, R.F. Dannals, J.M. Links, and H.N. Wagner, Jr.....	245
Radiation Dose Estimates for the Arterial Injection of Tc-99m Labeled HSA Microspheres and Macroaggregated Particles B.Y. Croft.....	260

KINETICS - WEDNESDAY AFTERNOON SESSION

Session Chairpersons: Katherine Lathrop and David Goodwin

The FDA's Requirements for Radiation Dosimetry of Radiopharmaceutical Drug Products N.M. Abel.....	267
Dosimetry Considerations in Patients with Renal Pathology C.S. Marcus and M.A. Koyle.....	274
Drugs that Alter Biodistribution and Kinetics of Radiopharmaceuticals J. Shani.....	291
Variations in Absorbed Doses From Fe-59 in Different Diseases P. Roth, E. Werner, K. Henrichs, U. Elsasser, and A. Kaul....	310
A Kinetic Model for the Dosimetry of Radiopharmaceuticals Contaminated by Mo-99 D.R. Shearer and J.C. Pezzullo.....	319
The Influence of Radioactive Contaminants on Absorbed Dose Estimates for Radiopharmaceuticals E.E. Watson and M.G. Stabin.....	331
Radiation Absorbed Dose Estimates for Rubidium-82 Determined from In Vivo Measurements in Human Subjects J.W. Ryan, P.V. Harper, V.S. Stark, E.L. Peterson, and K.A. Lathrop.....	346
Human Absorbed Dose Calculations for I-123 Labeled Phenyl Pentadecanoic Acid P.V. Kulkarni, G. Clark, J.R. Corbett, J.T. Willerson, and R.W. Parkey.....	359
A Comparison of Radiation Dosimetry for Several Potential Myocardial Imaging Agents E.E. Watson, M.G. Stabin, M.M. Goodman, F.F. Knapp, Jr., and P.C. Srivastava.....	371
Biokinetics and Dosimetry of I-131-Metaiodobenzylguanidine (mIBG) L. Jacobsson, S. Mattsson, L. Johansson, S. Lindberg, and M. Fjälling.....	389

PROBABILITY OF CAUSATION - A PAPER PRESENTED AT THE EVENING BANQUET

Probabilistic Causality and Radiogenic Cancers P.G. Groér.....	399
---	-----

MONOCLONAL ANTIBODIES - THURSDAY MORNING SESSION

Session Chairpersons: Rodney Bigler and Keith Eckerman

Dosimetry of Radiolabeled Monoclonal Antibodies Used for Therapy M.J. Myers, G.R. Hooker, and A.A. Epenetos.....	409
---	-----

A Compartmental Modeling Approach to the Radiation Dosimetry of Radiolabeled Antibody		
P.B. Zanzonico, R.E. Bigler, F.J. Primus, E. Alger, R. DeJager, S. Stowe, E. Ford, K. Brennan, and D.M. Goldenberg.....		421
Dosimetric Measurements and Radiobiological Consequences of Radioimmunotherapy in Tumor Bearing Mice		
B.W. Wessels, M.H. Griffith, E.W. Bradley, and B. Skibinski.....		446
Dosimetric Considerations in Radioimmunotherapy of Patients with Hepatoma		
P.K. Leichner, J.L. Klein, and S.E. Order.....		458
Distribution and Dosimetry of Indium-111 Labeled F(ab') ₂ Fragments in Humans		
P. Doherty, R. Schwinger, M. King, and M. Gionet.....		464
Chelate Chase of Radiopharmaceuticals Reversibly Bound to Monoclonal Antibodies Improves Dosimetry		
D.A. Goodwin, S.I. Smith, C.F. Meares, G.S. David, M. McTigue, and R.A. Finston.....		477
Cis-Platinum-193m: Its Microdosimetry and Potential for Chemo-Auger Combination Therapy of Cancer		
R.W. Howell, K.S.R. Sastry, H.Z. Hill, and D.V. Rao.....		493
 HEMATOPOIETIC SYSTEM AND MISCELLANEOUS DOSE ESTIMATION MODELS - THURSDAY AFTERNOON SESSION		
Session Chairpersons: Barbara Croft and Mark Cristy		
Aspects of the Dosimetry of Radionuclides Within the Skeleton with Particular Emphasis on the Active Marrow		
K.F. Eckerman.....		514
Bone Marrow Dosimetry for Monoclonal Antibody Therapy		
R.E. Bigler, P.B. Zanzonico, R. Leonard, M. Cosma, F.J. Primus, E. Alger, R. DeJager, S. Stowe, E. Ford, K. Brennan, and D.M. Goldenberg.....		535
Dose Point Kernels for Beta-emitting Radioisotopes		
W.V. Prestwich, L.B. Chan, C.S. Kwok, and B. Wilson.....		545
Effect of Tissue Inhomogeneity on Beta Dose Calculation		
C.S. Kwok, M. Irfan, M.K. Woo, and W.V. Prestwich.....		562
A Preliminary Model of the Circulating Blood for Use in Radiation Dose Calculations		
J.W. Poston, A. Aissi, T.Y. Hui, and B.M. Jimba.....		574
A Simple Dynamic Model for Calculating Radiation Absorbed Dose to the Bladder Wall		
C.-T. Chen, P.V. Harper, and K.A. Lathrop.....		587
An Age- and Sex-dependent Model for Estimating Radioiodine Dose to a Normal Thyroid		
G.G. Killough and K.F. Eckerman.....		613

Thyroid Cancer in the Marshallese: Relative Risk of Short-lived Internal Emitters and External Radiation Exposure E.T. Lessard, A.B. Brill, and W.H. Adams.....	628
---	-----

CLOSING SESSION - FRIDAY MORNING

Session Chairpersons: Hans D. Roedler and Roger J. Cloutier	
Radiolabeled Blood Cells: Radiation Dosimetry and Significance M. L. Thakur.....	648
An Assessment of the Risk to Patients from the Labelling of Leucocytes with Indium-111 A.A. Edwards and D.C. Lloyd.....	661
Variations in Absorbed Doses from Cr-51 in Investigations with Labelled Erythrocytes P. Roth, E. Werner, K. Henrichs, U. Elsasser, and A. Kaul.....	673
Radiobiological Half-lives for Carbon-14 and Hydrogen-3 Leucine in Man K.L. Classic, W.F. Schwenk, and M.W. Haymond.....	681
Summary.....	688
Panel and Discussion.....	691
List of Participants.....	701
Subject Index.....	708
Author Index.....	736

ABSTRACT

The focus of the Fourth International Radiopharmaceutical Dosimetry Symposium was to explore the impact of current developments in nuclear medicine on absorbed dose calculations. This book contains the proceedings of the meeting including the edited discussion that followed the presentations. Topics that were addressed included the dosimetry associated with radiolabeled monoclonal antibodies and blood elements, ultrashort-lived radionuclides, and positron emitters. Some specific areas of discussion were variations in absorbed dose as a result of alterations in the kinetics, the influence of radioactive contaminants on dose, dose in children and in the fetus, available instrumentation and techniques for collecting the kinetic data needed for dose calculation, dosimetry requirements for the review and approval of new radiopharmaceuticals, and a comparison of the effect on the thyroid of internal versus external irradiation. New models for the urinary bladder, skeleton including the active marrow, and the blood were presented. Several papers dealt with the validity of traditional "average-organ" dose estimates to express the dose from particulate radiation that has a short range in tissue. These problems are particularly important in the use of monoclonal antibodies and agents used to measure intracellular functions. These proceedings have been published to provide a resource volume for anyone interested in the calculation of absorbed radiation dose.

Proceedings of Previous Radiopharmaceutical Dosimetry Symposia:

1. RJ Cloutier, CL Edwards, and WS Snyder, eds. Medical Radionuclides: Radiation Dose and Effects, CONF-691212, USAEC Symposium Series 20, 1970, National Technical Information Service, Springfield, VA 22161.
2. RJ Cloutier, JL Coffey, WS Snyder, and EE Watson, eds. Radiopharmaceutical Dosimetry Symposium, HEW Publication (FDA) 76-0844, June 1976, Superintendent of Documents, U.S. Government Printing Office, Washington, DC 20402.
3. EE Watson, AT Schlafke-Stelson, JL Coffey, and RJ Cloutier, eds. Third International Radiopharmaceutical Dosimetry Symposium, HHS Publication FDA 81-8166, June 1981, Food and Drug Administration, Bureau of Radiological Health, Rockville, MD 20857.

NOTICES

The opinions expressed herein are those of the authors and do not necessarily reflect the opinions of Oak Ridge Associated Universities and its sponsoring institutions, the U.S. Food and Drug Administration, or the U.S. Department of Energy.

This report was prepared as an account of work sponsored by the United States Government. Neither the United States nor the U.S. Department of Energy, nor any of their employees, makes any warranty, express or implied, or assumes any legal liability or responsibility for the accuracy, completeness, or usefulness of any information, apparatus, product, or process disclosed, or represents that its use would not infringe privately owned rights. Reference herein to any specific commercial product, process, or service by trade name, mark, manufacturer, or otherwise, does not necessarily constitute or imply its endorsement, recommendation, or favoring by the U.S. Government or any agency thereof. The views and opinions of authors expressed herein do not necessarily state or reflect those of the U.S. Government or any agency thereof.

Printed in the United States of America
Available from
National Technical Information Service
U.S. Department of Commerce
5285 Port Royal Road
Springfield, VA 22161

NTIS price codes 99
Printed copy: A31
Microfiche copy: A01

Fourth International Radiopharmaceutical Dosimetry Symposium

**Proceedings of a Conference
Held at Oak Ridge, Tennessee**

November 5-8, 1985

Edited and Compiled by
Audrey T. Schlafke-Stelson
Evelyn E. Watson

SPONSORS

Oak Ridge Associated Universities
U.S. Food and Drug Administration
U.S. Department of Energy

April 1986

This report was prepared under contract number DE-AC05-76OR00033 between the U.S. Department of Energy and Oak Ridge Associated Universities.

(R) 100

ACKNOWLEDGMENTS

Publication of a book such as this combines the efforts of a great many people. The editors wish to gratefully acknowledge all who have assisted in preparing and printing this proceedings. The authors without whom we would have no book deserve our special thanks for submitting their manuscripts in time for us to meet our publication deadline. The Center for Drugs and Biologics and the Center for Devices and Radiological Health of the Food and Drug Administration and the Human Health and Assessments Division of the Department of Energy provided the necessary funds. The Office of Information Services of the Oak Ridge Associated Universities advised the editors and helped coordinate the tasks associated with the printing and binding.

Finally, we particularly wish to express our thanks to Fanny Smith and Martha Kahl for their work in transcribing the discussions from definitely imperfect recording tapes, to Fanny for retyping manuscripts and sections of manuscripts that could not be printed as received, and to Michael Stabin who provided invaluable help to the editors by interpreting ambiguous comments in the discussions and suggesting ways of expressing them more clearly.

Audrey T. Schlafke-Stelson
Evelyn E. Watson

IONIZING RADIATION: BENEFITS VS. RISKS

Henry N. Wagner, Jr., M.D.
Professor of Medicine, Radiology and Radiological Science,
and Environmental Health Sciences;
Director, Divisions of Nuclear Medicine
and Radiation Health Sciences
The Johns Hopkins Medical Institutions
615 North Wolfe Street
Baltimore, Maryland 21205-2179

ABSTRACT

Most of the material and social benefits we enjoy - from antibiotics to automobiles - involve some risks. Every advance in technology requires a similar weighing of benefits and risks. The use of ionizing radiation is no exception. No one has been identifiably injured by radiation within the levels set by the NCRP and ICRP in 1934. (1,2,3) No effects have been observed despite over 40 years of trying to find them. This fact and the level of natural radiation (average dose 102 millirems/year) help provide standards against which we can view the relative increases in exposure from manmade sources of radiation.(4) Because one person in five in the United States will die of cancer from all causes, it is impossible to detect small increases in some types of cancer from radiation.(5) A valid assumption is that any exposure to radiation carries some possibility of harm and should be kept below the level of the expected benefits. More is known about radiation toxicity than about any other potentially toxic substances. An obstacle to progress in the use of radioactive materials in biology and medicine is an exaggerated impression by the public of the risk of radiation. Several studies indicate that the public perceives the risk of radiation to be the greatest of all societal risks and at times does not distinguish peaceful from military uses of radiation.(6,7) It behooves scientists and physicians to inform the public about the benefits as well as the risks of procedures involving radiation. For example, many believe that discoveries concerning the biology of the mind are likely to be as revolutionary as the discoveries of atomic physics at the turn of the century and the revelations in molecular biology and genetics in the 1950s. For centuries, philosophers and psychologists have debated the relationship of the brain and the mind. Positron emission tomography (PET) is helping to break down this barrier, by making it possible to relate chemical processes in specific regions of the brain to human behavior, which is the function of the mind. (8,9,10,11)

The past 20 years have witnessed an explosion of new ways of looking at the structure and function of the human body, with the field of nuclear medicine playing a leading role. Portraying previously invisible body organs by mapping the distribution of radioactive tracers within the body after injection--nuclear imaging--was the first major advance in radiological imaging since the discovery of the x-ray by Roentgen in 1895.

THE BENEFITS

In the process of learning of the phenomenon of radiation and its potential beneficial uses, the "nuclear pioneers" also discovered the deleterious biological effects of uncontrolled exposure to radiation.

Radiation safety was recognized as an important issue of concern early in the development of this new technology. In 1928, at the Second International Congress of Radiology, an International Commission on Radiological Protection (ICRP) was established, originally under the name of the International X-Ray and Radium Protection Committee. Since then, this organization has been involved in establishing principles of radiation safety.

As knowledge and understanding of radiation accumulated, scientists developed increasingly sophisticated medical applications for the emerging technology. Today, approximately 10 million nuclear medicine procedures are performed annually in the United States alone. The "radioactive tracer" principle on which Nuclear Medicine is based is one of the best examples of the benefits of radiation for human beings. George von Hevesy, a Hungarian chemist who worked in many countries, was awarded the Nobel Prize in 1944 for his invention of the tracer principle in 1913, and for his subsequent pioneering use of tracers in biomedical research.

Among the earliest procedures involving the use of radioactive tracers in medicine was measurement of the uptake of radioactive iodine by the thyroid gland.(12) In the early 1940's it was found that the rate of uptake of iodine by the thyroid was greatly increased in patients with disease characterized by increased production of thyroid hormone, a disease that led to nervousness, tremor, weight loss and, in extreme cases, even death, the disease hyperthyroidism. Other patients exhibited decreased iodine uptake by the thyroid and had symptoms and signs of diminished thyroid function, the disease hypothyroidism. Since then, one organ system after another has been studied by the tracer principle, until today we can begin to examine the chemical reactions occurring in the living human brain and relate such findings to the functioning of the mind. The discovery of biologically important receptors throughout the body that bind specific chemicals and the development of monoclonal antibodies represent the two leading edges of nuclear medicine today. Ongoing research promises future advances which will have a dramatic impact on the diagnosis and treatment of diseases. Just as the pioneers in nuclear medicine were able to discover that some patients had over- or underactive thyroids, it is now possible to assess over- and underactivity of brain chemicals involved in anger, pain, anxiety and other mental states.

Many decades ago Pavlov said: "An important state of human thought will have been reached when the physiological and the psychological, the objective and the subjective are actually united." Radioactive tracer methods can now provide the needed objectivity. The study of nervous and mental disease, as well as that of other organs can be carried out at the molecular level.

Diseases, such as mental illnesses or retardation, now characterized by subjective tests, may soon be identified by biochemical measurements of the brain. The metabolic activity of the brain can be correlated to mental activity, as a result of the development of the deoxyglucose and other nuclear medicine tests.

The deoxyglucose test is also proving helpful in the evaluation of brain tumors. Initial research indicates that imaging by positron-emission tomography (PET) can reveal the level of glucose metabolism in brain tumors. If the tumor is malignant, the metabolic activity is usually high. In benign tumors, it is usually low.(13)

Metabolic characterization of brain tumors provides a way to monitor chemotherapy, which could have substantial advantages over current surgical treatment. Since modern treatment is often chemical, it is less than optimum to use only the anatomical information as the principal guide to treatment. Biochemical characterization of tumors is an idea whose time has come. Nuclear techniques are also beginning to be used to assist in the selection of appropriate patients for the surgical treatment of epilepsy.(14) While the study of the brain and the heart remain at the forefront of studies of human diseases with radioactive tracers, other important uses include the diagnosis of diseases of the lungs, gastrointestinal tract, endocrine, musculoskeletal, and genitourinary systems.

There is also considerable promise in the use of monoclonal antibodies labeled with radiotracers. It is even possible that receptor-binding drugs or monoclonal antibodies labeled with high levels of radioactivity may eventually be used therapeutically.(15,16)

New studies of the heart involve glucose and fatty acid metabolism. (17,18,19,20) Within 5-15 minutes after injection of a radioactive fat, the disappearance of radioactivity from the heart reflects oxidation of the fat to provide the energy used in the contraction of the muscles of the heart. In fasting patients with coronary artery disease, the heart muscle switches from its preference for fatty acids as a source of energy to glucose, the metabolism of which increases many-fold. Studies of this type help pinpoint specific abnormalities in both acquired and genetically determined heart disease, and help identify and establish the size of regions of myocardial infarction. After a heart attack, the locations and extent of myocardial injury are major determinants of the severity of associated disturbances of cardiac rhythm and mortality. Assessment of the amount of injury also aids in objective evaluation of the efficacy of treatment aimed at limiting the extent of myocardial injury.

Yet another example of current research is the development of antibodies characterized by their high degree of specificity in reacting with antigens. They can be used in several ways: as reagents for the measurement of chemical concentrations in blood; as indicators for measuring regional concentrations of chemicals in the living human body; as a way to concentrate a radioactive label within an organ; and as a way to detect, locate and possibly destroy cancers.

THE RISKS

Exposure to the human body from natural radiation occurs in two ways: external radiation from outside of the body and internal radiation from radioactive material within the body. (21,22) In the United States, the average person receives about 100 millirems of radiation dose annually. This is a reference against which additional radiation can be compared. (23)

Cosmic radiation from space varies considerably from one part of the country to another. (24) For example, it amounts to about 140 millirems/year in Colorado because of the high altitude, compared to 38 millirems in Florida, which is at sea level. The larger amount of air at the lower altitude absorbs much of the incoming cosmic radiation.

Naturally occurring radioactive elements result in internal radiation when they are inhaled or taken into our bodies in food and water. Internal radiation from naturally radioactive potassium, chiefly in muscle, amounts to 20 millirems/year in men compared to 15 millirems in women. One out of every 10,000 potassium atoms within our bodies is radioactive. Carbon-14 is another naturally-occurring isotope within our bodies. Thus it is literally true that

our bodies are irradiated by natural radioactivity from the time we are conceived until long after we have died.

PUBLIC PERCEPTION

Thus, a fundamental principle is that radiation is not just the result of human activities and can never be totally eliminated. The level of natural radiation exposure is one way to provide a standard against which we can compare the relative increases in exposure from manmade sources of radiation. A safe dose of radiation can be defined as one below which no deleterious effects would occur. Identifying the safe dose level is not a simple task because in most instances, the biological effects of radiation cannot be measured because radiation does not produce unique effects. Since one in five persons in the United States will die of cancer from all causes, it is impossible to measure what portion of these fatalities are attributable to radiation exposure. It is probable that less than one percent of cancer deaths are attributable to radiation, both natural and manmade.(22)

Because possible deleterious effects of low level radiation are too small to be measured, for decades an assumption has been made that any exposure to radiation carries some possibility of harm either to the person being irradiated or to subsequent generations. This is called the "zero threshold" hypothesis. A potential harmful agent, such as fire, has a "threshold"--a level below which no harmful effects occur, as, for example, when we sit in front of a fireplace. The "zero threshold" hypothesis states that any radiation exposure is harmful, even if only when large numbers of persons are exposed to it.

All regulatory agencies involved with radiation subscribe to the "zero-threshold" hypothesis. They have assumed that there is no safe dose of radiation and that every radiation dose is an overdose. Such statements occasionally lead to public confusion. For example, a statement such as, "We don't know everything about radiation," is often interpreted as, "We don't know anything about radiation," despite the fact that more is probably known about radiation toxicity than about any other potentially toxic substances. This knowledge is the result of the extreme sensitivity and accuracy with which radiation can be measured.

The lack of proper information and public education, coupled with the well-justified dread of nuclear war, has escalated public concern over radiation in recent years. Such concern was dramatically increased by the accident at the Three Mile Island nuclear power plant. This heightened sensitivity has resulted in widespread opposition to nuclear power and other peaceful uses of radiation.

Many believe that the risks from nuclear power and medical radiation have been overestimated. Lauriston Taylor, past-president of the National Council on Radiation Protection (NCRP), stated recently:

"No one has been identifiably injured by radiation while working within the first numerical standards set by the NCRP (National Council on Radiation Protection) and then the ICRP (International Council on Radiation Protection) in 1934.

"Let us stop arguing about the people who are being injured by exposure to radiation at the levels far below those where any effects can be found despite over 40 years of trying to find them. The theories about people being injured have still not led to the demonstration of injury and though considered as facts by some, must only be looked upon as figments of the imagination."

The sociologist Margaret Maxey has written:

"...despite the vast amount of radiobiological data, there is no conclusive scientific evidence to prove the existence or absence of a threshold. A moral argument which categorically condemns manmade uses of radioactive elements originates from, and depends upon, what is taken to be an unassailable scientific conclusion. But, in fact, it is only an untested theory, an extrapolated hypothesis, an ultra-conservative and protective rule of prudence."

The "zero-threshold" hypothesis for genetic effects was developed before there was clear-cut scientific evidence of the existence of naturally-occurring mechanisms for the effective repair of damage to genetic DNA. Such evidence now exists.

Recently the concept of a "practical threshold" for low-level radiation has been introduced. It is defined as a dose level below which the appearance of any possible harmful effect is in excess of the life expectancy of the exposed individual.(25) From the study of radium-dial painters, it has been concluded that if the radiation dose to bone is less than 39 millirem/day, the time of appearance of bone cancer exceeds the lifespan of the person.

An exaggerated perception of risk is not limited to radiation. Wildavsky stated in 1979 in The American Scientist:

"How extraordinary! The richest, longest-lived, best-protected, most resourceful civilization, with the highest degree of insight into its own technology, is on its way to becoming the most frightened. Has there ever been, one wonders, a society that produced more uncertainty more often about everyday life? (Uncertainty about) the land we live on, the water we drink, the air we breathe, the food we eat, the energy that supports us. Chicken Little is alive and well in America."

Even though we live longer and healthier lives, our awareness of risks has increased to a high level. As the public becomes more concerned with the dangers of nuclear war, their fear of all aspects of radiation and radioactivity increases to the point of genuine alarm. The fact that radiation cannot be perceived by our unaided senses, and has delayed effects, contributes to public anxiety. Some believe that no matter what the immediate benefit, the long-term risks of radiation are a violation of basic human rights and a moral evil.

People realize intuitively that life involves risk. They know that the felling of a tree for firewood carries with it the risk of injury from a chainsaw accident or by being struck by the tree as it falls. They are learning that activities they once took for granted as being totally safe do involve risk. Perception of risk can be healthy, but we can also make the mistake of letting pervasive doubt and skepticism interfere with rational decision-making. Most of us realize that new risks are the price of progress, but many forget that progress often decreases risk--for example, the risk of dying from diseases, such as typhoid fever and smallpox. It behooves scientists and physicians to better inform the public about the benefits as well as the risks of procedures involving radiation.

One of society's greatest needs today is to be better able to balance benefits and risks. Most of the material and social benefits we enjoy--from antibiotics to automobiles--involve some risk. In deciding to enjoy those benefits, we have also decided to accept the risks which they entail. Every advance in technology requires a similar weighing of benefits and risks. The use of radiation is no exception.

Balancing Risks and Benefits

The greatest obstacle to further progress in nuclear medicine is an exaggerated impression by the public of the risk of radiation. Several recent studies indicate that the public perceives radiation to be the greatest of all society risks--greater than the risk of war, crime, violence, smoking, driving an automobile, possessing a handgun or riding a motorcycle.

The medical benefits of radiation are enormous in terms of saving human lives by early diagnosis of disease, improving the quality of life and reducing the risks and costs associated with other diagnostic methods. Based on the results of ongoing research, the future promises major breakthroughs in nuclear medicine which will vastly improve our understanding of the structure and function of the human body and the diagnosis and treatment of diseases and conditions that continue to perplex the medical and scientific community.

These benefits greatly outweigh the risks associated with low-level medical use of radioisotopes. The safety of these radioactive drugs is due in part to their short half-lives, that is, the radioactivity of these substances decays in very short periods of time. In some cases, the half-lives are so short that the radiopharmaceuticals must be prepared in the hospitals where the studies are performed. Carbon-11, with a half-life of 20 minutes, is an example. Several leading hospitals, especially those in which medical research is conducted, have installed cyclotrons for the on-site preparation of these radioisotopes. This introduction of cyclotrons into hospitals represents another situation where not only must the instrument be operated safely, the public must perceive correctly that the operation is totally safe. Misconceptions of the safety of these low-level medical uses of radioisotopes can lead to excessive legislation and regulatory restraints on the handling of these substances. An example of this exaggerated concern is the proliferation of federal, state and local restrictions on the transportation of radioactive materials.

The U.S. Dept. of Transportation, which monitors all hazardous materials in transport, estimated that in 1977 alone, 2.5 million packages of radioactive materials were shipped by all modes of transportation. Between 1971 and 1979, of all reports received of release of hazardous substances, approximately 23 (0.5 percent) involved a radioactive substance. None of those incidents resulted in public health consequences such as those often associated with transportation accidents involving flammable liquids. Despite such an enviable safety record, regulatory bodies subscribing to the "zero threshold" hypothesis, and local governing bodies reacting to heightened public sensitivity threaten the availability of radiopharmaceuticals by restricting, and in many instances banning, the transportation of nuclear materials on roads within their jurisdiction. Such regulations do not contribute to public safety, but merely serve to prevent adequate doses of radiopharmaceuticals from being available for life-saving diagnostic tests. Because of the short half-lives of these radioactive substances, radiopharmaceuticals cannot be stockpiled. Therefore, physicians often order these drugs on an immediate as-needed basis, namely, when a patient is scheduled for a diagnostic procedure. Typically, the drugs are ordered in the afternoon of the day before they are used. When ordered, the drugs are then both manufactured and delivered during that night. This procedure is designed to provide for the drug's availability to the physician by

7:00 a.m. the next morning. The necessity of satisfying not only federal regulations on the shipment of these materials, but also a myriad of state, county and municipal requirements, each involving some form of licensing, registration or notification of shipment, severely limits, if not totally disrupts, the shipment of radiopharmaceuticals to physicians.

The ultimate result, if this trend of local regulation progresses, would most likely be that such medicine will be unavailable for diagnostic use in patients. These transportation roadblocks will also lead to more immediate results: insofar as compliance is often costly, these local laws and regulations will increase the cost of health care in this country, without commensurate benefit to the public. Delays in transportation will result in longer hospital stays for patients and unjustified delays in urgently needed medical care.

Efficient and affordable availability of radiopharmaceuticals can be maintained under a uniform national system of regulation of low-level nuclear material transportation. The proper handling of these radioisotopes can be assured without state and local regulation. States and localities which do undertake to impose individual regulatory schemes should exempt low-level medical use radioisotopes in order to permit the timely availability of these substances to the public.

Another issue that confronts the nuclear medicine community is the safe disposal of low-level nuclear waste. At present, only two disposal sites in Washington and South Carolina service all private generators of nuclear waste in the United States.

Federal law, passed within the last year, requires that each state prepare to assume responsibility for the low-level nuclear waste generated within its borders by January 1, 1986. States can comply with this mandate either by providing individual state waste repositories or by banding into regional pacts and establishing regional disposal facilities for common use.

The fact that so few disposal sites exist for servicing the entire nation necessitates the transportation of radioactive materials over long distances. Despite the safety record of nuclear materials in transportation, the public is concerned. Rather than impose overly restrictive transportation regulations to dissipate such concerns, the need for long distance transportaion of radioactive materials will be drastically reduced by the availability of local or regional disposal sites.

Some states are not acting with enough speed to meet the federal deadline and ensure that the issue of low-level radioactive waste disposal is optimally addressed to meet state needs. These states are exposing their citizens to the potential unavailability of radioactive drugs after January 1, 1986.

A related problem of disposal facing the nuclear medicine industry, as well as hospitals and medical centers utilizing radiopharmaceuticals, is that federal regulations, subscribing to the "zero threshold" hypothesis, require regulated disposal of materials of such low activity that they need not be considered radioactive.

Items such as syringes, containers, gloves and the like, once contaminated by very low levels of radioactivity must meet specific packaging requirements and be transported to official nuclear disposal sites despite the fact that they present no potential danger to the public.

Dr. Rosalyn S. Yalow, Nobel Prize winner in Medicine, testified before the Subcommittee on Energy Research and Production of the Committee on Science and Technology of the U.S. House of Representatives on November 7, 1979, addressing the need for redefinition of threshold levels of radioactivity requiring special handling and disposal. At that time, she illustrated how illogical existing regulations can be by the following analogy:

"As an adult, living, human being my body contains natural radioactivity; 0.1 microcuries K-40 and 0.1 microcuries C-14 are the predominant radioisotopes. According to the current rules of the Nuclear Regulatory Commission (NRC), if I were a laboratory animal who had received this amount of radioactivity as 'by-product material' and died with this radioactivity still in my body, I could not be buried, burned or disposed of in the garbage. My carcass would have to be packed into a small can, inside a larger can and transported to a site for disposal of radioactive waste. There I would needlessly occupy forever space that should be saved for significantly radioactive materials."

The number of nuclear waste disposal facilities required to appropriately handle this country's radioactive waste and the costs associated with disposal would decline if a more realistic assessment of hazards and risks of such low activity materials is incorporated in the regulatory process.

Radiopharmaceuticals are life-saving diagnostic tools, indispensable to optimum patient care. These benefits, along with foreseeable advances in the future, must be balanced against a rational evaluation of the hazards associated with radioactivity. If we lose sight of this balance and react to alarmist, factually unsubstantiated fears, we will jeopardize the progress made in understanding the structure and function of the human body through nuclear medicine.

Dr. Yalow closed her testimony to the House Subcommittee on Energy Research and Production with the following statement:

"It is time for cool heads and the wisdom of proven facts to determine policy. We need more realistic estimates of proven facts to determine policy. We need more realistic estimates of risk, and better education of the public about the entire field of radiation. We must begin teaching schoolchildren about rems and rads as well as about grams and centimeters."

SUMMARY

The fear of all aspects of radiation and radioactivity has increased to the point of genuine alarm. The fact that radiation cannot be directly perceived by the unaided senses and has long-delayed effects also contributes to public anxiety. Some believe that no matter what the benefits, the risks of radiation far outweigh them. Inadequate knowledge about matters concerning radiation impairs optimum decision-making by members of the public and professional groups.

Fears of radiation were increased considerably by the accident at Three Mile Island. It has resulted in a noticeable decrease in the numbers of persons applying for entrance into radiation-related programs, both medical and nonmedical; an increase in the number of persons refusing medical diagnostic procedures

involving radiation; increasing reluctance of regulatory agencies and institutional review boards to approve research protocols that involve human exposure to radiation; exaggerated perception by the public of the risk of transporting radioactive materials, such as radiopharmaceuticals; and disinclination of the public to develop facilities for the safe disposal of low-level radioactive wastes.

A lack of knowledge about radiation has become a problem in the following ways: (1) The virtual elimination of the nuclear option for generation of electricity could result in an unbalanced development of other options, such as the use of coal, which could aggravate the problem of "acid rain" or excessive carbon dioxide production; (2) Fear of medical radiation could result in misdiagnosis or neglected health care; (3) A shortage of workers in the radiation-related health professions could develop; (4) The public may not receive the benefits of biomedical research if scientists do not carry out experiments involving radioactive tracers if they have an unwarranted, exaggerated fear of the effects of radiation.

The United States political system is based upon the principle that the public has the right to participate in the formation of governmental policies. Few would deny the need for a better informed public. The need for better education of the public about the entire field of radiation is analogous to the need in the past to educate the public about the harmful and beneficial effects of microorganisms following their discovery in the late 19th century. Such educational efforts should be balanced and objective, the goal being to convey existing knowledge about both risks and benefits, in addition to identifying those areas where knowledge is incomplete.

"I know no safe depository of the ultimate powers of society but the people themselves; and if we think them not enlightened enough to exercise their control with a wholesome discretion, the remedy is not to take it from them but to inform their discretion."

Thomas Jefferson

References

1. BEIR, (1980) The Effects on populations of exposure to Low levels of Ionizing Radiation. Report of the Advisory Committee on the Biological effects of Ionizing Radiations. Washington, D.C., Division of Medical Science, National Academy of Sciences, National Research Council.
2. Yallow RS, Reappraisal of potential risks associated with low-level radiation. *Com. Mol Cell Biophys.*, 1:149-157., 1981
3. Cohen BL, Lee I-S, A catalog of risks. *Health Physics*, 36:707-722, 1979
4. Upton AC, The Biological effects of low-level ionizing radiation. *Scientific American*, 246:41-49, 1982
5. GAO, (1981), Problems in Assessing the cancer risks of low-level ionizing Radiation exposure, Vol 2. Report to the U.S. Congress by the Comptroller General. Gaithersburg, MD, U.S. General Accounting Office., XVIII-43
6. Slovic P, Fischhoff B, Lichtenstein S, Informing the public about the risks from ionizing radiation. *Health Physics* 41:589-598, 1981
7. Sinclair WK,: Effects of low-level radiation and comparative risk. *Radiology* 138:1-9, 1981
8. Wagner HN Jr, Burns HD, Dannals RF, Wong DF, Langstrom B, Duelfer T, Frost JJ, Ravert HT, Links JM, Rosenbloom SB, Lukas SE, Kramer AV, Kuhar MJ, Imaging dopamine receptors in the human brain by positron tomography, *Science* 221:1264-1266, 1983
9. Wong DF, Wagner HN Jr, Dannals RF, Links JM, Frost JJ, Ravert HT, Wilson AA, Rosenbaum AE, Gjedde A, Douglass KH, Petronis JD, Folstein MF, Toung JKT, Burns HD, Kuhar MJ: Effects of Age on Dopamine and Serotonin Receptors measured by Positron Tomography in the Living Human Brain. *Science* 226:1393-1396, 1984
10. Frost JJ, Wagner HN Jr, Dannals RF: Imaging Opiate Receptors in the Human Brain by Positron Tomography. *J Comput Assist Tomogr* 9:231-236, 1985
11. Phelps ME, Mazziotta JC: Positron emission tomography: Human brain function and biochemistry. *Science* 228:799-809, 1985
12. Hamilton JG, Soley MH: Studies in Iodine Metabolism of the Thyroid gland in situ by the use of Radio-iodine in normal subjects and in patients with various types of goiters. *Am J Physiol* 131:135-143, 1940-1941
13. Di Chiro G, Brooks RA, Bairamian D, Patronas NJ, Kornblith PL, Smith BH, Mansi L, Diagnostic and Prognostic value of Positron Emission Tomography using $[^{18}\text{F}]$ Fluorodeoxyglucose in Brain Tumors in Positron Emission Tomography, pages 291-309, Alan R. Liss, Inc., 1985
14. Kuhl DE, Engel J Jr, Phelps ME, Selin C: Epileptic patterns of local cerebral metabolism and perfusion in humans determined by Emission Computed tomography of ^{18}FDG and NH_3 , *Ann Neurol* 8:348-360, 1980
15. Larson SM: Radiolabeled Monoclonal Anti-tumor antibodies in Diagnosis and therapy, *J Nucl Med* 26:538-545, 1985

16. Keenan AM, Harbert JL, Larson SM: Monoclonal antibodies in Nuclear Medicine, J Nucl Med 26:531-537, 1985
17. Schelbert HR, Phelps ME, Hoffman E, Huang S-C, Kuhl DE: Regional myocardial blood flow, metabolism and function assessed noninvasively with positron emission tomography. Am J Cardiol 46:1269-1277, 1980
18. Schelbert HR: Radionuclide assessment of myocardial metabolism, in Freeman and Johnson's Clinical Radionuclide Imaging, 3rd edition, Crane and Stratton, 1984, p 563, vol. 1
19. Schelbert HR, Henze E, Schon HR, Keen R, Hansen HW, Selin C, Huang SC, Barrio JR, Phelps ME: C-11 palmitate for the noninvasive evaluation of regional myocardial fatty acid metabolism with positron computed tomography. III. In vivo demonstration of the effects of substrate availability on myocardial metabolism. Am Heart J 105:492-504, 1983
20. Freundlieb C, Hock A, Vysha K, Feinendegen LE, Machulla HJ, Stocklin G: Myocardial imaging and metabolic studies with (17-¹²³I) iodoheptadecanoic acid. J Nucl Med 21:1043-1050, 1980
21. HEW (1979): Report of the work group on exposure reduction. Interagency task force on the health effect of ionizing radiation. Washington, D.C., U.S. Department of Health, Education and Welfare, 1979
22. HEW (1976): The Biological effects of ionizing radiation: An overview, Barrett MH (ed) HEW Publications (FDA) 77-8004, Washington, D.C., U.S. Department of Health, Education and, Welfare, 1976
23. Brill AB, Adelstein JJ, Saenger EL, Webster EW: Low-level Radiation Effects: A Fact Book, The Society of Nuclear Medicine, Inc., N.Y. 1982
24. Oakley DT: Natural Radiation Exposure in the U.S. EPA report ORP/SID 7201, Washington, D.C., U.S. Environmental Protection Agency. 1972
25. Adelstein SJ: Radiation Risks in Nuclear Medicine edited by H.N. Wagner, Jr., Hospital Practice Publishing Co., Inc., New York, P74, 1975

DISCUSSION

SASTRY: Dr. Wagner, you have eloquently pointed out that the future of nuclear medicine is in the direction of neurobiological studies using PET scanners. Considering that these facilities are very expensive, do you envisage that they will be available at most medical centers across the country so that the results of such studies may be used by physicians in general for the benefit of their patients?

WAGNER: I think that in the next five years, we will see the use of positron emission tomography and cyclotrons in major medical centers. As I pointed out there are now 17 in the United States. I think it would be safe to predict that by another five years there could be 50 such major centers in the United States. I think throughout history advances made in medical centers have

diffused into the medical community and I think this will happen with PET. The use of dual probes, for example, may make it possible to carry out studies away from the medical center. We intend to put one of these probe systems into a methadone clinic, into the National Institute of Drug Abuse, and into the Maryland Psychiatric Research Institute.

Our cyclotron, even though it is very small, can produce enough radioactive tracers to keep 10 positron emission tomography systems occupied. Because one institution is not likely to have 10 PET scanners, positron emission tomography will be possible without a cyclotron. I think regional cyclotrons probably will be developed that will be run by industry. Although we are not particularly interested in doing this at Hopkins, a university that is interested in supplying a region with radioactive tracers will someday demonstrate that it is feasible and then industry will move into that area.

So I do think that, for the next five years, positron-emitting tracers will be used primarily in major medical centers but, within ten years, they will be much more widespread. As I have said before, by the year 2000, the major imaging in medicine will be anatomical imaging using magnetic resonance imaging as the major modality and chemical *in vivo* measurements using positron emission tomography.

One problem with the field of nuclear medicine that I would like to mention just occurred to me recently. Nuclear medicine is too "biochemical and abstract" for radiologists and too "imaging" for internists who are interested in molecular biology. We fit into some kind of a grey zone. In one sense this is nice because it gives us autonomy but it sometimes makes you feel very lonely and left out.

CLOUTIER: When you were talking about the risk, Henry, I was reminded that at one time people were saying that nuclear medicine would be selected over surgery for diagnosis because nuclear medicine is generally noninvasive. What accounts for the great fear of radiation today?

WAGNER: I think what you are driving at is that we run into situations where people talk about radiation risks in the most extreme circumstances of risks. In my experience, the people that need the most education about risk versus benefit of radiation are physicians. We continually have problems with our human investigation committee. Despite the fact that very complicated and extremely invasive procedures are performed all the time, we have long delays and lots of continued explanations if radioactive drugs are to be used. We believe in informed consent, but the risks should not be exaggerated.

As I said in my talk, I was really eager to get out of Turkey, or at least the part of Turkey where I was, because the tremendous air pollution there is really risky. This situation can happen. It happened in Turkey and yet they are smoking away, pumping out all this stuff from the chimneys - and they don't even have nuclear power.

CELLULAR VS. ORGAN APPROACHES TO DOSE ESTIMATES

S.J. Adelstein,¹ A.I. Kassis¹ and K.S.R. Sastry²

¹Harvard Medical School, Boston, MA 02115

²University of Massachusetts, Amherst, MA 01003

ABSTRACT

The cellular distribution of tissue-incorporated radionuclides has generally been neglected in the dosimetry of internal emitters. Traditional dosimetry assumes homogeneous distribution of radionuclides in organs of interest, while presuming that the ranges of particulate radiations are large relative to typical cell diameters. The macroscopic distribution of dose thus calculated has generally served as a sufficient approximation for the energy deposited within radiosensitive sites. However, with the increasing utilization of intracellular agents, such as thallium-201, it has become necessary to examine the microscopic distribution of energy at the cellular level. This is particularly important in the instance of radionuclides that decay by electron capture or by internal conversion with the release of Auger and Coster-Kronig electrons. In many instances, these electrons are released as a dense shower of low-energy particles with ranges of subcellular dimensions. The high electron density in the immediate vicinity of the decaying atom produces a focal deposition of energy that far exceeds the average dose taken over several cell diameters.

Radiobiologic experiments have shown that when the decay takes place in the vicinity of radio-sensitive sites the results are extremely toxic. Cell survival curves are of the high linear energy type, such as produced by alpha particles. More worrisome, is the increased yield of transformed and mutated cells seen with these decays when compared to beta-emission. In contrast, Auger-electron emission in an extracellular location contributes minimally to cytotoxic effects.

These studies point out the increasing need to take into account the microscopic distribution of dose on the cellular level as radionuclides distributed in cells become more commonplace, especially if the decay involves electron capture or internal conversion. As radiotracers are developed for the measurement of intracellular functions these factors should be given greater consideration.

In the calculations of absorbed dose for internal emitters, the cellular distribution of tissue-incorporated radionuclides has generally been neglected. Traditional dosimetry assumes homogeneous distribution of radionuclides in organs of interest and presumes that the particulate radiations are isotropic in their distribution and have ranges that are large relative to typical cell diameters. The macroscopic distribution of dose thus calculated has generally served as a sufficient approximation for the energy deposited within radiosensitive sites of cells. However, with the increasing use of radioindicators that are concentrated by cells, such as gallium-67 and thallium-201, it has become necessary to examine the microscopic distribution of energy at the cellular level. This is particularly important in the instance of radionuclides that decay by electron capture and internal conversion with the release of many Auger and Coster-Kronig electrons. Two factors must be taken into consideration, the intracellular content of these radionuclides (the concentration effect) and the consequence of their localization in the radiosensitive structures of the cell (the highly localized energy density phenomenon, HILED).

THE CONCENTRATION EFFECT

Several currently-used radiopharmaceuticals are highly concentrated in cells compared to their concentration in surrounding extracellular or intravascular fluids. Table 1 lists some typical internal and external concentrations for three radionuclides when Chinese hamster cells (V79) are incubated in vitro. In these instances, the cells concentrate radioactivity by factors of 100 to 1000.

Table 1: Cellular Concentration and Distribution of Some Auger-Electron Emitting Radioindicators by V79 Chinese Hamster Cells

<u>Radioindicator</u>	<u>Extracellular Concentration (MBq/ml)</u>	<u>Intracellular Concentration (mBq/cell)</u>	<u>Intracellular to Extracellular Concntr -Ratio</u>
Na ₂ ⁵¹ CrO ₄ (1)	0.40	230	1010
75Se-methionine (2)	0.76	144	330
201TlCl (3)	0.59	44	130

Each of these radionuclides emits a shower of Auger and Coster-Kronig (CK) electrons whose ranges in biological matter are small relative to cellular diameters (Table 2). Hence, considerable energy from the decay of these radionuclides is confined almost completely to the cell in which they are located. (For comparison, the intracellular contribution of such electrons from the decay of technetium-99m is included in Table 2).

Table 2: Range, Yield and Total Energy for Theoretical Auger and Coster-Kronig Electrons from Four Radionuclides

<u>Radionuclide</u>	<u>Range in Water (μm)</u>	<u>Average Yield (No./decay)</u>	<u>Average Total Energy per decay (keV)</u>
$^{51}\text{Cr}(1)$	≤ 0.65	5.4	3.6
$^{75}\text{Se}(2)$	≤ 2.5	7.4	5.7
$^{201}\text{Tl}(3)$	≤ 65 $(\leq 2.3)^*$	19.9	14.6 (12.6)*
$^{99\text{m}}\text{Tc}(4)$	≤ 7.0	4.0	1.0

* Does not include contribution from K-Auger electrons of range 65 μm .

Several lines of evidence suggest that these intracellular radionuclides are disproportionately responsible for the absorbed radiation dose received by cells concentrating them. First, when the cells are widely dispersed in culture fluid and the dose delivered calculated according to the average radionuclide concentration (essentially the extracellular activity) and the MIRD formulation, the apparent mean lethal doses (MLD) received by the cells (at 37% survival) are ridiculously low (Table 3). The mean lethal dose for x-ray exposure in these cells is 580 rads (2).

Table 3: Calculated Mean Lethal Dose (At 37% Survival) Received By V79 Cells From Radionuclides in The Culture Medium

<u>Radioindicator</u>	<u>Calculated MLD (rad)</u>
$\text{Na}_2^{51}\text{CrO}_4$	2.2
$^{75}\text{Se-methionine}$	19
$^{201}\text{TlCl}$	27

(The D_{37%} extra- and intracellular concentrations are given in Table 1.)

Second, when thallium-201 is injected into mouse testis where the cells are more closely packed (e.g. spermatogonial cells occupy a maximum of 17% of the testis volume), the MIRD formulation badly underestimates its radiotoxicity as compared with the beta-emitter, thallium-204 (5).

Thallium-201 is about four times more effective in reducing the number of sperm heads than the calculated dose of thallium-204 (Figure 1) based on the MIRD approach. Similar effects are found in case of intratesticular decays of the Auger electron emitter, iron-55, compared to the beta-emitting iron-59 distributed in the organ (6).

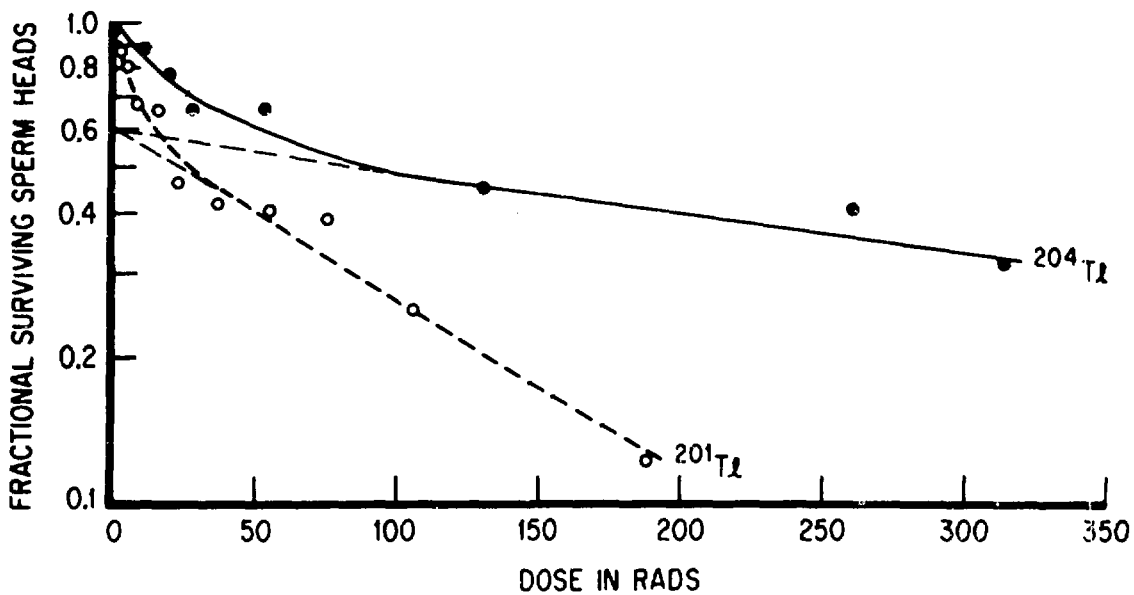
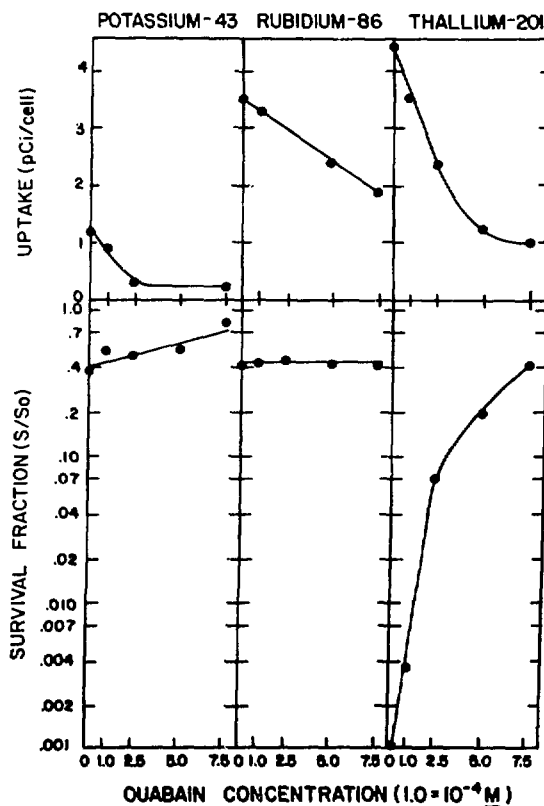
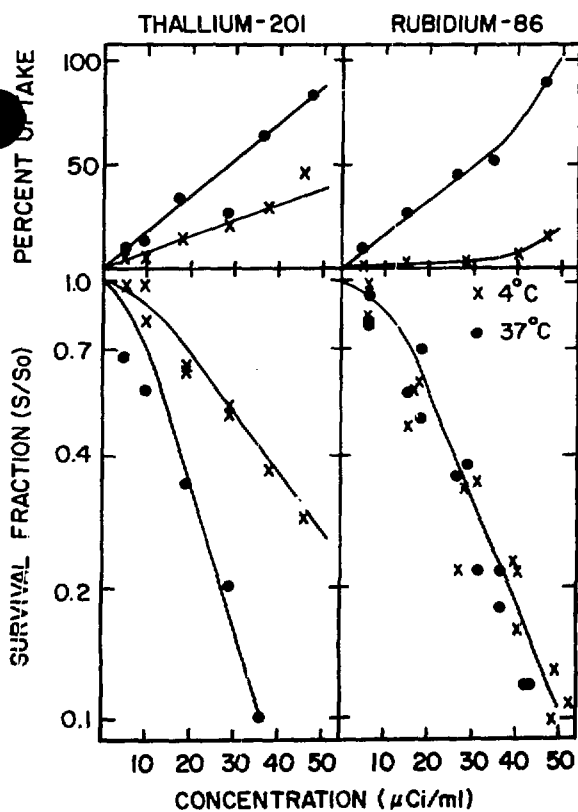


Figure 1. Sperm head survival as a function of calculated average dose to mouse testes from intratesticular injections of thallium-201 and thallium-204 as chlorides (5).

Third, exclusion of thallium-201 from V79 fibroblasts (while maintaining the extracellular concentration of the radionuclide) markedly reduces the radiotoxicity of this monovalent cation, while no similar result is observed with its congeners, potassium-43 and rubidium-86 (3). When the cells are treated with ouabain the intracellular concentration of thallium-201 drops e.g., from 3.5 to 2.3 pCi per cell; the survival fraction rises from 0.004 to 0.07. A similar drop in the intracellular concentration of rubidium-86 has no effect on survival (Fig. 2). When thallium-201 and rubidium-86 are excluded from the cells by lowering the temperature, the same comparative result is obtained (Fig. 3). These observations strongly support the proposition that the major absorbed dose for Auger-electron emitting thallium-201 is from the intracellular radionuclide while for the beta emitters it is from the extracellular decays.



Figures 2 (right) and 3 (left). Uptake and survival curves for V79 cells following 18-hr incubation with radioactive potassium congeners. On the right, uptake and survival fractions are plotted as a function of variable ouabain concentration in a constant concentration of radionuclide in the extracellular medium. On the left, uptake and survival fractions are plotted as a function of extracellular radionuclide concentration (3).

Correspondingly, the dose rate delivered to cells, as calculated by traditional MIRD dosimetry, is significantly less for thallium-201 than for potassium-43 and rubidium-86 when the cells are dispersed in the same concentration of radioactivity (Table 4A, Column 5). However, experimentally, under these circumstances thallium-201 has been found to have greater radiotoxicity. This last observation fits better with the degree of self-absorption from intracellular radioactivity than with the dose received from extracellular activity (Table 4A, Columns 2,3,4). In simulated tissues where the cells are packed closely together, these differences disappear due to the greater contribution to average dose provided by intracellular radioactivity (Table 4B).

Table 4: Dose Rates To Cells From 370 kBq/ml Average External Concentration of Radionuclide

A. DISPERSED CELLS

<u>Radionuclide</u>	Microdosimetry			
	<u>Cell To Itself</u>	<u>Other Cells to Cell</u>	<u>TOTAL*</u> <u>(rad/hr)</u>	<u>MIRD</u> <u>(rad/hr)</u>
201Tl	28.9	0.01	29.4	0.9
86Rb	2.0	0.13	10.7	11.1
43K	1.2	0.03	6.6	6.0

B. SIMULATED TISSUE GEOMETRY

201Tl	0.42	0.6	1.0	0.9
86Rb	0.03	14.1	14.2	14.2
43K	0.04	6.5	6.6	6.6

* The difference between the total value and the sum of the contributions in columns 3 and 4 is the contribution from the medium to the target cell.

The magnitude of this concentration effect leading to an underestimation of the calculated absorbed dose depends not only on the relative intracellular and extracellular concentrations of the radionuclide, on the range, energy and number of low energy electrons emitted, but also on the fraction of tissue occupied by cells sequestering the radioactivity. The greater the proportion of such cells in a tissue, the less the effect. Rao et al have calculated the dose-enhancement factors for thallium-201 for various fractions (*f*) of active cell volume. When *f* is negligible (great distance between cells) the enhancement is 31 times for cells concentrating the radionuclide 100-fold over the extracellular compartment (5). When *f* is 15%, it is 2.9; when 50%, it is 1.6, and when 70%, it is 1.4. For many tissues and many other radionuclides the values (and the corresponding dose error) could easily be 50 to 70%.

HIGHLY LOCALIZED ABSORBED ENERGY DENSITY

Some Auger-electron emitting radionuclides deposit relatively large amounts of energy in volumes of macromolecular dimensions, causing considerable damage to radiosensitive sites. An example is iodine-125 which, on the average, releases seventeen low energy electrons of 15 to 475 eV with ranges of 1 to 25 nm. Such low energy particles, say of 100 eV, deposit approximately 25 eV in spheres of radius 1 nm or $6 \text{ eV}/(\text{nm})^3$ or $6 \times 10^{21} \text{ eV}/\text{ml}$ corresponding to an "equivalent rad dose" of $\sim 10^8$ rad in that region(4). The differential profile of average absorbed energy density as a function of distance from the site of iodine-125 decay is given in Figure 4. It has been suggested that nuclear events depositing 300 eV or more energy in

regions of 3 to 5 nm can cause ≥ 10 ionizations in the region and lead to high LET-type biological effects (7).

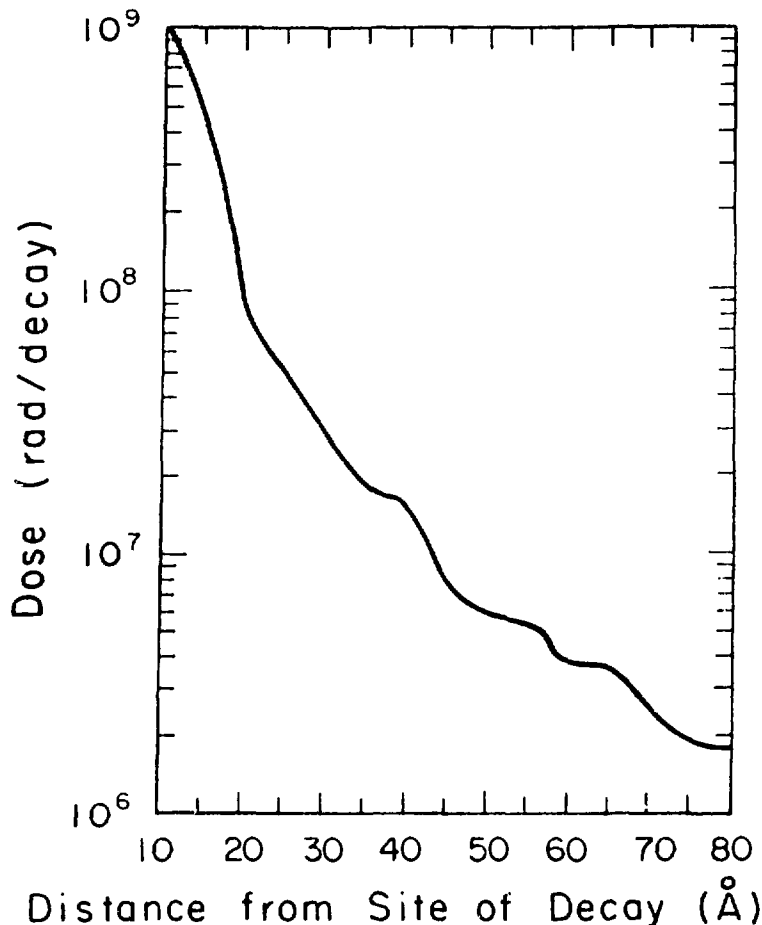


Figure 4. Differential profile of average absorbed energy density as a function of distance from the site of iodine-125 decay. For 10 \AA° , the absorbed energy density shown is for a sphere of this radius. Thereafter, the energy density in concentric spherical sheets of 5 \AA° thickness is given (4).

Indeed, severe molecular and biological effects have been observed when iodine-125 is incorporated into a number of compounds. When iodine-125 decays in gaseous alkyl halides (methyl and ethyl-iodide) or condensed halogenated pyrimidine bases (iodouracil), severe molecular fragmentation takes place with the production of one and two-carbon fragments(8,9). If iodine-125 is introduced into a constituent base of double stranded DNA-oligonucleotides, multiple strand breaks are produced in both strands upon decay, most of them within 5 to 6 nucleotides from the decay site(10). The frequency of strand breaks as a function of distance from the site is in agreement with the localized dose profile shown in Figure 4.

The biological effects are equally profound. In terms of cell sterilization, iodine-125 is much more effective per decay or per rad than either the beta-gamma emitter, iodine-131, or the beta emitter hydrogen-3 (Figure 5). Several differences among the three survival curves are noteworthy. First, there is a shoulder on the survival curves for tritium and

iodine-131 while for iodine-125 the curve is exponential throughout (as it is after exposure to alpha-particles); thus the survival curves after iodine-125 decay are high LET-like in their appearance. Second, the slope of the exponential portion of the survival curves is greater for iodine-125 than it is for the other radionuclides. We have found that, at the mean lethal uptake (D_{37}) of iodine-125 the total number of disintegrations is about 100/cell. Taking into account the Auger electron energy deposition pattern and the nuclear volume of V79 cells, the average absorbed dose to the nucleus is 67 rad; for the same cell line, the D_{37} for x-rays is 580 rads. Thus, the emanations from iodine-125 are about eight-times more effective than x-rays in reaching the same biological end point.

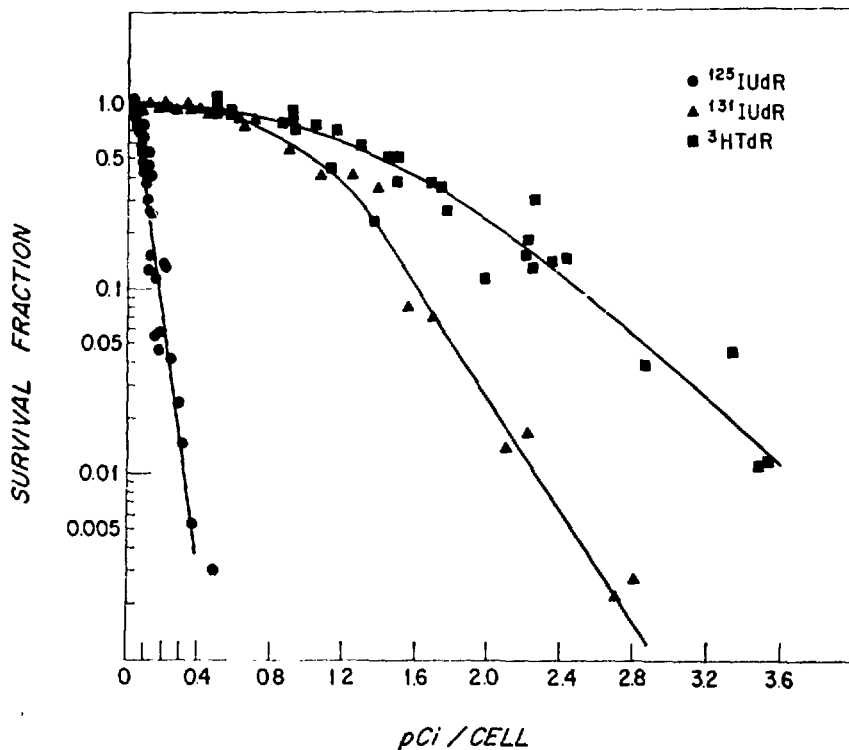


Figure 5. Survival curves for V79 cells after incorporation of radioactive deoxyribonucleoside precursors into their DNA. From left-to-right, the radionuclides are iodine-125, iodine-131 and hydrogen-3 (tritium).

Survival curves similar in appearance to iodine-125 are obtained with bromine-77 and iodine-123 which also decay by electron capture. Differences in the number of electrons emitted per decay, the energy deposited in 5nm spheres, and the D_{37} for survival are given in Table 5 (11). There is a regular inverse relationship between the amount of energy deposited in these macromolecular volumes (about 15 base pairs) and the number of decays required to sterilize a cell.

Table 5: Comparison of Electron Yields, Microscopic Energy Deposition and Cell Survival Among Auger Electron-Emitting Radiohalogens Incorporated into DNA

<u>Nuclide</u>	<u>Radiochemical Form (halodeoxyuridine)</u>	<u>Electron Yield Per Decay</u>	<u>Energy Deposited in 5nm Radius Spheres</u>	<u>D₃₇ (mBq/cells)</u>
Bromine-77	⁷⁷ BrUdR	7	300	4.8
Iodine-123	¹²³ IUDR	11	560	2.6
Iodine-125	¹²⁵ IUDR	20	1000	1.5

These Auger electron-emitting radiohalogens need not be incorporated directly into DNA. They can also produce similar biological effects when introduced into molecules that intercalate with DNA or into hormones that bind specifically with nuclear receptors (12,13). It has been suggested that radioactive decays taking place within 3 nm of the DNA duplex produce high LET-like effects with correspondingly elevated radiobiological effectiveness (14).

More worrisome, from the point-of-view of radiation protection, is the increased carcinogenesis and mutagenesis found *in vitro* with DNA-incorporated iodine-125 (15,16). Relative to tritiated thymidine (³HTdR), iodine-125 labeled iododeoxyuridine is a very efficient inducer of both malignant transformations in mouse BALB/3T3 cells and HPRT mutations in human diploid lymphoblasts. A three-fold increase in the yield of mutations or transformations was produced by only 8 and 20 total decays per cell respectively of ¹²⁵IUDR. Normalizing for survival, ¹²⁵IUDR is much more potent than either x-rays or ³HTdR.

CONCLUSION

The increasing use of intracellular radioindicators in nuclear medicine represents a new challenge for radiopharmaceutical dosimetry. The arguments presented in this paper demonstrate a need to take into account the microscopic distribution of dose at the cellular level, especially if the decay involves electron capture and internal conversion. For radionuclides deposited in the cytoplasm or uniformly throughout the cell, inaccuracies may be corrected by sufficient attention to self- and cell-to-cell irradiation. For radionuclides, positioned within 3 to 5 nm of the radiosensitive genome, corrections will be more problematic and must take into account the high-LET character of the radiation effects.

ACKNOWLEDGEMENT

The work from our laboratory cited in this paper was supported by grant R01-CA-15523 from the National Cancer Institute.

REFERENCES

1. Kassis, A.I., K.S.R. Sastry, S.J. Adelstein. Intracellular distribution and radiotoxicity of chromium-51 in mammalian cells: Auger-electron dosimetry. *J. Nucl. Med.* 26, 59-67, 1985.
2. Kassis, A.I., S.J. Adelstein, C. Haydock, K.S.R. Sastry. Radiotoxicity of ^{75}Se and ^{35}S : Theory and application to a cellular model. *Radiat. Res.* 84, 407-425, 1980.
3. Kassis, A.I., S.J. Adelstein, C. Haydock, K.S.R. Sastry. Thallium-201: An experimental and a theoretical radiobiological approach to dosimetry. *J. Nucl. Med.* 24, 1164-1175, 1983.
4. Sastry, K.S.R., D.V. Rao. Dosimetry of low energy electrons, in *Physics of Nuclear Medicine: Recent Advances*, edited by D.V. Rao, R. Chandra and M.C. Graham, pp. 169-208, AAPM Medical Physics Monograph No. 10, 1984.
5. Rao, D.V., G.F. Govelitz, K.S.R. Sastry. Radiotoxicity of Thallium-201 in mouse testes: inadequacy of conventional dosimetry. *J. Nucl. Med.* 24, 145-153, 1983.
6. Rao, D.V., K.S.R. Sastry, G.F. Govelitz, H.E. Grimmond and H.Z. Hili. Radiobiological effects of iron-55 and iron-59 in mouse testes, Biophysical dosimetry of Auger-electron emitters in vivo. *J. Nucl. Med.* (in press).
7. Goodhead, D.T., R.J. Munson, J. Thacker, R.Cox. Mutation and inactivation of cultured mammalian cells exposed to beams of accelerated heavy ions. IV. Biophysical interpretation. *Int. J. Radat. Biol.* 37, 135-167, 1980.
8. Carlson, T.R., R.M. White. Formation of fragment ions from $\text{CH}_3\ ^{125}\text{Te}$ and $\text{C}_2\text{H}_5\ ^{125}\text{Te}$ following the nuclear decay of $\text{CH}_3\ ^{125}\text{I}$ and $\text{C}_2\text{H}_5\ ^{125}\text{I}$. *J. Chem. Phys.* 38, 2930-2934, 1963.
9. Stöcklin, G., Chemical and biological effects of β -decay and inner-shell ionization in biomolecules, in *Proceedings of the Sixth International Congress of Radiation Research*, edited by S. Okada, M. Imamura, T. Teroshima and H. Yamaguchi, pp. 382-391, Tappan Publ., Tokyo, 1979.
10. Martin, R.F., W.A. Haseltine. Range of radiochemical damage to DNA with decay of iodine-125. *Science* 123, 896-898, 1981.
11. Kassis, A.I., K.S.R. Sastry, S.J. Adelstein. Intracellular localization of Auger electron emitters: Biophysical Dosimetry (in press).

12. Martin, R.F., T.R. Bradley, G.S. Hodgson. Cytotoxicity of an ^{125}I -labeled DNA-binding compound that induces double-stranded DNA breaks. *Cancer Res.* 39, 3244-3247, 1979.
13. Bloomer, W.D., W.H. McLaughlin, R.R. Weichselbaum, R.N. Hanson, S.J. Adelstein, D.E. Seitz. The role of subcellular localization in assessing the cytotoxicity of iodine-125 labeled iododeoxyuridine, iodotamoxifen and iodoantipyrine. *J. Radioanal. Chem.* 65, 209-221, 1981.
14. Goodhead, D.T., D.E. Charlton. Critical properties of radiation at low doses. Abstract of Papers, 33rd Ann. Mtg. Radiat. Res. Soc. Los Angeles, p. 121, 1985.
15. LeMotte, P.D., S.J. Adelstein and J.B. Little. Malignant transformation induced by incorporated radionuclides in BALB/5T3 mouse embryo fibroblasts. *Proc. Nat. Acad. Sci. (USA)* 79, 7763-7767, 1982.
16. Little, J.B., H.L. Liber, P.K. LeMotte. Iodine-125 and tritium mutagenesis and carcinogenesis *in vitro*. Abstract of Papers, 33rd Ann. Mtg. Radiat. Res. Soc. Los Angeles, p. 114, 1985.

DISCUSSION

HINES: You have shown the need to carefully consider the inhomogeneous distribution of the radionuclide and the subsequent absorbed dose calculation when the cell concentrates the radionuclide. Would you comment on the radiobiological effect of the uptake of the radionuclide by the cell wall?

ADELSTEIN: There is some experimental data that sheds some light on that. In our own laboratory we just simply use sodium iodide which is excluded from the cell and is in the surrounding media. As you would guess that's much less effective than incorporating the iodine into the cell nucleus. A number of years ago a group down in Florida under Kurt Hofer did some work with $I-125$ -labeled concanavalin A that selectively binds to cell membrane. They showed that it was essentially the same as excluding the material almost completely from the cell nucleus. I know there has been a certain amount of speculation as to whether the membrane radiation is an important part of radiosensitivity of the cell. We don't have any evidence of it so far.

BRODSKY: A beautiful paper. I am curious about something concerning radiation protection. For the past 10 years the NRC has had the responsibility of recommending bioassay procedures for the use of tritium. When this program was first started, there were some alarming reports in the literature that tritium was many times more radiotoxic than previously believed. In developing regulatory guidance for the conditions under which bioassay sampling of tritium workers should be carried out, I conducted literature reviews to examine the question of relative hazard of DNA precursors and other organic compounds labeled with $H-3$. Some of this review is included in NRC Publication No. NUREG-0938 (1983). I concluded that when the exposure route is via inhalation or ingestion, rather than injection, all $H-3$ labeled compounds can be treated the same as tritiated water for purposes of controlling worker exposure. I based this on the fact that laboratory experience shows the nonvolatility of those compounds in the biochemistry of DNA formation reduces probabilities of

exposure and that organic precursors of DNA tend to be converted to HTO or $3\text{H}_2\text{O}$ before transport to blood from the inhalation or ingestion route because tritium has the heavier molecular weight. Is there any information in your research or experience that would contradict these conclusions? We do not want to be more restrictive than necessary for safety in the handling of these compounds. Because we may be revising Regulatory Guide 8.20 which is our bioassay guide on I-125 and I-131, I would appreciate any new information on the relative hazards from compounds of these radionuclides also.

ADELSTEIN: Well, I can't answer the question completely. Let me try, though, in two ways. First of all, as you have seen from the survival curves that I've shown, tritium dosimetry is not surprising. Certainly the shape of the survival curves are of the low LET-type that you would expect. Secondly, Hermann Lisco and I did a piece of work about 100 years ago which has been mercifully neglected by the people who read the tritium literature, but it does relate to what you asked. There was an orthopedic surgeon by the name of Henry Banks who had permission to inject tritiated thymidine into a group of elderly people to study the migration of dividing cells in fractures of the hip. Hermann and I studied chromosomal aberration frequencies before and after the injection of tritiated thymidine in these patients. We predicted we would not see anything at that dose level and we didn't see anything. On the other hand, if you had a dire prediction you wouldn't have seen that either, because elderly patients have a rather high background of noise in terms of chromosomal frequencies. Nothing in my own personal experience tells me that there is anything wrong with your assumptions but I am unaware of the general literature.

WAGNER: Jim, when we first started doing lung scans, I calculated the radiation dose to the tissue adjacent to a particle and came up with something like hundreds of thousands of rads, which I'm sure is correct. At that time, which was over two decades ago, the conclusion I came to was that the averaging of radiation dose over tissue is really a mental exercise and not useful for estimating biological effects. The next circumstance I ran into was with respect to estimating the effective dose of I-125 versus I-131 in the treatment of hyperthyroidism. Standard dosimetry calculations would lead you to believe that you would see a greater effect from I-125 than from I-131, which is exactly opposite from the real situation.

You concluded your excellent talk by saying what we really should do is be aware of all these things. That brought to my mind the person who has a heart attack and goes home from the hospital and the doctor tells the patient to try and take it easy. The patient really needs to have something more specific. I'm going to challenge you to be a little more specific as to how we should be changing our ways of calculating radiation dose. We are taught that if you get one plutonium particle in your lung the probability of getting cancer is exceedingly high because of the delivered radiation dose; yet in nuclear medicine procedures, although you have documented that we're delivering billions of rads to cells, we're not observing these biological effects. My question then is, what guidelines should we take home? Should the whole concept of radiation dosimetry that we are now using be modified, or should we continue to go through these exercises that don't let us predict anything about observable biological behavior?

ADELSTEIN: Well, Henry, I think, if I may say it, that you learned half a lesson. First of all, let me comment on the old lung scanning dose. The fact is, the lung scanning dose probably overestimated by averaging the dose to the radiosensitive target since those particles in the lung were lodged in capillary endothelial cells. I don't know whether anybody ever calculated what the distances were to the cell nuclei, but by averaging, we probably overestimated and we probably overestimate the dose everytime we use I-125 if

material is extracellular. As a matter of fact, those calculations of dosimetry for treatment of thyrotoxicosis with iodine-125 were terribly flawed in terms of the premise made by people who did them originally. As you know, I-125 is concentrated in the follicles of the cells and they were trying to make some sort of estimation as to the dose to the perifollicular nuclei.

Now the reason I said you only learned half a lesson is that I thought I said you have to be most concerned when radionuclides that decay by this particular scheme are lodged in the genetic material itself. At the present moment, there are relatively few of them, but, as you and others begin to work with new compounds, I think you will need to pay attention to whether the receptors are internalized and brought to the cell nucleus. In the case of the neuroreceptors, I am not aware that they do that. Some hormone receptors, however, are internalized and brought into the region of the nucleus. Researchers today must be biologists as well as clinicians so they can understand the dynamics of these materials. I think they will need to pay some attention to radionuclides that are brought into cells. Although this is a new phenomenon in nuclear medicine, we are entering an era when more and more of these materials will be used.

If the distribution is quite heterogeneous, do we need to consider modifying the dosimetry? I don't think you ought to just watch out for it. I think you have to understand what the distributions are at a more microscopic level. By understanding the distributions at microscopic levels, one can make corrections in some instances. In other instances I just don't know what else to say except that we have observed phenomena that potentially are more hazardous than we have recognized.

THE MICRODOSIMETRY OF MONOCLONAL ANTIBODIES
LABELED WITH ALPHA EMITTERS

Darrell R. Fisher
Battelle, Pacific Northwest Laboratories
P. O. Box 999
Richland, WA 99352 U.S.A.

ABSTRACT

The recent discovery of new techniques for the production of monoclonal antibodies (MoAB) has opened up a number of potential new applications in cancer diagnosis and therapy. Monoclonal antibodies labeled with alpha-emitting radionuclides promise to be particularly effective therapeutic agents due to the efficient cell killing ability of highly ionizing, short-range alpha particle tracks localized at specific antigen sites within the tumor mass. For a radioimmunotherapy treatment plan to be effective, one must be able to estimate the absorbed radiation dose to both tumor cells and normal tissues in the body. However, conventional methods used in nuclear medicine for estimating absorbed doses and specific absorbed fractions for radiopharmaceuticals do not apply to alpha emitters owing to their short range and the large variations in the local distribution of energy at the cellular level that result.

Microdosimetric techniques developed for assessment of the radiological effects of internally deposited transuranic radionuclides take into account the statistical aspects of alpha particle track structure, energy distribution patterns, and radionuclide distribution within tissues, and provide a means for determining the number and frequency of cells irradiated, the probability densities in specific energy, and the average dose delivered to cells of interest. These techniques can be applied to the study of radiation absorbed dose from alpha-labeled monoclonal antibodies.

INTRODUCTION

Kohler and Milstein (1) were first to successfully utilize hybridization techniques for producing monoclonal antibodies (MoAB). This discovery opened the way for widespread clinical application of MoAB in immunological studies and in the use of radiolabeled MoAB in the diagnosis and treatment of many different neoplastic diseases (2).

The objective of radioimmunotherapy is to employ a monoclonal antibody specifically directed against selected tumor-associated antigens of malignant cells, couple the antibody to a radioisotope conjugate, and administer the complex to a cancer patient. Selective localization results in significantly higher concentrations of MoAB in neoplastic tissue than in normal tissue, allowing localized radiotherapy and/or external imaging of target tissues.

Research and clinical testing of radiolabeled monoclonal antibodies in cancer diagnosis and treatment is continuing at a rapid pace, as demonstrated by a recent international symposium (3). A variety of different MoAB, labeled with radionuclides such as I-131 (beta emission) or In-111 (electron capture), have been administered to human patients for treatment of a variety of cancer types (4). Photon emitters (Tc-99m, Ga-67) are excellent conjugates for

external imaging, whereas beta emitters (Sc-47, Cu-67, and Y-90), positron emitters (Cu-64, Br-77, and Zr-89) and alpha emitters (At-211, Bi-212) are preferred candidate radionuclides for therapy. Positron-labeled MoAB have potential for simultaneous imaging and therapy.

Alpha-emitting radionuclides have been considered for immunotherapy because they emit high-energy, short range helium nuclei that are highly effective in cell killing. Alpha-emitting MoAB cannot be imaged externally, but are thought to have potential for the most efficient in cell killing per unit administered activity. Their short range also offers the potential for higher tumor/normal tissue dose ratios and therefore greater therapy effectiveness with lower total patient doses and greater sparing of normal body tissues and organs.

Current research in alpha-labeled MoAB development is centered at the National Cancer Institute in Bethesda, Maryland. Work currently involves identifying and producing MoAB that are specific to tumor cell antigens but nonspecific to normal cells (5), selecting appropriate radionuclides, synthesizing and testing chelating agents to bind the MoAB to selected radioisotopes (6), the development of generators for short-lived radionuclides for clinical application (7), and the testing of radiclabeled MoAB for anti-tumor effectiveness (8).

Since the range of alpha particles in tissue is short (30-80 micrometers, depending on decay energy, or about 5-10 cell diameters), more than a single cell will probably be hit by an alpha particle emitted from the surface of a target cell wall. It is of interest, therefore, to quantify the dose to nearby cells as well as to cells on which the MoAB has attached. Furthermore, the dosimetric technique must account for the stochastic nature of alpha particle energy deposition and the geometry (size and distance) of target sites with respect to the alpha emitter (9). It may also be important to be able to determine the probability that cells are completely missed by alpha particles, hit once, twice, or hit many times.

With all radiotherapy, the ability to limit the undesired dose to normal tissues and organs of the body may determine the ultimate success or failure of treatment with radiolabeled MoAB (10). It is highly desirable to be able to estimate the absorbed radiation dose to both tumor cells and normal tissues. The range and ionization density of alpha particle tracks in tissue are complex; conventional methods used in nuclear medicine (11-13) for estimating absorbed doses and specific absorbed fractions for radiopharmaceuticals do not directly apply to alpha emitters.

This paper reviews concepts of microdosimetry as pertaining to internally deposited alpha emitters. The described method, developed for calculating the microdosimetry of alpha-emitting actinides, has potential for direct application to the dosimetry of alpha-labeled MoAB in clinical testing, treatment planning, and evaluation of therapy effectiveness.

ALPHA PARTICLE TRACKS AND ENERGY LOSS TO TISSUE

Charged-particle radiation interacts with atomic electrons of the matter through which it passes, and ionization/excitation energy is imparted with each interaction. The charge and mass of the particle, its initial energy, and the matter through which it travels determine the pattern of energy loss, the distance traveled, and the direction taken by the particle. Ionizations and excitations are produced when the energy is transferred from the particle to the medium. On the average, about 34 ev are expended for each ion pair produced; thus, many atoms or molecules are ionized by interactions with an alpha particle track.

Alpha particle tracks are characterized by a dense central core of primary ionizations along a straight path. A 5-MeV alpha particle travels about 38 μm in unit density material. Secondary low-energy electron tracks (delta rays) radiate from the central core with a penumbra diameter of about 100 nm. The relative specific ionization, or ionization density per unit track length, increases with distance traveled according to the familiar Bragg curve. The ionization density may become 2.5 times greater at the end of the track than at the beginning. The position of a target (cell or cell nucleus) along or near the track determines the amount of ionization energy that will be imparted to it by the track. The amount of energy imparted will be highly variable.

DOSIMETRIC QUANTITIES FOR SMALL TARGET SITES

The basic quantity that describes the energy imparted to matter is the absorbed dose. The absorbed dose is actually a mean value, sometimes called the "average dose." By definition, the absorbed dose D is the quotient of $d\bar{e}$ by $d\bar{m}$, where $d\bar{e}$ is the mean energy imparted by ionizing radiation to matter of mass $d\bar{m}$ (14):

$$D = d\bar{e}/d\bar{m}$$

The special name for the unit of absorbed dose is gray (1 Gy = 1 J/kg), although many dosimetrists still prefer to use the term "rad" (1 rad = 0.01 J/kg).

The specific energy (z) is a stochastic quantity with units similar to absorbed dose. It is defined as the quotient of e by m , where e is the energy imparted by ionizing radiation to matter of mass m (14):

$$z = e/m$$

The mean absorbed dose in a volume is equal to the mean specific energy, \bar{z} , in that volume:

$$D = \bar{z}$$

The ratio e/m is highly dependent upon target diameter. Figure 1 shows a 0.1- μm segment of a Monte Carlo track for a proton in water; primary ionizations are shown with x's, and secondary delta-ray interactions are shown with dots. The ionization energies imparted to four spherical targets with diameters varying from 5 to 50 nm are indicated. The difference in dose among the four sites is due primarily to the differences in target size. The dose can also vary according to the position of targets along or near the particle track.

Similarly, the dose to microscopic biological sites is determined by the amount of energy imparted to it by an intersecting particle. Each site will receive a unique amount of energy, and thus the dose to small sites may range from zero (if the site is missed) to many hundred gray.

For many target sites in an irradiated field, the variation in e/m increases as m decreases. Figure 2 shows dose, or specific energy density, as a function of the mass for which energy density is determined (15). The horizontal part of this figure shows the range of target sizes for which the absorbed dose (D) can be established in a single measurement.

The specific energy is a stochastic quantity. The dotted region represents the range in which statistical dose fluctuations are important. Each dot

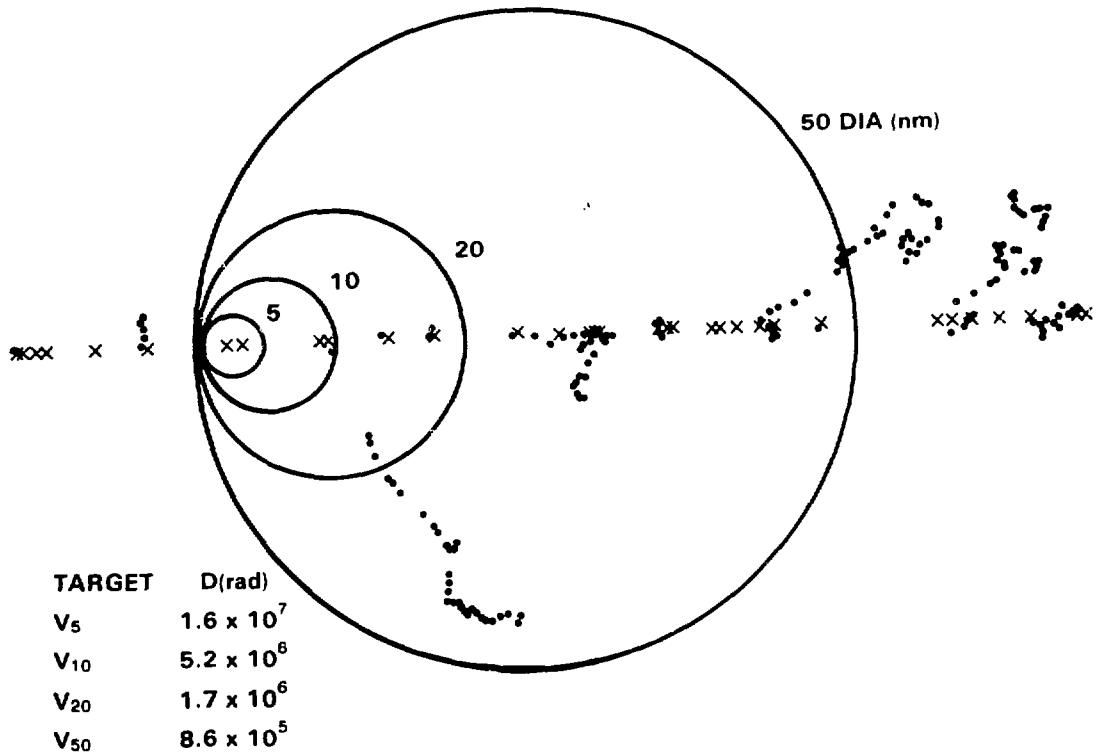


Figure 1. A Comparison of Doses to Microscopic Spheres Along the Path of a Hypothetical Proton Track.

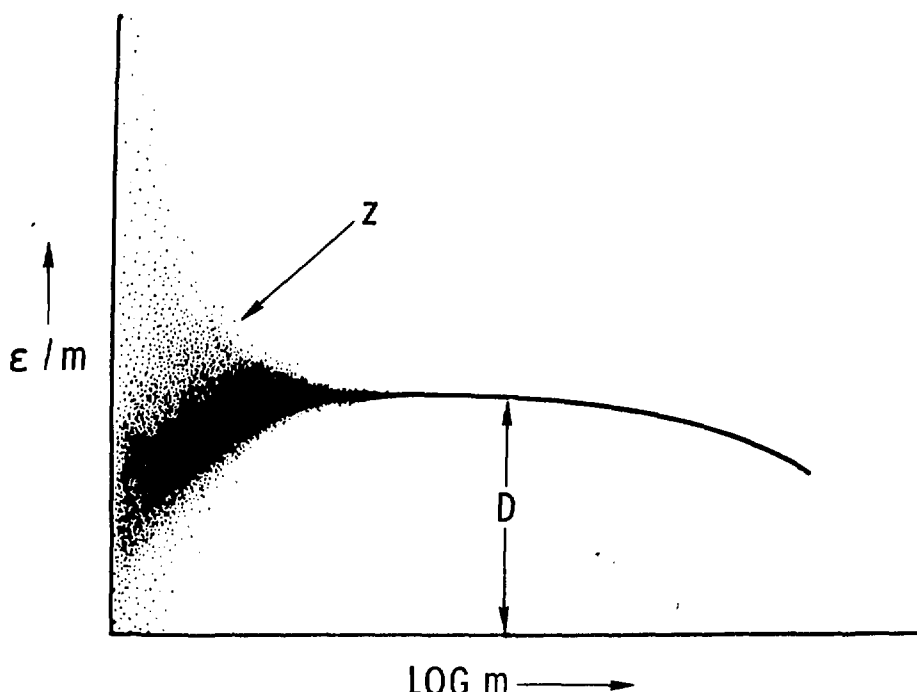


Figure 2. Variation in Dose as a Function of Target Mass. From Rossi (15). Used by permission.

represents the specific energy (z) for a single dose measurement or calculation. As one selects progressively smaller and smaller target sizes, the variations in the local dose become increasingly greater, and the average dose value becomes less and less indicative of the complete dose distribution. Thus, for very small sites, the concept of absorbed dose becomes increasingly abstract, and the dose is better represented by a distribution of doses in "specific energy." For a given target size mass, this distribution is called a "probability density in specific energy." If the probability density in specific energy is denoted by $f(z)$, then $f(z)dz$ is the probability that the specific energy received by a site lies in an infinitesimal range dz containing the value z . The density is a function of z rather than a single number, as with the absorbed dose.

The probability density includes the component $z=0$ and the delta function (δ) which is the probability that no energy is deposited. The delta function is equivalent to the fraction of unirradiated sites.

CALCULATING SPECIFIC ENERGY DENSITIES FOR ALPHA EMITTERS

Methods for calculating probability densities in specific energy for internally deposited alpha emitters were developed by Roesch (16), and were originally applied to the study of dose distribution and biological effects from inhaled transuranics. The first step involves characterizing the geometrical relationship between the distribution of alpha emitters and the distribution of target sites. Second, one must determine the density in specific energy for a target at any distance from the alpha source. All possible angles of intersection are considered. Third, one must determine from the spatial distribution of sources the probability that a point source exists at any given distance from the target. Fourth, the densities from all point sources are convoluted using Fourier transforms to construct a new specific energy density for the target population (the organ or tissue of interest). Accounted for are the low-energy delta ray components of the alpha track, and the relative specific ionization as a function of track length.

The geometrical relationship between the distribution of alpha-emitting sources and microscopic biological targets is an important consideration in internal microdosimetry. Computer codes have been written to incorporate the geometric distributions shown in Figure 3. These source-site configurations (or combinations thereof) are sufficient for modeling almost any natural biological arrangement in the body (9).

The computer codes written to accomplish these calculations are still in the development stage; however the results are of interest in demonstrating the principles involved in the internal microdosimetry of alpha-emitting radionuclides. Some examples are given below for Bi-212.

THE MICRODOSIMETRY OF BI-212

Bismuth-212 decays by alpha (34%) and beta (66%) emission with a half-life of 60.55 minutes. Most of the energy is lost by alpha emission (77%), with lesser amounts by beta, conversion electron, and Auger electron emission (16%). The beta-emission daughter (Po-212) immediately decays by emitting an 8.78 MeV alpha particle (half-life = 0.3 microseconds). Thus, more than 95% of the locally absorbed energy is deposited by alpha decay. In the following examples, only the 6.07 MeV alpha energy is included in the calculation, and the radiation energy from all other decay modes is omitted.

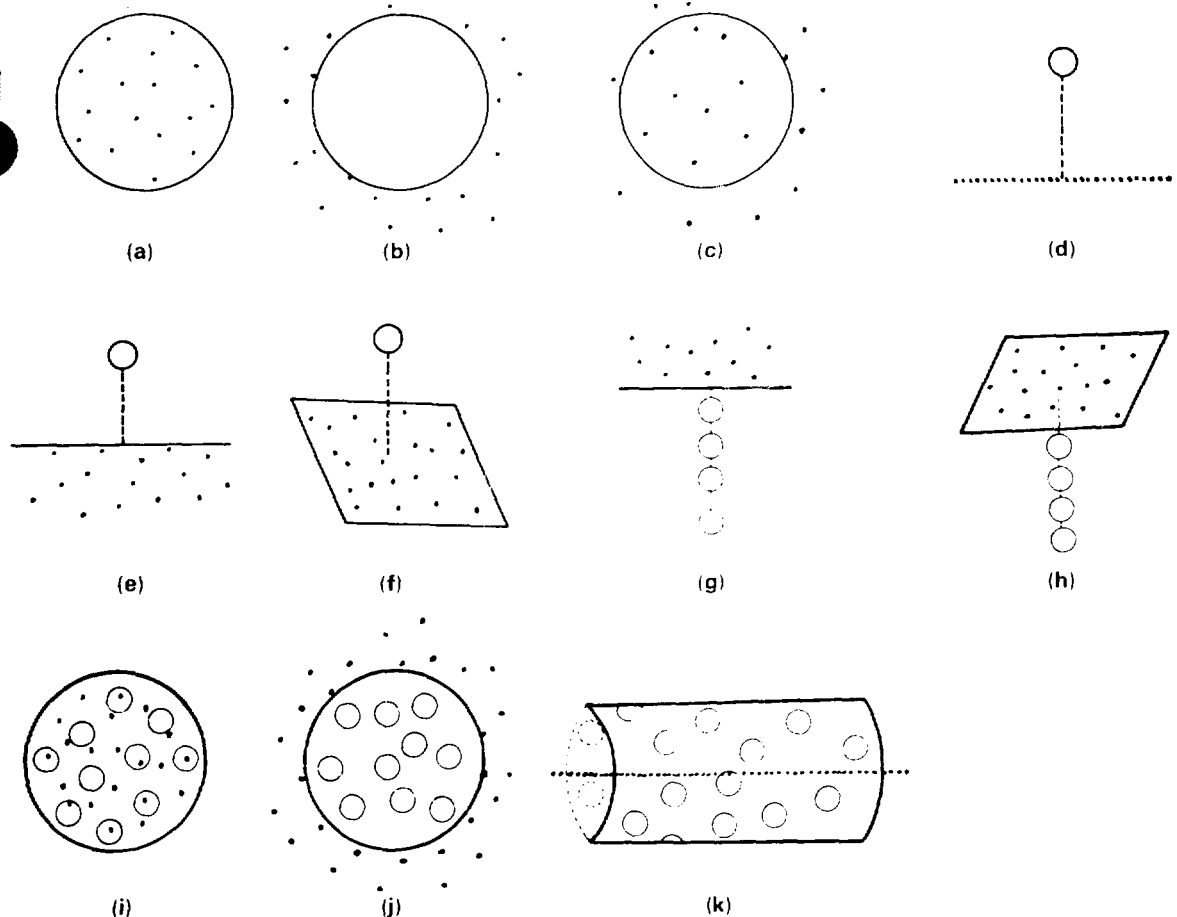


Figure 3. Geometrical Variations on the Spatial Distribution of Radioactive Particulates (small dots) and Biological Targets (small circles).

Monoclonal antibodies labeled with Bi-212 will attach to the surfaces of cells when the target antigen specific to that antibody is recognized. A target cell may be irradiated by activity on its own surface, or by activity on the surfaces of nearby cells. Consider first the case of Bi-212 located on the surface of the cell (dia. = $4.66 \mu\text{m}$). Figure 4 shows the probability density in specific energy (Gy) for three conditions: one alpha emitted, four alphas emitted, and ten alphas emitted, respectively. The average cell doses were found by calculation to be 0.57, 2.30, and 5.75 Gy, respectively (57, 230, and 575 rad). The delta functions (probability that the cell is completely missed by alpha radiation) were found to be 0.37, 0.026, and 0.0003, respectively.

Consider next the case involving irradiation of the cell by alpha emitters on the walls of neighboring cells. If the concentration of alpha activity per unit mass is known, the dose distribution in specific energy to randomly distributed target sites can be calculated. One alpha particle per source is assumed. If this concentration of alpha-emitting sources is 2.53 per 1,000 cubic micrometers of tissue, the resulting absorbed dose is 2.46 Gy (246 rad), and the specific energy distribution is illustrated in Figure 5. In this example, $\delta=0.111$, meaning that 11% of the target cells would likely be missed and 89% hit.

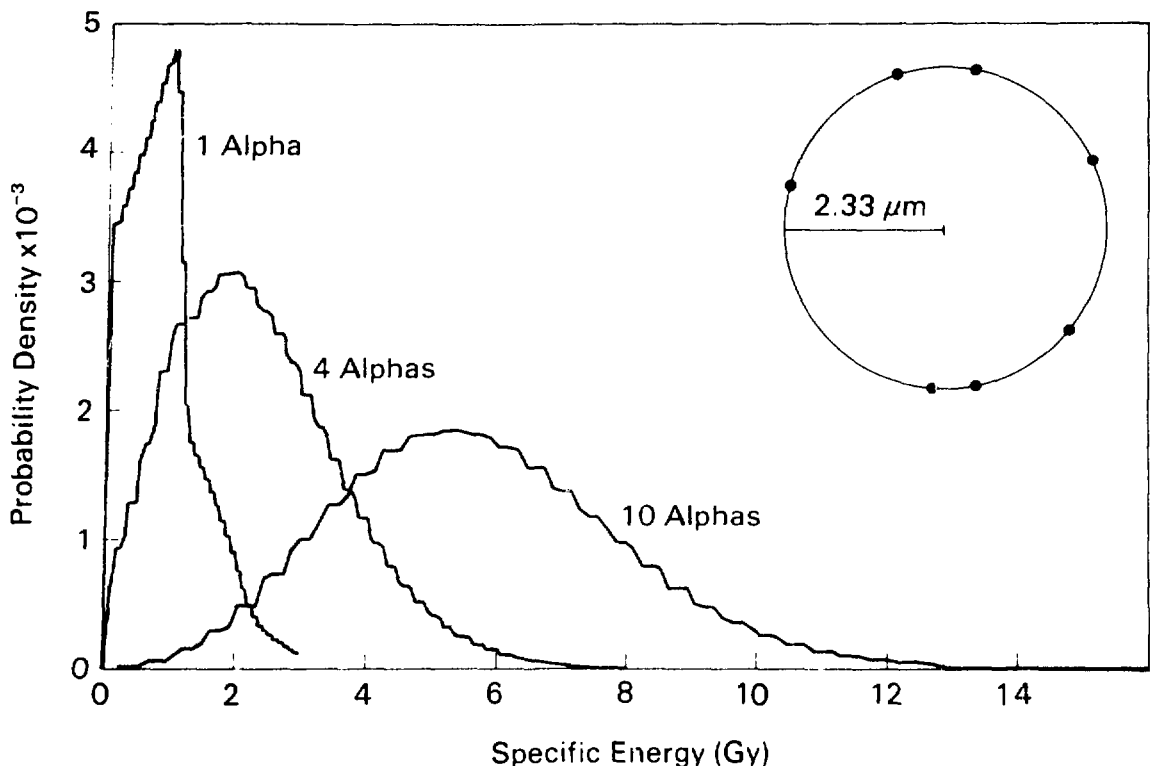


Figure 4. Probability Density in Specific Energy for a $2.33 \mu\text{m}$ Site Irradiated by Bi-212 Activity on the Cell Surface. The activity emits one, four, or ten alpha particles in any direction.

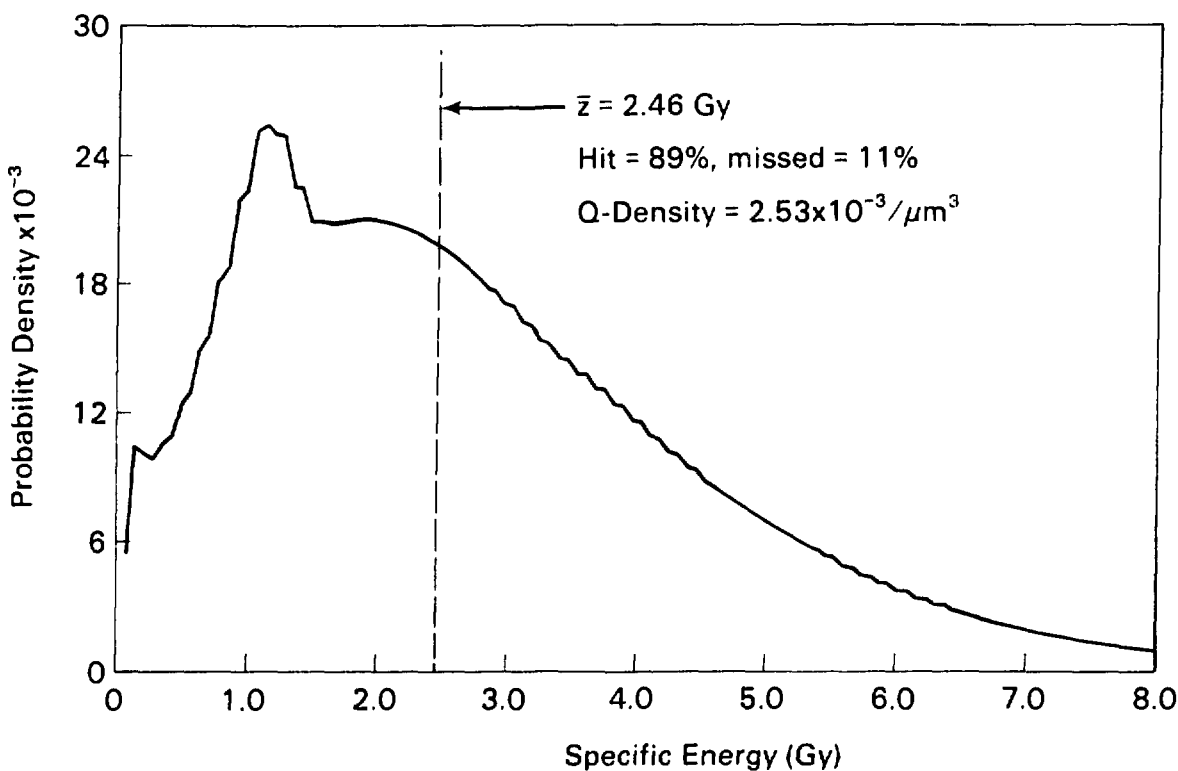


Figure 5. Probability Density in Specific Energy for Bi-212 in a Tumor Mass Delivering an Absorbed Dose of 2.46 Gy. The Q-Density is the concentration of MoAB emitting one alpha particle.

The absorbed dose to tissue may be varied by changing the concentration of alpha emitters. Figure 6 shows four probabilities in specific energy, and corresponding delta functions and absorbed doses for concentrations of 0.3, 2.5, 5.0, and 12.5 alpha-emitting sources per 1,000 cubic micrometers of tissue. At a dose of 12.32 Gy (1,232 rad), all sites are hit, whereas only 23.8% of the sites are hit with an absorbed dose of 0.29 Gy (29 rad).

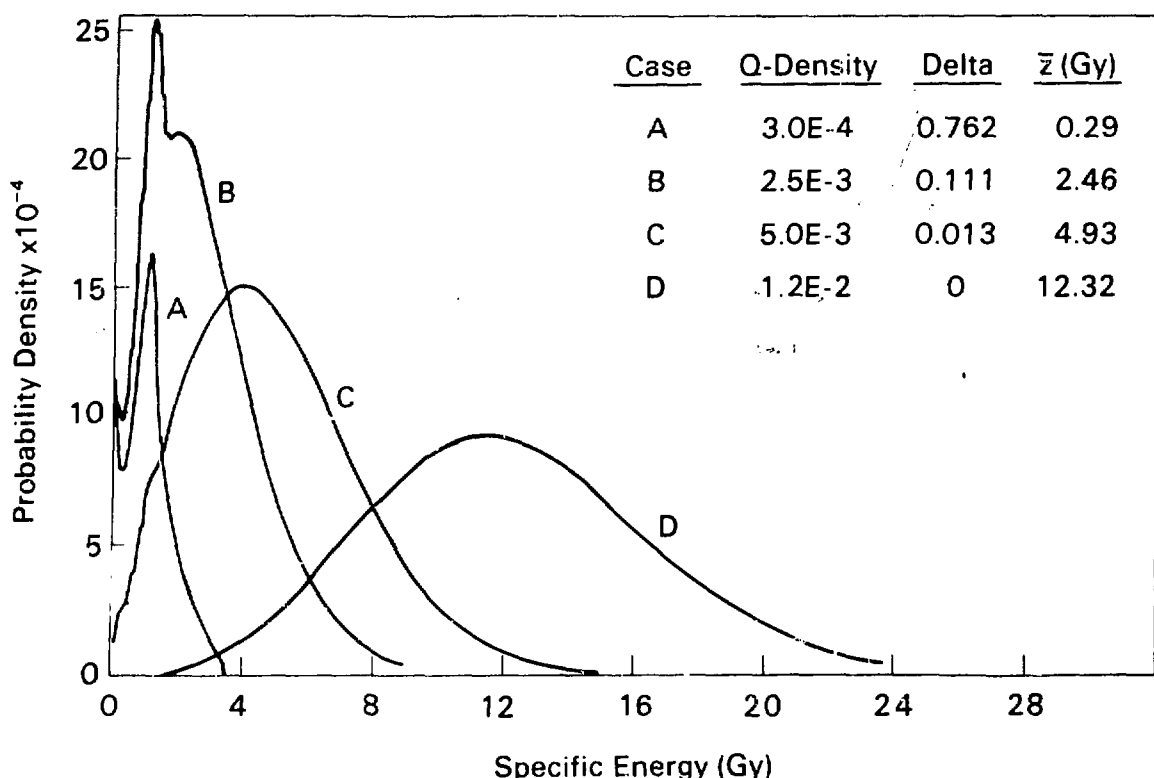


Figure 6. A Comparison of Probability Densities in Specific Energy for Four Concentrations of Bi-212 in a Tissue Mass.

Similar calculations may be performed for astatine-211 (half-life = 7.2 hr), an alpha-emitting halogen also considered to be a prime candidate for MoAB cancer therapy.

The shape of the probability density in specific energy provides clues to the potential effectiveness of the irradiation. The precise relationship between specific energy density and short-term or long-term biological effects is not known at this time, and further studies are needed to define the relationships. The curves are useful, however, for general comparisons of different irradiation conditions.

THE MICRODOSIMETRY OF PO-212 + BI-212

The half-life of Po-212 is less than one millionth of a second and thus for every three decays of Bi-212 there will be two 8.78 MeV alpha particles and one 6.07 MeV alpha particle. The higher energy alpha particle from Po-212

has a greater range and therefore will hit more cells along its path than the alpha particle from Bi-212. The absorbed dose to 4.66-micrometer-diameter cells from Po-212 located outside the cells was calculated to be 3.94 Gy (394 rad) for a Po-212 concentration of 2.53 alpha-emitting sources per 1,000 cubic micrometers of tissue. For this case, the delta function was found to be 0.01, meaning that 1% of the target cells would be missed and 99% would be hit. For the parent/daughter combination and a concentration of 2.53 Bi-212 parent atoms per 1,000 cubic micrometers of tissue, the resulting absorbed dose is 3.45 Gy (345 rad) and the delta function is 0.02.

AMOUNT OF ACTIVITY NEEDED TO INACTIVATE A CELL POPULATION

A simple calculation can be performed to determine the total concentration of Bi-212 needed to deliver a desired radiation dose, such that all the tumor cells will be inactivated.

From the examples above it was shown that a 3.45 Gy (345 rad) tumor dose could be achieved with an activity concentration of 2.53 Bi-212 parent atoms per 1,000 cubic micrometers of tissue. We assume that all atoms of Bi-212 decay. This corresponds to $\sim 2.5 \times 10^9$ alphas per cubic centimeter (or gram) of tissue. The total activity required is 13 μCi of Bi-212 per gram tissue, and 98% of the cells will be hit. If we assume that one gram of tissue corresponds to 1×10^9 cells, then 2.5 Bi-212 MoAB are required per targeted cancer cell. Ideally, one would like about ten times this amount for complete tumor eradication. Thus, about 135 μCi per gram tumor would result in an absorbed dose of about 35 Gy (3,500 rad), or about 25 alpha emissions per single cell, and complete cell killing.

CONCLUSIONS

The development of MoAB labeled with alpha-emitting radionuclides may provide an effective method for delivering a highly ionizing, short-ranged alpha particle to target cancer cells. Conventional dosimetric methods do not consider the great variation in local (microscopic) dose, the probability that cells are hit, or the microscopic nature of biological targets (cells and cell nuclei). Similarly, the concept of specific absorbed fraction does not apply to alpha emitters due to the local absorption of energy, the intense ionization along alpha particle tracks, and their short range.

Microdosimetric methods developed for assessing the radiobiological implications of incorporated alpha-emitting actinides have unique potential for direct application to the dosimetry of alpha-labeled monoclonal antibody therapy. Microdosimetry takes into account the stochastic nature of energy deposition in small sites, target hit probabilities, and the probable number of alpha-emitting MoAB needed to produce a desired effect.

The product of a microdosimetry calculation is a histogram--a statistical distribution of doses to small sites, rather than a simple average dose. However, the average dose can be determined from the distribution. It can then be compared to the probability density in specific energy or the absorbed dose from a different irradiation condition.

The precise relationship between specific energy density and resulting biological effects is not known. Clinical studies and in-vitro cell irradiation studies are needed to determine these relationships and to verify the general

effects predicted by theory. It is expected that microdosimetry will be useful in treatment planning and may help to explain the radiobiology of alpha-labeled MoAb cancer therapy.

REFERENCES

1. Kohler, G., and C. Milstein. Continuous cultures of fused cells secreting antibody of predetermined specificity. *Nature* 256. 495-497, 1975.
2. Oldham, R. K. Monoclonal antibodies in cancer therapy. *J. Clin Oncol.* 1. 582-590, 1983.
3. The American College of Radiology sponsored an international symposium on Labelled and Unlabelled Antibody in Cancer Diagnosis and Therapy, September 12-13, 1985, at the Johns Hopkins Medical Institutions in Baltimore, Maryland.
4. Dillman, R. O., and I. Royston. Monoclonal antibodies in the therapy of malignant diseases. In *Handbook of Monoclonal Antibodies--Applications in Biology and Medicine*, edited by S. Ferrone and M. P. Dierich, pp. 436-472, Noyes Publications, Park Ridge, New Jersey, 1985.
5. Colcher, D., P. Hand, M. Nuti, and J. A. Schlom. A Spectrum of Monoclonal Antibodies Reactive with Human Mammary Tumor Cells. *Proc. National Acad. Sci. (USA)* 78. 3199-3203, 1981.
6. Gansow, O. A., R. W. Atcher, D. C. Link, A. M. Friedman, R. H. Seevers, W. Anderson, D. A. Scheinberg, and M. Strand. Generator-produced Bi-212 Chelated to Chemically Modified Monoclonal Antibody for Use in Radiotherapy. *Amer. Chem. Soc. Sympos. Series* 241. 215-227, 1984.
7. Zucchini, G. L., and A. M. Griedman. Isotopic Generator for Pb-212 and Bi-212. *Int. J. Nucl. Med. Biol.* 9. 83-84, 1982.
8. Strand, M., D. A. Scheinberg, and O. A. Gansow. Monoclonal Antibody Conjugates for Tumor Imaging and Therapy. In *Cell Fusion: Gene Transfer and Transformation*, ed. by R. F. Beers, Jr., and E. G. Bassett, pp. 385-393, Raven Press, New York, 1984.
9. Fisher, D. Principles of Microdosimetry in Radiation Protection. PNL-SA-11959. Pacific Northwest Laboratory, 1984.
10. DeNardo, G. L., A. Raventos, H. H. Hines, et al. Requirements for a treatment planning system for radioimmunotherapy. *Int. J. Radiation Oncology Biol. Phys.* 11. 335-348, 1985.
11. Loevinger, R., and M. Berman. A Revised Schema for Calculating the Absorbed Dose from Biologically Distributed Radionuclides, NM/MIRD Pamphlet No. 1, Rev. Society of Nuclear Medicine, New York, 1976.
12. Snyder, W. S., M. R. Ford, C. G. Warner, and S. B. Watson. "S," Absorbed Dose Per Unit Cumulated Activity for Selected Radionuclides and Organs, NM/MIRD Pamphlet No. 11. Society of Nuclear Medicine, New York, 1975.
13. Berman, M. Kinetic Models for Absorbed Dose Calculations, NM/MIRD Pamphlet No. 12. Society of Nuclear Medicine, New York, 1977.

14. International Commission on Radiation Units and Measurements. Radiation Quantities and Units. ICRU Report 33, Washington, D.C., 1980.
15. Rossi, H. H. Microscopic Energy Distribution in Irradiated Matter, in Radiation Dosimetry, Vol. I, edited by F. H. Attix and W. C. Roesch, pp. 43-92, Academic Press, New York.
16. Roesch, W. C. Internal Microdosimetry. Radiat. Res. 70. 494-510, 1977.

DISCUSSION

ADELSTEIN: While you were giving the talk I was trying to think of the criteria you would have to use for therapeutic purposes. One must often kill all the cells in a tumor i.e., reduce the probability of any cell surviving to no higher than 10%. If you assume that a small number of alpha tracks inactivate a cell, what average number of transversals would be required to ensure that all cells receive at least that number? Is this number likely to be achieved by antibody therapy?

FISHER: I estimate that about three to four alpha particles through a cell will inactivate it and cause cell killing. Experiments at Argonne National Laboratory¹ have shown up to 15 may be required for flattened osteocytes. Recent work by Min, Cohn, and Simmons² at the Polytechnic of Central London confirm about three to four alpha particles will inactivate a cell. Because the particles can travel in 4-pi directions, to get those hits, you need three or four times that many alpha particles, so you need from nine to fifteen alpha emissions from the surface of the cell to be effective in killing that cell. This is well within the realm of therapy. There are probably 10,000 to 50,000 antigen sites on tumor cells. With normal efficiencies in getting the antibody to the specific antigen, 50 to 100 alpha emissions could be directed to an individual tumor site. I think this is a very good possibility.

One drawback with alpha emitters is that the range is only about 5 or 6 cell diameters. If you have a tumor with active cells that these alpha emitters cannot reach, you are not going to kill them. Another limitation is the half-life of the alpha emitter. Bismuth-212 has a one-hour half life so the delivery system has to be efficient and fast. Some solid tumors may not allow that.

DOHERTY: I have a question concerning what you said about alpha emitters providing mechanisms for getting a better tumor-to-blood ratio. I was wondering how you do it?

FISHER: A better tumor-to-normal tissue ratio. Well, first, the nature of monoclonal antibodies is that the activity is going to be attached specifically to tumor cells and nonspecifically to normal cells. Secondly, the range of these alpha particles is so short that the fraction of healthy tissue irradiated away from the tumor is going to be small.

¹Lloyd, E.L. and M.A. Gemmell. Survival of human osteosarcoma cells & normal human fibroblasts following alpha particle irradiation. Radiological & Environmental Research Division Annual Report, Argonne National Laboratory, Argonne, IL. Report #ANL-80-115, Part II, p 33-40, May, 1981.

²Min, T; P. Cohn, & J.A. Simmons. The sensitivity of three diploid human cell lines to alpha irradiation, IN: Proceedings of Second International Workshop on Lung Dosimetry. Cambridge, England, 9/2-6/85.

PHYSICAL AND CHEMICAL EVENTS THAT FOLLOW THE PASSAGE
OF A CHARGED PARTICLE IN LIQUID WATER

H. A. Wright, R. N. Hamm, and J. E. Turner
Health and Safety Research Division, Oak Ridge National Laboratory
Oak Ridge, Tennessee 37831

J. L. Magee and A. Chatterjee
Lawrence Berkeley Laboratory, University of California
Berkeley, California 94720

ABSTRACT

Biological effects of radiation are the result of a complicated sequence of events that begins with initial physical interactions that are complete by $\sim 10^{-15}$ s, followed by chemical interactions that begin at $\sim 10^{-11}$ s and are complete by $\sim 10^{-6}$ s, and followed by later biochemical and biological events, some of which may not occur for years. A central problem in radiation physics and radiation chemistry is to understand the details of the physical and chemical events that occur during that first microsecond following the passage of a charged particle. Significant progress has been made recently at linking early physical events with later chemical events. We have developed a Monte Carlo computer code to calculate the position and identity of each physical event that a charged particle (electron, proton, alpha) and all of its secondaries undergoes in traversing liquid water. The code then calculates the position and identity of each reactive chemical species (ion or radical) that is produced from these physical events and is present at 10^{-11} s, and then follows each reactant through the diffusion and chemical reaction stage of track development. This work will be discussed and examples of "pictures" of charged-particle tracks at various times will be shown.

INTRODUCTION

In radiopharmaceutical dosimetry or radiation protection dosimetry, the average dose in a macroscopic volume such as an entire organ is usually considered to be the relevant quantity. This average dose is then multiplied by an empirically determined weighting factor (Relative Biological Effectiveness, RBE, or Quality Factor, QF) for that particular type of radiation in order to estimate the biological response. The reason for the large variation in RBE (which can depend on type of radiation, effect considered, dose, dose rate, temperature, the degree of oxygenation, etc.) is still not understood but must depend on the details of the way the dose is deposited. If one considers the dose to a microscopic volume such as a single cell a few micrometers in diameter, the dose will not be the same in each cell. Some cells may receive no dose at all while others may receive doses that are orders of magnitude greater than the average dose to the entire organ. If one considers a volume with dimensions comparable to the diameter of a DNA molecule (i.e., a few nanometers), the variation in dose from one volume to the next is greater still. On this scale one must consider energy deposition by a single particle (electron, proton, etc.). However, there is even statistical variation in the deposition of energy along the trajectory of the particle. A proton or electron may go directly through the center of a DNA molecule and deposit no energy at all in the molecule. The picture gets even more complicated when one considers what happens after the energy is initially transferred from the particle to the medium. A complicated sequence of physical and chemical events occurs within the first microsecond. Biochemical and biological responses occur later. For example, within seconds enzymes can move in and start trying to repair damage that has occurred to the DNA molecule. Much has been learned about biological and biochemical reactions, but up until now very little has been known about initial physical and early chemical reactions in condensed matter.

We have recently made progress in understanding the details of the interactions that occur in liquid water within the first microsecond following the passage of a charged particle. In this paper we will discuss this work which describes the formation and chemical development of charged-particle tracks. It is the purpose of this paper to help provide some insight into the details of the complex sequence of physical and chemical interactions that radiation produces in condensed matter.

DISCUSSION OF EARLY PHYSICAL AND CHEMICAL INTERACTIONS IN MATTER

When a charged particle such as an electron or alpha particle traverses matter, it undergoes physical interactions with atoms or molecules of the material. These physical interactions result in energy transfer events that in general result in excitation or ionization of atoms or molecules of the material. The secondary electrons that are produced by ionization events may have substantial energy and may themselves produce further ionization or excitation events as they slow down. These physical events occur very rapidly. In a local region of space the physical interactions produced by a primary charged particle and all of its secondaries are complete in times of the order of 10^{-15} s. These physical events produce chemical changes within the track of the charged particle that result in chemically reactive ions or radicals that can diffuse through the medium and react with each other or with other molecules present. Diffusion and chemical reactions begin at times of the order of 10^{-11} s and are generally complete by 10^{-6} s. Thus the physical and chemical reactions that are produced by radiation are complete within the first microsecond, but these reactions can produce changes that may result in the induction of cancer decades later.

The collection of physical and chemical species produced by a charged particle is referred to as the track of the particle. Radiation of different qualities produces charged-particle tracks with different structures. For example, high-energy radiation can produce high-energy secondary electrons (delta rays) that can travel some distance laterally from the trajectory of the primary particle. Thus the track produced by a high-energy particle has a larger radius than that produced by a low-energy particle. High-LET (Linear Energy Transfer) radiation in general produces a more dense track than low-LET radiation. However, two particles of the same LET may produce quite different tracks. A 1-MeV proton, for example, has approximately the same LET in water as a 23-MeV alpha particle. However, since the alpha particle has a higher velocity, it can produce higher velocity delta rays. Therefore, the track it produces will have a larger radius than that of the proton. It is easy to see that studies of track structure are very important in attempting to understand the differences in the biological effects of different types of radiation. Studies of the "structure of tracks" are a central focus of the field of microdosimetry. Microdosimetry symposia typically have entire sessions devoted to such track structure studies (1).

Interactions between a charged particle and an atom or molecule can be measured in the gas phase. A charged particle penetrating a gas-filled chamber can undergo an interaction with a single atom or molecule and be scattered with a lower energy and new direction. A detector can then record the new energy and new direction of the incident particle as well as the energy and direction of secondary electrons that are produced. However, when an electron or other charged particle penetrates a condensed medium, such as liquid water, much of the energy transferred to the water appears first as a collective oscillation (plasmon) that involves a coherent oscillation of perhaps 10^9 electrons. The plasmon then decays into a specific energy transition (excitation or ionization) event which may be located nanometers (many molecular diameters) from the trajectory of the primary charged particle.

Since it is not possible, in general, to measure the details of individual interactions in condensed matter, much less is known about energy transfer mechanisms in condensed media. However, biological systems exist in condensed phase (solid or liquid), and therefore there is much interest in understanding interactions in such systems. We have recently made progress in understanding the physical and chemical interactions that occur in liquid water, a medium of much interest for biological systems. We have developed a set of differential inverse mean free paths (cross sections) for the initial physical interactions that occur in liquid water. We have constructed a model for reactions that occur during the pre-chemistry time to approximately 10^{-11} s. We have also developed a model to calculate quantities associated with the diffusion and chemical reaction stage following the passage of the charged particle. We have used this information to develop a computer code for performing calculations of the details of the physical and chemical interactions that follow the passage of a charged particle through liquid water. The code uses Monte Carlo techniques to simulate, event by event, the interactions that a particle undergoes in traversing liquid water. Thus the code determines the position and nature of every elementary energy transfer event. The code tabulates the position of each reactive chemical species (radical or ion) that is produced and then follows each of them individually as they diffuse through the medium and react with each other. This code can be used to calculate the transport of a charged particle through liquid water, the formation of the track during the physical stage, and the development of the track through the chemical stage of its evolution.

This program represents the first time that calculations have been made forward in time from the initial physical interactions through later chemical reactions. It therefore links radiation physics to radiation chemistry and

promises to make valuable contributions to understanding the mechanisms involved in producing biological effects of radiation. In order to discuss interactions that occur in liquid water, perhaps it is best to consider some characteristic distances and distance units as listed in Table 1. The

Table 1. Characteristic Distances

2.9 Å	= diameter of H ₂ O molecule
2 nm	= diameter of DNA helix
≥1 μm	= diameter of nucleus of biological cell
50 μm	= diameter of human hair
100 μm	= thickness of sheet of paper

diameter of the nucleus of a biological cell is generally a few microns. The range of a 5-keV electron is approximately 1 micron. However, if the DNA molecule is the sensitive site for damage within a cell, then the important distances to consider are only a small portion of the track of a 5-keV electron. Table 2 shows some characteristic times and reactions that occur during the physical stage of reaction of a charged particle in liquid water (2-4). Ionization and excitation events occur within 10^{-15} s. The vibrational

Table 2. Physical Interactions

10^{-18} s	Fast particle traverses atom
10^{-17} - 10^{-16} s	Ionization: $H_2O \rightarrow H_2O^+ + e^-$
10^{-15} s	Excitation: $H_2O \rightarrow H_2O^*$
10^{-14} s	Ion-molecule reactions: $H_2O^+ + H_2O \rightarrow H_3O^+ + OH$
10^{-14} s	Dissociation of excited molecules: $H_2O^* \rightarrow H + OH$
10^{-12} s	Hydration of electron: $e^- \rightarrow e_{aq}^-$
10^{-12} s	Light travels 300 μm, thickness of 3 sheets of paper

period of a water molecule is approximately 10^{-14} s, and some ion-molecule reactions and molecular dissociations can occur within this time period. Electrons can thermalize and become hydrated within 10^{-13} to 10^{-12} s. The hydrated electron is a reactive chemical species that is formed as several water molecules cluster around the negative electron. Since a reactive chemical species requires somewhat more than 10^{-12} s to diffuse a distance equal to the diameter of a water molecule, diffusion and chemical reactions are generally considered to begin at approximately 10^{-11} s. Table 3 shows some typical reaction times during the chemical stage of charged-particle track development. At very high concentrations, reactions can occur within 10^{-10} s since the reactants are close to each other. Reactions within a spur (a cluster of chemical species produced in a track by an energy loss of 100 eV or less) are generally complete in less than 10^{-7} s, and the remaining radicals are homogeneously distributed (i.e., initial spatial correlations are lost). For completeness, Table 4 shows some typical reaction times during the biological stage.

Table 3. Chemical Interactions

$10^{-12}\text{--}10^{-10}$ s	Interactions of e^-_{aq} and other radicals in high concentrations or in dense regions of charged particle tracks
10^{-10} s	Reactions of e^-_{aq} and other radicals with reactive solute at ~ 1 mol/L
$<10^{-7}$ s	Reactions in spur
10^{-7} s	Homogeneous distributions of radicals
10^{-7} s	Reactions of radicals with reactive solute at 10^{-3} mol/L
10^{-7} s	Light travels about 100 ft

Table 4. Biological Interactions

Seconds to hours	Enzyme repair of damaged molecules
Hours	Cell division affected
Days	Damage to central nervous system and GI tract
Several months	Kidney and lung damage
Years	Cancer induction or genetic damage

In the remainder of the paper we discuss some of the details of the code and the physical and chemical reactions produced by radiation. Then we give some details of charged-particle tracks at different stages of development. Finally, we describe some initial work toward applying the code to calculate effects on biological molecules such as DNA.

CALCULATIONS OF TRACK STRUCTURE DURING FIRST MICROSECOND

As mentioned in the introduction, some interactions of a charged particle and a molecule in gas phase can be measured directly. However, it is necessary to use a different approach for obtaining such information for liquid water. Our approach has been to develop a complex dielectric response function $\epsilon(w,q)$ for liquid water, where $\hbar w$ and $\hbar q$ are the energy and momentum transferred in a single event by a charged particle to the medium. In this manner collective effects in the condensed phase are included *a priori*. The macroscopic cross section (inverse mean free path), for any kind of interaction, can be obtained directly from $-Im(1/\epsilon)$, the negative of the imaginary part of $1/\epsilon$. Details of the development of the cross sections and the algorithm for treating initially delocalized collective oscillations in the condensed phase are described elsewhere (5-8).

We have used these cross sections to develop a Monte Carlo computer code to calculate the positions of the species that are produced in the track of a charged particle and are present at 10^{-15} s. These are ionized water molecules (H_2O^+), excited water molecules (H_2O^*), and subexcitation electrons (e^-). An example of a track of a 5-keV electron, starting at the origin and initially headed along the horizontal axis to the right, is shown in Fig. 1.

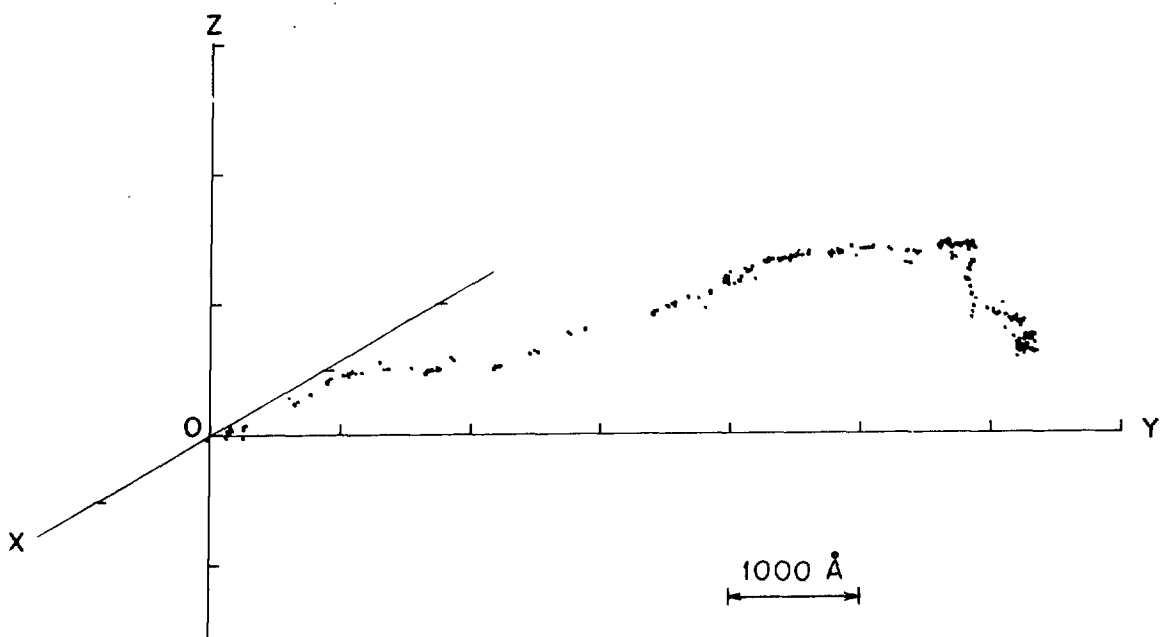


Fig. 1. Location of inelastic events produced by a 5-keV electron and all of its secondaries in liquid water. Original 5-keV electron started at the origin traveling toward the right along the horizontal axis. Ticks are 1000 Å apart.

Each point in the track represents the position of one of the two species H_2O^+ or $\text{H}_2\text{O}^\bullet$. The ticks on the axes are 1000 Å apart so the track is approximately 1 μm long. The model which we have developed to determine the position and identity of each reactive chemical species at the beginning of the chemical stage (10^{-11} s) is described elsewhere (9,10). The four reactive chemical species that are present at 10^{-11} s are the OH radical, the hydrated electron e_{aq}^- , the hydronium ion H_3O^+ , and the hydrogen radical H. Figure 2 shows an enlargement of the initial portion of the 5-keV electron track shown in Fig. 1 at 10^{-11} s where the positions and identities of the chemical species are shown. The ticks on the axes in this figure are 50 Å apart. For perspective, the diameter of the DNA helix is about 20 Å.

In order to simulate diffusion and chemical reactions, it is necessary to identify the chemical reactions that are to be considered significant, which we have taken to be those shown in Table 5. Each of the reactive species is allowed to undergo a diffusive jump. Then the distance between each pair is checked by the computer. If two species that can react according to Table 5 are close enough together, they are considered to react and are removed. After all pairs are checked, and those that have reacted are removed, the remaining reactants are jumped again and the process is repeated. Details of the schemes used to simulate this process are given elsewhere (10,11).

Three examples of 5-keV electron tracks are shown in Fig. 3. In each case the electron started at the origin traveling along the horizontal axis toward the right. In each case the points represent the positions of the reactive chemical species at 10^{-11} s. It is seen that the tracks are very different. It is noted that in general the tracks are far from just straight trajectories with a uniform density of energy losses along the track that would be expected from the stopping power alone.

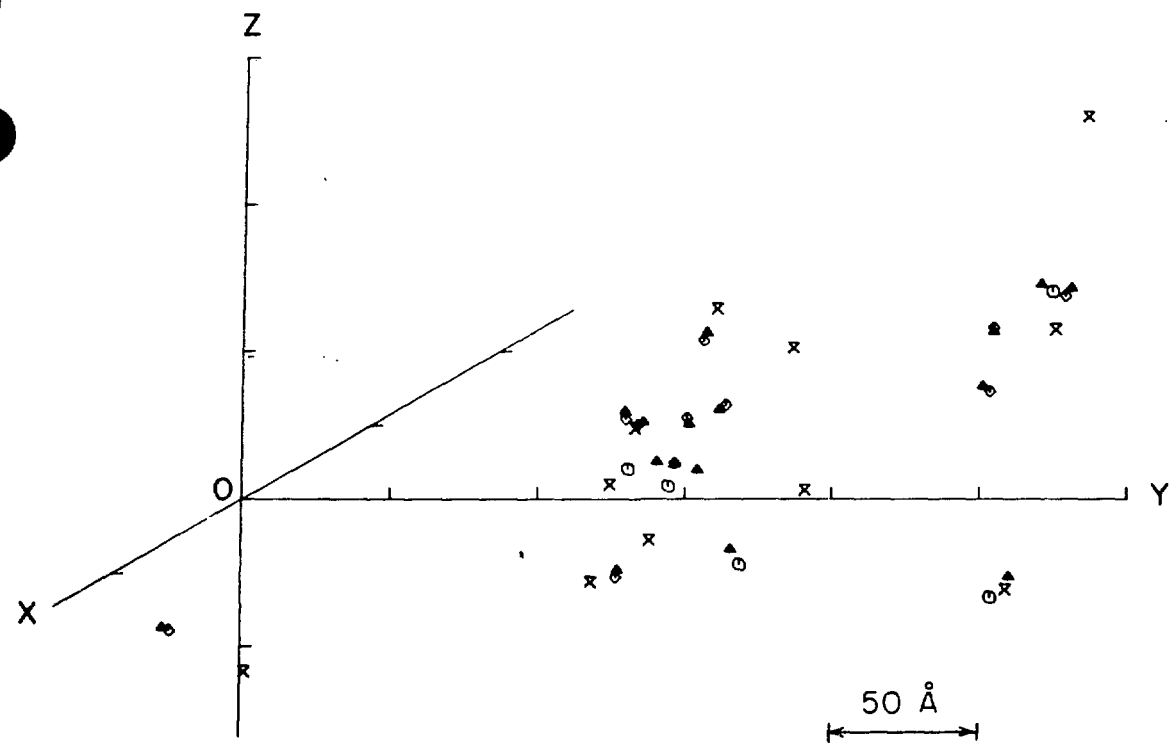


Fig. 2. Twenty-fold blown-up view of initial portion of track in Fig. 1, showing location of chemical species at 10^{-11} s. Legend: \circ , H; Δ , OH; \times , e^-_{aq} ; \diamond , H_3O^+ .

Table 5. Chemical Reactions at Times $>10^{-11}$ s

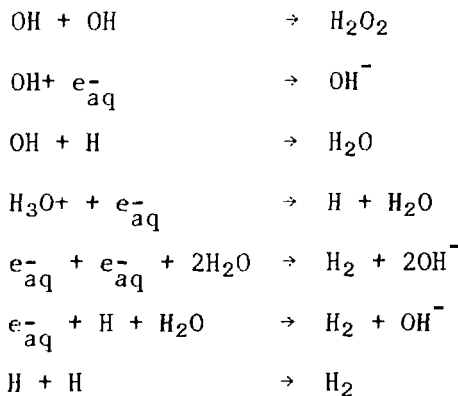


Figure 4 shows the chemical development of the top track in Fig. 3. At 10^{-11} s, the beginning of the diffusion and chemical reaction stage of track development, the track contained 1,174 distinct reactive species with positions as shown in the top left of Fig. 4. After 10 diffusive jumps of 2.5×10^{-12} s each, 985 reactants remained. Thus 189 species had already

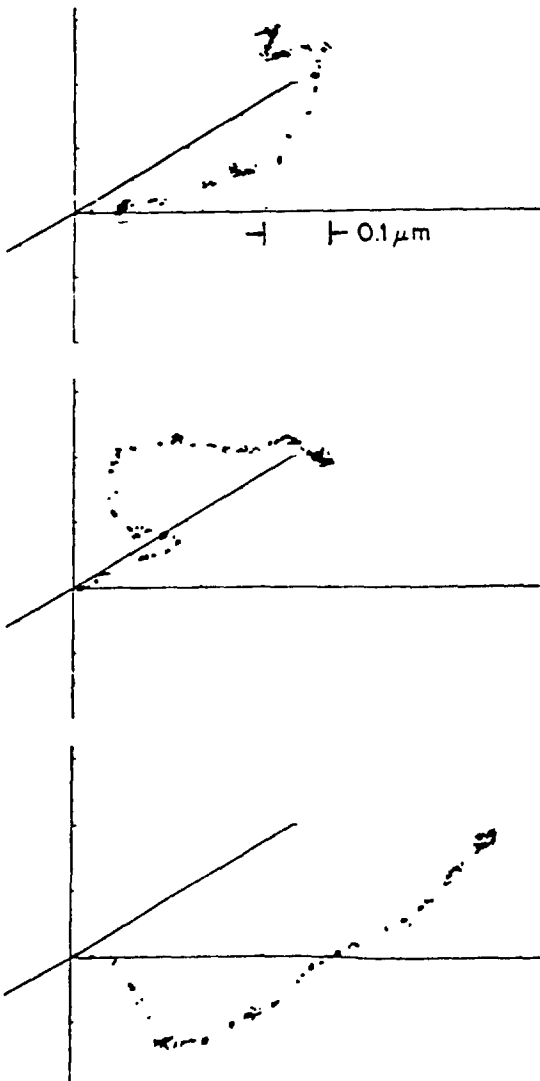


Fig. 3. Three examples of the spatial distribution of chemically active species present at 10^{-11} s around the tracks of 5-keV electrons in liquid water. In each case the electron started at the origin moving along the axis toward the right.

reacted and were removed. After 100 additional diffusive jumps, only 687 species remained. The number of the remaining species and their positions are shown at different times in the figure. Note that by 2.8×10^{-7} s there were only 410 species left, and they are essentially homogeneously distributed. Initial spatial correlations, considered important in many models for biological effects, no longer exist. By this time the reactants are sufficiently separated that further reactions occur infrequently. However, in any biological system there would be other molecules present that could also react with (scavenge) the species. In most cases the scavenge time would be much less than one microsecond, so this would terminate the chemistry stage of the track development.

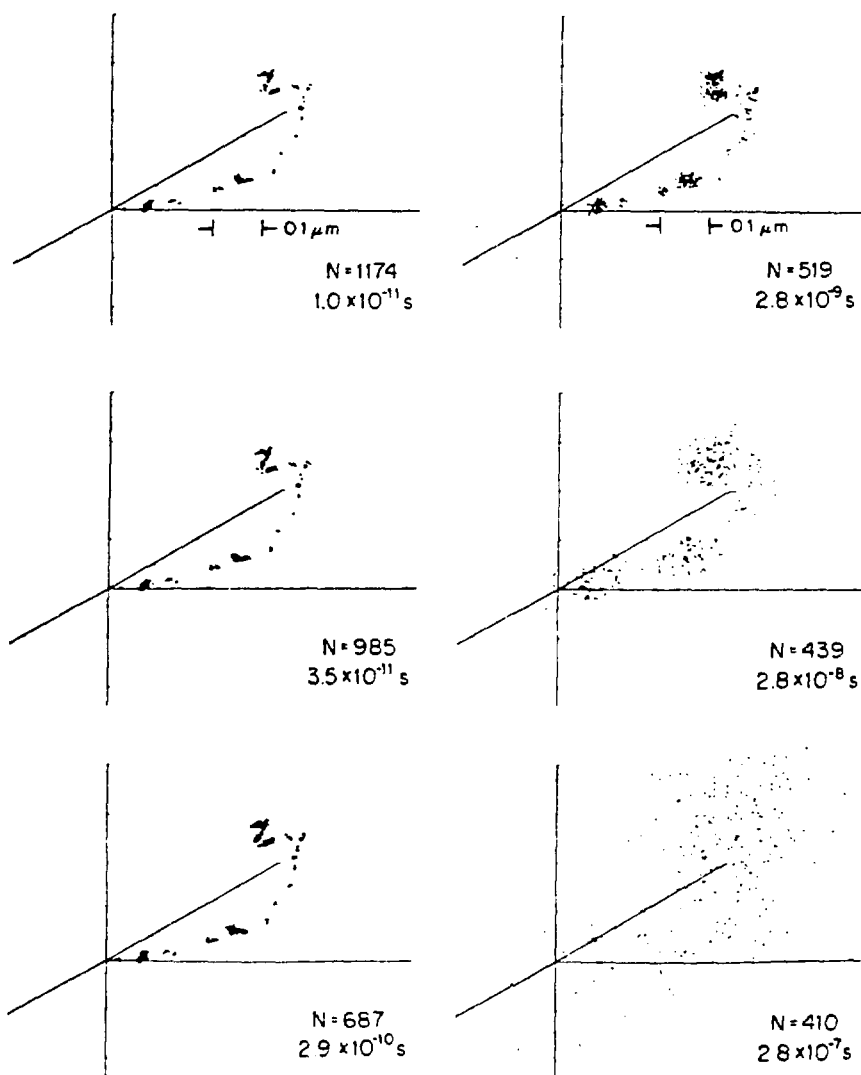


Fig. 4. Example of the chemical evolution of a 5-keV electron track showing the number, N , of species present at various times from 10^{-11} s to 2.8×10^{-7} s.

Figure 5 shows the track of a 20-keV electron at three different times during its development. A few high-energy electrons, or delta rays, can be seen along the track. The number of chemical species for this track at 10^{-11} s and at 2.8×10^{-7} s are shown in Table 6. It is noted that the most reactive species, OH and e^-_{aq} , have reduced drastically in number during the chemical reactions. Therefore, one sees that as the number of species is reduced due to chemical reactions, the relative numbers of each type of chemical species also changes. The more reactive species disappear more rapidly than the less reactive species.

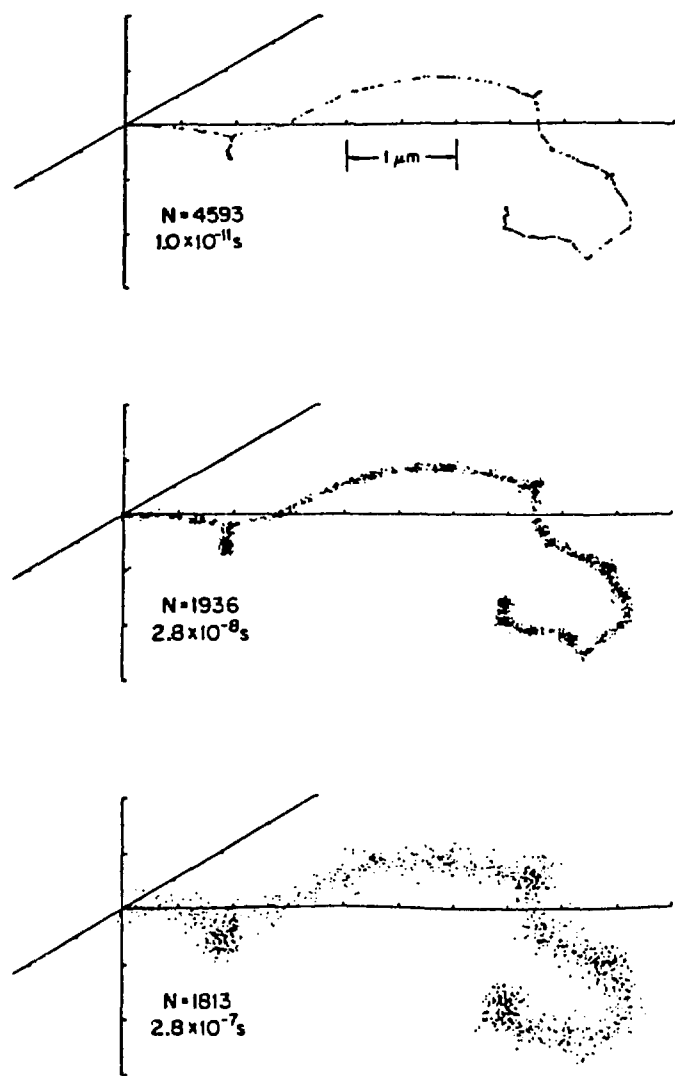


Fig. 5. Example of the chemical evolution of a 20-keV electron track showing the number, N , of species present at various times.

Table 6. Number of Chemical Species Present in the Track of a 20-keV Electron at Various Times

<u>Species</u>	<u>10^{-11} s</u>	<u>2.8×10^{-7} s</u>
e^-_{aq}	1247	205
H_3O^+	1242	1002
H	431	395
OH	1673	211
H_2	72	191
H_2O_2	72	383

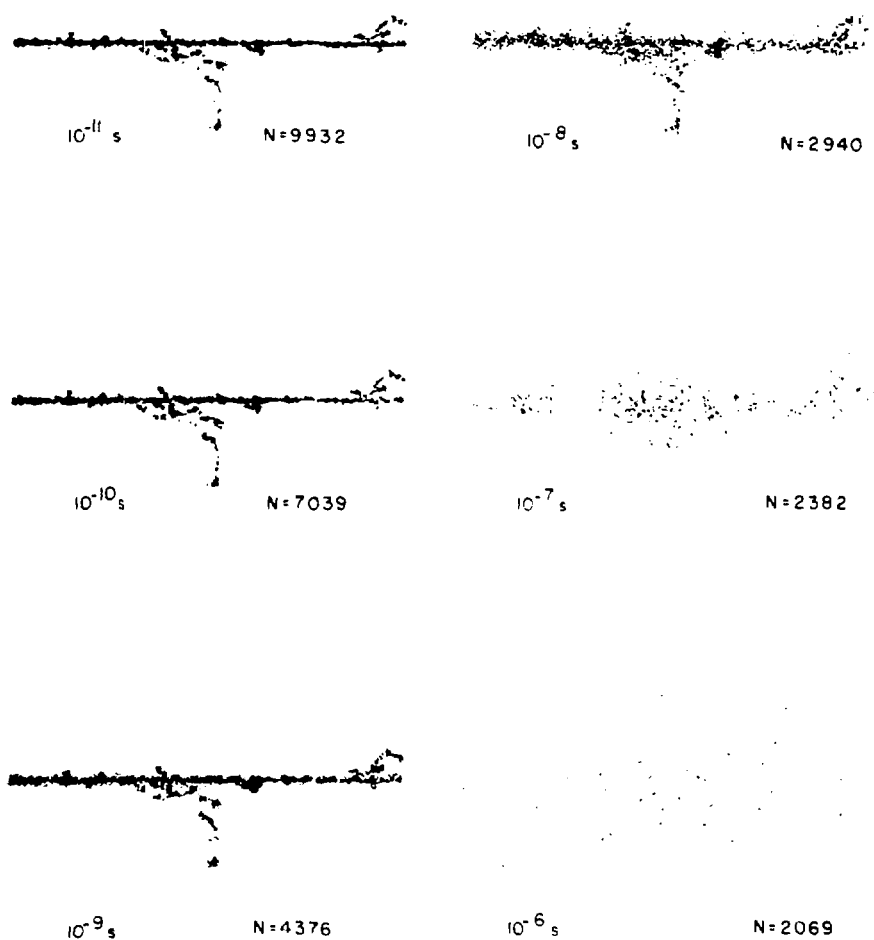


Fig. 6. Example of the chemical evolution of a segment of an 8-MeV alpha-particle track. The segment is $0.7 \mu\text{m}$ long.

For comparison between electron tracks and heavy-particle tracks, we show the development of an alpha-particle track in Fig. 6. This figure shows a $0.7\text{-}\mu\text{m}$ segment of the track of an 8-MeV alpha particle at different times during its evolution. High-energy secondary electrons (delta rays) are clearly seen.

As one final example, we will show a track of a proton in relation to a segment of a DNA molecule. Figure 7 shows the segment of the track of a 1-MeV proton with a portion of the center of the track enlarged.

Figure 8 shows a superposition of a simple model of a segment of a DNA molecule on this track. In this figure the points on the two helical strands represent alternating sugar and base sites. The proton could produce direct energy loss events within the DNA or could produce reactive species in the

1-MeV PROTON

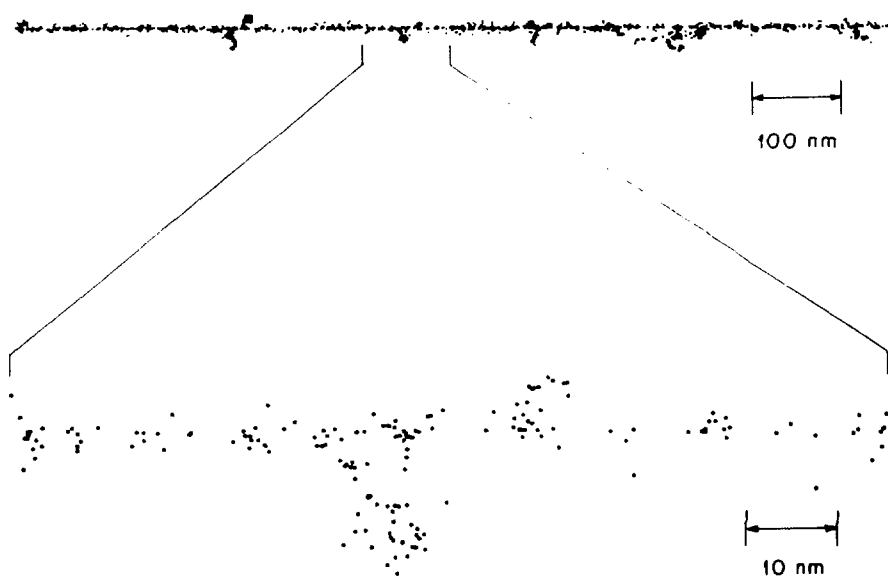


Fig. 7. Upper portion shows a 1000-nm segment of a 1-MeV proton track. Lower portion shows 10-fold blowup of a central portion of the segment, 100 nm in length.

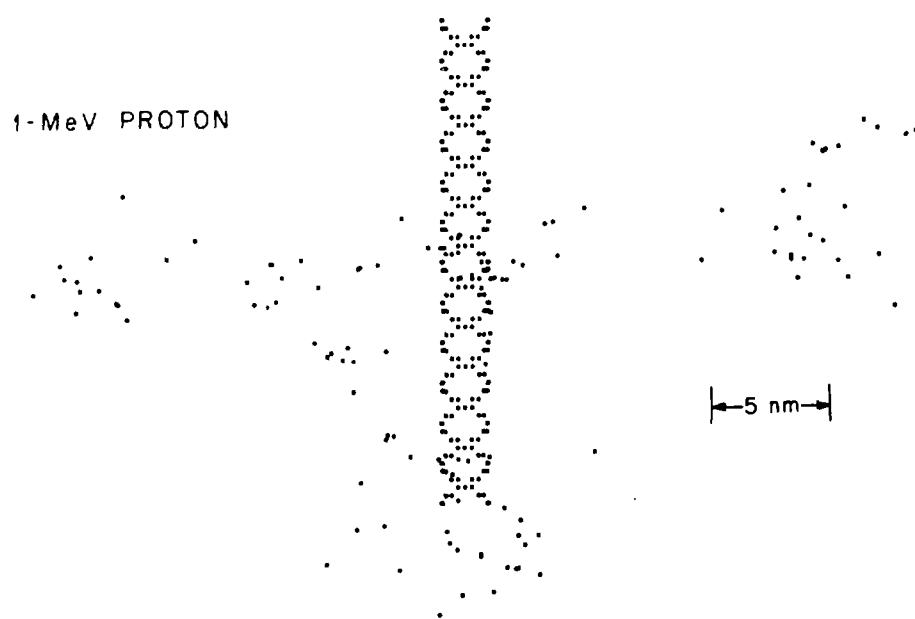


Fig. 8. Segment of double-stranded DNA near portion of track segment of the 1-MeV proton from Fig. 7. Dots in cylindrical array represent alternating bases and sugars in the two strands of the DNA.

medium (mostly water) surrounding the DNA which could diffuse over and react chemically with a site on the DNA. We have recently initiated a program to calculate direct physical and indirect chemical interactions produced in an irradiated medium containing DNA. In a biological system there would be other molecules with which the chemical reactants in the track could react and which, therefore, would act as scavengers for the reactive species. We take the scavenge time to be 10^{-8} s. The diffusion distance during this time is ~ 20 nm. We therefore consider a cylinder around the DNA of radius 20 nm and count the number of reactants that are in this cylinder due to the passage of the charged particle. This number will be, to first order, proportional to the dose in the cylinder, and thus we can compare results for different particles. In Fig. 9 we show the number of reactions between two reactants and the number between one reactant and a site on the DNA normalized to the total number of reactants in the cylinder for 1-MeV and 10-MeV protons and for 4-MeV alphas. The impact parameter is 0 (i.e., the particle passes through the center of the DNA). Since the alpha particle track is more dense, there are a greater number of reactions between reactants leaving fewer of them to react with DNA than for the proton tracks. Further results are being published elsewhere (11).

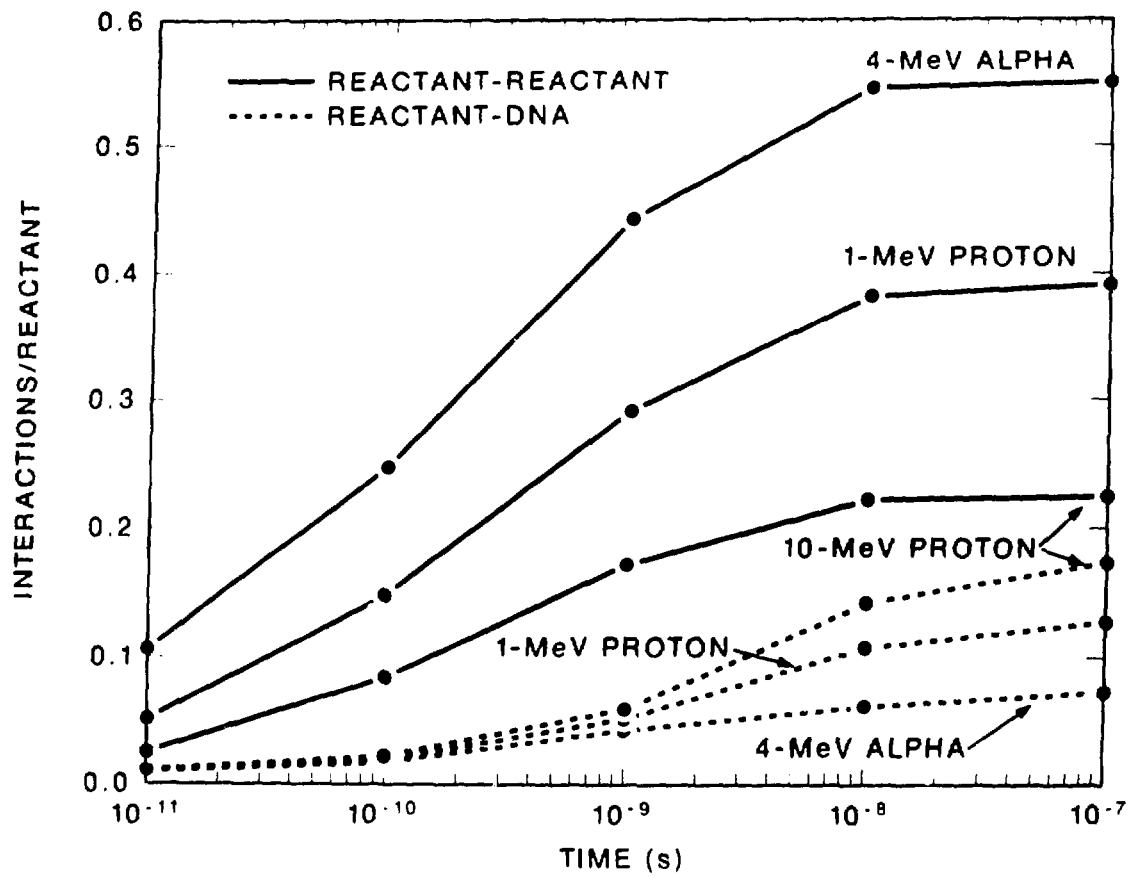


Fig. 9. Reactant-reactant and reactant-DNA interactions for various particles. Impact parameter = 0.

CONCLUDING REMARKS

Recent progress has been made at understanding radiation interactions in condensed media and at linking radiation physics with radiation chemistry. Although biological systems are very complicated and much more is to be

learned about mechanisms of biological action of radiation, the state of the art has advanced to the point that models for predicting biological response cannot ignore details of initial energy deposition (i.e., track structure). Whether in radiopharmaceutical dosimetry, or other radiation dosimetry considerations, average dose to an organ, or even to a single cell, may not be sufficient for determining effects. The field of microdosimetry is becoming increasingly important.

It is hoped that the program described in this paper can make significant contributions to identifying the mechanisms involved in producing biological effects of radiation.

ACKNOWLEDGMENT

Research sponsored by the Office of Health and Environmental Research, U.S. Department of Energy, under contract DE-AC05-84OR21400 with Martin Marietta Energy Systems, Inc., and contract W-7405-48 with the University of California, Lawrence Berkeley Laboratory.

REFERENCES

1. See, for example, Proceedings of Eighth Symposium on Microdosimetry, edited by J. Booz and H. G. Ebert, Commission of the European Communities Luxembourg, ISBN 92-825-3516-9, 1983.
2. Adams, G.E. and D.G. Jameson. Time effects in molecular radiation biology. *Radiat. Environ. Biophys.* 17. 95-113, 1980.
3. Chapman, J.D. and C.J. Gillespie. Radiation-induced events and their time scale in mammalian cells. *Advances in Radiation Biology*, Vol. 9, pp. 143-198, edited by I. T. Lett and H. Adler, Academic Press, 1981.
4. Mozumder, A. Advances in radiation chemistry, Vol. 1, pp. 1-102, edited by Ed. M. Burton and J. L. Magee, Wiley-Interscience, 1969.
5. Hamm, R.N., J.E. Turner, R.H. Ritchie, and H.A. Wright. Calculation of heavy-ion tracks in liquid water. *Radiation Research* (in press).
6. Hamm, R.N., H.A. Wright, R.H. Ritchie, J.E. Turner, and T.P. Turner. Monte Carlo calculation of transport of electrons through liquid water. In *Proceedings of the Fifth Symposium on Microdosimetry*, Verbania, Italy, September 22-26, 1975, pp. 1037-1050. Commission of the European Communities, Brussels, Belgium, 1976.
7. Ritchie, R.H., R.N. Hamm, J.E. Turner, and H.A. Wright. The interaction of swift electrons with liquid water. In *Proceedings of the Sixth Symposium on Microdosimetry*, Brussels, Belgium, May 22-26, 1978, pp. 345-354. Commission of the European Communities, Brussels, Belgium, 1978.
8. Hamm, R.N., R.H. Ritchie, J.E. Turner, and H.A. Wright. Inelastic cross sections for electron interactions in liquid water. In *Proceedings of the Workshop on the Interface Between Radiation Chemistry and Radiation Physics*, Argonne National Laboratory, September 9-10, 1982, pp. 32-36. ANL-82-88, Argonne National Laboratory, Argonne, Illinois, 1982.

9. Turner, J.E., J.L. Magee, R.N. Hamm, A. Chatterjee, H.A. Wright, and R.H. Ritchie. Early events in irradiated water. In *Seventh Symposium on Microdosimetry*, Oxford, U.K., edited by J. Booz, H. G. Ebert, and H. D. Hartfiel, pp. 507-517. Commission of the European Communities, Harwood, London, 1981.
10. Turner, J.E., J.L. Magee, H.A. Wright, A. Chatterjee, R.N. Hamm, and R.H. Ritchie. Physical and chemical development of electron tracks in liquid water. *Radiat. Res.* 96. 437-449, 1983.
11. Wright, H.A., J.L. Magee, R.N. Hamm, A. Chatterjee, J.E. Turner, and C.E. Klots. Calculations of physical and chemical reactions produced in irradiated water containing DNA. *Radiation Protection Dosimetry* (in press).

DISCUSSION

HAYDOCK: In simulating the formation of reactive species along the track of a charged primary particle, you have obviously accounted for the energy loss of this primary particle. How is this energy subsequently dissipated? In particular, is the energy entirely consumed in the formation of reactive species, or is the major fraction of the energy dissipated thermally? This thermal dissipation might result if most of the reactive species are created in states with high vibrational excitation energies. Can you specify as a function of time what fraction of primary particles energy has been thermalized and what fraction has been utilized as formation energy of reactive or stable chemical species?

WRIGHT: We do not explicitly keep track of the amount of energy that goes into heat. When a primary or secondary electron slows down to subexcitation energy, we assume that it is then thermalized and becomes hydrated. This energy would go directly into heat. Also, we have a parameter in the code to allow a fraction of the excitations that are produced to relax thermally. With a bit of effort we could probably identify, as a function of time, the fraction of the dose that is thermalized but we have not attempted to do so as yet.

SPERMATOGONIAL CELL KILLING BY RADICLABLED METHIONINE:
A COMPARATIVE STUDY OF THE EFFECTS OF Se-75, S-35, AND H-3

Dandamudi V. Rao and George F. Govelitz
Department of Radiology

University of Medicine and Dentistry of New Jersey, Newark, NJ 07103
and

Kandula S. R. Sastry and Roger W. Howell
Department of Physics and Astronomy

University of Massachusetts, Amherst, MA 01003

ABSTRACT

Spermatogenesis in the testes of mice offers an effective experimental model to investigate the biological effects and the dosimetry of Auger-electron emitters in vivo, aspects that are not yet well understood. Killing of the radiosensitive spermatogonia by intratesticularly localized radionuclides is the biological effect of interest, manifesting as reduced sperm-head population four to six weeks after the initial administration of the radionuclides. Our earlier studies showed that the average dose to the testis from the Auger-emitters, ^{201}Tl and ^{55}Fe , is about 3 times more effective in killing the sperm cells than the dose from their similarly distributed beta-emitting analogs, ^{204}Tl and ^{59}Fe , when these doses are calculated according to the conventional MIRD schema. We present here results of a comparative study of the effects of the Auger-emitter, ^{75}Se , and the beta-emitters, ^{35}S and ^3H , when these radionuclides are attached to the amino acid, methionine, and hence distributed similarly in the testis and in the cytoplasmic protein fractions of the spermatogonial cells. The sperm-head survival is assayed on the 36th day post-injection, when the sperm-head population reaches its minimum after the initial intratesticular administration of the radionuclides. In all the three cases, the survival fractions display similar dependence on the conventionally calculated average dose to the organ. These results show the adequacy of conventional dosimetry when ^{75}Se is localized in the cytoplasm of the cells, and emphasize the relative inefficiency of Auger electrons emitted from cytoplasmic decay sites in irradiating the radiosensitive DNA in the cells. Differences in the survival curves for the three radionuclides are understandable in terms of the respective dose rates to the nuclei of the spermatogonial cells.

INTRODUCTION

By virtue of their low energies and subcellular ranges in biological matter, Auger electrons from tissue-incorporated radionuclides decaying by orbital electron capture (EC) and internal conversion (IC) may locally and selectively irradiate radiosensitive sites in the nuclei of cells, depending on the localization of the radionuclides with respect to such sites (1). Therefore, the biological effects of Auger-electron emitters are not readily predictable. Conventional dosimetry (2,3) either ignores the low-energy Auger electrons or trivializes their possible importance by spreading their energies over macroscopic dimensions. Accordingly, the inherent assumption in this approach, that the average dose rates and cumulated doses to the cell nucleus and its constituents are the same as the values calculated for the organ as a whole, may not be valid in the case of Auger emitters. In view of these limitations, we have been engaged in an extended program of research aimed at an investigation of the biological effects of biomedically interesting Auger-emitters in vivo using spermatogenesis in mice as the experimental model. The "biological dosimetry" thus obtained provides the phenomenological basis for development of biophysically meaningful dosimetry of Auger emitters in vivo.

Our earlier studies with ^{201}Tl and ^{55}Fe , localized in the testes of mice, have revealed that the conventionally calculated average dose (2,3) to the organ from either of these Auger emitters is about three times more effective in killing the spermatogonial cells (4-6) than the average dose from their respective beta-emitting analogs, ^{204}Tl and ^{59}Fe , distributed similarly in the organ. Very recently, we have found that the average testicular dose from the Auger emitter ^{111}In , when introduced into the organ in the form of ^{111}In -oxine, is about five times more efficient in killing the sperm cells compared to the effects of irradiation of the organ by external X-rays (7). These results point to the inadequacy of conventional dosimetry of Auger emitters in vivo. The observed efficacies of these radionuclides are reasonably explained in terms of dose rate enhancement to the spermatogonial cells (4,5) and their nuclei (6,7) over the conventional estimates.

Recent radiobiological studies in vitro with Chinese hamster V79 lung fibroblasts have also revealed interesting and valuable information. When these cells are incubated for two doubling times (18 hr) with the radionuclides ^{75}Se , ^{201}Tl , and ^{51}Cr , the radionuclides are concentrated by the cells by factors of 650, 130, and 1000, respectively (8-10). The severe radiotoxic effects of ^{201}Tl are manifested only when this prolific Auger emitter is localized in the cells (9), demonstrating the efficacy of low energy Auger electrons for cell killing. Intracellular localization and distribution of ^{51}Cr have been related to the radiotoxicity of this Auger emitter in the same mammalian cell line (10). These studies clearly show that the actual dose rates to the cells in vitro are by far larger (11) than estimates based on the MIRD Schema (2), in agreement with our in vivo results.

The nuclear dose rate enhancement factors developed by us include several biophysically relevant parameters besides the nature of the Auger electron spectra following the EC and IC decay of the radionuclides. These are (1) the intracellular concentration factor n , being the ratio of the intracellular radionuclide concentration and the radionuclide concentration in the extracellular medium; (2) f_i , the fraction of the total volume of the organ occupied by the (spermatogonial) cells that have concentrated the radionuclide; (3) the size of the cell and its nucleus; (4) f_N , the fraction of the cellular volume occupied by cell nucleus; (5) r_N , the fraction of radioactivity in the cell localized in the nucleus; and (6) r_{Cy} , the cytoplasmic fraction of the intracellular activity (4-7,9).

In this paper, we consider the biological effects *in vivo* of ^{75}Se -selenomethionine, ^{35}S -methionine, and ^3H -methionine following intratesticular (i.t.) administration of these radiopharmaceuticals into the experimental mice. As shown by Kassis et al. (8), these analogs of the amino acid, methionine, are highly concentrated by the cells and are localized in the cytoplasmic protein fractions of the cells. Besides the fact that the Auger electrons from ^{75}Se (1,8) have very low energy, the beta rays from ^3H have a very low energy spectrum (12), and ^{35}S beta rays are not very energetic (8). The purpose of these studies is to examine the usefulness of our nuclear dose rate enhancement factors in the interpretation of radiobiological studies involving Auger emitters as well as soft beta emitters localized in the cells. Our results show that ^{75}Se is slightly less effective than ^{35}S , indicating the relative inefficiency of Auger emitters localized in the cytoplasm of the cell in irradiating the radiosensitive DNA in the nucleus of the cell. In contrast, ^3H in the cytoplasm is apparently more toxic than ^{35}S distributed similarly. Nuclear dose rate enhancement factors, presented for these radionuclides, show that the actual dose rates to the nucleus differ from the conventional values and that they depend on the concentration factor n . For large values of n , as implied by the *in vitro* studies, ^3H -methionine is only slightly more effective than ^{35}S -methionine.

EXPERIMENTAL MODEL, MATERIALS AND METHODS

EXPERIMENTAL MODEL

The fundamental biological process of spermatogenesis is complex yet tractable. The spermatogenic cycle in the mouse testis has been illustrated, for example, by Meistrich et al. (13). This process proceeds through three distinct phases involving cellular differentiation: renewal and proliferation of spermatogonial cells, meiosis, and development of mature spermatozoa. Mitotic proliferation of stem cells gives rise to type A₁ spermatogonia. These, in turn, divide and give rise to a succession of spermatogonial cells of types A₂, A₃, I_n, and B. Type B spermatogonia divide to become primary spermatocytes, which, through meiosis, become secondary spermatocytes. These cells form spermatids through a second reduction division. In the last phase, the spermatids proceed without further division through a series of morphological transformations to become sperm. The spermatogonial cells are the most sensitive to radiation, whereas the pre- and post-gonial cells are relatively more radioresistant (13). This differential radiosensitivity implies that the effects of radiation damage to the differentiated spermatogonia manifest themselves as reduced sperm-head population when counted after the time necessary (4 to 6 weeks in mice) for the spermatogonia to become spermatids. This forms the basis for the study of the biological effects of radiation in this *in vivo* model. The relevance of the mouse testis model to man has been pointed out (4,14,15).

MATERIALS

Male Swiss Webster mice, 9-10 weeks of age and 30 grams of average mass, are used in these studies. The average testis mass is 0.1 g. The radionuclides employed in this study are ^{75}Se , ^{35}S , and ^3H attached as radiolabels to the amino acid, methionine. The specific activities of the respective radionuclides are 2250 Ci/mmmole (^{75}Se), 1060 Ci/mmmole (^{35}S), and 83 Ci/mmmole (^3H). The radiomethionines were obtained from Amersham Corporation.

METHODS

The experimental procedures and protocols have been described in detail in our earlier papers (4-6). Only brief and relevant details are presented here. The radiopharmaceuticals were directly introduced into the right testes of the animals following a minor surgical procedure (4). The i.t. mode of administration, rather than the usual intravenous (i.v.) or intraperitoneal (i.p.) modes, is preferred because the i.t. mode needs injection of very small quantities of radioactivity. The large quantities involved in i.v. and i.p. modes primarily contribute to the non-target to target dose, and the whole body dose. These interference effects are not easily separable from the effect of intratesticulary localized activity alone. The i.t. mode essentially eliminates these problems and facilitates a delineation of the biological effects of low-energy electrons on spermatogenesis.

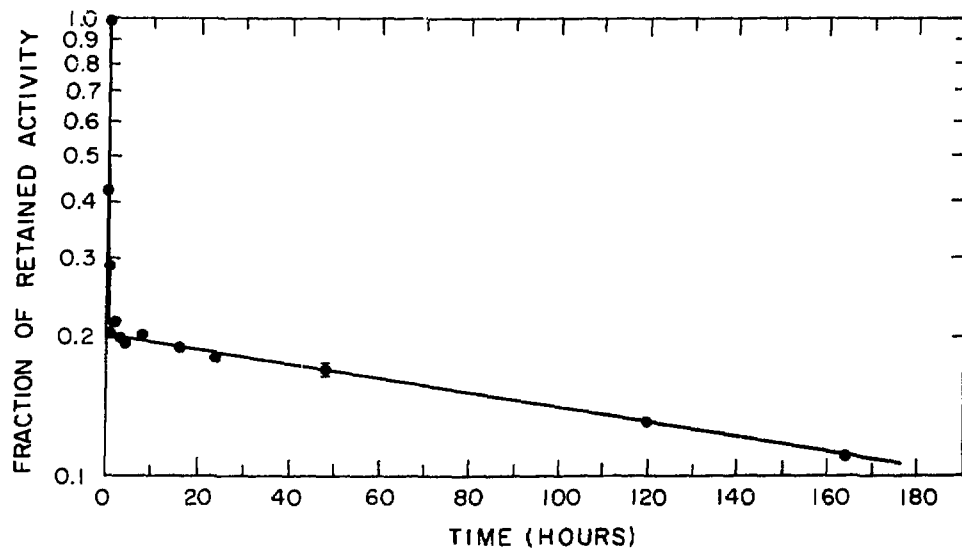


Figure 1. Biological clearance of ^{75}Se from mouse testis following intratesticular administration of ^{75}Se -selenomethionine. Error bar indicates the standard deviation of the mean.

All injections involved a standard volume of 3 μl . During the injection, the microsyringe needle was slowly moved along the long axis of the testis to facilitate a fairly even initial distribution of the solution in the organ. Mice that were left untouched or injected with normal saline or cold methionine were used as controls. Every aspect of the study involved mice in groups of at least five. The ^{75}Se radioactivity was measured by standard gamma ray spectroscopy while the ^{35}S and ^3H activities were measured using liquid scintillation spectroscopy.

The biological rates of clearance of the radionuclides from the testes, following i.t. injection of the radiopharmaceuticals into the testes of a group of mice, are first studied as described earlier (4-6). The optimal time

for sperm-head survival assay is then established for the radiopharmaceuticals. This is the time necessary (28-40 d) for the sperm-head count to reach the minimum following the initial i.t. administration of the radionuclide. For this purpose, several mice are given the same i.t. radionuclide injection dose. They are sacrificed over a period of several weeks. The testes are removed, weighed, and homogenized in one ml of deionized water, and sonicated for 30 seconds. The sperm heads are resistant to sonication. These are counted in a hemocytometer to a minimum of 200 under a microscope. The surviving sperm-head fraction, compared to the control animals, is determined. The minimum sperm-head count was reached on the 36th day post-injection, as in the case of our ⁵⁵Fe and ⁵⁹Fe studies (5,6). Animals injected with various amounts of the radiopharmaceuticals are sacrificed on the 36th day post-injection for sperm-head survival assay as a function of the radiation dose to the organ.

The macro- and microdistribution of the radionuclides in the testis are also studied. The former studies (6) ensure that the radionuclides are uniformly distributed in the organ. Frozen section autoradiography (4,6) is used for microdistribution studies. For this purpose 1 μ Ci of ³H-methionine was injected. The testes were removed 18 hr later and slides were prepared for autoradiography as described earlier (4,6). The grains were counted under a microscope in different regions of the seminiferous tubules from randomly selected sections and fields.

Table 1

Average Spectrum of Electrons Due to Auger (A) and Coster-Kronig (CK) Transitions per ⁷⁵Se Decay

Atomic Transition(s) Resulting in the Electrons	Yield	Average Energy (keV)	Range (μ m)
M _{4,5} A	1.35	0.017	0.0007
M _{4,5} A	2.61	0.029	0.0014
M _{1,2,3} CK, L ₁ CK	1.14	0.045	0.0020
M _{1,2,3} CK, L ₁ CK	0.37	0.098	0.0041
M _{1,2,3} A, M ₁ CK, L ₁ CK	0.18	0.147	0.0063
L _{1,2,3} A	1.31	1.176	0.086
K _A	0.42	9.476	2.46

RESULTS AND DISCUSSION

BIOLOGICAL CLEARANCE

Figure 1 shows the time dependence of ⁷⁵Se activity retained in the testis following i.t. administration of 0.5 μ Ci of ⁷⁵Se-selenomethionine. The pattern was the same for ³H-methionine and ³⁵S-methionine. The bulk of the activity (80%) was quickly eliminated with a biological half-life of 0.2 hr, while the remaining 20% stayed in the organ with a biological

half-life of 8.0 d. The effective half-lives for ^{75}Se , with the physical half-life of 120.4 d (12), are 8.3×10^{-3} d and 7.5 d, respectively, for the 80% and 20% components. For ^3H , with 12.35 y half-life (12), the corresponding values are 8.3×10^{-3} d and 7.99 d; and 8.3×10^{-3} d and 7.3 d for ^{35}S decaying with the physical half-life of 88.0 d (12).

RADIATION DATA

The average beta ray energy is 5.68 keV for ^3H (12) and 48.6 keV for ^{35}S (8). The average ranges of the respective beta groups are about 1 μm and 40 μm in unit density matter (16). For ready reference, the theoretical average Auger and CK electron spectrum (1,8) and the conversion electron spectrum (8) for ^{75}Se are given in Tables 1 and 2, respectively, along with the range of each electron group in unit density matter. The ^{75}Se decay is also accompanied by As K X-rays (10.66 keV) and L X-rays (1.28 keV), the

Table 2

Average Yield and Energies of Internal Conversion Electrons per ^{75}Se Decay

Group No.	Yield	Average Energy (keV)	Range (μm)
1.	0.0039	3.033	0.37
2.	0.0500	12.54	4.00
3.	0.0104	23.09	11.5
4.	0.0041	55.79	54.0
5.	0.0287	86.21	116.0
6.	0.0227	120.93	210.0
7.	0.0072	261.50	821.0

respective average yields being 0.544 and 0.014 per ^{75}Se decay. The complex gamma spectrum that follows ^{75}Se EC decay is given on p. 50, Reference (12). The absorbed fractions (ϕ_e) for electrons and beta rays emitted in the organ are calculated using the formulation of Sastry et al. (17) and Berger's scaled absorbed dose distribution (18) around point sources of monoenergetic electron emitters, and point sources of ^3H and ^{35}S in water. It is assumed that these emitters are uniformly distributed in the testis, treated as a sphere of unit density with a radius of 0.29 cm. These absorbed fractions for electrons in the organ are unity. The absorbed fractions (ϕ_γ) for the photons emitted in the organ are calculated as described earlier (6). These values for the L and K X-ray photons are 1.0 and 0.0775, respectively. For the gamma photons, $\phi_\gamma \approx 0.006$. The average electron energy emitted and absorbed (ϵ_e) in the organ is 13.94 keV per ^{75}Se decay in the organ, the photon energy deposited (ϵ_γ) being 2.91 keV. For ^3H , $\epsilon_e = 5.68$ keV, and 48.6 keV for ^{35}S .

CUMULATED RADIATION DOSE

The average radiation dose from intratesticular decays of the three radionuclides are calculated according to the conventional dosimetric approach (see, for example, Ref. (6): Equation 1) using the biological clearance data, the effective half-lives, the radiation data, and the absorbed fractions presented above. The cumulated dose for the first 13-d period is calculated for each case because of the long residence times of the radionuclides in the organ. The rationale for this has been pointed out (6,19). These 13-d cumulated average testicular doses are: 37.5, 4.56, and 13.1 rad per μCi of ^{35}S , ^3H , and ^{75}Se initially injected into the testis. About 17% of the total dose from ^{75}Se is from its penetrating radiations.

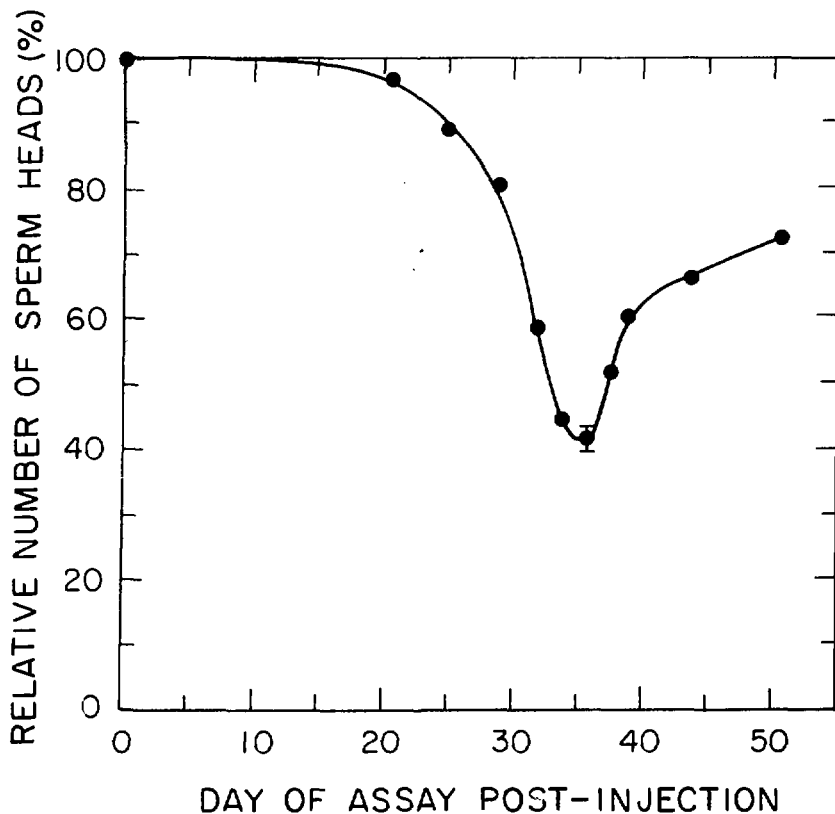


Figure 2. Relative sperm-head population in mice injected intratesticularly with 7.9 μCi of ^3H -methionine as a function of the post-injection time. The sperm-head survival is assayed on the 36th day post-injection, when the sperm-head population in mice exposed to the radionuclide attains the minimum value. The standard deviation of the mean is indicated by the error bar. There was no effect on the sperm-head population in the case of control mice injected with cold methionine.

SPERM-HEAD SURVIVAL

Data in Figure 2 show the relative sperm-head population in mice as a function of the time following the i.t. administration of 7.9 μCi of ^{35}S -methionine. The minimum sperm-head count is reached on the 36th day post-injection. This is the same for ^3H -methionine and for ^{75}Se -selenomethionine. Results of sperm-head survival assay, performed on this day, are shown in Figure 3 as a function of the conventionally calculated 13-d cumulated dose to testis for each radionuclide.

The shape of these survival curves (Figure 3) is the same as in the case of our ^{201}Tl and ^{55}Fe studies (4-6). This is not surprising because the same species of mice are used in all these studies. The lack of an initial shoulder and the presence of a sensitive component constituting about 25-30% of the surviving fraction, and a less sensitive component (70-75%) are the repeating features for the strain of the mice employed. Plausible reasons for this type of response were discussed earlier (4,6).

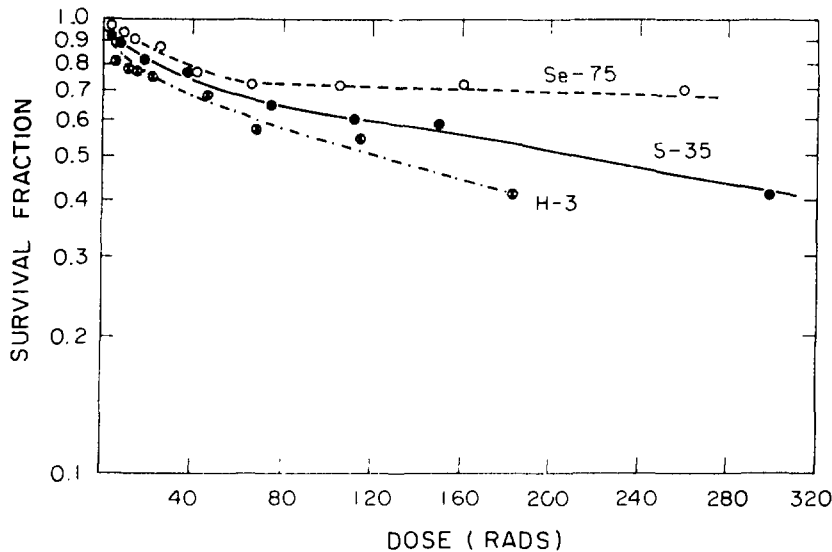


Figure 3. Sperm-head survival versus calculated average radiation dose to the organ from intratesticularly administered ^{75}Se , ^{35}S , and ^3H via the radiolabeled analogs of the amino acid, methionine.

EXPERIMENTAL 'RBE VALUES'

Although the survival curves for the three radionuclides (Figure 3) are similar, there are significant differences between them. For the sensitive (25%) component, the D_0 values (37% survival) are 9, 18, and 26 rad for ^3H , ^{35}S , and ^{75}Se , respectively. The D_0 values for the less sensitive (75%) component are 305 and 530 rad for ^3H and ^{35}S , respectively. Compared to the beta-emitter ^{35}S , values of 'relative biological effectiveness' (RBE) may be obtained from the D_0 values. These experimental 'RBE values' are 0.7 (^{75}Se) and 2.0 (^3H) for the sensitive component. For

the less sensitive component, the RBE value is 1.74 for ^{3}H relative to ^{35}S . A weighted average for the two components is 1.8 in the case of ^{3}H . For ^{75}Se , the D_0 value for the second component is apparently quite large. The nature of data in this region precludes an estimate of this parameter with any reasonable accuracy. Furthermore, it is the sensitive component occurring at low doses that is of much biophysical interest. Therefore, we consider the sensitive component only in case of ^{75}Se .

The data in Figure 3 show that ^{75}Se dose to the organ is somewhat less effective and ^{3}H dose slightly more effective than the average dose to the organ from ^{35}S . Since the organ doses may not necessarily be the actual doses to the nuclei of the spermatogonial cells, it is desirable to identify the above experimental RBE values as 'apparent RBE values' (Table 4). The discussion that follows indicates how the radionuclide localization in the cells may influence these values.

RADIONUCLIDE DISTRIBUTION

Our autoradiography results show that the radionuclides are distributed approximately uniformly in the basal 10 μm region of the tubules containing the spermatogonial cells, and the rest of the tubular and intertubular spaces. This indicates essentially uniform distribution of the radionuclides in the organ at the microscopic level as evidenced by autoradiography. The grains in the region of the spermatogonial cells may imply intracellular localization of the radionuclides. Kassis et al. (8) have shown that ^{35}S -methionine and ^{75}Se -selenomethionine are highly concentrated by V79 cells in culture, and are localized in the cytoplasm, presumably in the protein fractions. For such a distribution, they showed that an average decay of ^{35}S or ^{75}Se in the cytoplasm of V79 cells would deposit essentially the same energy in the nucleus of the same cell. This explains their finding that these radionuclides are essentially equally toxic. We consider below the implications of localization and concentration of the radionuclides in the cytoplasm of the spermatogonial cells in vivo.

NUCLEAR DOSE RATE ENHANCEMENT

When low-energy electrons are involved, the conventional dosimetry (2,3) may not be adequate as shown by our work on ^{201}Tl , ^{55}Fe , and ^{111}In -oxine (4-6,7). To account for the observed efficacies of these radionuclides localized in the spermatogonial cells, we introduced dose rate enhancement factors. Since the critically important DNA is in the cell nucleus, we consider the nuclear dose rate enhancement factors (N_N).

Let $A \mu\text{Ci}$ of radioactivity be in the testis of volume V at any instant. Then the average conventional dose rate (R_N)_{CON} (in keV/s) to the nucleus of volume v_N is given by

$$(R_N)^{\text{CON}} = N_0(A/V)\epsilon_e(1+\Delta)v_N$$

where N_0 = number of disintegrations per second per μCi , ϵ_e = average electron energy deposited in the organ per decay in the organ, and $\Delta = \epsilon_\gamma/\epsilon_e$, ϵ_γ being the average photon energy deposited in the organ per decay in the organ. The actual dose rate to the nucleus (R_N), on the average, is the sum of several contributions:

$$R_N = R_{NN} + R_{NCy} + R_{NO}$$

where R_{NN} is the dose rate to the nucleus from decays occurring in itself, R_{NCy} , the dose rate to the target nucleus from decays taking place in the cytoplasm of the cell containing the target nucleus, and R_{NO} , the dose rate to target nucleus from decays in the rest of the organ. For cytoplasmic localization, $R_{NN} = 0$. The term R_{NO} consists of contributions from electrons and photons emitted from decays external to the cell containing the target nucleus. Following the earlier work (4-7,9), we write the nuclear dose rate enhancement factor $N_N = R_N / (R_N)_{CON}$ as follows:

$$N_N = [\frac{(n/f_N) r_{Cy} \phi_{NCy}}{\{f_i(n-1) + 1\}} + \phi_{Ne} + \Delta] \frac{1}{(1 + \Delta)} \quad (1)$$

The parameters n , f_N , r_{Cy} , f_i and Δ have already been defined. The parameter ϕ_{NCy} is the fraction of electron energy emitted per decay in the cytoplasm that is absorbed in the nucleus, while ϕ_{Ne} is the fraction of electron energy absorbed in the target nucleus per decay external to the cell. For cytoplasmic localization, $r_{Cy} = 1$. The calculation of ϕ_{Ne} depends on the actual geometry of the cells in the organ. It is an adequate approximation to write $\phi_{Ne} = \epsilon' / \epsilon_e$. Here $\epsilon' = \epsilon_e - \epsilon''$, ϵ'' being the energy carried per decay by particles with very short ranges ($\leq 3 \mu\text{m}$) that cannot reach the nucleus of the spherical spermatogonial cells (6) of $12 \mu\text{m}$ diameter with the nucleus as a concentric sphere of $6 \mu\text{m}$ diameter. Electrons of 10 keV energy or less emitted external to the cell cannot reach the target nucleus. In the case of ^{75}Se decay external to the cell, the Auger and CK electrons (Table 1) and some of the conversion electrons (Table 2) cannot reach the target nucleus. Essentially no energy reaches the target nucleus from extracellular ^3H decay because of the very low probability of emission of beta particles in the high energy end of the spectrum. When ^{35}S decays external to the cell, about 13% of the beta particles with energies less than 10 keV cannot irradiate the target nucleus.

The absorbed fraction $\phi_{NCy} = \epsilon_{NCy} / \epsilon_e$, ϵ_{NCy} being the electron energy deposited in the target nucleus per decay in the cytoplasm of the cell. For the spermatogonial cell geometry, we have calculated ϵ_{NCy} for monoenergetic electrons emitted from decay sites distributed uniformly in the cytoplasm. These results, obtained by a calculation similar to the one described by Kassis et al. (8), are shown in Figure 4. From these generalized energy absorption curves, the energy deposited in cellular regions of interest by electrons emitted in specific source regions in the same cell can be readily estimated for radionuclides emitting a discrete or continuous spectrum of electrons. Data in Tables 1 and 2 are used for the calculation of ϵ_{NCy} in the case of ^{75}Se , while the complete beta spectra are used in the calculations for ^3H and ^{35}S .

The numerical values of the various parameters are: $f_N = 1/8$ for our cellular geometry; $\Delta = 0.209$, $\phi_{Ne} = 0.536$, $\epsilon_{NCy} = 0.28 \text{ keV}$, and $\phi_{NCy} = 0.02$ for ^{75}Se ; for ^3H , $\Delta = 0$, $\phi_{Ne} = 0$, $\epsilon_{NCy} = 0.22 \text{ keV}$, and $\phi_{NCy} = 0.039$; in the case of ^{35}S , $\Delta = 0$, $\phi_{Ne} = 0.97$, $\epsilon_{NCy} = 0.41 \text{ keV}$, and $\phi_{NCy} = 0.0084$. According to Green et al. (20), the region containing the spermatogonial cells, in a close packed tubular geometry, is at most 17% of the testicular volume. Our earlier studies show that f_i , the fractional volume of the testis occupied by spermatogonial cells, lies between 0.1 and 0.15 (4,6). For definiteness, we use the intermediate value $f_i = 0.13$. Then, the only variable parameter in equation 1 for N_N is n , the intracellular concentration factor.

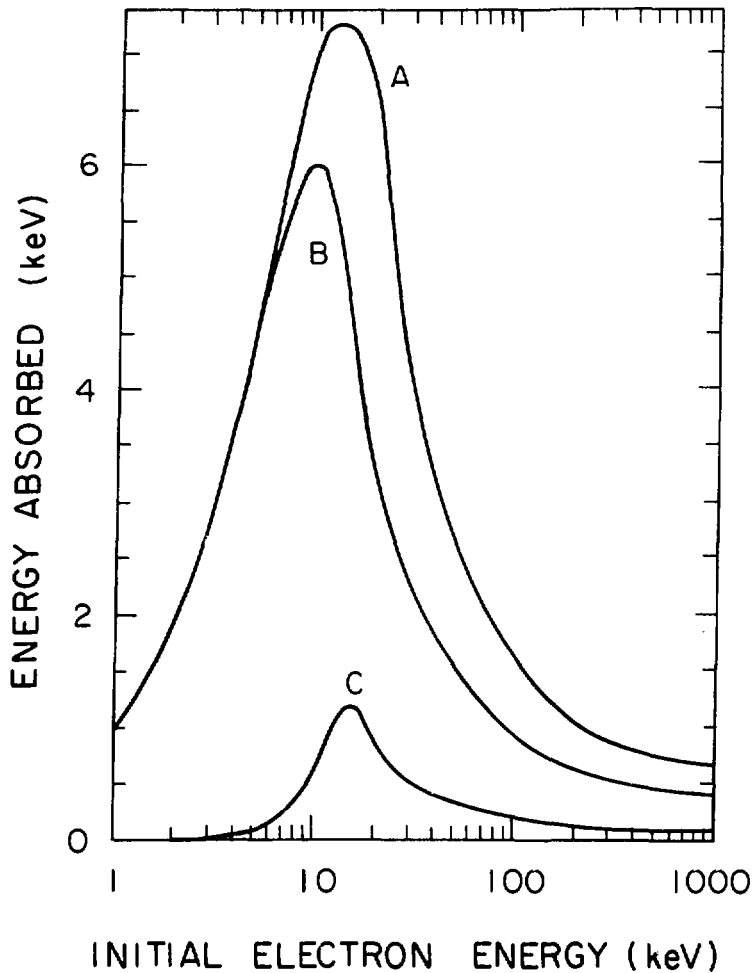


Figure 4. Average energy deposited per decay as a function of the initial energy of electrons emitted by hypothetical radionuclides uniformly distributed in different cellular regions of spermatogonial cells. Curve A: average energy absorbed in the cytoplasm per decay in the cytoplasm; Curve B: average energy deposited in the nucleus per decay in the nucleus; and Curve C: average energy absorbed in the nucleus per decay in the cytoplasm. The spermatogonial cell and its nucleus are assumed to be concentric spheres of diameter 12 μm and 6 μm , respectively, and of unit density.

In Table 3, we present the calculated nuclear dose rate enhancement factors (N_N) for each radionuclide as a function of n . Inspection of the Table shows that nuclear dose rates depend on n , and that they may be underestimated or overestimated by conventional dosimetric procedures in the case of Auger emitters as well as soft beta emitters such as ^{3}H and ^{35}S . For $n = 1$, the nuclear dose rate from ^{35}S is close to the conventional

value, and about 30% less than the conventional value in the case of ^{75}Se . The dose rate from ^3H is smaller by a factor of about 3 than the conventional dose rate. At high concentrations, nuclear dose rates from ^{75}Se and ^{35}S are larger than the conventional rates by a factor of 1.4 to 1.5, while the dose rate from ^3H is about 2.4 times larger.

Table 3

Calculated Average Nuclear Dose Rate Enhancement Factors

Intracellular Concentration Factor (n)	Nuclear Dose Rate Enhancement Factor (N_N)		
	^{75}Se	^{35}S	^3H
1	0.73	1.04	0.31
2	0.81	1.09	0.55
4	0.93	1.16	0.90
6	1.01	1.21	1.13
8	1.07	1.25	1.22
10	1.12	1.28	1.44
15	1.20	1.33	1.66
20	1.24	1.36	1.80
50	1.35	1.43	2.12
100	1.40	1.45	2.25
500	1.44	1.48	2.37
$n \rightarrow \infty$	1.45	1.49	2.40

The above deviations of nuclear dose rates from the conventional values must be taken into account to obtain more realistic RBE values. Accordingly, the 'apparent RBE' must be multiplied by the ratio of nuclear dose rate enhancement factors, $(N_N)_{\text{S}-35}/(N_N)_{\text{Se}-75}$ in case of ^{75}Se , and by the ratio $(N_N)_{\text{S}-35}/(N_N)_{\text{H}-3}$ for ^3H to obtain the 'corrected RBE'. These corrected RBE values are given in Table 4 for some values of n in the range 1 to 500. Only when $n \approx 1$, ^{75}Se is just as effective as ^{35}S , as far as the sensitive component is concerned; for n significantly larger than 1, the effectiveness is less by about 20-30% compared to ^{35}S . In contrast, ^3H is generally more effective than ^{35}S . The RBE values relative to ^{35}S are 6 for $n=1$ and 1.1 for very large values of n.

According to Kassis et al. (8,11), both ^{75}Se -selenomethionine and ^{35}S -methionine are concentrated by V79 cells in vitro by large factors: $n = 650$ (^{75}Se) and $n \approx 500$ (^{35}S). It is most reasonable to expect that the analog, ^3H -methionine, is also concentrated highly. The spermatogonial cells in vivo should also be expected to concentrate these radiopharmaceuticals. If the value of $n \geq 50$, it is reasonable to conclude that ^{75}Se is about 25% less toxic at low doses, and ^3H about 10-20% more toxic than ^{35}S at all doses.

Table 4

RBE Values for ^{75}Se -selenomethionine and ^3H -methionine
Compared to ^{35}S -methionine

Radio-pharmaceutical	Apparent RBE	n=1	Corrected RBE				500
			2	10	50		
^{75}Se -selenomethionine	0.7*	1.0	0.94	0.80	0.75	0.72	
^3H -methionine	1.8	6.0	3.6	1.6	1.2	1.1	

* For the sensitive component.

SUMMARY AND CONCLUSION

^{75}Se -selenomethionine, ^{35}S -methionine, and ^3H -methionine are radiolabeled analogs of the amino acid, methionine. When introduced into the mouse testis, they are distributed similarly in the cytoplasmic protein fractions of the spermatogonial cells as well as the rest of the organ. All of them have about the same effective half-life in the testis. Therefore, it has been possible to compare their relative efficacies for killing spermatogonial cells *in vivo*. Compared to ^{35}S , the apparent RBE value for ^3H is 1.8, and 0.7 for the sensitive component in the case of ^{75}Se , based on conventional dosimetry.

Nuclear dose rate enhancement factors are derived for each radionuclide. These depend on the intracellular concentration factor n. The actual dose rates to the nucleus may be very different from the conventional values, not only for the Auger emitter ^{75}Se , but also for soft beta emitters such as ^3H and ^{35}S localized in the cytoplasm of the cells. This is a finding of significance to the dosimetry of radionuclides *in vivo*. RBE values corrected for the effect of nuclear dose rate enhancement depend on n.

Our conclusion that ^{75}Se is somewhat less toxic than ^{35}S *in vivo* is valid essentially for all values of n greater than 1, and it is consistent with *in vitro* studies involving Auger emitters localized in the cytoplasm of cells (8,21). In contrast, ^3H toxicity relative to ^{35}S depends on the actual intracellular concentration. For large concentration factors, ^3H is only slightly more radioxic than ^{35}S .

ACKNOWLEDGEMENT

We are grateful to Venkata Lanka for the technical assistance. This work is supported by U.S. Public Health Service Grant No. CA32877.

REFERENCES

1. Sastry, K.S.R., and D.V. Rao. Dosimetry of low energy electrons, in Physics of Nuclear Medicine: Recent Advances, edited by D.V. Rao, R. Chandra, and M.C. Graham, pp. 169-208. American Association of Physicists in Medicine, Medical Physics Monograph No. 10, American Institute of Physics, 1984.
2. Loevinger, R., and M. Berman. A revised schema for calculating the absorbed dose from biologically distributed radionuclides, MIRD Pamphlet No. 1, revised, The Society of Nuclear Medicine, New York, 1976.
3. ICRU Report 32. Methods of assessment of absorbed dose in clinical use of radionuclides. International Commission on Radiation Units and Measurements, Washington D.C., 1979.
4. Rao, D.V., G.F. Govelitz, and K.S.R. Sastry. Radiotoxicity of Thallium-201 in mouse testes: Inadequacy of conventional dosimetry. J. Nucl. Med. 24. 145-153, 1983.
5. Rao, D.V., K.S.R. Sastry, G.F. Govelitz, H.E. Grimmond, and H.Z. Hill. Radiobiological effects of Auger-electron emitters in vivo: Spermatogenesis in mice as an experimental model. Radiat. Prot. Dosim. (in press).
6. Rao, D.V., K.S.R. Sastry, G.F. Govelitz, H.E. Grimmond, and H.Z. Hill. Radiobiological effects of iron-55 and iron-59 in mouse testes: Biophysical dosimetry of Auger-electron emitters in vivo. J. Nucl. Med. 26. 1456-1465. 1985.
7. Rao, D.V., H.E. Grimmond, and K.S.R. Sastry. Biological dosimetry of indium radiopharmaceuticals in mouse testes, in Proceedings of Forum on Microdosimetry of Radiopharmaceuticals, Committee on Effects of Ionizing Radiation, Medical Research Council, England, May 30, 1985.
8. Kassis, A.I., S.J. Adelstein, C. Haydock, and K.S.R. Sastry. Radiotoxicity of ⁷⁵Se and ³⁵S: Theory and application to a cellular model. Radiat. Res. 84. 407-425, 1980.
9. Kassis, A.I., S.J. Adelstein, C. Haydock, and K.S.R. Sastry. Thallium-201: An experimental and a theoretical radiobiological approach to dosimetry. J. Nucl. Med. 24. 1164-1175, 1983.
10. Kassis, A.I., K.S.R. Sastry, and S.J. Adelstein. Intracellular distribution and radiotoxicity of chromium-51 in mammalian cells: Auger-electron dosimetry. J. Nucl. Med. 26, 59-67, 1985.
11. Kassis, A.I., K.S.R. Sastry, and S.J. Adelstein. Intracellular localization of Auger-electron emitters: Biophysical dosimetry. Radiat. Prot. Dosim. (in press).
12. Martin, M.J., and P.H. Blichert-Toft. Radioactive atoms, Auger electron, α -, β -, γ -, and X-ray data. Nucl. Data Tables. A8, 1-198, 1970.
13. Meistrich, M.L., N.R. Hunter, N. Suzuki, P.K. Trostle, and H.R. Withers. Gradual regeneration of mouse testicular stem cells after exposure to ionizing radiation. Radiat. Res. 74, 349-362, 1978.

14. Gaulden, M.E. "Biological dosimetry" of radionuclides and radiation hazards. *J. Nucl. Med.* 24, 150-164, 1983.
15. Meistrich, M.L., and R.C. Samuels. Reduction in sperm levels after testicular irradiation of the mouse: A comparison with man. *Radiat. Res.* 102, 138-147, 1985.
16. Cole, A. Absorption of 20-eV to 50,000-eV electron beams in air and plastic. *Radiat. Res.* 38, 7-33, 1969.
17. Sastry, K.S.R., C. Haydock, A.M. Basha, and D.V. Rao. Electron dosimetry for radioimmunotherapy: Optimal electron energy. *Radiat. Prot. Dosim.* (in press).
18. Berger, M.J. Distribution of absorbed dose around point sources of electrons and beta particles in water and other media. *J. Nucl. Med. Suppl. No. 5, MIRD Pamphlet No. 7*, 5-23, 1971.
19. Mian, T.A., H.J. Glenn, T.P. Haynie, and M.L. Meistrich. Radiation dose and biological effects to mouse testis from sodium ^{32}P -phosphate. *Health Phys.* 42, 657-664, 1982.
20. Green, D., G.R. Howells, E.R. Humphreys, and J. Vennart. Localisation of plutonium in mouse testis. *Nature.* 255, 77, 1975.
21. Hofer, K.G., C.R. Harris, and J.M. Smith. Radiotoxicity of intracellular ^{67}Ga , ^{125}I and ^3H . Nuclear versus cytoplasmic effects in murine L1210 leukaemia. *Int. J. Radiat. Biol.* 28, 225-241, 1975.

DISCUSSION

WESSELS: I noticed a curious shape to the cell survival curves, they have a negative bend instead of a positive shoulder. Do you have a radiobiological explanation as to why an extrapolation number would be less than one for sensitivity to low doses? This is contrary to normal mammalian x-ray survival data.

RAO: Well, the spermatozoal cells are really sensitive to the radiation. For some reason there is no shoulder in the curve. It has been shown many times in all of our experiments and also by others. That's where you get this phenomenon.

WESSELS: In other words, it appears that the cells are more radiosensitive at low dose?

RAO: Exactly.

TRAVERSAL OF CELLS BY RADIATION AND ABSORBED FRACTION ESTIMATES FOR ELECTRONS AND ALPHA PARTICLES

K. F. Eckerman, J. C. Ryman, A. C. Taner, and G. D. Kerr
Health and Safety Research Division
Oak Ridge National Laboratory
P. O. Box X
Oak Ridge, Tennessee 37831

ABSTRACT

Consideration of the pathlength which radiation traverses in a cell is central to algorithms for estimating energy deposition on a cellular level. Distinct pathlength distributions occur for radionuclides: (1) uniformly distributed in space about the cell (referred to as μ -randomness); (2) uniformly distributed on the surface of the cell (S-randomness); and (3) uniformly distributed within the cell volume (I-randomness). For a spherical cell of diameter d , the mean pathlengths are $\frac{2}{3}d$, $\frac{1}{2}d$, and $\frac{3}{4}d$, respectively, for these distributions. Algorithms for simulating the path of radiation through a cell are presented and the absorbed fraction in the cell and its nucleus are tabulated for low energy electrons and alpha particles emitted on the surface of spherical cells. The algorithms and absorbed fraction data should be of interest to those concerned with the dosimetry of radionuclide-labeled monoclonal antibodies.

INTRODUCTION

In the dosimetry schema of the Medical Internal Radiation Dose (MIRD) Committee (1) and the dosimetry system of the International Commission on Radiological Protection (2) it is assumed that: 1. the nuclear transformations (decay events) occur uniformly within the geometric regions (generally organs) serving as source regions in the body, and 2. the absorbed dose in the radiosensitive sites of the target region can be approximated by the mean absorbed dose to the target. These assumptions allow the tabulation of so-called S-factors representing the absorbed dose in the target region per unit cumulated activity

in the source region for the anatomical model of the adult (3,4). The assumptions are not particularly limiting for penetrating radiations (photons); however, for particulate radiations it becomes necessary to consider the microscopic distribution of the radionuclide and the absorbed dose.

The amount of energy deposited within a cell depends on the path of the particulate radiation through the cell. Consideration of the distribution of path-lengths or chord-lengths in a convex body arises in a variety of disciplines and applications, for example, in estimating the energy deposition within the sensitive volume of a proportional counter. Chords are formed by the intersections of the convex body with straight lines, each of which is defined by a point and direction chosen at random from independent distributions. Distinct chord distributions occur for a point isotropic source of lines uniformly distributed in space about the convex body, on the surface of the body, and within the interior of the body. Failure to note the distinct nature of these distributions can result in misunderstanding of some aspects of the radiation transport processes.

DISTRIBUTION OF CHORD-LENGTHS

An excellent discussion of random traversal of convex bodies, including citations to the original literature, has been presented by Kellerer (5). Although there are many ways in which randomness of chords may arise in convex bodies, only three are of interest here:

1. Mean-free-path randomness (or μ -randomness). A chord of a convex body is defined by a point in space and a direction. The point and the direction are chosen randomly from independent uniform distributions. This kind of randomness results, for example, if the convex body is exposed to a uniform, isotropic field of straight lines.
2. Interior radiator randomness (or I-randomness). A chord is defined by a point in the interior of the convex body and a direction. The point and the direction are chosen randomly from independent uniform distributions. This kind of randomness results, for example, if the convex body contains a uniform distribution of point sources, each of which emits radiation isotropically.
3. Surface^{*} radiator randomness (or S-randomness). A chord is defined by a point on the surface of the convex body and a direction. The point and the direction are chosen randomly from independent uniform distributions. This kind of randomness results, for example, if the surface of a convex body contains a uniform distribution of point sources, each of which emits radiation isotropically.

The distribution of chords in a sphere associated with the various types of randomness is illustrated in Fig. 1.

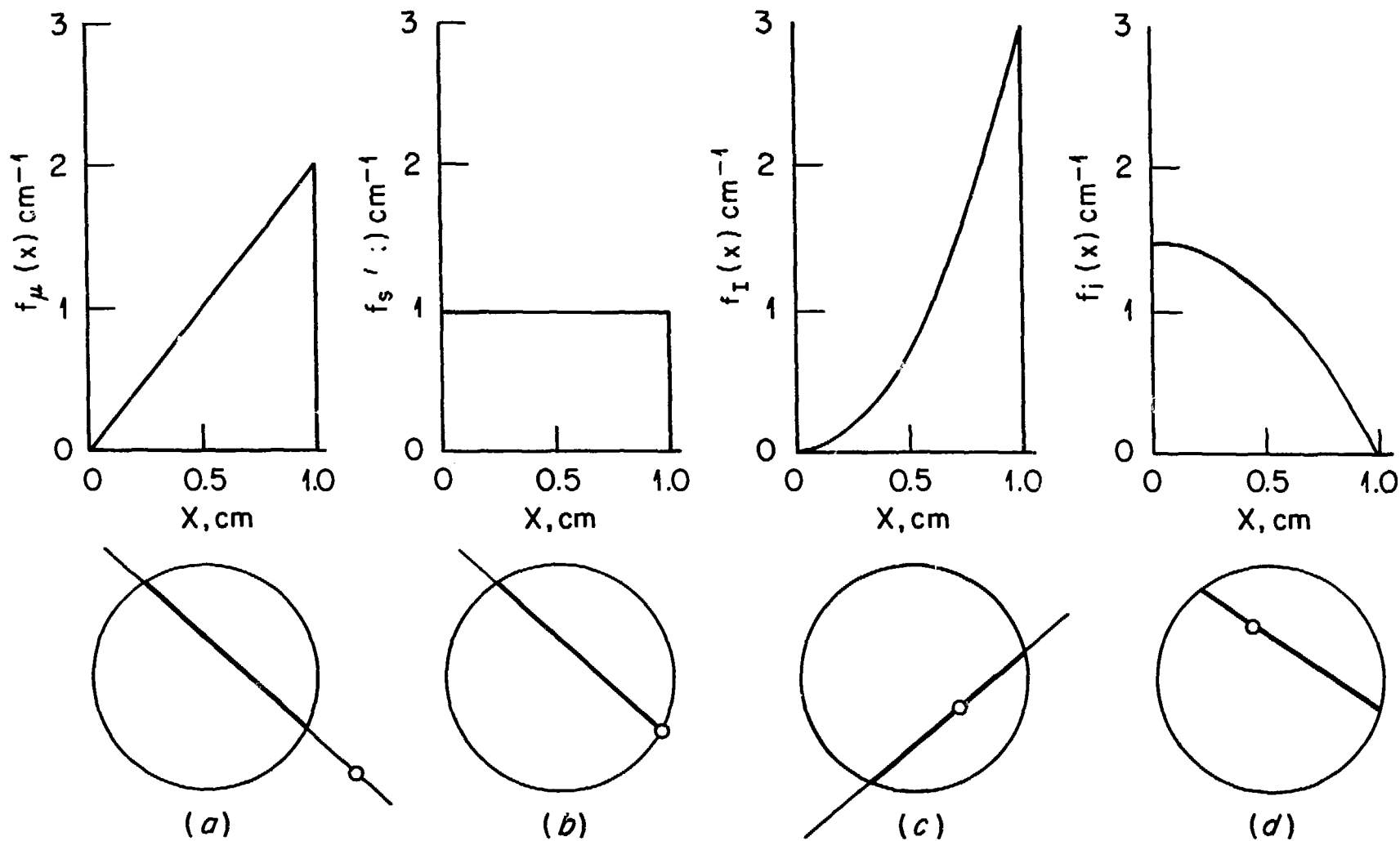


Figure 1. For a sphere of unit diameter the chord-length distribution for μ -randomness (a), S-randomness (b), and I-randomness (c) are illustrated. The ray-length distribution for I-randomness is shown in (d).

If radiation (electron or alpha particle) is emitted from radionuclides uniformly distributed in the space about a cell (convex body) then one is dealing with μ -randomness. However, if the emissions originate within or on the surface of the convex body then the chord distributions are determined by I- and S-randomness, respectively. The chord distributions for μ - and I-randomness in a convex body are related, in general, as (4):

$$f_I(x) = \frac{x}{\langle x \rangle_\mu} f_\mu(x) , \quad (1)$$

where

$f_I(x)$ and $f_\mu(x)$ denote the probability density functions for chord-lengths under I- and μ -randomness, respectively,

$\langle x \rangle_\mu$ denotes the mean value of the $f_\mu(x)$ distribution.

According to Kellerer (5), it remains an open question as to whether there exists a unique relationship between the chord distributions under μ - and S-randomness.

Equation 1 refers to the full chord; however, for radiations emitted within the convex body one is interested in the "half" chord or ray which defines the potential path of the particle. A chord of length s will give rise to a uniform distribution of rays of length x . That is, the conditional probability density function for ray-length x , given chord-length s , $f_i(x|s)$, is

$$f_i(x|s) = \frac{1}{s} , \quad 0 < x \leq s . \quad (2)$$

The probability density function for the ray-length distribution, $f_i(x)$, is then

$$f_i(x) = \int_x^\infty f_i(x|s) f_I(s) ds , \quad (3)$$

which yields, after substitution of Eq. 1 and 2,

$$f_i(x) = \frac{1}{\langle x \rangle_\mu} \left[1 - F_\mu(x) \right] , \quad (4)$$

where $F_\mu(x)$ is the cumulative distribution function defined as

$$F_\mu(x) = \int_0^x f_\mu(s) ds . \quad (5)$$

The probability density functions defining the chord-length distributions in a sphere can be expressed in analytical form. For a sphere of diameter d under μ -randomness the probability density function is simple and well-known,

$$f_{\mu}(x) = 2 \frac{x}{d^2} \text{ with } \langle x \rangle_{\mu} = \frac{2}{3} d . \quad (6)$$

For S-randomness the density is constant:

$$f_s(x) = \frac{1}{d} \text{ with } \langle x \rangle_s = \frac{1}{2} d . \quad (7)$$

From Eq. 1, the distribution for I-randomness is then

$$f_I(x) = \frac{3x^2}{d^3} \text{ with } \langle x \rangle_I = \frac{3}{4} d , \quad (8)$$

which from Eq. 4 results in the ray-length distribution

$$f_i(x) = \frac{3}{2d} \left[1 - \left(\frac{x}{d} \right)^2 \right] \text{ with } \langle x \rangle_i = \frac{3}{8} d . \quad (9)$$

The various distributions of chord- and ray-lengths in a sphere are depicted in graphic form in Fig. 1.

Note that the mean chord-length under μ -randomness, $\langle x \rangle_{\mu}$, is related to the volume, V , and surface area, S , of a convex body by Cauchy's theorem; $\langle x \rangle_{\mu} = 4 \frac{V}{S}$. Frequently Cauchy's theorem is applied incorrectly to S-randomness. As noted above the mean chord under μ -randomness exceeds that for S-randomness.

ABSORBED FRACTION ESTIMATES FOR CELLS

The fraction of the emitted energy which is deposited within the cell and within the cell's nucleus by alpha particles and electrons has been calculated assuming the particles originated on the cell surface (S-randomness) or were incident on the cell in an isotropic manner (μ -randomness). The energy deposition was estimated as the difference in energy of the particle on entrance to and exit from the region of interest. The range-energy relationships of Berger (6) for electrons in water and of Taner and Eckerman (7) for alpha particles in water were used in the calculations. The cell is represented as a sphere of diameter 20 μm with a concentric nucleus of 10 μm diameter. The mean chord through the cell under S-randomness is 10 μm and 13 μm for μ -randomness. We use Monte Carlo methods to simulate the flight of the particles. Some aspects of the simulation are discussed in Appendix A.

EMITTER ON CELL SURFACE

Because of spherical symmetry we need only consider a point isotropic source at a single location on the cell surface, e.g., $(0, -\frac{1}{2}d_0, 0)$, where d_0 denotes the diameter of the cell. From this location particles are considered to be emitted in a isotropic manner with direction cosines (u, v, w) outlined in Section A-4 of the Appendix. The parametric equation of the line passing through the point $(0, -\frac{1}{2}d_0, 0)$ with direction cosines (u, v, w) is

$$x = ut \quad (10a)$$

$$y = -\frac{1}{2}d_0 + vt \quad (10b)$$

$$z = wt \quad . \quad (10c)$$

Following the discussion in the Appendix, we note that the line intersects the cell at $t = 0$ (trivial solution) and at $t = |v|d_0$; the pathlength through the cell is $|v|d_0$.

The particle will pass through the cell nucleus (diameter of d_1) if the roots of the quadratic equation $At^2 + Bt + C = 0$ are real, where

$$A = 1 \quad , \quad (11a)$$

$$B = -d_0v \quad , \quad (11b)$$

$$C = \frac{1}{4}(d_0^2 - d_1^2) \quad . \quad (11c)$$

The pathlength through the nucleus is given by $|t_2 - t_1|$, where t_1 and t_2 denote the smaller and larger real roots, respectively, of the quadratic equation. The particle travels a distance t , prior to entering the nucleus and because of the symmetry travels the same distance to leave the cell after traversing the nucleus.

Let the initial energy and range of the particle be denoted as E_0 and R_0 , respectively. If R_0 is less than the available path-length t through the cell, then the particle will deposit all of its energy within the cell. However, if $R_0 > t$ then the deposited energy is given as $E_0 - E(t)$, where $E(t)$ denotes the energy of the particle after traveling a distance t . Particles traversing the nucleus must travel a distance t_1 to reach the nucleus. At this point the particle will be of energy $E(t_1)$ with a residual range of $R_0 - t_1$. In traversing the nucleus along the pathlength $t_2 - t_1$ the particle will deposit energy $E(t_1) - E(t_2)$ provided $t_2 - t_1$ is less than the residual range of the particle. If

the path in the nucleus exceeds the residual range, then the remaining energy would be deposited. The absorbed fraction is computed as the ratio of the total energy deposited and the total energy of all particles simulated.

CELL WITHIN AN ISOTROPIC FIELD

For an isotropic field (μ -randomness) the angle, θ , between the incident radiation and the normal to the surface element at the point of incidence is distributed on the region $0 \leq \theta \leq \frac{1}{2}\pi$ according to the density function

$$f_{\mu}(\theta) = 2 \sin \theta \cos \theta \quad (12)$$

To sample this probability density function we equate the random number ξ to the cumulative distribution F_{μ} which represents the probability that the angle of incidence is less than θ , namely $F_{\mu}(\theta) = \sin^2 \theta$. The resulting angle is $\theta = \sin^{-1}(\xi^{\frac{1}{2}})$ and thus the direction cosine (w) with respect to the normal is $w = \cos \theta = (1 - \xi)^{\frac{1}{2}}$. The angle δ is assumed to be uniform over the region $0 \leq \delta \leq 2\pi$ and the direction cosines u and v are obtained as discussed in Section A-4 and A-5 of Appendix A.

Evaluation of the pathlengths through the cell and its nucleus, as well as estimation of the energy deposition and the absorbed fraction follow the procedures discussed above.

RESULTS

The computed absorbed fraction data are presented in Tables 1 and 2 and are shown graphically in Figs. 2 and 3 for electrons and alpha particles, respectively. At the lower energies the absorbed fractions for the whole cell approach the values expected from geometric considerations, namely 1.0 for particles incident on the cell under μ -randomness and 0.5 under S-randomness (one-half the emitted particles enter the cell). The absorbed fraction in the cell nucleus is maximum in the region of 20 to 30 keV for electrons and at about 2 MeV for alpha particles. The energy dependence of the absorbed fractions for the low-energy electrons and alpha particles are qualitatively similar.

The basic concepts applicable to the random traversal of convex bodies and Monte Carlo simulation have been outlined. The algorithms and absorbed fraction data should be of interest to those concerned with the dosimetry of radionuclide-labeled monoclonal antibodies.

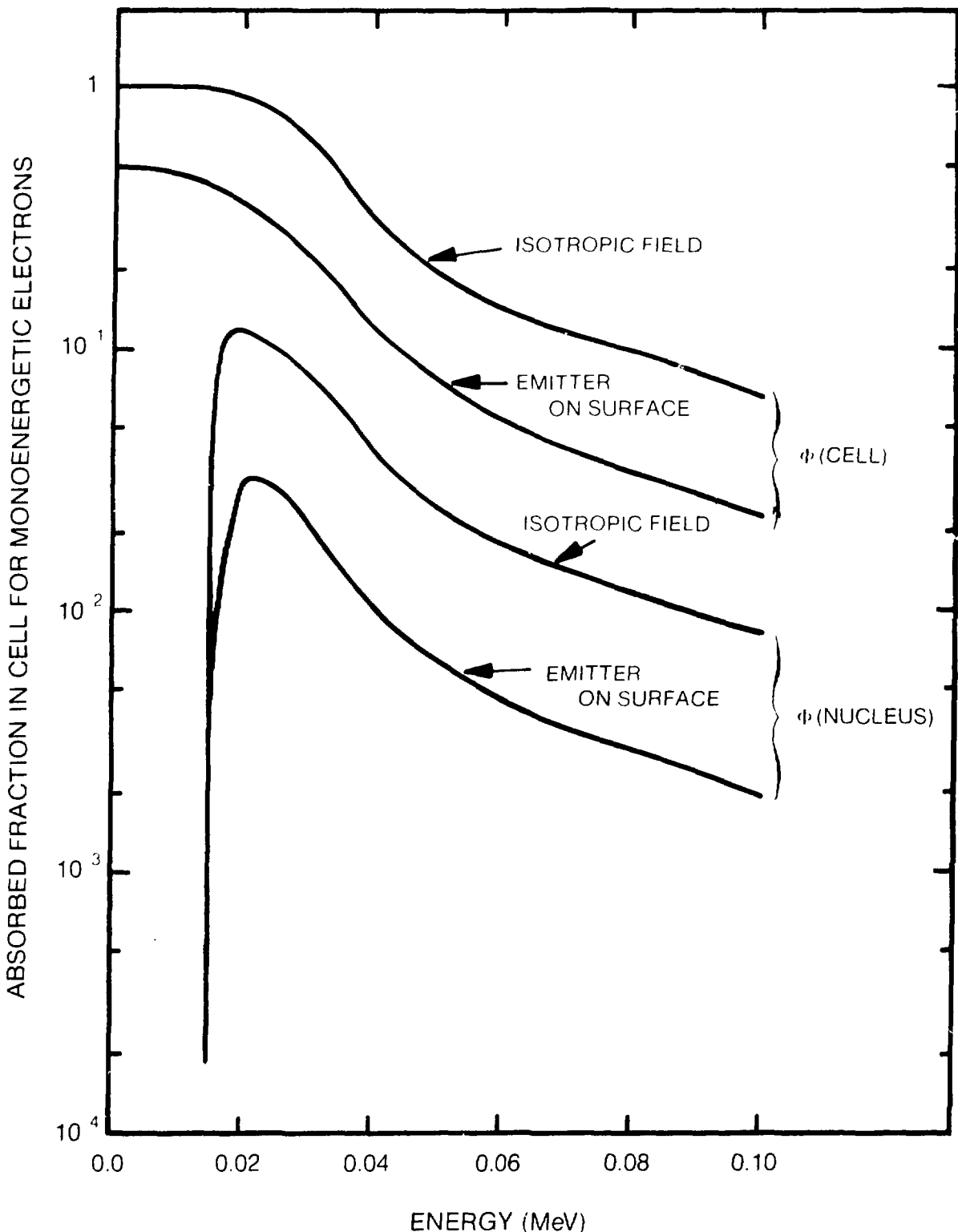


Figure 2. Absorbed fraction for monoenergetic electrons incident on cells under μ - and S-randomness.

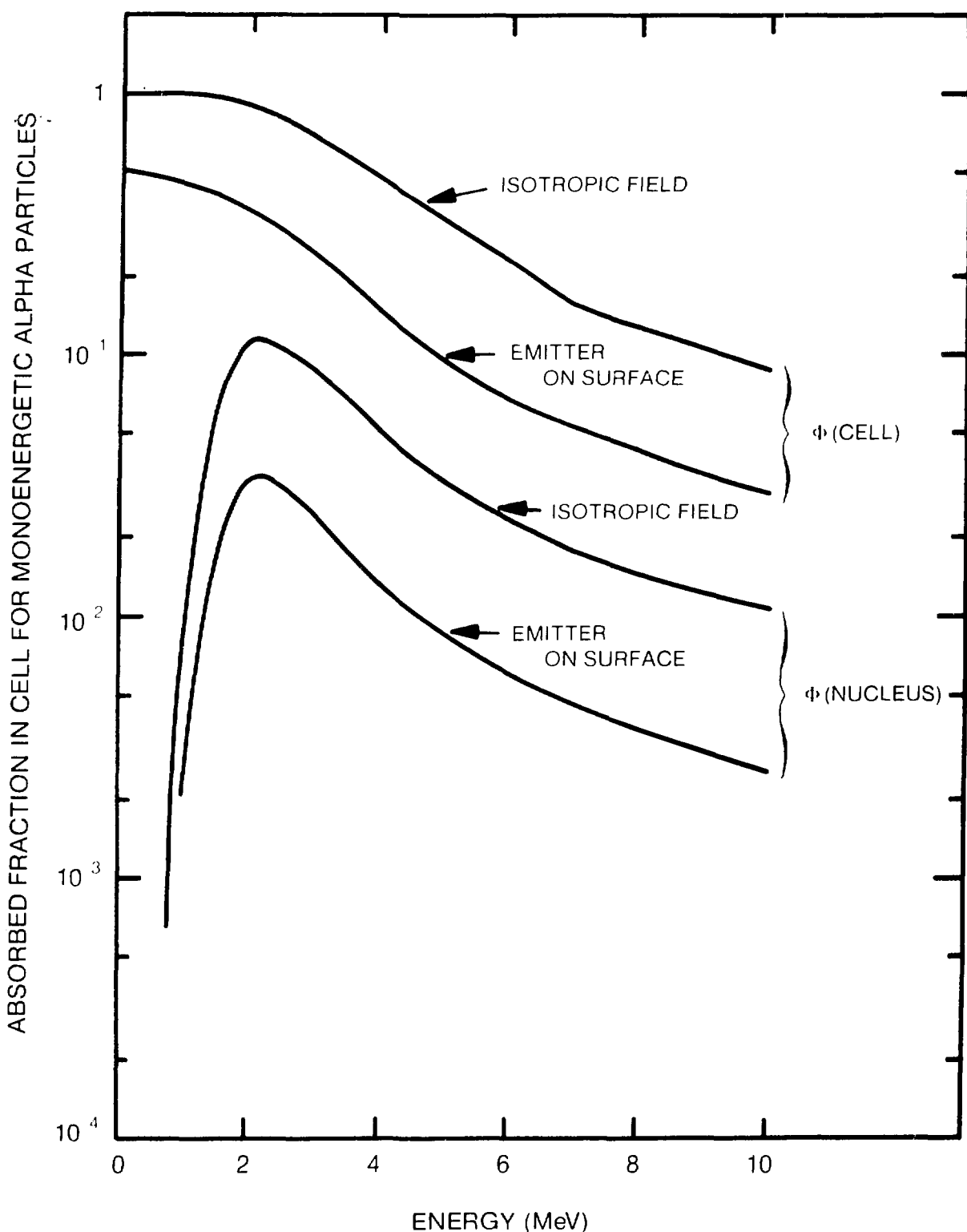


Figure 3. Absorbed fraction for monoenergetic alpha particles incident on cells under μ - and S-randomness.

Table 1. Absorbed fraction in cell for monoenergetic electrons

Energy (MeV)	Absorbed fraction	
	Cell	Nucleus
<u>Emitter on surface</u>		
0.015	0.420	5.46E-5
0.020	0.369	3.18E-2
0.030	0.227	2.11E-2
0.040	0.114	1.01E-2
0.050	0.075	6.52E-3
0.060	0.052	4.49E-3
0.080	0.034	2.99E-3
0.100	0.022	1.93E-3
<u>Isotropic field</u>		
0.015	0.970	2.68E-4
0.020	0.918	1.17E-1
0.030	0.647	7.87E-2
0.040	0.315	3.86E-2
0.050	0.196	2.25E-2
0.060	0.142	1.80E-2
0.080	0.097	1.17E-2
0.100	0.064	8.20E-3

Table 2. Absorbed fraction in cell for monoenergetic alpha particles

Energy (MeV)	Absorbed fraction	
	Cell	Nucleus
<u>Emitter on surface</u>		
0.8	0.444	1.94E-4
1.0	0.435	2.31E-3
1.5	0.400	1.51E-2
2.0	0.356	3.36E-2
3.0	0.247	2.41E-2
4.0	0.143	1.34E-2
5.0	0.094	8.24E-3
6.0	0.069	6.10E-3
7.0	0.052	4.46E-3
8.0	0.042	3.72E-3
10	0.029	2.52E-3
<u>Isotropic field</u>		
0.8	0.985	6.66E-4
1.0	0.976	8.55E-3
1.5	0.947	6.06E-2
2.0	0.893	1.13E-1
3.0	0.674	8.89E-2
4.0	0.389	4.97E-2
5.0	0.352	4.54E-2
6.0	0.222	2.72E-2
7.0	0.141	1.78E-2
8.0	0.124	1.49E-2
10	0.086	1.10E-2

ACKNOWLEDGEMENTS

Research sponsored by the Office of Health and Environmental Research, U.S. Department of Energy under contract DE-AC05-84OR21400 with the Martin Marietta Energy Systems, Inc.

APPENDIX A

MONTE CARLO TECHNIQUES FOR SIMULATION OF PARTICLES

Many of the Monte Carlo methods needed to simulate the flight of particulate radiations were developed in applications to neutron and photon radiation transport. Because present day micro- and minicomputers rival the computing power that was available during the developmental period, Monte Carlo methods can be widely applied to dosimetric problems. The algorithms present in this appendix are of general utility in applying Monte Carlo methods. We assume the reader has a general knowledge of Monte Carlo methods. For those who do not, we recommend the review article by Turner, Wright and Hamm (8) as a primer. We assume the existence of a random number generator yielding random numbers, ξ , uniform on the region $0 < \xi < 1$.

-1. EQUATIONS OF LINE AND SPHERE

The parametric equation of the line passing through the point (x_0, y_0, z_0) is given as

$$x = x_0 + ut \quad (A-1)$$

$$y = y_0 + vt$$

$$z = z_0 + wt$$

where the triplet (u, v, w) denote the direction cosines of the line. The equation of a sphere of diameter d centered at the origin is

$$x^2 + y^2 + z^2 = \frac{d^2}{4} \quad (A-2)$$

The intersections of the line and sphere can be found by substituting Eq. A-1 into Eq. A-2 and solving the resultant quadratic equation for t , i.e.,

$$A t^2 + B t + C = 0 \quad , \quad (A-3)$$

where,

$$A = u^2 + v^2 + w^2 ,$$

$$B = 2(x_0 u + y_0 v + z_0 w) ,$$

$$C = x_0^2 + y_0^2 + z_0^2 - \frac{d^2}{4} .$$

Note that the sum of the squares of the direction cosines is one, i.e., $A = 1$. If $B^2 - 4C < 0$ the line does not intersect the sphere; however, if $B^2 - 4C > 0$, then intersections occur at the points

$$(x_0 + ut_1, y_0 + vt_1, z_0 + wt_1)$$

and

$$(x_0 + ut_2, y_0 + vt_2, z_0 + wt_2) ,$$

where t_1 and t_2 denote the smaller and larger solutions, respectively, of the quadratic equation. The length of the line segment (chord) defined by the above points is $t_2 - t_1$ since $u^2 + v^2 + w^2 = 1$.

A-2. SAMPLING POINTS WITHIN A SPHERE

To randomly select points uniformly within a sphere we pick a point at random in the volume of a box enclosing the sphere. The sphere of radius $\frac{d}{2}$ d is enclosed by a box defined by the planes $x = \pm \frac{d}{2}$ d, $y = \pm \frac{d}{2}$ d, and $z = \pm \frac{d}{2}$ d. A point (x, y, z) is selected at random as

$$x = \frac{d}{2} (2\xi_1 - 1)$$

$$y = \frac{d}{2} (2\xi_2 - 1)$$

$$z = \frac{d}{2} (2\xi_3 - 1)$$

where ξ_1, ξ_2, \dots denote random numbers uniform on the region $0 < \xi < 1$. A test is performed to see if the point (x, y, z) lies within the sphere. If not, the point is rejected and a new point is selected. This method of sampling is referred to as the rejection method. The efficiency of the method in selecting points within a sphere is given by the ratio of the volume of the sphere to that of the box, i.e., $\frac{\pi}{6}$ or 52%.

A-3. SINE AND COSINE OF A UNIFORMLY DISTRIBUTED ANGLE

Frequently in Monte Carlo simulations one needs the sine and cosine of an angle uniformly distributed on the interval 0 to 2π . A random value for the angle δ can be obtained as $\delta = 2\pi \xi$ and the sine and cosine computed directly. It is often useful, however, to avoid evaluating these functions if possible. It can be shown that if δ is uniformly distributed over the interval 0 to 2π then

$$\cos \delta = \frac{x_1^2 - x_2^2}{x_1^2 + x_2^2}$$

$$\sin \delta = \frac{2x_1 x_2}{x_1^2 + x_2^2}$$

where $x_1 = 2\xi_1 - 1$, $x_2 = \xi_2$, and we reject the values if $x_1^2 + x_2^2 > 1$.

A-4. DIRECTION COSINES FOR ISOTROPIC SOURCE

An isotropic source emits radiation equally in all directions, i.e., each solid angle element receives the fraction $d\Omega/4\pi$. In spherical coordinates the fraction can be expressed as

$$\frac{d\Omega}{4\pi} = \frac{\sin \theta}{2} \frac{d\theta}{2\pi}$$

which is of the form $p(\theta, \delta) = p_1(\theta) p_2(\delta)$. Thus θ and δ are independent random variables which can be sampled separately from their respective functions. The probability density function p_2 is uniform over the region $0 \leq \delta \leq 2\pi$ and thus a random value is given by $\delta = 2\pi \xi$. The probability density function for θ is $p_1(\theta) = \frac{1}{2} \sin \theta d\theta$ which yields $\theta = \cos^{-1}(2\xi - 1)$. The direction cosines (u, v, w) are related to the spherical coordinate system as

$$u = \sin \theta \cos \delta$$

$$v = \sin \theta \sin \delta$$

$$w = \cos \theta .$$

Note that we obtain the sine and cosine of δ directly from the algorithm discussed above. If we denote $\cos \theta = x_3 = 2\xi - 1$ then $\sin \theta = [1 - \cos^2 \theta]^{\frac{1}{2}}$ and

$$u = [1 - x_3]^{1/2} \frac{x_1^2 - x_2^2}{x_1^2 + x_2^2}$$

$$v = [1 - x_3]^{1/2} \frac{2x_1 x_2}{x_1^2 + x_2^2}$$

$$w = x_3 .$$

A-5. DIRECTION COSINES FOR ISOTROPIC FIELD

The procedure to obtain the direction cosines for particles incident on the surface from an isotropic field was discussed in the text. For completeness we present the algorithm here. As noted in the text the direction cosine relative to the surface normal at the point of incidence is given as $\cos \theta = (1. - \xi_1)^{1/2}$ and thus $\sin \theta = \xi_1^{1/2}$. We have

$$u = \xi_1^{1/2} \frac{x_1^2 - x_2^2}{x_1^2 + x_2^2}$$

$$v = \xi_1^{1/2} \frac{2x_1 x_2}{x_1^2 + x_2^2}$$

$$w = (1. - \xi_1)^{1/2} .$$

Note that the z-axis, direction cosine w, of the Cartesian coordinate system is aligned along the normal to the surface. Appropriate rotation and translation of the coordinate system must be made as required by the problem.

REFERENCES

1. Loevinger, R. and M. Berman. A revised schema for calculating the absorbed dose from biologically distributed radionuclides. MIRD Pamphlet No. 1, Revised, Society of Nuclear Medicine, New York, 1976.
2. ICRP. International Commission on Radiological Protection. Limits for intake of radionuclides by workers, Annals of the ICRP, 2 No. 3/4, Pergamon Press, Elmsford, New York, 1979.
3. Snyder, W. S., M. R. Ford, and G. G. Warner. Estimates of specific absorbed fractions for photon sources uniformly distributed in various organs of a heterogeneous phantom, MIRD Pamphlet No. 5, Revised, Society of Nuclear Medicine, New York, 1978.
4. Snyder, W. S., M. R. Ford, G. G. Warner, and S. B. Watson. "S" absorbed dose per unit cumulated activity for selected radionuclides and organs, MIRD Pamphlet 11, Society of Nuclear Medicine, New York, 1975.

5. Kellerer, A. M. Consideration of the random traversal of convex bodies and solutions for general cylinders. Radiat. Res. **47**, 359-376, 1971.
6. Berger, M. J. Improved point kernels for electron and beta-ray dosimetry. Progress Report No. NBSIR 73-107, National Bureau of Standards, Washington, DC, 1973.
7. Taner, A. and K. F. Eckerman. Stopping power and point isotropic specific absorbed fraction data for alpha particles in tissue, in Report of Current Work of the Metabolism and Dosimetry Research Group, January 1, 1984 - June 30, 1985, pp. 109-116, edited by R. W. Leggett and B. P. Warren, ORNL/TM-9690, 1985.
8. Turner, J. E., H. A. Wright, and R. N. Hamm. A Monte Carlo primer for health physicists, Health Phys. **48**, No. 6, 717-733, 1985.

DISCUSSION

SASTRY: Dr. Eckerman: In one of your slides, you showed the absorbed fractions for electrons from radionuclides localized on surfaces of cells. If I recall correctly, these absorbed fractions peak at about 20-30 keV and drop drastically at higher energies. Does this imply that electrons of 20-30 keV are optimal for radioimmunotherapy?

ECKERMAN: Right, it would suggest that a higher fraction of the energy would be deposited in a nucleus if the emitted energy is in the neighborhood of 20 kiloelectron volts.

SPECT QUANTIFICATION OF REGIONAL RADIONUCLIDE DISTRIBUTIONS

RONALD J. JASZCZAK, Ph.D.

KIM L. GREER, N.M.T.

R. EDWARD COLEMAN, M.D.

P.O. Box 3949

Duke University Medical Center
Durham, North Carolina 27710

ABSTRACT

SPECT quantification of regional radionuclide activities within the human body is affected by several physical and instrumental factors including attenuation of photons within the patient, Compton scattered events, the system's finite spatial resolution and object size, finite number of detected events, partial volume effects, the radiopharmaceutical biokinetics, and patient and/or organ motion. Furthermore, other instrumentation factors such as calibration of the center-of-rotation, sampling, and detector nonuniformities will affect the SPECT measurement process. These factors are described, together with examples of compensation methods that are currently available for improving SPECT quantification. SPECT offers the potential to improve *in vivo* estimates of absorbed dose, provided the acquisition, reconstruction, and compensation procedures are adequately implemented and utilized.

INTRODUCTION

Although emission tomography using non-computerized techniques was first investigated nearly twenty-five years ago by Kuhl, et al [1], it has only been within the past few years that single photon emission computed tomography (SPECT) has emerged as a valuable clinical modality. Major factors resulting in this renewed interest in SPECT include the development of reliable, high-quality SPECT hardware devices, and the concurrent development of reasonably accurate reconstruction methods to compensate for inherent data acquisition limitations, such as the attenuation of photons and the detection of scattered photons. Quantitative SPECT measurements offers the potential for improved diagnostic, therapeutic, and dosimetric information.

As SPECT instrumentation has improved, a renewed interest has developed in new radiopharmaceuticals that could provide quantitative physiological information from SPECT scans. For example, within the last few years I-123 labeled compounds have been investigated as potential brain perfusion agents [2-5]. Furthermore, several groups are currently developing new Tc-99m labeled radiopharmaceuticals [6-7].

ABSORBED DOSE ESTIMATES AND SPECT

The objective of an internal dosimetric determination is to provide an estimate of the energy absorbed by various tissues within the body from exposure to ionizing radiation resulting from an internally administered radiopharmaceutical. The absorbed dose depends on many factors, including (1) the physical characteristics of the radionuclide, (2) the presence of radiochemical and/or radionuclidic impurities, (3) the biologic nature of the specific patient, and (4) the detailed uptake, regional biodistribution, and excretion for the organs of interest and the total body (i.e., the regional biokinetic properties of the radiopharmaceutical). To obtain dose estimates for each patient would present a formidable challenge. Thus, over the past two decades various models and mathematical approaches, such as the method developed by Loevinger and Berman [8-10], have been used to mathematically estimate absorbed dose.

Conventional planar imaging has been used in the past to estimate the *in vivo* biokinetics of certain organ systems for specific radiopharmaceuticals. However, it is not currently feasible to obtain accurate, absolute quantitative measurements of *in vivo* radionuclide distributions using planar imaging, except perhaps for a few specialized imaging situations. Quantitative planar imaging is limited by the effects of internally attenuated photons, inclusion of Compton scattered photons, and superposition of activities located at different depths within the patient. For situations where an isolated organ has a relatively large uptake of activity and is surrounded by negligible body activity, planar imaging can provide reasonably accurate quantitative information. In this case superposition is not a problem, and compensation for attenuation can be provided, for example, by using the geometric mean of opposing views [11].

Basically, SPECT maps the three dimensional concentration of a radiopharmaceutical by measuring the angular distributions, or projections, of gamma ray intensities emitted within the body. Besides providing true 3-D, or total organ imaging, SPECT is capable of eliminating overlying and underlying source activities, and offers the potential of quantitative measurements of regional biodistribution of radiopharmaceutical uptake within the patient. However, the problems associated with accurate SPECT quantification are formidable and require a thorough understanding of SPECT instrumentation design, and the physics involved with data acquisition and image reconstruction. In the following sections SPECT instrumentation approaches will be described together with methods to compensate for attenuation and scatter.

SPECT INSTRUMENTATION

Several devices (Fig. 1) are currently being developed for SPECT using both discrete-detector and camera-based approaches [12-24]. Since the sensitivity of a SPECT system is limited by the requirement to physically collimate the gamma radiation, a major objective of SPECT system design has been to utilize a large area of detector material (typically Tl-activated NaI) viewing the organ of interest. Discrete-detector approaches include (1) banks of closely spaced detectors such as the Mark IV system (Fig. 1-A) developed by Kuhl, et al [15], the Headtome-II system [16] that uses fan beam collimator vanes (Fig. 1-B) that rotate in front of a stationary discrete detector ring, and the Harvard multidetector system (Fig. 1-C) consisting of 12 scintillation counters that scan both radially and tangentially [17]. Other detector approaches (not illustrated in Fig. 1) include a multiple slice

system that uses a set of one-dimensional bar-type scintillation cameras [18], and a ring of stationary detectors that uses rotating slits to obtain a set of fan beam projections [19].

Camera-based SPECT approaches (Fig. 1-D through F) use one or more large-area, position-sensitive, NaI(Tl) scintillation crystals. The location of a gamma ray interacting with the crystal is determined using special electronic circuitry based on the application of the method developed by Anger [25,26]. The gamma camera rotates about the patient to acquire the projectional views necessary to reconstruct a 3-D representation of the radionuclide distribution. Besides single camera [12,14] systems (Fig. 1-D), dual camera [13] devices (Fig. 1-E), and even a triple camera SPECT system [21,22] consisting of a triangular arrangement of three rectangularly shaped gamma cameras have been developed and are commercially available. An interesting adaptation of a camera-based approach for SPECT imaging of the brain is the MUMPI system [23] that consists of a single annular NaI(Tl) crystal and rotating collimators to obtain the projection data (Fig. 1-F).

There are advantages and disadvantages to both discrete-detector and camera-based approaches. For example, devices using one or more rings of discrete detectors may have high-single slice volume sensitivity; however, they are usually optimized to scan only the brain, and typically a single scan results in a single slice, or at most a few noncontiguous sectional images. SPECT systems using a single scintillation camera will have a lower single-slice volume sensitivity; however, camera based approaches are capable of complete 3-D imaging of the entire organ volume using a single rotational scan about the patient. Furthermore, camera-based SPECT systems are quite versatile since both planar and SPECT images can be obtained with the same device. Most systems can scan both the head and the body by moving the camera radially towards or away from the axis of rotation. Spatial resolution and sensitivity can be varied by using different collimators. Because of these characteristics (and also the fact that the scintillation camera has evolved over the years into a highly optimized imaging device), most SPECT systems in clinical use today are based on gamma camera technology. Second generation camera-based SPECT systems, such as the MUMPI (23) or the device using three gamma cameras (21, 22) should have a single-slice sensitivity that is comparable to the sensitivity of a discrete-detector ring system, and a total organ sensitivity that is greater than a ring device.

FACTORS AFFECTING SPECT QUANTIFICATION

There are several classes of quantitative information potentially available from imaging a radionuclide distribution. The first, and perhaps the lowest, class consists of the determination of the number and locations of lesions within an organ. A second class of measurement consists of determining the dimensions (size, shape, and/or volume) of the radionuclide biodistribution of interest (lesion, chamber, or organ). A third class comprises the quantitative measurement of activity ratios (e.g., the ratio of radionuclide concentration within an organ to that of the surrounding body tissue). A fourth class consists of the measurement of the total amount of radionuclide within an organ and its variation with time. Finally, the fifth, and most difficult class consists of the absolute measurements of the radionuclide concentration as a function of time for small volume elements (voxels) within the body.

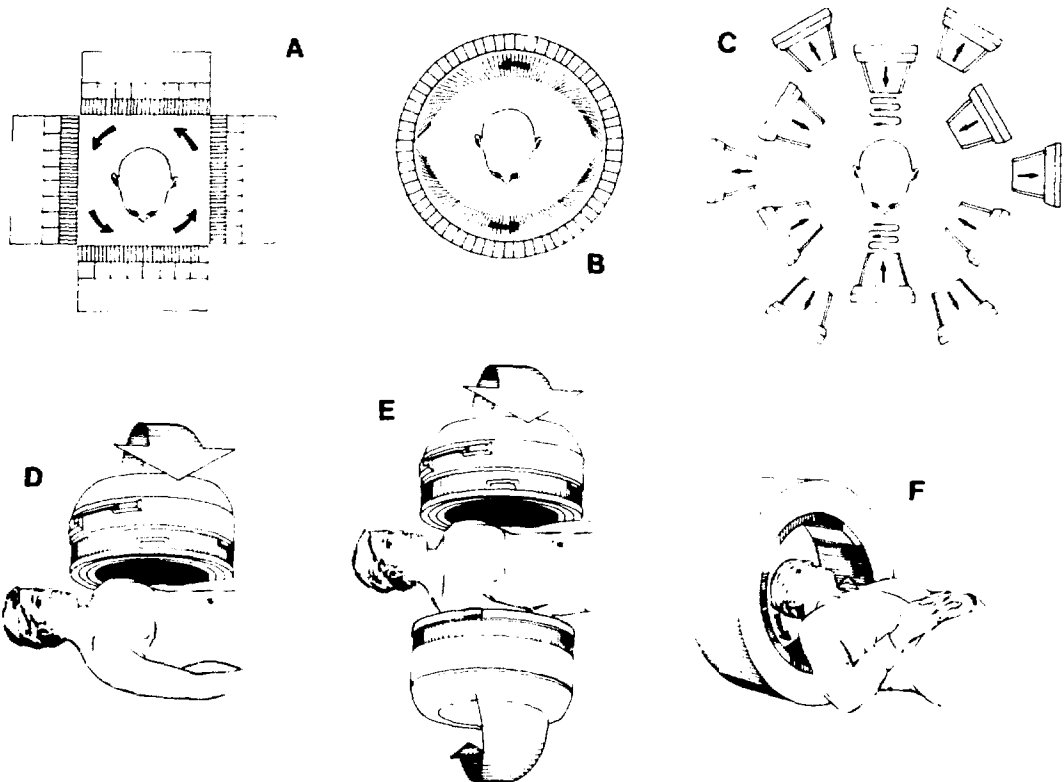
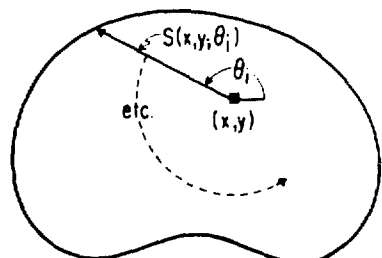


Figure 1. Approaches used in the design of SPECT instrumentation.
(Courtesy: Investigative Radiology 20 (1985)).



$$C_{att}(x,y) = \frac{1}{M} \sum_{i=1}^M \exp[-\mu \cdot s(x,y; \theta_i)]$$

$$f_1(x,y) = f(x,y) C_{att}(x,y)$$

FIRST ORDER CORRECTION

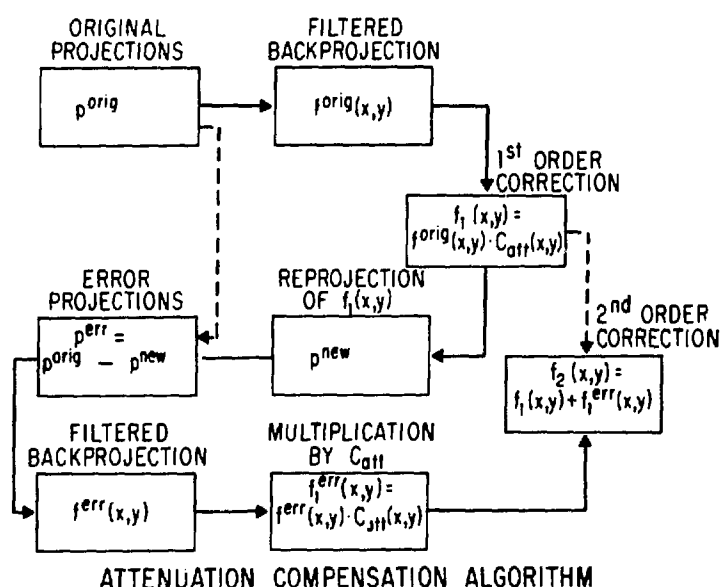


Figure 2. Attenuation compensation using post-processing methodology.

There are several factors that will directly, and indirectly, affect the SPECT measurement process. The relative importance of each factor will depend not only on the class of the quantitative information being determined, but also on the biokinetic properties (regional biodistribution and changes with time) of the particular radiopharmaceutical of interest. Thus, the extraction of reliable quantitative data using SPECT requires a thorough understanding of the mathematical and engineering characteristics of the data acquisition and image reconstruction methods, coupled with an understanding of the physical and biochemical nature of the radiation and radiopharmaceutical.

Depending on the specific application, the determination of the internal absorbed dose estimates might require, for example, either absolute regional concentrations or perhaps the total activity within the organ, its volume and location, and the change in activity with time.

There are many factors that affect SPECT quantification. Several of the major factors that affect camera-based SPECT systems are listed below.

I. Physical factors:

1. Characteristic energy (or energies) of the emitted photons.
2. Radiation decay as a function of time.
3. Attenuation of gamma photons within the patient.
4. The inclusion of scattered photons within the pulse height window of the detector.

II. Anatomical/physiological factors:

1. Source (organ) size and location within the body.
2. Patient and/or organ motion.
3. Biokinetic behavior of the radiopharmaceutical within the body.

III. SPECT system factors:

1. Camera/collimator energy and spatial resolutions.
2. Detection efficiency.
3. Changes in collimator geometric response with distance from the collimator surface.
4. Sensitivity variations across the camera surface.
5. Camera electronic variations, analog-to-digital convertor errors, and gantry mechanical variations with time and/or position.
6. Characteristics of the reconstruction process such as the shape of the filter function, values for the linear and angular sampling intervals, the accuracy of compensation methods for nonuniformities, attenuation and scatter, and the accuracy of edge-detection methods required for body contour and volumetric measurements.

Although additional factors may affect SPECT imaging, the above listing is adequate to indicate that accurate and precise quantification represents a challenge to the investigator. However, if well-designed and -built

instrumentation is used, and if the instrumentation is evaluated and calibrated using carefully implemented phantom and animal experiments, it is possible to attain a degree of quantification that is superior to that possible using conventional planar techniques.

It is beyond the scope of this paper to describe every factor affecting SPECT quantification. Many of these factors have been previously described as they affect SPECT [27-31]. In the following sections we will describe a few of the major factors that affect SPECT quantification.

ATTENUATION COMPENSATION

To perform quantitative SPECT imaging a compensation for photon attenuation must be made. For example, consider the imaging of a water-filled 20 cm diameter cylinder containing a uniform distribution of Tc-99m. Only about 25% of the total number of gamma photons emitted in the central region of the cylinder will be detected assuming an effective attenuation coefficient of 0.13 cm^{-1} for 140 keV photons. A value of 0.13 cm^{-1} is used, rather than the published narrow-beam value of 0.15 cm^{-1} , since the gamma camera pulse-height window includes a large number of events that have been scattered within the cylinder. In the absence of compensation for attenuation, the reconstructed transaxial image of the cylinder will appear to have decreased activity in its central region. With an appropriate compensation for attenuation, the SPECT image of the cylindrical radionuclide distribution would appear uniform.

The effect of attenuation results in a significant decrease in the measured projection data. Not only is there self-absorption within the target organ, but there is also attenuation in the surrounding body tissue. Furthermore, the attenuation coefficient is variable within the body, particularly within the thorax. Most compensation methods currently assume that the attenuation coefficient is constant, and hence will provide a less accurate compensation within regions such as the thorax where the value of the attenuation coefficient is variable. An accurate estimate of the body contour is also usually required. Three general approaches to attenuation compensation are described in the following sections.

Preprocessing Methods [11, 31-33]:

These approaches attempt to correct the measured projection data prior to image reconstruction. The arithmetic or geometric mean of opposing views is computed and used in a compensation equation that has been developed based on the assumption of a constant source activity. These approaches are relatively simple to implement; however, the quantitative accuracy is limited and they have the potential to generate streak artifacts in the presence of noisy data.

Intrinsic Compensation [31, 34-41]:

These approaches attempt to integrate the effect of attenuation directly into the reconstruction algorithm. One method is based on the use of an assumed or measured attenuation map as part of an interactive reconstruction algorithm. If an attenuation map is measured (for example, using a Tc-99m transmission source), then this approach offers the potential to accurately quantitate source activities even in the presence of nonuniform attenuation.

These methods are quite sophisticated, and presently have only been demonstrated on a few research SPECT systems with access to large computing facilities. Although a careful evaluation has yet to be performed, intrinsic compensation may result in improved absorbed dose estimates using SPECT.

Postprocessing Compensation [13, 42-44]

Postprocessing approaches first compute an image using a filtered back-projection algorithm and the assumption of no attenuation. Since this approach is used with several commercial SPECT systems, it will be more fully described. A first-order compensated image is determined by multiplying the original image by a correction matrix that has been mathematically computed using an independently measured or estimated body contour and an assumed constant attenuation coefficient. An element $C(x,y)$ of the correction matrix is equal to the reciprocal of the average attenuation along all rays from the pixel (x,y) to the boundary of the attenuating medium.

A further refinement of this method is to compute a second-order compensation by applying one further processing step (Figure 2). Using a reprojection algorithm a set of new projections are determined using the first-order image and the measured body contour. Error projections are obtained by subtracting the new reprojections from the the originally measured projection data. An error image is reconstructed, and the second-order image is determined by adding the error image to the first-order image. This second-order compensation has not been widely used since the computational requirements are increased; furthermore, image noise may also be increased. The first-order correction has been found to provide accurate measurements of activity within a uniform attenuating medium when used in conjunction with a scatter compensation algorithm [27]. Reasonable SPECT quantification has been demonstrated even within the nonuniformly attenuating canine thorax [45], if an average value for the effective attenuation coefficient has been empirically determined.

Effect of Finite Spatial Resolution

Although spatial resolution degrades with distance from the surface of parallel hole collimators, the spatial resolution in the reconstructed SPECT image plane is reasonably uniform. Furthermore, as a result of relatively fine sampling along the long axis of the patient, a camera-based SPECT system exhibits longitudinal resolution which is comparable to the resolution within the reconstructed plane.

It has been shown [28] that the SPECT measured image contrast for spherical sources placed within a uniform background source is degraded more for small diameter spherical sources as compared with larger diameter sources as a result of the finite resolution of the SPECT system. The image contrast C_{image} is defined as:

$$C_{image} = \frac{[(sphere\ counts/voxel) - (background\ counts/voxel)]}{background\ counts/voxel}. \quad (1)$$

The actual object contrast C_{obj} or "uptake ratio" (equal to the radionuclide concentration in the sphere Q_s minus the background concentration Q_b , divided by the background concentration) is related to the

SPECT-measured image contrast C_{image} as follows (assuming for the moment that the effect of Compton scattering is negligible):

$$C_{obj} = (Q_s - Q_b)/Q_b = C_{image}/CF_{avg}, \quad (2)$$

where CF_{avg} is an average contrast factor which compensates for the finite spatial resolution of the SPECT system [28]. This result is an extension of a similar result obtained for conventional nuclear medicine [46]. The contrast factor can be numerically computed if the system spatial resolution and the diameter of the sphere are known or can be measured. We have shown [28] that the published, tabulated values [46] for CF results in accurate SPECT-measured concentration ratios over a wide range of values. The contrast factor approaches unity for diameters greater than three or four times the SPECT spatial resolution (FWHM). This implies that for larger objects uptake ratios can be quantitated directly; however, careful compensation techniques (based on a determination of the object size) are required for smaller sources. It may be possible to measure the size of the source directly from the multi-slice SPECT data. Alternatively, complementary imaging modalities such as X-ray CT or ultrasound can be used. If the source dimensions cannot be readily determined, there remains only three options: 1) recognize and accept the inherent error of the measurement, 2) for isolated structures surrounded by little or no background activity, it is possible to measure the total radioactivity (in uCi) contained in the structure, 3) perform relative rather than absolute measurements by utilizing an internal standard that, for example, might be a known normal structure of the same size symmetrically located within the field-of-view.

SCATTER COMPENSATION

Consideration of scatter is important since its inclusion in the SPECT data set degrades the contrasts of lesions. This results in a major source of error in quantification of radionuclide activities. The use of NaI(Tl) as the primary detector for SPECT results in the inclusion of both scattered and non-scattered photons within the photopeak energy window. The use of Monte Carlo modeling [47,48] has been particularly useful in providing guidance in the development of scatter compensation procedures since it is possible to separately analyze the scattered and non-scattered components. A few of the approaches used to compensate for scatter are described below.

Use of an Average Scatter Fraction

This simple approach [28] can improve the accuracy of measurements of radionuclide uptake ratios made from attenuation-compensated SPECT images.

If Q_s is the radionuclide concentration within a hollow sphere, placed within a cylinder containing a uniform source distribution having a concentration Q_b , then the uptake ratio C_{obj} , can be estimated using this equation:

$$C_{obj} = (C_{image}/CF_{avg}) (1 + SF_{avg}), \quad (3)$$

where C_{image} is the SPECT-measured image contrast for the sphere, CF_{avg} is the contrast-loss factor previously described (reciprocal of the recovery coefficient) resulting from the system's spatial resolution, and SF_{avg} is the estimated value for the average scatter fraction in the reconstructed

SPECT image. Monte Carlo methodology [48] may be used to estimate SF_{avg}. For the measurement of uptake ratios, SF_{avg} need be only approximately known to obtain reasonable estimates. For example, changing SF_{avg} from 0.4 to 0.8 (a 100% increase) results in a 28% increase in the SPECT-measured uptake ratio. Thus, the use of an average scatter fraction is based on the assumption that relatively large errors in the estimated values of SF_{avg} result in smaller errors in the parameter being quantified. For the measurement of uptake ratios this assumption appears valid; however, the equation in its present form cannot be used to obtain absolute concentration levels.

Scatter Subtraction Method

This scatter-compensation method was proposed by Jaszczak, et al [27] and is based on the use of photons that are detected within a pulse-height window located below the primary photopeak. The method assumes that the shape of the reconstructed point spread function for events detected within the lower pulse-height window represents a reasonable approximation to the response of the true scatter component contained within the primary photopeak window. The method consists of subtracting a constant fraction of the image reconstructed with a low cut-off filter using the secondary pulse-height data from the image reconstructed using the photopeak pulse-height window. Alternatively, it would be possible to subtract a fraction of the lower energy projection data from the primary photopeak projection data. This method has been evaluated experimentally, and has demonstrated a marked improvement for SPECT quantification of absolute radionuclide concentrations [27]. A further refinement of this method would be to determine a position-dependent weighting function so that the amount of the "scatter image" subtracted is varied for different positions within the body contour.

Convolution methods

These techniques are based on a functional characterization of the scatter distribution [49, 50]. A convolution-subtraction technique has been proposed by Axelsson, et al [49] and consists of modeling the scatter component as a convolution of the measured projection data with an empirically derived function. The resulting scatter estimate is then subtracted from the original projections. Another approach, proposed by Floyd, et al [50], consists of a true deconvolution technique in which the scatter component is modeled as the convolution of the nonscatter projection data with an exponential function. An estimate of the true nonscatter projections is determined through deconvolution of the equation relating the nonscattered data to the measured projection data.

There are advantages and disadvantages to each scatter compensation approach. Some techniques are easy to implement. Other methods compensate only for scatter originating within the slice, and have not been extended to include compensation for a three dimensional scattering geometry. All methods have yet to be validated for nonuniformly attenuating media.

SPECT SYSTEM CALIBRATION

Besides the physical and mathematical factors described above, several system related alignment and calibration factors must be considered if SPECT quantification is to be accomplished. Many of these factors have been

previously described [51-53]. Two of the most important factors include compensation for regional sensitivity variations (i.e., flood nonuniformities), and alignment of the physical axis of rotation with the reconstruction matrix central ray (i.e., centering or offset calibration).

Problems associated with the implementation of nonuniformity compensation and central ray calibration will reduce the accuracy of the SPECT measurement and result in marked image degradation and artifacts.

The net effect of sensitivity variations (resulting from intrinsic camera or collimator imperfections) is to either increase or decrease the number of detected events at certain locations (or rays) within each projection set. If the sensitivity error is constant for all angular views, then the resulting image artifact will be a region of apparent increased or decreased activity that is circular or annular in appearance and symmetrically centered around the axis-of-rotation. Since SPECT tends to increase image contrasts as compared with the original contrasts determined from the projected data, small sensitivity errors will result in large reconstructed image errors.

The second factor, alignment of the central ray or offset voltage adjustment, is extremely important if high-quality, artifact-free images are to be obtained. Very slight positional misadjustments will produce observable effects since the peak signal will be distributed over a larger area (more pixels) in the reconstructed image. Small misalignments will result in a marked loss in spatial resolution; thus, the quantification of small objects will be degraded as a result of the change in the measured image contrast. Large misalignments will result in gross image artifacts and a completely useless SPECT study. For example, the point spread response in the reconstructed image will appear as a "ring" type structure. Accurate quantification would not be possible with such a SPECT device.

CONCLUSIONS

For certain *in vivo* procedures SPECT has the potential to provide improved estimates of internally absorbed doses as compared with planar imaging. However, SPECT currently has the following limitations:

1. Biodistributions that change relatively quickly with time (on the order of a few minutes) cannot be accurately determined in most situations.
2. Microscopic distributions cannot be estimated with SPECT since spatial resolution (FWHM) ranges between 0.8 to 2cm, depending on the system design and geometry.
3. The accuracy of the SPECT measurement is influenced by the calibration, and the compensation methods used to correct for physical factors affecting the data acquisition process.

Improved SPECT instrumentation and reconstruction methodology, coupled with the use of quantitative information supplied by complementary imaging modalities such as transmission computed tomography or magnetic resonance imaging, will improve the accuracy of SPECT measurements of radionuclide biodistribution activities.

ACKNOWLEDGEMENT

The authors thank Wendy Horton for her excellent secretarial support. This work was supported in part by PHS Grant Number CA33541 awarded by the National Cancer Institute, DHHS.

REFERENCES

1. Kuhl, D.E. and R.Q. Edwards: Image separation radioisotope scanning. Radiology 80. 653-662, 1963.
2. Winchell, H.S., R.M. Baldwin, and T.H. Lin: Development of I-123 labeled amines for brain studies: localization of I-123 iodophenylalkyl amines in rat brain. J. Nucl. Med. 21. 940-946, 1980.
3. Winchell, H.S., W.D. Horst, L. Braun, et al: N-isopropyl-[¹²³I] p-iodoamphetamine: Single pass brain uptake and washout; binding to brain synaptosomes; and localization in dog and monkey brain. J. Nucl. Med. 21. 947-952, 1980.
4. Kung, H.F. and M. Blau: Regional intracellular pH shift: A proposed new mechanism for radiopharmaceutical uptake in brain and other tissues. J. Nucl. Med. 21. 147-152, 1980.
5. Kung, H.F., K.M. Tramposch, and M. Blau: A new brain perfusion imaging agent: [I-123] HIPDM:N,N,N'-trimethyl-N'-(2-hydroxy-3-methyl-5-iodobenzyl)-1,3 propanediamine. J. Nucl. Med. 24. 66-72, 1983.
6. Kung, H.F., C.C. Yu, J. Billings, et al: New Tc-99m brain imaging agents. J. Nucl. Med. 25. P16, 1984.
7. Kung, H.F., M. Molnar, J. Billings, et al: Synthesis and biodistribution of neutral lipid-soluble Tc-99m complexes that cross the blood-brain barrier. J. Nucl. Med. 25. 326-332, 1984.
8. Loevinger, R.: A schema for absorbed-dose calculations for biologically-distributed radionuclides. MIRD Pamphlet No. 1, J. Nucl. Med. 9. Suppl. No. 1, 7-14, 1968.
9. Loevinger, R.M. and M. Berman: A formalism for calculation of absorbed dose from radionuclides. Phys. Med. Biol. 13. 205-216, 1968.
10. Loevinger, R. and M. Berman: A revised schema for calculating the absorbed dose from biologically distributed radionuclides, MIRD Pamphlet No. 1, Revised, pp. 3-10, Society of Nuclear Medicine, New York, 1976.
11. Sorenson, J.A.: Quantitative measurement of radiation in vivo by whole body counting, in Instrumentation in Nuclear Medicine Vol. 2. edited by G.H. Hine and J.A. Sorenson, pp. 311-348, Academic Press, New York, 1974.
12. Jaszcak, R.J., P.H. Murphy, D. Huard, and J.A. Burdine: Radionuclide emission computed tomography of the head with Tc-99m and a scintillation camera. J. Nucl. Med. 18. 373-380, 1977.

13. Jaszczak, R.J., L.T. Chang, N.A. Stein, and F.E. Moore: Whole-body single-photon emission computed tomography using dual, large-field-of-view scintillation cameras. *Phys. Med. Biol.* 24. 1123-1143, 1979.
14. Keyes, Jr. J.W., N. Orlandea, W.J. Heetderks, P.F. Leonard, and W.L. Rogers: The humongotron--A scintillation-camera transaxial tomograph. *J. Nucl. Med.* 18. 381-387, 1977.
15. Kuhl, D.E., R.Q. Edwards, A.R. Ricci, R.J. Yacob, T.J. Mich, and A. Alavi: The Mark IV system for radionuclide computed tomography of the brain. *Radiology* 121. 405-413, 1976.
16. Hirose, Y., Y. Ikeda, Y. Higashi, K. Koga, H. Hattori, I. Kanno, Y. Miura, and K. Uemura: A hybrid emission CT-HEADTOME II. *IEEE Trans. Nucl. Sci.* NS-29. 520-523, 1982.
17. Moore, S.C., M.D. Doherty, R.E. Zimmerman, and B.L. Holman: Improved performance from modifications to the multidetector SPECT brain scanner. *J. Nucl. Med.* 25. 688-691, 1984.
18. Stokely, E.M., E. Sveinsdottir, N.A. Lassen, and P. Rommer: A single photon dynamic computer assisted tomograph (DCAT) for imaging brain function in multiple cross-sections: *J. Comput. Assist. Tomogr.* 4. 230-240. 1980.
19. Rogers, W.L., N.H. Clinthorne, J. Stamos, K.F. Koral, R. Mayans, G.F. Knoll, J. Juni, J.W. Keyes Jr., and B.A. Harkness: Performance evaluation of SPRINT, a single photon ring tomograph for brain imaging. *J. Nucl. Med.* 25. 1013-1018, 1984.
20. Jaszczak, R.J., L.T. Chang, and P.H. Murphy: Single photon emission computed tomography using multiple-slice fan beam collimators. *IEEE Trans. Nucl. Sci.* NS-26. 610-618, 1979.
21. Lim, C.B., L.T. Chang, and R.J. Jaszczak: Performance analysis of three camera configurations for single photon emission computed tomography. *IEEE Trans. Nucl. Sci.* NS-27. 559-568, 1980.
22. Lim, C.B., S. Gottschalk, R. Walker, et al: Triangular SPECT system for 3-D total organ volume imaging: Design concept and preliminary imaging results. *IEEE Trans. Nucl. Sci.* NS-32(1). 741-747, 1985.
23. Logan, K.W. and R.A. Holmes: Missouri University multi-plane imager (MUMPI): A high sensitivity rapid dynamic ECT brain imager. *J. Nucl. Med.* 25. P105, 1984.
24. Gottschalk, S.C., D. Salem, C.B. Lim, et al: SPECT resolution and uniformity improvements by non-circular orbit. *J. Nucl. Med.* 24. 822-828, 1983.
25. Anger, H.O.: Scintillation camera with multichannel collimators. *J. Nucl. Med.* 5. 515-531, 1964.
26. Anger, H.O.: Scintillation camera. *Rev. Sci. Instr.* 29. 27-33, 1958.

27. Jaszczak, R.J., K.L. Greer, C.E. Floyd Jr., C.C. Harris, and R.E. Coleman: Improved SPECT quantification using compensation for scattered photons. *J. Nucl. Med.* 25. 893-900, 1984.
28. Jaszczak, R.J., R.E. Coleman, and F.R. Whitehead: Physical factors affecting quantitative measurements using camera-based single photon emission computed tomography (SPECT). *IEEE Trans. Nucl. Sci.* NS-28. 69-80, February, 1981.
29. Gullberg, G.T., J.A. Malko, and R.L. Eisner: Boundary determination methods for attenuation correction in single photon emission computed tomography, in *Emission Computed Tomography: Current Trends*, edited by P.D. Esser, pp. 33-53, Society of Nuclear Medicine, New York, 1983.
30. Soussaline, F.: The single photon tomograph, in *Radionuclide Imaging*, edited by D. Kuhl, pp. 153-184, Pergamon Press, Paris, 1983.
31. Budinger, T.F., G.T. Gullberg, and R.H. Huesman: Emission computer tomography, in *Image Reconstruction from Projections: Implementation and Applications*, edited by G.T. Herman, pp. 147-246, Springer-Verlag, Berlin, 1979.
32. Genna, S.: Analytical methods in whole-body counting, in *Clinical Uses of Whole-Body Counting*, pp 37-63, International Atomic Energy Agency, Vienna, 1966.
33. Kay, D.B. and J.W. Keyes Jr.: First order corrections for absorption and resolution compensation in radionuclide Fourier tomography. *J. Nucl. Med.* 16. 540-541, 1975.
34. Budinger, T.F. and G.T. Gullberg: Three-dimensional reconstruction in nuclear medicine emission imaging. *IEEE Trans. Nucl. Sci.* NS-21. 2-20, June, 1974.
35. Tretiak, O.J. and C. Metz: The exponential radon transform. *SIAM J. Appl. Math.* 39 (2). 341-354, 1980.
36. Gullberg, G.T. and T.F. Budinger: The use of filtering methods to compensate for constant attenuation in single-photon emission computed tomography, *IEEE Trans. Biomed. Eng.* BME-28(2). 142-157, 1981.
37. Bellini, S., M. Piacentini, C. Cafforio, et al: Compensation of tissue absorption in emission tomography, *IEEE Trans. Acoustics, Speech, and Signal Processing ASSP-27*. 213-218, 1979.
38. Soussaline, F.P., A. Cao, G. LeCoq, et al: An analytical approach to single photon emission computed tomography with attenuation effect. *Eur. J. Nucl. Med.* 7. 487-493, 1982.
39. Censor, Y., D.E. Gustafson, A. Lent, and H. Tuy: A new approach to the emission computed tomography problem: Simultaneous calculation of attenuation and activity coefficients, *IEEE Trans. Nucl. Sci.* NS-26. 2775-2779, April, 1979.
40. Floyd, C.E., R.J. Jaszczak, and R.E. Coleman: Inverse Monte Carlo: A unified reconstruction algorithm for SPECT. *IEEE Trans. Nucl. Sci.* NS-32(1). 779-785, February, 1985.

41. Miller, M.I., D.L. Snyder, and T.R. Miller: Maximum-likelihood reconstruction for single photon emission computed-tomography. *IEEE Trans. Nucl. Sci.* NS-32(1). 769-778, February, 1985.
42. Walters, T.E., W. Simon, D.A. Chesler, et al: Radionuclide axial tomography with correction for internal absorption, in *Information Processing in Scintigraphy*, Proceedings of the IVth International Conference, pp. 333-342, Orsay, 1975.
43. Chang, L.T.: A method for attenuation correction in radionuclide computed tomography system. *IEEE Trans. Nucl. Sci.* NS-25(2). 638-643, February, 1978.
44. Moore, S.C., J.A. Brunelle, and C.M. Kirch: An iterative attenuation correction for a single photon scanning multidetector tomography system. *J. Nucl. Med.* 22. P65, 1981.
45. Osborne, D., R.J. Jaszczak, K. Greer, M. Lischko, and R.E. Coleman: SPECT quantification of technetium-99m microspheres within the canine lung. *J. Comp. Assist. Tomogr.* 9. 73-77, 1985.
46. Whitehead, F.R.: Quantitative analysis of minimum detectable lesion-to background uptake ratios for nuclear medicine imaging systems, in *Medical Radionuclide Imaging Vol. I.*, pp. 409-434, International Atomic Energy Agency, Vienna, 1977.
47. Dresser, M.M. and G.F. Knoll: Results of scattering in radiosotope imaging. *IEEE Trans. Nucl. Sci.* NS-20. 266-272, 1973.
48. Beck, J.W., R.J. Jaszczak, R.E. Coleman, C.F. Starmer, and L.W. Nolte: Analysis of SPECT including scatter and attenuation using sophisticated Monte Carlo modeling methods. *IEEE Trans. Nucl. Sci.* NS-29. 506-511, February, 1982.
49. Axelsson, B., P. Msaki, and A. Israelsson: Subtraction of Compton-scattered photons in single-photon emission computerized tomography. *J. Nucl. Med.* 25. 490-494, 1984.
50. Floyd, C.E., R.J. Jaszczak, K.L. Greer, and R.E. Coleman: Deconvolution of Compton scatter in SPECT. *J. Nucl. Med.* 26. 403-408, 1985.
51. Jaszczak, R.J., K.L. Greer, and R.E. Coleman: SPECT system misalignment: Comparison of phantom and patient images, in *Emission Computed Tomography: Current Trends*, edited by P.D. Esser, pp. 57-70, Society of Nuclear Medicine, New York, 1983.
52. Greer, K.L., R.J. Jaszczak, C. Harris, and R.E. Coleman: Quality Control in SPECT. *J. Nucl. Med. Tech.* 13. 76-87, 1985.
53. Todd-Pokropek, A.: The mathematics and physics of emission computerized tomography (ECT), in *Emission Computed Tomography: Current Trends*, edited by P.D. Esser, pp. 3-31, Society of Nuclear Medicine, New York, 1983.

DISCUSSION

BIGLER: What general problems do you foresee for radionuclides such as I-131 that emit high energy photons and radionuclides such as Ga-67 that emit multiple photons?

JASZCZAK: Penetration, which I didn't have time to discuss, will make quantitation more difficult. The problem with the use of pure I-123 is not too bad even though it does have some high energy gamma rays. We've seen the results of the penetration; in fact, all brain images I showed were done with iodine- 123. But certainly, it's like Compton scatter. The penetration will give you background. The resolution probably won't be as good because you have to use thicker septa with different kinds of collimators. Again, I would like to say, if you can understand the system well enough and perhaps do phantom studies, simulations or whatever is necessary, you can convince yourself that you can reach the "level of quantification" you are interested in, be it total organ or regional quantification. If you can convince yourself that you can do it with a phantom, you have a chance of extending that to the in-vivo situation. If you can't do it with the phantom, I think it is very unlikely that you will succeed with the patient.

HARRIS: You listed the difficulties with SPECT quantitation even with the relatively abundant photons from Tc-99m. Given those difficulties, do you think there is any hope at all for SPECT quantitation with Ga-67 and other radionuclides with which we have severe dose limitations?

JASZCZAK: I think it would be extremely difficult except in whole organs of interest. It's like the iodine studies. I showed some nice iodine images, but these were all in phantoms where I was able to acquire adequate counts. In the patient scan with the HIPDM studies, we typically get 100,000 total counts per slice for the reconstructed image. With that kind of statistics, I cannot utilize 8 mm collimator resolution because I just don't have sufficient statistical accuracy. If your question is how much is in the liver, total liver or total organs, your region of interest is much larger.

MYERS: Because the resolution of conventional collimators increases significantly with depth, data are collected from a convex-lens-shaped volume rather than from a uniform disk. How does this affect attempts at quantitation?

JASZCZAK: I tried to show that in my presentation. I showed that if you use a ultrahigh resolution collimator, the gradient, in other words the change in resolution with distance, is on the order of a quarter of a millimeter per centimeter distance. But of course, you average with SPECT by scanning 360 degrees, and now there are algorithms that include it. For instance, the inverse Monte Carlo algorithms (reconstruction algorithm) we are working on at Duke with Dr. Floyd includes the effect of the divergence of the beam. Right now it is just an averaging process, but in the future I think these problems will be handled.

QUANTITATION OF RADIOPHARMACEUTICAL DISTRIBUTION FOR USE
IN DOSE ESTIMATES WITH POSITRON EMISSION TOMOGRAPHY

Edward J. Hoffman

Division of Nuclear Medicine and Biophysics
UCLA School of Medicine and Laboratory of Nuclear Medicine
University of California, Los Angeles
Los Angeles, CA 90024

ABSTRACT

Current PET systems provide a means of obtaining quantitative radiopharmaceutical distributions, which can be accurate for tissue volumes on the order of 1 cc. Properly calibrated PET systems can non-invasively measure amounts of positron emitter in all parts of the body, allowing dose estimations from data obtained with human subjects rather than performing estimates from activity distributions from test animals. Since these are usually rodents, species differences can be large enough to make this type of estimation irrelevant. Before testing in man, it can also be cost effective to measure activity distributions in non-human primates with PET (assuming less of a species difference than between man and rodents), since it would be unnecessary to kill animals to obtain data.

Typical measurements for developing dosimetry for new positron-emitting radiopharmaceuticals would start with a series of rectilinear scans with the PET system as a function of time, initially on non-human primates. This provides general distributions of activity as a function of time and allows one to choose appropriate areas for closer examination. If organs are clearly delineated in rectilinear scans of non-human primates, estimates of human doses can probably be made from that data. Because of species differences and small size of organs, tomographic scanning may not provide significant additional information. Studies could then proceed in man. As above, rectilinear scans as a function of time would define cross-sections to be defined by tomography. Details of studies would be dependent upon sophistication of dosimetry calculations. If calculations assume uniform whole organ distribution, rectilinear scans should provide adequate isotope concentrations and effective half-lives. If more detailed calculations are to be attempted, distributions can be localized to volumes on the order of 1 cc with tomography.

QUANTITATION IN PET

PET is unique among the Nuclear Medicine imaging modalities in that it is relatively easy to obtain quantitative isotope distributions from the images (1). The response of the detection system is essentially constant in resolution and efficiency as a function of depth (1-2). The methods of correcting for attenuation of the radiation in the body are relatively accurate and easy to implement (1, 3). Therefore, the interpretation of image data does

not have the difficulties of spatially variant responses in the image and the nature of the data is compatible with the requirements of standard reconstruction techniques (1).

Errors in the data due to background events can be small and relatively easy to remove in a properly designed system. PET has a unique source of background due to the fact that the localization of activity depends on the simultaneous or coincident detection of the two annihilation quanta for each event. The finite width of the timing window and the large flux of annihilation quanta on each detector results in accidental coincidences of unrelated quanta (1, 4). It is possible to simultaneously measure the accidentals rate and correct for this background, although there is a degradation in precision due to the fact that the true coincidence rate is derived from the difference between two independent measurements (1, 4). As in single photon imaging, scatter of the annihilation quanta leads to mispositioning of events and loss of contrast in the image. The scatter background is generally evenly distributed across the image and is generally not too large compared to the unscattered events (5). Corrections for the scatter background are estimated from models of scatter based on the behavior of the PET system with known objects, then, relatively simple corrections based on an average scatter background (5), or complex techniques based on deconvolving the response of the PET system (6) can be used to remove scatter.

Currently, the primary limitation on quantitation in PET is the limited resolution of the PET system and, in the near future, the limitation will be the intrinsic blurring due to the properties of the positron decay and annihilation, or the quantum efficiency in cases in which inadequate events are accumulated. The limited resolution of PET causes the isotope distribution for objects smaller than about 2 times the resolution of the system to be distributed over a wider area than their actual size (7). Therefore, quantitative concentrations cannot be measured for these small objects, although the net activity in the structure can still be determined. The theoretical limit on resolution depends on two factors inherent to positron decay. 1) The positron annihilates at some distance from the emitting nucleus, thus the resolution is reduced because of this mispositioning. The net effect of this blurring is a fraction of a millimeter for 18-F with a low energy positron and about 3.5-5 mm for 82-Rb with a relatively energetic positron (1). 2) The two annihilation photons are not emitted at exactly 180 deg, and there is mispositioning of 1.5-3.0 mm due to this factor (1).

The resolution can also be affected by the detection efficiency of the PET system, since enough events must be accumulated to form the image. Studies of the relationship between resolution and the signal to noise ratio in the image indicate that, for 18-F radiopharmaceuticals imaged with a 50 cm diameter PET system designed for brain imaging, resolutions of 3-4 mm will be possible in the near future with the doses that are in current use (8).

MEASUREMENT OF ISOTOPE DISTRIBUTIONS FOR DOSIMETRY

Since most nuclear medicine imaging does not allow accurate measurement of isotope distributions in the body of man, dose estimates are typically approximated from in vitro counting of isotope in organs of laboratory animals, usually rodents, that have been injected with the radiopharmaceutical. Better estimates of distributions could be made from non-human primates, but these animals are expensive and becoming more expensive. With PET it is possible to estimate the isotope distribution in non-human primates with a simple intravenous administration without sacrificing the animal. When the radiopharmaceutical goes to human trials, the isotope distribution can be measured directly in man.

An example of the procedure with the non-human primate is shown in figure 1. A rhesus monkey was given a rectilinear transmission scan on the NeuroECAT (5) for attenuation correction of the emission rectilinear scan. The transmission scan is obtained by placing a ring source in the field-of-view (FOV), taking a scan with nothing in place and then repeating the measurement with the subject in the FOV. The ratio of the two sets of data provides a correction for gamma-ray absorption and provides a low resolution x-ray image of the subject as is seen the the first panel of figure 1. The rectilinear image is obtained by stepping the patient bed through the FOV giving a whole body scan.. The transmission image provides anatomical landmarks for the emission image. The monkey was then injected with FDG and a series of rectilinear scans were taken. Three examples of pairs of lateral and AP views are shown in Figure 1.

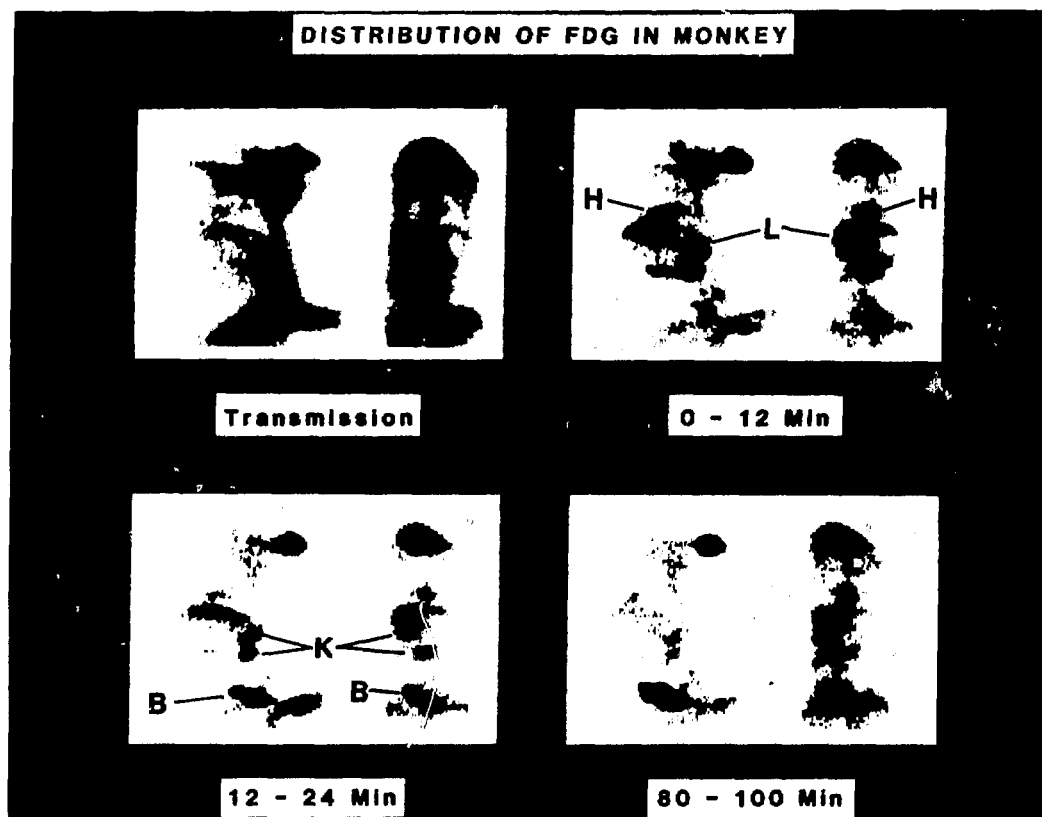


Figure 1. Distribution of FDG in a rhesus monkey as measured by a rectilinear scan with the NeuroECAT. The transmission scan is used to correct the emission scan for attenuation of the annihilation radiation and serves as a guide to the anatomy of the emission scan. The scans were collected for the times indicated below each view, which are measured from the time of injection. Several organs are clearly visible and time activity curves were obtained for the brain, kidneys (K), heart (H), bladder (B) and liver (L).

The isotope concentration is obtained from the image by drawing regions-of-interest (ROI) over the whole organ, an adjacent area is used to estimate the background per pixel and this background is subtracted from the organ ROI value. The ROI's are drawn on both AP and Lateral views and the same ROI's are used for all the scans to obtain the distribution as a function of time. The AP and Lateral views are used to obtain independent measurements of the same organ. The results of these measurements are shown in Figures 2 and 3. The pairs of values are the AP and lateral measurements, which are in generally good agreement with each other. The four kidney measurements for the two kidneys are also grouped. In the brain, heart and kidney there is a net accumulation of FDG with time, but decay reduces the total activity in the organ. The primary difficulty in these measurements is in estimating the proper background. The isotope accumulation in any one organ is the ratio of counts in the ROI for that organ divided by the total image counts times the amount of activity injected. Since there will be some species differences between man and monkey, more accurate tomographic imaging of the animal for dosimetry purposes would probably be just an academic exercise.

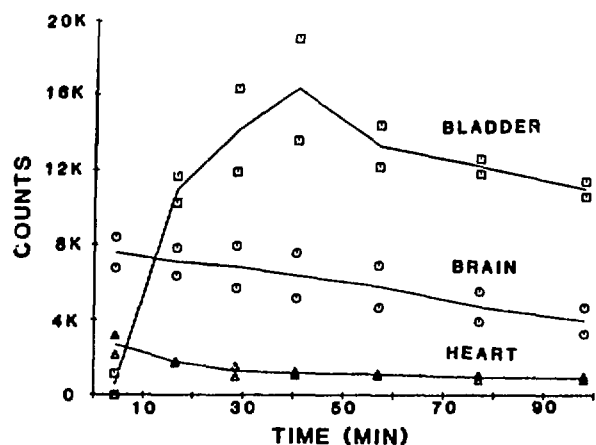


Figure 2. Time activity curves taken from the data displayed in Figure 1. Since AP and lateral views were available, data were obtained and plotted for both views. The solid line is the average of the two views for each organ.

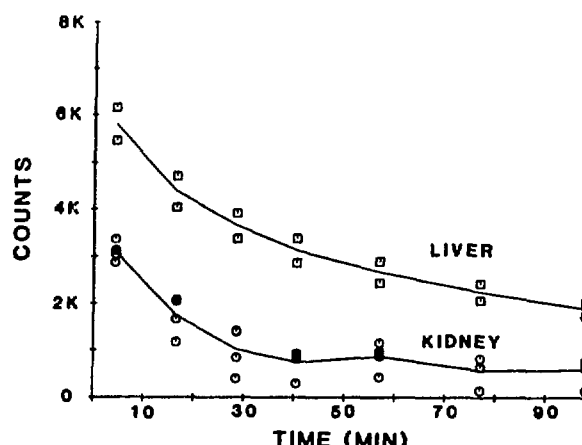


Figure 3. Time activity curves taken from the data displayed in Figure 1. Since both kidneys were visible all four curves (two AP and two lateral) were plotted together.

An example of the same type of imaging procedure in man is shown in Figure 4 in a series of AP rectilinear scans obtained with the ECAT II whole-body scanner (9). In newer whole-body systems, such as the ECAT III (10-11), it will be possible to simultaneously obtain several views for each rectilinear scan. The possibility of performing tomography on the whole body does exist, but would require a significant amount of data storage per determination (200 images [80 Kbytes/image] per whole-body scan [16 Mbytes] and 10 repeats [160 Mbytes]). It would be advisable to determine regions of high concentration of the radiopharmaceutical in the rectilinear scan and then return to those areas for detailed tomographic scans, such as those seen in Figure 5. The images in Figure 5 were obtained with the ECAT III (10-11) and demonstrate the detail with which activity can be localized in a modern PET system.

DISTRIBUTION OF FDG IN MAN

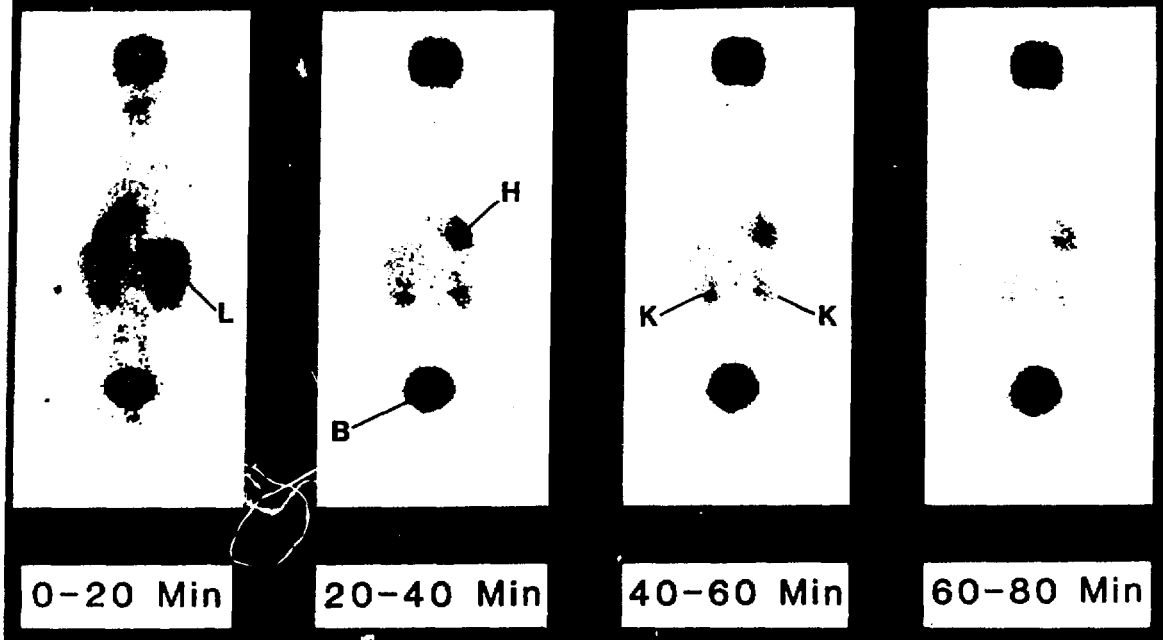


Figure 4. Distribution of FDG in man in measurement similar to that performed in Figure 1. Times of scans after injection indicated below each image.

For a number of isotopes in use in PET, a short half-life and rapid redistribution in the body make it difficult to estimate dosimetry. For such cases, it is necessary to take rapid dynamic scans of the isotope distribution to follow its time course in the body. An example of the ability of PET to perform this function is shown in figure 6 in which N-13 labelled ammonia is injected in a dog and we see the activity enter the right ventricle in a tomographic image and we can follow its course in 2 sec frames into the lung field, back into the left ventricle and to eventually be extracted in the myocardium.

DISCUSSION

The unique ability of PET to extract quantitative isotope distributions from its images allows a potential increase in the accuracy of dosimetry for positron emitting radiopharmaceuticals. The ability to noninvasively measure the isotope distribution in non-human primates allows accurate and cost effective initial evaluation of dosimetry. The ability to do the same measurement in man allows the dosimetry to be done with the correct subject. Rectilinear scans can be used for the general distribution and areas of high concentration can be concentrated on for detailed measurements. The dynamic capability of PET allows accurate dosimetry for shortlived isotopes that rapidly redistribute in the body. In general the proper use of PET in dosimetry studies can provide accurate and rapid dose estimations and reduce the possibility of excess exposure to radiation due to the approximations required in estimating dosimetry from organ counting from laboratory animals or approximations from scintillation cameras studies of man.

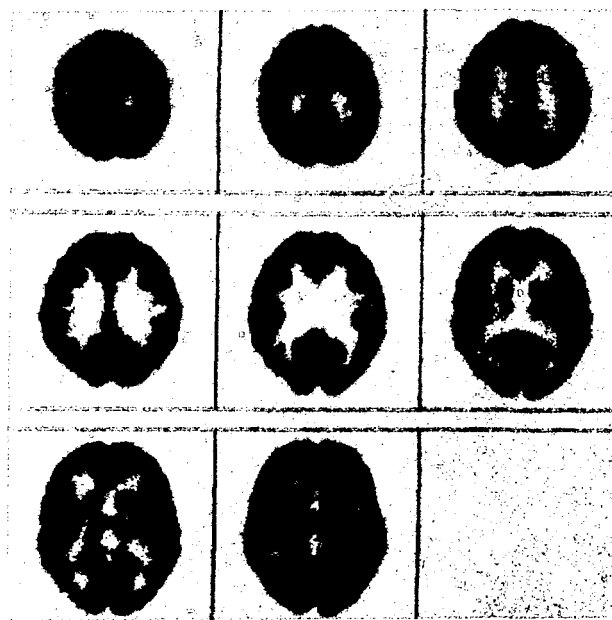


Figure 5. High resolution FDG brain scan obtained with the ECAT III PET system. Note the detailed structure seen in the convolutions of the cortex, and the clear resolution of the central nuclei such as the caudate, putamen and thalamus.

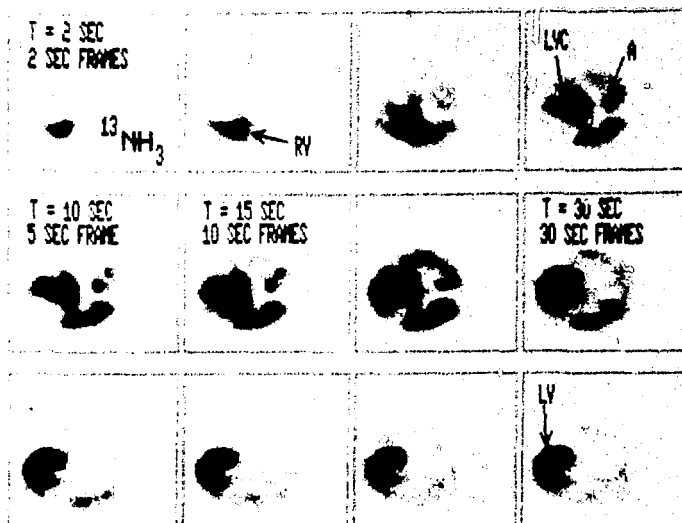


Figure 6. Dynamic tomographic heart scan of a dog following a bolus injection of ^{13}N -ammonia taken by the ECAT III. The initial time frames are 2 seconds and the progress of the activity can be followed as it enters the right ventricle (RV), moves to the lung field and then into the left ventricle (LV) followed by the extraction of the activity into the myocardium.

ACKNOWLEDGEMENTS

I would like to thank R Sumida, C Selin, H Hansen, F Aguilar, L Pang, and C Whitt for technical assistance, R Keen, J Cook, L McConnel, R Birdsall and N MacDonald for radiopharmaceutical preparation, and M Griswold and M Dahlbom for illustrations. This work was supported in part by Department of Energy Contract DE-AC03-76-SF00012 and National Institutes of Health Grants HL-29845-02, P01-NS15654-06 and R01-MH37916-03. PET data were collected in the Ahmanson Laboratory of Biochemical Imaging.

REFERENCES

1. Hoffman EJ, Phelps ME: Positron Emission Tomography: Principles and Quantitation. In "Tracer Kinetic Study of Cerebral and Myocardial Function: Positron Emission Tomography and Autoradiography". Phelps ME, Mazziotta JC and Schelbert H (Eds). Raven Press, New York, 1985.
2. Hoffman EJ, Huang SC, Plummer D and Phelps ME: Quantitation in Positron Emission Computed Tomography: 6. Effect of Nonuniform Resolution. *J Comput Assist Tomogr* 6:987-999, 1982.
3. Huang SC, Hoffman EJ, Phelps ME, Kuhl DE: Quantitation in Positron Emission Computed Tomography. 2. Effects of Inaccurate Attenuation Correction. *J Comput Assist Tomogr* 3:804-814, 1979.
4. Hoffman EJ, Huang SC, Phelps ME and Kuhl DE: Quantitation in Positron Emission Computed Tomography: 4. Effect of Accidental Coincidences. *J Comput Assist Tomogr* 5:391-400, 1981.
5. Hoffman EJ, Phelps ME and Huang SC: Performance Evaluation of a Positron Tomograph Designed for Brain Imaging. *J Nucl Med* 24:245-257, 1983.
6. Bergstrom M, Eriksson L, Bohm C, Blomquist G, Litton J: Correction for Scattered Radiation in a Ring Detector Positron Camera by Integral Transformation of the Projections. *J Comput Assist Tomogr* 7:42-50, 1983.
7. Hoffman EJ, Huang SC, Phelps ME: Quantitation in Positron Emission Computed Tomography: 1. Effect of Object Size. *J Comput Assist Tomogr* 3:299-308, 1979.
8. Phelps ME, Huang SC, Hoffman EJ, Plummer D, Carson RE: An Analysis of Signal Amplification Using Small Detectors in PET. *J Comput Assist Tomogr* 6:551-565, 1982.
9. Phelps ME, Hoffman EJ, Huang SC, Kuhl DE: ECAT: A new Computerized Tomographic Imaging System for Positron-Emitting Radiopharmaceuticals. *J Nucl Med* 19:635-647, 1978.
10. Hoffman EJ, Ricci AR, Van der Stee LMAM, Phelps ME: ECAT III: Basic Design Considerations. *IEEE Trans Nucl NS-30:729-733*, 1983.
11. Hoffman EJ, Phelps ME, Huang SC, Collard PE, Bidaut LM, Schwab RL, Ricci AR: Dynamic, Gated and High Resolution Imaging with the ECAT III. *IEEE Trans Nucl Sci NS-33*, February 1986.

DISCUSSION

BIGLER: Do you have any experience and/or opinions about time-of-flight in PET?

HOFFMAN: PET using time-of-flight is an attractive concept which allows one to obtain an effective increase in sensitivity. However, the practical application to this point in time has been disappointing. The detectors that one uses in time-of-flight are intrinsically less sensitive than the BGO detectors used in most PET systems. The gain in sensitivity from the time-of-flight technique does not overcome the loss of sensitivity due to the detector material.

JASZCZAK: Dr. Hoffman, could you please comment on the usefulness (if any) of having a spatial resolution that is the same axially as it is within (i.e., across the axis-of-rotation) the reconstructed plane?

HOFFMAN: The concept of equal resolution in all dimensions is desirable but difficult to achieve in PET. The image slice thickness in PET is usually fixed. However, the image resolution for an acceptable signal-to-noise ratio will vary by the choice of reconstruction filter because the total number of events per image will vary greatly from patient to patient and isotope to isotope. In SPECT, with continuous two-dimensional detectors, the axial resolution can be chosen to match the image resolution after the study.

MAXIMIZING PRECISION AND ACCURACY IN QUANTITATIVE AUTORADIOGRAPHIC DETERMINATION OF RADIOPHARMACEUTICAL DISTRIBUTION FOR DOSIMETRY CALCULATION

James L. Lear, M.D.,^{1,2} Kenneth Mido, M.D.,² Jeffrey Plotnick,³ and Russell Muth³
¹Nuclear Medicine Service, VA Medical Center, 3801 Miranda Ave., Palo Alto, CA 94304,
²Department of Radiology, Stanford University Medical Center, Stanford, CA 94305,
and ³Imagtronics, Ltd., 2 Morro Vista, Menlo Park, CA 94025

ABSTRACT

EXPOSURE OPTIMIZATION: We developed operational equations which relate ranges of film darkening or optical density produced by exposures from autoradiograms to the ranges of radiopharmaceutical concentration contained in the autoradiograms. The equations were solved and used to define ranges of optical density which were optimal for precise determination of radiopharmaceutical concentration. The solutions indicated that in order to maximize precision in determination of tracer concentration, autoradiograms should be produced with images that are less dark than are typically considered pleasing to the eye.

DIGITAL IMAGE ANALYSIS: Based upon these observations, a solid state image analyser was designed and developed for high spatial resolution, quantitative analysis of autoradiograms. The analyser uses a linear array of charge-coupled devices (CCD's) which mechanically scans the autoradiograms. The images are digitized into 512 X 512 or 1024 X 1024 pixels with 256 gray levels and directly mapped into memory. The system is therefore called a memory mapped, charge-coupled device scanner (MM-CCD). The images can be directly converted to represent tracer concentration or functional parameters and rapid region of interest analysis can be performed in single or multiple tracer studies. The performance of the system was compared to that of other commercially available image analysers, rotating drum densitometers and video camera digitizers. Values of tracer concentration using the MM-CCD scanner were generally greater than twice as precise and accurate as from the other systems.

BACKGROUND - EXPOSURE OPTIMIZATION

Quantitative autoradiography is a powerful tool for high spatial resolution determination of tissue concentrations of radiopharmaceuticals. In the technique, thin tissue sections containing radiolabeled compounds are placed in contact with photographic film. The emissions from the radionuclides produce exposures on the film, the magnitude of which are a direct function of the activity of the radionuclides and the length of time of the exposure. These exposures in turn cause the film to darken during development producing a visible image. The final images can be visually inspected for qualitative determination of regional concentration of radionuclides or analysed to determine tracer concentrations quantitatively. In quantitative analysis, standards with known radionuclide concentrations are usually used to determine the relationship between tracer concentration and film darkening, and this relationship is then applied to the images of interest.

Because autoradiography evolved with visual inspection being an important method of image analysis, autoradiographic images are traditionally produced with film darkesses designed to be pleasing to the eye. Despite the increasing use of quantitative analysis, little study has been done on how best to produce images optimized for quantitative analysis. The purpose of this investigation, therefore, was to explore the relationships of tracer concentration and film darkening, and to devise methods to produce images optimized for quantitative determination of tracer concentration.

In order to understand the details of this study, it is important to be fully aware of the terminology of exposure and film darkening. Exposure is defined as the amount of energy deposited per area of film emulsion. In tissue autoradiography therefore, it is the product of the effective local concentration of radionuclide and the length of time of contact with the film. If the radionuclide half-life is very long, effective concentration is simply the concentration at any time, while if the half-life of the radionuclide is short relative to the length of time of exposure, decay correction must be applied. Film darkening is a function of exposure and conditions of development. It is usually referred to in units of transmittance (T) or optical density (OD). T is defined as the intensity of light which passes through the film divided by the intensity of light incident on the film.

$$(1) \quad T = I_t / I_i$$

OD is defined as the negative logarithm of the transmittance and T is thus 10 to the negative OD power.

$$(2) \quad OD = -\log(T)$$

$$(3) \quad T = 10^{-OD}$$

OD is the most widely used parameter to describe film darkening and this is probaly because the human eye responds in a manner which is practically linear with OD . If a section of film has twice the OD of another section, it will appear twice as dark as another. Most instruments for measuring film darkening, however, have detectors which respond linearly to input light intensity which is equal to the light which passes through the film. They therefore respond directly to T rather than OD , although some have logarithmic circuits which convert their outputs to reflect OD .

METHODS - EXPOSURE OPTIMIZATION

The general relationship between film darkening and exposure was explored by placing standards with known tracer (^{14}C) concentrations, C , on two types of film frequently used in autoradiography, Kodak SB-54 and NMB for lengths of time ranging from 5 - 10 days. The products of ^{14}C concentration times duration of exposure and corresponding OD of the resulting images were recorded, the OD values having been measured using a spot microdensitometer. Corresponding values of T were also calculated.

From the results of these measurements, the relationship between T and C concentration was described in a general fashion. Operational equations were developed which defined how incremental differences in C within a tissue section caused incremental differences in T . Using the general assumptions the transmitted light intensity, I_t , would be the measured parameter resulting from autoradiographic exposure and that it would be highest in regions of zero exposure where $T = 1$, the operational equations were optimized with respect to maximizing precision of C determination from T measurements.

Because the range of C values within the tissue sections was found to be an important parameter used in optimizing exposure, typical ranges of values of C were measured in the brains of normal awake rats for several tracers used for measuring cerebral blood flow and glucose metabolic rate. Based upon these ranges, optimum ranges of film darkening were determined for high precision autoradiographic measurement of radiotracer concentration.

RESULTS - EXPOSURE OPTIMIZATION

Both Kodak SB-54 and NMB films had similarly shaped responses at low exposures. OD vs C was linear for OD values up to approximately .4 for SB-54 and .8 for NMB film. Above these values, OD became approximately logarithmic with respect to C until saturation values were reached. (See Figure 1).

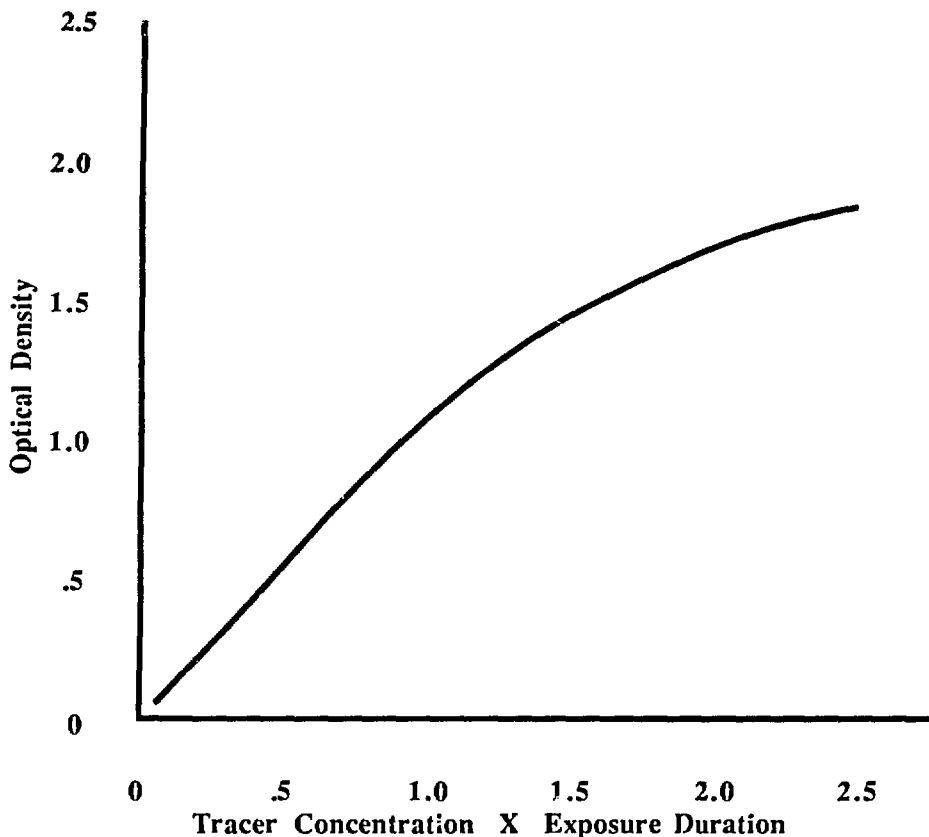


FIGURE 1 Optical density is plotted as a function of tracer concentration x length of time of contact with film (exposure duration) for a hypothetical film. The relationship is practically linear for light images but shows saturation for darker images. The optical density at which the linearity is lost, OD_m , varies with the film. Typical OD_m values run from .4 to .8.

- (4) $OD = k t C$ for $OD < OD_m$, where
 k = constant depending upon film and development conditions
 t = length of time of exposure
 OD_m = maximum value of linear film response range

The response of T with respect to C is therefore an inverse power relationship for exposures which produce OD values which are less than OD_m :

(5) $T = 10^{-k t C}$

An autoradiograph is produced by exposure from a tissue section containing a range of values of C, and will produce an image containing a range of values of T or OD. A parameter describing the range of interest must therefore be defined, and this derivation will use that range of values of C which includes the mean ± 2 standard deviations. C_h represents the highest value in the range, C_l

the lowest, and R the ratio, C_h / C_l .

When an autoradiograph is analyzed quantitatively, the gray scale contained in the image is digitized into discrete steps or gray scale levels. The total number of gray scales available to digitize the image is defined as D. In order to maximize the accuracy of determination of tracer concentration, the relationship between gray scale levels within D and values of C must be defined and optimized. Because of the inverse power relationship of detector response with C, accuracy will be a function of C, and some decision as to how precision should be maximized must be made.

One possibility, which will be referred to as Condition 1, is to maximize the average precision of C measurement over the range of C values in the tissue section. To maximize the average precision of C measurement over this range, the range should be spread over as many levels within D as possible. This is accomplished by maximizing the difference between the T values associated with C_l and C_h , or T_l and T_h respectively. This difference is referred to as T_d .

$$(6) \quad T_d = T_l - T_h$$

Figure 2 shows that for a given value of R, T_d is a function of where the image lies on the T curve.

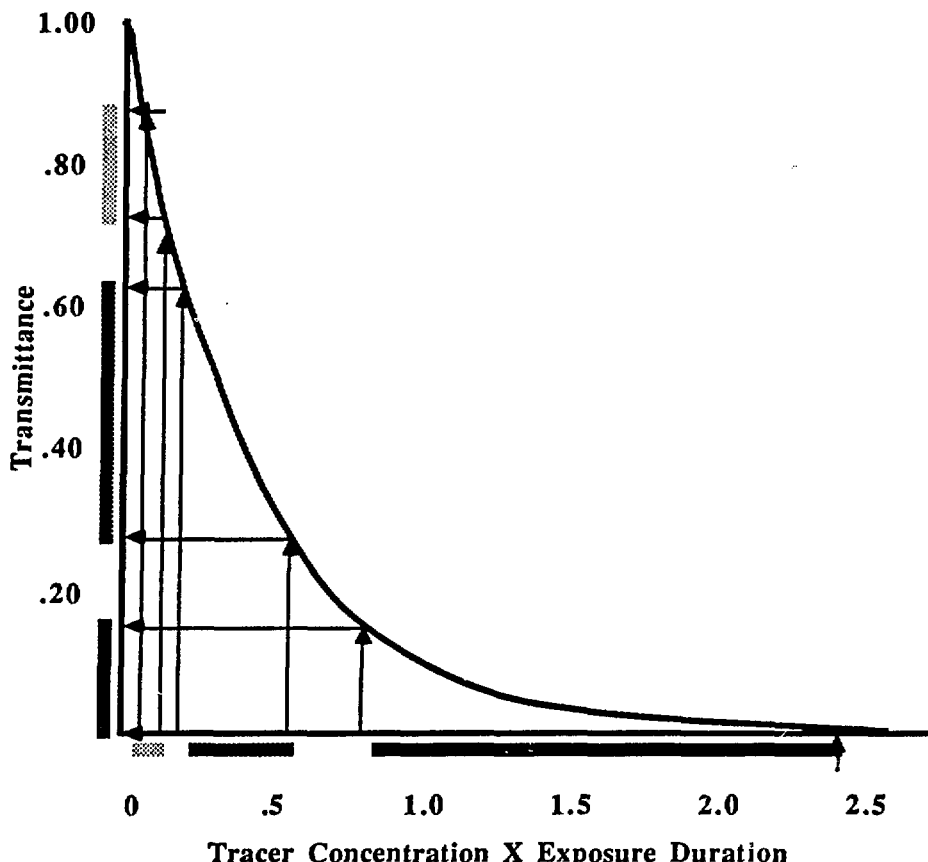


FIGURE 2 Illustration of effect of image darkness on T_d . The segments along the X axis represent tracer concentration x exposure duration with R values equal to 3. They differ only in their lengths of time of exposure and thus image darkness. The very short (lightest segment) and very long (darkest segment) exposures produce T_d values which are less than the intermediate length exposure as indicated by the corresponding segments along the Y axis.

For very light or dark images, T_d becomes small, indicating that a maximum can be found. This is done as follows. For OD values less than OD_l:

$$(7) \quad T_d = 10^{-(k_t C_l)} - 10^{-(k_t C_h)} \text{ or}$$

$$(8) \quad T_d = 10^{-(k_t C_l)} - 10^{-(R k_t C_l)}$$

Equation 8 can be maximized by finding the solution for the zero value of the first derivative.

$$(9) \quad 0 = k_t R C_l 10^{-(R k_t C_l)} - k_t C_l 10^{-(k_t C_l)}$$

$$(10) \quad k_t C_l = \log(R) / (1-R) \text{ or,}$$

$$(11) \quad OD_l = \log(R) / (R-1)$$

Equation 11 shows that for Condition 1, the optimum value of optical density of the image is a function of the range of tracer concentrations contained within the tissue section which was used to produce the image.

The sizes of the smallest resolvable steps in T (ΔT) are all equal to 1/D. The sizes of the corresponding steps in C, ΔC , are not uniform however, but rather are a function of C. ΔC is the product of the size of the incremental step in T (ΔT) and the first derivative of C with respect to T.

$$(12) \quad \Delta C = \Delta T \times (dC / dT) = (1/D) \times (dC/dT)$$

$$(13) \quad dC/dT = -\log(e) / T$$

For a given increment in D, the incremental steps in C will be larger in dark regions than in light regions of the image, making C measurements less precise in dark regions. (See Figure 3). Therefore, other optimization criteria which would improve the precision of measurement for C_h might be desirable at times. One such condition (Condition 2) for optimization might be to maximize *fractional* precision of C measurements in dark regions, i.e. minimize $\Delta C_l / (C_h - C_l)$. Substituting from equations 4, 9 and 10, we should maximize $10^{-(OD_h)} \times (C_h - C_l)$. By setting the first derivative equal to zero:

$$(14) \quad OD_l = 1 / (R \times \ln(10))$$

Another optimization strategy, Condition 3, might be to maximize the absolute precision of measurement of C_h. This condition is important because many detectors which can be used to analyse images have signal/noise characteristics inversely related to T. Condition 3 is met by minimizing ΔS , the size of the incremental step in C (ΔC) as a fraction of the image transmittance width, T_h - T_l.

$$(15) \quad \Delta S = \Delta C / (T_h - T_l)$$

$$(16) \quad \Delta S = \log(e) / D \times 1 / ((T_h - T_l) \times T)$$

Thus we should minimize $1 / ((T_h - T_l) \times T_h)$ or maximize $(T_h - T_l) \times T_h$. By substituting for T as in equation 6, and solving for the zero value of the derivative, the optimal condition can be determined.

$$(17) \quad K C_l = \log((R+1)/2R) / (1-R) \text{ or,}$$

$$(18) \quad OD_l = \log((2R)/R+1) / (R-1)$$

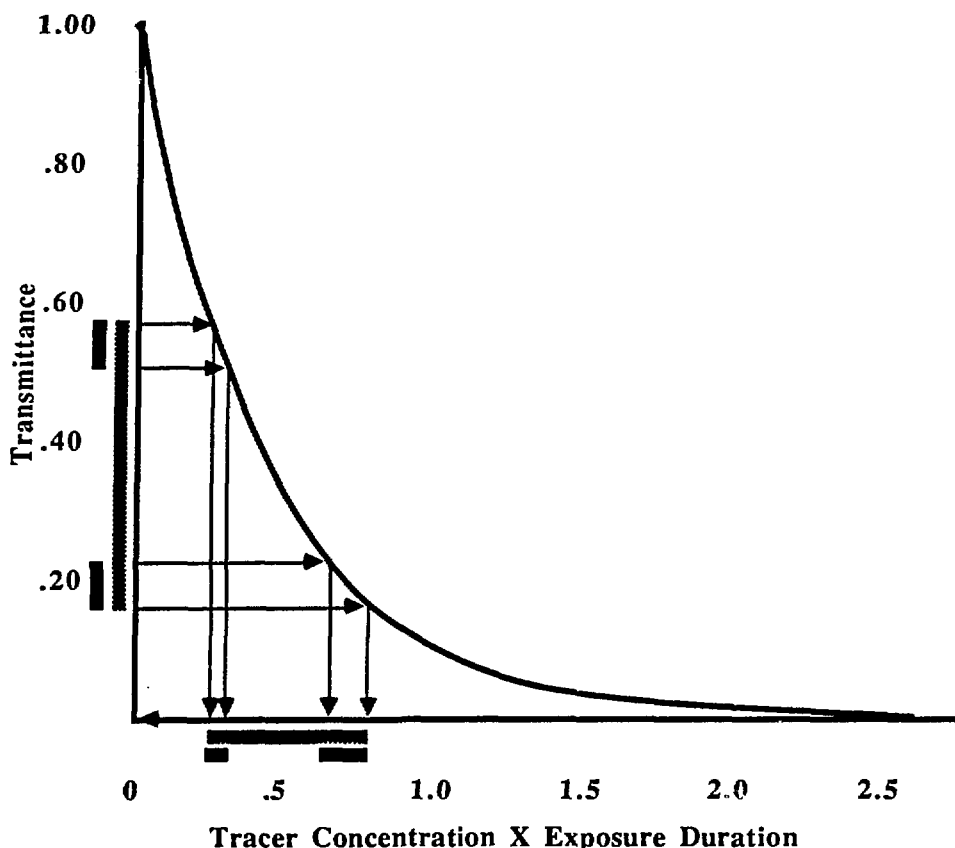


FIGURE 3 The hatched line along the X axis represents the S width of an image and has a corresponding T_d represented by the hatched line along the Y axis. ΔT , which is fixed in size, has corresponding ΔC values which differ in size depending on where it located within T_d as indicated by the pairs of solid lines.

Because Conditions 1, 2, and 3 show that optimal image darknesses are functions of R, it is useful to determine R for common experimental conditions. Table 1 contains the results of the studies to determine R values for several tracers used in cerebral blood flow and metabolism research. As can be seen, these values generally range from approximately 3 - 4.

TABLE 1

	<u>R</u>
^{14}C -iodoantipyrine	2.9
^{201}Tl -diethyldithiocarbamate	3.6
^{123}I -isopropylidoamphetamine	3.7
^{18}F -fluorodeoxyglucose	3.9
^{14}C -glucose	3.9

Table 2 contains values of OD, T, and ΔC for an R value of 3.9.

TABLE 2

	OD_h	OD_l	T_h	T_l	$T_f T_h$	$\Delta C_h/S$	$\Delta C_l/S$
Condition 1	.78	.20	.17	.63	.46	1.0	.27
Condition 2	.44	.11	.36	.78	.42	.84	.38
Condition 3	.27	.07	.53	.85	.32	.94	.59

Condition 1 causes the transmittance width of the image, $T_l - T_h$, to be .46. An image would thus occupy .46 of the total number of D values that a detector could provide. The precision of C measurement as indicated by $\Delta C/S$, is almost 4 times less in the dark regions as light regions for Condition 1. Condition 2 which yeilds an overall lighter image, has a transmittance width and therefore average precision, which is approximately 10% lower than Condition 1. The ratio of precisions for C_h and C_l improves to slightly greater than 2, precision for C_h improves by approximately 20% and precision for C_l worsens by 35%. Condition 3, which yields an even lighter image, has a transmittance width which is further reduced by approximately 30% to .34. The ratio of precision for C measurements between light and dark regions is reduced to less than 2. This is accomplished by a large, greater than 50%, reduction in precision in C_l measurement and a slight improvement in precision in dark regions as compared to Condition 1. Compared to Condition 2, precision of measurement for both C_h and C_l are lower for Condition 3, but transmittance in dark regions increases. If there is a fixed noise component (dark current noise) in the detector to be used for image analysis or if the noise in detector output is quantum limited by light input, a gain in signal/noise may be accomplished by going from Conditions 1 or 2 to Condition 3 which offsets the overall precision loss.

Although Conditions 1, 2, and 3 are appropriate for many experimental situations, other optimization schemes may be appropriate at times. For example, if the desired final parameter of measurement has a non-linear relationship with tracer concentration as with most local cerebral blood flow studies, the nonlinearity must be incorporated into the optimization equations and solution. Thus, the autoradiographer should carefully define the parameters of interest and their expected range in the tissue sections in order to create images optimized for quantitative analysis.

BACKGROUND - DIGITAL IMAGE ANALYSIS

In order to best utilize the information that autoradiograms contain, one must have a method of obtaining measurements of film density with high precision, accuracy, and spatial resolution. In early studies, quantitative analysis was performed by manually measuring density using a photomultiplier-based densitometer with a small, 100μ to 1000μ , aperture. Although this method was accurate, it was tedious, and tracer concentration maps of entire sections could not be obtained.

More recently, systems have been developed which can create digitized maps of density of entire sections. These systems generally use either scanning densitometers (1) or video cameras (2) as input devices. In order to understand the potentials and limitations of such systems, and to provide a basis for the development of an improved imaging system, it is important to be familiar with several important parameters describing performance. These include parameters related to spatial resolution, geometric accuracy, response uniformity and linearity, stability, and noise characteristics:

1) Spatial resolution (SR) describes the size of the matrix into which the image is digitized. The autoradiographs have inherent resolutions of 10μ to 20μ with ^3H and 50μ or higher with ^{14}C or other radionuclides. Video camera based systems generally have 256×256 to 512×512 image matrices, and therefore resolution is related to the size of the image being scanned. Scanning densitometers have apertures from 25μ to 100μ and can digitize entire autoradiographs.

2) Modulation transfer function (MTF) describes the response of the imaging system at a light-dark interface. If the value is less than 100%, artificial graying will occur at such boundaries. At resolution of 512×512 , most video camera systems have low MTF values. Scanning densitometers have complicated MTF values which are functions of scanning speed, scanning direction, and operating temperature.

3) Geometric linearity (GL) described how well the shape of scanned objects is preserved. Video cameras tend to have distortions which alter the image shape and density measurements. Scanning densitometers generally have excellent linearity.

4) Photometric uniformity (PU) describes how well the system preserves response across the image. Video camera systems generally have uniformity variations or "shading" of approximately 10%. Because the shading changes with light intensity, it is difficult to develop correction factors. Because scanning densitometers use a single small aperture, their uniformity is high when films are mounted properly.

5) Photometric linearity (PL) describes how well the response of the system linearly reflects light input. Video cameras have different degrees of photometric linearity depending on their design. Unfortunately, better photometric linearity is usually accompanied by lower dynamic range. Densitometers have very high photometric linearity.

6) Stability (PS) describes how response is preserved over time. It is usually temperature dependent and therefore varies with manufacturers for both video camera systems and scanning densitometers.

7) Dynamic range (DR) describes the range of response a system can generate. It is usually defined as the maximum output of the system divided by the smallest resolvable increment in response. Video camera systems generally have dynamic ranges of from 50 to 100 while scanning densitometers have values over 100.

8) Signal / noise ratio (SN) describes the fraction of the system's output which represents true data. It can be defined referenced to the peak or average noise in the signal. Video cameras usually have poor signal / noise characteristics, with values referenced to peak noise of $20/1$ - $30/1$. Data from such systems has to be improved by multiple averaging to be at all useful in quantitative autoradiography. Scanning densitometers are usually better, having values of approximately $100/1$.

9) Head room (HR) describes the difference between the amount of light which yields maximum system output and that which saturates the detector. It is limited by the dynamic range divided by the number of gray levels of the system. Video camera systems often have analog to digital conversion circuits with a greater number of gray levels than their dynamic range. Thus they have false gray levels and no head room. Although the photomultiplier detectors in some scanning densitometers have dynamic ranges which would permit headroom with typically used gray scale numbers, most devices have fixed outputs and thus have no usable headroom.

10) Gray scale resolution describes the number of digital steps into which the darkness of an image is divided. Almost all video camera and densitometer systems have 8 bit outputs, or 256 gray levels.

11) Scanning time (ST) describes the time necessary to digitize an image. Recent advances allow video images to be captured and digitized in less than 1 second, and some systems can

perform the necessary multiple frame averaging very quickly. Scanning densitometers generally have scan times on the order of several minutes because of the complicated image movement necessary to digitize the image.

METHODS - DIGITAL IMAGE ANALYSIS

Both video camera and scanning densitometer systems have been used in quantitative autoradiography. Reports have indicated that while either type of system can be used to digitize autoradiograms, problems with precision, accuracy, or speed exist (1,2). Video camera systems have precisions which limit the detection of differences in tracer concentration to approximately 3-4%, and scanning densitometers have coefficients of variation in tracer concentration measurement of 6-12%. Because inherent film response uniformity in autoradiography is greater than 99%, a more precise and accurate image analysis system could yield more precise and accurate tracer concentration maps.

We therefore undertook to develop an image analysis system using a new type of solid state detector, the charge-coupled device or CCD. CCDs are available in linear or matrix arrays of small detector elements. The upper limit of the number of elements available in matrix arrays with acceptable response characteristics was approximately 250 x 250 one year ago when this project was begun, although present technology has pushed this limit to approximately 400 x 400. Linear arrays were available with much greater numbers of usable elements along a given direction, up to approximately 1000 x 1000. Because ^{14}C autoradiographs have inherent resolution greater than 512 x 512 per in² and ^3H autoradiographs have greater than double the linear resolution, we chose to use a linear CCD array system.

In order to digitize an image, the linear array is moved beneath a lens to scan the image into a 512 x 512 matrix. A Digital Equipment Corporation PDP 11/23+ CPU is used to control the array movement. Data from the array is digitized into 8 bits and mapped directly into memory through direct memory access; the system is thus referred to as a memory-mapped charge coupled device (MM-CCD) scanner. Images are viewed in gray scale with user controlled contrast enhancement on a 512 x 512 high resolution monochrome monitor. Programs were written in Forth for typical image processing requirements of single and multiple tracer quantitative autoradiography. Transformation of density images into tracer concentration, blood flow, or glucose metabolism images is done by inputting arterial curve data and data from C-14 standards. Up to 4 images can be stored in random access memory and rapid fractional image subtraction can be performed to yield pure tracer concentration in multiple tracer studies.

RESULTS - DIGITAL IMAGE ANALYSIS

Performance of the system for tracer concentration measurement was evaluated by scanning an image repeatedly over 2 hours and comparing each scan with the first on a pixel to pixel basis. With gain set to allow precision of tracer concentration measurement to within 1%, coefficients of variation between pixels in different images were measured by subtracting the subsequent images from the first image and displaying the absolute value of the difference. Differences averaged less than 1 part in 256 for the early scans and increased to less than 3 parts in 256 over the two hours. Table 3 compares the characteristics of the MM-CCD scanner with the other types of systems. These data suggest that total accuracy and precision of tracer concentration measurements using the MM-CCD scanner are greater than twice those of the other systems.

The system was used to scan and digitize autoradiographs from a triple label study comparing the distributions of ^{14}C -iodoantipyrine (IAP), ^{123}I -isopropylidoamphetamine (IMP), and ^{201}Tl -diethyldithiocarbamate (DDC). The study was performed using simultaneous multiple radionuclide autoradiographic techniques (3). Images were converted from film density to radiopharmaceutical concentration, and concentration ratio images were then created. (See Figure 4).

TABLE 3

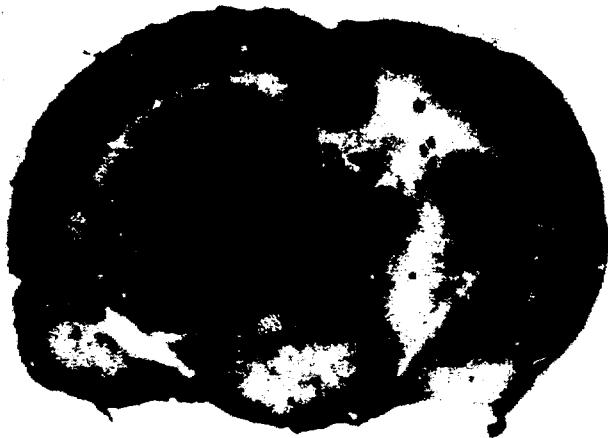
	SR	MTF	GL	PU	PL	PS	DR	SN	HR	ST
VC	50μ	30%	poor	10%	poor	good	100	30	none	fast
SD	25μ	>50%	good	1%	good	?	200	100	none	slow
MM-CCD	50μ	70%	good	1%	good	good	500	200	1.5	fast

DISCUSSION

This study has shown that dark images which are frequently produced in autoradiography to be pleasing to the eye or easy to photograph, are not optimal for precise quantitative determination of radiopharmaceutical concentration. Rather, the darkness of the image should be controlled and should be a function of expected ranges of tracer concentration within the tissue. A CCD based image analyser was designed and constructed specifically for quantitative autoradiographic determination of tracer concentration. Its performance was compared to existing image analysers and significant superiority with respect to accuracy and precision were found.

A**B**

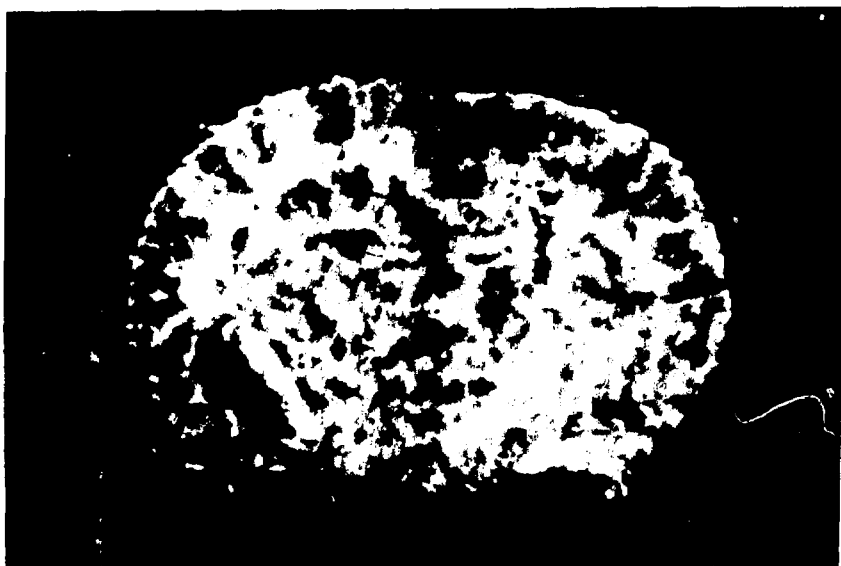
C



D



E



F



FIGURE 4 Images obtained from MM-CCD scanner using triple label quantitative autoradiography and exposure optimization. The images are from a coronal brain section from a normal rat which was awake during the tracer administration A) Local cerebral blood flow (LCBF) measured with IAP. B) LCBF measured with IMP. C) LCBF measured with DDC. D) A/C E) C/B F) A/B

ACKNOWLEDGEMENTS

Funding for these investigations was provided by the VA Research Administration Merit Review Program, the Stanford University Nuclear Medicine Special LATS fund, a Stanford University Biomedical Research Grant, and a grant from Imagitronics, Ltd.

REFERENCES

- 1 Gooch, C., Rasband, W., and Sokoloff, L. Computerized densitometry and color coding of ^{14}C deoxyglucose autoradiographs. *Ann Neurol* 7: 359-370, 1980.
- 2 Yonekara, Y., Brill, A., Som, P., Bennett, G., and Fand, I. Quantitative autoradiography with radiopharmaceuticals: Digital film analysis system by video densitometry. *J Nucl Med* 24: 231-237, 1983.
- 3 Lear, J., Ackermann, R., Kameyama, M., Carson, R., and Phelps, M. Multiple radionuclide autoradiography in evaluation of cerebral function. *J Cerebral Blood Flow Metabol* 4: 264-269, 1984.

DISCUSSION

BRILL: Jim, when one is doing autoradiographic film analysis, sometimes you are interested in the low contrast region and sometimes you are interested in the high contrast region. Of course, when you are doing a large number of the same types of studies, you optimize the procedure. However, often one studies

tissues in which wide ranges of contrast are encountered, all of which are of interest. In that circumstance, we use the same approach as that used in photography; that is, we adjust the f-stop of the densitometer lens for the different intensities and digitize several times to cover the wide latitude required. Can you comment on the efficacy of this method?

LEAR: If you are willing to forego the ability to scan the whole image and have the whole range there, you can do that.

ACQUISITION OF BIOKINETIC DATA FOR INTERNAL DOSE CALCULATIONS FOR SOME NOVEL RADIOPHARMACEUTICALS

Terry Smith, Giuseppe D. Zanelli and John C. W. Crawley

Radioisotopes Division
MRC Clinical Research Centre
Watford Rd, Harrow, Middlesex
HA1 3UJ, U.K.

ABSTRACT

In the U.K., the administration of radiopharmaceuticals to human patients and volunteers is controlled by The Medicines (Administration of Radioactive Substances) Regulations 1978 introduced to comply with the requirements of the European Communities Directive, and this control is implemented by the ARSAC (Administration of Radioactive Substances Advisory Committee). Estimation of radiation dose commitment, expressed as an effective dose equivalent, is a prior requisite to the application for a licence to administer radiopharmaceuticals and, therefore, in the case of novel radiopharmaceuticals is leading to an increasing awareness of the need for dosimetry-orientated studies. In this laboratory potential new radiopharmaceuticals are investigated initially by animal studies to assess the possible distribution in man, and subsequently in controlled volunteer studies designed to obtain the maximum possible amount of biokinetic data to allow accurate estimation of radiation dose. A variety of techniques are used for this purpose, including profile counting, partial and whole-body scanning by LFOV gamma camera and whole-body counting, in addition to the analysis of radioactivity in blood and excreta. The use of these techniques is illustrated for the acquisition of biokinetic data and subsequent dosimetry of three novel radiopharmaceuticals: ⁷⁷Br-p-bromospiperone (quantification of dopamine receptors in the brain); ⁹⁹Tc^m-porphyrins (location of sites of occult infection/inflammation); and ⁹⁹Tc^m DEPE (a possible novel blood pool marker for MUGA studies).

INTRODUCTION

In the U.K., the Medicines Regulations of 1978, which are concerned with the protection of the patient or volunteer in the administration of radioactive substances for clinical or research purposes, were introduced to comply with the requirements of Article 5(a) of the European Communities Directive. They require that any doctor or dentist wishing to administer a radioactive medicinal product to a human being must hold a certificate of authorization issued by the Health Ministers, who are advised by the Administration of Radioactive Substances Advisory Committee (ARSAC). Application for such a certificate should include an estimate of the radiation dose arising from a particular investigation and, for guidance, the ARSAC has listed doses, given as effective dose-equivalents, for a wide variety of commonly used radiopharmaceuticals. For newly developed radiopharmaceuticals, dose estimates must be determined. Since an important part of the work of our laboratory is concerned with development of

novel radiopharmaceuticals for clinical investigation, considerable emphasis is placed on accurate dosimetry, and studies designed to obtain as much dosimetry data as is reasonably practicable are performed for each substance. These normally involve initial investigations in animals to suggest possible distribution and retention patterns in man and to provide dose estimates for certification: subsequently, comprehensive studies on human volunteers are undertaken. This paper is confined to the latter studies and describes, with examples, our methods of internal dosimetry for intravenously administered radiopharmaceuticals in man.

METHODS

INSTRUMENTATION

A variety of techniques is available for investigating the distribution, long-term whole-body retention and excretion of radionuclides in human subjects.

Gamma Camera

Radioactivity distribution in different organs is examined using an IGE 400 AT gamma camera in the whole-body scanning mode or in the static mode for local uptake measurements. Anterior, posterior and left and right lateral whole-body scans are performed at appropriate times following administration of radioactivity and scan speeds are varied according to the activity present, scans generally taking between 7 and 15 min. Scan data are stored and subsequently processed using a Star computer in conjunction with the gamma camera, and hard copy on X-ray film is also available. For all organs with clearly defined uptake, a region-of-interest (ROI) facility is used to estimate the counts in both the anterior and posterior views and these are corrected for body background using a ROI positioned over the thigh. The geometric mean of corrected counts for the two views is then used to estimate the activity in a given organ as a proportion of the total-body content estimated in a similar manner. Where necessary, the radioactivity in the bladder and GI tract is also estimated in this way.

Profile Scanner

The distribution of radioactivity is also monitored using a Hybrid Scanner (1). In view of the combined use of the gamma camera, this scanner is used only to plot the profile of distribution in the longitudinal body axis. It consists of two cylindrical NaI crystal arrays, each 38 cm long and 5 cm in diameter, placed one above and one below the patient and perpendicular to the axis of motion. Each detector is fitted with a rectangular slit collimator giving a spatial resolution of about 2 cm in the scanning axis. The patient is scanned between the fixed detector assembly, each scan taking 15 min, and the combined response from the two detectors is used to produce the profile. Although the profile contains less information than gamma camera scans, it plays a useful role, for relatively simple distributions, in providing confirmation of the estimates of uptake by the gamma camera using relative peak areas.

The other main value of this instrument is as a high level whole-body counter for the early investigation periods when body activity content is high. It is employed for this purpose until the body activity has fallen to about 740 kBq (20 μ Ci), when retention measurements on both this scanner and a whole-body counter (see below) are normalized.

Whole-body Counter

Subsequent whole-body counting is performed with a multi-detector array consisting of 8 NaI detectors (10.2 cm dia x 7.6 cm) placed 4 above and 4 below a stationary couch within a cubicle made from 15 cm thick steel. This counter is routinely used for total-body potassium measurements (2) and therefore capable of measuring accurately a few nCi of activity. Its main contribution in our dosimetry studies is in examining long-term retention tails of long-lived radionuclides. A high sensitivity liquid scintillator whole-body counter (3) is also available if required.

Blood and Excreta Counters

Serial venous blood samples are withdrawn from the subject at appropriate times after administration of a radiopharmaceutical and whole-blood and plasma aliquots are counted against standards in an automatic gamma counter (LKB-Wallac 1280): their activities are expressed in terms of the percentage of the administered activity per litre. Where possible, complete collections of urine and faeces are made at least until most of the excretion has occurred. These samples are counted in a bulk-sample counter (4) comprising two opposing NaI crystals (12.7 cm dia x 5.0 cm) whose separation can be adjusted to accommodate containers of various sizes. This instrument, which can measure activities of less than 370 Bq (10 nCi), is also used in dosimetry studies on small animals for counting the entire carcass as well as individual organs.

DOSIMETRY MODEL

The aim of internal dosimetry studies is to establish biokinetic models from which values of cumulated activity (\bar{A}) in total body and organs can be derived and hence radiation doses determined. The most convenient starting point is the total-body retention equation since organ cumulated activities can be stripped from that of the total body to leave an estimate of residual body cumulated activity. However, the total-body retention as measured may include activity in GI tract and bladder which can lead to inaccuracy since this activity might be included twice in the dose calculation. A rapidly excreted substance could result in some bladder activity being recorded (as shown later) even though it may be feasible to make measurements immediately after the bladder has been emptied, while no similar expedient is possible for radioactivity excreted by the faecal route. In our method we aim at deriving an equation for total-body retention less the contents of the GI tract and bladder, since this is the pool of activity which is supplying the excretion pathways and its equation is therefore the one required to be fed into the GI tract and kidney-bladder models (Fig. 1). From the cumulative faecal and urinary activities, the fractions f_F and f_U eliminated by each excretion route can be determined. The actual total activity which enters the GI tract is then readily calculated as shown and, for purposes of dosimetry, can be assumed to enter the small intestine (SI) as a single input. The ICRP GI-tract model (5), modified to account for input to the SI, is used to estimate cumulated activity (\bar{A}) values for the gut segments. The kidney-bladder model is always used to estimate the cumulated activity of bladder contents where there is significant urinary excretion. In general, we use a mean bladder voiding period (t_v) of 3.5 h for this calculation, but this value is modified if the clinical investigation requires earlier or more frequent voiding. Except when there is sufficient uptake in kidneys to allow measurement by the ROI technique, this model is also used to estimate the kidney cumulated activity due to transit of urine: for this a renal transit time (t) of 5 min is used in the normal case but may be varied in pathological cases. To this contribution to the kidney \bar{A} value is also added its share, by weight, of that due to residual body activity.

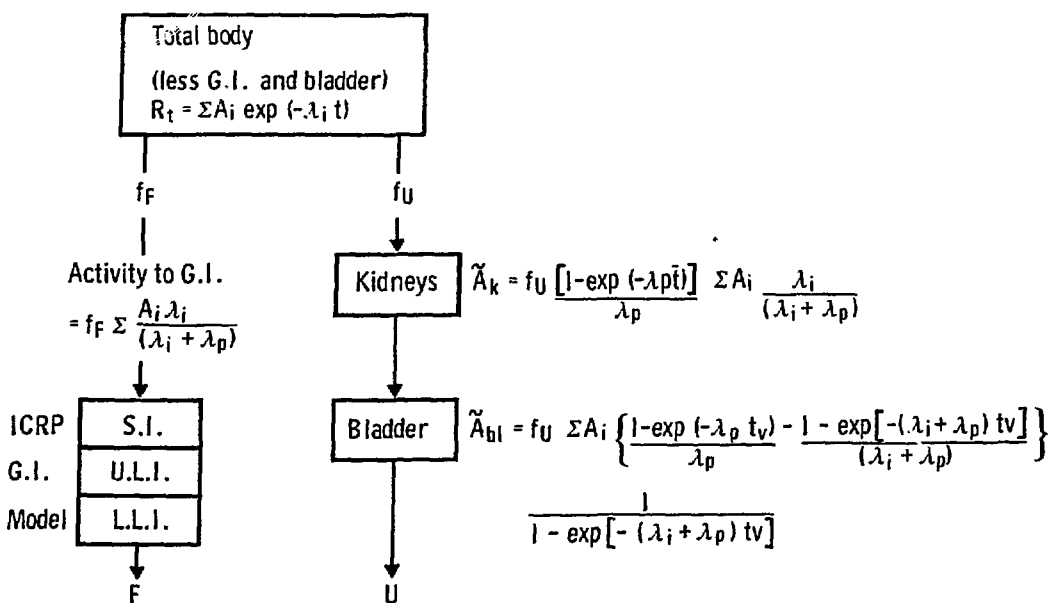


Figure 1. Dosimetry model for intravenously administered radiopharmaceuticals (λ_i and λ_p represent biological and physical decay constants respectively, t is the renal transit time and t_v the bladder voiding period.)

DOSE CALCULATION

Exponential equations are fitted to the biological retention data of selected measured source organs and the total body (less GI tract and bladder), from which cumulated activities are calculated. Values for GI tract, kidney and bladder are calculated from the models previously explained (Fig. 1) and the values of cumulated activity and mass of the residual body, which are unique for given radiopharmaceutical, are readily obtained by difference. A computer program uses these values in the standard dosimetry formula:-

$$\bar{D}_t = \sum \tilde{A}_s s_{t \leq s} + \tilde{A}_{RB} \left\{ \frac{m_{TB} s_{t \leq TB} - \sum m_s s_{t \leq s}}{m_{RB}} \right\}$$

where \bar{D} = dose
 \tilde{A} = cumulated activity
 S = dose per unit of cumulated activity
 m = mass
 t = target organ
 s = source organ
 TB = total body
 RB = remaining body

The expression in brackets in the above formula represents the estimated S value for the remaining body as source organ for the situation considered. Doses are calculated for all the listed ICRP target organs using a tape of S values obtained from the Oak Ridge National Laboratory, and for a number of additional

organs for which S values were specially calculated. S values for heart wall and heart contents were estimated from data in MIRD pamphlet 13 (6) and for breast as target organ from Cristy (7). The dose to gall-bladder wall was estimated using a model similar to that of MIRD dose estimate report No. 7 (8). From the list of organ doses an effective dose equivalent (EDE) is calculated using ICRP risk weighting factors (9). For this purpose no attempt is made to adjust the weighting factors to give a so-called somatic EDE. The EDE provide a single dose value which takes into account the non-uniform distribution and effects of a given radiopharmaceutical and is used here to allow comparison of doses from different radiopharmaceuticals; it is acknowledged, however, that this was not its intended use.

RESULTS

DOSE ESTIMATES FOR NOVEL RADIOPHARMACEUTICALS

^{77}Br -p-Spiperone

This neuroleptic agent has been labelled in our laboratory and used successfully to image dopamine receptors in the striatum of the brain by single photon emission computed tomography (SPECT) (10). The dosimetry of this substance, carried out on two male subjects given 18.5 MBq (500 μCi) i.v., has been reported elsewhere (11) and is therefore only briefly summarized here. It was rapidly taken up in liver and lungs (Fig. 2) where its retention was similar to

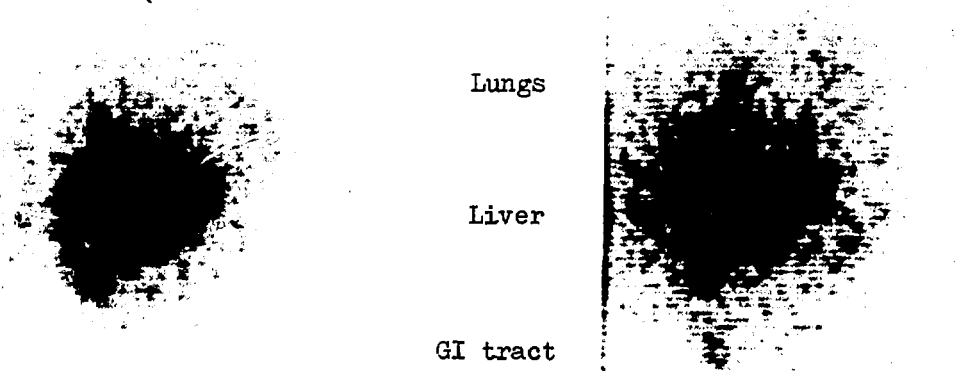


Figure 2. Distribution of ^{77}Br -p-bromospiperone in a normal male subject.
Left: anterior (2 h), right: anterior (68 h)

that of the total body (Fig. 3), at least over the first 3 days. These were the only readily identifiable organs with significant uptake for ROI measurements, other than GI tract and bladder, and the major excretory pathway was via urine. The dosimetry model is therefore relatively simple, as indicated in Fig. 4, in which solid boxes represent organs whose activity was measured and dashed boxes those whose activity was derived from models. The estimated EDE is $0.083 \text{ mSv} \cdot \text{MBq}^{-1}$ ($0.31 \text{ mrem} \cdot \mu\text{Ci}^{-1}$) with highest dose to liver ($0.25 \text{ mGy} \cdot \text{MBq}^{-1}$)

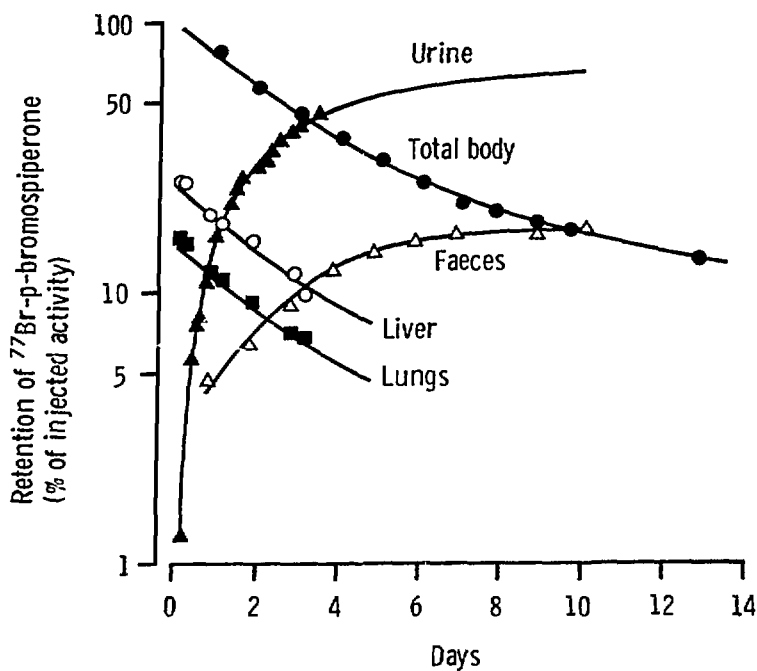


Figure 3. Biological retention of ^{77}Br -p-bromospiperone in a normal male subject.

(Reproduced from ref. 11 by kind permission of Nuclear Technology Publishing, U.K.)

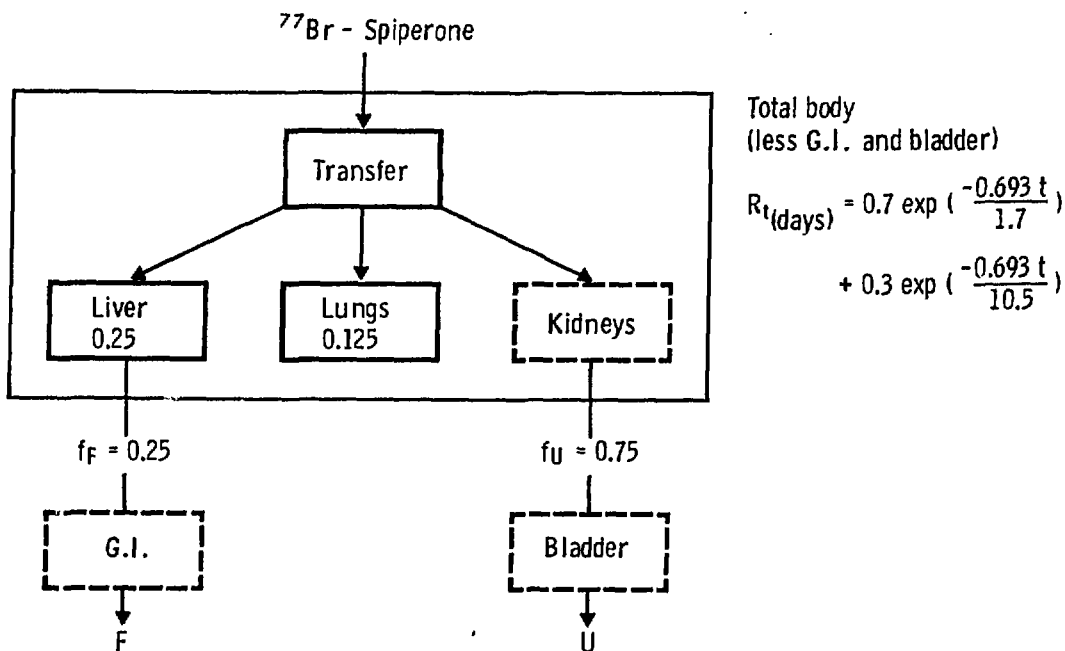


Figure 4. Dosimetry model for ^{77}Br -p-bromospiperone.



Lungs

Heart

Liver

Gallbladder

Kidneys



GI tract



Bladder



Heart

Liver

Gallbladder

Kidneys



GI tract



Bladder



Figure 5. Distribution of $^{99}\text{Tc}^{\text{m}}$ TPPS in a normal male subject.

Top left: anterior (15 min), Top right: posterior (30 min)
Bottom left: Rt. lateral (1.8 h), Bottom right: Lt. lateral (2h)

$0.94 \text{ mrad} \cdot \mu\text{Ci}^{-1}$). An administered activity of about 260 MBq (7 mCi) is required, giving an overall EDE of 22 mSv (2.2 rem). Despite the successful imaging of this radiopharmaceutical, the physical properties of ^{77}Br are not ideal for this application and more recently we have investigated the use of a ^{123}I -labelled pharmaceutical [(-)-N-(1-ethyl-2-pyrrolidinylmethyl)-2-hydroxy-6-methoxy benzamide hydrochloride: FLA 981, Astra Lakemedel AB, Sweden] which it is estimated will reduce the dose by a factor of 2.5 whilst giving higher counting efficiency.

$^{99}\text{Tc}^m$ Porphyrin (TPPS)

This synthetic porphyrin analogue, tetraphenylporphine sulphonate, was developed in our laboratory and is now used to investigate sites of infection and inflammation, mostly in gastrointestinal disorders (12). It is available in kit form requiring only the addition of $^{99}\text{Tc}^m$ -pertechnetate. In our clinical studies it is used simultaneously with ^{111}In -labelled leucocytes for comparison of the efficacy of the two substances. Dosimetry studies were performed on 2 male subjects given 74 MBq (2 mCi) $^{99}\text{Tc}^m$ TPPS i.v. Blood activity fell to 2 % dose per litre within 3 h and there was measurable uptake in several organs (Fig. 5) including the gallbladder, as shown more clearly in the right lateral view. Half of the administered activity was excreted in urine within the first 4 h, and after a day the organ with highest uptake was the kidney (Fig. 6).

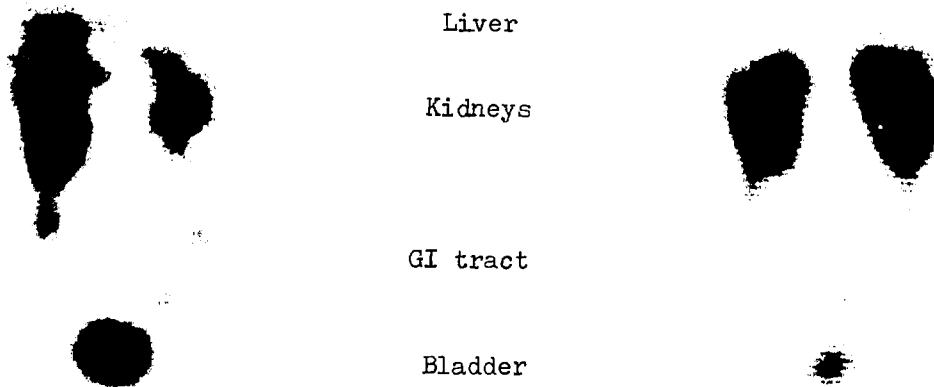


Figure 6. Distribution of $^{99}\text{Tc}^m$ TPPS in a normal male subject.
Left: anterior (23 h), Right: posterior (24 h)

Serial profiles (Fig. 7) showed that the urinary tract was the major excretion pathway and also that the uptake in kidneys increased with time. These observations are shown in detail in the retention curves (Fig. 8) which also indicate the good agreement between the various methods of estimating total-body retention. The dosimetry model, shown in Fig. 9, is more complex than that of

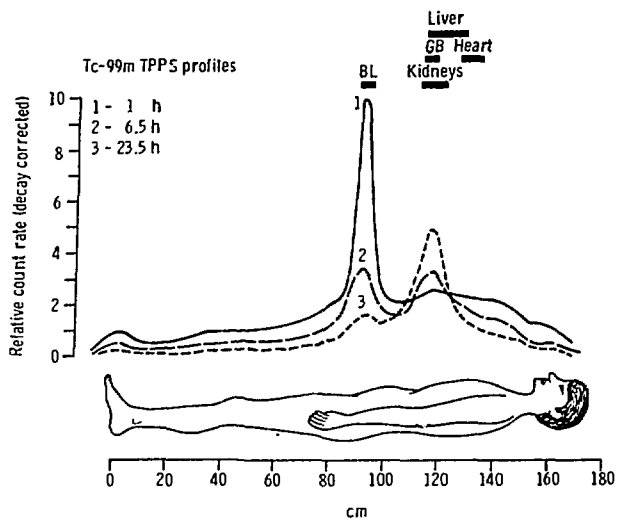


Figure 7. Profile distributions of $^{99}\text{Tc}^{\text{m}}$ TPPS in a normal male subject.

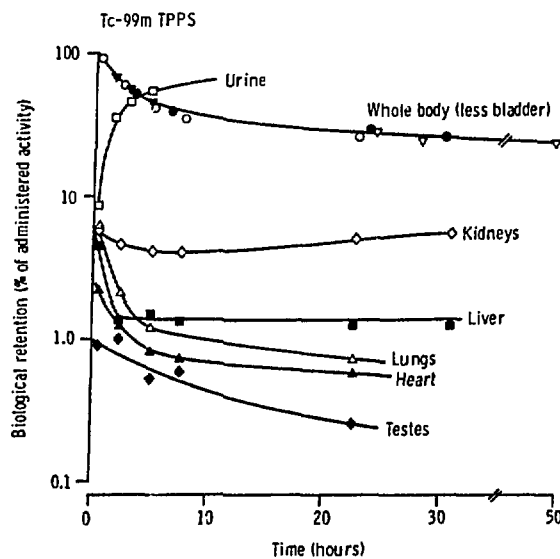


Figure 8. Biological retention of $^{99}\text{Tc}^{\text{m}}$ TPPS in a normal male subject.

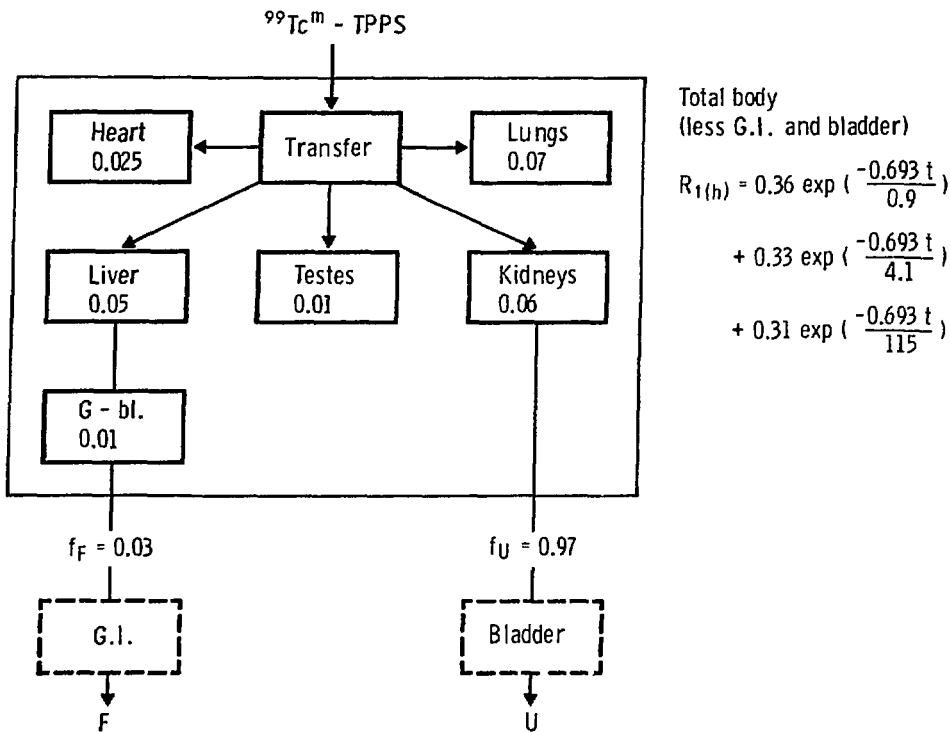


Figure 9. Dosimetry model for $^{99}\text{Tc}^m$ TPPS in a normal male subject

the previous example. In clinical investigations, gamma camera scans are made 2 and 4 h after administration and it is clear that the bladder must be emptied prior to scanning. For this reason a shorter bladder voiding period of 2 h has been used in the model of this substance and the dose estimates are presented in Table 1. Only those target organs which contribute to the EDE have been included.

Table 1. Dosimetry of $^{99}\text{Tc}^m$ TPPS in a normal male subject

Target organ	Dose		w_T
	mrad/ μCi	mGy/MBq	
Testes	0.0718	0.0194	0.25
Breast	0.0061	0.0016	0.15
Red marrow	0.0133	0.0036	0.12
Lung	0.0129	0.0035	0.12
Thyroid	0.0050	0.0014	0.03
Bone surfaces	0.0099	0.0027	0.03
Bladder wall (2 h void)	0.0959	0.0259	0.06
Kidneys	0.0790	0.0213	0.06
Gallbladder	0.0437	0.0118	0.06
ULI wall	0.0231	0.0062	0.06
LLI wall	0.0207	0.0056	0.06
Liver	0.0136	0.0037	-
Effective dose equivalent	0.038	0.0103	

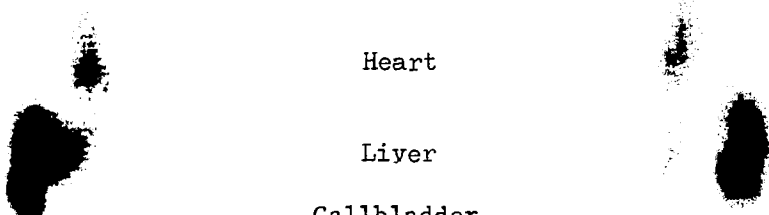
ded although doses to other organs are available. Because of the rapid elimination of activity in urine, the bladder wall receives the highest dose despite the shorter voiding period. Its influence on the EDE and also the contribution from bladder activity to the dose to female gonads are important factors to consider. The usual administered activity of this radiopharmaceutical in clinical studies is 74 MBq (2 mCi) giving an EDE of 0.8 mSv (80 mrem); this compares favourably with a value of 7.0 mSv (700 mrem) for an administered activity of 11 MBq (300 μ Ci) of ^{111}In -leucocytes.

$^{99}\text{Tc}^m$ DEPE

This lipophilic molecule with unit positive charge $[^{99}\text{Tc}^m(\text{DEPE})_2(\text{CNR})_2]^+$ was synthesized from diethylenephosphino ethane and isonitriles as a potential myocardial scanning agent. Preliminary investigations in animals were sufficiently encouraging to prompt studies in man. Unfortunately the human myocardium failed to take up this substance, which was subsequently found to be totally bound to plasma proteins, and the species difference is as yet unexplained. Nevertheless, the properties of this substance suggest it may have a useful role as an alternative blood pool marker, and successful MUGA studies have been carried out with it. Despite the current uncertainty regarding the eventual application of this substance, detailed dosimetry has been performed on a male subject given 220 MBq (6 mCi) i.v. for a MUGA study. The dosimetry results are presented here since there are some interesting differences between this substance and $^{99}\text{Tc}^m$ TPPS. The injected activity was retained in plasma with a half-life of about 3 h. Highest uptake occurred in the liver (10 %), from which activity was subsequently rapidly cleared, but highest concentration occurred in the gallbladder (Fig. 10). The main excretory pathway for this substance, in contrast to $^{99}\text{Tc}^m$ TPPS, was via liver, gallbladder and GI tract. More than 70 % was excreted by this route and this example particularly illustrates the need to correct the total-body retention for the large proportion of the administered activity in transit through the GI tract. In the example shown (Fig. 11) an estimated 20 % of the administered activity resided in the gut at 4.5 h. The profiles (Fig. 12) show the marked difference in redistribution of radioactivity compared with the previous example. The organs for which cumulated activities were measured (Fig. 13) or derived are indicated in the dosimetry model (Fig. 14) and, in this example, activities in several other organs were estimated from their relative blood content. The gallbladder receives the highest dose (Table 2) followed by segments of the GI tract, and this dose distribution leads to a higher EDE than the value of 0.007 mSv.MBq⁻¹ (0.026 mrem. μ Ci⁻¹) estimated for $^{99}\text{Tc}^m$ -labelled erythrocytes (13). It is interesting to note that for both the $^{99}\text{Tc}^m$ -labelled substances described, the liver dose does not contribute to the EDE even though in both cases liver uptake is substantial as evident from the scans. With $^{99}\text{Tc}^m$ TPPS a 20 % reduction in EDE can be achieved by reducing the bladder voiding period from 3.5 to 1 h, but with $^{99}\text{Tc}^m$ DEPE, which is largely excreted in faeces, no similar expedient exists and this is reflected in a somewhat higher EDE.

CONCLUSIONS

1. Our available instrumentation is satisfactory for the comprehensive acquisition of biokinetic data required for good dosimetry of novel radiopharmaceuticals.
2. For fairly long-lived radiopharmaceuticals such as ^{77}Br -spiperone the importance of prolonged whole-body counting is evident, whilst the studies on the $^{99}\text{Tc}^m$ -labelled substances TPPS and DEPE illustrate the need for accurate assessment of excretion pathways, with particular emphasis on the estimation of activity residing in GI tract and bladder. A model based



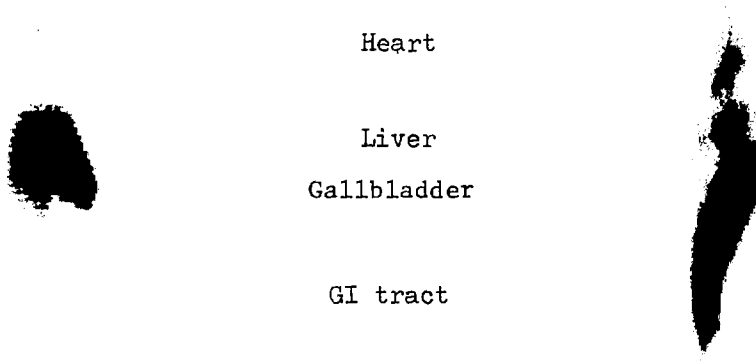
Heart

Liver

Gallbladder

GI tract

Bladder



Heart

Liver

Gallbladder

GI tract

Figure 10. Distribution of $^{99}\text{Tc}^{\text{m}}$ DEPE in a normal male subject.

Top left: anterior (45 min), Top right: posterior (1 h)
Bottom left: Rt. lateral (1.2 h), Bottom right: Lt. lateral (1.4 h)

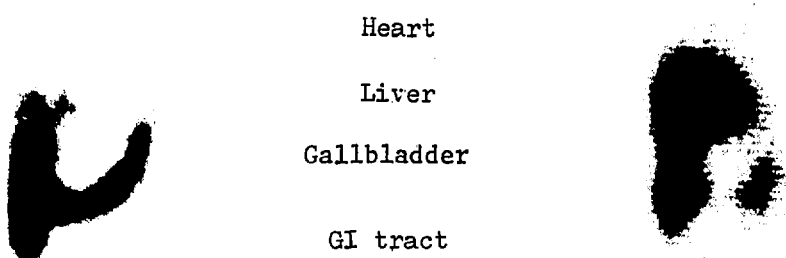
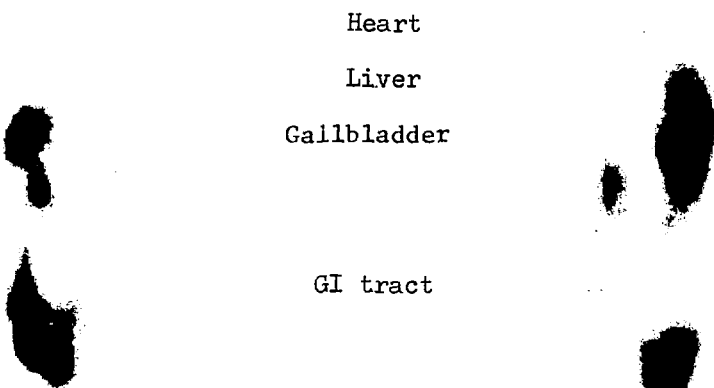


Figure 11. Distribution of $^{99}\text{Tc}^{\text{m}}$ DEPE in a normal male subject.

Top left: anterior (4.3 h), Top right: posterior (4.5 h)
Bottom left: anterior (20 h), Bottom right: anterior (44 h)

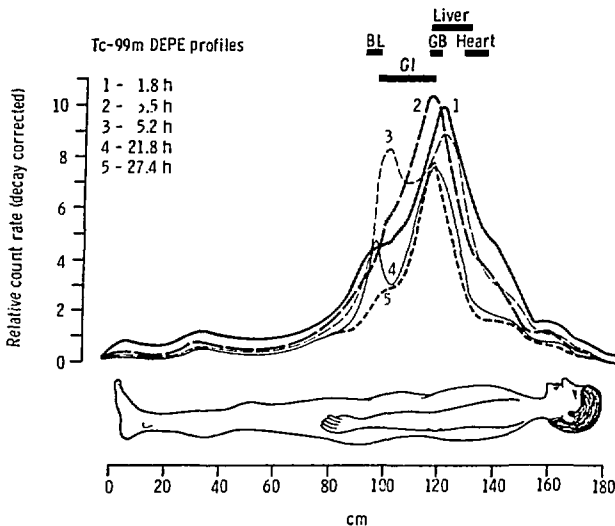


Figure 12. Profile distributions of $^{99}\text{Tc}^m$ DEPE in a normal male subject.

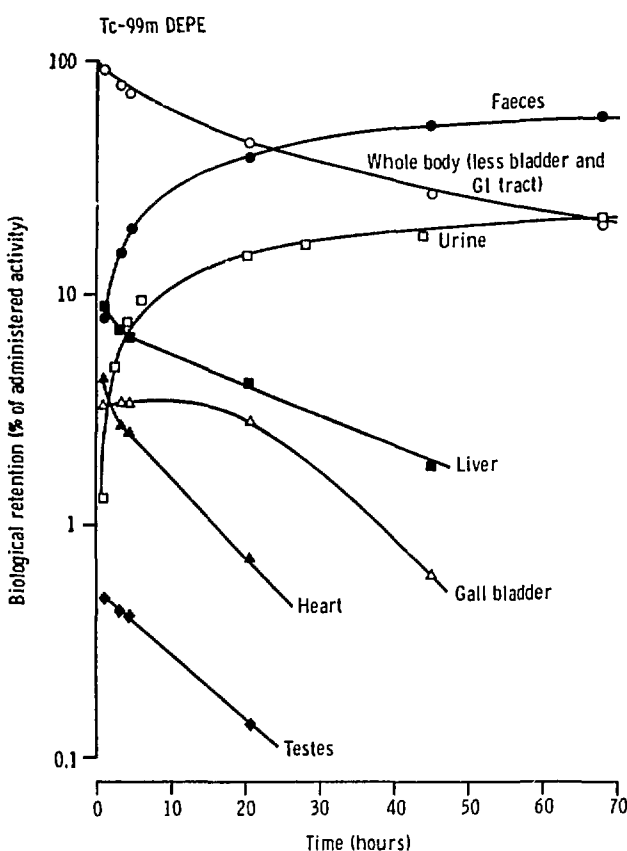


Figure 13. Biological retention of $^{99}\text{Tc}^m$ DEPE in a normal male subject.

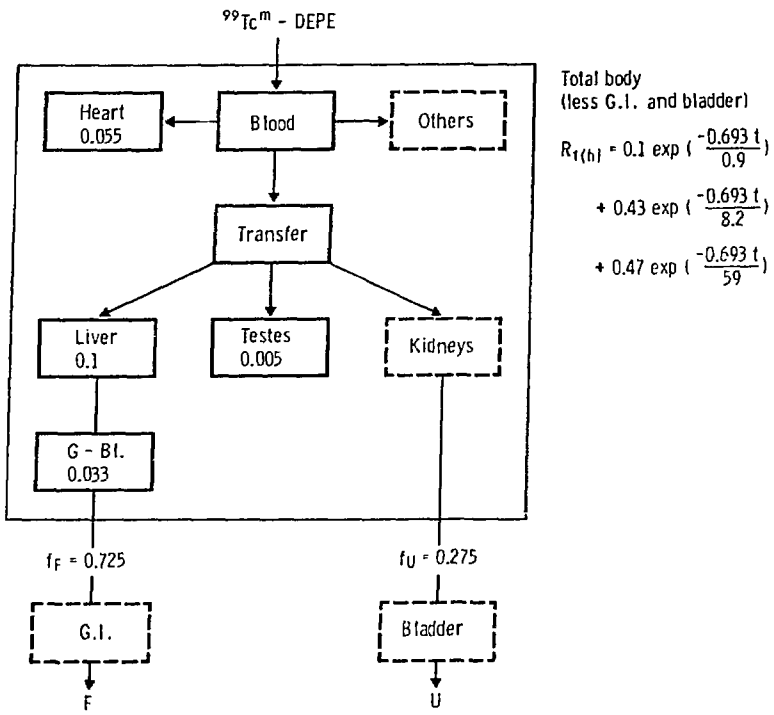


Figure 14. Dosimetry model for $^{99}\text{Tc}^m$ -DEPE in a normal male subject

Table 2. Dosimetry of $^{99}\text{Tc}^m$ -DEPE in a normal male subject

Target organ	Dose		w_T
	mrad/ μCi	mGy/MBq	
Testes	0.0455	0.0123	0.25
Breast	0.0106	0.0029	0.15
Red marrow	0.0222	0.0060	0.12
Lung	0.0224	0.0060	0.12
Thyroid	0.0084	0.0023	0.03
Bone surfaces	0.0084	0.0023	0.03
Gallbladder	0.1404	0.0379	0.06
ULI wall	0.1244	0.0336	0.06
LLI wall	0.0885	0.0239	0.06
SI wall	0.0719	0.0194	0.06
Bladder wall (3.5 h void)	0.0406	0.0110	0.06
Liver	0.0342	0.0093	-
Effective dose equivalent	0.0468	0.0126	

on organ blood content is convenient for radiopharmaceuticals with prolonged retention in the circulation.

3. Further work is required to consolidate our dosimetry technique and will involve methods of estimating and improving the accuracy of organ uptake measurements, possibly including investigations of the method of Fleming (14) and the use of single photon emission computed tomography.

ACKNOWLEDGEMENTS

We wish to thank Mr S.R.D. Oldland and Dr N. M. Patel for their assistance with the preparation of the radiopharmaceuticals discussed, and Dr N. Veall for his interest and advice.

One of us (T.S.) gratefully acknowledges the receipt of a generous contribution from Amersham International plc towards the cost of attendance at this meeting.

REFERENCES

Crawley, J.C.W., and N. Veall. The design and some clinical applications of a hybrid scanner, in Medical Radioisotope Scintigraphy, Vol. 1, pp. 105-112, International Atomic Energy Agency, Vienna, 1973.

Smith, T., R. Hesp, and J. Mackenzie. Total body potassium calibrations for normal and obese subjects in two types of whole body counter. Phys. Med. Biol. 24, 171-175, 1979.

Smith, T., and A.G. Cronquist. A versatile and economic whole-body counter based on liquid scintillation detector modules. Br. J. Radiol. 50, 332-339, 1977.

Cronquist, A.G., J. Mackenzie, and T. Smith. A high resolution bulk-sample counter with variable geometry. Int. J. Appl. Radiat. Isot. 26, 89-91, 1975.

ICRP Publication 30 (Part 1). Limits for intakes of radionuclides by workers. Ann. ICRP, 2, pp. 30-34, Pergamon Press, Oxford, 1979.

Coffey, J.L., M. Cristy, and G.G. Warner. Specific absorbed fractions for photon sources uniformly distributed in the heart chambers and heart wall of a heterogeneous phantom (MIRD pamphlet no. 13). J. Nucl. Med. 22, 65-71, 1981.

Cristy, M. Calculation of annual limits of intake of radionuclides by workers: significance of breast as an explicitly represented tissue. Health Phys. 46, 283-291, 1984.

Freeman, L.M., D.D. Patton, L. Rosenthal, G.V. Taplin, and E.M. Smith. Summary of current radiation dose estimates to humans from ^{123}I , ^{124}I , ^{126}I , ^{130}I and ^{131}I as sodium rose bengal (MIRD dose estimate report no. 7). J. Nucl. Med. 16, 1214-1217, 1975.

ICRP Publication 26. Recommendations of the International Commission on Radiological Protection. Ann. ICRP, 1, No 3, 1977.

D. Crawley, J.C.W., T. Smith, N. Veall, G.D. Zanelli, T.J. Crow, and F. Owen. Dopamine receptors displayed in living human brain with ^{77}Br -p-sipiperone.

Lancet, 2, 975, 1983.

11. Crawley, J.C.W., T. Smith, N. Veall, and G.D. Zanelli. Distribution, retention and radiation dosimetry of ^{77}Br -p-bromospiperone. Radiat. Prot. Dosim. 8, 147-153, 1984.
12. Bjarnason, I., G.D. Zanelli, T. Smith, N. Veall, and A.J. Levi. Intestinal imaging: comparison of ^{111}In -labelled leucocytes and $^{99}\text{Tc}^m$ porphyrin. Gut, 26, A553 (abstr.), 1985.
13. Johansson, L., S. Mattsson, and B. Nosslin. Effective dose equivalent from radiopharmaceuticals. Eur. J. Nucl. Med. 9, 485-489, 1984.
14. Fleming, J.S. A technique for the absolute measurement of activity using gamma camera and computer. Phys. Med. Biol. 24, 176-180, 1979.

DISCUSSION

BIGLER: What assumptions and/or measurements did you use to develop the radiation dose estimates for red bone marrow for your various radiopharmaceuticals?

SMITH: Red marrow? Unless the radioisotope is obviously concentrated in red marrow and, therefore, becomes a source organ, it is included as part of the remaining body, and the dose calculation to the red marrow is the result of dose contributions from the various selected organs which appeared in the box in these examples and also from the remaining body of which the red marrow would be part.

CLOUTIER: I want to compliment you on the collection of this data because it is definitely needed. I have a question about your use of the effective dose equivalent. As I recall, ICRP 26 suggested that the effective dose equivalent not be used for medical purposes. Does the use of effective dose equivalent in the United Kingdom mean effective dose equivalent will be used in the future?

SMITH: No, it does not. The latest is that the ICRP has recommended that a ICRP task group, which is at present updating ICRP 17 on doses from radiopharmaceuticals, use the effective dose equivalent as a crude estimate of detriment as a means for comparing doses from different radiopharmaceuticals.

QUANTITATIVE CLINICAL UPTAKE MEASUREMENTS USING CONJUGATE COUNTING

Katherine A. Lathrop

Robert D. Bartlett

Chen-Tu Chen

Jin-Shin Chou

Peter F. Faulhaber

Paul V. Harper

Violet J. Stark

The University of Chicago

5841 South Maryland

Chicago, Illinois 60637

ABSTRACT

While the use of conjugate counting for determination of organ uptake in human subjects has been extensively described, in the present study the determination of the organ uptake of ortho-iodohippurate presented several opportunities for validation of the *in vivo* counting data. Ortho-iodohippurate is distributed in the extracellular space, is largely extracted on each pass through the kidneys, and is not significantly deiodinated *in vivo*. Thus the kidney uptake rate should be proportional to the blood level, the appearance rate of activity in the bladder is equal to the disappearance rate from the kidneys, and direct measurement of activity in the urine after voiding provides an internal standard for imaging measurements of bladder activity. Since the activity levels in the kidneys, bladder, and remainder of the body changed fairly rapidly, especially in the first 20 to 30 minutes following injection, posterior images of the trunk including kidneys and bladder were obtained continuously using a gamma camera fitted with a diverging collimator for 30 minutes and then at intervals for several hours. Simultaneous conjugate counting determinations were made using a whole body scanning system previously described at these meetings. Imaging data corrected for decay and adjacent background were fitted by least squares methods to curves representing a sum of exponentials, and the curves were normalized to the conjugate uptake measurements. The uptake curves of the kidneys and bladder matched well with the direct measurements of the urinary excretion. Data were collected in 16 normal subjects, and the estimated absorbed dose was calculated for the kidneys, the bladder and the remainder of the body for seven radioisotopes of iodine.

INTRODUCTION

The estimation of radiation absorbed dose in a human receiving a radiopharmaceutical involves calculations with data taken from four areas, i.e., nuclear decay, physics, mathematical description of the human body, and biological distribution in human subjects. The calculation is a simple multiplication of two quantities: $D = \tilde{A}S$, where \tilde{A} is cumulated activity, and S is absorbed dose per unit cumulated activity. The challenge of the exercise is an accurate determination of these two quantities.

The term S is determined by the appropriate use of data about the physics of interaction with matter, nuclear emissions, and mathematical models for the human body. Determination and tabulation of data about nuclear decay and interactions of radiation with matter are adequate for most of the radioisotopes used or attempted for nuclear medicine. Availability of these data and the formulation of mathematical models for humans have resulted, by Monte Carlo calculation, in estimates and tabulation of values for S .

The term \tilde{A} is determined by data about the biological distribution, physical half-life, and the administered activity. Information about the two latter terms is readily available. Information about the biokinetic distribution of radiopharmaceuticals, however, is generally inadequate. The necessary data can, for the most part, be acquired in the clinical nuclear medicine facility, but the time required and the consequent expense may seem prohibitive for most installations at the present time.

"Dosimetry should be viewed with a sense of humor" is a quotation from Dr. Herbert Parker, one of the early workers in the field of radiation dosimetry. "Collection of biological data for dosimetry is a serious matter", if taken seriously will remove some of the humor from estimation of radiation doses, and will help nuclear medicine achieve the scientific status it deserves as a tool for the quantitative study of physiological and biochemical processes in the intact human.

This paper confines itself to the problem of determination of the biodistribution of a radionuclide in a human subject. The collection of quantitative biological data for a specific radiopharmaceutical, I-123-ortho-iodohippurate (o-IH), is presented but the methods have general applicability. Some details of the mathematical processing of the biological data and the absorbed dose values for o-IH labeled with seven radioisotopes of iodine are also presented.

METHODS AND MATERIALS

DEFINITION OF QUANTITATIVE BIOLOGICAL DISTRIBUTION

Quantitative biological distribution means knowing the quantity of activity, $\pm 5\%$, introduced into the subject, and accounting for 100% of this activity to within $\pm 5\%$ at various time intervals throughout its lifetime within the subject. Our experience has taught us that unsuspected errors may occur in quantitation unless the 100% recovery is obtained (1).

SELECTION OF RADIOPHARMACEUTICAL

Only radiopharmaceuticals of very high purity, both radiochemical and radionuclidic, are suitable for biodistribution studies. If radioactive contaminants are present in a commercially obtained preparation they must be reduced to levels that have no significant effect on the biodistribution pattern. Radioisotopes of the radionuclide being studied are not a problem when present in the same chemical combination and when the assay of activity is made by comparison with a known fraction of the preparation injected into the subject. Correction for other radionuclidic or radiochemical contamination requires exact knowledge of the amounts injected and of their biodistributions, which most frequently are not known. Their contribution to the observed distribution pattern must then be mathematically corrected in order to obtain the true distribution. Chemical or physical removal of the contaminants may prove to be a simpler process and the subject will receive less radiation.

For the study used here as an example for the collection of quantitative biological data, i.e., the distribution of o-IH, a high purity preparation, delivering low radiation dose to the subject but providing high count rates to give the most accuracy in the data, was needed. For these reasons, I-123 was chosen as the label. Interference from iodide distribution would be eliminated if 100% of the radioiodine was attached to the o-IH. Interference from other organic molecules binding with the radioiodine would be eliminated if removed prior to the exchange reaction between iodide and stable o-IH. Initially, a preparation meeting these requirements could not be obtained commercially. This resulted in our producing I-123 with the on-site cyclotron for use with repurified o-IH to give a preparation free of radioiodide and organic molecules such as ortho-iodobenzoate. An excellent commercial product became available late in the study and was used for the last four studies.

SELECTION OF SUBJECTS

The subjects were normal volunteers showing no evidence of renal disease and ranging in age between 20 and 70 years. Written informed consent was obtained from each prior to beginning the study. Of the sixteen subjects entered into the study, four were female. Four studies were not included in the data analysis, one because of a very high iodide content in the commercial preparation, one because of infiltration at the injection site, and two because of suspicious differences in uptake between left and right kidneys. The ratio for uptake between left to right kidneys, in the 12 subjects included in the study, was 1.03 ± 0.16 .

DATA COLLECTED

Data were collected from each subject for right and left kidney uptake, bladder uptake, whole body retention, thyroid uptake, blood and urine content. Subjects were positioned appropriately with respect to the imaging equipment used and an indwelling catheter was inserted into the antecubital vein of each arm. The radiopharmaceutical was delivered into the right arm. Samples of blood were withdrawn from the left arm at 2, 5, 10, 20, 40, 80, 160 minutes, and 24 hours after injection. Each sample was transferred to a previously weighed, heparinized test tube which was again weighed to provide, by difference, the weight of the blood. Samples were counted in a NaI well crystal, and were converted to % of injected I-123 per ml by comparison with 1 ml of a known fraction of the injection solution counted under the same conditions.

Radiation dose to the bladder wall was reduced by having the subject begin the study with a comfortably full bladder, and by making the first voiding, when possible, about two hours after injection of the radiopharmaceutical. Before and after voiding, images were taken throughout the study to determine residual activity and to correlate the activity determined by imaging with that found by direct assay of the urine.

Whole body and regional activities were determined with a whole-body conjugate count scanning system consisting of two banks of eight NaI detectors directly facing each other, through which the subject was passed on a moving bed. Data were collected and processed using a dedicated computer. This system and its use is described in the Proceedings of the Third International Symposium on Radiopharmaceutical Dosimetry (2).

The above system is not suited to collection of data during rapidly changing distribution of activity, which must be determined from indirect quantitation of dynamic curves obtained with a gamma camera fitted with a wide

angle diverging collimator to include the thyroid, kidneys, and urinary bladder. First, transmission images with both the whole body and camera systems were obtained to correct for differences in body thickness. The subject was then positioned under the gamma camera and made ready for injection of the radiopharmaceutical. With the recording system operating at the desired frame rate, the activity was administered, and data collection continued until kidney activities reached a fairly constant value. At this time, the subject was transferred to the whole-body system where data were collected to provide a single quantitative value that was used to calibrate the gamma camera curves. Urine was collected quantitatively, assayed, and used to confirm the bladder assay from the image data. This method is depicted in Figure 1.

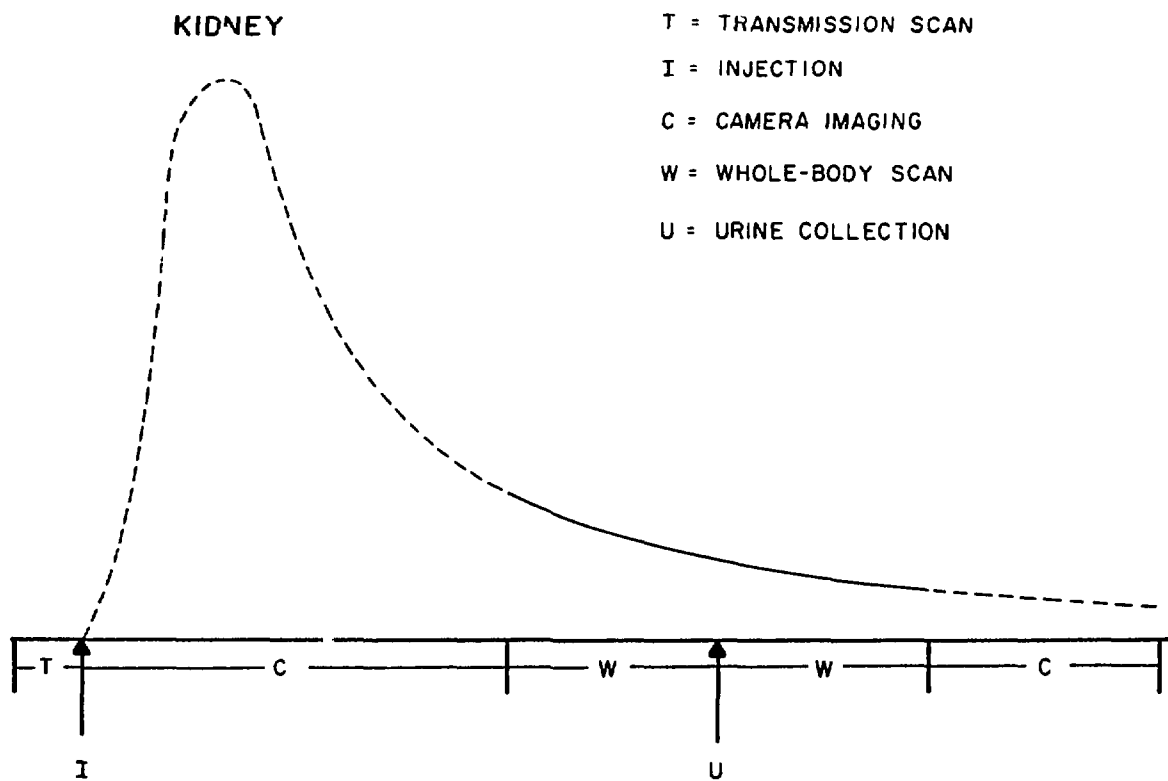


Figure 1. Graphic depiction of the technique employed to relate gamma camera counts to absolute in vivo measurements obtained with the conjugate count whole-body system. A transmission scan of the patient is made with the whole-body system previous to injection of the radiopharmaceutical. Imaging with the gamma camera is done continuously until counts versus time become fairly constant. Whole-body quantitative imaging is then done, the subject voids, and is again imaged to determine residual bladder activity. Gamma camera imaging is resumed continuously, or at intervals if more appropriate. Corresponding regions of interest from the camera and whole-body imaging system provide % injected activity per count in the camera image at the same time point determined by interpolation on the camera curve.

Agreement obtained for elimination of activity from the whole body based on actual counts and on recovered urine was good as shown in Figure 2. The data are from our first study, made with a commercial preparation containing 11% I-123-iodide. All other studies contained less than 1% radioiodide and showed 100% elimination within about five hours. The effect of substantial radioiodide in the radiopharmaceutical is shown in Table 1, with two studies made in the same individual. The first preparation contained 11% radioiodide, the second 1.5%. The significantly longer time required for complete elimination of activity in the urine and the higher retention in the blood when the larger quantity of iodide was used obviously have important implications for the reduction and estimation of absorbed dose.

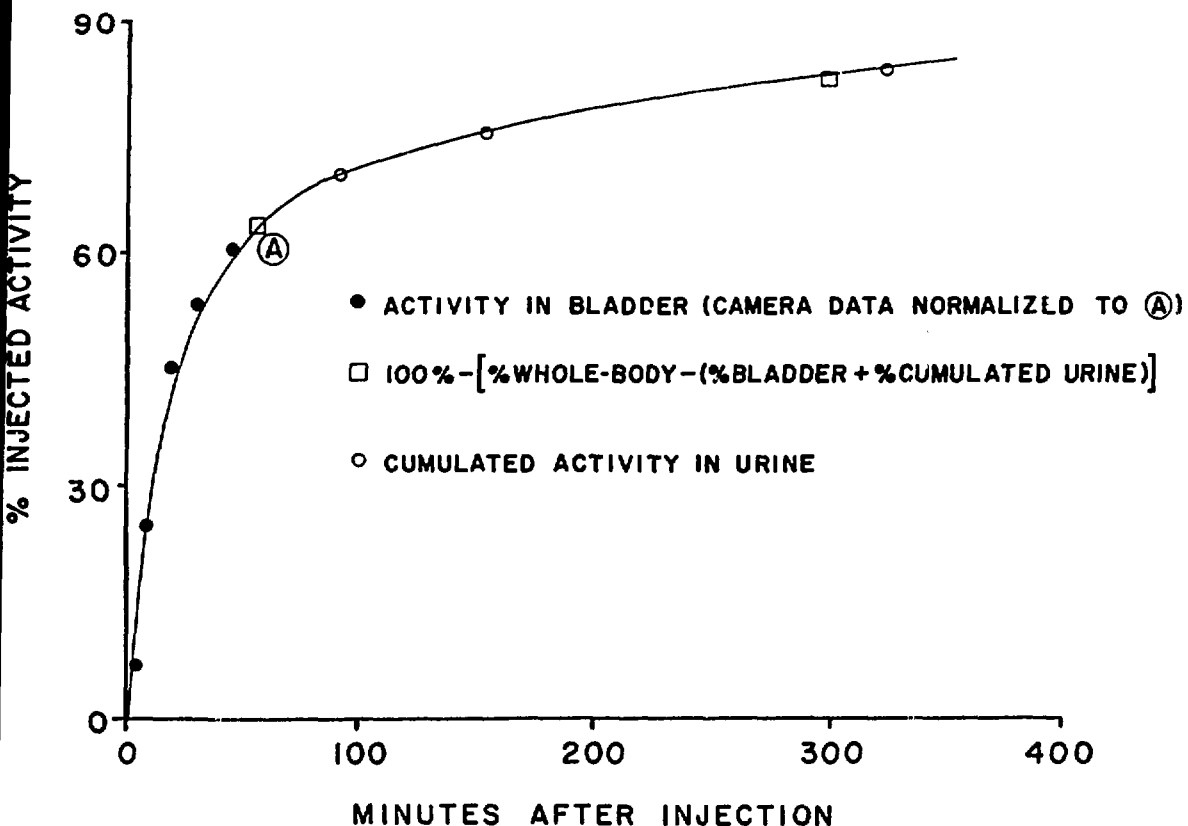


Figure 2. Urinary excretion of I-123 injected as o-IH obtained by direct assay of quantitatively recovered urine (open circles), by assay of in vivo bladder activity with the whole-body conjugate count system (open circles), and by gamma camera counts over the bladder corrected for background and for physical decay (solid circles). Point A was determined by direct assay of urine voided immediately after completion of the whole-body imaging. These data agree well with the decline in whole body counts (open squares).

Table I. Effect of Radioiodide Contamination on Distribution Pattern for Radio-o-Iodohippurate

140

11% Radioiodide				1.5% Radioiodide			
Time (m)	Urine (%IA)	Time (m)	Blood (%IA/g)	Time (m)	Urine (%IA)	Time (m)	Blood (%IA/g)
57	63	2	0.0053	140	94	2	0.0071
141	73	3	0.0077	250	98	3	0.0054
295	79	6	0.0057	554	99	5	0.0049
442	83	10	0.0046	1164	100	10	0.0027
743	88	22	0.0030			20	0.0014
983	91	42	0.0022			40	0.0006
1241	93	80	0.0015			98	0.00013
1518	95	158	0.0012			160	0.00007
1673	96	307	0.0010			320	0.00003
1883	97	464	0.0007				
2443	98						

The evidence for the accuracy of our methods and for the complete excretion of I-123 from o-IH within about five hours enabled us to proceed without the whole-body instrument when the system disintegrated due to a power failure. We turned to quantitation of activity in kidneys and bladder by using two gamma cameras, one below and one above the subject, to produce anterior and posterior images with individual data acquisition systems from which quantitation was obtained by a conjugate count calculation. A transmission image allowed correction for varying thickness of the body and the conjugate images for attenuation and differing depths for the kidneys. As much as 30% difference was observed between right to left kidney ratios determined by conjugate counting and the ratios of posterior counts alone. This finding has been verified by Choi et al. (3). This technique should, thus, be useful in the clinic to obtain kidney uptake as percent of injected activity from which the true, undistorted, ratio between kidneys may be determined.

The average curve for the right kidney of the 12 subjects is shown in Figure 3, and for the left kidney in Figure 4. Differences between the curves are not significant. The wide range for error bars in the early phase is due to sharper peaks in about the last one-third of the studies where more counts were available, but areas under the curves were similar.

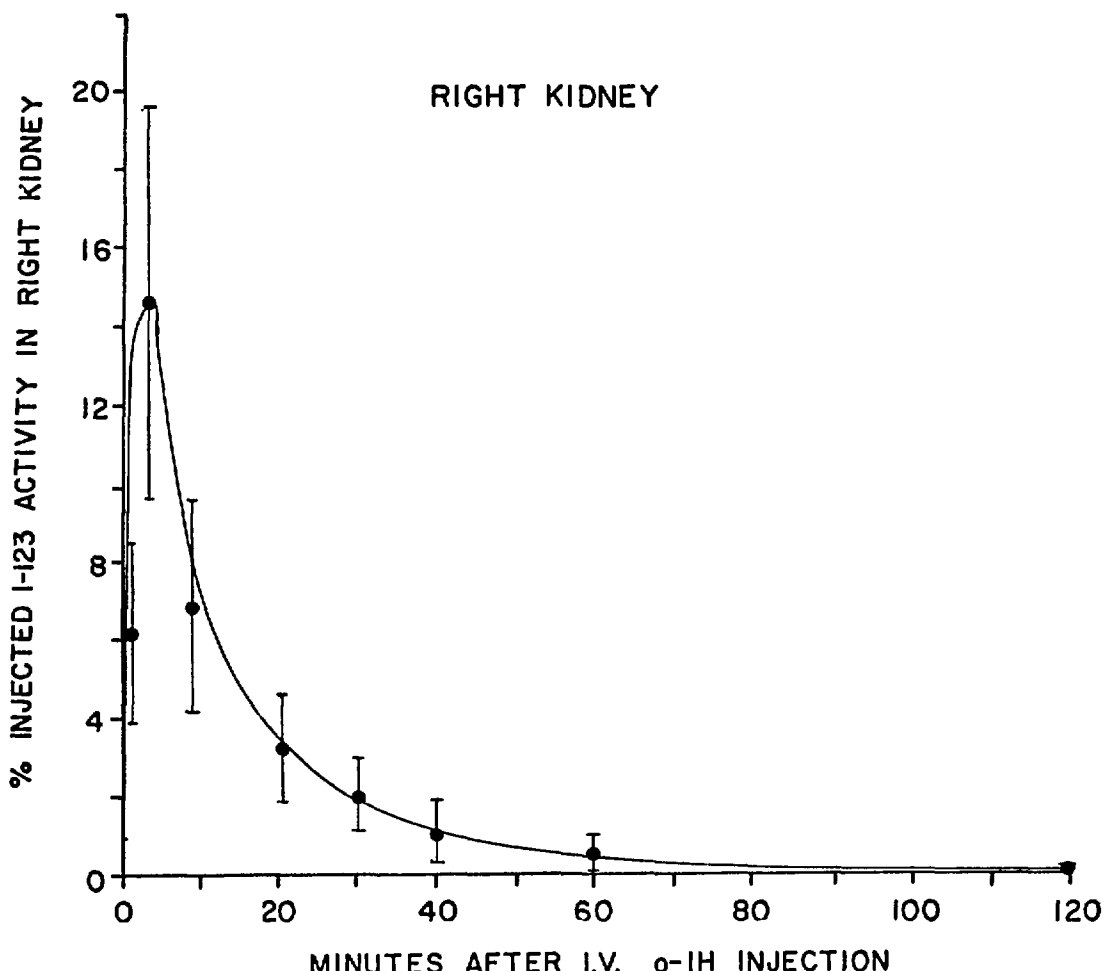


Figure 3. Mean curve of activity in right kidney of 12 normal subjects. The wide range for error bars at the earliest points is due to more available counts in about one-third of the studies. Areas under the individual curves were similar.

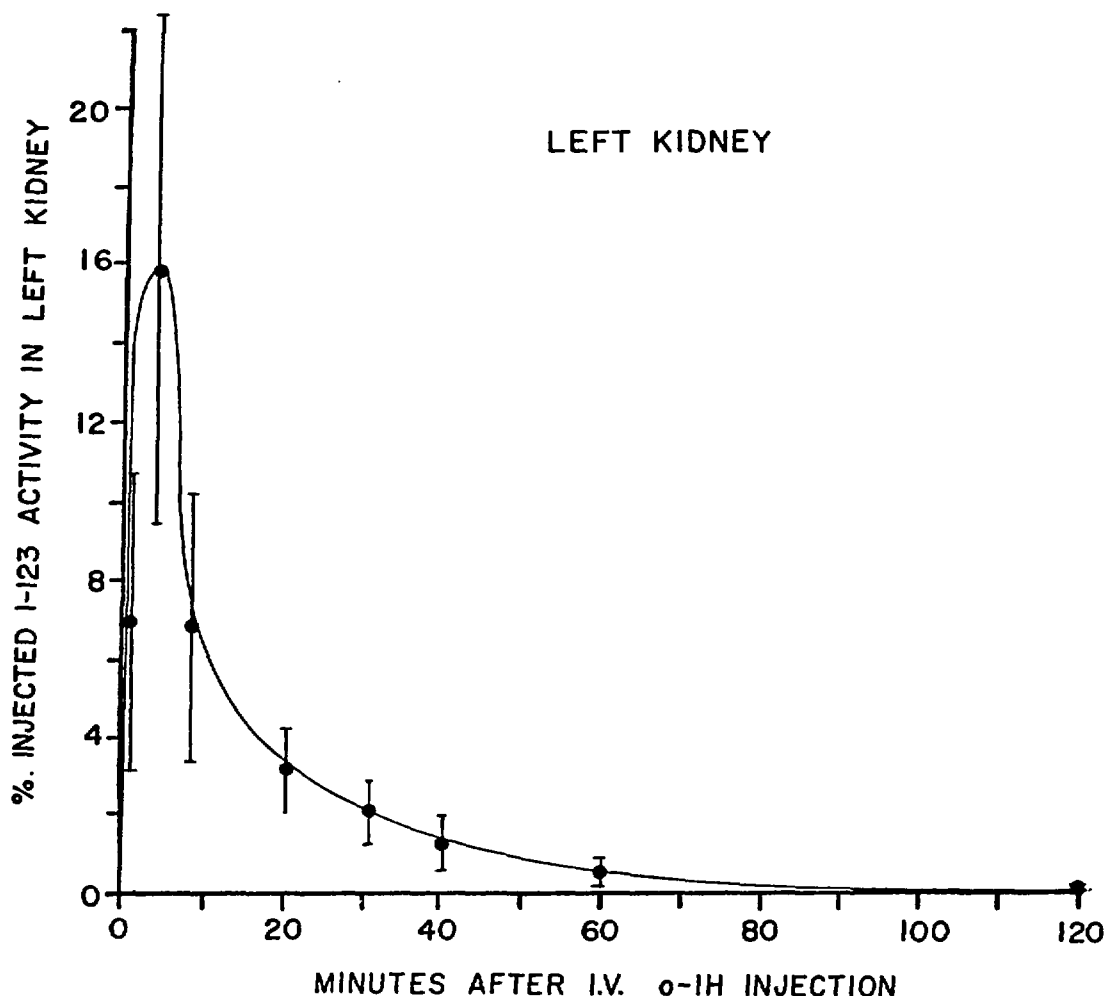


Figure 4. Mean curve for activity in left kidney of 12 normal subjects. See Figure 3 for explanation and comparison of curves. The mean for the ratio of uptake between left to right kidney was 1.03 ± 0.16 .

Activity in the thyroid, determined with a thyroid phantom, was consistent with the iodide contamination determined for the preparation. The thyroid could not be visualized with preparations containing around 0.1% iodide. Thus, no evidence was found for *in vivo* deiodination.

DATA ANALYSIS AND ESTIMATION OF ABSORBED DOSE

Using conjugate image data obtained with the whole-body counter or the two camera system and single camera data normalized to the conjugate data, conjugate count rates for both kidneys and the bladder were calculated, with corrections for adjacent background, attenuation, and physical decay. A simplified model was assumed to describe the kidney localization, consisting

of a monoexponential uptake and a biexponential washout commencing about 4 minutes after injection (kidney transit time). The parameters of this equation were determined by least squares fitting to the count data, making use of the observation that 100% of the activity is excreted through both kidneys. The coefficients of this equation for the right and left kidneys $A_K(\infty)_{\text{left}}$ and $A_K(\infty)_{\text{right}}$ are assumed, thus, to add up to 100%. Using this assumption the count data is converted to percent injected activity values and the least squares fitting is repeated, leading to the final equations (see example). The appearance of activity in the bladder may also be described by a biexponential expression. This was produced by least squares fitting of counting data as with the kidney curves, and normalized to 100% excretion. Assay of the voided urine agreed well with this curve, as well as with the excretion curve calculated analytically from the kidney curves. The expressions shown in this example, though not exact and not precisely consistent mathematically, appear to describe the distribution data with adequate accuracy. The expression for the remainder of the body was determined by difference and agreed well with whole-body counting data in cases where these were available. S values for the remainder of the body were calculated from the S value correction method (4).

Example:

Equation for kidney activity:

$$A_K(\infty) = A_K(t) \quad \text{For } \lambda_2 = \lambda_3 = 0 \quad T = \infty \quad \text{i.e., no washout}$$

$$A_K(t) = \begin{cases} A(\infty)(1-e^{-\lambda_1 t}) & t < 4m \\ A(\infty)(1-e^{-\lambda_1 t})(\alpha e^{-\lambda_2(t-4)} + \beta e^{-\lambda_3(t-4)}) & t \geq 4m \end{cases}$$

General constraints for curve fitting:

$$A_K(\infty)_{\text{left}} + A_K(\infty)_{\text{right}} = 100\% \text{ of injected activity}$$

$$40\% \leq A_K(\infty)_{\text{left}}, A_K(\infty)_{\text{right}} \leq 60\%$$

$$\alpha + \beta = 1 \quad 0 \leq \alpha, \beta \leq 1$$

A calibration factor, % injected activity per count, was determined by comparison of count data with a reference standard or by assumptions of 100% excretion and 100% passage through the kidneys.

From Count Data:

$$A_K(t)_{\text{left}} = 8784.6 (1-e^{-0.0693t}) (.699e^{-0.608(t-4)} + .301e^{-0.0725(t-4)})$$

$$A_K(t)_{\text{right}} = 9057.2 (1-e^{-0.0693t}) (.505e^{-0.847(t-4)} + .495e^{-0.0685(t-4)})$$

From % injected activity data:

$$A_K(t)_{\text{left}} = 49.97 (1 - e^{-0.0694t}) (.67 e^{-0.742(t-4)} + .343 e^{-0.0725(t-4)})$$

$$A_K(t)_{\text{right}} = 50.03 (1 - e^{-0.0622t}) (.55 e^{-0.715(t-4)} + .445 e^{-0.0638(t-4)})$$

For bladder (% injected activity):

$$A_B(t) = 19.3(1 - e^{-2.61(t-4)}) + 80.7(1 - e^{-0.034(t-4)})$$

For remainder of body (% injected activity):

$$A(t)_{\text{rem}} = 44.8 e^{-0.176t} + 55.2 e^{-0.0226t}$$

Figures 3 through 6 show the biological time concentration curves for the group studied. These curves were obtained from the average values of the equations for each subject evaluated at the intervals shown. The error bars thus represent largely differences between individual subjects rather than variation in the data for the individual subjects.

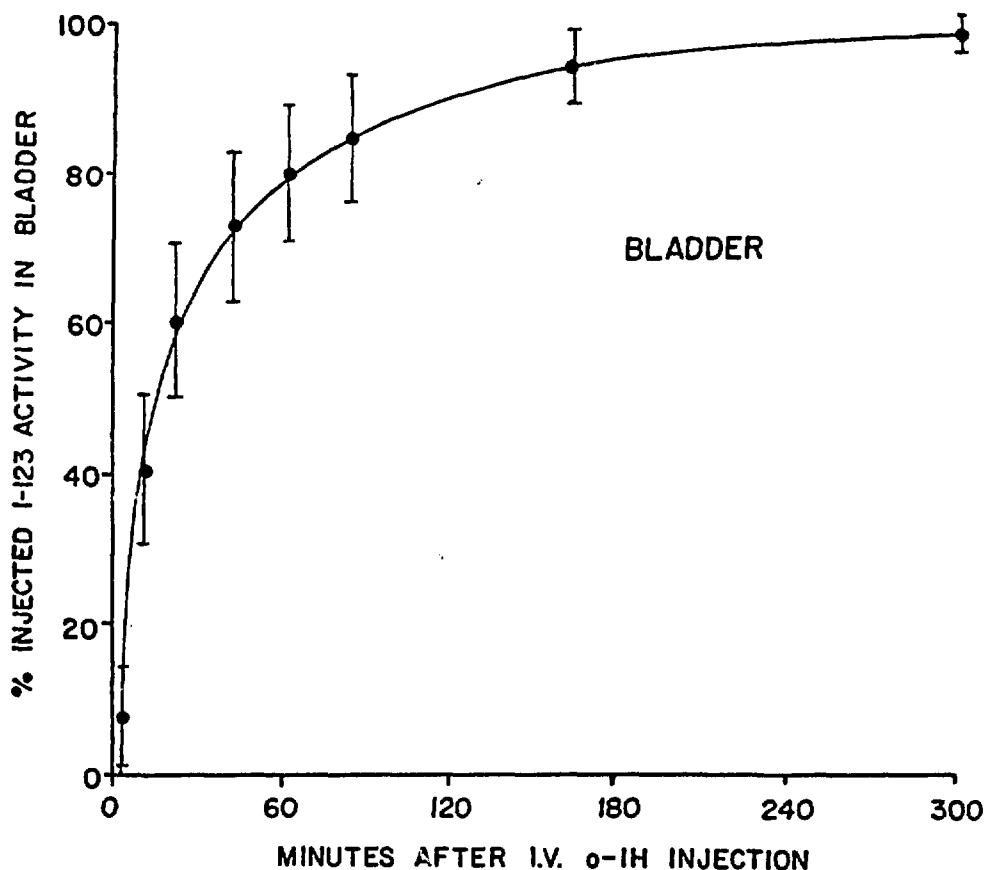


Figure 5. Mean curve of cumulative activity entering the bladder for 12 normal subjects. The individual curve for each subject was determined as shown in Fig. 2, and was also generated from the curves for the right and left kidneys. In all cases the agreement was excellent. The 12 individual curves were then averaged to obtain the one shown.

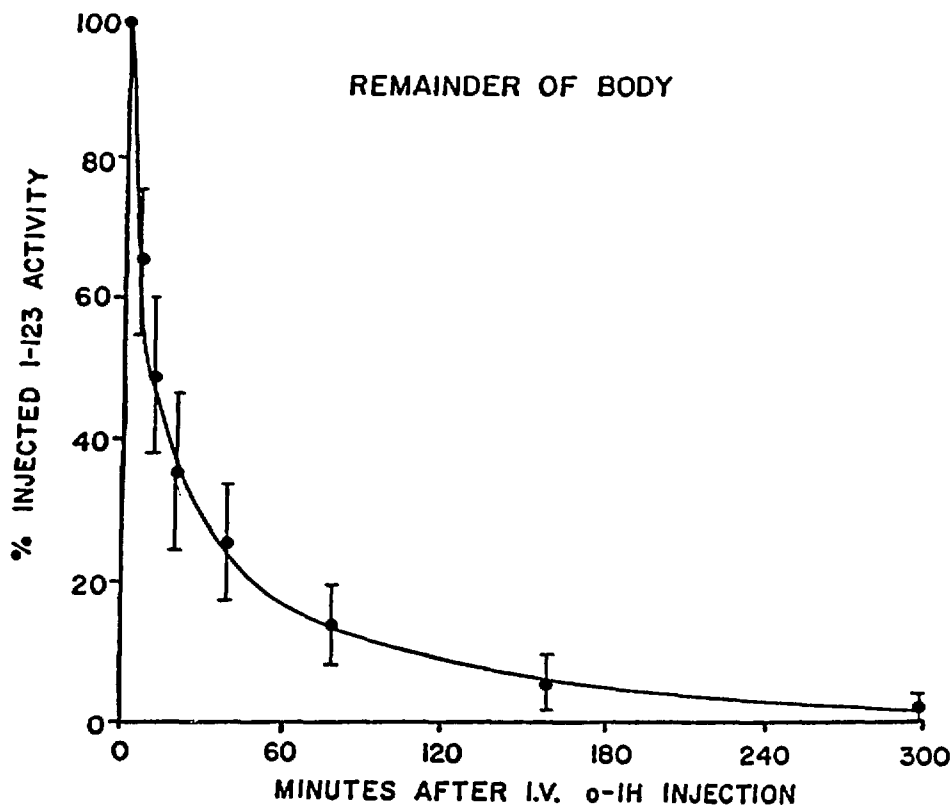


Figure 6. Mean curve for activity retained in the body for the 12 normal subjects. The curve for each subject was generated by subtracting activity in the source organs (kidneys and bladder) from 100% (A_0). The curve was verified with urinary excretion data and with whole-body counts. The 12 individual curves were then averaged.

The mean biologic curves determined for the twelve subjects were each corrected by the decay factor for each of the seven radioisotopes of iodine. The resulting curves were integrated to obtain the cumulated activity in μCi /mCi injected. These values are presented in Table 2. These values are very close for each isotope because of the short biological half-time. Only for I-132, with its 2.3 h physical half-life is a significant difference noted. The absorbed dose estimates calculated from these values and the S values are given in Table 3.

SUMMARY

Techniques have been presented with which $100\% \pm 5\%$ of administered activity can be accounted for within the human body. The method permits quantitation of the biokinetic distribution in various body regions, even in the presence of rapidly changing activity. Using I-123-ortho-iodohippurate to demonstrate application of the method, it was shown that the uptake and washout of I-123 from each kidney may be quantitatively determined from conjugate count data obtained with two gamma cameras; that I-123 administered as o-IH does not localize in the thyroid, indicating the absence of in vivo deiodination, and is completely excreted in the urine of normal subjects in about five hours; that the residence times for the radioisotopes of iodine when incorporated into o-IH are determined principally by the biological half-time; and that the radiation absorbed doses for various isotopes differ principally because of the radiation characteristics of the decay.

Table II. Source Organ Cumulated Activity
from I.V. Radioiodine-o-Iodohippurate

Organ	Iodine Radioisotope						
	I-123 (13h)	I-124 (4d)	I-125 (60d)	I-126 (13d)	I-130 (12h)	I-131 (8d)	I-132 (2.3h)
(μ Ci h/mCi injected)							
L. Kidney	22	22	22	22	22	22	21
R. Kidney	22	22	22	22	22	22	20
Bladder							
5m-2.4h	1500	1600	1600	1500	1500	1600	1100
2.4-4.8h	125	150	150	125	125	150	50
ROB†	980	1100	1110	980	980	1100	651

†Remainder of Body

Table III. Summary of Radiation Absorbed Dose From Ortho-Iodohippurate (o-IH). (N=12)

Radioisotope	Organ					
	Bladder Wall	Kidney	Red Marrow	Ovaries	Testes	Bdy Remainder
(mrads/mCi injected)						
I-123	490± 40	26± 8.0	7.5±0.62	19±0.92	12±0.55	4.7±0.55
I-124	3400±250	170±50.	33. ±3.6	110±4.6	85±3.8	28. ±3.3
I-125	380± 28	19± 5.9	2.5±0.57	5±0.28	3±0.24	1.7±0.37
I-126	1900±150	100±30.	14. ±1.6	38±1.6	33±1.4	12. ±1.5
I-130	4700±380	260±72.	57. ±4.8	180±8.5	160±7.1	54. ±4.3
I-131	2300±170	120±35.	16. ±2.1	44±1.9	33±1.6	11. ±2.0
I-132	4800±470	220±71.	47. ±3.2	120±7.7	120±6.3	44. ±3.8

REFERENCES

1. Lathrop, K.A. Quality control in animal biodistribution studies, in Quality Assurance of Pharmaceuticals Manufactured in the Hospital, edited by A. Warbick-Cerone and L.G. Johnston, pp 147-154, Pergamon Press, New York, NY, 1985.
2. Tsui, B.M.W., C.-T. Chen, N.J. Yasillo, C.J. Ortega, D.B. Charleston, P.V. Harper, and K.A. Lathrop. A whole-body scanning system for collection of quantitative in vivo distribution data in humans, in Proceedings of the Third International Symposium on Radiopharmaceutical Dosimetry, edited by E.E. Watson, A.T. Schlafke-Stelson, J.L. Coffey, and R.J. Cloutier, pp. 138-156. Bureau of Radiological Health, Rockville, MD, 1980.
3. Choi, H. and P.T. Kirchner. Importance of renal depth correction for quantitation of differential renal function. J. Nucl. Med. 26. P56, 1985.
4. Coffey, J.L. and E.E. Watson. Calculating dose from remaining body activity: a comparison of two methods. Med. Phys. 6. 307-308, 1979.

DISCUSSION

MARCUS: Are you aware of any commercial sources of I-123 or I-123-OIH that contain I-126, I-130, or I-131? I have contamination levels for I-124 and I-125, but not the other 3 radiocontaminants.

LATHROP: No, I can't tell you of any offhand.

CONSIDERATIONS REGARDING DOSIMETRY IN CHILDREN

David L. Gilday, M.D., Professor of Radiology, University of Toronto,
Deputy Radiologist-in-Chief, The Hospital for Sick Children, 555
University Avenue, Toronto, Ontario M5G 1X8

ABSTRACT

The most important consideration when deciding whether or not to perform a nuclear medicine procedure in a child is whether the benefit of the information obtained exceeds the potential risk. In most circumstances the potential benefits are well defined. No patient should be studied unless the question to be answered is clearly understood and there is a reasonable chance to answer it. To properly perform procedures in children one must not only have a schedule to scale the radiopharmaceutical dose to be administered to the child's body surface area but also one must have an established minimum dose for small babies and infants. There is no point in under-dosing the patient as then the information will not be obtained from the nuclear medicine study.

The value of nuclear medicine in the paediatric population cannot be underestimated. It is often the single most important test that can be performed diagnostically. For these reasons it is very important to understand the proper relationship of an adequate study versus the minimization of radiation.

The use of nuclear medicine in paediatric patients has undergone a rapid growth in the last ten years. This could lead to a potential increase in biological hazard secondary to radiation. When considering a radiological investigation involving a child one should always minimize the radiation dose provided that the necessary information desired from the procedure is not reduced. As a result of diagnostic paediatric nuclear medicine there have been no reported biological effects from its radiation. Paediatric patients present with a variety of diseases which are quite different from those seen in adults. They also respond in a different manner to illness. For example, they frequently have a very rapid downhill course and therefore diagnoses must be made quickly, efficiently and accurately. Because of this most diagnostic services have developed a close relationship between nuclear medicine, ultrasound, computed tomography, special procedures, magnetic resonance imaging and standard radiological investigations. Triage is the most important aspect of our investigation in children. This accomplishes both rapid investigation, the best utilization of resources and as a result the lessening of radiation exposure.

When considering the choice of various tests in the diagnostic imaging field one has two choices. One is to use non-ionizing radiation modalities such as ultrasound or MRI, or to use one of the ionizing radiation modalities. Quite frequently ultrasound is used for screening

as it is inexpensive and essentially a biologically neutral investigation. However, it quite frequently does not answer all of the presented problems in paediatrics. Paediatric nuclear medicine has a valuable role, especially in screening disease and often for making specific diagnoses.

The consideration of benefit versus risk in any test becomes far more important in paediatrics where the possibility of biological damage secondary to a nuclear medicine procedure is a possibility. Therefore, the paediatrician requesting the study and a nuclear medicine physician should assure themselves that a reasonable probability exists that the anticipated benefit from their examination will exceed the potential risk to the patient. As a first step in this decision-making process, it is essential that the nuclear medicine physician clearly understands the problem that the clinician wishes to have solved. Quite frequently the clinician doesn't have a clear idea of the problem that he wishes to have solved in the first place. A discussion can usually clarify the expected result from the test that is to be performed. In some patients more than one test may be in order such as a bone scan followed by a Gallium scan in a patient suspected of having osteomyelitis. The nuclear medicine physician should consider himself a consultant not only a service person. It is not necessary that there be a guarantee that the test will yield a "positive" result but only that the test will achieve clearer understanding of the disease process being studied. As a corollary to this, nuclear medicine should never be used as a screening procedure for healthy populations or even for routine use in certain diseases unless it can be known that its use has a reasonable probability of yielding significant decision-making clinical information.

A very important factor in performing nuclear medicine studies in paediatrics is to obtain diagnostic images. One could reduce the radioactive tracer administered to the patient to a negligible radiation dose but the diagnostic information may become negligible. Paediatric nuclear medicine departments have designed a variety of methods of determining the optimum radiopharmaceutical dose to be administered to the patient (1). By thus scaling the dose we maintain a relatively constant image quality which is excellent and satisfactory for interpretation. Although the radiation dose to the newborn for the appropriate amount of radiopharmaceutical is higher than in the older child, its value is considered to be less than that of a comparable diagnostic radiology examination. A minimum dose, however, is necessary to produce the proper images.

It is very useful to have a list available of potential radiation doses for the different procedures and for the different pharmaceuticals. One of the best descriptions is in Protection in Nuclear Medicine and Ultrasound Diagnostic Procedures in Children (Tables 1 through 9)(2).

The value of having a proper schema for administering radioactive materials to children cannot be underestimated. A review of administered radioactivity to children in a group of U.S. hospitals which were not primarily paediatric, showed that there was a very large variation in the amount of radioactivity given to a child at a certain age and weight as well as an inconsistency in any one institution in the method for determining the amount of radioactivity to administer (3). For this reason I would urge anybody doing these studies to follow a standard procedure such as the one illustrated in the Paediatric

Atlas of Nuclear Medicine (1). This is just one example, but the important thing is not whether you follow this particular method but have a valid method for estimating dose rather than by guesswork.

The other aspect of doing these studies which is very important to reduce the potential radiation doses is to obtain quality images so that repeat studies with re-administration of the tracer are not necessary. To this end, one must have good quality imaging equipment where one uses the appropriate choice of collimator sensitivity and resolution to obtain the diagnostic information that is necessary. Motion, which can be a distinct problem, should be avoided by either sedation or mild restraint or a combination of both. Severe restraint usually results, especially with the younger children, in their wiggling and fighting against the restraint. The sedation that we feel is the best is Nembutal intramuscularly given one half hour before the study is to be performed at a dose of 6 mg. per kg. to a value of 60 mg. and above that at 5 mg./kg. until a dose of 100 mg. is reached. It is essential to administer this intramuscularly so that the sedating effect is known exactly.

Nuclear medicine in the evaluation of paediatric disease has become a front-runner in the diagnostic armamentarium. The adjunct of SPECT and newer radiopharmaceuticals such as technetium-^{99m}-hexamethyl-propyleneamine oxine for cerebral perfusion studies has meant that it will become even more commonly used. Therefore, it is extremely important to consider all of the factors considered in this article in attempting to determine the best approach with the maximum diagnostic information for the least amount of radiation to the child. When this is done, one not only has a happy child because he has been examined carefully and treated well, but also the referring physicians have the appropriate information to best assess their patients' disease and results of therapy.

REFERENCES

1. Alderson, P., Gilday, D., and Wagner, R. *Atlas of pediatric nuclear medicine*. Mosby, December 1978.
2. Protection in nuclear medicine and ultrasound diagnostic procedures in children. NCRP Report No. 73, issued December 30, 1983.
3. Goetz, W.A., Hendee W.R., and Gilday, D.L. In vivo diagnostic nuclear medicine. Pediatric experience. Cl. Nuc. Med. Vol.8, No.9, 434-439, 1983.

DISCUSSION

DONG: Have you found any measurable effects of sedatives and anesthetics on the distribution of radiopharmaceuticals?

MILDAY: We don't use anesthetics. We use Nembutal which doesn't affect distribution the same way an anesthetic would. I think there is a significant difference. We've been very fortunate that in 15 years we've only had to use the general anesthetic to do a study and that was to do a CSF injection. The imaging actually took place 4 and 24 hours later when any anesthetic effect might have worn off. Nembutal is a fairly well-known sedative. Although we haven't quantitated uptake after Nembutal administrations in a large number of studies, it doesn't appear to change the distribution of a tracer.

A lot of the time, the study of acute dynamic processes doesn't require sedation; it's more often needed for longer studies such as total-body imaging. By the time you administer the sedation for these studies, the tracer is already where you want it to be. The shorter term studies where an effect might be seen usually don't require the same degree of anesthetic or sedative.

DONG: Can you use any other kind of sedative like chloral hydrate?

MILDAY: Yes, actually, you have a variety of alternatives. One difficulty is that if you give chloral hydrate, or if you give Nembutal as a suppository, it's amazing what that anal sphincter reflex does to get rid of the suppository. As the saying goes, you're up the creek without a paddle because you cannot re-administer. You don't know how much has been absorbed. With intramuscular Nembutal you know exactly how much was administered, so if you do need to re-sedate, you can because you know exactly what was absorbed by the patient. Another advantage of giving injections of something like Nembutal is that it is a very safe drug; it has very few reactions. In our hospital, the consensus of the anesthetists is that other sedatives are used only when the patient is allergic to Nembutal, which fortunately is very rare.

DONG: I think this is an important issue not only for clinical nuclear medicine but for research in nuclear medicine as well. We have been trying some new anesthetics at Hopkins that are similar, such as Brevital, when we do kinetic studies over a two-hour period. Some of our anesthesiologists are looking at effects on blood flow in sheep models and I think it's a very important issue.

MILDAY: I think you are absolutely right. If you are using something which is being administered during some period of time when there is a dynamic change, you must know whether the anesthesia is going to have an impact. As I said, most of the time when we use Nembutal or something like that, we are studying something which is not changing significantly with time during that period, but that's a very good point.

MERS: Is the rationale behind administering more activity than predicted to smaller patients simply on a weight-to-weight calculation based on the information density in the smaller images? Thus, the activity would follow a $\sqrt{W_1/W_2}$ law.

MILDAY: It is based on information density.

MERS: The liver will appear small.

MILDAY: That is a good point. I hadn't thought of bringing it out that way. I originally developed our technique from crude methods of determining information density. In 1972, we had a Picker Dyna camera which allowed us to

assign a region of interest to determine when a certain information density occurred. For example, we targeted a liver scan and reached our information density in four minutes. We then used that value to determine what the activity was in the patient's liver. Although I agree there may be differences from organ to organ, we used that as our model for developing a graph to determine how much activity to administer. Our technique has been modified slightly, but that is basically how we did it originally.

SAENGER: Dave, I didn't quite understand you. You said something about the risk of 10⁻³ as being unacceptable.

GILDAY: What I said was that in areas outside of pure medicine, that is, in the public health domain, a risk of one in ten thousand is an unacceptable risk to incur for routine testing or evaluations. I would agree that a risk of one in ten thousand is insignificant if you have carcinoma of the liver. That is quite different from a checkup or a chest x-ray or even if you have pain in the abdomen and you are having a study to evaluate that. I was speaking of the area of preventive medicine where a risk of one in ten thousand from a test is considered to be unacceptable.

SAENGER: For example, ICRP says that you have a risk of 10⁻⁴ per rem per year. Is it justified to characterize a risk of 1 in 10,000 as unacceptable in the use of radiation in individuals who are sick?

GILDAY: Gene, I got that data at a medicolegal conference a week ago. It was their consensus based on evaluations of different risks. A risk of one in 1,000,000 for a particular procedure or study does not require informed consent. A risk of one in 100,000 or less is the type where you have to get informed consent from the patient. Now this is in Ontario where we are under Canadian laws, not in the states; but I suspect that since our medical jurisprudence in the area of malpractice is behind the U.S., it's probably not that dissimilar. A risk of one in 10,000 would be considered to be a risk that would not be acceptable at the minimum informed consent level. Below that it really gets to be dicey, whether it's worth doing or not. You would really have to look at the risk-benefits.

SAENGER: I think that in the practice of medicine, generally, be it radiation or not, if we start applying criteria like that we're really going to have to see some consistent and worthwhile data to support what you are advocating.

HERSCOVITCH: Positron emission tomography is now being used to do clinical research studies in the pediatric population. Would you comment on exposing pediatric patients to ionizing radiation for a clinical research study when the patient may not specifically benefit from the study and also on the appropriateness of the recommended FDA guidelines for exposure of pediatric patients in clinical research programs using radiopharmaceuticals?

GILDAY: I'm not sure what the FDA guidelines are but I'll tell you what mine are--it's very simple. I look at the situation and ask if I would want my child to have that particular research study done and the answer to that is no. In our hospital we are not allowed to administer any form of ionizing radiation to a healthy child who has no disease. By the way, this is a very frustrating problem if you apply for research grants or submit any publications that involve a pediatric population because everybody always wants to know what your normal control group is and you just can't develop one. All our normal control groups have been highly coincidental. For example, we may study a patient who has cystic fibrosis, looking for the amount of strain on the left side of the heart under certain circumstances. If the patient has proven over a period of 2 or 3 years to have no sign of any abnormality with the heart, we are able to move that patient's study into a quasinormal category. I abide by our

stringent guidelines and I believe in them: A totally normal child should not suffer ionizing radiation, not because I believe it is going to cause anything, but because there should be no risk without benefit.

ABEL: The FDA is certainly a complex institution, one that I fail to understand at certain times, but as far as a guideline for giving the patient a dose, it's strictly a risk-benefit decision. I don't see how you can have any other guideline.

It's disturbing when we have to approve a drug without any pediatric dosage information in the package insert. I'm afraid that is one reason why the medical community often utilizes some other technique in the pediatric population. Some members of the FDA Radiopharmaceutical Advisory Committee are working diligently to provide us with dosage information for the pediatric population. Hopefully in the near future, pediatric dosage information for many of the approved radiopharmaceuticals will be available; however, if you are going to submit a study on an IND, the dosage would be determined by what you are trying to do, what the benefit is, and many other factors but the FDA assigns no upper or lower limit.

DOHERTY: If, as sometimes occurs, you need to give a patient a little bit higher dose than you would normally give under the guidelines, would it pop into your mind that a greater risk is involved? Would you then have to inform the parents of this child that the child is undergoing some risk? What do you define as the risk and how do you explain the risk to the parent? Is there a level above the normal dosage that you would go, say, 3, 4, or 5 times above? What is your cut-off and what risk have you incurred?

GILDAY: I'm not quite sure I understand the problem, and why we would have to increase the activity. Our administered doses are determined from two factors: 1) the amount of radiation the patient receives and 2) what is considered to be an acceptable level with no discernible risks associated with it. In only one very specific situation have we had to increase the administered activity beyond that. That is the liver scan for trauma where we do from time to time have to increase the dose by 50% because we are trying to get a flow study and the amount of technetium sulfur colloid that we normally would administer will not permit it. In that case, I don't think there is any significant change in the risk and do not consider it necessary to discuss with the parents that there is any change or any increase in risks. The risk from radiation is insignificant compared to the risk of missing a laceration of a vessel, the laceration of a kidney, the laceration of an artery, or trauma to the liver and the spleen. The risk of a blood transfusion, which is the method of treatment for a hepatic or splenic trauma if it does occur, or the risk of anesthesia in an operation, is far higher than the indiscernible risk of doing a radionuclide study. In our hospital and in most children's hospitals, this is a study that does not require informed consent.

MARCUS: It amazes me how people get upset over raising the dose 50% or even doubling it and don't worry in the least about repeating the study a few days later if it is appropriate. I think what people have to understand is that generally speaking the absorbed doses that are generated in nuclear medicine are small, and nobody has the faintest idea what they could possibly cause. It's not a matter of telling the parents this is the risk that your child will develop leukemia in the next five years. Anyone here who gives out research money knows that, no matter how much is spent, you can't get data on low-level radiation effects although people sit around making up probability of causation tables that are based on very little data at the low dose level. I am going to talk tomorrow about some circumstances in which we give rather large doses. The kidney in certain disease states receives up to several hundred rads. Till the diseases themselves are often life-threatening. We don't even know

what happens if we give a kidney 200 rad over a period of 2 months, because it is a very radioresistant organ. Perhaps we shouldn't get too worried about a little extra radiation. I don't believe anyone in nuclear medicine sits down with parents and tells them that their child is at increased risk.

GILDAY: I think you just echoed my point exactly, Dr. Marcus. We don't consider it a risk, but we have to allay fears rather than determine whether it's a 1 in 10,000 or 1 in 10,000,000 risk. It's a fact that it's an insignificant risk compared to the problem we are studying or else we wouldn't be doing the study.

SPECIFIC ABSORBED FRACTIONS AND S-FACTORS FOR CALCULATING
ABSORBED DOSE TO EMBRYO AND FETUS

U.Elsasser¹⁾, K.Henrichs²⁾, A.Kaul¹⁾, A.R.Reddy³⁾, H.D.Roedler¹⁾

- 1) Institute for Radiation Hygiene, Federal Health Office, Neuherberg/München, FRG
- 2) Institute for Radiation Protection, GSF, Neuherberg/München, FRG
- 3) Defense Laboratory, Jodhpur, India

ABSTRACT

The variation of specific absorbed fractions from maternal tissues to embryo/fetus is investigated for four different target masses and geometries. S-factors are calculated for selected radionuclides assumed to be distributed uniformly in fetal tissues represented by spheres from 1 mg to 4 kg. As an example, the dose to fetal tissues for iodine-131 and iron-59 is estimated based on human biokinetic data for various stages of pregnancy.

INTRODUCTION

The calculation of absorbed dose to embryo or fetus from administered radiopharmaceuticals requires knowledge of radionuclide biokinetics and the absorbed dose per unit cumulated activity in maternal source organs and in embryo or fetus.

Based on an anthropomorphic standard phantom (mass $m = 70$ kg), Smith and Warner (1) calculated S-factors for a sphere located in the center of the uterus with a radius of $r = 0.13$ cm and a mass $m = 9.2$ mg. This sphere is taken as an embryo model 10 - 14 days after conception.

Cloutier et al. (2) calculated specific absorbed fractions for the uterus as a target organ, based on an anthropomorphic phantom of mass $m = 58$ kg, to be used for calculating the dose to a fetus up to 3 months of age.

It is the purpose of this paper to investigate the age- and mass-dependence of fetal dose resulting from activity in maternal source organs. Additionally, for selected radionuclides, S-factors are derived for estimating the self-dose to organs or total body of the fetus.

As an example, the dose to fetal tissues for iodine-131 and iron-59 is estimated based on human biokinetic data for various stages of pregnancy.

METHODS

The dose to embryo or fetus is calculated by the formalism used by the Medical International Radiation Dose Committee of the Society of Nuclear Medicine (3).

The mean absorbed dose \bar{D} in a target region r_k is

$$\begin{aligned}\bar{D}(r_k \leftarrow r_h) &= \tilde{A}_h \sum_i \Delta_i \phi_i(r_k \leftarrow r_h) \\ &= \tilde{A}_h S(r_k \leftarrow r_h)\end{aligned}$$

where

$D(r_k \leftarrow r_h)$	mean absorbed dose in r_k
\tilde{A}_h	cumulated activity in source-region r_h
i	index for type and energy of radiation
Δ_i	equilibrium dose constant
$\phi_i(r_k \leftarrow r_h)$	specific absorbed fraction
$S(r_k \leftarrow r_h)$	mean dose in r_k per unit cumulated activity in r_h .

The dose to embryo or fetus results from the activity in the maternal source-organs and/or the activity in embryo or fetus itself, if the placental activity is neglected.

SPECIFIC ABSORBED FRACTIONS TO EMBRYO OR FETUS FROM ACTIVITY IN MATERNAL ORGANS

For estimating the dose to embryo or fetus from activity in maternal organs, specific absorbed fractions were calculated for the following target regions:

- total uterus,
- sphere ($m = 100$ g) located in the center of the uterus,
- sphere ($m = 1$ g) located in the center of the uterus,
- sphere ($m = 1$ g) located at the anterior pole of an ellipsoid representing the uterus.

The calculations were based on the specific absorbed fractions published by Berger (4) for isotropically emitting point sources. The integration over the source- and target-volumes was done by Monte-Carlo-methods for the phantom of 15 year old child ($m = 54.5$ kg) described by Cristy (5). A displacement of maternal organs due to fetal growth was not taken into consideration.

For photon energies above 50 keV the statistical errors could be limited to approximately 30 %; for lower energies, the statistical errors were within range of 50 to 100 %. In view of these uncertainties, the results did not differ significantly for the four different target regions.

In the following dose calculations, specific absorbed fractions for the uterus as a target were used.

S-FACTORS FOR SELF-IRRADIATION OF EMBRYO OR FETUS

It is assumed that embryo or fetus may be represented by spheres of radius r and density $\rho = 1 \text{ g/cm}^3$. Radius r depends on mass m of embryo or fetus according to:

$$r = \left(\frac{3m}{4\pi} \right)^{1/3}$$

For calculating absorbed fractions $\phi(r, E_i)$ for monoenergetic electrons, according to Berger (6) the following equation may be used, as based on the values of the scaled point kernel $F(\xi, E_i)$ tabulated by Berger (6):

$$\phi(r, E_i) = \int_0^d \left(1 - \frac{3}{2} \frac{x}{d} + \frac{1}{2} \left(\frac{x}{d} \right)^3 \right) \cdot F\left(\frac{x}{r_o}, E_i\right) dx$$

where

$$F(x/r_o, E_i) = 4\pi\rho x^2 \Phi(x, E_i) \quad \text{and } d = 2r$$

For β -electrons, the absorbed fractions are given by

$$\phi_\beta(r) = \int_0^d \left(1 - \frac{3}{2} \frac{x}{d} + \frac{1}{2} \left(\frac{x}{d} \right)^3 \right) \cdot F_\beta\left(\frac{x}{x_{90}}, E_i\right) dx$$

Values of $F_\beta(x/x_{90})$ for various radionuclides were published by Berger (7).

For photons, the absorbed fractions were calculated depending on mass m of embryo or fetus and photon energy E as follows:

- for $1 \leq m \leq 4000 \text{ g}$ and $30 \text{ keV} \leq E \leq 2750 \text{ keV}$, the values tabulated by Ellett (8) were used;
- for $1 \leq m \leq 4000 \text{ g}$ and $E < 30 \text{ keV}$ or $E > 2750 \text{ keV}$, the relation

$$\phi = \begin{cases} 1 - \frac{3}{8} \frac{s_m}{r} + \frac{1}{64} \left(\frac{s_m}{r} \right)^3 & s_m \leq 2r \\ .75 \frac{r}{s_m} & s_m > 2r \end{cases}$$

was used, where

$$S_m = 1.44 / \mu_{en}$$

μ_{en} energy absorption coefficient
r radius;

- for $m < 1$ g and $E \geq 50$ keV the above formula was used;
- for $m < 1$ g and $E < 50$ keV the absorbed fractions tabulated by Mehta (9) were adopted.

RESULTS

Table 1 shows S-factors for selected radionuclides used in clinical nuclear medicine.

FETAL RADIATION DOSE FROM IODINE-131

BIOKINETIC DATA

Activity concentration in the thyroid

For maternal iodine metabolism, the metabolic data for the adult reference man were used as given in ICRP Publication 30 (10):

"Of iodine entering the transfer compartment a fraction, 0.3, is assumed to be translocated to the thyroid while the remainder is assumed to go directly to excretion. Iodine in the thyroid is assumed to be retained with a biological half-life of 120 d and to be lost from the gland in the form of organic iodine. Organic iodine is assumed to be uniformly distributed among all organs and tissues of the body other than the thyroid and to be retained there with a biological half-life of 12 d. One-tenth of this organic iodine is assumed to go directly to faecal excretion and the rest is assumed to be returned to the transfer compartment as inorganic iodine."

For embryo or fetus up to week 12, it is assumed that the activity concentration is equal to that in the maternal body. Approximately from week 12 on, a selective accumulation of radioiodine in the fetal thyroid has been demonstrated. Published data are available on measurements of iodine-131 activity in the thyroid after diagnostic administration of iodine-131 approximately 24 h prior to therapeutic abortions, as well as from fallout after nuclear explosions. These data are summarized in Table 2. The uptake values for the maternal thyroid refer to 24 h after administration, if not stated otherwise. This also applies to most uptake values of the fetal thyroid. Therefore, all ratios of fetal and maternal activity concentrations may be regarded as 24 h values.

The fetal thyroid masses in Table 2 were extracted from the respective publications, or derived from a curve fit of fetal thyroid masses and are included in brackets. A number of 135 fetal thyroid masses as taken from Aboul Khair et al. (11), Beierwaltes et al. (12), Costa et al. (13), Eisenbud

Table 1: S-factors for self-irradiation of embryo or fetus represented by spheres of unit density and mass as indicated

mass (g)	⁵⁹ Fe		^{99m} Tc		¹¹¹ In		¹²³ I		¹³¹ I		²⁰¹ Tl		
	$\frac{\text{rad}}{\mu\text{Ci}\cdot\text{h}}$	$\frac{\text{Gy}}{\text{MBq}\cdot\text{h}}$											
159	0.001	71.4	19.3	3.8	1.0	6.6	1.8	4.8	1.3	92.5	25	6.8	1.8
	0.01	12.5	3.4	0.77	0.21	1.6	0.42	1.2	0.31	16.8	4.5	1.7	0.45
	0.1	2.0	0.54	0.21	0.056	0.45	0.12	0.34	0.092	2.9	0.78	0.51	0.14
	0.2	1.1	0.30	0.14	0.039	0.31	0.084	0.24	0.065	1.7	0.36	0.36	0.097
	0.4	0.62	0.17	0.087	0.024	0.19	0.051	0.15	0.039	0.93	0.25	0.22	0.058
	0.8	0.34	0.09	0.045	0.012	0.099	0.027	0.076	0.020	0.50	0.14	0.11	0.030
	1.0	0.28	0.075	0.037	0.0099	0.080	0.022	0.061	0.016	0.41	0.1	0.090	0.024
	2.0	0.14	0.039	0.019	0.0050	0.043	0.011	0.031	0.0083	0.21	0.057	0.045	0.012
	8.0	0.038	0.010	0.0050	0.0013	0.011	0.0030	0.0081	0.0022	0.053	0.014	0.011	0.0031
	10.0	0.031	0.0084	0.0040	0.0011	0.0091	0.0025	0.0065	0.0018	0.043	0.012	0.0090	0.0024
	100.0	0.0042	0.0011	$5.2 \cdot 10^{-4}$	$1.4 \cdot 10^{-4}$	0.0013	$3.5 \cdot 10^{-4}$	$7.9 \cdot 10^{-4}$	$2.1 \cdot 10^{-4}$	0.0047	0.0013	$9.2 \cdot 10^{-4}$	$2.5 \cdot 10^{-4}$
	1000.0	$6.0 \cdot 10^{-4}$	$1.6 \cdot 10^{-4}$	$7.6 \cdot 10^{-5}$	$2.0 \cdot 10^{-5}$	$2.0 \cdot 10^{-4}$	$5.3 \cdot 10^{-5}$	$1.9 \cdot 10^{-4}$	$2.9 \cdot 10^{-5}$	$5.3 \cdot 10^{-4}$	$1.4 \cdot 10^{-4}$	$9.6 \cdot 10^{-5}$	$2.6 \cdot 10^{-5}$
	2000.0	$3.4 \cdot 10^{-4}$	$9.1 \cdot 10^{-5}$	$4.3 \cdot 10^{-5}$	$1.2 \cdot 10^{-5}$	$1.1 \cdot 10^{-4}$	$3.1 \cdot 10^{-5}$	$5.9 \cdot 10^{-5}$	$1.6 \cdot 10^{-5}$	$2.8 \cdot 10^{-4}$	$7.5 \cdot 10^{-5}$	$4.9 \cdot 10^{-5}$	$1.3 \cdot 10^{-5}$
	4000.0	$1.9 \cdot 10^{-4}$	$5.2 \cdot 10^{-5}$	$2.5 \cdot 10^{-5}$	$6.8 \cdot 10^{-6}$	$6.7 \cdot 10^{-5}$	$1.8 \cdot 10^{-5}$	$3.3 \cdot 10^{-5}$	$9.0 \cdot 10^{-6}$	$1.5 \cdot 10^{-4}$	$4.0 \cdot 10^{-5}$	$2.5 \cdot 10^{-5}$	$6.8 \cdot 10^{-6}$

Table 2: Fetal to maternal activity concentration ratios C_F/C_M in the thyroid after single intake of iodine-131. All uptake data refer to 24 hrs, if not stated otherwise (see remark 4).

Fetal age (weeks)	Uptake(%)		Fet.thyr. mass(mg)	Act.conc.(%/g)		C_F/C_M	class 3)	Authors and adm.act. (μCi)
	Fetus 1)	mother 1)	2)	Fetus 1)	mother 1)			
13	0.01	38	5	2.0	1.9	1.05	1	T.C.Evans et al.
13	0.034	29	8	4.25	1.45	2.93	1	(15)
13	0.03	30	7	4.3	1.5	2.87	1	
14	0.03	-	15	2.0	1.5	1.33	2	
14	0.03	26	20	1.5	1.3	1.15	1	Usually
15	0.03	35	41	0.73	1.75	0.42	1	100 μCi
15	0.04	-	23	1.74	1.5	1.16	2	a few cases
15	0.04	30	45	0.90	1.5	0.60	1	with 500 μCi
15	0.025	-	58	0.43	1.5	0.29	2	
20	0.3	-	150	2.0	1.5	1.33	2	
21	0.24	-	187	1.28	1.5	0.85	2	
21	0.22	-	78	2.82	1.5	1.88	2	
22	0.8	61 4)	96	8.33	1.5	5.55	2	
23	1.1	-	220	5.0	1.5	3.33	2	
23	0.6	-	200	3.0	1.5	2.0	2	
24	1.5	41	225	6.67	2.05	3.25	1	
38*	1.3	19	944	1.38	0.95	1.45	1	
38*	3.0	-	1500	2.0	1.5	1.33	2	
13	0.15	26	(15)	10	1.3	7.7	2	R.E.Hedges et al. (20)
15	0.10	30	(40)	2.5	1.5	1.67	2	
15	0.40	-	(40)	10	1.5	6.67	3	500 μCi i.v.
15	5)	-	5)	0.80	1.5	0.53	2	S.A.Aboul
18	-	-	-	2.7	1.5	1.8	2	Khair et al.
19	-	-	-	1.5	1.5	1.0	2	(11)
19	-	-	-	0.96	1.5	0.64	2	20-40 μCi i.v.
14	0.088		(30)	2.93	1.5	1.95	3	L.Lampe .
14	0.014		(30)	0.47	1.5	0.31	3	et al.
14	0.094		(30)	3.13	1.5	2.09	3	(21)
16	1.33		(80)	16.7	1.5	11.1	3	30-40 μCi
17	1.21		(100)	12.1	1.5	8.1	3	oral
19	2.08		(150)	13.9	1.5	9.3	3	
23	1.02		(220)	4.64	1.5	3.1	3	
15	0.45	-	213	2.1	1.5	1.4	2	A. Costa et al. (13)
16	0.51	-	171	2.9	1.5	1.93	2	
17	0.8	-	133	1.5	4.0	2		
22	0.33	-	206	1.6	1.5	1.07	2	No inform.
26	5.68	-	511	11.1	1.5	7.4	2	on adm.
28	5.80	-	646	9.0	1.5	6.0	2	dose
16	-	-	-	0.12	1.5	0.08	3	E.M.Chap-
20	5)	-	5)	0.11	1.5	0.08	3	man et al.
32	-	-	-	4.83	1.5	3.22	3	(22)
								No inform.
								on adm.dose

Table 2 (continued)

Fetal age (weeks)	Fetus	Uptake(%) mother 1)	Fet.thyr. mass(mg) 2)	Act.conc.(%/g) Fetus mother 1)	C_F/C_M	class 3)	Authors and adm.act. (μ Ci)
13		-		2.13	1.42	2	
14	5)	-	5)	1.88	1.25	2	N.C.Dyer et al.(19)
14.5		-		3.11	2.07	2	
15		-		1.40	1.5	0.93	2
15		-		2.25	1.5	2.25	50 μ Ci oral
16		-		3.37	2.25	2	
20		-		6.50	4.33	2	
22		-		6.14	4.09	2	
26					2.5	2	P.Czerniak et al.(23) 6) no inform. on adm.dose

Remarks

- 1) Whenever the maternal uptake was not explicitly stated, a 30% uptake was assumed. For a thyroid mass of 20 g, this results in an activity concentration of 1.5%/g.
- 2) The fetal thyroid masses in brackets are those from the fit $m(t) = at^b$, $a = 3.72$; $b = 1.62$.
- 3) A definition of classes is given in the text.
- 4) Maternal uptake 96 hours post administration.
- 5) Fetal uptake and mass were measured, but not given in the publication.
- 6) Written in Hebrew. Not clear to the non-Hebrew reader whether maternal uptake, fetal weight and uptake are contained in the text.

Table 3: Fetal to maternal activity concentration ratios C_F/C_M after continuous intake of iodine-131

Fetal age (weeks)	Fetal thyroid mass (g)	Activity conc. in thyroid of fetus	of mother	C_F/C_M	Authors
26	0.21	4 100 *	3 300 *	1.3	M. Eisenbud et al. (14)
30	0.47	15	8.5	1.7	
30	0.64	13	1.6	8.2	
34	0.98	7.7	4.3	1.8	
38	2.5	4.2	27	1.6	
21	-	1.08	0.82	1.3	W.H.Beierwaltes et al. (12)

* I-131-albumin administered to the mother

al. (14), Evans et al. (15) were fitted as follows:

$$m(t) = at^b \quad (1)$$

$$m(t) = A(e^{Bt} - 1) \quad (2)$$

m fetal thyroid mass (mg)

t time (weeks)

a,b,A,B fit coefficients

Both functions are a suitable fit for $t = T - 10.5$ where T represents the week of pregnancy. The best estimates for the coefficients are

$$\begin{array}{lll} a & = & 3.72 \\ A & = & 26.5 \end{array} \quad \begin{array}{lll} b & = & 1.62 \\ B & = & 0.138 \end{array}$$

with correlation coefficients of

$$\begin{array}{ll} r^2 & = 0.82 \text{ for (1) and} \\ r^2 & = 0.73 \text{ for (2).} \end{array}$$

The fetal thyroid masses in brackets given in Table 2 are based on equation 1.

The ratios of activity concentrations in fetal and maternal thyroids C_F/C_M given in Table 2 are classified depending on the number of parameters measured. The parameters needed for calculating the ratios of activity concentrations are

- a) uptake of fetal thyroid
- b) mass of fetal thyroid
- c) uptake of maternal thyroid
- d) mass of maternal thyroid.

The classes were defined as follows:

class 1: a, b and c measured;

class 2: a and b measured;

class 3: a measured only.

These classes are indicated in the respective column of Table 2.

The mean values of activity concentration ratios in fetal and maternal thyroids are

- 1.68 (class 1, 8 cases)
- 2.36 (class 2, 31 cases)
- 4.17 (class 3, 11 cases)

Maternal thyroid mass was assumed to be 20 g (16). If no maternal uptake was stated, a value of 30% was assumed (10).

Table 3 summarizes activity concentration ratios C_F/C_M after continuous intake of iodine-131 from fallout. With one exception, these values do not differ significantly from those for single administration in Table 2. A publication of Beierwaltes et al. (17), containing data from 25 fetuses and a group of adults, was not included in Table 3 because the fetuses did not originate from the adults measured.

The following dose estimates are based on a mean value of C_F/C_M of 1.7 derived from measurements of a, b and c. The use of the remaining values, for which two or three out of four parameters had to be approximated by standard values, did not appear suitable for the present absorbed dose estimates.

Half-lives

The biological half-life of iodine in the thyroid is age-dependent. It measures approximately 120 d in adults (10) and only 15 d in newborns (18). An even shorter half-life during the fetal period is substantiated by measurements from Aboul Khair et al. (11). A re-evaluation of his data (radioiodine-tests 3 hours up to 6 days prior to therapeutic abortions) results in a mean half-life of 2.7 days for a mean fetal age of 17 weeks, without considering the low values for week 12 and 13. Due to the lack of additional data, a linear increase of the biological half-life of iodine in the thyroid is assumed to be from 2.7 days during week 17 up to 15 days at birth.

The decrease of fetal activity concentration due not only to physical decay and biological elimination but also to thyroid growth must be considered. The doubling time of the fetal thyroid mass according to equation 2 is approximately 5 weeks. Thus, a growth-corrected effective half-life of iodine-131 concentration in the fetal thyroid is used as of 1.9 days at week 17, and 4.6 days at birth.

ABSORBED DOSES

Based on the biokinetic data stated above, the cumulated activities and doses are:

- Total dose to embryo or fetus up to the 12th week:

$$A_{RB} = 12.9 \mu\text{Ci h}$$
$$D_{RB} = 12.9 \mu\text{Ci h} \cdot 1.1 \cdot 10^{-5} \text{ rad } \mu\text{Ci}^{-1} \text{ h}^{-1} = 0.14 \text{ mrad}/\mu\text{Ci} (0.038 \text{ mGy/MBq})$$

- Fetal thyroid dose at week 17

$$\tilde{A} = 1.44 \cdot 0.002 \cdot 45.6 \text{ h} \cdot 1 \mu\text{Ci} = 0.131 \mu\text{Ci h}$$
$$D = 0.131 \mu\text{Ci h} \cdot 3.56 \text{ rad } \mu\text{Ci}^{-1} \text{ h}^{-1} = 468 \text{ mrad}/\mu\text{Ci} (126 \text{ mGy/MBq})$$

- Fetal thyroid dose during final period of pregnancy

$$A = 1.44 \cdot 0.019 \cdot 110.4 \text{ h} \cdot 1 \mu\text{Ci} = 3.02 \mu\text{Ci h}$$
$$D = 3.02 \mu\text{Ci h} \cdot 0.539 \text{ rad } \mu\text{Ci}^{-1} \text{ h}^{-1} = 1.63 \text{ rad}/\mu\text{Ci} (440 \text{ mGy/MBq})$$

FETAL RADIATION DOSE FROM IRON 59

BIOKINETIC DATA

In this study biokinetic data for the healthy adult from the MIRD dose estimate report No. 11 (24) were adopted. Absorbed dose calculations for the fetus are based on the data published by Dyer and Brill (19) for fetal liver-uptake and fetal liver mass.

The available data, however, refer only to weeks 9 to 22 of pregnancy. During this period, the fetal erythropoiesis has to be attributed essentially to

the liver. For absorbed dose calculation it is assumed that approximately 12% of the fetal liver activity enters the storage compartment of the liver ($T_{eff} = 45$ d) and the remainder goes to the erythropoiesis compartment of the liver ($T_{eff} = 2.6$ d). From the data reported by Dyer and Brill (19), a doubling time of fetal liver mass of approximately two weeks may be derived and is again considered in calculating the growth-corrected effective half-life of iron concentration in the fetal liver ($1/45 + 1/14 = 1/10.7$). By adding both half-life components, an effective growth corrected half-life of 3.2 d is derived.

ABSORBED DOSES

The external dose to the uterus or to the fetal liver is $D = 1080 \mu\text{Ci} h^{-5} \cdot 3.44 \cdot 10^{-5} \text{ rad } \mu\text{Ci}^{-1} h^{-1} = 37 \text{ mrad}/\mu\text{Ci}$ (10 mGy/MBq). The age dependence of fetal liver dose is summarized in Table 4.

Table 4: Fetal liver dose for various ages

Age (weeks)	Fetal liver mass (g)	Fetal liver uptake (%)	S-factor ($\frac{\text{rad}}{\mu\text{Ci} \cdot \text{h}}$)	$\frac{\text{mrad}}{\mu\text{Ci}}$	$\frac{\text{mGy}}{\text{MBq}}$
9	0.15	0.074	1.16	95	26
11	0.54	0.171	0.49	92	25
11	0.36	0.101	0.72	80	22
13	1.2	0.514	0.23	144	39
14	2.5	0.665	0.13	93	25
14	2.2	0.713	0.14	107	29
14.5	4.5	0.779	0.068	59	16
15	3.6	0.681	0.088	66	18
15	4.0	0.822	0.074	67	18
16	5.6	0.642	0.055	39	11
20	9.3	1.66	0.032	63	17
22	15.1	2.26	0.023	60	16

SUMMARY AND CONCLUSIONS

Specific absorbed fractions from maternal organs to embryo/fetus represented by spheres of 1 g (central and anterior pole location) and 100 g do not differ significantly from those calculated for the total uterus as a target, if the statistical uncertainties due to the Monte Carlo calculations are taken into account.

S-factors for self-irradiation of embryo/fetus have been calculated and are tabulated for selected radionuclides used in clinical medicine.

Human fetal biokinetic data for iodine-131 and iron-59 were derived from published data for absorbed dose calculation.

Embryonal/fetal total body dose from iodine-131 up to the 12th week is approximately 150 mrad/ μ Ci (41 mGy/MBq); fetal thyroid dose varies from 0 mrad/ μ Ci (130 mGy/MBq) at week 17 to 1600 mrad/ μ Ci (440 mGy/MBq) during final period of pregnancy as compared to a maternal thyroid dose of approximately 1600 mrad/ μ Ci (440 mGy/MBq). These results are based on maternal thyroid take values of approximately 30 %.

Fetal liver dose from iron-59 during weeks 9 - 22 is approximately mrad/ μ Ci (22 mGy/MBq) as compared to maternal liver doses of approximately mrad/ μ Ci (12 mGy/MBq).

Biokinetic data from the human fetus are not available for further radiopharmaceuticals, and it is unlikely that such data could be measured in future the same manner as 15 years ago for iodine-131 and iron-59.

acknowledgements

This work was supported by the Ministry of the Interior of the Federal Republic of Germany (FV St.Sch. 972a). Thanks are due to Mrs. R. LeMar for assisting in the translation and to Mrs. I. Zeitlberger for typing the manuscript.

REFERENCES

Smith EM, GG Warner. Estimates of radiation dose to the embryo from nuclear medicine procedures. J.Nucl.Med. 17, 836-839, 1976

Cloutier RJ, EE Watson, WS Snyder. Dose to the fetus during the first three months from gamma sources in maternal organs, in: Radiopharmaceutical Dosimetry Symposium, edited by RJ Cloutier, JL Coffey, WS Snyder, EE Watson, pp. 370-375, HEW Publication (FDA) 76-8044, Bureau of Radiological Health, Rockville, Maryland 208057, 1976

Loevinger R, M Berman. A revised scheme for calculating the absorbed dose from biologically distributed radionuclides, MIRD Pamphlet No. 1 Revised, Society of Nuclear Medicine, New York, 1976

Berger MJ. Energy deposition in water by photons from point isotropic sources. MIRD Pamphlet No. 2, J.Nucl.Med. 9, suppl. 1, 1968

Cristy M. Mathematical phantoms representing children of various ages for use in estimates of internal dose, ORNL/NUREG/TM-367, 1980

Berger MJ. Improved point kernels for electron and beta-ray dosimetry, NBSIR-73-107, Washington, 1973

Berger MJ. Distribution of absorbed dose around point sources of electrons and beta particles in water and other media, MIRD Pamphlet No. 7, Society of Nuclear Medicine, New York, 1971

Ellett WH, RM Humes. Absorbed fractions for small volumes containing photon emitting radioactivity, MIRD Pamphlet No. 8, Society of Nuclear Medicine, New York, 1971

9. Mehta A. Personal communication, 1980
10. ICRP Publication 30. Limits for intakes of radionuclides by worker. Pergamon Press, Oxford, 1979
11. Aboul Khair SA, TJ Buchanan, J Crooks, AC Turnbull. Structural and functional development of the human fetal thyroid, Clin.Sci. 31, 415-421, 1966
12. Beierwaltes WH, R Crane, A Wegst, NB Stafford, EA Carr jr. Radioactive iodine concentration in the fetal human thyroid gland from fallout. J.Am.Med.Assoc. 173, 1895-1902, 1960
13. Costa A, F Cottino, M Dellepiane, GM Ferraris, L Lenare, G Magro, Patrito, G Zoppetti. Thyroid function and thyrotropin activity in mother and fetus. Curr.Top.Thyroid Res. 5, 738, 1965
14. Eisenbud M, Y Mochizuki, G Laurer. I-131 dose to human thyroids in New York City from nuclear tests in 1962. Health Phys. 9, 1291-1298, 1963
15. Evans TC, RM Kretschmar, RE Hodges, CW Song. Radioiodine uptake studies of the human fetal thyroid. J.Nucl.Med. 8, 157-165, 1967
16. ICRP Publication 23. Report of the Task Group on Reference Man, Pergamon Press, Oxford 1975
17. Beierwaltes WH, MTJ Hilger, A Wegst. Radioiodine concentration in fetal human thyroid from fallout. Health Phys. 9, 1263-1266, 1963
18. Hoffmann FO, CF Baes III. A statistical analysis of selected parameters for predicting food chain transport and internal dose of radionuclide ORNL/NUREG/TM-282, 1979
19. Dyer NC, AB Brill. Maternal-fetal transport of iron and iodine in human subjects. Adv.Exper.Med.Biol. 27, 351-366, 1972
20. Hodges RE, TC Evans, JT Bradbury, WC Keettel. The accumulation of radioactive iodine by human fetal thyroids. J.Clin.Endocrinol.Metabol. 1, 661-667, 1955
21. Lampé L, L Kertesz, J Dzvonyar. Über die Jodspeicherung der Schilddrüse des menschlichen Fetus. Zb. Gynäkol. 86, 905-908, 1964
22. Chapman EM, GW Gorner, D Robinson, RD Evans. The collection of radioactive iodine by the human fetal thyroid. J.Clin.Endocrinol.Metab. 8, 717-722, 1948
23. Czerniak P, N Soferman, S Chajchik. The passage of I-131 and P-32 from mother to fetus (in hebrew). Harefuah 69, 158-161, 1965
24. Robertson JS, RR Price, TF Budinger, UF Fairbanks, M Pollycove. Radiative absorbed doses from Iron-52, Iron-55, and Iron-59 used to study ferrokinetics. J.Nucl.Med. 24, 339-348, 1983

RADIOPHARMACEUTICALS IN BREAST MILK

P.J. Mountford and A.J. Coakley

Department of Nuclear Medicine, Kent and Canterbury Hospital, Canterbury,
Kent CT1 3NG, U.K.

ABSTRACT

An assessment has been made of the radiological hazards to an infant following the administration of a radiopharmaceutical to a breast feeding mother. Feeding should be discontinued after administration of most I-131 and I-125 compounds, Ga-67 citrate or Se-75 methionine, and for iodinated compounds where it was possible to resume feeding, a thyroid-blocking agent should be administered. For Tc-99m compounds, pertechnetate had the greatest excretion in milk and interruptions of 12hr and 4hr were considered appropriate for pertechnetate and MAA respectively. Other Tc-99m compounds, Cr-51 EDTA and In-111 leucocytes did not justify an interruption just on the grounds of their associated excretion in milk. The ingestion hazard could be minimised by reducing the administered activity, and in some cases, by the substitution of a radiopharmaceutical with lower breast milk excretion.

For Tc-99m lung and brain scans, the absorbed dose due to radiation emitted by the mother (i.e. when cuddling) was less than the ingested dose, but for a Tc-99m bone scan the emitted dose was greater. In all three cases, the emitted dose did not exceed 0.5mGy for the infant in close contact to the mother for one-third of the time. For In-111 leucocytes, the emitted dose was about 2mGy, and it was concluded that close contact should be restricted to feeding times during the first 3 days after injection.

INTRODUCTION

Administration of radiopharmaceuticals to a breast-feeding mother presents two radiological hazards to her infant. Firstly, radioactivity excreted in the milk will be ingested by the infant. This hazard can be minimised by recommending a period of interruption for breast feeding (1). Such recommendations and restrictions have to be based on published biokinetic measurements of radioactivity in breast milk. Opportunities to make such studies on a breast feeding mother occur infrequently and the collection of biokinetic data can present logistical difficulties. Most published data is confined to case reports scattered through the literature.

The second hazard is due to radiation emitted from the mother when the infant is in close proximity. The absorbed dose from cuddling can also be reduced by restricting the time spent by the infant in close contact with the mother. However, there is little data available on which to base appropriate restrictions.

This paper summarises the available measurements of the excretion of radiopharmaceuticals in breast milk, including some measurements made at our own hospital. A preliminary assessment has also been made of the dosimetry of the radiation emitted by a mother, after undergoing some of the more common nuclear medicine investigations.

EXCRETED RADIOACTIVITY

ASSESSMENT OF THE RADIOLOGICAL HAZARD

To evaluate the potential hazard to a newborn infant, the ingested activity could be compared with one-tenth of the annual limit of intake (ALI/10) appropriate to a newborn infant (2), or with the dose equivalent limit (3). To deduce the activity potentially ingested by an infant from measurements of the activity concentration (a_n) in expressed milk samples, it was necessary to assume values for the volume (V_n) of each feed, and the time between each feed. Published case reports describing this potential dose have varied in the values of these two latter parameters. In this report the potential ingested activities have been recalculated on a common basis, using the measured concentrations of activity in expressed samples as given in each case report. The total ingested activity (A) was given by:

$$A = a_1 V_1 + a_2 V_2 + a_3 V_3 + \dots + a_n V_n \quad (1)$$

To simplify the calculations, a constant volume (V) per feed and time (t) between each feed was assumed. In general, the expressed activity concentration has been found to follow a monoexponential decrease with time. Therefore equation (1) becomes a simple geometric progression and the total ingested activity could be calculated from:

$$A = \frac{a_1 V}{1 - \exp(-bt)} \quad (2)$$

From a total feed of 850ml per day (4), it was assumed that there was a 4hr interval between feeds resulting in a volume of 142ml per feed. It was assumed that the mother had last fed her infant 1hr before injection, and therefore for uninterrupted feeding, the next feed was 3hr after injection. Exponential curves were fitted by the least squares method, and values were taken from the fitted curves of the activity concentration (a_1) at 3 hr after injection and of the effective excretion decay constant (b). In several reports the excretion curve had not reached a maximum by 3hr, in which case measured concentrations at 4 hr intervals were substituted into equation (1) until the decay phase was reached.

The absorbed dose due to ingested activity depends on the chemical form of the activity, on the absorption from an infant's gastrointestinal tract, and on the anatomical distribution and retention in the newborn infant. In some reports more than one chemical form of activity in milk has been identified, and the distribution of these forms varied with time. There is little data available which describes the oral absorption, distribution and retention of radioactivity in the newborn infant. Therefore to calculate the absorbed dose to the newborn infant from ingested activity, it was assumed that the activity was in only one chemical form and that absorption was total unless otherwise stated. It was also assumed that the distribution and retention in an infant was the same as for an adult, and that the appropriate absorbed dose per unit activity and ALI/10 could be taken from MIRD Dose Estimate Reports (5 - 8) and from ICRP Publication 30 (2) respectively, with each

value corrected by a factor of 17 in line with the recommendations of the UK radiopharmaceutical administration licensing authority (ARSAC) (9). (On the basis of correction by body weight, this factor corresponded to a newborn infant's weight of about 4kg).

IODINATED COMPOUNDS

The half-life of breast milk excretion following injection of NaI-131 was very similar in two separate reports (10,11), and together with the half-life for iodinated hippuran was less than the half-lives for the other iodinated compounds listed in Table 1 (12-15). The I-131 activity after MAA injection did not reach a peak value until 25hr after injection. The half-lives of excretion after maternal injection of fibrinogen were very similar to the half-life of fibrinogen in blood. A second I-125 HSA case had an excretion half-life of about 2 days for measurements starting 3.5 days after injection (13).

Table 1. Summary of the excretion measurements of radioiodinated compounds including the total ingested activities, doses and effective half-lives for uninterrupted feeding

Compound	Reference	No. of cases	Half-life (hr)	Administered activity (MBq)	Ingested activity (MBq)	Dose (mGy) whole body	thyroid
NaI-131	10	1	7	0.4	0.09	0.29	528
	11	1	8	0.4	0.14	0.47	864
I-131 MAA	12	1	17*	7.4	1.4	4.6	8436
I-125 HSA	13	1	72	0.2	0.08	1.0	151
I-125 Fib.	14	1	80	3.7	0.19	0.4	666
I-125 OIH	15	1	4.8	0.4	0.01	0.02	35
I-131 IIM	15	6	4.5	0.4	0.01	0.04	74

*from 25hr after injection

The total activity ingested by an infant corresponding to the typically administered activities are also listed in Table 1. Iodine is absorbed rapidly and almost completely from the gastrointestinal tract and total absorption is assumed by ICRP30 for all compounds of iodine (2). The ALI/10 for a newborn infant was calculated to be 0.0006 MBq (16 nCi) for I-125 and I-131, and this limit will be exceeded by all the iodinated compounds, if breast feeding is not interrupted. The interruption necessary to reduce the ingested activity below the ALI/10 is far too long to maintain milk flow for all the compounds except for hippuran, where an interruption of 24hr would be appropriate.

Uptake of iodine by a newborn infant's thyroid can be double the value used (25%) for the calculated results in Table 1 (7). On the other hand, if a thyroid-blocking agent is administered to the mother, it may be excreted in breast milk in a concentration sufficient to reduce the infant's thyroid dose by a factor of 0.01 (16,17).

TECHNETIUM-99M COMPOUNDS

Following injection of the Tc-99m-labelled compounds listed in Table 2, the half-lives of radioactive excretion are all about 4 hr, with the exception of the single study of Tc-99m-labelled erythrocytes (12,14,15,18-25). It was assumed that the Tc-99m was excreted as free pertechnetate, although a small proportion associated with a protein precipitate has been identified in human milk after injections of MAA and DTPA (23,25). Differences in the fractional absorption of pertechnetate from the gastrointestinal tract have been reported, and ICRP30 assumes a fractional absorption of 80% which leads to an ALI/10 for a newborn infant of 18 MBq (0.5 mCi) (2,26). Injection of pertechnetate, MAA and plasmin lead to greater than 1% of the administered activity being excreted in breast milk. However for typically administered activities, the ALI/10 will only be exceeded after administration of pertechnetate (Table 2). Assuming complete absorption from the gut, total body doses of 0.9 mGy (90mrad) and 0.1 mGy (10 mrad) to the infant were calculated for an injection of 550 MBq (15 mCi) of pertechnetate for a brain scan and 75 MBq (2 mCi) of MAA for a lung scan. The dose to the stomach wall and to the thyroid could be as much as 20 - 25 times greater than these total-body doses (8,27). For the other Tc-99m compounds, the results in Table 2 show that the ALI/10 would not be exceeded for uninterrupted feeding, and the whole-body infant doses did not exceed 0.01 mGy (1 mrad) for typical injection activities (Table 2).

Table 2. Summary of the excretion measurements of Tc-99m compounds including the total ingested activities, doses and effective half-lives for uninterrupted feeding.

Compound	Reference	No. of cases	Half- life (hr)	Administered activity (MBq)	Ingested activity (MBq)	Whole body dose (mGy)
Pertechnetate	12,15,18, 19	5	5.2 (3.2-9.9)	550	15 (0.6-60)	0.9 (0.03-3.6)
MAA	15,20-24	13	3.8 (2.6-4.7)	75	1.5 (0.2-4)	0.1 (0.01-0.2)
DTPA	15,25	2	4.6 (3.7-4.6)	75	0.01 (0.008-0.011)	0.0006 (0.0005-0.0007)
EDTA	12	1	4.1*	75	0.18	0.01
MDP	15	2	4.3	550	0.17	0.01
red cells	15	1	7.7	550	0.03	0.002
plasmin	15	1	4.1	20	0.24	0.01

*second phase of a biexponential curve from 7 hr after injection.

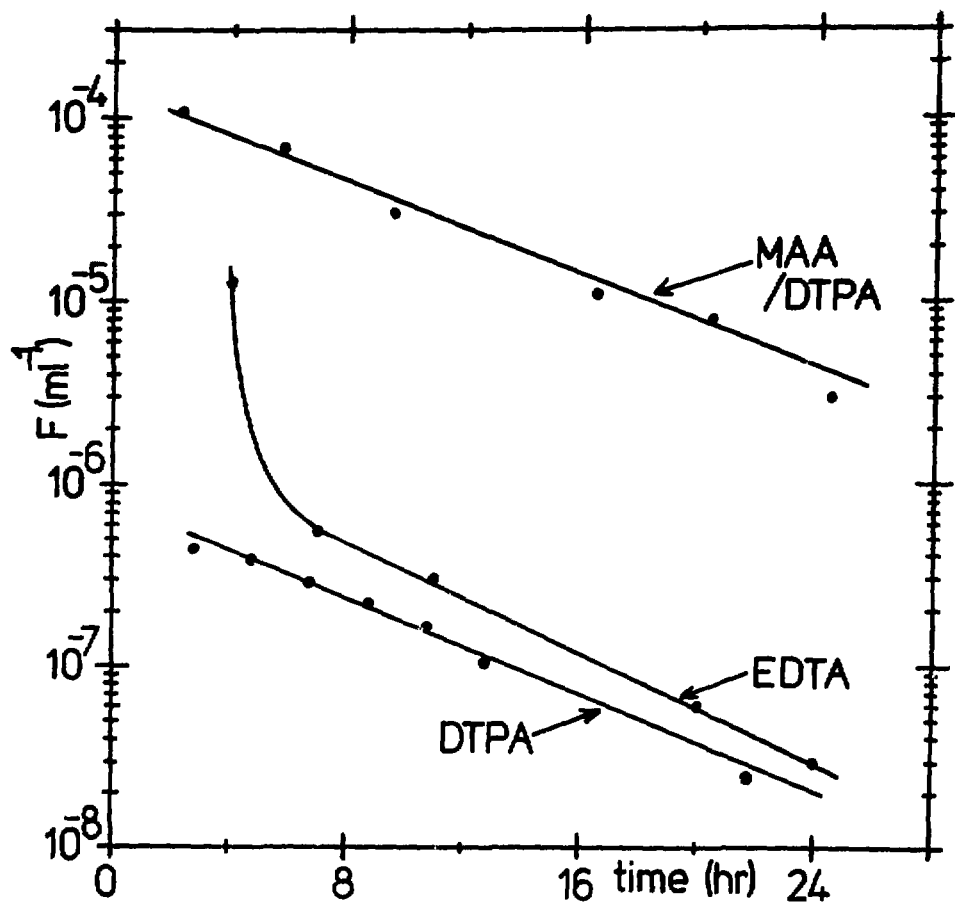


Fig. 1. A comparison of the variation in breast milk activity concentration (F) with time after administration of Tc99m DTPA aerosol/Tc99m MAA (23), Tc99m EDTA (12) and Tc99m DTPA i.v. (25).

All the excretion measurements summarised in Table 2 showed a mono-exponential decrease in activity concentration with time, except for Tc-99m EDTA which showed an early rapid decrease followed by a second slower phase ($T_{1/2} = 4.1$ hr) (12). Although the glomerular filtration of EDTA and DTPA are similar, no early fast excretion of greater concentrations of activity were found in two separate studies of DTPA (12,15,25) (Fig. 1). Also shown in Fig. 1 is a comparison between MAA and DTPA demonstrating the negligible contribution to the total excreted activity in breast milk of a DTPA aerosol when used with MAA for a combined ventilation/perfusion lung scan (23,25). There is no published data describing the excretion of radioactivity in breast milk after a Tc-99m gluconate injection. However gluconate has a slower renal clearance than DTPA, and as pertechnetate is selectively concentrated in breast milk, Tc-99m DTPA should be regarded as the agent of choice for brain scanning a lactating mother.

OTHER RADIOPHARMACEUTICALS

Sufficient data to allow the calculation of the potential ingested activity from 3 hr have been published for Ga-67 citrate (28), Se-75 methionine (29), Cr-51 EDTA (14,15) and In-111 leucocytes (30).

The earliest measurement of breast milk Ga-67 activity concentration was at 72 hr after injection, and the calculations in Table 3 are based on an extrapolated value at 3 hr. The proportion of Ga-67 activity excreted in breast milk was large, and for an administered activity of 150 MBq (4 mCi), will lead to more than 40 MBq (1.1 mCi) ingested by a breast-fed infant. Other published data of Ga-67 excretion in breast milk do not contain enough measurements for separate analysis, but the activity concentrations were consistent with those on which the calculations in Table 3 were based (31-33). ICRP30 assumes a fractional absorption after ingestion of Ga-67 of only 0.1% and the ALI/10 for a newborn infant was calculated to be 1.8 MBq (0.05 mCi) (2). This fractional absorption may be too low for Ga-67 excreted in breast milk because it has been shown that this activity is contained primarily in the lactoferrin-rich protein fraction (33). Although the exact fate of Ga-67 bound to lactoferrin after ingestion is unknown, total absorption was assumed for dosimetric purposes. Intravenous administration of Ga-67 citrate will also result in Ga-67 binding to lactoferrin, and the corresponding absorbed dose per unit activity was corrected for body weight to yield a total body-dose to an infant of 48 mGy (4.8 rads) (6).

Methionine is present in human milk and the study of breast milk excretion after Se-75 methionine identified 90% of the excreted activity associated with protein (29). ICRP30 assumes that 80% of all selenium compounds other than elemental selenium and selenides are absorbed after oral ingestion, and that the retention of selenium is not affected markedly by its chemical form (2). Therefore the ALI/10 for Se-75 methionine ingested by a newborn infant was calculated to be 0.12 MBq (0.003 mCi). Se-75 was excreted in a bioexponential curve with a decrease in activity concentration of 2 from 5 hr to 29 hr after injection, and therefore the total excretion at 3 hr and 7 hr was derived from graphical data and added to the calculated total excretion from 11 hr. It was found that from 3 hr after injection, 10% of the injected activity was excreted in breast milk (Table 3). A large absorbed dose per unit activity (37 mGy/MBq for a newborn infant) is associated with Se-75 (5), and thus despite the low activity of 10 MBq administered in clinical studies, a newborn infant will receive a dose of 37 mGy (3.7 rads) if feeding is resumed at 3 hr.

For Cr-51 EDTA, it was assumed that the stability of the compound after intravenous administration is high enough for it to be excreted in this form and not absorbed from the gastrointestinal tract of a child (15). Three cases of Cr-51 EDTA excretion have been reported (14-15). Only one case contained

data earlier than three hr after injection, and it showed a monoexponential decrease in activity concentration up to about 40hr (15). Therefore it was considered valid to extrapolate the values at 3hr in the other two cases from their exponential curves. The Cr-51 activity in milk was excreted with a short effective half-life (mean value 7.8hr) and at a very low initial concentration (typically about 10^{-6} ml $^{-1}$ of the injected activity), resulting in a total ingested activity of about 0.3 kBq (8 mCi).

Table 3. Summary of the excretion data for Ga-67 citrate, Se-75 methionine, Cr-51 EDTA, and In-111 leucocytes including ingested activities, doses and half-lives for uninterrupted feeding.

Compound	References	No. of cases	Half-life (hr)	Administered activity (MBq)	Ingested activity (MBq)	Whole Body dose (mGy)
Ga-67 Citrate	28	1	69	150	41	48
Se-75 methionine	29	1	78*	10	1	37
Cr-51 EDTA	14,15	3	7.8	0.03	0.0003	0.000008
In-111 leucocytes	30	1	82\$	20	0.024	0.08†

*from 29hr

\$from 13hr

†dose equivalent (mSv)

The exact form of In-111 in breast milk after an In-111 leucocyte scan was uncertain, although no cell-bound activity could be identified, and with the exception of the early (2.2hr) measurement, only a minor proportion was associated with the protein precipitate (30). From experiments on rats and comparative toxicity studies between oral and intravenous administration of indium, ICRP30 assumed a fractional absorption from the gastrointestinal tract of 2% for all compounds of indium (2). This assumption yielded an ALI/10 for a newborn infant of 1.2MBq (0.03mCi). The In-111 activity concentration increased from 2.2hr to a peak value at about 13hr after injection (Fig. 2). The interpolated excretion at 3, 7 and 11hr was added to the calculated total excretion from 15hr. The total activity from 3hr and onwards was very small, and was two orders of magnitude less than the ALI/10. Even if total absorption from the gut was assumed and the anatomical distribution was the same as for intravenous administration of In³⁺ in the adult, then using the dose equivalent per unit activity given in the DISS ARSAC guidance notes and corrected for body weight (9), the total body dose equivalent to the infant was calculated to be only 0.08mSv (8mrem).

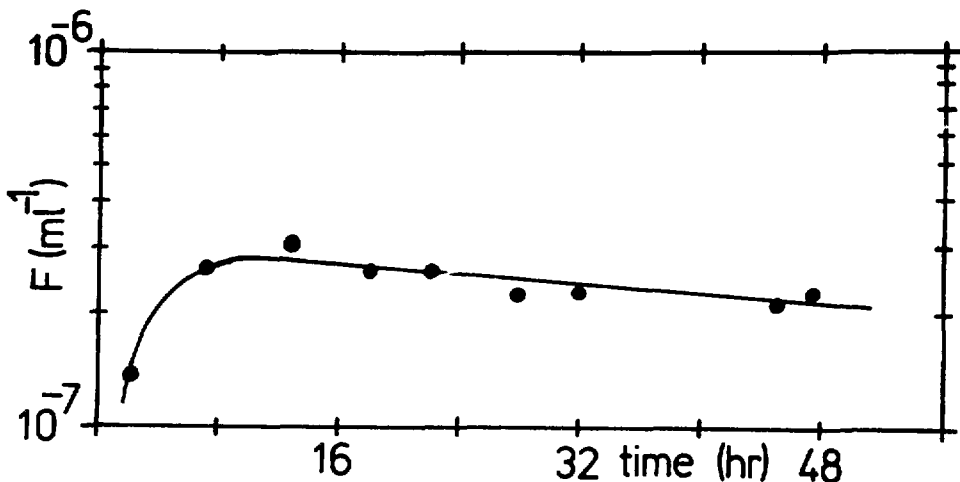


Fig. 2. The variation of breast milk activity concentration (F) with time after reinjection of In-111 oxine leucocytes (30).

EMITTED RADIATION

Two separate studies have been carried out as a preliminary investigation of the potential dose of emitted radiation received by an infant while in close contact with the mother. Firstly, a LiB thermoluminescent dosimeter (TLD) was secured under each breast and about 2.5 cm above the navel of 4 female patients. With the patient sitting, these sites corresponded approximately to the position of the head and lower limbs of an infant when being cuddled. These patients had respectively a Tc-99m ventilation/perfusion lung scan, a Tc-99m brain scan, a Tc-99m bone scan, and an In-111 leucocyte scan. The administered activities and radiopharmaceuticals are given in Table 4. Each TLD was secured to the patient immediately after injection and was removed about 24hr later. Although the sensitivity of LiB TLD is not as low as other types of TLD, it was readily available and could be obtained in very thin sachets designed for measuring low energy mammography doses. Therefore it was well suited to measuring the lower energy scattered radiation emitted from a patient. Furthermore, its response to the low-energy X-rays emitted by Tc-99m and In-111 was not less than 90% of its response to their respective gamma radiation (34).

The potential close contact absorbed dose (CCAD) to an infant was calculated from the measured TLD dose (T) using the following relation:

$$\text{CCAD} = \frac{T[1 - \exp(-kt_2)]}{[1 - \exp(-kt_1)][1 - \exp(-kt_3)]} \quad (3)$$

where k was the effective decay constant of the dose rate at the site of measure, t_1 was the time for which the TLD was irradiated, t_2 was the duration of each period of close contact and t_3 was the time between the start of each of these periods. Although this approach was naive in assuming that t_2 and t_3 never varied, that the first period of close contact was immediately after injection and that the dose rate was at a maximum at that time, it was

considered that such an approach should yield a good indication of the magnitude of a CCAD. Furthermore, where it may be considered necessary to restrict the close contact between a mother and her infant, then appropriate simple guidelines could be derived from the above equation.

Values of CCAD derived from the TLD measurements assuming a value of 20 min for t_2 and 1hr for t_3 are given in Table 4 for each of the three sites of measurement. Although only one set of measurements were conducted, the results suggested that the variation of dose across the surface of the mother was likely to depend on the radiopharmaceutical administered. The brain and bone scan patients were of similar build and were given the same activity of Tc-99m (550MBq), therefore differences in the anatomical distribution of activity and its redistribution with time must have been responsible for the CCAD for the brain scan being about twice that of the bone scan. The left and right breast CCAD's of the brain scan compared to the lung scan were in the ratio of the administered activities. Relatively higher CCAD'S at the site above the navel (patient sitting) for the bone scan may partly be explained by bladder activity. The greater CCAD at the right breast site compared to the left for the In-111 leucocyte scan (ILLS) was due to the greater accumulation of activity in the liver and the posterior position of the spleen. The ILLS yielded the greatest CCAD despite the low administered activity (14MBq), and for the values used in equation 3 above, the right CCAD was 40% of the dose limit for a member of the public (3).

Table 4. Calculated values of the absorbed dose (CCAD) to a newborn infant cuddled for 20min in every hour assuming the dose rate was at a maximum immediately after injection when cuddling started.

Scan	Administered activity (MBq)	Compound	Absorbed dose (mGy)		
			Right breast	Mid-line (navel)	Left breast
Brain	550	Tc-99m gluconate	0.42	0.32	0.52
Lung	37	Tc-99m DTPA (aerosol)	0.05	0.04	0.08
	75	Tc-99m MAA			
Bone	550	Tc-99m medronate	0.26	0.23	0.25
Leucocyte	14	In-111 leucocytes	2.10	0.40	1.37

For the second part of the study, measurements were made of the exposure rate close to the left and right breasts of a series of female patients undergoing routine Tc-99m radiopharmaceutical investigations. A Wallac RD-8 survey meter was used for these measurements. Its detector is a Geiger-Muller tube with a non-uniform energy response decreasing to zero at about 30keV (35). It was calibrated crudely in terms of absorbed dose by comparing its response at the surface of a diffuse flood source of Tc-99m surrounded with scattering material, to that of the absorbed dose at the same position measured by a TLD. The accuracy of these measurements was limited by the angular response of the meter and the difference between the scattered

radiation spectrum emitted from a patient and from the flood source. Nevertheless, it can be seen from Table 5 that the absorbed dose rates at the breast surface, corresponding to the time when a patient leaves the department, are roughly in the ratio of the administered activity, apart from a bone scan where the activity is spread much more uniformly through the body and where there is a longer time between injection and scan.

Table 5. Measurements of the absorbed dose rates at the breast surface of a series of female patients undergoing Tc-99m radiopharmaceutical studies.

Scan	Administered activity	Compound	No. of patients	Time after injection (hr)	Dose rate ($\times 10^{-2}$ mGy/hr)	Right Breast	Left Breast
Brain	550	Gluconate	6	2	9.7 ± 3.8	9.5 ± 4.0	
Lung	37 + 75	DTPA+MAA	6	0.5	1.6 ± 1.0	1.6 ± 1.0	
Bone	550	Methronate	22	3.5	4.8 ± 1.6	4.9 ± 1.6	
Renal	75	DTPA	8	0.5	1.7 ± 0.6	1.7 ± 0.6	
Thyroid	100	Ethylene	8	0.5	2.9 ± 1.4	3.0 ± 1.3	
Liver	75	Colloid	2	0.5	1.9 ± 0.5	2.4 ± 0.8	

DISCUSSIONS AND CONCLUSIONS

Major assumptions have been made in deriving the potential radiation doses from ingested activities and from radiation emitted from a mother. However, in nearly all cases, these assumptions should have led to an overestimate of the doses. When more accurate information becomes available concerning the chemical form of breast milk radioactivity, their absorption from the gastrointestinal tract of the infant, and their subsequent anatomical distribution and retention, then it would be appropriate to modify these dosimetric calculations. It has also been assumed that the milk concentrations measured in expressed samples, which are smaller in volume than feeds, represent the concentrations to be found in the latter. However it has been noted in several reports that where the expressed samples vary widely from the same mother, the excretion concentration follows a quite smooth mono-exponential curve.

There are no criteria for an acceptable radiation dose to a newborn infant. The ALI was derived for classified radiation workers. Thus a weight-corrected ALI/10 should not be regarded as a standard to be attained, and radiation doses to the newborn should always be minimised.

For iodinated hippuran, an interruption for a minimum period of 24hr is needed to ensure that the ALI/10 is not exceeded. For all other compounds reviewed, a prolonged period of interruption to breast feeding is indicated, and in practice, this may result in the cessation of milk flow.

Of the Tc-99m procedures, the greatest ingested dose was from pertechnetate administration. A delay in resuming breast feeding of 12hr (i.e. three effective half-lives) will reduce the dose to about 12% of that given in Table 2. During this period, milk should be expressed and discarded. It will also allow for the variation in excretion after pertechnetate injection. The data given in Table 2 for pertechnetate excretion includes brain studies

(12,18,19) and a thyroid study (15). If the former only are considered, the mean proportion of activity excreted is much lower (0.6%, range 0.1-0.8%). The single thyroid study excreted the much larger value of 11% of the activity injected. Indeed one report has described some breast milk measurements on two thyroid cases where the integral activity excreted over 24hr (calculated for a daily feed of 850ml) would exceed the injected activity (36). However a delay of 12hr in that case still provides an adequate reduction in the activity concentration. The thyroid-blocking agent administered to pertechnetate brain scan patients may play a role in reducing the breast milk excretion compared to a thyroid scan patient.

For uninterrupted breast feeding following Tc-99m MAA administration, it is unlikely that the ALI/10 could be approached even in extreme circumstances. However an interruption of 4hr, during which period a sample of milk should be expressed and discarded, will leave a wide margin. For the other Tc-99m compounds, for Cr-51 EDTA and for In-111 (leucocytes), the calculations indicate that it is not essential to interrupt breast feeding. However it may be reasonable to recommend a brief period of interruption, partly to reassure the mother, and partly because there is a paucity of data in the first hour or two after injection. Some reports have shown in fact that the concentration of Tc-99m activity is rising during the first few hours after injection, but has usually reached its peak value at about 2 hours after injection (14,15,19,21,36). The relatively large release of radioactivity into breast milk after Ga-67 injection and long half-life have led other authors to suggest a breast feeding interruption of 14 days (28,32). Such a long period is almost certainly impractical to maintain milk flow, and the same conclusion was drawn from the Se-75 data.

With the simple recommendation of nursing and cuddling an infant for one-third of the time each hour, the CCAD for Tc-99m investigations will be less than the ingested dose for lung and brain studies but not for a bone scan. However in the latter case, the CCAD will only be about 5% of the dose equivalent limit, and it could be decreased further by issuing more restrictive instructions during the 4hr period in which breast feeding is interrupted. The CCAD measured from the ILLS patient (Table 4) was the largest of the values derived. If breast feeding was resumed at 4 hr after injection, then advising the mother to cuddle the infant only at nursing times (i.e. 20 minutes every 4 hours) for the first 3 days (i.e. one half-life) will reduce the CCAD by about 40%.

Interruption of breast feeding and reduction of nursing time are not the only methods of reducing the total dose to an infant (1). Firstly, the activity injected into the mother should be reduced to the minimum compatible with yielding a diagnostic result. The activity of Tc-99m MAA and In-111 can be reduced to one-half and one-third respectively of that used in Table 2, with corresponding reductions in the ingested dose and the CCAD. Secondly, an alternative radiopharmaceutical can sometimes be used which has either an associated lower breast milk activity concentration or has more favourable dosimetric properties. Examples of such alternatives are Tc-99m DTPA instead of Tc-99m gluconate or pertechnetate for brain scanning, an ILLS instead of Ga-67 for localising infection, and I-123 instead of I-131 which should lead to a reduction in thyroid dose by a factor of 0.01 (7). If In-111 platelets can be shown to produce a low breast milk concentration similar to In-111 leucocytes, then they could be used instead of plasmin for detection of deep vein thrombosis.

In our department, several breast-feeding patients are referred for investigation each year. Therefore it is surprising that such little data describing breast milk excretion has been reported world-wide. In

particular, it has been noted that data is absent for some compounds in common use, such as Tc-99m tin colloid, Tc-99m gluconate and Tl-201 chloride. It should be within the scope of any nuclear medicine department to conduct 24hr studies of such excretions, particularly since mothers should be encouraged to express milk samples during periods of interruption in order to maintain milk flow. These conclusions would suggest there is a need to collate such data from as many centres as possible, particularly as this review has shown that guidelines for many radiopharmaceuticals need not be as restrictive as has been concluded elsewhere (24).

ACKNOWLEDGEMENTS

The co-operation and help provided by Mr. B.F. Wall of the National Radiological Protection Board in conducting the TLD measurements is gratefully acknowledged.

REFERENCES

1. Coakley A.J., and P.J. Mountford. Nuclear medicine and the nursing mother. *Brit. Med. J.* 291, 159-160, 1985.
2. ICRP Publication 30. Limits for Intakes of Radionuclides by Workers. Pergamon Press, Oxford, 1980.
3. ICRP Publication 26. Recommendations of the International Commission on Radiological Protection. Pergamon Press, Oxford, 1977.
4. ICRP Publication 23. Report of the Task Group on Reference Man. Pergamon Press, Oxford, 1975.
5. MIRD Dose Estimate Report No. 1. Summary of current radiation dose estimates to humans from Se-75-methionine. *J. Nucl. Med.* 14, 49-50, 1973.
6. MIRD Dose Estimate Report No. 2. Summary of current radiation dose estimates to humans from Ga-66, Ga-67, Ga-68 and Ga-72 citrate. *J. Nucl. Med.* 14, 755-756, 1973.
7. MIRD Dose Estimate Report No. 5. Summary of current dose estimates to humans from I-123, I-124, I-125, I-126, I-131, and I-132 as sodium iodide.
8. MIRD Dose Estimate Report No. 8. Summary of current radiation dose estimates to normal humans from Tc-99m as sodium pertechnetate. *J. Nucl. Med.* 17, 74-75, 1976.
9. DHSS Health Notice HN(84)5. Notes for guidance on the administration of radioactive substances. Appendix 1, Parts A and B, DHSS, London, 1984.
10. Nurnberger, C.E., and A. Lipscomb. Transmission of radioiodine (I-131) to infants through human maternal milk. *JAMA* 150, 1398-1400, 1952.
11. Weaver, J.C., and R.L. Dobson. Excretion of radioiodine in human milk. *JAMA* 173, 872-875, 1960.

11. Weaver, J.C., and R.L. Dobson. Excretion of radioiodine in human milk. *JAMA* 173, 872-875, 1960.
12. Wyburn, J.R. Human breast milk excretion of radionuclides following administration of radiopharmaceuticals. *J. Nucl. Med.* 14, 115-117, 1973.
13. Bland, E.P., J.S. Crawford, M.F. Docker, and R.F. Farr. Radioactive iodine uptake by thyroid of breast-fed infants after maternal blood-volume measurements. *Lancet* ii, 1039-1041, 1969.
14. Mattson, S., L. Johansson, B. Nosslin, and L. Ahlgren. Excretion of radionuclides in human breast milk following administration of I-125 fibrinogen, Tc-99m MAA and Cr-51 EDTA, in *Proceedings of the Third Radiopharmaceutical Dosimetry Symposium*, edited by E.E. Watson, A.T. Schlafke-Stelson, J.L. Coffey, and R.J. Cloutier, pp 102-110, HHS Publication FDA 81-8166, 1981.
15. Ahlgren, L., S. Ivarsson, L. Johansson, S. Mattsson, and B. Nosslin. Excretion of radionuclides in human breast milk after the administration of radiopharmaceuticals. *J. Nucl. Med.* 26, 1085-1090, 1985.
16. Veall, N., and T. Smith. Excretion of I-125 in breast milk following administration of fibrinogen. *Br. J. Radiol.* 53, 512-513, 1980.
17. Bowring, C.S., P.L. Ormsby, and D.H. Keeling. Excretion of I-125 in breast milk following administration of labelled fibrinogen. *Br. J. Radiol.* 53, 513, 1980.
18. Rumble, W.F., R.L. Aamodt, A.E. Jones, R.I. Henkin, and G.S. Johnston. Accidental ingestion of Tc-99m in breast milk by a 10 week-old child. *J. Nucl. Med.* 19, 913-915, 1978.
19. Pittard, W.B., K. Bill, and B.D. Fletcher. Excretion of technetium in human milk. *Pediatrics* 94, 605-607, 1979.
20. Tribukait, B., and G.A. Swedjemark. Secretion of Tc-99m in breast milk intravenous of marked macroaggregated albumin. *Acta Radiol [Oncol]* 17, 379-382, 1978.
21. Pittard, W.B., R. Merkatz, and B.D. Fletcher. Radioactive excretion in human milk following administration of technetium Tc-99m macroaggregated albumin. *Pediatrics* 70, 231-234, 1982.
22. Berke, R.A., E.C. Hoops, J.C. Kereiakes, and E.L. Saenger. Radiation dose to breast-feeding child after mother has Tc-99m MAA lung scan. *J. Nucl. Med.* 14, 51-52, 1973.
23. Mountford, P.J., F.M. Hall, C.P. Wells, and A.J. Coakley. Breast-milk radioactivity after a Tc-99m DTPA aerosol/Tc-99m MAA lung study. *J. Nucl. Med.* 25, 1108-1110, 1984.
24. HPA Topic Group Report 39. *Radiation Protection Procedures in the Use of Tc-99m*. Hospital Physicists' Association, London, 1984.
25. Mountford, P.M., A.J. Coakley, and F.M. Hall. Excretion of radioactivity in breast milk following injection of Tc-99m DTPA. *Nucl. Med. Commun.* 6, 341-345, 1985.

26. Hays, M.T. Tc-99m pertechnetate transport in man: absorption after subcutaneous and oral administration: secretion into saliva and gastric juice. *J. Nucl. Med.* 14, 331-335, 1973.
27. ICRP Publication 17. Protection of the patient in radionuclide investigations. Pergamon Press, Oxford, 1971.
28. Tobin, R.E., and P.B. Schneider. Uptake of Ga-67 in the lactating breast and its persistence in milk. *J. Nucl. Med.* 17, 1055-1056, 1976.
29. Taylor, D.M., V.R. McCready, and D.O. Cosgrove. The transfer of L-selenomethionine to human milk and the potential radiation dose to a breast-fed infant. *Nucl. Med. Commun.* 2, 80-83, 1981.
30. Mountford, P.J., and A.J. Coakley. Excretion of radioactivity in breast milk after an indium-111 leucocyte scan. *J. Nucl. Med.* 26, 1096-1097.
31. Larson, S.M., and G.L. Schall. Gallium 67 concentration in human milk. *JAMA* 21, 171-172, 1970.
32. Greener, A.W., P.J. Conte, and K.D. Steidley. Update on gallium-67 concentration in human breast milk. *J. Nucl. Med.* 11, 171-172, 1970.
33. Hoffer, P.B., J. Huberty, and H. Khayam-Bashi. The association of Ga-67 and lactoferrin. *J. Nucl. Med.* 18, 713-717, 1977.
34. Langmead, W.A., and B.F. Wall. A TLD system based on lithium borate for the measurement of doses to patients undergoing medical irradiation. *Phys. Med. Biol.* 21, 39-51, 1976.
35. White, D.F., D.R. Blundell, K. Callowhill, and W.J. Illes. Instrument evaluation no. 5: Wallac OY Universal Radiation Survey Meter Type RD-8. NRPB-IE5, HMSO, London, 1976.
36. Ogunleye, O.T. Assessment of radiation dose to infants from breast milk following the administration of Tc-99m pertechnetate to nursing mothers. *Health Phys.* 45, 149-151, 1983.

DISCUSSION

MATTSSON: Thank you for an interesting lecture and for pointing out that the external radiation from the mother for some radiopharmaceuticals can contribute significantly to the irradiation of the child. I also want to take this opportunity to warn nuclear medicine physicians about the hazards of using 125-I-fibrinogen for investigations in nursing mothers. If this radiopharmaceutical has to be used, breastfeeding must be interrupted for at least three weeks, otherwise the absorbed dose by the thyroid of the child may be as high as 0.5 Gy.

MOUNTFORD: Do you think interrupting feeding for three weeks is practical?

MATTSSON: No, I don't think so.

RADIATION EXPOSURE TO PARENTS NURSING THEIR CHILD DURING TREATMENT WITH 131-I-META-IODOBENZYL GUANIDINE FOR NEUROBLASTOMA

H.R. Marcuse, J. van der Steen, H.J.M. Maessen,
C.A. Hoefnagel and P.A. Voûte.

The Netherlands Cancer Institute (Antoni van Leeuwenhoek Huis)
Plesmanlaan 121, 1066 CX Amsterdam, The Netherlands

ABSTRACT

After 22 treatments involving eight patients the radiation dose equivalent received by parents is described. Patients received 1.5-5.5 GBq I-131 as MIBG by 1-24 hours infusion. Selection for therapy was made after a diagnostic examination of MIBG uptake with quantities less than 40 MBq. The decision for treatment was based on estimations of the radiation dose delivered to the tumor and to normal organs and the general condition of the patient. The hospital is licenced to discharge patients if a number of conditions concerning the administered radioactivity are satisfied. It is shown that the dose equivalent to the parent can be kept to an acceptable level of approximately 1 mSv per treatment. This dose equivalent is mainly due to external radiation since blocking the parent's thyroid leads to negligible dose equivalent from internal contamination.

INTRODUCTION

It can be a problem for children to have to stay a few days isolated in a room with minimal contact with nurses and visitors. In children's hospitals the parents are involved as much as possible in the nursing of their child. Therefore the presence of one parent in the nursing room during the treatment with MIBG labelled with GBq I-131 was piloted.

RADIATION PROTECTION METHODS

The measures taken to keep the dose equivalent received by the parent as far as possible below the annual limit for members of the public (5 mSv) will be described elsewhere (1).

The most relevant steps taken in the hospital are:

- a) Protecting the parent's thyroid by 100 mg KI solution per day from one day before treatment and during the stay in the isolation room.
- b) Wearing special clothing in the isolation room, a nurse's apron, and disposable gloves.
- c) Measuring external radiation dose by pocket dosimeter.

- d) Urine sampling and counting to estimate the committed dose equivalent for total body irradiation (2).

After discharge from the hospital the patient exposes and contaminates the environment by his body burden. The most relevant criteria and assumptions in the decision to discharge a patient after the application of more than ten times the annual limit of intake (ALI) as a radionuclide having an effective half-life (T_e) of five days or more, are:

- e) If a fast excretion period exists, the period with a rapid excretion rate of more than 50% of the body burden per day must have passed.
- f) We assume patients spill 1% of the excreted activity at home and 1% of the spill will be ingested by the inhabitants of the house. To keep contamination of the inhabitants under 5% of the dose equivalent for members of the public (5 mSv), the body burden at the time of discharge must be less than $(T_p/T_p-T_e) * 50 * ALI$. T_p = physical half-life of the radionuclide.
- g) $\dot{X} \cdot T_e$, the product of the exposure rate \dot{X} in mR/h at a distance of 1 meter to the patient and the effective half-life in hours, both at the time of discharge, may not be more than 500 mR. Making appropriate estimations about a 'mean distance' for the home contacts to the patient after discharge, the value of $\dot{X} \cdot T_e$ gives a guidance for the exposure that can be expected to the contact resulting in a dose equivalent of 5 mSv.

RESULTS

Table 1 contains the details of eight patients treated 22 times for neuroblastoma with ^{131}I -MIBG.

Figure 1 gives the average dose equivalent to the parent, measured by pocket dosimeter when staying in the nursing room. The first bar represents the average of all 22 treatments on the first day of the hospitalization, the second bar on the second day and the third on the third day. The fourth bar represents the average dose on the fourth day for 17 treatments that lasted four days or more. The next bar gives the average total for all 22 treatments, regardless of the number of days before discharge. The last eight bars are dual and represent the average for the individual patients from Table 1. The left side of the bar indicates the dose by external radiation and the right side represents the committed dose equivalent, resulting from the urine sampling mentioned at d).

Figure 2 gives the potential average dose equivalent to the parent after discharge of the patient. The left side of the dual bars represents the dose equivalent by internal contamination caused by the expected spill from the patient's body burden as mentioned at f). The dose equivalent from external radiation emerging from the child at home is estimated in the right side of the bars in a way as indicated at g).

DISCUSSION

Nursing a child in hospital leads to negligible parent internal contamination, except in Case IV, where during one of the 5 treatments the mother did the urine sampling and became contaminated herself.

Table 1. Patients treated for neuroblastoma.

patient/age	site/indication	dose(GBq)	results	nursed by
I male 4	soft tissue/ progressive	2.2	temporary regression	father
II female 5	abdomen + bone/ progressive	1.7/2.1/1.7	temporary regression/ good palliation	mother
III male 2	bone/ progressive	2.0/3.9/3.9 + chemotherapy	temporary regression/ good palliation	mother
IV male 7	bone/ residual disease	1.5/3.9/3.7 3.8/3.8	regression	mother
V female 12	bone + abdomen/ residual disease	3.7/3.6/3.7	complete remission	father
VI male 5	abdomen/ recurrent	3.7/5.5/5.5 5.5	regression	father
VII male 4	abdomen/ progressive	3.7	-	father
VIIImale 4	bone + bone marrow/ residual disease	3.7/3.7	-	gr. mother

Table 2. Total dose equivalent per treatment.

patient	III	VIII	I	VII	II	VI	IV	V
age	2	4	4	4	5	5	9	12
total uSv/GBq	502	768	505	378	662	258	403	227
GBq administered	9.8	7.4	2.2	3.7	6.1	20.2	16.7	11.0
number of treatments	3	2	1	1	3	4	5	3
mSv per treatment	1.6	2.8	1.1	1.4	1.3	1.3	1.3	0.8

Figure 1. Average dose equivalents in μSv delivered to parents in hospital per GBq ^{131}I -MIBG administered to children.

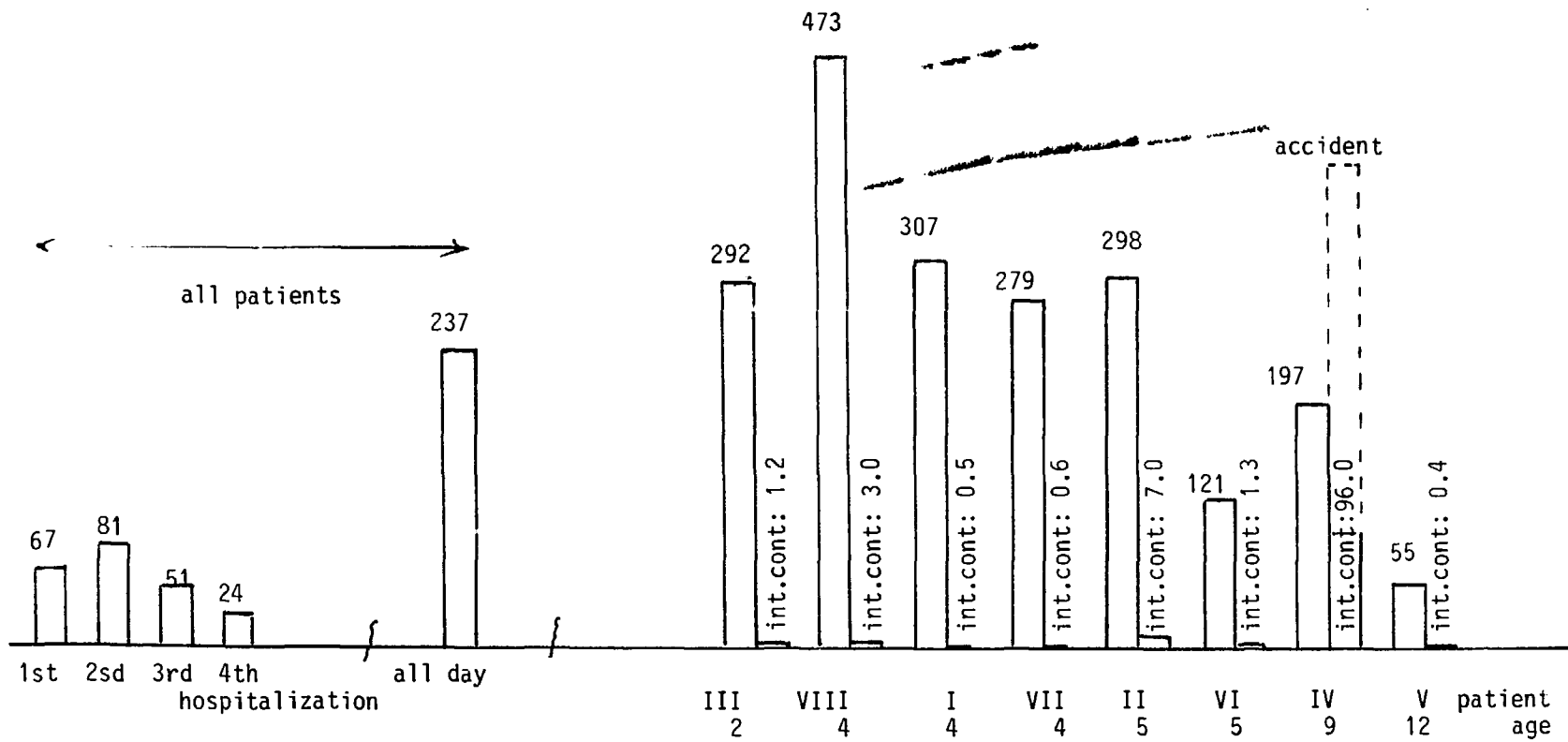
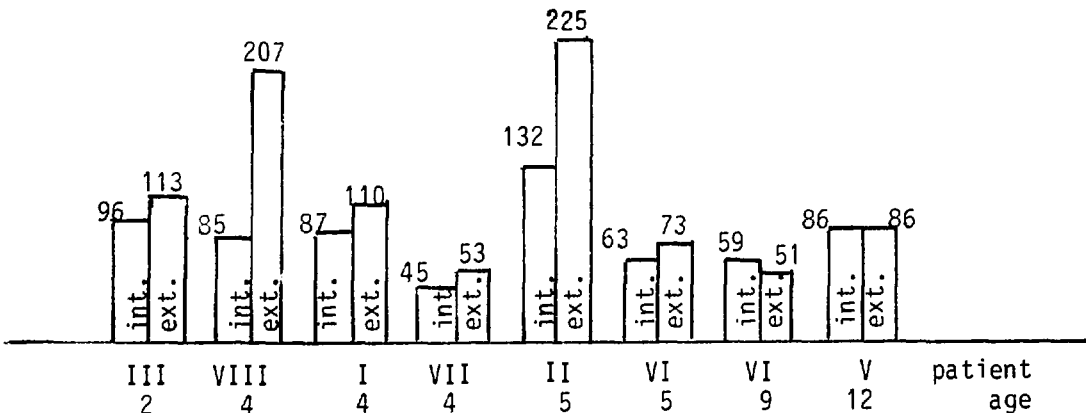


Figure 2. Average dose equivalent in μ Sv to parents
after discharge
per GBq administered to children.



This 'accident' did not result in an unacceptable equivalent dose for the mother.

External exposure is the main radiation source to the parents. It could not be related to the day of the treatment or the time spent in isolation. It may be related to the age and the amount of care the child needs.

In Table 2 all equivalent doses during stay in hospital and after discharge are taken together. The conclusion from this account is that MIBG treatment with large amounts of radioactivity and with the participation of one parent can be safe.

ACKNOWLEDGMENT

The authors appreciate the cooperation with Drs H.A.Selling and C.M.Gispen-Vos from the Ministry of Housing, Physical Planning and Environment in the development of the discharge rule.

REFERENCES

1. van der Steen, J., H.J.M. Maessen, C.A. Hoefnagel and H.R. Marcuse. Radiation protection during treatment of children with ^{131}I -meta-iodobenzylguanidine. *Health Physics*. accepted for publication.
2. ICRP 1979, "Limits for intakes of radionuclides by workers", ICRP Publication 30 (1), Annals of the ICRP 2, No 3/4 Oxford: Pergamon Press.

MEDICAL CONCERNS IN THE APPLICATION OF ULTRASHORT-LIVED
RADIONUCLIDES

H. William Strauss, M.D., John Gill, M.D., D. Douglas Miller,
M.D., Ronald Callahan, Ph.D., and David Elmaleh Ph.D.

Division of Nuclear Medicine, Department of Radiology,
Massachusetts General Hospital, Boston, MA 02114

ABSTRACT

The dosimetry of ultrashort-lived radionuclides is dependent on the biodistribution and residence time of the materials eluted from the generator. Since the half-life of the daughter usually precludes any serious chemical manipulations, the eluates are usually infused in the chemical form available directly from the generator, typically simple ions. As a result, the factors that will define dosimetry are:

1. Decay scheme of the daughter
2. Progeny of the daughter
3. Decay scheme of the parent
4. Radiocontaminants of the parent
5. Breakthrough of the parent
6. Biodistribution of the radionuclides

The half-life of the daughter is usually sufficiently short that it does not contribute significantly to the radiation burden. The half-life of the parent, associated radiocontaminants or the progeny, on the other hand, may contribute substantially to the radiation burden of the patient. Many of these agents, including osmium, germanium, and mercury have long biological half-lives and specific organ localization which contribute to the radiation burden.

The short physical half-lives of ultrashort-lived agents require that the radionuclides be eluted directly from the generator into the patient. This places severe constraints on the quality control procedures that can be performed prior to administration of a dose. Although this problem must be addressed with all of the generator systems, the severity of the problem increases when the half-life of the parent nuclide is long compared to the daughter. For example, in the Rb-81/Kr-81m generator, the half-life of parent Rb-81 is only 4.7 hours. Breakthrough of the parent radionuclide to the eluate will result in a relatively modest radiation burden. With Hg-195/Au-195m or the Os-191/Ir-191m systems, where the parent biological and physical half-lives are much longer (Hg-195 $T_{\frac{1}{2}}$ = 2.5 days and Os-191 $T_{\frac{1}{2}}$ = 14 days), each microcurie of parent in the eluate results in a greater radiation burden.

To determine breakthrough, the generator is eluted and the eluate immediately placed in a dose calibrator. The initial activity measured represents the daughter, while activity remaining after the daughter has decayed through 10 half-lives represents breakthrough of the parent. If the parent breakthrough is acceptable and the volume passed through the column is less than that associated with a high incidence of parent elution, the next dose is administered directly to the patient.

The behavior of the progeny of daughter products must be understood, since these agents build up on the generator column between elutions. In the case of Ir-191m, the daughter Ir-191 is stable and is not present in large enough quantities to cause any toxicity. In the case of Kr-81m, the daughter Kr-81 has a half life of 10E6 years and is therefore not a significant radiation burden. The Au-195m however, decays to a radioactive progeny which has a half-life of 185 days. This decay-product radionuclide, unfortunately, has a long biological half-life, and concentrates primarily in the kidneys. When a Hg/Au generator is eluted after a prolonged interval, the quantity of daughter-progeny Au-195 in the eluate can be substantial (hundreds of microcuries) and may result in a significant radiation burden to the patient. To minimize this problem, the generator is usually pre-eluted to "waste" immediately prior to use. Even with this caveat, the quantity of Au-195m infused should be limited to 300mCi or less/patient to minimize the radiation burden to the kidneys from in-vivo generation of Au-195 to <5 rads.

Although these radiopharmaceuticals can be employed to study the right heart, the amount of radionuclide entering the left heart is limited with Kr-81m and Ir-191m: >90% of the dose of krypton will be cleared by the lungs during a single transit through the normal pulmonary capillary bed (by the same "preferred solubility" mechanism as that of xenon), while with Ir-191m, the normal transit time through the right heart and pulmonary capillaries of about 8 seconds will result in loss of about 75% of the injected activity (about 2 physical half-lives). Au-195m, on the other hand, with its 30 second half-life, permits visualization of both the right and left heart with a high photon flux, but with minimal radiation burden to the patient.

DESCRIPTION OF SPECIFIC GENERATOR SYSTEMS AND THEIR APPLICATIONS

KRYPTON-81m

In 1968 Yano and Anger (1) proposed the use of the Rubidium-81/Krypton-81m generator system to image the blood pool. The 4.7 hour half-life cyclotron-produced Rb-81 [alpha particle bombardment of a Br-79 target ($\alpha, 2n$)] is adsorbed to a column, and the 13 second daughter, inert gas Kr-81m produced. If the column is filled with dextrose, the resulting solution of dextrose/Kr-81m can be injected intravenously to determine right ventricular function and pulmonary perfusion, or intra-arterially to determine regional cerebral perfusion or myocardial perfusion. If the generator is opened to the air, the resulting gas can be inhaled to define regional ventilation. The 190 keV energy of the Kr-81m is well suited for imaging with low or medium energy collimators available on most scintillation cameras. Kr-81m is particularly useful for the repetitive evaluation of right ventricular function due to its short effective half-life (i.e. $T_{\frac{1}{2}}$ effective = $(T_{\frac{1}{2}} \text{ biological} * T_{\frac{1}{2}} \text{ physical}) / (T_{\frac{1}{2}} \text{ biological} + T_{\frac{1}{2}} \text{ physical})$). The short effective half-life comes from the combination of short physical half-life and short biological half-life due to the evolution of the radionuclide from the blood into the alveolus during its passage through the lung. As a result, no significant activity enters the left heart. The short

effective half-life results in a low radiation burden/MBq, which permits a large dose to be administered/injection.

Kr-81m right heart studies require high doses of Rb-81 on the infusion generator. The costs of producing the parent radionuclide, coupled with its short physical half-life make this an expensive nuclide. To market the generator at a reasonable price, primarily intended for use with inhalation imaging, the manufacturer elected to make the generator with 5 mCi of rubidium on the column. As a result, the photon flux available from the typical commercial generators is low. The detected photon flux of about 5000 cts/sec available from infusions of Kr-81m from this generator are less than 25% of that from Tc-99m during an equilibrium study. These low photon fluxes generate "noisy" images, which preclude the determination of regional wall motion of the right ventricle. If larger generators become available, Kr-81m will be useful for the determination of right heart function.

The ultrashort physical half-life of Kr-81m led to the development of a new approach to measure regional myocardial perfusion. Since the radio-nuclide decays in a shorter interval than the transit through the myocardial bed, images recorded during continuous infusion of Kr-81m are dominated by its input function - myocardial perfusion. The biological half-life of the agent in the myocardium is approximately 30 seconds, while its physical half-life is 13 seconds giving an effective half-life of 9 seconds. As a result, the usual inert gas clearance approach to measurement of regional myocardial perfusion with this nuclide is dominated by the physical decay of the nuclide, rather than the biological clearance due to perfusion. Therefore, a static image recorded during continuous infusion of the agent at the root of the aorta depicts the regional distribution of myocardial perfusion.

IRIDIUM-191m

Ir-191m is a generator-produced 4.7 second half-life radionuclide with gamma photons of 129 keV and X-rays of 65 keV. The parent, reactor produced Os-191, has a half-life of 15 days. The short half-life of the iridium product makes it difficult to characterize the chemical form of the Group VIII element. Although this generator was originally described in 1968 by Yano and Anger (1,2) for the determination of pulmonary perfusion, it was not until the recent work of Treves (3,4) that a generator practical for human use was developed. The radionuclide is associated with a radiation burden of 3-5 mrad/mCi while providing a high photon flux (the majority of the radiation burden stems from the "breakthrough" of the parent Os-191 into the Ir-191m eluate). Improvements in the column material recently suggested by Knapp et al (5) indicate that the radiation burden may be reduced by 10 to 100 fold. The combination of high photon flux and exceptionally low radiation burden are well suited to the pediatric population to evaluate shunts and ventricular function.

Although the agent can be used in adults, the intrathoracic transit time of 8-10 seconds is relatively long compared to the 4.7 second half-life. As a result, right heart data is recorded with a photon flux 2-4 fold greater than that of the left heart. To visualize the left heart well, the count rate from the right heart must be very high. This high photon flux may actually present a problem for Anger-type scintillation cameras, since count rates in excess of 100,000 counts/second result in dead time of the camera, and a non-linear relationship between activity in the field of view and counts recorded. The multi-crystal gamma camera, or the multi-wire proportional chamber described by Lacy et al (6) are able to take advantage of the

very high count rates offered by Ir-191m, since these instruments can process maximum count rates of 500-800,000 counts/second.

GOLD-195m

Gold-195m is a 30.5 second half-life daughter of the 40.5 hour, cyclotron produced, Hg-195. Au-195m has a 262 keV gamma photon which is 68% abundant. The chemical form of the gold eluted from the column is not well characterized, but it is likely that this Group IB nuclide is ionic. The half-life of Au-195m is long with reference to the central circulation time, and permits high quality studies of the left and right heart to be recorded. The combination of short half-life and high photon energy led Mena et al (7) to suggest that Au-195m could be i.o.-injected with Tl-201 at the time of bicycle exercise studies to permit an evaluation of global and regional function in conjunction with assessment of myocardial perfusion. The procedure described by Mena consisted of recording an Au-195m first pass ventricular function study, reprocessing the camera for Tl-201 and 5 minutes later recording myocardial perfusion data.

As with other short half-life generator-produced radionuclides, the radiation burden to the patient is primarily the result of "breakthrough" of the parent Hg-195. Since mercury compounds localize in the kidneys, the radiation burden from breakthrough increases the renal dose. Although improvements in the generator column and eluate have resulted in a marked decrease in the breakthrough problem, a limit of 300 mCi total dose is usually employed to minimize the radiation burden to the kidneys.

An additional problem, unique to the Au-195m generator system, is the decay of Au-195m to a long-lived daughter, Au-195 ($T_{\frac{1}{2}}$ physical 190 days). This decay process is continuously underway on the generator, which results in a high concentration of Au-195 in the initial eluate from the generator. Biodistribution studies in animals suggest Au-195 localizes in the kidneys, adding to the potential radiation burden from breakthrough of the parent Hg-195. To minimize the build up of Au-195, the column should be pre-eluted within 10 minutes of use.

RUBIDIUM-82

Rubidium-82 is a 75 second half-life positron-emitter; daughter of cyclotron-produced Sr-82 (Rb-85 ($p,4n$) - $T_{\frac{1}{2}}$ physical 25 days). The production of the parent Sr-82 requires a high-energy cyclotron, and is accompanied by the production of small quantities of Sr-85 as a radiocontaminant. Since strontium radionuclides localize in bone and have a long biological half-life, the generator system has been refined to minimize the "breakthrough" of the parent in the eluate. The generator is tested for breakthrough by the prior elution method described above. A maximum of 0.001 μ Ci Sr-82/mCi Rb-82 results in a radiation burden of 0.019 rads/mCi to the kidney and 0.001 rads/mCi to the total body.

Rubidium-82, a member of Group IA, is eluted from the generator as a monovalent cation. The agent behaves as a Sapirstein tracer (e.g. the regional distribution of the radionuclide is proportional to perfusion in organs with high extraction). The radionuclide is concentrated in tissues by the Na-K ATPase pump and has a myocardial extraction between 65 and 75%. As with other generator produced ultrashort-lived nuclides, quality control is by pre-elution calibration and direct infusion of the dose to the patient.

Myocardial imaging with this radionuclide requires fast acquisition of data. Images recorded during the first 1-2 minutes after intravenous administration depict the blood pool distribution of the radionuclide (if images are recorded with gating, ejection fraction and regional wall motion can be determined), while images recorded after 2 minutes depict regional perfusion. Reasonable quality images can be recorded for 4-6 half-lives after infusion, 1-2 half-lives are consumed with clearance, and the remainder for myocardial perfusion. Although images of this positron-emitting nuclide can be recorded with a single photon camera (see below) the highest quality images are recorded with a multi-slice positron tomograph.

Recent studies by Gould and Mullani (8) demonstrated the ability to measure absolute as well as relative myocardial perfusion from Rb-82 PET images with a time-of-flight positron camera. A limitation of this approach to calculating absolute flow, is the problem of diffusion limitation at myocardial blood flows $>2x$ baseline (flow rates commonly observed with dipyridamole infusions). At these perfusion levels, the deposition of Rb-82 in tissue will underestimate regional perfusion. However, since coronary disease is associated with a marked decrease in perfusion, the non-linearity of the measurement in the higher ranges are not of great importance clinically. Selwyn and his colleagues (9) have made several unique observations with the Rb-82 PET imaging technique: 1. In patients with CAD, marked changes in regional myocardial perfusion were observed during the performance of mental arithmetic. These changes were of similar severity to those induced by exercise. 2. Following restoration of perfusion to zones of ischemia, prolonged abnormalities in cation uptake were observed, presumably due to disturbances in cation transport and trapping.

If a PET camera is unavailable, images can be recorded with an Anger scintillation camera with a specially constructed high energy tungsten collimator. The sensitivity of this single photon approach, however, is about 0.1% that of the positron technique. Even with this low sensitivity, the quality of the images is similar to that of Tl-201.

Overall, these ultrashort-lived agents offer an extremely useful approach to the repetitive evaluation of patients with rapidly changing states. The high photon flux and low radiation burden make the agents attractive for use in acute care environments, where increasing concerns about radiation dose to the hospital staff have been observed. Since the patients have no significant residual radioactivity at the conclusion of these studies, there is no need to implement radiation precautions for the staff. This should lead to increased acceptance of the studies, enhanced utilization, and improved patient care as a result of more detailed monitoring of cardiac function.

REFERENCES

1. Yano Y., H.O. Anger. Ultrashort-lived radioisotopes for visualizing blood vessels and organs. *J. Nucl. Med.* 9, 2-6, 1968.
2. Yano Y. Radionuclide generators: Current and future applications in nuclear medicine, in *Radiopharmaceuticals*, edited by G. Subramanian, B.A. Rhodes, J.F. Copper, and V. Scdd, pp 236-245, Soc. Nucl. Med. Inc., New York, NY, 1975.
3. Cheng C., S. Treves, A. Samuel, and M.A. Davis. A new osmium-191 iridium-191m generator. *J. Nucl. Med.*, 21, 1169-1176, 1980.

4. Treves S., C. Cheng, A. Samuel, et al. Iridium-191m angiography for the detection and quantitation of left to right shunting. *J. Nucl. Med.*, 21, 1151-1157, 1980.
5. Brihaye, C., T.A. Butler, F.F. Knapp, Jr., M. Guillaume, E.E. Watson, and M.G. Stabin. A new osmium-191 Ir-191m radionuclide generator system using activated carbon. *J. Nucl. Med.* (In Press).
6. Lacy, J.L., M.S. Verani, A. Packard, et al. Minute to minute assessment of left ventricular function with a new multiwire gamma camera and a ultrashort-lived isotope Ir-191m. *J. Am. Coll. Cardiol.*, 5, (2), 388, 1985.
7. Mena I., K.A. Narahara, R. DeJong, and J. Maublant. Gold-195m, an ultrashort-lived generator produced radionuclide: Clinical applications in sequential first pass ventriculography. *J. Nucl. Med.*, 24, 139-144, 1983.
8. Mullani, N.A., K.L. Gould, R.A. Goldstein, et al. Gated blood pool and myocardial perfusion imaging by PET after a single IV injection of rubidium-82. *Circulation*, 70, (Supp II: II-24), 1984. Abstract.
9. Selwyn, A.P., G. Forese, K. Fox, K. Jonathan, and R. Steiner. Patterns of disturbed myocardial perfusion in patients with coronary artery disease: regional myocardial perfusion in angina pectoris. *Circulation*, 64, pp 83-90, 1981.

DISCUSSION

HARRIS: There is an additional dosimetry consideration with using the Rb-82 generator. The 30 millicuries of Sr-82 is frequently accompanied by about 200 millicuries of Sr-85. When the generator is packaged in the usual Tc-99m generator shield, the Sr-85 increases the radiation level in the vicinity of the generator.

STRAUSS: I agree with you, Craig. When we obtained our rubidium generator, we had to modify our license to allow us to possess the 200 millicuries of Sr-85; however, the breakthrough of strontium from the system is now low enough that it does not present a serious dosimetry consideration.

MARCUSE: Do you have some difficulties in finding the ventricular volume and, when calculating the ejection fractions, do you have some particular techniques for subtracting background?

STRAUSS: When we calculate ejection fractions, with either the iridium approach or technetium red cells, we use the conventional method of identifying background in the lungs and subtracting that from the left ventricular time-activity curve. We are not using any special approaches to make these measurements, these are all done with commercially available programs on our nuclear medicine computer systems.

MANSPEAKER: With the Os/Ir generator, what is the typical duration of the study and what would be the resulting volume of the infusion to the patient? What are the clinical implications of infusing this volume of fluid into a patient suffering from congestive heart failure?

STRAUSS: Studies can be done with the osmium-iridium generator in either the bolus or continuous infusion modes. At present, the generator is eluted with saline at pH 2, with some additional potassium iodide (to increase the elution efficiency). The eluate is neutralized (using two syringes) by online mixing with base at the time of elution-injection. Bolus studies are typically done with volumes less than 10 ml (3-5 ml elution and 5 ml flush), and would not present a problem to patients in heart failure. To date, the continuous infusion studies have only been done in animals. Infusion rates between 10 and 25 ml/minute, without additional buffer solution, have been used for both the coronary and renal perfusion studies. Higher infusion rates do not increase the count rate. Regardless of the infusion rate, a steady state count rate is achieved within about 15 seconds of initial visualization of activity in the field-of-view. The duration of the infusion is then determined by the count density desired in the images. If a single measurement is contemplated, the total measurement should be completed within 1 minute. Patients in mild heart failure should be able to tolerate a 25 ml volume. Patients in severe failure, however, would present a problem.

MYERS: This is more of a comment than a question. You don't seem to have addressed directly the radiation dosimetry of the ultrashort-lived radionuclides. For this you need to know the distribution of activity on a quantitative basis. Could I suggest one approach to this involving a two stage process? Firstly, a known amount of a long-lived biologic analog is imaged in the patient to approximate the biologic distribution of the ultrashort-lived radionuclide (assumed to be in equilibrium). Secondly, as a separate phantom experiment or calculation, the imaging characteristics of the long-lived biologic analog and the short-lived radionuclide are related. As an example, for Kr-81m lung imaging, a known amount of Tc-99m-MAA acts as the biologic analog and camera counts from regions of interest in the patient may be acquired. The imaging properties of Kr-81m and Tc-99m are related in a phantom experiment such that the camera is calibrated directly in terms Kr-81m in the patient. Acquisition can then be performed until the required dose is reached. Calibrating the gross input of the ultrashort-lived radionuclide is quite inaccurate because of losses in the delivery system.

STRAUSS: You are actually getting to the crux of an issue which I chose to avoid. The problem of actually computing absorbed dose from these ultrashort-lived tracers is a fair one, but in my experience with our own radiation safety committee and Dr. Ted Webster, who I think is fairly knowledgeable in the area of dosimetry, the major issues are not the doses from the ultrashort-lived nuclide itself. Dr. Webster feels that with something such as Ir-191m with a 5 sec. half-life or with Rb-82 with it's 75 sec. half-life, the dosimetry from that nuclide is not the one of major concern. His major interest has been the other things that will come through or, as in the case of the gold-195m, the progeny production and the half-life and biodistribution of the progeny in the patient. While I believe it is important to know the dosimetry from the tracer and certainly its calibration, I did not mention the issue which is certainly a major problem. I don't think anyone at this moment has a system where we can calibrate the actual dose as it is being administered to the subject. Squibb is evaluating a system to do this for their rubidium generator, and I am aware of some work Barry Wessels and his colleagues are doing on the iridium system so that one can actually calibrate the dose as it is being administered. One issue that has come up with iridium is where do you measure the dose? Do you do it at the catheter port? In our system we have always used catheters threaded into the patient's central circulation. Do you make the measurement at the entry port, let's say in the jugular? With an iridium infusion, the intensity of your photon flux is highly variable depending on where you measure it. If you take the measurement at the catheter exit port, that is one thing; if you take it in the right ventricle or left ventricle or some other place in the patient, that is quite different.

WONG: I would like to ask what precautions you think are necessary with respect to breakthrough of the parent for ultrashort-lived isotopes; then I have a quick comment about our experience with Kr-81m.

STRAUSS: I think the way we have approached this and the way our committees have found satisfactory is to pre-elute. Most of these generators have a characteristic breakthrough with increasing volumes through the generator. If you know how many milliliters you put through the unit, you can determine approximately where you are on the potential breakthrough curve. Another thing we do after about 10 half-lives is to pre-elute and check the eluate with the dose calibrator for breakthrough. When you have documented where you are on the breakthrough curve, the next elution can go into the patient.

WONG: I basically agree with most of that. I would like to add that recently we have been making our own Rb-81 generators at Hopkins for Kr-81m. Not only do we pre-elute, but we also find differences depending on how we pack the generators. Some of the data can be found in the November 1985 issue of the American Journal of Cardiology. Another thing which we've done, although I think that with very consistent quality control it is unnecessary, is add a second peanut downstream as a trap. Then you actually can count to see how much is really there. We've decided other systems, such as alarm systems, detection systems, are probably impractical.

I think your comments concerning the dosimetry were quite appropriate. We have certainly found, and the people who work with oxygen-15 water would also agree, that the highest dose area is at the injection site. That can be quite high, but, of course, it is a radioresistant area. I think that the factors concerning elution, speed, volume, and characteristics are important when you specify the dosimetry.

PROBLEMS IN RADIATION ABSORBED DOSE ESTIMATION FROM POSITRON EMITTERS

G.F. Powell, P.V. Harper, C.S. Reft, C.-T. Chen, and K.A. Lathrop

University of Chicago Hospitals and Clinics
5841 S. Maryland
Chicago, IL 60637

ABSTRACT

The positron emitters commonly used in clinical imaging studies for the most part are short-lived, so that when they are distributed in the body the radiation absorbed dose is low even though most of the energy absorbed is from the positrons themselves rather than the annihilation radiation. These considerations do not apply to the administration pathway for a radiopharmaceutical where the activity may be highly concentrated for a brief period rather than distributed in the body. Thus, high local radiation absorbed doses to the vein for an intravenous administration and to the upper airways during administration by inhalation can be expected. For these geometries, beta point source functions (FPS's) have been employed to estimate the radiation absorbed dose in the present study. Physiologic measurements were done to determine other exposure parameters for intravenous administration of O-15 and Rb-82 and for administration of O-15-CO₂ by continuous breathing. Using FPS's to calculate dose rates to the vein wall from O-15 and Rb-82 injected into a vein having an internal radius of 1.5 mm yielded dose rates of 0.51 and 0.46 (rad·g / μCi·h), respectively. The dose gradient in the vein wall and surrounding tissues was also determined using FPS's. These results, along with the physical parameters determined by bolus injection experiments, indicate the need to reduce exposure time by saline flushing to remove activity from the site of injection as quickly as possible. Administration of O-15-CO₂ by continuous breathing was also investigated. Using ultra-thin thermoluminescent dosimeters (TLD's) having the effective thickness of normal tracheal mucosa, experiments were performed in which 6 dosimeters were exposed to known concentrations of O-15 positrons in a hemicylindrical tracheal phantom having an internal radius of 0.96 cm and an effective length of 14 cm. The dose rate for these conditions was 3.4 (rads / h) / (μCi / cm³). Calculations performed using FPS's to support the TLD results demonstrate little difference between doses for activity in the hemicylindrical model either airborne or coated on the walls. This calculation was necessary because O-15-CO₂ exchanges with water in the tracheal wall. Experiments in which low concentrations of O-15-CO₂ were administered to volunteers revealed that additional activity present in the trachea due to this reaction was 4.8 ± 0.6 times higher than would be observed without this phenomenon. Aside from these considerations, a correction had to be made for the virtual absence of O-15-CO₂ in expired air. Using these values to calculate the dose to the tracheal mucosa due to the administration of O-15-carbon dioxide for 30 minutes at a concentration of 1 μCi / cm³ gave 4.1 rads. The tracheal dose was used as an example here because it can be easily approximated by a hemicylinder. However, activity seen in the nasopharynx of a volunteer who participated in O-15-CO₂ studies to determine the effects of mouth and nose breathing was 7.1 ± 2.7 times higher than would have been observed during mouth breathing without an uptake phenomenon and 8.5 ± 1.0 times greater for the nose breathing experiment. Thus, the dose to the nasopharynx from the inhalation of O-15-CO₂ should be examined along with other areas in the upper airways.

INTRODUCTION

The majority of radionuclides used in nuclear medicine emit principally medium energy

gamma radiation and little particle radiation so that even with fairly long half-lives, radiation absorbed doses are low. The positron emitters in current use for imaging emit primarily particle radiation which results in a much higher locally absorbed radiation dose rate. The factor which largely balances this increase is the short physical half-lives of the agents: e.g., oxygen-15, carbon-11, nitrogen-13, rubidium-82 and flourine-18. Substantial millicurie quantities of these agents distributed in the body result in tolerable radiation absorbed dose levels.

For shorter lived materials, particularly oxygen-15 (122 s) and rubidium-82 (75 s) where 50 to 100 mCi result in moderate absorbed doses in source organs when using conventional methods for estimation of the absorbed dose, the radiation exposure along the route of administration becomes important. Here, when the exposure time is short compared with the physical half-life of the nuclide, or where continuous administration directly from a production facility is being carried out, the compensating effect of the short half-life is lost, and very high, if brief, exposures are given to the upper airway mucosa from administration by inhalation, and to the vein wall from intravenous administration.

These cases, which fall outside the MIRD formalism, are the basis for the present report. In each case there are two aspects to consider. First, the beta dose to the wall of the organ in question from its contents (gamma dose is negligible in comparison) and second, the concentration of activity and the exposure time resulting from the administration parameters, e.g., respiration, blood flow, injection rate, etc.

INTRAVENOUS ADMINISTRATION

INTRODUCTION

Explicit calculations of beta dose to the surface of a cylindrical volume containing the emitter are not available in the literature. The factors to be considered are the following:

1. radius of the vein;
2. concentration of the radionuclide;
3. energy and spectral shape of the emitter; and
4. exposure time, determined by
 - a. rates of injection, and
 - b. blood flow.

Combining these considerations, the dose gradient for any vein radius can be calculated from the beta point source function (FPS) of the nuclide, for the vein wall and extending into the surrounding tissues to the end of the beta particle range.

PHYSIOLOGICAL MEASUREMENTS

Consider first the concentration of emitter and the exposure time. Assume that activity is being injected into the vein at a constant rate of 'A' mCi / s in a small volume. Assume a blood flow rate of 'B' ml / s and further assume complete mixing in the vein. Then, the concentration 'C' of activity in the vein is, $C = A/B$ mCi / ml. To determine blood flow and vein radius, a small bolus of known volume containing $\sim 500 \mu\text{Ci}$ of Tc-99m was injected into a typical vein, and the length and movement of the bolus was determined by imaging at short intervals (0.10 to 0.15 s) with a gamma camera. The observed length of the bolus together with its known volume allowed calculation of the vein radius and this together with the observed motion of the bolus permitted calculation of the flow rate 'B' and the exposure time.

It is of interest that the vein exposure appears to be independent of the injection rate for a given amount of activity. For instance, injection at half the rate reduces the concentration by half but doubles the exposure time. Thus, bolus injection and continuous infusion give equal exposure for the same activity injected under the assumptions given above.

In a typical example, 0.5 ml of Tc-99m DTPA was injected in 0.7 s into a rather large antecubital vein. Following injection, the leading end of the bolus moved at 8.6 cm/s. The length of the bolus at the end of injection was 10.3 cm. Correcting for the flow during the 0.7 s injection period gave a corrected bolus length of 4.3 cm, assumed to be 0.5 ml (i.e. the same volume as the

injected bolus), giving a flow rate of 58 ml / min and an exposure time of 0.5 s. Data from two such measurements are shown in Table I.

Table I. Results of Bolus Injection Measurements

Vein	Bolus Volume (ml)	Injection Time (s)	Initial Bolus Length (cm)	Bolus Movement [†] (cm / s)	Corrected Bolus Length (cm)	Vein Radius (mm)	Vein Flow Rate (ml / m)
Antecubital	0.5	0.7	10.3	8.6	4.3	1.9	58.
Forearm*	0.2	0.6	9.6	0.0	9.6	0.8	12.**

[†]Bolus movement during injection.

*Vein was compressed during administration.

**Vein flow rate after release of vein compression.

The radiation absorbed dose to the vein wall for a given concentration and exposure time was then calculated using point source functions (FPS's).

POINT SOURCE FUNCTION CALCULATIONS FOR A CYLINDRICAL VEIN

A Point Source Function (FPS) is defined as the rads per disintegration at a distance x from a point source emitting beta particles in a homogeneous medium. Ideally, these fuctions may, in general, be used for both positrons and negatrons. Several FPS's are described in the literature(1,2,3). For the following calculations, the Loevinger FPS (1) was employed because it appeared easier to integrate and is perhaps the best known FPS. The FPS of Loevinger et al. is usually represented by $J(x)$ and is defined for allowed beta spectra (i.e., beta particles come out of the nucleus radially without angular momentum) as

$$J(x) = \frac{k}{(v x)^2} \left\{ c \left[1 - \frac{v x}{c} e^{\{1-(vx/c)\}} \right] + v x e^{\{1-vx\}} \right\} \quad \text{rads/disintegration, where}$$

[]=0 for $x > (c/v)$.

The value of v is the apparent attenuation coefficient, c is a correction term dependent only on the maximum beta energy, e is the natural log value 2.71828..., and k is a normalization constant derived from the consideration that the average energy imparted per disintegration by a point source to a surrounding homogeneous medium is equal to the average energy of the beta spectrum. Thus,

$$k = \bar{E}_\beta (\text{MeV}) / \int_0^\infty 4 \pi \rho x^2 J(x) dx$$

where \bar{E}_β represents the average energy of the beta spectrum and ρ is the density of the medium.

With appropriate conversion factors, the resulting expression for k is

$$k = 1.275 \times 10^{-9} v^3 \rho^2 \bar{E}_\beta \alpha \quad \text{rads/disintegration, where}$$

$$\alpha = [3c^2 - (c^2 - 1)e]^{-1}$$

with v expressed in cm^2/g and ρ in units of g/cm^3 . Of course, it is sometimes preferable to express v in units of cm^{-1} . However, care should be taken so that any term " $v x$ " is dimensionless.

As noted by Loevinger (1), the term $-v R_0 e^{\{1-vx\}}$, where R_0 is the continuous slowing down approximation (c.s.d.a.) range of the betas in the medium, may be included within the large brackets of the $J(x)$ expression for values of x , where $R_0 / 2 \leq x < R_0$, since this term allowed a better fit of Loevinger's experimental data for values of x in this range. However, because of the slight change in calculated dose and the large increase in complexity of integration of the FPS, this term was omitted in the present calculations.

Integration of $J(x)$ to determine the dose to a point on the wall of a cylinder from activity in the cylindrical volume elements is non-trivial. This was accomplished by approximating activity in a

vein with a large array of parallel line sources. For a single line source in a homogenous medium, the dose rate to a point "P" a perpendicular distance h_0 from a line source (S -> Figure 1.) is given by

$$D(P) = \int_{-y_{\max}}^{+y_{\max}} \xi J(r) dy$$

$$\text{where } r^2 = h_0^2 + y^2$$

and ξ is the number of disintegrations per unit length. The magnitude of y_{\max} is given by the equation

$$y_{\max}^2 = R_o^2 - h_0^2$$

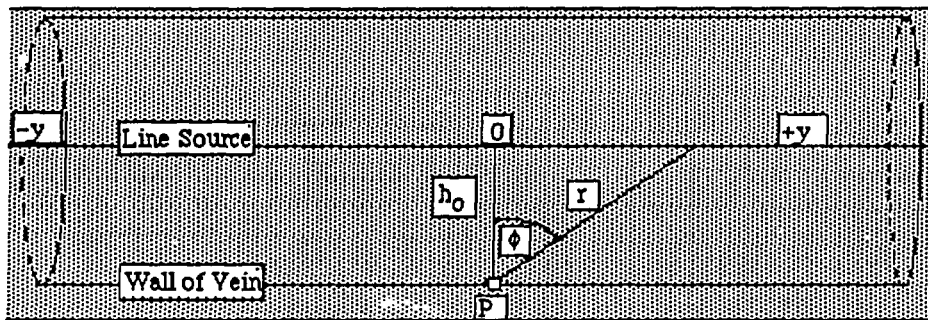


Figure 1. Geometry used for line source array calculations. A single line source is shown located in a vein. The medium is considered homogeneous.

Of course, for the case of $h_0 > R_o$, $D(P)$ is zero. Using symmetry, $D(P)$ may be written as

$$D(P) = 2 \xi \int_0^{y_{\max}} J(r) dy$$

Integration of the above expression yields

$$D(P) = 2 k \xi [(c/v h_0) \tan^{-1} \{ [(c/v h_0)^2 - 1]^{1/2} \} - (e/v) \sqrt{2\pi} [E_1(2h_0v/c) - E_1(2)] + (e/v) \sqrt{2\pi} [E_1(2vh_0) - E_1(2vR_o)]] \quad h_0 < c/v$$

$$D(P) = 2 k \xi (e/v) \sqrt{2\pi} [E_1(2vh_0) - E_1(2vR_o)] \quad c/v < h_0 < R_o$$

$$D(P) = 0 \quad h_0 \geq R_o$$

where $E_1(x)$ represents the exponential integral. The exponential integral is defined as

$$E_1(z) = \int_z^\infty \frac{e^{-t}}{t} dt \quad (|\arg z| < \pi)$$

where the value of z may have a complex phase angle component. However, this is not the case here and the equation may be represented as $E_1(x)$ where x is a real number. Fortunately, good approximation formulas for $E_1(x)$ may be found in the literature (4).

To estimate the dose from Rb-82 and O-15 injected intravenously, a 444 line source array was employed. Rb-82 decays by electron capture and positron emission, while O-15 is a pure positron emitter. Only the beta dose contributed by the two prominent positrons (beta 4 and beta 5) was considered in the evaluation of Rb-82 dose. The information used for these calculations is provided in Table II. Figure 2 provides a comparison of the calculated vein wall dose and classical approximation which simply assumes that the dose rate to the wall of the vein is half of the value of Δ_i , the equilibrium dose rate constant for the emitted particles (6). From Figure 2 it is clear that a classical approach is not valid where the particle range significantly exceeds the vein radius. Figure 3 shows the calculated depth dose rates from injected Rb-82 and O-15 for a vein with a diameter of 3 mm.

Table II. Data Used to Calculate Vein Wall and Depth Dose Rates

Beta Emitter	n_i^* (n/dis)	v^{**} (cm ² /g)	R_0^{***} (g/cm ²)	\bar{E}_β^\dagger (MeV)	$\Delta_i^{\ddagger\dagger}$ (rad·g/μCi·h)
O-15	1.	9.2	0.82	0.72	1.53
Rb-82, Beta 4	0.115	5.8	1.1	1.06	0.259
Beta 5	0.828	3.9	1.7	1.42	2.51

Note: The density of the medium was 1.06 g/cm³, the density of blood and the Loevinger c value was 1.

* n_i = the average number of betas per disintegration. Data taken from MIRD Pamphlet No. 10 (5).

** v = the apparent attenuation coefficient calculated using the formula provided by Loevinger (1).

*** R_0 = the c.s.d.a. (continuous slowing down approximation) range, extrapolated from data given by Bochkarev (3).

† \bar{E}_β = the average energy of the positrons. Data taken from MIRD Pamphlet No. 10 (5).

†† Δ_i = equilibrium dose rate constant. Data taken from MIRD Pamphlet No. 10 (5).

CALCULATION OF VEIN DOSE

For the cases cited in Table I, the β dose to the vein wall surface from intravenously injected O-15 and Rb-82 may be calculated from the values in Tables I and II and in Figure 2. As an example, assume that an equal concentration of activity (100 mCi/ml) injected into each vein replaces an equivalent volume of the blood but does not disturb the blood flow. The resulting exposure time is given by

$$\text{Calculated Exposure Time (s)} = \text{Bolus Volume (ml)} / \text{Venous Flow rate (ml/s)}.$$

The dose to the wall of the vein may be estimated by multiplying the calculated dose rate (g·rad)/(μCi·h) by the activity concentration (in units of μCi/ml, assuming 1 ml = 1 g) and the exposure time (expressed in hours). Table III gives a summary of the results of the dose calculations for the parameters in Table I.

Table III. Summary of the Results of Vein Wall Dose Calculations

Vein	Bolus Volume (ml)	Vein Radius (mm)	Venous Flow Rate (ml / min)	Amount Injected (mCi)	Calculated Exposure Time (s)	Vein Wall Dose (rads)	O-15	Rb-82
Antecubital	0.5	1.9	58.	50.	0.5	8.1	8.7	
Forearm	0.5	0.8	12.	50.	2.5	37.	33.	

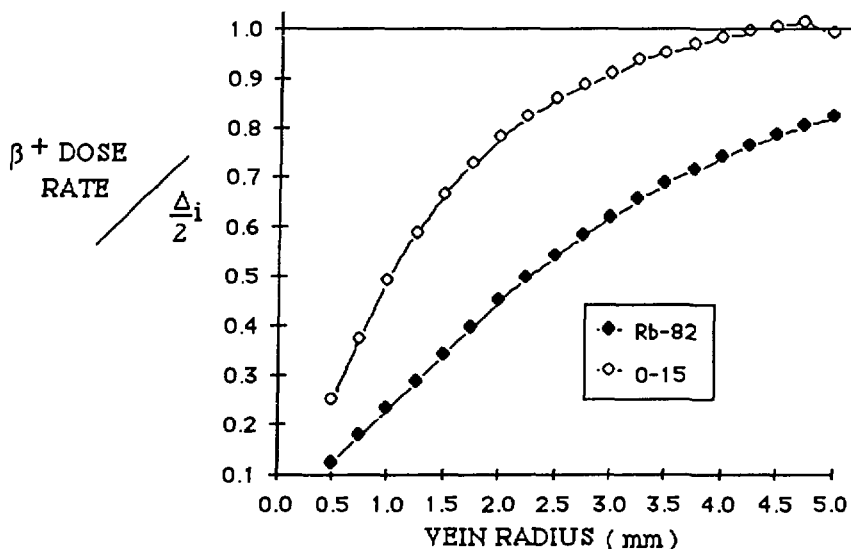


Figure 2. Calculated dose rate to the inside surface of the vein wall as a function of vein radius.

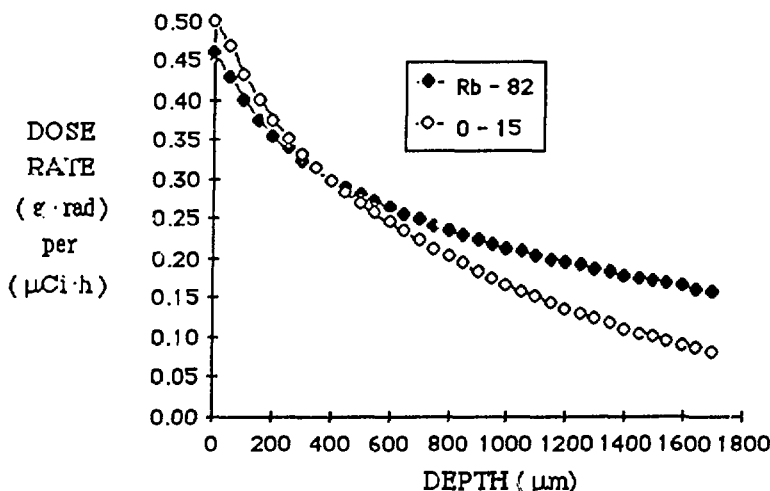


Figure 3. Positron dose rate to the wall (i.e., DEPTH = 0) and surrounding tissues of a vein (3mm in diameter) due to a bolus injection of O-15 or Rb-82.

DISCUSSION OF VEIN DOSE CALCULATIONS

It may be argued that the calculated exposure times shown in Table III may not be realized in clinical practice. Additional factors that must be considered in any realistic dose calculation are:

1. Due to vein elasticity, rapid injection of a large bolus increases the radius of the vein and the venous flow rate.
2. Compression of the vein during administration stops the blood flow and therefore, can significantly increase the dose by increasing exposure time.
3. The available concentration of the activity affects the choice of the administration method.

As mentioned above, reducing the concentration of the beta emitter will not decrease the dose

because the exposure time is increased. It is also clear that injection of activity into a vein with a slow flow rate can greatly increase the dose. Therefore, it is advisable to follow any injection of a positron emitter with a saline "flush" to aid in the removal of the bolus from the injection site and allow the activity to proceed quickly to larger veins with greater venous flow rates.

ADMINISTRATION BY INHALATION

INTRODUCTION

The usual assumption used in the majority of dose calculations involving administration by inhalation is that the dose to the upper airways is small compared with the lung dose. It has also been usually assumed that the administered nuclides do not adhere to the walls of the airways. Recent evidence has shown that, at least in the case of the administration of O-15-CO₂ by continuous breathing, such adherence does occur (7,8). Again, explicit descriptions of dose calculations are not found in the literature. For the present study, the exposure parameters involved in the administration of O-15-CO₂ by continuous breathing are presented and the approach used to calculate the dose to tracheal mucosa is described.

Two major considerations in the calculation of the dose to the tracheal mucosa due to the administration of O-15-CO₂ by continuous breathing are:

1. A correction to account for the virtual absence of O-15-CO₂ in expired air.
and
2. The effect of activity adhering to the wall of the trachea due to the exchange of O-15-CO₂ with water in the tracheal mucosa.

These factors determine the geometry of the source distribution (aside from the physical dimensions) and the time parameters (aside from the actual administration period). Both of these must be incorporated with FPS calculation results and/or physical measurements to determine the tracheal dose.

PHYSIOLOGICAL MEASUREMENTS

The adherence of O-15-CO₂ to the tracheal mucosa was investigated using low levels of activity in continuous breathing experiments with 6 volunteers. The data were collected using a Searle Positron Two Camera system (9) and an Ohio Nuclear 150 data acquisition system. The Positron Camera System consists of two scintillation cameras connected in coincidence. Imaging was done using the stationary mode usually in the lateral projection with a plane of focus located in the middle of the subject as determined by focussing on a point source. Data were collected at a rate of 5 seconds per frame. Using a ⁶⁸Ge-⁶⁸Ga sheet source, field flood and subject transmission images were recorded to correct the data for camera sensitivity and attenuation of the annihilation radiation in the subject. Singles rates were also monitored to correct the data for dead time losses. A review of the data analysis procedures is provided in the Appendix. Figure 4 shows the results of a continuous breathing study. The majority of the studies were performed with the subject breathing through a simple mouthpiece in the sidearm of a corrugated tube through which the labeled activity and breathing gas passed to waste. One experiment (No. 5) was performed using a breathing mask with the subject breathing through his mouth. Two "nose breathing" experiments (No. 4 and No. 6) were performed with the same mask. No apparent differences in the tracheal uptake were observed. It was determined that the ratio of the CO₂ taken up in the tracheal wall to that which would have been observed under conditions of no uptake was $4.8 \pm .6$ (See Table IV). This ratio was calculated taking into consideration the virtual absence of O-15-CO₂ in expired air.

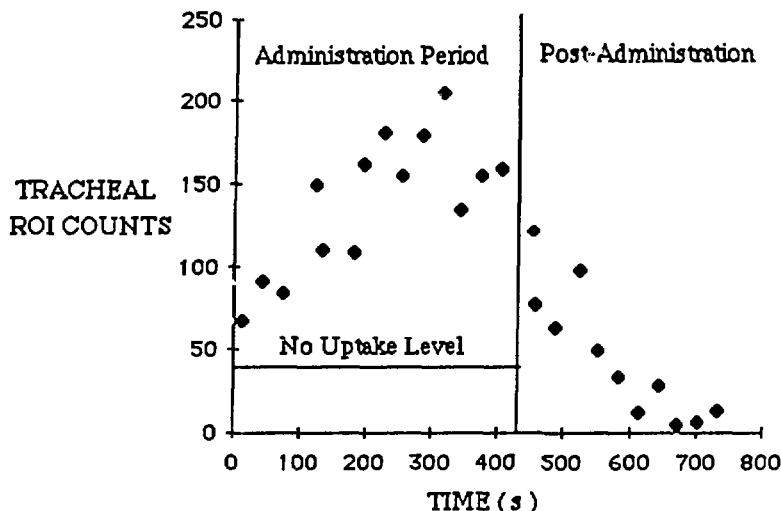


Figure 4. Tracheal uptake results of a O-15-CO₂ breathing study (No. 3 in Table IV). The data represent the corrected tracheal region of interest (ROI) counts as outlined in the Appendix. The "No Uptake Level" refers to tracheal ROI counts in the absence of uptake in the tracheal wall as determined in molecular O-15-O₂ experiments or by extrapolation of the data back to the first breath.

TABLE IV. Summary of O-15-CO₂ Continuous Breathing Studies

STUDY NUMBER	TRACHEAL GAS (ROI COUNTS)	EQUILIBRIUM BUILDUP (ROI COUNTS)	UPTAKE RATIO
1	37. ± 6.1 [^]	190. ± 14. ^{††}	5.0 ± 0.90
2	15. ± 4.4*	64. ± 8.0 ^{††}	4.2 ± 1.3
3	35. ± 10. [†]	170. ± 20. ^{**}	4.9 ± 1.5
4	3.4 ± 0.42*	17. ± 3.9 ^{**}	5.0 ± 1.3
5	16. ± 3.1*	93. ± 23. ^{**}	5.9 ± 1.9
6	13. ± 4.1*	47. ± 12. ^{**}	3.7 ± 1.9
AVE. RATIO =			4.8 ± .61

[^]Combined least squares monoexponential fit and extrapolation. Poisson statistics assumed.

*Determined by O-15-O₂ studies corrected for virtual absence of O-15 labeled CO₂ in expired air.

[†]Determined by extrapolation of the data back to the first breath.

^{††}Determined by least squares fit. Poisson statistics assumed.

**Average value of corrected ROI counts at equilibrium buildup level.

DOSE MEASUREMENTS AND CALCULATIONS FOR A TRACHEAL PHANTOM

Introduction

Dose to the tracheal mucosa from activity present only in the tracheal gas was determined by direct measurements in a tracheal phantom and by calculations using modified point source functions. Each technique will be described in detail, beginning with the dose measurements.

TLD Measurements in a Tracheal Phantom

Experiments were performed with thermoluminescent dosimeters (TLD's) in a hemicylindrical

phantom, constructed similarly to the model used by Goddard and Ackery (10) for calculating the dose from labeled xenon gases. Since betas may be significantly attenuated in a thick TLD, ultra-thin TLD's were used. Table V provides a summary of the important characteristics of these TLD's.

Table V. Characteristics of Ultra-Thin TLD's Used
in O-15-CO₂ Dose Measurements in a Tracheal Phantom

Type of TLD*	LiF (7)-Teflon Discs
Diameter	6 mm
Thickness	20 μm
Weight	1.44 \pm .27 mg
Effective Z	8.3
Minimum Detectable Dose	.6 rads
Density	2.54 g/cm ³
Calibration	Individually with Co-60

*Manufactured by Teledyne Isotopes, 50 Van Buren Ave., Westwood, N.J., 07675.

The tracheal phantom employed was made of lucite and was approximately tissue equivalent. The internal radius of the tracheal phantom was 0.96 cm and the effective length was 14 cm with a 10 cm insert used to complete the hemicylindrical geometry (See Figure 5). Six TLD's having approximately the effective thickness of normal tracheal mucosa (i.e., 50 μm , (11)) were placed in the center on the flat hemicylindrical surface and a known concentration of O-15-CO₂ was passed over these TLD's at a predetermined rate. These TLD's had been individually calibrated with Co-60. The calibration was also tested by using the TLD's to determine the dose rate from a known standard uranium metal sheet source. The results of two experiments with O-15 positrons are shown in Table VI.

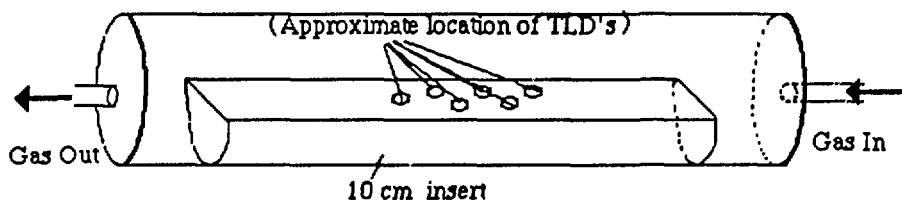


Figure 5. Schematic of the hemicylindrical tracheal phantom.

TABLE VI. Results of TLD Measurements in the Tracheal Phantom

O-15-CO ₂ concentration ($\mu\text{Ci}/\text{cm}^3$)	Exposure Time (minutes)	TLD Dose*	rads/h per $\mu\text{Ci}/\text{cm}^3$
6.3 \pm 0.32	8.0 \pm 0.1	2.8 \pm 0.3	3.3 \pm 0.4
17.9 \pm 0.73	10.0 \pm 0.1	10.0 \pm 0.3	3.4 \pm 0.17

*Average of six dosimeters

Calculation With Point Source Functions

The second approach employed both the Loevinger (1) and Bochkarev (3) FPS's. The Bochkarev FPS is represented by

$$\psi(r) = \{1/(4\pi r^2)\} W(r) \quad (\text{MeV/g}), \text{ and}$$

$$W(r) = .25 W_0 e^{-10X} + .75 W_0 e^{-2X} + K X e^{-X} \quad (\text{MeV cm}^2/\text{g}), \text{ where}$$

$$X = r v \quad \text{and} \quad W_0 = |\bar{E}_\beta/dr| \quad (\text{MeV cm}^2/\text{g}).$$

K is found by satisfying the same normalization condition as the value of k in the Loevinger FPS evaluation and is given by

$$K = \bar{E}_\beta v - .4 W_0 \text{ (MeV cm}^2/\text{g}).$$

Of the two FPS's, the Bochkarev is considered more accurate, especially for short distances through which betas are attenuated (3). For purposes of convenience W_0 and K may be expressed in units of (MeV / cm). The values for the apparent attenuation coefficient are usually different and thus, v_B and v_L will be used to denote the Bochkarev and Loevinger apparent attenuation coefficients, respectively.

A line source array approximation of the activity was employed to represent the activity present in a hemicylindrical model. Figure 6 shows the geometry used to describe the dose contribution from a single line source to a point P located at a depth of h_{oi} , perpendicular to the flat surface of the hemicylinder. Both FPS's required a slight modification to account for the geometric fall off in intensity of the activity located in the hemicylindrical volume while neglecting physical attenuation until the positrons reached the tissue equivalent medium. The resulting equations were simply,

$$J(x,d) = \frac{x^2}{(x+d)^2} J(x), \quad \text{and}$$

$$\psi(x,d) = \frac{x^2}{(x+d)^2} \psi(x),$$

where x is the distance in which the intensity of positrons emitted toward a point P in a tissue equivalent medium from a point on the line source (located above the medium) is physically attenuated and d is the pathlength in which only geometrical (i.e. $1/r^2$) falloff occurs. Since the gas in the trachea does not appreciably attenuate the positrons, these corrections were used. Tissue-air interface effects were ignored.

To calculate the dose to the point P (See Figure 6) from a single line source located in a hemicylindrical tracheal model, the solutions using the Bochkarev and Loevinger formalisms are:

$$D(P)_B = 2 \xi \int_0^{s_{\max}} \psi(x,d) ds, \quad \text{and}$$

$$D(P)_L = 2 \xi \int_0^{s_{\max}} J(x,d) ds,$$

respectively, where ξ denotes the dis/cm along the line source and s_{\max} is determined by the condition that x must be less than the c.s.d.a. range (R_0) of the betas and s_{\max} must be less than or equal to one-half the length of the hemicylinder.

From Figure 6 it can be seen that the following relationships exist:

$$\begin{aligned} x &= h_0 \sec \phi \\ d &= z_0 \sec \phi \\ s &= (h_0 + z_0) \tan \phi, \quad \text{and therefore,} \\ ds &= (h_0 + z_0) \sec^2 \phi d\phi. \end{aligned}$$

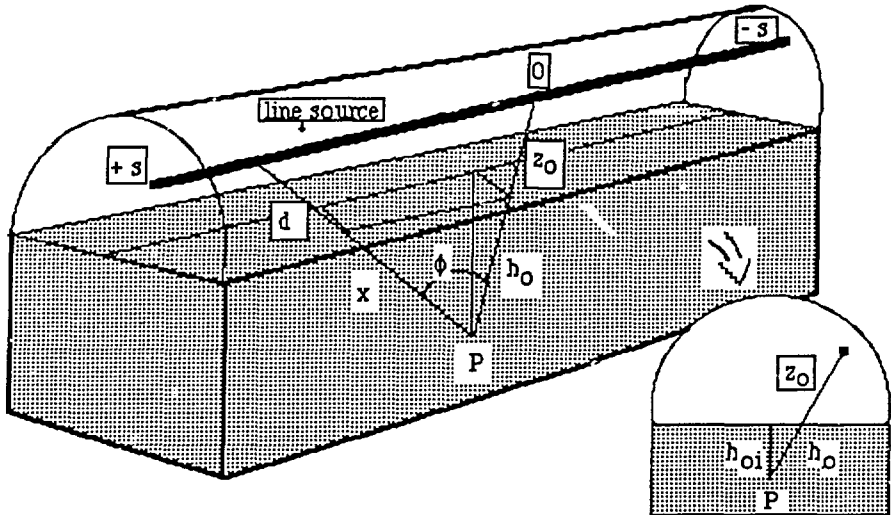


Figure 6. Schematic of a line (segment) source located in the hemicylindrical tracheal model. Note that the h_{0i} , the perpendicular depth of P , and h_0 are in the same plane.

Substituting these relationships into the $D(P)_B$ equation yields

$$D(P)_B = \frac{2 \xi}{4\pi (h_0 + z_0)} \left[.25 W_0 \int_0^{\phi_{\max}} e^{-10 v_B h_0 \sec \phi} d\phi \right. \\ \left. + .75 W_0 \int_0^{\phi_{\max}} e^{-2 v_B h_0 \sec \phi} d\phi \quad 0 < h_0 < R_0 \right. \\ \left. + K v_B h_0 \int_0^{\phi_{\max}} \sec \phi e^{-v_B h_0 \sec \phi} d\phi \right]$$

where $\phi_{\max} = \cos^{-1}(h_0/R_0)$ except when this quantity gives a value of s greater than one-half the length of the hemicylinder. The first two integrals in the equation above may be recognized as Sievert integrals $F(\vartheta, x)$ (12) of the form

$$F(\vartheta, x) = \int_0^\vartheta e^{-x \sec \phi} d\phi$$

A lookup table for discrete x values from 0 - 10 and discrete ϑ values from 10° to 90° (13) was used for these calculations. $F(\vartheta, x)$ formulas for $\vartheta < 5^\circ$ along with appropriate extrapolation formulas (14,15) were also employed for desired values of x and ϑ . The third integral in the $D(P)_B$ equation was solved using Simpson's approximation.

Integration of the two exponential terms in the $D(P)_L$ equation required the substitutions for x , d , s , and h_0 mentioned above, but was not necessary for the other term in the $J(x, d)$ expression. Noting the limits on the values in the Loevinger FPS, the resulting expressions for $D(P)_L$ are

$$D(P)_L = \frac{2 \xi k}{(z_0 + h_0)} \left[\frac{c}{v_L^2} \tan^{-1} \sqrt{\left(\frac{c}{v_L h_0} \right)^2 - 1} \right. \\ \left. - \frac{e h_0}{v_L} \int_0^{\phi_{\max 1}} \sec \phi e^{\left\{ -\frac{v_L h_0}{c} \sec \phi \right\}} d\phi \right. \\ \left. + \frac{e h_0}{v_L} \int_0^{\phi_{\max 2}} \sec \phi e^{\left\{ -v_L h_0 \sec \phi \right\}} d\phi \right]$$

$0 < h_0 < c/v_L$

and

$$D(P)_L = \frac{2 \xi k}{(z_0 + h_0)} \left[\frac{e h_0}{v_L} \int_0^{\phi_{\max 2}} \sec \phi e^{\left\{ -v_L h_0 \sec \phi \right\}} d\phi \right]$$

$c/v_L \leq h_0 < R_0$

where $\phi_{\max 1} = \cos^{-1}\{h_0/(c/v_L)\}$ and $\phi_{\max 2} = \cos^{-1}\{h_0/R_0\}$ except, of course, in the event that when used in the equation $s = (z_0 + h_0) \tan \phi$, s is greater than one-half the length of the hemicylinder. The integrals in the $D(P)_L$ expression were solved using Simpson's approximation.

To demonstrate the use of the above equations, activity present in the hemicylindrical tracheal model was replaced by an equivalent array of 474 line sources. The data used for the Loevinger calculation are shown in Table II. The O-15 data for the $D(P)_B$ equation were not readily available. However, Bochkarev (3) did provide the necessary data for P-32 which is a β^- emitter having average and maximum energy values approximately the same as O-15. Thus, because of the similarity, the P-32 data were used as a first approximation of the actual O-15 values (See Table VII).

Table VII . Physical Parameters Used in the Bochkarev Expression $D(P)_B$
to Calculate the Dose from O-15

W_0 (MeV cm ² / g)	K (MeV cm ² / g)	R_0 (g / cm ²)	v_B (cm ² / g)
2.4	5.9	0.82	9.8

The calculated and measured doses for the hemicylindrical tracheal phantom are in good agreement (See Figure 7).

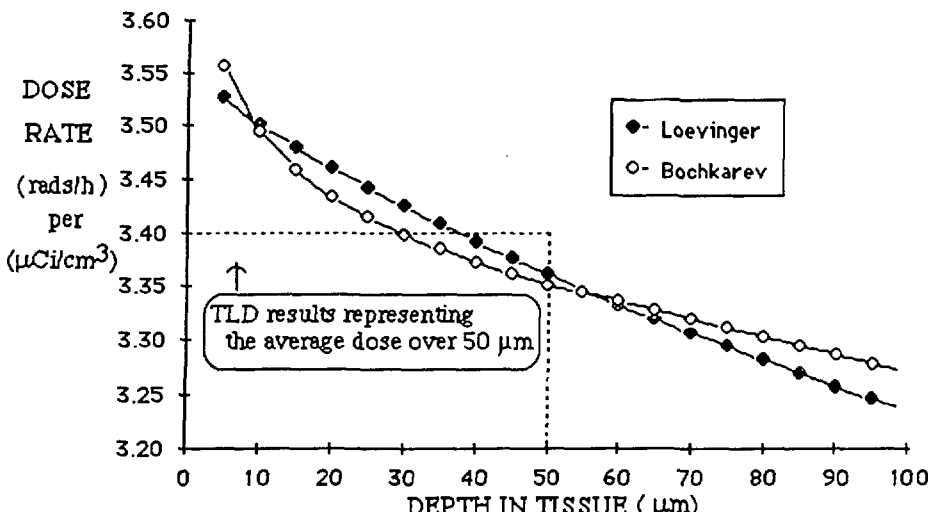


Figure 7. Comparison of Loevinger and Bochkarev FPS calculations for the O-15 dose rate from the tracheal gas to the tissue equivalent walls of a hemicylinder with an internal radius of 0.96 cm and a total length of 14. cm. A comparison with the TLD measurements is also provided.

Application of Point Source Functions to Activity Coated on the Inside of a Hemicylinder

Another calculation was performed using the Bochkarev FPS assuming that the originally airborne acitivity was concentrated into an array of 80 line souces and located along the walls of the tracheal phantom. This approach yielded a dose rate of $3.4 \text{ (rads/h)/(μCi/cm}^3)$ for the average of the dose rate values for $5, 10, 15...50 \mu\text{m}$ depths in the tracheal wall, with the volume here referring to the original airborne activity. This value differs little from the $3.48 \text{ (rads/h)/(μCi/cm}^3)$ calculated for the airborne activity and the TLD measurements. Therefore, for an estimation of the dose to the tracheal mucosa, it does not matter if the activity is airborne or coated on the walls of the hemicylinder.

CALCULATION OF TRACHEAL DOSE

These results may be used to estimate the tracheal dose. To demonstrate the use of the results, the tracheal dose from a 30 minute O-15-CO₂ continuous breathing study is presented. For these calculations it was assumed that the subject had a trachea with the same dimensions as the tracheal phantom and the breathing gas activity was $1 \mu\text{Ci/cm}^3$. Using TLD results and accounting for the virtual absence of O-15-CO₂ in expired air yields a dose of $0.85 \pm 0.04 \text{ rads}$. Accounting for the uptake of O-15-CO₂ in the trachea yields a dose of $4.1 \pm 0.5 \text{ rads}$ to the tracheal mucosa. This value has been confirmed by Meyer et. al. (7). However, Bigler et al. (8), using the results of mucus activity measurements from dogs breathing O-15-CO₂ and an unspecified method of calculation, reported a dose that was less than one-half this value.

DISCUSSION OF TRACHEAL DOSE RESULTS

The above calculation does not incorporate the attenuating effect of the $5 \mu\text{m}$ layer of mucus on the wall of the trachea. However, as can be seen from Figure 7, inclusion of this factor would not change the calculated dose by more than a few percent. A trachea with a larger radius would also have a higher dose rate than a trachea with a small radius for the same activity concentration in the tracheal gas.

The tracheal dose was used as an example here because the tracheal geometry can be easily approximated by a hemicylinder. However, the nasopharyngeal dose may be higher. An uptake

ratio of 7.1 ± 2.7 was determined for a mouth breathing experiment and a value of 8.5 ± 1.0 for a nose breathing experiment using the same subject. The dose to the nose also should be investigated because of the prolonged exposure that could result during a continuous breathing study.

CONCLUSIONS

Injection or inhalation of a positron emitter requires careful consideration of the dose along the route of administration. Estimation of the dose to these pathways from commonly used positron emitters may be calculated using point source functions and the results of physiological measurements. The use of line sources to approximate activity located in the volume of these routes facilitates the calculations.

ACKNOWLEDGEMENT

The assistance given by Peter Faulhaber and Bob Bartlett in the O-15-CO₂ subject studies is very much appreciated. Dr. J.W. Ryan also deserves our appreciation for his help in the bolus injection measurements. Special thanks go to Violet Stark for her assistance with this work.

REFERENCES

1. Loevinger, R., E.M. Japha, and G.L. Brownell. Discrete Radioisotope Sources in Radiation Dosimetry, edited by G.J. Hine and G.L. Brownell, pp. 693-799, Academic Press, New York, 1956.
2. Spencer, L.V. Energy Dissipation by Fast Electrons. Natl. Bureau of Standards Monograph No. 1, Washington D.C., 1959.
3. Bochkarev, V.V., G.B. Radzievsky, L.V. Timofeev, and D.A. Demianov. Distribution of Absorbed Energy from a Point Beta-Source in a Tissue Equivalent Medium. Intl. J. Applied Rad. and Isotopes 23. 493-504, 1972.
4. Gautschi, W., W.F. Cahill. Exponential Integral and Related Functions, in Handbook of Mathematical Functions, edited by M. Abramowitz and I.A. Stegun, pp. 227-251, Dover Publications, Inc., New York, 1965.
5. Dillman, L.T., F.C. Von der Lage. Radionuclide Decay Schemes and Nuclear Parameters for Use in Radiation-Dose Estimation. MIRD Pamphlet No.10, New York, Society of Nuclear Medicine, 1975.
6. Snyder, W.S., M.R. Ford, G.G. Warner, and S.B. Watson. "S", Absorbed Dose per Unit Cumulated Activity for Selected Radionuclides and Organs. MIRD Pamphlet No. 11, New York, Society of Nuclear Medicine, 1975.
7. Meyer, E., Y.L. Yamamoto, A.C. Evans, J. Tyler, M. Diksic and W. Freindel. Radiation Dose to the Trachea from Inhaled O-15-CO₂ (Abstract), J. Nucl. Med. 26(5): P62, 1985.
8. Bigler, R.E., G. Sqourous, P.B. Zanzonico, M. Cosma, R.W. Leonard, and J.R. Dahl. Radiation Dose to the Respiratory Airway Linings from Inhalation of [¹⁵O] - Carbon Dioxide (Abstract), J. Nucl. Med. 26(5): P62, 1985.

9. Muehllehner, G., F. Atkins, and P.V. Harper. Positron Camera with Longitudinal and Transverse Tomographic Ability, in Medical Radionuclide Imaging, Vol I. pp. 291-307, IAEA, Vienna, 1977.
10. Goddard, B. A., and D.M. Ackery. Xenon-133, ^{127}Xe , and ^{125}Xe for Lung Function Investigations: A Dosimetric Comparison. Journal of Nuclear Medicine 16, 780-786, 1975.
11. Snyder W.S., M.J. Cook, E.S. Nasset. Report of Task Group on Reference Man, ICRP Pub. 23. p. 157, New York, Pergamon Press, 1975.
12. Sievert, R.M. Die Intensitätsverteilung der Primären γ -Strahlung in der Nähe Medizinischer Radium Präparate. Acta Radiol. 1, 89-128, 1921.
13. Stegun, I.A. Miscellaneous Functions, in Handbook of Mathematical Functions, edited by M. Abramowitz and I.A. Stegun. pp. 997-1030, Dover Publications, Inc., New York, 1965.
14. Morgan, K.Z., and L.C. Emerson. Dose from External Sources of Radiation, in Principles of Radiation Protection, edited by K.Z. Morgan and J.E. Turner. pp. 268-297, Robert E. Krieger Publishing Co., Huntington, New York, 1973.
15. Rockwell, T.,III. Reactor Shielding Design Manual, Van Nostrand, Princeton, 1956.

APPENDIX

INTRODUCTION

Continuous breathing study data were collected using a Searle Positron Two Camera System and an Ohio Nuclear 150 Data System. These data were presented as two dimensional tomographic frames at a rate of 5 seconds per frame.

To determine the relative activity present in the trachea due to the administration of O-15-CO₂ or O-15-O₂, a region of interest (ROI) containing p_T pixels was placed over the trachea and a nearby background ROI having p_B pixels was selected in the neck tissues. The number of counts in these ROI's were recorded for each frame.

Analysis of the data required consideration of the following:

1. The non-uniform sensitivity of the positron camera across the field of view.
2. Attenuation of the 511 keV annihilation photons in the subject.
3. Dead time count losses due to high singles rates and the paralysability of the camera system.
4. Subtraction of tracheal background activity due to the exchange of O-15-CO₂ in the lungs and the subsequent introduction of O-15-H₂O into the blood pool.
5. Additional counts due to "leakage" of energetic positrons penetrating the tubing used in the delivery system and annihilating in the camera's field of view.
6. Correcting the counts recorded in the background ROI due to imperfect imaging of activity in the trachea.
7. Random counts due to high singles rates.

Each of these items is discussed below. Items 4-6 are addressed in the discussion of background subtraction. The equation for the corrected tracheal counts is also provided.

CAMERA SENSITIVITY AND SUBJECT ATTENUATION

Correction for non-uniform camera sensitivity and subject attenuation was done by recording flood and subject transmission images. The ratio of the flood count rate divided by the transmission count rate is the correction factor for a selected ROI. Care was taken to ensure that a ROI did not include anatomical areas with large differences in attenuation (e.g. part of the background ROI in the neck containing part of the shoulder). The magnitude of these correction factors for the trachea and background ROI's was usually between 2.5 - 4. for lateral views. If the singles rates were high, flood and transmission data had to be corrected for dead time losses.

DEAD TIME LOSSES

Correcting for dead time count losses necessitated recording the singles rates on each camera head during data acquisition. To determine the necessary correction factor, a dead time study monitoring the decay of ^{11}C in a water phantom was performed before or shortly after each study.

BACKGROUND SUBTRACTION

Subtraction of the tracheal background activity from the counts in the tracheal ROI requires a more rigorous approach using background ROI data. The quantity that must be determined first is the actual counts, $b_B(I)$, in a displayed background ROI due only to $\text{O-15-H}_2\text{O}$ from the exchange of O-15-CO_2 in the lungs.

Let $b_B(I)$ be defined as the counts in a positron emission tomogram, background region of interest (ROI) for a particular frame "I". This ROI has a fixed number of pixels, p_B . In general,

$$b_B(I) = B(I) - X_B(I) - S_t(I) \quad (1)$$

where $B(I)$ is defined as the total counts in the displayed background ROI, $X_B(I)$ is the contribution of counts due to positron "leakage" in the delivery system, $S_t(I)$ represents the contribution of counts due to imperfect imaging of activity in adjacent "hot" ROI's for the airways.

For evaluation of the counts in the tracheal ROI due to O-15-CO_2 exchange, the background region of interest was located near the trachea. Therefore, the quantity $S_t(I)$ may be estimated by

$$S_t(I) = k R_T t(I) \quad (2)$$

where R_T is the attenuation and sensitivity correction factor for the tracheal ROI determined from the flood and transmission measurements, $t(I)$ represents the true (background corrected) counts in the displayed tracheal ROI, and k is a proportionality constant. Equation (2) states that background ROI counts due to imperfect imaging of activity in the trachea are proportional to the true activity in the trachea at the time the counts were recorded.

It is useful to define the quantities

$$B(I)^* = B(I) - X_B(I), \text{ and} \quad (3)$$

$$T(I)^* = T(I) - X_T(I). \quad (4)$$

The values $B(I)$ and $X_B(I)$ have been previously defined. $T(I)$ represents the total counts in the tracheal ROI and $X_T(I)$ represents the contribution of counts seen in the tracheal ROI due to positron leakage in the delivery system. $B(I)^*$ and $T(I)^*$ are the displayed counts in the tracheal and background ROI's, respectively, corrected for positron leakage in the delivery system. With a two dimensional imaging system it is impossible to directly measure the effect of positron leakage

activity in the subject because of the difficulty in separating the sources contributing to the registered counts. Therefore, the effect of the leakage is measured with the subject in place and activity flowing through the delivery system prior to administration. These values are defined as $X_B(0)$ and $X_T(0)$ and are related to $X_B(I)$ and $X_T(I)$, respectively, by the equations

$$X_B(I) = F(0) X_B(0) / F(I), \text{ and} \quad (5)$$

$$X_T(I) = F(0) X_T(0) / F(I) \quad (6)$$

where $F(0)$ is the dead time correction factor for $X_B(0)$ and $X_T(0)$, and $F(I)$ is the dead time correction factor for the frame I under consideration. Of course, after cessation of administration $X_B(I)$ and $X_T(I)$ are zero because there is no activity in the delivery system.

Using equation (3), equation (1) may be written

$$b_B(I) = B(I)^* - k R_T t(I). \quad (7)$$

The true displayed counts $t(I)$ in a tracheal ROI in frame I may be determined by

$$t(I) = T(I)^* - b_T(I) \quad (8)$$

where $b_T(I)$ represents the true displayed background in the tracheal ROI due to the exchange of activity in the lungs and the subsequent introduction of labeled water into the blood and tissues. Filling equation (8) into equation (7) yields

$$b_B(I) = B(I) - k R_T (T(I)^* - b_T(I)) \quad (9)$$

$$= B(I) - k R_T T(I)^* + k R_T b_T(I). \quad (10)$$

Another fundamental assumption employed is that

$$R_T b_T(I) / p_T = j R_B b_B(I) / p_B \quad (11)$$

Equation (11) simply states that for any frame "I", the true background activity per pixel in the tracheal ROI is directly proportional to the activity per pixel in the background ROI by some scale factor j . Rearrangement of this equation yields

$$b_T(I) = [(j R_B p_T) / (R_T p_B)] b_B(I). \quad (12)$$

The quantity j is not easily determined. If after administration, there is no uptake present in the trachea and only background activity is present, the value of j can be calculated by using equation (11). Under these conditions, $T(I)$ and $B(I)$ values are equal to $b_T(I)$ and $b_B(I)$, respectively. This approach is useful for O-15-O₂ studies. However, in O-15-CO₂ studies there is appreciable uptake. Fortunately, the value of j is approximately 1 for most subjects and this value was always used as a first approximation in the calculations. Variation in subject anatomy did make it necessary to calculate j using data collected 5-6 minutes after O-15-CO₂ administration. At this time, the activity in the trachea was reduced by decay and biological removal and the majority of the recorded counts were due to background activity.

Using equations (10) and (12) and simple algebra yields

$$b_B(I) = [B(I)^* - k R_T T(I)^*] / [1 - (k j p_T R_B / p_B)]. \quad (13)$$

Equation (13) can then be used in equation (12) provided the values of k and j can be evaluated.

The value of k is easily determined by noting that during the first few seconds of administration b_B is zero. Thus for this initial period I_{in} ,

$$B(I_{in})^* = k R_T T(I_{in})^*. \quad (14)$$

This yields

$$k = B(I_{in})^* / (R_T T(I_{in})^*) . \quad (15)$$

The value of k is usually on the order of 0.02 - 0.05. However, if the imaging system is not focussed well, the value of k can be greater.

RANDOMS

If the randoms were uniformly distributed in the tomographic displays, the background subtraction method would also include the subtraction of the appropriate number of registered randoms. Under this condition, the background ROI would contain the same number of randoms per pixel as the tracheal ROI. However, in the experiments reported here, randoms were not significant because singles rates were kept low.

CORRECTED TRACHEAL COUNTS

Using equations (4), (8), and (12), the corrected counts present in the trachea $T_c(I)$ is given by

$$T_c(I) = R_T \{f_x/f_f\} F(I)[T(I) - X_T(I) - j(p_T/p_B) (R_B/R_T) b_B(I)] \quad (16)$$

$$= R_T \{f_x/f_f\} F(I) t(I) \quad (17)$$

where $\{f_x/f_f\}$ is the ratio of the dead time correction factors for the transmission and flood images.

DISCUSSION

CLOUTIER: Is the point dose at the site of injection really important in estimating risk? We would not expect a nonstochastic effect at the doses mentioned. Should we therefore worry about stochastic effects and perhaps talk about gram-rads as a measure of the number of cells at risk?

HARPER: You can always make the dose look lower by averaging it over a larger volume of tissue. Perhaps this is the wrong thing to say, but this is common practice in radiation protection circles. We were trying to look at the highest dose to the endothelium of the vessel and to the tracheal mucosa. Now, how you interpret these numbers, what use you make of them in dealing with the administration of isotopes, I don't know. As I said, my suggestion is that one should worry about them a little.

RADIATION DOSE ESTIMATES FOR COPPER-64 CITRATE IN MAN

J.E. Crook, J.E. Carlton, M. Stabin, and E. Watson
Oak Ridge Associated Universities
P.O. Box 117
Oak Ridge, Tennessee 37831

ABSTRACT

Tumor imaging agents suitable for use with positron emission tomographs are constantly sought. We have performed studies with animal-tumor-bearing models that have demonstrated the rapid uptake of copper-64. The radiation dose estimates for man indicate that the intravenous administration of 7.0 mCi would result in radiation doses to the kidney of 9.8 to 10.5 rads with other organs receiving substantially less radiation.

INTRODUCTION

The role of copper in health and disease is, with few exceptions, not clearly defined. The notable exceptions are Wilson's disease and Menkes' kinky hair syndrome. In the former, patients have an excess of tissue copper that results in cirrhosis and a deterioration of the central nervous system resulting in movement disorders as well as a diminution of intellectual capacities. The Menkes' syndrome derives part of its name from the abnormal texture of the hair. Unlike Wilson's disease, Menkes' syndrome results from a deficiency of tissue copper. In addition to the changes in hair texture, seizures, growth and mental retardation as well as a progressive cerebral and cerebellar degeneration, all contribute to the early demise of the affected individual.

Pertinent to the role of copper in the development of cardiovascular disease in man are those findings pointing out the striking similarities between copper deficient rats and individuals with cardiac and/or vascular disease (1). These similarities include sudden death, electrocardiographic changes and fibrotic hearts and blood vessels.

Perhaps most intriguing of all, are those investigations that have sought to link changes in serum copper concentrations with progression or remission of lymphomatous disease activity. This, coupled with reports of an avidity of tumors for copper (2), led to the present investigation.

MATERIALS AND METHODS

Copper-64 was obtained as the chloride in 0.2 N HCl from Oak Ridge National Laboratory, Oak Ridge, Tennessee. The ^{64}Cu is produced by neutron activation of CuO enriched in ^{63}Cu . The specific activity of the ^{64}Cu chloride solution was approximately 1 mCi/ μg Cu. For our studies the ^{64}Cu was converted to the citrate form by adding sodium citrate to appropriate volumes of the radioactive

material and neutralizing with 0.2 N NaOH. This solution was filtered through a sterile 0.22 μ Millipore^R filter to remove any particulate material.

Copper-64 as the citrate was administered by tail vein injections to adult tumor bearing rats. Tissue distribution studies were performed utilizing three different strains of rats and three different tumor lines. The Morris 5123C hepatoma is a subline of the original 5123 tumor induced by the ingestion of N-2-fluorenylphthalic acid and was transplanted to the Buffalo rat. The Reuber H-35 hepatoma was transplanted in the American Cross Irish (ACI) rat. The R-4047 (Ward colon tumor) is a tumor originally induced by the oral administration of dimethylhydrazine and was utilized as a transplantable tumor in the Fischer 344 rat. The size of the experimental groups of animals was limited to four. Serial timed experiments for maximum uptake were performed only with the 5123C hepatoma. The animals were sacrificed by exsanguination under light anesthesia. The tissue samples were weighed and assayed by gamma counting. The results were normalized to a body weight of 250 grams and averaged.

For calculations of the estimated radiation dose to Reference Man from administration of copper-64, tissue distribution data for all tissues were pooled. The normalized data were extrapolated to man as follows:

$$\frac{\% \text{ admin. activity}}{\text{organ (man)}} = \frac{\% \text{ admin. activity}}{\text{g tissue (animal)}} \cdot \frac{\text{TB mass (animal)}}{\text{TB mass (man)}} \cdot \text{organ mass (man)}$$

where TB represents total body and organ mass in man is expressed in grams.

The MIRD technique (3) was used for the calculations, and correction for activity in surrounding organs and the remainder of the body was made according to the technique described by Cloutier et al. (4). The S values were taken from MIRD Pamphlet No. 11 (5).

The calculations were based on the assumption that uptake was immediate and that the percentage of the administered activity measured in each tissue at 30 minutes was the initial uptake. The distribution was assumed to remain the same until total decay of the radionuclide occurred; thus, the effective half-time in each organ would be equal to the physical half-life.

RESULTS AND DISCUSSION

The distribution data for the three transplanted tumor animal studies are shown in Table 1. The Reuber H-35 hepatoma and the Morris 5123C exhibited the highest levels of copper-64 uptake. The R-4047 transplanted colon carcinoma had the lowest tumor concentration of copper-64, taking up only 40% as much of the radioactive copper as the Reuber hepatoma which exhibited the highest concentration. The data in Table 1 confirms other investigators findings that copper radionuclides have tumor seeking properties (2). Timed, sequential tissue distribution studies of copper-64 in Buffalo rats bearing the Morris hepatoma are shown in Table 2. The results revealed uptake at two hours with little change over a 24-hour time period.

As noted in Table 1, the tumor-to-blood ratio is low. However, this is not especially troublesome since the copper-64 is used in positron emission studies using the ECAT-IITM positron tomograph.

Table 1

The 24-Hour Distribution of Copper-64 in Rats Bearing Various Transplanted Tumors

Tissues	Morris 5123C Hepatoma	Reuber H-35 Hepatoma	R-4047 Colon Cancer
Tumor concentration (%/g)*	2.0 ± 0.2	3.0 ± 0.2	1.2 ± 0.1
Ratio tumor concentration to that in:			
Liver			
Liver	1.0 ± 0.1	1.8 ± 0.1	0.8 ± 0.0
Spleen	3.3 ± 0.6	3.2 ± 0.3	3.0 ± 0.2
Kidney	0.4 ± 0.0	0.8 ± 0.1	0.7 ± 0.1
Lung	3.6 ± 0.5	6.3 ± 0.4	2.7 ± 0.2
Muscle	25.0 ± 3.6	61.0 ± 7.5	19.0 ± 1.2
Femur	11.0 ± 1.1	12.0 ± 0.8	5.2 ± 0.1
Marrow	1.6 ± 0.2	2.3 ± 0.1	1.6 ± 0.0
Blood	3.5 ± 0.8	6.8 ± 0.6	2.7 ± 0.2

* Percent administered dose/g normalized to body weight of 250 g.
Four animals per group.

Table 2

Tissue Distribution of Copper-64 in Rats Bearing Morris 5123C Hepatomas at Various Time After Intravenous Administration of Copper-64 Citrate

Tissues	Time (hrs)				
	2	4	6	12	24
Tumor concentration (%/g)*	1.6	1.8	1.6	1.7	2.0
Ratio tumor concentration to that in:					
Liver					
Liver	0.8	1.1	0.9	0.8	1.0
Spleen	3.7	3.5	2.5	2.9	3.3
Kidney	0.1	0.2	0.3	0.2	0.4
Lung	3.1	3.8	3.1	3.4	3.6
Muscle	13.0	24.0	23.0	21.0	26.0
Femur	7.3	8.3	9.1	8.8	10.6
Marrow	2.1	2.1	1.6	1.3	1.6
Blood	2.4	2.3	2.5	2.0	3.5

* Percent administered dose/g normalized to body weight of 250 g.

The estimated radiation dose to the organs listed in Table 3 for copper-64 are low enough that the Food and Drug Administration has granted an Investigational New Drug exemption for the intravenous administration of 7.0 mCi per subject which would result in radiation doses to the kidney of 9.8 to 10.5 rads.

Table 3

**Radiation Dose Estimates for the Administration of
Copper-64 Citrate to the Standard Man***

<u>Organ</u>	<u>Rads/mCi</u>	<u>mGy/MBq</u>
Heart Wall	0.10	0.028
Kidneys	1.4	0.39
Liver	0.44	0.12
Lungs	0.12	0.033
Muscle	0.047	0.013
Ovaries	0.11	0.030
Skeleton	0.084	0.023
Red Marrow	0.18	0.048
Spleen	0.14	0.037
Testes	0.12	0.032
Total Body	0.098	0.026

* Based on tissue distribution of copper-64 citrate in the rat.

SUMMARY

Copper-64, a positron emitter, can be reactor produced in a high specific activity form. We have confirmed its tumor seeking properties in transplanted tumor animal models. Also, it has been demonstrated that the uptake by tumor tissue is rapid compared to gallium-67. Due to its relatively long half-life (12.7 hrs), it could be transported to positron emission tomography centers for use as a tumor seeking agent.

ACKNOWLEDGEMENTS

This report is based on work performed under Contract No. DE-AC05-76OR-00033 between the U.S. Department of Energy, Office of Energy Research, and Oak Ridge Associated Universities. The helpful support of F.F. Knapp, Jr., Ph.D., of the Nuclear Medicine Technology Group, Health and Safety Research Division, Oak Ridge National Laboratory for supplying copper-64 is appreciated.

REFERENCES

1. Klevay, L.M. Interaction of copper and zinc in cardiovascular disease. Annals N.Y. Acad. Sci. 355, 140-151, 1980.
2. Raynaud, C., et al. Lung cancer diagnosis with ^{67}Cu : Preliminary results. J. Nucl. Med. 14, 947-950, 1973.
3. Loevinger, R. and M. Berman. A Revised Schema for Calculating the Absorbed Dose from Biologically Distributed Radionuclides. MIRD Pamphlet No. 1, Revised. New York, The Society of Nuclear Medicine, 1976.
4. Cloutier, R.J., E.E. Watson, R.H. Rohrer, and E.M. Smith. Calculating the radiation dose to an organ. J. Nucl. Med. 14, 53-55, 1973.
5. Snyder, W.S., M.R. Ford, G.G. Warner, and S.B. Watson. "S," Absorbed Dose Per Unit Cumulated Activity for Selected Radionuclides and Organs. MIRD Pamphlet No. 11. New York, The Society of Nuclear Medicine, 1975.

DISCUSSION

MARCUS: Have you investigated the possibility of long-lived radiocontaminants in your Cu-64? I have followed a patient for some years who many years ago volunteered for a Cu-64 study and ended up several months later with a body burden of europium-154, a bone-seeker with a long half-life and a hard beta emission. His was also a reactor-produced product and I wondered if you had any long-lived contaminants. Europium-154 is a terrible thing to have sitting in your bones.

CROOK: Yes, I should have pointed that out. We looked into the problem in preparing the IND. We have not had any problems, but we are certainly exquisitely aware of the possibility and want to continue to watch for it.

ZANZONICO: A European group recently reported in Cancer Research on the subcellular distribution of radiocopper in tumor-bearing rodents as determined by cell fractionation. These studies indicated that a significant amount of copper is associated with DNA. In view of the electron mode of decay of copper-64, and the associated emission of very short range and very densely ionizing Auger electrons, have you performed any microdosimetric calculations to estimate the absorbed dose specifically to the DNA?

CROOK: I haven't and we've not focused on that particular point. One thing I didn't point out is a potential mechanism of action for Cu-64. The heart is the most heartily endowed organ with mitochondria which use copper as part of the cytochrome oxidase change, so it may well be a reflector mirror of mitochondrial activity in the myocardial cells, but concerning your particular question we haven't entertained that.

MARCUSE: By what criteria do you select the pixels in your tomograms as belonging to the localization where radioactive uptake is to be measured and what kind of background subtraction is appropriate for your studies? If you have a cross section through the lung or another part of the thorax, the amount of background subtraction is critical. How do you do your edge detection? In our institution, we have the most trouble with this. If we do more background subtraction, we have a smaller volume with a higher amount of activity and get a higher dose.

CROOK: Well, I think you shouldn't feel as though you are the lone oarsman in your boat. As I understand the second part of your question, it partly depends on how valiant and stalwart a defender of your data you choose to be. I didn't point out these were attenuation corrected and nongated studies. A tremendous amount of effort is needed for work in the thorax and certainly all the problems aren't solved. As far as your particular question concerning techniques for edge detection, the problems with PET are not short-lived.

N-13 LABELED AMINO ACIDS: BIODISTRIBUTION, METABOLISM AND DOSIMETRIC CONSIDERATIONS

Karen C. Rosenspire and Alan S. Gelbard
Memorial Sloan-Kettering Cancer Center
1275 York Ave.
New York, NY 10021

ABSTRACT

With the growing interest in "metabolic imaging" and with the increasing number of cyclotron/PET facilities, more studies are being performed in animal and humans using short-lived positron-emitting radionuclides. Amino acids labeled either with N-13 or C-11 are one group of compounds being used to study in vivo regional organ (i.e., brain and heart) or tumor metabolism. Of the studies previously reported using C-11 or N-13 labeled amino acids (methionine, alanine, valine, glutamate, glutamine and tryptophan), imaging was restricted mainly to the organ or tissue of interest with little information obtained about the whole-body distribution of the label. Such data are important for studying interorgan transport of amino acids and for determining accurate dosimetric measurements after intravenous injection of labeled amino acids.

The goals of our study were to compare the distribution of several N-13 L-amino acids and N-13 ammonia in tumor-bearing mice and to determine the metabolic fate of the label in vivo. The following amino acids were enzymatically labeled using N-13 ammonia: glutamine, glutamate, methionine, α -aminobutyric acid, valine and leucine.

Mice bearing either the Ridgeway Osteogenic Sarcoma (ROS) or Sarcoma-180 (S-180) tumors subcutaneously were injected either intraperitoneally or in the retro-orbital venous plexus with the various L-(N-13) amino acids or N-13 ammonia to determine differences in distribution based on route of injection as well as to look at differences in distribution between the agents. Animals were sacrificed at various times and the % dose/gram and % dose/organ were determined for each tissue. In addition, the short-term metabolic fate of labeled nitrogen derived from N-13 ammonia and glutamine was determined in tumors and blood of glutaminase-sensitive (S-180) and resistant (ROS) tumor-bearing mice.

The distribution studies using retro-orbital injection, show most of the label (% dose/organ) accumulates in the liver and muscle regardless of agent, however, there were differences between agents (i.e., the % dose/organ for heart and brain from N-13 ammonia was higher than the labeled amino acids). The distributions from the intraperitoneal route of injection were quantitatively different from the retro-orbital route. Such differences can be explained by the fact that intraperitoneally administered agents are absorbed, enter the hepatic portal system and are metabolized by the liver and then circulated through the body. Thus extrapolation of radiation absorbed dose in humans from animal distribution data of such metabolically active

compounds can be in error when administration is via another route. Metabolic fate studies in blood and tumor after N-13 ammonia or N-13 glutamine administration show most of the label is metabolized in 5 minutes. A large portion of the metabolized label in tumor and blood was found as N-13 urea.

INTRODUCTION

With the growing interest in "metabolic imaging" and with the increasing number of cyclotron/PET facilities, more studies are being performed in animals and humans using short-lived positron-emitting radionuclides. Amino acids labeled either with N-13 or C-11 are one group of compounds being used to study regional organ (brain, heart, liver, pancreas (1-7) or tumor metabolism (8-10).

In the studies mentioned above, imaging was restricted mainly to the organ or tissue of interest with little information about whole-body distribution of the label. Since these labeled amino acids may be involved in a wide variety of metabolic pathways located in different types of cells, more information is needed about interorgan transport and metabolism to determine accurate dosimetric measurements.

MATERIALS AND METHODS

Tissue distribution and blood clearance studies were carried out in mice with the following N-13 labeled compounds: ammonia, glutamine (amide labeled; neutral amino acid), glutamate (acidic amino acid), methionine (a sulfur containing amino acid), α -aminobutyric acid (a nonmetabolizable amino acid), valine and leucine (branched chain amino acids). The amino acids were enzymatically labeled in high specific activity using N-13 ammonia as previously described (11,12).

The Sarcoma-180 (S-180) tumor was implanted in female B6D2F1 mice (18-20 g) by injecting 10 million cells subcutaneously. The Ridgeway Osteogenic Sarcoma (ROS tumor was implanted subcutaneously in female AKD2F1 mice (18-20 g) by trocar needle. For some studies, both the ROS and S-180 tumor-bearing mice were treated with Pseudomonas 7A glutaminase (150 IU/kg) 3 days after implantation. Glutaminase is a glutamine-depleting enzyme used in phase I clinical trials in cancer patients (13-15). The S-180 tumor is sensitive to glutaminase treatment while the ROS tumor is resistant to such treatment (16,17). The mice were fed ad libitum and were not fasted before use.

One week after implantation, mice were injected either intraperitoneally or in the retro-orbital venous plexus with 0.05-0.20 mCi/0.1 ml N-13 ammonia or one of the L-(N-13) amino acids and killed by cervical dislocation at various time intervals. Tissues were removed, counted for radioactivity and weighed.

The short-term metabolic fate of labeled nitrogen derived from N-13 ammonia and glutamine was determined in deproteinized extracts of tumors and blood using HPLC (12). Mice were injected intraperitoneally with 15-180 mCi in 1.5 ml of N-13 glutamine or ammonia and killed at 1, 5 or 10 minutes. Tumor and pooled chest blood were homogenized in cold 1% picrate, centrifuged and the supernatant analyzed by cationic exchange HPLC (12).

RESULTS AND DISCUSSION

After retro-orbital injection, the N-13 label of ammonia and the various amino acids is rapidly cleared from the blood (Fig 1). These studies show that most of the label accumulates in the liver (7-23 % dose/organ) and muscle (12-38% dose/organ)(Tables 1-7). The highest N-13 levels in liver were after N-13 ammonia administration; the lowest from N-13 leucine and valine. There were differences between agents for other tissues as well. N-13 activity in brain was highest after N-13 ammonia administration. The concentration of label in brain was moderate after injection of N-13 leucine, valine or methionine. These results are consistant with previous studies of brain uptake of C-14 labeled amino acids in rats (18). Heart uptake of label from the amino acids differs in mice from that observed in humans (2). After N-13 glutamate or leucine administration in mice the % dose in heart is about 0.7 and 0.6 respectively, compared to % dose in human heart of 5.7% (2) and 3-4% respectively. Such differences in amino acid uptake are known to exist between species. Thus, as a result of species differences in distribution of labeled amino acids, there are problems in extrapolating accumulated absorbed dose in mice to humans leading to overestimations or underestimations. For all N-13 amino acids and N-13 ammonia, tumor concentration of the N-13 label ranged from 1.17 (for leucine) to 6.06 (for glutamate) % dose/gram. These values in tumor are comparable to those reported for other labeled amino acids (19-22).

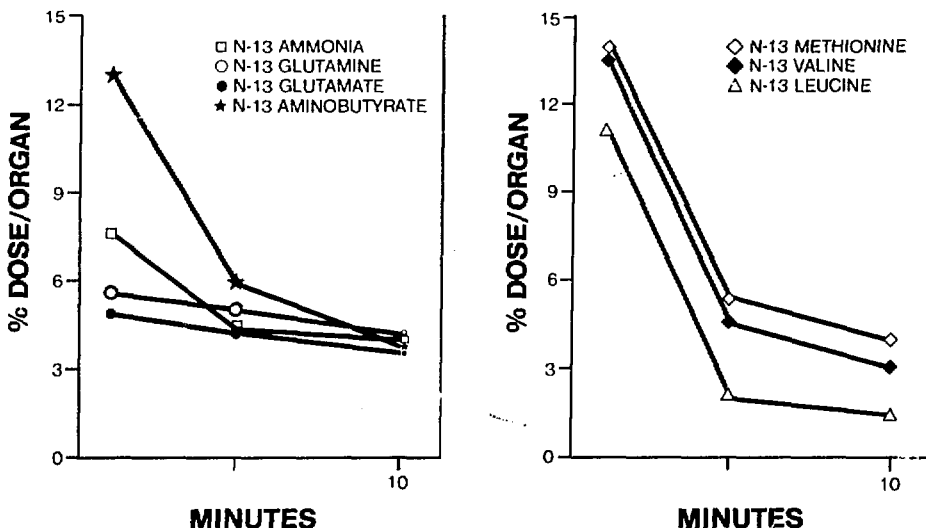


FIG. 1. Blood activity versus time after retro-orbital injection of N-13 ammonia, glutamate, glutamine, α -aminobutyrate, methionine, leucine and valine.

The distributions from the retro-orbital route of administration were quantitatively different from the intraperitoneal route. Concentrations of N-13 activity in heart and brain 10 minutes after N-13 ammonia or glutamine injection were 2-4 times lower after intraperitoneal injection than by retro-orbital. On the other hand, blood and liver concentrations of N-13 activity after intraperitoneal injection are higher probably due to the slow rate of absorption of the intraperitoneally administered material. Thus extrapolating radiation absorbed dose (from intraperitoneal injection) in mice to humans (where route of administration is intravenous) can lead to errors in estimation. Such differences may be explained by the fact that intraperitoneally administered agents are first absorbed into the portal circulation, and hence may be absorbed and metabolized by the liver prior to circulation through the body. It should be noted that injection into the retro-orbital venous plexus is similar to an intravenous injection with about a 60 sec period of time required for the activity to get across the capillary membrane of the venous plexus and into the blood (Fig. 2).

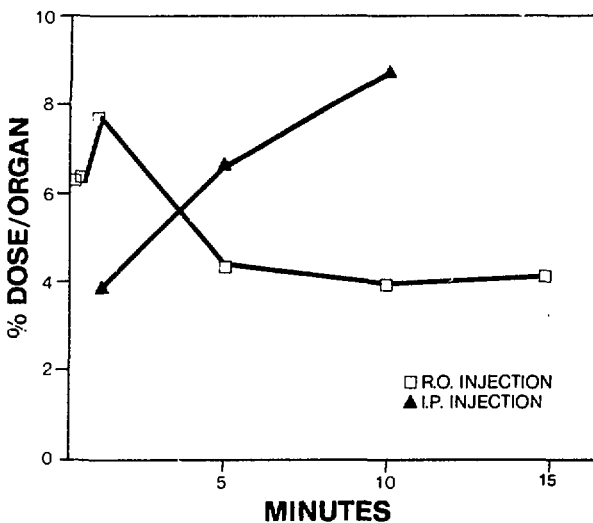


FIG. 2. Comparison of blood activity versus time after injection of N-13 ammonia by retro-orbital or intraperitoneal route of administration.

The results of tissue distribution studies of N-13 ammonia and L-(amide-N-13)glutamine after intraperitoneal injection in control and glutaminase treated mice are shown in Tables 8-11. The distribution studies were carried out 3 days after glutaminase treatment, allowing sufficient time for glutamine to be depleted from the blood as well as for glutaminase to be cleared as well. Differences in tissue distribution between control and treated animals were slight. After N-13 ammonia, both the S-180 and ROS tumors in glutaminase treated mice had significantly higher % dose/organ. However, the % dose/gram values were not different indicating that the significance in the % dose/organ values were due to larger tumors. Although the data in Tables 8-11 appears to indicate a discrepancy between the % dose/gram and % dose/organ data in control and treated mice for other tissues, this may be explained by the glutaminase treatment. This treatment causes ammonia toxicity and weight loss such that the treated animals lost approximately 2 to 3 grams leading to a reduction in some organ weights.

Metabolic fate studies were performed in ROS and S-180 tumor-bearing mice after intraperitoneal injection of either N-13 ammonia or N-13 glutamine (Tables 12-14). At 1, 5 and 10 minutes after injection of N-13 ammonia, approximately 85, 35 and 2%, respectively, of the label is present in protein-free extracts of blood as N-13 ammonia. Conversely, 4, 20 and 83% of the label in blood is in the form of N-13 urea at these time points. Thus for at least the first 5 minutes, a significant amount of N-13 ammonia is available for delivery to the tumor. The percentage of N-13 ammonia found in both the ROS and S-180 tumors decreased with time as the percentage of N-13 urea increased. We were unable to demonstrate the *in vitro* formation of N-13 urea from N-13 ammonia in S-180 tumor slices (12). There are two explanations for our findings of N-13 urea in the tumors. First is endogenous production of N-13 urea from an intermediate of the urea cycle formed elsewhere and transported into the tumor. For example, kidney cells can synthesize urea from citrulline (23); muscle can convert arginine to urea (24) and brain can convert glutamine (25,26) or aspartate (27) to urea. The second explanation may be influx of N-13 urea from blood to tumor.

Five minutes after N-13 glutamine administration, most of the label in the tumors was in a metabolized form. Many tumors are known to contain high levels of glutaminase (28), and our data (Table 13) suggest that the ROS and S-180 tumors hydrolyze the amide group of glutamine. By 10 minutes, both tumor lines show that >30% of the label has been metabolized to N-13 urea.

At five minutes after intraperitoneal injection of N-13 ammonia or N-13 glutamine, only about 0.7% of the label recovered in either tumor was in protein. In contrast, a preliminary study was performed on the metabolic fate of the N-13 label in the ROS tumor 5 minutes after retro-orbital injection of labeled methionine. Methionine has a more limited metabolic fate than ammonia and glutamine. The protein precipitate accounted for 14.1% of the N-13 activity. HPLC analysis of the supernatant showed 90% of the label as N-13 methionine. Thus a much higher percentage of the N-13 activity from N-13 methionine was incorporated into protein than from N-13 glutamine. Even though the N-13 methionine and glutamine were administered by different routes, the percent activity incorporated into protein can be compared since it is calculated as a percent of total radioactivity in the tumor and not as a percent of the administered dose. [For a comprehensive review of N-13 as a biochemical tracer see reference 29].

SUMMARY

The organ distribution and metabolic fate studies show the importance of interpreting the interorgan relationships of these metabolically active N-13 labeled amino acids. As we have shown, the organ distribution of the N-13 label changes as a function of route of injection and the specific amino acid injected.

Depending on the metabolic pathway involved, different tissues are involved (i.e., liver, kidney, etc.). Since positron-emitting radionuclides have up to a 4 mm range in tissue before annihilation (30), a high fraction of the energy deposited is in the organ in which the annihilation takes place. Thus a significant portion of the radiation absorbed dose to a particular organ is due to radioactivity within the organ rather than from an adjacent organ. While the localization of the N-13 activity may be in different parts of the cell (i.e., nucleus for nucleic acid synthesis, mitochondria and cytosol for urea synthesis, etc.) the range of the positron is large enough to be assumed to be evenly distributed.

The following points must be kept in mind when considering radiation absorbed dose using metabolically active agents like N-13 ammonia and N-13 amino acids. There are considerable species differences in the tissue distribution of the N-13 labeled amino acids resulting in overestimation or underestimation of radiation absorbed dose. In addition, there are different tissue distributions by different routes of administration of the radiopharmaceutical. Therapeutic regimen(s) may affect the distribution of the N-13 label.

ACKNOWLEDGEMENTS

The interest and support of Dr. John S. Laughlin is much appreciated. The cooperation of the staff of the Cyclotron Facility is gratefully acknowledged. We also thank Ms. Sabina F. DeRicco and Mr. Edward Nieves for technical assistance. This investigation was supported by National Institute of Health Grants CA-33732, CA-34603 and the United States Department of Energy Contract DE-AC02-77EV04268.

REFERENCES

1. Comar, D., Cartron, J.-C., Maziere, M. and Marazano C. Labeling and metabolism of methionine-methyl-C-11. *Eur. J. Nucl. Med.* 1. 11-14, 1976.
2. Gelbard, A.S., Benua, R.S., Reiman, R.E., McDonald, J.M., Vomero, J.J. and Laughlin, J.S. Imaging the human heart after administration of L-(N-13) glutamate. *J. Nucl. Med.* 21. 988-991, 1980.
3. Henze, E., Schelbert, H.R., Barrio, J.R., Hansen, H.W., MacDonald, N.S., and Phelps, M.E. Evaluation of myocardial metabolism, with N-13 and C-11 labeled amino acids and positron computed tomography. *J. Nucl. Med.* 23. 641-652, 1982.
4. Knapp, W.H., Helus, F., Ostertag, H., Tillmans, H. and Kubler, W. Uptake and turnover of L-(N-13) glutamate in the normal human heart and in patients with coronary artery disease. *Eur. J. Nucl. Med.* 7. 211-216, 1982.
5. Bading, J.R., Daly, J.M., Gelbard, A.S. and Benua, R.S. A kinetic imaging study of human hepatic metastases by hepatic artery injection of N-13 L-glutamate. *J. Nucl. Med.* 26. P109, 1985.
6. Hubner, K.F., Andrews, G.A., Buonocore, E., Hayes, R.L., Washburn, L.C., Collman, I.R. and Gibbs, W.D. Carbon-11-labeled amino acids for the rectilinear and positron tomographic imaging of the human pancreas. *J. Nucl. Med.* 20. 507-513, 1979.
7. Syrota, A., Duquesno, N., Paraf, A. and Kellerschon, C. The role of positron emission tomography in the detection of pancreatic disease. *Radiology* 143. 249-253, 1982.
8. Kubota, K., Matsuzawa, T., Ito, M., Ito, K., Fujiwara, T., Abe, Y., Yoshioka, S., Fukuda, H., Hatazawa, J., Iwata, R., Watuanuke, S. and Ido, T. Lung tumor imaging by emission tomography using C-11 L-methionine. *J. Nucl. Med.* 26, 37-42, 1985.
9. Reiman, R.E., Huvos, A.G., Benua, R.S., Rosen, G., Gelbard, A.S. and Laughlin, J.S. Quotient imaging with N-13 L-glutamate in osteogenic sarcoma: Correlation with tumor viability. *Cancer* 48. 1976-1981, 1981.

10. Knapp, W.H., Helus, F., Sinn, H., Ostertag, H., Georgi, P., Brandeis, W.-E. and Braun, A. N-13 L-glutamate uptake in malignancy: Its relationship to blood flow. *J. Nucl. Med.* 25. 989-997, 1984.
11. Cooper, A.J.L. and Gelbard, A.S. The use of immobilized glutamate dehydrogenase to synthesize N-13 labeled L-amino acids. *Anal. Biochem.* 111. 42-48, 1981.
12. Rosenspire, K.C., Gelbard, A.S., Cooper, A.J.L., Schmid, F.A. and Roberts, J. N-13 Ammonia and L-(amide-N-13)glutamine metabolism in glutaminase-sensitive and glutaminase-resistant murine tumors. *Biochim. Biophys. Acta.* In Press.
13. Warrell, R.P., Chou, T.-C., Gordon, C., Tan, C., Roberts, J., Sternberg, S.S., Phillips, F.S. and Young, C.W. Phase I evaluation of succinylated Acinetobacter glutaminase-asparaginase in adults. *Cancer Res.* 40. 4546-4551, 1980.
14. Kien, C.L. and Holcenberg, J.S. Amino acid utilization and urine protein excretion in children treated with succinylated Acinetobacter glutaminase-asparaginase. *Cancer Res.* 41. 2056-2062, 1981.
15. Holcenberg, J.S., Camitta, B.M., Borella, L.D. and Ring, B.J. Phase I study of succinylated Acinetobacter L-glutaminase-L-asparaginase. *Cancer Treat. Rep.* 63. 1025-1030, 1979.
16. Greenberg, D.M., Blumenthal, G. and Ramadan, M.-E. A. Effect of administration of the enzyme glutaminase in the growth of cancer cells. *Cancer Res.* 24. 957-963, 1964.
17. Schmid, F.A. and Roberts, J. Antineoplastic and toxic effects of Acinetobacter and Pseudomonas glutaminase-asparaginases. *Cancer Chemother. Rep.* 58. 829-840, 1974.
18. Oldendorf, W.H. Brain uptake of radiolabeled amino acids, amines, and hexoses after arterial injection. *J. Am. Physiol.* 221. 1629-1639, 1971.
19. Kubota, K., Yamada, K., Fukada, H., Endo, S., Ito, M., Abe, Y., Yamaguchi, T., Fujiwara, T., Sato, T., Ito, K., Yoshioka, S., Hatazawa, J., Matsuzawa, T., Iwata, R. and Ido, T. Tumor detection with carbon-11 labeled amino acids. *Eur. J. Nucl. Med.* 9. 136-140, 1984.
20. Lembares, N., Dinwoodie, R., Gloria, I., Lathrop, K.A., Bautovich, G. and Harper, P.V. Nitrogen-13 ammonia and glutamate as possible tumor localizing agents. *J. Nucl. Med.* 14. 630, 1973.
21. Spolter, L.S., Cohen, M.B., MacDonald, N.S., Troulman, B. and Chang, C.C. Tumor uptake of N-13 NH₃, L-glutamine, and L-glutamic acid. *J. Nucl. Med.* 14. 456, 1973.
22. Gelbard, A.S., Kaseman, D.S., Rosenspire, K.C. and Meister, A. Enzymatic synthesis of carbamyl phosphate, L-citrulline, and N-carbamyl L-aspartate labeled with either N-13 or C-11. *Int'l. J. Nucl. Med. Biol.* 12. 235-242, 1985.
23. Mullin, J.M., Cha, C.-J. M. and Kleinzeller, A. Metabolism of L-lactate by LLC-PK1 renal epithelia. *Am. J. Physiol.* 242. C41-C45, 1982.

24. Pardridge, W.M., Duducgian-Vartavarian, L., Casanello-Ertl, D., Jones, M.R. and Kopple, J.D. Arginine metabolism and urea synthesis in cultured rat skeletal muscle cells. *Am. J. Physiol.* 242. E87-E92, 1982.
25. Betz, A.L. and Gilboe, D.D. Effect of pentobarbital on amino acid and urea flux in the isolated dog brain. *Am. J. Physiol.* 224. 580-587, 1973.
26. Drewes, L.R., Conway, W.P. and Gilboe, D.D. Net amino acid transport between plasma and erythrocytes and perfused dog brain. *Am. J. Physiol.* 233. E320-E325, 1977.
27. Sadashivudu, B. and Rao, T.I. Studies on functional and metabolic role of urea cycle intermediates in brain. *J. Neurochem.* 27. 785-794, 1976.
28. Knox, W.E., Linder, M. and Friedell G.H. A series of transplantable rat mammary tumors with graded differentiation, growth rate, and glutaminase content. *Cancer Res.* 30. 283-287, 1970.
29. Cooper, A.J.L. , Gelbard, A.S. and Freed, B.R. Nitrogen-13 as a biochemical tracer, in *Advances in Enzymology and Related Areas of Molecular Biology*, V.57, edited by A. Meister, pp. 251-356, John Wiley and Sons Inc., New York, 1985.
30. Cho, Z.H., Chan, J.K., Ericksson, L., Singh, M., Graham, S., MacDonald, N.S. and Yano, Y. Positron ranges obtained from biomedically important positron-emitting radionuclides. *J. Nucl. Med.* 16. 1174-1176, 1975.

DISCUSSION

BRILL: Have you, or others that you could identify, conducted tumor imaging studies in animals on defined diets, with and without restriction of the particular amino acid being studied? Is it possible to significantly alter C-11 or N-13 amino acid uptake in the normal pancreas or tumor by deprivation of that amino acid for periods (of some length) before the study?

ROSEN SPIRE: We have performed tissue distribution studies of N-13 glutamine in mice following glutaminase treatment. Glutaminase depletes circulating levels of glutamine. Studies, measuring enzyme levels before and after glutamine depletion in cell cultures, have been done by us and others. However, glutamine, being a nonessential amino acid, would be difficult to deplete by diet alone in an animal; thus, amino-acid depleting enzymes are beneficial. Other agents which may alter N-13 or C-11 amino acid distribution would be drugs like DON (a glutamine antagonist) or methionine sulfoximine (a glutamine synthetase inhibitor). I would expect that depending on the amino acid, treatment would be necessary over a period of several weeks.

Table 1

DISTRIBUTION OF N-13 AMMONIA IN ROS AND S-180 TUMOR-BEARING MICE AFTER RETRO-ORBITAL VENOUS PLEXUS INJECTION

Tissue	% dose/gram + S.E.		% dose/organ + S.E.	
	S-180	ROS	S-180	ROS
1 Min				
Blood	5.07+0.63	3.55+0.64	7.70+0.90	6.96+1.25
Heart	21.34+4.39	19.16+6.67	1.98+0.34	2.12+0.29
Liver	13.31+0.23	8.66+0.93	14.54+0.83	13.26+3.30
Muscle	3.76+1.15	2.60+0.20	21.32+3.42	26.99+2.39
Tumor	2.35+0.50	3.62+0.34	0.85+0.10	1.08+0.18
Pancreas	48.20+8.10	20.33+1.27	0.66+0.01	0.54+0.04
Brain	5.66+0.22	4.57+0.00*	2.31+0.03	1.79+0.09
n	4	4	4	4
5 Min				
Blood	2.82+0.09	2.50+0.16*	4.38+0.18	4.84+0.22
Heart	13.51+0.90	12.81+1.16	1.48+0.15	1.77+0.16
Liver	10.89+0.74	10.88+0.91	12.12+0.99	14.43+1.43
Muscle	4.26+0.70	2.57+0.41	34.49+5.95	25.78+3.71
Tumor	2.76+0.24	3.25+0.26	2.73+0.61	1.05+0.20*
Pancreas	11.85+2.58	9.54+1.99	0.44+0.01	0.54+0.02
Brain	3.48+0.15	3.21+0.17	1.36+0.96	1.43+0.07
n	6	5	6	5
10 Min				
Blood	2.55+0.22	1.93+0.06	3.95+0.28	3.59+0.14
Heart	10.33+0.96	12.18+1.34	1.09+0.08	1.42+0.10*
Liver	6.95+0.81	6.93+0.59	8.68+1.13	9.90+0.38
Muscle	4.66+0.61	3.97+1.26	37.43+4.17	35.38+8.71
Tumor	2.96+0.32	3.64+0.17	1.47+0.09	1.21+0.11
Pancreas	22.24+0.81	15.64+2.53	0.58+0.02	0.48+0.02*
Brain	3.27+0.16	1.86+1.56	1.18+0.03	1.32+0.05
n	4	4	4	4

* P less than 0.05

Table 2

TISSUE DISTRIBUTION OF N-13 GLUTAMATE IN ROS AND S-180 TUMOR-BEARING MICE AFTER RETRO-ORBITAL VENOUS PLEXUS INJECTION

Tissue	% dose/gram + S.E.		% dose/organ + S.E.	
	S-180	ROS	S-180	ROS
1 Min				
Blood	3.21+0.37	3.41+0.83	4.87+0.50	5.69+0.97
Heart	4.31+0.31	3.24+0.55	0.44+0.03	0.34+0.03
Liver	18.75+1.28	14.90+1.90	21.03+1.49	18.85+0.43
Muscle	1.64+0.07	1.45+0.27	12.93+0.60	12.67+1.38
Tumor	1.95+0.22	4.72+0.59*	0.67+0.14	0.97+0.18
Pancreas	21.80+4.20	16.80+1.10	0.76+0.17	0.80+0.14
Brain	1.24+0.22	1.34+0.06	0.50+0.09	0.52+0.03
n	<u>4</u>	<u>4</u>	<u>4</u>	<u>4</u>
5 Min				
Blood	2.82+0.19	2.34+0.21*	4.21+0.22	3.87+0.19
Heart	6.00+0.52	4.34+0.52	0.61+0.03	0.46+0.03*
Liver	11.20+0.33	11.88+1.10	12.15+0.39	14.80+0.47*
Muscle	2.46+0.15	1.67+0.23*	19.03+0.81	14.20+1.23*
Tumor	2.91+0.15	6.06+1.19	0.99+0.11	1.63+0.18*
Pancreas	25.85+0.95	22.40+3.40	1.09+0.03	1.17+0.14
Brain	1.32+0.07	1.49+0.21	0.53+0.04	0.58+0.07
n	<u>4</u>	<u>4</u>	<u>4</u>	<u>4</u>
10 Min				
Blood	2.33+0.25	2.13+0.31	3.67+0.36	4.21+0.49
Heart	6.35+0.49	5.89+1.32	0.70+0.05	0.65+0.11
Liver	9.16+0.43	8.97+0.82	11.09+0.61	15.00+1.17*
Muscle	4.17+0.76	2.67+0.58	33.70+5.61	27.30+5.32
Tumor	3.75+0.15	7.19+1.48	2.69+0.64	1.57+0.20
Pancreas	70.20+17.70	50.95+2.65	1.12+0.16	1.47+0.72
Brain	1.72+0.16	2.14+0.58	0.67+0.08	0.89+0.27
n	<u>6</u>	<u>4</u>	<u>6</u>	<u>4</u>

* P less than 0.05

Table 3

TISSUE DISTRIBUTION OF L-(AMIDE-N-13) GLUTAMINE IN ROS AND
S-180 TUMOR-BEARING MICE AFTER RETRO-ORBITAL VENOUS PLEXUS
INJECTION

Tissue	% dose/gram + S.E.		% dose/organ + S.E.	
	S-180	ROS	S-180	ROS
1 Min				
Blood	3.60+0.03	2.79+0.09*	5.61+0.15	5.56+0.09
Heart	6.97+0.45	4.93+0.22*	0.72+0.06	0.64+0.02
Liver	17.50+2.39	14.83+0.64	20.83+3.68	22.75+1.28
Muscle	2.82+0.24	1.49+0.12*	22.53+1.65	15.35+0.95*
Tumor	1.75+0.36	2.67+0.15	0.75+0.20	0.87+0.07
Pancreas	25.85+5.05	21.70+3.60	1.00+0.16	0.85+0.19
Brain	1.43+0.04	1.35+0.14	0.59+0.01	0.55+0.07
n	4	4	4	4
5 Min				
Blood	3.49+0.13	3.37+0.50	4.97+0.26	6.44+0.78
Heart	10.00+0.78	6.91+0.81*	0.86+0.09	0.76+0.07
Liver	13.83+0.83	12.10+0.78	12.83+1.34	17.80+1.32*
Muscle	3.71+0.60	2.37+0.23	27.54+4.77	23.68+2.43
Tumor	2.09+0.23	4.27+0.19*	0.92+0.25	1.14+0.32
Pancreas	50.20+11.40	28.80+1.80	0.48+0.08	0.67+0.04
Brain	1.32+0.24	1.31+0.10	0.51+0.12	0.57+0.05
n	4	4	4	4
10 Min				
Blood	3.06+0.37	2.39+0.51	4.20+0.48	4.09+0.45
Heart	8.70+0.72	7.42+1.17	0.87+0.07	0.85+0.04
Liver	10.34+0.96	12.37+1.78	11.01+1.84	16.65+0.27
Muscle	3.76+0.65	3.18+0.81	24.48+3.50	27.85+4.03
Tumor	2.39+0.40	5.12+0.86	3.19+1.56	1.24+0.32
Pancreas	46.65+0.15	41.73+7.47	0.98+0.09	0.83+0.28
Brain	1.47+0.02	1.20+0.38	0.57+0.00	0.49+0.18
n	4	4	4	4

* P less than 0.05

Table 4

TISSUE DISTRIBUTION OF N-13 METHIONINE IN ROS AND S-180
TUMOR-BEARING MICE AFTER RETRO-ORBITAL VENOUS PLEXUS
INJECTION

Tissue	% dose/gram + S.E.		% dose/organ + S.E.	
	S-180	ROS	S-180	ROS
1 Min				
Blood	10.14+2.58	7.74+1.06	14.25+3.27#	5.51+2.91
Heart	10.68+4.88	6.74+1.68	0.67+0.15#	0.83+0.15
Liver	6.94+1.52	8.85+0.52	10.95+1.93	12.84+1.29
Muscle	1.71+0.23	2.74+0.47	17.47+3.58	28.86+6.74
Tumor	2.16+0.38	3.76+0.59	7.17+3.33	2.56+1.22
Kidneys	15.36+2.79	10.02+1.03	6.37+0.61	3.64+0.34
Pancreas	18.91+5.39	21.14+3.25	1.29+0.25	2.21+0.44
Brain	2.92+0.74	2.31+0.19	1.18+0.29	1.00+0.10
n	4	4	4	4
5 Min				
Blood	2.93+0.10	2.76+0.25	5.34+0.52	5.87+0.90
Heart	6.13+0.68	4.56+0.37	0.80+0.14	0.67+0.11
Liver	11.61+0.70	9.80+1.12	17.44+3.93	14.43+1.30
Muscle	2.84+0.16	2.53+0.32	27.05+3.22	28.01+5.15
Tumor	3.07+0.17	3.47+0.55	4.93+1.89	2.22+1.03
Kidneys	10.82+0.15	7.57+1.92	4.42+0.05	3.07+0.62
Pancreas	37.98+0.78	31.67+4.02	2.70+1.08	3.94+0.89
Brain	2.11+0.11	1.73+0.10*	0.84+0.05	0.71+0.05
n	4	4	4	4
10 Min				
Blood	1.95+0.12	1.82+0.13	3.99+0.32	3.84+0.49
Heart	5.23+0.51	4.56+0.30	0.65+0.13	0.55+0.02
Liver	10.65+0.58	8.10+0.60*	19.07+5.34	11.21+0.69#
Muscle	3.41+0.43	2.76+0.23	35.97+4.04	29.87+2.43
Tumor	3.73+0.59	3.44+0.29	10.86+5.82	2.54+1.17
Kidneys	9.95+0.76	7.27+0.92	4.29+0.32	2.65+0.46
Pancreas	45.71+9.22	36.01+6.15	3.06+0.96	3.06+0.98
Brain	1.99+0.17	2.03+0.08	0.78+0.11	0.75+0.01
n	3	4	3	4

*P less than 0.05

n = 3

Table 5

TISSUE DISTRIBUTION OF N-13 LEUCINE IN ROS AND S-180 TUMOR-BEARING MICE AFTER RETRO-ORBITAL VENOUS PLEXUS INJECTION

Tissue	% dose/gram + S.E.		% dose/organ + S.E.	
	S-180	ROS	S-180	ROS
1 Min				
Blood	5.94+0.58	6.60+0.45	11.28+0.09	14.23+2.44
Heart	6.20+0.88	6.61+0.68	0.75+0.12	0.88+0.04
Liver	7.69+0.59	6.63+1.33	12.08+2.39	10.18+1.18
Muscle	2.68+0.68	3.37+0.53	26.91+8.53	36.82+5.50
Tumor	1.52+0.27	2.13+0.63	5.07+2.33	1.16+0.17
Kidneys	8.99+0.75	8.95+0.77	3.23+0.15	3.30+0.16
Pancreas	22.00+9.18	12.99+1.68	0.94+0.19	1.84+0.75
Brain	2.12+0.19	2.88+0.13	0.83+0.07	0.75+0.04
n	$\bar{3}$	$\bar{3}$	$\bar{3}$	$\bar{3}$
5 Min				
Blood	0.87+0.07	1.19+0.06	1.99+0.02	3.37+0.03*
Heart	3.85+0.22	4.67+0.27	0.71+0.05	0.61+0.01
Liver	5.36+0.49	4.40+0.25	10.14+0.43	8.46+0.71
Muscle	1.73+1.14	1.78+0.20	20.47+0.37	26.11+1.62
Tumor	1.17++0.01	2.02+0.62	3.08+0.87	2.18+1.33
Kidneys	6.93+0.26	7.39+0.17	3.14+0.16	3.23+0.47
Pancreas	22.21+3.91	19.63+0.11	2.65+0.59	4.46+0.04
Brain	1.55+0.21	1.40+0.04	0.65+0.08	0.64+0.03
n	$\bar{2}$	$\bar{2}$	$\bar{2}$	$\bar{2}$
10 Min				
Blood	0.66+0.03	0.73+0.03	1.40+0.02	1.85+0.23
Heart	4.31+0.28	4.34+0.14	0.56+0.02	0.63+0.02
Liver	5.89+0.83	4.73 #	10.47+1.22	10.06+0.95
Muscle	1.77+0.25	1.64+0.10	19.87+3.57	21.47+0.71
Tumor	1.27+0.13	2.24+0.00	2.98+0.93	1.46+0.81
Kidneys	7.54+0.74	7.51+0.25	3.27+0.09	2.76+0.17
Pancreas	31.82+3.50	23.01+3.60	3.67+0.18	4.47+0.65
Brain	1.56+0.17	1.51+0.20	0.61+0.08	0.61+0.13
n	$\bar{2}$	$\bar{2}$	$\bar{2}$	$\bar{2}$

* P less than 0.05

n = 1

Table 6

TISSUE DISTRIBUTION OF N-13 VALINE IN ROS AND S-180 TUMOR-BEARING MICE AFTER RETRO-ORBITAL VENOUS PLEXUS INJECTION

Tissue	% dose/gram \pm S.E.		% dose/organ \pm S.E.	
	S-180	ROS	S-180	ROS
1 Min				
Blood	7.21 \pm 0.56	6.91 \pm 0.52	13.63 \pm 1.12	13.65 \pm 1.13
Heart	5.70 \pm 1.75	3.70 \pm 0.26	0.63 \pm 0.14	0.46 \pm 0.03
Liver	5.80 \pm 0.52	4.94 \pm 0.35	8.88 \pm 1.68	7.28 \pm 0.34
Muscle	3.46 \pm 0.83	2.19 \pm 1.11	31.62 \pm 4.00	22.41 \pm 1.13
Tumor	2.16 \pm 0.36	3.54 \pm 0.84	4.67 \pm 1.43	1.29 \pm 0.13
Kidneys	7.59 \pm 0.74\$	7.49#	3.40 \pm 0.37\$	2.54#
Pancreas	25.84 \pm 1.16\$	17.58#	2.57 \pm 0.11\$	2.33#
Brain	1.02 \pm 0.28\$	0.63#	0.42 \pm 0.12\$	0.25#
n	4	3	4	3
5 Min				
Blood	4.07 \pm 1.42	3.10 \pm 0.37	4.56 \pm 0.55	6.90 \pm 1.43
Heart	3.74 \pm 0.39	3.72 \pm 0.46	0.45 \pm 0.08	0.48 \pm 0.08
Liver	7.59 \pm 0.66	6.23 \pm 0.22	9.12 \pm 1.20	9.96 \pm 0.82
Muscle	4.29 \pm 0.71	3.14 \pm 0.30	37.97 \pm 6.51	36.20 \pm 7.38
Tumor	3.76 \pm 0.32	3.71 \pm 0.35	8.08 \pm 2.92	1.70 \pm 0.30
Kidneys	9.63 \pm 1.07\$	10.93 \pm 0.05\$	3.32 \pm 0.60\$	4.11 \pm 0.12\$
Pancreas	52.92 \pm 8.73\$	39.38 \pm 1.94\$	4.97 \pm 2.27\$	8.67 \pm 0.93\$
Brain	1.49 \pm 0.01\$	1.10 \pm 0.01\$*	0.47 \pm 0.09\$	0.48 \pm 0.02\$
n	4	4	4	4
10 Min				
Blood	1.63 \pm 0.06	1.49 \pm 0.10	3.07 \pm 0.44	3.16 \pm 0.47
Heart	3.76 \pm 0.23	3.92 \pm 0.41	0.47 \pm 0.06	0.46 \pm 0.05
Liver	8.40 \pm 0.83	7.75 \pm 0.69	13.79 \pm 3.67	10.86 \pm 1.48
Muscle	3.79 \pm 0.16	2.88 \pm 0.34	36.31 \pm 2.99	32.19 \pm 5.93
Tumor	3.29 \pm 0.06	3.12 \pm 1.04	9.03 \pm 3.81	3.52 \pm 1.55
Kidneys	8.40 \pm 0.03\$	10.90 \pm 1.12\$	3.41 \pm 0.15\$	3.90 \pm 0.16\$
Pancreas	61.14 \pm 4.39\$	30.97 \pm 3.80\$	7.06 \pm 0.45\$	9.98 \pm 0.70\$
Brain	1.23 \pm 0.01\$	1.11 \pm 0.01\$	0.44 \pm 0.05\$	0.47 \pm 0.05\$
n	4	4	4	4

* P less than 0.05

n = 1

\$ n = 2

Table 7

TISSUE DISTRIBUTION OF N-13 α -AMINOBUTYRIC ACID IN ROS AND S-180 TUMOR-BEARING MICE AFTER RETRO-ORBITAL VENOUS PLEXUS INJECTION

Tissue	% dose/gram + S.E.		% dose/organ + S.E.	
	S-180	ROS	S-180	ROS
1 Min				
Blood	5.41+0.75	6.32+0.48	13.09+1.94	9.90+1.27
Heart	4.06+0.84	4.67+0.41	0.60+0.08	0.48+0.12
Liver	7.43+1.31	8.85+1.27	13.84+3.43	10.73+2.98
Muscle	1.67+0.62	2.11+0.30	25.20+3.98	15.11+1.39\$
Tumor	1.81+0.45	2.55+0.23	0.95+0.25	1.98+1.14
Kidneys	n.d.	n.d.	n.d.	n.d.
Pancreas	27.19+5.15	28.35+4.64\$	2.68+1.24\$	1.70+0.74
Brain	0.73+0.07	0.72+0.07	0.33+0.02	0.24+0.04
n	$\frac{4}{4}$	$\frac{4}{4}$	$\frac{4}{4}$	$\frac{4}{4}$
5 Min				
Blood	3.20+0.48	3.80+0.28	5.84+1.40	8.43+1.41
Heart	5.41+1.31	4.81+0.17	0.54+0.09	0.63+0.09
Liver	14.14+2.22	14.50+1.03	15.50+1.92	22.82+4.95
Muscle	4.61+1.03	2.70+0.17	30.11+1.08	32.12+7.01
Tumor	3.50+0.23	3.74+0.30	7.73+4.07	1.29+0.23
Kidneys	n.d.	n.d.	n.d.	n.d.
Pancreas	23.06+3.98\$	31.98+2.07\$	1.50+0.33\$	4.26+3.08\$
Brain	0.72+0.08\$	0.70+0.03\$	0.28+0.05\$	0.28+0.02\$
n	$\frac{4}{4}$	$\frac{4}{4}$	$\frac{4}{4}$	$\frac{4}{4}$
10 Min				
Blood	1.96+0.30	2.54+0.25	3.96+0.44	5.96+1.29
Heart	3.11+0.54	4.21+0.39	0.39+0.06	0.56+0.11
Liver	11.61+2.79	12.25+1.74	16.36+5.26	23.38+4.69
Muscle	3.48+1.06	3.08+0.28	35.99+10.39\$	37.15+7.71
Tumor	2.92+0.63	4.91+0.67	4.17+2.92	3.24+1.23
Kidneys	n.d.	n.d.	n.d.	n.d.
Pancreas	30.44+5.39	29.96+1.67	2.42+0.55	3.71+1.54
Brain	0.82+0.19	0.73+0.06	0.27+0.06	0.26+0.02
n	$\frac{4}{4}$	$\frac{4}{4}$	$\frac{4}{4}$	$\frac{4}{4}$

* P less than 0.05

n = 2

\$ n = 3

n.d. not determined

Table 8

TISSUE DISTRIBUTION OF N-13 AMMONIA IN CONTROL AND
GLUTAMINASE-TREATED ROS AND S-180 TUMOR-BEARING MICE AFTER
INTRAPERITONEAL ADMINISTRATION

Tissue	<u>% dose/gram + S.E.</u>			
	S-180		ROS	
	Control	Treated	Control	Treated
1 Min				
Blood	1.63+0.57	4.65+0.84*	2.43+0.51	3.79+0.87
Heart	1.29+0.20	3.25+0.40*	1.27+0.15	5.91+3.05
Liver	14.50+0.77	27.00+7.56	15.63+1.05	15.38+2.03
Muscle	1.32+0.51	0.77+0.20	1.12+0.48	0.96+0.48
Tumor	0.50+0.15	1.97+0.93	0.48+0.08	1.60+0.68
Pancreas	22.17+5.36	15.44+7.34	24.76+6.41	46.80+1.55*
Brain	0.21+0.03	0.77+0.49	0.14+0.03	0.27+0.07
n	5	4	4	4
5 Min				
Blood	4.46+0.47	5.63+0.92	3.76+0.20	5.13+1.54
Heart	5.03+0.50	5.09+0.50	4.23+0.15	5.01+0.65
Liver	14.33+1.14	15.98+0.79	15.38+1.22	15.33+0.84
Muscle	2.46+0.33	2.67+0.32	2.30+0.86	2.10+0.18
Tumor	3.13+0.77	4.16+1.19	3.68+0.21	3.92+0.44
Pancreas	15.05+0.73	18.73+1.14*	14.43+0.78	17.55+2.37
Brain	0.73+0.09	0.90+0.07	0.65+0.02	0.86+0.07
n	4	4	4	4
10 Min				
Blood	5.87+1.04	5.69+2.84	3.42+0.12	3.89+1.37
Heart	5.53+0.30	10.26+4.57	5.04+0.18	5.04+0.59
Liver	10.54+0.87	16.06+5.25	12.66+1.63	10.19+0.21
Muscle	3.23+0.70	2.54+0.81	2.49+0.16	2.55+0.40
Tumor	3.90+0.43	3.94+1.76	4.06+0.16	4.23+0.65
Pancreas	15.87+1.09	27.87+12.52	17.71+1.69	14.07+0.55
Brain	0.84+0.03	1.65+0.64	0.86+0.06	0.98+0.05
n	3	4	4	3

* P less than 0.05

Table 9

TISSUE DISTRIBUTION OF N-13 AMMONIA IN CONTROL AND
 GLUTAMINASE-TREATED ROS AND S-180 TUMOR-BEARING MICE AFTER
 INTRAPERITONEAL ADMINISTRATION

Tissue	% dose/organ + S.E.			
	S-180		ROS	
	Control	Treated	Control	Treated
1 Min				
Blood	3.85±0.37	6.90±1.66	3.39±0.55	6.90±1.68
Heart	0.13±0.02	0.26±0.08	0.08±0.01	0.26±0.08
Liver	14.86±1.15	20.35±3.00	16.80±1.51	20.40±3.01
Muscle	6.33±1.10	9.17±4.57	4.67±1.56	9.19±4.59
Tumor	1.05±0.74	0.35±0.11	0.12±0.05	0.35±0.11
Pancreas	2.16±0.52	5.78±1.77	2.57±0.32	5.78±1.77
Brain	0.08±0.01	0.10±0.03	0.05±0.00	0.10±0.03
n	5	4	4	4
5 Min				
Blood	6.75±0.68	6.37±0.44	6.06±0.17	9.26±2.90
Heart	0.52±0.04	0.57±0.09	0.42±0.01	0.57±0.09
Liver	12.74±1.33	18.98±0.72	19.08±0.90	18.98±0.72
Muscle	19.48±2.79	19.50±1.91	25.27±6.62	19.50±1.91
Tumor	0.77±0.16	1.30±0.37	1.00±0.43	1.30±0.37
Pancreas	1.35±0.10	2.43±0.43	1.74±0.29	2.44±0.43
Brain	0.21±0.02	0.29±0.04	0.21±0.02	0.29±0.04
n	4	4	4	4
10 Min				
Blood	8.82±1.39	7.37±2.42	5.86±0.11	7.37±2.42
Heart	0.58±0.02	0.64±0.05	0.51±0.03	0.64±0.05
Liver	7.35±0.32	12.80±0.25*	15.25±1.78	12.80±0.25
Muscle	25.30±5.43	25.37±3.48	23.42±0.37	25.37±3.48
Tumor	0.90±0.08	2.29±0.24*	0.89±0.10	2.29±0.24*
Pancreas	1.28±0.04	2.34±0.18*	1.95±0.15	2.34±0.18
Brain	0.33±0.01	0.36±0.02	0.33±0.01	0.36±0.02
n	3	4	4	3

* P less than 0.05

Table 10

TISSUE DISTRIBUTION OF L-(AMIDE-N-13) GLUTAMINE IN CONTROL
AND GLUTAMINASE-TREATED ROS AND S-180 TUMOR-BEARING MICE
AFTER INTRAPERITONEAL ADMINISTRATION

Tissue	% dose/gram \pm S.E.			
	S-180		ROS	
	Control	Treated	Control	Treated
1 Min				
Blood	1.12 \pm 0.12	4.66 \pm 0.75*	3.46 \pm 0.98	1.46 \pm 0.47
Heart	0.29 \pm 0.04	0.77 \pm 0.12*	0.52 \pm 0.16	0.53 \pm 0.13
Liver	9.85 \pm 0.79	11.16 \pm 1.12	9.98 \pm 0.86	8.44 \pm 1.68
Muscle	1.91 \pm 0.77	5.63 \pm 2.56	6.43 \pm 2.43	5.71 \pm 1.34
Tumor	0.50 \pm 0.26	0.73 \pm 0.19	5.08 \pm 2.24	1.30 \pm 0.32
Pancreas	37.02 \pm 4.83	25.21 \pm 3.31	25.40 \pm 4.14	30.45 \pm 6.02
Brain	0.09 \pm 0.04	0.35 \pm 0.10	0.09 \pm 0.04	0.20 \pm 0.06
n	4	4	4	4
5 Min				
Blood	3.86 \pm 0.70	12.20 \pm 2.89	3.42 \pm 0.22	5.95 \pm 1.61
Heart	2.88 \pm 0.57	3.52 \pm 0.50	3.13 \pm 0.17	4.35 \pm 0.44
Liver	20.78 \pm 1.24	15.33 \pm 2.02	16.98 \pm 1.31	17.47 \pm 0.91
Muscle	1.60 \pm 0.23	4.38 \pm 0.60	6.40 \pm 2.64	3.53 \pm 0.76
Tumor	3.09 \pm 0.48	2.19 \pm 0.49	2.31 \pm 0.53	2.71 \pm 0.87
Pancreas	33.48 \pm 2.78	22.28 \pm 4.27	28.83 \pm 1.45	33.23 \pm 4.40
Brain	0.47 \pm 0.06	0.62 \pm 0.06	0.49 \pm 0.04	0.63 \pm 0.09
n	4	4	4	3
10 Min				
Blood	2.86 \pm 0.21	7.31 \pm 1.52	3.09 \pm 0.16	5.35 \pm 0.84
Heart	4.70 \pm 0.60	6.08 \pm 1.45	4.90 \pm 0.37	5.11 \pm 0.41
Liver	17.50 \pm 1.68	15.72 \pm 2.92	15.23 \pm 1.06	13.20 \pm 2.07
Muscle	7.15 \pm 1.89	2.58 \pm 0.52	2.37 \pm 0.13	3.72 \pm 0.38
Tumor	4.01 \pm 0.22	4.12 \pm 0.91	2.83 \pm 0.33	3.34 \pm 0.50
Pancreas	34.53 \pm 2.71	31.25 \pm 6.52	29.60 \pm 1.56	29.25 \pm 2.65
Brain	0.78 \pm 0.08	1.05 \pm 0.22	0.72 \pm 0.07	0.78 \pm 0.08
n	4	4	4	4

* P less than 0.05

Table 11

TISSUE DISTRIBUTION OF L-(AMIDE-N-13) GLUTAMINE IN CONTROL
AND GLUTAMINASE-TREATED ROS AND S-180 TUMOR-BEARING MICE
AFTER INTRAPERITONEAL ADMINISTRATION

Tissue	% dose/organ \pm S.E.			
	S-180		ROS	
	Control	Treated	Control	Treated
1 Min				
Blood	5.08 \pm 1.42	2.61 \pm 0.73	1.76 \pm 0.31	10.71 \pm 1.90*
Heart	0.06 \pm 0.02	0.06 \pm 0.01	0.03 \pm 0.01	0.14 \pm 0.05
Liver	9.93 \pm 0.30	9.72 \pm 1.90	10.46 \pm 0.06	15.65 \pm 1.01*
Muscle	49.75 \pm 18.72	61.00 \pm 17.16	14.89 \pm 6.15	37.52 \pm 11.35
Tumor	1.59 \pm 0.77	0.48 \pm 0.10	0.05 \pm 0.01	0.54 \pm 0.23
Pancreas	2.51 \pm 0.77	3.21 \pm 0.85	3.97 \pm 0.73	3.28 \pm 0.48
Brain	0.04 \pm 0.01	0.06 \pm 0.02	0.02 \pm 0.01	0.13 \pm 0.03*
n	<u>4</u>	<u>4</u>	<u>4</u>	<u>4</u>
5 Min				
Blood	4.93 \pm 0.38	17.34 \pm 7.09	6.18 \pm 1.06	22.62 \pm 6.18
Heart	0.33 \pm 0.03	0.72 \pm 0.25	0.29 \pm 0.05	0.41 \pm 0.04
Liver	16.23 \pm 0.20	31.80 \pm 9.59	23.39 \pm 1.77	19.40 \pm 0.90
Muscle	46.11 \pm 18.65	33.90 \pm 5.53	8.97 \pm 3.10	41.14 \pm 7.29*
Tumor	0.72 \pm 0.15	2.36 \pm 0.90	0.40 \pm 0.07	0.91 \pm 0.07*
Pancreas	3.01 \pm 0.36	4.74 \pm 1.16	3.61 \pm 0.49	2.69 \pm 0.33
Brain	0.15 \pm 0.01	0.36 \pm 0.16	0.18 \pm 0.02	0.23 \pm 0.01
n	<u>4</u>	<u>4</u>	<u>4</u>	<u>3</u>
10 Min				
Blood	4.51 \pm 0.18	9.37 \pm 1.31*	4.56 \pm 0.09	13.74 \pm 2.79*
Heart	0.54 \pm 0.01	0.61 \pm 0.04	0.47 \pm 0.01	0.77 \pm 0.17
Liver	15.28 \pm 1.45	16.95 \pm 3.02	20.38 \pm 1.29	18.68 \pm 3.39
Muscle	17.90 \pm 0.95	33.93 \pm 2.59*	56.98 \pm 15.07	25.13 \pm 4.82
Tumor	0.79 \pm 0.22	1.93 \pm 0.82	0.65 \pm 0.20	1.55 \pm 0.27*
Pancreas	2.48 \pm 0.51	2.00 \pm 0.28	4.69 \pm 0.34	3.41 \pm 0.51
Brain	0.29 \pm 0.03	0.26 \pm 0.01	0.25 \pm 0.04	0.39 \pm 0.09
n	<u>4</u>	<u>4</u>	<u>4</u>	<u>4</u>

* P less than 0.05

TABLE 12
DISTRIBUTION OF N-13 AMONG VARIOUS TUMOR METABOLITES AFTER
INTRAPERITONEAL INJECTION OF N-13 AMMONIA

<u>Metabolite</u>	Percentage of N-13 in S-180 Tumor (mean \pm S.E.)		
	<u>1 Min (n=3)</u>	<u>5 Min (n=3)</u>	<u>10 Min (n=2)</u>
Ammonia	58.0 \pm 18.7	13.5 \pm 3.8 a)	7.7 \pm 3.5
Urea	16.0 \pm 12.6	45.5 \pm 11.5 b)	58.5 \pm 0.2
Neutral Amino Acids c)	25.4 \pm 6.6	38.9 \pm 7.5	31.9 \pm 3.9
Basic Amino Acids d)	0.1 \pm 0.0	0.9 \pm 0.6	0.5 \pm 0.1
Acidic Amino Acids	0.2 \pm 0.1	0.5 \pm 0.3	f)
Citrulline e)	0.1 \pm 0.0	0.2 \pm 0.1	f)
Very Acidic Fraction	0.2 \pm 0.1	0.7 \pm 0.8	1.6 \pm 0.4

<u>Metabolite</u>	Percentage of N-13 in ROS Tumor (mean \pm S.E.)		
	<u>1 Min (n=3)</u>	<u>5 Min (n=3)</u>	<u>10 Min (n=3)</u>
Ammonia	22.5 \pm 1.8	3.0 \pm 0.3 a)	1.4 \pm 0.4
Urea	38.3 \pm 3.9	55.6 \pm 5.8 b)	66.9 \pm 9.7
Neutral Amino Acids	32.7 \pm 1.7	36.0 \pm 7.4	26.9 \pm 8.7
Basic Amino Acids	0.8 \pm 0.3	1.0 \pm 0.4	0.6 \pm 0.1
Acidic Amino Acids	f)	0.4 \pm 0.3	f)
Citrulline	8.6 \pm 2.9	1.6 \pm 0.5	2.3 \pm 1.3
Very Acidic Amino Acids	0.9 \pm 0.6	1.9 \pm 0.8	1.9 \pm 0.1

a) >90% of the label was found in ammonia after treatment with urease

b) >94% of the label was present as L-(amide-N-13) glutamine

c) Arginine plus ornithine

d) Glutamate plus aspartate

e) Nucleotides, nucleosides, diphosphates, nucleoside triphosphates, adenylosuccinate, carbamyl phosphate

f) None detected

Table 13

DISTRIBUTION OF N-13 AMONG VARIOUS TUMOR METABOLITES AFTER INTRAPERITONEAL INJECTION OF L-(AMIDE-N-13) GLUTAMINE

<u>Metabolite</u>	Percentage of N-13 in S-180 Tumor (mean \pm S.E.)		
	1 Min (n=2)	5 Min (n=5)	10 Min (n=2)
Ammonia	1.7 \pm 1.6	8.5 \pm 0.4 a)	5.2 \pm 1.3
Urea	36.8 \pm 36.8	6.3 \pm 1.0 b)	30.5 \pm 17.2
Neutral Amino Acids	55.4 \pm 43.7	64.6 \pm 5.6	63.3 \pm 18.9
Basic Amino Acids	0.4 \pm 0.2	11.4 \pm 3.0	c)
Acidic Amino Acids	c)	2.3 \pm 1.4	c)
Citrulline	0.4 \pm 0.2	2.4 \pm 0.6	c)
Very Acidic Fraction	5.6 \pm 5.5	4.8 \pm 1.4	1.1 \pm 0.4

<u>Metabolite</u>	Percentage of N-13 in ROS Tumor (mean \pm S.E.)		
	1 Min (n=3)	5 Min (n=3)	10 Min (n=4)
Ammonia	9.7 \pm 4.5	9.6 \pm 2.6 a)	4.3 \pm 0.8
Urea	61.1 \pm 7.2	26.0 \pm 3.3 b)	32.3 \pm 3.3
Neutral Amino Acids	15.2 \pm 4.5	26.4 \pm 18.7	57.4 \pm 1.0
Basic Amino Acids	5.7 \pm 1.8	10.5 \pm 6.0	1.5 \pm 1.3
Acidic Amino Acids	c)	11.4 \pm 8.6	c)
Citrulline	3.8 \pm 2.4	11.0 \pm 3.1	1.4 \pm 0.6
Very Acidic Fraction	2.1 \pm 1.7	5.5 \pm 2.0	3.1 \pm 0.5

a) Following treatment with urease, >90% of the label was found as N-13 ammonia

b) >97% of the label was present as L-(amide-N-13) glutamine

c) None detected

Table 14

DISTRIBUTION OF RADIOACTIVITY IN BLOOD AFTER INTRAPERITONEAL
INJECTION OF N-13 AMMONIA OR N-13 GLUTAMINE

<u>Metabolite</u>	Percentage of N-13 from N-13 Ammonia Administration (mean \pm S.E.)		
	<u>1 Min (n=3)</u>	<u>5 Min (n=3)</u>	<u>10 Min (n=3)</u>
Ammonia b)	85.3 \pm 1.4	35.3 \pm 11.4	1.8 \pm 0.7
Urea c)	4.5 \pm 0.4	20.2 \pm 7.4	82.7 \pm 1.9
Neutral Amino Acids	8.2 \pm 1.4	41.4 \pm 10.9	13.0 \pm 2.1
Basic Amino Acids	a)	1.3 \pm 0.9	0.7 \pm 0.2
Acidic Amino Acids	a)	0.1 \pm 0.1	a)
Citrulline	0.2 \pm 0.2	0.5 \pm 0.3	1.5 \pm 0.3
Very Acidic Fraction	0.2 \pm 0.1	0.9 \pm 0.5	0.2 \pm 0.1

<u>Metabolite</u>	Percentage of N-13 from N-13 Glutamine Administration (mean \pm S.E.)		
	<u>1 Min (n=4)</u>	<u>5 Min (n=4)</u>	<u>10 Min (n=3)</u>
Ammonia b)	0.5 \pm 0.1	0.6 \pm 0.1	1.8 \pm 0.7
Urea d)	0.1 \pm 0.1	0.7 \pm 0.1	13.8 \pm 2.8
Neutral Amino Acids	99.3 \pm 0.2	94.7 \pm 2.1	83.4 \pm 2.6
Basic Amino Acids	0.1 \pm 0.1	0.2 \pm 0.1	0.6 \pm 0.6
Acidic Amino Acids	a)	a)	a)
Citrulline	0.1 \pm 0.1	0.3 \pm 0.3	a)
Very Acidic Fraction	0.1 \pm 0.1	0.1 \pm 0.1	0.4 \pm 0.3

a) None detected

b) After urease treatment, 80-92% of the radioactivity was converted to N-13 ammonia

c) After glutaminase treatment, most of the radioactivity in this fraction was due to L-(amide-N-13)glutamine (approx. 92% at 1 and 5 min. and 71% at 10 min.)

d) After urease treatment, at least 98% of this fraction was due to L-(amide-N-13)glutamine

DOSIMETRY OF D- AND L-ENANTIOMERS OF ^{11}C -LABELED TRYPTOPHAN AND VALINE

L.C. Washburn, B.L. Byrd, T.T. Sun, J.E. Crook,
K.F. Hubner*, J.L. Coffey**, and E.E. Watson
Oak Ridge Associated Universities
P.O. Box 117
Oak Ridge, Tennessee 37831

ABSTRACT

We have previously reported the radiation dosimetry of ^{11}C -labeled DL-tryptophan and DL-valine, as well as clinical pancreatic imaging studies with these agents. Because of significant uptake in both normal pancreas and in pancreatic tumors (thought to be due to the presence of the D-enantiomer), differential diagnosis of pancreatic carcinoma was not feasible. High-performance liquid chromatographic (HPLC) methods were developed for rapid resolution of ^{11}C -labeled DL-tryptophan and DL-valine. Radiation dose estimates to the various organs in man were calculated for the D- and L-enantiomers of ^{11}C -labeled tryptophan and valine, based on tissue distribution data in rats. The dose estimates were sufficiently low that 20-mCi doses of each of the enantiomeric amino acids were approved by the FDA for intravenous administration to humans.

INTRODUCTION

^{11}C -Labeled amino acids, in conjunction with positron emission tomography (PET), have shown potential as agents for pancreatic imaging (1-6), tumor localization (7-9), and measurement of regional cerebral protein synthesis (10,11). The most widely used and generally applicable procedure for production of ^{11}C -labeled amino acids is our high-temperature, high-pressure modification of the Bücherer-Strecker synthesis (12,13). This synthetic technique produces amino acids labeled with ^{11}C in the carboxyl group and yields racemic mixtures of those amino acids having an asymmetric center. Clinical studies of ^{11}C -labeled DL-tryptophan and DL-valine for differential diagnosis of pancreatic carcinoma were disappointing because of significant uptake of these racemic mixtures in both normal pancreas and in pancreatic carcinoma (4). The uptake by pancreatic tumors was quite unexpected based on the well-known ability of [^{75}Se]L-selenomethionine to permit diagnosis of tumors as defects in normal pancreatic images (14). This finding was thought to be due to the presence of the D-enantiomers, which were reported by Tamemasa and co-workers (15) to selectively localize in tumor tissue. A high-performance liquid chromatographic (HPLC) method was developed in our laboratory for rapid resolution of ^{11}C -labeled DL-valine (16) and later adapted for resolution of ^{11}C -labeled

* Present address: University of Tennessee Memorial Research Center and Hospital, 1924 Alcoa Highway, Knoxville, Tennessee 37920

** Present address: Nuclear Pharmacy, Inc., 4272 Balloon Park Road, NE, Albuquerque, New Mexico 87109

DL-tryptophan and DL-leucine (17). These HPLC techniques have yielded clinically useful quantities of the D- and L-enantiomers of ^{11}C -labeled tryptophan and valine for diagnostic studies in patients with pancreatic carcinoma.

In the second symposium in this series, we presented data on the radiation dosimetry of ^{11}C -labeled DL-tryptophan and DL-valine (18). In this paper we describe animal tissue distribution studies and the resulting radiation dosimetry data for the resolved D- and L-enantiomers of these ^{11}C -labeled amino acids.

MATERIALS AND METHODS

Tissue distribution studies were carried out in male and female Fischer rats (8-20 weeks old) using the ^{14}C -labeled analogs of the four enantiomeric ^{11}C -labeled amino acids of interest in this study. L-Tryptophan [side chain-3- ^{14}C] and L-valine[1- ^{14}C] both were obtained from New England Nuclear, Boston, MA, whereas D-tryptophan [carboxyl- ^{14}C] and D-valine[1- ^{14}C] were synthesized using our modified Bücherer-Strecker synthesis (12,13) and resolved by HPLC using a chiral mobile phase (16,17). Each of the enantiomeric ^{14}C -labeled amino acids was administered to male and female rats via the tail vein at levels of 0.01 - 0.19 mg and 2.6 - 5.0 μCi per kg of animal weight. Each experimental group consisted of five animals. At 30 minutes after injection the rats were killed by exsanguination under light ether anesthesia. Weighed tissue samples were dissolved in NCS tissue solubilizer (Amersham/Searle, Arlington Heights, IL) and assayed by liquid scintillation counting. The results were normalized to a body weight of 250 g and averaged.

For calculations of the estimated radiation dose to Reference Man from administration of ^{11}C -labeled D- and L-tryptophan and D- and L-valine, male and female tissue distribution data for all tissues common to both sexes were pooled. The normalized data were extrapolated to man as follows:

$$\frac{\% \text{ admin. activity}}{\text{organ (man)}} = \frac{\% \text{ admin. activity}}{\text{g tissue (animal)}} \cdot \frac{\text{TB mass (animal)}}{\text{TB mass (man)}} \cdot \frac{\text{organ mass (man)}}{\text{TB mass (man)}}$$

where TB represents total body and organ mass in man is expressed in grams.

The MIRD technique (19) was used for the calculations, and correction for activity in surrounding organs and the remainder of the body was made according to the technique described by Cloutier et al. (20). The S values were taken from MIRD Pamphlet No. 11 (21).

The calculations were based on the assumption that uptake was immediate and that the percentage of the administered activity measured in each tissue at 30 minutes was the initial uptake. The distribution was assumed to remain the same until total decay of the radionuclide occurred; thus, the effective half-time in each organ would be equal to the physical half-life.

RESULTS AND DISCUSSION

The 30-minute tissue distribution data for ^{14}C -labeled D- and L-tryptophan is given in Table 1 and that for D- and L-valine is shown in Table 2. Uptake differences between the D- and the L-enantiomer of each amino acid are greater for those organs that utilize the naturally occurring L-amino acids for protein or peptide synthesis and/or are active in amino acid transport (i.e., pancreas, liver, brain, bone marrow, and small intestine). Furthermore, these differences are much greater for D- and L-valine than for D- and L-tryptophan, likely due at least in part to the faster urinary excretion for D-valine than for any

Table 1

Tissue Distribution of ^{14}C -Labeled D- and L-Tryptophan
in Male and Female Fischer Rats at 30 Minutes Postinjection

Tissue	D-Tryptophan		L-Tryptophan	
	Male	Female	Male	Female
Pancreas	7.60 ± 0.09*	8.06 ± 0.28	14.80 ± 0.44	13.77 ± 0.50
Liver	0.81 ± 0.02	0.93 ± 0.03	1.46 ± 0.03	1.58 ± 0.12
Spleen	0.53 ± 0.04	0.68 ± 0.03	0.81 ± 0.03	0.96 ± 0.02
Kidney	1.62 ± 0.05	1.62 ± 0.10	1.08 ± 0.02	1.04 ± 0.04
Lung	0.39 ± 0.03	0.65 ± 0.04	0.47 ± 0.01	0.75 ± 0.04
Muscle	0.25 ± 0.01	0.25 ± 0.01	0.23 ± 0.01	0.23 ± 0.01
Heart	0.33 ± 0.03	0.43 ± 0.03	0.38 ± 0.00	0.43 ± 0.02
Brain	0.11 ± 0.01	0.13 ± 0.01	0.23 ± 0.01	0.26 ± 0.01
Marrow	0.79 ± 0.10	0.63 ± 0.02	1.00 ± 0.04	0.89 ± 0.08
Blood	0.26 ± 0.06	0.30 ± 0.08	0.25 ± 0.01	0.29 ± 0.01
S. Intestine	0.90 ± 0.03	0.96 ± 0.05	1.58 ± 0.05	1.70 ± 0.08
Testis	0.18 ± 0.02	-	0.17 ± 0.00	-
Ovary	-	0.70 ± 0.07	-	0.90 ± 0.08

* Percent administered activity/g ± S.E.; normalized to a body weight of 250 g; values are averages of 5 animals.

Table 2

Tissue Distribution of ^{14}C -Labeled D- and L-Valine
in Male and Female Fischer Rats at 30 Minutes Postinjection

Tissue	D-Valine		L-Valine	
	Male	Female	Male	Female
Pancreas	2.30 ± 0.09*	2.46 ± 0.10	10.87 ± 0.47	10.16 ± 0.30
Liver	0.16 ± 0.01	0.17 ± 0.01	1.11 ± 0.05	1.16 ± 0.05
Spleen	0.32 ± 0.01	0.33 ± 0.01	0.84 ± 0.07	0.85 ± 0.02
Kidney	0.57 ± 0.01	0.65 ± 0.04	0.75 ± 0.05	0.71 ± 0.03
Lung	0.39 ± 0.01	0.43 ± 0.03	0.58 ± 0.08	0.50 ± 0.01
Muscle	0.18 ± 0.01	0.20 ± 0.01	0.23 ± 0.02	0.22 ± 0.01
Heart	0.34 ± 0.01	0.33 ± 0.02	n.d.	n.d.
Brain	0.04 ± 0.00	0.04 ± 0.00	0.12 ± 0.01	0.14 ± 0.01
Marrow	0.31 ± 0.01	0.27 ± 0.01	1.45 ± 0.04	1.09 ± 0.06
Blood	0.10 ± 0.03	0.06 ± 0.03	0.16 ± 0.01	0.16 ± 0.01
S. Intestine	0.36 ± 0.02	0.43 ± 0.02	1.77 ± 0.09	1.74 ± 0.11
Testis	0.09 ± 0.00	-	0.14 ± 0.01	-
Ovary	-	0.37 ± 0.01	-	0.70 ± 0.04

* Percent administered activity/g ± S.E.; normalized to a body weight of 250 g; values are averages of 5 animals.

of the three other enantiomeric amino acids studied (data not shown).

Because there were no apparent sex differences in the distribution data for any of the four enantiomeric amino acids studied, the male and female data for all tissues common to both sexes were pooled for the calculations of radiation dose (Table 3). Based on our previously reported studies of the time course of biodistribution for the radiolabeled racemic mixtures of tryptophan and valine (1,2,18), the assumption of immediate organ uptake for the enantiomeric amino acids seems reasonable for the dose calculations. Likewise, in view of the 20.4-minute half-life of carbon-11, the assumption of complete decay in situ also appears to be valid.

Table 3

Estimated Dose to Reference Man from Intravenous Administration
of ^{11}C -Labeled D- and L-Tryptophan and D- and L-Valine

Organ	Radiation Dose* (rads/mCi)			
	D-Tryptophan	L-Tryptophan	D-Valine	L-Valine
Total Body	0.012	0.011	0.012	0.011
Pancreas	0.14	0.25	0.046	0.19
Liver	0.023	0.035	0.008	0.028
Spleen	0.018	0.020	0.012	0.022
Kidney	0.035	0.023	0.016	0.019
Lung	0.014	0.017	0.012	0.014
Marrow	0.016	0.017	0.012	0.021
S. Intestine	0.026	0.042	0.013	0.009
Testis	0.009	0.010	0.009	0.007
Ovary	0.017	0.019	0.011	0.011

* Based on the tissue distribution of the ^{14}C -labeled amino acids 30 minutes following intravenous administration to male and female rats, assuming immediate uptake and no further change in distribution.

The radiation dose estimates for those organs utilizing L-amino acids in protein or peptide synthesis and/or amino acid transport are generally somewhat higher for the L-forms of both amino acids and somewhat lower for the D-forms than reported previously for the respective DL-mixtures (18). Estimates for other organs are similar regardless of the stereoisomeric form of the amino acid.

The estimates of radiation dose for ^{11}C -labeled D- and L-tryptophan and D- and L-valine are all sufficiently low that the U.S. Food and Drug Administration has approved, under Investigational New Drug status, the intravenous administration of 20-mCi doses of each enantiomeric amino acid. Administration of this amount of each ^{11}C -labeled amino acid would produce radiation doses to the critical organ, the pancreas, of 2.8 rads for $[^{11}\text{C}]$ D-tryptophan, 5.0 rads for $[^{11}\text{C}]$ L-tryptophan, 0.9 rads for $[^{11}\text{C}]$ D-valine, and 3.8 rads for $[^{11}\text{C}]$ L-valine.

ACKNOWLEDGEMENTS

This report is based on work performed under Contract No. DE-AC05-76OR-00033 between the U.S. Department of Energy, Office of Energy Research, and Oak Ridge Associated Universities. It was also supported by National Pancreatic Cancer Project Grant No. CA29490.

REFERENCES

1. Washburn, L.C., T.T. Sun, B.L. Byrd, R.L. Hayes, and T.A. Butler. DL-[Carboxyl- ^{11}C]tryptophan, a potential agent for pancreatic imaging: production and preclinical investigations. *J. Nucl. Med.* 20, 857-864, 1979.
2. Washburn, L.C., B.W. Wieland, T.T. Sun, R.L. Hayes, and T.A. Butler. [$1-^{11}\text{C}$]DL-Valine, a potential pancreas-imaging agent. *J. Nucl. Med.* 19, 77-83, 1978.

3. Hubner, K.F., G.A. Andrews, E. Buonocore, R.L. Hayes, L.C. Washburn, I.R. Collmann, and W.D. Gibbs. Carbon-11-labeled amino acids for the rectilinear and positron tomographic imaging of the human pancreas. *J. Nucl. Med.* 20, 507-513, 1979.
4. Hubner, K.F. and E. Buonocore. Positron emission tomography of the abdomen. In *Alimentary Tract Radiology*, 3rd Edition, edited by A.R. Margulis and H.J. Burhenne, Vol. 2, pp. 2486-2494, The C.V. Mosby Company, St. Louis, Missouri, 1983.
5. Kirchner, P.T., J. Ryan, M. Zalutsky, and P.V. Harper. Positron emission tomography for the evaluation of pancreatic disease. *Semin. Nucl. Med.* 10, 374-391, 1980.
6. Syrota, A., D. Comar, M. Cerf, D. Plummer, M. Mazière, and C. Kellershohn. [¹¹C]Methionine pancreatic scanning with positron emission computed tomography. *J. Nucl. Med.* 20, 778-781, 1979.
7. Hayes, R.L., L.C. Washburn, B.W. Wieland, T.T. Sun, R.R. Turtle, and T.A. Butler. Carboxyl-labeled ¹¹C-1-aminocyclopentanecarboxylic acid, a potential agent for cancer detection. *J. Nucl. Med.* 17, 748-751, 1976.
8. Washburn, L.C., T.T. Sun, B.L. Byrd, R.L. Hayes, and T.A. Butler. 1-Aminocyclobutane[¹¹C]carboxylic acid, a potential agent for tumor localization. *J. Nucl. Med.* 20, 1055-1061, 1979.
9. Hubner, K.F., S. Krauss, L.C. Washburn, W.D. Gibbs, and E.C. Holloway. Tumor detection with 1-aminocyclopentane and 1-aminocyclobutane[¹¹C]carboxylic acid using positron emission computerized tomography. *Clin. Nucl. Med.* 6, 249-252, 1981.
10. Phelps, M.E., J.R. Barrio, S.C. Huang, R. Keen, N.S. MacDonald, J.C. Mazziotta, C. Smith, and L. Sokoloff. The measurement of local cerebral protein synthesis in man with positron computed tomography (PCT) and C-11 L-leucine. *J. Nucl. Med.* 23, P6, 1982.
11. Barrio, J.R., R.E. Keen, S.-C. Huang, R.A. Hawkins, and M.E. Phelps. Cerebral protein synthesis rates in vivo: estimation via biochemical analyses and tracer kinetic modeling. *J. Nucl. Med.* 26, P6-P7, 1985.
12. Washburn, L.C., T.T. Sun, B.L. Byrd, R.L. Hayes, T.A. Butler, and A.P. Callahan. High-level production of C-11-carboxyl-labeled amino acids. In *Radiopharmaceuticals II*, pp. 767-777, The Society of Nuclear Medicine, New York, 1979.
13. Hayes, R.L., L.C. Washburn, B. W. Wieland, T.T. Sun, J.B. Anon, T.A. Butler, and A.P. Callahan. Synthesis and purification of ¹¹C-carboxyl-labeled amino acids. *Int. J. Appl. Radiat. Isot.* 29, 186-187, 1978.
14. Youngs, G.R., J.E. Agnew, G.E. Levin, and I.A.D. Bouchier. A comparative study of four tests of pancreatic function in the diagnosis of pancreatic disease. *Q.J. Med.* 42, 597-618, 1973.
15. Tamemasa, O., R. Goto, and T. Suzuki. Preferential incorporation of some ¹⁴C-labeled D-amino acids into tumor-bearing animals. *Gann* 69, 517-523, 1978.
16. Washburn, L.C., T.T. Sun, B.L. Byrd, and A.P. Callahan. Production of L-[carboxyl-¹¹C]valine by HPLC resolution. *J. Nucl. Med.* 23, 29-33, 1982.

17. Washburn, L.C., T.T. Sun, B.L. Byrd, and A.P. Callahan. Resolution of [¹¹C]DL-leucine and [¹¹C]DL-tryptophan by high-performance liquid chromatography. *J. Labelled Comp. Radiopharm.* 22, 135-142, 1985.
18. Washburn, L.C., J.L. Coffey, E.E. Watson, T.T. Sun, and R.L. Hayes. Radiation dosimetry of some ¹¹C-labeled amino acid pharmaceuticals. In *Radiopharmaceutical Dosimetry Symposium*, edited by R.J. Cloutier, J.L. Coffey, W.S. Snyder and E.E. Watson, pp. 441-451, U.S. Department of Health, Education and Welfare, Washington, D.C., 1976.
19. Loevinger, R. and M. Berman. A Revised Schema for Calculating the Absorbed Dose from Biologically Distributed Radionuclides. MIRD Pamphlet No. 1, Revised. New York, The Society of Nuclear Medicine, 1976.
20. Cloutier, R.J., E.E. Watson, R.H. Rohrer, and E.M. Smith. Calculating the radiation dose to an organ. *J. Nucl. Med.* 14, 53-55, 1973.
21. Snyder, W.S., M.R. Ford, G.G. Warner, and S.B. Watson. "S," Absorbed Dose Per Unit Cumulated Activity for Selected Radionuclides and Organs. MIRD Pamphlet No. 11. New York, The Society of Nuclear Medicine, 1975.

DISCUSSION

ZANZONICO: Have you taken into account the radiation dose associated with carbon-11 incorporated with the volatile, and therefore rapidly eliminated, metabolite of C-11 labeled tryptophan and valine, namely, CO₂? If so, how have you done this?

WASHBURN: Decarboxylation of amino acids labeled in the carboxyl group is quite significant in small animals such as the rat, and our biodistribution data, of course, reflect this decarboxylative loss of radiolabel. However, we have shown that practically no decarboxylation occurs in man for any of the C-11 labeled amino acids that we have studied, including tryptophan and valine. The result of this is that the estimated radiation doses to Reference Man based on rat biodistribution data may be somewhat low. On the other hand, although good pancreas uptake of C-11 labeled amino acids in man has been observed, our experience has been that the specificity of uptake by the human pancreas is less than that by the rat pancreas. As a result, the estimated radiation doses to the critical organ, the pancreas, may be too high. These two factors thus operate in opposite directions and tend to cancel each other out.

SASTRY: My question has to do with basic radiation physics and chemistry. In your studies, you have attached C-11, a positron emitter, to D- and L-enantiomers of tryptophan and valine. These molecules are optically active and have a sense of "handedness". Because beta decay involves parity nonconservation, the positrons have a right-handed helicity. One may therefore expect that some of this helicity of positrons may be transferred to the amino acid residues. As a result, if one starts with an equal population of D- and L-enantiomers, one may expect a relative preponderance of one isomer over the other. Have you found any evidence for this in your studies?

WASHBURN: We have observed no difference in the sizes of the HPLC peaks for the two enantiomers of either C-11 labeled amino acid studied, which indicates that there is no stereoselectivity in the production of C-11 labeled amino acids by the modified Bücherer-Strecker synthesis.

CONSIDERATIONS FOR DOSIMETRY CALCULATIONS WITH NEURORECEPTOR BINDING RADIOLIGANDS

Dean F. Wong, Alden N. Bice, Thomas Beck, Robert F. Dannals,
Jonathan M. Links, and Henry N. Wagner, Jr.

The Johns Hopkins Medical Institutions

Divisions of Nuclear Medicine and Radiation Health Sciences

Departments of Radiology and Environmental Health Sciences

Tower Basement

600 N. Wolfe Street

Baltimore, Maryland 21205

ABSTRACT

Neuroreceptor binding radiotracers have unique characteristics which must be considered in absorbed dose calculations. In this article we outline some of the important issues to be considered such as the high specific binding to various receptor bearing tissue regions, the receptor kinetics, the specific activity of the injected ligand and the presence of competing unlabeled substances. As an example of these considerations we have shown the outline of the measurements for animal and human biodistribution data of the D2 dopamine receptor binding ligand ^{11}C -3N-methylspiperone (NMSP) and we calculated the absorbed doses for the important body organs. This includes dose estimates using various species including mice, followed by primate and human data. Because of the selective uptake of NMSP to brain regions such as the basal ganglia we calculated values specifically for these areas in the cerebellum. Since kinetic modeling and therapeutic drug monitoring employ competing unlabeled ligands such as haloperidol which alter the NMSP distribution we estimated the dose in both unblocked and cases blocked with haloperidol. In such cases the doses were about 50% lower in the blocked cases for the basal ganglia. Target organs such as the bladder using external probes and a model based upon changing urine volumes suggests a 30% decrease from mouse estimates.

Abnormalities in neuroreceptors have been implicated in neuropsychiatric and neurological disorders (1,2). Also the possible application to drug therapy has motivated the study of such neuroreceptor systems.

Hence, the considerable interest in labeling multiple ligands for receptor and neurotransmitter imaging in human brain *in vivo* with both PET and potentially SPECT makes these dosimetry considerations very timely.

ISSUES IN RECEPTOR PHARMACOLOGY

Neuroreceptors have a class of pharmacologic properties which define their presence based upon various interacting ligands. These properties include saturability, stereospecificity competition, selective distribution and protein-like behavior. Important neuroreceptor properties are outlined in Table 1.

Table 1. Some criteria for receptor binding.

1. Saturability by competing ligands
2. Appropriate pharmacology: Stereospecific blocking by competing isomers
3. Appropriate regional distribution of ligand for receptors studied
4. Heat lability; irreversible thermal denaturation

Historically, the characteristics of these receptors were first examined in tissue homogenates via in vitro binding studies of tritium labeled ligands or other radiolabeled ligands with long physical half-lives. Several receptor types were defined using these radiotracers as markers and comparing their displacement or competition with either the same unlabeled ligand or competing ligands. A partial summary of receptors discovered in this manner are listed in Table 2 (1).

Table 2. Partial list of important neuroreceptor systems

Dopamine	D ₁
	D ₂
Adrenergic	α
	β
Serotonin	S ₁ (multiple subtypes)
	S ₂
Histamine	
GABA	
Opioid	kappa
	mu
	sigma
cholecystokinin	
Glycine	
Cholinergic	muscarinic
	nicotinic

More recent studies of the in vivo distribution of receptors have been performed principally in rodents and primates. These studies and others have indicated a difference in the distribution of receptors from that measured in vitro. These in vivo measurements usually consisted of gamma-ray counting or

scintillation counting of injected tritiated compounds. Presently, with the availability of compact medical cyclotrons, receptor binding ligands are routinely synthesized and labeled with low atomic weight radionuclides, e.g. ^{11}C and ^{18}F (which do not radically change the pharmacologic properties of these ligands). This new class of positron-emitting radiopharmaceuticals has allowed the external, non-invasive imaging of the distribution of several receptor types in animals and humans via positron emission tomography (2,3).

The recent success of imaging human neuroreceptors has been based upon demonstration of the appropriate receptor pharmacology, first in rodent studies and non-human primates, and subsequently in human beings using the same labeled ligand. Since competition with unlabeled ligands for receptor binding is an important criterion, both the animal and the human studies require such an *in vivo* demonstration. More importantly, in human studies, where only external imaging is used to estimate absolute receptor density and other receptor parameters, competition studies are helpful and often essential. That is, often multiple human studies are required, each with sufficient injected radioactivity to achieve statistically acceptable tomographic images. An example of such an *in vivo* competition study is shown in Figure 1.



JOHNS HOPKINS UNIVERSITY

Figure 1. Unblocked and blocked PET scans: these are two PET scan studies done in the same individual. The one on the left shows the uptake of C11-NMSP in the caudate and putamen 45 minutes post injection with no prior competing substance. The image on the right is also 45 minutes post injection but with the prior administration of 7 mg of unlabeled haloperidol which blocked the uptake of C11-NMSP.

This demonstrates the effect of prior ingestion of a competing unlabeled ligand, haloperidol, on the uptake of the N-methylspiperone (NMSP) tracer in brain regions. The differences in activity distribution in unblocked and blocked receptor uptake tracer studies may also be relevant in dosimetric calculations.

PET IMAGING OF RECEPTORS

Typical human positron emission tomography (PET) imaging studies have consisted of the injection of sufficient radioactive material (15-20 mCi) to allow measurement of the time course of the tracer. The time course of measurement must be sufficiently long to allow for a high degree of specific to non-specific binding in the simplest case, or to provide a sufficient depiction of the physiological distribution to allow estimation of kinetic parameters in more sophisticated models. A typical time course with the D₂ dopamine receptor binding ligand ¹¹C-3N-methylspiperone is shown in Figure 2.

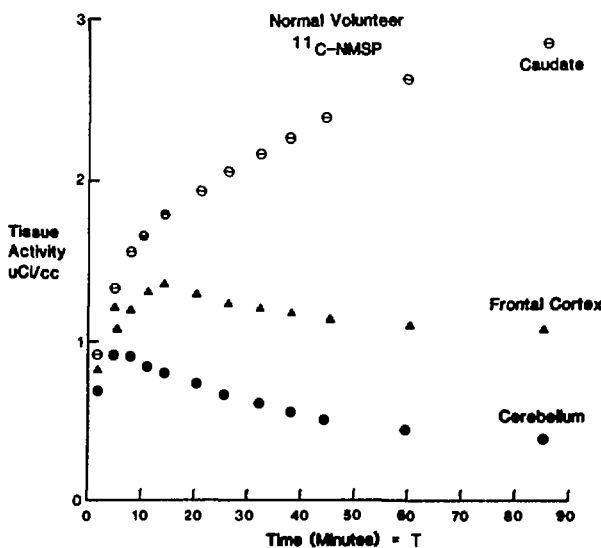


Figure 2. Time activity curve of C11-NMSP in the human brain. The upper curve shows the increasing binding to the caudate and putamen because of the high concentration of D₂ dopamine receptors and its essentially irreversible binding to these receptor sites. The lower curve shows the early wash-in and progressive wash-out from non-specific sites in the cerebellum. The middle curve shows the intermediate binding to the lower affinity S₂ serotonin sites which are principally located in the frontal cortex and other cortical regions.

A recently developed technique used to estimate absolute receptor density involves imaging neuroreceptors that are unblocked and then blocked (4,5) by competition with unlabeled competing ligands. This technique emphasizes the requirement that sufficient radioactivity be administered and multiple PET studies be performed to provide optimal quantification of receptors. Realistic estimations of receptor parameters are imperative to optimize the research potential of this technique. Clearly, the level of activity which may be administered is dependent upon dosimetry considerations. Thus, it is important that accurate estimates be performed of the absorbed dose from neuroreceptor binding positron-emitting radiopharmaceuticals.

GENERAL CONSIDERATIONS FOR DOSIMETRY ESTIMATES

INTRODUCTION

The labeling of human neuroreceptors for in vivo imaging has resulted in a new opportunity for studying neuropsychiatric disorders and the effects of drugs on such receptors. Since these receptor binding radioligands have a biodistribution which can be predicted by their receptor pharmacology, certain considerations apply to these studies that may be somewhat unique in dosimetry studies. The preference of receptors in specific parts of various organs allows for increased concentrations of radionuclides in subregions of these organs. These local concentrations can be altered by the presence of a competing ligand for the receptor sites. The usual assumption of a homogeneous activity distribution within the organ may be inaccurate with neuroreceptor binding compounds.

The ligand candidates for neuroreceptor imaging ideally should be evaluated for dosimetry with the same radiolabel as that to be used in practice. Although many such ligands may be available in a tritiated or ^{14}C label form, the exact chemical form should be studied whenever possible to ensure that the biological course is appropriately measured. Differences in the radiolabel position, or in the inserted nuclide (e.g. ^{18}F for hydrogen) could radically affect receptor binding and distribution properties or the metabolic fate of the label, thereby confounding the biodistribution and modifying the absorbed dose. In the case of ^{11}C labeled tracers, the 20 min. half-life makes it challenging to do biodistributions, especially in multiple rodent studies. In practice, biodistribution measurements only can be performed up to about 1.5 to 2 hours post injection. In addition to the physical half-life limitations, successful biodistribution measurements are dependent upon the specific activity of the labeled ligand and the time in transporting the tracer from the production site to the biodistribution facility. Thus, it may be necessary to employ longer lived radionuclides to obtain sufficient time-activity information. In such cases biological similarities must be demonstrated between the short and long-lived tracer.

The injected mass of the prospective ligand is another important consideration. Since receptor-binding radiotracers concentrate in the receptor tissue in an amount dependent upon the total mass of the ligand injected, it is useful to examine the tracer residence times for the approximate range of injected mass that is to be used in human studies. Similarly, if unlabeled, competing ligands are also to be injected, then measurement of the activity distribution with them present is also necessary to accurately assess the total absorbed dose. Furthermore, it is clearly appropriate to use the same injected ligand mass per unit body weight (e.g. $\mu\text{g}/\text{kg}$) in each dosimetric measurement when multiple productions of the radiolabeled compound are being used.

Rodents are the most common species for screening the pharmacological properties of new ligands and similarly appropriate for initial dosimetry estimations. However, the GI tract or the bladder are often the critical organ, therefore more specific absorbed dose measurements in dogs or non-human primates are required. Although human biodistributions are the most desirable, there are limitations in which organ measurements can be performed especially when only a head but not a whole-body PET scanner is available. In this case, the use of external probes (vide infra) can provide useful measurements in humans.

SPECIFIC EXAMPLES: ^{11}C -N-METHYLPIPERONE

The mouse biodistributions were obtained in triplicate up to 120 min. post injection of the tracer at 10 $\mu\text{g}/\text{kg}$. (Previous studies determined that in mice the mass of 1-10 $\mu\text{g}/\text{kg}$ had the same binding in vivo.) Table 3 shows the absorbed dose estimates based upon MIRD S-factors.

Table 3.

^{11}C -N-Methylspiperone
Dosimetry per mCi in mrads (from mouse distributions)

<u>Target Organ</u>	<u>Total Doses</u>
Eyes	3.4 mrads
Brain	< 10 mrads*
Lung	60.8 mrads
Liver	42.8 mrads
Kidneys	71.3 mrads
Bladder	98.4 mrads* (no voiding)
Stomach	40.6 mrads
Small intestine	36.0 mrads
Upper LI	31.3 mrads
Lower LI	30.3 mrads
Bone marrow	12.7 mrads
Ovaries	34.6 mrads
Testes	12.4 mrads
Total body	15.4 mrads
Spleen	14.5 mrads

*based on human estimates (see text)

More accurate absorbed dose measurements of the GI tract were obtained from rhesus monkey studies. These gave dose estimates which were within 15% of our mouse GI tract estimates (6).

Human biodistributions: Specific measurements of selected brain parts and the bladder were made in several human volunteers.

Brain activity distributions were obtained from serial PET scans performed after the intravenous injection of 15-20 mCi of ^{11}C -NMSP. Brain activity distributions were also measured in subjects where 7.5 mg of

haloperidol were administered orally 4 hours prior to the ^{11}C -NMSP. (Haloperidol, a neuroleptic, which binds to D-2 dopamine receptors, competes with NMSP for receptor sites.)

Figure 3 shows a typical set of PET images of the distribution of ^{11}C -labeled NMSP in minutes post injection. Each column corresponds to a different level in the brain; the cerebellum, the basal ganglia and the frontal cortex respectively, each separated by 32 mm. Each row is a different time post injection.

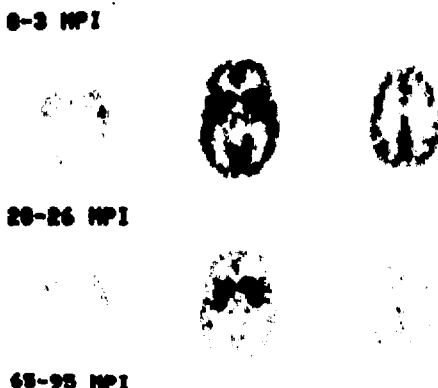


Figure 3. ^{11}C -labeled NMSP PET images corresponding to 3 different levels in the brain at 0-3, 20-26, and 65-95 minutes post-injection. The first column shows the appearance of the tracer in the lowest slice, passing through the cerebellum and the washout of the tracer from the non-specific sites. The middle column of images shows the progressive binding to the caudate and putamen where D2 dopamine receptors are prevalent. The third column shows the intermediate binding and then dissociation from the frontal cortical regions as a function of time. Each of the three columns represent images separated by 32 mm, which is determined by the physical characteristics of our CTI NeuroECAT scanner.

To estimate the amount of energy absorbed by the caudate, putamen, and whole brain from ^{11}C -NMSP we employed the absorbed fraction method. Absorbed fractions for the caudate, putamen and whole brain as source regions of annihilation gammas and the caudate, putamen and whole brain as target regions were those calculated previously (7). The specific absorbed fraction for the whole brain as the source region for 511 keV gammas and the eyes as the target region were taken from Eckerman et al. (8). All betas were assumed to have an absorbed fraction of 1.0.

From the serial PET scans the observed mean counts/pixel in the tomographic images were converted to $\mu\text{Ci}/\text{ml}$ estimates for brain tissue. Cumu-

lated activities were calculated by numerical integration of the time-activity curves. Owing to the fact that the highest concentration of ^{11}C -NMSP (other than the caudate and putamen) in the brain is in the frontal cortex, the cumulated activity for the whole brain was calculated conservatively using frontal cortex activity estimates for areas of the brain other than the corpus striatum. All cumulated activities were increased by 10% to conservatively account for the additional absorbed dose which occurred after cessation of serial PET measurements, i.e., 100 minutes post ^{11}C -NMSP injection. In calculating the caudate and putamen cumulated activities a recovery coefficient value (vide infra) of .5 was included (9, 10). Cumulated activities in the eyes were difficult to estimate owing to the difficulty in defining the loss of quantitation for these small structures. Again, the activity/ml in the frontal cortex was taken as an estimate of the activity/ml in the eye.

Table 4 shows the absorbed dose in mrads/mCi of injected ^{11}C -NMSP for the caudate, putamen and whole brain. The average dose per mCi of injected ^{11}C -NMSP for the caudate, putamen and whole brain are 93, 96 and 36 mrads, respectively.

Table 4 also shows similar estimates of the absorbed dose per mCi of ^{11}C -NMSP injected for subjects with haloperidol present. Both the whole brain and corpus striatum absorbed doses are decreased compared with studies employing no haloperidol. The average absorbed dose per mCi of ^{11}C -NMSP administered for the caudate, putamen and whole brain are 54, 56 and 32 mrads, respectively.

Table 4.

^{11}C -NMSP

Human Dosimetry Estimates

average dose (\pm 1 S.D.)
mrads/mCi

	<u>caudate</u>	<u>putamen</u>	<u>whole brain</u>
control (N=8)	93.3 (31.1)	96.0 (31.8)	35.5 (11.3)
haladol (N=4) block	53.8 (16.7)	55.5 (16.7)	32.3 (9.7)

Doses are brain \rightarrow caudate
 brain \rightarrow putamen
 brain \rightarrow brain

The absorbed dose for the eyes for eight subjects was also estimated. Since there are serious partial volume problems with eye activity measurements and since the eyes were only occasionally visible due to positioning, we conservatively estimated the eye self-dose by using the time activity curve of the frontal cortex for a cc of tissue. The dose was calculated to be 88 ± 26 (1 S.D.) mrads/mCi of ^{11}C -NMSP injected.

Bladder Distributions:

The bladder is one organ where errors are often encountered in absorbed dose estimations. These errors result from the use of published tabulations

of S-factors or specific absorbed fractions which were calculated assuming a fixed bladder content volume (of 200 ml). Recall that the value of S is dependent upon the amount and composition of the absorbing medium between the source of radiation and the target organ, on the energy and type of particle(s) emitted and on the size, shape and composition of the target and source organ. In the case of irradiation of the bladder (wall), changing the volume of the bladder contents results in a change in the absorbed dose received from the radioactivity within the bladder content. For bladder wall dose estimation it is necessary to estimate the change in bladder content volume over time since the S-factors also change. It is also helpful to determine the arrival time of activity in the bladder.

How can the required data be obtained to accurately assess the bladder dose? Among the methods are: 1) the use of a well-collimated external probe over the bladder, 2) PET measurements of the bladder, 3) bladder catheterization or 4) animal studies.

For the bladder dosimetry data to be presented below we have used a single, external probe over the bladder of normal volunteers participating in a PET study. Bladder time-activity data were acquired from six normal subjects (and 1 patient) during NMSP studies. After positioning the supine subject in the PET device a 2" x 2" NaI crystal was positioned above the bladder (as shown in Fig. 4) using external body landmarks. A tapered lead collimator provided a diverging field of view encompassing the bladder. (Fig. 4)

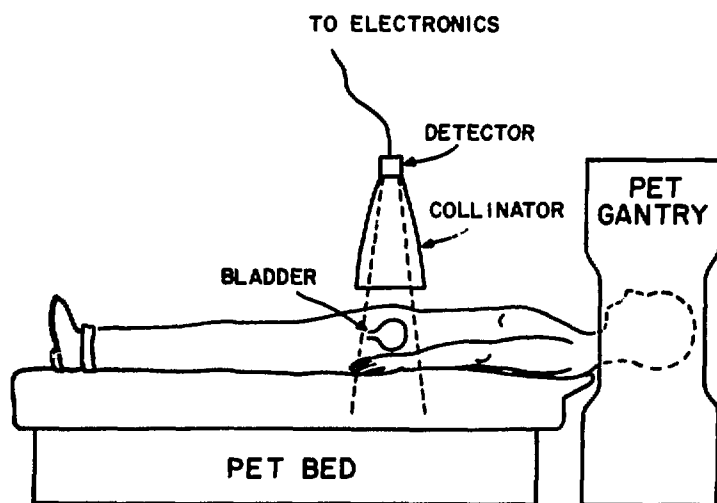


Figure 4. Bladder probe arrangement: Bladder measurements can be estimated from probe measurements in human studies when only PET measurements of the head are available.

Bladder activity was continuously monitored (and the data stored on a microcomputer) from the time of ^{11}C -NMSP injection to completion of the PET procedure (105-120 minutes post-injection). To calculate the dose to the bladder wall from the contents a linear production rate was assumed for the urine, i.e.,

$$V_{\text{urine}} = V_0 + kt$$

where V_0 is the volume of urine in the bladder at the time of tracer injection, k is the linear rate constant and t is the time post-injection. The linear rate constant is determined from the measured final urine volume and a specified starting urine volume. In our PET protocols, subjects last void at least 20-30 minutes prior to the NMSP injection (to allow positioning time and angiocatheter insertion). Given normal residual urine volumes in the bladder and normal urine production rates (11) subjects are expected to have at least 20 ml of urine in their bladder when the tracer is injected. For the bladder calculations below starting urine volumes of 20, 30 and 40 ml were assumed.

From the urine production rate the volume of urine in the bladder could be estimated conservatively (at each time point after tracer injection). Given an estimate of the volume of the bladder contents at each time point the "instantaneous" dose to the bladder wall from the contents could be calculated. For the dose due to penetrating radiation, i.e., the annihilation photons, the empirical formula of Snyder (12) was employed.

$$D_Y(v) = 2 \times [7.44 \times 10^{-6} e^{-0.00192V} + 2.38 \times 10^{-5} e^{-0.0342V}] \text{ rads/ } \mu\text{Ci-min}$$

The factor of 2 accounts for the two annihilation photons per decay.

For the nonpenetrating radiation, it was assumed that the dose to the bladder wall was one-half that of the bladder contents far from the wall.

Integration of the "instantaneous" dose yielded dose estimates for the bladder wall during the PET procedure. (During the integration procedure corrections were applied for the different detection efficiency of the external probe to different bladder volumes.) The total dose estimates were increased by an additional (conservative) 10% to account for the dose received after cessation of measurements. Note that after 100 minutes post-injection only 3% of the ^{11}C injected activity remains.

Table 5 shows the estimated bladder wall dose per 20 mCi of injected ^{11}C -NMSP for three starting volumes. In all instances, a larger starting volume in the bladder provides a lower dose to the bladder wall.

Table 5. Bladder Dosimetry

¹¹C-NMSP Dosimetry (Human Estimates)

Bladder Dose (N=5)*
mrads/mCi
(starting bladder volume (ml))

Subject	20	30	40	final bladder volume (ml)
1	28	24	20	(395)
2	83	64	60	(225)
3	53	43	39	(355)
4	133	114	102	(200)
5	195	155	130	(200)
Avg.	98.4	80.0	70.2	(275)
Sd.	59.6	48.0	40.5	(83.1)

*Bladder dose from bladder contents only

OTHER SOURCES OF RADIATION: CT SCANS

Depending on the PET scanning devices available some anatomical alignment may be necessary to demonstrate various structures which require imaging. For example, in the case of ¹¹C-NMSP and the three-plane CTI NeuroECAT PET scanner, it has been found helpful to first do an alignment with a limited non-contrast CT scan. This is done to maximize the position of the middle plane of the PET scanner to pass through the basal ganglia where D2 dopamine receptors are located, the upper plane to pass through the frontal cortex where S2 serotonin receptors are concentrated and the bottom plane to pass through the cerebellum where non-specific binding is measured (since both S2 serotonin and D2 dopamine receptors are essentially absent there). These alignment procedures require anywhere between 5 to 10 CT slices for localization. Other methods such as skull x-rays may also be considered for alignment prior to PET scanning. These procedures add to the overall radiation dose especially to the head as in the neuroreceptor PET imaging studies.

Using dosimetric calculations for Siemens Somatom DR-3 CT scanner typical CT mean doses to the whole brain are in the order of 1-2 rads. The assumptions and dosimetry calculations are discussed below.

The brain is assumed to be reasonably represented by a right circular cylinder. When irradiated by the Siemens Somotrom DR-3 CT system the cylindrical "brain" is irradiated uniformly in a narrow band extending around the circumference.

Measured dose data indicate that the dose on the surface, within the irradiated volume, is uniform around the circumference. It can also be assumed that the dose on any radius is uniform from the axis to the surface.

These conditions would not hold if: 1) Scan rotation is more or less than 360°, the two shortest scan times in the DR-3, are less than 360°. 2) The brain is not located on the axis of rotation. (This should result in a relatively small error for typical conditions.) 3) Differences in absorption of overlying structures distort the dose uniformity. Certainly the brain is not a right circular cylinder and the absorption of the skull varies greatly. These last difficulties will be ignored for the first attempt.

Dose measurements were taken with TLDs in a cylindrical Plexiglas phantom with dimensions length = 150 mm; radius = 75 mm. Data were taken on the axis and on a line parallel to the axis at a depth of 1 cm. This results in dose profiles along these two lines, generated for a centrally located slice.

For the purposes of this discussion the following geometry is assumed: The three dimensional coordinates have the origin at the center of the cylindrical phantom. The x-ray plane is the plane of irradiation which is the scan plane and passes through the origin. The z axis is the axis of rotation and the phantom axis. Thus the dose profiles measured were on the z axis and at a radius of 6.5 cm parallel with the z axis.

The assumed symmetry suggests that the average dose along any radius is reasonably represented by the mean of the central axis and surface doses at that point. A mean dose profile was then plotted as the average dose along the z axis. The average volume dose is then the integral of average dose along this line divided by the length of the integration line.

Average doses were obtained by using a Simpson's estimate of the integral for slice widths of 2, 4, and 8 mm at 125 kVp 360° scan rotation. See Table 6.

Table 6. Calculation of mean dose to brain from X-ray CT

Expressed as mrads per mAs

<u>Slice width</u>	<u>mean dose</u>
2mm	0.173 mrad/mAs
4mm	0.221 mrad/mAs
8mm	0.311 mrad/mAs

Typical HEAD scan with Siemens Somatom DR-3

Factors: 10 slices, 8 mm slice width 449 mAs
Mean Dose = 10 slices x .311 mrad/mAs x 449 mAs
Mean Dose = 1.4 rads

The total mean brain dose for a given head CT scan is then

$$\bar{D} = n \times D_i \times Q$$

where

- \bar{D} = mean total brain organ dose
 D_i = average brain dose/slice
 n = number of slices within brain
 Q = mAs per scan

For example: A head study done with 16 slices with 8 mm slice width and 449 mAs/scan at 125 kVp would be:

$$\bar{D} = 16 \text{ slices} \times \frac{.311 \text{ mrad}}{\text{mAs-slice}} \times 449 \text{ mAs}$$

$$\bar{D} = 2234 \text{ mrad}$$

Hence, the total dose to the brain for a typical ^{11}C -NMSP study including a control PET scan with 20 mCi, a competition study with unlabeled haldol with 20 mCi injected and a localizing CT scan gives a total whole brain dose in the order of about 2.7 rads. See Table 7.

Table 7.

Typical Total Doses to Whole Brain
for the ^{11}C -NMSP Tracer Including a CT Scan

	<u>rads</u>
control PET @ 20 mCi	0.69
haldol PET @ 20 mCi	0.65
CT scan	1.4
Total dose to whole brain	2.7

PARTIAL VOLUME EFFECTS

Inherent in the PET imaging procedure is the possibility of underestimating the true activity concentration because of the finite resolution of the scanner. By using radioactive spheres with known concentrations which are imaged in the PET scanner or realistic human phantoms (9), an estimation of the "recovery coefficient" can be obtained for various structures. More recent methods using simulation calculations to directly estimate the partial volume effect have also been employed (13). These may be important in small structures where PET imaging is used to estimate the activity time integral. Rough estimates of this correction factor are in the order of 50-100% underestimation of the true counts in a PET neuroECAT imaging device with a full width at half maximum resolution of 8 mm x 8 mm x 15 mm. However, the calculation of the overall loss of quantitation is somewhat complex since it is also a function of the background radioactivity which, as seen in Figure

2, is a variable function of time. Hence, conservative estimates by doubling PET estimated doses may be appropriate. In the case of ^{11}C -NMSP the individual doses are relatively small so conservative estimates are tolerable although with some radioligands highly conservative estimates may lead to restrictions on the activity which can be injected.

Issues for Further Study

This paper has been an initial attempt to outline an approach to estimate the absorbed dose from a neuroreceptor binding radiotracer. Issues that might be considered in future dosimetry studies include the application of kinetic modelling to actual residence time calculations and more accurate models for measurement of local dose and microdosimetry. Improvement in both these areas will allow more accurate risk assessment of neuroreceptor binding radiotracers.

CONCLUSIONS

Dosimetry estimates of neuroreceptor binding ligands require consideration of such varied issues as pharmacology, receptor distribution and positron emission. These considerations make this dosimetry rather unique and worthy of extensive discussion and evaluation.

ACKNOWLEDGEMENT

This work was supported in part by PHS grant NS15080. We thank the cyclotron group including Drs. Hayden Ravert, Allan Wilson and Mr. Fred Gilbart; and the PET scanning group, Steve Herda and Martin Stumpf; Kate Prendergast and Madleen Murrell. A special thanks for discussions with Dr. Thomas Mitchell.

REFERENCES

1. Yamamura H.I., S.J. Enna, M.J. Kuhar. Neurotransmitter Receptor Binding, second edition, Raven Press, 1985.
2. Wagner HN, Jr, Burns HD, Dannals RF, Wong DF, et al. Imaging dopamine receptors in the human brain by positron tomography. *Science* 221:1264-1266, 1983.
3. Wong D.F., H.N. Wagner, Jr, R.F. Dannals, et al. Effects of age on dopamine and serotonin receptors measured by positron tomography in the living human brain. *Science* 26:1393-1396, 1984.
4. Wong DF, Gjedde A., Wagner, HN Jr. Quantification of Neuroreceptors in the Living Human Brain. Part I. Association Rate of Irreversibly Bound Ligands. *J Cereb. Blood Flow and Metab.* (in press, March/April, 1986).

5. Wong DF, Gjedde A., Wagner HN Jr., et al. Quantification of Neuroreceptors in the Living Human Brain. Part II. Assessment of Receptor Density and Affinity Using Inhibition Studies. *J. Cereb. Blood Flow and Metab.* (in press, March/April, 1986)
6. Personal communication: Dr. Lundquist, Uppsala University, Sweden.
7. Bice A.N., J.M. Links, D.F. Wong, H.N. Wagner, Jr. Absorbed fractions for dose calculations of neuroreceptor PET studies. *Eur J Nucl Med* 11:127-131, 1985.
8. Eckerman K.F., M. Cristy, G.G. Warner. Dosimetric evaluation of brain scanning agents. In the Proceedings of the Third International Radiopharmaceutical Dosimetry Symposium, Oct. 7-10, 1980, Oak Ridge Tennessee. Edited by Watson E., Schlafke-Stelson A., Coffey J., Cloutier R. pp 527-540.
9. Wong DF, Links JM, Molliver ME, et al. An anatomically realistic brain phantom for quantification with positron tomography. *J Nucl Med* 25:p105, 1984.
10. Mazziotta, J.C., M.E. Phelps, D. Plummer, D.E. Kuhl. Quantitation in positron emission computed tomography: 5. Physical-anatomical effects. *J Comput Assist Tomogr* 5:734-743, 1981.
11. Campbell's Urology, vol. 1, 4th edition. Harrison J.H., Gittes R.F., Perlmutter A.D., Staney T.A., Walsh P.C., eds. W.B. Saunders Company, Philadelphia, Pa., 1978.
12. Snyder W.S., M.R. Ford. Estimation of dose and dose commitment to the bladder wall from a photon emitter present in urine. Health Physics Division Annual Progress Report, period ending July 31, 1973. ORNL-4903.
13. Bice A.N., D.F. Wong, H.N. Wagner, Jr. A method for estimating recovery coefficients in positron emission tomography. *J Nucl Med* 26(5):p36, 1985.

DISCUSSION

HINES: The slide you showed concerning the calculation of the absorbed dose from x-ray CT may not be correct in that I do not believe the dose is additive for the number of slices. Also, I am not certain that you have included cross-scatter from adjacent primary slices.

WONG: Dr. Hines' comments are appreciated; however, the dose in our simplified expression is integrated over the entire brain volume; i.e. the absorbed dose from scattering is also included. Certainly, as he states, the primary contribution cannot be simply additive; however, within the simplifying assumptions used in our work, the integral doses are indeed additive. However, we do feel that our method of estimating the organ dose could be refined further. We are currently working on relatively refined computer models of organ dose in CT with an anthropomorphic conceptual phantom.

RADIATION DOSE ESTIMATES FOR THE ARTERIAL INJECTION OF Tc-99m
LABELED HSA MICROSPHERES AND MACROAGGREGATED PARTICLES

Barbara Y. Croft, Ph.D.
Department of Radiology
University of Virginia
Charlottesville, Virginia 22908

ABSTRACT

Particles of human serum albumin, such as macroaggregated albumin or microspheres, have been injected intra-arterially for the following indications: to examine tumor perfusion prior to and during chemotherapy, to examine coronary artery perfusion, and in the diagnosis of peripheral vascular disease. The region of distribution of the particles is localized according to the artery selected for injection.

The radiation dose is affected by the distribution of the radioactivity in time and space and the physical parameters of the radionuclide. In addition, the radiation dose estimate takes into account the mass and geometry of the perfused volume. In certain cases, there is a significant amount of shunting of the injected particles; the radiation dose conferred by the shunted particles is to the lung tissue.

INTRODUCTION

Quite a number of nuclear medicine laboratories have been using the arterial injection of technetium-99m labeled particles, in the size range which blocks capillaries, to visualize blood flow. Such use is not covered in the package inserts because intra-arterial injection is not described. Most users have applied to the FDA for IND's to cover intra-arterial injection.

The single most common use for intra-arterial injection is to visualize the area of perfusion of a catheter implanted arterially for the delivery of a chemotherapeutic agent to a tumor (1). The more the agent can be made to perfuse only the tumor on its first pass, the more successful the therapy and the less likely the damage of other tissues by the chemotherapeutic agent. The distribution of radioactivity shows the perfusion pattern and allows the correct placement of the catheter; radioactive tracer methods are superior to angiography because the radioactivity can be injected at the same flow rate as the chemotherapeutic agent, perfectly tracing its distribution.

Intra-arterial particle injection has been used to trace the perfusion of the coronary arteries (2). The particles are injected at the time of coronary artery catheterization and imaged afterward. The technique seems to have proven itself to be quite safe. That thallium-201 is more often the radionuclide used to delineate coronary artery circulation is because its use does not require a catheter for injection.

Besides the coronary arteries, the circulation of other major arteries has been studied with intra-arterial particles. The arterial circulation of the legs (3) and carotid arteries (4) have been extensively studied. Radiolabeled particles have been used for cardiac output measurements after injection into the left ventricle (5).

Each of the above mentioned techniques will be outlined as to the patterns most commonly seen and sample dose calculations offered for each. For a particular patient, the radiation dose estimate must depend on the amount of tissue affected and the percentage of the radionuclide that is distributed to that tissue. It should be noted that when one is discussing the safety of intra-arterially injected particles, the number of particles injected and the radiation dose are both important.

A number of different particles have been used for intra-arterial injection. Since it is not possible to know for which one the reader would desire a radiation dose estimate, a table of biological and effective half lives would have to be drawn up, such as that shown in Table 1. It should be noted that the half lives are for the particles in the lungs, the only organ for which there is data commonly available.

TABLE 1 Half-lives in the lungs

Source of numbers was package inserts and manufacturers' technical services. Where both biological and effective half-lives were given, both are stated below even if inconsistent.

Particle	T-biol	T-phys	T-eff
3-M microspheres	13 hr	6 hr	4.1 hr
Squibb MAA	2-3 hr	6 hr	1.76 hr or less
NEN MAA	30%:1.5 hr;60%:8 hr	6 hr	

TUMOR ARTERIAL CATHETER INJECTION, OFTEN IN LIVER

For chemotherapeutic agents which are rapidly removed from the blood, there is the possibility of delivering more of the agent to the tumor and less to the rest of the patient if the agent is placed in the blood supply of the tumor. In some patients, the agent is supplied directly after the arterial supply to the tumor is occluded. In these patients it is useful to know whether the agent is actually being delivered to the tumor as well as what normal tissue is also being perfused by the cytotoxic drug. It is sometimes possible, depending on the catheter size, to use arteriography to look at perfusion in the area of the catheter, but the flow rates that must be employed are much greater than those normally used in the delivery of the chemotherapeutic agent, so the x-ray images may not represent the perfused area correctly. In this setting, radioactive particles have been used successfully (6). Most of the tumors in question have been intrahepatic (1,7,8,9) although some work has been done with pelvic and peripheral tumors (10).

After injection into a hepatic artery catheter, the patterns of distribution are several. Depending on the catheter position and the perfusion patterns in the patient, most of the liver may be perfused, only the tumor may be perfused, or there may be perfusion of organs outside the liver such as the stomach or small bowel. Occasionally there is shunting to the venous circulation and the lungs are visible. Since the extrahepatic activity seen on the images represents areas which will be exposed to high concentrations of cytotoxic agent, it is important for these to be seen and identified. The

catheter tip is often moved so that other tissue will not be exposed. Pulmonary uptake has been associated with gastrointestinal toxicity of the chemotherapeutic agent (11); in 14 patients studied lung uptake was under 10% in 11.

The same kinds of observations have been made after injection of particles into peripheral arterial catheters (10). The possibility of shunting so that radioactivity is found in the lungs may be a normal occurrence, not associated with tumor neovascularity (10).

Typically 1 to 5 mCi of Tc-99m labeled particles in 0.5 ml are injected into the catheter in imitation of the flow rate of the chemotherapeutic agent. Because of the variety of arteries used for infusion and the variety of patterns seen, it is necessary to make dose estimates for a number of different circumstances. In hepatic artery perfusion, the target organ is usually the liver, but the lungs and portions of the intestine should also be considered. When other arteries are perfused, the muscles may be the target organ, along with the lungs. The table below should provide a means for calculating dose to the liver, lungs and muscles, depending on the percent of the dose that lodges in each of these organs. Macroaggregated albumin labeled with Tc-99m is the imaging agent of choice, in part because the MAA seems to be able to be pushed through the catheter better than microspheres which lodge in the catheter (12).

For the radiation dose estimates (Table 2), spherical regions of 10, 40, and 100 grams were chosen as representative. The radioactivity was assumed to be uniformly distributed in the region, so that the standard calculation for small spheres with uniformly distributed activity (13) could be used. Actually, of course, the activity in the intestines might well be considered to be distributed in an annular ring around the intestinal contents. This would require its own calculation.

TABLE 2 Dose to various organs after injection into liver arterial catheter
 f indicates fraction of injected dose deposited in the organ in question. T indicates the effective half-life of the material in the organ in question.
 $\tilde{A} = 1.44E+03 T \mu\text{Ci}\cdot\text{hr}/\text{mCi}$

Organ	"S" factors for Tc-99m	Dose rads/mCi for Tc-99m	References
Liver	4.6E-05	6.62E-02 fT	(14)
Lungs	5.2E-05	7.49E-02 fT	(14)
Intestines			(13, p.30, 15)
10g	4.25E-03	6.12 fT	
40g	1.16E-03	1.67 fT	
100g	5.51E-04	0.79 fT	

CORONARY ARTERIES

A great deal of the interest focused on the heart is focused directly on the coronary arteries. It is presumed that if the perfusion of an area by the arterial circulation is patent, then the myocardium is viable. Thallium-201 thallous chloride is injected intravenously, usually after exercise, to determine myocardial perfusion. Thallium is useful but it is expensive, the examinations take several hours, thallium is not a good imaging nuclide, and the activity doses are not large enough for good counting statistics because of radiation dose limitations. The injection of Tc-99m labeled particles, either human serum albumin microspheres or macroaggregated albumin particles, during

coronary angiography, provides another method for studying myocardial perfusion. Should one wish to study the distribution of flow from the various arteries perfusing the myocardium, more than one radionuclide label can be used. Iodine-131, indium-111, and indium-113m have been used in combination with Tc-99m.

Kirk et al.(16) injected approximately 20,000 microspheres in the 30 micron size range labeled with 3 mCi Tc-99m into the left coronary artery. They injected a maximum of 800,000 I-131 macroaggregated albumin particles in 150 μ Ci into the right coronary artery. They estimated a radiation dose of 1.7 rads to the heart from 3 mCi of Tc-99m and 0.87 rads from 150 μ Ci of I-131. An estimated 3500 patients were studied between 1971 and 1977.

Kolibash et al.(2) injected approximately 50,000 macroaggregated albumin particles labeled with 1 mCi of Tc-99m into the left coronary artery and 100,000 particles labeled with 300 μ Ci of In-111 into the right coronary artery. Patients with by-pass grafts were injected differently to assess graft patency. At the time of writing, over 2500 patients had been examined.

The MIRD Heart Task group used a new heart model to refine the estimates of the specific absorbed fraction from radioactivity in the heart contents and in the heart muscle (17). Table 4 of that paper has been used in the preparation of the dose estimates given in Table 3. The estimates of the cumulated activity for Tc-99m MAA, Tc-99m microspheres, I-131 MAA, In-113m MAA and In-111 MAA include effective half-lives from the package inserts for the materials or the worst-case estimate of an effective half-life equal to the physical half-life of the radionuclide. Output data has been taken from MIRD publications (15).

TABLE 3 Dose to heart wall from radioactivity in the heart wall
f is the fraction in the organ in question; T is the effective half-life of the material in question in the organ in question.

Nuclide	"S" factor for nuclide	Dose rads/mCi	References
Tc-99m	1.78E-04	0.256 fT	(15, p 62; 17)
In-111	4.72E-04	0.680 fT	(15, p 66; 17)
In-113m	9.37E-03	1.34 fT	(15, p 66; 17)
I-131	1.52E-03	2.18 fT	(15, p 75; 17)

OTHER ARTERIES, FOR THE STUDY OF PERfusion

In order not only to visualize, but also to quantitate, perfusion in several regions of the body: extremities and brain in particular, it has seemed useful to employ Tc-99m-labeled macroaggregated albumin (MAA) or human albumin microspheres (HAM), injected intra-arterially. Because the distribution of the particles is fixed, it can be studied carefully. If resting and stress imaging is desired, then another radionuclide, such as In-113m HAM, is injected. The use of particles intra-arterially in the extremities has been well documented (3,18,19,20,21). Use for carotid artery perfusion is less common (4,22,23,24). In addition microspheres have been used to quantitate cardiac output in human beings (5). Other methods for obtaining the same or similar information use Tl-201 or Xe-133 where muscles are involved and Xe-133 or Tc-99m pertechnetate, and more recently I-123 iodoamphetamine, for the brain.

To assess arterial perfusion in peripheral vascular disease, 5 to 10 mCi of Tc-99m HAM are injected either intra-aortically below the level of the renal

arteries or directly into the femoral artery. A like amount of In-113m HAM would be used if necessary. Several patterns can be observed (3). The tracer is distributed between the point of injection and the toes. In a patient with no peripheral vascular disease, the activity is distributed in the muscle mass, with relatively less in the nonmuscular regions. In patients with ischemia and diabetes, the activity is distributed more in proportion to skin surface. A third pattern of diffuse activity shows an increase in the knees and ankles, with activity visible in the muscles. There also several patterns of localization with less in one particular muscle, a concentration in the region of an ulcer or in the region of a diseased bone. If the patient is injected while hyperemic, then there is an increase in the relative amount of activity that appears in muscle.

For such a variety of patterns, dose estimates can only be made very generally. One can estimate radiation dose (Table 4) based on the muscle mass in the legs and the general cylindrical shape of the muscles. One leg was assumed to be an ellipsoid of 10 kg and to be roughly of the shape of the ellipsoids used for the calculations of absorbed doses from uniformly distributed activity.

TABLE 4 Dose to one leg from particles injected into femoral artery
 f is the fraction in the organ in question; T is the effective half-life of the material in question in the organ in question. See Table 2 for lung dose, in the event of shunting.

Material	"S" factor for nuclide	Dose rads/mCi	References
Tc-99m HAM	8.84E-06	1.273E-02 fT	(15, p 62; 25, p 37)
In-113m HAM	3.96E-05	5.70E-02 fT	(15, p 66; 25, p 37)

Carotid artery injection is made to assess perfusion patterns in the brain. If the patients have had bypass surgery, then the patterns of perfusion will reflect their surgery as well as the state of their disease (4). Common carotid injection reaches the area perfused by the external and internal carotid branches, so parts of the scalp, face, and nose are visualized along with the perfused parts of the brain. A dose of 5 mCi of Tc-99m HAM containing about 80,000 particles is injected. The radiation dose estimates are calculated according to an estimate of the amount of tissue perfused by the particles. The various affected parts of the brain were assumed to be spheres or thick ellipsoids for the dose calculation (25)(Table 5).

TABLE 5 Dose to brain segments from particles injected into carotid arteries
 f is the fraction in the organ in question; T is the effective half-life of the material in question in the organ in question.

Region size	"S" factor for Tc-99	Dose rads/mCi	References
Tc-99m			(15, p 62; 25, p 37)
300 gram	2.03E-04	.2923 fT	
500 gram	1.31E-04	.1886 fT	
1 kg	7.24E-05	.1043 fT	

The measurement of cardiac output to individual organs in human subjects is not often performed. Lavender et al. (5) reported on a series of seven patients injected during angiography with approximately 4 million 15 micron Tc-99m HAM.

Whole-body emission and transmission scans were performed to estimate the relative distribution of radioactivity throughout the body. From the percentages of blood flow to the various organs, radiation doses can be calculated (see Table 6), using MIRD tables of S values (14).

TABLE 6 Dose from Tc-99m particles used to measure cardiac output

Organ	Fraction to that organ	S factor for Tc-99m	Dose rads/mCi	References
Head	14.8%	1.77E-05	3.77E-03 T	(15, p 62; 25)
Heart	4.8	1.78E-04	1.23E-02 T	(15, p 62; 17)
Kidneys	20	1.9E-04	5.47E-02 T	(14)
Spleen	6.0	3.3E-04	2.85E-02 T	(14)
Rest of body	54	2.0E-06 total body	1.55E-03 T	(14)

REFERENCES

1. Thrall, J. H., Gyves, J. W., Ziessman, H. A., et al. Hepatic arterial chemotherapy: pharmacokinetic rationale and radionuclide perfusion imaging. Nucl. Med. Annual 1984. 211-226.
2. Kolibash, A. J., Tetelman, M. R., Olsen, J. O., et al. Intracoronary radiolabeled particulate imaging. Sem. Nucl. Med. 10. 178-186, 1980.
3. Siegel, M. E., and Stewart, C. A. The role of nuclear medicine in evaluating peripheral vascular disease. Nucl. Med. Annual 1984. 227-271.
4. Etani, H., Kimura, K., Iwata, Y., et al. Internal carotid occlusion: assessment, by Tc-99m-tagged microspheres, of bypass from superficial temporal to middle cerebrsi artery. J. Nucl. Med. 22. 856-860, 1981.
5. Lavender, J. P., Maseri, A., Davies, G. J., et al. The distribution of cardiac output in man recorded by intraventricular injection of microspheres. J. Nucl. Med. 22. P30, 1981.
6. Kaplan, W. D., D'Orsi, C. J., Ensminger, W. D., et al. Radionuclide angiography to predict patient response to hepatic artery chemotherapy. Cancer Treatment Reports 64. 217-1222, 1980.
7. Bledin, A. G., Kantarjian, H. M., Kim, E. E., et al. Tc-99m-labeled macroaggregated albumin in intrahepatic arterial chemotherapy. Am. J. Roentg. 139. 711-715, 1982.
8. Yang, P. J., Thrall, J. H., Ensminger, W. D., et al. Perfusion scintigraphy (Tc-99m MAA) during surgery for placement of chemotherapy catheter in hepatic artery: concise communication. J. Nucl. Med. 23. 1066-1069, 1982.
9. Ziessman, H. A., Wahl, R. L., Juni, J. E., et al. The utility of SPECT for Tc-99m MAA hepatic arterial perfusion scintigraphy. Amer. J. Roentg. 145. 747-751, 1985.
10. Kantarjian, H. M., Bledin, A. G., Kim, E. E., et al. Arterial perfusion with Tc-99m macroaggregated albumin (MAAAP) in monitoring intra-arterial chemotherapy of sarcomas. J. Nucl. Med. 24. 297-301, 1983.
11. Kaplan, W. D., Come, S. E., Takvorian, R. W., et al. Pulmonary uptake of technetium-99m macroaggregated albumin: a predictor of gastrointestinal toxicity

- during hepatic artery perfusion. J. Clin. Oncol. 2. 1266-1269, 1984.
12. Plauche, W. E., Foreman, J. B., and Carter, R. D. Comparison of Tc-99m MAA and Tc-99m HAM as intra-arterial perfusion scanning agents in patients receiving infusion chemotherapy. J. Nucl. Med. 23. P97, 1982.
13. Ellett, W. H., and Humes, R. H. Absorbed fractions for small volumes containing photon-emitting radioactivity. MIRD Pamphlet No. 8. J. Nucl. Med. 12, Suppl. No. 5, 1971.
14. Snyder, W. S., Ford, M. R., Warner, G. G., et al. "S," absorbed dose per unit cumulated activity for selected radionuclides and organs. MIRD Pamphlet No. 11. Society of Nuclear Medicine, 1975.
15. Dillman, L. T., and Von der Lage, F. C. Radionuclide decay schemes and nuclear parameters for use in radiation-dose estimation. MIRD Pamphlet No. 10. Society of Nuclear Medicine, 1975.
16. Kirk, G. A., Adams, R., Jansen, C., et al. Particulate myocardial perfusion scintigraphy: its clinical usefulness in evaluation of coronary artery disease. Sem. Nucl. Med. 7. 67-84, 1977.
17. Coffey, J. L., Cristy, M., and Warner, G. G. Specific absorbed fractions for photon sources uniformly distributed in the heart chambers and heart wall of a heterogeneous phantom. MIRD Pamphlet No. 13. J. Nucl. Med. 22. 65-71, 1981.
18. Siegel, M. E., and Wagner, H. N., Jr. Radioactive tracers in peripheral vascular disease. Sem. Nucl. Med. 6. 253-278, 1976.
19. Siegel, M. E., Giargiana, F. A., Jr., White, R. I., Jr., et al. Peripheral vascular perfusion scanning. Correlation with the arteriogram and clinical assessment in the patient with peripheral vascular disease. Am J. Roentg. 125. 628-633, 1975.
20. Siegel, M. E., Williams, M., Giargiana, F. A., et al. A useful, objective criterion for determining the healing potential of an ischemic ulcer. J. Nucl. Med. 16. 993-995, 1975.
21. Mullinix, F. M., Burt, R. W., Schauwecker, D. S., et al. Evaluation of leg perfusion with Tl-201, Tc-99m microspheres, and angiography. J. Nucl. Med. 23. P27, 1982.
22. Kennedy, J. C., Swanson, L., Taplin, G. V. Assessment of the cerebral microcirculation (basic and clinical studies). J. Nucl. Med. 8. 267, 1967.
23. Verhas, M., Schoutens, A., Demol, O., et al. Use of Tc-99m-labeled albumin microspheres in cerebral vascular disease. J. Nucl. Med. 17. 170-174, 1976.
24. Murphy, E. S., Cervantes, C. R., Maass, R. E. Radicalbumin macroaggregate brain scanning. A histopathologic investigation. Am. J. Roentg. 102. 88-92, 1968.
25. Brownell, G. L., Ellett, W. H., and Reddy, A. R. Absorbed fractions for photon dosimetry. MIRD Pamphlet No. 3. J. Nucl. Med. Suppl. No. 1. 1968.

THE FDA'S REQUIREMENTS FOR RADIATION DOSIMETRY OF
RADIOPHARMACEUTICAL DRUG PRODUCTS.

N.M. Abel, Reviewing Pharmacist
Division of Oncology and Radiopharmaceutical Drug Products
Office of Drug Research and Review
Center for Drugs and Biologics
Food and Drug Administration
Rockville, MD. 20857

ABSTRACT

The primary concern of the Office of Drug Research and Review of the Food and Drug Administration in the field of radiation dosimetry is to ensure that radiopharmaceutical drug products are safe when used as investigational drugs (INDs) and are both safe and effective when a new drug application (NDA) is approved. In order to accomplish this, the sponsor of either an IND or applicant in the case of a NDA must provide information that clearly describes the radiation dose that a patient will receive from the administration of the drug. The submitted numerical estimates of the radiation dose should be based on an absorbed fraction method of radiation dose calculation, such as the system set forth by the Medical Internal Radiation Dose (MIRD) Committee of the Society of Nuclear Medicine or the system set forth by the International Commission on Radiological Protection (ICRP).

This presentation will describe in detail the data that a sponsor of an IND needs to submit to satisfy the regulatory requirements. Examples will be given of common mistakes and omissions by sponsors in their presentation of data.

The Food, Drug, and Cosmetic Act as amended by the U.S. Congress in 1938 established a requirement that new drugs (drugs not generally recognized as safe) be demonstrated to be safe and require an approved New Drug Application (NDA) before they can be shipped in interstate commerce (marketed). In 1962, the Act was amended to require that new drugs be demonstrated to be both safe and effective before a New Drug Application could be approved for marketing. Effectiveness must be demonstrated through adequate and well-controlled investigations, including clinical investigations, conducted by experts qualified to conduct such studies. The 1962 Amendments created a legal instrument called the Notice of Claimed Investigational Exemption for a New Drug, commonly referred to as the IND, in order that the drug may be shipped in interstate commerce for the purpose of conducting the required investigations. The IND has another important purpose--it established requirements for protection of human subjects in clinical research from unreasonable and unnecessary risk.

The Food and Drug Administration is concerned with the safety and efficacy of drugs. In the investigative phase of any drug, the primary concern is with the safety of the drug upon its initial introduction into human subjects.

Phase I studies (i.e., those which include the first use of the drug in man) document the safety and establish a dosage range. These first studies should describe the biodistribution of the drug and furnish the initial data for the estimation-in the case of a radiopharmaceutical-of the radiation dose to the subject, including the doses to be expected to localize in the critical organs. Later studies (including Phase II and III) should also document the safety and efficacy in patients. Information such as differences in radiation dosimetry from normals to patients should become apparent in these studies.

Some of the necessary information that is required in order to make an estimate of the radiation absorbed dose to the subject are the drug's physical characteristics and chemical and radiochemical purity. A detailed description of the composition of the drug and its biodistribution in animals (unless by happenstance human data are available) are just two of the many important factors that are utilized in radiation dose calculations.

Let us review some of the more important Food and Drug Administration's requirements regarding INDs. As part of its regulatory function the U.S. Food and Drug Administration recognizes its responsibility in ensuring that safeguards are used in testing drugs. The assurance of the safety and effectiveness of a drug rests in large part on scientific evidence provided by adequate and well controlled studies and other information supplied by responsible investigators. Foreign data, if gathered in the same responsible fashion, may be used. However, this evidence is obtained largely under the provisions of the IND. Some of the principal requirements of the IND are:

1. Complete composition of the drug.
2. Results of all preclinical investigations.
3. Protocol for the planned investigation.
4. Qualifications of investigators.
5. Notification of adverse reactions.
6. Annual progress reports.
7. Protection of the human subject
 - a. By Institutional Review Board (IRB) & Radiation Safety Committee approval.
 - b. By informed consent.

Of these items the second statement, the results of all preclinical investigations, is the most relevant to the field of radiation dosimetry for a radiopharmaceutical drug product which is intended to be used as a diagnostic imaging agent. Up to this time it has been rare for radiopharmaceutical drug products to exhibit any toxicity other than that produced by the radiation hazard. However, in the case of some of the newer materials being investigated, this may not always be the case.

Most radiopharmaceutical drug products are diagnostic agents and thus used only once or with extremely limited repetition. The preclinical toxicology and pharmacology requirements should be, and are, considerably less stringent than for drugs which are to be used continually. Therefore the evaluation of the safety of these products is sometimes restricted to the radiation dose alone.

The IND Application Form 1571, Parts #6d and #10a, derive from the Code of Federal Regulations (Title 21 Part 312.1) which says,

If the drug is a radioactive drug, sufficient data must be available from animal studies or previous human studies to allow a reasonable calculation of radiation absorbed dose upon administration to a human being

and later on,

If the drug is a radioactive drug, the clinical pharmacology stage (Phase I, II studies) must include studies which will obtain sufficient data for dosimetry calculations. These studies should evaluate the excretion, whole-body retention and organ distribution of the radioactive material.

Therefore, to satisfy this requirement, the sponsor should submit all information available to him derived from preclinical investigations and any clinical studies and experience and propose a study in which the necessary information regarding human distribution can be gathered.

Personnel at the Food and Drug Administration responsible for reviewing and commenting on the adequacy of this data have interpreted the regulation as requiring the sponsor to provide the following in order to determine whether the absorbed dose is correct and that the sponsor and the investigator(s) realize the possible risk from the radiation exposure.

- (a) All radioactive material included in the drug either as essential material or as a significant contaminant or impurity shall be included when determining the total radiation dose and dose commitments. If the labeled product is not one hundred percent bound to the ligand thru the life of the product, then the percentage of free isotope (at least at the time of labeling and at the expiry of the coupled product) should be determined and that percentage of free isotope noted.
- (b) The numerical definition of dose should be based on an absorbed fraction method of radiation absorbed dose calculation, such as the system set forth by the Medical Internal Radiation Committee (MIRD) of the Society of Nuclear Medicine, or the system set forth by the International Commission on Radiological Protection (ICRP). The method utilized by the sponsor should be the one which provides the highest estimate of the absorbed dose.
- (c) The equations used in such calculations should be given in full, with numerical substitutions. Any assumptions made in order to use these calculations should be stated clearly and fully documented. These calculations concern biodistribution and effective half-lives and must be based upon the highest dose to be administered. If certain physiological conditions, e.g., thyroid accumulation, urinary bladder emptying, intestinal obstruction, and gall bladder absence, change the absorbed dose, a worst case calculation should be made and presented. In actuality, the worst case situation should always be assumed. If measures, such as blocking the thyroid, are to be taken to overcome some of these conditions, absorbed doses in both instances should be presented. The calculations should be for the highest possible amount of radioactive drug to be administered, e.g., if the dosage schedule includes a range, the upper limit of that range is the one to utilize. The calculations should be at the time of expiry (TOE) in most cases in order to provide for the upper limit of radioactive contaminants. This includes the free isotope as mentioned in part a and its absorbed dose based upon the

biodistribution of the free isotope. In general, these are a help to both the FDA reviewer and the investigator (1) by assuring us that the doses to be given represent safety and (2) by assuring us that the investigator is aware of the radiation hazards in his use of the drug.

- (d) Radiation doses from other procedures such as x-ray procedures, CT and other administered radiopharmaceuticals that are part of the research study (i.e., which would not have occurred but for the study) should be included. If there is a possibliliy of follow up studies, this should be considered for inclusion in the dose calculations.

The final estimate should be a table outlining the absorbed dose to the organs of interest and total body from the principal isotope, radioactive contaminants, other isotopes utilized in the study and include absorbed doses from other imaging modalities.

Returning to the necessary preclinical (animal) biodistribution (in the event that there are no human studies available to the sponsor from which to provide distribution data), studies are required to determine the biological distribution, translocation, and the route and extent of excretion of the product. This information is essential for meaningful dosimetry calculations. Dosimetry calculations on animal data should be determined prior to initiating human studies. The organ distribution studies should be carried out in an appropriate species, not one which does not accurately predict human biodistribution. In general, it is desirable to assay for the concentration of the radiopharmaceutical at selected time intervals in all major organs and tissues so that the organs (tissues) receiving the highest radiation absorbed doses can be identified. With a diagnostic radiopharmaceutical employed for imaging purposes, the organ (tissue) receiving the highest radiation absorbed dose is often, but not always, the same as the organ (tissue) of primary interest which is to be imaged.

In phase I studies involving a diagnostic radiopharmaceutical, initial studies in man should demonstrate normal biodistribution, the organs receiving the maximum concentration of the radiopharmaceutical, the clearance half-time, the routes of excretion and optimal imaging or sampling times. A small number of normal (Phase I) and diseased subjects (Phase II) is usually sufficient. The latter group is necessary to demonstrate altered distribution due to disease.

Regarding doses to be administered to the subjects, the proposed dose in Phase I or in other later studies should be determined with the following considerations in mind:

- a. The initial proposed dose should be the lowest one that is needed to obtain the desired information. This will insure that the radiation absorbed dose will also be kept as low as possible. Determination of this dose should be based upon other human studies with the isotope, animal biodistribution studies of the radiopharmaceutical in question plus other relevant physical factors.
- b. An adequate number of usable particles or photons should be available to ensure statistically meaningful images or counting results with the instrumentation likely to be employed clinically. Imaging time per view (or sample counting time) must be kept within reasonable limits, e.g., to prevent image degradation due to patient motion.

c. Doses for future studies should be based upon the results from the initial studies and other relevant information.

In phase I studies involving a therapeutic radiopharmaceutical, the study should be primarily designed to obtain biodistribution data in man utilizing tracer quantities of the proposed product. Such studies should initially be performed in normal adult volunteers and then in patients with the disease in which use of the therapeutic radiopharmaceutical is intended. The purpose of these studies is to permit projection of absorbed radiation dose to the intended target organ(s) or tissue(s) and to critical organ(s) or tissue(s) at therapeutic doses. Such studies should include blood clearance data, excretion data, organ distribution data (from external imaging and quantitation or from limited biopsy sampling). Evaluation of bone marrow distribution may be particularly important since the radiation dose to the marrow may be the limiting toxicity.

With regard to therapeutic doses, after the performance of the tracer biodistribution studies and calculation of projected therapeutic radiation doses, studies to determine the proper therapeutic dose should be undertaken (assuming that the therapeutic ratio is not unacceptably low). A reasonable starting dose might be at the lower limit of the calculated dose range expected to produce a therapeutic response and one that is within tolerable limits for normal tissues. The drug dosage may be reasonably increased thereafter until a dose (or dose range) is found which produces the desired therapeutic effect without inducing disabling toxicity.

If the radiopharmaceutical is used to treat a neoplastic disease, the therapeutic schedules should include maximally tolerated doses for a period of time sufficient to allow recognizable neoplastic regression (i.e., as compared with the natural progression of the neoplasm which would be expected in the absence of effective therapy).

Some of the other factors with which the dosimetry evaluation is often concerned with include items such as the source of an isotope. The approved radiopharmaceuticals are for specific isotopes attached to a specific ligand or in specific solution or capsule. Many isotopes have radioactive contaminants. The approved products have specifications as to limits of these radioactive contaminants. Both the type of contaminants and the percentage of the contaminants can and will vary from supplier to supplier depending on the method of production of the isotope and the time of expiry of the product.

Often the sponsor of an IND makes references to a Drug Master File that the supplier has filed with the Food and Drug Administration. There are no approved Drug Master Files (DMFs). DMFs may not directly relate to the quality of the product though often they do provide manufacturing criteria for that product. The sponsor of every IND should clearly identify his specifications for the isotope throughout its life and determine whether the product to be utilized will meet those specifications.

The stability of the labeled product should also be determined throughout the possible life of the product. It is quite conceivable that the percentage of free isotope can increase during the product's shelf life. Adequate testing should be carried out (both *in vitro* and *vivo*) and limits of free isotope should be set.

With respect to approved drugs, the Food and Drug Administration approves the labeling of both diagnostic and therapeutic radioactive drug products which includes directions to the physician for proper use of the product. Such labeling includes a recommended amount (expressed in both the International System and the older system known as the centimeter-gram-second system) or range of doses for those indications for which the radiopharmaceutical has been shown to be safe and effective.

As with non-radioactive drugs, the Food and Drug Administration continues to follow experience in use of the drug after marketing. If circumstances show that doses (either the prescribed dose or the radiation absorbed dose) originally approved should be changed (up or down) as a result of clinical experience or the introduction of more sophisticated measurement instrumentation, the official labeling may be modified. Similarly, if newer radiopharmaceutical drug products are introduced which show improvement over existing products in terms of greater diagnostic or therapeutic effectiveness at the same radiation absorbed dose or equal effectiveness at lesser doses, the Food and Drug Administration may initiate action to withdraw approval of the product or certain indications for that product on the basis of relative safety.

A few of the more common errors or omissions in IND submissions regarding the dosimetry calculation include the following:

- a. Not listing all of the contaminants of the product.
- b. Not accounting for a 100% distribution in the preclinical studies.
- c. Not utilizing the worst case situation.
- d. Using methods of calculating dosimetry which lead to a lower radiation dose estimate.
- e. Listing the radiation dose in rads per μ Ci instead of rads per dose that will be administered to the subject.
- f. Not listing assumptions utilized in the calculations.
- g. Listing activity per unit in a variety of ways, i.e., per gram of organ, per gram of body weight, per gram with no explanation, per gram of the organ in relationship to body weight, per anything without a step by step explanation of how this per unit of activity was selected.

The problem that is most disconcerting is that the sponsor does not adequately explain his method, assumptions and calculations so that the reviewer can follow his logic. It is almost impossible on our part to make such assumptions for the sponsor. Therefore, in many cases where a reviewer can not follow the logic or pathway of reasoning used by the sponsor, the result may be that the start of a study will be delayed or that the study will be stopped until further explanation is received from the sponsor.

In conclusion, radiation absorbed doses from radioactive drug products are thoroughly and carefully evaluated by the Food and Drug Administration in the determination of the safety of the product prior to the start of the clinical study.

DISCUSSION

HARPER: Please comment on FDA jurisdiction in cases where radiopharmaceuticals are manufactured and used completely within an institution. Is an IND required in such cases?

ABEL: If an approved product is to be manufactured in the hospital and used completely within the institution, no IND is required. If the product is an

investigational drug, it would depend on whether it is a labeled antibody (if the isotope is obtained out of state or not) or a labeled drug. The researcher should call or write the FDA to ascertain if an IND is necessary when using an unapproved or unlicensed product.

MITCHELL: Mr. Abel, you mentioned that risk estimates are made at the FDA on the basis of dosimetry provided by the investigators. Could you tell us the source of dose-effect data on which your risk projections are made? Do you use the NIH probability of causation tables? We know that genetic and carcinogenic effects of radiation are not additive but may be recovered from. Do you take into consideration that radionuclides produce radiation over a long period of time and that the total dose is less effective than the same dose given over a short period of time, such as in x-ray or atomic weapon exposure?

ABEL: (a) We do not base our safety review (i.e., risk estimate) on probability tables or dose-effect data. Our decisions are made upon the possible benefits of a study with respect to the risks involved. That includes not only the risks from radiation exposure but other parameters. It is very difficult to list all the factors involved in a decision; however, the decision is much like a clinical one when the physician makes a decision to perform a procedure.

(b) The possible effect from a certain amount of radioactive exposure is taken into account when ascertaining the risk/benefit for a particular population in a study. The time frame over which the radiation is delivered is certainly a factor we take into account.

DOSIMETRY CONSIDERATIONS IN PATIENTS WITH
RENAL PATHOLOGY

Carol S. Marcus and Martin A. Koyle
Divisions of Nuclear Medicine
and Urology
Harbor-UCLA Medical Center
1000 West Carson Street
Torrance, CA 90509

ABSTRACT

Adult dosimetry is generally performed for normal individuals and these are the absorbed dose calculations sent to FDA and listed on package inserts. However in a variety of circumstances pathophysiologic state may significantly alter the biodistribution and kinetics of a radiopharmaceutical, and radiation doses calculated for normal individuals may not be appropriate approximations for these patients. Examples of disease states that merit consideration include kidney abnormalities such as acute tubular necrosis (ATN) and various degrees of obstruction.

In addition, the presence of certain pathophysiologic states often guarantees that the patient will have multiple studies over a period of days, weeks, months, or years. In order to have a true appreciation for the radiation dose commitment to such patients, it is important to examine dose totals from multiple nuclear medicine studies. Examples of renal disease states that commonly involve "polyradiopharmacy" include ureteral obstruction, progressive renal insufficiency, and kidney transplantation.

Dosimetry calculations will be presented for I-123, I-124, I-125, and I-131 labeled hippuran in moderate and severe ATN, acute and chronic near-total obstruction, and renal transplants. In addition, a nuclear medicine examination profile will be presented for patients receiving renal transplants at Harbor-UCLA Medical Center from January, 1985 through May, 1985. This profile was constructed by retrospectively examining the records of 20 randomly-chosen transplant patients and recording all nuclear medicine procedures performed up to July, 1985. A total of 172 studies was performed, of which 69 were Tc-99m-DTPA flows, 62 were hippurans, and 22 were indium-111-oxine-platelets. The dosimetric contribution of all studies was assessed. The importance of the hippuran component will be discussed.

INTRODUCTION

The absorbed dose commitment to patients undergoing renal nuclear medicine studies may vary by several orders of magnitude. The factors that cause such variability of dose include the type and activity of radiopharmaceutical administered, whether the patient is an adult or a child, the underlying renal pathophysiology, and whether the disease category itself commits the patient to multiple nuclear medicine procedures.

The nuclear medicine physician is responsible for the administration of radiopharmaceuticals, and should be aware of the approximate absorbed dose involved in each procedure. In practice, this goal is often not attained. The commonest source of dosimetry information is the package insert, and this usually contains dosimetry for normal adults only. In the case of renal procedures, this is often insufficient for clinical purposes. In addition, the recent availability of I-123-orthiodohippurate (OIH) for renal function and imaging studies has given the nuclear medicine physician an alternative to I-131-OIH. The advertisement for I-123-OIH which has been appearing in the Journal of Nuclear Medicine from April, 1985 to this writing (Oct., 1985) contains a flow and function study in a renal transplant patient, and states that the radiopharmaceutical is "particularly useful in obstructed patients". On the basis of our dosimetry calculations and clinical experience with I-123-OIH, we have concluded that this compound should not be used for flow studies, has limited use in transplant patients, should not be used in obstructed patients, and the administered activity should be half that suggested by the manufacturer. Clearly there is a discrepancy here, and we are presenting our dosimetry so that practitioners of nuclear medicine may make an informed choice of radiopharmaceutical in a particular clinical setting.

In addition to the dosimetry calculations for individual procedures, we have addressed a problem that has largely been ignored in nuclear medicine, and that is the absorbed dose commitment to patients who are virtually guaranteed multiple nuclear medicine procedures because of their particular disease state. We have chosen to make these calculations for renal transplant patients at our institution. Although such absorbed dose profiles will probably differ significantly between institutions, we believe that our general conclusions will be widely applicable.

MATERIALS AND METHODS

I-123-OIH PREPARATIONS

The I-123-OIH used at our institution was prepared in house using I-123 obtained exclusively from Crocker Laboratories at the University of California at Davis. The I-123 was made using the reaction: I-127 ($p,5n$) Xe-123 (which decayed with a 2 hr. half-life to I-123). This product contained no contaminant I-124. It did contain I-125, which at time of expiration (T.O.E.) reached a maximum level of 1.4% (1). This value was used for our dosimetry.

The I-123-OIH which is commercially available (NephroflowTM, Medi + Physics, Inc.) utilizes I-123 made by the reaction: Te-124 ($p,2n$) I-123. This product contains I-124 as its most important contaminant. According to the

package insert, the maximum I-124 level at time of calibration (T.O.C.) is 4.8% and at T.O.E. is 12.9%. We used a value of 10% for our dosimetry calculations.

I-123-OIH ADMINISTRATION AND IMAGING PROCEDURES

Over a 10-month period we administered our in-house preparation of I-123-OIH to 126 patients. Nine patients were children aged 1.4 mos. to 4 yrs. weighing 3.2-18 kg. Activity administered was 100-600 μ Ci. Of the adult patients, about half were renal transplant recipients. Activity administered was mainly 500 μ Ci, although a few patients early in our series received activities up to 5 mCi.

Images were acquired on a gamma camera and were subsequently processed by minicomputer. This resulted in flow images at 10 sec. intervals for 60 sec. following intravenous bolus administration of the radiopharmaceutical, followed by 1 min. images for 20 min. and renogram curves. One 300,000 count image was obtained at the termination of the study.

TC-99M-DTPA STUDIES

Adult Tc-99m-DTPA flow and function studies were performed using 15 mCi administered activity and the same imaging protocol as described for I-123-OIH.

IN-111-OXINE-PLATELET STUDIES

After appropriate signed consent was obtained, 500 μ Ci autologous labeled platelets were administered intravenously and images of the chest, abdomen, and pelvis were obtained at 24 hrs. A few patients had images performed at 48 or 72 hrs. These studies were performed in transplant patients initially to assess rejection, but later were used to assess rejection or cyclosporin A toxicity. The dosimetry for this procedure included the contaminant In-114m/In-114 found in the Amersham In-111-oxine product (2).

OTHER NUCLEAR MEDICINE PROCEDURES

A small number of a variety of other standard nuclear medicine procedures was performed in our transplant patients. These include I-131-OIH (600 μ Ci per administration), Tc-99m-RBC's (20 mCi), Tc-99m-DMSA (4 mCi), Tl-201(3 mCi), Ga-67 (5 mCi), In-111-oxine-WBC's (500 μ Ci), Tc-99m-MAA (2 mCi), Tc-99m-HIDA (2 mCi), and Tc-99m-MDP (25 mCi).

MIRD DOSIMETRY

All dosimetry was performed using MIRD "S" tables (3) or published sources based on this methodology (4-7). Unpublished pediatric "S" values for I-123, I-124, I-125, and I-131 were kindly supplied by Michael Stabin of the Radio-pharmaceutical Internal Dose Information Center, ORAU.

Biodistribution and kinetic models are discussed in detail in (8). Briefly, our model for moderate acute tubular necrosis (ATN) was taken from Elliot and Britton (6) who assumed a renal transit time of 4 hrs. For severe ATN (as occurs frequently in transplants), we assumed 100% uptake and $T_B = T_p$ where T_B is biological half-time and T_p is physical half-life.

For acute, near-total obstruction with 50% uptake in the obstructed kidney we assumed $T_B=T_p$ in the affected kidney. For chronic, near-total obstruction with 5% uptake in the obstructed kidney we again assumed $T_B=T_p$ in the affected kidney. All assumptions are conservative, and actual clinical cases often fall between these idealized categories.

RENAL TRANSPLANT PATIENT ABSORBED DOSE PROFILES

This study was entirely retrospective to avoid any bias in performing imaging procedures. Twenty renal transplant patients were chosen at random, and their nuclear medicine and clinical records were intensively reviewed. All patients had received transplants between Jan., 1985 and May, 1985, and nuclear medicine studies were included up to July, 1985. Renal pathology was assessed in each patient in order to appropriately estimate hippuran dosimetry. No patients had a normally functioning transplant at the time of hippuran imaging.

RESULTS

I-123-OIH ADMINISTERED ACTIVITY

We attempted to obtain renal flow images in addition to function studies in adult patients early in our series. The minimum practical administered activity (MPAA) for a passable quality flow study was found to be about 3 mCi of I-123-OIH. As many of the patients in whom we wished to perform renal flow studies had some degree of ATN, we decided that the absorbed dose was too high and continued to perform flow studies with Tc-99m-DTPA. The MPAA for a renal function study with good renal images was found to be about 500 μ Ci; this was found earlier by Elliot and Britton (6). The MPAA for pediatric studies was found to be about 200 μ Ci. Pediatric doses were scaled down using a nomogram based on the 3/2 power of body weight (5).

OIH DOSIMETRY

The absorbed dose per procedure in adults with various states of renal function is seen in Table 1. Doses are for pure I-123-OIH, I-123-OIH with 1.4% I-125-OIH, I-123-OIH with 10% I-124-OIH, and I-131-OIH. Note that absorbed doses from I-123-OIH and I-123-OIH with 1.4% I-125-OIH are easily justifiable regardless of pathology, whereas doses from I-123-OIH + 10% I-124-OIH are into the "double digit" rad range for acute obstruction and transplant with severe ATN. These doses are all based on 500 μ Ci administered activity, and not the 1 mCi activity recommended by the commercial manufacturer. The comparative absorbed doses for I-131-hippuran were also calculated assuming a 500 μ Ci administered activity. Note that these doses are considerably higher, and that in cases of acute obstruction and transplant with severe ATN, the doses are prohibitively high.

In cases of renal obstruction, we calculated absorbed dose to the affected kidney assuming no resolution of the obstruction and assuming resolution in one week (e.g. by passing a stone, surgical intervention, or percutaneous nephrostomy). Resolution makes a difference in the dosimetry of I-124-OIH, I-125-OIH, and I-131-OIH because of the relatively long effective half-lives of these radiopharmaceuticals. The dosimetry of I-123-OIH is not affected because all the absorbed dose is delivered in less than a week.

Table 1. Comparison of Absorbed Dose from the Different OIH Radiopharmaceuticals

<u>Renal Pathology</u>	<u>Adult Absorbed Dose, Rad/Procedure</u>			
	<u>500 µCi pure I-123-OIH</u>	<u>500 µCi I-123-OIH +1.4% I-125-OIH</u>	<u>500 µCi I-123-OIH +10% I-124-OIH</u>	<u>500 µCi I-131-OIH</u>
Normal kidneys	0.035	0.035	0.055	0.50
Moderate ATN	0.56	0.57	0.97	3.0
Near-total obstruction with 50% uptake in obstructed kidney; no resolution	3.2	6.8	18	210
Near-total obstruction with 50% uptake in obstructed kidney; resolution in 1 week	3.2	3.5	9.8	79
Near-total obstruction with 5% uptake in obstructed kidney; no resolution	0.32	0.68	1.8	21
Near-total obstruction with 5% uptake in obstructed kidney; resolution in 1 week	0.32	0.35	0.98	7.9
Transplant with severe ATN; no recovery	6.4	14	37	420
Transplant with severe ATN; recovery in 3 weeks	6.4	7.8	30	270

In Tables 2a and 2b we list the absorbed doses to children from pure I-123-OIH and I-123-OIH with 10% I-124-OIH contamination. Because of the MPAA of 200 μ Ci, these doses can occasionally be quite high, especially in acute obstruction and severe ATN.

NUCLEAR MEDICINE PROCEDURE PROFILES IN RENAL TRANSPLANT PATIENTS

The breakdown of nuclear medicine procedures in our renal transplant patients is seen in Table 3. A total of 172 studies was performed, of which 69 were Tc-99m-DTPA renal flows, 53 were I-123-OIH function studies, 9 were I-131-OIH function studies, and 22 were In-111-oxine platelets for assessing rejection or cyclosporin A toxicity.

The distribution of renal pathology seen with OIH imaging in our 20 transplant patients is seen in Table 4. Note that the predominant condition is severe ATN post transplant (39 cases), and that none of the 62 OIH studies was performed on patients with transplants showing normal renal function. This is because normal function is usually assessed by serum creatinine and urine output, and nuclear medicine studies are not ordered on patients with normally functioning transplants in our institution. In fact, 80% of the transplants in these patients eventually showed normal or near-normal function. Of the 4 that failed to function, 2 demonstrated primary non-function and 2 were rejected despite medical therapy.

The total body and kidney dosimetry for the average renal transplant patient, the average uncomplicated renal transplant patient, the average moderately complicated renal transplant patient, and the average complicated renal transplant patient is presented in Tables 5, 6, 7, and 8, respectively. Because I-131-OIH made a relatively large contribution to kidney absorbed dose, and because it was no longer used after I-123-OIH became available in our laboratory, dosimetry was calculated with and without the I-131-OIH contribution. Note also that all our I-123-OIH was free of I-124-OIH. Had commercial I-123-OIH been used, at the 1 mCi recommended administered activity, kidney absorbed dose per OIH study in patients with severe ATN and recovery in 3 weeks would have been 7.7 times higher than it was in our series. This is an important consideration, because 63% of our OIH studies were performed in patients with severe ATN.

In comparison to OIH absorbed doses, the contribution of Tc-99m-DTPA to whole body and renal absorbed dose is very low. In cases of severe ATN with no excretion of Tc-99m-DTPA, total body or kidney dose from 15 mCi of Tc-99m-DTPA is only about 260 mrad.

DISCUSSION AND CONCLUSION

Dosimetry considerations in patients with renal pathology essentially center around the dose contribution of OIH. Other radiopharmaceuticals contribute relatively little to absorbed dose, regardless of underlying pathology, and present no need for concern.

In patients with severe ATN or acute obstruction with a high degree of uptake in the affected kidney, I-131-OIH should probably not be used at all, especially in small children. I-123-OIH contaminated with significant levels of I-124-OIH should probably not be used, either. It certainly should not be used in activities sufficient for flow studies. In these patients, a large amount of information may be obtained with a Tc-99m-DTPA study, and usually this information is sufficient for the clinician to make a diagnostic or therapeutic decision.

Table 2a. Comparison of Pediatric Absorbed Dose for Pure I-123-OIH and I-123-OIH Contaminated with 10% I-124-OIH

<u>Renal Pathology</u>	<u>Newborn; Rad/Procedure</u>	<u>1 Yr; Rad/Procedure</u>		<u>5 Yr; Rad/Procedure</u>		
	200 µCi pure I-123-OIH	200 µCi I-123- OIH +10% I-124- OIH	200 µCi pure I-123-OIH	200 µCi I-123- OIH +10% I-124- OIH	215 µCi pure I-123-OIH	215 µCi I-123- OIH +10% I- 124-OIH
Normal kidneys	0.14	0.22	0.046	0.078	0.039	0.059
Moderate ATN	2.8	4.4	0.84	1.5	0.56	0.96
Near-total obstruction with 50% uptake in ob- structed kidney; no resolution	16	79	4.8	29	3.2	18
Near-total obstruction with 5% uptake in ob- structed kidney; no resolution	1.6	7.9	0.48	2.9	0.32	1.8
1 kidney, severe ATN: no resolution	31	160	9.6	58	6.3	36

Table 2b. Comparison of Pediatric Absorbed Dose for Pure I-123-OIH and I-123-OIH Contaminated with 10% I-124-OIH

Renal Pathology	<u>10 Yr; Rad/Procedure</u>		<u>15 Yr; Rad/Procedure</u>		<u>18 Yr; Rad/Procedure</u>	
	300 µCi pure I-123-OIH	300 µCi I-123- OIH +10% I-124- OIH	435 µCi pure I-123-OIH	435 µCi I-123- OIH +10% I-124- OIH	500 µCi pure I-123-OIH	500 µCi I-123- OIH +10% I- 124-OIH
Normal kidneys	0.039	0.058	0.044	0.063	0.035	0.055
Moderate ATN	0.56	0.94	0.82	1.2	0.56	0.97
Near-total obstruction with 50% uptake in ob- structed kidney; no resolution	3.2	17	3.4	18	3.2	18
Near-total obstruction with 5% uptake in ob- structed kidney; no resolution	0.32	1.7	0.34	1.8	0.32	1.8
1 kidney, severe ATN, no resolution	6.4	35	6.8	36	6.4	37

Table 3. A Survey of Nuclear Medicine Procedures Performed in 20 Renal Transplant Patients

	$\bar{x} \pm s_x$	Range	Median	n
Average no. of procedures per pt.	8.6±6.0	4-25	5	20
Average no. of procedures per 2-transplant pt.	21±4.0	17-25	21	3
Average no. of procedures per transplant	7.5±3.7	4-16	5	23
Average no. of OIH procedures per pt. (I-131-OIH + I-123-OIH)	3.1±2.9	1-12	2	20
Average no. of mCi I-123-OIH per pt.	1.3±0.89	0.5-3	1	20
Average no. of mCi I-131-OIH per pt.	0.27±0.84	0-3.6	0	20
Average no. of mCi Tc-99m per pt. (mainly DTPA)	63±52	0-180	48	20
Average no. of mCi In-111-oxine per pt. (mainly platelets)	0.52±0.22	0.22-1.2	0.5	20
Average no. of mCi Tl-201 per pt.	0.60±1.2	0-3	0	20
Average no. of mCi Ga-67 per pt.	0.25±1.1	0-5	0	20

Table 4. Distribution of Renal Pathology Seen with OIH Imaging in 20 Renal Transplant Patients

<u>Renal Pathology</u>	<u>I-123-OIH</u>	<u>I-131-OIH</u>
Very poor function pre-transplant	-	1
No function post-transplant (severe ATN)	39	2
Mild function post-transplant (moderately severe ATN) ¹	7	3
Moderate function post-transplant (mild-moderate ATN)	6	4
Total	53	9 (post-transplant)

¹For dosimetry purposes, patients with mild function and those with moderate function were combined and considered characteristic of moderate ATN.

Table 5. Total-Body and Kidney Dosimetry for the Average Renal Transplant Patient (n = 20)

Radiopharmaceutical	Total mCi Administered per Pt.	Total-Body Absorbed Dose, Rad	Kidney Absorbed Dose, Rad
I-123-OIH ¹	1.3	0.069	22
I-131-OIH ²	0.27	0.19	53
Tc-99m-DTPA ³	63	1.1	1.1
In-111-oxine platelets ⁴	0.52	0.34	0.68
Tl-201 Cl	0.60	0.14	0.14
Ga-67 Citrate	0.25	0.065	0.065
Total absorbed dose per patient:		1.9	77
Total absorbed dose per patient, excluding the 9 I-131-OIH studies:		1.7	24

¹All I-123-OIH and I-131-OIH dosimetry was weighted in terms of pathophysiological state. The I-123 used here was free of I-124. The I-125 contribution was included in the dosimetry.

²Used before I-123-OIH became available.

³A small quantity of Tc-99m was administered in approximately dosimetrically equivalent form, e.g. Tc-99m-NaTcO₄.

⁴This includes a small quantity of In-111-oxine-WBC's. The dosimetry includes the contribution from In-114m/In-114.

Table 6. Total Body and Kidney Dosimetry for the Average Uncomplicated Renal Transplant Patient (n = 14)

<u>Radiopharmaceutical</u>	<u>Total mCi Administered per Pt.</u>	<u>Total-Body Absorbed Dose, Rad</u>	<u>Kidney Absorbed Dose, Rad</u>
I-123-OIH	0.89	0.046	15
I-131-OIH	-	-	-
Tc-99m-DTPA	34	0.59	0.59
In-111-oxine platelets	0.54	0.34	0.68
Tl-201 Cl	0.64	0.15	0.15
Ga-67 Citrate	-	-	-
Total absorbed dose per pt.:		1.1	16

Table 7. Total-Body and Kidney Dosimetry for the Average Moderately Complicated Renal Transplant Patient (n = 3)

<u>Radiopharmaceutical</u>	<u>Total mCi Administered per Pt.</u>	<u>Total-Body Absorbed Dose, Rad</u>	<u>Kidney Absorbed Dose, Rad</u>
I-123-OIH	1.8	0.094	30
I-131-OIH	-	-	-
Tc-99m-DTPA	89	1.5	1.5
In-111-oxine platelets	0.67	0.43	0.86
Tl-201 Cl	1.0	0.24	0.24
Ga-67 Citrate	1.7	0.44	0.44
Total absorbed dose per pt.:		2.7	33

Table 8. Total-Body and Kidney Dosimetry for the Average Complicated Renal Transplant Patient (n = 3)¹

<u>Radiopharmaceutical</u>	<u>Total mCi Administered per Pt.</u>	<u>Total-Body Absorbed Dose, Rad</u>	<u>Kidney Absorbed Dose, Rad²</u>
I-123-OIH	2.8	0.14	46
I-131-OIH	1.8	1.3	350
Tc-99m-DTPA	160	2.8	2.8
In-111-oxine platelets	0.84	0.54	1.1
Tl-201 Cl	-	-	-
Ga-67 Citrate	1.7	0.44	0.44
Total absorbed dose per pt.:		5.2	400
Total absorbed dose per pt., excluding the 9 I-131-OIH studies:		3.9	50

¹Each received a second transplant

²Absorbed dose divided between each of the 2 kidney transplants per patient.

In renal transplant patients, most of whom have some degree of ATN post transplant, often severe ATN, one may justify a single I-123-OIH study, free of I-124-OIH, to document areas of transplant infarction and necrosis. Tc-99m-DTPA is the radiopharmaceutical of choice for studying renal flow. As filtration function recovers before secretory function in these patients, Tc-99m-DTPA is also the radiopharmaceutical of choice for early evaluation of obstruction and ureteral leaks.

The use of nuclear medicine procedures in patients whose underlying pathology predicts the occurrence of multiple studies, such as the transplant patients depicted here, deserves careful consideration. Procedures should be evaluated in terms of the integrated expected renal absorbed dose from multiple studies, not only on a single procedure basis.

This whole issue of OIH dosimetry will hopefully disappear with the availability of Tc-99m compounds which are secreted by the kidney. This is really the best solution to the problem, and one which we hope will soon be accomplished.

ACKNOWLEDGEMENTS

The authors wish to thank the following individuals for their contributions to this project:

Mr. Michael Stabin of the Radiopharmaceutical Internal Dose Information Center, ORAU, for his help in obtaining and interpreting certain of the pediatric "S" values;

Mr. John Kuperus for synthesis of and information pertaining to I-123-OIH;

Mr. Arnold Go and Mr. Arnulfo Pleyto for technical assistance in imaging and data processing;

Miss Pat Twomey for clinical records and patient follow-up;

Drs. Ismael Mena and Jacob Rajfer for constructive suggestions;

Mrs. Dorothy Tamura for secretarial services;

Mr. Neil Abel of the F.D.A. for prompting us to initiate portions of this study.

REFERENCES

1. Personal communication with Dr. Manuel Lagunas-Solar, Crocker Laboratories, University of California at Davis, June, 1985.
2. Marcus, C.S., M.G. Stabin, E.E. Watson, and J.H. Kuperus: Contribution of contaminant indium-114m/indium-114 to indium-111-oxine blood dosimetry. *J. Nucl. Med.* 26, 1091-1093, 1985.
3. NM/MIRD Pamphlet no. 11: "S", Absorbed Dose per Unit Cumulated Activity for Selected Radionuclides and Organs, SNM, New York, 1975.
4. NCRP Report no. 70: Nuclear Medicine-Factors Influencing the Choice and Use of Radionuclides in Diagnosis and Therapy, NCRP, Bethesda, MD, 1982, Appendix B.
5. NCRP Report no. 73: Protection in Nuclear Medicine and Ultrasound Diagnostic Procedures in Children, NCRP, Bethesda, MD, 1983, pp 7-14 and 46-50.

6. Elliott, A.T. and K.E. Britton: A review of the physiological parameters in the dosimetry of I-123 and I-131 labelled hippuran. Int. J. Appl. Radiat. Iso. 29, 571-573, 1978.
7. Kaul, A., K. Oeff, H.D. Roedler, et al.: Radiopharmaceuticals-Biokinetic Data and Results of Radiation Dose Calculations. Informationsdienst für Nuklearmedizin, Berlin, 1973, p. 193.
8. Marcus, C.S., and J.H. Kuperus: Pediatric renal I-123-orthoiodohippurate dosimetry. J. Nucl. Med. 26, 1211-1214, 1985.

DISCUSSION

MARCUSE: If a renal transplant is successful and the child returns to normal life expectancy, do you have any idea of the implications of doses of several hundreds of rads in the kidneys? What effect on kidney function might be expected in 10-20 years?

MARCUS: That's a good question, Dr. Marcuse. I have no idea. I know that the bad effects of cyclosporin A probably outweigh anything I am doing to them with radiation. That stuff is really toxic. Most of the time data on genitourinary tumors include bladder. In the case of severe ATN, the hippuran doesn't go to the bladder. The patient is getting a kidney dose without a bladder dose. I suppose we would readily see any huge incidence of renal cell carcinoma because it's not such a common tumor, but I really don't know what to expect. It's only been relatively recently that we could keep these renal transplants going pretty well and I really doubt that many of these are going to live out a natural life span with no problems. But I can't answer what to expect from several hundred rads. I have told our urologist, that in the old days he irradiated kidneys before he transplanted them to stop graft-vs.-host reaction and today he doesn't need to because we are doing it for him. This may change now that we are not using I-131 hippuran.

HARPER: Do you have any feeling for the size of the population who have received triple-digit radiation doses to the kidneys?

MARCUS: I don't know how many renal transplants are done in the United States, Dr. Harper. Of the renal transplants that have been done, a lot of them, especially before I-123 hippuran became available, got high doses with I-131 hippuran. Many years ago when renograms were done without much imaging, patients got very small amounts of I-131 hippuran. Later, when people could put the pictures on a computer and do regions of interest, the dose increased. I think in the old days it was a little safer for the patients than it became some years later. After starting my present appointment at a busy county hospital and seeing so many children get hippuran studies that showed congenital UPJ obstruction or something like that, I finally put an end to I-131 hippuran studies in my department. Unless I was on hand to evaluate each one, many were getting unnecessary exposure. I thought it was easier to stop the whole thing than try to educate the whole house staff. If my experience is similar to others, I suppose tens of thousands and maybe more patients than that have gotten high doses because most physicians don't calculate those things. Technetium-99m DTPA gives the patient in total renal failure only about 260 millirad total-body dose and kidney dose. You can tell almost everything you want to know from a DTPA study and that's what I use. Even in the transplant patients, filtration function comes back before secretion and DTPA is the best agent for looking for ureteral kinks or anything else.

S. SRIVASTAVA: In terms of radionuclidic purity, the AECL iodine-123 which is produced by a (p, 2n) reaction on a gaseous Xe-124 target is probably the best. Have you utilized I-123 from this source? The I-123 we produce at Brookhaven, is quite low in I-125 contamination (<0.2% at shipment). As you mentioned, up to 1.5% I-125 contamination doesn't contribute very significantly to the dose to the kidneys. However, this could be further minimized by using I-123 from the above-mentioned sources.

MARCUS: The dose from I-125 is certainly not in the league with I-124. We have been looking into getting the AECL material because of shipping problems. The national labs usually do not follow a rigorous, every single week routine.

MOUNTFORD: What method do you use to calculate the injection activity for pediatric investigations?

MARCUS: In David Gilday's talk yesterday, he showed a table by Webster that he photographed out of NCRP 73, one of the NCRP books that was based on the three-halves power of body weight. It's a very standard way of reducing activity for children, and we use the Webster table for all our pediatric procedures. The only variation is we must decide where to stop. That is, what is our minimum practical administered activity? From our experience we have found if we want to see anything we have to use around 200 microcuries. If you just want a renogram, of course, you can use less; but, if you want to get a picture of the kidneys to look at areas of infarct or necrosis, you need at least a 100, but 200 microcuries is better.

FRITZBERG: I would like to make some comments. First, as one who has spent several years developing a Tc-99m replacement for iodinated hippuran, I must say that I was not aware of the magnitude of the doses to the kidney in diseased states. I don't feel that I am alone in this and would encourage dissemination of these results. Second, a Tc-99m replacement should be available in the near future. Its value appears now to be greater than we have appreciated.

DRUGS THAT ALTER BIODISTRIBUTION AND KINETICS OF RADIOPHARMACEUTICALS

Jashovam Shani

Radiopharmacy Program, School of Pharmacy,
University of Southern California, Los Angeles, CA 90033

ABSTRACT

Target localization and organ biodistribution of radiopharmaceuticals (RPs) may be altered by non-radioactive drugs whose pharmacological mechanisms compete with the RPs for the same retention processes. Originally referred to as "side effects" or "incompatibilities", such interactions became a major concern in evaluating Nuclear Medicine procedures, as they might cause interpretation of the latter to be without value or misleading. With accumulated experience, some interactions were intentionally included in Nuclear Medicine procedures and became an additional tool in differential diagnosis. Moreover, due to the ability of some RPs to compete with therapeutic agents, Nuclear Medicine studies shifted from anatomical-physiological to more pharmacologically-pathologically-based procedures that can also monitor the stage of disease, and follow its treatment (1).

During the past thirty years many reports on drug-RP interactions have been published and reviewed (2), mostly classified on the basis of their radiopharmacodynamic or radiopharmacokinetic characteristics. The first group represents modification of the drug's action on the body due to system/receptor saturation with a RP. The second group modifies the reaction of the body to the RP by changing the RP's metabolism and biodistribution (3). Because some RPs are utilized to evaluate more than one organ/system each, and as Nuclear Medicine physicians and scientists usually focus in imaging specific body systems, alteration of the biodistribution of RPs by drugs is classified in this review by organ, with sub-classification by the drug causing the change. The systems covered are: myocardium (with emphasis on cardiotoxic drugs); brain; red blood cells and blood pool; reticuloendothelial system (with emphasis on hepatotoxic agents and the effect of aluminum-containing drugs); hepatobiliary system (cholinergic, anti-cholinergic and enzyme-stimulating drugs); bone (drugs affecting phosphate and fluoride distribution); ^{67}Ga in tumor and abscesses; gastrointestinal system (especially drugs affecting gastric motility and acid secretion); thyroid; kidney; lungs (with emphasis on pulmonary fibrosis due to drug abuse); pancreas and adrenal. Tentative mechanisms are proposed for most interactions, emphasizing those which enhance the excretion of the RP, thus decreasing its radiation absorbed dose to the patient.

The aim of this review, therefore, is not only to illustrate some crucial pharmacological issues in Nuclear Medicine imaging, but to emphasize the possible input that alterations of RP biodistribution by drugs may have in achieving better and safer diagnosis, disease staging and monitoring of the patient's response to therapy.

MYOCARDIAL IMAGES WITH PHOSPHATE RPs

Infarcted myocardium (MYO) is characterized by a central necrotic zone surrounded by an ischemic zone. The uptake of $^{99\text{m}}\text{Tc}$ -pyrophosphate ($^{99\text{m}}\text{Tc}$ -PYP) in the ischemic tissue is affected by drugs, and the pathophysiological basis for this uptake is dependent on the level of damage, as represented by the tissue blood flow.

While the central necrotic cells of the MYO do not exhibit calcification and do not demonstrate PYP uptake, the peripheral zone of the necrotic MYO, with its ischemia due to diminished blood flow, allows influx of calcium and takes up phosphate.

High levels of calcium and phosphate existing in this poorly-perfused tissue exceed the solubility of calcium phosphate and lead to its precipitation in an amorphous form, which is later converted to hydroxyapatite, which in turn chemisorbs the $^{99m}\text{Tc-PYP}$ (4).

Drugs that heal myocardial infarct by decreasing its oxygen requirement or by increasing its oxygen supply will decrease myocardial uptake of phosphates. In this respect, hydrocortisone and methylprednisolone in pharmacological doses stabilize the cell's lysosomal membrane by increasing the blood flow into the cells, consequently diminishing myocardial necrosis. These drugs prevent myocardial cells from progressing into ischemic necrosis even if their administration is initiated six hours after coronary occlusion, suggesting that therapy might still be effective when started up to six hours after onset of the occlusion. It also suggests that some myocardial injury is reversed by these drugs, and that its clinical progress may be followed up by using $^{99m}\text{Tc-PYP}$ (5,6).

The two glucocorticoids mentioned above reverse fresh myocardial infarct by improving the collateral blood flow into the infarcted area, thus increasing its metabolic response, especially elevating pyruvate necessary to maintain the generation of energy-producing substances. Methylprednisolone also increases cell survival time, which results in greater salvage of ischemic myocardium. In addition, methylprednisolone increases PYP excretion by increasing the glomerular filtration rate, resulting in lower blood and normal-zone myocardial PYP, and consequently in altering myocardial PYP tissue uptake indirectly (7). However, one published report suggested that glucocorticoids given during myocardial infarct might delay the healing process and cause formation of ventricular aneurysms (8).

Some cardiotoxic drugs were shown to cause increased deposition of $^{99m}\text{Tc-PYP}$ due to their damaging the MYO, not necessarily infarcting it, e.g. - adriamycin (doxorubicin) (9,10), daunorubicin and rubidomycin (11). Even though the data obtained for the localization of the $^{99m}\text{Tc-PYP}$ in the drug-treated patients (and with doxorubicin also the localization of ^{131}I -heptadecanoic acid in dogs (12)) are inconsistent, some authors suggest that it might be a reliable method for monitoring cardiac damage during treatment with cardiotoxic drugs (9,13-14).

MYOCARDIAL IMAGES WITH NON-PHOSPHATE RPs

At least five different groups of cardiac drugs have been used in conjunction with myocardial uptake of non-phosphate RPs in patients with coronary artery disease. The use of these clinical agents was aimed at aiding in the evaluation of the extent of ventricular dysfunction.

Nitroglycerin and similar nitrates dilate venous blood vessels, increase coronary collateral flow and reduce venous return to the heart. In Nuclear Medicine studies they minimize exercise-induced abnormalities of left ventricular (LV) wall motion and ejection fraction by reducing myocardial oxygen demand, reducing ischemia and permitting improvement in ventricular function (15-17). Two other nitrates which were shown to improve LV performance in ischemic patients were isosorbide dinitrate (18) and sodium nitroprusside (19), both decreasing ischemia in acute myocardial infarct.

Dipyridamole is a potent coronary vasodilator which has been used as a pharmacological exercise substitute for thallium scintigraphy, as it increases myocardial ^{201}Tl uptake by increasing its regional blood flow (20). The increased rate depends on the condition of the blood vessel, and was much higher in the healthy artery (73% increase) than in the stenotic one (50% increase) (21). Similar results were obtained when dipyridamole was administered to patients with coronary artery disease and the myocardial blood flow evaluated by ^{133}Xe (22). An effect similar in intensity to that of dipyridamole (60% increase) (23) was obtained by isoproterenol, which elevates the uptake of ^{67}Ga (24), ^{201}Tl and a ^{99m}Tc -tetracycline derivative (25), and reverses the decrease in uptake caused by propranolol (26). Similar increases are reported by the diuretic agents furosemide, ethacrynic acid and bicarbonate, which increase the renal excretion of ^{201}Tl , thus changing its kinetic pattern (27).

The effect of three commonly used anti-arrhythmic agents - quinidine, procainamide and disopyramide on LV function was assessed using radionuclide angiography in 17 patients, each of whom received all three drugs in random sequence. While no statistically significant differences were found in resting ejection fraction or in the ejection fraction response to exercise among the three drugs or between any drug and the controls - a 85% reduction in ventricular ectopic beats was found in 60% of the disopyramide patients and in 40% of the other patients (28).

Propranolol, a beta-receptor antagonist, alleviates ischemic heart disease by a different mechanism than nitrates: it has only little direct effect on peripheral vascular tone and on coronary flow, but decreases heart rate and contractility. This made it useful in evaluating LV function in healthy subjects and in patients with coronary artery disease, utilizing quantitative radionuclidic angiography (17,29). The study showed that while in resting patients oral propranolol in therapeutic doses produced no change in ejection fraction and regional wall motion, in myocardial infarction patients the ejection fraction and cardiac output during exercise were significantly lower (30). Another sympathomimetic drug known to improve myocardial function in congestive heart failure is the β_1 receptor agonist dobutamine, which was used as a pharmacological alternative to exercise. Radionuclidic studies combined with this drug are being conducted (31).

Digoxin therapy is used to increase myocardial contractility, but the consecutive scintigraphic results are variable. In one study it did not affect the ejection fraction at rest and at peak exercise in ischemic patients, but provided improved ventricular function at peak exercise in patients with well-preserved LV function at rest (32). Other studies demonstrated 10-22% reduction in ^{201}Tl accumulation in heart muscle after digoxin and ouabain (in small rodents) (27). The RPs used for those studies were ^{201}Tl , $^{99\text{m}}\text{Tc-HSA}$, $^{99\text{m}}\text{TcO}_4$ and $^{99\text{m}}\text{Tc-RBC}$. In addition, diphenylhydantoin (dilantin), an anti-epileptic drug which is used in treating digitalis-induced arrhythmias, caused a significant decrease (39%) in ^{201}Tl MYO uptake, as compared with the control group (33).

In a retrospective study in 62 patients who had ^{201}Tl cardiac imaging, myocardium-to-background ratios were calculated in patients taking propranolol, nitroglycerin, isosorbide dinitrate, digoxin, hydrochlorothiazide or quinidine. While no drug consistently affected that ratio, the lowest one was achieved with digoxin. The authors concluded that none of the commonly used cardiac drugs altered ^{201}Tl uptake to an extent that would cause erroneous image assessment, but that the Nuclear Medicine physician should be aware of such a possibility (34). Some preliminary studies reported that pentobarbital anesthesia increased the concentration of ^{125}I -16-iodohexadecanoic acid in the heart of rats by 94% if the barbiturate was administered 2 hours before the RP, while hepatic radioactivity was markedly reduced (35). An interesting dual mechanism for a cardioactive drug which increases the myocardial uptake of ^{201}Tl was described for grisorixin, an ionophore antibiotic of the nigericin group. Being used clinically as a coronary vasodilator, in doses above 60 $\mu\text{g}/\text{kg}$ it appears to be a potent positive inotropic agent. As an ionophore, grisorixin has the ability to complex and transport monovalent cations across biological membranes, and is a preferential potassium carrier, rather than sodium, and presents a high affinity also for thallium, thus increasing the MYO/background ratio in ^{201}Tl scintigrams (36,37).

BRAIN IMAGING WITH PERTECHNETATE

The classical case of one RP affecting the biodistribution of another, was demonstrated by $^{99\text{m}}\text{Tc-Sn-pyrophosphate}$, altering the consecutive images obtained with $^{99\text{m}}\text{TcO}_4$ for brain studies. If done within a 24 h interval, all brain images show an abnormal pattern, demonstrating increased activity in selected areas. This is due to the fact that tin binds to the erythrocytes, and as a consequence the pertechnetate undergoes intracellular reduction and labels the RBC during the pertechnetate brain imaging (38,39).

A few groups of drugs were reported to apparently alter blood-brain barrier (BBB) penetration of RPs:

Radiographic contrast agents e.g. renografin, administered for cerebral angiography, increased capillary permeability and enhanced $^{99m}\text{TcO}_4$ concentration in healthy brains and in brains with tumors up to six hours after injection (40).

Some cancer chemotherapeutic agents may lead to erroneous brain scans. In one study an abnormal $^{99m}\text{TcO}_4$ scan was obtained in a patient undergoing methotrexate therapy, apparently due to drug-induced ventriculitis (41).

Glucocorticoids are also known to disrupt BBB uptake of RPs, but in the opposite direction: they decrease visualization of intracerebral lesions and prevent visualization of brain tumors by $^{99m}\text{TcO}_4$. This is explained by the ability of glucocorticoids, e.g. dexamethasone, to decrease the degree and extent of the associated cerebral edema in the tumor and the surrounding brain tissue, thus reflecting improvement in the clinical neurologic status of the patient, reducing the extracellular fluid volume and altering the localization of pertechnetate (42).

An interesting finding in this system was that cerebral blood flow did not change under the influence of drug treatment regimens which significantly lower the systemic blood pressure. This was shown with propranolol and metyldopa treatment of hypertensive patients and evaluation of the cerebral blood flow using ^{133}Xe washout: no significant variation was monitored between the control and the drug-treatment groups (43). Another important observation is the effect of ACTH, propranolol and metyrapone on the biodistribution of radioiodinated-isopropyl-p-iodo-amphetamine (IAMP). While propranolol and ACTH decreased IAMP uptake by the brain, metyrapone caused a significant decrease in the RP's concentration in the kidneys, spleen, gut and stomach, but not in the brain. The authors concluded that while the exact mechanism of these competitions were not clear, their implication in imaging with IAMP is of clinical importance (44).

A case study pointing to a potential hazard in non-ventilated laboratories could be seen in a brain scan of a 15 year-old schoolboy who inhaled toluene which was the solvent of a glue he had been sniffing at school. The brain scan showed a large area of increased uptake, consistent with an infarction. As toluene and similar organic solvents are so common in clinical laboratories, it would be desirable to determine the worker's occupational exposure to such solvents (45).

RECEPTOR IMAGING OF THE BRAIN

Neuroreceptor PET imaging makes it possible to attempt to relate cerebral functions to specific receptor-bound neurotransmitters. The goals of such studies are to estimate the receptor affinity and density in healthy and pathological conditions as well as to assess their competitive binding rate with specific drugs. In one study carried out in baboons ^{11}C -suriclone, an anti-anxiety drug which is known to bind to the benzodiazepine receptor complex with high affinity, was displaced from its receptors in the cerebral cortex and the cerebellum by an experimental benzodiazepine antagonist Ro-151788 (46). In another study in healthy volunteers the caudate/cerebellum uptake of ^{11}C -n-methyl-spiperone, a dopaminergic agent, was dramatically decreased by the neuroleptic drug haloperidol, in a dose-dependent response (47). The number of brain receptor types studied in animals is too numerous to detail here, and is indicative of the tremendous effort put into this type of kinetic competitive study, which is aimed at using clinical drugs for proving malfunction of a specific receptor for specific neurotransmitters (115).

RED BLOOD CELLS (RBC) AND BLOOD POOL

A variety of drugs was reported to alter RBC labeling efficiency, and consequently blood pool visualization, in various *in vivo* models. Heparin causes poor *in vivo* RBC labeling, and consequently decreases the activity in the heart and increases renal uptake and excretion. In comparison, RBC labeled *in vitro* have significantly greater retention in the blood pool, with correspondingly higher LV counting rates (48). Significant uptake of ^{99m}Tc -heparin by the liver (28%) and the kidneys (45%)

was reported by Kulkarni et al (49), while some other authors suggested that heparin might have contributed to the poor in vivo labeling of RBC, due to unidentified mechanism (50,51). The superiority of ACD over heparin for RBC labeling was demonstrated both in vivo and in vitro in healthy volunteers, where the use of ACD resulted in lower non-target activity (52).

A mechanistic approach for reduction in the RBC labeling efficiency was suggested for other drugs as well : hydralazine and methyl-dopa were reported to decrease in vivo labeling of RBC, possibly through their oxidation of the stannous ion existing in the RBC kit (53). This implies that every drug which might be reduced by the Sn^{++} , competes with pertechnetate for its reducing agent in the kit, and diminishes the ability of $^{99m}\text{TcO}_4^-$ to get reduced efficiently in order to bind to the RBC. Animal studies showed that the antihypertensive drug prazosin, as well as the cardioactive drug digoxin, demonstrated a significant reduction in RBC tagging with ^{99m}Tc (54). However, two other cardiac drugs, lidocaine and quinidine, were found not to alter RBC labeling efficiency by pertechnetate (53).

Another factor which is apt to reduce RBC labeling efficiency is RBC antibody formation. When incubated with antibodies prior to labeling, RBC labeling efficiency dropped from 95% to 73% (54). The mechanism of this phenomenon is not completely understood.

RETICULOENDOTHELIAL SYSTEM (RES) AND COLLOIDAL RPs

The major issue discussed in relation to preferential colloid uptake is the effect of aluminum ion on colloid distribution. High plasma Al causes marked alteration in biodistribution of a variety of ^{99m}Tc -labeled compounds. As ingested Al is usually not absorbed from the alimentary tract, its level in the blood is kept at concentrations below 4 ppm (55). When these levels exceed 10 ppm (e.g. - due to renal failure), the biodistribution pattern of at least 3 RPs may be altered:

a) $^{99m}\text{Tc-S-colloid}$: Aluminum causes flocculation of the colloid, and formation of a S-colloid macroaggregate, leading to extraction of the S aggregate in the lung and to a consequential increase in lung activity. In patients with plasma Al level of over 30 $\mu\text{g}/\text{ml}$ -white colloidal material can be observed microscopically (55).

b) $^{99m}\text{Tc-diphosphonate}$: In the presence of above 20 $\mu\text{g}/\text{ml}$ Al in plasma, this bone agent is mostly concentrated in the liver, possibly by formation of a submicroscopic complex in which it is trapped (56,57). In rats injected 20 $\mu\text{g}/\text{kg}$ Al, increased soft tissue uptake and progressive degradation of bone scan images occurred, even though Millipore filtration could not show any colloidal particles in the preparation (58).

c) $^{99m}\text{Tc-pertechnetate}$: In hyperaluminemia, $^{99m}\text{TcO}_4^-$ fails to leave the vascular space, and as a consequence, no stomach or bladder are seen. This should be alarming in high-risk patients, i.e. those under prolonged dialysis, where slow Al excretion and higher incidental Al intake may cause critical changes in Al balance (59).

The two major Al sources reported to affect RP biodistribution are the excess of this ion in the eluate of the Mo-Tc generator, and Al ions in antacid preparations containing aluminum hydroxide.

Another group of drugs that increase lung uptake of colloidal RPs are RES stimulants. Such agents, i.e. heparin, thyroid hormones, vitamin B₁₂, dextrose, steroids and triglycerides, increase the number of intravascular macrophages which settle in the lung. They do so by mobilizing a large number of phagocytic cells from the liver, spleen and bone marrow into the vascular spaces, where they are trapped in the pulmonary capillary bed and exercise their ability to phagocytize colloidal particles (60,61). Enhanced lung phagocytic activity was also noticed in rats after administration of *E. coli* endotoxin, and a marked depression was noticed after RES blockade with gelatin (62). No in vivo alteration in particle size occurred in that study, and the radioactivity was distributed over individual cells and not in clumps as with blockade by macroaggregated albumin (62).

In contrast, single doses of chemotherapeutic agents, given singly or in combination, cause only minimal and transient changes in the biodistribution of radiocolloids in liver of cancer patients (63). Prolonged treatment with methotrexate against psoriasis is hepatotoxic, but these reactions cannot be reliably evaluated by ^{99m}Tc -S-colloid (64). Immunosuppressive and chemotherapeutic agents have been reported to alter bone marrow imaging with ^{99m}Tc -S-colloid, due to their ability to expand the bone marrow to peripheral sites. This expansion is secondary to marrow injury, and is transient, ending after termination of the treatment (65).

A few reports on reversal of the normal liver/spleen biodistribution of colloids were published in patients undergoing general anesthesia. Children who had a diagnostic surgical procedure under anesthesia with halothane, demonstrated extreme slowing of the hepatic arterial flow due to specific increase in the hepatic vasoconstrictor tone at the arterial, sinusoidal and venous levels, leading to reduction in systemic arterial pressure and in hepatic blood flow, upon which colloid extraction is dependent. For that reason, hepatotoxic anesthetics like halothane, methoxyfluorane and enflurane may induce such changes in the liver that will either image as hepatitis and hepatic necrosis or diminish liver uptake of the colloidal marker (66). Methoxyfluorane (penthrane) reduced splanchnic blood flow by 50% due to arterial hypotension and increased splanchnic vascular resistance, but this study was not documented with RPs (67).

Some pharmacologic agents that change splenic size in man and animals include epinephrine, which causes contraction of an enlarged spleen; steroids, causing a dramatic decrease in the size of a spleen involved by sarcoidosis; anti-malarial agents and chemicals (e.g. ethyl palmitate) which cause splenic destruction. Scan-documented changes in splenic size has important diagnostic and prognostic significance (68).

HEPATOBILIARY RPs

Hepatobiliary imaging with the various imino diacetic acid analogues (e.g. HIDA, PIPIDA) is highly dependent on endogenous physiological factors, mainly gallbladder-emptying stimulants and inhibitors. Cholecystokinin (CCK) and its synthetic octapeptide analogue sincalide are gallbladder contractors, serving as cholecystagogues, and are used to increase gallbladder contraction and intestinal motility when the bladder is not visualized shortly after an imino diacetic acid derivative dose (69). It may also be used before the RP is administered, to empty a full gallbladder, or after a study is completed which demonstrates a cystic duct but no bowel activity. The latter situation is common in early common bile duct obstruction, ileus, and after administration of narcotic analgesic, which may cause a functional obstruction of the sphincter of Oddi. Administration of CCK prevents a false positive diagnosis of surgical common bile duct obstruction. Another analogue of CCK, ceruletid, is an cholescytokinetic gallbladder contractor. It is a decapeptide which is qualitatively identical in activity to CCK (70). In comparison, somatostatin and many drugs are known as bile release inhibitors, preventing the emptying of the bile into the duodenum, and obliterating gallbladder response to meals or to sham feeding (71). This inhibitory effect of somatostatin on gallbladder emptying may be due to decreased release of CCK or suppression of gallbladder muscle response to direct stimuli (72). Some of the pharmacological agents affecting such cholescintigraphic studies are the following:

Phenobarbital, when given in neonatal jaundice for at least five days prior to HIDA scans, enhances and accelerates biliary excretion in cholestatic jaundice, but has no effect in extrahepatic biliary atresia. Phenobarbital is a potent inducer of hepatic microsomal enzymes and has been shown to enhance canalicular blood flow. This choleretic effect is independent from the enzyme induction, as it acts on the whole hepatic transport system for organic anions (73). In spite of its being an inducer of hepatic enzymes, phenobarbital did not alter liver uptake of ^{67}Ga when pre-administered on six consecutive days before the Ga administration (74). As could be expected, cholinergic stimulants, e.g. bethanechol, induce gallbladder emptying 25-fold above control values (75).

Apparently the mode of administration of the intervening drug has to do with the significance of its effect on distribution of the relevant RP. Thus, when the

chemotherapeutic agent 5-fluorodeoxyuridine (5-FUDR) was infused directly via the hepatic artery, in the treatment of certain hepatic tumors, all hepatobiliary scintigraphies looked abnormal with nonvisualization of the gallbladder at 1 hour, identified as gallbladder dysfunction presumably due to chemical cholecystitis (76).

Nicotinic acid "and a variety of other vitamins" were described as causing false positive HIDA scans, and were thought to interfere with conjugation of HIDA with glutathione for its excretion (77). Later in vitro studies suggested that nicotinic acid did not have an inhibitory effect on hepatic transport of biliary imaging agents, and actually stimulated hepatic uptake of PIPIDA (78).

Morphine, as well as other narcotics (e.g. meperidine) administered in therapeutic doses, was found to increase the intrabiliary pressure and consequently to slow down the transfer kinetics of ^{99m}Tc -HIDA into the bile canaliculi, and the entire process of gallbladder emptying was shown occasionally, suggesting complete obstruction (1,2). Cholinergic blockers, e.g. atropine, reduce gallbladder emptying by about 25% from the control value (75). Interestingly enough, alcohol also inhibits gallbladder contractile response in man (79) and delays the rate of gastric emptying and the release of endogenous CCK (80). In alcoholics a marked increased uptake of ^{99m}Tc -HIDA was noticed due to drug-induced membrane alteration, suggesting that ^{99m}Tc -HIDA became a sensitive monitor of functional changes in the hepatobiliary system (81).

BONE IMAGES WITH PHOSPHATE RPs

Uptake of phosphates and phosphonates by the bone is a complex process, and is therefore affected by a large variety of drugs. In general, this uptake depends on the rate and amount of blood flow, on passive diffusion via capillaries into the extravascular spaces, on sequestration of the phosphate by organic and mineral bone components, on bone mineralization, on acid-base relationship, fluid pressure in the bone and on parathyroid activity. Each of these factors may be affected by a therapeutic drug and alter the retention of the labeled phosphate in the bone matrix.

Parathyroid hormone given IV is known to promote calcium and phosphate resorption from bone, and so does dihydrotachysterol given orally and 1,25-dihydroxy-vit D, vit D's major metabolite. In addition, the latter increases intestinal absorption of calcium and phosphate, thus promoting bone mineralization, and its overall effect depends on the extracellular concentrations of Ca and phosphate (4). It was shown by Carr et al that tissue distribution of ^{99m}Tc -pyrophosphate is modulated favorably by prior IV administration of vit D₃ in pharmacological doses. Vit D₃ administered IV to rats decreased uptake of the RP by bone, but did not decrease its uptake by an experimental infarct, thus causing a significant increase in the ratio of uptake by infarct/bone and improving the images which previously were degraded by the uptake of the overlapping ribs (82,83). In general, long-term steroid therapy depletes bone minerals, and as a consequence causes a remarkable decrease in skeletal uptake of bone imaging RPs in such patients (84).

Altered biodistribution of ^{99m}Tc -pyrophosphate and other phosphates were also reported in patients with chronic iron overload, resulting from either repeated transfusions or hemochromatosis. Such scans are characterized by reduction of bone uptake, increased renal activity and a significant increase in soft-tissue accumulation of ^{99m}Tc -labeled phosphates (85). Similar results were reported in patients with thalassemia major, whose decreased hemoglobin synthesis led to serum iron excess (86). Mechanistically it has been suggested that metal ions, such as Ca and Fe, might facilitate the dissociation of ^{99m}Tc from the carrier ligand and produce in vivo a ^{99m}Tc form that carries the activity to the kidneys. This is the case with Tc-HEDP and Tc-pyrophosphate, which upon in vitro mixing turns into ^{99m}Tc -gluconate and clears via the kidneys. It is believed that serum ferritin, which was elevated in all the patients reported, was the readily available source of that iron (87).

Another common source of such iron is iron-dextran, which explains the concentration of ^{99m}Tc -phosphate at the site of intramuscular injection of iron-dextran

complex, i.e. - the gluteal muscle (88). Mechanistically, reduced ^{99m}Tc occupies the unfilled coordination sites in the iron of the ferric hydroxide as it is released from the iron dextran complex, resulting in deposition of the ^{99m}Tc -phosphate complex in the site of the iron-dextran injection. In this complex the dextran is merely the carrier for the iron, and when infused prior to administration of ^{99m}Tc -Sn-pyrophosphate, bonding between the two complexes will achieve blood-pool labeling and eliminate bone uptake. It was shown that such a double complex and blood pool labeling are formed only with iron dextran, not with dextran itself, and that the activity obtained stays mainly in the plasma (89,90).

In a retrospective study in children receiving chemotherapy for various malignant diseases, who had bone scans within one week afterwards, an intense renal parenchymal uptake was noted with ^{99m}Tc -pyrophosphate. The drugs reported were cyclophosphamide, vincristine and doxorubicin, and although no apparent decrease in renal function was noticed, it was suggested that the effect might be due to the antimitotic activity of those drugs (91). In a case reported by Sorkin et al, the authors interpreted a diffuse increased uptake of ^{99m}Tc -diphosphonate in the soft tissue of the extremities as due to hyperemia secondary to melphalan and actinomycin D chemoperfusion which the patient had received 4 days earlier (92). A variety of chemotherapeutic agents was demonstrated to cause reduced uptake of bone RP by metastatic lesions, so much so that ^{99m}Tc -EHDP was suggested for assessment of response of bone metastases to anti-cancer treatment (93).

High renal uptake of bone-seeking phosphates was also noticed in patients taking osmotic diuretics, which inhibit the normal tubular resorption of the bone agent (2), and in a patient receiving a contrast material for urography just prior to performing the scan (94). In the latter case, a repeat bone scan yielded a normal partition of this agent.

A comprehensive study on the effect of steroid hormones in 24 h whole-body retention of ^{99m}Tc -diphosphonate (a sensitive indicator of skeletal metabolism) was conducted in oophorectomized women. The estrogen-treated group had significantly lower retention and lower rate of bone loss than the untreated group, indicating suppressed skeletal metabolism due to the estrogen treatment. The highest uptake of diphosphonate was recorded in women who defaulted from the estrogen therapy. This higher uptake was due to a rebound period of accelerated skeletal metabolism and bone loss. These findings suggested that whole-body retention of diphosphonate be used in monitoring skeletal metabolism in cases of estrogen supplementation (95). Another study reported bilateral breast uptake of ^{99m}Tc -pyrophosphate in a prostatic cancer patient who had developed gynecomastia after receiving diethylstilbestrol therapy (96).

BONE IMAGES WITH ^{18}F

Of the various bone agents used clinically, two were used for kinetic studies : ^{99m}Tc -diphosphonate and ^{18}F . Diphosphonate is taken up by the skeleton with very little accumulation in soft tissues. Uptake is almost exclusively in bone, and it is therefore a good RP for modeling bone kinetic studies. This skeletal tracer clearance technique prompted Sagar et al (97) to utilize diphosphonate uptake in kinetic studies in dogs and define a seven-compartment model for this RP.

Another bone agent used for kinetic studies is ^{18}F . Charkes evaluated a five-compartment model for ^{18}F kinetics in rats, and noticed that the initial fluoride distribution was similar to that of ^{77}Br , a known extracellular fluid tracer (98). Hence, the reliability of ^{18}F studies in following-up regression of bone metastases was questioned in at least one study, in which patients undergoing chemotherapy or hormonal therapy showed the same abnormal ^{18}F uptake in spite of roentgenographic evidence of improvement and regression of the metastases. The authors suggested that short-term radionuclidic bone studies in patients under drug therapy should be interpreted cautiously (99).

⁶⁷Ga IN TUMORS AND ABCESSES

Two categories of drugs were related to ⁶⁷Ga accumulation and re-distribution. The first includes cations, e.g. Fe and Ga, competing with radiogallium due to a "carrier effect" as based on their proton number. Hagan et al (100,101) have shown that Fe⁺³ exerts a highly discriminative effect on ⁶⁷Ga uptake in tissues: Fe increases tumor ⁶⁷Ga uptake but reduces ⁶⁷Ga retention in healthy tissue, thus permitting a shortened ⁶⁷Ga-scanning procedure and reduced radiation dose to the patient. This dual phenomenon, which was noticed in the tissue before it was noticed in blood, was considered by the authors to be a "false carrier effect" and was caused by the fact that "Fe binds to both malignant and nonmalignant tissue much faster than does Ga". In contrast, non-radioactive Ga, being a true carrier, had an opposite effect : it decreased Ga uptake by both tumor and non-tumored tissue, but its effect in the tumor was much more dramatic. The mechanism of this observation is not entirely clear. It is neither simply a matter of valence, nor is there a constant trend in the competition between the various metals studied, i.e., Fe, Ga, Mn, Sc etc. It seems that the dominant factor in this complex is the bonding between the metal and the plasma or tissue protein, as ⁶⁷Ga binding to non-malignant tissues in the first few hours after injection is so labile that it is easily displaced by carrier Ga or by false carriers, while Fe is quickly and tightly bound, and consequently not easily displaced (102,103).

The Ga-related false-carrier effect in tumors is much different from that in abcesses : ⁶⁷Ga concentration in an abcess developed experimentally in a rabbit decreased to a much greater extent over a 24 h period after iron-dextran injection than ⁶⁷Ga concentration observed in tumor during the same time period. In this study, the iron-dextran lowered the whole-body retention of ⁶⁷Ga in both the normal and the abcess-bearing animals (104). Hence, the abcess-to-muscle ratio increased two-fold in iron-dextran-treated rabbits as compared to non-treated ones, provided the iron-dextran was administered 24 h after the ⁶⁷Ga. In such a case the ⁶⁷Ga concentrated in the abcess, and the injected Fe replaced the ⁶⁷Ga only in the floating transferrin complex and enhanced ⁶⁷Ga elimination (105).

Due to the practical importance of such a competition in decreasing the background and increasing abcess-to-muscle ratio of ⁶⁷Ga, various Fe-complexes were experimented with as carriers for the iron : iron-sorbitol-citrate was shown to lower soft-tissue background when administered 1 h before ⁶⁷Ga-citrate, resulting in early diagnosis and improved quality of the scans. As the iron-sorbitol was injected 1 h before the ⁶⁷Ga, the authors suggested that it saturated the free transferrin, thus enhancing the lesion-to-background ratio (106). Desferoxamine given to rats 5 h following administration of ⁶⁷Ga, was found to reduce the whole-body radiation dose by 25% by forming a metal-chelate excreted through the kidney, but was too toxic for human use. Another chemical which complexes ⁶⁷Ga, hastens its renal clearance and increases its abcess to soft-tissue concentration is tricatecholamide which forms a complex which is rapidly excreted with ⁶⁷Ga (107). This approach of formation of excretable chelates with ⁶⁷Ga for reduction of radiation dose can be utilized with a variety of chelating agents, obtaining a variety of quantitative results (108,109).

The second category of agents related to ⁶⁷Ga accumulation includes a variety of agents and drugs that cause abnormal Ga accumulation in specific tissues showing inflammatory changes. This is the case in patients developing abnormal lung accumulation of ⁶⁷Ga due to pulmonary interstitial fibrosis after cancer chemotherapy. Patients with normal chest radiography, who received multiple cycles of chemotherapy with a 3-4 drug combination including vincristine, methotrexate, procarbazine, prednisone and cyclophosphamide, demonstrated a diffuse bilateral lung uptake of ⁶⁷Ga. As cyclophosphamide was included in all drug combinations - it was suggested that this drug was most likely the cause for that altered biodistribution (110), but animal studies suggested that bleomycin might be another responsible agent. Similar enhanced lung scans were obtained after long-term intravenous administration of talc in drug abusers (111) and in patients receiving oily contrast agents used in lymphangiography (112).

One unusual mechanism by which a chemotherapeutic agent alters ^{67}Ga biodistribution is that of methotrexate, vincristine, and mechllorethamine, which cause localization of ^{67}Ga in the bone and its enhanced excretion by the kidneys due to their ability to inhibit iron incorporation into RBCs. This increases serum iron levels and causes saturation of the Ga-binding sites in the serum by iron atoms. This effect of methotrexate, which is noticed even after single doses of the drug, indirectly reduces radiation dose to the patient (113,114). Another mechanism promoting non-specific uptake of ^{67}Ga by the liver is due to drugs elevating the enzymatic activity of the liver microsomal system, e.g. phenobarbital. Even though the increase of ^{67}Ga uptake by the mouse liver in one study (74) was not impressive, such an effect of liver activation should always be in mind.

A series of reports connect ^{67}Ga uptake to hormones involved in the brain-to-breast pathway: steroids (dexamethasone) given prior to, or on the day of the ^{67}Ga scan, caused significant suppression of the ^{67}Ga intake in tumors of the CNS (116), while another steroid (diethylstilbestrol) caused retention of the RP in the metastatic breast apparently due to high concentration of lactoferrin in the breast (117). Phenothiazine tranquilizers, e.g. prochlorperazine and chlorpromazine, which depressed the hypothalamic prolactin-inhibiting factor and cause hyperprolactinemia, were also reported to cause enhanced breast ^{67}Ga uptake (118), and similar results were reported also by other authors (119), emphasizing the involvement of ^{67}Ga in the hormonal balance of the hypothalamus-breast axis.

GASTROINTESTINAL (GI) SYSTEM IMAGES

The effect of drugs on two physiological parameters of the GI system has been reported: acid secretion and gastric emptying, as evaluated utilizing Nuclear Medicine procedures. Cimetidine, an anti- H_2 drug, is a model agent for affecting acid secretion, but its effect is somewhat controversial. While Sagar claims that cimetidine inhibits the excretion of $^{99\text{m}}\text{TcO}_4$ into the gastric content by 47% concomitantly with the acid output, and that the difference in $^{99\text{m}}\text{Tc}$ content between the gastric juice and the stomach wall in the cimetidine-treated animals is 2.5 times greater than in control dogs (120), Schwesinger reports "no effect" for cimetidine in a similar model (121). Part of this discrepancy is due to the controversy over what is the cellular site for $^{99\text{m}}\text{TcO}_4$ concentration, suggested to be mainly the mucus-secreting epithelial cells of the gastric mucosa rather than the acid secreting parietal cells (122). Obviously, retention of $^{99\text{m}}\text{TcO}_4$ by the gastric mucosa improves the quality of images of the upper GI tract, performed by pertechnetate, thus improving the target-to-nontarget ratio (123) when imaging for Meckel's diverticulum.

Gastric emptying time was evaluated by various RPs under the effect of drugs. In one study $^{99\text{m}}\text{Tc}$ -labeled-resin-oatmeal was utilized for evaluating gastric emptying time in diabetic gastroenteropathy, secondary to gastric atony, treated by metoclopramide. This dopamine-antagonist stimulates gastric motility independent of vagal innervation and shortens the gastric emptying time in the atonic stomach, bringing it to almost normal values, but does not affect gastric emptying in healthy subjects (124). Use of the $^{99\text{m}}\text{Tc}$ -labeled resin may help to predict which patient will benefit from a pharmacological intervention by this drug (125). In a more detailed study where different markers were given simultaneously for the liquid component (113In-DTPA) and the solid component ($^{99\text{m}}\text{Tc-S-colloid}$) of the stomach content, metoclopramide accelerated the emptying of both markers (125). In a similar study where $^{99\text{m}}\text{Tc-S-colloid-DTPA}$ chicken liver and $^{111}\text{In-DTPA}$ solution were given to healthy men, morphine caused significant inhibition of gastric emptying of both components, probably due to relaxed gastric smooth muscle (124,126). A study in healthy volunteers who received the same two markers demonstrated that somatostatin, a naturally-occurring gut hormone which inhibits insulin and glucagon secretion, also inhibits gastric emptying, and drugs affecting somatostatin release into the plasma may slow the emptying of gastric content significantly (127).

Gastrointestinal bleeding as evaluated by $^{99\text{m}}\text{TcO}_4$ or by $^{99\text{m}}\text{Tc-S-colloid}$ can also be modified by drugs. If $^{99\text{m}}\text{Tc-S-Coll}$ is being injected into patients with

active GI bleeding, a portion of the RP will penetrate through the rupture and will not reach the colloid target organs, thus distorting the typical colloidal biodistribution (128). Epinephrine was used at one time intra-arterially to control bleeding in hemorrhagic gastritis, but was discontinued because of tachyphylaxis, epinephrine-induced vasospasm and rebound hyperemia. A safer pharmacological way to control GI bleeding is by vasopressin (pitressin), which is used as a therapeutic vasoconstrictor administered intraarterially, but also produces sustained reduction of splanchnic blood flow and is used for controlling bleeding and restoring colloidal scans (129).

Gastrointestinal bleeding caused by Meckel's diverticulum is imaged by $^{99m}\text{TcO}_4$, as this RP is taken up by the parietal cells of the ectopic gastric mucosa and aids in identifying them. Pre-medication with parietal cell stimulants, e.g. - pentagastrin, increases the uptake of pertechnetate, while drugs that antagonize parietal cell secretion, e.g. glucagon, which prevents washout of the intraluminal activity, decrease its level (130,131).

THYROID SCANS

Since the first extensive review of factors influencing uptake of iodide by the thyroid (132), many reports and reviews have been published, and the reader is referred to reference (3) as a comprehensive one. The major group of drugs decreasing thyroïdal uptake of iodide consists of an array of minerals which resemble iodide in size and are capable of replacing its trapping, though not organification, in the thyroid. Some of those anions, e.g. Br^- , SCN^- , ClO_4^- and TcO_4^- are being used clinically, the latter two for intentional thyroid blocking. It was reported as early as 1952 that the monovalent anions thiocyanate (SCN^-) and perchlorate (ClO_4^-) are strong competitors of iodide for its active transport mechanism into the thyroid, and it is known today that such a competition is also valid for other anions and in other tissues, e.g. the salivary glands and the choroid plexus, and is dependent in part on the ionic size (133).

A second group of drugs decreasing thyroïdal uptake are those containing inorganic and organic iodine. Uptake of radioiodide is significantly decreased even if the "cold" iodide (e.g. Lugol's solution) is given a few hours later. Not only is this characteristic shared by some anti-tussives and vitamin-mineral preparations (134), but also by organic molecules containing iodine, e.g. contrast agents. Iodinated contrast agents that are strongly bound to serum proteins, e.g. iodipamide, alter iodide biodistribution for months after their administration, and in the case of oil-soluble iodinated contrast agents, e.g. lipiodol, for years (135). A prolonged retention is also reported for iodinated organic molecules administered and absorbed externally, e.g. vioform and betadine (136). Special consideration must be given to drugs that lower radioiodine uptake due to thyrotoxicosis, i.e. amiodarone. Apparently this drug initially inflates the thyroid-hormone stores due to iodine excess, then discharges the hormone into the circulation (137).

A third group of drugs decreasing thyroïdal uptake are hormonal or pharmacological preparations which interfere with the thyroid activity. This group contains the clinically-useful antithyroid drugs propylthiouracil, which decreases iodide uptake by the thyroid due to its inhibition of thyroid hormone synthesis and carbimazole, which confers radioprotection by forming disulphide bonds with thyroïdal cell proteins (138). Also included are thyroid preparations which specifically compete by feedback on the thyroid activity; drugs which suppress release from the hypophysis, i.e. phenylbutazone (139) and drugs which involve the hypothalamus-hypophyseal-thyroidal metabolic pathway. Some of these agents are used clinically for regulation of thyroid activity.

The fourth group of drugs altering the radioiodine uptake by the thyroid is a non-uniform one, ranging from centrally-active to diuretic agents. Friedell noticed as early as 1958 that tranquilizing agents, particularly meprobamate and benactyzine, decreased thyroid activity as measured by the uptake of ^{131}I , due to their central inter-neuronal blocking activity (140). Similar results were obtained after intake of adrenal and gonadal steroids, as well as after ACTH, probably due to suppression

of TSH formation and increased renal radioiodine clearance. Although most steroids inhibit radioiodine uptake, estrogens have not demonstrated this effect, and human studies of thyroidal uptake of radioiodine are inconclusive (2).

KIDNEY SCANS

Three major categories of drugs altering kidney function have been reported. The first one demonstrates the dependence of kidney function on acid-base balance and the alteration of the latter by drugs. A typical example in this category is the influence of biochemical and physiological factors, e.g. tubular blockade, changes in hydration and acid-base balance on renal localization of ^{99m}Tc -DMSA. Both osmotic diuresis and dehydration by water deprivation resulted in a slower plasma clearance in rats, while acidosis markedly increased background due to increased liver accumulation and higher plasma protein binding of the RP. Alkalizing the urine by sodium bicarbonate (pH 9.2) or its acidification by NH_4Cl (pH 5.9) significantly reduced DMSA retention, but there was no significant change in the DMSA uptake after induction of mannitol diuresis or after probenecid, given by gavage, in order to achieve proximal tubular blockage (141).

In patients with unilateral renal artery stenosis, administration of the antihypertensive drug captopril decreases glomerular filtration in the affected kidney by interruption of autoregulatory mechanisms, as visualized by ^{99m}Tc -DTPA or by ^{131}I - o -iodohippuran. This decrease is reversed after discontinuation of the drug (142).

Hence, diuretic radionuclide urography became an accepted method for evaluating various nephrourethral obstructions and for quicker clearance of the RP. It seems that diuresis radiorenography not only enables differentiation between mechanical and functional obstructive uropathy assisting in patient management (143,144), but affects renal function and uptake. Its sensitivity and specificity for detection of obstruction is over 90%, but it is unreliable in patients with poor renal function (145). On the other hand, probenecid (a general inhibitor of tubular secretion) inhibits the urinary secretion of some renal radiopharmaceuticals, but this inhibition is not common to all RP used (146).

Cisplatin is an example of a chemotherapeutic agent, used clinically for treating a variety of cancers, which interferes with the clinical uptake of radiogallium, in that renal uptake is increased while liver uptake is markedly decreased (135). In consecutive experiments by the same group, cisplatin caused a reduced uptake of radiogallium in tumors of tumor-bearing dogs, suggesting that the effect of the drug on ^{67}Ga uptake is related to the altered cellular protein synthesis by this nephrotoxic drug (147). Diuretics and hypertonic solutions can reduce the renal toxicity of this drug significantly as shown with ^{131}I -iodohippurate (148), and when used as a RP (^{99m}Pt -cisplatin), reduce its background levels and consequently the radiation absorbed doses (149). The impact of another nephrotoxic agent, the immunosuppressive drug cyclosporin A, on kidney images was studied by Klintmalm et al (150). It was demonstrated that the drug mimics acute tubular necrosis or rejection in ^{99m}Tc -DTPA and ^{131}I -iodohippuran studies, and that the interpretation of such scans in the transplant patient should be done with great caution. The drug's nephrotoxicity and consequently the altered biodistribution of the RPs can often be reversed by reducing the drug's dose (151).

LUNG SCANS

Asthmatic patients show expected alteration in ventilation lung scans, as they represent a frequently-medicated group. The two RPs utilized for monitoring therapy in such patients are ^{99m}Tc -DTPA-aerosol and ^{133}Xe , and when the scan is performed immediately after a bronchodilator drug, a dramatic relief in ventilation effort can be demonstrated. One factor which may complicate the scan even further is a possible pharmaceutical antagonism between the bronchodilator and the $^{99m}\text{TcO}_4^-$, in case both are being given as aerosols (152).

There is a correlation between the biodistribution of ^{133}Xe and the amount of fat in the liver. The fattier the liver - the more ^{133}Xe is retained (dissolved) in it, due to the higher partition coefficient of the ^{133}Xe in the adipose tissue (153). It was documented that heavier (i.e. fatter) subjects show a greater uptake of the radioxenon than leaner ones (154). The partition coefficient of triglycerides for ^{133}Xe is somewhat higher, and drugs such as clofibrate, which interfere with the conversion of triglycerides into fatty acids in the liver, may actually enhance xenon retention (155).

Drug addicts comprise a very special group of patients with altered biodistribution of lung RPs. Measurement of regional lung function with ^{133}Xe and $^{99\text{m}}\text{Tc}$ -albumin microspheres in narcotic (heroin) addicts without respiratory symptoms revealed abnormalities of regional perfusion in 73% of the subjects and abnormal regional ventilation in 27% of them, characterized by delayed clearance of the gas. The authors suggested that the abnormal regional perfusion was due to septic emboli, to edema or to foreign body granulomas being developed after repeated parenteral use of abused drugs. In these patients the pulmonary bed serves as a filter to the foreign bodies incidentally injected, e.g. cotton fibers and talc crystals (156). As cotton wool is used by addicts as a filter in their syringes, fibers of this material may be inadvertently injected. In the lung, talc and cotton wool emboli induce a granulomatous reaction which, in turn, alters both ventilation and perfusion studies (2,18). In other systems, e.g. bone, $^{99\text{m}}\text{Tc}$ -phosphate scintigraphy in heroin addicts is more sensitive than radiography in the diagnosis of acute osteomyelitis (157).

Pulmonary interstitial fibrosis was also diagnosed after various drugs, e.g. bleomycin, nitrofuran, cyclophosphamide, mitomycin and other chemotherapeutic agents. This is considered a non-specific effect which increases ratiogallium uptake in the lungs. Many of these pulmonary fibrosis scans were performed with ^{133}Xe or $^{99\text{m}}\text{Tc}$ -MAA (135).

PANCREAS SCANS

Apparently the pancreatic uptake of ^{75}Se -selenomethionine is hardly used today and is not easily altered by drugs, particularly not in animal models. In a comprehensive survey, the influence of pre-treatment with 16 various drugs on the uptake of this RP by the rat pancreas was studied. Only propylthiouracil, when administered for 3 consecutive days prior to the RP, resulted in a 17% increase in the pancreatic uptake and seven other agents resulted in significant decreases in that uptake (158). In a similar set of experiments in mice and dogs, growth hormone depressed the pancreatic uptake by 13%, and so did some drugs which stimulate growth hormone production. The authors suggest that hypothalamic factors may be important in balancing the function of the exocrine pancreas, and that drugs which interfere with the hypothalamus-pituitary axis may alter pancreatic functions (153).

ADRENAL SCINTIGRAPHY

Adrenal cortex imaging is performed with iodinated cholesterol derivatives and is known to be suppressed by dexamethasone. Two daily injections of this steroid suppressed the uptake of both $^{19-131\text{I}}$ -cholesterol (NM-145) and $^{6\beta-19}$ -nor-iodocholesterol (NP-59), and administration of this glucocorticoid analog before and after dexamethasone was advocated in aldosterone-producing adenoma (159-161).

A physiological approach for intensifying adrenal visualization is the use of synthetic ACTH (162). Drugs that alter ACTH or prostaglandin levels result in alteration of cholesterol uptake in the adrenal cortex, and in turn, in steroid hormone biosynthesis and secretion. Metyrapone, a steroid hydroxylase inhibitor which elevates pituitary ACTH release, increases adrenal cholesterol uptake, while glucocorticoids (e.g. dexamethasone) which lower ACTH plasma levels, reduce adrenal cholesterol uptake (163). Hormonal changes in the adrenal's environment sensitive balance may

alter, by a feedback or by a pathological intervention, its steroid uptake and build-up, and physicians should be aware of drugs that may unbalance this process.

Imaging of the adrenal medulla can be easily affected by drugs. MIBG, which was originally suggested for imaging myocardium, is an analogue of the neuroblocking agent guanethidine, and concentrates in the chromaffin cells of the adrenal medulla. Reserpine, a catecholamine-depleting tranquilizer, blocks norepinephrine uptake in the storage vesicles, i.e. the chromaffin granules of the adrenal medulla, and lowers MIBG uptake. This happens because both MIBG and reserpine share the same storage mechanism in the adrenal medulla (164). Animal experiments have shown that phenoxybenzamine and cocaine, both potent inhibitors of catecholamine and guanethidine uptake, inhibit MIBG medullary uptake by about 40% (165), suggesting that drugs which have the same mechanism will have a similar inhibitory effect. In addition, some commonly used sympathomimetic agents, including pseudoephedrine, phenylephrine and amphetamine cause a great decrease in ^{125}I -MIBG concentration in the rat cardiac tissue, mainly the left atrium (166).

In conclusion, there seems to be a growing awareness in the Nuclear Medicine community to the possibility of utilizing pharmacological agents in conjunction with Nuclear Medicine procedures. The major reasons for such combined studies are to aid in diagnosis, to minimize bodily exposure to the radiopharmaceutical used, and to explore mechanisms of localization of new receptor-binding RPs. Such goals will not only develop RPs of higher specificity, but will enhance the integration between Nuclear Medicine diagnosis and the pharmacological evaluation of the disease process.

ACKNOWLEDGEMENTS

The author wishes to acknowledge helpful discussions of this work with Carol S. Marcus, M.D., Ph.D. and Walter Wolf, Ph.D. This work was supported in part by grant DE-FG03-84-ER-60219 from the U.S. Department of Energy, Office of Health and Environmental Research.

REFERENCES

1. Sefczek, D.M., Sharma, P., Isacs, G.H., Brodmerkel, G.J., Adatepe, M.H., Powell, O.M. and Nichols, K.: J. Nucl. Med. 26, 51-53, 1985.
2. Hladik, W.B., Nigg, K.K. and Rhodes, B.A.: Sem. Nucl. Med. 12, 184-218, 1982.
3. Avery, G.S.: Drugs 14, 132-146, 1977.
4. Wahner, H.W. and Dewanjee, M.K.: J. Nucl. Med. 22, 555-559, 1981.
5. Libby, P., Maroko, P.R., Bloor, C.M., Sobel, B.E. and Braunwald, E.: J. Clin. Investi. 52, 599-607, 1973.
6. Masters, T.N., Harbold, N.B., Hall, D.G., Jackson, R.D., Mullen, D.C., Daugherty, H.K. and Robicsek, F.: Amer. J. Cardiol. 37, 557-563, 1976.
7. Schneider, R.M., Hayslett, J.P., Downing, S.E., Berger, H.J., Donabedian, R.K. and Zaret, B.L.: Circulation 56, 1029-1034, 1977.
8. Bulkley, B.H. and Roberts, W.C.: Amer. J. Med. 56, 244-250, 1974.
9. Chacko, A.K., Gordon, D.H., Bennett, J.M., O'Mara, R.E. and Wilson, G.A.: J. Nucl. Med. 18, 680-683, 1977.
10. Alexander, J., Dainiak, N., Berger, H.J., Goldman, L., Johnstone, D., Reduto, L., Duffy, T., Schwartz, P., Gottschalk, A. and Zaret, B.L.: New Eng. J. Med. 300, 278-283, 1979.
11. Samuels, L.D., Lewis, B., Weiss, A. and Naperstak, E.: JNM 20, 651, 1979.
12. Styles, C.B., Noujaim, A.A., Jugdutt, B.I., Sykes, T.R., Bain, G.O., Shuithay, T.K. and Hooper, H.R.: J. Nucl. Med. 24, 1012-1018, 1983.
13. Lentle, B.C., Scott, J.R., Noujaim, A.A. and Jackson, F.I.: Sem. Nucl. Med. 9, 131-143, 1979.
14. Gorton, S.J., Wilson, G.A., Sutherland, R., Schenk, E., Chacko, A.K., Durakovic, A. and Bennett, J.M.: J. Nucl. Med. 21, 518-522, 1980.

15. Rozanski, A., Berman, D., Levy, R., Maddahi, J., Garcia, E., Gutman, J. and Waxman, A.: *J. Nucl. Med.* 22, p 83, 1981.
16. Borer, J.S., Bacharach, S.L., Green, M.V., Kent, K.M., Johnston, G.S. and Epstein, S.E.: *Circulation* 57, 314-320, 1978.
17. Steingart, R.M., Wexler, J.P. and Blaufox, M.D.: *Sem. Nucl. Med.* 11, 80-88, 1981.
18. Stephens, J.D., Dymond, D.S. and Spurrell, R.A.J.: *Circulation* 61, 536-542, 1980.
19. Shah, P.K., Berman, D., Pichler, M., Shellock, F., Maddahi, J., Waxman, A. and Swan, H.J.C.: *J. Nucl. Med.* 20, 640, 1979.
20. Lyons, K.P., Lyons, J., Eugene, J., McColgan, S., Gelezunas, V. and Swan, L.: *J. Nucl. Med.* 25, p 69, 1985.
21. Chaudhuri, T.K., Sorenson, S. and Groves, B.M.: *JNM* 22, p 41, 1981.
22. Port, S., Lassar, T.A., Patel, S., Ray, G. and Schmidt, D.H.: *J. Nucl. Med.* 24, p 75-76, 1983.
23. Hamilton, G.W., Narahara, K.A., Yee, H., Ritchie, J.L., Williams, D.L. and Gould, K.L.: *J. Nucl. Med.* 19, 10-16, 1978.
24. Sasaki, T., Kojima, S. and Kubodera, A.: *J. Nucl. Med.* 7, 545-548, 1982.
25. Zambova, B., Stojanora, D., Stokie, D., Tadzer, I. and Bogdanova, V.: *Eur. J. Nucl. Med.* 8, 10-11, 1983.
26. Zaret, B.L.: *Circulation* 53 (Supp I) 126-129, 1976.
27. Lameijer, W. and Zwieten, P.A.: *Arch Toxicol.* 42, 33-41, 1979.
28. Wisenberg, G., Zawadowski, A.G., Gebhardt, V.A., Prato, E.S., Goddard, M.D., Nichol, P.H., Rechntzer, P.A. and Gryle-Becker, B.: *JNM* 25, 1161, 1984.
29. Berger, H.J., Lachman, A., Giles, R.W., Sands, M., Zito, R., Goodyer, A.V.N. and Zaret, B.L.: *J. Nucl. Med.* 22, p. 16, 1981.
30. Port, S., Cobb, F.R. and Jones, R.H.: *Circulation* 61, 358-366, 1980.
31. Schachner, E.R., Oster, Z.H., Cicale, N.R., Sacker, D.F., Son, P., Atkins, H.L. and Brill, A.B.: *Eur. J. Nucl. Med.* 6, 585-586, 1981.
32. Firth, B.G., Dehmer, G.J., Corbett, J.R., Lewis, S.E., Parkey, R.W. and Willerson, J.T.: *Amer. J. Cardiology* 46, 481-490, 1980.
33. Freeman, M., Palac, R., Virupannavar, S., Mason, J., Barnes, W.E., Eastman, G., Loeb, H. and Kaplan, E.: *J. Nucl. Med.* 24, p. 54, 1983.
34. Waschek, J., Hinkle, G., Basmadjian, G., Allen, E.W. and Ice, R.D.: *Amer. J. Hosp. Pharm.* 38, 1726-1728, 1981.
35. Brown, L.E., Mangner, T.J., Marsh, D.D., Otto, C.A., Wieland, D.M. and Beierwaltes, W.H.: *J. Nucl. Med.* 22, p 73, 1981.
36. Moins, N., Gachon, P. and Maublant, J.: *J. Nucl. Med.* 23, 330-336, 1982.
37. Maublant, J.C., Moins, N., Gachon, P., Ross, M.R. and Davidson, W.D.: *J. Nucl. Med.* 26, 626-629, 1985.
38. Chandler, W.M. and Shuck, L.D.: *J. Nucl. Med.* 16, 518-519, 1975.
39. McRae, J., Sugar, R.M., Shipley, B. and Hook, G.R.: *JNM* 15, 151-155, 1974.
40. Rosenthal, L., Ambhanwong, S. and Stratford, J.: *Radiology* 92, 1467-1472, 1969.
41. Makler, P.T., Gutowicz, M.F. and Kuhl, D.E.: *Clin. Nucl. Med.* 3, 22-23, 1978.
42. Fletcher, J.W., George, E.A., Henry, R.E. and Donati, R.M.: *J. Amer. Med. Assn.* 232, 1261-1263, 1975.
43. Quaife, M.A., Wulf, B.G., Gust, W.F., Consigny, P.M. and Grissom, R.L.: *J. Nucl. Med.* 24, P130, 1983.
44. Som, P., Oster, Z.H., Yamamoto, K., Meinken, G.E., Srivastava, S.C., Yonekura, Y., Ebner, S.A., Atkins, H.L., Brill, A.B., Fawwaz, R.A., Alderson, P.O., Coffey, J., Carlton, E. and Hubner, K.F.: *Intern. J. Nucl. Med. Biol.* 12, 185-186, 1985.
45. Lamont, C.M. and Adams, F.G.: *Eur. J. Nucl. Med.* 7, 387-388, 1982.
46. Frost, J.J., Dannals, R.F., Ravert, M.T., Wilsom, A.A., Links, J.M., Trifiletti, R., Synder, S.H. and Wagner, H.N.: *J. Nucl. Med.* 26, p 52, 1985.
47. Wong, D.F., Wagner, H.N., Coyle, J. et al, *J. Nucl. Med.* 26, p 52-53, 1985.
48. Rao, S.A., Knobel, J. and Collier, B.D.: *J. Nucl. Med.* 26, p 95-96, 1985.
49. Kulkarni, P.V., Parkey, R.W., Wilson, J.E., Lewis, S.E., Buja, L.M., Bonte, F.J. and Willerson, J.T.: *J. Nucl. Med.* 21, 117-121, 1980.

50. Hegge, F.N., Hamilton, G.W., Larson, S.M., Ritchie, J.L. and Richards, P.: J. Nucl. Med. 19, 129-134, 1978.
51. Thrall, J.H. and Swanson, D.P.: J. Nucl. Med. 20, 1214-1215, 1979.
52. Porter, W.C., Dees, S.M., Freitas, J.E. and Dworkin, H.J.: J. Nucl. Med. 24, 383-387, 1983.
53. Zimmer, A.M., Spies, S.M. and Majewski, W.: 2nd Inter. Symp. Radiopharmacology, Chicago, Illinois, Sept. 1981.
54. Lee, H.B., Wexler, J.P., Scharf, S.C. and Blaufox, M.D.: J. Nucl. Med. 24, 397-401, 1983.
55. Bobinat, D.D., Sevrin, R., Zurbiggen, M.T., Spolter, L. and Cohen, M.B.: J. Nucl. Med. 15, 1220-1222, 1974.
56. Chaudhuri, T.K.: Intern. J. Nucl. Med. Biol. 3, 37, 1976.
57. Jaresko, G.S., Zimmer, A.M., Pavel, D.G. and Spies, S.M.: J. Nucl. Med. Technol. 8, 160-161, 1980.
58. Zimmer, A.M. and Pavel, D.G.: Radiology 126, 813-816, 1978.
59. Wang, T.S.T., Fawwaz, R.A., Esser, P.D. and Johnson, P.M.: J. Nucl. Med. 19, 381-383, 1978.
60. Mikhael, M.A. and Evans, R.G.: J. Nucl. Med. 16, 22-27, 1975.
61. Saba, T.M.: Arch Intern. Med. 126, 1031-1052, 1970.
62. Quniones, J.D.: J. Nucl. Med. 14, 443-444, 1973.
63. Kaplan, W.D., Drum, D.E. and Lokich, J.J.: JNM 21, 84-87, 1980.
64. Geronemus, R.G., Auerbach, R. and Tobias, H.: Arch. Derm. 118, 649-651, 1982.
65. Henry, R.E., Fletcher, J.W., Solaric-George, E. and Donati, R.M.: J. Nucl. Med. 15, 343-348, 1974.
66. Berger, P.E., Culhan, J.A.G., Fitz, C.R. and Harwood-Nash, D.C.: Radiology 118, 303-306, 1976.
67. Libonati, M., Malsch, E., Price, H.L., Cooperman, L.H., Baum, S. and Harp, J.R.: Anesthesiology 38, 466-472, 1973.
68. Spencer, R.P., Lange, R.C., Schwartz, A.D. and Pearson, H.A.: J. Nucl. Med. 13, 211-214, 1972.
69. Freeman, L.M., Sugarman, L.A. and Weissmann, H.S.: Sem. Nucl. Med. 11, 186-193, 1981.
70. Krishnamurthy, G.T., Turner, F.E., Mangham, D., Bobba, V.R., White, S.A. and Langrell, K.: J. Nucl. Med. 24, p 38, 1983.
71. Rock, E., Rattner, Z., Malmud, L.S. and Fisher, R.S.: JNM 22 p 88, 1981.
72. Levin, G., Malmud, L.S., Rock, E., Brady, S., Maurer, A.H. and Fisher, R.S.: J. Nucl. Med. 24, p 39, 1983.
73. Majd, M., Reba, R.C. and Altman, R.P.: Sem. Nucl. Med. 11, 194-204, 1981.
74. Hubbard, T., Larson, S.M. and Allen, D.R.: JNM 19, 1089-1090, 1978.
75. Fisher, R.S., Roek, E., Rattner, Z. and Malmud, L.S.: JNM 22, p 29, 1981.
76. Housholder, D.F., Hynes, H.G., Dakhil, S.R. and Marymont, V.: J. Nucl. Med. 26, 474-477, 1985.
77. Richards, A.G. and Brighouse, R.: J. Nucl. Med. 22, 746, 1981.
78. Shafer, R.B., Knodell, R.G., Stanley, L.N. and Elson, M.K.: J. Nucl. Med. 23, p. 28, 1982 and Eur. J. Nucl. Med. 8, 12-14, 1983.
79. Fisher, R.S., Malmud, L.S., Brody, S., DeVegvar, M.L. and Ryan, J.: J. Nucl. Med. 23, p 27, 1982.
80. Malmud, L.S., Brody, S., Ryan, J., DeVegvar, M.L. and Fisher, R.S.: J. Nucl. Med. 23, 689, 1982.
81. Coenegracht, J.M., Oei, T.L. and Van Breda Uriesman, P.J.C.: Eur. J. Nucl. Med. 8, 140-144, 1983.
82. Carr, E.A., Carroll, M. and Montes, M.: Life Sciences 22, 1261-1274, 1978.
83. Carr, E.A., Carroll, M. and Montes, M.: J. Nucl. Med. 22, 526-534, 1981.
84. Powell, M.L. in Handbook of Clinical Nucl. Med. (Martin, P., ed.), Medical Examination Publ. Co., N.Y. pp 238-262, 1977.
85. Parker, J.A., Jones, A.G., Davis, M.A., McIlmoyle, G. and Tow, D.E.: Clin. Nucl. Med. 1, 267-268, 1976.
86. Choy, D., Murray, I.P.C. and Hoschl, R.: Radiology 140, 197-202, 1981.

87. McRae, J., Hambright, P., Valk, P. and Bearden, A.J.: *J. Nucl. Med.* 17, 208-211, 1976.
 88. VanAntwerp, J.D., Hall, J.N., O'Mara, R.E. and Hilts, S.V.: *J. Nucl. Med.* 16, 577, 1975.
 89. Jones, A.G., Francis, M.D. and David, M.A.: *Sem. Nucl. Med.* 6, 3-18, 1976.
 90. Charkes, N.D.: *J. Nucl. Med.* 20, 794-795 (1979).
 91. Lutrin, C.L., McDougall, I.R. and Goris, M.L.: *Radiology* 128, 165-167, 1978.
 92. Sorkin, S.J., Horii, S.C., Passalqua, A. and Braunstein, P.: *Clin. Nucl. Med.* 2, 451, 1977.
 93. Citrin, D.L., Bessent, R.G., Tuohy, J.B., Greig, W.R. and Blumgart, L.H.: *The Lancet* 1, 1132-1133, 1974.
 94. Crawford, J.A. and Gumerman, L.W.: *Clin. Nucl. Med.* 3, 305-307 (1978).
 95. Fogelman, I., Bessent, R.G., Cohen, H.N., Hart, D.M. and Lindsay, R.: *The Lancet* 2, 667-670, 1980.
 96. Ramsingh, P.S., Pujara, S. and Logic, J.R.: *Clin. Nucl. Med.* 2, 206, 1977.
 97. Sagar, V.V., Piccone, J.M. and Charkas, N.D.: *J. Nucl. Med.* 20, 1257-1261, 1979.
 98. Charkes, W.D., Brookes, M. and Makler, P.T.: *J. Nucl. Med.* 20, 1150-1157, 1979.
 99. Kampffmeyer, H.G., Dworkin, H., Carr, E.A. and Bull, F.E.: *Clin. Pharmacol. Therap.* 8, 647-657, 1967.
 100. Hagan, P.L., Halpern, S.E., Stern, P.H., Dabbs, J.E. and Gordon, R.: *Invest. Radiol.* 16, 229-233, 1981.
 101. Stern, P.H., Halpern, S.E., Hagan, P.L. and Chen, A.: *Invest. Radiol.* 17, 386-393, 1982.
 102. Hayes, R.L., Byrd, B.L., Rafter, J.J. and Carlton, J.E.: *J. Nucl. Med.* 21, 361-365, 1980.
 103. Anghileri, L.J., Thouvenot, P., Brunotte, F., Marchal, C. and Robert, J.: *Intern. J. Nucl. Med. Biol.* 9, 195-196, 1982.
 104. Oster, Z.H., Larson, S.M. and Wagner, H.N.: *J. Nucl. Med.* 17, 356-358, 1976.
 105. Larson, S.M., Mahler, D. and Allen, D.R.: *Nuklearmedizin* 17, 95-98, 1978.
 106. Smith, F.W. and Dendy, P.P.: *Brit. J. Radiol.* 54, 398-402, 1981.
 107. Moerlein, S.M., Welch, M.J. and Raymond, K.N.: *JNM* 23, 501-506, 1982.
 108. Oster, Z.H., Som, P., Sacker, D.F., Cicale, N., Brill, A.B. and Atkins, H.L.: *J. Nucl. Med.* 22, p 44, 1981.
 109. Hoffer, P.: *J. Nucl. Med.* 21, 282-285, 1980.
 110. MacMahon, H. and Bekerman, C.: *Radiology* 127, 189-193, 1978.
 111. Bekerman, C., Hoffer, P.B., Bitran, J.D. and Gupta, R.G.: *Sem. Nucl. Med.* 10, 286-301, 1980.
 112. Lentle, B.C., Castor, W.R., Khaliq, A. and Dierich, M.: *J. Nucl. Med.* 16, 374-376, 1975.
 113. Chilton, H.M., Witcofski, R.L., Watson, N.E. and Heise, C.M.: *J. Nucl. Med.* 22, 1064-1068, 1981.
 114. Fletcher, J.W., Herbig, F.K. and Donati, R.M.: *Radiology* 117, 709-712, 1975.
 115. Wagner, H.N., Dannals, R.F., Frost, J.J., Wong, D.F., Ravert, H.T., Wilson, A.A., Links, J.M., Burns, H.D., Kuhar, M.J. and Snyder, S.H.: in RPs and labelled compounds. IAEA Publ., Vienna 503-512 (1985).
 116. Waxman, A.D., Beldon, J.R., Richli, W., Tanasescu, E.D. and Siemsen, J.K.: *J. Nucl. Med.* 19, 480-482, 1978.
 117. Ajmani, S.K. and Pircher, F.J.: *J. Nucl. Med.* 19, 560-561, 1978.
 118. Stepanas, A.V. and Maisey, M.N.: *Brit. J. Radiology* 49, 379-380, 1976.
 119. Kim, Y.C., Brown, M.L. and Thrall, J.H.: *Radiology* 124, 169-175, 1977.
 120. Sagar, V.V. and Piccone, J.M.: *J. Nucl. Med.* 21, p 67, 1980.
 121. Schwesinger, W.H., Straw, J.D. and Chaudhuri, T.K.: *JNM* 22, p 87, 1981.
 122. Williams, J.G.: *J. Nucl. Med.* 24, 633-636, 1983.
 123. Yeker, D., Buyukunal, C., Benli, M., Buyukunal, E. and Urganciooglu, I.: *Eur. J. Nucl. Med.* 9, 316-319, 1984.
 124. Prokop, E.K., Caride, V.J., Winchenbach, K., Troncale, F.T. and McCallum, R.W.: *J. Nucl. Med.* 24, p 57, 1983.

125. Domstad, P.A., Kim, E.E., Coupal, J.J., Beihn, R., Yonts, S., Choy, Y.C., Mandelstam, P. and Deland, F.M.: *JNM* 21, 1098-1100, 1980.
 126. Frank, E.B., Lange, R., Plankey, M. and McCallum, R.W.: *J. Nucl. Med.* 23, p 21, 1982.
 127. McCallum, R.W., Saltzman, M.B., Plankey, M., Lange, R., Walesky, H. and Sherwin, R.: *J. Nucl. Med.* 23, p 21, 1982.
 128. Alavi, A. and McLean, G.K.: *Sem Nucl. Med.* 11, 216-223, 1981.
 129. White, R.I., Harrington, D.P., Novak, G., Miller, F.J., Giargiana, F.A. and Sheff, R.N.: *Radiology* 111, 549-557, 1974.
 130. Khettry, J., Effmann, E., Grard, R.J. and Treves, S.: *Radiology* 120, 629-631, 1970.
 131. Sfakianakis, G.N., Anderson, G.F., King, D.R. and Boles, E.T.: *J. Nucl. Med.* 22, 678-683, 1981.
 132. Slingerland, D.W.: *J. Clin. Endocrinol.* 15, 131-141, 1955.
 133. Wyngaarden, J.B., Wright, B.M. and Ways, P.: *Endocrinology* 50, 537-549, 1952.
 134. Kohn, L.A. and Nichols, E.B.: *New Engl. J. Med.* 253, 286-287, 1955.
 135. Lentle, B.C., Scott, J.R., Noujaim, A.A. and Jackson, F.I.: *Sem. Nucl. Med.* 9, 131-143, 1979.
 136. Magalotti, M.F., Hummon, I.F. and Hierschbiel, E.: *Amer. J. Roentogenology, Radium Therapy and Nucl. Med.* 81, 47-64, 1959.
 137. Leger, A.F., Frogu, P., Rougier, P., Laurent, M.F., Tubiana, M. and Savoie, J.C.: *J. Nucl. Med.* 24, 582-585, 1983.
 138. Connell, J.M.C., Hilditch, T.E., McCruden, D.C., Robertson, J. and Alexander, W.D.: *Eur. J. Nucl. Med.* 9, 464-466, 1984.
 139. Linsk, J.A., Paton, B.C., Persky, M., Isaacs, M. and Kupperman, H.L.: *J. Clin. Endocrin.* 17, 416-423, 1957.
 140. Friedell, M.T.: *J. Amer. Med. Assn.* 167, 983-984, 1958.
 141. Yee, C.A., Lee, H.B. and Blaufox, M.D.: *JNM* 22, 1054-1058, 1981.
 142. Oei, H.Y., Geyskes, G.G., Mees, E.J.D. and Puijlaert, C.B.A.: *J. Nucl. Med.* 25, p 36, 1984.
 143. Koff, S.A., Thrall, J.H. and Keyes, J.W.: *J. Urol.* 122, 451-454, 1979.
 144. Domstad, P.A.: *J. Nucl. Med.* 21, 700-701, 1980.
 145. Majd, M., Kass, E.J., Gainey, M.A., Belman, A.B. and Burnette, D.G.: *J. Nucl. Med.* 23, p 14-15, 1982.
 146. Antar, M.A. and Jones, A.N.: *J. Nucl. Med.* 26, p 131, 1985.
 147. Noujam, A.A., Terner, U.K., Turner, C.J., Nieuwenhuyze, B. and Lentle, B.C.: *Intern. J. Nucl. Med. Biol.* 8, 289-293, 1981.
 148. Wieler, H., Rabs, U., Burger, R. and Hengst, W.: *Eur. J. Nucl. Med.* 8, A70, 1984.
 149. Litterst, C.L.: *Toxicol. Appl. Pharmacol.* 61, 99-108, 1981.
 150. Klintmalm, G.B.G., Klingensmith, W.C., Iwatsuki, S., Schroter, G.P.J. and Starzl, T.E.: *J. Nucl. Med.* 22, p 37, 1981.
 151. Kim, E.E., Gutierrez, C., Sandler, C.M., Flechner, S.M., Van Buren, C.T. and Kahon, B.D.: *J. Nucl. Med.* 24, p 129, 1983.
 152. Chopra, S.K., Taplin, G.V., Sashkin, D.P., Trevor, E. and Elam, D.: *J. Nucl. Med.* 18, 606, 1977.
 153. Sutherland, J.B., McCarthy, D.S., Mark, R.J. and Thorlakson, T.K.: *J. Can. Assn. Radiol.* 29, 82-84, 1978.
 154. Susskind, H., Atkins, H.L., Cohn, S.H., Ellis, K.J. and Richards, P.: *J. Nucl. Med.* 18, 462-471, 1977.
 155. Shafer, R.B. and Bianco, J.A.: *J. Nucl. Med.* 20, 450-452, 1979.
 156. Soil, J.S., McKusick, K.A. and Wagner, H.N.: *J. Amer. Med. Assn.* 224, 1717-1720, 1973.
 157. Mojano-Lopex, V., Miskew, D. and Sansi, P.: *Eur. J. Nucl. Med.* 6, 17-21, 1981.
 158. Cottrall, M.F. and Taylor, D.M.: *Nucl. Med.* 20, 187-190, 1981.
 159. Sarkar, S.D., Cohen, E.L., Beierwaltes, W.H., Ice, R.D., Gill, S.P. and Gold, E.N.: *J. Nucl. Med.* 17, 563, 1976.

160. Hoefnagels, W.H., Claessens, R.A., Corstens, F.H., Drayer, J.T., Kazen, J. and Kloppenborg, P.W.: Nucl. Med. 20, 76-81, 1981.
161. Gross, M.D., Shapiro, B. and Freitas, J.E.: J. Nucl. Med. 26, 43-48, 1985.
162. Thrall, J.H., Gross, M., Freitas, J.E. and Beierwaltes, W.H.: Applied Radiology/Nucl. Med. 9, 115-123, 1980.
163. Gross, M.D., Valk, T.W., Swanson, D.P., Thrall, J.H., Grekin, R.J. and Beierwaltes, W.H.: Sem. Nucl. Med. 11, 128-148, 1981 and J. Nucl. Med. 22, 12-17, 1981.
164. Wieland, D.M., Brown, L.E., Tobes, M.C., Rogers, W.L., Marsh, D.D., Mangner, T.Y., Swanson, D.P. and Beierwaltes, W.H.: J. Nucl. Med. 22, 358-364, 1981.
165. Guilloteau, D., Bauliev, J.L., Huguet, F., Viel, C., Chambon, C., Valat, C., Bauliev, F., Itti, R., Pourcelot, L., Narcisse, G. and Besnard, J.C.: Eur. J. Nucl. Med. 9, 278-281, 1984.
166. Sherman, P.S., Fisher, S.J., Wieland, D.M. and Sisson, J.C.: J. Nucl. Med. 26, p 35, 1985.

DISCUSSION

FRITZBERG: I am concerned about your suggestion that nicotinic acid caused poor Tc-99m HIDA uptake because of GSH conjugation interference. Our work and that of Adrian Nunn with HPLC analysis showed no change in the behavior of Tc-99m iminodiacetate agents in rat bile. What evidence supports conjugation of GSH in the excretion of these agents? I would also add that phenobarbital (Nembutal) markedly reduces gastric motility in dogs and rabbits. As Dr. Gilday mentioned the use of Nembutal in infants, perhaps this effect may be operative and cause concern in hepatobiliary studies.

SHANI: My suggestion was based on a communication by Richards et al (J Nucl Med 22:746, 1981), entitled "Nicotinic Acid - A Cause of Failed HIDA Scanning" which indicated that the mechanism through which the liver excretes HIDA entails a preliminary conjugation with glutathione in the liver cells. The authors tentatively suggested that nicotinic acid interfered with the secretion of HIDA through its toxic effect on the liver cells and that in their study nicotinic acid was the only culprit interfering with the excretion of HIDA. After the nicotinic acid was withdrawn, a normal HIDA scan could be obtained in the patient.

VARIATIONS IN ABSORBED DOSES FROM ^{59}Fe IN DIFFERENT DISEASES

P. Roth, E. Werner, K. Henrichs
Gesellschaft für Strahlen - und Umweltforschung
Paul- Ehrlich-Str. 20
D-6000 Frankfurt am Main, FRG

U. Elsasser, A. Kaul
Bundesgesundheitsamt, Institut für Strahlenhygiene
Ingolstädter Landstr. 1
D-8042 Neuherberg, FRG

ABSTRACT

The biokinetics of radiopharmaceuticals administered *in vivo* may vary considerably with changes in organ functions. We studied the variations in absorbed doses from ^{59}Fe in 207 patients with different diseases, in whom ferrokinetic investigations were performed for diagnostic purposes.

370 kBq ($10\mu\text{Ci}$) ^{59}Fe , bound to autologous transferrin, were injected intravenously. Concentration of ^{59}Fe in blood plasma was measured for 2 weeks and in whole blood for 3 months. External counting over liver, spleen, and sacrum and whole-body counting was carried out for 3 months. A linear compartmental model was assumed to describe radioiron kinetics in man. Transfer rate constants and organ retention functions were estimated from the tracer data by use of the computer program SAAM-25 run on a UNIVAC-1108 computer. From the cumulated activities of the source regions, organ doses and effective dose equivalents (D_E) were calculated according to the MIRD concept.

Radiation doses to the bone marrow were highest in patients with deserythropoietic anaemias (mean 38 nSv/Bq, range 19 - 57 nSv/Bq) and in haemolytic anaemias (mean 21 nSv/Bq, range 7 - 35 nSv/Bq), whereas lower and rather constant values were found in other diseases (mean values between 9 and 13 nSv/Bq). The highest organ doses, the greatest differences with respect to diagnosis and also the largest variations within each group of patients were found for liver and spleen (e. g. in aplastic anaemia; liver: 66 nSv/Bq, range 29 - 104 nSv/Bq; spleen: 57 nSv/Bq, range 34 - 98 nSv/Bq. In iron deficiency; liver: 13 nSv/Bq range 12 - 14 nSv/Bq; spleen: 19 nSv/Bq, range 18 - 20 nSv/Bq). Lower organ doses and smaller variations within and between the groups of patients were found for the gonads (means 3 - 7 nSv/Bq), the kidneys (means 10 - 13 nSv/Bq), the bone (means 4 - 7 nSv/Bq), the lung (means 8 - 12 nSv/Bq), and the total body (means 6 - 8 nSv/Bq). In patients with chronic bleeding absorbed doses decrease concomitantly to the extent of blood loss. The D_E is not markedly affected by the variations in organ doses but is fairly constant for different diseases (mean values from 10 to 15 nSv/Bq). The results of this study in general confirm the findings of the MIRD Dose Estimate Report No. 11. However, in certain clinical conditions the variations in absorbed doses from ^{59}Fe can be significantly larger than anticipated.

INTRODUCTION

Ferrokinetic investigations with radioiron are a useful diagnostic tool for the characterization and investigation of haematological disorders (1,2,3). The biokinetics of radiopharmaceuticals may be different under different pathological conditions and consequently so may be the radiation doses to the patients investigated. We studied the variations in absorbed doses from ^{59}Fe in patients in whom ferrokinetic investigations were performed for diagnostic purposes.

PATIENTS

A total of 207 investigations with ^{59}Fe was performed in patients with various haematological disorders. The distribution of the patients according to diagnosis is shown in Table 1.

Table 1. Distribution of the patients investigated according to diagnosis

DIAGNOSIS	NUMBER OF PATIENTS
HYPPOPLASTIC ANAEMIA	19
HAEMOLYTIC ANAEMIA	12
DYSERYTHROPOIETIC ANAEMIA	12
RENAL FAILURE WITHOUT DIALYSIS	28
RENAL FAILURE HAEMODIALYSIS	9
RENAL FAILURE PERITONEAL DIALYSIS	12
IRON DEFICIENCY BL* < 5	16
BL* 5 - 25	45
BL* 25 - 105	29
BL* > 105	13
OTHER DISEASES	12
TOTAL	207

*BL: MEAN DAILY BLOOD LOSS (ML/DAY)

IRON KINETICS

The ferrokinetic investigations were performed with 370 kBq ($10 \mu\text{Ci}$) ^{59}Fe bound to autologous transferrin (4). After intravenous injection serial plasma samples were measured for 2 weeks.

^{59}Fe activity in red blood cells was measured for a period of 3 - 4 months. Sequential in vivo organ measurements over liver, spleen, and sacrum were performed with a special organ counting device (5). Whole body retention of ^{59}Fe was measured for 3 - 4 months with a whole-body counter (6).

A compartmental model was assumed to describe iron kinetics in man (7). The model chosen (Figure 1) is characterized by the central role of the plasma as the transport compartment from which two distinct iron circuits emerge: iron entering the erythroid pathway either leaves the bone marrow in mature red cells or is involved in ineffective erythropoiesis. In course of the latter these defective cells or cell fragments are phagocytosed and processed by the reticuloendothelial cells (RE cells) of the bone marrow. The iron is then either rapidly released to the plasma again or stored within the RE cells as ferritin (8). The iron in the red cells of the peripheral blood will also reflux to the plasma via the RE cell compartment at the end of the lifespan of the erythrocytes. On the other side there is a bi-directional exchange between the plasma iron and the parenchymal iron stores. A direct transfer of iron from the red blood cell compartment to the tissue stores occurs in haemolysis inside the vascular tree. Iron losses

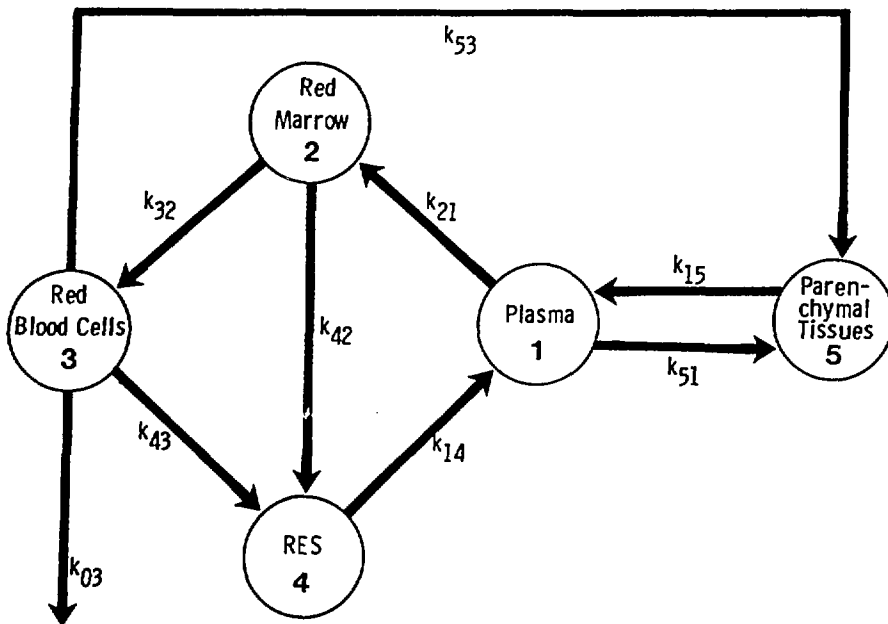


Fig. 1. Compartmental model of iron kinetics in man.

k_{ij} = fractional transfer rates between compartments, k_{03} = excretion rate due to blood losses, RES = Reticuloendothelial System.

by bleeding are represented by a transfer from the red blood cell compartment to the exterior.

The compartmental model of iron kinetics is assumed to be linear, i. e. the distribution of the ^{59}Fe can be described by a set of first order linear differential equations with constant coefficients:

$$\frac{d}{dt} Q_i(t) = \sum_j k_{ij} \cdot Q_j(t) - \sum_j k_{ji} \cdot Q_i(t) \quad (I)$$

where $Q_i(t)$ is the ^{59}Fe activity in compartment i at time t and k_{ij} is the fractional turnover rate from compartment j to compartment i .

The ^{59}Fe activities of the plasma and red cell samples are proportional to the activities in the respective compartments, whereas the external organ measurements have activity contributions from more than one compartment:

$$Q_l(t) = \sum_j s_{lj} \cdot Q_j(t) \quad (II)$$

where l refers to liver, spleen or sacrum and s_{lj} are summation coefficients. Whole-body measurements are special cases of external counting with the sum-

mation coefficients all being unity. For the estimation of the rate constants k_{ij} and the summation coefficients s_{ij} from the tracer data the computer program SAAM25 (Simulation Analysis And Modelling) was used (9). The program determines iteratively a set of parameter values by a non-linear least square fitting procedure that provides a best fit of the model solutions to the experimental data. The quantitative analysis of external organ measurements requires a careful calibration of the counting device to correct for different dimensions of the organs, different depths of tissue and count rate contributions from other organs (5). The SAAM program has some special advantages that make it very suitable for the analysis of tracer data, in that more than one observable (retention or clearance curve) can be analyzed simultaneously, and in that the measured quantities may also be linear combinations of compartments (as in the organ measurements).

From the transfer rates the compartment sizes and the intercompartmental iron fluxes can be calculated for steady-state conditions.

DOSE CALCULATIONS

The calculations of absorbed doses were based on the method described in MIRD Pamphlet No. 1, revised (10). The mean absorbed dose $\bar{D}(r_k)$ in any target region r_k is given by:

$$\bar{D}(r_k) = \sum_h \tilde{A}_h \cdot S(r_k \leftarrow r_h) \quad (\text{III})$$

where \tilde{A}_h is the cumulated activity in source region h , $S(r_k \leftarrow r_h)$ is the absorbed dose in target region r_k from any source region r_h , and h is the number of source regions. The source organs for ^{59}Fe were liver, spleen, red marrow, lung, kidneys, and residual.

From the organ doses $\bar{D}(r_k)$ the effective dose equivalent D_E was calculated by:

$$D_E = \sum_k w_k \cdot \bar{D}(r_k)$$

where w are the risk weighting factors as described in ICRP Publication No. 26 (11).

The required S values were taken partly from MIRD Pamphlet No. 11 (12). For those organs, for which individual organ masses were available (liver, spleen, total body) S values corrected for the masses were used (13). Liver and spleen masses were determined sonographically at the beginning of the investigation. From the fractional turnover rates k_{ij} the cumulated activities \tilde{a}_i in the compartments can be determined:

$$(a) \quad \begin{pmatrix} \tilde{a}_1 \\ \tilde{a}_2 \\ \vdots \\ \tilde{a}_5 \end{pmatrix} = (K - \lambda I)^{-1} \cdot Q(0) \quad (\text{IV})$$

where K is the matrix of the fractional turnover rates, I is the unity matrix, and λ is the physical decay constant for ^{59}Fe .

The contributions of the compartments to the activities in the source organ are shown in Table 2. The values for the fractions of the blood compartments, s_{11} (= plasma) and s_{13} (= erythrocytes), were taken from ICRP-Publication 23 (14). The contributions of compartment 4, s_{14} (= RES), and compartment 5, s_{15} (= parenchymal iron stores) to the liver and spleen activities were determined individually from the organ measurements.

Table 2. Fractional distribution of the compartments to the activities in source organs

SOURCE ORGANS	COMPARTMENTS				
	PLASMA (1)	ERYTHROCYTES (3)	RED MARROW (2)	RES (4)	PARENCHYMAL TISSUES (5)
LIVER (a)	$S_{a1} \cdot \tilde{\alpha}_1$	$S_{a3} \cdot \tilde{\alpha}_3$	-	$S_{a4} \cdot \tilde{\alpha}_4$	$S_{a5} \cdot \tilde{\alpha}_5$
LUNG (b)	$S_{b1} \cdot \tilde{\alpha}_1$	$S_{b3} \cdot \tilde{\alpha}_3$	-	-	-
SPLEEN (c)	$S_{c1} \cdot \tilde{\alpha}_1$	$S_{c3} \cdot \tilde{\alpha}_3$	-	$S_{c4} \cdot \tilde{\alpha}_4$	$S_{c5} \cdot \tilde{\alpha}_5$
KIDNEYS (d)	$S_{d1} \cdot \tilde{\alpha}_1$	$S_{d3} \cdot \tilde{\alpha}_3$	-	-	-
RED MARROW (e)	$S_{e1} \cdot \tilde{\alpha}_1$	$S_{e3} \cdot \tilde{\alpha}_3$	$1.0 \cdot \tilde{\alpha}_2$	-	-
RESIDUAL (f)	$(1 - \sum S_{11}) \tilde{\alpha}_1$	$(1 - \sum S_{13}) \tilde{\alpha}_3$	-	$(1 - S_{a4} - S_{c4}) \cdot \tilde{\alpha}_4$	$(1 - S_{a5} - S_{c5}) \cdot \tilde{\alpha}_5$

RESULTS AND DISCUSSION

The results of the dose calculations for ferrokinetic investigations with ^{59}Fe are summarized in Table 3. The table shows the mean values and ranges for the most relevant organ doses and the effective dose equivalents for the different groups of patients. The group of patients "other diseases" was included only for completeness. Because of its heterogeneity, the mean values for this group are of little significance. The highest organ doses were found for bone marrow, liver, and spleen. The radiation dose to the bone marrow was highest in patients with dyserythropoietic anaemias with a mean value of 38 nSv/Bq (range 19 - 57 nSv/Bq) followed by the patients with haemolytic anaemias (mean value 21 nSv/Bq, range 7 - 35 nSv/Bq). In other diseases, the bone marrow dose is fairly constant with mean values ranging from 9 to 13 nSv/Bq. The highest organ doses, the greatest differences with regard to diagnosis, and also the largest variations within each group of patients were found for liver and spleen. The liver doses were highest in the patients with hypoplastic anaemias (mean value 66 nSv/Bq, range 29 - 104 nSv/Bq). The mean liver doses in haemolytic anaemias (34 nSv/Bq) and dyserythropoietic anaemias (27 nSv/Bq) were about half of that but with large individual variations. Nearly identical mean values were found for spleen doses in these groups of patients. Whereas ^{59}Fe accumulation in the spleen is usually a consequence of increased red cell sequestration, ^{59}Fe may enter the liver either via the plasma (bound to transferrin) or in the course of intravascular haemolysis. So, despite the nearly identical mean values for liver and spleen doses in these diseases, the radiation doses to these two organs may differ by a factor of 10 in a particular patient. Much lower organ doses and much smaller variations between and within the groups of patients were found for the gonads (mean values 3 - 7 nSv/Bq), the kidneys (mean values 10 - 13 nSv/Bq), the bone (mean values 5 - 7 nSv/Bq), the lung (mean values 8 - 12 nSv/Bq) and the total body (mean values 6 - 8 nSv/Bq). Normally, only small amounts of iron are excreted from the body (about 0.03 % of body iron content per day). However, in patients with chronic bleeding, absorbed doses decrease concomitantly to the extent of blood loss (Table 3).

Table 3. Organ doses and effective dose equivalents (D_E) to patients undergoing ferrokinetic investigations with ^{59}Fe .
Mean values and ranges (nSv/Bq)

DIAGNOSIS	ORGAN DOSE (nSv/Bq)							D_E (nSv/Bq)
	BONE MARROW	LIVER	SPLEEN	GONADS	KIDNEYS	BONE	LUNG	
HYPOPLASTIC ANAEMIA	9 (5 - 13)	66 (29-104)	57 (34-98)	3 (1 - 5)	11 (10-13)	5 (3 - 6)	8 (7 - 9)	15 (11-18)
HAEMOLYTIC ANAEMIA	21 (7 - 35)	34 (8 - 61)	34 (2 - 65)	4 (3 - 6)	11 (3 - 13)	6 (5 - 8)	10 (7 - 11)	12 (9 - 16)
DYSERYTHROPOIETIC ANAEMIA	38 (19 - 57)	27 (8 - 46)	29 (13-45)	3 (2 - 4)	10 (9 - 12)	7 (6 - 9)	8 (7 - 10)	14 (12-15)
RENAL FAILURE WITHOUT DIALYSIS	13 (10- 17)	13 (10- 17)	22 (13-32)	6 (5 - 7)	12 (11-13)	6 (5 - 7)	11 (10-12)	10 (9 - 11)
RENAL FAILURE HAEMODIALYSIS	12 (10- 15)	16 (6 -25)	29 (17-41)	5 (5 - 6)	11 (10-12)	6 (5 - 7)	10 (9 - 11)	10 (8 - 11)
RENAL FAILURE PERITONEAL DIALYSIS	12 (10- 14)	14 (10- 18)	25 (10-41)	7 (3 - 11)	12 (11-14)	5 (5 - 8)	11 (10-12)	11 (8 - 12)
IRON DEFICIENCY BL* < 5	13 (12- 14)	13 (12- 14)	19 (19-20)	6 (5 - 7)	11 (11-12)	6 (5 - 7)	11 (10-11)	10 (9 - 10)
BL* 5 - 25	12 (11- 12)	11 (10- 11)	18 (17-18)	6 (5 - 7)	13 (12-13)	6 (5 - 7)	12 (12-13)	9 (8 - 10)
BL* 25 - 105	9 (8 - 10)	7 (5 - 9)	11 (9 -14)	4 (3 - 5)	8 (6 - 9)	4 (3 - 5)	7 (6 - 9)	6 (5 - 7)
BL* > 105	7 (6 - 8)	4 (3 - 5)	6 (4 - 8)	2 (2 - 3)	5 (3 - 6)	3 (2 - 3)	4 (2 - 4)	4 (3 - 5)
OTHER DISEASES	18 (5 - 32)	26 (7 - 45)	23 (9 -37)	5 (4 - 7)	12 (10-13)	7 (5 - 8)	10 (9 -12)	11 (10-12)

*BL: MEAN DAILY BLOOD LOSS (ML/DAY)

The calculation of the effective dose equivalent is not markedly affected by the variations in organ doses. For all the pathological conditions investigated, it is fairly constant within and between the groups of patients (mean values between 10 and 15 nSv/Bq).

A task group of the MIRD Committee recently published a dose estimate report for radioactive iron isotopes in ferrokinetic investigations (15). The authors assume also a compartmental model for iron kinetics in man which in its essential parts is similar to the one proposed in the present study. The only major difference is that the red blood cell compartment is assumed to retain the iron for 120 days, after which time the iron is transferred to the rapidly equilibrating tissue compartment. This assumption, however, is seriously jeopardized in many situations in which ferrokinetic investigations are required. In almost all diseases, the red cell life span is shortened to varying extents. Additional blood losses may further reduce the residence time of red blood cells in the circulation. A half-time of as short as 13 days was found in our patients with occult blood losses of more than 105 ml/day. The tracer data, on which the dose calculations in the MIRD report are based, were collected from different studies with different experimental procedures. It should be emphasized, for example, that the radioiron should not be administered directly, but that a proper labelling procedure for the transferrin be employed (4). Nevertheless, the dose estimates of the present study and the values of the MIRD report show quite a close agreement for the comparable groups of patients, for example for the patients with iron deficiency anaemia. On the other hand variations in organ doses with regard to diagnoses are much larger in the present study than in the MIRD report. This could be partly due to the different diseases studied, but it is more likely that it is a result of the more elaborate data acquisition and analysis in this study. Especially iron excretion by blood losses may be a dose reducing factor in many diseases and is often more important than the normal iron excretion rate of about 0.5 mg/day. Dose calculations based on the even less realistic ICRP model for iron kinetics have recently been reviewed critically (16). The ICRP model is a non-circulating first order model, with compartments represented by organs (liver, spleen, other soft tissue) rather than physiological compartments. The ICRP model seems not to describe iron kinetics adequately, even not for radiation protection purposes. Whereas for ^{59}Fe the differences in dose calculations for different models and different diseases may still be tolerable (as the relatively constant D_E values show), this will be completely different for other radioactive iron isotopes. The disagreement between the models for absorbed doses increases with the half-life of the radioisotopes. Since some radioactive isotopes of iron are potentially important as internal contaminants in both occupational and environmental settings, a realistic model for iron metabolism is of major importance in radiation protection, whereas individual variations in the biokinetic parameters are of less significance.

The authors gratefully acknowledge the skillful technical assistance of Ms. H. Hahn, Ms. U. Tacke, and Mrs. B. Moock.

This work was supported in part by grant St. Sch. 757i, Bundesminister des Inneren.

REFERENCES

1. Finch, C. A., K. Deubelbeiss, J. D. Cook, J. W. Eschbach, L. A. Harker, D. D. Funk, G. Marsaglia, R. S. Hillman, S. Glickter, J. W. Adamson, A. Ganzioni, and E. R. Giblett, Ferrokinetics in man. Medicine. 49.17 - 53 1970.

2. Cavill, I., C. Ricketts, J. A.F. Napier, and A. Jacobs. Ferrokinetics and erythropoiesis in man: Red-cell production and destruction in normal and anaemic subjects. *Br. J. Haemat.* 35. 33 - 40, 1977.
3. Berzuini, C., P. Colli Franzone, M. Stefanelli, and C. Viganotti. Iron kinetics: Modelling and parameter estimation in normal and anaemic states. *Comp. Biom. Res.* 11. 209 - 227, 1978.
4. Cavill, I. The preparation of ^{59}Fe -labelled transferrin for ferrokinetic studies. *J. Clin. Path.* 24. 472 - 474, 1971.
5. Roth, P. and E. Werner. Einsatz von Teilkörperzählern für Organmessungen bei Ferrokinetikuntersuchungen, in *Medizinische Physik '81*, edited by E. Bunde, pp. 737 - 741, A. Hüthig Verlag, Heidelberg, 1981.
6. Werner, E., S. M. Morsy, W. Stahlhofen, and W. Pohlit. A whole-body counter with invariant response, in *Diagnosis and Treatment of Incorporated Radionuclides*, pp. 231 - 235, International Atomic Energy Agency, Vienna, 1976.
7. Werner, E., P. Roth, and J. P. Kaltwasser. Ferrokinetik. Der Nuklear-mediziner. 4. 141 - 160, 1981.
8. Fillet, G., J. D. Cook, and C. A. Finch. Storage iron kinetics. VII: A biological model for reticuloendothelial iron transport. *J. Clin. Invest.* 53. 1527 - 1533, 1974.
9. Foster, D. M. and R. C. Boston. The use of computers in compartmental analysis: The SAAM and CONSAM programs, in *Compartmental Distribution of Radiotracers*, edited by J. S. Robertson, pp. 73 - 142, CRC Press, Boca Raton, Florida, 1983.
10. Loevinger, R., and M. Berman. A revised schema for calculating the absorbed dose from biologically distributed radionuclides. *MIRD Pamphlet No. 1*, Revised, New York, Society of Nuclear Medicine, 1976.
11. Recommendations of the International Commission of Radiation Protection. *ICRP Publication 26*, Pergamon Press, Oxford, 1976.
12. Snyder, W. S., M. R. Ford, G. G. Warner, and S. B. Watson. "S", Absorbed dose per unit cumulated activity for selected radionuclides and organs. *MIRD Pamphlet No. 11*, New York, Society of Nuclear Medicine, 1975.
13. Roedler, H. D., and A. Kaul. Dose to target organs from remaining body activity: results of the formally exact and approximate solution. In *Radio-pharmaceutical Dosimetry Symp.*, HEW Publ.(FDA) 76 - 8044, pp. 155 - 163, 1976.
14. Snyder, W. S. (Chairman). Report of the Task Group on Reference Man. *ICRP Publication 23*, Pergamon Press, New York, 1975.
15. Robertson, J. S., R. R. Price, T. F. Budinger, V.F. Fairbanks, and M. Pollicove. Radiation absorbed doses from iron-52, iron-55, and iron-59 used to study ferrokinetics. *MIRD Dose Estimate Report No. 11*. *J. Nucl. Med.* 24. 339 - 348, 1983.
16. Johnson, J. R., and D. W. Dunford. Comparison of the ICRP and MIRD models for Fe metabolism in man. *Health Physics*. 49. 211 - 219, 1985.

DISCUSSION

BRILL: Would you indicate the previous dose estimates with which your findings disagreed? I wonder if the lack of fine structure, such as a delay line in the bone marrow, may account for some of the discrepancies. In particular, do you differ significantly from the MIRD dose estimates?

ROTH: The dose estimates of our study and the values given in MIRD Dose Estimate Report No. 11 agree quite well for comparable groups of patients. The variations in organ doses with regard to different diseases, however, are much larger in the present study than in the MIRD report. There are large discrepancies with regard to ICRP 17. Dose calculations, based on the ICRP model for iron metabolism should no longer be used, because the present data, as well as the results of the MIRD report, show that the ICRP model does not describe iron kinetics adequately.

The introduction of a delay line in the bone marrow compartment would be required for iron isotopes with a short half-life such as Fe-52. For Fe-59 this seems to be of little significance for the dose calculations.

A Kinetic Model for the Dosimetry of Radiopharmaceuticals Contaminated by Mo-99

Douglas R. Shearer, Ph.D. and John C. Pezzullo, Ph.D.
Rhode Island Hospital, Providence, RI

Introduction

Radiopharmaceuticals tagged with Tc-99m may become contaminated with breakthrough products from the Mo-99/Tc-99m generator. If a fraction of the contaminant becomes bound to the radiopharmaceutical, the dose to the radiopharmaceutical target organ from the contaminant must be considered. The dose to the contaminant target organ may then be calculated as the sum of the doses from a) the initially unbound contaminant, and b) the contaminant later released by degradation of the radiopharmaceutical.

This paper presents a model which takes the above processes into account. The model is illustrated with clinical data derived from Mo-99 contaminated radiopharmaceuticals.

Method

For simplicity, the model assumes only two compartments with simple exponential elimination. If adequate biological data is available, the model can be extended appropriately. The compartments shown in Fig. 1 are the target organ (A) for the radiopharmaceutical and the organ (B) which takes up the unbound contaminant.

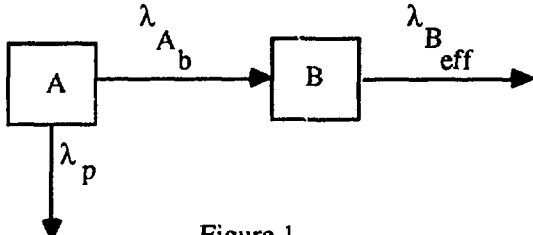


Figure 1

The rate constants shown in Figure 1:

$$\lambda_{A_b} = \lambda_{A_{eff}} - \lambda_p \quad (1)$$

and

$$\lambda_{B_{eff}} = \lambda_{B_b} + \lambda_p \quad (2)$$

Where:

λ_{A_b} = the biological decay constant for the target organ

$\lambda_{A_{eff}}$ = the effective decay constant for the target organ

λ_p = the physical decay constant for the contaminant

$\lambda_{B_{eff}}$ = the effective decay constant for the organ which takes up the unbound contaminant

λ_{B_b} = the biological decay constant for the organ which takes up the unbound contaminant

For the contaminant which is initially bound to the radiopharmaceutical, the kinetics can be described by:

$$[A] = [A_0] e^{-\lambda_{A_{eff}} t} \quad (3)$$

$$\frac{d[B]}{dt} = [A] \lambda_{A_b} - [B] \lambda_{B_{eff}} \quad (4)$$

Where:

$[A]$ = the activity of contaminant in the target organ at any time t ,

$[A_0]$ = the initial activity of contaminant in the target organ,

$[B]$ = the activity of contaminant in organ B at any time t .

This leads to an expression for the activity of contaminant in organ B at any time t :

$$[B] = [A_0] \cdot \frac{\lambda_{A_b}}{\lambda_{B_{eff}} - \lambda_{A_{eff}}} \left\{ e^{-\lambda_{A_{eff}} t} - e^{-\lambda_{B_{eff}} t} \right\} \quad (5)$$

Integration of this expression from $t=0$ to $t=\infty$ yields the cumulative activity $\tilde{[B]}$

$$\tilde{[B]} = [A]_0 \frac{\lambda_{A_b}}{\lambda_{A_{\text{eff}}} * \lambda_{B_{\text{eff}}}} \quad (6)$$

In the general case, only a fraction of the contaminant will be bound to the radiopharmaceutical. The remainder is free and assumed to be directly taken up by organ B.

Thus, the activity of contaminant in organ B at any time t is given by:

$$\begin{aligned} \tilde{[B]} &= f [A]_{\text{tot}} e^{-\lambda_{B_{\text{eff}}} t} \\ &+ (1-f) [A]_{\text{tot}} \frac{\lambda_{A_b}}{\lambda_{B_{\text{eff}}} - \lambda_{A_{\text{eff}}}} \left\{ e^{-\lambda_{A_{\text{eff}}} t} - e^{-\lambda_{B_{\text{eff}}} t} \right\} \end{aligned} \quad (7)$$

where:

f = the fraction of contaminant which is directly taken up by organ B,

$(1-f)$ = the bound fraction of contaminant which is taken up directly by the target organ A, and

$[A]_{\text{tot}}$ = the total activity of administered contaminant.

The cumulative activity in the organs is then given by:

$$\tilde{[B]} = [A]_{\text{tot}} \left\{ \frac{f}{\lambda_{B_{\text{eff}}}} + \frac{(1-f)}{\lambda_{A_{\text{eff}}} * \lambda_{B_{\text{eff}}}} \right\} \quad (8)$$

and

$$\tilde{[A]} = [A]_{\text{tot}} \frac{(1-f)}{\lambda_{A_{\text{eff}}}} \quad (9)$$

Thus, the kinetics of organ B can be described as a combination of the two curves given by equations (3) and (5), and sketched in Fig. 2. The relative contribution of each curve depends on the fraction of contaminant bound to the pharmaceutical.

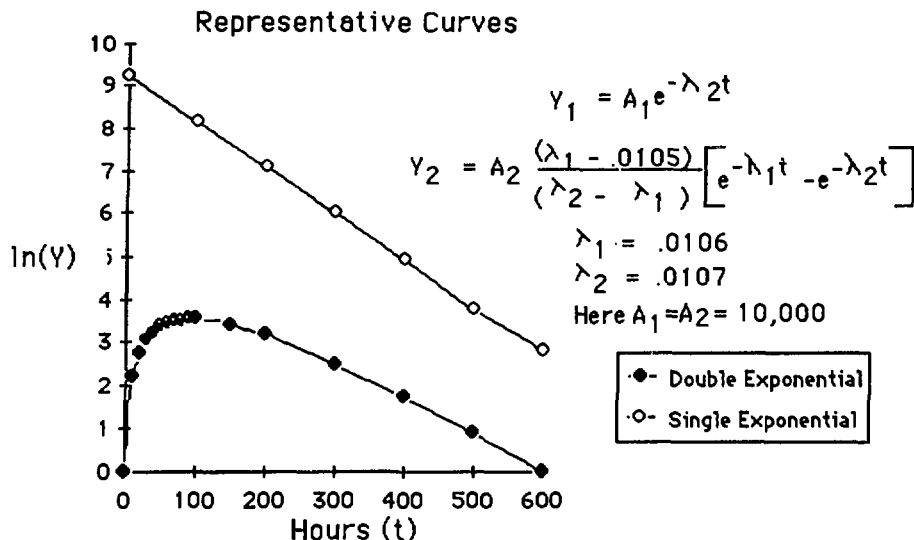


Figure 2

The shape of the curve described by equation (5) is determined by the values of $\lambda_{A_{eff}}$ and $\lambda_{B_{eff}}$ if λ_p is a constant. The minimum values of these parameters are constrained by the condition:

$$\lambda_{A_{eff}} \text{ and } \lambda_{B_{eff}} \geq \lambda_p \quad (10)$$

The time of maximum uptake by organ B (t_{max}) is given by:

$$t_{max} = \frac{1}{\lambda_{B_{eff}} - \lambda_{A_{eff}}} \ln \left\{ \frac{\lambda_{B_{eff}}}{\lambda_{A_{eff}}} \left[1 - \frac{f}{(1-f)} \frac{\left(\frac{\lambda_{B_{eff}}}{\lambda_{A_{eff}}} - \frac{\lambda_{A_{eff}}}{\lambda_{A_b}} \right)}{\lambda_{A_b}} \right] \right\} \quad (11)$$

It should be noted that equation (5) becomes indeterminate when

$$\lambda_{A_{eff}} = \lambda_{B_{eff}}$$

In this case, equation (5) reduces to:

$$[B] = [A]_0 t \lambda_{A_b} e^{-\lambda_{B_{eff}} t} \quad (12)$$

and equation 7 can be written as:

$$[B] = f [A]_{\text{tot}} e^{-\lambda_B^{\text{eff}} t} + (1-f) [A]_{\text{tot}} e^{-\lambda_{A_b}^t} - \lambda_{A_b}^t e^{-\lambda_B^{\text{eff}} t} \quad (13)$$

This expression is useful with data where λ_{A_b} is approximately equal to λ_B^{eff} and curve-fitting programs may not converge to give physically useful values for the equation parameters.

$$\tilde{[B]} = \frac{f [A]_{\text{tot}}}{\lambda_B^{\text{eff}}} + \frac{(1-f) [A]_{\text{tot}} \lambda_{A_b}}{\lambda_B^{\text{eff}}^2} \quad (14)$$

and the time of maximum uptake (t_{\max}) is given by:

$$t_{\max} = \frac{(1-f) \lambda_{A_b} - f \lambda_B^{\text{eff}}}{(1-f) \lambda_{A_b} \lambda_B^{\text{eff}}} \quad (15)$$

The above expressions can be used to supply values of $[A]$ and $[B]$, which depend on the rate constants of the biological processes involved, the physical decay constant of the contaminant and the fraction of bound and unbound contaminant.

The dose to an organ is given (1) as:

$$\text{Dose (rads)} = \tilde{[A]} S \quad (16)$$

where:

$\tilde{[A]}$ is the cumulative activity in the organ, and

S is the absorbed dose per unit cumulative activity (rads/ μCi hour).

Application

Sixteen subjects were injected with Tc-99m labeled radiopharmaceuticals containing Mo-99 as shown in Table I.

Table I
Patient Data

Patient	Age	Wt.(lbs)	Radiopharmaceutical
A	41	100	MDP ^a
B	24	115	MDP ^a
C	68	140	MDP ^a
D	38	120	MDP ^a
E	46	150	MDP ^a
F	84	150	MDP ^a
G	68	160	MDP ^a
H	10	50	MDP ^a
I	75	123	SC ^b
J	75	92	SC ^b
K	75	100	SC ^b
L	48	184	SC ^b
M	1	15	DTPA ^c
N	59	140	MAA ^d
O	38	130	DISIDA ^e
P	63	230	TcO ₄

a = Tc-99m Medronate - bone imaging agent

b = Sulfur colloid liver imaging agent

c = Diethylenetriaminepentaacetic acid chelate - kidney imaging agent

d = Aggregated Albumin lung imaging agent (size range of particles between 15 and 90 microns).

e = Disofenin gall bladder imaging agent

The quantity of Mo-99 associated with each radiopharmaceutical at the time of administration was confirmed by two independent assays of the radiopharmaceutical vials, which agreed to better than 18% in all cases, and usually to better than 10%.

Ten to fourteen days after administration, the collection of biological clearance data from fourteen of the patients was begun using a Gamma camera set on a 20% Tc-99m window. Between two and six measurements were taken from patients over a period of approximately three weeks. The original Tc-99m had decayed by this time, leaving only the Tc-99m produced from the decay of Mo-99. The only detectable Mo-99 was found to be in the liver. The activity of Mo-99 in the liver images was quantitated by using phantoms containing a known activity of Mo-99 uniformly dispersed in water. The Tc-99m levels were allowed to reach equilibrium before measurement. Phantom dimensions were chosen to simulate the range of liver sizes to be expected.

The results of a single exponential least squares fit to the patient data are shown in Table II.

Table II
Single Exponential Model Results

Patient	Radiopharm.	Mo-99 @ t=0 determined by vial assay (mCi)	Extrap. Mo-99 activity @ t=0 (mCi)	Eff. Half-Life in Liver (hrs.)
A	MDP	3.52 ± .63	No Data	No Data
B	MDP	3.52 ± .63	2.18 ± .28	46.3 ± 0.5
C	MDP	2.22 ± .09	1.41 ± .11	52.1 ± 0.7
D*	MDP	2.48 ± .10	9.94 ± 2.5	34.3 ± 1.2
E	MDP	2.63 ± .11	2.24 ± .09	54.5 ± 0.5
F*	MDP	2.62 ± .11	3.57 ± .08	44.9 ± 0.5
G	MDP	2.74 ± .11	1.73 ± .05	60.5 ± 0.5
H*	MDP	0.94 ± .06	3.16 ± .18	48.7 ± 0.2
I	SC	0.47 ± .05	0.27 ± .03	64.3 ± 1.0
J*	SC	0.53 ± .04	2.30 ± .57	42.0 ± 1.4
K	SC	0.59 ± .04	No Data	No Data
L*	SC	0.59 ± .04	1.14 ± .13	48.2 ± 1.0
M*	DTPA	0.40 ± .01	2.07 ± .04	40.8 ± 0.7
N	MAA	0.74 ± .09	Data too poor for estimation	
O	DISIDA	0.74 ± .03	0.31 ± .02	55.4 ± 5.5
P	TcO ₄	3.31 ± .21	1.64 ± .11	61.6 ± 0.2

It can be seen that for six of these patients (denoted by an *) the extrapolated activity is greater than the assayed activity by factors of 1.4, 2.9, 3.4, 4.0, 4.3 and 5.2. These discrepancies are greater than can be explained by experimental or calculational errors.

Thus the single exponential model is not appropriate for these cases and therefore is not generally adequate for labeled radiopharmaceutical cases.

The data can be fitted to equations (7) or (13) with

$$\lambda_p = 0.0105 \text{ hr.}^{-1} \text{ for Mo-99}$$

where it has been assumed that all the administered dose was partitioned between the liver and the radiopharmaceutical target organ. All free molybdenum was assumed to be immediately taken up by the liver. This is probably an overestimate.⁽⁴⁾ Because of the scarcity of data points due to the delay between administration of the Mo-99 and the start of biological measurements, and the lack of information on the fraction of Mo-99 tagged to the radiopharmaceuticals, it is possible to get adequate fits to the data using many values of f. This in turn leads to different values for the effective half-lives and cumulative activity.

Values of the dose to the liver in rads, the effective half-life in the liver, and the target organ dose have been determined assuming different fractions of free molybdenum (f). Values of S have been taken from MIRD tables⁽¹⁾ and adjusted as required for pediatric cases⁽²⁾. The dose to the organ from Tc-99m in equilibrium with Mo-99 has not been included, but would increase the tabulated doses by approximately 9%.

Values for the patients given MDP are given in Table III. Results for the sulfur colloid patients and others are given separately in Tables IV and V. The column labeled Single

Exponential Fit gives the results which would be obtained by extrapolating the data from the patients back to the time of administration. The columns labeled Not Applicable (N/A) are those for which the extrapolated single exponential line lay below that fraction of the administered activity at $t = 0$.

Table III
MDP Patients

Pt.	Single Exponential Model						Two Compartment Model													
	$f = 0.8$						$f = 0.5$						$f = 0.2$				$f \approx 0.1$			
	Liver Dose rads	Liver Teff hrs.	Bone Dose rads	Liver Dose rads	Liver Teff hrs.	Bone Dose rads	Liver Dose rads	Liver Teff hrs.	Bone Dose rads	Liver Dose rads	Liver Teff hrs.	Bone Dose rads	Liver Dose rads	Liver Teff hrs.	Bone Dose rads	Liver Dose rads	Liver Teff hrs.	Bone Dose rads		
B	72.7	46	0	----	N/A	----	63	38	16	40	35	25	33	34	29					
C	53	52	0	----	N/A	----	46	45	11	30	43	17	25	42	19					
D	243	34	0	66	42	4	50	40	10	37	38	15	33	37	17					
E	87	54	0	85	52	5	65	51	12	46	50	18	39	49	20					
F	116	45	0	75	46	5	56	44	12	39	42	12	34	41	23					
G	75	60	0	----	N/A	----	67	55	14	46	53	14	39	53	23					
H	232	49	0	----	----	----	See Text													

Table IV
Sulfur Colloid Patients

Pt.	Single Exponential Model				Two Compartment Model							
			$f = 0.8$		$f = 0.5$		$f = 0.2$		$f = 0.1$			
	Total Liver Dose (rads)	Liver Teff (hrs)	Total Liver Dose (rads)	Liver Teff (hrs)	Total Liver Dose (rads)	Liver Teff (hrs)	Total Liver Dose (rads)	Liver Teff (hrs)	Total Liver Dose (rads)	Liver Teff (hrs)		
I	12.4	64	---	N/A	---	20.3	57	20.6	55	20.8	55	
J	69.6	42	21.4	55	22.8	56	22.4	49	23.4	52		
L	39.6	48.2	24.3	55	26.0	57	25.4	48	27.2	56		

Table V
Other Patients

Pt.	Single Exponential Model				Two Compartment Model					
			f = 0.8		f = 0.5		f = 0.2		f = 0.1	
	Total Dose (rads)	Liver Teff (hrs)	Total Dose (rads)	Liver Teff (hrs)	Total Dose (rads)	Liver Teff (hrs)	Total Dose (rads)	Liver Teff (hrs)	Total Dose (rads)	Liver Teff (hrs)
M (DTPA)	365	40.8	79	56	55	59	30	57	24	54
O (DISIDA)	12.5	55	21.2	46	15.7	44	11.1	42	9.6	41
P (Pertechnetate)	72.9	62	---N/A---		---N/A---		---N/A---		---N/A---	

It can be seen that the single exponential model, while fitting the limited data available, gives a wide range of estimated doses and effective half-lives of Mo-99 in the liver, in addition to overestimating the administered activity in six cases. The two-compartment model gives adequate fits to the clearance data in all but one case and takes the known administered activity into account. Liver doses for the same nominal administered activity are smaller with less variation, and the range of effective half-lives is also slightly decreased. That is, the mean dose for the MDP patients decreases from 98.3 ± 37.7 rads to 57.8 ± 7.8 rads for the case of 50% tagging. These values were derived from the results of patients B, C, D, E, F, and G. The mean effective half-life also decreases from 48.7 ± 7.9 hours to 45.5 ± 5.9 hours. Similarly for the sulfur colloid patients the mean liver dose decreases from 35.3 ± 18.6 rads to 23 ± 2.3 rads for the case of 50% tagging. The corollary is that the target organ dose now has to be considered. Due to the smaller S value for bone (1.4×10^{-4} for MDP assumed to be equally distributed between the cortical and cancellous bone (3), compared with 5×10^{-4} for the adult liver), the sum total of dose is generally decreased. In the case of the sulfur colloid patients, the contaminant can be thought of as being released from one type of cell and taken up by another in the same organ, leaving the dose approximately the same.

In one case (Patient H) the data could not be fitted by the model. A more complex model must then be considered. It is probable that there are several components to the release process from both the radiopharmaceutical target organ and the liver. The simplest case is to assume no biological elimination for a period of time while the radiopharmaceutical is broken down, after which the contaminant is instantaneously made available for release. Thus, 75% of the administered contaminant is assumed to be immediately taken up by the liver⁽⁴⁾ with only physical decay until catastrophic release occurs. Thus a slow component consisting of only the physical decay is followed by a fast component made up of the physical and biological components. The effective decay constant for the liver (fast component) is taken as that determined by the single exponential fit. The interval of time before biological release of the contaminant (T_{rel}) is given by the

intersection point of the fitted single exponential curve and a single exponential curve assuming only physical decay of 75% of the total administered activity.

$$T_{\text{rel}} = \frac{1}{\lambda_{B_{\text{eff}}}^* - \lambda_p} \ln \left\{ \frac{[A]_0^*}{.75 [A]_{\text{tot}}} \right\} \quad (17)$$

where:

$\lambda_{B_{\text{eff}}}^*$ = the effective decay constant from the single exponential fit.

$[A]_0^*$ = the extrapolated initial activity from the single exponential fit.

The dose in this case is given by:

$$D = S_{\text{liver}} \left\{ \frac{.75 [A]_{\text{tot}} (1 - e^{-\lambda_p t_{\text{rel}}}) + \frac{[A]_0^* e^{-\lambda_{B_{\text{eff}}}^* t_{\text{rel}}}}{\lambda_{B_{\text{eff}}}^*}}{\lambda_p} \right\} \quad (18)$$

where S_{liver} is the absorbed dose per unit cumulative activity for the liver.

Doses have been calculated using this model for the 6 patients with the anomalous activities derived from the single exponential fit. The results are given in Table VI.

If a fraction of the molybdenum is assumed to be taken up by the target organ (e.g., bone) a similar process may occur, thus decreasing the dose to the liver. Due to the lack of early data, such a calculation has not been attempted.

Table VI
Catastrophic Release from the Liver

Patient	Radio-pharmaceutical	Assumed Initial Mo-99 Activity (mCi)	Dose (Rads)	Time to Release T_{rel} (hours)
D	MDP	1.86	77	183
F	MDP	1.97	85	121
H	MDP	0.71	66	401
J	SC	0.40	18	296
L	SC	0.44	21	245
M	DTPA	0.30	82	299

Discussion

Although the above example does not validate the proposed model, it does point out limitations of the single exponential approach which may give a considerable overestimate of the administered dose. For a more definitive evaluation of the model, the following work should be carried out:

The degree of Mo-99 tagging to clinically used Tc-99m labeled radiopharmaceuticals, prepared as used clinically, should be determined. Preliminary work has been carried out in this department and indicates that, at least for MDP and sulfur colloid preparations, Mo-99 does tag to the radiopharmaceutical.(5)

The kinetics of well-defined Mo-99 tagged radiopharmaceuticals should be studied in an animal model and the results compared with the theory.

Clinically, in cases where molybdenum contamination is discovered, not only should the amount of administered Mo-99 be determined but the radiopharmaceutical should also be assayed chromatographically to determine the fraction of bound Mo-99. Biological measurements should be performed as soon as possible, preferably starting within 24 hours after administration, to determine the way in which Mo-99 is taken up and excreted from the target organ and the liver.

If these procedures are not followed, dose estimates may be considerably in error.

References

1. MIRD Committee Pamphlet #11. Society of Nuclear Medicine (1975).
2. Cristy,M., Mo-99 and Tc-99m S-factors for children. Metabolism and Dosimetry Group, ORNL, Health and Safety Research Division. (1985)
3. Subramaniam, J. G.; McAfee, G. Blair, R.J., et al. J. Nuc. Med., **16**, 8; 744-755 (1975).
4. Sorenson, L.B. and Archambault, M. Visualization of the liver by scanning with Mo-99 (Molybdate) as tracer. J. Lab & Clin. Med., **62**, 2; 330-339 (1963).
5. Finan, J., Nuclear Medicine Department, P. I. Hospital, Private Communication.

DISCUSSION

CROFT: This is a wonderful piece of work. I can really appreciate the trouble that collecting all this data and making the calculations represent. Could you tell me how this breakthrough occurred and give those of us in clinical nuclear medicine practice some hints about how to avoid it?

SHEARER: The breakthrough was due to a faulty generator. The only way to minimize the consequences of this rare event is to meticulously perform the standard molybdenum-99 breakthrough tests before administration.

S. SRIVASTAVA: In your Table II, the Mo-99 assayed in the vials ranged between about 0.5 to 3.5 mCi. This must have been due to a very unusual situation;

Mo-99 breakthrough is usually never more than about 10^{-5} to 10^{-6} of the Tc-99m activity. If I recall correctly, the accepted limit is only 0.1 mCi per mCi Tc-99m. Assay systems are good enough to detect Mo-99 breakthrough at this level to prevent the Tc from being used in patients if the breakthrough exceeds this limit. Also, is your total dose based on that due to Tc-99m and Mo-99 or just the Mo-99 contamination?

SHEARER: The regulatory limits state that the eluate must not contain more than 1 microcurie of molybdenum-99 for each millicurie of technetium-99m; the total activity administered to the patient must not contain more than 5 microcuries of molybdenum-99. The doses reported here do not include the contribution due to the original technetium-99m administered with the radiopharmaceutical nor the contribution from the technetium-99m in equilibrium with the molybdenum-99 which would increase the dose by 8 or 9% as stated in the written text.

THE INFLUENCE OF RADIOACTIVE CONTAMINANTS ON ABSORBED DOSE ESTIMATES FOR RADIOPHARMACEUTICALS

Evelyn E. Watson and Michael G. Stabin
Oak Ridge Associated Universities
Oak Ridge, Tennessee 37831

ABSTRACT

Several popular radiopharmaceutical products contain low levels of radioactive contaminants. These contaminants increase the radiation absorbed dose to the patient without any increased benefit and, in some cases, with a decrease in image quality. The importance of a contaminant to the radiation dosimetry picture is a function of 1) the contaminant level, 2) the physical half-life of the contaminant, 3) the organ uptake and the biological half-time of the contaminant in the various body systems, and 4) the decay mode, energy, etc. of the contaminant. The general influence of these parameters is discussed in this paper; families of curves are included that reflect the changing importance of contaminant dosimetry with respect to the primary radionuclide as a function of these variables. Several specific examples are also given of currently used radiopharmaceutical products which can contain radioactive contaminants ($I-123$, $In-111$, $Tl-201$, $Ir-191m$, $Rb-82$, $Au-195m$).

INTRODUCTION

Radionuclidic impurities, either as byproducts in accelerator- or reactor-produced radionuclides, or as breakthrough of the parent radionuclide from a radionuclide generator, may be of significant concern in nuclear medicine applications (1-4). These impurities increase the radiation dose to the patient often without any increase and, sometimes with a significant decrease, in image quality. The image quality is usually most seriously affected when the impurity emits high energy photons or has a different biodistribution than the primary radionuclide. The additional radiation dose is sometimes inconsequential; however, in other instances, it constitutes the major fraction of the total organ dose, particularly if the radionuclidic impurities have half-lives significantly longer than that of the primary radionuclide. For this reason, the influence of the radioactive contaminants on the radiation dose estimates for radiopharmaceuticals needs to be considered.

CALCULATION OF RADIATION DOSE ESTIMATES

The general equation that describes the radiation dose to a target organ from a single source organ is (5):

$$\bar{D} = A(0) \tau S \quad (1)$$

where \bar{D} is the mean dose to the target organ,
 $A(0)$ is the administered activity,
 τ is the residence time in a source organ, and
 S is the mean dose to the target per unit cumulated activity.

The S value is the summation of the products of the mean energy emitted per nuclear transition, Δ_i , and the specific absorbed fraction, Φ_i .

The importance of a radioactive contaminant to the risk a patient receives from a nuclear medicine procedure can be studied by defining the ratio of absorbed dose from the contaminant to the dose from the primary radionuclide:

$$\frac{D_c}{D_r} = \frac{A_c(0) \tau_c S_c}{A_r(0) \tau_r S_r} \quad (2)$$

where the subscripts c and r refer to the contaminant and the primary radionuclide, respectively. For simplicity, we will consider the situation where the elimination of the radioactive material can be described by a single exponential. Under this condition, the residence time can be calculated by:

$$\tau = 1.443 f \cdot T_{eff} \quad (3)$$

where f is the fraction of initial activity, $A(0)$, in the source organ and T_{eff} is the effective half-time of activity in the source organ. The effective half-time is defined by the equation

$$T_{eff} = \frac{T_p \cdot T_b}{T_p + T_b} \quad (4)$$

where T_p are the physical half-life and the T_b biological half-time of the radionuclide in the source organ. If the biological half-time of the contaminant is equal to that of the primary radionuclide, the absorbed dose ratio may be expressed as

$$\frac{D_c}{D_r} = \frac{[A_c(0) \cdot f_c] (T_p)_c (T_p + T_b)_r S_c}{[A_r(0) \cdot f_r] (T_p)_r (T_p + T_b)_c S_r} \quad (5)$$

The ratio of $[A(0) \cdot f_c]/[A(0) \cdot f_r]$ is the contaminant level in the organ, and Eq. 5 may be simplified slightly by defining this ratio as L :

$$\frac{D_c}{D_r} = \frac{L (T_p)_c (T_p + T_b)_r S_c}{(T_p)_r (T_p + T_b)_c S_r} \quad (6)$$

From these equations, we can see that the importance of a radioactive contaminant to the radiation dose an organ receives is directly proportional to the contaminant level and the S value of the contaminant but inversely proportional to the sum of the physical half-life and biological half-time of the contaminant. In the situation where the biological half-time is the same for both the primary radionuclide and the contaminant and where the biological half-time is also short compared to the physical half-lives of both radionuclides, the dose ratio is not affected by the physical half-lives because they will cancel out of the equation. If the biological half-time is long compared to the physical half-lives, however, the dose ratio is very sensitive to the physical half-lives of the two radionuclides. Thus, the

influence of the contaminant depends on (1) the contaminant level, (2) the physical half-lives of the contaminant and the primary radionuclide, (3) the organ uptake and biological half-time of the radiopharmaceutical in the body systems, and (4) the decay mode, energy, and other physical factors of the contaminant that are summed up in the S value. If the contaminant is not chemically associated with the pharmaceutical, its effect on the total radiation dose also depends on its own biological half-time. In addition, the distribution of the contaminant within the body will probably be different from that of the primary radionuclide.

Another factor to consider is that the relative contaminant level will not remain constant because the half-life of the contaminant is different from that of the primary radionuclide. If the half-life of the contaminant is longer (which often occurs), the relative contaminant level increases; if it is shorter, the relative contaminant level decreases. Figure 1 illustrates how the contaminant level for Tl-201 can vary over time. The curves in Fig. 1 show the relative activity from 70 hours before calibration to 70 hours after time of calibration (TOC). As shown in Table 1, time of expiry (TOE) for Tl-201 is 6 days after TOC which is much greater than 70 h. Calculations show that the Tl-202 fraction of the total activity has almost tripled by time of expiry. The Tl-200 is almost gone by TOE but, at 70 h before TOC, has a higher relative activity than the Tl-202. Therefore, the user must be aware that dose estimates calculated for the radiopharmaceutical at TOC will not be applicable for all times after receipt of the radionuclide. If the contaminant half-life is longer, the radiation dose may increase and, if the contaminant has photon emissions of higher energy than that of the primary radionuclide, the image quality may also deteriorate. In this situation, the physician will want to exercise care in deciding whether or not the benefit from the study outweighs the risks associated with it.

In Table 1 are listed contaminant levels that may be found in various radionuclide preparations commonly used in nuclear medicine. Contamination of an I-123 pharmaceutical with I-125 will increase considerably over time: 3% at TOC and about 13% at TOE. An I-123 pharmaceutical contaminated with I-124 and Na-24 shows a similar pattern: 6% at TOC and about 15% at TOE. The contaminant level of Ga-66 in a Ga-67 preparation decreases because of its shorter half-life but the Zn-65 will increase somewhat. Marcus et al. (2) have shown that the In-114+In-114m contamination will vary from sample to sample but the values shown Table 1 are representative of those commonly found.

Xenon-133 is contaminated with several radionuclides: Xe-133m, Xe-131m, Kr-85, and even some I-131. In its dose estimate report on xenon (6), the MIRD Committee gave estimates for Xe-131m and Xe-133m that can be used to help assess the contribution that these contaminants make to the total radiation dose from studies performed with Xe-133.

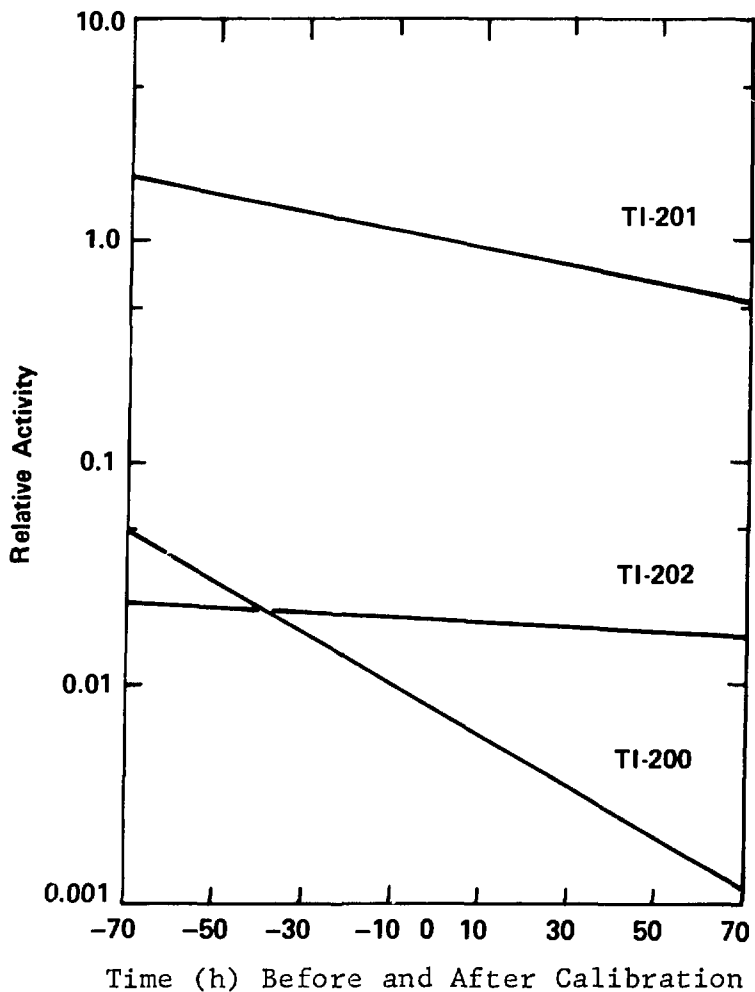


Fig. 1. Relative activity of Tl-200, Tl-201, and Tl-202 as a function of time before and after supplier's calibration time if the Tl-201 preparation contains 0.75% Tl-200 and 1.9% Tl-202 at calibration.

Table 1. Changes in Contaminant Levels as a Function of Time

<u>Radionuclide*</u>	<u>Time of Expiry</u>	<u>Approximate % of Total Activity</u>		
		<u>At 4 h Before TOC</u>	<u>At TOC</u>	<u>At TOE</u>
I-123	30 h after TOC	97.4	97.0	87.3
I-125	TOC	2.3	2.9	12.7
I-121/Te-121		0.3	0.1	0
I-123	30 h after TOC	94.8	94.0	85.3
I-124	TOC	4.2	5.0	13.65
Na-24		0.98	1.0	1.05
Ga-67	14 d after manufacture	99.8	99.8	96.4
Ga-66		0.03	0.02	0
Zn-65		0.2	0.2	3.6
Tl-201	6 d after TOC	97.7	97.8	97.1
Tl-200	(but not to exceed 9 d)	1.1	1.0	0.09
Tl-202		0.96	1.0	2.8
Pb-201	after manufacture)	0.16	0.13	0
Pb-203		0.13	0.13	0.07
In-111 DTPA	7 d after TOC	99.8	99.8	99.0
In-114m + In-114		0.1	0.1	0.5
Zn-65		0.1	0.1	0.5
In-111 oxine	7 d after TOC	99.9	99.9	99.7
In-114m + In-114		0.06	0.06	0.30
Xe-133	14 d after TOC	98.1	98.1	95.5
Xe-133m	(but not to exceed 21 d)	0.31	0.30	0.02
Xe-131m		1.5	1.5	4.1
Kr-85	after manufacture)	0.06	0.06	0.37
I-131		0.01	0.01	0.02

* Primary radionuclide followed by contaminants.

SPECIFIC EXAMPLES

Let us now consider the effects of contamination level and biological half-time on the ratio of the dose from the contaminant to the dose from the primary radionuclide in the situation where the contaminant and the primary radionuclide are isotopes.

I-123 WITH I-125

Figure 2 shows that for I-125 contamination the absorbed dose ratio for the total body being irradiated by the total body continues to increase as the biological half-time increases; however, at the maximum level of I-125 contamination expected at TOE ($L = 0.145$) and with a biological half-time of 10 hr, which is a reasonable half-time in the total body, the absorbed dose from the I-125 is about 0.17 of the absorbed dose from the I-123.

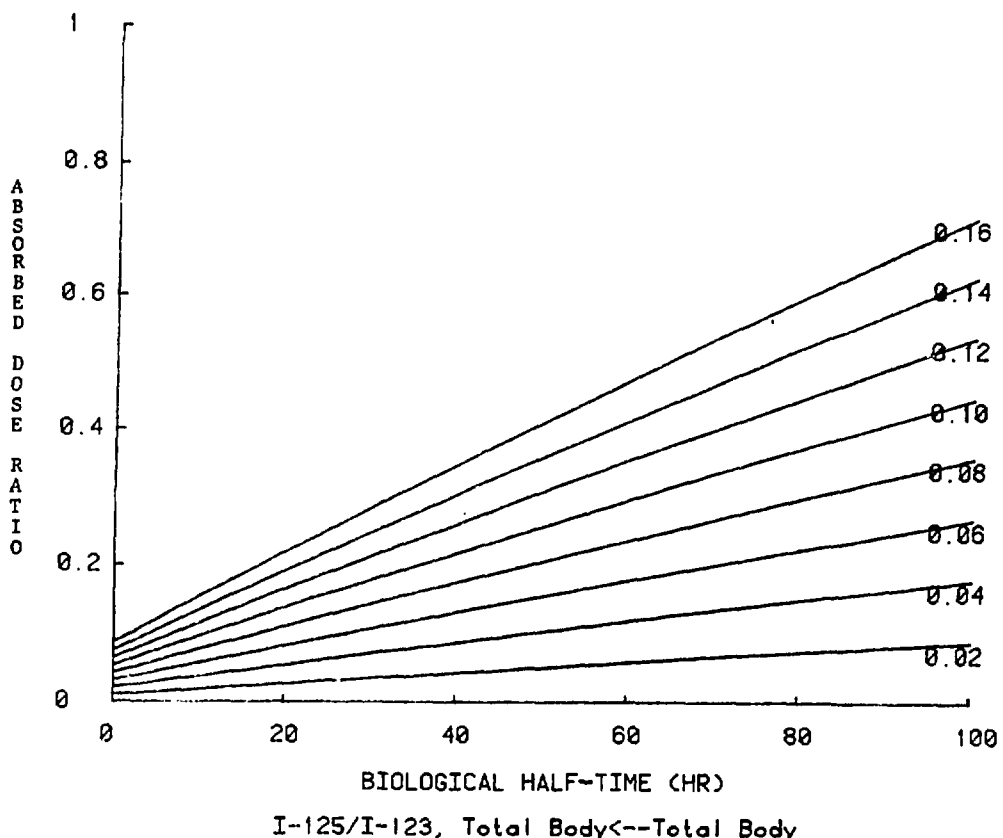


Fig. 2. Absorbed dose ratios for the total body irradiating the total body as a function of biological half-time for different ratios of I-125 to I-123.

The situation is considerably different for the thyroid as shown in Fig. 3 because the biological half-time of iodide in the thyroid can be as long as a hundred or more days. Because the physical half-life of I-125 (60 days) is much longer than that of I-123 (13 h), the absorbed dose to the thyroid from the I-125 will be about equal to the dose from I-123 at a 3% level of contamination and may be 6 times the dose from I-123 at the level that is possible at TOE. We can also see from Fig. 3 that biological half-times longer than the 100 days shown will result in an even larger absorbed dose ratio.

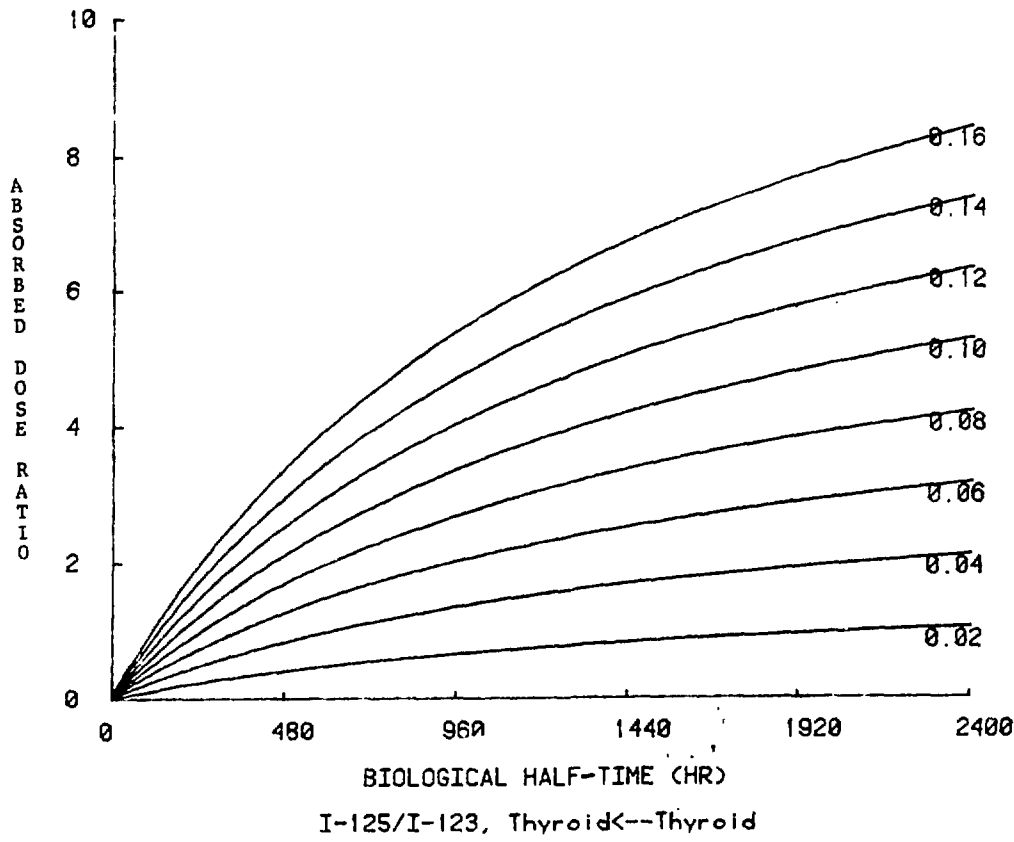


Fig. 3. Absorbed dose ratios for the thyroid irradiating the thyroid as a function of biological half-time for different ratios of I-125 to I-123.

I-123 WITH I-124

The I-124 contaminant will result in an absorbed dose to the thyroid more than twice that from I-123 at TOC if L equals 0.053 and an absorbed dose approximately 7 times the I-123 dose at TOE if L equals 0.16. Also of interest in Fig. 4 is the fact that, unlike the situation with I-125 contamination, longer biological half-times have little effect on the absorbed dose ratio.

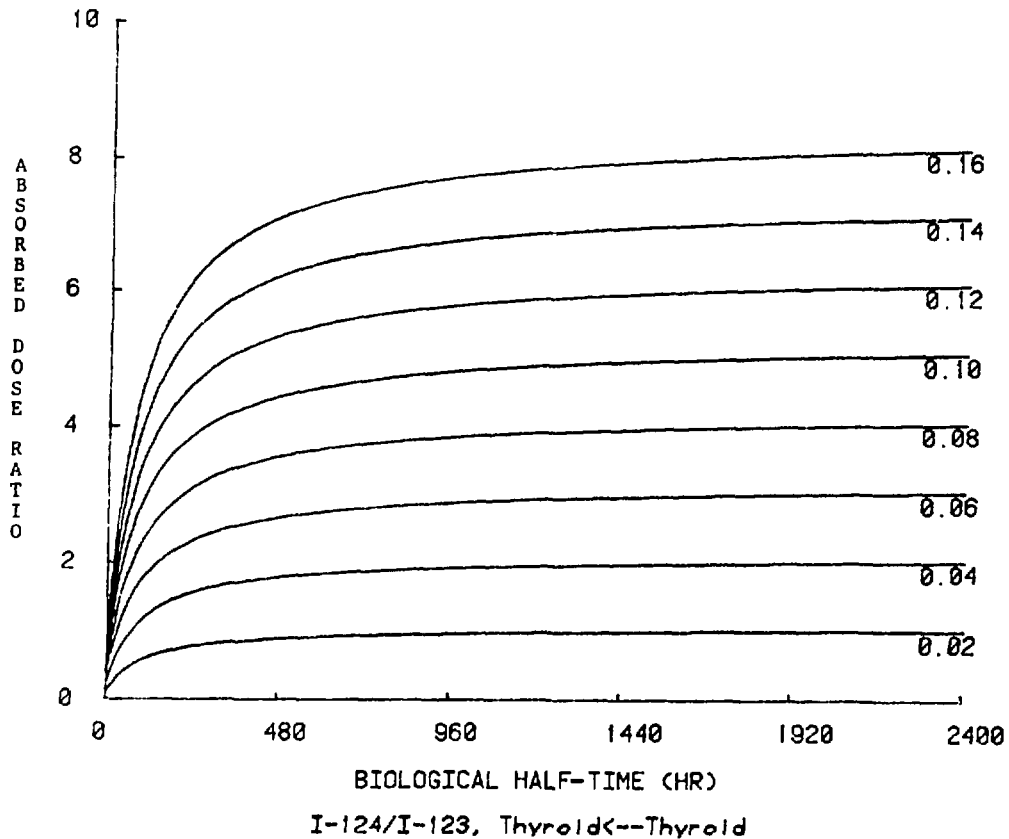


Fig. 4. Absorbed dose ratios for the thyroid irradiating the thyroid as a function of biological half-time for different ratios of I-124 to I-123.

Tl-201 WITH Tl-200+Tl-202

As we would expect, Fig. 5 shows that the absorbed dose ratio for the heart wall is low for Tl-200 and decreases with longer biological half-times.

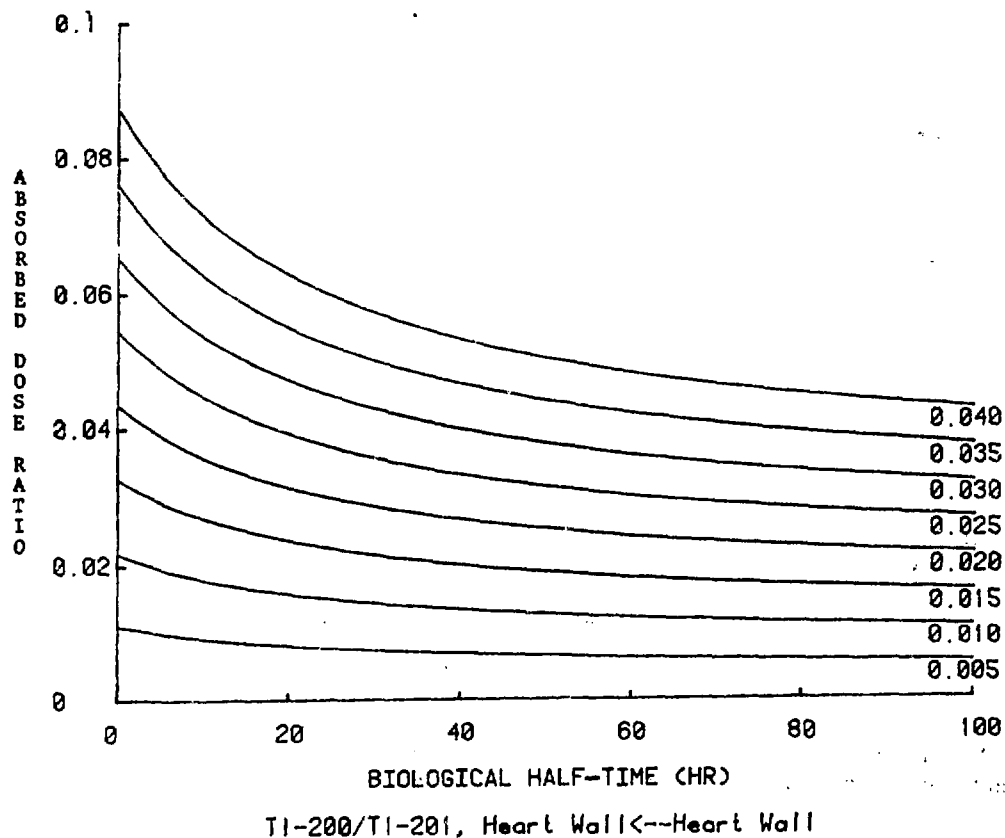
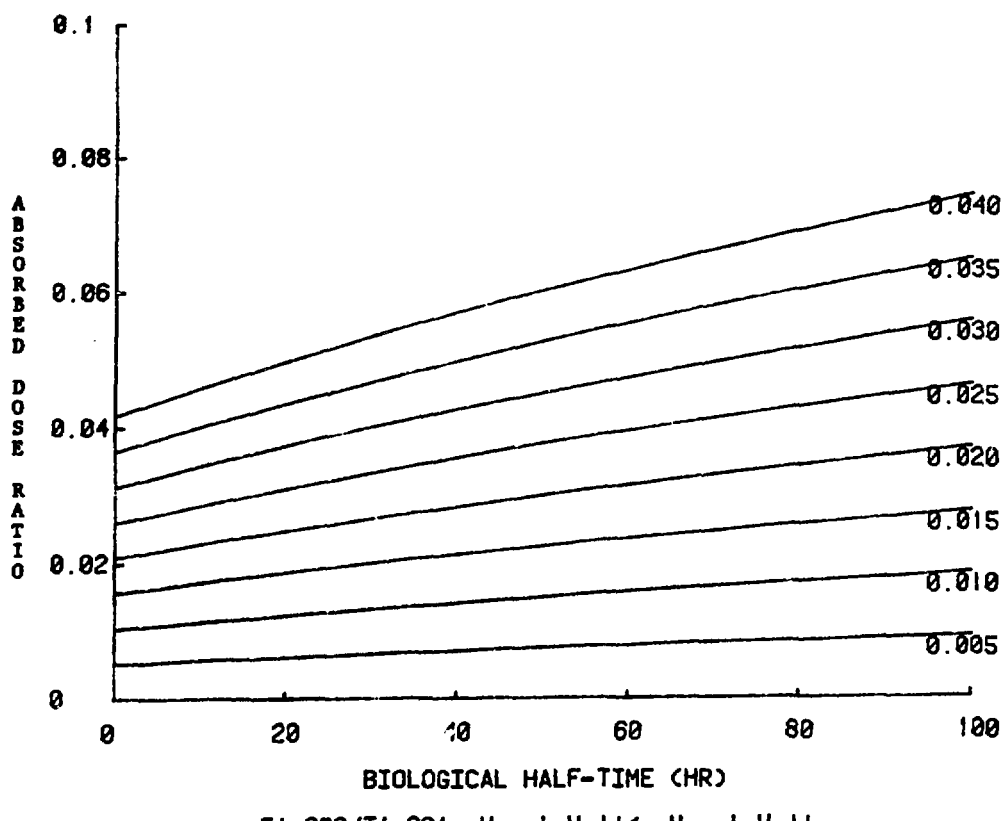


Fig. 5. Absorbed dose ratios for the heart wall irradiating the heart wall as a function of biological half-time for different ratios of Tl-200 to Tl-201.

The dose ratio for the Tl-202 contamination is also low but, as shown in Fig. 6, increases with longer biological half-times. Comparisons of this type are more difficult for contaminants such as the lead isotopes found in Tl-201 preparations because of the different biological behavior; however, Table 2 shows the contribution of the different contaminants at the levels that might be seen at TOC.



Tl-202/Tl-201, Heart Wall--Heart Wall

Fig. 6. Absorbed dose ratios for the heart wall irradiating the heart wall as a function of biological half-time for different ratios of Tl-202 to Tl-201.

Table 2. Absorbed Dose from a Tl-201 Preparation Including Contaminants

Organ	mGy/MBq of Tl-201 Preparation*					
	Tl-201	Tl-200	Tl-202	Pb-203	Pb-201	Total
Liver	0.15	0.0023	0.0070	0.0026	0.00089	0.17
Kidneys	0.32	0.0038	0.010	0.0011	0.00046	0.35
Ovaries	0.13	0.0016	0.0054	0.00059	0.00038	0.13

* Estimated contaminant levels at time of calibration. The activity of the radioactive leads was divided equally between the two isotopes.

In-111 WITH In-114m+In-114

Indium-111 is used in various forms (DTPA, labeled platelets, leukocytes, etc.), and the critical organs will be determined by the type of material administered. For illustration, we have shown in Fig. 7 the dose ratios for In-114m+In-114 contamination in an In-111 preparation where the organ of interest is the red marrow. As with other contaminants that have physical half-lives much longer than the half-life of the primary radionuclide, the biological half-time strongly affects the absorbed dose ratio.

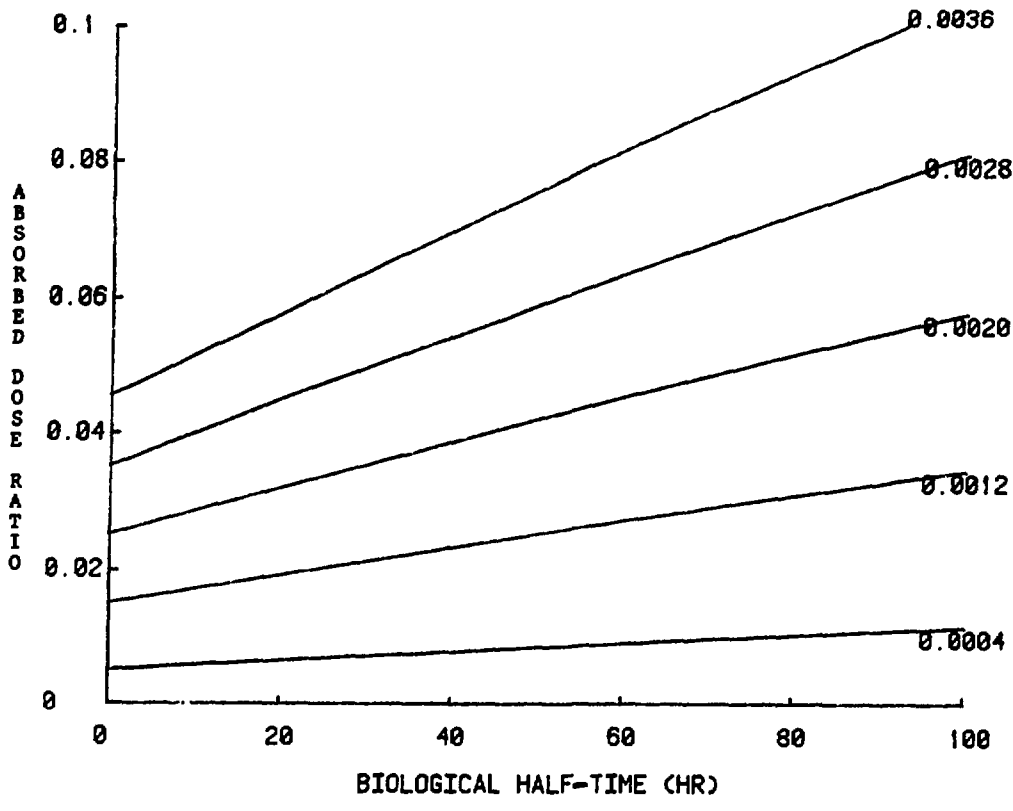


Fig. 7. Absorbed dose ratios for the red marrow irradiating the red marrow as a function of biological half-time for different ratios of In-114m + In-114 to In-111.

CONTAMINATION IN GENERATOR-PRODUCED RADIONUCLIDES

Technetium-99m

Generator-produced radionuclides are sometimes contaminated with radionuclides that are eluted with the primary radionuclide. As presented by Shearer in this proceedings, Mo-99 breakthrough must be considered in the calculation of dose from Tc-99m preparations. Table 3 shows some other ultrashort-lived radionuclides and the contaminants that may be present as well as the estimated dose from them.

Table 3. Possible Contaminants in Some Ultrashort-Lived Radionuclide Preparations (7)

Ultrashort-lived radionuclide	Primary contaminant	Physical half-life	Mode of decay*	Activity of contaminant, kBq/MBq of radiopharmaceutical	Absorbed dose contribution from contaminant, mGy/MBq of radiopharmaceutical
Kr-81m	Rb-81	4.6 hr	EC	1	0.32 (heart) 0.11 (lungs)
Rb-82	Sr-82	25.0 days	Ec	1	51 (marrow) 22 (bone surfaces)
Ir-191m Au-195m	Os-191 Hg-195m	15.4 days 41.6 hr	Beta minus IT	0.05 1	0.54 (vein) 2.6 (kidney) 0.73 (spleen)

*EC, electron capture; IT, isomeric transition.

Iridium-191m

A comparison of the absorbed doses from Ir-191m, Os-191, and Ir-192 for an Os-191/Ir-191m generator is shown in Table 4. For most organs, the doses from the contaminants are as great or greater than the doses for the Ir-191m; however, all of the doses are low.

Table 4. Estimates of Absorbed Doses from Ir-191m, Os-191 and Ir-192 per Injected 2 ml-bolus of Ir-191m*

Organ	μGy per Injection			
	From Ir-191m	From Os-191	From Ir-192	Total
Bladder wall**	-----	26	26	52
Brain	0.91	0.59	3.0	4.5
Small intestine	-----	10	21	31
Heart walls	5.9	3.8	12	22
Kidneys	26	40	49	115
Liver	15	58	18	92
Lungs	8.0	4.3	13	25
Ovaries	15	8.8	22	46
Red marrow	15	9.4	21	46
Spleen	8.0	34	54	97
Testes	11	6.9	19	37
Thyroid	25	22	40	87
Total body	13	9.4	18	40

* 40 GBq Os-191 generator; a "typical" injection bolus containing 5300 MBq Ir-191m; 0.063 MBq Os-191 breakthrough ($2.1 \times 10^{-4}\%$ /bolus); 0.013 MBq Ir-192.

** 4.8 h voiding interval

Although Au-195m has not been used to any great extent in the U.S., some studies are being performed with this generator-produced radionuclide in Europe. The contamination of the Au-195m preparations with Hg-195, Hg-195m, and Au-195 has been a major problem from the standpoint of image quality, but, as shown in Fig. 8, the absorbed dose from the contaminants such as Au-195 must also be taken into account unless the contaminating radionuclide is rapidly eliminated from the body.

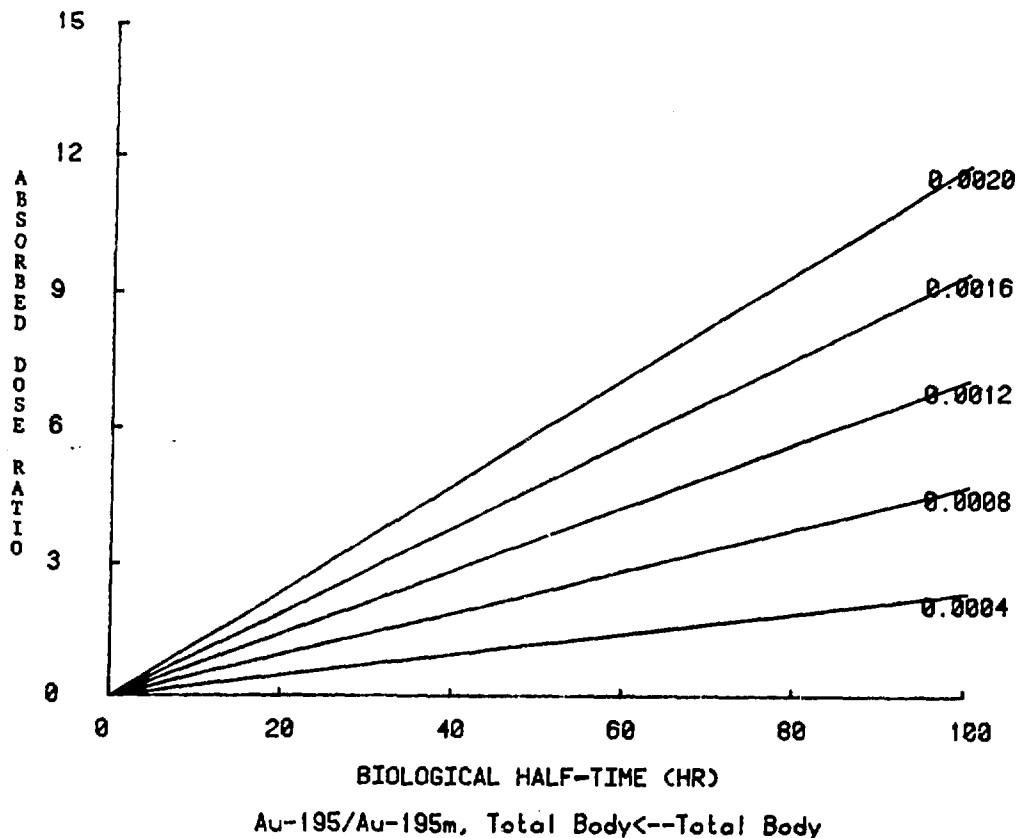


Fig. 8. Absorbed dose ratios for the total body irradiating the total body as a function of biological half-time for different ratios of Au-195 to Au-195m.

SUMMARY

Although we only examined a few situations that may be encountered with radioactive contaminants in radiopharmaceuticals, this analysis does show that radionuclidic impurities in radiopharmaceutical preparations should be considered from the standpoint of the absorbed dose as well as from the other problems such as image degradation that may result from different distributions of activity within the body or from photons that detract from image quality. The absorbed dose from contaminants with physical half-lives longer than that of the primary radionuclide may sometimes be considerably greater than the dose from the primary radionuclide. Although the cost of totally eliminating radionuclidic impurities also must be taken into account in the manufacturing process, the user can prevent some problems by not administering the product after the TOE.

ACKNOWLEDGEMENT

This article is based on work supported by contract number DE-AC05-76-OR00033 between the U. S. Department of Energy and ORAU and Interagency Agreement No. FDA 224-75-3016 with the Food and Drug Administration.

REFERENCES

1. Palmer, D.W. and S.A. Rao. A simple method to quantitate iodine-124 contamination in iodine-123 radiopharmaceuticals. *J. Nucl. Med.* 26, 936-940, 1985.
2. Marcus, C.S., M.G. Stabin, E.E. Watson, and J.H. Kuperus. Contribution of contaminant indium-114m/indium-114 to indium-111 oxine blood dosimetry. *J. Nucl. Med.* 26, 1091-1093, 1985.
3. Husak, V. and J. Vlcek. Long-lived ^{99}Tc in generator-produced $^{99\text{m}}\text{Tc}$, its determination and significance. *Int. J. Appl. Radiat. Isotop.* 30, 165-170, 1979.
4. Colombetti, L.G. and V. Husak. Study of the purity of $^{99\text{m}}\text{Tc}$ sublimed from fission ^{99}Mo and the radiation dose from the impurities. *Int. J. Appl. Radiat. Isotop.* 25, 35-41, 1974.
5. Loevinger, R. and M. Berman. A revised schema for calculating the absorbed dose from biologically distributed radionuclides. MIRD Pamphlet No. 1, Revised. Society of Nuclear Medicine, New York, 1976.
6. Atkins, H.L., J.S. Robertson, B.Y. Croft, B. Tsui, H. Susskind, K.J. Ellis, M.K. Loken, and S. Treves. MIRD Dose Estimate No. 9, Estimates of radiation absorbed doses from radioxenons in lung imaging. *J. Nucl. Med.* 21, 459-465, 1980.
7. Watson, E.E. Problems unique to dose estimation for ultrashort-lived radionuclides, in Single-Photon Ultrashort-lived Radionuclides; proceedings of a symposium held at Washington, D.C., May 9-10, 1983, CONF-830504, edited by Peter Paras and J.W. Thiessen, pp. 296-303, Office of Scientific and Technical Information, U.S. Dept. of Energy, Oak Ridge, TN, 1985.

DISCUSSION

MATTSSON: It is evident that we will have to think about systems to limit the amount of radioactive impurities in radiopharmaceuticals. At the 1980 Oak Ridge dosimetry symposium, we proposed to limit the contribution to the effective dose equivalent (H_e) from impurities in Tc-99m-radiopharmaceuticals to 10% of the contribution from Tc-99m itself. Do you think this is a realistic system and can it be used also for other radionuclides?

WATSON: For Tc-99m this appears to be reasonable, but contaminants associated with other radionuclides will have to be examined on an individual basis.

**RADIATION ABSORBED DOSE ESTIMATE
FOR RUBIDIUM-82
DETERMINED FROM IN VIVO MEASUREMENTS
IN HUMAN SUBJECTS**

James W. Ryan
Paul V. Harper
Violet S. Stark
Erma L. Peterson
Katherine A. Lathrop
The University of Chicago
5841 South Maryland Avenue
Chicago, Illinois 60637

ABSTRACT

Radiation absorbed doses from rubidium-82 injected intravenously were determined in two young men, aged 23 and 27, using a dynamic conjugate counting technique to provide data for the net organ integrated time-activity curves in five organs: kidneys, lungs, liver, heart, and testes. This technique utilized a tungsten collimated Anger camera and the accuracy was validated in a prestwood phantom. The data for each organ were compared with conjugate count rates of a reference Ge-68/Ga-68 standard which had been calibrated against the Rb-82 injected. The effects of attenuation in the body were eliminated. The MIRD method was used to calculate the organ self absorbed doses and the total organ absorbed doses.

The mean total absorbed doses were as follows (mrads/mCi injected): kidneys 30.9, heart walls 7.5, lungs 6.0, liver 3.0, testes 2.0 (one subject only), red marrow 1.3, remainder of body 1.3 and, extrapolating to women, ovaries 1.2. This absorbed dose to the kidney is significantly less than the pessimistic estimate of 59.4 mrads/mCi, made assuming instantaneous uptake and complete extraction of activity with no excretion by the kidneys, which receive 20% of the cardiac output. Further, in a 68 year old man the renal self absorbed dose was approximately 40% less than the mean renal self absorbed dose of the younger men. This decrease is probably related to the decline in renal blood flow which occurs with advancing age but other factors may also contribute to the observed difference.

INTRODUCTION

Rubidium-82 (Rb-82) is a short lived ($T_{1/2} = 75$ seconds) positron emitting radionuclide produced from a long lived strontium-82 (Sr-82) generator. Clinically it has applicability in imaging of the myocardium, brain, and kidneys. Several estimates of the radiation absorbed dose to humans based on extrapolation of animal data in humans and estimates of physiological functions have been published, but there have been no direct measurements of the biokinetic distribution in humans (1-4).

The kidneys have the greatest uptake of Rb-82. The pessimistic estimate of the renal absorbed dose based on assumptions of instantaneous uptake and complete extraction of activity with no excretion by the kidneys, which receive 20% of the cardiac output, is 59.4 mrads/mCi. However, this estimate is too high because the short physical half-life of Rb-82 results in

significant decay of activity during injection and transit through the circulation; other factors may also contribute to decreasing the pessimistic estimate.

After obtaining informed consent, two healthy young men, aged 23 and 27, were studied in a protocol which measured the counts versus time over five organs: kidneys, lungs, liver, heart, and testes. Blood disappearance curves were constructed from the assayed samples of venous blood. The MIRD method was used to calculate organ absorbed doses. In addition we similarly calculated the renal self dose from Rb-82 in a 68 year old man.

MATERIALS AND METHODS

A Sr-82/Rb-82 generator with infusion system was supplied by E. R. Squibb & Sons, Princeton, N.J. (5). A dose calibrator (Capintec CRC 22) was used to measure the injected activity of Rb-82 and a 5" NaI well counter was used in assay of blood specimens. Rb-82 and Ge-68/Ga-68 standards were imaged with a single Anger gamma camera (Siemens, Pho Gamma IV) equipped with a tungsten collimator designed for 0.511 MeV photons (6). During data acquisition this collimator was slowly rotated by a motor drive in order to obliterate the collimator pattern on the images without loss of resolution. Data were recorded for subsequent analysis on an Ohio Nuclear 160 Data Acquisition System.

DATA COLLECTION

The gamma camera was peaked at 0.511 MeV with a Ge-68/Ga-68 source and a 20% window was used for data acquisition. For injection of tracer an 18 gauge indwelling catheter was placed in an antecubital vein of the subject and normal saline was slowly infused throughout the study. The subject, after fasting 10-12 hours, was positioned supine on an imaging table and did not move during each organ imaging sequence. To reduce room background the generator and infusion assembly were located outside the imaging room during the study. The camera was placed below the table to begin imaging each organ from the posterior view. The initial 10 ml of eluate from the generator was discarded. Then 30 mCi in approximately 15 ml was collected in a syringe and placed in a shielded dose calibrator containing a glass vessel to convert the positrons to annihilation radiation. When 16 mCi was recorded, a stopwatch was started and the syringe was transferred to a stopcock assembly for injection into the subject. At exactly 75 seconds after starting the stopwatch, 8 mCi of Rb-82 was injected rapidly followed by a 10 ml flush of saline. The injection and flush were completed in 5-6 seconds. Imaging was begun at the start of injection and data were acquired in frame mode (10 seconds/frame) for 10 minutes.

After completion of the organ imaging in the posterior view when essentially all of the injected Rb-82 activity had decayed, the reference standard of Ge-68/Ga-68 which had been calibrated against Rb-82 in the dose calibrator was imaged. This standard, 17 mm in length, was housed in a 6 mm cylindrical plastic container covered with 8 mm of paraffin. It was placed on the skin anteriorly over the organ of interest, and approximately 10,000 counts were acquired. Without moving the reference source, the gamma camera was repositioned for imaging the organ from the anterior view. The reference source was again imaged until approximately 10,000 counts were obtained, then removed, and a second injection of Rb-82 was made followed by imaging. The Rb-82 injection and imaging sequence was repeated, as described above, for each of the five organs to obtain a conjugate image pair of each organ with

two identical injections of Rb-82: one for the anterior view and the other for the posterior view.

After completion of the five organ studies, an additional injection of Rb-82 was given as described above, and serial venous blood samples were obtained from the opposite arm at 1, 2, 4, 6, 8, and 10 minutes. These were assayed using a well counter and an injection standard.

DATA ANALYSIS

The Rb-82 images obtained serially with each injection were summed over the entire sequence, and a region of interest (ROI) was drawn over the organ and independently over the adjacent background. Each organ ROI was drawn to conform to the anatomic boundaries as determined visually from the images. To account for the transit of tracer through the central circulation in the heart and lung studies, the first 30 seconds were analyzed separately from the remainder of the summed data for these organs. The net organ counts corresponding to a net integrated Rb-82 time-activity curve were obtained from the summed data for each view using the organ and background ROI's. A comparison of this technique with an analysis of the data on a frame by frame basis using the same ROI's in a renal study showed no significant difference, indicating that the background to organ activity ratio remained constant throughout the study. Therefore, only summed data were analyzed except for first 30 seconds of data after injection in the heart and lung studies which were analyzed separately. The geometric mean of the anterior and posterior net counts ("conjugate counts") was calculated for each organ. For the Ge-68/Ga-68 reference standard data, rectangular ROI's were drawn to enclose the activity focus on the images, and the geometric mean net count rate ("conjugate count rate") of the reference standard was calculated. Room background was negligible in these ROI's. The cumulated activity (\bar{A}) from Rb-82 in each of the five organs was determined from comparison of the Rb-82 conjugate counts in each organ with the corresponding reference source conjugate count rates. The MIRD method was used to calculate organ self doses and the total absorbed doses. S values were obtained from references (7) and (8). The S values for the heart as a source organ in reference (8) were also used in a reciprocal manner with the heart as a target organ to calculate the total absorbed heart doses. The dose for the remaining body activity was calculated using the S value correction method (9). Source organ activities were used to calculate absorbed doses to the red marrow and ovaries.

CONJUGATE COUNTING TECHNIQUE

The conjugate counting method was presented at the last symposium (10). Briefly, if an organ is thin and does not have significant self absorption and the photon attenuation is monoexponential in the overlying body tissues, then the net count rates for each of the two opposite views can be expressed as follows:

$$C_1 = A E e^{-\mu x}$$

$$C_2 = A E e^{-\mu(T-x)},$$

$$\text{and the conjugate count rate} = \sqrt{C_1 \cdot C_2} = A E e^{(-\frac{\mu T}{2})},$$

where A = activity, E = efficiency, T = body thickness, x = depth to center of organ, and μ = attenuation coefficient for 0.511 MeV photons (and in Figure 1 d = organ thickness).

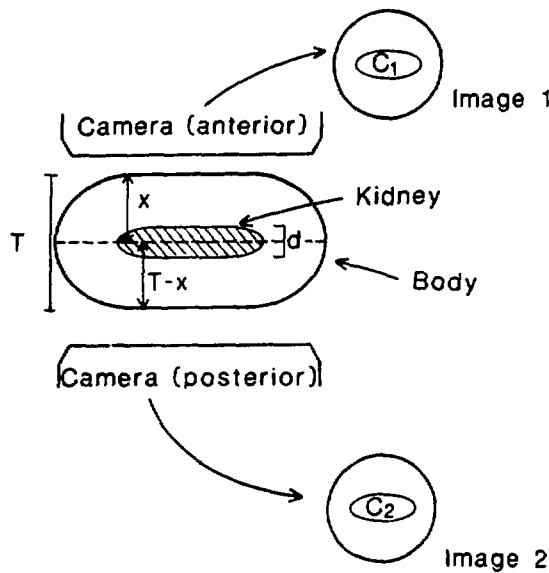


Figure 1

Diagrammatic representation of conjugate counting method.

Thus, the net conjugate count rates are independent of the depth of the source, allowing the net conjugate count rates from an organ of interest to be compared with those of a reference source placed on the surface of the body over the organ.

With our tungsten collimated Anger camera we measured the attenuation coefficient (μ) for 0.511 MeV photons in prestwood as a tissue equivalent material using the sealed reference source of Ge-68/Ga-68 previously described but without the paraffin cover. The attenuation was monoexponential with $\mu = 0.0889 \text{ cm}^{-1}$. A similar but slightly lower value ($\mu = 0.0752 \text{ cm}^{-1}$) was determined using a sheet source of Ge-68/Ga-68.

The correction factor (F) which adjusts for self absorption within a source of thickness "d" is:

$$F = \frac{\sinh \frac{\mu d}{2}}{\frac{\mu d}{2}}$$

For $\mu = 0.0889 \text{ cm}$,

$$\begin{aligned} F &\approx 1.00 \text{ for } d < 3 \text{ cm} \\ F &\approx 1.01 \text{ for } d = 4 \text{ to } 5 \text{ cm} \\ F &\approx 1.05 \text{ for } d = 12 \text{ cm} \\ F &\approx 1.14 \text{ for } d = 20 \text{ cm} \end{aligned}$$

For example, in the adult kidney which is approximately 4 cm thick, $F = 1.01$ and thus there is no significant error if we assume no renal self absorption.

RESULTS

An example of the self dose calculation for the left kidney in subject #1 illustrates the method used in this dynamic conjugate counting technique (Figure 2).

Rb-82 DATA (8 mCi)

Posterior View, Kidney ROI = 1366 pixels = 42,681 counts
(summed) Bkg. ROI = 1366 pixels = 19,766 counts
Net kidney count (600 sec) = 22,915 counts

Anterior View, 1478 pixels
(summed) Net kidney count (600 sec) = 15,406 counts

Net Conjugate Counts in Kidney from 8 mCi Rb-82,

$$\sqrt{22,915 \times 15,406} = \underline{\underline{18,789 \text{ counts}}}$$

Ge-68/Ga-68 REFERENCE STANDARD DATA (125.1 μCi):

Net posterior count rate = 1,264 counts/min

Net anterior count rate = 10,372 counts/min

Net conjugate count rate = $\sqrt{1,264 \times 10,372} = \underline{\underline{3,621 \text{ counts/min}}}$

Thus, the reference standard of Ge-68/Ga-68 which was calibrated in the dose calibrator as equivalent to 125.1 μCi of Rb-82 yielded 3,621 conjugate counts/minute. For 8 mCi Rb-82 injected, the 18,789 net conjugate counts in the kidney from Rb-82 were equivalent to 649.09 $\mu\text{Ci-min}$ as derived in the following equation:

$$\frac{125.1 \mu\text{Ci}}{3,621 \text{ counts/minute}} = \frac{125.1 \mu\text{Ci-min}}{3,621 \text{ counts}} = \frac{\tilde{A} (\mu\text{Ci-min})}{18,789 \text{ counts}}$$

$$\tilde{A} = 649.09 \mu\text{Ci-min in left kidney}/8 \text{ mCi}$$

$$\tilde{A} = 10.82 \mu\text{Ci-hr in left kidney}/8 \text{ mCi}$$

$$\tilde{A} (\text{both kidneys}) = 2 \times 10.82 \mu\text{Ci-hr} = 21.64 \mu\text{Ci-hr} \text{ (assuming equal uptake bilaterally)}$$

$$S = 9.5E-3 \text{ rads}/\mu\text{Ci-hr}$$

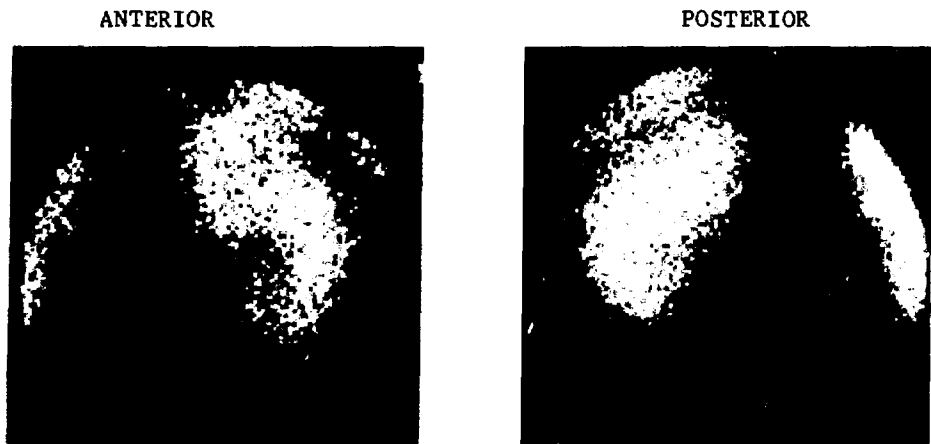
$$D = \tilde{A}S = (21.64) (9.5E-3) = 205.55 \text{ rads}/8 \text{ mCi}$$

$$D = 25.69 \text{ mrads}/\text{mCi Rb-82 injected (self absorbed dose)}$$

The calculation of the total dose to the kidneys also includes contributions from the four other source organs and from the remaining body activity. Calculations were performed in a similar way for other organs. The cumulated activities (\tilde{A}) and organ self doses are shown in Table 1, and the total organ absorbed doses are shown in Table 2.

For the liver study the background region was drawn adjacent to the right lobe inferiorly. The right kidney activity was assumed to be equal to the left kidney activity and was subtracted from the liver activity prior to the liver self absorbed dose calculation. The correction factor (F) for a liver thickness of 20 cm is 1.14.

Calculations for the testes were similar although in one subject the net posterior count was zero so that no absorbed dose calculations were performed for this subject. A partial circumferential background region was used with each view. No correction factor (F) is required.



Ge-68/Ga-68
Reference
Standard with
Regions of
Interest



Figure 2.

Summed images with ROI's of left kidney (Rb-82)
and corresponding Ge-68/Ga-68 reference standard. The reference
standard is located on the anterior surface of the body over the kidney.

For the heart and lung studies it was necessary to account for the initial bolus transit through the central circulation following injection. Inspection of the serial images showed that the bolus activity was present in

the heart and great vessels during the first 30 seconds of data acquisition (3 frames), so that these data were analyzed separately from the remaining time sequence. For the heart studies activity in the cardiac ROI's detected in the first 30 seconds was allocated to the heart chambers, while all subsequent cardiac activity was classified as heart wall activity. A circumferential background ROI was drawn around the entire heart in each view. The correction factor (F) for a heart thickness of 12 cm is 1.05.

Table 1
Summary of Cumulated Activities and Self Doses*

	\tilde{A} ($\mu\text{Ci}\text{-hrs}/\text{mCi}$)		\tilde{AS} (mrads/ mCi)		Mean Self Dose (mrads/ mCi)
	<u>Subject #1</u>	<u>Subject #2</u>	<u>Subject #1</u>	<u>Subject #2</u>	
Kidneys	2.70	3.53	25.69	33.57	29.63
Liver	1.58	1.49	2.68	2.53	2.61
Lungs	2.09	1.81	6.05	5.26	5.65
Heart Chambers	0.55	0.50	**	**	**
Heart Walls	0.55	0.44	5.31	4.25	4.78
Remainder of body	22.53	22.23	1.12	1.11	1.12
Testes	0.009	***	0.74	***	0.74

*: No correction factors (F) were used in these data.

**: Heart chamber self dose was not calculated.

***: No calculation done as net posterior count was zero.

Table 2
Summary of Total Absorbed Doses from Rubidium-82*

<u>Target Organ</u>	<u>Subject #1</u> mrads/ mCi	<u>Subject #2</u> mrads/ mCi	<u>Average</u> mrads/ mCi	<u>Average</u> Rads/40 mCi
Kidneys	26.9	34.8	30.9	1.24
Heart Wall	8.1	6.9	7.5	0.30
Lungs	6.4	5.6	6.0	0.24
Liver	3.0	3.0	3.0	0.12
Remainder of Body	1.3	1.3	1.3	0.05
Testes	2.0	--	2.0	0.08
Ovaries	1.2	1.2	1.2	0.05
Red Marrow	1.3	1.3	1.3	0.05

* No correction factors (F) were used in these calculations.

The lung studies required additional refinement of the initial 30 seconds of data. The right lung was analyzed in each subject and the lung ROI was determined from a previously obtained transmission scan and from the vascular blush in the lung during the first transit of the bolus. This ROI overlapped the subclavian vein, superior vena cava, a portion of the right heart, and the right pulmonary artery and vein. From inspection of the images, the bolus had not entered the pulmonary circulation during the first 10 seconds so that no counts in the first frame were used for dose calculations. On the second and third frames a significant portion of the activity in the lung ROI was judged to be present in the large vessels and heart. This activity was estimated to be 70% of the total counts in the lung ROI in the second frame and 35% in the third frame and was subtracted from the total lung ROI counts in each of these frames. From 31 seconds to 10 minutes, all activity in the lung ROI was

accepted as lung activity. The right lung was considered to be 16% larger than the left (11). Some of the initial activity of the bolus transit was accounted for in the calculation of the heart chamber activity as a source organ contributing to the lung dose. Background for the lung study was chosen from a portion of the body surface on the right lateral chest wall. The density of the lungs is approximately 0.3 so that the lung correction factor (F) is minimal.

The whole body self dose was calculated using the S value correction method for the remaining body activity (9). In our study, the remainder of body includes all of the body except the kidneys, liver, heart, and lungs. The testes were included in the remainder of the body for this calculation, but estimates of self dose to the testes were also made in the two subjects. In the second subject background exceeded organ counts in the posterior view, making the net count zero in this view. Using the data from the first subject as testes source organ activity, the calculated doses to the target organs from the testes were negligible. Therefore, there was no significant error from including the testes in the remainder of the body activity. Calculations for absorbed doses in red marrow and ovaries were performed using the MIRD method.

Values for the venous blood samples were averaged for the two subjects and plotted (Figure 3). The average percent injected dose in the blood was 6.6% at 1 minute, 8.3% (peak) at 2 minutes, and 3.4% at 10 minutes post injection.

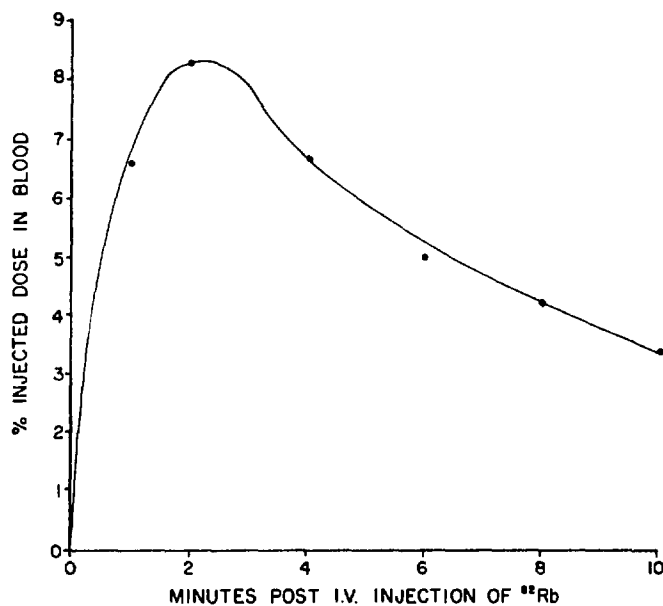


Figure 3
Mean Rb-82 activity in estimated blood volume in two subjects.

Prior to this protocol the renal self dose was determined in a 68 year old man using a similar technique but infusing the Rb-82 activity slowly over 60 seconds. The injected dose of 10.77 mCi was corrected for physical decay during infusion and the calculated self absorbed dose to the left kidney was 17.0 mrads/mCi.

DISCUSSION

The dynamic conjugate counting technique utilizing identical rapid bolus injections of Rb-82 and an Anger camera equipped with a rotating tungsten collimator for imaging proved to be an excellent technique for determining the integrated net organ time-activity curves for Rb-82, a short lived positron emitting radionuclide. This technique eliminated the effects of attenuation. Comparison of these data with a known source of Ge-68/Ga-68 provided \bar{A} for use in the MIRD method. This technique was validated experimentally by showing that attenuation of 0.511 MeV photons was monoexponential in a prestwood phantom with both a small reference source and a sheet source.

The kidneys receive the highest radiation absorbed dose from Rb-82, and in the two protocol subjects the calculated total absorbed dose to the kidneys is approximately one half of the pessimistic estimate. Most of the total renal absorbed dose is due to the self dose, which in turn is dependent upon several variables, including renal blood flow, renal uptake of Rb-82, excretion or washout of activity from the kidneys, and the physical decay of the agent during injection and during transit through the circulation before it fully localizes in the kidneys.

An interesting finding was the decrease in self absorbed dose to the kidney in the 68 year old man compared with the average dose to the men in their twenties. A larger series would be needed to confirm this observation, but the decline in renal blood flow which occurs with advancing age is probably responsible for this difference, at least in part (12). In one study of men of various ages with no known renal disease admitted to Baltimore hospitals, renal blood flow determined by the plasma diodrast clearance method varied widely in each age group, but the mean renal blood flow declined after age 30, and overall the renal blood flow after age 50 was significantly less than in the preceding age groups (Figure 4) (13).

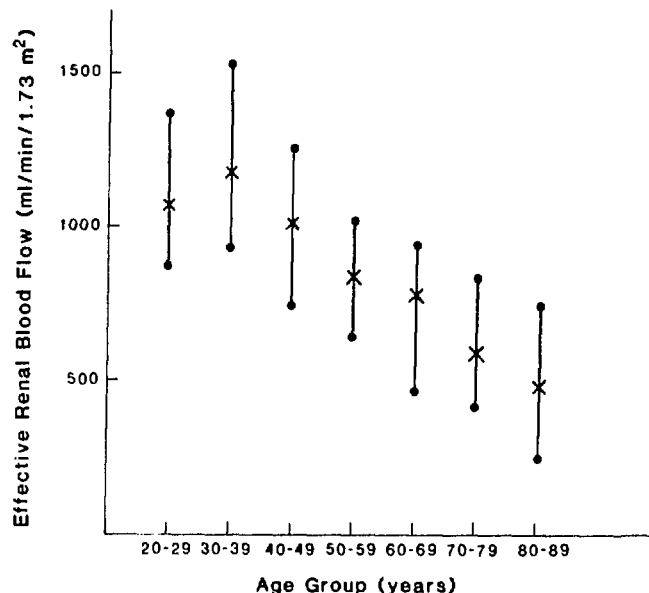


Figure 4
Age related effective renal blood flow
(plasma diodrast clearance) in men from reference (13).

Thus, in older subjects and in patients with decreased renal blood flow from any cause, clinical imaging with Rb-82 will result in less renal uptake of tracer and a smaller renal absorbed dose than observed in our protocol.

We also calculated the maximum renal uptake of Rb-82 in the left kidney as a percent of the injected dose in these three subjects. The results were 8.8%, 7.1%, and 5.9% respectively in the subjects aged 23, 27, and 68 years. These values show less variation than the renal self dose data, and in the older subject the decrease in renal self dose is substantially greater than can be accounted for by the maximum Rb-82 uptake in his kidney. Since the self absorbed dose is proportional to the area under the net integrated time-activity curve and is decreased out of proportion to the peak value in the older man, a more rapid washout of renal Rb-82 activity is suggested in the older person compared with the younger men. Further observations will be necessary to substantiate this possibility in older subjects.

The dose estimates to the lungs and heart involve decisions about the circulating activity ("blood pool") following injection of a tracer. This subject is not yet well developed and in retrospect more rapid frame intervals would have been useful in analysis of the first 30 seconds of data acquisition. In the heart data, activity in the heart chamber was arbitrarily separated from heart wall activity at 30 seconds after injection, but some Rb-82 activity persists in the blood throughout the duration of the study as shown in Figure 3. High resolution PET methods should prove helpful in separating the sources of the heart activity. The method of background subtraction also may need to be modified in the future. The right lateral chest wall was used as the background region for the lung calculations and a circumferential background was used for the cardiac calculations.

The absorbed doses to the liver and testes appear to carry the highest degree of uncertainty of the estimates in this protocol. The correction factor (F) of 1.14 for a 20 cm thick liver is the largest organ correction factor in this study, but the liver thickness is not uniform throughout and the correction factor may need to be modified as a result.

If the whole body self dose were estimated from the assumptions of instantaneous tracer distribution in the whole body without excretion following injection, \bar{A} would be 30 $\mu\text{Ci}\text{-hrs}/\text{mCi}$ and the whole body self dose would be 1.53 mrads/mCi. The remainder of the body activity calculations with the S value correction method result in lower \bar{A} values and a lower mean self absorbed dose of 1.12 mrads/mCi in the remainder of body. In a preliminary presentation of these data the remainder of body activity calculations were not utilized, and calculations for the heart as a target organ were not included (14). The remaining body activity is the major contributor to the calculated doses to the testes, ovaries, and red marrow and it is the next highest source organ dose to the kidneys, lungs, and liver after the self absorbed doses.

There have been some technical problems with this approach. The 0.7765 MeV peak of Rb-82 contributed to septal penetration and scatter in the images. Choice of ROI's was subjective. Some differences were observed by varying the size of the ROI's over the reference source, and the ones used in these calculations were chosen to minimize scatter in the ROI's. If larger ROI's were used over this source, the organ absorbed doses would have been reduced by 10-20%. On the other hand if larger ROI's were used for organ data, the absorbed doses would have been somewhat increased.

The total absorbed dose from the Rb-82 injections should also include the radioactive strontium (Sr-82, Sr-85) breakthrough, and Neirinckx et al. showed

that there was <10E-9/ml breakthrough in the Squibb generator (5). The two subjects in our protocol were studied on consecutive days when the generator column contained an average of 55.8 mCi Sr-82 and 190.7 mCi Sr-85. The total volume (160 ml) injected into each subject for this protocol contained 0.0092 μ Ci Sr-82 and 0.0315 μ Ci Sr-85. According to a personal communication from Hoop to Yano cited in reference (2), these activities would result in a total absorbed dose of <4.9 mrads to the bone, <4.4 mrads to the red marrow, and <0.81 mrads to the whole body in each subject.

The rapid bolus injection technique which was used in this study provided a rapid input function and the net organ conjugate counting yielded time-activity curves which approximated an impulse response to instantaneous injection. Although this bolus technique is not routinely performed in clinical studies where, instead, a prolonged Rb-82 infusion is given with monitoring by the infusion system, the estimated radiation doses will be the same for either method.

For comparison, 2.0 mCi of Tl-201 injected intravenously gives the following absorbed doses (rads): kidneys 2.4, liver 1.1, testes 1.0, ovaries 0.4, whole body 0.4.

SUMMARY

Radiation absorbed doses from Rb-82 were determined using a dynamic conjugate counting technique to provide quantitative data for construction of time-activity curves. This technique utilized a tungsten collimated Anger camera and was validated in a prestwood phantom. The count data for each organ were compared with the count data of a reference Ge-68/Ga-68 standard which had been calibrated against the Rb-82 injection in order to obtain uptake values. The effects of attenuation in the body were eliminated. The MIRD method was used to calculate the organ self absorbed doses and the total organ absorbed doses.

In two young adult men aged 23 and 27 the mean total absorbed doses were as follows (mrads/mCi injected): kidneys 30.9, heart walls 7.5, lungs 6.0, liver 3.0, testes 2.0 (one subject only), red marrow 1.3, remainder of body 1.3, and extrapolating to women, ovaries 1.2. The organ of highest Rb-82 absorbed dose is the kidney and the measured renal dose is significantly less than the pessimistic estimate of 59.4 mrads/mCi. Further, in a 68 year old man the renal self absorbed dose was approximately 40% lower than the mean renal self absorbed dose of the younger men. This is probably due in part to the decline in renal blood flow which occurs with advancing age, especially after age 50, but other factors also may contribute to the observed difference. Thus, in older patients who are at increased risk of acute coronary disease, the renal uptake of Rb-82 from myocardial perfusion studies is decreased and sequential studies can be obtained as indicated with less renal exposure than observed in our protocol subjects.

We wish to acknowledge the collaborative support from Ms. Meg L. Graff and Dr. Marion Meeks of the E.R. Squibb & Sons Company, Princeton, NJ, which supported this study in part.

REFERENCES

1. Budinger, T.F., Y. Yano, and B. Hoop. A comparison of $^{82}\text{Rb}^+$ and $^{13}\text{NH}_3$ for myocardial positron scintigraphy. J. Nucl. Med. 16. 429-431, 1975.

2. Yano, Y., P. Chu, T.F. Budinger, P.M. Grant, A.E. Ogard, J.W. Barnes, H.A. O'Brien, Jr., and B. Hoop, Jr.. Rubidium-82 generators for imaging studies. *J. Nucl. Med.* 18. 46-50, 1977.
3. Yen, C.K., Y. Yano, T.F. Budinger, R.P. Friedland, S.E. Derenzo, R.H. Huesman, and H.A. O'Brien. Brain tumor evaluation using Rb-82 and positron emission tomography. *J. Nucl. Med.* 23. 532-537, 1982.
4. Kearnott, K.J. Radiation absorbed dose estimates for positron emission tomography (PET): K-38, Rb-81, Rb-82, and Cs-130. *J. Nucl. Med.* 23. 1128-1132, 1982.
5. Neirinckx, R.D., J.F. Kronauge, G.P. Gennaro, and M.D. Loberg. Evaluation of inorganic adsorbents for the Rubidium-82 generator. I. Hydrous SnO₂. *J. Nucl. Med.* 23. 245-249, 1982.
6. Harper, P.V., K.A. Lathrop, H. Krizek, N. Lambares, V. Stark, and P.B. Horfer. Clinical feasibility of myocardial imaging with ¹³NH₃. *J. Nucl. Med.* 13. 278-280, 1972.
7. Snyder, W.S., M.R. Ford, G.G. Warner and S.B. Watson. MIRD Pamphlet No. 11: "S" absorbed dose per unit cumulated activity for selected radionuclides and organs, pp 126-127, Society of Nuclear Medicine, New York, 1975.
8. Coffey, J.L. and E.E. Watson. S values for selected radionuclides and organs with heart wall and heart contents as source organs. Third International Dosimetry Symposium, edited by E.E. Watson, A.T. Schlafke-Stelson, J.L. Coffey, R.J. Cloutier, pp. 563-594, Bureau of Radiological Health, Rockville, Md., 1981.
9. Coffey, J.L. and E.E. Watson. Calculating dose from remaining body activity: A comparison of two methods. *Med. Physics* 6. 307-308, 1979.
10. Tsui, B.M.W., C.T. Chen, N.J. Yasillo, C.J. Ortega, D.B. Charleston, P.V. Harper, and K.A. Lathrop. A whole body scanning system for collection of quantitative in vivo distribution data in humans, in Third International Radiopharmaceutical Dosimetry Symposium, edited by E.E. Watson, A.T. Schlafke-Stelson, J.L. Coffey, R.J. Cloutier, pp. 138-156, Bureau of Radiological Health, Rockville, Md., 1981.
11. Coffey, J.L., M. Cristy and G.G. Warner. MIRD Pamphlet No. 13: Specific absorbed fractions for photon sources uniformly distributed in the heart chambers and heart wall of a heterogeneous phantom. *J. Nucl. Med.* 22. 65-71, 1981.
12. Schuster D.W. and V.L. Schuster. Renal clearance, in The Kidney: Physiology and Pathophysiology, edited by D.W. Seldin and G. Giebisch, pp. 365-395. Raven Press, New York, 1985.
13. Davies, D.F. and N.W. Shock. Age changes in glomerular filtration rate, effective renal plasma flow, and tubular excretory capacity in adult males. *J. Clin. Invest.* 29. 496-507, 1950. Also referenced in Biological Handbook, Respiration and Circulation, edited by P.L. Altman and D.S. Ditmer, pp. 426-427, Federation of American Societies for Experimental Biology, Bethesda, Md., 1971.
14. Ryan J, P. Harper, V. Stark, E. Peterson, and K. Lathrop. Radiation absorbed dose estimate for Rb-82 using in vivo measurements in man. *J. Nucl. Med.* 25. P94, 1984.

DISCUSSION

MARCUSE: In your scintigrams of the left kidney, the presence of the heart suggests a coordinate in the field of view dependent on background subtraction, where I understood you applied a homogeneous background subtraction. Do you think that the background subtraction method can influence your dosimetric results in a significant way?

RYAN: Background subtraction is pretty much an arbitrary procedure as we defined it. Our camera field of view is a smaller standard field-of-view camera. We are not able to put multiple organs in the field of view at the same time. We tried several ways of making the background correction. I think that the surrounding background would probably give the best estimates of the background. We would be happy to have suggestions as to other ways of doing it, but this was the best way that we could come up with.

HUMAN ABSORBED DOSE CALCULATIONS FOR
¹²³I LABELED PHENYL PENTADECANOIC ACID

Padmakar V. Kulkarni, Ph.D., Geoffrey Clark, Ph.D., James R. Corbett, M.D.,
James T. Willerson, M.D.^{**} and Robert W. Parkey, M.D.^{*}

Departments of Radiology and Internal Medicine, Cardiology Division
The University of Texas Health Science Center at Dallas
5323 Harry Hines Blvd., Dallas, TX 75235

ABSTRACT

I-123 labeled fatty acids have been proposed for studying myocardial metabolism by scintigraphic methods. With the availability of clean I-123 and the advent of single photon emission tomography, I-123 labeled fatty acids would be well suited to study regional myocardial viability or metabolism in humans. We have studied I-125 and I-123 labeled iodophenyl pentadecanoic acid (IPPA) in laboratory animals -- rats and dogs. Clinical studies are in progress with I-123 (IPPA). We have studied the pharmacokinetics of this tracer in male Sprague-Dawley rats at 0.25, 0.5, 1, 3, 6, and 24 hours postinjection. The cumulated doses, due to both the "pure" I-123 and a version contaminated with 1.4% I-125, in various organs and the total body in humans are estimated. The average dose to organs for humans injected with I-123 IPPA with "pure" I-123 and contaminated I-123 respectively, are (rads to organ per mCi injected): heart wall (0.0507, 0.0514), liver (0.0792, 0.0875), kidneys (0.0479, 0.0561), thyroid (0.0517, 0.0638), ovaries (0.0427, 0.0561), testes (0.0307, 0.0309), total body (0.0386, 0.0392).

INTRODUCTION

In order to be approved for human use, a new radiopharmaceutical must first be tested in animals. The kinetic data from the animal studies are then extrapolated to calculate the radiation absorbed dose to humans. This paper describes our calculations for radiation dose estimation to a human injected with I-123 iodophenyl pentadecanoic acid (IPPA) for medical imaging purposes. The IPPA was prepared by our proposed method (1,2,3,).

The model used for this calculation is based on the formalism of the MIRD Committee (4). The experimental subjects were groups of male Sprague-Dawley rats ranging from 180-200 grams total body weight. The data used are the measurements of the radioactivity distributions for various rat organs which were performed sequentially and are presented in Table 1.

The cumulated doses in humans due to both the "pure" I-123 PPA and a version contaminated with 1.4% I-125 are presented as well as the steps and assumptions involved with the calculation.

The mean absorbed dose $\bar{D}(r_k \leftarrow r_h)$ is expressed as the rad to a target organ r_k from a radionuclide distributed uniformly in a source organ r_h and has been formulated by the MIRD Committee (4,5) as

$$\bar{D}(r_k \leftarrow r_h) = (1/m_k) \tilde{A}_h \sum_i \Delta_i \phi_i(r_k \leftarrow r_h) \quad [1]$$

where \tilde{A}_h ($\mu\text{Ci}\cdot\text{hr}$) is the cumulated activity in the source organ r_h ; m_k is the mass of the target organ in grams; Δ_i ($\text{g-rad}/\mu\text{Ci}\cdot\text{hr}$) is the mean energy emitted per unit cumulated activity for the type of radiation under consideration; and $\phi_i(r_k \leftarrow r_h)$ is the absorbed fraction of the energy for target organ r_k for particles i emitted from source organ r_h .

The MIRD Committee (5) has noted that the term \tilde{A}_h embodies most of the biological data whereas the other terms on the right-hand side of [1] are concerned with physical and anatomical data. Therefore the quantity $S(r_k \leftarrow r_h)$ has been introduced and is defined as

$$S(r_k \leftarrow r_h) = (1/m_k) \sum_i \Delta_i \phi_i(r_k \leftarrow r_h). \quad [2]$$

The values of S for photons have been estimated and tabulated by the MIRD Committee (5) using Monte Carlo techniques (6) for a human phantom based on the organ data of the reference man. The tables of these S -value estimates for many radionuclides common to medicine (5) are used to calculate the mean absorbed dose using the equation

$$\bar{D}(r_k \leftarrow r_h) = S(r_k \leftarrow r_h) \tilde{A}_h \quad [3]$$

Thus acceptance of the assumptions made above reduces the problem to estimating the cumulated activity \tilde{A}_h of the source organ and calculating the mean absorbed dose by plugging \tilde{A}_h into equation [3]. The total absorbed dose to a given target organ can then be calculated by summing the contributions from all source organs. The rat data is extrapolated to humans by assuming that a given organ will have the same disappearance (or uptake) curve, and thus the same cumulated activity as the same organ in a rat.

ABSORBED DOSE ESTIMATION

CUMULATED ACTIVITIES

The cumulated activities \tilde{A}_h were estimated by making a semi-log plot of the data for each organ in Table 1 as a function of time. The curves were then resolved into components (7). In this form the data could express the activity as a function of time in terms of a sum of exponentials, e.g.,

$$A_h(t) = \sum_j A_j \exp[-(\lambda_p + \lambda_j) t] \quad [4]$$

where A_j is the value of the j th component at $t=0$; λ_p is the physical decay constant of the particular radionuclide and λ_j is the biologic disappearance (or uptake) constant of the j th exponential component.

All the curves were resolved into two or three components. The blood, thyroid, and remainder curves have negative A_j 's to account for the slower uptake of the radionuclide. All other organs were assumed to have instantaneous uptake. The curves from which the cumulated activities were calculated are shown in Figures 1-9 and the disappearance constants and A_j 's for each organ are presented explicitly in Table 2.

TABLE 1

DISTRIBUTION OF RADIOACTIVITY (% INJECTED DOSE PER GRAM OF TISSUE) IN RAT
ORGANS AT VARIOUS TIMES AFTER INJECTION OF I-125 LABELED PPA

<u>Organ</u>	<u>Time After Injection</u>						
	<u>1 min</u>	<u>15 min</u>	<u>30 min</u>	<u>1 hr</u>	<u>3 hr</u>	<u>6 hr</u>	<u>24 hr</u>
Heart Wall	3.46	3.23	3.00	1.40	0.83	0.33	0.25
Blood	0.56	0.72	0.67	0.56	0.48	0.23	0.18
Lungs	1.46	1.24	1.20	0.80	0.91	0.49	0.66
Liver	2.31	2.34	2.59	1.65	1.27	0.41	0.53
Spleen	1.96	0.95	0.79	0.68	0.78	0.31	0.34
Kidneys	0.85	0.86	0.91	0.70	0.80	0.31	0.32
Stomach	0.28	0.40	0.31	0.27	0.42	0.13	0.19
Thyroid	0.67	0.97	0.86	1.47	1.68	1.31	2.84
% Injected Radioactivity Excreted in Urine							
Urine	--	--	3.79	11.92	5.76	7.16	46.53

TABLE 2

INITIAL ACTIVITIES AND BIOLOGICAL DISAPPEARANCE CONSTANTS
OF EXPONENTIAL COMPONENTS

<u>Organ</u>	<u>(% injected activity/gm tissue)</u>			<u>(1/hr)</u>		
	<u>A_1</u>	<u>A_2</u>	<u>A_3</u>	<u>λ_1</u>	<u>λ_2</u>	<u>λ_3</u>
Heart Wall	1.95	1.51	0.34	1.5395	0.4495	0.0133
Blood	0.255	-0.3	0.6	0.0096	2.7726	0.4077
Lungs	0.9	3.70	----	0.0144	4.16	-----
Liver	0.55	2.6	----	0.004	0.533	-----
Spleen	0.36	0.64	1.0	0.0133	0.4621	6.931
Kidneys	0.32	0.63	----	0.0015	0.4332	-----
Stomach	0.26	0.23	----	0.0078	0.4616	-----
Thyroid	-4.0	5.0	----	0.033	0.0001	-----
Remainder	122	-69	----	0.0415	0.2768	-----

Note that the data in Table 1 is for the IPPA labeled with I-125. This fact required that the physical decay constants be interchanged for the I-123 calculation. As well, the data is presented in units of % injected activity per gram of tissue. Therefore, the data had to be multiplied by the weight of the organ or tissue. The values used in this

conversion and their sources are listed in Table 3. The value for the mass of the contents of the heart was calculated from the mass of the heart wall given in Table 3 assuming that the ratio of heart-contents mass to heart-wall mass were the same for rats as for humans, i.e. 1.44 (11).

TABLE 3
AVERAGE RAT ORGAN MASSES
(200 gm male Sprague-Dawley or closest approximation)

<u>Organ</u>	<u>Rat Organ Weight (gm)</u>	<u>Reference</u>
Heart Wall	0.8	8
Heart Contents	1.2	see text
Lungs	1.43	avg. 8 & 9
Liver	10.34	10
Spleen	0.675	10
Kidneys	1.55	avg. 8,9,10
Stomach Wall	1.0	8
Thyroid	0.0154	8
Remainder	183	see text

To obtain the total cumulated activity \tilde{A}_h , the activity function $A_h(t)$ was then integrated from time $t=0$ to infinity. The results are presented in Table 4 in units of % injected activity for each organ.

The estimation of the cumulated activity for the remainder of the body required a further assumption. The data on urine was used as well as the total activity of all the organs in Table 1. The total-body activity function $A_{hTB}(t)$ was obtained using the equation

$$A_{hTB}(t) = \{100 \exp[-\lambda_p t] - \sum_j A_j(t) m_j - A_{ur}(t)\} \quad [5]$$

where m_j is the mass of the rat organ j ; $A_j(t)$ is the value of activity found in Table 1 for organ j (modified for the appropriate physical decay constant); $A_{ur}(t)$ is the value for the urine sample from Table 1; and the value A_{hTB} is expressed in % injected activity. The values A_{hTB} were calculated for each time presented in the data of Table 1 and plotted, Figures 1-9.

The above calculation assumed that all of the activity not in the organs listed in Table 1 was distributed uniformly throughout the rest of the body, and that the only disappearance of activity was due to the physical decay of the isotope and urination. The components of the disappearance curve for the remainder of the body were then resolvable.

S Values

The S values used were obtained from the tables of S values found in the MIRD pamphlet #11 (5) with the following exceptions. The S values for the cases of the heart wall and heart contents being the source organs were taken from reference (11). The S values for the cases where the

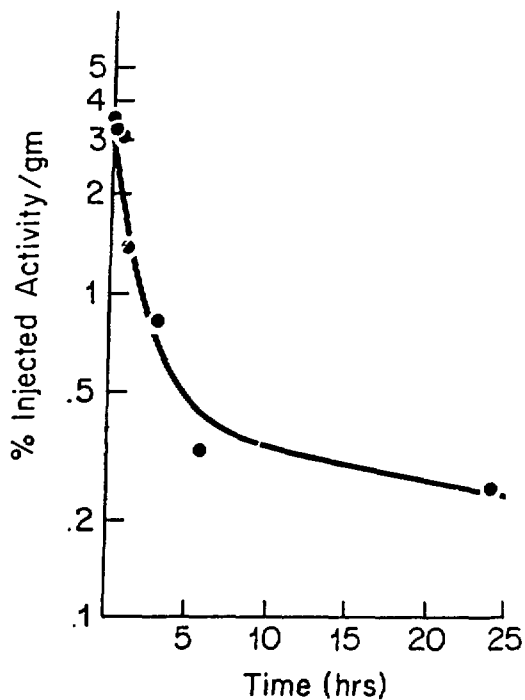


Figure 1

Plot of data in Table 1 for rat heart wall. The solid line is the function $A_h(t)$ described by equation [4] and the parameters of Table 2.

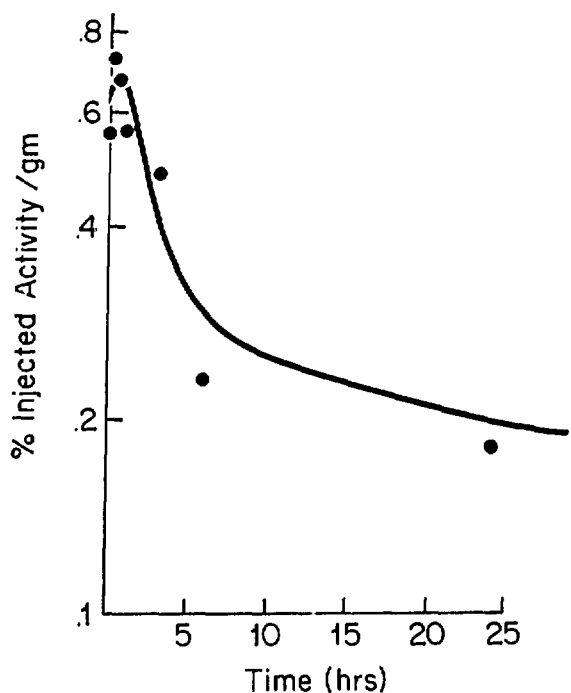


Figure 2

Plot of data in Table 1 for rat blood (heart contents). The solid line is the function of $A_h(t)$ described by equation [4] and the parameters of Table 2.

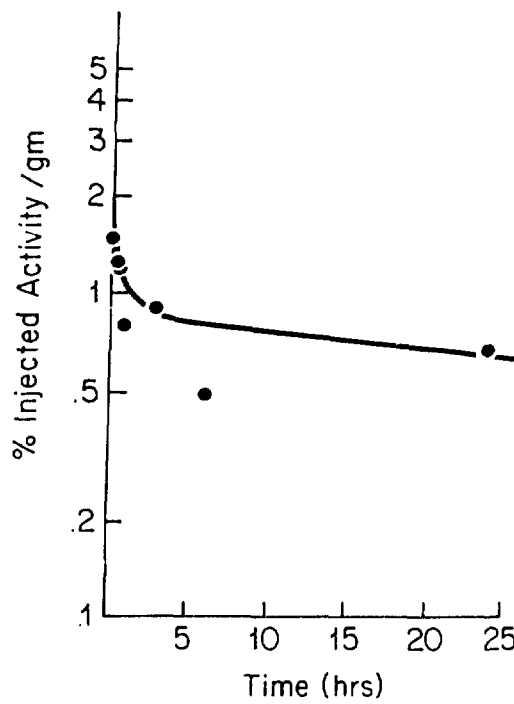


Figure 3

Plot of data in Table 1 for rat lungs. The solid line is the function of $A_h(t)$ described by equation [4] and the parameters in Table 2.

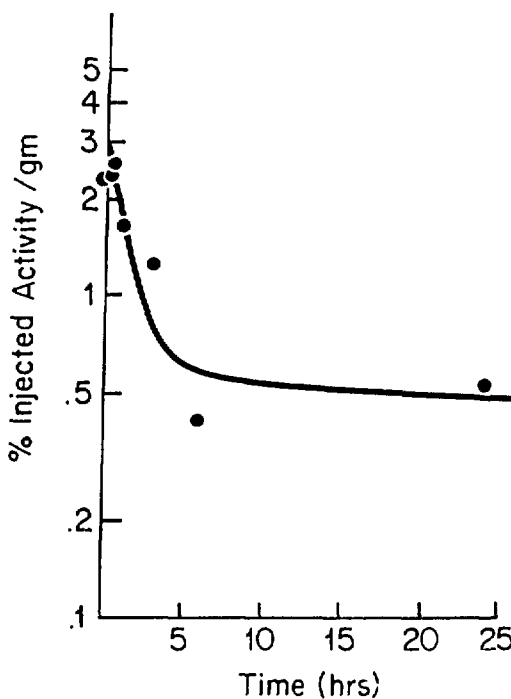


Figure 4

Plot of data in Table 1 for rat liver. The solid line is the function of $A_h(t)$ described by the equation [4] and the parameters in Table 2.

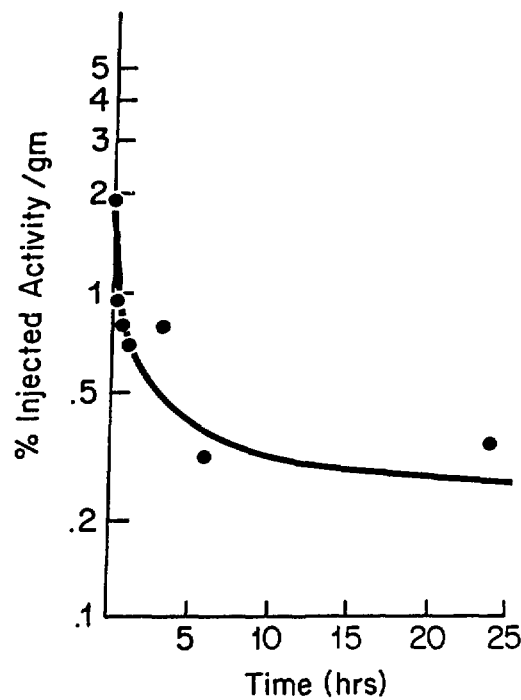


Figure 5

Plot of data in Table I for rat spleen.
The solid line is the function $A_h(t)$
described by equation [4] and the
parameters of Table 2.

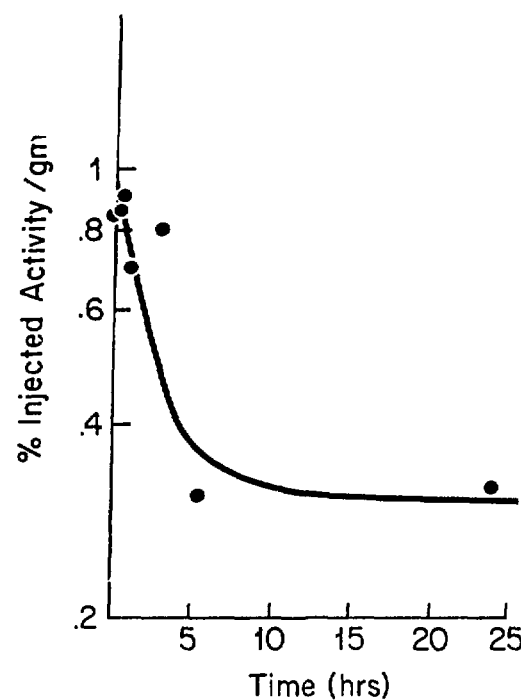


Figure 6

Plot of data in Table I for rat kidneys.
The solid line is the function $A_h(t)$
described by equation [4] and the
parameters in Table 2.

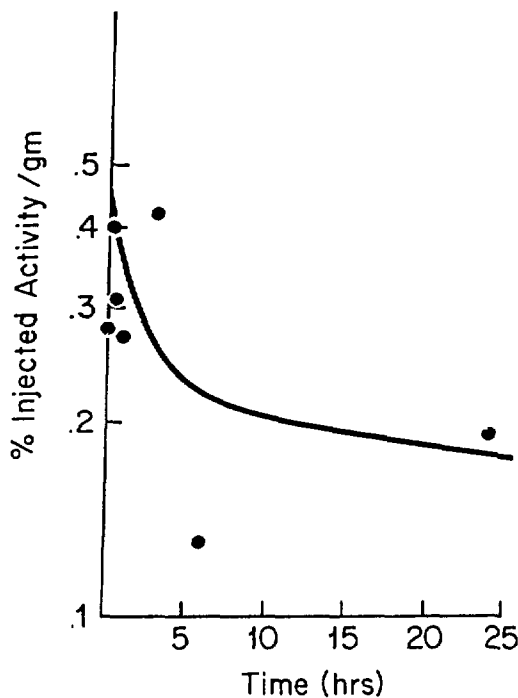


Figure 7

Plot of the data in Table 1 for rat stomach. The solid line is the function of $A_h(t)$ described in equation [4] and the parameters in Table 2.

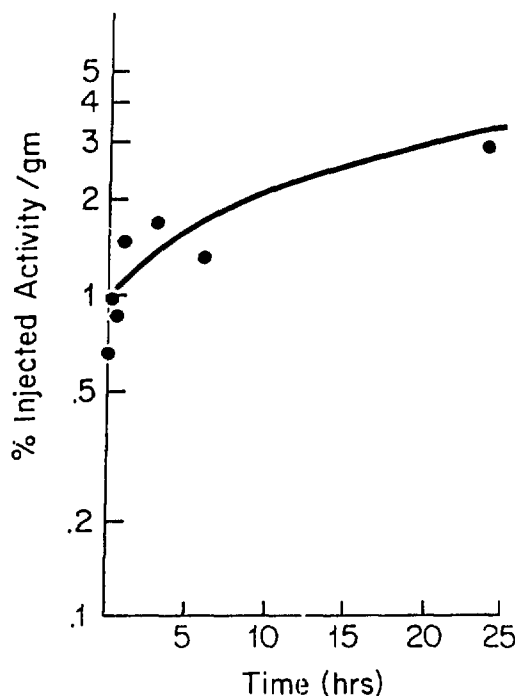


Figure 8

Plot of the data in Table 1 for rat thyroid. The solid line is the function $A_h(t)$ described by equation [4] and the parameters in Table 2.

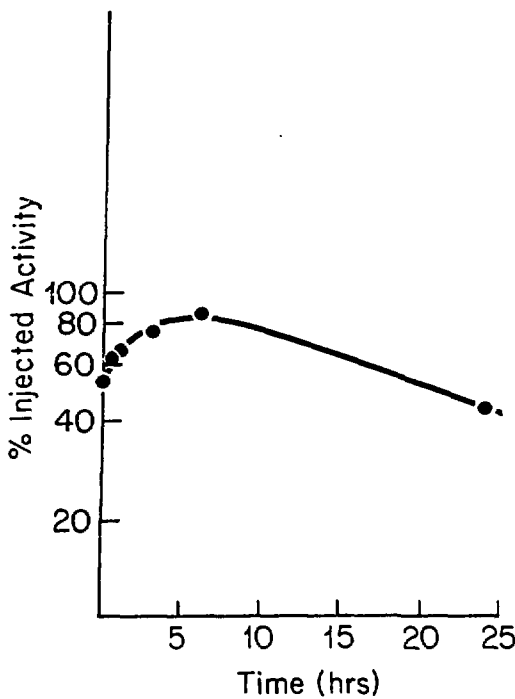


Figure 9

Plot of data points obtained by applying equation [5] to obtain values of $A_{hTB}(t)$ for various points in time. The solid line is the function $A_h(t)$ for the remainder of the body resolved from these points by applying equation [4] to obtain the parameters in Table 2.

stomach wall was the target organ were applied using the principle of reciprocity, e.g.,

$$S(r_k \leftarrow r_h) = S(r_h \leftarrow r_k). \quad [6]$$

As well, the S values for the cases of the heart wall being the target organ were also a result of the application of reciprocity except for where the heart wall and heart contents were the source organs.

Total Average Dose to Target Organs

Cloutier et al (12) have pointed out that if the total-body dose is to be properly taken into account then a simple summation of equation [3] over all the source organs is not sufficient. The simple summation method results in an overestimation of the total average dose of target organ k , D_k , since the total-body component of the source organ dose is counted twice. Instead it is suggested that the equation

$$D_k = \tilde{A}_h^* S(r_k \leftarrow r_h) + m_{TB} (\tilde{A}_{rem}/m_{rem}) S(r_k \leftarrow TB) \quad [7]$$

be used. Here m_{TB} is the mass of the total body of the animal (200 gm for the rat) and \tilde{A}_{rem} and m_{rem} are the cumulated activities and masses of the portion of the total body not including the specified source organs. The value \tilde{A}_h^* is a modified cumulated activity and is defined as

$$\tilde{A}_h^* = \tilde{A}_h - (m_h/m_{rem}) \tilde{A}_{rem}. \quad [8]$$

\tilde{A}_h^* compensates for that part of the total-body cumulated activity included within each source organ's cumulated activity. The computed values for \tilde{A}_h^* are shown in Table 4.

TABLE 4
CUMULATED ACTIVITIES

	\tilde{A}_h (% injected activity-hour per gm tissue)	\tilde{A}_h (% injected activity-hr)	\tilde{A}_h^* (% injected activity-hr)			
Organ	I-125	I-123	I-125	I-123	I-125	I-123
Heart Wall	29.26	9.32	23.41	7.46	11.80	7.25
Heart Conts.	26.61	5.44	31.93	6.53	14.51	- 0.54
Lungs	61.29	14.27	87.64	20.41	66.89	11.99
Liver	127.1	10.62	1314.2	109.8	1164.1	48.92
Spleen	27.61	6.79	18.64	4.58	8.84	0.61
Kidneys	161.5	7.13	250.3	11.05	227.75	1.92
Stomach Wall	26.7	0.92	26.7	0.92	26.54	- 4.97
Thyroid	1915.5	39.67	29.5	0.611	29.3	0.52
Remainder	14.5	5.89	26.55	1077.6	-----	-----
Total body	-----	-----	-----	-----	2902.7	1177.7

Equation [7] was applied to the modified cumulated activities of the source organs and the total average doses to the target organs were calculated. Table 5 shows the values of D_k in humans (in units of rads/millicurie administered) for IPPA labeled with "pure" I-123 and a "contaminated" isotopic mixture containing 1.4% I-125. The radionuclidian purity is given as I-123 > 98.6% and contamination of I-125 < 1.4%, within 24 hours postcalibration as per University of California at Davis, Crocker Nuclear Laboratory specifications.

TABLE 5

TOTAL AVERAGE DOSE TO ORGANS FOR HUMANS INJECTED WITH I-123 PPA

<u>Target Organ</u>	<u>D_k (rads to organ per mCi injected)</u>	<u>"contaminated" I-123 (1.4% I-125) -</u>
	<u>"pure" I-123</u>	
Heart Wall	0.0507	0.0514
Lungs	0.0494	0.0502
Liver	0.0792	0.0875
Kidneys	0.0479	0.0561
Thyroid	0.0517	0.0638
Ovaries	0.0427	0.0561
Testes	0.0307	0.0309
Total Body	0.0386	0.0392

REFERENCES

1. Kulkarni P. and R.W. Parkey: A new radioiodination method utilizing an organothallium intermediate: Radioiodination of phenyl pentadecanoic acid (PPA) for potential applications in myocardial imaging. J Nucl Med 23:P105, 1982
2. Chien K.R., E. Han, J. White, and P. Kulkarni: In vivo esterification of a synthetic I-125 labeled fatty acid into cardiac glycerolipids. Am J Physiol 245:H693-H697, 1983
3. Rellas J.S., J.R. Corbett, P. Kulkarni, C. Morgan, M.D. Devous, L. M. Buja, L. Bush, R.W. Parkey, J.T. Willerson, S.E. Lewis: Iodine-123 phenylpentadecanoic acid: Detection of acute myocardial infarction and injury in dogs using an iodinated fattyacid and single-photon emission tomography. Am J Cardiol 52:1326-1332, 1983
4. Loevinger R. and M. Berman: A schema for absorbed dose calculations for biologically-distributed radionuclides. MIRD pamphlet No. 1, revised. Society of Nuclear Medicine, 1976
5. Snyder, W.S., M.R. Ford, G.G. Warner, and S.B. Watson: "S", absorbed dose per unit cumulated activity for selected radionuclides and organs. MIRD pamphlet No. 11. Society of Nuclear Medicine, 1975

6. Snyder, W.S., M.R. Ford, and G.G. Warner: Estimates of specific absorbed fractions for photon sources uniformly distributed in various organs of a heterogeneous phantom. MIRD pamphlet No. 5, revised. Society of Nuclear Medicine, 1978
7. Smith, E.M.: Dose estimation techniques, in Nuclear Medicine Physics Instrumentation, and Agents, edited by F.D. Rollo, pp. 513-543, C.V. Mosby Co., St. Louis, 1977
8. Hebel R. and Stromberg M.W., Anatomy of the Laboratory Rat, The Williams and Wilkins Co., Baltimore, 1976
9. Handbook of Biological Data, edited by W.S. Spector, W.B. Saunders Co., Philadelphia, 1956
10. CRC Handbook of Laboratory Animal Science, Vol. III, edited by N.H. Altman and E.C. Melby, The CRC Press, Cleveland, 1974
11. Coffey J.L. and E.E. Watson: S values for selected radionuclides and organs with the heart wall and heart contents as source organs, in Third International Radiopharmaceutical Dosimetry Symposium, Bureau of Radiological Health, p. 563, 1981
12. R.J. Cloutier, E.E. Watson, R.H. Rohrer, and E.M. Smith: Calculating the radiation dose to an organ. J Nucl Med 14:53-55, 1973

DISCUSSION

STABIN: Dr. Kulkarni, I was wondering whether you normalized your percent per gram values for body weight before you converted them to percent per organ?

KULKARNI: If by normalized you mean the weight of the human organ to the weight of the body, no.

BRILL: One of the major contributions of Mones Berman was to point out that the data for different organs in the body which metabolize a particular tracer can be fit most properly by different linear combinations of the same set of exponential coefficients. You fit each compartment independently and did not take advantage of that constraint. I wonder why you chose to do so?

KULKARNI: We followed the standard calculation procedure; we didn't do anything different from what was standard procedure.

BRILL: Perhaps I did not express myself properly. If, in the solution of a compartmental model, three exponential terms can be stripped from the data, each compartment should share the same lambdas and just have different linear combinations of those lambdas. Instead, you fit each set of data independently. I think you lose a degree of the internal constraints that are within the data when you do that. I would suggest that perhaps you might try doing it the other way. I don't think the data will turn out to be greatly different, but I think it is a more elegant way of doing it.

A COMPARISON OF RADIATION DOSIMETRY FOR SEVERAL POTENTIAL MYOCARDIAL IMAGING AGENTS

E.E. Watson¹, M.G. Stabin¹, M.M. Goodman², F.F. Knapp, Jr.², P.C. Srivastava²

¹ Oak Ridge Associated Universities, P.O. Box 117, Oak Ridge, Tennessee 37831

² Oak Ridge National Laboratory, P.O. Box X, Oak Ridge, Tennessee 37831

ABSTRACT

Although myocardial imaging is currently dominated by Tl-201, several alternative agents with improved physiologic or radionuclidic properties have been proposed. Based on human and animal studies in the literature, the metabolism of several of these compounds was studied for the purpose of generating radiation dose estimates. Dose estimates are listed for several I-123-labeled free fatty acids, an I-123-labeled phosphonium compound, Rb-82, Cu-64, F-18 FDG (all compounds which are taken up by the normal myocardium), and for Tc-99m pyrophosphate (PYP) (which localizes in myocardial infarcts). Dose estimates could not be generated for C-11 palmitate, but this compound was included in a comparison of myocardial retention times. For the I-123-labeled compounds, I-124 was included as a contaminant in generating the dose estimates. Radiation doses were lowest for Rb-82 (gonads 0.3-0.4 Gy/MBq, kidneys 8.6 Gy/MBq). Doses for the I-123-labeled fatty acids were similar to one another, with IPPA being the lowest (gonads 15 Gy/MBq, heart wall 18 Gy/MBq). Doses for Tc-99m PYP were also low (gonads 4-7 Gy/MBq, heart wall 4 Gy/MBq, skeleton 15 Gy/MBq). The desirability of these compounds is discussed briefly, considering half-life, imaging mode and energy, and dosimetry, including a comparison of the effective whole body dose equivalents.

INTRODUCTION

The study of myocardial perfusion is currently dominated by Tl-201, which is used to produce both planar and tomographic reconstructions of images of the myocardium. Its emission energies are not ideal (low abundance 137 and 165 keV gammas and 70-80 keV X-rays from Hg-201), but its biological properties (3-4% uptake in the myocardium with an initial 4.4 hour biological half-time (1,2)) make it a very useful agent. The myocardium may extract thallium by activation of the sodium potassium ATPase system (?). Several other radioactive agents have been developed for myocardial imaging, but have not been as useful for various reasons. Potassium-43 is rapidly cleared by the blood and efficiently extracted by the myocardium; however, it is rapidly cleared from the myocardium, precluding imaging more than one hour post injection. Cesium-129 is another potassium analog which has a slightly longer radioactive half-life, but it is not efficiently extracted by the myocardium. Nitrogen-13 ammonia ($^{13}\text{NH}_3$) has a very short radioactive half-life, and has a complex metabolic behavior which makes it difficult to use for quantitative studies.

In the past few years, a variety of myocardial imaging agents have emerged that employ radionuclides with more favorable imaging characteristics which are attached to radiopharmaceuticals that take advantage of other cellular uptake mechanisms. Several of these utilize some of the cell energy cycles to enter the myocardial cells. For example, F-18 fluorodeoxyglucose is a glucose analog which enters the cell's normal glucose cycle, but does not complete the glycolytic pathway. Other radionuclides (usually I-123) have been attached to modified fatty acids, which are taken up by the cells through their fatty acid metabolic pathways and retained. Some, being monovalent cations, are believed to employ some of the same metabolic pathways as thallium. Still other radiopharmaceuticals have been observed to be taken up in the normal or infarcted myocardium. Most of these new products employ a radionuclide which has more favorable imaging characteristics than Tl-201. If they are to find widespread application, they must also be easy to obtain and store, and must show at least similar, or more desirable, imaging and radiation dose characteristics. In this paper, the radiation doses received by patients from these compounds will be discussed and compared. Some discussion will also be developed which compares the availability and expected biological properties with those of Tl-201.

AGENTS WHICH LOCALIZE IN THE HEALTHY MYOCARDIUM

1) F-18 Fluorodeoxyglucose (FDG)

Radiation dose estimates for ^{18}FDG may be calculated using a combination of the dog data of Gallagher et al. (4) and the human data of Jones et al. (5). Jones et al. provided data for uptake and retention of ^{18}FDG in the urinary bladder, brain, and remainder of the body while Gallagher et al. provided uptake values for lungs, heart, brain, ovaries, spleen, liver, pancreas, and kidneys and collected urine samples at 60 and 135 minutes. Jones et al. monitored the activity in the urinary bladder with a collimated probe during the first 120 minutes post injection and estimated cumulated activity by integrating under the curves. These values, however, are only applicable for the experimental schema used by the investigators (which involved voiding the bladder and drinking two glasses of water before injection, no voiding for two hours, and voiding at the end of two hours). For this reason, the biological half-time for elimination through the urine from the data of Gallagher et al. was used to estimate bladder dose in the two general cases of regular 2.0 hour and 4.8 hour voiding after injection. The standard MIRD formulas were used, applying the remainder of the body correction proposed by Cloutier et al. (6). The dose estimates in Table 1 use the values for brain uptake from the data of Jones et al. and the uptake values for the other organs and the remainder of the body from the data of Gallagher et al., assuming that the effective half-time in all of these organs is equal to the physical half-time of ^{18}F . Myocardial uptake predicted by the data of Gallagher et al. is 3.5%, and the effective half-time would be 1.8 hours.

TABLE 1
Radiation Dose Estimates For F-18 FDG

Organ	Estimated Radiation Absorbed Dose			
	2.0 hour*		4.8 hour*	
	rad mCi	mGy MBq	rad mCi	mGy MBq
Bladder	0.86	0.23	1.7	0.46
Brain	0.064	0.017	0.064	0.017
Heart Wall	0.23	0.061	0.23	0.061
Kidneys	0.076	0.020	0.077	0.021
Liver	0.062	0.017	0.064	0.017
Lungs	0.067	0.018	0.068	0.018
Ovaries	0.062	0.017	0.082	0.022
Pancreas	0.094	0.025	0.095	0.026
Red Marrow	0.054	0.014	0.058	0.016
Spleen	0.14	0.039	0.14	0.039
Testes	0.068	0.018	0.084	0.023
Total Body	0.054	0.015	0.060	0.016

* Bladder voiding interval

Dose to the 'Total Body' is dose to the whole body from all source organs plus any activity uniformly distributed in the remainder of the body.

2) Radiolabeled Free Fatty Acids

A. I-123 15-(p-iodophenyl)-3-R,S-methylpentadecanoic acid (BMIPP)

A radiolabeled fatty acid would be very useful as a myocardial imaging agent if the compound is rapidly extracted by the myocardium and retained for a significant period of time, i.e., long enough that enough of the compound is removed from the blood to minimize interference from activity in the heart chambers. The fatty acid molecule is degraded in the mitochondria of the cells by progressive release of 2-carbon segments in the form of acetyl coenzyme A (acetyl Co-A); this process is referred to as β -oxidation. The acetyl Co-A molecules are ultimately broken down in the citric acid cycle into carbon dioxide and hydrogen atoms (7), which will not be selectively retained by the myocardial cells. Researchers at Oak Ridge National Laboratory (ORNL) have developed modified fatty acid molecules that do not participate in the fatty acid metabolism, but are still efficiently extracted by the myocardial cells. Early efforts involved tellurium-123, which had an attractive gamma energy for imaging but a long physical half-life, a high production cost, and a low specific activity (8). Attention was then given to the preparation of iodine-123 labeled fatty acids modified with nonradioactive tellurium. The difficulty of preparing these compounds led to the investigation of the use of radioiodinated iodophenyl- and iodovinyl-substituted fatty acids which employ methyl-branching as the structural abnormality that would inhibit β -oxidation and thus "trap" the fatty acid molecule in the myocardium.

Detailed distribution studies were performed at ORNL in female Fisher rats for one such compound, I-123 labeled BMIPP. The I-125 labeled compound

was administered to the rats, which were sacrificed at various time intervals, for times up to 3 days. Excretion data were also obtained over this time period. Organ retention data were extrapolated from % kg injected activity per gram in the rat to % injected activity per organ in the human, and least squares fit to one or two compartment uptake and elimination models. Whole-body retention, from the % of injected activity in the excreta, was extrapolated directly to humans from the animal values. Radiation dose estimates were calculated based on the residence times for I-123 using the standard MIRD technique and the remainder of the body correction. For this compound, and all of the I-123 labeled compounds, a contaminant level of 5% I-124 was assumed so that the dose estimates would be more representative of what might be expected in practice. The I-124 contribution to the total dose to any organ for these compounds is typically half or more. Dose estimates are listed in Table 2. Myocardial uptake was 2.9%; elimination was biphasic, with 86% having an effective half-time of 2.8 hours, and 14% having an effective half-time of 8.0 hours.

TABLE 2

Radiation Dose Estimates For I-123 BMIPP*

Organ	Estimated Radiation Absorbed Dose			
	2.0 hour**		4.8 hour**	
	rad mCi	mGy MBq	rad mCi	mGy MBq
Bladder	0.19	0.050	0.38	0.10
Stomach	0.050	0.014	0.050	0.014
Small Intestine	0.19	0.052	0.19	0.052
Upper Large Intestine	0.42	0.11	0.42	0.11
Lower Large Intestine	0.61	0.16	0.61	0.16
Heart Wall	0.094	0.025	0.094	0.025
Kidneys	0.069	0.019	0.069	0.019
Liver	0.076	0.021	0.076	0.021
Lungs	0.058	0.016	0.058	0.016
Ovaries	0.12	0.033	0.13	0.035
Red Marrow	0.068	0.018	0.069	0.019
Testes	0.045	0.012	0.049	0.013
Thyroid	0.28	0.075	0.28	0.075
Total Body	0.053	0.014	0.055	0.015

* 5% I-124 contamination assumed. 0.48% free iodide assumed; treated as in MIRD Dose Estimate Report No. 5 (25% uptake).

** Bladder voiding interval.

Dose to the 'Total Body' is dose to the whole body from all source organs plus any activity uniformly distributed in the remainder of the body.

B. I-123 15-(p-iodophenyl)-3,3-dimethylpentadecanoic acid (DMIPP)

This agent, prepared similarly to BMIPP, was also studied by ORNL researchers in female Fisher rats. The study techniques and data reduction techniques were identical to those for BMIPP, described above. Radiation dose estimates are listed in Table 3. Myocardial uptake was 2.5% and retention was

biphasic, with 91.6% having an effective half-time of 3.0 hours and 8.4% having an effective half-time of 9.8 hours.

TABLE 3
Radiation Dose Estimates For I-123 DMIPP*

Organ	Estimated Radiation Absorbed Dose		
	2.0 hour**		
	rad mCi	mGy MBq	
Bladder	0.13	0.035	0.16
Stomach	0.10	0.027	0.10
Small Intestine	0.72	0.19	0.72
Upper Large Intestine	1.7	0.46	1.7
Lower Large Intestines	2.6	0.70	2.6
Heart Wall	0.083	0.022	0.083
Kidneys	0.11	0.029	0.11
Liver	0.19	0.051	0.19
Lungs	0.056	0.015	0.056
Ovaries	0.44	0.12	0.44
Red Marrow	0.11	0.031	0.11
Spleen	0.068	0.018	0.068
Testes	0.040	0.011	0.041
Thyroid	3.4	0.91	3.4
Total Body	0.085	0.023	0.086

* 5% I-124 contamination assumed. 6.4% free iodide assumed; treated as in MIRD Dose Estimate Report No. 5 (25% uptake).

** Bladder voiding interval.

Dose to the 'Total Body' is dose to the whole body from all source organs plus any activity uniformly distributed in the remainder of the body.

C. I-123 Phenylpentadecanoic acid

Iodine-123 Phenylpentadecanoic acid (IPPA) is another fatty acid which has been investigated as a myocardial imaging agent. Kulkarni et al. (9) published detailed distribution studies performed in Sprague-Dawley rats. Their values of % injected activity per gram of tissue were converted to % kg injected activity per gram, using an average body weight of 0.19 kg. These results were then analyzed using the same methods as for BMIPP and DMIPP. Radiation dose estimates based on these assumptions are listed in Table 4. Predicted myocardial uptake was 3.0%, with 89% having an effective half-time of 0.79 hours and the remaining 11% having an effective half-time of 9.2 hours. Studies done in human subjects (10-12) also showed a biexponential clearance of this compound from normally perfused myocardium. The half-lives for the two compartments were given, however the fractions associated with each half-life and the total myocardial uptake were not given. The values were between 10 and 15 minutes (0.17-0.25 hours) for the short-lived fraction and about 80 minutes (1.3 hours) for the long lived fraction.

TABLE 4
Radiation Dose Estimates For I-123 IPPA*

Organ	Estimated Radiation		Absorbed Dose	
	2.0 hour**		4.8 hour**	
	rad mCi	mGy MBq	rad mCi	mGy MBq
Bladder	0.25	0.067	0.57	0.17
Heart Wall	0.067	0.018	0.067	0.018
Kidneys	0.12	0.033	0.12	0.033
Liver	0.12	0.032	0.12	0.032
Lungs	0.11	0.029	0.11	0.029
Ovaries	0.048	0.013	0.054	0.015
Red Marrow	0.048	0.013	0.048	0.013
Spleen	0.060	0.016	0.061	0.016
Testes	0.034	0.0094	0.042	0.011
Total Body	0.040	0.011	0.044	0.012

* 5% I-124 contamination assumed. No free iodide considered.

** Bladder voiding interval.

Dose to the 'Total Body' is dose to the whole body from all source organs plus any activity uniformly distributed in the remainder of the body.

D. C-11 Palmitate

Carbon-11 labeled palmitic acid is another free fatty acid which has been studied in humans and animals as a potential myocardial imaging agent. Carbon-11 is a short lived (20.4 min) positron emitter. Although many papers have discussed the metabolism of this agent in the myocardium, no detailed distribution studies were found which could be used to generate a comprehensive set of radiation dose estimates. Reske et al. (13) found that the biological behavior of C-11 palmitate was similar to that of I-123 IPPA but that levels in tissues were generally lower, with the exception of the liver. Most researchers (14-18) found a biexponential elimination curve for the myocardium. In the dog studies, the short half-time was between 3 and 5 minutes, and the long half-time was between 150 and 360 minutes. In the human studies, the short half-time was between 6 and 14 minutes, and the long half-time, as reported in one study (14), was 157 minutes.

3) I-123 (E-1-Iodo-1-Penten-5-yl) Triphenylphosphonium Iodide

Phosphonium cations labeled with I-123 have been suggested as myocardial perfusion agents, as these cations penetrate the hydrophobic core of the myocardial cell membrane. Detailed distribution studies were performed in female Fischer rats at ORNL, where the compound was developed. Animals were sacrificed at various times up to three days, and urine and feces samples were collected each day. Data reduction techniques were identical to those used for I-123 BMIPP and DMIPP. Radiation dose estimates are listed in Table 5. The resulting curve for the heart predicts a myocardial uptake of 4.5% of the injected activity with an effective half-time of 10.5 hours.

TABLE 5

Radiation Dose Estimates For I-123
(E-1-Iodo-1-Penten-5-vl) Triphenylphosphonium Iodide*

Organ	Estimated Radiation		Absorbed Dose	
	2.0 hour**		4.8 hour**	
	rad mCi	mGy MBq	rad mCi	mGy MBq
Bladder	0.15	0.042	0.21	0.057
Stomach	0.13	0.034	0.13	0.034
Small Intestine	0.39	0.10	0.39	0.10
Upper Large Intestine	0.79	0.21	0.79	0.21
Lower Large intestine	1.2	0.32	1.2	0.32
Heart Wall	0.46	0.12	0.46	0.12
Kidneys	0.19	0.051	0.19	0.051
Liver	0.071	0.019	0.071	0.019
Lungs	0.087	0.023	0.087	0.023
Ovaries	0.23	0.061	0.23	0.061
Red Marrow	0.15	0.040	0.15	0.040
Spleen	0.088	0.024	0.088	0.024
Testes	0.10	0.027	0.10	0.027
Thyroid	4.0	1.1	4.0	1.1
Total Body	0.12	0.031	0.12	0.032

* 5% I-124 contamination assumed. 7.1% free iodide assumed; treated as in MIRD Dose Estimate Report No. 5.

** Bladder voiding interval.

Dose to the 'Total Body' is dose to the whole body from all source organs plus any activity uniformly distributed in the remainder of the body.

4) Rubidium-82

Rubidium-82 is thought to be a potassium analog. This radionuclide is a short-lived (76 seconds) positron emitter which can be obtained from a Sr-82/Rb-82 generator system (parent half-life 25.6 days). The Rb-82 is rapidly extracted by the myocardium; the short half-life permits closely spaced repeat studies. Kefratt (19) published detailed distribution studies for Rb-86 in Sprague-Dawley rats. Ryan et al. (20) collected distribution data in two adult men for Rb-82. Radiation dose estimates in Table 6 use the data of Ryan et al. where possible and fill in the other organ radiation doses from the data of Kefratt. The dose estimates based on extrapolation of the rat data to Rb-82 in humans agreed fairly well with those based on the human data. Data obtained from one generator system suggested contamination levels of 10^{-7} and 2.5×10^{-7} for Sr-82 and Sr-85, respectively (35). The dose estimates in Table 6 include radiation doses from these contaminants, with the following assumptions:

- 1) 50% of the strontium is taken up by bone and retained with an infinite biological half-time; the activity is assumed to be uniformly distributed throughout the bone volume (21).

- 2) 0.5% of the strontium is taken up in the testes and retained with a 1.5 day biological half-time.
- 3) The remaining 49.5% is uniformly distributed in the remainder of the body and retained with a biological half-time of 1.5 days.

Rb-82 produced in the bone by decay of Sr-82 is assumed to stay in the bone, while Rb-82 produced in the remainder of the body is considered free and is treated like the injected Rb-82. Neither Kearnott nor Ryan et al. gave the uptake fractions and effective half-times for Rb-82 in the myocardium; they only listed the cumulated activities. The uptake fraction may be inferred from the cumulated activity values because the effective half-time is probably equal to the physical half-life. Kearnott's value (rats) for the heart wall was 1.4 $\mu\text{Ci}\text{-hr}/\text{mCi}$, while that of Ryan et al. (humans) was 0.55 $\mu\text{Ci}\text{-hr}/\text{mCi}$. From this, the uptake fraction is either 4.6% or 1.8%, respectively. The latter value is probably to be preferred because it came from human subjects. The effective half-time would then be 1.27 minutes, or 0.0212 hours.

TABLE 6
Radiation Dose Estimates For Rb-82

<u>Organ</u>	<u>Estimated Radiation Absorbed Dose</u>	
	<u>mrad</u> <u>mCi</u>	<u>μGy</u> <u>MBq</u>
Adrenals	3.6	0.97
Stomach	3.2	0.86
Small Intestine	5.3	1.4
Upper Large Intestine	3.2	0.86
Lower Large Intestine	3.2	0.86
Heart Wall	7.0	1.9
Kidneys	32	8.6
Liver	3.2	0.86
Lungs	6.4	1.7
Ovaries	1.4	0.38
Pancreas	2.3	0.62
Trabecular Bone	0.0092	0.0025
Cortical Bone	0.015	0.0041
Red Marrow	1.4	0.38
Testes	1.1	0.30
Total Body	1.6	0.43

Dose to the 'Total Body' is dose to the whole body from all source organs plus any activity uniformly distributed in the remainder of the body.

5) Copper-64

Copper-64 is a relatively long-lived (12.7 hours) positron emitter. Similarities between the effects produced in animal tissues due to copper deficiencies and those in humans due to heart disease have caused some to speculate that copper metabolism is important in the formation of ischemic heart disease (22-26). Distribution studies were performed in rats at the

Medical and Health Sciences Division (MHSD) of Oak Ridge Associated Universities (ORAU). Cu-64 levels in the liver, spleen, kidneys, lungs, muscle, bone, and marrow were determined at 0.5, 1, 2, 4, 6, 12, 24, and 26 hours post injection. Residence times were determined by least squares fitting of the % injected activity per organ values at these times (extrapolated from the % kg injected activity per gram in the rat) to one compartment exponential elimination curves. Radiation dose estimates were calculated as in the above cases. The estimates are listed in Table 7. Activity in the heart was estimated for only two time points in these distribution studies; the maximum uptake fraction, which occurred at 26 hours, was 0.43%. The effective half-times in all of the other organs were very long (8.7-12.7 hours), possibly indicating that myocardial retention would also be long.

TABLE 7
Radiation Dose Estimates For Cu-64

<u>Organ</u>	<u>Estimated Radiation Absorbed Dose</u>	
	<u>rad</u> <u>mCi</u>	<u>mGy</u> <u>MBq</u>
Heart Wall	0.10	0.028
Kidneys	1.4	0.39
Liver	0.44	0.12
Lungs	0.12	0.033
Muscle	0.047	0.013
Ovaries	0.11	0.030
Skeleton	0.084	0.023
Red Marrow	0.18	0.048
Spleen	0.14	0.037
Testes	0.12	0.032
Total Body	0.098	0.026

Dose to the 'Total Body' is dose to the whole body from all source organs plus any activity uniformly distributed in the remainder of the body.

6) Tc-99m Labeled Cations

Because many compounds accumulate in the myocardium which are not clearly potassium analogs but are monovalent compounds at physiological pH, several researchers have concentrated on the development of monovalent cations labeled with Tc-99m (27). The availability and excellent imaging characteristics of this radionuclide make it attractive for any nuclear medicine procedure, and many procedures are currently done with Tc-99m labeled compounds.

Early efforts to produce Tc-99m labeled cations resulted in the development of two technetium (III) complexes, $\text{tr-[Tc-99m(DIARS)}_2\text{X}_2]$, (where DIARS represents the α -phenylene-bis(dimethylarsine) ligand and X is a chloride or bromide) and $\text{tr-[Tc-99m(DMPE)}_2\text{Cl}_2]$ (where DMPE represents the 1,2-bis(dimethylphosphino)ethane ligand). Although these agents showed promising distributions in dogs and rats, in humans the hepatic uptake was very high, and interfered with the myocardial images. Work with technetium (I) complexes resulted in the development of $[\text{Tc-99m(DMPE)}_3]$, $[\text{Tc-99m(TMP)}_6]$ (where TMP represents trimethyl-phosphite), and $[\text{Tc-99m(POM-POM)}_3]$ (where

POM-POM represents 1,2-bis(dimethoxyphosphino)ethane), which again showed promising results in several animal species, but which cleared very slowly from the human bloodstream. Another such compound, [Tc-99m(TBIN)₆] (where TBIN represents t-butylisonitrile), exhibited early lung uptake, with late (approximately one hour post injection) clearance to the liver and myocardium. Although this compound provided the best myocardial images from the Tc-99m cationic species, the images were difficult to interpret. The hypothesis that the Tc-99m labeled species are being reduced *in vivo* to a neutral technetium (II) species which may precipitate in colloidal form, thus explaining the liver uptake, has led some to develop technetium (III) complexes with redox potentials which will inhibit *in vivo* reduction. Results of these efforts are still forthcoming.

In summary, although much work has been done, no Tc-99m labeled agent has been produced which can be used routinely to image the myocardium. Because distribution data are not available for any of these experimental agents which would allow calculation of even preliminary dose estimates, these agents were not considered in the comparison developed in this paper.

AGENTS WHICH LOCALIZE IN THE INFARCTED MYOCARDIUM

1) Tc-99m Pyrophosphate

Although Tc-99m pyrophosphate was initially used as a bone imaging agent, researchers have found that it is taken up in the infarcted myocardium (28, e.g.). Radiation dose estimates for Tc-99m pyrophosphate in Table 8 are based on the distribution and retention data of Subramanian et al. (29) and on the data of Bonte et al. (28) for the dog myocardium. For the myocardium, an uptake fraction of 1.27×10^{-3} and an effective half-time of 6.02 hours were assumed.

TABLE 8
Radiation Dose Estimates For Tc-99m Pyrophosphate

Organ	Estimated Radiation		Absorbed Dose	
	2.0 hour*		4.8 hour*	
	rad mCi	mGy MBq	rad mCi	mGy MBq
Bladder	0.098	0.026	0.23	0.061
Heart Wall	0.015	0.0041	0.015	0.0041
Kidneys	0.047	0.013	0.047	0.013
Ovaries	0.019	0.0051	0.025	0.0068
Skeleton	0.055	0.015	0.056	0.015
Red Marrow	0.042	0.011	0.044	0.012
Testes	0.013	0.0036	0.017	0.0047
Total Body	0.019	0.0051	0.021	0.0056

* Bladder voiding interval.

Dose to the 'Total Body' is dose to the whole body from all source organs plus any activity uniformly distributed in the remainder of the body.

2) Other Compounds

Evidence exists (30,31) that enhanced F-18 FDG uptake may occur in areas of ischemic but viable myocardium. Radiation dose estimates for F-18 FDG are listed in Table 1. Evidence exists that In-111 and Tc-99m labeled antimyosin (Fab fragments of antibodies directed against human cardiac myosin) will also selectively locate in infarcted myocardial tissue (32,36,37,e.g.). This raises the possibility of using labeled antibodies for myocardial infarct imaging, although enough data to calculate radiation dose estimates were not found in the literature.

DISCUSSION

Three basic parameters may be compared to estimate the desirability of these agents: (1) the availability of the radionuclide, (2) the image quality obtainable with the radiopharmaceutical, and (3) the radiation dose received by the patient from a typical procedure. The first parameter includes the cost and ease of procurement as well as the physical half-life. The second parameter considers the photon energy, the effective half-life of the radiopharmaceutical at the imaging site, and the type of detector which may be used for imaging.

AVAILABILITY

In general, a generator-based radionuclide will be less expensive and will present fewer logistic problems than either an accelerator-produced or reactor-produced radionuclide. A product utilizing Tc-99m would probably be the most attractive because of its low expense, widespread availability, and good imaging energy. At this time, no such product has been demonstrated, although at least two groups (27) are working on this approach. Infarct imaging with Tc-99m PYP will probably continue but cannot answer all of the questions involved with evaluation of myocardial perfusion. The Sr-82/Rb-82 generator would make the ultrashort-lived Rb-82 widely available in a generator with a long shelf life. The extremely long shelf life of this generator would, however, bring up questions of long term product sterility.

The half-lives of the accelerator- and reactor-produced radionuclides, F-18, I-123, and C-11 are 1.8 hours, 13.2 hours, and 0.34 hours, respectively. Besides the expense, the additional problems associated with the production and transport of these isotopes increases with decreasing radionuclide half-life and increasing distance of the nuclear medicine facility from the production facility. This would make I-123 the most attractive isotope for institutions which do not have an in-house production facility.

IMAGE QUALITY

The principal photon energies for Rb-82, Cu-64, F-18 and C-11 are the 0.511 MeV photons, the annihilation radiation from the positron emissions. These radionuclides could be used in PET studies, which can provide excellent anatomical detail. The principal photon energy of I-123 (159 keV) is within the optimum range of nuclear medicine cameras, allowing I-123 labeled compounds to be used for planar or tomographic imaging with SPECT. Iodine-123 has two problems associated with its use, both of which are manageable. First, free iodide will concentrate in the thyroid, causing unnecessary radiation dose to the patient and possible interferences on images. Secondly, accelerator-produced I-123 usually contains significant levels of I-124 (and possibly other contaminants) which also produce unwanted radiation doses and can cause image degradation. The use of a thyroid-blocking agent will reduce

the thyroid dose from free iodide; the choice of a radiopharmaceutical which has been produced with good quality control can minimize the amount of free iodide and contaminants. Some control of the latter problem can be exerted on site, as Palmer and Rao (33) have shown that a simple laboratory method can be used to quantitate the I-124 level in I-123 samples.

Increasing the fraction of administered activity taken up in the myocardium would offer significant advantages over the relatively low 3-4% value for Tl-201. The effective half-time for myocardial retention is also important because performance of stress/redistribution studies depends on having a significant amount of activity in the myocardium 2-4 hours post injection. Table 9 lists the uptake fractions and effective half-times in the myocardium for the compounds studied. Rb-82 showed the lowest uptake fraction, 1.8%. Because of the short effective half-time, repeat studies could be performed over short time periods without interference from earlier studies; continuous infusion studies would also be possible. Presumably, myocardial washout may be inferred through multiple studies, but could not be observed directly. Both BMIPP and DMIPP show about 2.5-3.0% uptake in the myocardium, with the majority of the activity having a short (2-3 hour) half-time and the remainder (about 10%) having a longer (8-10 hour) half-time. I-123 IPPA has an uptake fraction of about 3%; most of the activity has a relatively short effective half-time (0.79 hours) while the remainder (about 12%) has a long effective half-time (9.2 hours). F-18 FDG has a slightly higher uptake fraction, but a much shorter effective half-time. I-123 triphenylphosphonium iodide has an uptake fraction of 4.5% and an effective half-time of over 10 hours.

TABLE 9

Uptake Fractions And Effective Half-Times In The Myocardium
Of The Compounds Studied In This Paper

Compound	Uptake Fraction	Effective Half-Time	
F-18 FDG	0.035		1.8 hours
I-123 BMIPP	0.029	86%	2.8 hours
		14%	8.0 hours
I-123 DMIPP	0.025	91.6%	3.0 hours
		8.4%	9.8 hours
I-123 IPPA	0.030	89%	0.84 hours
		11%	9.2 hours
C-11 Palmitate	No data		0.05-0.08 hour 2.5-6.0 hours
I-123 Triphenyl- phosphonium Iodide	0.045		10.5 hours
Rb-82	0.018*		0.021 hours
Cu-64	0.0043		No data
Tc-99m PYP	0.0013		6.01 hours

* Deduced from cumulated activity results in human subjects (19).
Result from animal studies (20) would be 0.046.

RADIATION DOSE

To compare the radiation doses from these radiopharmaceuticals properly, some estimate must be made of the amount of activity to be used per study. Table 10 shows the radiation dose to the critical organ and the gonads based on an assumed amount of activity per study for each compound for which radiation dose estimates could be obtained. The assumed values for activity per study were taken from various sources, including estimations from researchers who developed some of the compounds and quoted values in journal articles and abstracts. In addition, the committed effective whole body dose equivalent, as defined in ICRP 26 (34), was calculated for each compound and is also listed in Table 10. This parameter provides an at-a-glance estimate of the radiation dose from a compound, taking into account the relative risk of irradiation of specific tissues.

The highest critical organ doses are seen for I-123 triphenyl-phosphonium iodide and I-123 DMIPP because of the thyroid doses (150-200 mGy per study). This value is highly dependent on the amount of free iodide and I-124 contaminant in the product. Because these parameters are controllable to some degree, the actual doses seen in practice may not be this high. Radiation dose to the lower large intestine and bladder were relatively high for I-123 DMIPP, I-123 triphenylphosphonium iodide, and F-18 FDG.

The results in Table 10 show that the gonadal dose (in this table, the average of testicular and ovarian dose) is lowest for Rb-82 (0.10 mGy). I-123 IPPA is the next highest, with 0.92 mGy; F-18 FDG, I-123 BMIPP, I-123 DMIPP, I-123 triphenylphosphonium iodide, Cu-64, and Tc-99m PYP have similar gonadal estimates, approximately 5-10 mGy per study. The I-123 DMIPP gonadal dose is about a factor of three higher than BMIPP. This is because for these compounds ovarian dose is primarily determined by activity in the GI tract; excretion data on the two compounds suggest that about 16% of the activity is excreted through the feces for BMIPP while 74% is excreted through the feces for DMIPP.

The effective whole body dose equivalents are lowest for I-123 IPPA and Rb-82, both under 1 mSv. The contaminants Sr-82 and Sr-85 did not contribute significantly to the radiation dose estimates for Rb-82, because of the low values assumed for their breakthrough. As with all products containing long-lived contaminants, and especially with these because of their affinity for bone and the possibility of administering large amounts of activity during repeat or continuous infusion studies, the dosimetry picture can change significantly if the contaminant levels change. F-18 FDG, I-123 BMIPP, and Tc-99m PYP all have values between 1 and 10 mSv, with Tl-201 having a value near 10 mSv. I-123 triphenylphosphonium iodide and I-123 DMIPP have the highest effective whole body dose equivalents, at 18 and 24 mSv, respectively.

TABLE 10
Some Radiation Dose Characteristics Of The Compounds
Studied In This Paper

Compound	Assumed Average Activity/Study (MBq)	Estimated Radiation Dose (mGy)		Committed Effective WB Dose Equivalent (mSv)
		Critical Organ	Gonads	
¹⁸ FDG	180	Bladder 83	4.0	8.3
¹²³ I BMIPP	180	LLI 29	4.3	7.1
¹²³ I DMIPP	180	LLI 130 Thyroid 160	12	24
¹²³ IPPA	40	Bladder 4.8	0.82	0.92
¹²³ I Triphenyl-phosphonium Iodide	180	LLI 58 Thyroid 200	7.9	18
⁸² Rb	300	Heart Wall 4.5	0.12	0.69
⁶⁴ Cu	260	Kidneys 100	8.1	14
^{99m} Tc PYP	550	Bladder 34 Skeleton 8.2 Red Marrow 6.6	3.2	4.7
²⁰¹ Tl	100	Kidneys 32	14	8.3

CONCLUSIONS

Table 11 summarizes the comparisons made above. The compounds were given a rather arbitrary ranking of low to high availability, based on the expense and difficulty anticipated with acquisition of the radionuclide. The biological distribution parameters of uptake fraction and effective half-time, as well as the effective whole body dose equivalent, were compared with Tl-201.

F-18 FDG may be difficult to obtain unless an accelerator is near the location where the studies will be performed. The distribution and radiation dose characteristics were either about equal or inferior to those of Tl-201. The free fatty acids labeled with I-123 were all assigned a 'medium' availability. BMIPP and DMIPP have somewhat lower uptake fractions than Tl-201 and similar effective half-times in the myocardium for the majority of the activity taken up by the myocardium. In both compounds, about 10% of the initial activity in the myocardium has a long (8-10 hours) effective half-time. The radiation dose for DMIPP, based on the preliminary animal studies, is higher than that for Tl-201, and that for BMIPP is about the same as that for Tl-201. I-123 IPPA has a lower radiation dose than Tl-201, however, the effective half-time for the majority of the activity is short. All of the I-123 triphenylphosphonium iodide taken up by the myocardium has a long effective half-time; its radiation dose is predicted to be higher than most

of the other agents and Tl-201, but follow-up human studies should be performed to see whether or not this result predicted from animal models is valid. Myocardial uptake for Rb-82 was only 1.8%; its effective half-time in the myocardium is limited by its short physical half-life. The use of multiple studies or continuous infusion techniques might make it usable for perfusion studies. Tc-99m PYP gives different information than Tl-201, and seems well suited for the studies it is designed to perform. Not enough data are available to evaluate C-11 palmitate or Cu-64 against the other agents.

TABLE 11

Comparison Of The Compounds Studied In This Paper
Based On Availability, Distribution, And Radiation Dose

Compound	Availability	Distribution Parameters	Radiation Dose
		Relative To Tl-201	Relative To Tl-201
18FDG	Low	"same uptake shorter T_{eff}	"same
123I BMIPP	Medium	lower uptake "same T_{eff}	"same
123I DMIPP	Medium	lower uptake "same T_{eff}	higher
123IPPA	Medium	"same uptake shorter T_{eff}	lower
11C Palmitate	Low	uncertain	uncertain
123I Triphenyl- phosphonium Iodide	Medium	"same uptake longer T_{eff}	higher
82Rb	High	lower uptake shorter T_{eff}	lower
64Cu	Medium	lower uptake (uptake, T_{eff} uncertain)	higher
99mTc PYP	High	lower uptake longer T_{eff} (restricted information)	lower

This article is based on work supported by contract number DE-AC05-76OR00033 between the U.S. Department of Energy and ORAU and Interagency Agreement No. FDA 224-75-3016 with the Food and Drug Administration. Research is also supported by the Office of Health and Environmental Research, U.S. Department of Energy, under contract number DE-AC05-84OR21400 with Martin Marietta Energy Systems, Inc.

REFERENCES

- 1) Samson G., F.J.Th. Wackers, A.E. Becker, et al.: Distribution of thallium-201 in man. Nuklearmedizin, Verhandlungsbericht der 14. International Jahrestagung der Gesellschaft fur Nuclear Medizin, D. Oeff and H.A.E. Schmide eds., Medico-Informationschirnste, Berlin, pp 385-389, 1978.
- 2) Garcia E., J. Maddahi, D. Berman, and A. Waxman: Space-time quantitation of sequential thallium-201 myocardial scintigrams: description and application of a new method. J Nucl Med 21(6):P62, 1980.
- 3) Walker J. and D. Margouleff: A Clinical Manual of Nuclear Medicine. Appleton-Century-Crofts, East Norwalk, CT 1984.
- 4) Gallagher B.M., A. Ansari, H. Atkins, et al.: Radiopharmaceuticals XXVII: ¹⁸F-labeled 2-deoxy-2-fluoro-d-glucose as a radiopharmaceutical for measuring regional myocardial glucose metabolism in vivo: tissue distribution and imaging studies in animals. J Nucl Med 18(10):990-996, 1977.
- 5) Jones S., A. Alavi, D. Christman, et al.: The radiation dosimetry of 2-[F-18]fluoro-2-deoxy-d-glucose in man. J Nucl Med 23(7):613-617, 1982.
- 6) Cloutier R., E. Watson, R. Rohrer, et al.: Calculating the radiation dose to an organ. J Nucl Med 14(1):53-55, 1973.
- 7) Guyton A.: Textbook of Medical Physiology. W. B. Saunders Company, Philadelphia, PA, 1976.
- 8) Knapp F.F. and M.M. Goodman: The design and biological properties of iodine-123 labeled β -methyl-branched fatty acids. From the "Workshop on Radiolabeled Free Fatty Acids", Academic Hospital, Free University, Amsterdam, The Netherlands, July 6, 1984. Published in the European Heart Journal, February, 1985.
- 9) Kulkarni P., G. Clark, J. Corbett, et al.: Human absorbed dose calculations for ¹²³I labeled phenyl pentadecanoic acid. In Proceedings: Fourth International Radiopharmaceutical Dosimetry Symposium, Nov 5-8, 1986, Oak Ridge Associated Universities, Oak Ridge, TN.
- 10) Reske S., R. Knopp, H. Machulla et al.: Clearance-patterns of 15(p-I-123 phenyl-)pentadecanoic acid (IP) in patients with CAD after bicycle exercise. J Nucl Med 24(5):P13, 1983.
- 11) Reske S., D. Koischwitz, H. Machulla et al.: Myocardial turnover of (123I-phenyl-)pentadecanoic acid (IP) in patients with CAD. Eur J Nucl Med 8(5):A5, 1983.
- 12) Dudczak R., R. Schmoliner, P. Angelberger et al.: Myocardial studies with I-123 p-phenylpentadecanoic acid (PPA) in patients with coronary artery disease (CAD) and cardiomyopathy (CMP). J Nucl Med 23(5):P35, 1982.
- 13) Reske S., W. Sauer, H.-J. Machulla, and C. Winkler: 15(p-[¹²³I] iodophenyl)pentadecanoic acid as tracer of lipid metabolism: comparison with [1-¹⁴C]palmitic acid in murine tissues. J Nucl Med 25(12):1335-1342, 1984.
- 14) Notohamiprodjo G., A. Schmid, G. Spohr, et al.: Comparison of

¹¹-C-palmitic acid (CPA) and ¹²³I-heptadecanoic acid (IHA) turnover in human heart. J Nucl Med 26(5):P88-89, 1985.

- 15) Wijns W., M. Schwaiger, S. Huang, et al.: Effects of inhibition of -oxidation on tissue kinetics of C-11 palmitate in normal myocardium. J Nucl Med 26(5):P89, 1985.
- 16) Hoffman E., M. Phelps, E. Weiss, et al.: Transaxial tomographic imaging of canine myocardium with ¹¹C-palmitic acid. J Nucl Med 18(1):57-61, 1977.
- 17) Schon H., H. Schelbert, G. Robinson, et al.: Extraction and turnover of C-11 palmitate in normal myocardium. J Nucl Med 22(6):P57, 1981.
- 18) Henze E., R. Grossman, S. Huang, et al.: Myocardial uptake and clearance of C-11 palmitic acid in man: effects of substrate availability and cardiac work. J Nucl Med 23(5):P12-13, 1982.
- 19) Kearnott K.: Radiation absorbed dose estimates for positron emission tomography (PET): K-38, Rb-81, Rb-82, and Cs-130. J Nucl Med 23(12):1128-1132, 1982.
- 20) Ryan J., P. Harper, V. Stark, et al.: Radiation absorbed dose estimate for Rb-82 using *in vivo* measurements in man. J Nucl Med 25(5):P94, 1984.
- 21) Committee 2 of the International Commission on Radiological Protection: Limits for Intakes of Radionuclides by Workers. ICRP 30. Pergamon Press, New York, 1979.
- 22) Klevay L.M.: The role of copper and zinc in cholesterol metabolism. In Draper H.H., ed. Advances in Nutritional Research - I. Plenum Publishing Corp., New York, 1977.
- 23) Harris E.D., J.K. Rayton, J.E. DeGroot: A critical role for copper in aortic elastin structure and synthesis. Adv Exp Med Biol 79:543-559, 1977.
- 24) Klevay L.M.: Interaction of copper and zinc in cardiovascular disease. Ann NY Acad Sci 355:140-151, 1980.
- 25) Klevay L.M.: Coronary heart disease: the zinc/copper hypothesis. Am J Clin Nutr 28:764-774, 1975.
- 26) Crook J.E., J.E. Carlton, E.C. Holloway: Copper-64 citrate as a potential myocardial imaging agent. J Nucl Med, in press.
- 27) Deutsch E.: Cardiovascular radiopharmaceuticals. In Proceedings, Southeastern Chapter of the Society of Nuclear Medicine Meeting, October 24-26, 1985, Hollywood, Florida. Section X.
- 28) Bonte F., R. Parkey, K. Graham, J. Moore: Distributions of several agents useful in imaging myocardial infarcts. J Nucl Med 16(2):132-135, 1975.
- 29) Subramanian G., J. McAfee, R. Blair, et al.: Technetium-99m-methylene diphosphonate - a superior agent for skeletal imaging: comparison with other technetium complexes. J Nucl Med 16(8): 744-755, 1975.
- 30) Sochor H., M. Schwaiger, H. Hasen, et al.: Assessment of myocardial injury after reperfusion with Tl-201, Tc-99m pyrophosphate (PP1) and F-18

deoxyglucose (FDG). J Nucl Med 25(5):P38, 1984.

- 31) Rigo P., C. De Landsheere, D. Raets, et al.: Demonstration by positron tomography and ¹⁸F deoxyglucose of regional myocardial viability after myocardial infarction: influence of fibrinolysis and revascularization. J Nucl Med 26(5):P87, 1985.
- 32) Yasuda A., B. Khaw, J. Gold, et al.: Comparison of image characteristics of In-111-antimyosin and Tc-99m antimyosin in patients with acute myocardial infarction. J Nucl Med 26(5):P88, 1985.
- 33) Palmer D. and S. Rao: A simple method to quantitate iodine-124 contamination in iodine-123 radiopharmaceuticals. J Nucl Med 26(8): 936-940, 1985.
- 34) International Commission on Radiological Protection: Recommendations of the International Commission on Radiological Protection. ICRP 26. Pergamon Press, New York, 1977.
- 35) Gennaro G.P., R.D. Neirinckx, B. Berner et al.: Radionuclide Generators. American Chemical Society, Washington, D.C. 1984.
- 36) Khaw B.A., G.A. Beller, E. Haber: Localization of cardiac myosin-specific antibody in myocardial infarction. J Clin Invest 58:439-446, 1976.
- 37) Khaw B.A., J.T. Fallon, H.W. Strauss, E. Haber: Myocardial infarct imaging with Indium-111-diethylene triamine pentaacetic acid-anti-canine cardiac myosin antibodies. Science 209:295-297, 1980.

BIOKINETICS AND DOSIMETRY OF ^{131}I -METAIODOBENZYLGUANIDINE (MIBG).

L. Jacobsson, S. Mattsson, L. Johansson, S. Lindberg and M. Fjälling.

Departments of Radiation Physics and Nuclear Medicine, University of Göteborg
Sahlgren Hospital, S-413 45 Göteborg and FOA 451, S-901 82 Umeå, Sweden.

ABSTRACT

In connection with clinical ^{131}I -MIBG studies of patients with suspected sporadic pheochromocytoma or multiple endocrine neoplasia (MEN II), quantitative biokinetic data have been collected in order to improve the present estimates of absorbed dose to various organs and tissues as well as of the effective dose equivalent and its variation from patient to patient. We find considerably higher liver uptake than earlier published, but our estimates of the uptake in the thyroid and in the normal adrenal medulla show lower values than earlier reported.

This results in the following absorbed dose per activity unit administered (mGy/MBq) (mean and typical range):

Liver: 0.83 (0.50 - 1.2); Spleen: 0.61 (0.17 - 1.3); Salivary glands: 0.22 (0.082 - 0.41); Thyroid (blocked): 0.1; Total body: 0.082 (0.055 - 0.12). The effective dose equivalent was estimated to be 0.20 (0.1 - 0.3) mSv/MBq when the thyroid is adequately blocked.

INTRODUCTION

The affinity of iodine-131-metaiodobenzylguanidine (^{131}I -MIBG) for adrenal-medullary-like cells (1) has proven useful in the scintigraphic localization of pheochromocytoma (2) and the assessment of adrenal medullary hyperplasia (3). It has also been found that MIBG concentrates in another adrenergic tumour, namely neuroblastoma (4), and recent case reports indicate that it is also taken up in other tumours with neurosecretory granules (5).

Tumours as well as hyperplastic adrenals have a high uptake of ^{131}I -MIBG and may respond to treatment with large activities of the radiopharmaceutical. There is therefore an increasing interest in this compound both for diagnosis and therapy.

At The Third Radiopharmaceutical Dosimetry Symposium in Oak Ridge in 1980 The University of Michigan group (6) presented calculations of absorbed dose for ^{131}I - and ^{123}I -MIBG mainly based on experimental data from animals. Since then the main interest in the dosimetry of radioiodine-labelled MIBG has been directed towards its potential use for therapy and has therefore mainly been restricted to absorbed dose calculations to adrenergic tumours and to the whole body (2, 7). Although a large number of patients has hitherto undergone diagnostic studies using ^{131}I -MIBG there is still very limited quantitative information on the biokinetics and dosimetry of ^{131}I -MIBG. There is therefore a

need to improve our knowledge on the absorbed dose to various organs and tissues as well as on the effective dose equivalent and its variation in normal patients and in patients with hyperplasia or adrenal tumours. It may also be of interest to compare the biokinetics of ^{131}I -MIBG from various manufacturers.

In case of therapy there is of course still interest in improving the absorbed dose calculations to guarantee that a therapeutic activity can be given without causing too much irradiation of other organs and tissues in the body. The irradiation of the liver and the salivary glands may be critical.

PATIENTS AND METHODS

Fifty-seven patients were included in the study; all with suspected sporadic pheochromocytoma or MEN II. They were given 20 or later 40 MBq of ^{131}I -MIBG (Institutt for Energiteknikk, Kjeller, Norway) i.v. for measurements (8) using a gamma camera. Fourteen of them were also followed for two weeks with measurements by a whole-body scanner (2 NaI(Tl)-detectors, 12 cm Ø x 10 cm) in a low-background room. Samples of blood and urine taken from these patients were also analysed.

Using the gamma camera the activity present in the various organs has been estimated by means of conjugate counting and comparison with phantom measurements.

To reduce the thyroid uptake of ^{131}I , the patients were given 200 mg KI immediately before injection and then 2 x 100 mg daily for 10 days.

RESULTS AND DISCUSSION

RETENTION IN THE WHOLE BODY

Figure 1 shows for 14 patients the fraction of the injected activity which is present in the total body at various times after injection. Between one and four days after injection the retention curve is almost exponential with an effective half-life of 28 ± 8 hours. This fraction extrapolated to the time of injection corresponds to $(63 \pm 10)\%$ of the injected activity. Initially there is a faster elimination rate corresponding to an effective half-life of about 3 hours for $(36 \pm 10)\%$ of the injected activity. The relative magnitude of these components is assumed to be dependent on the patients' kidney- and liver function. A minor component (1%) has an effective half-life of about 8 days.

The distribution of the activity within the body is quite constant during the whole measurement period (0-14 days) indicating approximately the same half-life in all organs with a significant uptake.

Most of the ^{131}I activity which leaves the body is excreted via the urine. In the first 15 minutes after the injection about 10% of the activity is excreted and after 5 days between 66 and 91% of the activity has been excreted via the urine. Analysis of blood samples shows that 1.5% of the injected activity is present in the total-blood volume. The retention in whole blood up to 14 days after injection is described by a single exponential function corresponding to an effective half-life of 32 hours as a mean for 6 patients. Half of the activity is found in plasma and the other half in the blood cells.

Gamma-camera pictures show the uptake of ^{131}I mainly in the liver, salivary glands and spleen. Sometimes there is also a visible uptake in the lungs and

heart, colon and the empty bladder. This is in agreement with earlier reports (9, 10).

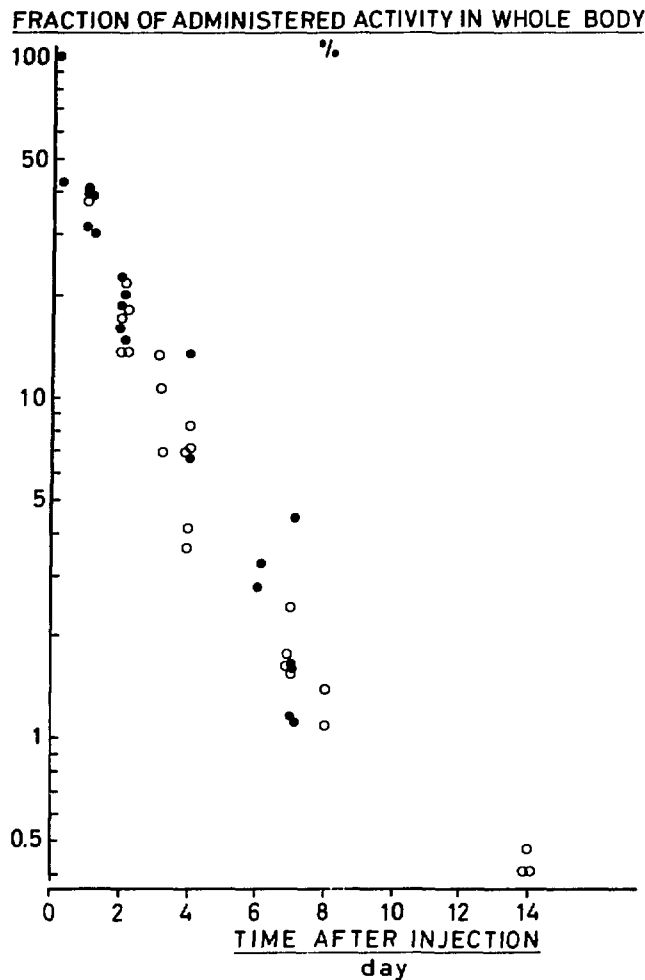


Figure 1. Retention of ^{131}I in the whole body of 14 patients injected with ^{131}I -MIBG. For 7 of the patients (•) the first measurement (100%) was carried out before any excretion of activity. For the other 7 (○) the first measurement was carried out 24 hours after injection and for these patients the 24-hour value was normalized to the mean value for the rest of the group (37.5%).

UPTAKE AND RETENTION IN LIVER, SPLEEN AND SALIVARY GLANDS

^{131}I -MIBG is uniformly taken up in the liver and reaches its maximum very soon (≈ 15 min) after i.v. injection.

About one third of the total-body activity of ^{131}I is found in the liver. A minor component ($\approx 15\%$ of the injected activity) is rapidly eliminated ($T_{\text{eff}} \approx 3\text{h}$) from the liver. The retention in the liver is however dominated by

a component having an effective half-life of between 22 and 34 hours with a mean value of (28 ± 3) hours. (Fig. 2). This uptake, extrapolated to the time of injection, corresponds to between 9 and 50% of the injected activity (mean: 21%, S.D.: 9%), (Fig. 2). As for the whole body, a smaller part (0.3%) is retained with considerably longer half-life (≈ 8 days).

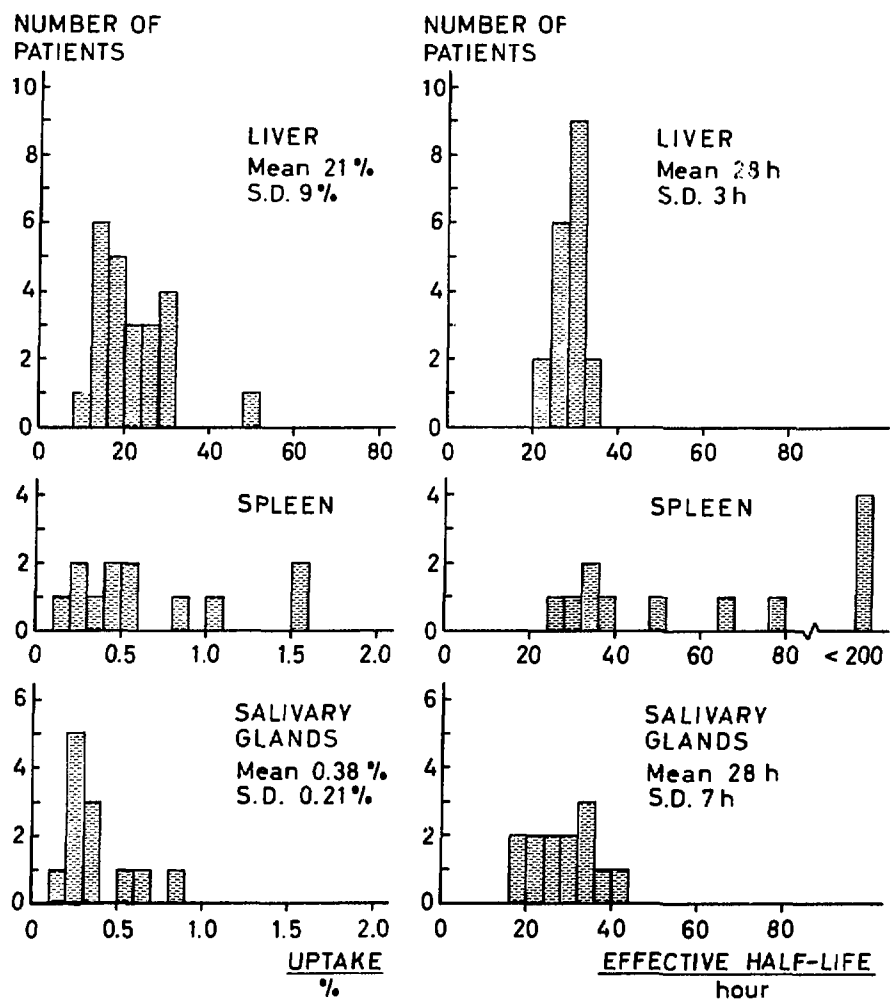


Figure 2. Uptake of ^{131}I in liver, spleen and salivary glands in patients who have received ^{131}I -MIBG i.v. The figure shows the extrapolated uptake at the time of injection as well as effective half-life for the fraction which dominates the retention curve between 1 and 4 days after injection.

Splenic uptake is seen in all individuals. (Fig. 2). A varying fraction [$(0.6 \pm 0.5)\%$ of the injected activity] is retained with effective half-lives which vary by a factor of 10 between patients (1-8 days). The apparently long half-life for some of the patients may be explained by a continuous trapping of ^{131}I -MIBG-labelled blood cells in the spleen.

The salivary glands are normally also visualized in all patients. Other studies (11) have indicated that this uptake may be caused by a probable neu-

ronal uptake of ^{131}I -MIBG in the rich sympathetic innervation rather than by uptake of free iodide.

The retention of ^{131}I -MIBG in the salivary glands may be described by an effective half-life of (28 ± 7) days for $(0.4 \pm 0.2)\%$ of the injected activity. (Fig. 2).

ESTIMATED MAXIMAL UPTAKE IN THE THYROID

With adequate "blocking" the thyroid is not visible on the scintigrams during the measurement period. This indicates a number of counts over the thyroid which is less than about 10% above the surrounding tissue "background", which therefore means that the activity concentration in the thyroid is always less than twice that of the surrounding tissue.

The maximal thyroid uptake may also be estimated in the following way: The uptake of ^{131}I in the thyroid is supposed to be dependent on the amount of free iodide. At injection the fraction of ^{131}I present as $^{131}\text{I}^-$ was normally 2-3% and never exceeded 5% of the total activity. The in vivo degradation of ^{131}I -MIBG was assumed to be very low because we found a very small fraction of the ^{131}I in urine in the form of $^{131}\text{I}^-$ ($\approx 5\%$) compared with that of ^{131}I -MIBG and its metabolites other than ^{131}I -iodide. Five percent of the ^{131}I -MIBG activity is therefore assumed to be available for the thyroid uptake. With the thyroid blocking regime used, at the most 0.1% of the available $^{131}\text{I}^-$ is assumed to be taken up by the thyroid (12).

The effective half-life of ^{131}I in the thyroid is assumed to be 7 days. These assumptions lead to a result which is in agreement with the observation that the thyroid is not seen on the scintigrams if it is properly "blocked". Without blocking, 300 times higher thyroid uptake may be reached.

UPTAKE AND RETENTION IN ADRENALS AND PHEOCHROMOCYTOMAS

Twenty-nine patients (no longer suspected for pheochromocytoma) show no visible uptake ($<0.05\%$) in the adrenal medulla. For 16 patients the adrenal medulla is visible; 13 patients have been used for quantitative calculations, showing uptake values up to 0.17%. (Fig. 3). This group ("unverified uptakes") may include persons with normal and hyperplastic adrenals and possibly some with small intra-adrenal pheochromocytomas. In 11 surgically proven pheochromocytomas (in 10 patients) the uptake was 0.02% - 22%. The effective half-life in the pheochromocytomas was 40 - 200 hours and for the unverified adrenal uptakes 35 - 85 hours. (Fig. 3).

The uptake per gram of tissue in intra-adrenal pheochromocytomas is given in Figure 4 showing a wide range of uptake values. For the calculation of the absorbed dose in normal adrenals, we have used an uptake value of 0.02% and an effective half-life for ^{131}I of 65 hours.

^{123}I -MIBG scintigraphy is reported to visualize the normal adrenal medulla in most patients (13). The better counting statistics and better spatial resolution make quantification of uptake possible, and may have implications in the investigation of dosimetry.

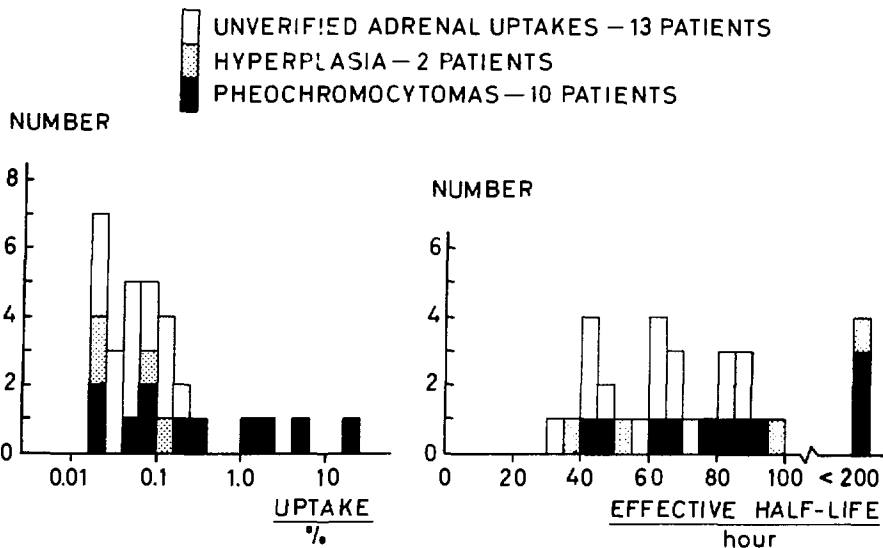


Figure 3. Uptake (extrapolated to the time of injection) and effective half-life of ^{131}I in adrenals and pheochromocytomas measured between 4 and 7 days after injection. For some patients more than one "uptake" is indicated in the figure. Eight of the pheochromocytomas from 7 patients were intra-adrenal and in 2 patients 2 extra-adrenal tumours were found. Eight visible uptakes in 5 patients not used for quantitative calculation because the number of counts was less than 10% over the background, Twenty-nine patients showed no visible uptake (<0.05%).

COMPARISON OF UPTAKE BETWEEN DIFFERENT ORGANS AND TISSUES

Using standard masses of the various organs (14) for which uptake data have been measured, the initial uptake per mass of organ relative to the mean activity concentration in the total body has been calculated and the results are presented in Table 1.

A comparison with earlier publications (7, 10, 13) shows that we have found a considerably higher liver uptake than those earlier presented. On the other hand our estimated thyroid uptake is lower. The uptake in the spleen is about the same as those reported earlier. The uptake in the normal adrenal medulla is considerably lower in our studies. The mean absorbed dose to various organs per injected activity unit calculated from our biokinetic data using standard MIRD methods (15, 16) are given in Table 2 for the case of adequate thyroid blocking. The effective dose equivalent has been estimated to be 0.2 mSv per MBq.

Without blocking, the mean absorbed dose to the thyroid may be as high as 26 mGy/MBq increasing the effective dose equivalent to 0.9 mSv/MBq.

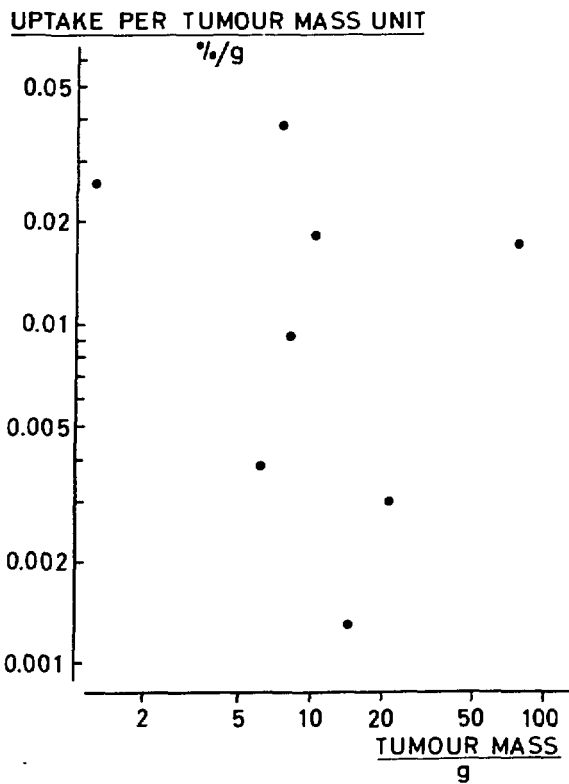


Figure 4. Mean concentration of ^{131}I in 8 intra-adrenal pheochromocytomas from 7 patients.

Table 1 Relative uptake and cumulated activity (\tilde{A}) per injected activity (A_0) in various organs

Organ	Mass g	Relative extrapolated uptake at inj per organ mass unit	$\frac{\tilde{A}}{A_0}$ hour
Total body	70000	1	30 (20-42)
Liver	1800	14	10 (6-15)
Salivary glands	85	3.5	0.16 (0.06-0.30)
Adrenals (normal)	4	\approx 3.5	\approx 0.02
Spleen	180	2.3	0.8 (0.2-1.7)
Lungs	1000	\approx 1.8	\approx 0.9
Thyroid (blocked)	20	\approx 2	\approx 0.01
Blood	5200	0.34	0.71

Table 2 Mean absorbed dose in various organs and effective dose equivalent

Organ	Absorbed dose mGy/MBq	
Liver	0.83	(0.50 - 1.2)
Spleen	0.61	(0.17 - 1.3)
Salivary glands	0.22	(0.082 - 0.41)
Lungs	~0.16	(0.08 - 0.30)
Adrenals*	~0.2	
Thyroid (blocked)	~0.1	
Bone marrow	0.065	(0.046 - 0.087)
Gonads { ♀	0.057	(0.042 - 0.075)
♂	0.052	(0.038 - 0.068)
Bladder wall	~0.6	
Total body	0.082	(0.055 - 0.12)
Effective dose equivalent	0.20	(0.1 - 0.3) mSv/MBq

*The mean absorbed dose to the adrenal medulla may be about 10 times higher than the mean value for the total adrenal.

REFERENCES

1. Wieland, D.M., J.-L. Wu, L.E. Brown, T.J. Manger, D.P. Swanson and W.M. Beierwaltes. Radiolabeled adrenergic neuron-blocking agents: Adrenomedullary imaging with ^{131}I -iodobenzylguanidine. *J. Nucl. Med.* 21. 349-353, 1980.
 2. Sisson, J.C., M.S. Frager, T.W. Valk, M.D. Gross, D.P. Swanson, D.M. Wieland, H.C. Tobes, W.H. Beierwaltes and N.W. Thompson. Scintigraphic localization of pheochromocytoma. *N. Eng. J. Med.* 305. 12-17, 1981.
 3. Valk, T.W., M.S. Frager, M.D. Gross, J.C. Sisson, D.M. Wieland, D.P. Swanson, T.J. Manger and W.H. Beierwaltes. Spectrum of pheochromocytoma in multiple endocrine neoplasia. A scintigraphic portrayal using ^{131}I -metaiodobenzylguanidine. *Ann. Intern. Med.* 94. 762-767, 1981.
 4. Treuner, J., U. Feine, D. Niethammer, W. Muller-Schaumberg, J. Meinke, E. Eibach, R. Dopfer, Th. Klingebul and St. Grumbeck. Scintigraphic imaging of neuroblastoma with ^{131}I -m-iodobenzylguanidine. *Lancet* i. 333-334, 1984.

5. Beierwaltes, W.H. Horizons in radionuclide therapy: 1985 update. *J. Nucl. Med.* 26. 421-427, 1985.
6. Swanson, D.P., J.E. Carey, L.E. Brown, R.C. Kline, D.M. Wieland, J.H. Thrall and W.H. Beierwaltes. Human absorbed dose calculations for iodine-131 and iodine-123 labeled meta-iodobenzyl-guanidine (mIBG): A potential myocardial and adrenal medulla imaging agent. In: Proc. of The Third International Radiopharmaceutical Dosimetry Symposium. Health and Human Services Publication FDA 81-8166, Rockville, Maryland, 1981, 213-224.
7. Sisson, J.C., B. Shapiro, W.H. Beierwaltes, J.W. Glowniak, M. Nakajo, T.J. Mangner, J.E. Carey, D.P. Swanson, J.E. Copp, W.G. Satterlee and D.M. Wieland. Radiopharmaceutical treatment of malignant pheochromocytoma. *J. Nucl. Med.* 25. 197-206, 1984.
8. Lindberg, S., I. Ernest, M. Fjälling and L. Jacobsson. The value of late images in ^{131}I -metaiodobenzylguanidine (^{131}I -MIBG) scanning of the adrenal medulla. *J. Nucl. Med.* 26. A28, 1985 (abstr).
9. Nakajo, M., B. Shapiro, J. Copp, V. Kalff, M.D. Gross, J.C. Sisson and W.H. Beierwaltes. The normal and abnormal distribution of the adrenomedullary imaging agent m (I-131) iodobenzylguanidine (131-I-MIBG) in man: Evaluation by scintigraphy. *J. Nucl. Med.* 24. 672-682, 1983.
10. McEwan, A.J., B. Shapiro, J.C. Sisson, W.H. Beierwaltes and D.M. Ackery. Radio-iodobenzylguanidine for the scintigraphic location and therapy of adrenergic tumours. *Sem. Nucl. Med.* 15. 132-153, 1985.
11. Nakajo, M., B. Shapiro, J.C. Sisson, D.P. Swanson and W.H. Beierwaltes. Salivary gland accumulation of meta (131-I) iodobenzylguanidine. *J. Nucl. Med.* 25. 2-6, 1984.
12. Jacobsson, L., S. Mattsson and B. Nosslin. Measurements of the effect of thyroid blocking in patients investigated with ^{125}I -fibrinogen. In: Radiation Protection, A Systematic Approach to Safety, Vol I (Ed. by International Radiation Protection Society). Pergamon Press Oxford 1980, 279-281.
13. Lynn, M.D., B. Shapiro, J.C. Sisson, D.P. Swanson, T.J. Mangner, D.M. Wieland, L.J. Myers and W.H. Beierwaltes. Portrayal of pheochromocytoma and normal human adrenal medulla by 123-I-meta-iodobenzylguanidine (123-I-MIBG). *J. Nucl. Med.* 25. 436-440, 1984.
14. International Commission on Radiological Protection. Report of the Task Group on Reference Man. ICRP Publication 23, Pergamon Press, 1975.
15. Snyder, W.S., M.R. Ford, G.G. Warner and S.B. Watson. "S" absorbed dose per unit cumulated activity for selected radionuclides and organs. MIRD Pamphlet No 11, Society of Nuclear Medicine, New York, 1975.
16. Ellett, W.H. and R.M. Humes. Absorbed fractions for small volumes containing photon-emitting radioactivity. MIRD Pamphlet No 8. *J. Nucl. Med.* 12. (Suppl 5). 25-32, 1971.

DISCUSSION

MOUNTFORD: What experience have you had in using I-131-mIBG for therapy?

MATTSSON: We have mainly used it for diagnostic purposes. Our experience with therapy is limited to three patients: two with pheochromocytomas and one child with neuroblastoma. Several other groups have more knowledge about the therapeutic use of this compound, mainly the Ann Arbor group and, also, an English group in South Hampton.

FUEGER: There is a group in Tubingen that is working with neuroblastoma cases. They are doing therapy with large doses and intravenous injections.

MARCUSE: Several authors have reported that uptake by adrenal-medulla tumor tissue competes so much with the myocardium that the myocardium may disappear from the scintigram if a tumor exists. Will removal of patients with dubious myocardial uptake in your series significantly change the results you found for the absorbed dose per MBq administered?

MATTSSON: We are quite aware of this situation, but we think that this investigation and many other investigations have shown some of these patients are without the disease which they were investigated for and the uptake and retention parameters for the liver are very constant between the different groups of patients.

SHEN: We at University of Michigan have performed more than 400 diagnostic studies with I-131-mIBG. It is normally taken up by the salivary glands, thyroid, heart, liver, and about 10% of normal adrenal medulla. Besides marked species differences in I-131-mIBG uptake, we have also noted that in patients with pheochromocytoma who have elevated norepinephrine levels, the cardiac uptake and plasma norepinephrine levels have an inverse relationship. This demonstrates that the biokinetics of I-131-mIBG may be different in patients with pheochromocytoma from those without pheochromocytoma. I suspect this may be generally true for radiopharmaceuticals with biokinetics that differ in patients with disease and those without disease. This, then, is an important factor to be taken into account when calculating dose estimates for patients with a given disease. Furthermore, they are likely to be subjected to repeated follow-up studies as is done for patients with malignant pheochromocytoma.

PROBABILISTIC CAUSALITY AND RADIogenic CANCERS*

Peter G. Groér
Center for Epidemiologic Research
Oak Ridge Associated Universities
P. O. Box 117
Oak Ridge, Tennessee 37831-0117

*This paper is based on an evening lecture delivered at this symposium

ABSTRACT

A review and scrutiny of the literature on probability and probabilistic causality shows that it is possible under certain assumptions to estimate the probability that a certain type of cancer diagnosed in an individual exposed to radiation prior to diagnosis was caused by this exposure. Diagnosis of this causal relationship like diagnosis of any disease--malignant or not--requires always some subjective judgments by the diagnostician. It is, therefore, illusory to believe that tables based on actuarial data can provide objective estimates of the chance that a cancer diagnosed in an individual is radiogenic. It is argued that such tables can only provide a base from which the diagnostician(s) deviate in one direction or the other according to his (their) individual (consensual) judgment. Acceptance of a physician's diagnostic judgment by patients is commonplace. Similar widespread acceptance of expert judgment by claimants in radiation compensation cases does presently not exist. Judicious use of the present radioepidemiological tables prepared by the Working Group of the National Institutes of Health or of updated future versions of similar tables may improve the situation.

INTRODUCTION

"Mathematical reasoning and deductions are a fine preparation for investigating the abstruse speculations of the law." Thomas Jefferson as quoted by I. J. Good (2).

The President of the United States signed the so-called Orphan Drug Act (Public Law 97-414) on January 4, 1983. The purpose of this act was amendment of federal law regulating the development of drugs to facilitate especially the development of drugs for rare diseases and conditions. Section 7(b) of this bill directed the Secretary of Health and Human Services to "devise and publish radioepidemiological tables that estimate the likelihood that persons who have or have had any of the radiation-related cancers and who have received specific doses prior to the onset of such disease developed cancer as a result of these doses." Section 7(b) was attached to the Orphan Drug Act since earlier bills introduced by Senator Orrin Hatch of Utah were not reported out of the respective committees (1). These earlier bills followed several hearings on this subject at which experts in radiobiology and radioepidemiology testified. Some preliminary quantitative estimates of the "Probability of Causation" (PC)--to be explained subsequently--were presented

and the feasibility of detailed and extensive calculations leading eventually to published radioepidemiological tables was deliberated. All these preparations culminated finally in the publication of the report by the National Institutes of Health ad hoc Working Group (1) which is termed "NIH-report" below. More background information and a brief enumeration of related activities by other scientific panels and committees can be found in this report.

The NIH-report and other related reports were--in the opinion of this author--somewhat superficial in their treatment of the relevant, underlying concepts of probability and causality. This opinion and involvement with scientific groups concerned with PC and its possible applications led to the scrutiny of the literature dealing with these concepts and to the thoughts expressed below. The reader should keep in mind that this paper was written with the benefits of hindsight.

PROBABILITY

"The most important questions of life are, for the most part, really only problems of probability." Pierre Simon de Laplace

Uncertainty is part of the human condition. Therefore, it is not surprising that references to probability as a measure of uncertainty and as an important ingredient of decision making under uncertainty can be found in the ancient and modern literature on natural philosophy, physics, mathematics, and statistics. "Probability is the very guide of life" from Cicero's *De Natura* (2) appears to be one of the earliest known quotations. Remarkable is the following quote by James Clark Maxwell (3): "They say that Understanding ought to work by the rules of right reason. These rules are, or ought to be, contained in Logic; but the actual science of logic is conversant at present only with things either certain, impossible, or entirely doubtful, none of which (fortunately) we have to reason on. Therefore, the true logic for this world is the calculus of Probabilities, which takes account of the magnitude of the probability which is, or ought to be, in a reasonable man's mind." The adjective "fortunately" made me reflect on determinism and free will and the qualifying "reasonable" made me ponder the irrational fears of modern man often rooted in uncalibrated uncertainty assessments.

Man's initially informal involvement with probability eventually produced formal definitions of this concept and led to a calculus of probability. Gambling was the early motivation for formalization of probabilistic ideas. It is, therefore, not surprising to find the ratio of favorable cases to the total number of equally likely cases as a definition of probability in early writings on the subject. Another definition stated that probability was the limit of a long-run relative frequency. But how long is a long run and--as John Maynard Keynes put it--"In the long run, we shall all be dead." In his *Ars Conjectandi* (1713), James Bernoulli suggested that probability is a "degree of confidence" that a person attaches to an event conditional on his background knowledge about this event. This revolutionary idea was adopted by some and rejected by others during the following two centuries. In modern parlance probability is the "degree of belief" of a person in a statement on the basis of all the relevant information about this statement considered by him. Over two hundred years after the "Art of Guessing" was published, de Finetti (4) established the connection between frequency and degree of belief. In the same paper, he also gives--somewhat oversimplified--a recipe for the elicitation of a probability: "Let us suppose that an individual is obliged to evaluate the rate p at which he would be ready to exchange the possession of an arbitrary sum S (positive or negative) dependent on the

occurrence of a given event E, for the possession of the sum pS; we will say by definition that this number p is the measure of the degree of probability attributed by the individual considered to the event E, or, more simply, that p is the probability of E." This implies that a person could assign any value of p to a given event at a certain time and that other persons could assign different values of p to the same event. This freedom in the assigning of probabilities is only constrained by the requirement of coherence. This requirement was first introduced by Ramsey (5) in 1926. Coherence places restrictions on the relationships between a person's degrees of belief. In terms of a trivial example, coherence requires you to assign $p = 0.6$ to "tails" if you assigned a probability of 0.4 to the outcome "heads" for the toss of a warped coin which cannot stand on edge.

Some people object to the idea of assigning subjective or personal probabilities to unique events, like the death of an individual of a certain age during a given year, and prefer to maintain the long-run frequency definition of probability. Erwin Schrödinger, one of the founders of quantum mechanics, comments on this very issue: ". . . I do admit, that the readiness with which we physicists and many others who use the theory (of probability) in practice adopt frequency as the basis, does mean taking things a little too easy. There are grave objections to this, mainly that we thereby cut ourselves off from ever applying rational probability considerations to a single event" (6). If one agrees with Schrödinger, how should one evaluate a probability for a "single" event? de Finetti (4) has important advice: "It is thus that one readily evaluates probabilities in most practical problems, for example, the probability that a given individual, let us say Mr. A, will die in the course of the year. If it is desired to estimate directly under these conditions what stakes (or insurance, as one would prefer to say in this case) seem to be equitable, this evaluation would seem to us to be affected with great uncertainty, . . . one must consider other events, for example, the deaths, during the year, of individuals of the same age and living in the same country as Mr. A. Let us suppose that among these individuals about 13 out of 1,000 will die in a year, if, in particular, all the probabilities are judged equal, their common value is $p = 0.013$, and the probability of death for Mr. A is 0.013; if in general there are reasons which make the chances we attribute to their deaths vary from one individual to another, this average value of 0.013 at least gives us a base from which we can deviate in one direction or the other in taking account of the characteristics which differentiate Mr. A from other individuals." Lindley states the same idea slightly differently (7): "From the actuary's point of view, death is also a statistical event, since he considers a large population of people at risk, and can consider the event to be repeated as each person dies: although it is hard to be dogmatic about the death of a single person, one can be reasonably sure about the proportions of people dying in a population within a specified period." These quotations make it clear that the probabilities of unique events can only be approximated by the frequency of events judged to be "exchangeable" (4). "Exchangeable" is here a technical term which implies an "identity for all practical purposes" of two or more events. (A customer who returns a defective item and accepts another item of the same kind and of hopefully better quality from the merchant makes such an "exchangeability" judgment.) More precisely, there are three distinct and successive phases (4) involving personal or subjective judgments that lead to probability estimates for unique events. The first is the selection of a class of "similar" events including the one under consideration; the second, the prediction of the frequency in a future interval, is usually based on the judgment that the frequency has remained the same over some period of time; the third involves the comparison of the probability of the unique event (e.g., the death of Mr. A) with the probabilities for the events in the class chosen earlier.

This comparison becomes more difficult in the same proportion as the events in the chosen class become more numerous. de Finetti (4) illustrates this with the following example: "If one must give an estimate of the thickness of a sheet of paper, he can very easily arrive at it by estimating first the thickness of a packet of n sheets in which it is inserted, and then by estimating the degree to which the various sheets have the same thickness. The thickness (of the packet) can be evaluated the more easily the larger the packet; the difficulty of the subsequent comparison of the sheets is on the contrary diminished if one makes the packet thinner by saving only those sheets judged to have about the same thickness as the sheet that interests us."

A quite outlandish example of a probability assessment for a truly unique event was reported by Borch (8). He read that the Scottish whiskey producer Cutty Sark offered an award of one million British pounds to the captor of the Loch Ness monster. After somebody in the upper echelons of the company had doubts about the wisdom of this generous offer, Cutty Sark approached Lloyd's of London. As usual Lloyd's agreed to cover the risk for a premium of 2,500 pounds during the period from 1 May 1971 to 30 April 1972. The insurance slip specified that "In the event of loss hereunder, the monster shall become the property of the underwriters hereon." This made the contract essentially risk free for Lloyd's marine underwriters.

This extraordinary example shows that probabilities for unique events are assessed by responsible people often in the absence of directly relevant observed frequencies. In less extreme cases the probability assessor finds himself in more amenable circumstances where he can use frequency data or probabilities of related events to infer the probability of the event under consideration. Since probabilities once assessed have to obey certain rules (see e.g. (7)), the situation of a probabilist is in this regard analogous to a surveyor who derives certain distances from other actually measured distances and angles according to the laws of Euclidean geometry. de Finetti (4) remarks: "The fact that a direct estimation is not always possible constitutes the reason for the utility of the logical rules of probability; their practical end is to relate an evaluation, itself not very accessible, to others by means of which the determination of the first evaluation is made easier and more precise." We will show below that it is this feature of probability laws which makes estimation of the Probability of Causation possible.

Before proceeding to a discussion of causality it seems useful to reiterate that personal judgments need to be made to assess probabilities of unique events. Such judgments are necessary to determine, for instance, the class of events whose frequency permits calculation of a base value "from which we can deviate in one direction or the other" to establish a numerical value characteristic for an individual who is not quite "exchangeable" with members of a class and to single out characteristics (like age, sex, country, race) relevant to the definition of this class of similar events. While the reasons for some such judgments can be explained, the reasons for others, like the reasons for assigning probabilities without frequency data, remain unknowable. Inscrutable processes in the brain of the probability assessor produce certain numerical values when such an elicitation is demanded. On this point we quote Poincaré as cited by de Finetti (4): "The calculus of probability rests on an obscure instinct, which we cannot do without; without it science would be impossible, without it we could neither discover a law nor apply it." Despite its obscurity this instinct seems to guide Lloyd's underwriters and also medical diagnosticians quite successfully. However, only trust and confidence in the expertise of the physician can induce a comfortable acceptance of a diagnosis by the patient. Trust can make up for lack of scrutability.

CAUSALITY

"The law of causality, I believe, like much that passes muster among philosophers, is a relic of a bygone age, surviving, like the monarchy, only because it is erroneously supposed to do no harm..." Bertrand Russell

This citation is from a paper (9) written around 1913, slightly more than a decade before a spring-tide of probabilistic ideas entered physics with the advent of quantum mechanics. With this theory "deterministic" causality, deemed superfluous by Russell, died forever, but it took another thirty-five years before Good (10) wrote the first general paper on probabilistic causality. The second author to treat this subject in detail was Suppes (11) who referenced Good's earlier work and developed the idea of a probabilistic cause in a formally different manner. Since his treatment is more easily adapted to the paradigm of the NIH report we will follow his approach.

Suppes (11) defined first a prima facie cause for an event C_T , which in the context of this paper, can be interpreted as Cancer diagnosed at time T after exposure to an organ dose D_t of ionizing radiation at time $t < T$.

The event D_t is a prima facie cause of the event C_T if and only if $p(D_t) > 0$,

$$p(C_T/D_t) > p(C_T) \text{ and } t < T. \quad (1)$$

This definition of a cause at "first sight" is also contained in ref. (1) although in a somewhat different and unconventional notation. $p(C_T/D_t)$ is a conditional probability and the symbols are interpreted as "the probability of C_T given a prior exposure to D at t ." In contrast to (1) Suppes (11) points out that a prima facie cause can be a spurious cause if there is another event, for instance, an exposure to a chemical at time $d < t$ so that $p(C_T/D_t, A_d) = p(C_T/A_d)$ if $p(D_t, A_d) > 0$. This implies that knowledge of other exposures is necessary before D_t can be singled out as the sole cause for C_T . In the absence of data, only judgment can resolve this issue. Other conditioning information for probabilities is usually indicated by the letter H --short for "history"--to the right of the vertical conditioning stroke, e.g., $p(C_T/D_t, H)$. H is important for assessments of probabilities and causes alike and includes here the exposure history of the individual. Already John Stuart Mill stated: "The statement of the cause is incomplete unless in some shape or other we introduce all the conditions."

Suppes (11) gives a much more refined differentiation of causes. Such detail is beyond the scope of this paper and the interested reader should consult both Good(10) and Suppes (11) for further details on probabilistic causality. Subsequently, we will only use Equ. (1) to derive a formula for Probability of Causation.

PROBABILITY OF CAUSATION

"The notion of "cause" thus depends on the notion of probability, and it follows also from the same subjective source as do all judgments of probability." Bruno de Finetti

Victor P. Bond (12) was the first one to use the concept of PC in the context of compensation for late effects after exposure to ionizing radiation. He also coined this term and used it for the first time in unpublished testimony before the Senate Committee on Labor and Human Resources. Credit

for an apparently independent rediscovery of PC goes to Oftedal et al (13) who pointed out that "'Baye's (sic) Law' is applicable" and did not(!) use Bayes' Theorem to derive their PC formula.

We will use this theorem (7) to derive a formula for PC. First we need to introduce some notation for the events under consideration:

C = Spontaneous or radiogenic cancer diagnosed in an individual after exposure to organ dose D .

$R(\bar{R})$ = Radiogenic (spontaneous) cancer in the same individual.

$D(\bar{D})$ = Exposure (no exposure) to organ dose D .

H = "History" of the individual. This includes other relevant information like age at exposure and diagnosis, other exposures, e.g., to background radiation or toxic chemicals. In most formulas below, H is left out and only inserted at the end of the derivation to simplify the formulas.

According to Bayes' Theorem (7) we have:

$$p(R/C,D) = p(C/R,D)p(R/D)/p(C/D)$$

This simplifies immediately to:

$$p(R/C,D) = p(R/D)/p(C/D) \quad (1)$$

$$\text{since } p(C/R,D) = 1$$

The last equation is expressed in words: If it were known that an individual has a radiogenic cancer then by implication and therefore with certainty he has cancer. If it is assumed that an exposed individual can only suffer from R or \bar{R} but not simultaneously from both forms of cancer then

$$p(C/D) = p(R/D) + p(\bar{R}/D) \text{ or}$$

$$p(R/D) = p(C/D) - p(\bar{R}/D) \quad (2)$$

If simultaneous occurrence of R and \bar{R} in an individual is assumed a slightly different derivation of PC becomes necessary. This was pointed out by Lindley (14). Since R is not directly observable a further assumption (14,15)

$$p(\bar{R}/D) = p(\bar{R}/\bar{D}) \quad (3)$$

is necessary to approximate $p(\bar{R}/D)$ by the frequency of cancer in a cohort of otherwise exchangeable individuals with no exposure to D . Since there can be no radiogenic cancers without exposure to D

$$p(\bar{R}/\bar{D}) = p(C/\bar{D}) \quad (4)$$

This gives finally using equs. (1) through (4) and inserting H , assumed to be identical for all probabilities,

$$p(R/C,D,H) = [p(C/D,H) - p(C/\bar{D},H)]/p(C/D,H) \quad (5)$$

The probability of a radiogenic cancer given diagnosis of cancer after a prior exposure to D and H --called "Probability of Causation" (for D)--can be expressed according to (5) in terms of other probabilities.

The NIH-report (1) describes in considerable detail how PC, as defined in equ. (5) can be approximated by looking at the frequencies of certain types of cancer in the U.S. population and certain exposed populations like, for example, the Japanese A-bomb survivors. If the claimant is judged to be exchangeable with the individuals in the exposed and unexposed groups then his PC would follow directly from these frequencies. If there are reasons to assume that the individual differs from the individuals in the reference groups, the compensation board or court may "deviate in one direction or the other" in taking account of the personal characteristics of the claimant. Such an adjustment is based on an obscure and, therefore, inscrutable process in the brains of the experts. The experts can enumerate their reasons why they decided to deviate from the PC-value based on frequencies but could offer no explanation how they arrived at the adjusted numerical value for the PC if they decided or were required to announce their final value. Because of the inscrutability of this final step only trust by the victim in the experts' judgment can lead to acceptance. The fact that it is now possible to use frequency based PC-values from the NIH-report should enhance the confidence in PC-assessments made by experts since the "evaluation, itself not very accessible" has been related to other probabilities about which we are more certain. The radiation expert can, like a diagnosing physician, order a test--from the NIH-tables--and come up with a final answer after consideration of the test result. Allowing a final adjustment of the PC by an expert or experts eliminates the criticism that claimants should not be treated like faceless members of a statistical collective.

It may be illustrative at this point to give a slightly modified example from the NIH-report (1, p. 220). The modifications are parenthesized. In this example, a liver cancer was diagnosed in a 59 year old man who received a dose of 10 rad of low LET radiation to the liver (from a diagnostic scan) at age 31. (It is further known that the patient received an intravenous injection of about 20 ml of Thorotrast which contained several grams of ^{232}Th at age 23.) The NIH-report lists a PC of 8 percent for the dose of 10 rads in this case. Experts with knowledge of the Thorotrast injection would not accept the 8 percent but would judge the PC to be lower because of the known carcinogenic effects of Thorotrast. If only the fact of the injection is considered quantification of the decrease seems impossible. After consideration of the available epidemiologic evidence on liver cancer in Thorotrast patients a quantitative adjustment is feasible after some effort. The costs of the time and effort to collect necessary data and to analyze them has to be considered. Consideration of this trade-off is important as Good (16) has emphasized. He dubbed this idea the principle of type II rationality and remarked that it is often perceived as a threat to "conventional logic" since a shortcut is taken. In other words, calculations have to stop at some point. It is not cost effective to strive for greater detail and precision. Consider in this context that penalties for speeding tickets are scaled according to integer miles per hour over the speed limit. Following this advice we conclude this paper with a discussion of some difficulties of the approach outlined above.

DIFFICULTIES AND CONCLUSIONS

"When one comes down to particular instances, everything becomes more complicated." Albert Camus

"Mankind always sets itself only such problems as it can solve..." Karl Marx

During a lifetime an individual can be exposed to many suspected carcinogens. Background radiation, radiation from medical diagnostic procedures or

radiation therapy, Rn-daughters in the basement of his house, chemicals at his workplace, asbestos in the elementary school's cafeteria, chemicals in drinking water, chemicals in the atmosphere after a tank truck overturned or chemical plant malfunctioned, and allegedly even saccharin in the cup of mountain grown coffee are possibilities. It is clearly impossible to have sufficient epidemiologic data for all of these alleged carcinogens and combinations thereof. Therefore, it is also impossible to find always the "correct" partition (17) into subpopulations of individuals exchangeable in all respects with the claimant. Often such partitions are legislated (15,17) and the resulting laws or regulations contradict available evidence (e.g., the requirement of equal retirement contributions for men and women). To push things to the extreme consider an individual who underwent a sex change operation!

This shows that only "verage probabilities as suggested by de Finetti (4) and in the PC-context by Bond (18) can be calculated. Fine tuning has to be done through expert judgment and the idea of "objective" PCs collected in tables is, therefore, illusory.

The PC calculus could be extended somewhat following Laplace's ideas (19) but such an extended calculus will be subject to similar criticisms as the simple one. It appears that a compromise is the only way out of this dilemma. The PC values from the NIH-report should be accepted as average values derived from available epidemiologic information. Experts, like a physician after the receipt of laboratory tests, can then deviate "in one direction or the other in taking account of the characteristics" of the individual requesting compensation. How the PC value should be linked to the amount of the compensation is not clear at this time. Some suggestions were already made (17). The most reasonable in our opinion involves scaling of the compensation, maybe in a stepwise fashion, starting with a maximum amount at PC values over 90% and ending with a tenth of this amount for PC values less than 10%. This is a thorny issue and further thought is required.

An obvious shortcoming of this approach and of a compensation scheme based solely on PC in general is the awarding of equal amounts for equal PC values at different ages of cancer diagnosis. A young cancer victim deserves more than an older victim with the same PC value. Additional scaling based on the loss of expected length of life (20) seems required and the details of such a scheme need to be worked out. The PC approach to compensatory issues seems to be a step in the right direction but will require trust in the judgment of the experts by the claimants if lengthy litigations are to be avoided.

ACKNOWLEDGMENT

Before and after the evening lecture on which this paper is based I have benefitted from discussion with and critical comments by Richard E. Barlow, Dennis V. Lindley, I. J. Good, Michael Fry, Joop Thiessen, and Victor P. Bond. The remaining mistakes, errors of judgment and vagueness should be blamed on the author who thanks the organizing committee of this symposium for inviting him. The research on which this paper is based concerns work undertaken as part of the Health and Mortality Study of Department of Energy workers being conducted by Oak Ridge Associated Universities with the collaboration of the School of Public Health, University of North Carolina at Chapel Hill under Contract No. DE-AC05-76OR00033 between the Department of Energy, Office of Energy Research, and Oak Ridge Associated Universities.

REFERENCES

1. "Report of the National Institutes of Health ad hoc Working Group to Develop Radioepidemiological Tables," NIH Publication No. 85-2748 (for sale by the Superintendent of Documents, U.S. Government Printing Office, Washington, D.C. 20402).
2. Good, I. J. Probability and the Weighing of Evidence, Charles Griffin and Company Limited, London, 1950.
3. Jeffreys, H. Theory of Probability, 3rd edition, Oxford at the Clarendon Press, 1961.
4. de Finetti, B. Foresight: Its Logical Laws, Its Subjective Sources in Studies in Subjective Probability, edited by H. E. Kyburg and H. E. Smokler, pp. 53-118, Robert E. Krieger Publishing Company, Huntington, New York, 1980.
5. Ramsey, F. P. Truth and Probability in Studies in Subjective Probability, edited by H. E. Kyburg and H. E. Smokler, pp. 23-52, Robert E. Krieger Publishing Company, Huntington, New York, 1980.
6. Schrödinger, E. The foundation of the theory of probability. Proc. Royal Irish Acad. 51, Sect. A, 51-66, 1947.
7. Lindley, D. V. Making Decisions, p. 22, Wiley-Interscience, London, New York, 1978.
8. Borch, K. The monster in Loch Ness in New Developments in the Applications of Bayesian Methods, edited by H. Aykac and C. Brumat, pp. 273-278, North Holland Publishing Company, Amsterdam, New York, Oxford, 1977.
9. Russell, B. On the notion of a cause. Proc. Aristotelian Society, 13, 1-26, 1913.
10. Good, I. J. A causal calculus (I and II), Brit. J. Phil. Science, 11, 305-318, 1961 and 12, 43-51, 1962.
11. Suppes, P. A probabilistic theory of causality. Acta Phil. Fennica, 24, 1-130, 1970.
12. Bond, V. P. The medical effects of radiation, in National Association of Compensation Claimants Attorneys (NACCA), 13th Annual Convention, Miami Beach, W. H. Anderson Company, Cincinnati, 1959.
13. Oftedal, P. et al. On the probability of radiation being the cause of leukemia. Br. J. Radiol., 41, 711-712, 1968.
14. Lindley, D. V. Letter to Peter G. Groér, November 7, 1985.
15. Good, I. J. Letter to Peter G. Groér, October 21, 1985.
16. Good, I. J. Good Thinking, p. 16, University of Minnesota Press, Minneapolis, 1983.

17. Oversight Committee on Radioepidemiological Tables, "Assigned Share for Radiation as a Cause of Cancer--Review of Radioepidemiological Tables Assigning Probabilities of Causation" (Final Report), National Academy Press, Washington, D.C., 1984.
18. Bond, V. P. Causality of a given cancer after known radiation exposure in Technology and Fairness, Symposium held at the National Academy of Engineering, Washington, D.C., June 3-4, 1985, to be published by the National Academy Press, Washington, D.C.
19. Laplace, P. S. de, "Mémoire sur la probabilité des causes par les événements," Mémoires...par divers Sarans 6, 621-656, 1774.
20. Barlow, R. E. Letter to Peter G. Groér, October 2, 1985.

DOSIMETRY OF RADIOLABELED MONOCLONAL ANTIBODIES USED FOR THERAPY

M.J. Myers, G.R. Hooker, and A.A. Epenetos

Department of Medical Physics, Hammersmith Hospital,
DuCane Road, London W12, UK

ABSTRACT

The present state of radiotherapy using labeled antibodies is reviewed. From the point of view of dosimetry, antibody therapy does not seem to have reached a stable and practicable enough state to provide an input to any but rather tentative dosimetry models. These, therefore, should not be taken too far until the problems of antibody targeting have been more fully developed.

Some of the instrumental techniques for acquiring dosimetric data under clinical conditions are discussed as are some of the techniques of therapy in use today.

INTRODUCTION

For therapeutic applications of radiolabeled antibodies all the data that are required in practice in order to calculate the radiation dose at a site in the body are the activity at the site, the time course of the activity, and a tabulation of the radiations emitted by the radionuclides involved. These data can then be plugged into some standard formulations to produce an answer that, although of limited accuracy, would have sufficient validity to allow the therapeutic procedure to be judged effective or not.

Theoretically then, the dosimetry involved in the use of radiolabelled monoclonal antibodies could be dismissed as a trivial exercise. After all, if the specific antibody can be tailored to target onto a specific tumor site, the calculation of the local radiation dose, which might be on a microscopic or a macroscopic level depending on the radionuclide used and the geometry of the isolated target to be treated, should be a simple one with no accompanying embarrassing complications of high doses to marrow or liver or bladder since the antibody would bypass these organs.

In addition, for therapy there should be, among the relatively large and diverse selection available, a radioactive label that can be attached to the antibody in order to deliver a large enough activity at an appropriate dose rate locally to the tumor site.

In practice this new tool is only just beginning to be understood and presently employed antibodies clearly are not yet specific enough. Their distribution in the blood and other organs is still at too high a level relative to tumor uptakes to yield the required safe target to nontarget ratio. Because of this, predictions based on any elaborate system of dosimetry in which levels of uptake and time course in target and normal tissue areas are assumed should be approached with caution. New approaches are being

tried in dosimetry at the cellular or subcellular level in preparation for the use of radionuclides with extremely short range emissions deposited near the cell surface and affecting few neighbouring cells. This may be the method of choice for future dosimetry. However today, in individual clinical situations where measurements are actually performed to determine the behaviour of the radiolabel, calculations little different from those traditionally employed for 'conventional' radiopharmaceuticals are still applicable.

Perhaps the therapeutic system coming closest to the ideal radiolabelled antibody situation is the well established one of radioiodine treatment of thyroid metastases (despite its being associated with a high blood background). Here there is an active and very specific mechanism of radionuclide uptake with high target to nontarget ratios. Levels of 0.1-0.5 %/g of the administered dose can be achieved. This may be compared with levels generally of an order of magnitude less than in the present use of antibodies. The dosimetric problems of thyroid metastasis therapy, as there might be with the use of antibodies, are confined to ones of ascribing a volume of distribution and a half-life of uptake and disappearance to localised isolated regions of uptake, and estimating the levels of activity in the blood. Presumably the mature stage of the iodine technique, where dosimetry is scarcely performed and a standard activity based on a rule of thumb is administered, will be reached ultimately with the antibody technique - assuming of course that by that time the use of radionuclides as the labels for antibody therapy still exists and has not been replaced by drugs.

A system of dosimetry for the therapeutic use of radiolabeled antibodies is thus perhaps necessary in this intermediate stage as a guide to how far we have gone along the path towards the ideal state (when dosimetry is no longer a problem). It is debatable then, in this changing situation, how accurate the dosimetry should be since any practical long term therapy will ultimately have to involve levels of safety of orders of magnitude above those achieved now. Administrations that are at present resulting in liver uptakes of 20-30% or bone marrow doses of hundreds of cGy need not be taken as indicating the real potential of the technique. Only a situation resulting in thousands of cGy being received by the tumor and perhaps less than tens of cGy to the sensitive organs would need to be looked at carefully. Hopefully then, today's endeavours will be outdated and redundant in a few years. At present we need to continue with less than optimum conditions while we mark time before real tumor specificity is achieved.

PRESENT STAGE OF DOSIMETRY

The dosimetric calculations arising from the use of radiolabeled antibodies requires answers to the same questions as asked with other more conventional radionuclides and radiopharmaceuticals, that is: where is the activity; how long does it stay there; what, where, and how is the energy deposited?

What does distinguish the use of antibodies from that of conventional radiopharmaceuticals may be: (a) the specific nature of the final distribution in the target which may be either a uniform or nonuniform distribution throughout or around the tumor mass or the individual cells themselves; (b) the specific time courses associated with the radionuclide and with the antibody in the target and normal tissues as a function of uptake and removal; (c) the specific radionuclides used to label the antibody.

As more imagination is being employed in trying to label the antibody, more exotic dose calculations involving the possibilities of microdosimetry are involved.

The questions thus asked in the context of the use of radiolabelled antibodies and especially in the context of their use in therapy are as follows:

1. About the antibody itself:

How specific is it?

How much of it reaches the target and what is the tumor to normal uptake ratio?

How much of the antibody can be administered with the same efficiency without an immune reaction?

What are the dissociation kinetics of the complex?

How is the radiolabeled antibody to be delivered to the target?

What conditions in the delivery (e.g. temperature effects) alter the uptake?

2. About the radionuclide label:

What radionuclide is to be used and what specific activity can be achieved?

What is its half-life in relation to the kinetics involved?

How does the label itself affect the antibody either through its presence or its radiations?

How do the conditions of labeling and administration affect the antibody?

3. About the target and normal tissues:

What is the size and the state of the target in terms of perfusion and necrosis?

How is the target spatially distributed? Are the normal tissues relatively close? How is the radionuclide deposited relative to the target?

What is the ultimate fate of the radionuclide?

Many of the techniques and much of the technology enabling quite accurate dosimetry are generally available today. Functional location may be performed by radionuclide imaging, anatomical delineation by X-ray computerised tomography, ultrasound, or nuclear magnetic resonance. The kinetics and quantitation of radioactivity distributions may be estimated using a number of techniques involving whole-body gamma camera imaging. The theory on which the conventional dosimetry is based is also being confirmed by direct measurement (1). However, the physical extent of the uptake in small tumors or remnants after surgery is still extremely difficult to measure and to monitor after therapy. There are also questions about quantitation of activity that are introduced by not accounting for all the activity in a region because of unknown amounts of scattered or attenuated radiation. In the case of very small targets with a reasonable uptake, the lack of knowledge can mean that we may often deliver 1/5 to 5 times the required dose while the level of quantitation might have an error of 50 to 100%. More accurate microdosimetry calculations might also introduce large correction factors to the average dose calculations.

DATA ACQUISITION FOR DOSIMETRY

The instruments and techniques needed to acquire the information about activity and distributions are well established. Since a quantitative answer is required about how much activity (in MBq) is at each site, a simple gamma camera imaging technique giving answers in counts per second will not suf-

fice. Methods based on the combining of opposed computer acquired digital gamma camera views with correction for attenuation are then required. It has been found that complicated corrections for the distribution of the activity predicted by theory are not necessary and sufficiently accurate results can be obtained using relatively simple phantoms and a small range of calibration factors.

The main practical inaccuracies in the whole approach stem from the poor spatial resolution of the camera which is, in the case of direct imaging of lower energy radionuclides such as In-111, of the order of 15 ± 3 mm and, for the commonly used medium energy radionuclides like I-131, about 20 ± 5 mm. Often however, the entire distribution has to be analysed and a whole-body image with significantly poorer resolution has to be acquired using a scanning gamma camera. The lack of resolution means that the activity associated with a tumor is not correctly measured and also that accurate sizing of the site is impossible. In addition, it should be borne in mind that three-dimensional 'tubes' through the body rather than two-dimensional areas of activity are being imaged. Thus, it could be considered that the activity in a $1.5 \times 1.5 \times 25$ cm volume containing both normal and abnormal tissue appears in the region of interest from each small area of localised activity on the two-dimensional image. This inclusion of activity from normal tissues reduces the contrast in the image and reduces the apparent increase in uptake by the lesion of the labeled antibody. It is one of the main reasons for using more complicated tomographic acquisition and processing techniques.

All the emitted radiations are subject to varying degrees of absorption and scattering in the process of escaping from the body and registering as a count in the imaging device. Methods of correction for these attenuation processes involve either a transmission image or an analysis based on the buildup factors involved (2). Measurements in the body are related to previously established calibration measurements obtained using a model system involving known configurations of target and background. Errors in quantitating activity in a wide range of volumes and backgrounds of $\pm 5\%$ can be achieved in a well defined situation. However because of varying tissue back-ground this accuracy would not be expected to be achieved *in vivo*.

The regions that are to be quantitated are outlined and defined using the computer display system. The definition of the outline employs either a computer edge-detection algorithm, which is generally more accurate, or an operator judgement in which case the choice is rather arbitrary since color or intensity settings are often determined by the maximum count in the whole image quite independently of the region of interest.

A problem that affects higher energy radionuclides such as I-131 is the scattering of an amount of activity out of the immediate region to a significant and unknown extent (3). A loss of counts from the source is therefore expected. It is more acute for smaller sources and also depends on the depth of the source. Since the effect would be expected to occur also in the phantom used to derive the calibration factors, the breakdown in the relationship between counts and activity may not be so acute. Another practical difficulty that arises is the correspondence of regions of interest in anterior and posterior views of organs and tumors and in transmission images since the outlines often appear quite differently on the images.

The use of single photon emission computerised tomography for location and quantitation of uptakes does offer some improvements because of its ability to examine volumes free of overlying and underlying activity. However, unless some rather complicated measures (special collimators, elliptical orbits, etc.) are taken, the resolution is usually degraded by the reconstruction process and, with circular orbits, by having to image at non-optimal distances from the patient. In addition, quantitative results are not easily attained because of difficulties in correcting for attenuation. It would, in addition, be impractical to image the whole body in this way (Fig.1).



Figure 1. Whole-body distribution of In-111 labeled H17E2.
Numerous sites of uptake are of interest for dosimetric purposes and require computer analysis over the field of the whole-body image.

For investigating the kinetics of the labelled antibody, that is in establishing the half-life (or half-lives or rate constants) of disappearance of the activity, it is not really necessary to obtain a quantitative estimate at each time of imaging. A relative count in a specified region of interest will suffice. The geometric mean of the counts from two conjugate views obtained at the various times is quite accurate enough for these kinetics, assuming that the redistribution of activity within the differently attenuated regions of the body has only a marginal effect.

Questions of 'how much' and 'how long' can thus be answered with accuracies of the order of $\pm 10\%$. These imaging measurements are of course usually supported by timed blood and perhaps urine collections in which the activity can be expressed in terms of the percentage of the initial activity administered.

The volume of distribution of activity is not shown with sufficient accuracy by either of the nuclear medicine techniques, planar imaging or SPECT. Activities distributed in volumes of 1 mm^3 or 1 cm^3 would appear as having the same area in the image, and volumes of, say, 2 cm^3 and 5 cm^3 would be barely differentiated. This degree of inaccuracy would have a drastic effect on any dosimetric calculations since knowledge of the activity per gram is essential. Volumes down to 30 ml , at which level the error is about 10%, can be estimated with SPECT (4) using a simple though instrument-specific thresholding technique. For example, this may be useful for determining the volume of a liver. However it is volumes considerably smaller than this, corresponding to tumor diameters less than a few centimeters, that we would eventually like to examine.

Positron emission tomography is another technique with an improved (in nuclear medicine terms) spatial resolution of less than 10mm and an accurate though laborious method of quantitation of activity. This technique has the obvious limitations of requiring expensive specialised equipment and a positron emitting radionuclide with a half-life of the order of days as the label and has an even more limited volumetric field of view than the SPECT technique.

Because in all the techniques described above the limited relative spatial resolution for small sources renders the volume determinations unacceptably inaccurate, we have to make the leap to a more morphological imaging technique to obtain the information about volumes of radionuclide distributions. Three imaging modalities - x-ray CT, ultrasound, and magnetic resonance imaging - have found an application in evaluating volumes for dosimetric purposes (combined with monitoring the progress of the therapy). This introduces the assumption that the anatomical volume, for example, an x-ray computerised tomography image, will correspond to the functional image. In practice, the relationship between the distribution of labeled antibody throughout a solid tumor and the distribution of attenuation constants may be rather tenuous.

Measurement for therapy will usually proceed in two stages, a diagnostic one followed by the therapeutic application. This is especially true when we are dealing with a relatively unfamiliar technique of administration or a situation where the uptake is unpredictable or a new antibody or radionuclide. In the diagnostic stage the required monoclonal antibody is labeled with relatively low activities of the therapeutic label or, often, with an equivalent radionuclide able to be safely administered at a higher activity because it emits gamma rather than beta emissions. Thus, I-123 ($13 \text{ hr } T_{1/2}$, 169 keV gammas) has been used in place of I-131 and In-111 ($68 \text{ hr } T_{1/2}$, 171 keV gammas) in place of Y-90. The use of lower energy radionuclides alleviates the problems of scatter discussed above and more accurate localisation can be made especially when the therapeutic agent is exclusively a beta emitter. The higher energy beta emitters such as Y-90 or P-32 can of course be imaged with the gamma camera using a window set to receive x-rays resulting from the electrons but not in any quantitative way. Often two radionuclides are used in the preliminary investigative stage. One labels the proposed specific antibody and the other, which can be distinguished in terms of its energy, the control antibody.

It is useful after the therapeutic activity dose has been given to check that the predicted distribution and kinetics actually have been achieved. This check is usually impossible to carry out soon after therapy using a camera because the high activities involved would swamp the sensitive gamma camera (use might even be made of an old rectilinear scanner with low sensitivity high resolution collimators to image the body in the first few days

after therapy). Alternatively, as a simple check, a collimated counter or a dose-rate meter held at a fixed distance from both sides of the body, so that a geometric mean of the readings can be calculated, can be employed to determine whole-body elimination rates.

DOSIMETRIC CALCULATIONS

Radiolabels for antibody therapy have been chosen on the grounds of availability, economics, and ease of labeling as well as physical properties of appropriate half-life and therapeutically efficient, usually beta, emissions. Alpha emitters also have been suggested but no reports of their use have yet appeared.

Up to now I-131 has been very widely used for radiolabeled antibody therapy. Even though this is a rather old-fashioned radionuclide its performance as a therapeutic agent for macroscopic tumors still holds good. It is as a label for the antibody that it is found wanting since it tends to lose its attachment to the antibody especially after systemic administration where the free iodine proves an embarrassment both in the blood and the marrow and to the unblocked thyroid. Of the beta emitters with appropriate half-lives measured in days, Y-90 (used as a bifunctional chelate) has been suggested as a strong candidate for therapy as has P-32 which involves a more complicated method of attachment.

Radionuclides such as these can be handled with sufficient accuracy to monitor the progress of antibody applications in therapy. In present day situations standard MIRD formulations and conventional dose calculations for small tumors can be carried out. Although patients will not conform to the MIRD standard organ configurations and 'S' values will not be available for calculation of contributions of nonpenetrating radiations to normal organs probably some good assumptions can be made using the MIRD tables to fit a given case.

VALUE OF MODELING

A number of papers have appeared in which the dosimetry of a particular situation (for example anti-ferritin in hepatoma (5)) or a range of hypothetical situations (for example a multitude of untried radionuclides (6)) has been calculated. In addition to these a variety of models will be presented later at this symposium. As with any model the conclusions reflect to a large extent the initial assumptions so that any predictions made have to be viewed with these assumptions in mind.

An example of how dependent the predictions are on the conditions of uptake and kinetics used in the calculations may be taken from the literature (6). Here absorbed dose calculations are made for a 500 g solid tumour in a standard liver with a 3:1 tumor/non-tumor uptake of whole antibody at 12 hours that increases to a plateau value of 10:1 at 48 hrs. The doses in cGy to tumor, liver, and whole body for 3.7 GBq activity administered are 1700, 200, and 200, respectively, for Y-90. After scaling to an equal whole-body dose and rounding up, the corresponding doses for I-131 are 700, 400, and 200.

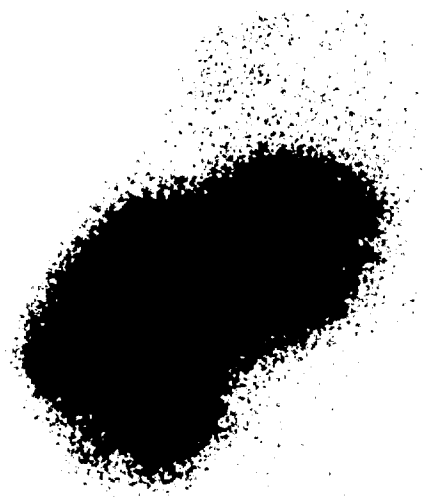


Figure 2. Numerous small metastases appearing in the liver after i.v. injection of In-111 labeled H17E2. Details of dosimetry appear in the text.

Based on an actual example, using In-111 labeled monoclonal antibody to placental alkaline phosphatase (Figure 2), the following conditions were found.

About 30% of the activity went to the liver and liver metastases with a short uptake time and long release time; the uptake in the 10g tumor was about 0.5% giving an estimated 3:1 target to normal tissue ratio; the uptake in the bone marrow treated as a subcompartment of the blood was 15% with a half-life of 18 hrs. Standard MIRD type calculations gave corresponding doses to the tumor, liver, and bone marrow for 2.4 GBq of Y-90 of 4000, 2400, 200 cGy, respectively, and 8000, 3000, and 200 cGy for 8 GBq of I-131. Corresponding figures for 3 GBq of P-32 are 11000, 3600, and 200.

What conclusions can be drawn from this comparison of two similar calculations where presumably the dosimetric calculations are reasonably correct and follow standard procedures and yet come to very different conclusions? What guidance in the development of radiolabeled antibodies can they give? In the one, Y-90 is clearly superior to I-131, in the second, it is the reverse with the added complication that the liver is over-dosed. The differences result obviously from the assumed values for tumor size and kinetics and emphasise the basing of the data on an established range of clinical situations.

CAVITY THERAPY WITH LABELED ANTIBODIES

One manoeuvre that has met with some apparent success is that of cavity administration of labeled antibodies. The rationale here is that if intravenous administration of the antibodies leads to too small an uptake due to dilution and dissociation (though enroute binding to free antigens is not always a problem), then direct placing of the antibody into a cavity with little or no communication with other body compartments would enhance the

antibody's chance of reaching the target. This rather limited form of therapy has been applied to the peritoneum in the treatment of ovarian cancers and in the pericardium and pleural cavities to treat malignant effusions. Although it has been calculated that after introduction of 2000 - 4000 MBq of I-131 labeled antibody into the cavity, doses of the order of 5000 cGy have been delivered to tumors with doses of the order of tens of cGy to the blood and organs such as the liver, enhancement of the target to non-target ratio has not yet been sufficient and consistent enough to justify the approach against more commonly used procedures employing P-32. In such a technique the uniform distribution of only 1 GBq of P-32 labeled chromic chloride particles would deliver an estimated 8000 cGy to the surface of the cavity with only a few cGy delivered to the blood (7). Obviously it would be hoped that the use of an antibody leads to a more directed targeting of the activity and consequently that the rest of the cavity would be spared, but it is uncertain whether the overall result of what is an expensive and complicated procedure produces any better results than the simple one. Both methods seem to suffer from non-uniformity of distribution of the activity due to trapping in pockets and folds of the cavity though this is less permanent in the case of the antibody.

Sufficiently large numbers of patients have not been treated to date to compare this form of therapy in terms of survival though it has been found that 6 out of 6 patients with intra-abdominal stage III ovarian cancer are well 6-24 months after treatment though 3 out of 4 patients with stage IV extra-abdominal disease had died but had benefited symptomatically for 3-6 months after treatment. Adverse symptoms appearing after greater than 4000 MBq were administered were diarrhoea and cytopenia. In the treatment of pleural and pericardial effusions all patients have shown resolution and no evidence of recurrence except where the primary was antibody negative.

However, with improvements in techniques or labeling, Figure 3, it is likely that this intermediate method and the dosimetric methods associated with it may be replaced by one involving intravenous imaging and different problems in dosimetry.

Figure 3. Intraperitoneal ovarian cancers localised for therapy using intravenous rather than direct cavity administration of radiolabeled antibody.



DOSIMETRY AT THE CELLULAR LEVEL

The radiation dose, say to a tumor, is usually calculated by considering the tumor as a collection of cells and determining the average dose or energy deposited in the volume of the tumor. However the cytocidal properties of the radiation lie in the dose received by individual cells and the concept of an averaged dose may not be adequate to describe this. Essentially each cell could receive a dose from the radioactive atoms very near to (on the surface of or within) the cell itself and a dose from atoms at a distance from it. Usually we consider only the latter case since the radiations dealt with are either penetrating gamma rays or beta rays with a range of the order of millimeters in tissue. However the presence and contribution of low-energy electrons (Auger, Coster-Kronig etc.) with energies less than, say, 10 keV are increasingly being considered (8). These radiations have a range of perhaps 10nm to 10 μ m and obviously affect only the cell itself (diameter about 10 μ m) and possibly its near neighbours. The target tumor cells are therefore receiving a total radiation dose that may be substantially underestimated by conventional dosimetry. Two factors increase the significance of this cellular or microdosimetry aspect. Firstly the labeled antibody concentrates (or ought to concentrate) at the target cells rather than dispersing uniformly in the environment of the target. Secondly the radionuclide used as a label for the antibody may be chosen for its low energy, low range radiations, in order to exclusively treat the tumor cells themselves and spare the normal tissue. Depending on the degree of concentration of the activity around the cells and depending on the energy associated with the short range radiations the dose calculated using microdosimetric techniques may be many times that derived from the standard averaging calculations.

Radionuclide labels chosen for close range irradiation of tumor cells should act at or near the cell surface. It is unlikely that access will be gained to the cell nucleus. Alpha particles would probably remain on the cell surface and for maximum efficiency of irradiation have an energy of 1-2 MeV and a range of the order of a cell diameter (10-15 μ m). Auger and low energy conversion electrons with energies 5-50 keV (range 1-50 μ m) would also be suitable for irradiating a single cell and some of its closely packed neighbours.

Since a number of Auger and similar energy electrons are usually associated with a radionuclide, the dosimetry would be based on the sum of each separate product of number of disintegrations, mean energy, and probability of deposition. In practice only those emissions with a relatively high abundance need to be considered. In a simplified scheme the probability of deposition is obtained from the geometry of the situation, assuming a point emitter at the surface or at a mean position within the cell, emitting energy over a volume defined by an estimate of its path length (usually assumed to be straight). The degree of overlap of this volume and the volume of the cell or the cell and its neighbours yields the probability of deposition. The calculation of the degree of overlap may be a simple one (9) or it might involve a more complex Monte Carlo computer simulation. The microdosimetry of alpha emitters will have been dealt with earlier in this symposium.

Therapy of this nature would involve a radical departure from conventional medium energy beta therapy and no realistic antibody labelling technique employing specific Auger or alpha emitters with suitable half-lives (since it is debatable whether 28-day T_1 I-125 or 7.2 hr T_1 At-211 would really be practical) has been described?

CONCLUSIONS

A wide variety of practical therapeutic applications with different radiolabeled antibodies has yet to be achieved. Until adequate targeting with uptakes at least ten times those yet attained is demonstrated, then dosimetric models should not be made over-elaborate or be firmly established. In any case practical methods of data acquisition to feed into calculations for dosimetry are well established and should be accurate enough to cope practically with any eventual outcomes. What new dosimetric techniques are perhaps required to sit ready in the wings are at the cellular level involving yet to be applied low energy emission radionuclides. Again the appropriate antibody has to be established to provide basic data for further models.

REFERENCES

1. Wessels, B.W., B.W. Bacha, and S.M. Quadri. Microdosimetric TLD measurement of tumor associated antibody therapy. J. Nucl. Med. 25, P39, 1984.
2. Wu, R.K., J.A. Siegel. Absolute quantitation of radioactivity using the build-up factor. Med. Phys. 11, 189-192, 1984.
3. Clarke, L.P., J.F. Malone M. Casey. Quantitative measurement of activity in small sources containing medium energy radionuclides. Brit. J. Radiol. 55, 125-133, 1982.
4. Tauxe, W.N., F. Soussaline, and A.E. Todd-Pokropek. Determination of organ volume by SPECT. J. Nucl. Med. 23, 984-987, 1982.
5. Leichner, P.K., J.L. Klein, J.B. Garrison et al. Dosimetry of I-131 labelled anti-ferritin in hepatomas: a model for radioimmunoglobulin dosimetry. Int. J. Onc. Biol. Phys. 7, 323-333, 1981.
6. Wessels, B.W. R.D. Rogus. Radionuclide selection and model absorbed dose calculations for radiolabeled tumor associated antibodies. Med. Phys. 11, 638-645, 1984.
7. Boye, E., M.W. Lindegaard, E. Paus et al. Whole body distribution of radioactivity after peritoneal administration of P-32 colloids. Brit. J. Radiol. 57, 395-402, 1984.
8. Rao, D.V., G.F. Govelitz, and K.S.R. Sastry. Radiotoxicity of thallium-201 in mouse testes: inadequacy of conventional dosimetry. J. Nucl. Med. 24, 145-153, 1983.

DISCUSSION

HARPER: I was disturbed by what you said about the difficulties in determining the nuclide distribution encountered with monoclonal antibodies, in which your group relied on rectilinear scanning although tomographic methods were available. Although the more powerful PET and SPECT methods have limited fields of view (particularly PET), with some sacrifice of temporal and spatial resolution, the field of view of a PET imaging device can be extended by moving

the patient longitudinally during the procedure and presenting the data in a manner analogous to that used with the scanning Anger camera. If this approach is feasible, it should provide improved data without greatly increased labor.

MYERS: I would like to correct your impression that we are using exclusively rectilinear scanning at Hammersmith. We in part use scanning cameras and planar imaging as well as SPECT and planar imaging. Because the large number of antibody studies required for accurate dosimetry (and perhaps some quantitative repeat studies at both a diagnostic and a therapeutic stage using both a specific- and a nonspecific-labeled antibody) are difficult to fit into the department's routine, the more sophisticated and time-consuming techniques like SPECT or PET might not get the attention they deserve.

MARCUS: I think Dr. Harper made a very interesting point. Paul, what radionuclide do you think you would put on the monoclonals?

HARPER: Gallium-68

THAKUR: Yes, Dr. Harper, Ga-68 could be used to label monoclonal antibodies for PET imaging, but some problems in doing that effectively are the short half-life of Ga-68, the volume in which it is eluted, and the cationic impurities the solution contains. Why can't In-111 monoclonal antibodies be used and the data of the type you are suggesting be acquired in the SPECT mode?

HARPER: Using the same scan?

THAKUR: Right.

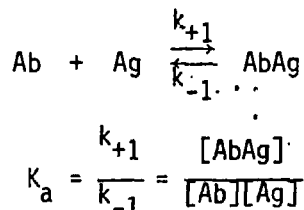
A Compartmental Modeling Approach to the
Radiation Dosimetry of Radiolabeled Antibody

P.B. Zanzonico and R.E. Bigler
New York Hospital-Cornell Medical Center
and Memorial Sloan-Kettering Cancer Center
525 East 68th Street
New York, NY 10021

F.J. Primus, E. Alger, R. DeJager,
S. Stowe, E. Ford, K. Brennan, and D.M. Goldenberg
Center for Molecular Medicine and Immunology
University of Medicine and Dentistry
100 Bergen Street
Newark, NJ 07103

ABSTRACT

Essential for the calculation of absorbed doses from systemically administered radiolabeled antibody is the determination of the total number of nuclear transformations (i.e. cumulated activity) in specified "source regions." Compartmental analysis (using biodistribution data augmented with a priori physiological information), unlike simply integrating empirical "time-activity" curves, may enable one to calculate the cumulated activity in "unsampled" as well as "sampled" source regions. These may include microscopic source regions (e.g. the intracellular space, cell surface, and extracellular space) important for microdosimetry calculations. Of particular importance is the interaction between the "anti-tumor" antibody (Ab) and the "tumor" antigen (Ag):



where k_{+1} and k_{-1} are the association and dissociation rate constants, respectively, and K_a is the association equilibrium constant. If, in vivo, $L(\text{bound} \leftarrow \text{free})$ and $L(\text{free} \leftarrow \text{bound})$ represent the fractional rates of association of Ag and Ab and of dissociation of the AgAb complex, respectively, then

$$L(\text{bound} \leftarrow \text{free}) = k_{+1}[\text{Ag}] \quad L(\text{free} \leftarrow \text{bound}) = k_{-1}$$
$$= k_{-1} K_a [\text{Ag}]$$

If it is assumed that total $[\text{Ag}] \gg$ total $[\text{Ab}]$, then the first as well as the second of these rate constants are essentially constant and the associated compartmental model is thereby linear. Because the parameters k_{+1} , k_{-1} , K_a , and total $[\text{Ag}]$ can, in principle, be evaluated in vitro, compartmental analysis can be used to theoretically assess the clinical efficacy (in terms of the differential cumulated activity between tumor and normal tissue) of any potential "anti-tumor" antibody.

INTRODUCTION

Accurate and precise radiation dosimetry is crucial to the successful therapeutic application of systemically administered radionuclides, including of course radionuclides in the form of radiolabeled antibody. In marked contrast to the diagnostic application of radiopharmaceuticals, where absorbed dose estimates simply provide an approximate measure of the potential radiation hazard (i.e. risk) inherent in a particular procedure, the results of dosimetric calculations for radionuclide therapy may actually dictate the course of therapy: the absorbed dose estimates (in terms of rad/mCi, for example) for the target tissue (i.e. tumor) indicate the minimum administered activity required to produce a significant therapeutic effect and the maximum administered activity which will not produce prohibitive normal tissue morbidity. Our collective experience suggests that, even under the most favorable circumstances (e.g. using a truly tumor-specific "anti-tumor" antibody), the latter quantity is not likely to greatly exceed the former quantity. As with all anticancer therapeutic modalities, the therapeutic index of systemic radionuclide therapy is therefore marginal, indicating that such therapy cannot proceed in an optimum manner without heretofore unattained accuracy and precision in internal radionuclide dosimetry.

The difficulties inherent in generating accurate and precise absorbed dose estimates are exacerbated when dealing with radiolabeled antibody because of the marked qualitative as well as quantitative differences in pharmacokinetics among different individuals, different antibodies, different radionuclides, etc. Accordingly, radiation dosimetry of sufficient accuracy and precision for therapeutic application of radiolabeled antibody will certainly have to be performed on a case-by-case basis. Because of the variable factors enumerated above and the generally limited and at times imprecise biodistribution data available for individual patients, we believe the most expeditious and systematic approach to calculating absorbed dose will be based upon physiologically rational compartmental modeling, rather than simply integrating "time-activity" curves. In this way, important a priori information (e.g. antigen concentration and antigen-antibody rate and equilibrium constants) can be incorporated into the estimation of cumulated activities, improving the overall accuracy and precision of absorbed dose estimates.

OVERVIEW OF INTERNAL RADIONUCLIDE DOSIMETRY: THE "MIRD" FORMALISM

The calculation of radiation absorbed doses to various organs and tissues from systemically administered radionuclides is most expeditiously accomplished by considering separately the physical and the biological components of this calculation. Thus, one can determine separately the absorbed dose to a given "target region" per nuclear transformation in a given "source region" (the "physical" component) and the total number of nuclear transformations which actually occur in that source region (the "biological" component). As formulated by the Medical Internal Radiation Dose (MIRD) Committee of the Society of Nuclear Medicine (1, 2), the former quantity is represented by " $S(r_k \times r_h)$," mean absorbed dose (in rad) to a target region r_k per unit cumulated activity (in $\mu\text{Ci}\cdot\text{hr}$) of a radionuclide uniformly distributed in a source region r_h ; the latter quantity is represented by " $\bar{\lambda}_h$," the cumulated activity (in $\mu\text{Ci}\cdot\text{hr}$) of the radionuclide in source region r_h . Accordingly, the mean absorbed dose, $D(r_k \times r_h)$, to a target region r_k from a radionuclide uniformly distributed in a

source region r_h is given by the following equation:

$$\bar{D}(r_k \leftarrow r_h) = \lambda_h S(r_k \leftarrow r_h) \quad (1).$$

Since there are generally a number of source regions, the total mean dose, $\bar{D}(r_k)$, to target organ r_k is given by the following equation:

$$\bar{D}(r_k) = \sum_h \lambda_h S(r_k \leftarrow r_h) \quad (2).$$

The quantity $S(r_k \leftarrow r_h)$ is a physical quantity, related to the nuclear properties of the particular radionuclide under consideration, the geometrical orientation of the target organ r_k and the source organ r_h , and the mass density and elemental composition of the target organ r_k , the source organ r_h , and the intervening tissues. The determination of the values of $S(r_k \leftarrow r_h)$ is an extremely difficult problem and is beyond the scope of this paper. Nevertheless, for a specified anthropomorphic anatomic model (i.e. "Reference Man"), the values of $S(r_k \leftarrow r_h)$ for many radionuclides and target organ-source organ pairs have been tabulated (2). On the other hand, knowing the physical half-life of the particular radionuclide under consideration, the quantity λ_h is a biological quantity, related to the pharmacokinetics of the particular radiopharmaceutical under consideration.

The determination of the values of λ_h in man for systemically administered radioiodinated "anti-tumor" antibody is the subject of this paper.

DETERMINATION OF CUMULATED ACTIVITIES

THE "EMPIRICAL" APPROACH

The traditional, purely empirical approach (1,2) to the determination of λ_h (e.g. in $\mu\text{Ci}\cdot\text{hr}$) is represented by equation (3):

$$\lambda_h = \int_0^\infty A_h(t) dt \quad (3)$$

where $A_h(t)$ is the uncorrected (for radioactive decay) amount of activity (in μCi) in source region r_h at time t post-administration (in hr). If, as is often done, one corrects the amount of radioactivity in source region r_h for radioactive decay from the time of administration of the radiopharmaceutical, equation (3) can be reformulated as equation (4):

$$\lambda_h = \int_0^\infty e^{-\lambda t} q_h(t) dt \quad (4)$$

where λ is the physical decay constant (in hr^{-1}) of the particular radionuclide under consideration and $q_h(t)$ is the distribution function for source region r_h , that is, the corrected (for radioactive decay) amount of radioactivity (in μCi) in source region r_h at time t post-administration (in hr). In general, it is assumed that the distribution function can be approximated by a sum of exponentials to within an accuracy adequate for absorbed dose calculations:

$$q_h(t) = \sum_j A_{hj} e^{-\lambda_j t} \quad (5)$$

where A_{hj} is the value (in μCi) of the j th exponential component at time $t=0$ and λ_j is the biological disappearance constant (in hr^{-1}) of the j th exponential component. Substituting the expression for $q_h(t)$ in equation (5) into equation (4) and evaluating the resulting definite integral yields equation (6):

$$\hat{\chi}_h = \sum_j \frac{A_{hj}}{\lambda + \lambda_j} \quad (6).$$

In practice, the parameters (i.e. A_{hj} , λ_j) of the distribution function, $q_h(t)$, for each of any number of source regions r_h for the radionuclide derived from any radiopharmaceutical under consideration are generally determined according to the following paradigm or some variation thereof: the amount or concentration of radioactivity in any number of tissues or organs (i.e. source regions r_h) of a selected animal model system at various times t post-administration is measured, for example, by radioassay in vitro of weighed serial necropsy samples; the resulting "time-activity" data for each such source region r_h are fit to a time-dependent function of the form of that in equation (5) (generally "by eye," by exponential "curve stripping," or by a "least squares" fitting algorithm) to yield values of A_{hj} and λ_j for the particular animal model system under consideration; the resulting values of A_{hj} and λ_j are each adjusted for the respective differences in fractional mass of each source organ or tissue r_h between the particular animal model system and, for example, "Reference Man" (3), to yield values of A_{hj} and λ_j for man. Substituting the values of A_{hj} and λ_j thus derived and the value of λ for the particular radionuclide under consideration into equation (6), the value of $\hat{\chi}_h$ for each respective source region r_h is calculated. Substituting the resulting values of $\hat{\chi}_h$ and the tabulated values (2) of $S(r_k+r_h)$ for the particular radionuclide under consideration and the appropriate target region-source region pairs into equation (2), the value of $D(r_k)$ for any particular target region r_k is calculated.

THE "PHYSIOLOGICAL" APPROACH

An alternative, "physiological" approach to the determination of $\hat{\chi}_h$ is based upon compartmental analysis (4), wherein the particular biologic system under consideration is treated conceptually as an assortment of interconnected compartments each consisting of an ensemble of identical chemical or physical units. Each such ensemble may somehow be localized in an identifiable anatomic entity (e.g. the liver), an identifiable functional entity (e.g. the reticuloendothelial system), or an identifiable physical entity (e.g. the extracellular space). Any such anatomically, functionally, or physically localized ensemble constitutes a compartment. Such an ensemble may not, however, actually be localized in any such identifiable entity and its existence as a discrete compartment is then purely conceptual. In the body, compartments tend to remain

constant in terms of size of the ensemble (i.e. number of chemical or physical units), while undergoing continual turnover, by net rate of input equaling net rate of output, resulting in a dynamic equilibrium, or "steady state." The existence of a dynamic equilibrium, or steady state, together with the identifiability of specific compartments and detectability of the flux of a non-perturbing tracer through various such compartments, are implicit assumptions of compartmental analysis. A compartmental model is thus characterized by the number of compartments and by transition probabilities, or "exchange rates," between compartments, and may be represented mathematically by a set of first-order ordinary differential equations (5):

$$\frac{dF(i,t)}{dt} = \sum_{\substack{j=0 \\ j \neq i}}^n [L(i,j,t)F(j,t) - L(j,i,t)F(i,t)] \quad (7)$$

where $F(i,t)$ and $F(j,t)$ are functions corresponding to the amount of tracer in compartments i and j , respectively, at time t and $L(i,j,t)$ and $L(j,i,t)$ are the fractional exchange rates to compartment i from compartment j and to compartment j from compartment i , respectively. The exchange rates are generally constant with time (i.e. non-varying), yielding a set of linear differential equations and a so-called linear compartmental model (6):

$$\frac{dF(i,t)}{dt} = \sum_{\substack{j=0 \\ j \neq i}}^n [L(i,j)F(j,t) - L(j,i)F(i,t)] \quad (8).$$

In a whole-body compartmental model for systemically administered antibody (See below.), however, the finite antigen concentration and the resulting saturability of antigenic binding sites requires non-linear differential equations (See equation (7) above and equations (9)-(14) below.) to explicitly represent the antigen-antibody interactions (i.e. a non-linear compartmental is required).

To derive a compartmental model the solution of which agrees with experimental data that correspond to discrete values of $F(i,t)$, the number of compartments and the values of $L(i,j)$ must be determined. There is actually no unique model for a given set of data since any model can always be modified beyond the "resolution" possible from the data by, for example, the introduction of additional compartments. In practice, however, one generally develops a model having a minimum number of compartments. The "solution" of a compartmental model (i.e. the determination of values of the model parameters), even for relatively simple models, is a formidable computational task and is beyond the scope of this paper; the interested reader is referred to References 4-6. Suffice it to say, however, that compartmental models for systemically administered radiolabeled "anti-tumor" antibody are sufficiently complex as to require computers for their solution.

The actual compartmental modeling-based calculation of cumulated activities can be accomplished by the method of Bigler and Sgouros (7), as presented in Figure 1. In order to calculate χ_h , the cumulated activity in source region r_h , for example, one introduces two "virtual" compartments, h_1 and h_2 , connected to compartment h (representing source region r_h) and their associated exchange rates, $L(h,h_1)$, $L(h_1,h)$ and $L(h,h_2)$, $L(h_2,h)$, respectively, such that

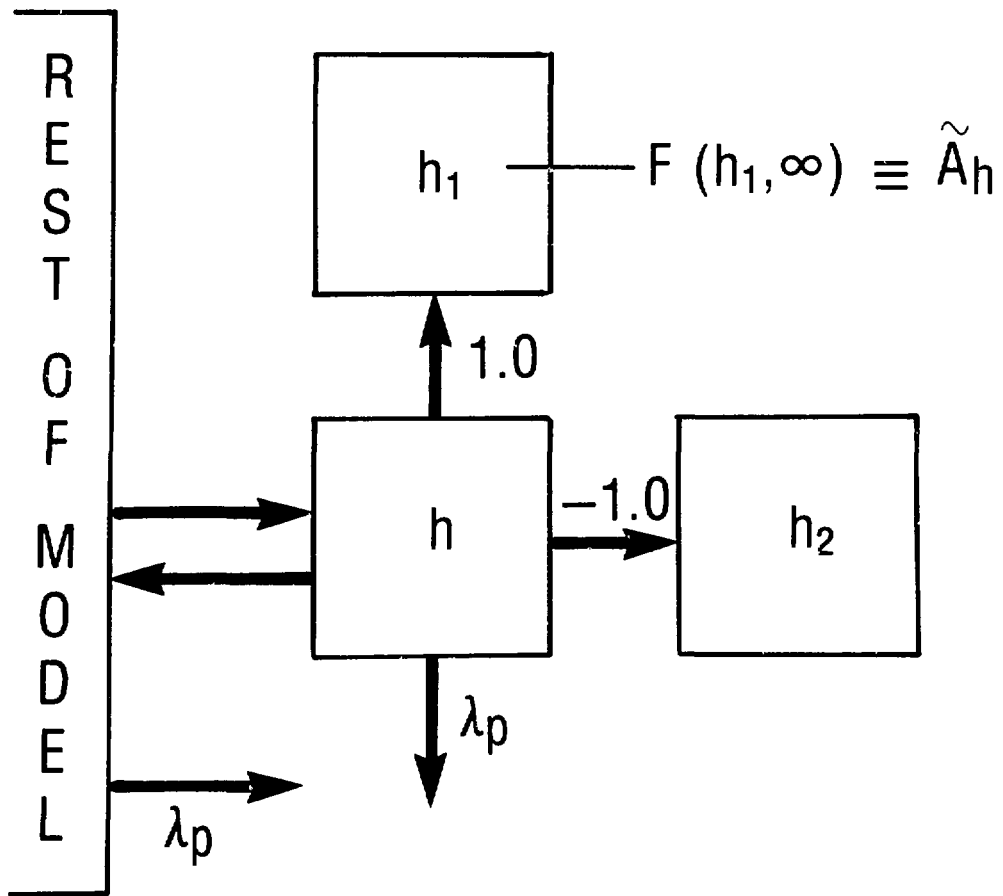


Figure 1. Method of calculating cumulated activities directly from a compartmental model.

$$\begin{aligned}
 L(h, h_1) &\equiv 0 \text{ hr}^{-1}, \\
 L(h_1, h) &\equiv 1 \text{ hr}^{-1}, \\
 L(h, h_2) &\equiv 0 \text{ hr}^{-1}, \\
 L(h_2, h) &\equiv -1 \text{ hr}^{-1}
 \end{aligned} \tag{9}.$$

In addition, in order to account for radioactive decay, one must introduce an additional elimination exchange rate, $L(0, i)$, connected to each compartment i of the model such that

$$L(0, i) \equiv \lambda \tag{10}$$

where λ is the physical decay constant (in hr^{-1}) of the particular radionuclide under consideration. Then, if the administered activity is expressed in μCi and all exchange rates are expressed in hr^{-1} , the content of virtual compartment h_1 at "infinite" time (i.e. $F(h_1, \infty)$) is numerically equal to A_h in $\mu Ci\cdot hr$; virtual compartment h_2 is introduced to continually re-supply compartment h with whatever amount of tracer is transferred from compartment h to compartment h_1 , thereby leaving the amount of tracer in compartment h unperturbed by the presence of compartments h_1 and h_2 . Implicit in this method of calculating cumulated activities is the ability to calculate the content of any compartment at any arbitrary time (i.e. the ability to calculate, for example, $F(h_1, t)$).

In practical terms, however, "infinite" time is any time which is long relative to the physical half-life of the particular radionuclide under consideration.

COMPARTMENTAL MODELING OF RADIOIODINATED "ANTI-TUMOR" ANTIBODY

A PROPOSED MODEL

We will now present our current whole-body compartmental model for systemically administered radioiodinated "anti-tumor" antibody (actually, monoclonal antibody directed against tumor-associated carcinoembryonic antigen (CEA) (8-12)) in tumor-bearing "Reference Man" (3). Our proposed model, presented in literal terms below and in the familiar diagrammatic form in Figure 2, is based on a critical survey of the literature and incorporates a number of implicit and explicit assumptions. We must emphasize that it is highly tentative and that it has not as of yet been validated.

Like all substance administered systemically via intravenous injection, antibodies are initially distributed among tissues in relation to perfusion and fractional cardiac output after passing through the pulmonary circulation (13). Because of their high molecular weight and polarity, plasma-borne proteins such as antibodies diffuse only slowly in most tissues across the patent capillary endothelium into the extravascular space. This occurs more rapidly in some tissues than in others, however. For most visceral tissues, including brain, lung, heart, kidney, small intestine, large intestine, and stomach, the mass-normalized exchange rates for transfer of antibody from the vascular to the extravascular space are all quite comparable and typically of the order of $2 \times 10^{-5} hr^{-1}$ per gram of tissue (14); accordingly, these tissues collectively constitute what may be termed a "rapidly exchanging tissue" compartment (15). Since the combined mass of the tissues composing this compartment is approximately 3,500 gm (i.e. 5% of the total body mass of "Reference Man") (3), its exchange rate for vascular space-to-extravascular space transfer of antibody is $0.070 hr^{-1}$, corresponding to a half-time of approximately 10 hr. For most non-visceral tissues, including adipose tissue, bone, cartilage, muscle, and skin, the mass normalized exchange rate for transfer of antibody from the vascular to the extravascular space are likewise all quite comparable and typically of the order of only $6 \times 10^{-7} hr^{-1}$ per gram of tissue (14); accordingly, these tissues collectively constitute what may be termed a "slowly exchanging tissue" compartment (15). Since the combined mass of the tissues composing this compartment is approximately 48,000 gm (i.e. 75% of the total body mass of "Reference Man") (3), its exchange rate for vascular space-to-extravascular space transfer of antibody is $0.020 hr^{-1}$, corresponding to a half-time of approximately 35 hr.

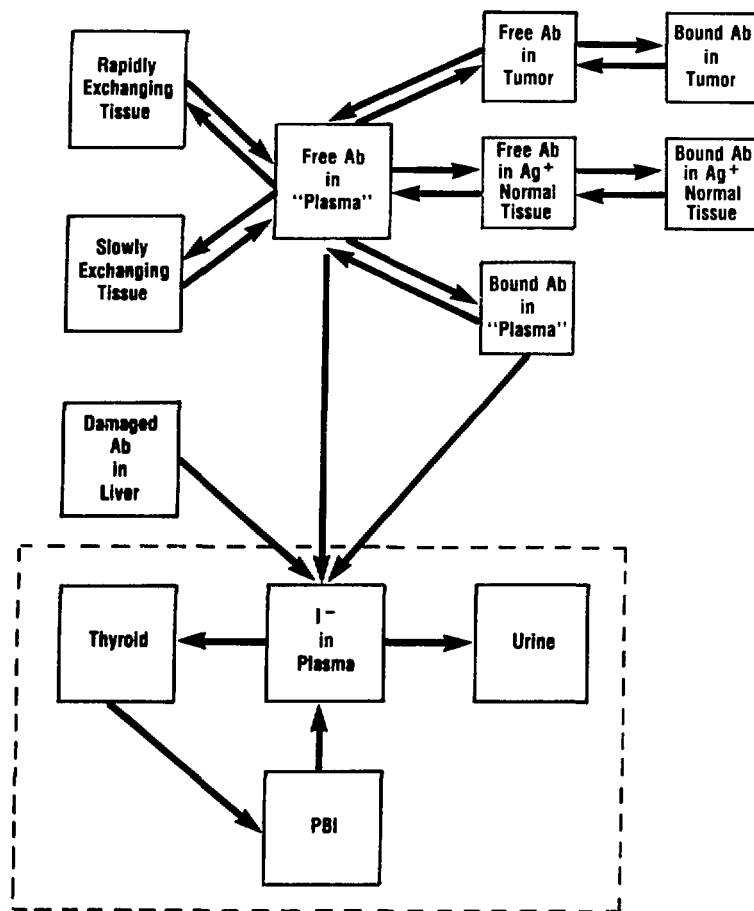


Figure 2. A proposed whole-body compartmental model for systemically administered radioiodinated "anti-tumor" anti-body in tumor-bearing "Reference Man."

Assuming a uniform distribution ratio (i.e. the ratio of the total amount of radioiodinated antibody in the extravascular compartment to that in the vascular compartment) of 1.4 at equilibrium (14), application of the law of mass action immediately yields a reverse exchange rate (i.e. the exchange rate for extravascular space-to-vascular space transfer of antibody) of 0.050 hr^{-1} (half-time: 14 hr) and of 0.014 hr^{-1} (half-time: 48 hr) for the "rapidly exchanging tissue" compartment and for the "slowly exchanging tissue" compartment, respectively.

In tissues (i.e. bone marrow, liver, lymph nodes, and spleen) of the

reticuloendothelial system (16), the characteristic sinusoidal vasculature, with large inter-endothelial cell pores (fenestrae) and/or no basement membrane (basal lamina), allows much faster exchange of antibody to occur between the vascular and the extravascular spaces. The rapidity of this process allows one to effectively combine, or "lump," the plasma and the reticuloendothelial system (specifically, bone marrow, lymph nodes, and spleen) into a single compartment (which may be nominally referred to as "plasma") with respect to systemically administered antibody. The notable exclusion of the liver from this lumped compartment is based principally on the unique microscopic anatomy of the hepatic vasculature: besides typical endothelial cells, it contains fixed macrophages, or Kupffer cells, which voraciously phagocytose any circulating debris, including damaged, or denatured, protein (16). Together with the large fractional cardiac output to the liver (i.e. ~ 0.25 (16)), this will result in extremely rapid hepatic localization of systemically administered antibody which is in any way damaged (14, 17). Though the proportion of damaged antibody in a radioiodinated antibody preparation can be minimized by insuring that there are only several iodine atoms per antibody molecule (18), for example, a small, but significant, amount of damaged radioiodinated antibody is likely to be present despite scrupulous radiochemical purification. Thus, within the limits of temporal resolution currently achievable, we may assume that at the precise time of intravenous administration of a radio-iodinated antibody preparation (i.e. at "zero" time), the proportion of administered antibody corresponding to undamaged and to damaged antibody are in the "plasma" compartment and in the "liver" compartment, respectively. In addition, the incorporation of an explicit "liver" compartment into a whole-body compartmental model has the following practical advantage: the large size of the liver makes it particularly amenable to absolute quantitation by non-invasive (i.e. scintigraphic) methods applicable to man (19), yielding data which can be used directly in "solving" the model for individual patients.

The compartmental model developed thus far, though somewhat elaborate, is rather conventional in the sense that it is a linear compartmental model (i.e. the exchange rates are constant). However, besides non-specific, and therefore non-saturable, localization of circulating antibody, it interacts specifically with the antigenic binding sites against which it is directed in the antigen-positive tissues. In the most general case, as typified by that of antibody directed against tumor-associated CEA (8-12), the antibody can bind to antigen in target tissue (i.e. tumor), where it is generally present in highest concentration, in antigen-positive normal tissues (i.e. the stomach, small intestine, and large intestine), and in plasma, where it is generally present in lowest concentration. We have not yet incorporated into the model any compartments corresponding to antigenic binding sites. As a consequence of the finite concentration of antigenic binding sites and the resulting saturability thereof, the rates of association of the antigen and antibody and of dissociation of the antigen-antibody complex are not constant but are dependent on the actual concentrations of antigen, of antibody, and of antigen-antibody complex. If "Ag," "Ab," and "AgAb" represent antigen, antibody, and antigen-antibody complex, respectively, then the antigen-antibody interaction can be represented by the following reaction, characteristic of any reversible bimolecular binding reaction (20):



where k_{+1} is the association rate constant (e.g. in $\text{sec}^{-1}\text{M}^{-1}$) and k_{-1} is the dissociation rate constant (in sec^{-1}). Accordingly, the gross, as opposed to net, rates of conversion of Ab to AgAb and of AgAb to Ag and Ab are given by

equations (10) and (11), respectively:

$$\frac{d[Ab]}{dt} = (k_{+1}[Ag])[Ab] \quad (12)$$

$$\frac{d[AgAb]}{dt} = k_{-1}[AgAb] \quad (13).$$

Equations (10) and (11) can be re-arranged to yield equations (12) and (13), giving fractional rates of conversion of Ab to AgAb and of AgAb to Ag and Ab, respectively:

$$\frac{\frac{d[Ab]}{[Ab]}}{dt} = k_{+1}[Ag], \quad (14),$$

$$\frac{\frac{d[AgAb]}{[AgAb]}}{dt} = k_{-1} \quad (15).$$

If one now identifies an "Ab" (i.e. "'free' Ab") compartment and an "AgAb" (i.e. "'bound' Ab") compartment within an antigen-positive tissue, then the exchange rates for "free" Ab-to-"bound" Ab transfer and for "bound" Ab-to-"free" Ab transfer of Ab are given, by definition, by equations (12) and (13), respectively. Because the Ag (i.e. "'free' Ag") concentration is not constant, the former exchange rate is not constant and a non-linearity is thereby introduced. If $[Ag]_0$ is the total Ag concentration in an antigen-positive tissue (e.g. in mol/kg, that is, in M), V_d is the volume of distribution of AgAb in the antigen-positive tissue (in l), and $F(t)$ is the amount of AgAb in the antigen-positive tissue (i.e. the model-derivable content of the "AgAb" compartment) at time t post-administration (in mol), then equation (12) can be reformulated entirely in terms of experimentally or theoretically evaluable quantities to yield a time-varying, but evaluable, expression for this exchange rate:

$$\begin{aligned} \frac{\frac{d[Ab]}{[Ab]}}{dt} &= k_{+1}[Ag] \\ &= k_{+1}([Ag]_0 - [AgAb]) \\ &= k_{+1}([Ag]_0 - \frac{F(t)}{V_d}) \end{aligned} \quad (16).$$

As a first approximation, we can assume that V_d is simply equivalent to the wet mass (in kg) of the antigen-positive tissue. In contrast to equation (14), the reverse exchange rate, that is, the exchange rate for "bound" Ab-to-"free" Ab transfer of Ab is given by equation (13) and is therefore constant. Approximate values of the pertinent parameters for CEA and anti(CEA) antibody, required for the simulation studies described below, are presented in Table 1.

If the values of k_{+1} , k_{-1} , and $[Ag]_0$ do not vary significantly among antigen-positive normal tissues, these, of course, may be combined into a single "antigen-positive normal tissue," resulting in lumped "'free' Ab" and lumped "'bound' Ab" compartments. The forward and reverse exchange rates between the "plasma" compartment and the "'free'" Ab compartment may be assumed to be equal to the forward and reverse exchange rates, respectively, between the "plasma"

Table 1

Compartmental Model-based Computer Simulation of the Time-dependent Tissue Distribution of Systemically Administered ^{131}I -"anti-tumor" Antibody in Tumor-bearing "Reference Man": Values of Pertinent Antibody-Antigen Parameters (8-12)

	Plasma	Ag+ Normal Tissue*	Tumor	
k_{+1} ($\text{hr}^{-1}\text{M}^{-1}$)	2.89×10^{-8}	2.89×10^{-8}		2.89×10^{-8}
k_{-1} (hr^{-1})	0.0289	0.0289		0.0289
K_a (M^{-1})	1×10^{10}	1×10^{10}		1×10^{10}
$[\text{Ag}]_0$ (M)	5×10^{-10}	5×10^{-9}		5×10^{-7}
Tissue mass (gm)	3,000	1,000	100	1,000
Amount of Ag (mol)	1.5×10^{-9}	5×10^{-9}	5×10^{-8}	5×10^{-7}

* For CEA, Ag+ normal tissues are stomach, small intestine, and large intestine.

compartment and the "rapidly exchanging tissue" or "slowly exchanging tissue" compartments as appropriate for the particular tissue or tissues composing the "antigen-positive normal tissue." Tumor, in this respect, may generally be characterized as a "rapidly exchanging tissue" (14, 15).

Because of the prohibitively large size (typically at least twice the molecular weight of the antibody itself) of circulating antigen-antibody complex, we shall assume, for the moment, that it is effectively excluded from the extravascular space of all tissues, except those of the RE system. As is the case for antibody itself, the rapidity of the exchange of antigen-antibody complex between the vascular and the extravascular spaces of tissues of the RE system, due to their porous sinusoidal vasculature, allows one to effectively lump the plasma and the RE system into a single compartment (which may nominally be referred to as "bound antibody in 'plasma'") with respect to circulating antigen-antibody complex.

As plasma-borne radioiodinated antibody and antigen-antibody complex are distributed in the body, they are concurrently catabolized, resulting, ultimately, in the production of inorganic radioiodide. While the precise sites of protein catabolism have apparently not yet been definitively identified, the principal site appears to be the RE system, including bone marrow, liver, lymph nodes, and spleen (21-24). The liver, in particular, is an extremely active and quantitatively important site, with some evidence indicating that protein cata-

bolism may actually occur within the Kupffer cells. In addition, some de-iodination, if not actual catabolism, of radioiodinated proteins occurs in plasma. There is evidence, as well, that the kidney and the small and large intestines may be important sites of protein catabolism. On the basis of the preponderance of evidence, however, we shall identify the "liver" compartment and the "plasma" compartment (i.e. the lumped plasma, lymph node, and spleen compartment) as the sites of catabolism and de-iodination of antibody and antigen-antibody complex. The exchange rates for de-iodination, which we shall assume are uniform among all tissues of the RE system and which we shall further assume are identical for antibody and for antigen-antibody complex, can be approximated as the rate constant for the monoexponential clearance of activity from the liver following systemic administration of radioiodinated antibody (See Figure 9b.). The reverse exchange rates, that is, the exchange rates for re-iodination, are identically zero, mainly because of simple dilution of the liberated radioiodide.

The inorganic radioiodide thus produced must, of course, be incorporated into the compartmental model. Its distribution, metabolism, and excretion can be described entirely by a simplified, linear version of the whole-body compartmental model of Singh et al. (25). Once produced by de-iodination, inorganic radioiodide is "instantaneously" distributed in the volume of distribution of iodide. This appears to be equivalent to the total-body extracellular space, giving rise to an extracellular space compartment for iodide (nominally referred to as "plasma") connected directly to the "liver" compartment and the "free" and "bound" antibody "plasma" compartments. From the "plasma" compartment, iodide enters the "thyroid" compartment. The exchange rate for extracellular space-to-thyroid transfer of iodide, in the absence of radiation damage to and "blocking" (26) of the thyroid, is 0.0074 hr^{-1} (25). However, we must actually use a one hundred-fold lower value of the exchange rate, 0.000074 hr^{-1} , because effective "blocking" reduces thyroid localization of radioiodide to 1% of its "unblocked" value (26). The reverse process (i.e. thyroid-to-extracellular space transfer of iodide) is negligible in the absence of radiation damage to the thyroid, yielding an exchange rate of zero. Iodide, once in the thyroid, is eventually organified and irreversibly secreted into the plasma as protein-bound iodine with an exchange rate of 0.00063 hr^{-1} . Plasma-borne protein-bound iodine (the "protein-bound iodine (PBI)" compartment) undergoes spontaneous re-conversion to inorganic iodide at an exchange rate of 0.03 hr^{-1} . Finally, inorganic iodide in the "plasma" compartment is excreted in the urine at an exchange rate of 0.057 hr^{-1} .

We have implemented our compartmental model using Berman's SAAM ("Simulation, Analysis, and Modeling") computer code (version 27) (5); we have actually used the "conversational," or interactive, form of the code, CONSAAM, which is running on our VAX 11/780 computer facility.

We have simulated the quantitative in vivo behavior of systemically administered radioiodinated "anti-tumor" antibody in tumor-bearing "Reference Man" (3) as a function of what appear to be two critical parameters (27, 28): amount of administered antibody and size of the tumor. The results of this simulation analysis are presented graphically in Figures 3-7. In Figures 3 and 4, the percent administered activity at "equilibrium" (i.e. 100 hr post-administration) as antigen-antibody complex per gram of antigen-positive tissue is plotted, on a log-log graph, as a function of the amount of administered antibody for "Reference Man" bearing 100- and 1,000-gm tumors, respectively. As the amount of administered antibody is increased, the most accessible antigenic sites, those circulating in plasma, are saturated first, with decreasing con-

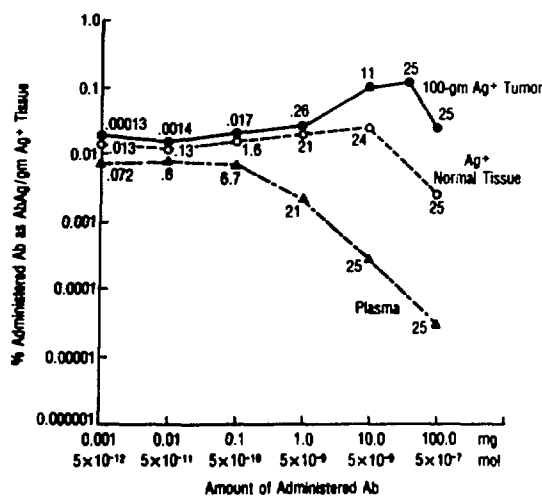


Figure 3. The percent administered activity at "equilibrium" (i.e. 100 hr post-administration) as AgAb per gram of Ag⁺ tissue as a function of the amount of administered Ab for "Reference Man" bearing a 100-gm tumor.

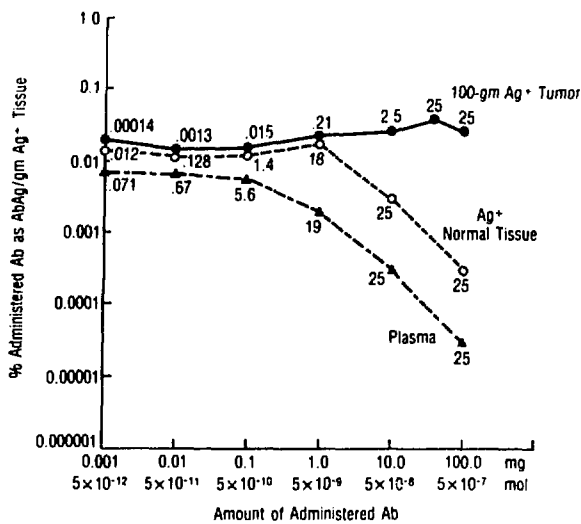


Figure 4. The percent administered activity at "equilibrium" (i.e. 100 hr post-administration) as AgAb per gram of Ag⁺ tissue as a function of the amount of administered Ab for "Reference Man" bearing a 1,000-gm tumor.

centration of percent administered antibody bound to antigen as the amount of administered antibody is increased. At the same time, as an increasing amount of circulating antibody remains unbound to circulating antigen, the concentrations of percent administered antibody bound to antigen in tissues having less accessible binding sites first increase and then decrease as these sites, too, eventually are saturated. Because the concentration of antigen is greatest in tumor, it achieves the highest concentration among antigen-positive tissues of percent administered antibody bound to antigen at its optimum antibody dose. However, the maximum concentration in tumor and in antigen-positive normal tissue is several-fold less in the case of the 1,000-gm tumor than that in the case of the 100-gm tumor. This is presumably due to "mass balancing" of the total available antibody among the total number of antigenic binding sites. Note that at very high antibody doses, when the antigenic sites in all tissues are saturated, the concentration of percent administered antibody bound to antigen decreases in parallel in all antigen-positive tissues in direct proportion to the antibody dose. Note further that "saturation" of antigenic binding sites occurs not at 100%, but at 25%, receptor occupancy (The number next to each data point in Figures 3 and 4 represents the percent receptor occupancy.); that is, the maximum percent of antigenic binding sites which can bind antibody is 25%. At equilibrium, this value is dependent solely on the affinity of binding between the antigen and antibody (expressed as the association equilibrium constant, K_a , for example), which is assumed to be constant among all antigen-positive tissues (See Table 1.).

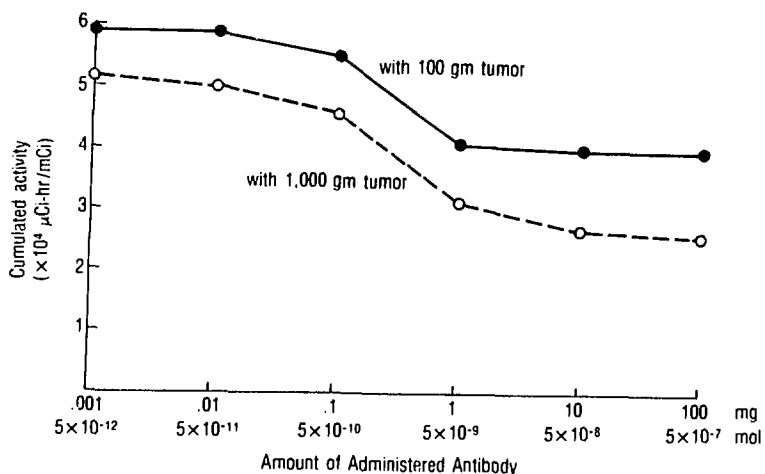


Figure 5. The cumulated activity in blood per unit administered activity of ^{131}I -"anti-tumor" Ab as a function of amount of administered Ab for "Reference Man" bearing a 100- or 1,000-gm tumor.

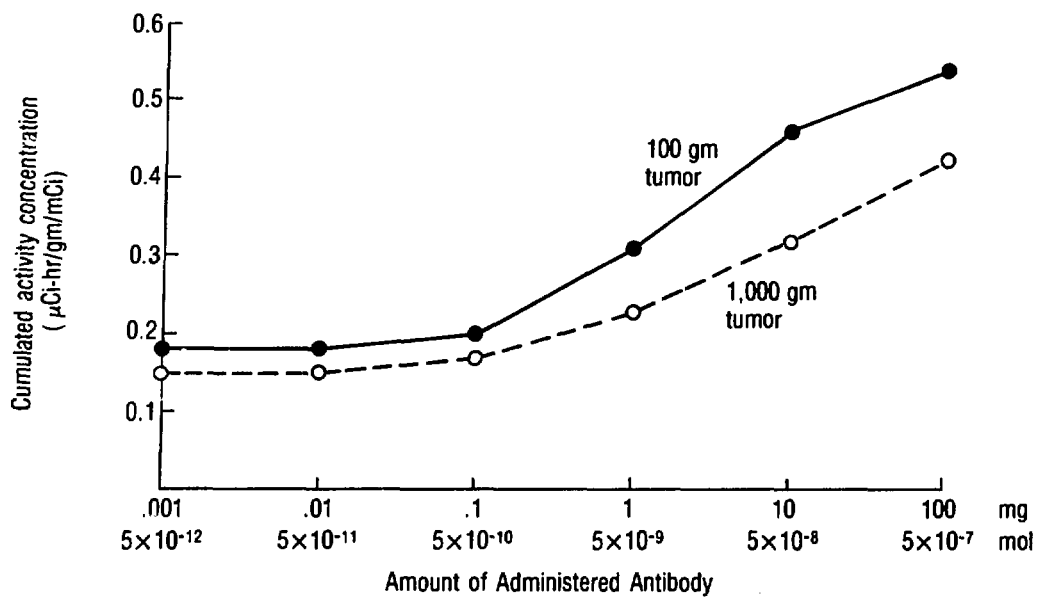


Figure 6. The cumulated activity concentration in tumor per unit administered activity of ^{131}I - "anti-tumor" Ab as a function of amount of administered Ab for "Reference Man" bearing a 100- or 1,000-gm tumor.

In Figures 5, 6, and 7, the cumulated activity or cumulated activity concentration in blood, in tumor, and in "rest of the body" (i.e. the total body, excluding blood and tumor, but including antigen-positive normal tissue), respectively, per unit I131 administered activity are plotted as a function of amount of administered activity for "Reference Man" (3) bearing a 100- or 1,000-gm tumor. The cumulated activity in blood (Figure 5) decreases sigmoidally and the cumulated activity concentration in tumor (Figure 6) and the cumulated activity in the "rest of the body" (Figure 7) appear to increase sigmoidally as a function of amount of administered antibody. In the case of the 1,000-gm tumor, the slight decrease in cumulated activity in the "rest of the body" at antibody doses exceeding 1 mg, or 5×10^{-9} mol, is presumably somehow related to the aforementioned "mass balancing" of total available antibody among the total number of antigenic binding sites. In any case, the data presented indicate that increasingly more favorable cumulated activity distributions, in terms of maximizing radiation absorbed dose to the target tissue (i.e. tumor) and minimizing radiation absorbed dose to non-target (i.e. normal) tissues, is achieved with increasing antibody dose. Note, however, that even at the highest antibody dose, the cumulated activity concentration in blood is greater than that in tumor, suggesting that prohibitive bone marrow morbidity will occur if one attempts to deliver a tumoricidal radiation dose. Thus, the presence of circulating antigen, while not contraindicating "equi-

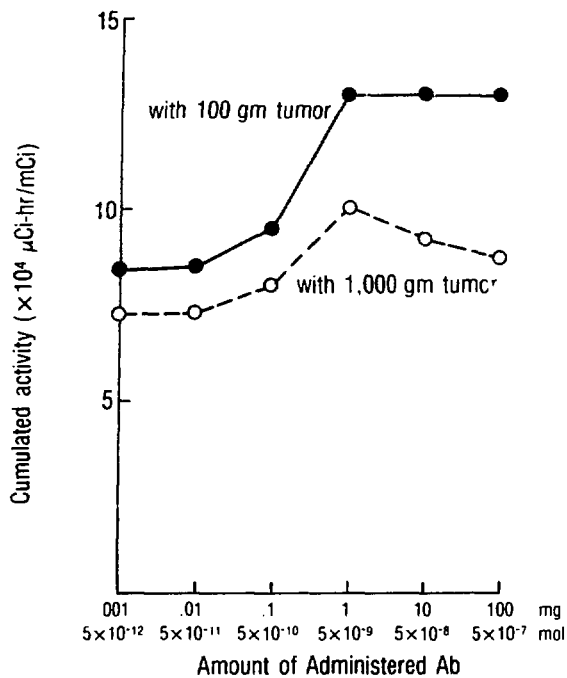


Figure 7. The cumulated activity in "rest of the body" per unit administered activity of ^{131}I - "anti-tumor" Ab as a function of amount of administered Ab for "Reference Man" bearing a 100- or 1,000-gm tumor.

librium" radioimmunoimaging (See Figures 3 and 4.), appears to contraindicate radioimmunotherapy, at least with an isotope as short-lived as I131.

CLINICAL STUDIES

In collaboration with Dr. David Goldenberg and his associates at the Center for Molecular Medicine and Immunology at the University of Medicine and Dentistry in Newark, New Jersey, we have collected serial biodistribution data from patients in Phase I clinical trials of ^{131}I -labeled anti (CEA) monoclonal antibody for treatment of metastatic colon carcinoma (29). In one patient in particular, serial blood and urine activity concentration data were collected to 120 hr post-administration, with liver and thyroid activity data collected at 48 hr and at 96 hr post-administration. Blood and urine activity concentrations were converted to total blood and urine activities (in percent of administered activity) using the calculated total blood volume (3) and the measured total void volume, respectively. Liver and thyroid activities (in percent of administered activity) were estimated by multiplying the fraction of total counts on an anterior whole-body scan (Omega 500, Technicare Corp.) in regions of interest corresponding to the liver and to the thyroid, respective-

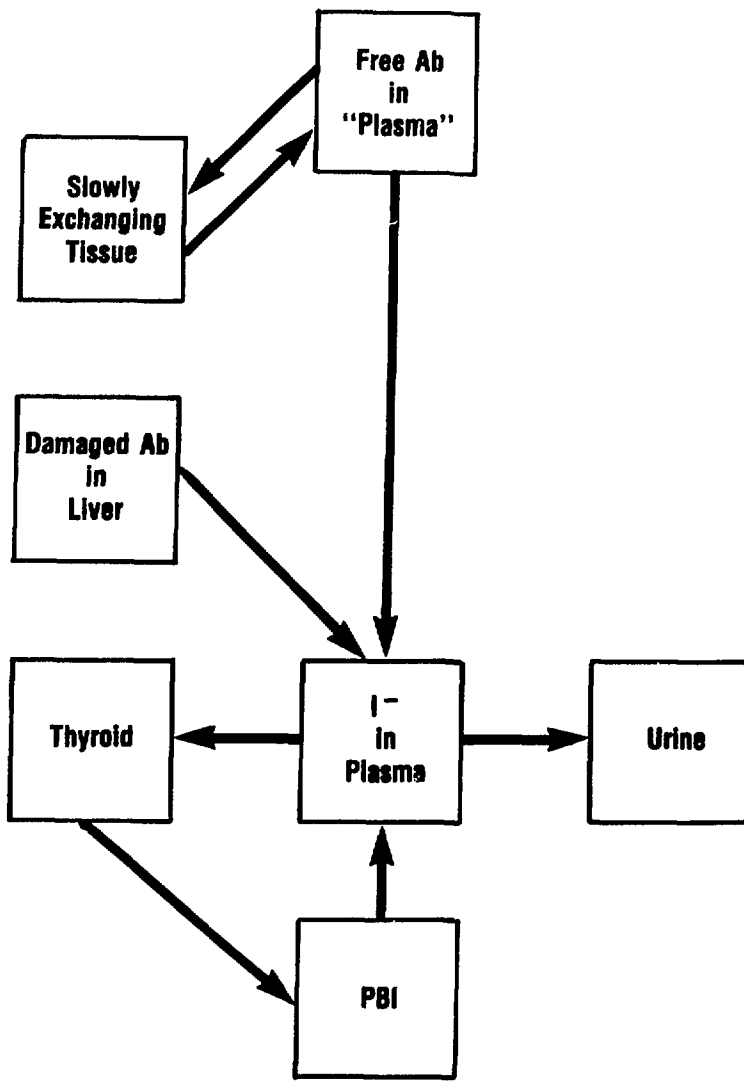
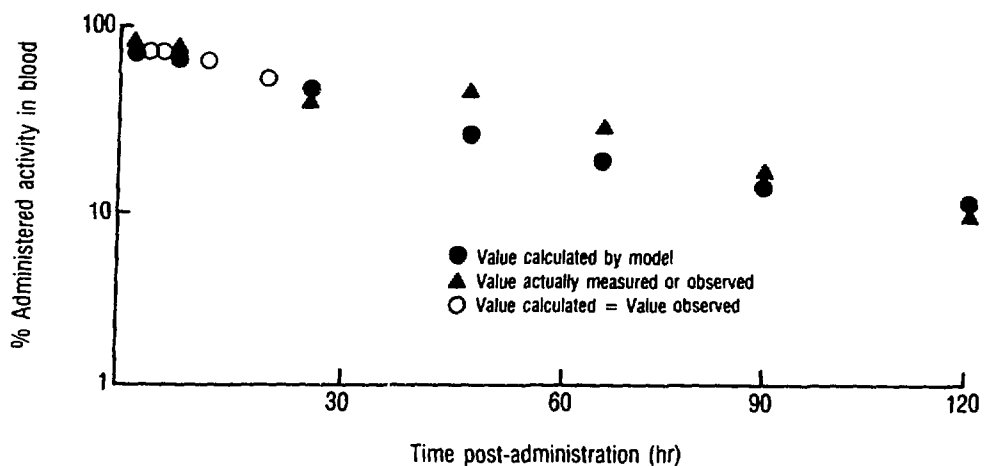
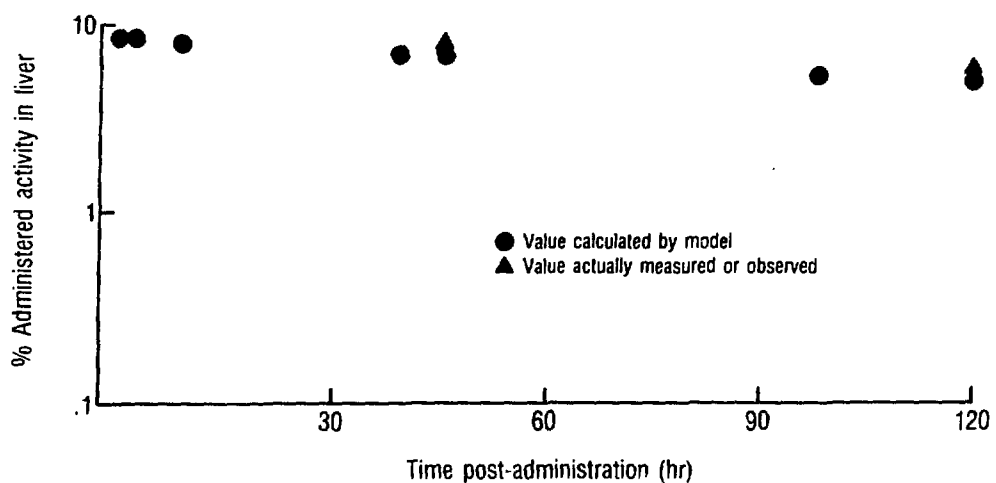


Figure 8. The "optimum" model for ^{131}I -anti (CEA) Ab administered to a patient with metastatic colon carcinoma.

ly, by the percent total-body retention (determined from the cumulative urinary excretion data). Not unexpectedly, the rather limited biodistribution data actually collected were not sufficient to resolve all the compartments of the complete compartmental model (Figure 2) when we attempted to optimize the values of the exchange rates by "fitting" the model to the observed data. Accordingly, the optimum model (Figure 8) for this patient was much simpler, with no antigen-positive tissue compartments and "rapidly exchanging tissue" compartment. In Figure 9 (a-d), the results of this analysis are summarized in graphical form: the measured and the model-derived values of the percent administered activity in blood (Figure 9a), in liver (Figure 9b), in thyroid (Figure 9c), and in urine (Figure 9d) versus time post-administration (in hr) are plotted on semi-log graphs. In general, the agreement between the measured and the model-

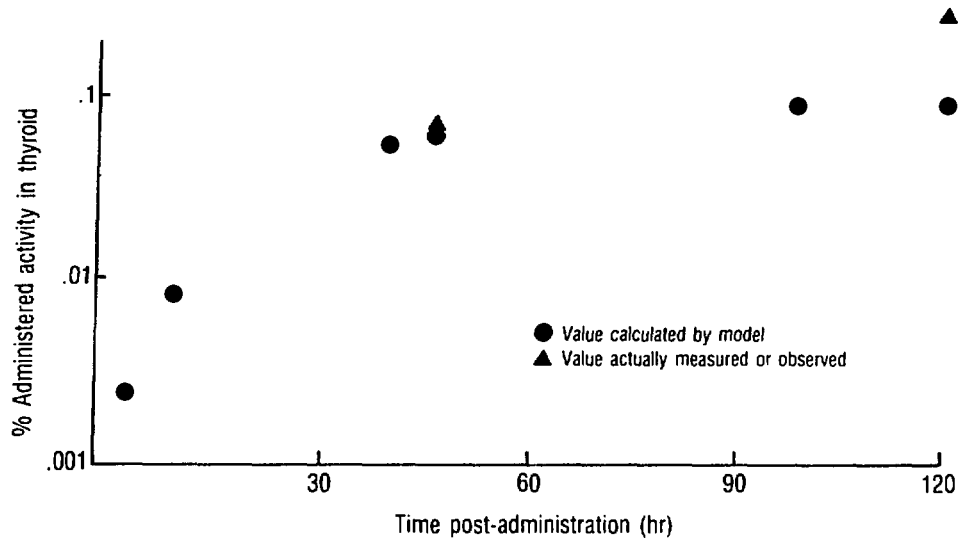


(a)

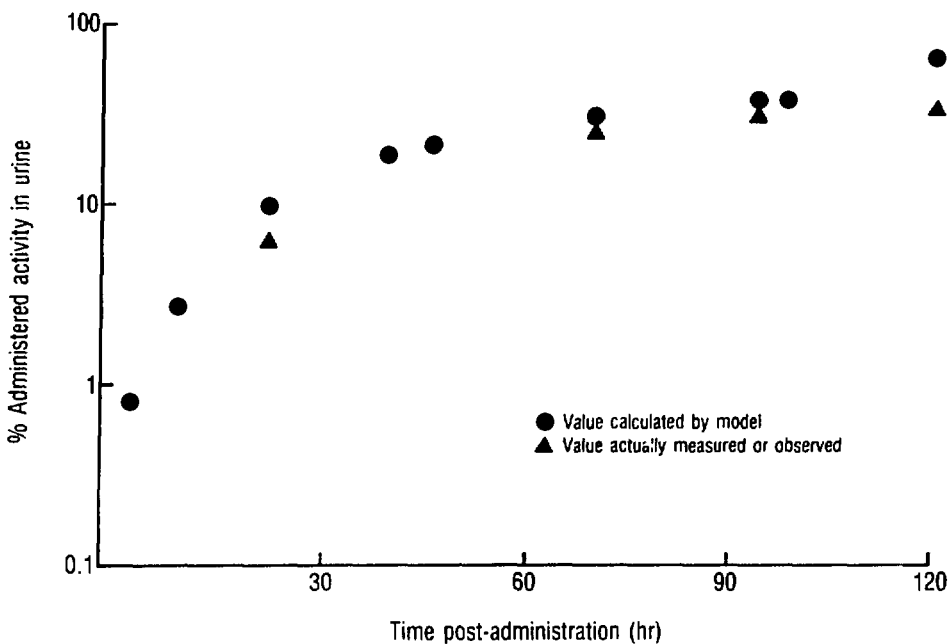


(b)

Figure 9. The measured and the model-derived values of the percent administered activity of ^{131}I -anti(CEA) Ab in blood (a) and in liver (b) versus time post-administration for a patient with metastatic colon carcinoma.



(c)



(d)

Figure 9 (continued). The measured and the model-derived values of the percent administered activity of ^{131}I -anti (CEA) Ab in thyroid (c) and in urine (d) versus time-post-administration for a patient with metastatic colon carcinoma.

derived values is remarkably good. Note, as previously discussed, that the value of the "zero" time intercept, 10%, and of the "slope" (i.e. rate constant), 0.0070 hr^{-1} , of the liver time-activity curve (Figure 9b) may be equated with the percent of damaged, or denatured, antibody in the administered antibody preparation and the rate of hepatic protein de-iodination, respectively.

The resulting optimized compartmental model was then used to directly calculate the cumulated activities (in $\mu\text{Ci}\cdot\text{hr}$) in various source regions, including the bone marrow, the liver, the thyroid, and the total body, by the previously described method of Bigler and Sgouros (7). The cumulated activity in bone marrow was actually calculated by multiplying the cumulated activity concentration in the "plasma" compartment by the total mass of red marrow (1,500 gm) of "Reference Man" (3), the nominal "plasma" compartment actually being a lumped compartment consisting of plasma, bone marrow, lymph nodes, and spleen. The cumulated activities calculated by compartmental analysis and calculated by the familiar method of simply integrating the empirical time-activity curves have been tabulated, together with the associated absorbed doses (calculated using the pertinent formulas in Reference (30)), in Table 2.

Table 2

Cumulated Activities and Associated Absorbed
Doses for a Patient with Metastatic Colon
Carcinoma Receiving 50 mCi ^{131}I -anti(CEA) Ab

Tissue	Based on compartmental analysis		Based on integration of curves	
	λ ($\mu\text{Ci}\cdot\text{hr}$)	\bar{D} (rad)	λ ($\mu\text{Ci}\cdot\text{hr}$)	\bar{D} (rad)
Bone marrow	5.9×10^5	170	6.7×10^5	180
Liver	6.0×10^5	200	-	-
Thyroid	9.3×10^3	220	-	-
Total body	5.8×10^6	58	5.3×10^6	52

SUMMARY and CONCLUSIONS

A reasonably realistic, but highly tentative, generalized whole-body model for systemically administered radioiodinated "anti-tumor" antibody has been formulated. This model incorporates the saturable, and therefore non-linear, interaction between antigen and antibody in plasma, in antigen-positive normal tissue, and in tumor. In addition, it incorporates the catabolism of the antibody and the circulating antigen-antibody complex and the subsequent distribution, metabolism, and excretion of the inorganic radioiodide thus produced. Note that this model also incorporates explicitly microscopic source regions (i.e. the extracellular space and the cell surface), which are completely unresolvable by any imaging modality, but whose cumulated activities are essential for microdosimetric calculations.

In computer-executed simulation studies, we have determined the optimum antibody dose, in terms of maximizing the "equilibrium" antibody concentration in tumor relative to that in plasma and in antigen-positive normal tissue, for different size tumors. However, in terms of maximizing the cumulated activity concentration in tumor relative to that in other tissues, it appears that the larger the antibody dose, the larger the absolute and relative cumulated activity concentration in tumor. Nevertheless, the presence of circulating antigen, while not contraindicating "equilibrium" radioimmunoimaging, contraindicates radioimmunotherapy, at least with an isotope as short-lived as I^{131} , because the cumulated activity in blood, even at the highest antibody dose, exceeds that in tumor.

Using a simplified, linear version of our whole-body compartmental model, we have analyzed clinical biodistribution data for I^{131} -anti(CEA) antibody. The agreement between the measured and the model-derived values of percent administered activity in blood, in liver, in thyroid, and in urine at various times post-administration are in general remarkably good. Finally, using the compartmental model thus optimized, we have developed and applied a method for calculating cumulated activities (in μ Ci-hr) directly from a model; the cumulated activities calculated by this method and by simply integrating the empirical time-activity curves are comparable.

ACKNOWLEDGEMENTS

This work was supported by National Cancer Institute contract N01-CM-37565.

REFERENCES

1. Loevinger, R. and M. Berman. A schema for absorbed dose calculations for biologically distributed radionuclides. MIRD Pamphlet No. 1, J. Nucl. Med. 9, Suppl. No. 1, 1968.
2. Snyder, W.S., M.R. Ford, G.G. Warner, and S.B. Watson. "S," absorbed dose per unit cumulated activity for selected radionuclides and organs. MIRD Pamphlet No. 11, Society of Nuclear Medicine, New York, 1975.
3. International Commission on Radiological Protection. Report of the Task Group on Reference Man, ICRP Publication 23, Pergamon Press, New York, 1975.
4. Shipley, R.A. and R.E. Clark. Tracer Methods for In Vivo Kinetics, Academic Press, New York, 1972.
5. Berman, M., E. Shahn, and M.F. Weiss. The routine fitting of kinetic data to models - A mathematical formalism for digital computers. Biophys. J. 2, 275-287, 1962.
6. Berman, M., M.F. Weiss, and E. Shahn. Some formal approaches to the analysis of kinetic data in terms of linear compartmental systems. Biophys. J. 2, 289-298, 1962.

7. Bigler, R.E. and G. Sgouros. Radiation dosimetry for zinc-63 for oral, IV, and jejunal tube administration. *J. Nucl. Med.* 24, P40, 1984.
8. Gold, P. and S.O. Freedman. Demonstration of tumor-specific antigens in human colon carcinomata by immunological tolerance and absorption techniques. *J. Exp. Med.* 121, 439-462, 1965.
9. Gold, P. and S.O. Freedman. Specific carcinoembryonic antigens of the human digestive tract. *J. Exp. Med.* 122, 467-481, 1965.
10. LoGerfo, P., F.P. Herter, J. Braun, and H.J. Hansen. Tumor associated antigen with pulmonary neoplasms. *Ann. Surg.* 175, 495-500, 1968.
11. Pusztaszeri, G. and J.P. Mach. Carcinoembryonic antigen (CEA) in non digestive cancerous and normal tissues. *Immunochemistry* 10, 197-204, 1973.
12. Zamchek, N. The present status of CEA in diagnosis, prognosis, and evaluation of therapy. *Cancer* 36, 2460-2468, 1975.
13. Winchell, H.S. Mechanisms for localization of radiopharmaceuticals in neoplasms. *Semin. Nucl. Med.* 6, 371-378, 1976.
14. Dewey, W.C. Vascular-extravascular exchange of I¹³¹ plasma proteins in the rat. *Am. J. Physiol.* 197, 423-431, 1959.
15. O'Connor, S.W. and W.F. Bale. Accessibility of circulating immunoglobulin G to the extravascular compartment of solid rat tumors. *Cancer Res.* 44, 3719-3723, 1984.
16. Bloom, W. and D.W. Fawcett. *A Textbook of Histology*. 10th edition, W.B. Saunders Company, Philadelphia, 1975.
17. McFarlane, A.S. *Progress in Biophysics*. volume 7, p 115, Pergamon Press, New York, 1957.
18. Eckelman, W.C., C.H. Paik, and R.C. Reba. Radiolabeling of antibodies. *Cancer Res.* 40, 3036-3042, 1980.
19. Myers, M.J., J.P. Lavender, J.B. deOliveira, and A. Maseri. A simplified method of quantitating organ uptake using a gamma camera. *Br. J. Radiol.* 54, 1062-1067, 1981.
20. Berzofsky, J.A. and I.J. Berkower. Antigen-antibody interaction. in *Fundamental Immunology*. Paul, W.E. (Editor), pp 595-644, Raven Press, New York, 1984.
21. Berson, S.A., R.S. Yalow, S.S. Schreiber, and J. Post. Tracer experiments with I¹³¹ labeled serum albumen: Distribution and degradation studies. *J. Clin. Endocrinol. Metab.* 14, 746-767, 1954.
22. Andersen, S.B. *Metabolism of Human Gamma Globulin*. F.A. Davis Company, Philadelphia, 1964.
23. Birke, G., R. Norberg, and L.O. Plantin (Editors). *Physiology and Pathophysiology of Plasma Protein Metabolism*. Pergamon Press, New York, 1969.

24. Rothschild, M.A. and T. Waldman (Editors). *Plasma Protein Metabolism: Regulation of Synthesis, Distribution, and Degradation*. Academic Press, New York, 1970.
25. Singh, B., S.M. Sharma, M.C. Patel, K.V. Raghavencran, and M. Berman. Kinetics of large therapy doses of ^{131}I in patients with thyroid cancer. *J. Nucl. Med.* 15, 674-678, 1974.
26. Becker, D.V. Physiological basis for the use of potassium iodide as thyroid blocking agent: Logistic issues in its distribution. *Bull. N.Y. Acad. Med.* 59, 1003-1008, 1983.
27. Carrasquillo, J.A., K.A. Krohn, P. Beaumier, R.W. McGuffin, J.P. Brown, K. E. Hellstrom, I. Hellstrom, and S.M. Larson. Diagnosis of and therapy for solid tumors with radiolabeled antibodies and immune fragments. *Cancer Treat. Rep.* 68, 317-328, 1984.
28. Larson, S.M. Radiolabeled monoclonal anti-tumor antibodies in diagnosis and therapy. *J. Nucl. Med.* 26, 538-545, 1985.
29. Goldenberg, D.M., F. DeLand, E. Kim, S. Bennett, F.J. Primus, J.R. van Nagel, N. Estes, P. DeSimone, and P. Rayburn. Use of radiolabeled antibodies to carcinoembryonic antigen for the detection and localization of diverse cancers by external photoscanning. *N. Engl. J. Med.* 298, 1384-1388, 1978.
30. Bigler, R.E. and G. Sgouros. Biological Analysis and Dosimetry for ^{150}O -labeled O_2 , CO_2 , and CO gases administered continuously by inhalation. *J. Nucl. Med.* 24, 431-437, 1983.

DISCUSSION

BRILL: Pat, do I understand correctly that if one can make measurements, one can establish principles by simulating a complicated model for the interactions you described and predict the kinds of dose distributions encountered? You have a heterogeneous tumor distribution in different extracellular fluid beds with different perfusions, etc. The complexity of calling tumor, "tumor" instead of the multiple sites in which tumor is located, poses real problems in terms of dosimetry for individual patients. It seems to me that what you've said is, if you can make the measurements that Mel Myers was anguish about, you can use models of varying complexities - much more complex than you were talking about today - to simulate and model and compute the data. Is that correct?

ZANZONICO: That is correct, and I think the advantage of using a modeling approach is that one can use it basically to constrain your data to conform to known biological information. For example, studies of the interaction between antibody and antigens, both *in vivo* and *in vitro* have resulted in a tremendous data base for those types of interactions; therefore, we have certain information concerning those types of interactions. That information base can be superimposed on data that we can collect from individual patients. Even though relatively large uncertainties may exist in that data, if we can constrain that data to be consistent with *a priori* biological information, I think we can make the data much more useful and the results derived from that data more accurate. This is not a panacea - you know - garbage in is garbage

out; but the point is we are actually introducing additional a priori data when using a model. Anytime you have more data, assuming it is reasonably reliable, you expect better results.

KWOK: Are there any significant differences between your whole body compartmental model and that assumed in the SAAM program?

ZANZONICO: The SAAM program is basically a calculational device. It does not propose any model for any tracer; it just provides the mathematics to solve for the model you may propose. SAAM does not have a specific model associated with it. It is simply the calculator that does the number-crunching for you, but you have to introduce to it the desired model.

HARRIS: I have always been bothered by compartmental analyses that use single-valued rate constants for exchange between compartments; these implicitly define linear or exponential transfer. Experimental data frequently suggest time-dependent or concentration-dependent rate coefficients. Would you comment on how this concern is handled in your modeling?

ZANZONICO: The model I propose, and I think it is somewhat unique in this respect, does include time-dependent rate constants. The particular time-dependent rate constants it includes are the specific antibody-antigen interactions, because the actual rate of association of antibody and antigen depends on the instantaneous concentration of free antigen, not the total concentration which is a constant, but the instantaneous concentration of free antigen. As antibody binds to antigen and as the concentration of free antigen decreases, the actual association rate will decrease and that has been included in this model for each of the three antigen-positive tissues. In other cases, for example in the model of Singh which may be adaptable to the case of antitumor antibodies, a term for incorporation of iodine into the thyroid is included which takes into account radiation damage to the thyroid and accelerated release of iodide from the thyroid. That is a nonlinear term, and any interaction which warrants a nonlinear term of that nature can be incorporated into this model. Up to now, the only such interaction that has warranted that sort of nonlinear term has been the interaction between antibody and antigen. As more data become available, if additional interactions warrant nonlinearities, they can be incorporated, and again that demonstrates the flexibility of a modeling approach.

SASTRY: In your model, you have used some rate constants. Would you expect these to be the same for in vivo situations under different pathological conditions?

ZANZONICO: Each of those arrows in the diagrams depicting the model corresponds to a number which is an exchange rate. The actual values were collected from a variety of sources in the literature, and Frankly included exchange rates in animal systems. The idea is that this is a first guess. What SAAM does in calculating exchange rates, in a real case, is begin with those values as an initial guess, and by iterative approach adjust the value of the individual exchange rates to give the best fit between observed and calculated values. All you really need to do is start out with a good guess. It can be argued that even if you are within a order of magnitude that is a good enough guess. Presumably, when you introduce data, the model will converge on the actual value, so we are not depending blindly on any particular sets of values of exchange rates. Those are simply our initial guesses. You have to start somewhere and you do this by introducing some reliable or reasonable initial guesses. But, you must also introduce data for each individual case, and then the model will do the calculation for each case. For example, one may know from the literature, a mean value of the rate of disappearance of iodine from the thyroid. Presumably, you could use that value

to calculate cumulated activities for a particular patient. It would be best to start off with that as a first guess and use some sort of iterative program for fitting your observed data for that patient about that initial guess to give you the exact value for that patient. A similar thing is done with compartmental modeling. You start off with an initial guess and then by putting in data you converge to the "actual" true value for that particular patient. So we will need biodistribution data and the more the better for each individual patient.

DOSIMETRIC MEASUREMENTS AND RADIOPHYSICAL CONSEQUENCES OF
RADIOIMMUNOTHERAPY IN TUMOR BEARING MICE

B.W. Wessels, M.H. Griffith,
E.W. Bradley and B. Skibinski,
The George Washington University Medical Center
Washington, D.C. 20037

ABSTRACT

With the development of the hybridoma technology, the production of highly specific tumor associated monoclonal antibodies has provided new optimism for the adjuvant delivery of therapeutic radiation doses via radioimmunotherapy. This effort has been for the most part led by members of the nuclear medicine and immunology scientific communities. These investigators have generated biodistribution data which is usually expressed in terms of percent injected dose (activity) /gram, localization indices and antibody affinity constants. These terms are not readily interpreted into a radiation therapy physics or radiobiological framework in which absorbed dose, dose rate, tumor growth delay and control are used to characterize dose response.

We have used a modified form of the well-established TL dosimetry technology to measure the dose resulting from radioimmunotherapy experiments in tumor bearing mice. Our laboratory has designed and tested a miniature CaSO₄:Dy TLD which fits conveniently inside a 20 gauge needle for the direct implantation of the dosimeter in an animal model undergoing radiolabeled antibody therapy. Direct measurement of absorbed dose from beta and gamma radiation in the animals may be obtained upon removal of the dosimeter at animal sacrifice or by surgery. This absorbed dose data may then be related to antibody affinity and localization data obtained by serial biodistribution studies. Using p96.5 melanoma antibody with a Brown Tumor Model in athymic mice, localization indices measured in the range of 2 to 4 and scored 4 to 7 days post antibody injection, yielded a tumor dose/whole body dose ratio of 1.10 ± 0.08 (no enhancement). The dose to liver showed marker time-dependent enhancement relative to the whole body, however. An outline of suggested control radiobiological experiments to be performed in conjunction with radioimmunotherapy experiments has been included in order to provide comparative dose response data.

I. INTRODUCTION

The administered dose for radioimmunotherapy has been commonly quoted in radionuclide activity units ($\mu\text{Ci}/\text{kg}$ body weight) and biodistribution results have been tabulated in units of percent injected dose per gram. No precise correlation exists for estimating these data in terms of absorbed radiation dose delivered to the tumor or critical normal organs. MIRD dosimetry for these animal studies does not accurately represent the absorbed dose deposited in a tumor or other organs due to substantial uncertainties in the actual geometric organ size, spatial distribution of heterogeneous antibody uptake in an organ, or the relative proximity of adjacent organs. Hence, an accurate correlation to radiobiological tumor dose response does not currently exist for radioimmunotherapy studies in tumor bearing animals.

A method has been developed (1) for the direct verification of absorbed radiation dose in animals through the use of teflon-imbedded, $\text{CaSO}_4:\text{Dy}$ thermoluminescent dosimeters (TLD) which have been modified to fit inside a 20 gauge needle. These sterilized mini-TLD ($0.2 \times 0.4 \times 5 \text{ mm}$) may be directly implanted into a variety of animal organs in which dosimetric information is desired. The dosimeters may be recovered upon sacrifice of the animal or by surgical removal. These dosimeters have been cross-calibrated under 4 MV x-ray radiation with a dosimeter whose calibration is traceable to NBS radiation standards. The TLD dosimeters have been shown to be linear in response ($\pm 5\%$) from 10 to 2000 cGy for I-131, Re-186, P-32 and Y-90 radionuclides. Calibration of these TLD in a thin-walled tumor phantom and relative cross calibrations to 4MV x-ray irradiation has been previously discussed (2).

II. METHODS AND MATERIALS

a. Labeling Studies and Antibody Purification

Radiolabeling experiments with I-131 or I-125 used with chloramine-T method in which typically 50-500 μg of antibody in 100 μl was labeled with 10 mM of chloramine-T for five minutes at 0°C. After the reaction was extinguished with a molar excess of sodium dithionite, purification of the fresh preparation included G-75 Sephadex column chromatography (0.6 x 20 cm) (Figure 1) to rid the antibody of free iodine. The labeled fraction was rechromatographed on a Sepharose 6B column (2 x 100 cm) (Figure 2) to assess the amount of unwanted colloid formation or label-free iodine.

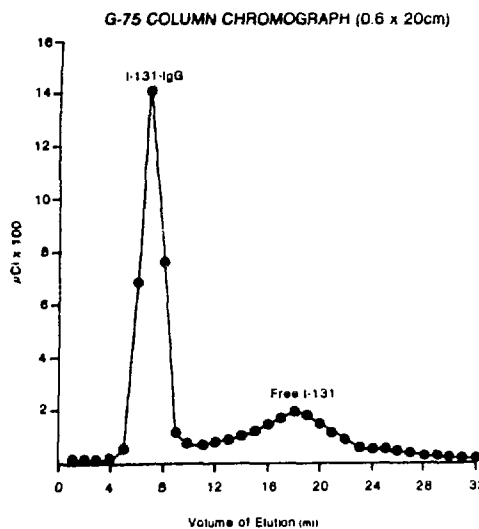


Figure 1 - Activity vs Volume of elution profile showing an 85% radiochemical yield of purified I-131-IgG (Fractions 5-9) and free iodide peak (Fractions 15-23)

Both affinity column chromatography with an Affi-gel 15 protein A column (Figure 3) and *in vitro* binding affinity studies (Figure 4) were performed to determine the radiolabeled antibody immunoreactivity (20 - 30%). Similar studies were performed as acceptance criteria for all radiolabeled antibody used in these studies and produced either internal or external to our laboratory.

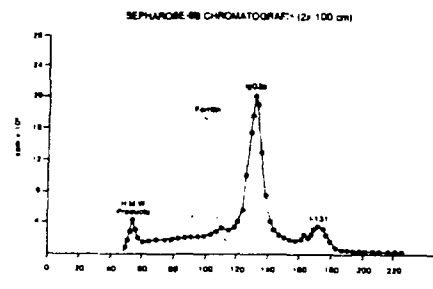


Figure 2 - Activity vs. Volume of elution profile showing size exclusion of high molecular weight colloid (Fractions 48-58) purified IgGa - I-131 (Fractions 120-140) and free iodide (Fractions 164-182). Ferritin was used as molecular weight marker (440 kd).

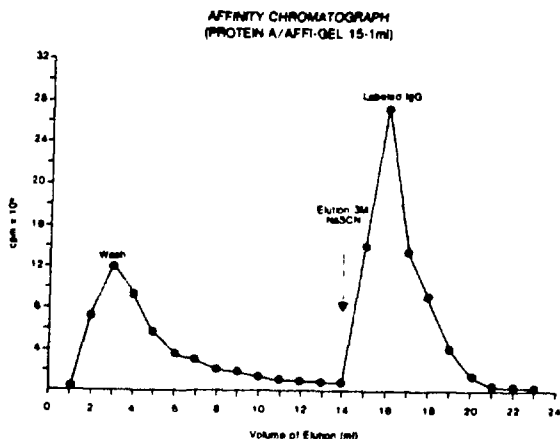


Figure 3 - Activity vs Volume elution profile. Column is loaded with purified Sephadex column fraction of labeled IgG washed with 0.2% PBS (Volumes 1-14), and eluted with 3M NaScn (Volumes 15-23). Final labeled preparation includes dialysis against 0.2% PBS to remove salt (NaScn).

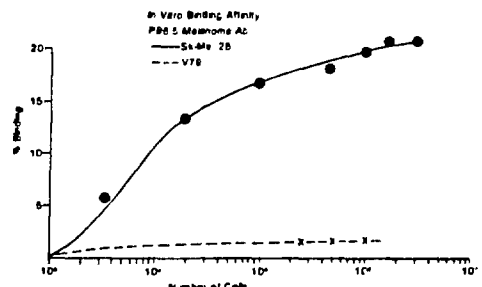


Figure 4 - Percent cell binding vs number of cells for *in vitro* binding affinity test. Black closed circles indicate a 20% binding affinity for SK-Mel-28 target cells at saturation and 2% non-specific uptake in the control cell line (V79) (Shown as X).

b. In Vivo Biodistribution Measurements

Immunodeficient athymic nude mice (BALB/c; male; 5-6 weeks old) were used in all experiments to host either Brown or M21 melanoma human xenografts. Both lines were obtained as minced frozen tumor samples from Hybritech, Inc.. At Hybritech, these tumors were kept as both frozen samples and as a transplant in mouse colony. These tumor lines originate from human melanoma explants received by Giovanella of Houston, Texas in 1982 and are maintained in tissue culture.

In our laboratory, the tumor colony was maintained by injecting 0.1 - 0.2 ml of minced tumor fragments (5×10^6 cells) subcutaneously into either hind flank of the athymic mice four to seven days before the tail vein injection of the radiolabeled antibody. Typically, 50 - 500 μ Ci of 100-300 μ l of I-131 labeled p96.5 or ZME-018 antibody to melanoma was injected with 1 mg of unlabeled human serum albumin (HSA) as carrier into tumor bearing athymic mice. Mice were serially sacrificed in four to six fold redundancy per data point, and biodistribution of radiolabeled antibody was assessed on a per organ basis for time ranging from 1 to 239 hours at regular 12-24 hour intervals (Figures 5 and 6).

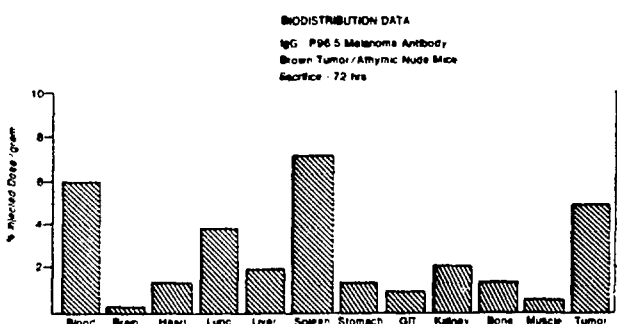


Figure 5 - Percent injected dose/gm vs organ site containing radio-labeled antibody and associated activity. Sacrifice time is 72 hrs.

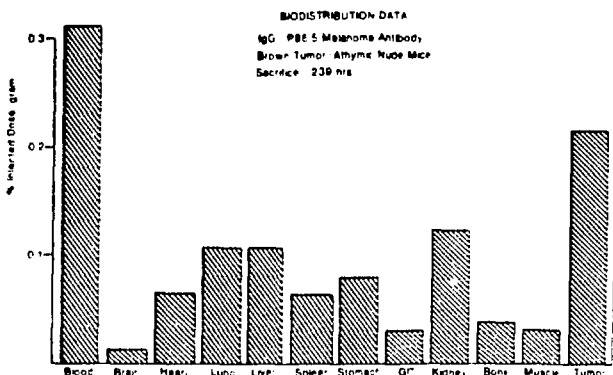


Figure 6 - Percent injected dose/gm vs organ site containing radio-labeled antibody and associated activity. Sacrifice time is 239 hrs.

In addition, dose calibration measurements of the whole animal were taken and compared to the sum of the activity measured in the biodistribution experiments (Figure 7). This data showed reasonable agreement for the clearance of whole I-131 labeled IgG from tumor bearing animals as assessed by these two methods.

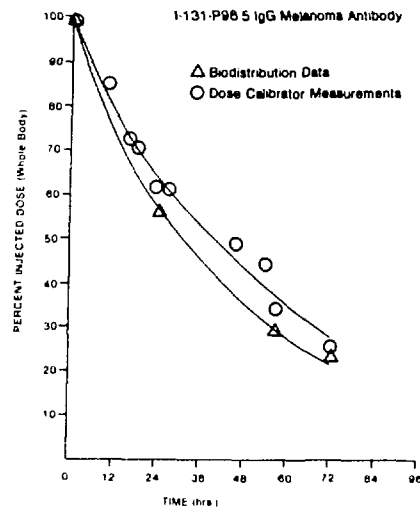


Figure 7 - Comparison of dose calibrator measurements of mouse total body activity vs time with serial, summated biodistribution data (mouse total body) vs time for I-131-IgG.

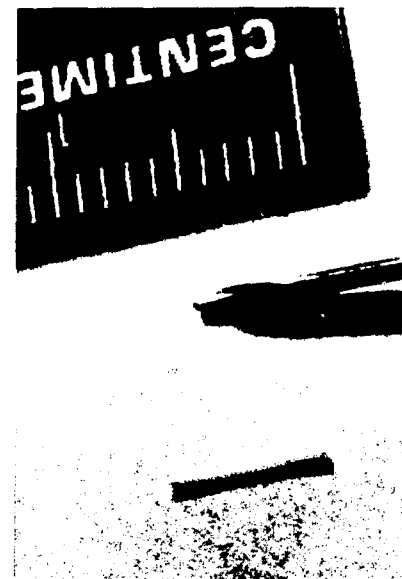


Figure 8 - Tip of 20 gauge needle with miniature TL dosimeter in place for implantation procedure. A second dosimeter is shown below overall length comparison (5mm).

c. TLD Radioimmunotherapy Measurements in Mice

An important endpoint for the procedure of accurately sizing and calibrating the mini-TL dosimeters is to implant the dosimeters *in vivo* such that absorbed dose measurements may be obtained for animals undergoing radioimmunotherapy. After sterilization through autoclaving at 250°C for one hour or soaking ten minutes in 90% methanol, TLD may be inserted into a 20 gauge needle for the subsequent implantation procedure (Figure 8).

A sterilized wire push rod is fitted in behind the TLD from Luer-Lok end to indicate its relative position in the needle. The wire stylus is used as push rod to insert the TLD after the needle is in place in the appropriate organ. The needle and push rod are then withdrawn leaving the TLD imbedded in tissue. Microtome tissue sections of implanted areas indicate that a minimal amount of inflammatory reaction is noted. The TLD appears to be completely inert to its surrounding environment as a result of its teflon support matrix and encapsulation. No degradation in dose is observed with external irradiated control TLD implanted in animals for a week or more.

Using the Brown tumor bearing mouse model, eight anatomical sites are routinely implanted a) subcutaneously in the left hind flank; b) two in the tumor; c) subcutaneously in the left shoulder; d) subcutaneously in the right shoulder; e) intraperitoneal GI; f) liver; g) subcutaneously 1 cm above tumor and; h) subcutaneously 1 cm toward midline from the tumor. After time periods ranging from 12-240 hours, the mice were sacrificed and the dosimeters carefully recovered noting their exact anatomical location. The recovered dosimeters are then washed in Radiac Wash (neutrally soapy water at room temperature) to remove surface contamination. The TLD is then counted in a NaI well counter over the major energy peak or beta bremsstrahlung spectrum (50 KeV - 200 KeV) to detect residual activity as a health physics survey. All TLDs are washed until the detected activity is less than twice background. The TLDs are heated and counted for light output by the TLD reader in a similar manner as described in performance of the phantom work. No unusual browning or discoloration of the TLD was noted in most of the dosimeters after readout if care was taken to remove all extraneous tissue or liquid matter. Dosimeters that had any degree of browning were excluded from the study.

III. RESULTS

a. TLD Organ Dose Measurements

The measurement of absorbed dose to individual organs in tumor bearing athymic mice receiving radioimmunotherapy dose of radiolabeled antibody was performed using I-131 - p96.5 melanoma antibody. Typical results are shown in Tables 1 and 2. TLD measurements of absorbed dose for dosimeters located in the left and right shoulder regions, non-tumor bearing hind flank and GI show reasonable agreement with MIRD calculations assuming uniform distribution of activity throughout the body for a cylindrical geometry with dimensions approximately those of a 22 g mouse. Regions of increased activity uptake such as the liver and the tumor show corresponding enhancement of absorbed dose for these regions. This variation of dose to a target organ was calculated through the use of a factor which is defined in the following manner:

$$(1) \quad \beta = \frac{D_{\text{organ}}}{\bar{D}_{\text{ext}}}$$

$$\text{where } \bar{D}_{\text{ext}} = \frac{(D_{\text{rt.shoulder}} + D_{\text{lt.shoulder}} + D_{\text{lt.flank}} + D_{\text{1 cm above tumor}})}{4}$$

and D_T = TLD measured absorbed dose in organ (tumor)

By this method, a uniform average "external" or "subcutaneous" dose may be defined by these four dosimeters and mathematically compared to the organs of interest. The ratio of organ (tumor) to D_{ext} shows this variation from the average dose measured by the dosimeters placed at four different regions of uniform uptake in the animal (Equation 1). Two confirming experiments were performed in normal mice to verify the TLD sensitivity to change in a) total activity injected; and b) integrated wash-out curves between two types of antibody fragments.

Table 1

TL DOSIMETER DATA			
TLD Number	Location	Measured Dose (cGy)	ϵ
1	Rt. Hind Flank	63	0.63
2	Lt. Hind Flank (Tumor)	130	1.29
3	Lt. Shoulder	106	1.08
4	Lower GI Tract	115	1.15
5	Liver	144	1.43
6	Control	0.25	0.0029

$$\bar{D}_{\text{Ext}} = 100.3 \text{ cGy}$$

$$\epsilon = \frac{\text{Organ Dose}}{\bar{D}_{\text{Ext}}}$$

Table 2

TL MICRODOSIMETER DATA			
TLD Number	Location	Measured Dose (cGy)	ϵ
1	Rt. Hind Flank	7.3	0.91
2	Lt. Hind Flank (Tumor)	6.8	0.85
3	Lt. Shoulder	8.7	1.09
4	Lower GI Tract	7.2	0.89
5	Upper GI Tract	5.8	0.73
6	Upper GI Tract	5.3	0.67
7	Control	0.666	0.065

$$\bar{D}_{\text{Ext}} = 6.0 \text{ cGy}$$

$$\epsilon = \frac{\text{Organ Dose}}{\bar{D}_{\text{Ext}}}$$

b. Dosimetry for Linear Increases in Activity in Normal Mice

First, in order to demonstrate TLD response to changes in injected activity of radiolabeled monoclonal antibody, an experiment was designed in which 10 μCi and 400 μCi of p96.5 IgG was administered through the tail vein into two separate groups of normal mice. The total-body activity was monitored by corrected dose calibrator measurements of the mice vs time up to 72 hours. In each group, 6 standard mini-TLD were injected into the animal at six different sites within one hour after antibody injection. A mathematical ratio was derived by integrating the area under the time-activity curve for the 400 μCi group (cumulated activity) and dividing the integrated area under the 10 μCi time activity curve as shown in Equation 2a.

$$(2a) \text{Dose Ratio} = \frac{\text{IgG Time Activity Integration (400 } \mu \text{Ci})}{\text{IgG Time Activity Integration (10 } \mu \text{Ci})}$$

$$(2b) = \frac{\text{TLD Measured Average Dose (400 } \mu \text{Ci})}{\text{TLD Measured Average Dose (10 } \mu \text{Ci})}$$

If the IgG time activity curve for the normal mice was similar for both 10 μCi and 400 μCi injections, the resultant cumulated activity ratio (CAR) should be 40 to 1 (See Figure 9).

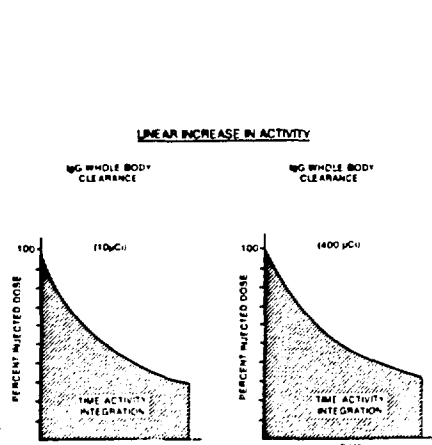


Figure 9 - Comparison of two different activities for the clearance of labeled IgG in normal mice.

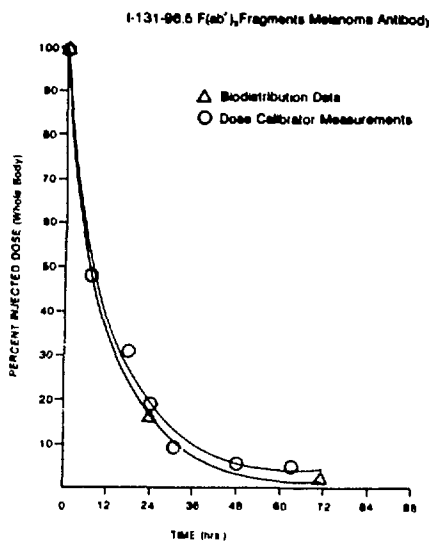


Figure 10 - Comparison of dose calibrator measurements of mouse total body vs time with serial, summated biodistribution data (mouse total body) vs time for I-131- F(ab')₂.

The TLD readings in these animals should reflect a similar result, since the measured dose is in proportion to the cumulated activity for the two groups. TLD measurement ratio was found to $40 \pm 8\%$ for absorbed doses measured in the $400 \mu\text{Ci}$ injected animals compared with the $10 \mu\text{Ci}$ injected animals (Equation 2b).

c. Dosimetry Comparison of IgG and F(ab')₂ Clearance in Normal Mice

A similar experiment was performed in normal mice to compare the absorbed dose ratio measured by TLD for mice receiving the same activity but different antibody fragments (IgG and F(ab')₂ p96.5 melanoma antibody). F(ab')₂ fragments clear faster than whole IgG (See Figure 10).

$$(3) \quad \text{Dose Ratio} = \frac{\text{IgG Time Activity Integration}}{\text{F(ab')}_2 \text{ Time Activity Integration}} \\ = 3.70 \pm 0.4$$

Again, a ratio of the integrated time activity curves for IgG (idealized in Figure 11) and F(ab')₂ (idealized in Figure 12) was computed at 3.7 ± 0.4 (Equation 3) and compared to the corresponding ratio of TLD measured integrated dose (Equation 4).

$$(4) \quad \text{Dose Ratio} = \frac{\text{IgG TLD Whole Body Average}}{\text{F(ab')}_2 \text{ TLD Whole Body Average}} \\ = 4.21 \pm 0.4$$

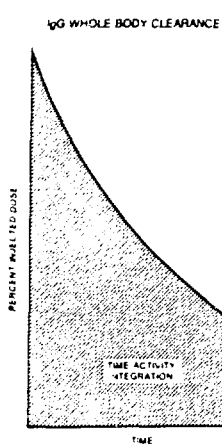


Figure 11 - Idealized time activity integration curves for IgG whole body clearance.

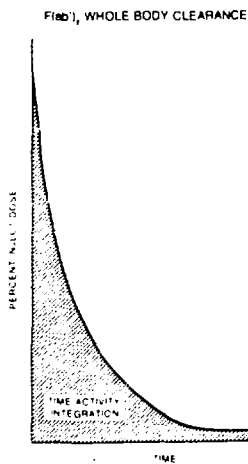


Figure 12 - Idealized time integration curves for $F(ab')_2$ whole body clearance.

These ratios showed reasonable agreement and further demonstrated the applicability of this system to dose measurement problems related to radiolabeled monoclonal antibody clearance.

Results for dose enhancement in tumor relative to the whole body have been mixed for this Ab/tumor system. For I-131 labeled p96.5 administration, statistical significant groups of tumor bearing mice ($N=6$) showed a $\beta = 1.10 \pm 0.08$. This indicates no significant dose enhancement to the tumor for localization indices of IgG - 2-4, tumor size of 50 - 200 mg with localization times ranging 72 -240 hours and radiolabeled antibody doses of 50 - 500 μ Ci. However, localization on a per organ basis was compared to TLD measurements for sacrifice times ranging from a corresponding increased initial activity in the liver (see Figure 13). Hence, when activity enhancement can be demonstrated, the TLD method does respond significantly to increases in local organ activity in a time dependent manner.

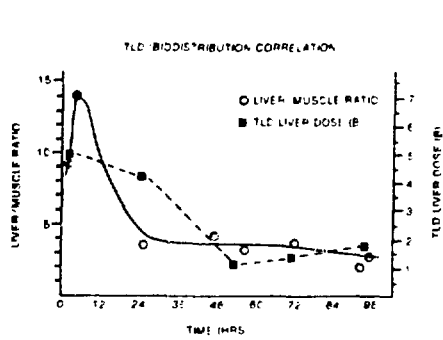


Figure 13 - Comparison of serial biodistribution data for liver and muscle to TLD Liver Dose Ratio (β_L). Two data sets show reasonable correspondence between biodistribution data and TLD measurements in liver at early and late times.

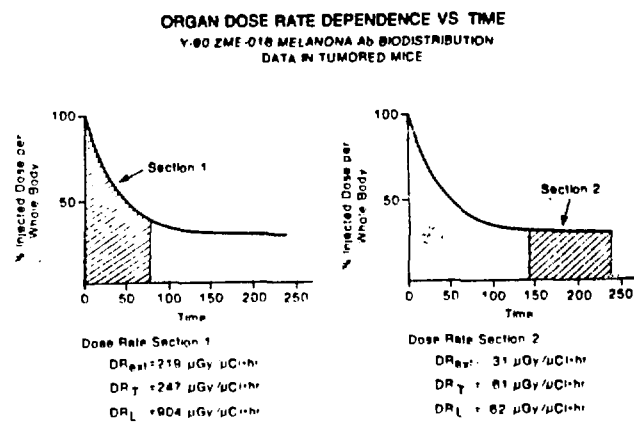


Figure 14 - Dose rate analysis for TLD integrated dose data - Sec. 1 (0-72 hrs.) and Section 2 (140-230 hrs.) Sec. 2 data was taken by post-implanting the TLD 140 hrs. after the injection of antibody and removing dosimeters upon sacrifice (240 hrs.).

d. In Vivo Dose Rate Measurement

Further preliminary experiments were performed using post implantation of TLD dosimeter many hours after Ab injection. Figure 14 shows the implantation of TLD in tumor bearing animals ($N=2$) at time zero and 140 hours post Ab injection. This figure also shows a comparison of time averaged dose rate to the tumor (D_T), liver (D_L) and D_{ext} for different regions of the time activity curve.

IV. DISCUSSION

For the past two decades, thermoluminescent dosimeters have been used extensively for a variety of health physics (3) and radiation therapy physics purposes (4). The application of this technique to in vivo dose measurements for radioimmunotherapy adds yet another dimension to the overall versatility of this well-known radiation dosimeter. However, special attention must be paid to the uniformity of dosimeter fabrication and the onset of energy dependent calibration factors with decreasing beta particle energy. In addition, care must be maintained with respect to physical handling of the TLD, the removal of animal matter and residual radioactivity and the potential optical opacity changes in the crystal material to insure accurate dose assessment.

V. SUGGESTION FOR FUTURE STUDIES - Correlation of Radiobiological Data with Radioimmunotherapy Results

The radiobiology of tumor dose-response curves and the technology of measuring integrated dose to organs in animal systems undergoing radioimmunotherapy is still in its infancy. A majority of the animal data presently available (5,6,7,8) use tumor growth delay (TGD) vs. the total administered radiolabeled antibody activity as the criteria for therapeutic response in animals. Absorbed dose in cGy delivered to the tumor, dose rate, fractionation schedule, or comparison of the tumor response to a standard external beam dose delivery is either not accurately known or specified. The use of the in vivo TL dosimeters would provide a valuable link in the correlation of this information. Although there is a wealth of radiobiological information regarding the treatment response of many tumor models to external beam (9,10) and brachytherapy irradiation (11), the radiosensitivity for tumors undergoing radioimmunotherapy has not been systematically correlated with the radiation absorbed dose delivered to the tumor and the administered activity of the radiolabeled antibody.

We strongly recommend that investigators interested in quantitating the effects of radioimmunotherapy engage in a systematic radiobiological evaluation of their Ab/tumor model. Table 3 is a summary of suggested experiments to be performed in order to obtain the necessary radiobiological data.

Table 3

Radiobiological Quantitation of
Radioimmunotherapy in Animals

Suggested Experiments

1. Normal Tissue Tolerance Studies
2. Single fraction external beam irradiation
 - a) Tumor Growth Delay (TGD) b) Tumor Control Dose (TCD)
3. Multiple Hyperfractionation External Beam Irradiation
 $5 - 10 \times 600$ cGy
4. Low dose rate implant brachytherapy
5. Whole body animal toxicity - radiolabeled MoAb - Establish LD_{50/30}
6. Radioimmunotherapy - Examine TGD and TC₀₅₀ in terms of tumor size and injected Ab mass.
7. Combine External Beam and Adjuvant Radioimmunotherapy.

ACKNOWLEDGEMENT

The authors wish to express their appreciation to the Hybritech Corp. for the supply of antibody and tumor explants necessary for this work. Thanks is also due to Mary Vallely for her support in manuscript preparation. This work was supported in part by a grant from the National Cancer Institute (NIH2 SO RR05359-22)

REFERENCES

1. Wessels, B.W., Bacha, P., Quadri, S.N. 1984. Microdosimetric TLD measurements for tumor associated antibody therapy. Journal of Nuclear Medicine 25(5):39.
2. Wessels, B.W., and Griffith, M.H. 1985. Miniature TLD absorbed dose measurements in tumor phantom models. Journal of Nuclear Medicine (Submitted Sept. 1985).
3. Cameron, J.R., Suntharalingam N., Kennedy, G.G. (eds). 1968. Thermoluminescence Dosimetry, University of Wisconsin Press, Madison.
4. Oberhofer, M., Schramann, A. (eds). 1981. Applied Thermoluminescent Dosimetry, Adam Hilger, Bristol, England.

5. Goldenberg, D.M., Gaffar, S.A., Bennett, S.J. and Beach, J.L. 1981. Experimental radioimmunotherapy of a xenografted human colonic tumor (GW-39) producing carcinoembryonic antigen. *Cancer Research* 41:4354-4360.
6. DeNardo, S.J., Jungerman, J.A., Denardo, G.L. et al. 1982. The choice of radionuclides for radioimmunotherapy. International Symposium of the Developing Role of Short-Lived Radionuclides, Washington, D.C. DOE Publication.
7. Zalcberg, J.R., Thompson, C.H., Lichtenstein, M. and McKenzie, I.F.C. 1984. Tumor Immunotherapy in the Mouse with the Use of ¹³¹I-Labeled Monoclonal Antibodies. *Journal of the National Cancer Institute* 72:697-704.
8. Fawwaz, R.A., Wang, T.S.T., Srivastava , S.C., et al. 1984. Potential of Palladium-109-labeled antimelanoma monoclonal antibody for tumor therapy. *Journal of Nuclear Medicine* 25(7):796-799.
9. Rofstad, E.K. 1985. Human tumor xenografts in radiotherapeutic research. *Radiotherapy and Oncology* 3:35-46.
10. Denekamp, J. 1979. Experimental Tumor Systems: standardization of end-points. *International Journal of Radiation Oncology Biology Physics* 5:1175-1184.
11. Gutin, P.H., Phillips, T.L., Hosobuchi, Y. et al. 1981. Permanent and removable implants for the brachytherapy of brain tumors. *International Journal of Radiation Oncology Biology Physics* 7:1371-1381.

DOSIMETRIC CONSIDERATIONS IN RADIOIMMUNOTHERAPY OF PATIENTS WITH HEPATOMA

Peter K. Leichner, Jerry L. Klein, Stanley E. Order
The Johns Hopkins Oncology Center
Department of Radiation Oncology
600 N. Wolfe Street
Baltimore, Maryland 21205

ABSTRACT

Dosimetric studies of I-131 labeled antiferritin have provided the foundation for preparative and administrative aspects of radiolabeled antibody treatment of patients with hepatoma. Tumor response to I-131 labeled anti-ferritin IgG was encouraging and radioimmunotherapy with Y-90 labeled anti-ferritin IgG was recently initiated. For these patients, In-111 labeled antiferritin IgG was used as the imaging agent, with administered activities ranging from 0.8 - 7 mCi. Serial gamma camera imaging from 30 minutes to 6 days post injection demonstrated that 5-30% of the administered activity localized in hepatomas (8/12 patients). The mean value of the effective half-life in the tumor and liver was 2.8 d. Disappearance curves for the blood circulation, spleen, and other normal tissues were biphasic such that 50% of the activity disappeared within 24 hours post injection. The eight patients who demonstrated sufficient tumor localization were subsequently treated with Y-90 labeled antiferritin IgG. Administered activities were dependent on tumor volume and uptake of radiolabeled IgG and ranged from 8 - 20 mCi. The remaining patients were treated under other existing protocols.

INTRODUCTION

Detailed dosimetric studies for patients with hepatoma who received treatment with I-131 labeled polyclonal antiferritin IgG, anti-AFP, or the combination of antiferritin and anti-AFP administered in a bolus, have been reported (1-3). It was determined that antiferritin provided more than three times the radiation absorbed dose in hepatomas than did anti-AFP. Antiferritin has, therefore, remained the antibody of choice in the radioimmunotherapy of hepatomas. Additionally, these studies demonstrated that the fraction of the administered activity that localized in hepatomas was directly proportional to tumor volume and that multiple infusions re-saturated hepatomas. These results and a study of the toxicity associated with the administration of I-131 labeled antiferritin (4) led to the treatment regimen of administering 30 mCi on Day 0 and 20 mCi on Day 5 following the first injection. For this schedule, mean values of the absorbed dose were 1100 rads in the tumor, 230 rads in normal liver, and 45 rads of total-body irradiation. The mean value of the initial (maximum) tumor dose rate was 4.5 rads/hour.

Absorbed dose considerations indicated that higher initial tumor dose rates would be achieved by radiolabeling antiferritin with Y-90 rather than I-131. This report presents preliminary data for the biodistribution and

absorbed-dose estimates for Y-90 labeled antiferritin IgG, based on in-vivo quantitation of In-111 labeled antiferritin IgG (labeling chemistry for both isotopes developed and patented by Hybritech, Inc., La Jolla, California).

METHODS AND MATERIALS

Patients were x-ray CT scanned 1 to 7 days prior to the administration of radiolabeled antiferritin IgG. Livers were scanned at contiguous 8-mm intervals with an 8-mm slice thickness while patients suspended respiration at resting lung volume. Transaxial slices were stored on magnetic tape in 256 x 256 matrices and analyzed on a minicomputer. Semi-automatic computer software was used to define a region of interest (ROI) corresponding to the whole liver in each slice, and a histogram of the CT numbers within each slice was generated. A global histogram was then obtained by summing over the histograms for each slice. Whole liver and tumor volumes were computed on the basis of the CT number distributions in global histograms, the known pixel size, number of pixels, and slice thickness.

To determine tumor localization kinetics and disappearance curves, patients were administered 0.8 - 7 mCi of In-111 labeled antiferritin. Whole-body imaging was, in general, carried out at 30 minutes, 2, 4, 24, and 92 hours following infusion. Effective half-life measurements for tumor-bearing and normal organs were based on serial gamma camera images. The method of conjugate gamma camera views (4-6) was applied for in-vivo quantitation of In-111 labeled antiferritin in hepatomas, normal liver, and spleen. The fraction of the administered activity in these tissues was determined in this manner.

The administered activities of Y-90 labeled antiferritin ranged from 8 - 20 mCi and were dependent on tumor volume and uptake of radiolabeled antiferritin within the tumor. Imaging of Y-90 bremsstrahlung was carried out to qualitatively monitor the biodistribution of Y-90 labeled antiferritin. Total urinary excretion of Y-90 was monitored over the first 48 hours following injection. In-111 and Y-90 activities were measured in a well-type scintillation counter whose calibration was traceable to the National Bureau of Standards.

Radiation absorbed-dose estimates for Y-90 labeled antiferritin were based on the assumption of uniform distribution of activity, the physical characteristics of the isotope (7), the activity in tumor-bearing and normal tissues, and the computed volumes of these tissues.

RESULTS

Tumor and normal liver targeting of In-111 and Y-90 labeled antiferritin was rapid, and maximum activity in these tissues was achieved in less than 30 minutes following infusion. The disappearance curves for both tissues were characterized by single exponential terms, and the effective half-life was 2.8 ± 0.3 days, the same as the physical half-life of In-111. Disappearance curves for blood, spleen, femur, and other tissues were biphasic and characterized by the sum of two exponential terms. There was initially rapid clearance of radiolabeled antiferritin from the circulation and normal organs such that 50% of the activity was cleared within 24 hours following infusion. This was followed by a slower disappearance component corresponding to an effective half-life of 2.8 days.

In the first four patients, the maximum tumor dose ranged from 4-6 rads/-hour, corresponding to an absorbed dose of 400-600 rads for complete disappearance of the isotope. This dose rate was in the same range as previously achieved with I-131 and lower than expected. However, all patients who had received I-131 labeled antiferritin had previously been treated with external-beam irradiation (2100 rads). Therefore, a smaller dose of 900 rads of external beam, administered in three fractions, was applied to the tumor prior to a second infusion of In-111 labeled antiferritin. This resulted in doubling the fraction of the administered activity that was in hepatomas, but did not increase uptake of radiolabeled antibody in normal liver. In four patients studied to date, following external beam, the fraction of the administered activity in hepatomas ranged from 10% to 30%, in normal liver from 5% to 8%, and in the spleen from 2% to 4%. The initial dose rates in the tumor ranged from 10 to 17 rads/hour, corresponding to an absorbed dose of 900 to 1700 rads. The absorbed dose in normal liver ranged from 260 to 640 rads, and the absorbed dose in the spleen ranged from 50 to 200 rads. The kidneys were difficult to visualize in In-111 images because of low count rates, and the absorbed dose was much lower than for the spleen. This was consistent with urinary excretion for the first 48 hours post injection. Urinary excretion of Y-90, chelated or bound to protein, in this time period ranged from 0.2% to 2.2% of the administered activity. There was no free Y-90 in the urine, as determined from thin-layer chromatography.

DISCUSSION

It has been demonstrated in the H-4-II-E rat hepatoma model that targeting of hepatomas by radiolabeled antiferritin depends on tumor vascularity, permeability of tumor vasculature, and ferritin synthesis and secretion within the tumor (8-10). The preliminary results reported in this article suggest that external-beam irradiation increased the permeability of tumor vascularity. Increased permeability resulted in increased tumor uptake of radiolabeled antiferritin, as determined from quantitative In-111 studies prior to and following 900 rads of external beam. Quantitation of the activity of In-111 labeled antiferritin IgG in conjunction with tumor volumetrics made it possible to compute the administered activity of Y-90 labeled antiferritin that maximized tumor irradiation and reduced the absorbed dose in normal tissues. Studies are underway to improve treatment planning in an effort to optimize therapy with Y-90 labeled antibodies.

REFERENCES

1. Leichner, P.K., J.L. Klein, E.K. Fishman, S.S. Siegelman, D.S. Ettinger, and S.E. Order. Comparative tumor dose from I-131 labeled polyclonal antiferritin, anti-AFP, and anti-CEA in primary liver cancers. *Cancer Drug Delivery* 1. 321-328, 1984.
2. Leichner, P.K., J.L. Klein, S.S. Siegelman, D.S. Ettinger, and S.E. Order. Dosimetry of I-131 labeled antiferritin in hepatoma: specific activities in the tumor and liver. *Cancer Treat. Rep.* 67. 647-658, 1983.
3. Leichner, P.K., J.L. Klein, J.B. Garrison, R.E. Jenkins, E.L. Nickoloff, and S.E. Order. Dosimetry of I-131 labeled antiferritin in hepatoma: a model for radioimmunoglobulin dosimetry. *Int. J. Radiation Oncology Biol. Phys.* 7. 323-333, 1981.

4. Thomas, S.R., H.R. Maxon, and J.G. Kereiakes. In-vivo quantitation of lesion radioactivity using external counting methods. Med. Phys. 3. 253-255, 1976.
5. Thomas, S.R., M.J. Gelfand, S. Burns, C. Purdom, J.G. Kereiakes, and H.R. Maxon. Radiation-absorbed dose estimates for the liver, spleen, and metaphyseal growth complexes in children undergoing gallium-67 citrate scanning. Radiology 146. 817-820, 1983.
6. Hammond, N.D., P.J. Moldofsky, M.R. Beardsley, and C.B. Mulhern, Jr. External imaging techniques for quantitation of I-131 F(ab')₂ fragments of monoclonal antibody in humans. Med. Phys. 11. 778-783, 1984.
7. Dillman, L.T. and F.C. Von der Lage. Radionuclide decay schemes and nuclear decay parameters for use in radiation-dose estimation, Medical Internal Radiation Dose Committee (MIRD), pamphlet no. 10, p. 59, The Society of Nuclear Medicine, New York, 1975.
8. Rostock, R.A., J.L. Klein, K.A. Kopher, and S.E. Order. Selective tumor localization in experimental hepatomas by radiolabeled antiferritin antibody. Int. J. Radiation Oncology Biol. Phys. 9. 1345-1983.
9. Rostock, R.A., J.L. Klein, K.A. Kopher, and S.E. Order. Variables affecting the tumor localization of I-131 antiferritin in experimental hepatoma. Am. J. Clin. Oncol. 6. 9-18, 1984.
10. Rostock, R.A., K.A. Kopher, T.W. Bauer, and J.L. Klein. Factors that affect antiferritin localization in four rat hepatoma models. Cancer Drug Delivery 2. 139-145, 1985.

DISCUSSION

MARCUSE: If by using CT volumetrics you find no response or only partial response after treatment, could that be caused by necrotic and nonviable tissue that possibly is not recognized in the CT scan by CT numbers?

LEICHNER: It has been our experience in the Phase I-II trials that patients who do not respond to one treatment modality (for example, external-beam irradiation and/or chemotherapy) may subsequently respond to I-131 antiferritin IgG. Additionally, patients who do not respond to one or two cycles of radiolabeled antibody may respond to further cycles. Therefore, I do not believe that lack of distinction between necrotic and viable tumor tissues in CT slices of hepatoma patients is a major factor in determining the number of non-responders. However, this cannot be ruled out completely and may occur in a small fraction of the patient population.

GRADY: Perhaps ECT with Tc-99m-sulfur colloid would be useful for showing circulation and viability of liver cancer. Does the use of a vasoconstrictor into the hepatic artery enhance concentration of antibody in tumor?

LEICHNER: If I understand you correctly, the question is whether hepatic artery infusion increases tumor localization of radiolabeled antibodies. We have only a very limited experience with this. However, available data for three patients demonstrate clearly that such infusions do not increase tumor localization. The biodistribution of radiolabeled antiferritin IgG following intrahepatic infusion was the same as that observed for intravenous administration.

HINES: Have you been able to image with In-111 during the Y-90 therapy? If you have, did you see a difference in the kinetics of the antibody when comparing the In-111 pretreatment data with the In-111/Y-90 treatment data?

LEICHNER: Imaging of In-111 antiferritin is relatively easy, even after administration of Y-90 antiferritin, because the latter has no photopeaks. To date, the maximum administered activity of Y-90 antiferritin has been 30 mCi. This has not affected the disappearance curves of In-111 antiferritin.

ZANZONICO: You showed an image demonstrating increased tumor localization of a radiolabeled antibody induced by external irradiation of the tumor to a dose of 900 rad and stated that this resulted from radiation-induced increased capillary permeability to the plasma-borne antibody, which is a rather well-known effect of radiation. However, another rather well-known effect of radiation is what may be termed a "reactive hyperemia", that is, a radiation-induced increase in blood volume in the irradiated tissue. Since this, too, could have resulted in an apparent increase in tumor localization of an "anti-tumor" antibody following irradiation of the tumor, have you performed any "blood pool" radionuclide study (e.g., using Tc-99m red blood cells) to verify that the observed increase in tumor localization of antibody following tumor irradiation was, in fact, due to increased capillary permeability and not an increase in local blood volume?

LEICHNER: Studies in experimental hepatoma using polyclonal antiferritin and experimental melanoma using monoclonal antibodies have demonstrated that the increase in tumor uptake following irradiation is due to increased binding at the tumor site rather than blood flow.

WESSELS: Can you comment on the TBI (total body irradiation) for your Y-90 labeled antiferritin treatment with particular reference to bone marrow dose and dose rate?

LEICHNER: An estimate of the mean absorbed dose to marrow and blood from Y-90 labeled antiferritin IgG in the blood circulation can be made, using the model of Cloutier and Watson¹. According to this model and the disappearance curves for In-111 labeled antiferritin, the estimated dose to the blood ranges from 4 to 7 rads/mCi of Y-90 antiferritin, and the dose to the marrow from 0.4 to 0.7 rads/mCi of Y-90 antiferritin.

SCHLESINGER: Can a dose of 600-1000 rads, which can presently be delivered to a tumor by radioactively labeled monoclonal antibodies, really have a therapeutic effect in view of the well known doses of 6000-7000 rads needed in intracavitary therapy (due to low dose rates) and a dose of at least 10,000 rads needed for radioiodine therapy of thyroid cancer? Maybe the effects observed are not due to radiation?

LEICHNER: A very important concept in the evolution of radiotherapy has been well summarized by Fletcher in his 1977 Erskine Memorial Lecture². To assume that you can deliver an "all-or-none" cancerocidal dose to a lesion with a single dose or within a short period of time is incorrect. I believe that this concept applies to radioimmunotherapy in particular. Our Phase I-II study of antiferritin IgG in hepatomas has demonstrated that cyclic therapy results in a 50% response³.

OLKOWSKI: How many patients with massive hepatoma were cured by radiolabeled antibodies and 900 R of external radiation?

LEICHNER: None.

OLKOWSKI: This is a major point. During the past 15 years, people have been

trying to cure patients with metastatic disease by adjuvant immunotherapy with no results. I hope we will not repeat this with antibodies labeled with radiopharmaceuticals in an attempt to cure patients with massive, malignant disease. We should rather concentrate on the use of labeled antibodies to detect early lesions in high risk individuals that are not detectable by other means (for instance, symptomatic patients with glioma suspected in the brain stem) to improve the diagnosis and the cure rate. Technologies are available to detect 0.5 cm lesions in experimental animals.

LEICHNER: Your comment was, in part, discussed in my earlier response. I wish to add that all patients in the hepatoma protocol are inoperable and that all other forms of therapy have been less successful than the treatment results obtained in our Phase I-II study. One promise radioimmunotherapy holds out is that results can be greatly improved as we gain a better understanding of the physics, chemistry, and biology inherent in this treatment modality.

FRITZBERG: Can you compare the efficacy of Y-90 and I-131 for therapy with antiferritin at this time?

LEICHNER: The number of patients currently entered in the Y-90 antiferritin protocol is too small and follow-up too short to make a statistically valid comparison with I-131 antiferritin.

¹Cloutier R.J. and E. Watson. Radiation dose from radioisotopes in the blood. In Medical Radionuclides: Radiation Dose and Effects, AEC Symposium Series No. 20, Cloutier, R.J., Edwards, C.L. and Snyder, W.S., eds., Oak Ridge, Conf-691212, 1970.

²Fletcher, G.H. The evolution of the basic concepts underlying the practices of radiotherapy from 1949 to 1977. Radiology 127:3-19, 1978.

³Order, S.E., G.B. Stillwagon, J.L. Klein, et al. Iodine 131 antiferritin, a new treatment modality in hepatoma: A radiation therapy oncology group study. J. Clin. Onc. 3:1573-1582, 1985.

DISTRIBUTION AND DOSIMETRY OF INDIUM-111
LABELED F(ab')₂ FRAGMENTS IN HUMANS

P. Doherty, R. Schwinger, M. King, M. Gionet

Department of Nuclear Medicine

University of Massachusetts Medical Center

Worcester, MA

ABSTRACT

The purpose of this study was to obtain quantitative biodistribution data in patients injected with the indium-111 labeled F(ab')₂ fragments of mouse monoclonal antibody. From this data dosimetric calculations were made for the individual organs. We also evaluated the quantitative properties of SPECT in this application and compared it with the more conventional two view planar technique in both phantom and patient studies.

For one antibody (19-9) the mean dose in rads/mCi for the organs of highest accumulation, namely, the liver and kidneys was 3.2 and 2.6 respectively. Preliminary data from another antibody (OC 125) showed much higher blood levels and a significantly lower liver dose of 2.3 indicating that antibody type is another significant determinant in dosimetry. The SPECT approach, particularly in the presence of background activity, was more accurate in the phantom studies and resulted in larger estimated doses in the patient studies. Also, SPECT has the added advantage of providing an index of organ volume, which has to be balanced with the fact the planar is more rapid, and does not require special hardware.

INTRODUCTION

Monoclonal antibodies, directed against a variety of tumor associated antigens, are now available in sufficient quantities that a number of investigators are using these radiolabeled reagents for *in vivo* diagnostic and therapeutic patient studies (1-5). Thus, it is important that quantitative data on their distribution and dosimetry in humans be obtained, so that accurate predictions as to the possibility of using this as a successful approach to radioimmunotherapy can be assessed.

In humans, the situation is very complex. This is because of the presence of multiple factors which govern the biodistribution of monoclonal antibodies, related to both the antibodies themselves and the status of the host. The most important of these are the type and stability of the radiolabel, the characteristics of the antibody (isotype, whole antibody vs. fragments, immunoreactivity, dose, etc.), the presence of circulating antigen with associated immune complex formation, cross reactivity with other tissues, the

presence of antibodies to mouse proteins, the use of unlabeled antibody, and the catabolic capacity of the organs.

In this study, we estimate the dose to normal tissues associated with the use of the $F(ab')_2$ fragments of two monoclonal antibodies (19-9, OC 125) labeled with In-111 (6). Using this approach the factors relating to label stability, immunoreactivity, and antigen antibody complex formation have already been described (7).

During the course of studying the first group of patients it became clear that when regions of interest were being drawn to outline the organ boundaries for the calculation of the % distribution in the liver, spleen, and kidneys, a certain error was unavoidable due to the superposition of adjacent activity. In order to overcome this problem and assess its influence on the measurements, we evaluated the potential of SPECT imaging as an alternative for these quantitative studies since it minimizes the contribution of activity in adjacent organs and surrounding tissues. To check the relative accuracy of these two methods a series of phantom studies were performed and this was followed by a comparative study in patients.

METHODS

We have previously characterized the properties of our SPECT system, the Picker dyna-scan (8). Briefly, the system consists of a single 61 tube detector with a 38 cm. wide, 9.5 mm thick crystal and two stage uniformity correction. Gantry motion is microprocessor controlled. The gantry is interfaced to a DEC Gamma-11 computer system with the SPETS-11 software package for circular and body contouring acquisition, image reconstruction and display. An array processor (Analogic AP400) has been integrated into the computer system. The collimator was of a medium energy, medium sensitivity, parallel hole type.

In all of the phantom work we made an effort to approximate the clinical imaging situation with similar levels of radionuclide activity and comparable imaging times. The Alderson phantom is an abdomen shaped plastic shell which allows realistic organ shaped hollow plastic inserts and 1 to 5 cm hollow plastic spheres to be imaged within the shell. Two imaging techniques were then used; a planar technique, and a circular rotation SPECT acquisition.

The planar technique (9-11) employs 5 minute, 64 x 64 word mode anterior and posterior images with anterior transmission images using a Co-57 flood for attenuation correction. The anterior and posterior images are combined using the formula:

$$N_C(x,y) = [4.*[N_a(x,y)*N_p(65-x,y)]^{1/2} + [N_a(x,y)+N_p(65-x,y)]/2]/5$$

where $N_a(x,y)$ and $N_p(x,y)$ are the computer acquired anterior and posterior images respectively, and $N_C(x,y)$ is the combined result. This combination of arithmetic mean (average of sum) and geometric mean (square root of product) was empirically determined to yield uniform sensitivity throughout the field of view for point sources of In-111. In order to correct this result for attenuation, it is necessary to know the pixel by pixel thickness of the phantom. This is determined from the natural log of the ratio of anterior Co-57 transmission scans with and without the phantom in place. To account for scatter buildup as well as absorption, this was modeled as a quadratic relation:

$$t(x,y) = a_t + b_t \ln(i(x,y)/i_0(x,y)) + c_t [\ln(i(x,y)/i_0(x,y))]^2$$

where $t(x,y)$ is the pixel by pixel phantom thickness, and $i(x,y)$ and $i_0(x,y)$ are the transmission scans with and without the phantom respectively. The coefficients of this equation were determined from a least-squares fit to attenuation data using the same source, camera, and collimator. This effective thickness was then used to determine the attenuation correction from a second quadratic relation:

$$s(x,y) = a_s + b_s t(x,y) + c_s t(x,y)^2$$

where $s(x,y)$ is the estimated activity per pixel in microcuries. The coefficients of this relation were also determined from a least-squares fit to data for the fractional count per pixel for In-111 in a point source attenuated with increasing thickness of absorber. The quadratic coefficients used to determine the pixel by pixel phantom thickness and the activity in microcuries from the estimated thickness have been previously determined for similar geometry, isotope, camera, collimator, and energy window. A five millicurie Co-57 flood source was used for the transmission scans with the contribution of the In-111 into the Co-57 energy window subtracted from the transmission scan with the phantom in place. The geometry of the phantom was arranged such that the spheres of activity did not overlap in the anterior and posterior views. The use of the SPECT system for this procedure facilitated accurate registration of the two views.

The second technique consisted of first performing a SPECT acquisition using 64 views, 64x64 pixel word mode matrix, and 30 seconds per view. The reconstruction approach used was that available in the SPETS-11 package and the filter a Shepp-Logan with a cutoff at the Nyquist frequency. An important aspect of accurate quantitation in SPECT is the use of a method to compensate for internal photon absorption. In these studies we used a post-reconstruction technique developed by Chang (12).

The total activity in a volume of interest from the SPECT study was determined by summing counts in variable regions of interest over contiguous transverse sections and multiplying by an appropriate calibration factor (related to camera, collimator, energy window, and reconstruction algorithm). The calibration factor was determined by scanning a point source of Indium-111 of known activity in air. The regions of interest were defined by an experienced operator using a lower threshold level of 30 to 50%. The count rate and area of activity in the regions were recorded for each slice, whose thickness was usually 12 cm. The total activity and organ volume were computed by adding together the values from the individual slices with corrections being made for decay.

To check the accuracy of these techniques with extended sources the phantom was imaged with liver, spleen, and kidney "organs" in place. To simulate the clinical situation more accurately, we used a dog model in which six 0.3 ml vials containing 2.5 to 50 μ Ci of In-111 were placed in the abdomen. Imaging was performed prior to and following the I.V. injection of 1.1 mCi of In-111 labeled antibody.

In the patient studies 1 mg of the $F(ab')_2$ fragments of two antibodies 19-9 and OC 125 were labeled with 1-2 mCi of In-111. They were infused intravenously over 45 minutes. Whole-body biological clearance was evaluated using digitized whole-body scans (13). The individual organ distribution was estimated using the planar technique at multiple time points from 1 to 72 hours following the injection. In five patients both planar and SPECT acquisitions were obtained. Blood and urine clearance was estimated by counting serial samples along with an aliquot of the injected dose in a gamma well counter.

The dose to the organs and the rest of the body was calculated using the conventional MIRD approach (14,15). Besides those assumptions inherent in the MIRD approach to internal dosimetry, the following assumptions were made in calculating the absorbed dose to the liver, spleen, kidneys and rest of body. First, the uptake in all organs was assumed instantaneous and equal to the average value of the measurements made at all time points. Thus, with the exception of the rest of the body, no biological clearance was assumed. This assumption was used since it was unlikely to underestimate the radiation dose, and plots of the uptake as a function of time did not strongly indicate clearance from these organs. The uptake in the rest of the body was assumed to be that of the initial dose minus the sum of the uptakes in liver, spleen, kidneys and the cumulative excretion of the urine. This was fit with a least squares program (16), to one or two exponentials and the best fit used to model the clearance from whole body.

RESULTS

When the planar and SPECT estimates of activity for the small isolated volumes are compared, both perform well in the absence of background activity (Fig. 1a, b). With the addition of background activity to the phantom, the SPECT estimates remained accurate while the planar technique showed degraded performance with a reduced slope and correlation coefficient (Fig. 1c, d).

The organ phantom data point out several results. Figure 2a shows the variability of the planar technique to estimate organ activity. Note that the plotted line is not the regression line, but the line of unity. The regression coefficients for this data are 1.60, -56.3, and .96 (slope, intercept, correlation coefficient). The two points at 750 microcuries actual activity represent the liver phantom with partial overlapping of kidneys and spleen and point to the problem with the planar approach when organs are in close proximity. Neglecting these two points, the slope, intercept and correlation coefficient are 1.03, 36.1, and .96 respectively. In contrast the SPECT estimated activities (Fig. 2b) demonstrate the ability of this technique to accurately determine total activity for an organ sized volume of interest due primarily, as can be seen on the images (Fig. 3), to the isolation of the organs on the transverse sections. The slope, intercept, and correlation coefficient for SPECT are 0.99, 2.92, and 10.99.

In the animal model both imaging techniques accurately estimated vial activities (Fig. 2c) when they were placed in the abdomen initially. However, the two lowest activity vials were indistinguishable from background in both planar views (Fig. 4). Therefore, it was necessary to use regions of interest determined from the pre-injection image. This effect of added background has prominent effects on the planar estimates (Fig. 2d) whereas the SPECT transverse section images visualized all six vials and accurately estimated their respective activities.

In the 6 patient studies using the $F(ab')_2$ fragments of the 19-9 antibody, the mean body clearance as calculated from the digitized whole-body scans was 160 hours with the only significant loss of activity being via the urine at a mean rate of 0.26% per hour. The blood clearance which was biexponential showed a $T_{1/2}$ alpha of 1.9 hours and a $T_{1/2}$ beta of 19.3 hours. The organ distribution, in terms of the % injected dose, was calculated using the planar technique and the mean dose expressed in rads/mCi. In 5 patients using the OC 125 antibody a comparison between the SPECT and planar estimates was obtained and in these cases the lower levels in the liver were associated with higher blood levels (Table I).

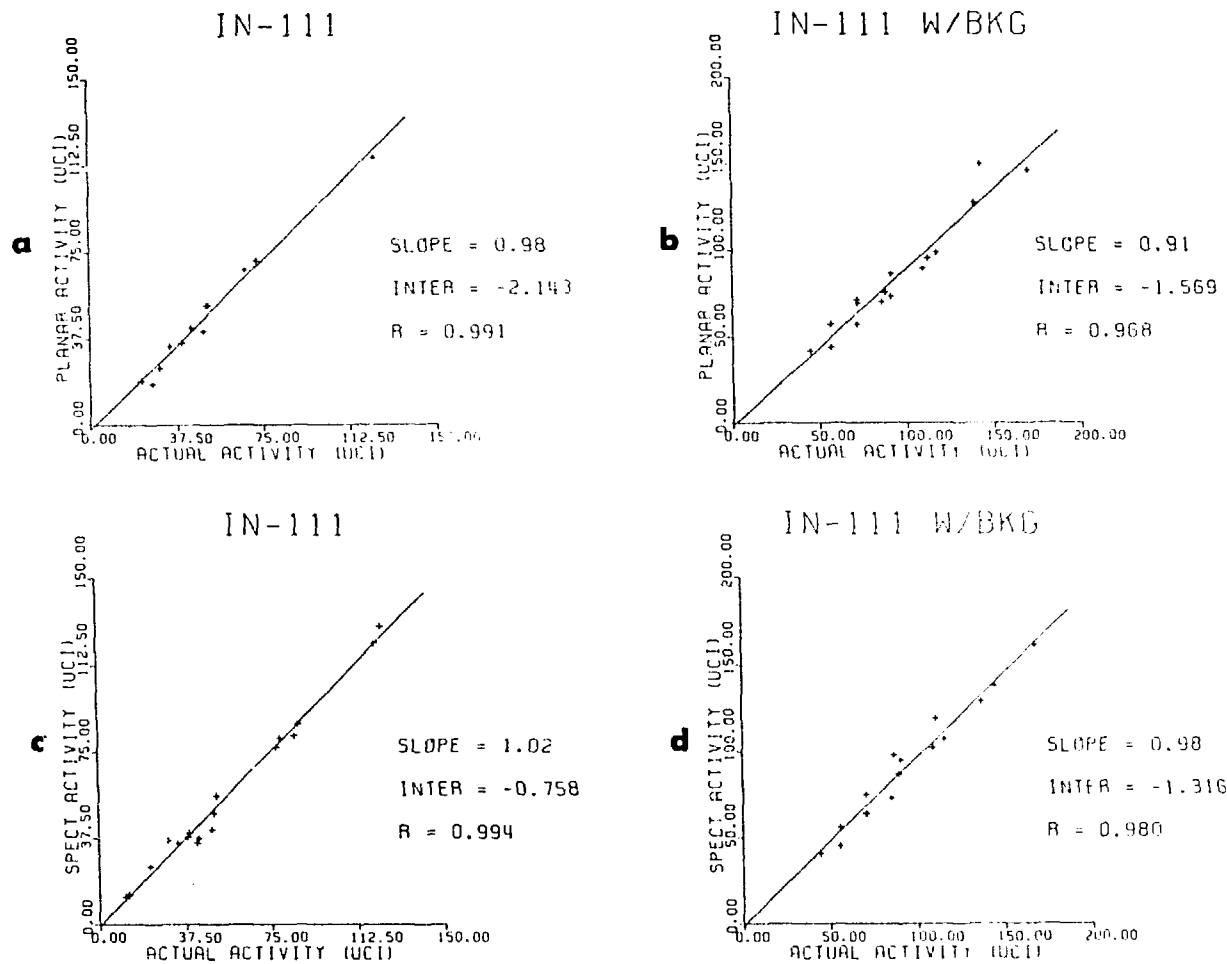
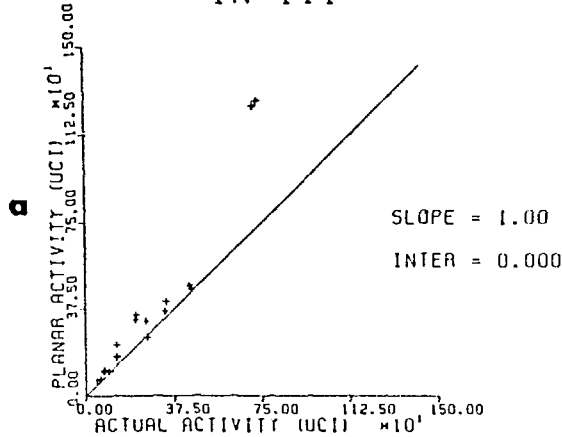
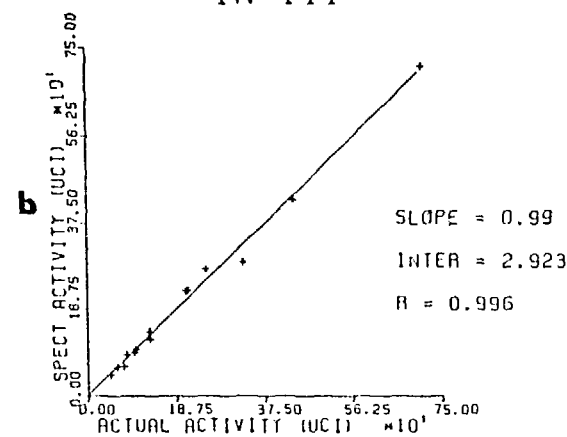


Fig. 1. Relationships between planar and SPECT estimated activities and actual activities in small spheres in phantom. a) planar, b) planar with background activity, c) SPECT, d) SPECT with background activity.

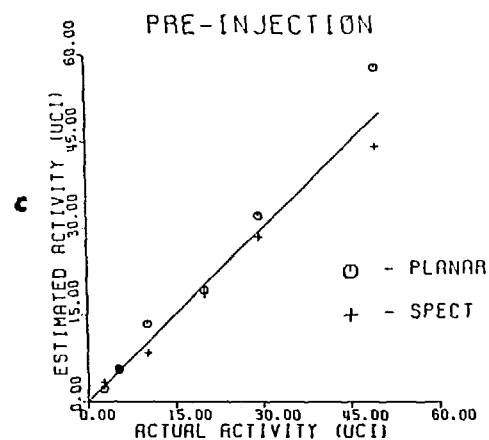
IN-111



IN-111



PRE-INJECTION



POST-INJECTION

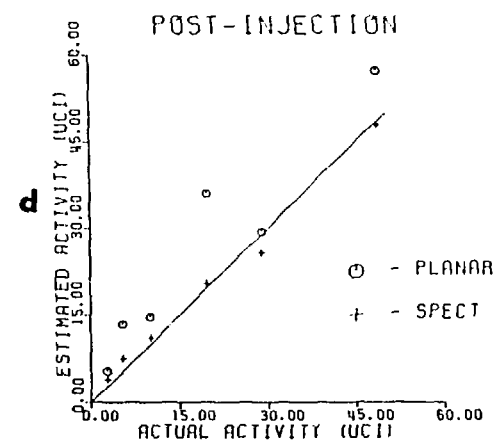


Fig. 2. Relationships between planar (a) and SPECT (b) estimates for Alderson organ phantoms and actual activities. Relationship between actual and measured activities in vials in animals model both before (c) and after (d) injection of background activity.

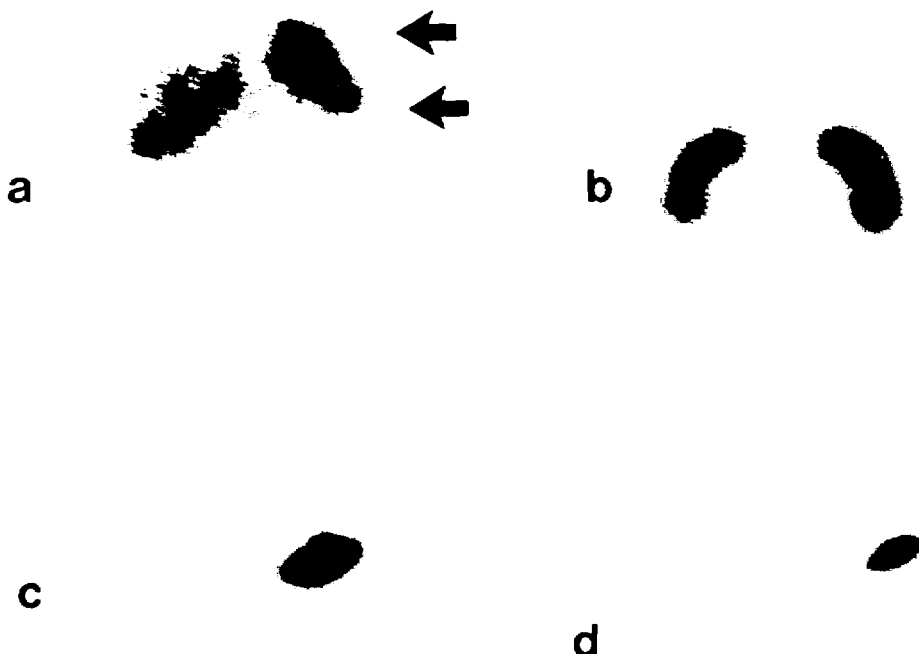


Fig. 3. Planar and SPECT images of 'organs' in phantom, a) anterior view, b) posterior view, c), d) transverse section images corresponding to arrows in (a).

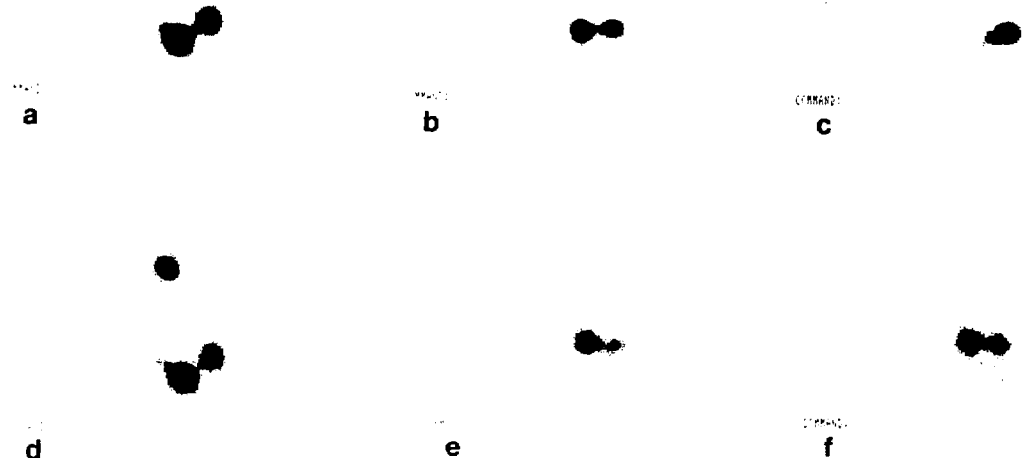


Fig. 4. Planar and SPECT images of In-111 filled vials in dogs' abdomen. a) anterior image before injection of labeled antibody, b), c) transverse section images through vials in (a), d) anterior image 30 minutes post-injection. The transverse section images through vials in (d) and shown in (e) through the vials in the lower part of the abdomen and (f) through those in the upper abdomen adjacent to the liver.

Table I

Dosimetry for Major Organs in Patients Using 19-9 (n=6)
and OC 125 (n=5) Antibodies

	Antibody - F(AB') ₂ of 19-9			Antibody - F(AB') ₂ of OC 125		
Organ	% Dose Planar	Rads/ mCi	% Dose Planar	Rads / mCi	% Dose SPECT	Rads/ mCi
Liver	23.3 ± 9.9	3.2	15.1 ± 4.4*	2.3	19.0 ± 3.9**	2.8
Spleen	1.3 ± 0.8	1.6	1.3 ± .9	1.7	2.1 ± 0.9	2.2
Kidneys	4 ± 2.4	2.6	3.5 ± 1.6	2.3	2.5 ± 1.1	1.8
Rest of Body	71.4 ± 10.2	0.4	80.1 ± 4.7*	0.4	76.4 ± 4.2**	0.4

* Different from planar measurement of 19-9 by t-test with $p \leq .05$

** Different from planar measurement of OC 125 by t-test with $p \leq .05$

DISCUSSION

The accuracy of the whole-body counting method using a gamma camera has been shown to be of the order of ± 10% (17) and in our cases where there was a complete collection of urine, the values for whole-body clearance were in good agreement. In the case of the planar method, used to determine the organ uptake, the major problem relates to the presence of overlapping and juxtaposed organs; the tendency being to overestimate the absolute amount of activity which is more prominent for small organs and exaggerated by the presence of background activity. This influence of overlapping and background contribution appears to be less of a problem for the SPECT approach which, while having the added attraction of providing an index of organ volume (18), has the drawback of being more difficult to perform.

A source of error common to both the planar and SPECT methods is the accuracy with which the organ boundaries are drawn, using the manual technique. The phantom studies indicate this error is probably less than 5%. A more reproducible approach may be to use a computer based edge detection algorithm. One explanation as to why the liver levels are significantly lower with the planar technique may be related to the constant background correction factor used, which would tend to overestimate its contribution when a large organ occupies the major portion of the field of view. SPECT allows three-dimensional definition of the volume of interest and thus has no need for background correction.

Overall, SPECT does appear to hold promise as a tool for quantitative data collection in humans for dosimetry applications in the case of monoclonal antibodies since the rates of change in biodistribution are relatively slow. In this study, while there were not large differences in the case of small organs, SPECT's ability to detect and separate small areas of activity suggest that its major advantage may well be in the estimation of tumor volume and dosimetry, particularly in the abdomen. Since we did not attempt to resolve very small volumes of activity, the problems of Compton scattering, septal penetration, and the finite spatial resolution of the camera were not critical. Techniques for subtraction of Compton scattered photons (19-21) and resolution recovery (22-23) have been shown to be useful in SPECT imaging when

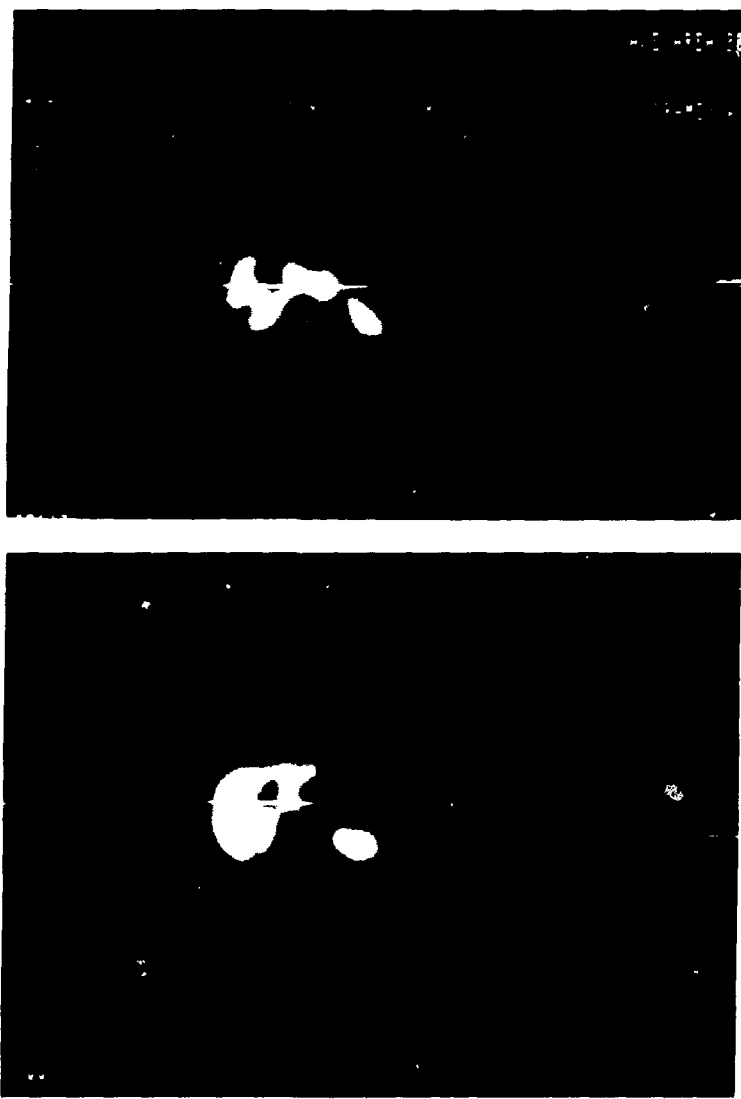


Fig. 5. The SPECT images in the patients showed that in the liver the distribution of the activity is heterogeneous on the early studies with a prominent amount of the activity being present in the portal venous system (top). As the blood pool level drops, the activity becomes more homogenously distributed throughout the parenchyma (bottom).

higher image contrast is a major concern. However, before it becomes more routinely applied, further work on the influence of the approach used for attenuation correction, the type of filter used in the reconstruction process, and its accuracy with small volumes which have low-target to background ratios needs to be done.

In general, what happened within the first few hours following the injection of the fragments into the patients dictated that portion of the injected dose which would settle in the organs. Over the next 72 hours, a very slow progressive build up occurred in the liver associated with a fall in blood pool and splenic activity. Thus, the assumption of instantaneous organ uptake used in the dose calculations did not lead to a significant overestimation of organ dose. The activity in the kidneys remained fairly constant over time. The major component of the injected dose was distributed uniformly in the interstitium with the only identifiable focal accumulation being in the blood pool and bone marrow. The extent of marrow uptake is difficult to calculate from the scans with any degree of confidence. To use a worst case estimate and calculate the dose based on the assumption that rest of the body dose was equivalent to the marrow dose would provide a very large overestimation since on the images, the marrow activity was slight but did appear to increase with time.

The time dependent inhomogeneity of activity in the liver documented by the SPECT images (Fig. 5) may not be very important when calculating liver dose from a predominantly gamma emitter such as In-111 but would need to be taken into consideration if attempts were used to extrapolate from this data as to what dose one might expect if one were to use a beta emitter such as Yttrium-90 (24).

In this preliminary study there were significant differences in the organ distribution between the two antibodies. Also, within both groups there was some overlap in individual patient results. These results suggest that there are no simple rules which can be employed across the board to predict the dosimetry for one antibody based on results from another and that data will have to be obtained for each one separately in each patient.

ACKNOWLEDGMENTS

The authors thank D. Hnatowich for his help and support, M. Rusckowski and J. McGann for their assistance with antibody labeling and sample counting. We are grateful to Centocor for supplying the antibodies and Medi-Physics for the ^{111}In used in this study and to L. Desai for her assistance in the preparation of this paper. This investigation was aided in part by grants from the American Cancer Society (PDT-274) and NCI CA 33029.

REFERENCES

1. Rainsbury, R.M., R.J. Ott, J.H. Westwood, et al. Localization of metastatic breast carcinoma by a monoclonal antibody chelate labeled with indium-111. *Lancet* 934-938, 1983.
2. Mach, J., J. Chatal, J. Lumbroso, et al. Tumor localization in patients by radiolabeled monoclonal antibodies against colon carcinoma. *Cancer Res.* 43, 5593-5600, 1983.
3. Moldofsky, P.J., J. Powe, C.B. Mulhern, et al. Metastatic colon carcinoma detected with radiolabeled $F(ab')_2$ monoclonal antibody fragments. *Radiology* 149, 549-555, 1983.

4. Carrasquillo, J.A., K.A. Krohn, P. Beaumier, et al. Diagnosis of and therapy for solid tumors with radiolabeled antibodies and immune fragments. *Cancer Treat. Rep.* 68, 371-378, 1984.
5. Courtenay-Luck, N., A.A. Epenetos, K.E. Halnan, et al. Antibody-guided irradiation of malignant lesions: three cases illustrating a new method of treatment. *Lancet* 1441-1443, 1984.
6. Hnatowich, D.J., W.W. Layne, R.L. Childs, D. Lanteigne, M.A. Davis, T.W. Griffin, P.W. Doherty. Radioactive labeling of antibody: a simple and efficient method. *Science* 220, 613-615, 1983.
7. Hnatowich, D.J., T.W. Griffin, C. Kosciuczyk, M. Rusckowski, R.L. Childs, J.A. Mattis, D. Shealy, P.W. Doherty. Pharmacokinetics of an indium-111 labeled monoclonal antibody in cancer patients. *J. Nucl. Med.* 26, 849-958, 1985.
8. King, M.A., R.B. Swinger, P. Esser, et al. Preliminary characterization of the properties of a new rotating SPECT imaging system. In: Emission Computed Tomography: Current Trends, Society of Nuclear Medicine, New York, 91-104, 1983.
9. Myers, M.J., J.P. Lavender, J.B. DeOliveira, A. Maseri. A simplified method of quantitating organ uptake using a gamma camera. *Brit. J. Rad.* 54, 1062-1067, 1981.
10. Macey, D.J., R. Marshall. Absolute quantitation of radiotracer uptake in the lungs using a gamma camera. *J. Nucl. Med.* 23, 731-735, 1982.
11. Graham, L.S., R. Neil. In vivo quantitation of radioactivity using the Anger camera. *Radiology* 112, 441-442, 1974.
12. Chang, LT. A method for attenuation correction in radionuclide computed tomography. *IEEE Trans. Nucl. Sci.* 25, 638-643, 1978.
13. King, M.A., P.W. Doherty. A computer program for reconstruction of images from a scanning gamma camera. *Computer Programs in Biomedicine* 14, 115-120, 1982.
14. Loevinger, R., M. Berman. A schema for absorbed-dose calculations for biologically-distributed radionuclides. *J. Nucl. Med.*, Supplement 1, 7-14, 1968.
15. Snyder, W.S., M.R. Ford, G.G. Warner, S.B. Watson. "S", absorbed dose per unit cumulated activity for selected radionuclides and organs. MIRD Pamphlet No. 11, Society of Nuclear Medicine, New York, 1975.
16. Gomeni, R., C. Gomeni. Automod: A polyalgorithm for an integrated analysis of linear pharmacokinetic models. *Comput. Biol. Med.* 9, 39-48, 1979.
17. Goodwin, D.A., R.A. Finston, S.I. Smith. Distribution and dosimetry of In-111 labeled leukocytes and platelets in humans. Third International Radiopharmaceutical Dosimetry Symposium. Conference Proceedings, p 88-100, 1980.
18. Strauss, L.G., J.H. Clorius, T. Frank, G. Van Kaick. Single photon emission computerized tomography (SPECT) for estimates of liver and spleen volume. *J. Nucl. Med.* 25, 81-85, 1984.

19. Beck, J.W., R.J. Jaszczak, R.E. Coleman, C.F. Starmer, L.W. Nolte. Analysis of SPECT including scatter and attenuation using sophisticated Monte Carlo modeling methods. IEEE Trans. Nucl. Sci. 29, 506-511, 1982.
20. Axelsson, B., P. Msaki, A. Israelsson. Subtraction of Compton-scattered photons in single-photon emission computerized tomography. J. Nucl. Med. 25, 490-494, 1984.
21. Pang, S.C., Genna, S. The effect of Compton scattered photons on emission computerized transaxial tomography. IEEE Trans. Nucl. Sci. 26, 2772-2774, 1979.
22. Gottschalk, S.C., D. Salem, C.B. Lim, R.H. Wake. SPECT resolution and uniformity improvements by noncircular orbit. J. Nucl. Med. 24, 822-828, 1983.
23. King, M.A., R.B. Schwinger, P.W. Doherty, B.C. Penney. Two-dimensional filtering of SPECT images using the Metz and Wiener filters. J. Nucl. Med. 25, 1234-1240, 1984.
24. Hnatowich, D.J., F. Virzi, P.W. Doherty. DTPA-coupled antibodies labeled with Yttrium-90. J. Nucl. Med. 26, 503-509, 1985.

DISCUSSION

FRITZBERG: Your data that shows 19 to 23% localization of $F(ab')_2$ In-111 antibodies in the liver seem high assuming lack of the Fe portion responsible for liver uptake. How do these values compare with whole antibody and is the reduction as expected?

DOHERTY: I also have this problem with the liver and what goes on within it with the various nuclides and the various antibodies. I think that someone showed during the first day of this symposium that the uptake of the blood pool agents in the liver was approximately 10 to 15 percent. We're not all that much higher with our liver uptake. I'm not quite sure that a large amount of the liver activity in the early phases isn't due to the blood pool. You have the pool in the liver early on and you don't have it later, but it's not a major thing. We know that the indium comes off at a rate of 9% per day, and that it doesn't come off more for $F(ab')_2$'s than for whole antibodies. I think that you get "colloidal-type" uptake in the liver only in relation to what happens with protein; that is, if you have a lot of carbohydrate on your protein, the rubbish signals the liver to take it out. If you're using $F(ab')_2$ you don't have the carbohydrate component, so you don't have that particular problem. If you have iodine, you have a different situation altogether because you deiodinate up to 50% within a very short period of time.

FRITZBERG: Secondly, I want to comment on SPECT imaging. The liver has many nonuniform aspects from the vascular system and biliary system. Interpretation of SPECT images of the liver will be difficult.

DOHERTY: I totally agree with that.

GRADY: You have partly answered my question which relates to the RE system and the uptake of the colloid. I have seen a large amount of distribution generally wherever there are RE cells if you administer any kind of colloid or

free yttrium chloride that forms a colloid. Perhaps if we preload the patient or animal with a large quantity of nonradioactive albumin colloid, we might decrease the uptake in liver. I think some people have tried it, but I don't know how thoroughly it has been done. Have you an opinion on whether this is feasible to clear liver concentration of Y-90?

DOHERTY: I do have an opinion. Being an Irishman, I have a good healthy respect for the liver's capacity to get rid of junk, usually of the alcoholic variety. I don't think it is a feasible or practical procedure in a human. I think you can in animals; certainly it has been shown that you can give oils and other stuff, but I think in a human it would be a waste of time. I think it is possible to "saturate" a healthy person's liver and it will still be able to get rid of a little bit of floating junk.

CHELATE CHASE OF RADIOPHARMACEUTICALS REVERSIBLY
BOUND TO MONOCLONAL ANTIBODIES IMPROVES DOSIMETRY

D.A. Goodwin^{1, 2}, S.I. Smith², C.F. Meares³,
G.S. David⁴, M. McTigue¹, R.A. Finston²

(1) Veterans Administration Medical Center
3801 Miranda Avenue
Palo Alto, California 94304

(2) Stanford University School of Medicine
Stanford Health Physics Office
Stanford, California 94305

(3) Department of Chemistry
University of California, Davis
Davis, California 95616

(4) Hybritech, Inc.
San Diego, California 92121

ABSTRACT

One hundred micrograms of monoclonal antibody (MoAb) CHA255 with a binding constant K_b of 4×10^9 was complexed with indium-111 labeled BLEDTA II, BLEDTA IV, benzyl EDTA, and an EDTA conjugate of Fab. The 24-hour tumor and organ distribution in BALB/c mice bearing KHJJ tumors was studied for each compound alone, the antibody complex, and 3 hours following a chelate chase of the antibody complex. Whole-body biological half-life was measured for 7 days with and without a chelate chase for each antibody complex. The 24-hour whole-body counts dropped 20-60 percent within 3 hours of administering the chelate chase. Blood concentration fell over 89 percent within 3 hours of administering the chase and there was a decrease in concentration in all organs, except the kidneys, of 10 to 85 percent. Theoretical equivalent human doses were calculated from the 24-hour organ concentrations, effective half-life, and MIRD 11 "S" values (absorbed dose per cumulated activity). Liver and spleen were the target organs, with the dose ranging from 0.50 to 3.91 rads per millicurie. The reduction in organ radiation dose varied up to 95 percent following the chelate chase. Rapid selective renal clearance of chelate labeled radiopharmaceuticals by competitive inhibition (chelate chase) of their reversible binding to monoclonal antibodies, greatly improves the radiation dosimetry of tumor imaging agents.

INTRODUCTION

The tumor uptake of covalently-radiolabeled monoclonal antibodies and their fragments is directly related to the integral of blood concentration over time, the highest tumor concentrations being obtained with whole antibody which has the longest biological half-life in the plasma (1,2,3). Higher tumor to background ratios can be obtained with $F(ab')_2$ or Fab Fragments that disappear more rapidly than whole antibody from the blood but only at the cost of a lower absolute tumor concentration (1,2). Tumor concentration of whole antibody reaches a maximum in approximately 1 to 2 days but the majority continues to circulate for many days after due to the slow excretion of covalently labeled proteins. This prolonged retention of activity adds a large amount of useless radiation exposure to normal tissue, especially liver, spleen, and bone marrow.

Ideally, for both maximum tumor concentrations and tumor to background ratios combined with minimum radiation exposure, blood levels should be maintained as high as possible for periods up to 24 hours followed by rapid selective lowering of the blood and whole-body radioactivity at the time of imaging. We describe a chelate chase technique utilizing reversible binding of chelate-labeled radiopharmaceuticals by anti-chelate monoclonal antibodies for enhancing tumor images while reducing the radiation exposure.

MATERIALS AND METHODS

A. MONOCLONAL ANTIBODY

The production and characterization of antibodies against metal chelates have been previously reported (4). Briefly, in order to make antibodies against indium-EDTA, an antigen was prepared by conjugating (L)SCN-C₆H₄-CH₂-EDTA (parathiocyanato benzyl EDTA) (5) to keyhole limpet hemocyanin using the methods of Meares et al. (6). After addition of indium 3+, there was approximately 0.1 mg of attached chelate per milligram of protein. To prepare antibody producing hybridoma cell lines, spleen cells from BALB/c mice (multiply immunized with the antigen) were fused with a variant of the P3.653 myeloma cell line using the technique of Gerhard (7). The resulting hybridomas were screened by radioimmunoassay (8) for their ability to bind indium-111 (L)-NH₂-C₆H₄-CH₂-EDTA or iodine-125 bovine serum albumin bearing nonradioactive indium EDTA groups.

Binding constants for indium chelates were determined in triplicate by equilibrium dialysis and Scatchard analysis of a series of antibody and chelate solutions (9). The binding constants for metal chelates other than indium (L)-benzyl EDTA were determined by equilibrium dialysis in competition with indium 3+-(L)-benzyl EDTA (4). Based on their high titres and affinities, two IgG₁ antibodies from clones CHA255 and CHB235 were selected for use in this study.

B. ANIMAL STUDIES

1. Biological Half-life

Whole-body counting of mice was carried out using two opposed 3-inch sodium iodide scintillation detectors (Picker Corp.). Thirty to 40 microcuries of indium-111 were injected intravenously and a minimum of 10,000 counts was obtained for each point. The animals were counted immediately following injection, at 3 hours and 5 hours on the first day, and daily for the subsequent 6 to 7

days. At least three animals were used for each compound. The counts were decay corrected and the biological disappearance plotted on a logarithmic ordinate scale of percent remaining versus the arithmetic abscissa scale of time. Indium-111 BLEDTA IV was studied alone and complexed with 1, 10, 50 and 100 micrograms of CHA255. Indium-111 benzyl EDTA was studied alone and complexed with 10 and 100 micrograms of CHA255.

The effect of 0.5 mg (0.9 micromoles) of intravenous nonradioactive indium benzyl EDTA on the whole body biological half-life of In-111 BLEDTA IV, In-111 benzyl EDTA, and In-111 Fab complexed with either 10 or 100 micrograms of CHA255 was studied at 3 hours and at 22 hours following injection. In some cases 70 micrograms of human transferrin conjugated with 4.23 nanomoles of non-radioactive indium benzyl EDTA (chelate/HTr molar ratio 5:1) was used as the flushing agent.

2. Mouse Organ Distribution Studies

Tumor and organ assays were carried out 24 hours following intravenous injection in BALB/c mice bearing KHJJ tumor in the flank as described previously (10). Uptake of indium-111 BLEDTA IV CHA255 complex was measured in the tumor, blood and liver for concentrations of CHA255 of 1, 10, 50, and 100 micrograms and the percent dose per gram plotted versus the antibody concentration. A minimum of three mice was used for each experimental determination. In-111 labeled BLEDTA IV alone was also studied.

Detailed 24-hour tumor and organ distribution studies were carried out for indium-111 labeled benzyl EDTA, BLEDTA II, BLEDTA IV, and Fab, both with and without 100 micrograms of CHA255. Three to six mice were injected for each determination. In each of the experimental groups, the effect of a flushing dose of 0.5 mg of nonlabeled indium 3+ benzyl EDTA was studied when given three hours prior to sacrifice. The 24-hour concentrations were determined in the blood, heart, lungs, liver, spleen, kidneys, tumor, muscle, bone, skin, and gut. The percent dose per gram organ was calculated and the tumor to organ ratio was determined.

Organ cumulated activities (\tilde{A}) were calculated using the measured biological half-life of whole-body radioactivity and concentration of radioactivity in five selected organs (lungs, liver, spleen, kidneys, and red marrow) at the times of interest. The combined activity in the five organs was subtracted from the total-body activity to give an "organ" called "Rest of Body" in which the activity was assumed to be uniformly distributed. The organ doses were then calculated using the "S" values (absorbed dose per unit cumulated activity) from MIRD 11 (11). The "S" value for total body was used for the "Rest of Body".

In the half-life and distribution studies the antibody was always present in molar equivalence or in molar excess over the EDTA groups. Antibody to EDTA group molar ratio varied from 1:1 to 60:1. It should be noted that the molar concentration of the carrier-free indium-111 labeled chelate present was much lower than total chelate concentration, resulting in antibody to indium-111 molar ratios from 60:1 to 9000:1.

3. Imaging

Whole-body pinhole images of mice were made with the gamma camera immediately following and 24 and 48 hours after intravenous injection with approximately 500 microcuries of indium-111 labeled compounds. The animals were sedated with chloral hydrate, and 200,000 counts were obtained in all images with the pinhole positioned three inches above the posterior aspect of the

mouse. The percent of the injected dose remaining was calculated from the decay corrected count rates on the images expressed as a fraction of the count rate obtained immediately following injection. Indium-111 labeled compounds or compounds complexed with 100 micrograms of antibody were studied. Images were also made 3 hours and 24 hours following a flushing dose of 0.5 mg of non-radioactive indium 3+ benzyl EDTA. Note that in the imaging studies a larger amount of indium-111 chelate than used in the distribution studies was complexed with 100 micrograms of antibody to obtain the larger amount (500 pci) of activity, resulting in an antibody to EDTA molar ratio less than 1:1 (0.14:1). However the antibody to indium-111 molar ratio still greatly exceeded 1:1 (70:1). The images were stored digitally, enabling later region of interest analysis.

RESULTS

A. MONOCLONAL ANTIBODIES

The binding constants for various metal chelates to the monoclonal antibodies have been published elsewhere (4). The antibodies were amazingly selective for indium: simply changing the metal from indium 3+ in the chelate decreased the antibody binding constant K_b by more than three orders of magnitude. Monoclonal antibody CHA255, which had the highest binding constant for indium-111 chelate ($K_b=4\times 10^9$), was selected for use in these experiments. CHB235 ($K_b=1.1 \times 10^8$) was also studied.

B. ANIMAL STUDIES

1. Biological Half-life

One microgram of CHA255 had no measurable effect on the BLEDTA IV half-life which was approximately 5 hours, with a small amount having a longer terminal half-life. Increasing the amount of antibody had a profound effect; 10 micrograms increased the half-life to 2.1 days; 50 micrograms to 2.4 days; 100 micrograms to 4 days. In comparison 100 micrograms of CHB235 had little effect. Ten micrograms CHA255 increased the half-life of In-111 benzyl EDTA from approximately 1 hour to 6.8 hours and 100 micrograms increased the half-life to 2.3 days.

Intravenous administration of 0.5 mg of nonradioactive indium 3+ benzyl EDTA 22 hours following administration of the BLEDTA IV complex promptly lowered the remaining whole-body radioactivity 54 percent (from 65 percent to 30 percent remaining) within 3 hours. It was noted that following the rapid response to flushing, the activity remaining in the body decayed at about the same rate as the initial activity prior to flushing.

The effect of antichelate antibody and chase on the whole-body biological half-life of In-111 labeled Fab fragments is seen in Figure 1. Antibody increased Fab $T_{1/2}$ from 2.3 to 8.4 days. A nonradioactive indium benzyl EDTA chase at 24 hours caused a prompt reduction in whole-body activity of 12 percent in 7 hours and 16 percent in 24 hours. The remaining activity disappeared with a $T_{1/2}$ of 6.3 days. An In chelate transferrin chase had a more profound and lasting effect: 19 percent drop in 7 hours, 33 percent in 24 hours. The effect continued, producing a disappearance curve similar to Fab alone with a $T_{1/2}$ of 3.1 days.

2. Mouse Distribution and Dosimetry

When BLEDTA IV was complexed with increasing amounts of anti-chelate antibody the tumor concentrations exceeded both blood and liver concentrations until the concentration of binding sites reached 10^{-7} moles (50 micrograms) at which point the blood concentration exceeded the tumor concentration. It

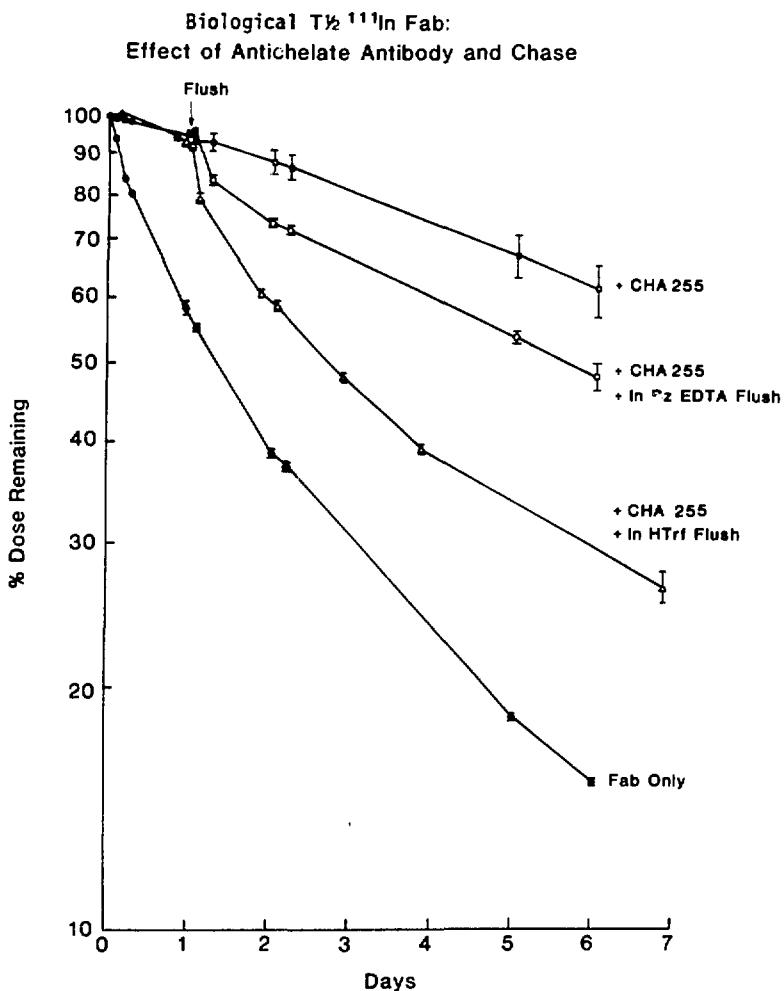


Figure 1

Whole-body counts, 3 mice in each group following intra-venous In-111 chelate labeled Fab fragments. Complexing In-111 Fab with antibody greatly prolongs half-life: chelate chase 24 hours later causes prompt excretion. (Points = mean \pm 1 S.D.)

was noted that at no time did the liver concentration exceed the tumor concentration. At a concentration of 3×10^{-8} moles of binding sites (equivalent to 7 mg/3 liters for human subjects), adequate tumor concentrations were achieved (3 percent per gram) at a point at which neither the blood nor liver concentration exceeded the tumor concentrations.

Measurements obtained for indium-111 benzyl EDTA at 3 hours showed concentrations in all organs were less than 1 percent per gram. Complexation with the anti-chelate antibody markedly increased all organ concentrations, even at 24 hours, most notably the blood and the tumor. Liver concentrations were less than half that of the blood. The flushing dose (0.5 mg nonradioactive In benzyl EDTA) lowered the blood concentrations by more than 99 percent, lowered the liver concentrations by 78 percent, with a drop of 55 percent in the tumor concentration. This produced an acceptable tumor concentration of 5 percent/gram with tumor/blood ratio greater than 45:1 and high tumor/organ ratios.

The reduction in radiation dose to the organs as a result of the chelate chase is shown in Table 1. The average radiation dose was reduced 86 percent.

Table 1

Reduction in Radiation Dose Following Chelate Chase of
In-111 Benzyl EDTA-CHA255 Complex (100 µg)

ORGAN	Estimated Radiation Dose (rad/mCi)		
	WITHOUT CHASE	WITH CHASE	% REDUCTION
Lung	0.25	0.03	88
Liver	0.61	0.03	95
Spleen	0.50	0.10	80
Kidney	0.48	0.06	88
Red Marrow	0.26	0.04	85
Rest of Body	0.19	0.03	84

One hundred micrograms CHA255 produced a marked increase in all organ concentrations of BLEDDTA II at 24 hours, especially in the blood and the tumor. The flushing dose of 0.5 mg nonradioactive benzyl EDTA produced a 90 percent drop in the blood levels 3 hours after administration, a 58 percent drop in the liver concentration, with only a 46 percent drop in the tumor concentration. This produced a good tumor concentration of over 5 percent/gram with markedly increased tumor/organ ratios (tumor/blood ratios were greater than 7:1). The organ dose reduction from the chase is shown in Table 2 and averaged 49 percent.

Table 2

**Reduction in Radiation Dose Following Chelate Chase of
In-111 BLEDTA II-CHA255 Complex (100 µg)**

<u>ORGAN</u>	<u>Estimated Radiation Dose (rad/mCi)</u>		
	<u>WITHOUT CHASE</u>	<u>WITH CHASE</u>	<u>% REDUCTION</u>
Lung	0.46	0.22	52
Liver	0.68	0.43	37
Spleen	1.27	0.64	50
Kidney	1.07	0.44	59
Red Marrow	0.53	0.27	49
Rest of Body	0.39	0.20	49

A similar result was obtained with In-111 BLEDTA IV antibody complex. Once again the antibody markedly increased all organ concentrations, especially the tumor and blood and the flushing dose decreased most organ concentrations to a greater extent than the tumor, preserving a good tumor concentration with marked increased tumor/organ ratios with a tumor/blood ratio of greater than 5:1. An average radiation dose reduction of 37 percent from the chase is shown in Table 3.

Table 3

**Reduction in Radiation Dose Following Chelate Chase of
In-111 BLEDTA IV-CHA255 Complex (100 µg)**

<u>ORGAN</u>	<u>Estimated Radiation Dose (rad/mCi)</u>		
	<u>WITHOUT CHASE</u>	<u>WITH CHASE</u>	<u>% REDUCTION</u>
Lung	0.30	0.12	60
Liver	0.78	0.65	17
Spleen	0.66	0.41	38
Kidney	0.61	0.61	0
Red Marrow	0.28	0.11	61
Rest of Body	0.21	0.14	33

The organ distribution of In-111 Fab and In-111 Fab-antibody complex, with and without chelate chase, is shown in Table 4. The carrier function of the antibody caused a marked increase in blood concentration resulting in a doubling in tumor concentration, however, the tumor to blood ratio was less than one. This was improved to 3.5:1 by the chelate chase with no lowering of tumor uptake. The complex produced an increase in liver concentration that was not reduced by the chase. The reduction in organ radiation dose produced by the chase is shown in Table 5.

Table 4

In-111 Mouse IgG Fab Fragment-Antibody Complex
24 HR Organ & Tumor Concentration

	In-111 IgG Fab (N=4)			In-111 IgG Fab + 100 µg CHA255 (N=4)			In-111 IgG Fab + 100 µg CHA255: 3 Hrs Post Flush (N=4)		
	%/gm	S.D.	T/O Ratio	%/gm	S.D.	T/O Ratio	%/gm	S.D.	T/O Ratio
Blood	0.47 ± 0.04		9.31	9.90 ± 0.66		0.92	3.26 ± 0.52		3.45
Heart	1.51 ± 0.12		2.88	2.17 ± 0.26		4.19	1.29 ± 0.22		8.67
Lungs	0.93 ± 0.11		4.70	4.31 ± 0.29		2.11	2.15 ± 0.31		5.21
Liver	7.42 ± 0.47		0.58	34.66 ± 5.51		0.26	37.31 ± 2.53		0.30
Spleen	3.13 ± 0.26		1.41	3.16 ± 0.39		2.88	2.87 ± 0.63		3.93
Kidneys	85.48 ± 13.29		0.05	4.90 ± 0.25		1.86	28.59 ± 3.43		0.39
Tumor	4.34 ± 0.64			9.07 ± 0.92			11.16 ± 1.92		
Muscle	0.31 ± 0.06		14.16	1.03 ± 0.04		8.86	0.64 ± 0.10		17.55
Bone	1.09 ± 0.15		3.97	1.15 ± 0.18		7.93	0.79 ± 0.03		14.12
Skin	0.85 ± 0.22		5.38	1.19 ± 0.14		7.72	0.96 ± 0.17		11.72
Gut	0.86 ± 0.17		5.14	1.15 ± 0.36		8.27	1.57 ± 0.05		7.08

Table 5

**Reduction in Radiation Dose Following Chelate Chase of
In-111 Fab CHA255 Complex (100 µg)**

In-111 Fab + ANTI-CHELATE ANTIBODY

Estimated radiation dose (rad/mCi)

<u>Organ</u>	<u>Without Chase</u>	<u>With Chase</u>	<u>% Reduction</u>
Lung	0.50	0.39	22
Liver	3.91	3.90	0
Spleen	0.87	0.81	7
Kidney	1.07	3.10	0
Red Marrow	0.44	0.35	17
Rest of Body	0.41	0.54	0

There was a significant lowering of lung, red bone marrow, and whole-body dose with a modest increase in the kidney dose.

The dose excretion relationship of BLEDTA IV complex and In benzyl EDTA appears nearly logarithmic with respect to the flushing dose of In benzyl EDTA (Fig. 2). This suggests the kidney is competing for the flushing chelate, lowering the blood concentration before flushing is complete.

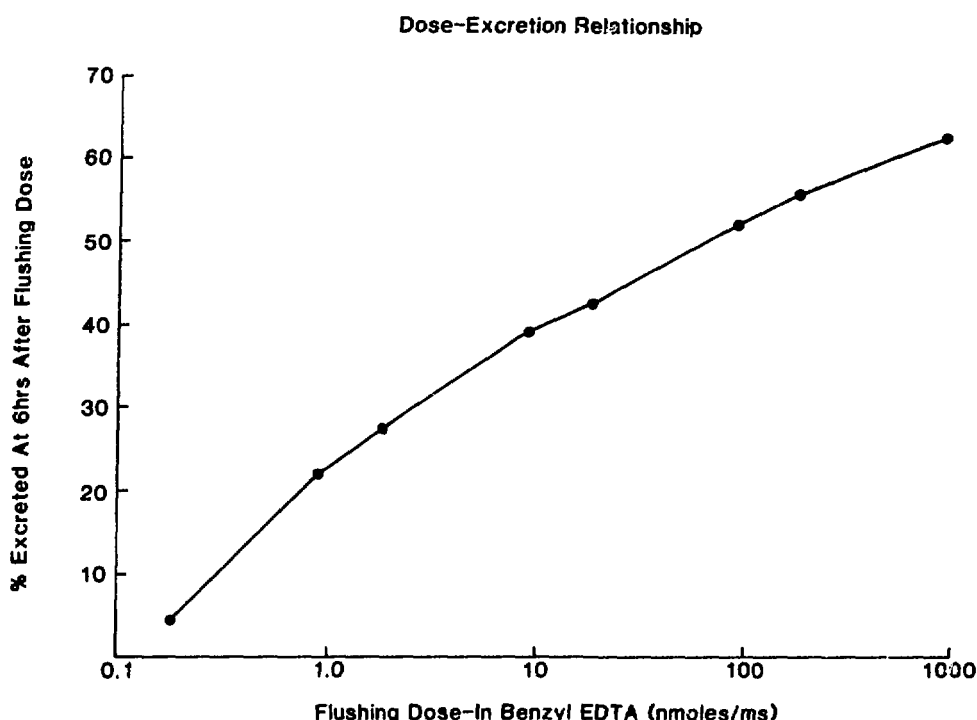


Figure 2

3. Animal Imaging

Posterior whole body images of tumor mice obtained following In-111 benzyl EDTA antibody complex with and without chelate chase are shown in Figure 3. The antibody caused 67 percent retention at 24 hours (A) and 52 percent at 48 hours (C). The image 3 hours after the chase (B) shows a striking redistribution in the kidneys (K), urinary bladder (BL), and gallbladder (GB). Twenty-four hours later (D) this had cleared, with only 9.6 percent of the activity remaining. ROI analysis showed 18 percent of the total activity was in the tumor, and 3.6 percent in the liver. Half-life curves taken from the digitized images compared to In-111 benzyl EDTA alone are shown in Figure 4.

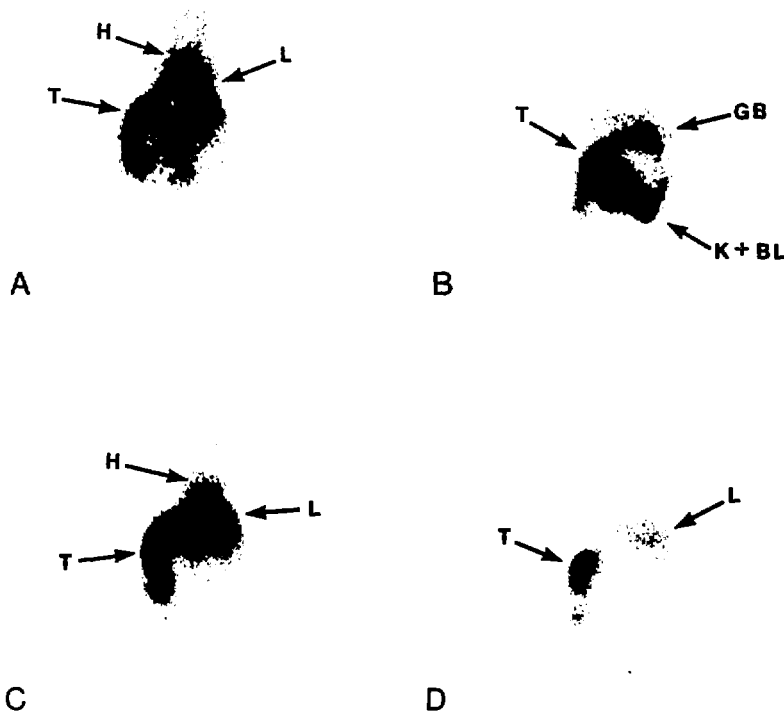


Figure 3

Posterior pinhole images of tumor mice: 200k counts in each image following intravenous 500 μ ci In-111 benzyl CHA255 complex (100 μ g). A: 67% remaining at 24 hours; H=heart, L=liver, T=tumor. B: 27% remaining at 24 hours, 3 hours after chelate chase; GB = gallbladder, K+BL=kidneys+bladder, T=tumor. C: 52% remaining at 48 hours; H=heart, L=liver, T=tumor. D: 9.6% remaining at 48 hours, 27 hours following chelate chase; T=tumor contained 18%, L=liver contained 3.6%.

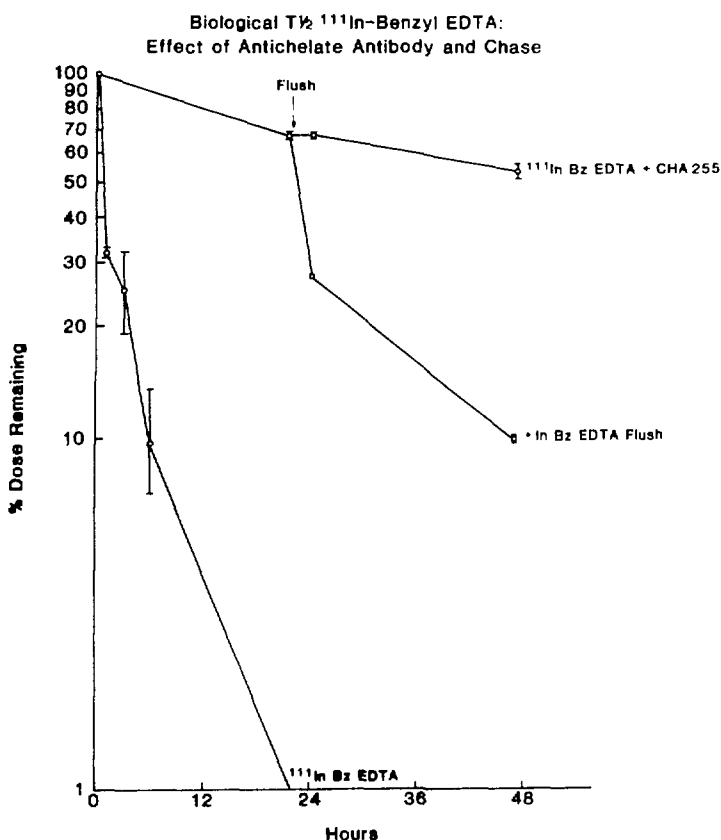


Figure 4

DISCUSSION

Tumor imaging with radiolabeled monoclonal antibodies produces a very large nontarget background activity in the blood pool, liver and spleen (12,13). Since the target specificity and absolute concentration are more than adequate, reducing the background would produce an enhanced image with lower radiation exposure. Several approaches to this problem are currently undergoing investigation: 1) Fab and $\text{F}(\text{ab}')_2$ fragments (1,2), 2) second antibody (14,15), 3) lymphoscintigraphy (16,17), 4) metabolizable chelates (18) and 5) monoclonal antibodies as reversible carriers (19).

Since Fab and $F(ab')_2$ fragments disappear much more rapidly from the plasma than whole antibody, being excreted more rapidly by the kidneys (20) while retaining the specific binding site, they produce much higher target to background ratios and lower radiation dose. However their use is inevitably associated with a lower target uptake, apparently due to the shorter residence time in the circulation (3). In some studies the target (tumor) uptake was from 3 to 24 times higher with whole antibody than with Fab (1,2).

The use of a second antibody is effective in lowering the blood background quickly but produces high liver background and radiation dose, as essentially none of the activity is excreted (14,15).

Another method of avoiding large amounts of circulating activity is the simple expedient of administering the labeled monoclonal subcutaneously (21). This provides very high concentrations to the lymphatics as well as avoiding circulating antigen. This approach, while producing increased concentrations in the lymphatics, is limited to those lymph nodes draining accessible injection sites, and also does not lower the radiation exposure.

Recently we have investigated the use of metabolizable chelates for labeling an anti-mouse lymphoma monoclonal antibody. These contain an enzyme cleavable link such as an ester group between the protein and the chelate (18). Initial results show a more rapid drop in blood levels and whole-body activity compared to stable chelate, with a modest reduction in tumor concentration. This method results in lower radiation exposure due to excretion of the metabolized chelate.

The properties of our anti-chelate monoclonal CHA255, with its remarkable preference for indium benzyl EDTA, have provided us with an ideal carrier for In-111 chelate labeled radiopharmaceuticals (22). The present study has shown it is possible to alter profoundly the pharmacokinetics of In-111 chelate-labeled tracers as well as to provide a new degree of control over the timing of excretion. The reversible equilibrium binding of haptens by antibodies allows competitive inhibition by the introduction of a nontoxic, nonradioactive chelate at a predetermined time. In contrast to their usually rapid excretion, small molecular weight haptens (such as drugs) may circulate for many days when bound to antibodies (23,24). In addition, monoclonal antibodies being monospecific do not form large aggregates providing the antigen molecule contains less than three determinants (chelate groups). Since most chelate labeled biological molecules retain optimum function and have adequate specific radioactivity when labeled with 3 chelates or less per molecule, this should not be a problem (17,25).

Varying either the amount of antibody, its specificity, or its affinity will change the pharmacokinetics and the effect of the flushing agent. For example, decreasing the sensitivity to the metal ion may make it possible to flush with Fe or Ca EDTA, potentially less toxic ions than In.

Our results using human transferrin conjugated with nonradioactive In-benzyl EDTA as a chelate chase showed that much less was required to produce the same flushing effect. This was anticipated since we had previously shown that chelate labeled In-111 transferrin had a prolonged circulation time and thus would have a higher effective inhibitor concentration than In-benzyl EDTA (Fig. 2). Only 1/200 the molar amount of In-EDTA bound to transferrin compared to In-benzyl EDTA was needed to produce the same lowering of whole-body activity. A possible problem with the use of this type of flushing agent is the potential for antigenicity. This may be minimized by the small amounts required and the use of human protein carriers.

In the present work, we have clearly demonstrated that the use of anti-chelate antibody for reversibly binding benzyl EDTA, chelate derivates of bleomycin and chelate labeled Fab will greatly prolong the circulating half-time. Furthermore we have shown that prior to imaging, a chelate chase can be administered to reduce the blood background and radiation exposure. A schematic illustration of this two-step approach to reversible radiolabeling is shown in Figure 5.

REVERSIBLE RADIOLABELING

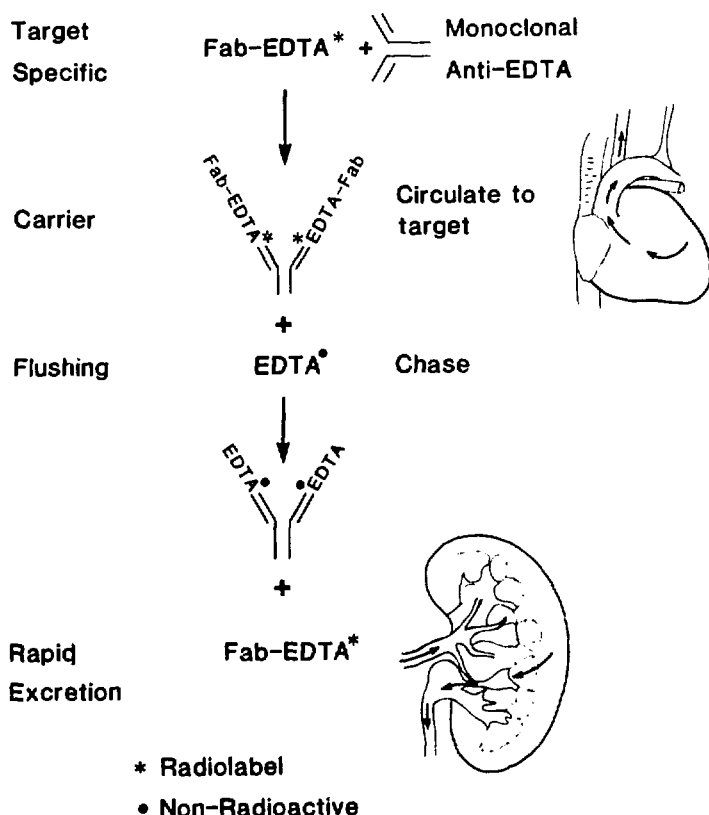


Figure 5

Complexing a rapidly excreted chelate labeled Fab fragment greatly prolongs its circulation time during which localization in its target may occur. After a preselected interval, a chase with an excess of a competing nonradioactive chelate displaces Fab allowing rapid renal excretion.

We have calculated the theoretical equivalent human doses from the biological half-lives and organ concentrations obtained in these experiments. The liver and spleen were the target organs with the dose ranging from 0.50 to 3.91 rads per millicurie. The average organ radiation dose was decreased up to 95 percent following the chelate chase. These results have very important implications in radioimmunotherapy where the limiting factor is radiation to normal tissue.

Since the antibody used in these experiments had no specificity for the tumor, it is presumed to accumulate passively. In this work we have not demonstrated specific uptake of the BLEDTA derivatives, benzyl EDTA or Fab independent of the carrier antibody. Double label experiments are planned using Co-57-teta labeled antibody (26), with In-111 labeled BLEDTA and tumor specific In-111 Fab to elucidate the delivery role, if any, of the carrier antibody. It is postulated that the antibody may act in a way analogous to endogenous carrier proteins for low molecular weight hormones (such as thyroxin binding globulin and transcartin) by reducing renal excretion, thus promoting prolonged circulation times and increasing the biological half-life.

Extension of the present work to develop bispecific antibodies either by hybridoma technology (27) or chemical recombination (28) may provide further improvements. These hybrid immunoglobulins could be engineered to contain one chelate binding site, and one target specific site. Such molecules would have many potential uses, including immunodiagnostic procedures, and targeted delivery of drugs.

We have developed a novel use for metal chelate specific monoclonal antibodies as radiopharmaceutical carriers. These molecules allowed rapid selective renal clearance of chelate labeled radiopharmaceuticals by competitive inhibition with a nonradioactive chelate chase (flushing dose) at the time of imaging. This markedly improved both tumor images and radiation dosimetry in mice and has great potential for human use.

ACKNOWLEDGEMENTS

This work was supported in part by a grant from the Veterans Administration (DAG) and PhS Grants number CA28343 (DAG) and CA16861, RCDA CA00462 (CFM).

REFERENCES

1. Wilbanks A.B., J.A. Peterson, S. Miller, L. Kauffman, D. Ortendahl, and I.L. Ceriani. Localization of mammary tumors *in vivo* with ^{131}I -labeled Fab fragments of antibodies against mouse mammary epithelial (MME) antigens. *Cancer* 48:1768-1775, 1981.
2. Wahl R.L., C.W. Parker, and G.W. Philpott. Improved radioimaging and tumor localization with monoclonal $\text{F}(\text{ab})_2$. *J. Nucl. Med.* 24:316-325, 1983.
3. Nelp W.B., J.F. Eary, P. Beaumier, K.A. Krohn, I. Hellstrom, and K.E. Hellstrom. Antibody deposition in tumor in relation to blood clearance using a nephrectomized mouse model. *J. Nucl. Med.* 26:67, 1985. Abstract.

4. Reardan D.T., C.F. Meares, D.A. Goodwin, M. McTigue, G.S. David, M.R. Stone, J.P. Leung, R.M. Bartholomew, and J.M. Frincke. Antibodies against metal chelates. *Nature* 316:265-268, 1985.
5. DeRiemer L.H., C.F. Meares, D.A. Goodwin, and C.I. Diamanti. BLEDTA II: Synthesis of a new tumor visualizing derivative of Cobalt (III) bleomycin. *J. Lab. Compd. Radiopharm.* 18:1517-1534, 1981.
6. Meares C.F., D.T. Reardon, M.T. McCall et al. Conjugation of antibodies with bifunctional chelating agents bearing isothiocyanate or bromoacetamide groups and subsequent addition of metal ions. *Anal. Biochem.* 142: 68-78, 1984.
7. Gerhard W. Monoclonal antibodies. Kennett R., McKearn T.J., and Bechtol K.G., editors, 370, 1980, Plenum, New York.
8. Wang R., E.D. Sevier, R.A. Reisfeld, and G.S. David. Semi-quantitative solid-phase radioimmunoassay for carcinoembryonic antigen. *J. Immun. Meth.* 18:157, 1977.
9. Eisen H.N. Equilibrium dialysis for measurement of antibody-hapten affinities. *Meth. Med. Res.* 10:106-114, 1964.
10. Goodwin D.A., M.W. Sundberg, C.I. Diamanti et al. Indium-111 radiopharmaceuticals in cancer localization. In 18th Annual Clinical Conference Monograph: Radiologic and Other Biophysical Methods in Tumor Diagnoses. Chicago, Yearbook Medical Publishers, 57-88, 1975.
11. Snyder W.S., M.R. Ford, G.G. Warner, and S.B. Watson. "S" absorbed dose per unit cumulated activity for selected radionuclides and organs. MIRD pamphlet #11. Soc. Nucl. Med., 1975. New York.
12. Burcheil S.W. and B.A. Rhodes, editors. Radioimmunoimaging and Radioimmunotherapy, 1983. Elsevier, New York.
13. DeLand F.H., E.E. Kim, G. Simmons, and D.M. Goldenberg. Imaging approach in radioimmunodetection. *Cancer Res.* 40:3046-3049, 1980.
14. Goodwin D.A., C.F. Meares, C.I. Diamanti et al. Use of specific antibody for rapid clearance of circulating blood background from radiolabeled tumor imaging proteins. *Eur. J. Nucl. Med.* 9:209-215, 1984.
15. Begent R.H.J., A.J. Green, K.D. Bagshawe, B.E. Jones, P.A. Keep, F. Searle, R.F. Jewkes, G.M. Barratt, and B.E. Ryman. Liposomally entrapped second antibody improves tumour imaging with radiolabeled (first) antitumour antibody. *Lancet* 2:739-742, 1982.
16. Weinstein J.N., R.J. Parker, A.M. Keenan et al. Monoclonal antibodies in the lymphatics: Toward the diagnosis and therapy of tumor metastases. *Science* 218:1334-1337, 1982.
17. Goodwin D.A., C.F. Meares, M.J. McCall, M.K. Haseman, M. McTigue, C.I. Diamanti, and W. Chaovapong. Chelate conjugates of monoclonal antibodies for imaging lymphoid structures in the mouse. *J. Nucl. Med.* 26:493-502, 1985.
18. Haseman M.K., D.A. Goodwin, C.F. Meares, M.S. Kaminski, T.G. Wensel, M.J. McCall, and R. Levy. Metabolizable In-111 chelate conjugated anti-idiotype

monoclonal antibody for radioimmunodetection of lymphoma in mice. Submitted
J. Nucl. Med.

19. Goodwin D.A., C.F. Meares, M. McTigue, and M.R. Stone. Hapten monoclonal antibody complexes as drug carrier systems. Amer. Chem. Soc. Annual National Meeting, Miami Beach, Florida, 48, 1985. Abstract.
20. Arend W.P. and F.J. Silverblatt. Serum disappearance and catabolism of homologous immunoglobulin fragments in rats. Clin. Exp. Immunol. 22: 502-513, 1975.
21. Epenetos A.A. Antibody guided lymphangiography in the staging of cervical cancer. Br. J. Cancer 51:805-808, 1985.
22. Goodwin D.A., C.F. Meares, G.S. David, M. McTigue, M.J. McCall, J.M. Frincke, M.R. Stone, R.M. Bartholomew, and J.P. Leung. Monoclonal antibodies as reversible equilibrium carriers of radiopharmaceuticals. Int. J. Nucl. Med. Biol., 1985. In Press.
23. Schmidt D.H., B.M. Kaufman, V.P. Butler, Jr. Persistence of hapten-antibody complexes in the circulation of immunized animals after a single intravenous injection of hapten. J. Exp. Med. 139:278-294, 1974.
24. Berson S.A., R.S. Yalow, A. Bauman, M.A. Rothschild and K. Newerly. Insulin- I^{131} metabolism in human subjects: Demonstration of insulin binding globulin in the circulation of insulin treated subjects. J. Clin. Invest. 35:170, 1956.
25. Goodwin D.A., C.F. Meares, C.I. Diamanti et al. Biological properties of molecules labelled with metal ions using bifunctional chelates. In Medical Radionuclide Imaging, IAEA Vienna, Vol. 2, 61-69, 1976.
26. Moi M.K., C.F. Meares, M.J. McCall, W.C. Cole, and S.J. DeNardo. Copper chelates as probes of biological systems: Stable copper complexes with a macrocyclic bifunctional chelating agent. Anal. Biochem. 148:249-253, 1985.
27. Milstein C. and A.C. Cuello. Hybrid hybridomas and their use in immuno-histochemistry. Nature (London) 305:537-540, 1983.
28. Brennan M., P.F. Davison, and H. Paulus. Preparation of bispecific antibodies by chemical recombination of monoclonal immunoglobulin G₁ fragments. Science 229:81, 1985.

**CIS-PLATINUM-193m: ITS MICRODOSIMETRY AND POTENTIAL FOR
CHEMO-AUGER COMBINATION THERAPY OF CANCER**

Roger W. Howell and Kandula S.R. Sastry

Department of Physics and Astronomy

University of Massachusetts, Amherst, MA 01003

and

Helene Z. Hill and Dandamudi V. Rao

Department of Radiology

University of Medicine and Dentistry of New Jersey, Newark, NJ 07103

ABSTRACT

Cis-Platinum is widely used in chemotherapy of cancer. Its usefulness is limited by its chemotoxic effects. The action of this drug involves its binding to DNA base sequences. The overwhelming evidence for the cytoidal effects of DNA-incorporated ^{125}I through localized irradiation of the intranuclear radiosensitive sites by the numerous low energy Auger electrons from its decay suggests the interesting prospect of chemo-Auger combination therapy using cis-Pt labeled with suitable radionuclides. In this approach, the localized action of Auger electrons augments the chemical action of cis-Pt for cell killing. Accordingly, possibilities exist for a reduction of the chemotoxicity of the drug. The radionuclides ^{195}mpt and ^{193}mpt are natural candidates in this regard since both are prolific emitters of low energy Auger electrons by virtue of their decay modes. Preliminary studies with cis- ^{195}mpt on experimental mouse tumor models are encouraging. The problem with ^{195}mpt is its low specific activity. In contrast, ^{193}mpt can be produced at a much higher specific activity, even carrier-free, compared to ^{195}mpt . Monte Carlo calculations show that about 25 Auger electrons are to be expected per decay of ^{193}mpt . The microdosimetry of these electrons indicates that the localized absorbed energy density around the decay site is more than in the case of ^{125}I . These considerations point to the promise of cis- ^{193}mpt for chemo-Auger combination therapy. The cellular dosimetry of ^{193}mpt , localized on the surfaces of cells, is also discussed in the context of the current interest in radioimmunotherapy.

INTRODUCTION

Since the discovery of the antitumor activity (1) of the platinum coordinated complex, cis-dichlorodiamineplatinum II, this compound, generally known as cis-platinum, has been widely used in the chemotherapy of various types of cancer including lymphomas, lung carcinoma, and genitourinary, head and neck cancers (see Ref. (2) and articles therein). Severe nausea and vomiting, myelosuppression, impairment of hearing, and nephrotoxicity are amongst the several toxic side effects that limit the utility of this drug (2). Intense research efforts are going on to find ways of mitigating the limitations.

In this paper, we suggest chemo-Auger combination therapy as a prospective new approach towards a reduction of the chemotoxic effects of cis-Pt while maintaining therapeutic efficacy. The basis for this idea stems from numerous radiobiological experiments *in vitro*, which have repeatedly emphasized the high LET type cell killing by the decay of ^{125}I when incorporated into the DNA of proliferating cells (3-7). Although ^{125}I decay by orbital electron capture (EC) and internal conversion (IC) does not involve emission of high LET radiations, the inner atomic shell vacancies produced in the residual atom by the primary EC and IC decay modes result in copious emission of electrons because of atomic Auger processes (8,9). A large number of these Auger electrons have very low energies (~ 200 eV), intermediate LET values (~ 25 keV/ μm), and extremely short ranges (a few nm) in biological matter (8). Accordingly, when the decay occurs inside or within 2-3 nm of the DNA duplex, the collective effect of the highly localized irradiation of the radiosensitive DNA by the low energy electrons results in high LET type molecular damage and cell killing. There is now general agreement that the severe damage of the DNA molecule (10) is because of the highly localized energy density (HILED) prevailing around the site of the decay of the radionuclide (8,11,12). Experiments *in vitro* with the Auger-emitter, ^{77}Br , bound to the DNA of V79 Chinese hamster lung fibroblasts (13), and with ^{201}Tl , a prolific Auger-electron emitter, localized in these cells (14) have demonstrated severe cytoidal effects. There is now clear evidence for the enhanced efficacy of cell killing by Auger-electron emitters such as ^{201}Tl and ^{55}Fe *in vivo*, as revealed by the recent studies of Rao et al. (15-17) in the mouse testis model.

The above developments not only draw attention to the necessity of improvement in biological risk estimates of the several radionuclides decaying by EC and IC in Nuclear Medicine (18) but also point out a possible role for such radionuclides in therapy. The therapeutic prospects are particularly interesting when the radionuclide can be transported by a molecular carrier to the DNA and attached to the double helix. The action of cis-Pt is generally accepted to involve its binding to the guanine base sequences in the DNA (19-21) rather than intercalation between base pairs. The twin radionuclides ^{193}mPt and ^{195}mPt decaying by IC (22,23) are Auger-emitters. The specificity of the drug-DNA interaction ensures that either of these radionuclides can be bound to the double helix when used in the form of cis- ^{193}mPt and cis- ^{195}mPt . At present very limited data are available regarding the Auger-electron emissions from ^{193}mpt and ^{195}mpt (24,25). We present here complete Auger and Coster-Kronig (8,9) electron spectra for these radionuclides based on Monte Carlo calculations. About 25 such electrons should be expected on the average from the decay of either radionuclide. Microdosimetric calculations show that the HILED in the immediate vicinity of the decay sites of the radionuclides is substantially in excess of values reported for ^{125}I (8,12). Preliminary studies are performed on experimental tumor bearing mice using cold cis-Pt alone (10-15 mg per kg of body weight), and with the same cold drug dose containing about

100 μ Ci of 195m Pt as cis- 195m Pt. Mice treated with the drug containing the radiolabel display prolonged survival relative to those receiving cold cis-Pt alone.

The theoretical and experimental results presented here point out the potential of the chemo-Auger combination approach in improving the overall efficacy of cis-Pt. The utility of 195m Pt is limited because of its low theoretical specific activity. In contrast, 193m Pt can be produced at a much higher specific activity, and even as a carrier-free radionuclide. Thus cis- 193m Pt offers a high promise for chemo-Auger combination therapy. Finally, in view of recent interest in radioimmunotherapy, the cellular dosimetry of 193m Pt localized on the surfaces of cells is presented.

THEORETICAL ESTIMATES

MONTE CARLO CALCULATION OF THE ELECTRON SPECTRA

Monte Carlo methods are employed to calculate the average Auger electron spectra resulting from the decay of 193m Pt and 195m Pt. Computer simulation of the nuclear and atomic transitions is accomplished with a program similar to that of Charlton and Booz (26). The calculations have been performed on the Nuclear Physics VAX-11/750 computer facility of the University of Massachusetts.

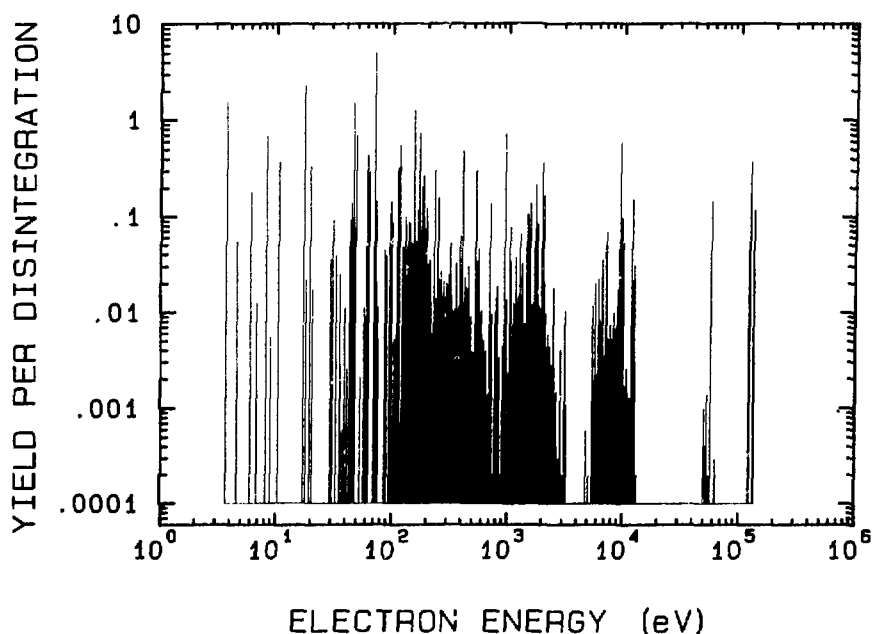


Figure 1. Average electron spectrum from the decay of 193m Pt based on Monte Carlo calculations. Electrons from internal conversion and atomic Auger, Coster-Kronig, and super Coster-Kronig processes are included.

Atomic and Nuclear Decay Processes

The 4.3 day 149.7 keV isomeric state of ^{193}mpt decays to the very long-lived (50 y) ground state of ^{193}Pt by way of three cascade transitions of energies 135.5 keV, 12.6 keV, and 1.64 keV, all of which are highly internally converted (22). The respective IC probabilities are 99.89%, 99.33%, and 99.99%. The γ -emission probabilities are essentially negligible.

The radionuclide ^{195}mpt undergoes several isomeric transitions in reaching the stable ground state of ^{195}Pt (23). The 4.02 d 259.3 keV metastable state of ^{195}Pt decays almost exclusively (99.76%) to the 129.79 keV level via the highly converted (99.9%) 129.5 keV M4 transition. The 129.79 keV level decays either directly to the ground state (8%) by an E2 transition, or to the 98.9 keV first excited state (92%) by a 30.89 keV mixed M1+E2 transition, the IC probabilities being 63.7%, and 97.5%, respectively. The 98.9 keV M1+E2 transition from the first excited state occurs with a probability of 92.5% per decay, 87.7% of which is internally converted. The E2/M1 mixing ratio is -0.021 for the 30.89 keV transition, and -0.130 for the 98.9 keV transition (23). Since the above transitions are not totally converted, γ -rays with an average yield of 0.16 are emitted per decay of ^{195}mpt .

As a result of each IC process, a vacancy is produced in an inner atomic shell or subshell. These vacancies in the inner atomic orbitals are energetically unstable, and are filled by electrons in higher energy levels. The complex series of atomic vacancy cascades that occur involve four competitive processes : radiative X-ray transitions, and non-radiative transitions of the Auger, Coster-Kronig (CK), and super-CK type, all of which move the primary vacancies to higher shells or subshells. The distinction between the various processes may be found, for example, in a recent review by Sastry and Rao (8). The X-ray transitions dominate the filling of the K-shell vacancies, and constitute an important pathway in the case of L-shell vacancies. Such transitions only move the initial vacancy to higher shells and subshells. The non-radiative transitions involve multiplication of vacancies in the higher shells and subshells since two new vacancies are produced for each filled vacancy. Whenever energetically possible, super-CK transitions dominate the other types. Thus, as the inner shell vacancies move upward to the valence and near valence shells of the atom, copious emission of electrons occurs. Since the transition energies are very small for the higher shell transitions, the electrons ejected possess very small energies and extremely short ranges (a few nanometers) in biological matter (8). It is this phenomenon that makes these radionuclides interesting from a microdosimetric point of view.

Monte Carlo Method

The Monte Carlo calculation simulates the decay of an unstable isotope using random selection processes. In general, at any stage of the decay, the simulated decay process proceeds by randomly selecting a transition from the set of all possible transitions for the nuclear and atomic configuration at that stage. As the random selections are made, data concerning the emitted radiations are recorded. The selection process continues until the ground state of the isotope is reached.

An explicit description of how Monte Carlo methods were used to compute the electron spectrum of ^{193}mpt follows; the spectrum of ^{195}mpt was determined similarly. A disintegration is defined as the set of all transitions involved in the decay of ^{193}mpt to its ground state. We

describe how the computer code handles a single nuclear transition and the atomic cascades that follow. The metastable state ^{193}mpt decays, in principle, by either γ -emission or IC via the 135.5 keV transition to the 14.3 keV level in ^{193}Pt . A decision is made based on the experimental total internal conversion coefficient α (22,23). A random number between 0 and 1 is generated by the computer; all random numbers generated in the program lie in this range. If this number is less than $1/(1+\alpha)$, γ -emission is chosen, otherwise internal conversion is selected. In the case of ^{193}mpt , α is very large compared to 1 for each transition and hence γ -emission is ignored. The IC transitions create vacancies in inner atomic shells. The shell in which the vacancy occurs is chosen using theoretical subshell conversion coefficients α_i , and a new random number. The subshell conversion coefficients are normalized to create a set of probabilities for determining the vacancy position by summing them for the IC transition of interest, and dividing each α_i by the sum, so that the sum of the probabilities is 1. As an example, consider a hypothetical IC transition where $\alpha_K = 100$, $\alpha_{L1} = 200$, $\alpha_{L2} = 300$, $\alpha_{L3} = 400$, and all other subshell coefficients are 0. Upon summing the coefficients and dividing each one by the sum we obtain probabilities $p_K = 0.1$, $p_{L1} = 0.2$, $p_{L2} = 0.3$, and $p_{L3} = 0.4$. If the random number falls between 0 and 0.1, a K-shell vacancy is created, while random numbers between 0.1 and 0.3, 0.3 and 0.6, 0.6 and 1.0, represent creation of an L₁-, L₂-, L₃-shell vacancy respectively. After choosing the particular IC transition as described, the properties of the ejected electron and the dynamic subshell vacancy distribution are recorded.

At this stage, in the ^{193}mpt analysis, the Pt nucleus would be in the 14.3 keV state with a single vacancy in one of the atomic subshells. This vacancy is filled either by a radiative or a non-radiative transition depending on the value of the new random number and the fluorescent yield ω_i of the subshell in which the vacancy resides. If the random number is less than ω_i ($0 \leq \omega_i \leq 1$) a radiative transition is chosen, otherwise a non-radiative transition is chosen. Let us assume that a radiative transition is chosen. The relative probabilities for all possible radiative transitions which fill the vacancy are constructed by summing the theoretical radiative rates of those transitions which fill the vacancy, and dividing each one by the sum. A random number is generated and a transition is chosen and recorded in the same manner as described for IC transitions.

A new vacancy in a higher atomic subshell is created as a result of the radiative transition. As described earlier, a vacancy may be filled by either a radiative or a non-radiative transition. Assume that on this occasion a non-radiative transition is selected. The set of theoretical non-radiative transition rates corresponding to all possible ways of filling the vacancy (Auger, CK, super-CK) are summed, and each transition rate is divided by the sum. Yet another random number is generated and a transition is selected in the manner described earlier. Following a non-radiative transition, two new vacancies are created in higher subshells. After several of these transitions, multiple vacancies exist in the atomic subshells, thus invalidating the theoretical transition rates which are based on the assumption of frozen orbitals. In order to compensate for this, correction factors based on the fraction of electrons remaining in the subshells are applied to each transition rate prior to normalizing them as described previously (see Estimates and Assumptions). It is important to keep in mind that, during this cascade process, the innermost vacancy is always under consideration for the vacancy filling process.

The innermost vacancy moves toward the valence or near valence subshells until no more electrons are available for transitions. When this occurs all

subshells are refilled with their requisite number of electrons. The 12.6 keV and the 1.6 keV cascade nuclear transitions that follow are treated in the same manner, completing a single disintegration of ^{193}mpt . Ten thousand nuclear disintegrations are considered in these calculations, involving a total of 252630 atomic transitions.

Table 1A. Hypothetical Vacancy Distribution

M3	xxxx
M2	xx
M1	xx
L3	xxxx
L2	xx
L1	xx
K	xx

Table 1B. Correction Factors for Multiple Vacancies Based on the Diagram in Table 1A

Transition	Correction Factor
KL ₁ L ₂ (A)	1
KL ₂ L ₃ (A)	1/4
KL ₃ L ₃ (A)	0
KL ₃ M ₂ (A)	1/2 * 1/4 = 1/8
KM ₃ M ₃ (A)	(3!/2!(3-2)!) / (4!/2!(4-2)!) = 1/2
KL ₃ (K)	1/4

Input Data

Both theoretical and experimental data were used in the Monte Carlo code.

IC: Experimental total IC coefficients α were obtained from Nuclear Data Sheets (22,23). Theoretical subshell IC coefficients α_i were obtained from Rösel (27). In those cases where transitions are of mixed multipolarity, the theoretical subshell IC coefficients are appropriately corrected for such admixtures.

Auger-CK: K-,L-shells. There are no CK transitions for the K-shell. Theoretical radiationless transition rates for Z=78 computed by Chen et al. (28) were used for K-, and L-shell relative transition probabilities.

M-,N-shells. Theoretical transition rates of McGuire were used for M- and N-shell relative probabilities (29,30).

O-shell. The O-shell transitions are of the CK type and rigorous calculations are not yet available. Following Kassis et al. (14), the O-shell relative transition probabilities were estimated using statistical weight arguments based solely on the number and distribution of electrons available to the vacancy to be filled; all quantum mechanical effects were ignored in this first approximation (see Estimates and Approximations).

Energies: The electron binding energies compiled by Sevier (31) and the $Z/(Z+1)$ rule are used to obtain the energies of electrons from the Auger and CK transitions (8,26,32).

X-ray: K- and L-shell theoretical radiative rates are given by Scofield (33). Manson and Kennedy (34) calculate M-shell X-ray emissions for electric dipole transitions. N-shell X-ray emission is negligible.

Fluorescence Yield: Fluorescence yield data are obtained from Bambynek et al. (9).

For Z=78, experimental values are only available for the K-shell. Theoretical fluorescence yields, interpolated from the tables of Ref. (9) were used for the L- and M-shells.

Range: The ranges of electrons in unit density matter were computed using equation 1 (35).

Estimates and Assumptions

After numerous Auger and CK transitions, multiple vacancies exist within the atomic shells. The theoretical transition rates used in this work assume frozen orbitals, making them inaccurate when multiple vacancies exist. Hence, an empirical correction for each transition is made based on the fraction of electrons remaining in the orbitals involved (36). This is

Table 2

Summary of Average Electron Spectrum Due to Auger (A) and Coster-Kronig (CK) Transitions in the Decay of ^{193}mpt

Atomic Transitions Resulting in the Electrons	Yield per 10000 Decays	Ave. Energy (keV)	Range (nm)
$N_{6,7} A' M_2 CK, N_{2,4} CK, O_2 CK$	25709	0.005	0.5
$N_{6,7} A' O_2 CK, N_1 CK$	30782	0.016	0.9
$L_1 CK, M_{2,4} CK, N_{1,2} CK, O_1 CK$	2271	0.031	1.5
$L_1 CK, M_3 CK, N_1 CK, O_{1,3} CK$	25848	0.046	2.0
$N_{6,7} A' M_{1,3} CK, N_{1,2,3} CK, O_2 CK$	61569	0.069	2.9
$N_{1,3} CK, O_1 CK$	5331	0.096	4.0
$N_{4,5} A' N_{1,3,5} CK, M_{1,2} CK$	12131	0.117	4.9
$N_{4,5} A' N_{1,3,4,5} CK, M_{1,2,3} CK$	16473	0.151	6.5
$N_{4,5} A' N_{1,2,3,4,5} CK$	17346	0.177	7.7
$N_{4,5} A' M_{1,2} CK, N_{2,4,5} CK$	6551	0.232	10
$N_{3,4,5} A' L_1 CK, M_{1,2,3} CK, N_{1,2,3,4} CK$	3761	0.297	14
$N_{2,3} A' L_1 CK, M_{1,2,3} CK, N_{1,2,3} CK$	8004	0.405	20
$M_{4,5} A' N_{1,2,3} A' M_{1,2} CK, N_{1,2} CK$	6334	0.579	32
$M_{4,5} A' L_2 CK, M_{1,2} CK$	834	0.855	55
$M_{1,2,3,4,5} A' L_{1,2} CK, M_1 CK$	16671	1.64	140
$M_{1,2,3,4,5} A' L_1 CK$	3669	2.15	210
$M_1 A$	137	3.14	390
$L_3 A$	6	4.84	790
L_A	4564	7.59	1700
L_A	372	10.9	3100
K_A	48	55.4	52000

illustrated in Tables 1A and 1B. Consider the hypothetical vacancy distribution shown in Table 1A, and assume the transitions listed in Table 1B are allowed under the frozen orbital approximation. The correction factors computed are given in Table 1B. Theoretical transition rates, corrected appropriately by such factors, are used in the calculations.

Table 3

Atomic Shell Vacancy Distributions For
10000 Decays of ^{193}mpt

Transition Energy (keV)	Shell Vacancies														
1.64	N1 7397	N2 792	N3 93	N4 21	N5 9	N67 1	O1 1423	O2 122	O3 13	O4 2	O5 1	P1 126			
12.64	M1 6149	M2 989	M3 546	M4 17	M5 12	N1 1559	N2 217	N3 123	N4 7	N5 4	O1 317	O2 30	P1 24		
135.5	K 1508	L1 1738	L2 409	L3 3860	M1 499	M2 103	M3 1219	M4 36	M5 50	N1 134	N2 20	N3 293			
	N4 12	N5 40	O1 28	O2 4	O3 43	O4 1	P1 3								

Theoretical data available for transitions involving the N₆- and N₇-subshells are presented as a combined value, N₆₇, since the binding energies for these shells are very nearly the same. Accordingly, the computer code treats N₆₇ as a single subshell containing fourteen electrons in the initial state.

The lifetimes of the intermediate nuclear states in ^{193}mpt are 9.7 ns (1.64 keV) and 2.5 ns (14.3 keV) (22), and for ^{195}mpt , 0.67 ns (129.79 keV) and 0.163 ns (98.90 keV) (23). These are much longer than the time scale ($\sim 10^{-15}$ s) in which the atomic transitions occur. It is therefore, reasonable to assume that the atom recovers its normal electronic configuration after each IC transition.

For the sake of a self-consistent approach, all Auger and CK energies are computed using the Z/(Z+1) rule. This assumption leads to some problems in that certain transitions listed in the theoretical rates had to be eliminated since the Z/(Z+1) rule yielded negative electron energies. The transitions thus excluded are L₁L₂N₃, M₁M₂N₂, M₂M₃N₂, M₁M₃O₂, and N₁N₂N₆₇, comprising about 4%, 4%, 1%, 1%, 4%, respectively, of the total radiationless transition rate for the subshell in question. Exclusion of these transitions does not have a major effect on the spectrum as a whole.

Results of Monte Carlo Calculation

A complete summary of the radiations expected from the decay of ^{193}mpt is presented in this work. In view of the existing data for ^{195}mpt (24,25), we only summarize the Auger electron spectrum for this radionuclide. A log-log plot of the average yield of Auger, CK and conversion electrons is shown in Figure 1 as a function of the electron energy for ^{193}mpt . Table 2 is a summary of the complex Auger and CK electron spectrum. This spectrum, in spite of our limitations of treatment of the O-shell CK transitions, compares well with available experimental data on the Auger electron spectrum for stable Pt (37). Our calculation predicts an average yield of about 25 Auger and CK electrons per ^{193}mpt decay (Table 2). The ranges of various electron groups in unit density matter (35) are also included in Table 2. The primary atomic vacancy distribution due to the IC process is given in Table 3, and the average IC electron spectrum is presented in Table 4. The average K, L, and M X-ray yields are 0.15, 0.23, and 0.05 per decay of ^{193}mpt , with the energies 68.3 keV, 10.1 keV, and 2.1 keV, respectively.

Table 4

Average Yield of Internal Conversion Electrons for ^{193}mpt

Transition Energy (keV)	Yield per 10000 Decays	Ave. Energy (keV)	Range (μm)
1.64 keV	10000	1.0	0.07
12.63 keV	10000	10.0	2.7
135.50 keV	1508	57.1	56
135.50 keV	8492	126	211

The average Auger and CK spectrum for ^{195}mpt (Table 5) is very similar to the ^{193}mpt (Table 2) except that about 29 Auger and CK electrons are expected, on the average, per ^{195}mpt decay. Photon and internal conversion electron yields and energies may be found in the literature (24,25).

LOCALIZED ENERGY DEPOSITION

The pattern of localized energy deposition by the electrons around the decay site of ^{193}mpt is computed at the nanometric level using an approach described earlier (13,38). For unit density matter, and energies from 20 eV to 20 MeV, Cole (35) has experimentally found that the electron energy E (in keV) and the range R (in microns) are related by

$$E = 5.9 (R + 0.007)^{0.565} + 0.00413 R^{1.33} - 0.367 \quad (1)$$

Differentiation of equation 1 yields equation 2, the rate of energy

$$\frac{dE}{dR} = 3.333 (R + 0.007)^{-0.435} + 0.0055 R^{0.33} \quad (2)$$

Table 5

**Summary of Average Electron Spectrum Due to Auger (A) and Coster-Kronig (CK)
Transitions in the Decay of ^{195}mpt**

Atomic Transitions Resulting in the Electrons	Yield per 10000 Decays	Ave. Energy (keV)	Range (nm)
$\text{N}_{6,7} \text{ A}' \text{ M}_2 \text{ CK}' \text{ N}_{2,4} \text{ CK}' \text{ O}_2 \text{ CK}$	30244	0.005	0.5
$\text{N}_{6,7} \text{ A}' \text{ O}_2 \text{ CK}' \text{ N}_1 \text{ CK}$	39761	0.017	0.9
$\text{L}_1 \text{ CK}' \text{ M}_{2,4} \text{ CK}' \text{ N}_{1,2} \text{ CK}' \text{ O}_1 \text{ CK}$	1805	0.033	1.5
$\text{L}_1 \text{ CK}' \text{ M}_3 \text{ CK}' \text{ N}_1 \text{ CK}' \text{ O}_{1,3} \text{ CK}$	15103	0.047	2.1
$\text{N}_{6,7} \text{ A}' \text{ M}_{1,3} \text{ CK}' \text{ N}_{1,2,3} \text{ CK}' \text{ O}_2 \text{ CK}$	65782	0.069	2.9
$\text{N}_{1,3} \text{ CK}' \text{ O}_1 \text{ CK}$	2724	0.096	4.0
$\text{N}_{4,5} \text{ A}' \text{ N}_{1,3,5} \text{ CK}' \text{ M}_{1,2} \text{ CK}$	8865	0.119	5.0
$\text{N}_{4,5} \text{ A}' \text{ N}_{1,3,4,5} \text{ CK}' \text{ M}_{1,2,3} \text{ CK}$	19902	0.152	6.5
$\text{N}_{4,5} \text{ A}' \text{ N}_{1,2,3,4,5} \text{ CK}$	20615	0.176	7.6
$\text{N}_{4,5} \text{ A}' \text{ M}_{1,2} \text{ CK}' \text{ N}_{2,4,5} \text{ CK}$	8992	0.234	11
$\text{N}_{3,4,5} \text{ A}' \text{ L}_1 \text{ CK}' \text{ M}_{1,2,3} \text{ CK}' \text{ N}_{1,2,3,4} \text{ CK}$	4376	0.296	14
$\text{N}_{2,3} \text{ A}' \text{ L}_1 \text{ CK}' \text{ M}_{1,2,3} \text{ CK}' \text{ N}_{1,2,3} \text{ CK}$	9237	0.405	20
$\text{M}_{4,5} \text{ A}' \text{ N}_{1,2,3} \text{ A}' \text{ M}_{1,2} \text{ CK}' \text{ N}_{1,2} \text{ CK}$	4943	0.609	34
$\text{M}_{4,5} \text{ A}' \text{ L}_2 \text{ CK}' \text{ M}_{1,2} \text{ CK}$	976	0.872	56
$\text{M}_{1,2,3,4,5} \text{ A}' \text{ L}_{1,2} \text{ CK}' \text{ M}_1 \text{ CK}$	30886	1.65	142
$\text{M}_{1,2,3,4,5} \text{ A}' \text{ L}_1 \text{ CK}$	7187	2.12	209
$\text{L}_3 \text{ A}$	1655	5.96	1120
L_A	5861	7.15	1520
L_A	5494	8.87	2200
L_A	1540	10.9	3100
K_A	270	57.1	56000

expended as the electron traverses an infinitesimal path dR of its range in the continuously slowing down approximation.

Consider an electron of energy E emitted in a decay process. As the particle moves radially outward, the energy absorbed in a sphere of radius r , centered around the site of decay, is obtained by integrating dE/dR along a radial path up to the surface of the sphere. At this distance r from the decay site, the electron has a residual range $R(E) - r$ and an energy $E(R(E)-r)$, evaluated from equation 1. The energy $\epsilon_E(r)$ deposited by the electron of initial energy E in this sphere is

$$\epsilon_E(r) = E - E(R(E)-r), \quad 0 \leq r \leq R(E)$$

while the energy absorbed $\Delta\epsilon_E(r)$ in the annular region of the spherical shell with radii r and $r + \Delta r$ is given by

$$\Delta\epsilon_E(r) = (\Delta r) \frac{dE}{dR} \Big|_{R(E)-r} \quad 0 \leq r \leq R(E)$$

Hence, for Auger-electron emitters, the average energy absorbed, $\xi(r)\Delta r$, in a shell of radius r and thickness Δr centered on the decay site of an Auger-emitter is given by

$$\xi(r)\Delta r = (\Delta r) \sum_i n(E_i) \frac{dE}{dR} \Big|_{R(E_i)-r} \quad (3)$$

where $n(E_i)$ is the yield per decay of the i^{th} Auger electron group of energy E_i .

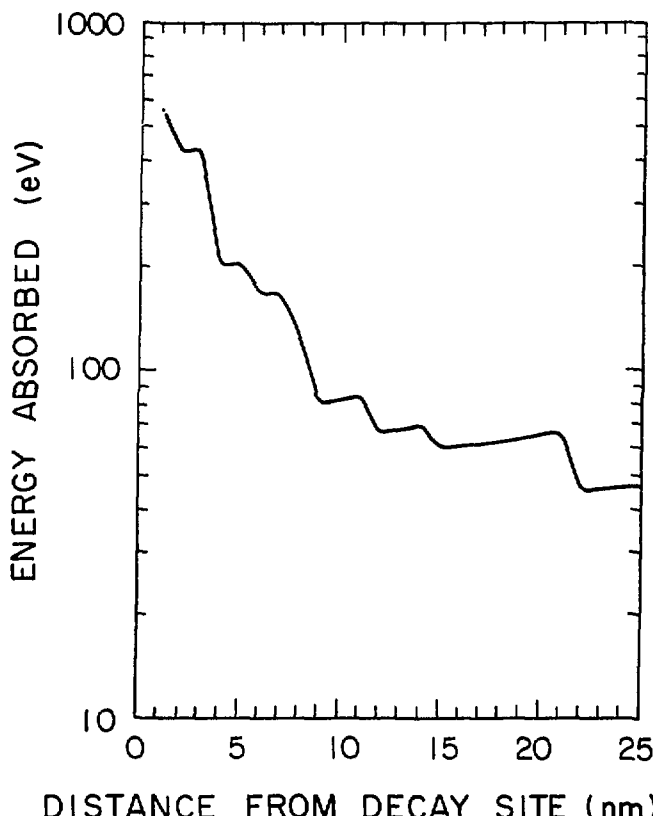


Figure 2. Differential spatial distribution of absorbed energy in unit density matter around the decay site of ^{193}mPt . The average absorbed energy in concentric spherical shells of thickness 1 nm is plotted as a function of the radial distance from the ^{193}mPt decay site. Note the sharp discontinuities as various electron groups reach the end of their range (see Table 2).

Using the electron data in Tables 2 and 4, and equation 3, we have calculated the average energy deposited in annular regions of unit density matter, of thickness 1 nm, up to radial distances of 25 nm centered around a ^{193}mpt decay site (Figure 2). Figure 3 shows the differential profile of the locally absorbed energy density. The pattern of localized energy deposition around the decay site of ^{195}mpt is essentially the same as for ^{193}mpt .

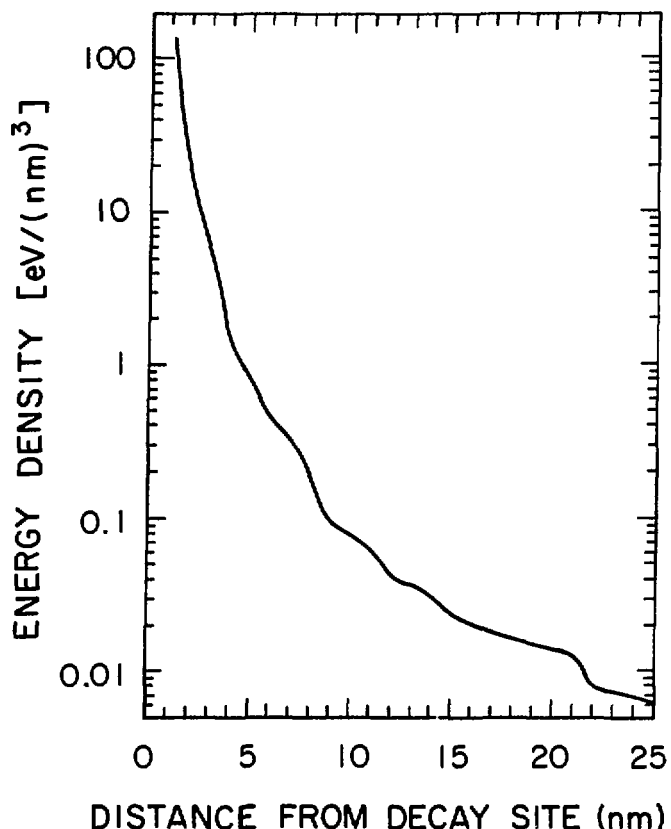


Figure 3. Differential profile of the average absorbed energy density in the vicinity of the decay of ^{193}mpt . The results shown are derived from the data in Figure 2.

SPECIFIC ACTIVITIES

Suitability of a radioisotope for therapy depends, in part, on the specific activity attainable. Two key factors, target enrichment and reaction cross section, are limitations imposed by the isotope itself and determine the resultant specific activity upon bombardment of the target.

^{195}mpt is produced by irradiating stable ^{194}Pt with neutrons according to the reaction $^{194}\text{Pt}(n,\gamma)^{195}\text{mpt}$. The cross section for this reaction is only 0.09 barn (39). ^{193}mpt may be produced similarly by the reaction $^{192}\text{Pt}(n,\gamma)^{193}\text{mpt}$ which has a cross section of 2 b (39). For a neutron flux $\Phi = 2.5 \times 10^{15}$ neutrons/cm²s, and bombardment time $t = 36$

hours, for example, one can compute the activity A produced by the familiar relation

$$A = f(N\sigma\Phi)(1 - e^{-(\ln 2)t/T}) \quad (4)$$

where f is the enrichment factor of the target Pt isotope of interest, N the number of Pt atoms in one mg $\approx 3 \times 10^{18}$ per mg, σ the reaction cross section, and T the half-life of the radioplatinum isotope. Use of the above cross sections in equation 4 gives the following initial specific activities with f = 1: A = 4 mCi/mg for ^{195}mpt and 90 mCi/mg for ^{193}mpt . For f = 0.33 (^{194}Pt) and f = 0.008 (^{192}Pt) in natural Pt, the corresponding specific activities are 1.3 mCi/mg and 0.7 mCi/mg. With the available enrichments of f = 0.95 (^{194}Pt) and f = 0.57 (^{192}Pt), the yields are 3.8 mCi/mg (^{195}mpt) and 50 mCi/mg (^{193}mpt). Higher specific activities are attainable with higher neutron fluxes and longer bombardment times. The relative specific activities of the two radionuclides remain the same for the same irradiation conditions.

Besides the fact that ^{193}mpt may be obtained at an order of magnitude higher specific activity than ^{195}mpt through neutron irradiation, ^{193}mpt may also be produced carrier-free by reactions such as $^{192}\text{Os}(\alpha, 3n)^{193}\text{mpt}$, followed by chemical separation. Stable ^{192}Os has a natural abundance of 41% (Ref. (39), p. 112). This reaction peaks at about 40 MeV α -particle energy in the laboratory frame, with a cross section of about 0.5 b. This suggests that very high specific activity *cis*- ^{193}mpt can be synthesized. In view of these considerations, *cis*- ^{193}mpt is much more useful for therapeutic purposes than *cis*- ^{195}mpt , which, of course, is the preferred radiopharmaceutical for imaging purposes because of its high yield of useful photons (24,25).

POTENTIAL OF ^{193}mpt FOR RADIOIMMUNOTHERAPY

The advent of monoclonal antibodies that may bind specifically to antigens on the surfaces of tumor cells has evoked much interest in radioimmunotherapy. In this approach, therapeutically suitable radionuclides, attached to appropriate antibodies, are transported and bound to the tumor cell surfaces using the antibodies as molecular carriers. The cell killing is done by the action of the radiations. Inspection of the electron spectra for ^{193}mpt (Tables 2 and 4) shows that several electrons have ranges of the order of cellular dimensions. Thus ^{193}mpt offers possibility of localized irradiation of the intracellular radiosensitive sites. Furthermore, the prospect of obtaining this radionuclide in carrier-free form makes it a particularly attractive candidate for this purpose.

Sastray et al. (40) have examined the cellular dosimetry of electron-emitting radionuclides localized on cell surfaces. Consider an array of cells of unit density and spherical shape, each of volume v_0 . Let us assume that a fraction p of the cells are labeled, with a_0 being the average radioactivity (in μCi) per labeled cell, uniformly distributed on the cell surface. The average dose rate D_k (in rad/hr) to the labeled cell is given by (40)

$$D_k = (a_0/v_0) \sum \Delta_k (\phi_{ii} + p\phi_{oi})_k \quad (5)$$

where $\Delta_k = 2.13 \times 10^{-3} n_k E_k$ for the kth particle emitted by a radionuclide emitting several monoenergetic electrons of energies E_k (keV) and yield n_k per decay. ϕ_{ii} is the self-absorbed fraction for

radiations emitted from decays on the surface of the labeled cell (i^{th} labeled cell to itself), and ϕ_{oi} is the contribution from other labeled cells to the i^{th} target cell. The average dose rate D_n to the unlabeled cell, and D to any cell are given by

$$D_n = (a_o/v_o) p \sum \Delta_k (\phi_{oi})_k \quad (6) \quad \text{and}$$

$$D = (a_o/v_o) p \sum \Delta_k (\phi_{ii} + \phi_{oi})_k \quad (7)$$

Sastray et al. (40) have tabulated the absorbed fractions ϕ_{ii} and ϕ_{oi} for finite clusters of cells in close packed cubic arrays. Using the data in Tables 2 and 4, we have calculated the average dose rates, D_L , D_n , and D , for one pCi of ^{193}mpt assumed to be uniformly distributed on the surfaces of labeled cells of $10 \mu\text{m}$ diameter. Results are presented in Table 6 for several different cluster diameters d .

Table 6

Summary of Average Dose Rates to Labeled and Unlabeled Cells
(in rad/hr per pCi of ^{193}mpt on cell surface)

Cell diameter = $10 \mu\text{m}$

$d(\mu\text{m})$	D_L	D_n	D
50	$24.3 + 32.8 \text{ p}$	32.8 p	57.1 p
108	$24.3 + 62.1 \text{ p}$	62.1 p	86.4 p
200	$24.3 + 118 \text{ p}$	118 p	142 p
400	$24.3 + 217 \text{ p}$	217 p	241 p
1000	$24.3 + 297 \text{ p}$	297 p	321 p
2000	$24.3 + 328 \text{ p}$	328 p	352 p
5000	$24.3 + 341 \text{ p}$	341 p	365 p

Inspection of Table 6 shows that the labeled cells receive a dose rate of about 24 rad/hr, while the dose rate to unlabeled cells depends on the fraction p of the cells labeled. If we assume that 10% of the cells are labeled, then the dose rate to labeled cells in a $50 \mu\text{m}$ diameter cluster of cells is about 28 rad/hr, and about 58 rad/hr for a $5000 \mu\text{m}$ diameter cluster. These two sizes of clusters represent a microscopic tumor containing about 100 cells, and a macroscopic one with about 10^8 cells, respectively. The dose rates to unlabeled cells are about 3 rad/hr and 34 rad/hr, for the respective clusters. If we simply assume an effective half-life of 24 hr for the radioactivity in the tumor, the cumulated doses to labeled cells in the two respective clusters are about 1000 and 2000 rad. The corresponding doses to the unlabeled cells are 100 and 1200 rad. These estimates indicate that the tumor cells may be killed quite efficiently through localized action.

For ^{193}mPt with its physical half-life of 4.3 d, about 2×10^{-4} radioactive atoms need to be bound to the cell surface in order that the activity on the surface is 1 pCi. Binding sites in excess of this are believed to exist on tumor cell surfaces.

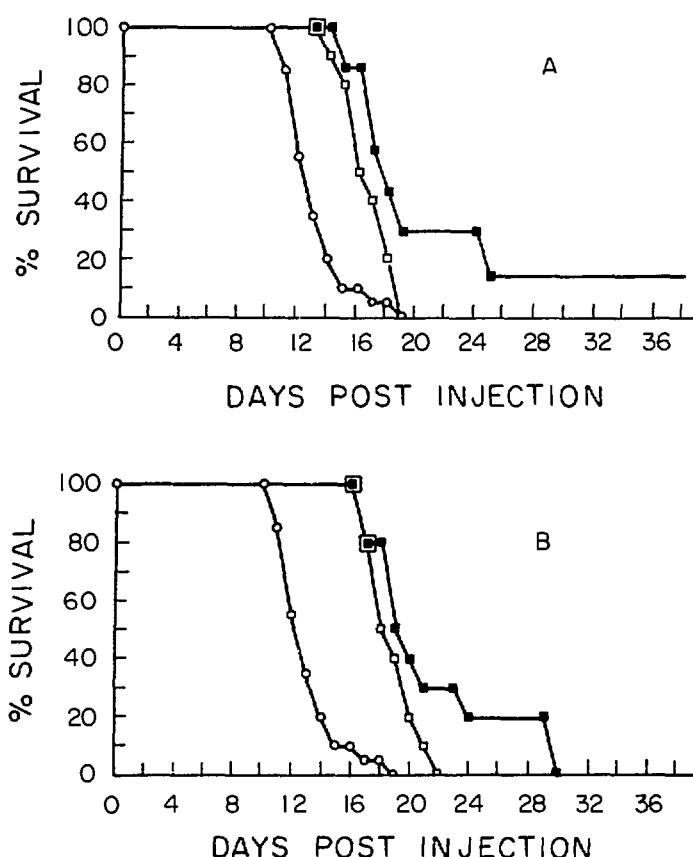


Figure 4. Survival of tumor bearing mice treated with cold cis-Pt, or with the same cold drug dose containing cis- ^{193}mPt . The open squares are for the cold drug alone. The solid squares are for the drug containing cis- ^{193}mPt . The open circles are for untreated animals serving as controls. Figures A and B represent the data for two different drug doses administered: 10 mg and 15 mg of cis-Pt per kg of body weight, respectively.

PRELIMINARY EXPERIMENTAL STUDIES

MATERIALS AND METHODS

C57BL/GJ mice, each weighing 20 grams, were injected intraperitoneally (i.p.) with 5×10^6 B16 melanoma cells. One day later, varying doses of cold cis-Pt (5 mg/kg to 25 mg/kg body weight) were administered through the i.p. mode. It is found that the animals die of toxicity when the dose level exceeds 15 mg/kg. Subsequently, mice, in groups of 10 were injected with the same number of melanoma cells. One day after this, the tumor bearing mice were given cold cis-Pt at doses of 10 or 15 mg/kg alone or the same drug doses containing cis-^{195m}Pt (80 μ Ci or 120 μ Ci, respectively). The biological clearance of the radioactivity was studied using a gamma camera. The survival of the animals was followed for over 30 days following the administration of the drug. Untreated mice served as controls.

EXPERIMENTAL RESULTS

The biological clearance studies revealed that 65% of injected activity was eliminated from the body with a biological half-life of 2 hours, while the rest had a half-life of 9 days. Using these and the nuclear data for ^{195m}Pt (25), the whole-body dose to the mouse from the injected activity is estimated to be about 60 rads for 10mg/kg and 90 rads for 15 mg/kg cis-Pt doses containing the radiolabel. The radiation doses received by the non-solid tumors may be somewhat higher but they are significantly smaller than conventional radiation therapy doses of about 1000 rads to the tumors.

The fraction of the mice surviving is plotted in Figure 4 as a function of the post-injection time. These data show that the radiolabeled drug has extended the life span of the animals more than the cold cis-Pt alone.

DISCUSSION AND CONCLUSION

We have presented here complete Auger and CK electron spectra from the IC decays of ^{193m}Pt and ^{195m}Pt. The average number of electrons emitted per decay of ^{193m}Pt is about 25 (Table 2), and about 29 (Table 5) from ^{195m}Pt decay. Microdosimetric calculations show that the HILED around the decay site (Figure 3) is very large indeed. For example, in a unit density sphere of 1 nm diameter around the decay site, over 600 eV of energy may be deposited, on the average, per decay of either radionuclide (Figure 2). This is roughly twice the value of about 300 eV (8) in a similar sphere in the case of ¹²⁵I. Therefore, these radionuclides bound to DNA bases via cis-^{193m}Pt and cis-^{195m}Pt should be highly effective in cell killing. Our preliminary results do indicate increased survival of tumor bearing mice treated with cis-Pt containing cis-^{195m}Pt compared with those treated with the cold drug at the same dose. This is encouraging. Although these initial experiments do not constitute direct evidence for the HILED mechanism as being responsible for the cell killing effects, it is a very likely explanation consistent with our current knowledge of the radiobiology of Auger-emitters in the DNA. Systematic studies with radiolabeled cis-Pt are needed to improve our understanding.

The limited theoretical specific activity of ^{195m}Pt poses a problem in that the platinum toxicity is always dominant. The prospect that ^{193m}Pt can be obtained at very high specific activities, in principle, indicates the potential of cis-^{193m}Pt for chemo-Auger combination therapy. With the

localized action of low energy electrons providing the cell killing mechanism, *cis*-¹⁹³mpt augments the chemical action of *cis*-Pt. This suggests that the dose of cold *cis*-Pt may be significantly reduced while maintaining therapeutic efficacy, with a reduction in the chemotoxic effects of the drug. ¹⁹³mpt can be made essentially carrier-free, and when localized on cell surfaces, it can effectively irradiate the radiosensitive targets in the cell. These considerations augur well for radioimmunotherapy with ¹⁹³mpt.

ACKNOWLEDGEMENT

This work is supported by U.S. Public Health Service Grant No. CA32877.

REFERENCES

1. Rosenberg, B., L. Van Camp, J.E. Trosko, and V.H. Mansour. *Nature*. 222, 385-386, 1969.
2. Proceedings of the National Cancer Institute Conference on *cis*-Platinum and Testicular Cancer, in *Cancer Treat. Rep.* 63(9,10), 1979, edited by T. Anderson, N. Javadpour, and L. Zswelling.
3. Krisch, R.E. Lethal effects of iodine-125 decay by electron capture in Escherichia coli and bacteriophage T₁. *Int. J. Radiat. Biol.* 21, 167-189, 1972.
4. Hofer, K.G., and W.L. Hughes. Radiotoxicity of intracellular tritium, ¹²⁵Iodine and ¹³¹Iodine. *Radiat. Res.* 47, 94-109, 1971.
5. Chan, P.C., E. Lisco, H. Lisco, and S.J. Adelstein. The radiotoxicity of iodine-125 in mammalian cells. II. A comparative study on cell survival and cytogenetic responses to ¹²⁵IUDR, ¹³¹IUDR, and ³HTdR. *Radiat. Res.* 67, 332-343, 1976.
6. Hofer, K.G., C.R. Harris, and J.M. Smith. Radiotoxicity of intracellular ⁶⁷Ga, ¹²⁵I and ³H. Nuclear versus cytoplasmic effects in murine L1210 leukaemia. *Int. J. Radiat. Biol.* 28, 225-241, 1975.
7. Warters, R.L., K.G. Hofer, C.R. Harris, and J.M. Smith. Radionuclide toxicity in cultured mammalian cells: Elucidation of primary site of radiation damage. *Curr. Top. Radiat. Res. Q.* 12, 389-407, 1977.
8. Sastry, K.S.R., and D.V. Rao. Dosimetry of low energy electrons, in *Physics of Nuclear Medicine: Recent Advances*, edited by D.V. Rao, R. Chandra, and M.C. Graham, pp. 169-208. American Association of Physicists in Medicine, Medical Physics Monograph No. 10, American Institute of Physics, 1984.
9. Bambynek, W., B. Crasemann, R.W. Fink, H.-U. Freund, H. Mark, C.D. Swift, R.E. Price, and P.V. Rao. X-ray fluorescence yields, Auger, and Coster-Kronig transition probabilities. *Rev. Mod. Phys.* 44, 716-813, 1972.
10. Martin, R.F., and W.A. Haseltine. Range of radiochemical damage to DNA with decay of iodine-125. *Science*. 212, 896-898, 1981.
11. Hofer, K.G., G. Keough, and J.M. Smith. Biological toxicity of Auger emitters: Molecular fragmentation versus electron irradiation. *Curr. Top. Radiat. Res. Q.* 12, 335-354, 1977.

12. Charlton, D.E. The range of high LET effects from ^{125}I decays. Radiat. Res. (to be published).
13. Kassis, A.I., S.J. Adelstein, C. Haydock, K.S.R. Sastry, K.D. McElvany, and M.J. Welch. Lethality of Auger electrons from the decay of Bromine-77 in the DNA of mammalian cells. Radiat. Res. 90, 362-373, 1982.
14. Kassis, A.I., S.J. Adelstein, C. Haydock, and K.S.R. Sastry. Thallium-201: An experimental and a theoretical radiobiological approach to dosimetry. J. Nucl. Med. 24, 1164-1175, 1983.
15. Rao, D.V., G.F. Govelitz, and K.S.R. Sastry. Radiotoxicity of Thallium-201 in mouse testes: Inadequacy of conventional dosimetry. J. Nucl. Med. 24, 145-153, 1983.
16. Rao, D.V., K.S.R. Sastry, G.F. Govelitz, H.E. Grimmond, and H.Z. Hill. Radiobiological effects of Auger electron emitters in vivo: Spermatogenesis in mice as an experimental model. Radiat. Prot. Dosim. (in press).
17. Rao, D.V., K.S.R. Sastry, G.F. Govelitz, H.E. Grimmond, and H.Z. Hill. Radiobiological effects of iron-55 and iron-59 in mouse testes: Biophysical dosimetry of Auger-electron emitters in vivo. J. Nucl. Med. (in press).
18. Auger cascades and nuclear medicine: Editorial. The Lancet, Vol II, No. 8454, pp. 533-534, September 7, 1985.
19. Goodgame, D.M.L., I. Jeeves, F.L. Phillips, and A.C. Skapski. Possible mode of action of anti-tumor platinum drugs: X-ray evidence for cis binding by platinum of two inosine 5'-monophosphate molecules via the N(7) position. Biochim. Biophys. Acta. 378, 153-157, 1975.
20. Dehand, J., and J. Jardanov. Interaction of cis-diaminotolueneplatinum (II) with nucleosides: Evidence for guanosine O(6).N(7) chelation by platinum. J. Chem. Soc. Chem. Commun. No. 15, p. 598, 1976.
21. Kelman, A.D., and H.J. Peresie. Mode of DNA binding of cis-platinum(II) antitumor drugs: A base sequence dependent mechanism is proposed. Cancer Treat. Rep. 63, 1445-1452, 1979.
22. Shirley, V.S. Nuclear data sheets for A=193. Nucl. Data Sheets. 32, 593-679, 1981.
23. Harmatz, B. Nuclear data sheets for A=195. Nucl. Data Sheets. 23, 607-669, 1978.
24. Lange, R.C., R.P. Spencer, and H.C. Harder. The antitumor agent $\text{cis-Pt}(\text{NH}_3)_2\text{Cl}_2$: Distribution studies and dose calculations for ^{193}mPt and ^{195}mPt . J. Nucl. Med. 14, 191-195, 1973.
25. Schlesinger, T., and W. Wolf. Dosimetry of Pt-195m: cis-dichlorodiammine-platinum (II) and other platinum compounds, in Proceedings of Radiopharmaceutical Dosimetry Symposium, edited by R.J. Cloutier, J.L. Coffey, W.S. Snyder, and E.E. Watson, pp. 452-462, U.S. Department of Health Education, and Welfare, Rockville, Maryland, 1976.
26. Charlton, D.E., and J. Booz. A Monte Carlo treatment of the decay of ^{125}I . Radiat. Res. 87, 10-23, 1981.

27. Rösel, F., H.M. Fries, K. Alder, and H.C. Pauli. Atomic Data Nucl. Data Tables 21, 291-514, 1978.
28. Chen, M.H., B. Crasemann, and H. Mark. Relativistic radiationless transition probabilities for atomic K- and L-shells. Atomic Data Nucl. Data Tables. 24, 13-37, 1979.
29. McGuire, E.J. M-shell Auger, Coster-Kronig, and radiative matrix elements, and Auger and Coster-Kronig transition rates in j-j coupling. Research Report SC-RR-710835, Sandia Laboratories, 1972.
30. McGuire, E.J. N-shell Auger, Coster-Kronig, and radiative matrix elements, and Auger and Coster-Kronig transition rates in j-j coupling. Research Report SAND-75-0443, Sandia Laboratories, 1975.
31. Sevier, K.D. Low Energy Electron Spectrometry, pp. 356-373, Wiley-Interscience, New York, 1972.
32. Chung, M.F., and L.H. Jenkins. Auger electron energies of the outer shell electrons. Surf. Sci. 22. 479-485, 1970.
33. Scofield, J.H. Relativistic Hartree-Slater values for K and L X-ray emission rates. Atomic Data Nucl. Data Tables. 14, 121-137, 1974.
34. Manson, S.T., and D.J. Kennedy. X-ray emission rates in the Hartree-Slater approximation. Atomic Data Nucl. Data Tables. 14, 111-120, 1974.
35. Cole A. Absorption of 20-eV to 50,000-eV electron beams in air and plastic. Radiat. Res. 38, 7-33, 1969.
36. Krause, M.O., and T.A. Carlson. Vacancy cascade in the reorganization of krypton ionised in an inner shell. Phys. Rev. 158(1), 18-24, 1967.
37. Palmberg, P.W., G.E. Rich , R.E. Weber, and N.C. MacDonald. Handbook of Auger electron spectroscopy, p. 145, Physical Electronics Ind., Inc., Edina, Minnesota, 1972.
38. Kassis, A.I., S.J. Adelstein, C. Haydock, and K.S.R. Sastry. Radiotoxicity of ⁷⁵Se and ³⁵S: Theory and application to a cellular model. Radiat. Res. 84, 407-425, 1980.
39. Lederer, C.M., J.M. Hollander, and I. Perlman, Table of Isotopes, Sixth Edition, p. 116, Wiley, New York, 1967.
40. Sastry, K.S.R., C. Haydock, A.M. Basha, and D.V. Rao. Electron dosimetry for radioimmunotherapy: Optimal electron energy. Radiat. Prot. Dosim. (in press).

DISCUSSION

NEACY: In the closely-packed cell model, were the radionuclides assumed to be within the cells or on the surface of the cells?

HOWELL: On the surface of the cells.

NEACY: Were the presented dose figures for the entire cell or for the DNA material within the cell?

HOWELL: The figures were for the entire cell.

WRIGHT: Over what time span does the Auger cascade occur?

HOWELL: The Auger cascades occur in a time scale of 10^{-15} seconds and all of the Auger electrons following each conversion process should be emitted simultaneously.

WRIGHT: Then that is short compared to the prompt chemistry, so the cascade would behave essentially like a high-LET particle.

HOWELL: They should.

ZANZONICO: You stated that in Dr. Sastry's dosimetric tissue model, it was assumed that cells are arranged in a close-packed cubic array. What is the fractional interstitial space of this array for cells of the size you are considering? How does this value compare to values in the literature for fractional extracellular spaces in various mammalian tissues?

HOWELL: The fractional volume occupied by the cells in a close-packed cubic array is 74% of the volume. Therefore the interstitial space would occupy 26%. To answer the second part of your question, this depends on the tissues you are considering and the cells of interest in the organ. About 74% is the maximum volume occupied by the cells in a highly cellular organ. This value may be smaller in other organs.

ROSENSPIRE: Do you have any comments on dose to critical organs other than tumor? We have done distribution studies in mice using N-13 labeled cis-Pt and have found high levels in kidney, lung and blood.

HOWELL: We did not calculate the dose to any particular organs except the whole body. The whole-body dose is 60 rad. The mice did not die of chemotoxicity or radiotoxicity so the dose to the kidneys shouldn't be more than this.

MATTSSON: Can you see any possibility of producing the Auger electrons from platinum by irradiating nonradioactive cis-Platinum in the tumor by low energy photons? Perhaps, it will at least work for superficial tumors.

SASTRY: Yes, indeed, provided there are a sufficient number of Pt atoms. You can, in principle, use synchrotron radiation tuned to the K- or L- shell binding energies in Pt. The photoelectric effect induced in the atom will be followed by copious Auger electron emission. I am not aware of any such studies. The Brookhaven group is attempting to excite such Auger cascades in iodine atoms incorporated into the DNA of cells. Perhaps Dr. Brill may have some comments on the status of the Brookhaven studies.

BRILL: The experiments are in progress but I don't have any details on it. Since Pt is a heavy element, K-shell excitation should result mostly in x-ray emission and only a few Auger electrons.

SASTRY: The K-shell fluorescence yield in Pt, a heavy element, is almost 1. Transitions in the L-shell and above are all of the Auger type.

HARRIS: The fluorescent yield (w_k) (K-shell) for Pt-193 is approximately 0.955. It doesn't really affect the Auger production which is from the L-shell upward.

RAO: Some experiments have been done at New Hampshire with external radiation using *cis*-Pt and no enhanced effects were noted.

SASTRY: The New Hampshire work you have mentioned is not done with photons of optimal energies.

ASPECTS OF THE DOSIMETRY OF RADIONUCLIDES WITHIN THE SKELETON
WITH PARTICULAR EMPHASIS ON THE ACTIVE MARROW

K. F. Eckerman
Health and Safety Research Division
Oak Ridge National Laboratory
P. O. Box X
Oak Ridge, Tennessee 37831

ABSTRACT

Epidemiological surveys on man and results from animal experiments have shown that two tissues associated with the skeleton are of primary concern with respect to cancer induction by ionizing radiation. These are the cells on or near endosteal surfaces of bone, from which osteosarcomas are thought to arise, and hematopoietic bone marrow, which is associated with leukemia. The complex geometry of the soft tissue-bone intermixture makes calculations of absorbed dose to these target regions a difficult problem. In the case of photon or neutron radiations, charged particle equilibrium may not exist in the vicinity of soft tissue-bone mineral interface. In this paper a general study of the dosimetry of radionuclides within the skeleton is presented. Dosimetric data consistent with the MIRD schema and reflecting the physical and anatomical parameters defining the energy deposition are tabulated for the relevant target regions.

INTRODUCTION

Calculation of absorbed dose in the tissues of the skeleton is a complex problem because charged particle equilibrium may not exist within the vicinity of soft tissue-bone mineral interfaces. Treatment of this problem has been hampered by difficulties in modeling the microscopic-intricate intermixture of soft tissue and bone. Most estimates of absorbed dose in organs of the body from photon radiation are based on transport calculations made for a mathematical analogue of the body with a homogeneous representation of the skeleton (1-3). While the homogeneous skeleton is adequate for transport considerations (i.e., appropriate scatter and absorption properties are assigned), the accompanying assumption of charged particle (electronic) equilibrium is often not satisfied

in skeletal tissues. The transport of energy by secondary electrons must be considered in deriving realistic estimates of absorbed dose in soft tissues close to bone mineral, in particular the active marrow.

This problem was first studied in 1949 by Spiers (4) and later by Spiers and others (5-9) using simple geometrical models (e.g., thin slabs, cylinders, and spherical cavities) to approximate the interface geometry. These studies demonstrated that for photon energies less than about 200 keV, electronic equilibrium does not exist and electrons liberated in mineral regions may contribute significantly to the absorbed dose in soft-tissue regions of the skeleton. Snyder et al. encountered the intractable geometry of trabecular bone in their Monte Carlo studies of photon transport and elected to formulate their calculation of absorbed dose in marrow in a conservative manner (1). They partitioned the total energy deposition in the homogeneous skeleton among various skeletal tissues, including active marrow, using skeletal mass fractions. The potential for an overestimate of absorbed dose in the active marrow was noted (see pp. 20 of Ref. 1):

"... it is assumed that the marrow absorbs energy per gram as efficiently as does bone. This assumption is not grossly wrong at energies of 200 keV or more, but is increasingly inaccurate at energies below 100 keV. The effect is to somewhat overestimate the dose to marrow and to somewhat underestimate the dose to bone. This difficulty results from the failure to find ways to program the intricate mixture of bone and marrow spaces in a more realistic fashion."

The potential overestimate has been considered by Rosenstein (3), Kramer (10), Ashton and Spiers (11), and Kerr (12), who indicate that for photon energies less than 100 keV the error is 300% or more. Rosenstein and Kramer apply an energy-dependent correction factor to values computed using the homogeneous skeleton. The correction factor assumes electronic equilibrium (marrow is considered to be a small cavity in the homogeneous skeleton) and includes consideration of the enhancement due to photoelectrons from bone, as indicated by Spiers (13). No computational approach existed which formulated the absorbed dose to the skeletal tissues at risk in terms of the relevant physical and anatomical variables defining the energy deposition.

The problems in formulating the absorbed dose in the active marrow from photon radiation are similar to those encountered in the dosimetry of beta emitters incorporated in bone. For beta emitters Spiers and co-workers reduced the intractable three-dimensional geometry to one dimension through use of measured distributions of chord-lengths in trabeculae and marrow cavities of trabecular bone (14-16). Clearly this approach to the geometry can be applied to secondary electrons liberated by photon interactions in the skeleton.

THE DISTRIBUTION OF CELLS AND TISSUES OF THE SKELETON AT RISK

The skeleton is a complex structure composed of bone, yellow or fatty marrow, red or active marrow, and assorted connective tissues. Throughout the discussion, "bone" refers to the skeletal mineral and adjacent cells and fluid remaining when the skeleton is stripped of its cartilage, periarticular tissue, and marrow. Bone can be divided into two categories, structural bone and metabolic bone. "Structural" refers to the mechanical function of the skeleton, while "metabolic" refers to the role the bone mineral plays in regulating the extracellular calcium levels, particularly in blood plasma.

In the mature skeleton, two bone types are reasonably distinct in terms of appearance as well as retention of bone seekers (17-19). Cortical bone is the hard, compact bone found largely in the shafts of the long bones. Trabecular bone, sometimes referred to as cancellous bone, is the soft, spongy bone composed of a lattice-work of fragile appearance and located at the interior of the flat bones and the ends of the long bones. In general, cortical and trabecular bone may be distinguished in terms of their surface-to-volume ratios, which are usually about 4 times larger for trabecular bone. Cortical bone constitutes about four-fifths, or about 4 kg, of the skeletal mineral in the mature skeleton while the remaining fifth or 1 kg is associated with trabecular bone (17). The high surface-to-volume ratio of trabecular bone arises from the interlacing splinters of bone (trabeculae) which form cavities in which the active marrow is found. The dominant microscopic structure of cortical bone is the Haversian system or osteon, which is a roughly cylindrical volume or canal containing blood vessels, osteoblasts (bone-forming cells), and undifferentiated cells. These canals are typically 50 microns in diameter (17) and, with their supporting channels, serve to supply nutrients to the interior of cortical bone.

There is now general agreement that two cell populations in the skeleton are at risk, namely, the hematopoietic stem cells of marrow and the osteogenic cells of the skeleton, particularly those on the endosteal surfaces of bone (18). Since blood cells are found in various stages of maturation within the active marrow, this tissue is of primary concern as the target tissue with respect to induction of leukemia. The osteogenic cells are the precursors of osteoblasts, which are involved in the formation of new bone, and osteoclasts, which are involved in the resorption of bone. Thus, osteogenic cells constitute the target tissue of concern with respect to induction of bone cancer. Committee 2 of the ICRP (20) has assumed that the hematopoietic stem cells are uniformly distributed within the marrow space of trabecular bone, and the dose equivalent in these cells is taken as the average dose equivalent in the marrow

space. For the osteogenic cells, the Committee now recommends that the dose equivalent be calculated as an average over endosteal tissues up to a distance of 10 μm from bone surfaces (20). Since cortical and trabecular bone contribute about equally to the skeletal surface area, half of the endosteal tissues are assumed to be associated with trabecular bone and half with cortical bone (17). The dose to the osteogenic cells is usually referred to as the bone surface dose, but this is a misnomer since the dose calculation is actually made for the mass of soft tissue within 10 μm of the interface between bone and soft tissue, rather than for just the bone surface.

ABSORBED FRACTION DATA FOR ELECTRONS IN TRABECULAR BONE

Because the structure of trabecular bone cannot be described in simple geometrical terms, Spiers (13,21-22) introduced a method of calculating the energy deposition in which the geometries of the trabeculae and marrow cavities are represented by the distributions of chord-lengths across them. The chord-length distributions for trabeculae and marrow cavities were obtained by optically scanning the trabeculation under conditions of μ -randomness (the different types of randomness are discussed in a paper by Eckerman et al. in this proceedings). If the track of a particle through each trabecula and cavity is assumed to be straight, then the total track in trabeculation can be approximated by alternating chord-lengths in trabeculae and cavities selected randomly from the measured distributions.

DISTRIBUTION OF CHORD-LENGTHS

Measurements of the chord-length distributions in trabecular bone for up to nine bones in several species (15, 16, 23) have been reported by the Bone Dosimetry Research Unit, University of Leeds, UK, under the direction of Professor Spiers. Mean chord- and ray-lengths for the trabeculae and marrow cavities of several trabecular bones of the skeleton of man are summarized in Table 1. The chord distributions for the lumbar vertebra and the parietal bone are shown in Fig. 1. Note that the parietal bone of the adult skeleton appears to be distinct from other trabecular bones as suggested by ratios of mean chord-lengths given in Table 1.

The chord distributions were measured under μ -randomness and thus correspond to the pathlength of radiation incident on the regions in an isotropic manner. For particles originating with the marrow space and the trabeculae the relevant randomness is I-randomness. It has been shown that the distributions for μ - and I-randomness are related, in general, as (24):

ORNL-DWG 83-14992

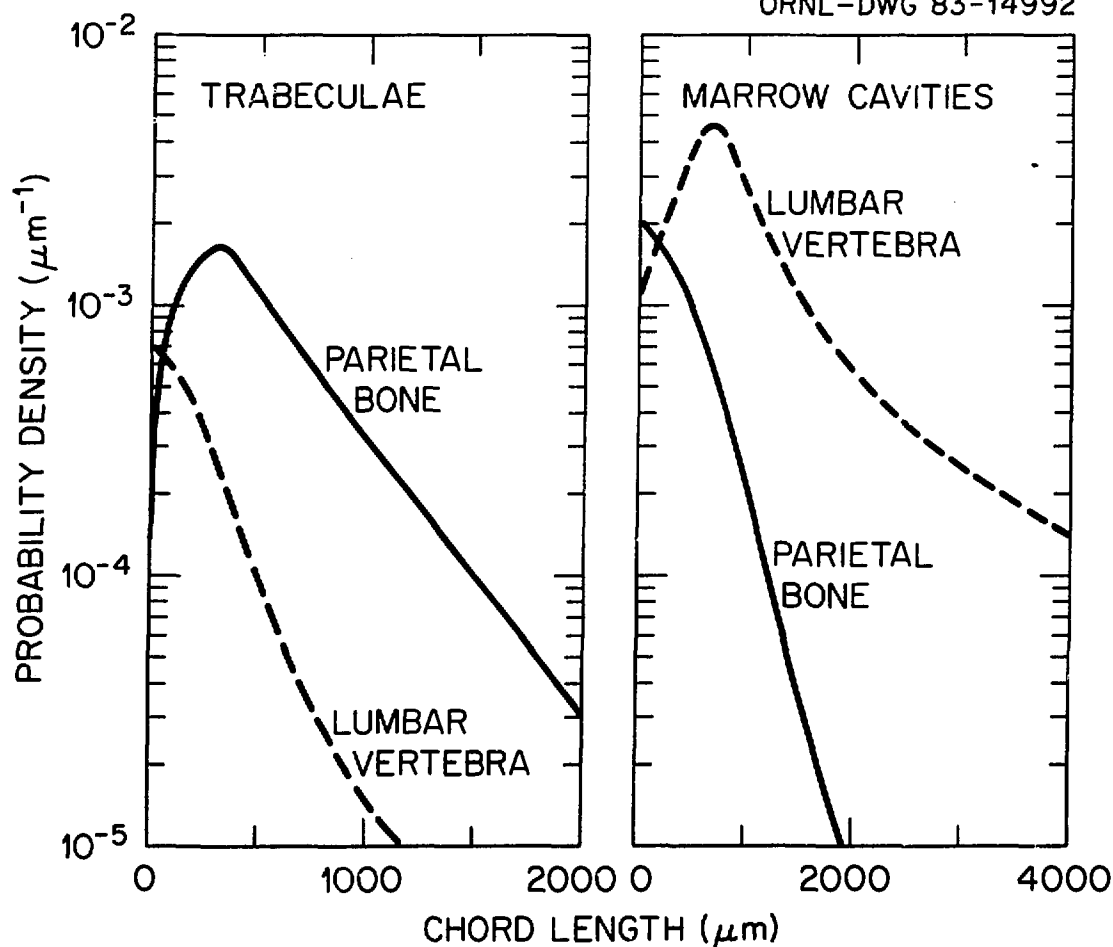


Figure 1. Illustration of measured chord-length distributions for μ -randomness in the trabeculae (left) and marrow cavities (right) of the lumbar vertebra and parietal bone from a 44-year-old male.

Table 1. Mean chord- and ray-lengths (μm) for trabeculae and marrow cavities in various bones of man

Bones	Trabeculae ^a			Marrow Cavities ^a			Ratio of mean chord lengths $\langle t \rangle_\mu : \langle l \rangle_\mu$
	$\langle t \rangle_\mu$	V_μ	$\langle t \rangle_i$	$\langle l \rangle_\mu$	V_μ	$\langle l \rangle_i$	
44-year-old male^b							
Parietal	511	0.570	401	389	0.784	347	1.31
Cervical vertebra	279	0.719	240	910	0.894	861	0.307
Lumbar vertebra	247	1.11	260	1228	1.12	1299	0.201
Rib	265	1.49	330	1706	1.09	1786	0.155
Iliac crest	242	0.675	203	904	0.647	745	0.268
Femur head	232	0.665	193	1157	0.901	1099	0.200
Femur neck	314	0.914	301	1655	0.905	1576	0.190
9-year-old child^c							
Parietal	539			306			0.272
Cervical vertebra	162			906			0.179
Lumbar vertebra	168			857			0.196
Rib	231			1123			0.204
Iliac crest	180			744			0.242
Femur head & neck	249			616			0.404
20-month-old child^b							
Parietal bone	566	1.21	625	255	2.90	500	2.22
Lumbar vertebra	188	1.04	192	736	0.987	731	0.255
Rib	191	1.22	212	559	1.04	569	0.342
Iliac crest	181	1.43	206	575	0.873	539	0.315
Femur	197	0.865	184	789	1.10	830	0.250

^{a)} Notation: $(\langle t \rangle_\mu, V_\mu)$ and $(\langle l \rangle_\mu, V_\mu)$ denote the mean and the fractional variance under μ -randomness for the trabeculae and marrow cavities, respectively. $\langle t \rangle_i$ and $\langle l \rangle_i$ denote the mean ray-length for trabeculae and cavities, respectively. Lengths are in units of μm .

^{b)} Values were computed from the chord-length distributions of Ref. 23.

^{c)} See Ref. 15.

$$f_I(x) = \frac{x}{\langle x \rangle_\mu} f_\mu(x) , \quad (1)$$

where

$f_I(x)$ and $f_\mu(x)$ denote the probability density functions for chord-lengths under I - and μ -randomness, respectively,

$\langle x \rangle_\mu$ denotes the mean value of the $f_\mu(x)$ distribution.

Eq. 1 refers to the full chord; however, we are interested in "half" chords or rays formed by particles originating inside the convex body. A chord of length x , selected from $f_I(x)$, will give rise to rays whose lengths are uniformly distributed between 0 and x , i.e., any point on the chord could serve to define the ray. Thus the chord distribution under μ -randomness and Eq. 1 allows selection of the path-lengths needed to simulate the path of particles within trabecular bone.

COMPUTATIONAL METHOD FOR ESTIMATING ABSORBED FRACTIONS

The absorbed fraction in target region r_k of radiation energy emitted within source region r_h is defined as the energy imparted to r_k divided by the total energy emitted in r_h . Thus $\varphi(r_k \leftarrow r_h)$ embodies the transport of the radiation under consideration as well as the geometric relationship of the source and target regions. The absorbed fraction data presented here are for monoenergetic electrons emitted uniformly (by mass) and isotropically within the trabeculae and cavities of trabecular bone. The target regions of interest are the red (active) marrow, for which we average the energy deposition over the marrow cavities, and the endosteal tissues within 10 μm of the surfaces of bone.

The representation of a typical path of an electron of energy E and range in marrow R_{RM} is illustrated in Fig. 2. By use of chord-length distributions the three-dimensional geometry has been reduced to one dimension. Furthermore, the two media considered in the problem (bone and marrow) can be reduced to a single medium as the ratio of the range of electrons in marrow, R_{RM} , to that of bone, R_{TB} , is nearly constant over electron energies of interest here, that is,

$$\frac{R_{RM}}{R_{TB}} \approx 1.75 \quad . \quad (2)$$

For irradiation of the active marrow by electrons originating within trabeculae, Monte Carlo sampling is used to select a chord-length, t , from the probability density function, $f_I(t)$, for the bone under consideration. A ray-length, t' , is

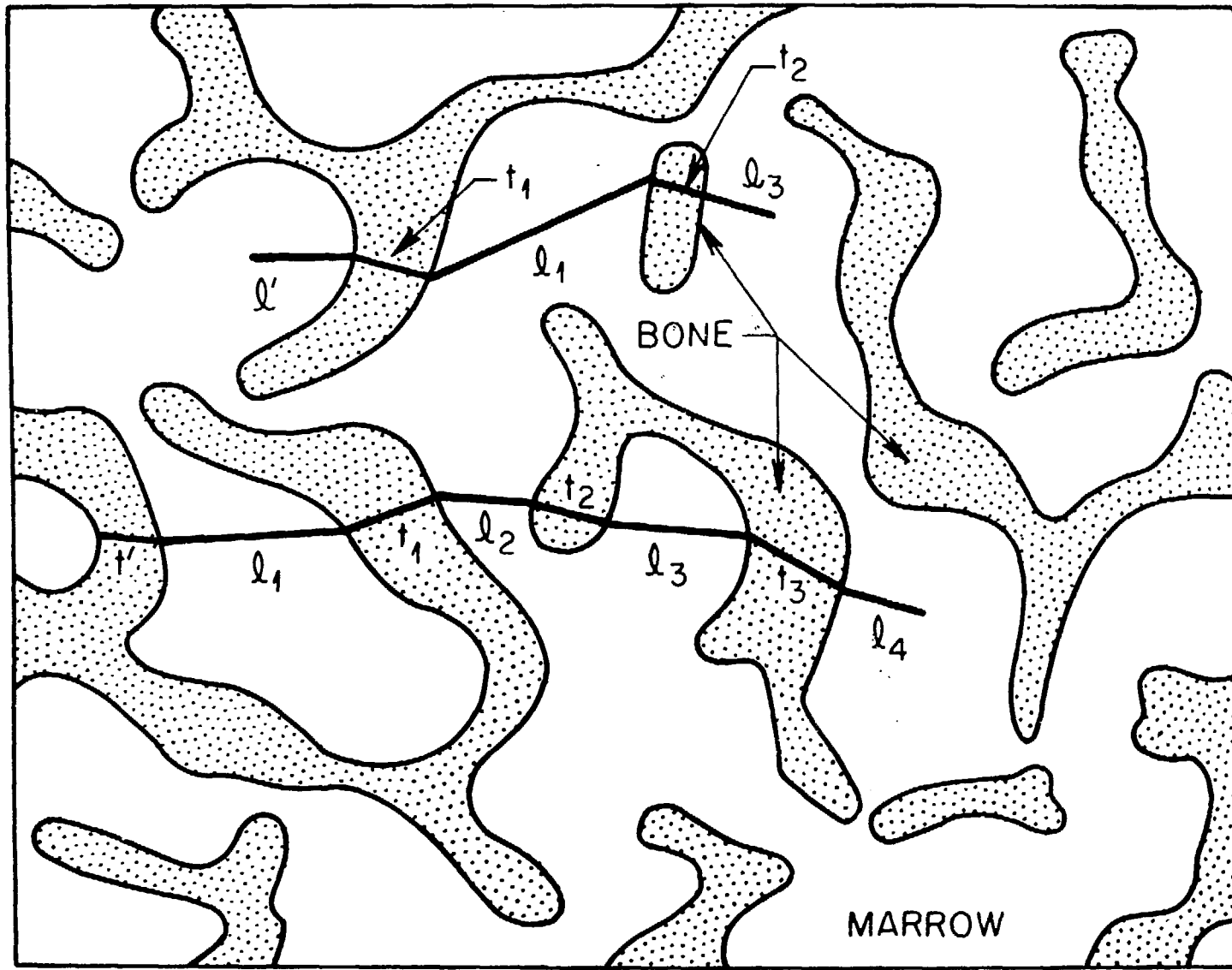


Figure 2.

Illustration of typical tracks for electrons originating in trabecular bone (bottom) and marrow cavities (top).

then determined as $t' = \xi t$, where ξ is a random number uniform on the region $0 < \xi < 1$. The electron is tracked as it alternately passes through marrow cavities along lengths l_1, l_2, \dots and trabeculae along chords t_1, t_2, \dots selected by Monte Carlo sampling of the probability density functions $f_\mu(l)$ and $f_\mu(t)$, respectively. The electron is tracked until

$$1.75(t' + t_1 + t_2 + \dots) + (l_1 + l_2 + \dots) \geq R_{RM} , \quad (3)$$

i.e., all of its energy has been deposited. The energy deposition in trabeculae (t 's) and marrow cavities (l 's) is calculated as the difference between the energy on entering and leaving a trabecula or cavity, in each case being determined from the residual range of the electron at that point in its track. The range-energy relationship was taken from Berger (25). By tracking a large number of electrons in this manner the absorbed fraction, $\varphi(RM \leftarrow TB)$, is obtained by dividing the total energy deposited in marrow cavities by the total energy of electrons simulated.

For electrons emitted within marrow cavities, the calculations proceed as above with selection of a chord-length from the probability density function $f_I(l)$ and determination of a ray-length l' as noted above. The electron is tracked until

$$(l' + l_1 + l_2 + \dots) + 1.75(t_1 + t_2 + \dots) \geq R_{RM} . \quad (4)$$

The energy deposition in trabeculae and marrow cavities and the absorbed fraction, $\varphi(RM \leftarrow RM)$, are determined as discussed above. Typically ten to seventy thousand electrons were tracked in each of the calculations of the absorbed fraction. The statistical errors in the Monte Carlo calculations were less than 1% in each case.

The absorbed fraction data for the parietal bone and lumbar vertebra of the skeleton of a 44-year old male are shown in Fig. 3. At low electron energies, $\varphi(RM \leftarrow TB)$ approaches zero and $\varphi(RM \leftarrow RM)$ approaches unity. This limiting behavior reflects the fact that at low energy the range of electrons is small relative to the mean ray-lengths, $\langle t \rangle_i$ and $\langle l \rangle_i$, and thus the energy is locally deposited. At high energies, $\varphi(RM \leftarrow RM) \approx \varphi(RM \leftarrow TB)$ and the behavior is described as

$$\lim_{E \rightarrow \infty} \varphi(RM \leftarrow TB) \approx \varphi(RM \leftarrow RM) \approx \frac{\langle l \rangle_\mu}{\langle l \rangle_\mu + 1.75 \langle t \rangle_\mu} . \quad (5)$$

i.e., the absorbed fraction is simply the fractional track length in the

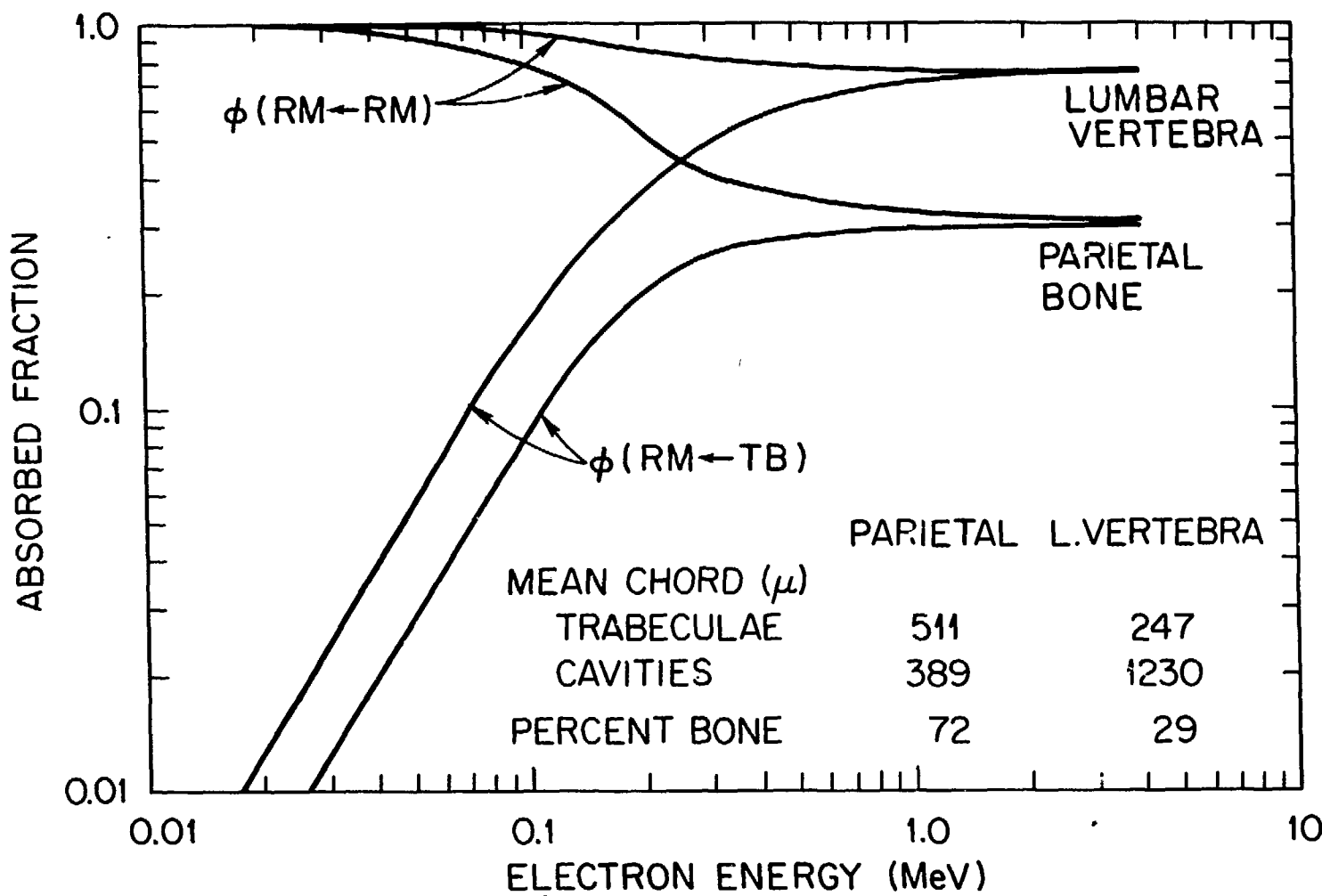


Figure 3. Absorbed fractions for active marrow from monoenergetic electrons emitted uniformly in the trabeculae, $\phi(RM \leftarrow TB)$, and active marrow, $\phi(RM \leftarrow RM)$, of lumbar vertebra and parietal bone from the skeleton of a 44-year-old male.

marrow cavities. The equality of the absorbed fractions at high energy arises as electrons traverse multiple trabeculae and cavities, thus establishing an energy deposition pattern which is largely independent of the electron's origin.

The complete results of the calculations for the parietal bone of the skull and the lumbar vertebra are given in Tables 2 and 3 for a 44-year old male and a 20-month old child, respectively. Although rather sharp distinctions are evident in the absorbed fraction data between the parietal bone and lumbar vertebra of either the child or the adult, the distinction with age is less pronounced. Further tabulation of the age dependence of various parameters characterizing the skeleton is given in Table 4.

ABSORBED DOSE PER UNIT PHOTON FLUENCE

In the anthropomorphic phantom the skeleton is represented as a uniform mixture of its component tissues, namely, cortical bone, trabecular bone, fatty marrow, active (hematopoietic) marrow, and osteogenic cells adjacent to the surfaces of both cortical and trabecular bone ("bone surface"). To estimate the energy deposition in these regions by photons, one must consider the energy transport by secondary electrons arising from photon interactions within the regions and from electrons entering the regions from skeletal components in the immediate vicinity of the target, e.g., bone adjacent to the target.

Consider the trabeculation of a bone experiencing a fluence, $\Psi(E)$, of photons of energy E . Let $m(TB)$, $m(RM)$, and $m(BS)$ denote the mass of bone (trabeculae), marrow, and endosteal tissue adjacent to the surface of the trabeculation. If we index the type of interaction by i and the region in which it occurred by r , $r = TB$ or RM , then the absorbed dose in active marrow, $D(RM)$, and in the endosteal tissue, $D(BS)$, per unit fluence can be expressed as

$$\frac{D(RM)}{\Psi(E)} = \sum_r \frac{m(r)}{m(RM)} \sum_i \int_0^\infty \varphi(RM \leftarrow r, T_i) (i/\rho)_r n_r(T_i) T_i dT_i \quad (6)$$

$$\frac{D(BS)}{\Psi(E)} = \sum_r \frac{m(r)}{m(BS)} \sum_i \int_0^\infty \varphi(BS \leftarrow r, T_i) (i/\rho)_r n_r(T_i) T_i dT_i \quad (7)$$

where

$\varphi(RM \leftarrow r, T_i)$ is the absorbed fraction in RM from r for electrons of energy T_i .

$(i/\rho)_r$, $i = \nu, \sigma$, and k , denotes the mass attenuation coefficients in medium r for the photoelectric, Compton, and pair-production interactions, respectively.

Table 2. Absorbed fraction, ϕ , in active marrow, RM, and bone surface, BS, from a uniformly distributed source of monoenergetic electrons in trabeculae, TB, and marrow of the parietal bone and lumbar vertebra of a 44-year-old male.

Electron energy (MeV)	Parietal bone				Lumbar Vertebra			
	$\phi(RM \leftarrow TB)$	$\phi(RM \leftarrow RM)$	$\phi(BS \leftarrow RM)$	$\phi(BS \leftarrow TB)$	$\phi(RM \leftarrow TB)$	$\phi(RM \leftarrow RM)$	$\phi(BS \leftarrow RM)$	$\phi(BS \leftarrow TB)$
0.010	1.95(-3)	0.994	1.05(-1)	1.95(-3)	3.94(-3)	0.999	3.87(-2)	2.94(-3)
0.015	3.29(-3)	0.990	9.67(-2)	3.29(-3)	7.81(-3)	0.997	3.77(-2)	6.56(-3)
0.020	5.77(-3)	0.983	9.11(-2)	5.77(-3)	1.29(-2)	0.996	3.51(-2)	1.17(-2)
0.030	1.23(-2)	0.969	7.88(-2)	1.14(-2)	2.59(-2)	0.991	3.06(-2)	2.08(-2)
0.040	1.98(-2)	0.950	6.97(-2)	1.54(-2)	4.34(-2)	0.985	2.82(-2)	2.90(-2)
0.050	2.94(-2)	0.927	6.55(-2)	1.85(-2)	6.26(-2)	0.979	2.75(-2)	3.32(-2)
0.060	4.03(-2)	0.901	6.10(-2)	2.04(-2)	8.25(-2)	0.971	2.68(-2)	3.56(-2)
0.080	6.34(-2)	0.854	5.28(-2)	2.18(-2)	1.31(-1)	0.953	2.51(-2)	3.91(-2)
0.10	8.80(-2)	0.794	5.09(-2)	2.37(-2)	1.83(-1)	0.935	2.58(-2)	4.24(-2)
0.15	1.53(-1)	0.654	4.52(-2)	2.65(-2)	3.12(-1)	0.888	2.82(-2)	4.24(-2)
0.20	1.99(-1)	0.538	4.08(-2)	2.84(-2)	4.17(-1)	0.848	2.78(-2)	3.87(-2)
0.30	2.58(-1)	0.415	3.87(-2)	2.98(-2)	5.47(-1)	0.808	2.84(-2)	3.44(-2)
0.40	2.71(-1)	0.376	3.60(-2)	2.96(-2)	5.97(-1)	0.793	2.90(-2)	3.23(-2)
0.50	2.76(-1)	0.358	3.50(-2)	3.00(-2)	6.25(-1)	0.779	2.86(-2)	3.32(-2)
0.60	2.82(-1)	0.346	3.35(-2)	3.05(-2)	6.48(-1)	0.767	2.85(-2)	3.30(-2)
0.80	2.88(-1)	0.335	3.37(-2)	3.09(-2)	6.74(-1)	0.765	2.87(-2)	3.32(-2)
1.0	2.93(-1)	0.327	3.30(-2)	3.09(-2)	6.90(-1)	0.757	2.88(-2)	3.23(-2)
2.0	2.97(-1)	0.317	3.19(-2)	3.11(-2)	7.17(-1)	0.747	2.94(-2)	3.26(-2)
3.0	3.00(-1)	0.311	3.18(-2)	3.11(-2)	7.22(-1)	0.747	2.90(-2)	3.23(-2)
4.0	3.01(-1)	0.308	3.15(-2)	3.11(-2)	7.27(-1)	0.744	2.88(-2)	3.22(-2)

Table 3. Absorbed fraction, ϕ , in active marrow, RM, and in bone surface, BS, from a uniformly distributed source of monoenergetic electrons in the trabeculae, TB, and marrow space of the parietal bone and lumbar vertebra of a 20-month old child.

Electron energy (MeV)	Parietal Bone				Lumbar Vertebra			
	$\phi(RM \leftarrow TB)$	$\phi(RM \leftarrow RM)$	$\phi(BS \leftarrow TB)$	$\phi(BS \leftarrow RM)$	$\phi(RM \leftarrow TB)$	$\phi(RM \leftarrow RM)$	$\phi(BS \leftarrow TB)$	$\phi(BS \leftarrow RM)$
0.01	1.62(-3)	0.990	1.62(-3)	1.40(-1)	4.66(-3)	0.997	4.66(-3)	5.99(-2)
0.015	3.44(-3)	0.981	3.44(-3)	1.33(-1)	9.90(-3)	0.995	9.90(-3)	5.68(-2)
0.02	6.09(-3)	0.969	6.09(-3)	1.21(-1)	1.65(-2)	0.992	1.65(-2)	5.26(-2)
0.03	1.24(-2)	0.947	1.14(-2)	1.01(-1)	3.39(-2)	0.984	3.16(-2)	4.62(-2)
0.04	1.91(-2)	0.920	1.47(-2)	9.04(-2)	5.67(-2)	0.973	4.24(-2)	4.19(-2)
0.05	2.80(-2)	0.889	1.74(-2)	7.98(-2)	3.01(-2)	0.962	4.83(-2)	3.94(-2)
0.06	3.46(-2)	0.858	1.79(-2)	6.97(-2)	1.12(-1)	0.949	5.37(-2)	3.75(-2)
0.08	5.12(-2)	0.789	2.00(-2)	5.28(-2)	1.74(-1)	0.922	5.83(-2)	3.49(-2)
0.10	7.09(-2)	0.724	2.29(-2)	5.73(-2)	2.34(-1)	0.892	5.68(-2)	3.52(-2)
0.15	0.106	0.591	2.44(-2)	4.67(-2)	3.74(-1)	0.829	5.30(-2)	3.65(-2)
0.20	0.130	0.501	2.61(-2)	4.21(-2)	4.70(-1)	0.786	4.78(-2)	3.95(-2)
0.30	0.154	0.401	2.67(-2)	3.76(-2)	5.58(-1)	0.750	4.37(-2)	4.11(-2)
0.40	0.168	0.354	2.79(-2)	3.49(-2)	5.94(-1)	0.730	4.20(-2)	4.23(-2)
0.50	0.176	0.328	2.80(-2)	3.34(-2)	6.26(-1)	0.722	4.16(-2)	4.25(-2)
0.60	0.179	0.308	2.75(-2)	3.26(-2)	6.38(-1)	0.718	4.12(-2)	4.11(-2)
0.80	0.181	0.283	2.79(-2)	3.18(-2)	6.51(-1)	0.706	4.09(-2)	4.12(-2)
1.0	0.188	0.267	2.80(-2)	3.09(-2)	6.62(-1)	0.708	4.18(-2)	4.19(-2)
2.0	0.196	0.238	2.82(-2)	2.96(-2)	6.78(-1)	0.698	4.12(-2)	4.13(-2)
3.0	0.199	0.224	2.82(-2)	2.92(-2)	6.81(-1)	0.696	4.12(-2)	4.13(-2)
4.0	0.201	0.221	2.82(-2)	2.89(-2)	6.84(-1)	0.696	4.09(-2)	4.10(-2)

Table 4. Summary of descriptive parameters for the skeleton of man.

Descriptive Parameter	Age (yr)					
	0	1	5	10	15	Adult
Skeleton¹						
Volume (cm ³)	288	813	1935	3309	5466	7155
Mass (kg)	0.351	1.138	2.709	4.633	7.652	10.0
Density (g/cm ³)	1.22	1.40	1.40	1.40	1.40	1.40
Bone mineral						
Calcium ² (g)	28	99.8	219	396	806	1000
Mass ³ (kg)	0.140	0.499	1.095	1.980	4.030	5.000
Fraction ⁴	0.399	0.438	0.404	0.427	0.527	0.500
Active Marrow						
Mass (kg)	0.047	0.150	0.320	0.610	1.050	1.120
Fraction ⁴	0.134	0.132	0.118	0.132	0.137	0.112
Inactive Marrow						
Mass (kg)	-	0.020	0.140	0.590	1.550	2.380
Fraction ⁴	-	0.018	0.052	0.127	0.203	0.238
Other tissues⁵						
Mass(kg)	0.164	0.469	1.154	1.453	1.022	1.5
Fraction ⁴	0.467	0.412	0.426	0.314	0.133	0.150
Trabecular bone⁶						
Mass (kg)	0.140	0.200	0.219	0.396	0.806	1.000
Fraction ⁴	0.176	0.438	0.081	0.085	0.105	0.100
S/V ⁷ (cm ² /cm ³)	-	220	-	225	-	190
Cortical bone⁸						
Mass (kg)	-	0.299	0.875	1.584	3.224	4.000
Fraction ⁴	-	0.263	0.323	0.342	0.421	0.400
Surface Area (m²)						
Trabecular	1.5	2.2	2.4	4.4	7.7	6.0
Cortical	-	0.45	1.3	2.4	4.8	6.0
Total	1.5	2.6	3.7	6.8	12	12

¹ See Ref. 26.² See Ref. 27.³ Computed assuming 0.2 g-Ca per g bone mineral.⁴ Mass fraction in the skeleton.⁵ Difference between skeletal mass and identified tissues.⁶ All bone is trabecular at birth; 40% at one year, 20% thereafter.⁷ Surface to volume ratio, see Ref. 15.⁸ Based on trabecular bone mass and S/V ratio of 220 through age 10, 190 at age 15, and 120 for the adult.

* The adult S/V ratio for cortical bone was applied to all ages.

$n_r(T_i) dT_i$ denotes the number of electrons of energy between T_i and $T_i + dT_i$ liberated in region r per interaction i.

The mass ratios which appear in the equation can be related to the mean chord lengths of the trabeculae, $\langle t \rangle$, and marrow space, $\langle l \rangle$, as measured by scanning the trabeculation in an isotropic manner. The ratios expressed in terms of the measured chord-lengths are

$$\frac{m(TB)}{m(RM)} = \frac{\rho_{TB}}{\rho_{RM}} \frac{\langle t \rangle}{\langle l \rangle} \quad (8)$$

$$\frac{m(TB)}{m(BS)} = \frac{\rho_{TB}}{\rho_{RM}} \frac{\langle t \rangle}{4d} \quad (9)$$

$$\frac{m(RM)}{m(BS)} = \frac{\langle l \rangle}{4d} \quad (10)$$

where ρ_{TB} and ρ_{RM} denote the density of bone and marrow and d is the distance over which the endosteal tissue is averaged, i.e., in ICRP Publication 30 (20) a value of 10 μm is considered appropriate.

Soft-tissue adjacent to surfaces of trabecular bone represent about one half the total endosteal tissue of the skeleton. The remaining tissue is associated with the surfaces of cortical bone where it is contained within small cavities (largely the Haversian canals of about 50 μm diameter) within the bone matrix (17). The dose-response function for this component of the endosteal tissue is computed as

$$\frac{D(BS)}{F(E)} = \int_0^\infty (i/\rho)_r n_r(T_i) T_i S(T_i) dT_i \quad (11)$$

where $S(T_i)$ denotes the ratio of the mass stopping power for soft tissue to that of bone at energy T_i . The total dose to endosteal tissues is the average of that indicated by Eqs. 7 and 11 since trabecular and cortical bone contribute about equally to the total endosteal tissue mass in the skeleton.

A complete set of dose response functions for the skeleton is given in Table 5 and those for the active marrow are shown in Fig. 4. These data can be applied to photon fluence estimates derived from Monte Carlo transport calculations in mathematical analogues of the body (1,26) to estimate absorbed dose. Variations with incident photon energy in the ratio of absorbed dose in active marrow to the equilibrium dose (kerma) in soft-tissue are indicated in Fig. 5. These ratios are maximal at photon energies in the region of 50 to 60 keV and are higher for the thick trabeculae and small marrow cavities of the parietal bone than for the thinner trabeculae-larger marrow cavities of other bones. The

Table 5. Absorbed dose in active marrow, D(RM), and in bone surface, D(BS), per unit fluence, $\Psi(E)$, of monoenergetic photons in the skeleton.

Photon energy (MeV)	D(RM or BS)/ $\Psi(E)$, Gy per photon/m ²					
	Parietal Bone		Lumber Vertebra		Cortical	Total ¹
	D(RM)	D(BS)	D(RM)	D(BS)	D(BS)	D(BS)
0.010	6.30(-16)	8.47(-16)	6.14(-16)	9.43(-16)	5.32(-15)	3.13(-15)
0.015	2.71(-16)	4.17(-16)	2.61(-16)	4.98(-16)	2.45(-15)	1.47(-15)
0.020	1.53(-16)	2.98(-16)	1.43(-16)	3.39(-16)	1.39(-15)	8.65(-16)
0.030	7.49(-17)	2.00(-16)	6.44(-17)	2.12(-16)	6.11(-16)	4.12(-16)
0.040	5.04(-17)	1.42(-16)	4.11(-17)	1.51(-16)	3.41(-16)	2.46(-16)
0.050	4.18(-17)	1.09(-16)	3.31(-17)	1.10(-16)	2.20(-16)	1.65(-16)
0.060	3.93(-17)	8.75(-17)	3.11(-17)	8.69(-17)	1.57(-16)	1.22(-16)
0.080	4.15(-17)	6.61(-17)	3.45(-17)	7.03(-17)	1.03(-16)	8.67(-17)
0.10	4.79(-17)	6.32(-17)	4.22(-17)	6.76(-17)	8.51(-17)	7.64(-17)
0.15	7.16(-17)	7.96(-17)	6.74(-17)	8.90(-17)	8.80(-17)	8.85(-17)
0.20	9.88(-17)	1.05(-16)	9.57(-17)	1.22(-16)	1.10(-16)	1.16(-16)
0.30	1.57(-16)	1.65(-16)	1.54(-16)	1.98(-16)	1.67(-16)	1.83(-16)
0.40	2.15(-16)	2.26(-16)	2.10(-16)	2.65(-16)	2.24(-16)	2.45(-16)
0.50	2.72(-16)	2.85(-16)	2.66(-16)	3.30(-16)	2.80(-16)	3.05(-16)
0.60	3.28(-16)	3.38(-16)	3.19(-16)	3.94(-16)	3.34(-16)	3.64(-16)
0.80	4.28(-16)	4.37(-16)	4.15(-16)	5.09(-16)	4.33(-16)	4.71(-16)
1.0	5.19(-16)	5.25(-16)	5.03(-16)	6.12(-16)	5.22(-16)	5.67(-16)
1.5	7.13(-16)	7.23(-16)	6.91(-16)	8.37(-16)	7.09(-16)	7.73(-16)
2.0	8.79(-16)	8.89(-16)	8.50(-16)	1.03(-15)	8.69(-16)	9.49(-16)
3.0	1.17(-15)	1.18(-15)	1.12(-15)	1.36(-15)	1.15(-15)	1.26(-15)
4.0	1.43(-15)	1.44(-15)	1.37(-15)	1.65(-15)	1.42(-15)	1.54(-15)
5.0	1.69(-15)	1.70(-15)	1.59(-15)	1.93(-15)	1.68(-15)	1.81(-15)
6.0	1.94(-15)	1.95(-15)	1.82(-15)	2.20(-15)	1.94(-15)	2.07(-15)
8.0	2.46(-15)	2.46(-15)	2.26(-15)	2.74(-15)	2.47(-15)	2.61(-15)
10.0	2.99(-15)	2.99(-15)	2.70(-15)	3.28(-15)	3.03(-15)	3.16(-15)

¹ Total represents the bone surface response of the skeleton and is computed as the average of the lumbar vertebra and cortical responses.

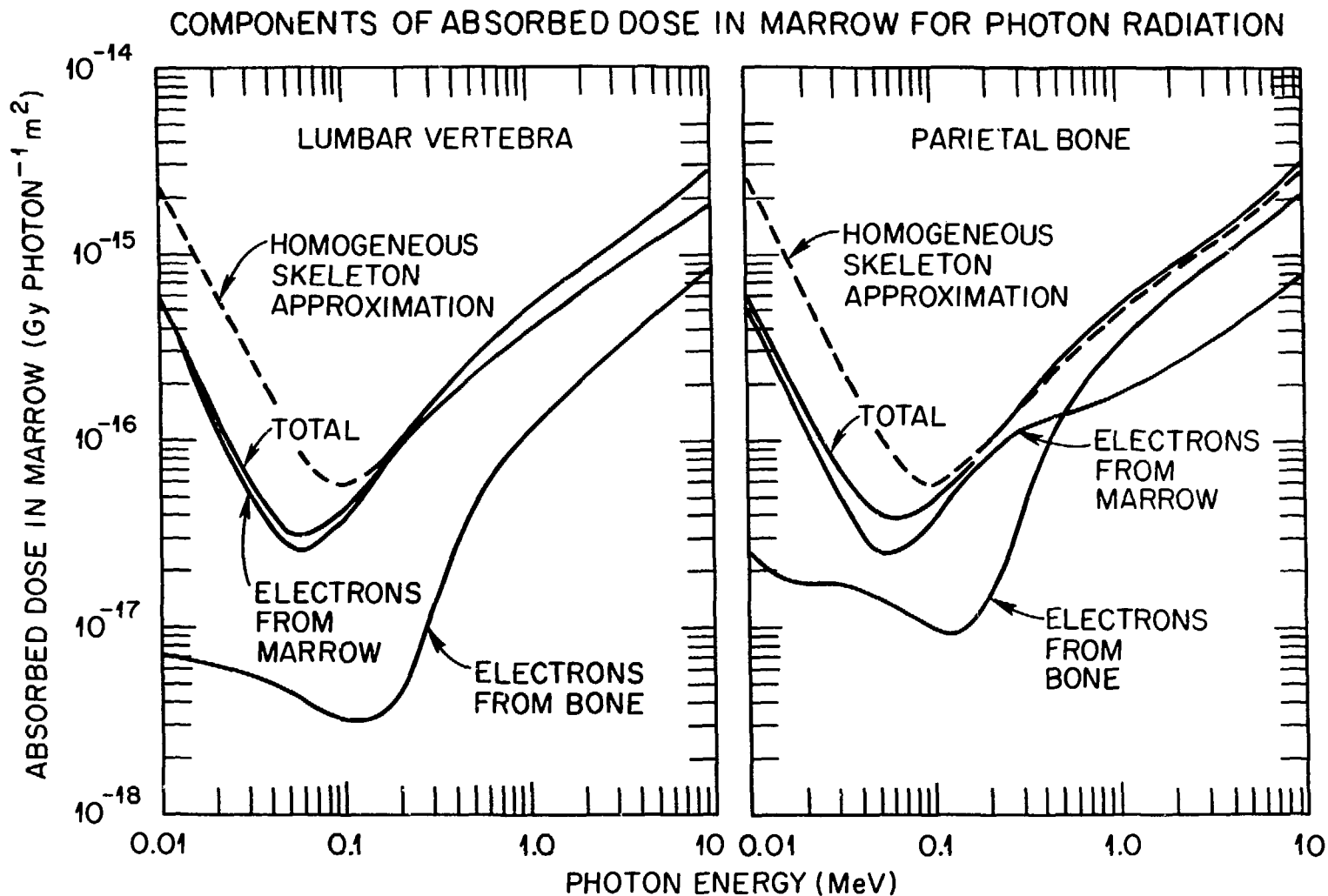


Figure 4. Components of the absorbed dose in marrow from photon radiations. The dotted curve assumes the active marrow absorbs energy per unit mass at the rate for the homogeneous skeleton approximation.

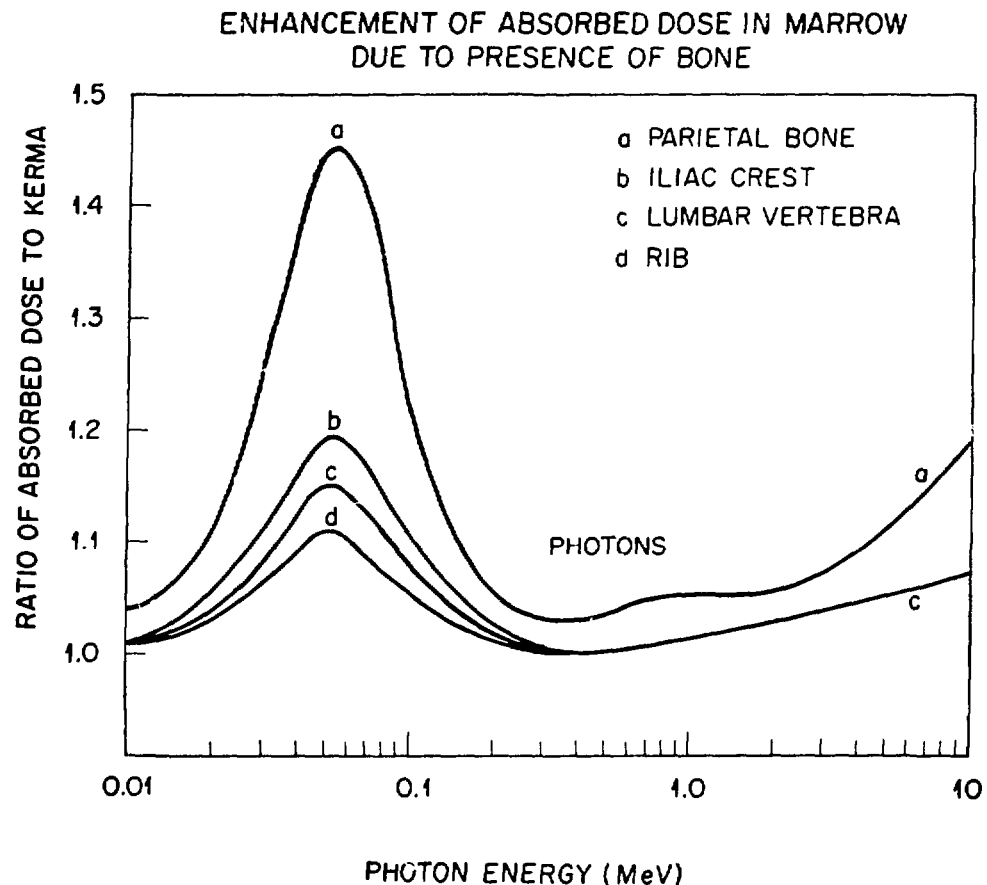


Figure 5. Illustration of the effects of the microstructure of trabecular bone on energy deposition in active marrow for various bones of the adult skeleton.

ratios at low energy conform to the general features indicated by Spiers (13). However, the parietal bone exhibits a substantially higher enhancement of the marrow dose than other trabecular bones. This enhancement should be considered in deriving skeletal average values for the diagnostic x-ray region. Enhancement of dose in the high energy (pair production) region is also indicated in our calculations. Enhancement is small, about 5%, for most trabecular sites but approaches 20% for the parietal bone. Considering the highly stylized analogue of the skeleton used in photon transport calculations, we recommend that the skull be treated as a separate bone region and data for the parietal bone in Table 5 be applied to estimate marrow dose. The lumbar vertebra appears to be representative of other trabecular sites.

DISCUSSION

Data on microstructure of trabecular bone has been used to estimate absorbed fractions for electrons in trabecular bone using a formulation similar to that set forth by Spiers (13). Absorbed fraction estimates are developed for electrons arising within the trabeculae or the marrow cavity itself. These data were applied to the secondary electrons arising from photon interactions within the skeleton in deriving dose-response functions which reflect the microstructure of trabecular bone. These functions overcome one of the well known limitations in current dosimetric formulations.

ACKNOWLEDGMENT

Research sponsored by the Office of Health and Environmental Research, U.S. Department of Energy under contract DE-AC05-84OR21400 with the Martin Marietta Energy Systems, Inc.

REFERENCES

- [1] Snyder, W. S., M. R. Ford, and G. G. Warner, "Estimates of Specific Absorbed Fractions For Photon Sources Uniformly Distributed In Various Organs of a Heterogeneous Phantom, Medical Internal Radiation Dose Committee, Pamphlet No. 5, Revised (Society of Nuclear Medicine, New York) 1978.
- [2] Poston, J. W. and W. S. Snyder, "A model for exposure to a semi-infinite cloud of a photon emitter," Health Phys. 26, 287, 1974.
- [3] Rosenstein, M., Organ Doses in Diagnostic Radiology, U.S. Department of Health, Education and Welfare Report FDA 76-8030 (Washington, DC: U.S. Government Printing Office) 1976.

- [4] Spiers, F. W., "The influence of energy absorption and electron range on dosage in irradiated bone," Brit. J. Radiol. 12, 521, 1949.
- [5] Spiers, F. W., "Dosage in irradiated soft tissue and bone," Brit. J. Radiol. 26, 38, 1953.
- [6] Woodard, H. Q. and F. W. Spiers, "The effect of x rays of different qualities on the alkaline phosphates of living mouse bone," Brit. J. Radiol. 26, 38, 1953.
- [7] Charlton, D. E. and D. V. Cormack, "Energy dissipation in finite cavities," Radia. Res., 17, 34, 1962.
- [8] Aspin, N. and H. E. Johns, "The absorbed dose in cylindrical cavities within irradiated bone," Brit. J. Radiol. 36, 350, 1963.
- [9] Howarth, J. L., "Calculation of the absorbed dose in soft-tissue cavities in bone irradiated by x-rays," Rad. Res. 24, 158, 1965.
- [10] Kramer, R., Ermittlung von Konversionsfaktoren Zwischen Korperdosen und Relevanten Strahlungskenngrößen bei Externer Roentgen- und Gamma-Bremsstrahlung, Gesellschaft für Strahlen- und Umweltforschung GSF-Bericht-S-566, 1979.
- [11] Ashton, T. and F. W. Spiers, "Attenuation factors for certain tissues when the body is irradiated omnidirectionally," Phys. Med. Biol. 24, 950, 1979.
- [12] Kerr, G. D., "A Review of organ doses from isotropic fields of γ -Rays," Health Phys. 39, 3, 1980.
- [13] Spiers, F. W., "Transition-zone dosimetry," Radiation Dosimetry (edited by F. H. Attix and E. Tochlin) Vol. 3, pp. 809-867 (Academic Press; New York, NY) 1969.
- [14] Spiers, F. W., "Beta dosimetry in trabecular bone," Delayed Effects of Bone-Seeking Radionuclides (edited by C. W. Mays et al.) pp. 95-108 (U. of Utah Press; Salt Lake City, UT) 1969.
- [15] Beddoe, A. H., P. J. Darley, and F. W. Spiers, "Measurements of trabecular bone structure in man," Phys. Med. Biol. 21, 589, 1976.
- [16] Beddoe, A. H., "Measurements of the microscopic structure of cortical bone," Phys. Med. Biol. 22, 298, 1977.
- [17] ICRP Publication 23, Report of the Task Group on Reference Man, Pergamon Press, Oxford, 1975.
- [18] ICRP Publication 11, Task Group on Radiosensitivity of Tissues in Bone, Pergamon Press, Oxford, 1968.
- [19] ICRP Publication 20, Alkaline Earth Metabolism in Adult Man, Pergamon Press, Oxford, 1972.
- [20] ICRP Publication 30, Limits for Intakes of Radionuclides by Workers, (Pergamon Press: Oxford), 1979.

- [21] Whitwell, J. R. and F. W. Spiers, "Calculated beta-ray dose factors for trabecular bone," Phys. Med. Biol. 21, 16, 1976.
- [22] Spiers, F. W., J. R. Whitwell and A. H. Beddoe, "Calculated dose factors for radiosensitive tissues in bone irradiated by surface-deposited radionuclides," Phys. Med. Biol. 23, 481, 1978.
- [23] Whitwell, J. R., Theoretical Investigations of Energy Loss by Ionizing Particles in Bone, Ph.D. Thesis, University of Leeds, Leeds, UK, 1973.
- [24] Kellerer, A. M., "Consideration on the Random Traversal of Convex Bodies and Solutions for General Cyclinders," Radia. Res. 47, 359-376, 1971.
- [25] Berger, M. J., "Improved Point Kernels for Electron and Beta-ray Dosimetry," NBSIR 73-107, 1973.
- [26] Cristy, M., Mathematical Phantoms Representing Children of Various Ages for Use in Estimate of Internal Dose. NUREG/CR-1159, ORNL/NUREG/TM-367, 1980.
- [27] Leggett, R. W., K. F. Eckerman, and L. R. Williams, "Strontium-90 in bone: A case study in age-dependent dosimetric modelling," Health Phys. 43, 307-322, 1982.

DISCUSSION

FISHER: What are the ratios of trabecular/cortical bone for different parts of the skeleton?

ECKERMAN: Both bone types are present in the various bones of the skeleton. Data on the distribution within the skeleton is given in Table 16 (p 67) of the Reference Man report (ICRP Publication 23, 1975). We have not identified similar information for the nonadult; however, other information, e.g., data on the thickness of cortical bone, suggests that the distribution might be similar to that of the adult. We currently assume in dosimetric calculations, as shown in our Table 4, that all bone is trabecular at birth; 40% at one year, and 20% (the adult value) thereafter.

Bone Marrow Dosimetry for Monoclonal Antibody Therapy

R.E. Bigler, P.B. Zanzonico

R. Leonard, and M. Cosma

New York Hospital-Cornell Medical Center
and Memorial Sloan-Kettering Cancer Center
525 East 68th Street
New York, NY 10021

F.J. Primus, E. Alger, R. DeJager,
S. Stowe, E. Ford, K. Brennan, and D.M. Goldenberg
Center for Molecular Medicine and Immunology
University of Medicine and Dentistry
100 Bergen Street
Newark, NJ 07103

ABSTRACT

Immunoglobulins must permeate through the basement membrane of capillaries in order to enter the extracellular space (ECS) of tissue. Since the process is quite slow, the blood plasma activity in various organs contributes considerably to the radiation dose of the dose-limiting tissues. In bone marrow the basement membrane is absent and the blood circulation is functionally open. Therefore blood plasma and marrow ECS maintain equal concentrations of labeled immunoglobulins. A combination of factors including intravenous administration, slow absorption into most tissues, slow breakdown and elimination of labeled immunoglobulin, and rapid entry into bone marrow ECS as well as known radiosensitivity of marrow led us to expect this tissue would prove to be the primary tissue at risk for systemic monoclonal antibody therapy. We have developed and applied in a Phase I clinical study of ^{131}I labeled CEA antibody a procedure for estimation of radiation dose to red bone marrow. Serial measurements of blood plasma and total body retention (by difference with urinary loss and/or whole-body counting) are carried out. Binding of labeled antibody to the cellular components of blood is verified to be very low. Needle aspiration bone marrow biopsies are obtained and corrected for circulating blood content. A hematocrit is taken and the activity concentration in the acellular fraction is checked to verify it matches a concurrent plasma measurement. The washed cellular fraction is then checked to verify there is no substantial absorbed activity (e.g. by antigens expressed on stem cells or other premature elements of bone marrow). (Note: If radionuclides, such as ^{125}I , having a large portion of the available energy emitted in the form of short range radiations are used, the risk to stem cells should be carefully evaluated by means of cellular level dosimetry due to considerable heterogeneity in dose distribution anticipated for such radionuclides.) We have observed bone marrow depression at doses greater than 400 rad. This limited experience can be compared to exten-

sive experience of the use of ^{131}I for treatment of thyroid cancer, wherein a blood dose limitation of 200 rad has been recommended. If no special procedures are used to reconstitute marrow after radiation treatment, this dose level represents a much greater than generally recognized limitation to radio-labeled monoclonal antibody therapy.

INTRODUCTION

Bone marrow toxicity is the most clinically important and the most consistently and frequently encountered toxicity associated with currently available systemic cancer therapy (1, 2). For example, 14% of all deaths among cancer patients are due to infections caused by neutropenia secondary to iatrogenic myelosuppression (3). In addition, a small percentage (0.6%) of cancer deaths is attributable to hemorrhage caused by thrombocytopenia secondary to iatrogenic megakaryosuppression (3). Clearly, therefore, the potential bone marrow toxicity of any proposed systemic anticancer therapeutic modality, including of course radiolabeled "anti-tumor" antibody, must be thoroughly evaluated. Such evaluation is particularly pressing in light of the likely utilization of radiolabeled "anti-tumor" antibody as adjuvant therapy in patients previously or concurrently treated with conventional antineoplastic agents and therefore already at risk for bone marrow suppression.

The hematopoietic bone marrow (4) contains precursor cell (i.e. stem cell) populations which supply the cellular components of blood through continual proliferation (i.e. cell renewal) and concomitant differentiation and migration of the resulting terminally differentiated (i.e. functional) blood cells into the systemic circulation. Briefly, a common stem cell, termed a "pluripotential stem cell" (or "colony forming unit-spleen (CFU-S)"), gives rise to several series of committed stem cells, the megakaryoblastic, erythroblastic, myeloblastic, monoblastic, and lymphoblastic series, which proliferate and differentiate, yielding megakaryocytes and then platelets, erythrocytes, granulocytes (i.e. eosinophils, basophils, and neutrophils), monocytes and then macrophages, and lymphocytes, respectively. The cells composing this steady-state cell renewal system, which typically exhibit cell cycle times of the order of days (4) (comparable to that of many types of human cancer cells (5)), may therefore be characterized as rapidly proliferating as well as undifferentiated. This is the biological basis of the bone marrow toxicity of current antineoplastic agents: the mechanisms of these agents are generally related to a relative non-specific cytotoxicity among rapidly proliferating cells (5). This is also the radiobiological basis of the exquisite radiosensitivity of bone marrow (6, 7): according to the classic "law of Bergonie and Tribondeau," the radiosensitivity of cells is directly related to their rate of proliferation and indirectly related to their relative state of differentiation. This, of course, further necessitates the thorough evaluation, in the form of accurate and precise absorbed dose estimates, of the hazard to bone marrow associated with systemically administered radionuclides, including of course radionuclides in the form of "anti-tumor" antibody. For example, among patients treated with ^{131}I -iodide for thyroid carcinoma, serious bone marrow depression was observed in 21% of patients receiving bone marrow absorbed doses exceeding 200 rad (including fatal bone marrow depression in 6% of these cases), but in only 3% of patients receiving bone marrow absorbed doses less than 200 rad (8).

In most mammalian tissues, the patent vascular endothelium effectively restricts vascular space-extravascular space exchange of circulating proteins (9). In contrast, the characteristic sinusoidal vasculature of bone marrow (10), with large pores (i.e. fenestrae up to 100 nm wide) and absent or discontinuous basement membrane (i.e. basal lamina), allows free flow of plasma through the marrow parenchyma (i.e. "transparenchymal plasma flow" (11)) and,

as a result, rapid (i.e. within several minutes after intravenous administration) equilibration of large molecules such as proteins (12) and even particulate matter (13-15) between plasma and the marrow extracellular space. Thus, even in the absence of bone marrow expression of the putative tumor-associated antigen against which a particular antibody is directed (16), we anticipate significant non-specific localization of systemically administered "anti-tumor" antibody in marrow. Of course, if any of the diverse stem cell populations of bone marrow were to express the tumor-associated antigen (17), avid and prolonged localization of antibody in marrow, associated with the antigen-positive stem cell population, would be expected. We therefore anticipate, relative to most non-target (i.e. normal) tissues and especially with shorter lived radionuclides, moderately to extremely high cumulated activities and associated absorbed doses in bone marrow following systemic administration of radiolabeled "anti-tumor" antibody.

Theoretical considerations and clinical and experimental data thus strongly suggest that bone marrow will, in general, constitute the critical, or dose-limiting, normal tissue associated with radiolabeled antibody therapy of cancer. For example, in initial clinical trials of ^{131}I -labeled Fab fragments of antibody directed against human melanoma-associated antigen p97 for treatment of disseminated melanoma (18, 19), the maximum cumulative administered activity, 800 mCi, induced prohibitive bone marrow suppression (absorbed dose: 230 rad), imposing an absorbed dose limit of 11,000 rad to tumor. While recent clinical advances (e.g. prophylactic antibiotic therapy, use of "protected environments," granulocyte transfusions (1, 2)) may eventually increase the practical absorbed dose limit (\sim 200 rad (9)) for bone marrow, it will probably remain the critical normal tissue associated with systemically administered radiolabeled "anti-tumor" antibody therapy.

CLINICAL STUDIES

MATERIALS AND METHODS

Ten patients thus far have participated in Phase I clinical trials of ^{131}I -labeled murine monoclonal antibody directed against tumor-associated carcinoembryonic antigen (CEA) (20) for treatment of metastatic colon carcinoma, currently being conducted at the Center for Molecular Medicine and Immunology at the University of Medicine and Dentistry of New Jersey in Newark, NJ. Each patient typically received a total administered activity of 100-200 mCi ^{131}I , administered in four consecutive weekly administered activities of 25-50 mCi each. Peripheral whole blood samples were obtained from 0.5 hr to 120 hr post-administration and all urine was collected from 0 hr to 96 hr post-administration. Several ml samples of whole blood and of urine were counted in a calibrated automatic gamma well-counter (counting efficiency for ^{131}I : ~30%) and the count rate concentrations (in cpm/ml), corrected for radioactive decay from the time of antibody administration, were converted to activity concentrations (in $\mu\text{Ci}/\text{ml}$). The activity concentration in urine was converted to total activity (in μCi) eliminated per 24-hr interval using the values of sequential total 24-hr void volumes (in ml), all urine per each 24-hr interval having been pooled prior to counting. The total-body retention (in μCi) at 24-hr intervals was calculated as the difference between administered activity (in μCi) and the cumulative decay-corrected activity (in μCi) in the sequential 24-hr void volumes. The values of administered activity (in μCi), blood activity concentration (in $\mu\text{Ci}/\text{ml}$), and total body-retention (in μCi) were converted to the corresponding equivalent values for "Reference Man" by normalization to a 70-kg body mass (21).

Based on visual inspection of semi-log scatter plots and using Berman's SAAM computer code (22), the time-dependent activity concentration in blood, $[A_{B1}(t)]$, was fit to a bi-exponential function and the time-dependent total body retention, $A_{TB}(t)$, was fit to a monoexponential function (23):

$$[A_{B1}(t)] = (A_{B1})_1 e^{-(\lambda_{B1})_1 t} + (A_{B1})_2 e^{-(\lambda_{B1})_2 t} \quad (1),$$

$$A_{TB}(t) = A_{TB} e^{-\lambda_{TB} t} \quad (2)$$

where $(A_{B1})_1$ and $(A_{B1})_2$ are the "zero' time" values (in $\mu\text{Ci}/\text{ml}$) of the first and second components, respectively, and $(\lambda_{B1})_1$ and $(\lambda_{B1})_2$ are the biological disappearance constants (in hr^{-1}) of the first and second components, respectively, of the time-dependent activity concentration (in $\mu\text{Ci}/\text{ml}$) in blood and A_{TB} is the "'zero' time" value (in μCi) and λ_{TB} is the biological disappearance constant (in hr^{-1}) of the time-dependent total body retention (in μCi). The cumulated activity concentration (in $\mu\text{Ci}\cdot\text{hr}/\text{ml}$) in blood, $[\hat{A}_{B1}]$, and the cumulated activity ($\mu\text{Ci}\cdot\text{hr}$) in the total body, $\hat{\chi}_{TB}$, were calculated as follows (23):

$$\begin{aligned} [\hat{A}_{B1}] &= \int_0^\infty [A_{B1}(t)] e^{-\lambda t} dt \\ &= \frac{(A_{B1})_1}{(\lambda_{B1})_1 + \lambda} + \frac{(A_{B1})_2}{(\lambda_{B1})_2 + \lambda} \end{aligned} \quad (3),$$

$$\begin{aligned} \hat{\chi}_{TB} &= \int_0^\infty A_{TB}(t) e^{-\lambda t} dt \\ &= \frac{A_{TB}}{\lambda_{TB} + \lambda} \end{aligned} \quad (4)$$

where λ is the physical decay constant (in hr^{-1}) of the particular radionuclide under consideration (0.0036 hr^{-1} for ^{131}I).

As previously discussed, the sinusoidal vasculature of bone marrow, with large fenestrae and discontinuous basal lamina, allows free transparenchymal plasma flow through the marrow and, as a result, rapid equilibration of circulating antibody between plasma and the marrow extracellular space (10-15). In the absence of specific antibody binding to antigen expressed by the cellular elements of blood and of bone marrow, we can therefore equate the activity concentrations and the cumulated activity concentrations in blood and in marrow. Preliminary clinical results basically support this supposition. Following intravenous administration (at 18 and at 96 hr post-administration) of ^{131}I -anti(CEA) antibody to patients with metastatic colon carcinoma, the percent initial whole sample radioactivity for blood samples and for bone marrow aspirate samples associated with the washed pellet, and therefore possibly associated with cellular elements, was only 0.23-1.7% and 1.8-3.6%, respectively. While suggesting the possibility of antibody binding to small populations of cells (e.g. stem cells) in blood and in bone marrow, which would necessitate accurate cellular radiation dosimetry to insure that, in particular, one or more critical stem cell populations in marrow were not receiving cytocidal absorbed doses, these results basically indicate little or no specific antibody

binding to cellular antigen. In addition (at 18 and at 96 hr post-administration), the activity concentration in whole marrow aspirate samples was 55-93% (typically ~90%) of that in corresponding whole blood samples. The assumption that the activity concentrations and the cumulated activity concentrations in blood and in bone marrow are equal therefore appears well-founded, yielding equation (5):

$$[\bar{\lambda}_{RM}] = [\bar{\lambda}_{B1}] \quad (5)$$

where $[\bar{\lambda}_{RM}]$ is the cumulated activity concentration (in $\mu\text{Ci}\cdot\text{hr}/\text{ml}$) in red marrow ("RM"). An implicit assumption in the development of equation (5) is that the percent extracellular spaces in blood (i.e. the plasmacrit) and in marrow are equal. This assumption was verified by directly measuring the percent extracellular space in whole blood samples, yielding values of 67-69%, and in whole marrow aspirate samples, yielding values of 69-77%. The total cumulated activity (in $\mu\text{Ci}\cdot\text{hr}$) in red marrow, $\bar{\lambda}_{RM}$, is then given by equation (6):

$$\bar{\lambda}_{RM} = [\bar{\lambda}_{RM}] m_{RM} \quad (6)$$

where m_{RM} is the mass of red marrow, 1,500 gm, for "Reference Man" (21).

A modified version of the "MIRD" formalism (23) was used for the actual absorbed dose calculations. The modification provides an additional "source" term that accounts for radioactivity contained in the remainder of the body (24). The equations used are (24):

$$\bar{D}(r_k) = \sum_h \bar{\lambda}_h S(r_k \leftarrow r_h) + \bar{\lambda}_{Rem} S(r_k \leftarrow r_{Rem}) \quad (7),$$

$$S(r_k \leftarrow r_{Rem}) = \frac{m_{TB}}{m_{Rem}} [S(r_k \leftarrow r_h) - \sum_h \frac{m_h}{m_{TB}} S(r_k \leftarrow r_h)] \quad (8),$$

$$\bar{\lambda}_{Rem} = \bar{\lambda}_{TB} - \sum_h \bar{\lambda}_h \quad (9),$$

$$m_{Rem} = m_{TB} - \sum_h m_h \quad (10)$$

where $\bar{D}(r_k)$ is the mean absorbed dose (in rad) in target region r_k ; $\bar{\lambda}_h$, $\bar{\lambda}_{Rem}$, and $\bar{\lambda}_{TB}$ are the cumulated activities (in $\mu\text{Ci}\cdot\text{hr}$) in source region r_h , in the remainder of the body ("Rem") and in the total body ("TB"), respectively; $S(r_k \leftarrow r_h)$, $S(r_k \leftarrow r_{Rem})$, and $S(r_k \leftarrow r_{TB})$ are the S-factors (in $\text{rad}/\mu\text{Ci}\cdot\text{hr}$) (25) for the target region r_k and the source region r_h , for target region r_k and the remainder of the body, and for target region r_k and the total body, respectively; m_h , m_{Rem} , and m_{TB} are the masses (in gm) of target region r_h , of the remainder of the body, and of the total body, respectively. The calculations represented by equations (7)-(10) were actually performed by a FORTRAN computer code written by Mr. George Sgouros of our laboratory and running on our PDP 11/70 computer facility.

RESULTS AND CONCLUSIONS

Presented in Tables 1-4 are the results of the kinetic and dosimetric analyses of systemically administered ^{131}I -anti(CEA) antibody in patients with metastatic colon carcinoma. Note that the results of these analyses are presented separately for patients with and without human "anti(mouse)" antibody (HAMA). One of the major practical difficulties associated with the systemic administration of murine antibody to humans is the rapid induction of circulating HAMA. In the current series of patients, 40% (4/10) thus far have developed HAMA, usually within 1 to 2 weeks of the first administration of antibody. From the standpoint of *in vivo* tumor localization of "anti-tumor" antibody, the major consequence of high HAMA titers in plasma is the rapid formation of circulating immune complexes. For example, within 60 min post-administration of ^{131}I -anti(CEA) antibody to HAMA positive patients, only 5% of the plasma-borne radioactivity is in the form of native antibody; in contrast, in HAMA negative patients, 98% of the plasma-borne activity is still in the form of native antibody at 8 d post-administration. Immune complex formation results in dramatic alterations in the kinetics and biodistribution of the administered antibody, with rapid clearance from plasma into the spleen and markedly reduced extrasplenic (including tumor) localization. Note, in Table 1, that the half-times, $(T_{B1})_1$ and $(T_{B1})_2$, for blood clearance of ^{131}I -anti

Table 1

Parameters for Blood and for Total Body for Kinetics of Systemically Administered ^{131}I -anti(CEA) Antibody in Patients with Metastatic Colon Carcinoma

	Blood				Total Body	
	1st component*		2nd component*		λ_{TB}	T_{TB}
	$(\lambda_{B1})_1$	$(T_{B1})_1$	$(\lambda_{B1})_2$	$(T_{B1})_2$		
	(hr^{-1})	(hr)	(hr^{-1})	(hr)	(hr^{-1})	(hr)
HAMA positive	0.13	5.3	0.033	21	0.041	17
HAMA negative	0.032	22	0.012	59	0.014	50

* The "'zero' time" intercept of the second component, $(A_{B1})_2$, is typically 3-5% of the "'zero' time" intercept of the first component, $(A_{B1})_1$.

(CEA) antibody are three to four times shorter in HAMA positive than in HAMA negative patients; the half-time for total body elimination, T_{TB} , is likewise three times shorter in HAMA positive patients than in HAMA negative patients.

The radiation dosimetry for red marrow and for total body of systemically administered ^{131}I -anti(CEA) antibody in patients with metastatic colon carcinoma are presented for individual patients in Table 2 and in summary form in Table 3. As expected, the HAMA positive patients, because of more rapid blood clearance and total body elimination of the administered activity, exhibit sub-

Table 2

Parameters for Blood and for Total Body for
Radiation Dosimetry of Systemically Administered
 ^{131}I -anti(CEA) Antibody in Patients with Metastatic Colon Carcinoma

Patient	HAMA	Total administered activity (mCi)	Red Marrow		Total Body	
			$\bar{\alpha}_{\text{RM}}^*$ ($\mu\text{Ci}\cdot\text{hr}$)	\bar{D}_{RM} (rad)	$\bar{\alpha}_{\text{TB}}^*$ ($\mu\text{Ci}\cdot\text{hr}$)	\bar{D}_{TB} (rad)
1	-	164	1.7×10^5	450	9.8×10^6	96
2	-	122	1.9×10^6	440	3.2×10^6	31
3	-	110	1.5×10^6	390	9.2×10^6	91
4	+	103	6.6×10^5	230	3.1×10^6	30
5	+	104	3.9×10^5	130	6.6×10^6	65
6	-	204	3.4×10^6	630	1.1×10^7	100
7	-	151	3.9×10^6	980	1.6×10^7	160
8	+	166	1.6×10^5	59	3.8×10^6	38
9	+	157	8.6×10^5	250	4.5×10^6	44
10	-	124	2.3×10^6	420	1.3×10^7	130

* Normalized to the body mass of "Reference Man" (70 kg).

Table 3

Summary of Radiation Dosimetry of
 ^{131}I -anti(CEA) Antibody in Patients with Metastatic Colon Carcinoma

Mean absorbed dose per unit administered activity (rad/mCi)		
	Red Marrow	Total Body
HAMA positive	1.4	0.36
HAMA negative	3.8	0.71

stantially lower cumulated activities and absorbed doses than the HAMA negative patients.

The relation between bone marrow absorbed dose and bone marrow toxicity, based on clinical signs and symptoms of bone marrow suppression, is summarized in Table 3 for the current series of patients. Moderately severe to severe

Table 4

Correlation of Bone Marrow Absorbed Dose
with Bone Marrow Toxicity for ^{131}I -anti(CEA)
Antibody in Patients with Metastatic Colon Carcinoma

Patient	Total marrow absorbed dose (rad)	Clinical manifestation of marrow toxicity
1	450	None
2	440	None
3	390	None
4	230	None
5	130	None
6	630	Moderately severe neutropenia, requiring hospitalization, of 1 week's duration
7	980	Severe neutropenia, requiring hospitalization, of 1 month's duration
8	59	None
9	250	Transient thrombocytopenia
10	420	Moderately severe neutropenia and thrombocytopenia of 1 week's duration

bone marrow toxicity was observed only at absorbed doses exceeding 400 rad. Any generalizations one may infer from these data are, of course, confounded by the differences in previous clinical history among these patients, including most notably the nature and extent of previous cytotoxic therapy. For example, note that two patients who received marrow absorbed doses of 450 and 440 rad, respectively, exhibited no significant marrow toxicity. Nevertheless, this limited clinical experience can be compared to extensive clinical experience with ^{131}I -iodide for treatment of thyroid carcinoma (9), wherein a blood absorbed dose limit of 200 rad has been recommended, and to additional clinical experience with ^{131}I -anti(p97) Fab antibody fragment for treatment of malignant melanoma (19), wherein a marrow absorbed dose of 230 rad induced prohibitive marrow suppression. Accordingly, if reconstitution of bone marrow will not be attempted, a marrow absorbed dose limit of 200 rad is recommended, with perhaps an absolute upper limit of 400 rad under extenuating circumstances. In the absence of HAMA, the presence of which would appear to contraindicate systemic administration of radiolabeled "anti-tumor" antibody altogether (19), a marrow absorbed dose limit of 400 rad generally imposes a total administered activity limit of approximately 100 mCi (See Table 3.).

ACKNOWLEDGEMENTS

This work was supported by National Cancer Institute contract N01-CM-37565 and grant CA-39841.

REFERENCES

1. Hoagland, H.C. Hematologic complications of cancer chemotherapy. in Perry, M.C. and J.W. Yarbro. *Toxicity of Chemotherapy*. pp 433-448, Grune and Stratton, New York, 1984.
2. Creaven, P.J. and E. Mihich. The clinical toxicity of anticancer drugs and its prediction. *Semin. Oncol.* 4, 147-163, 1977.
3. Inagaki, J., V. Rodriguez, and G.P. Bodey. Cause of death in cancer patients. *Cancer* 33, 568-573, 1974.
4. Weiss, L. The life cycle of blood cells. in Weiss, L. *Histology: Cell and Tissue Biology*, 5th edition. pp 474-497, Elsevier Biomedical, New York, 1983.
5. Pratt, W.B. and R.W. Ruddon. *The Anticancer Drugs*. Oxford University Press, New York, 1979.
6. International Atomic Energy Agency and the World Health Organization. *Manual on Radiation Haematology*. Technical Report Series No. 123, International Atomic Energy Agency, Vienna, 1971.
7. DeBernardo, E. The effects of radiation on the cellular components of the immune system. in Pizzarello, D.J. *Radiation Biology*. pp 193-204, CRC Press, Boca Raton, FL, 1983.
8. Benua, R.S., N.R. Cicale, M. Sonenberg, and R.W. Rawson. The relation of radioiodine dosimetry to results and complications of metastatic thyroid cancer. *Am. J. Roentgenol.* 87, 171-182, 1962.
9. Dewey, W.C. Vascular-extravascular exchange of ^{131}I plasma proteins. *Am. J. Physiol.* 197, 423-431, 1959.
10. Tavassoli, M. and Y.M. Yoffey. *Bone Marrow: Structure and Function*, Alan R. Liss, New York, 1983.
11. Yoffey, J.M. Lymphocyte loading of bone marrow sinusoids. *Adv. Microcirc.* 7, 49-67, 1977.
12. Michelson, K. Determination of inulin, albumin, and erythrocyte spaces in the bone marrow of rabbits. *Acta Physiol. Scand.* 77, 28-35, 1969.
13. Zamboni, L. and D.C. Pease. The vascular bed of red bone marrow. *J. Ultrastructure Res.* 5, 65-85, 1961.
14. Hudson, G. and J.M. Yoffey. Reticulo-endothelial cells in the bone marrow of the guinea-pig. *J. Anatom.* 97, 409-416, 1963.
15. Hudson, G. and J.M. Yoffey. Ultrastructure of reticuloendothelial elements in guinea-pig bone marrow. *J. Anatom.* 103, 515-525, 1968.
16. Sulitzeanu, D. Human cancer-associated antigens: Present status and implications for immunodiagnosis. *Adv. Cancer Res.* 44, 1-42, 1985.

17. Carrel, S., A. Schmidt-Kessen, J.-P. Mach, D. Heumann, and C. Girardet. Expression of common acute lymphoblastic leukemia antigen (CALLA) on human malignant melanoma cell lines. *J. Immunol.* 130, 2456-2460, 1983.
18. Larson, S., J. Carrasquillo, and K. Krohn. Radiotherapy with "anti-p97" iodinated monoclonal antibodies in melanoma. in Raynaud, C. Proceedings of the Third World Congress of Nuclear Medicine and Biology. pp 3666-3669, Pergamon Press, Paris, 1982.
19. Carrasquillo, J.A., K.A. Krohn, P. Beaumier, R.W. McGuffin, J.P. Brown, K.E. Hellstrom, I. Hellstrom, and S.M. Larson. Diagnosis and therapy for solid tumors with radiolabeled antibodies and immune fragments. *Cancer Treat. Rep.* 68, 317-328, 1984.
20. Primus, F.J., K.D. Newell, A. Blue, and D.M. Goldenberg. Immunological heterogeneity of carcinoembryonic antigen: Antigenic determinants on carcinoembryonic antigen distinguished by monoclonal antibodies. *Cancer Res.* 43, 686-692, 1982.
21. International Commission on Radiological Protection. Report of Task Group on Reference Man. ICRP Publication 23. Pergamon Press, New York, 1975.
22. Berman, M.E., E. Shahn, and M.F. Weiss. The routine fitting of kinetic data to models - A mathematical formalism for digital computers. *Biophys. J.* 2, 275-287, 1962.
23. Loevinger, R. and M. Berman. A revised schema for calculating the absorbed dose from biologically distributed radionuclides. MIRD Pamphlet No. 1, revised. Society of Nuclear Medicine, New York, 1976.
24. Bigler, R.E. Dosimetry for evaluation of the biologic effects of radiation treatment using internally deposited radionuclides and labeled compounds. in: Radiopharmaceutical Dosimetry Symposium, R. J. Cloutier, J. L. Coffey, W. S. Snyder, and E. E. Watson, editors. HEW Publ. (FDA) 76-8044, Rockville, MD, pp. 221-229, 1976.
25. Snyder, W.S., M.R. Ford, and G.G. Warner. "S," Absorbed dose per unit cumulated activity for selected radionuclides and organs. MIRD Pamphlet No. 11. Society of Nuclear Medicine, New York, 1975.

DISCUSSION

RAO: You said that when you have a cluster of cells, the cells on the surface will get less dose than the cells from the center. Dr. Doherty pointed out this morning that the distribution of monoclonal antibodies is rather nonuniform in tumors with more at the surface and less at the center. In that case we would expect a higher dose at the surface of the tumor than at the center. Is that not correct?

BIGLER: Maybe the point you are missing is that these are just the nuclei of the cells at those positions. We are using an approximation as to where the activities are on the cell surface. Cell surfaces are touching in the cluster containing 17 total cells. This small cluster works rather well for the I-125; but, if you have an 80-keV electron you need 50 or so cells before the dose at the center becomes static. The surface dose, of course, will depend upon the energy of the beta, so if you use yttrium-90 or some radionuclide like that, the surface will be very macroscopic on something like a one-gram tumor.

DOSE POINT KERNELS FOR BETA-EMITTING RADIOISOTOPES

W. V. Prestwich and L. B. Chan
McMaster University, Hamilton, Ontario

C.S. Kwok and B. Wilson
Ontario Cancer Research Foundation, Hamilton, Ontario

ABSTRACT

Knowledge of the dose point kernel corresponding to a specific radionuclide is required to calculate the spatial dose distribution produced in a homogeneous medium by a distributed source. Dose point kernels for commonly used radionuclides have been calculated previously using as a basis monoenergetic dose point kernels derived by numerical integration of a model transport equation. The treatment neglects fluctuations in energy deposition, an effect which has been later incorporated in dose point kernels calculated using Monte Carlo methods.

This work describes new calculations of dose point kernels using the Monte Carlo results as a basis. An analytic representation of the monoenergetic dose point kernels has been developed. This provides a convenient method both for calculating the dose point kernel associated with a given beta spectrum and for incorporating the effect of internal conversion. An algebraic expression for allowed beta spectra has been accomplished through an extension of the Bethe-Bacher approximation, and tested against the exact expression. Simplified expressions for first-forbidden shape factors have also been developed.

A comparison of the calculated dose point kernel for ^{32}P with experimental data indicates good agreement with a significant improvement over the earlier results in this respect.

An analytic representation of the dose point kernel associated with the spectrum of a single beta group has been formulated. The construction of the dose point kernel for any specific radionuclide, using this representation as a basis, may be accomplished easily by anyone with access to a modest microcomputer.

INTRODUCTION

The estimation of dose from a distributed source is an important aspect of the application of labelled monoclonal antibodies to radio-immunotherapy. A major contribution to the dose arises from beta particles. The source may be described mathematically by a function giving the activity concentration at each position in the source. The dose produced at a specific site may then be calculated as the linear superposition of contributions from each volume element in the distribution treated as a point source. This process is summarized by the equation:

$$D(\vec{r}_s) = \int K(r) a(\vec{r}^l) d^3\vec{r}^l \quad (1)$$

where $D(\vec{r}_s)$ is the dose at the site specified by the co-ordinate \vec{r}_s , $a(\vec{r}^l)$ is the activity concentration at a point \vec{r}^l in the source distribution and $K(r)$ is the dose point kernel. This quantity corresponds to the dose produced by a point source of unit activity at a distance $r = |\vec{r}_s - \vec{r}^l|$. Integration extends over the region occupied by the source.

It is clear from equation (1) that the dose point kernel plays a fundamental role in the calculation. This quantity is a characteristic function of the radioisotope. It may be determined from the beta spectrum of the radioisotope, provided the dose point kernels for monoenergetic electrons propagating in the medium of interest have been established.

This work reports progress made in the development of an analytical representation for the dose point kernel of beta sources in a water medium.

MONOENERGETIC DOSE POINT KERNELS

A convenient quantity is the scaled point kernel, defined through the relationship:

$$F(E, x) = \frac{R(E)}{E} \cdot 4\pi\rho r^2 K(E, r) \quad (2)$$

In equation (2), $R(E)$ is the CSDA range for an election of energy E , $K(E, r)$ is the dose point kernel, and x is the ratio of the distance r to the CSDA range. To the extent that radiative stopping is negligible the scaled point kernel will satisfy the constraint:

$$\int F(E, x) dx = 1 \quad (3)$$

With the inclusion of radiative stopping, the integral is less than one, if the resultant photon dose is not included. The correction only amounts to 2% at 5 Mev. In this work all dose point kernels are constrained to satisfy condition (3).

In CSDA theory the dose point kernel vanishes for $x > 1.0$. More realistic calculations using Monte Carlo methods allow for range straggling. A compilation of dose point kernels in water for thirty-six energies from 0.5 keV. to 10 MeV is given in NBSIR-73.⁽¹⁾ In this case significant dose terminates at about $x = 1.2$. It is convenient to introduce an effective fractional residual range, $u = 1.2 - x$. In terms of this co-ordinate, it was noted that the dose point kernels qualitatively resemble the probability density function corresponding to the log normal distribution.

Quantitatively, it has been found possible to represent the mono-energetic dose point kernels by

$$F(E, x) = G(E, x) + L(E, x) \quad (4)$$

where

$$L(x) = \frac{A}{\sqrt{2\pi}\sigma_u} \exp - \left(\frac{(\mu - \ln u)^2}{2\sigma_l^2} \right) \quad (5)$$

and

$$G(x) = \frac{B}{\sqrt{2\pi}\sigma_1} \exp - \left(\frac{(x - x_0)^2}{2\sigma_1^2} \right) \cdot m(x) \quad (6)$$

The modifying function, $m(x)$, was chosen to truncate $G(x)$, and is given by

$$\begin{aligned} m(x) &= 1, \quad x < 0.9 \\ m(x) &= (4 - x/0.3)^2, \quad x > 0.9 \end{aligned} \quad (7)$$

The parameters A , μ , σ , σ_1 and x_0 are all functions of energy, expressed as a power series in $z = \ln(E/\epsilon)$. The co-efficients are given in Table 1. For the region below 10 keV, only the function $L(x)$ was necessary. Because it is more physically meaningful, the mode, x_m was used rather than the mean in characterizing $L(x)$. The relationship is given by

$$\mu = \ln(1.2 - x_m) + \sigma^2 \quad (8)$$

The value of B is determined by the unit area constraint.

Examples of the fitted functions are given in Fig. 1, 2 and 3. For the region $0 < x < 0.90$, which accounts for approximately 95% of the energy absorption, the average deviation between the calculated function and the Monte Carlo data is 2%. The largest deviation, 7% occurs at the end of the range. In addition, the Monte Carlo data exhibits a rather sharp drop at $x = 0$, which is not reproduced by the function, leading to deviations of about 4%.

BETA DOSE POINT KERNELS

For a beta spectrum $N(E)$, the dose point kernel satisfies

$$4\pi\rho r^2 K(r) = \int N(E) \cdot \frac{E}{R(E)} F(E, \frac{r}{R(E)}) dE \quad (9)$$

For convenience a scaled point kernel for the spectrum can be defined by

$$F(x) = 4\pi\rho r^2 R_0 D(r)/\bar{E} \quad (10)$$

where \bar{E} is the average energy and R_0 is the CSDA range for the end-point energy.

The CSDA range was fitted in two regions, 0.5 to 10 keV, and 10 keV to 3 MeV. The form is given as

$$\ln R = a + bx + cx^2 + dx^3 \quad (11)$$

where $x = \ln E/\epsilon$. The parameters are listed in Table 2. The values are within .3% for the low energy region, where the input data from NBSIR 73-107⁽²⁾ were used. A maximum deviation of 3% occurs at 3 MeV for the high energy region, using the data from NBSIR-82-2550A.⁽²⁾

Table 2. Range Parameters

Degree	$E < 10$ keV	10 keV $< E > 3$ MeV
0	-7.851513	-0.814245
1	+0.848241	+1.247420
2	+0.172400	-0.130086
3	-0.011319	-0.010436
ϵ	0.1 keV	1 MeV

Table 1. Co-efficients of the Polynomial Representation of Monoenergetic Dose Point Kernel Parameters

Parameter	$10 \text{ keV} \leq E \leq 10 \text{ MeV}$								$\epsilon = 1 \text{ MeV}$	
	Degree									
	0	1	2	3	4	5	6	7		
X_M	0.666738	0.022788	0.008434	0.001308						
	0.349450	0.026841	0.005712	-0.000854						
	0.676841	0.019970	-0.021141	-0.019877	-0.005072	0.001338	0.000937	0.000116		
	0.417371	-0.142187	0.041947	0.017131	-0.002159	-0.001051				
	-0.006268	8.789530	1.939269	-1.927159	-0.533682	0.158315	0.068728	0.006391		
$.5 \text{ keV} \leq E \leq 8 \text{ keV}$								$\epsilon = 0.1 \text{ keV}$		
X_M	0.374759	0.057090								
σ	0.088089	0.240107	-0.054706	0.004809						

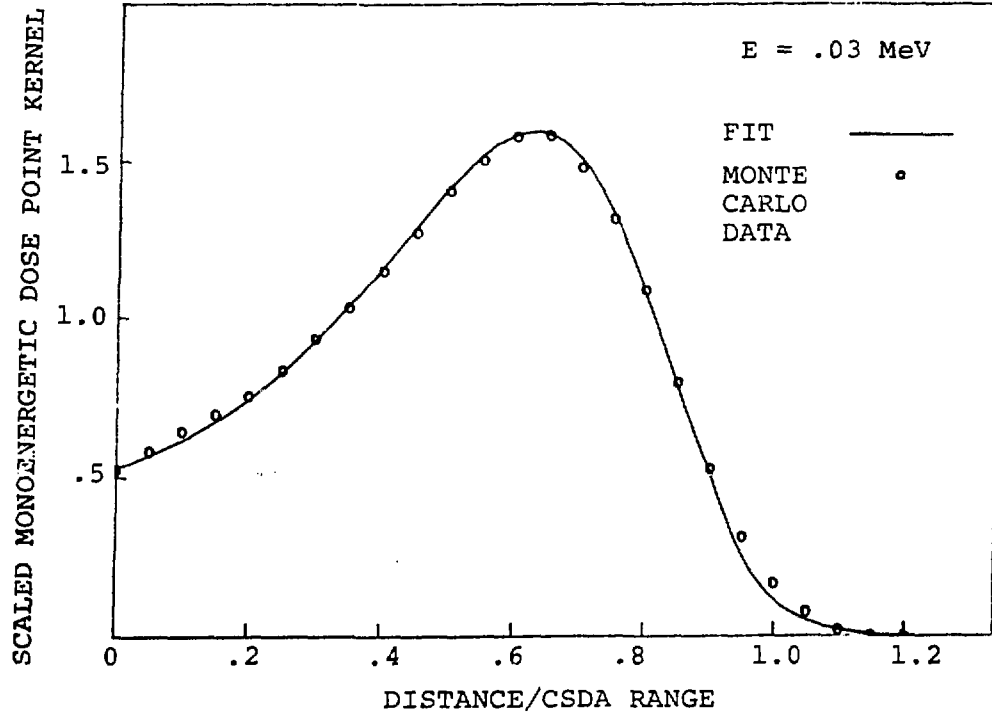


Fig. 1 Scaled dose point kernel for 0.03 MeV electrons in water.

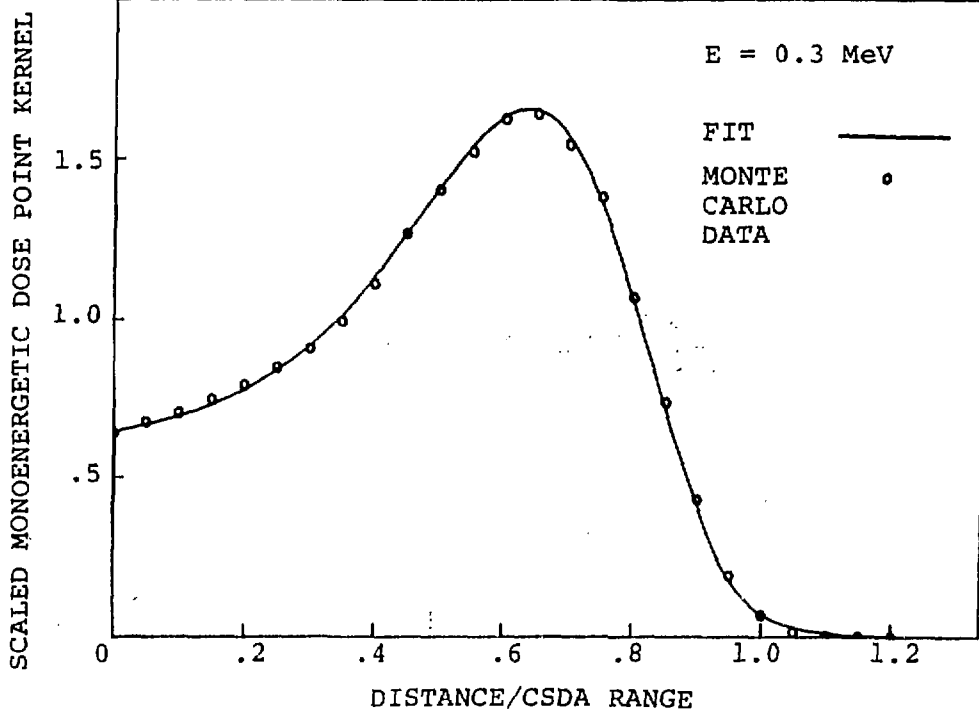


Fig. 2 Scaled dose point kernel for 0.3 MeV electrons in water.

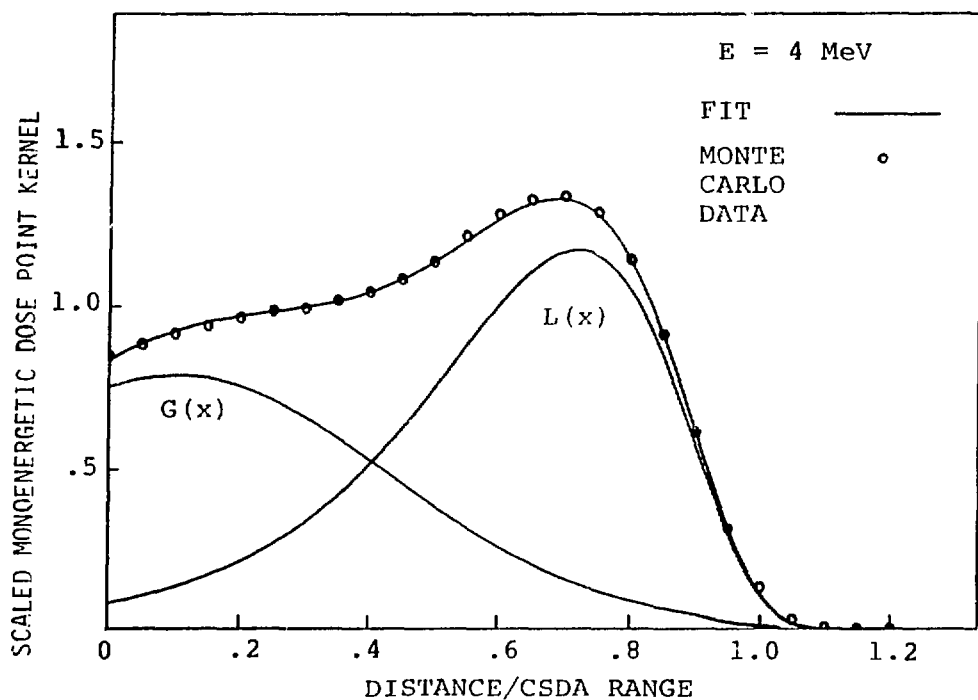


Fig. 3 Scaled dose point kernel for 4 MeV electrons in water. The lognormal and modified Gaussian components produce the fitted curve.

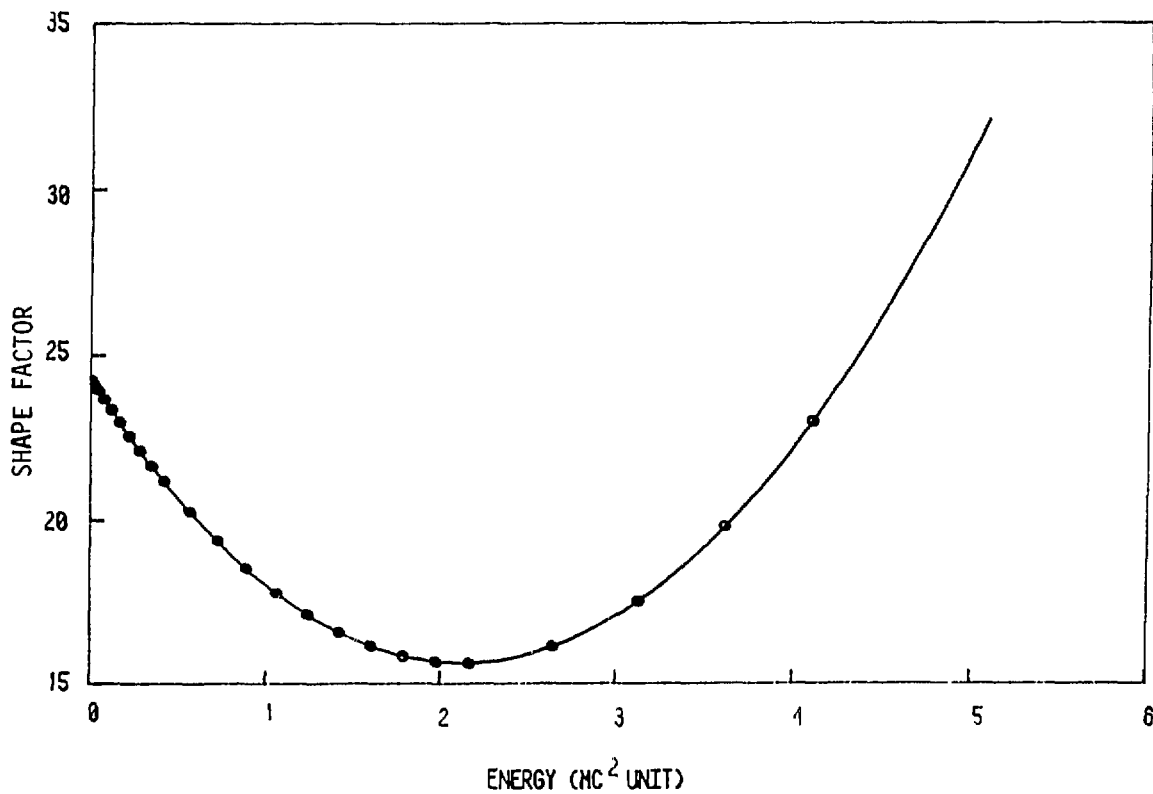


Fig. 4 The shape factor for a first-forbidden unique transition. Data points are the tabulated values.

The beta spectrum may be written as

$$N(E) = N_0 F(Z, W) \cdot S_\lambda \cdot pW (E_0 - E)^2 \quad (12)$$

where $W = E + M_e C^2 - V_0$, and $p = \sqrt{W^2 - 1}$, for $E < V_0$. The quantity V_0 is the screening potential. For energies less than the screening potential, the spectrum was approximated by the unscreened value multiplied by a correction factor. The latter is the ratio of the screened to unscreened values at $E = V_0$. The screening potential was taken to be

$$V_0 = 1.13 \alpha^2 Z^{4/3} M_e C^2. \quad (13)$$

In equation (12), N_0 is a constant required to normalize the area of the spectrum to unity, and was determined by numerical integration. The Fermi function $F(Z, W)$ and the shape factor S_λ are in general quantities determined by the electron wave function at the nucleus involving complex gamma functions.

In this work a modified version of the Bethe-Bacher approximation⁽³⁾ was used to calculate the Fermi function. The modification is

$$F(Z, W) = F_B(Z, W) \cdot [1 + (a\xi + b\xi^2)(1 - e^{-cp})] \quad (Z > 50) \quad (14)$$

where

$$\begin{aligned} \xi &= Z - 50 \\ a &= .405 \times 10^{-3} \\ b &= 2.23 \times 10^{-5} \\ c &= 1.26 \end{aligned}$$

and $F_B(Z, W)$ is the Bethe-Bacher value. The approximation was tested against the exact expression, which was calculated on a CYBER computer using a previously developed algorithm⁽⁴⁾ for the complex gamma function. Agreement is better than 0.6% for energies up to 3 MeV and atomic numbers up to 100.

The shape factor S_0 is unity for allowed and first-forbidden non-unique transitions. For first-forbidden unique transitions

$$S_1 = L_0 q^2 + 9L_1 \quad (15)$$

where q is the neutrino momentum and L_0 and L_1 are quantities involving both the complex gamma function and the hypergeometric function. We have fitted the tabulated values⁽⁵⁾ to functions of the form

$$L_0 = a + bp \quad (16)$$

and

$$\begin{aligned} 9L_1 &= [c + mp + g \exp(-\lambda, p - \lambda_2 p^2)] p^2 & p < 1.4 M_e C \\ L_1 &= c + mp & p > 1.4 M_e C \end{aligned} \quad (17)$$

where p is the electron momentum. A comparison between the exact shape factor for $Z = 40$, $E_0 = 5 M_e C^2$, and that obtained using equations (16) and (17) is presented in Fig. 4.

RESULTS

Calculations of beta dose point kernels have been performed previously.^(6,7) These, however, were based upon monoenergetic dose point kernels obtained by the method of moments solution of the electron transport

equation.⁽⁸⁾ As shown in Fig. 5, since energy fluctuations were not taken into account, a less disperse function is obtained than for the Monte Carlo results.

In Fig. 6 is presented a comparison between experimental values⁽⁹⁾ for ^{32}P , and various calculated dose point kernels. The experimental data was converted from air to water medium using the method described by Cross.⁽⁶⁾ The values based upon the Monte Carlo data are seen to be in good agreement with experiment throughout the range of the measurement. Beta dose point kernels for ^{14}C , ^{35}S , and ^{203}Hg based upon the transport calculations⁽⁶⁾ are compared with the present results in Fig. 7, 8 and 9. Since the effect of energy fluctuations results in range straggling, the general tendency in the present results is a slight lowering of the dose near the source of some 5% and an increase in the distance over which the energy is dissipated.

In general both calculations indicate a sharply decreasing component near the origin superimposed upon a more slowly varying component. The magnitude of the first component depends upon energy and atomic number. It is negligible for the high energy ^{32}P , but significant for the lower energy ^{35}S . We have investigated the possibility of obtaining analytical representations for the beta dose point kernels, in the form

$$F(x) = L(x) + Be^{-\lambda x} . \quad (18)$$

In this case, the fractional residual range is written

$$u = c(Z, E_0) - x \quad (19)$$

where $c(Z, E_0)$ is a fitted cut-off parameter. Several examples of the fitted results are shown in Figures 10 to 15. Parameter values are given in Table 3.

Table 3. Beta Dose Point Kernel Parameters

Isotope	Avg. Energy	c	x_m	σ	β	λ
^{14}C	49.5	1.56	-1.33	0.322	2.13	37.0
^{32}P	695.0	1.40	-0.06	0.281	0.00	-
^{35}S	48.8	1.57	-1.57	0.331	3.78	44.7
^{131}I (β_1)	69.3	1.56	-1.50	0.330	4.30	47.2
^{131}I (β_2)	86.9	1.56	-1.18	0.315	3.80	48.6
^{131}I (β_3)	97.9	1.56	-1.01	0.305	3.51	48.2
^{131}I (β_4)	191.8	1.34	-0.85	0.367	1.80	60.9
^{203}Hg	58.2	1.59	-1.78	0.332	4.81	46.2

The fitted values are typically within 4% of the calculated values for $0 < x < 0.7$, for which 99.8% of the energy is dissipated. The deviations are less than 20% out to $x = 1.0$. Beyond this point, both the fitted and calculated functions are rapidly approaching zero, the value at $x = 1.0$ being smaller than at $x = 0.0$ by five orders of magnitude.

For a composite spectrum such as ^{131}I , the dose point kernel may be written

$$4\pi\rho r^2 K(r) = \sum_i \beta_i \bar{E}_i \cdot F(E_i, \frac{r}{R_i}) / R_i \quad (20)$$

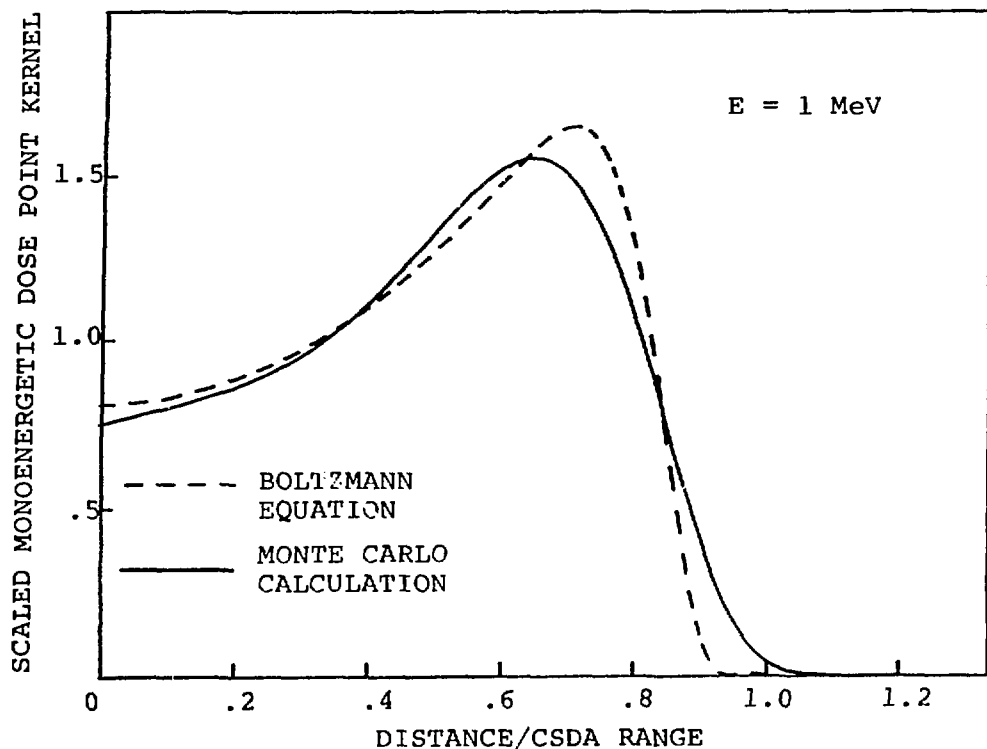


Fig. 5 Monoenergetic dose point kernels for 1 MeV electrons calculated from transport theory (dashed line) and the Monte Carlo technique (solid curve).

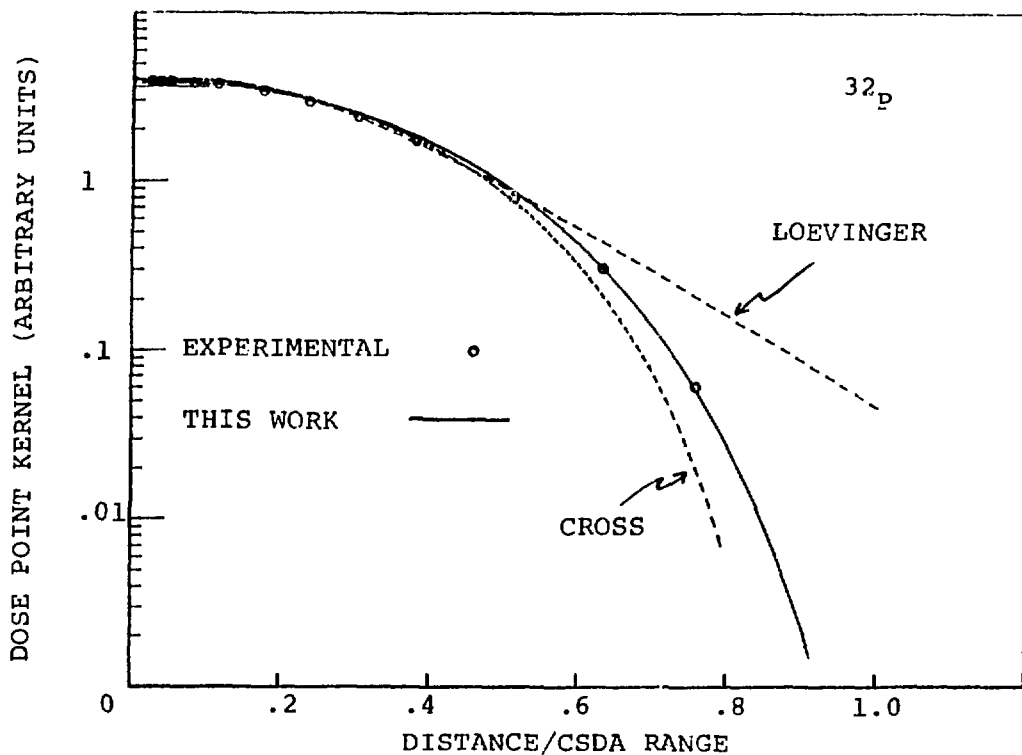


Fig. 6 The dose point kernel for ^{32}P . The solid curve represents the calculation in this work.

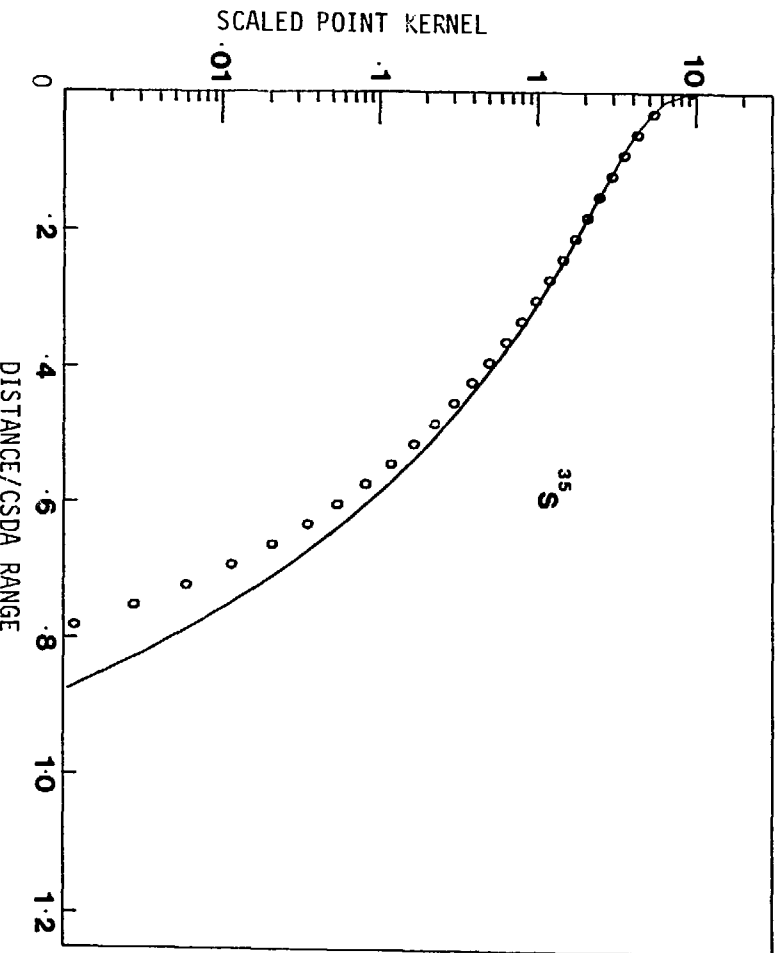


Fig. 8 Beta dose point kernel for ^{35}S .

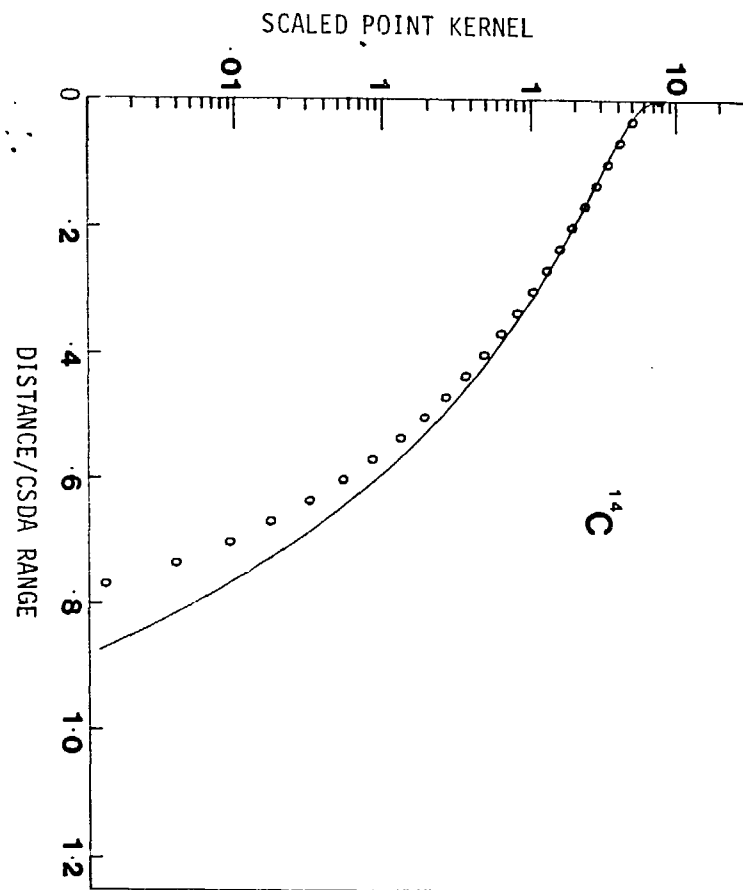


Fig. 7 Beta dose point kernel for ^{14}C . (smooth curve - Monte Carlo, circles - transport calculations).

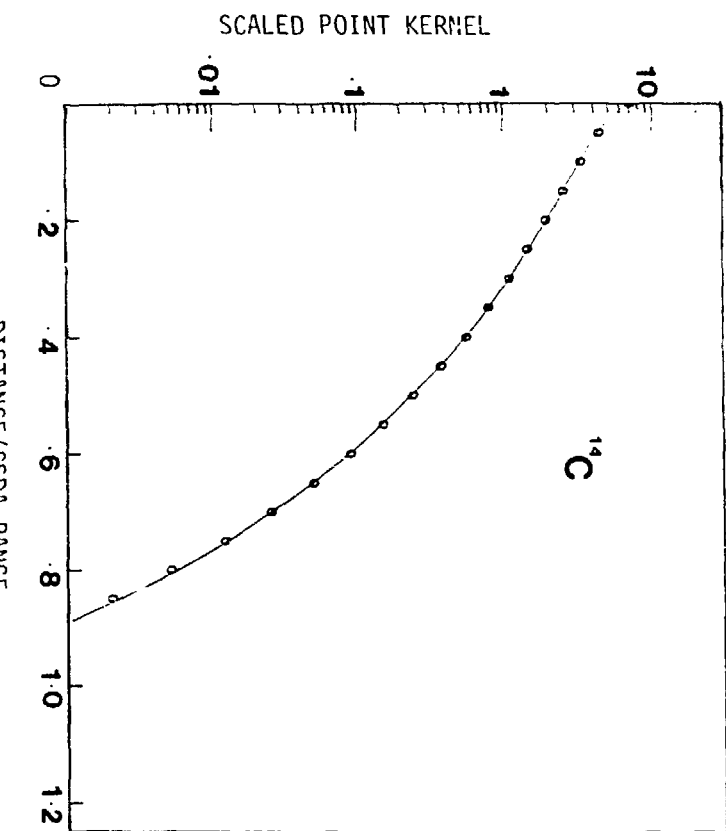


Fig. 10 Comparison of the analytic dose point kernel (smooth curve) with calculations (circles) for ^{14}C .

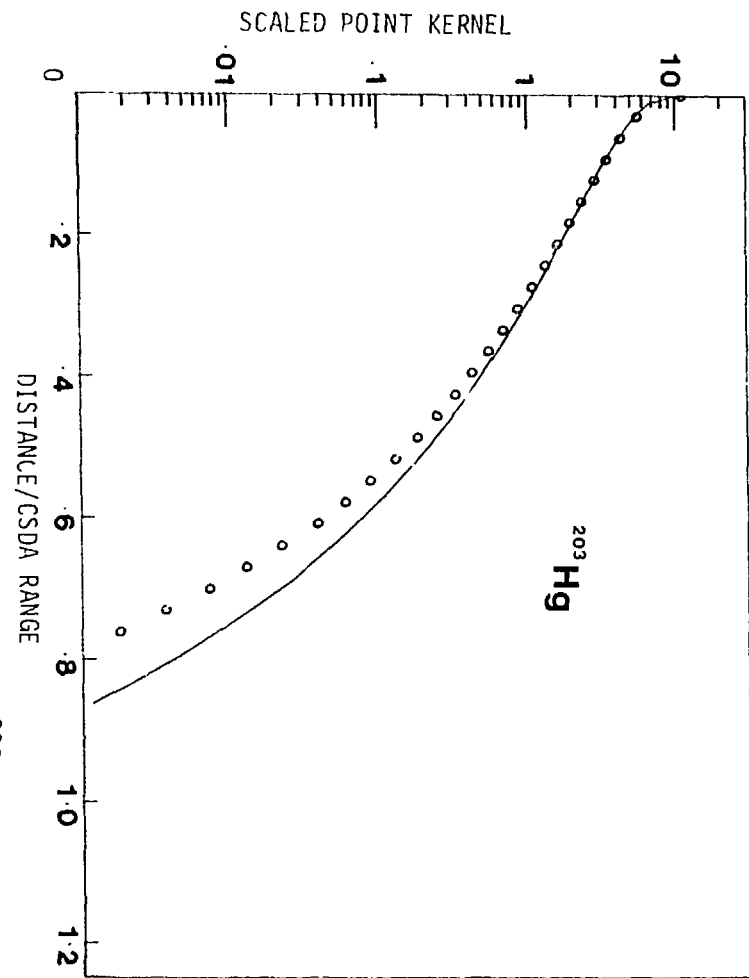


Fig. 9 Beta dose point kernel for ^{203}Hg .

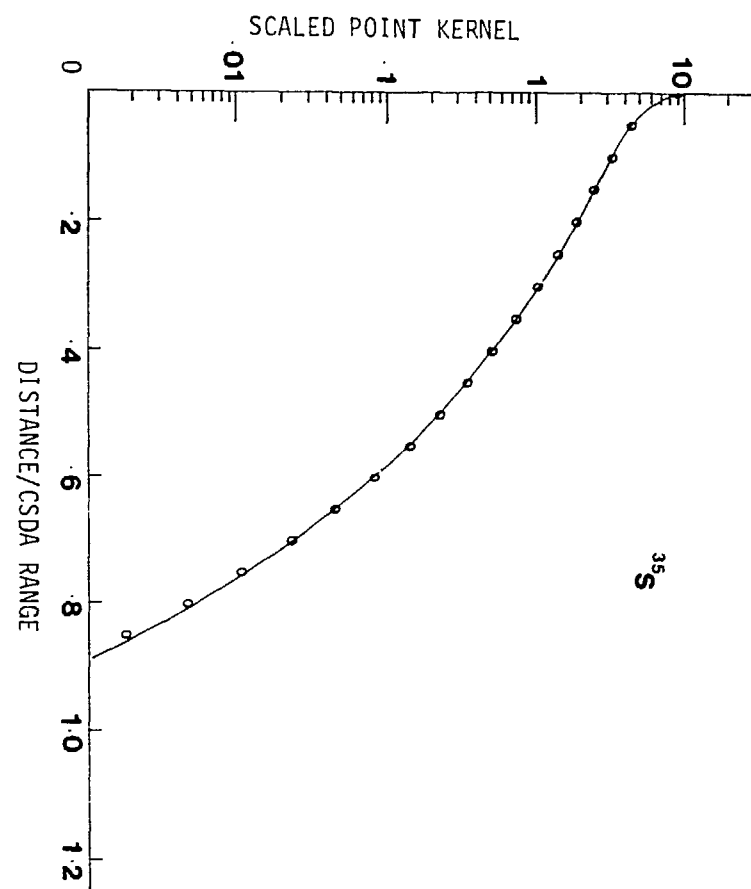
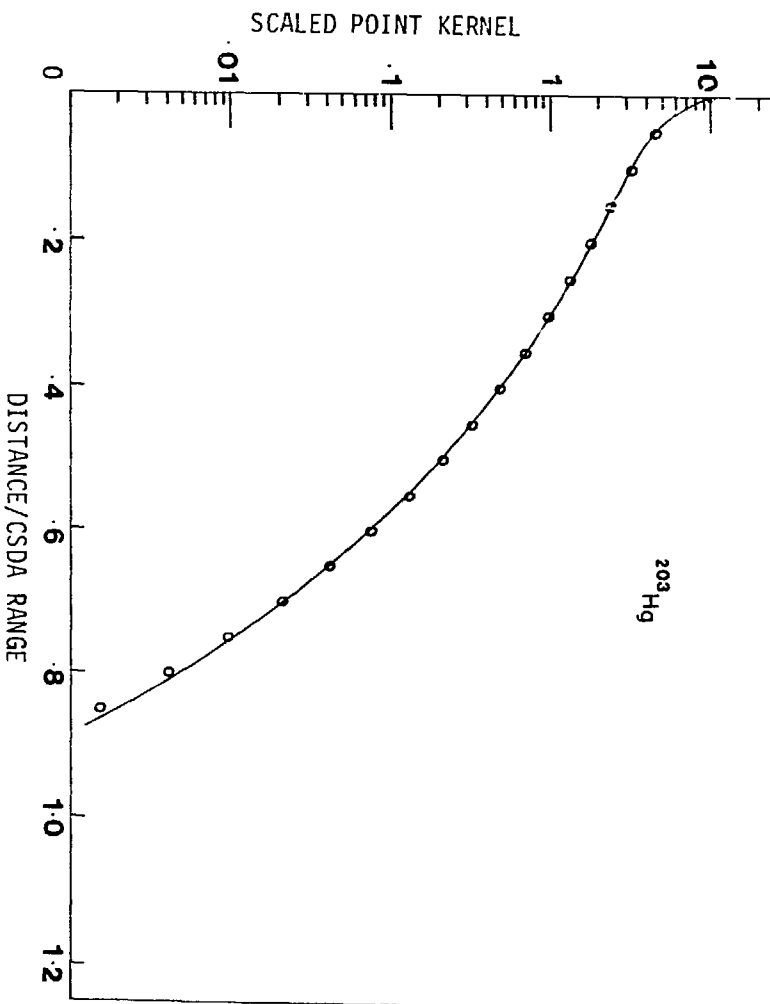


Fig. 11 Fitting of the ^{35}S dose point kernel.

Fig. 12 Fitting of the ^{203}Hg dose point kernel.

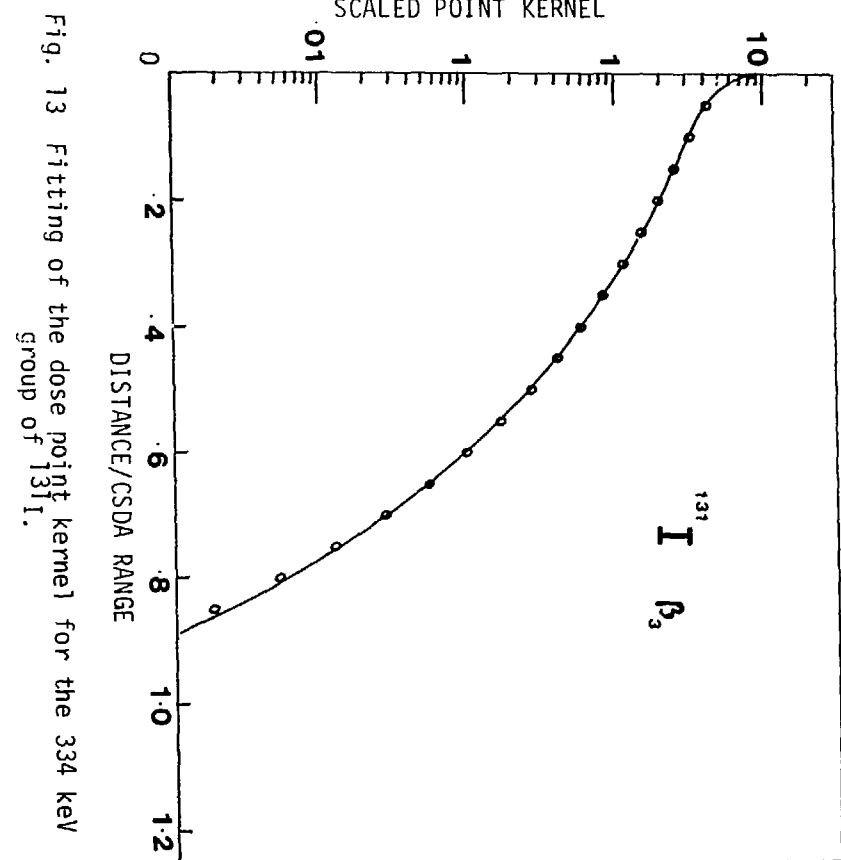
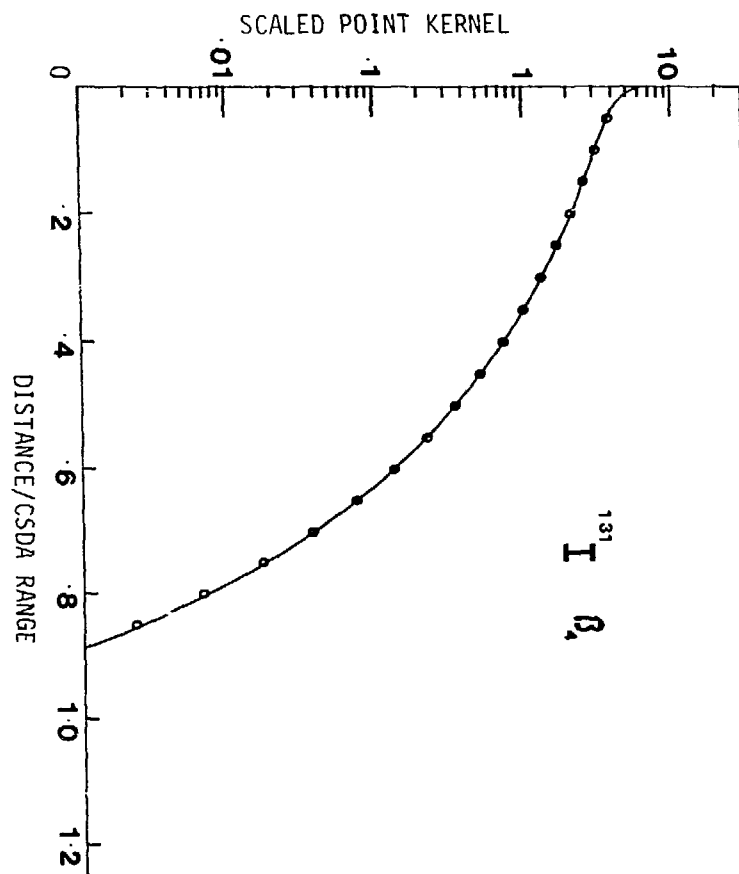


Fig. 14 Fitting of the dose point kernel for the 607 keV group of ^{131}I .

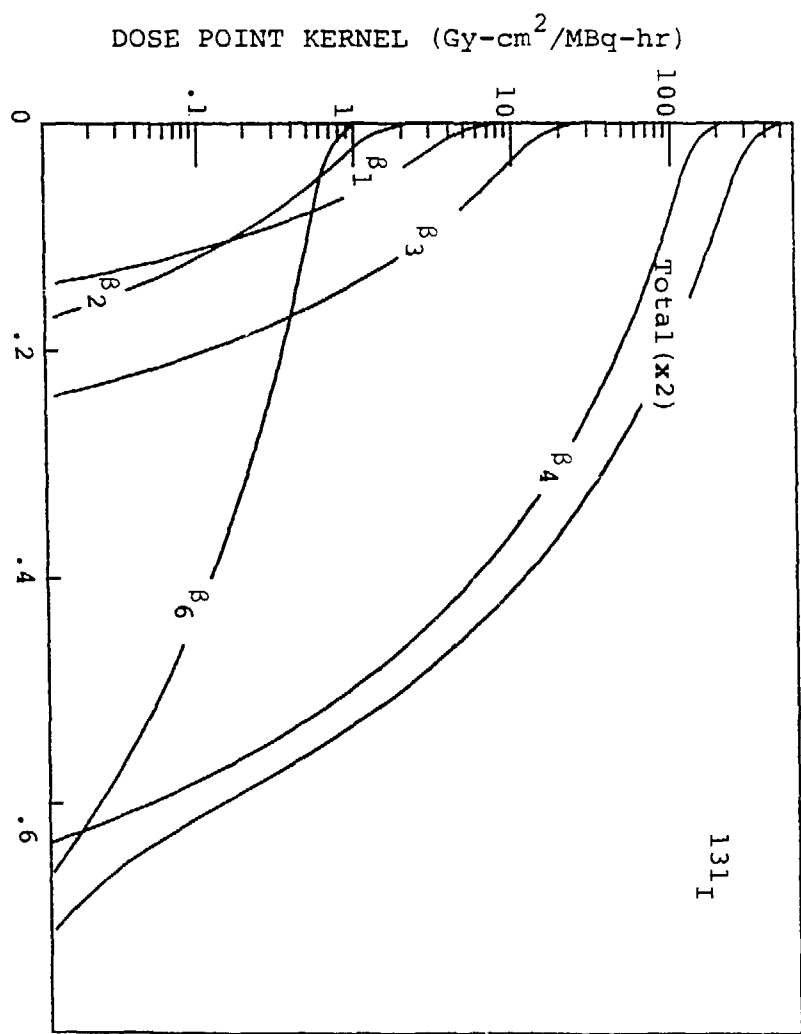


Fig. 15 Fitting of the ^{32}P dose point kernel.

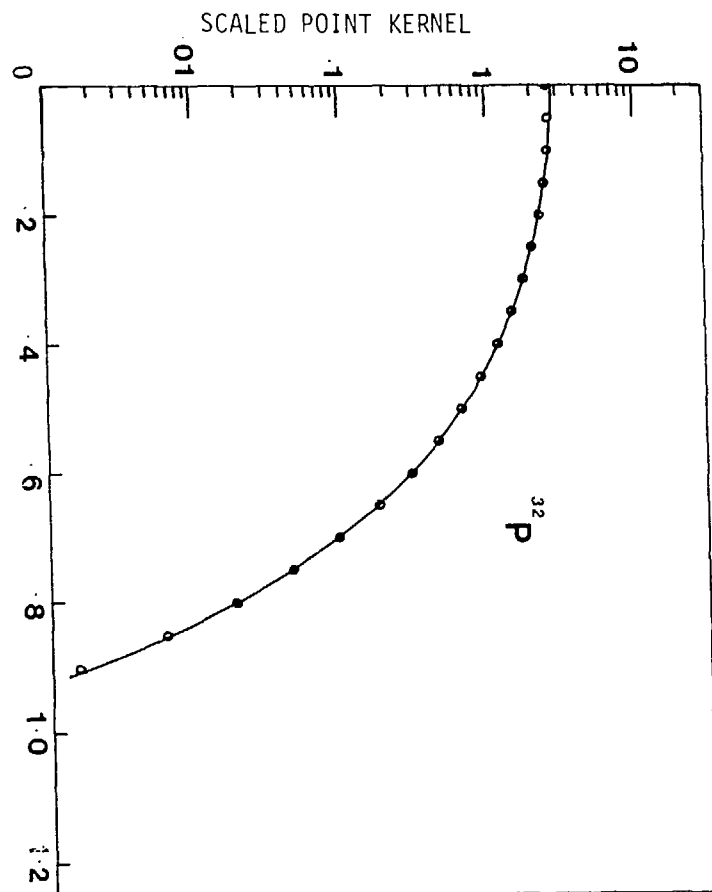


Fig. 16 Composition of the ^{131}I dose point kernel.

where β_i, E_i are the fractional intensity and average energy for the beta group with end point energy E_i and maximum C.S.D.A. range R_i . This procedure is illustrated in Figure 16, for ^{131}I .

CONCLUSIONS

It is possible to represent the monoenergetic dose point kernels calculated using the Monte Carlo method by analytic functions to a reasonable accuracy. The representation used here is awkward in that it involves a truncated Gaussian curve. We intend to investigate the use of a log normal curve to replace this component.

The beta dose point kernel for ^{32}P obtained using the Monte Carlo results is in good agreement with experiment. In general, beta dose point kernels are expected to be more diffuse than those presented in previous tabulations.^(6,7)

A reasonably accurate analytic representation of beta dose point kernels has been developed for specific radionuclides. Further work is required to generalize this approach so that the parameters of the representation are determined as functions of the atomic number and end-point energy for a beta transition of a specific type.

REFERENCES

1. Berger, M.J. Improved Point Kernels for Electron and Beta-Ray Dosimetry. Progress Report No. NBSIR 73-107, Center for Radiation Research, National Bureau of Standards, Washington, D.C. 20234 (May 1973).
2. Berger, M.J. and S.M. Seltzer. Stopping Powers and Ranges of Electrons and Positrons, 2nd edition. Report No. NBSIR 82-2550-A, U.S. Department of Commerce, National Bureau of Standards, Washington, D.C. 20234 (December 1982).
3. Bethe, H.B. and R.F. Bacher. Nuclear physics. A. Stationary states of nuclei. Reviews of Modern Physics Volume 8, No.1; pp. 82-229 (April 1936).
4. Kuki, H. Algorithm 421, Complex gamma function with error control. Com. of the A.C.M. 15, pp 262-267, 1972.
5. Rose, M.E. Tables of Forbidden β -Decay Functions: Beta and Gamma-ray Spectroscopy, edited by K. Siegbahn, pp. 884-903. North Holland Publishing Co., Amsterdam, 1959.
6. Cross, W.G., H. Ing, N.O. Freedman and J. Mainville. Tables of Beta-Ray Dose Distribution in Water, Air and Other Media. Report No. AECL-7617, Atomic Energy of Canada Limited, Chalk River, Ontario (September 1982).
7. Berger, M.J. Distribution of absorbed dose around point sources of electrons and beta particles in water and other media. Journal of Nuclear Medicine, Vol. 12, Supplement No. 5, MIRD Pamphlets No. 7-8, pp.7-23 (March 1971).
8. Spencer, L.V. Energy Dissipation by Fast Electrons. Monograph No. 1, National Bureau of Standards, 1959.
9. Clark, R.K., S.S. Brar, and L.K. Marinelli. Ionization of air by beta rays from point sources. Radiology 64, 94-104 (January 1955).

DISCUSSION

WERNER: Was your choice of the fitting function a guess or the result of a theoretical analysis?

KWOK: It is just a guess. The shape of the function inspired us to choose this function.

HINES: You made a comment about the deviation in the tail region of the P-32 beta spectra. Could you comment on the importance of that tail when you are going to do a convolution over a reasonable-sized object? This deviation should not be very important for a point source but could become important when one is doing convolutional calculations for distributed sources.

KWOK: I don't recall whether I have a slide with me which shows the difference between convolving a specified activity distribution with, say, the Loevinger expression or our new expression. But I can remember that using our expression you normally observe a higher dose rate away from the source. In order to have conservation energy, you may have a slight overestimation of dose rate if you use the Loevinger expression near the source.

SASTRY: Dr. Kwok, I would like to have some clarification. Have you simply fitted Berger's results to useful functional forms, or do you have new results on beta-ray dosimetry?

KWOK: If you have a big computer, you can predict the dose point kernel accurately using Berger's compilations. However, if you have only a small computer, you will have problems, especially when you want to look at a beta emitter or an emitter with a large number of monoenergetic electrons. Berger's compilation doesn't give you scaled dose point kernels for beta emitters; you have to do it yourself.

SASTRY: Did Berger do any beta spectra?

KWOK: As far as I know, he did some for Spencer's original compilation, not for his Monte Carlo calculations. I don't know why he didn't do it himself; he probably thought that it would be too complicated.

SASTRY: I thought Berger's calculations were Monte Carlo calculations.

KWOK: Berger's calculations for scaled dose point kernels were published twice. In 1971 he published his results based on Spencer's calculations and in 1973, he published his results based on the Monte Carlo calculations. I don't know which publication you are referring to - the latter? Yes, that was based on Monte Carlo, and we based our fitting to his Monte Carlo.

BRODSKY: Did I understand you to say that the normal distribution has two parameters and that you used three parameters for the lognormal distribution - the mean, the height and the dispersion? I know that for probability density functions both the normal and lognormal distributions can be fitted by two parameters. The mean μ and standard deviation σ fix the normal function; the geometric mean (and median) μ_g , and the standard geometric deviation S_g (or otherwise the σ_g in $\ln X$) fix the lognormal curve functions. If three parameters, including height, were needed to fit frequency functions (rather than probability density functions), would you not need to use three parameters for both normal or lognormal fitting? Why did you not use the geometric mean and standard geometric deviation as two of the three parameters in fitting the lognormal frequency functions?

KWOK: The lognormal function of each cell has two parameters, but you have to consider the amplitude. I had to introduce the Gaussian function and you can assume the amplitude of the lognormal function to be equal to the standard expression.

EFFECT OF TISSUE INHOMOGENEITY ON BETA DOSE CALCULATION

C.S. Kwok^{1,2}, M. Irfan¹, M.K. Wool¹, W.V. Prestwich²

¹Hamilton Regional Cancer Centre
Ontario Cancer Foundation
711 Concession Street
Hamilton, Ontario
Canada L8V 1C3

²McMaster University
1200 Main Street
Hamilton, Ontario
Canada L8N 3Z5

ABSTRACT

Appropriate monoclonal antibodies labelled with beta-emitting nuclides of high specific activity have been suggested for treatment of specific tumors. In a homogeneous medium the radiation dose rate distribution R due to a distributed activity distribution C can be calculated by convolution of the beta dose point kernel of the radionuclide in soft tissue with C. Prototype computer programs using Fast Fourier Transform techniques have been developed to evaluate the three dimensional spatial convolution efficiently.

To study the effect of tissue inhomogeneity on R, we simulated a soft tissue-bone interface by a polystyrene (PST)-aluminum (Al) interface and considered the backscattering of beta rays from a point source and a plane source of ^{32}P . LiF thermoluminescent dosimeters were used. With the point source at the PST-Al interface, R at 0-31, 125-156, and 283-314 mg/cm² separations from the interface were increased by $(12 \pm 3)\%$, $(8 \pm 2)\%$, and $(3 \pm 2)\%$, respectively, compared with a PST-PST interface. With the plane source, the increases were $(8 \pm 3)\%$, $(6 \pm 3)\%$, and $(5 \pm 5)\%$ for separations of 23-58, 150-184, and 277-311 mg/cm², respectively. With the point source at a PST-air interface to simulate soft tissue-air interface, R at 0-31, 139-170, and 283-314 mg/cm² from the interface were decreased by $(25 \pm 4)\%$, $(11 \pm 7)\%$, and $(5 \pm 2)\%$, respectively. The changes in R have also been measured with degraded spectra of ^{32}P . Comparison of the experimental data with Monte Carlo calculation and the "Two-Group" method of calculation will be discussed.

I. INTRODUCTION

One of the most severe limitations in the delivery of tumorcidal radiation doses is the risk of injury to normal tissues surrounding the target volume. Recent advances in the development of monoclonal antibodies

against tumors have reawakened interest in using such antibodies as carriers of intense ionizing radiation emitted by radionuclides. A number of beta-emitting nuclides such as ^{131}I , ^{67}Cu , ^{109}Pd , and ^{90}Y (1-4) having short ranges of penetration have been suggested.

Radioimmunotherapy modelling calculations based on Medical Internal Radiation Dose (MIRD) type dosimetry gives reasonable estimates of gamma-emitting radionuclides in comparing the absorbed doses from organ to organ in humans, but fails to be predictive when examining particulate radiation in the subcentimeter range at tumor boundaries, for tumor heterogeneities, and at organ interfaces. In the MIRD formalism, particulate radiation is simply treated as nonpenetrating. Since it is envisioned that antibody therapy will be performed predominately by particulate radiation, substantial uncertainty in computing dose deposition will become a major factor in determining tumor dose response to therapy.

This paper presents some experimental data and Monte Carlo calculation results pertinent to the calculation of radiation doses to tumors and normal tissues with the various beta-emitting nuclides likely to be used for the labelling of the antibody in the presence of tissue inhomogeneity. The types of tissue inhomogeneity include bone and air cavity.

II. METHODS

1. Microdosimetry of Distributed Beta Sources in Homogeneous Volume of Soft Tissue

From experiments of tumor localization by radiolabelled monoclonal antibodies, it is known that vascularization in the tumor is an important factor for the antibody distribution (5,6). High concentration of radioactivity is normally found at the periphery of tumor nodules. Necrotic areas of the tumor show diffuse and very low concentrations of radioactivity. This highlights the inadequacy of the MIRD system in calculating doses arising from nonuniformly distributed sources of particulate radiations.

The dose rate distribution $\vec{D}(\vec{r})$ produced by a nonuniform activity concentration $C(\vec{r}_s)$ in a homogeneous volume of soft tissue is given by

$$\vec{D}(\vec{r}) = \int_{\text{Source Volume}} C(\vec{r}_s) J(|\vec{r} - \vec{r}_s|) d^3 r_s \quad [1]$$

Source
Volume

where $J(r)$ gives the dose rate at different distances from a point source of unit activity. Loevinger's empirical formula (7) has been used commonly for J but more accurate expressions of J for several radionuclides in water have recently been obtained by us (8).

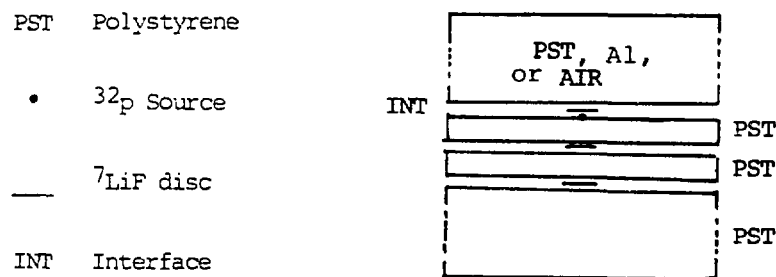
Using Fast Fourier Transform numerical techniques (9,10), we have developed prototype computer programs (11) on a PDP 11/34 computer to evaluate the convolution integral in equation [1] for any given activity distribution C of beta-emitting nuclides. The input format of C can be an analytic expression or a three-dimensional matrix.

2. Effect of Tissue Inhomogeneity on Beta Point Source Dose Distribution

To solve the problem of beta dosimetry in heterogeneous media, it is usual to employ the realistic and, in principle, accurate Monte Carlo method. A few sophisticated Monte Carlo codes for charged particle transport (12-16) have been discussed in the literature. These codes however are too time consuming for routine dosimetry. Some of them are not flexible enough to be applied to problems other than those they are designed for. The Electron-Gamma-Shower (EGS) code (14, 15) is an exceptionally flexible computer package which was originally designed for high energy physics applications but has recently been modified and corrected for low energy electron transport (15).

Simpler empirical or semi-empirical methods, providing for rather fast estimates, have been proposed for routine dosimetry for heterogeneous media (17-20). Such methods are generally of limited accuracy and are valid only for special cases.

To study the effect of bone and air cavity on the beta dose distribution in soft tissue, we have performed experiments for two well-defined geometries of activity and boundary conditions. We simulated a plane soft tissue-bone interface by a polystyrene-aluminum interface and measured the backscattered beta rays in polystyrene (PST) from a point source of ^{32}P . ^{7}LiF thermoluminescent dosimeters (5mm diameter teflon discs of thickness 0.13 mm and mass thickness 31 mg/cm²) positioned at three different separations from the interface were used. A plane PST-air interface was also used to simulate a soft tissue-air interface. This is shown schematically in Figure 1.



Max. Kinetic Energy of electrons at the interface
is in the range 1.64-1.70 MeV

Figure 1. Geometrical arrangement of dosimetry system used to measure the change in beta point source dose distribution in polystyrene due to the presence of a plane polystyrene-aluminum interface or a plane polystyrene-air interface.

In either interface, the point source of ^{32}P could be positioned at the interface or separated from the interface by known thickness of PST plates. Thus, measurements with beta rays of degraded energies at the interface could be made.

From the above measurements, we determined the following ratio:

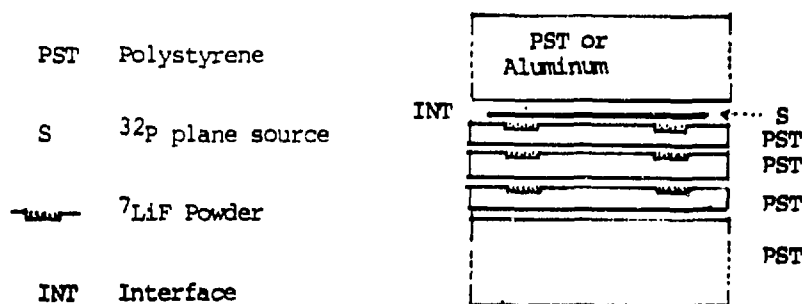
$$\frac{D_R}{R} = \frac{\text{Dose rate per unit activity for PST-nonPST interface}}{\text{Dose rate per unit activity in homogeneous PST phantom}} \quad [2]$$

Note that the quantity in the numerator was measured at the same location when the selected portion of the phantom was replaced by the nonPST substance under investigation.

3. Effect of Tissue Inhomogeneity on Beta Plane Source Dose Distribution

Thin circular sources of ^{32}P , about 7.5 cm in diameter and within 5% variation in source strength, have been prepared by soaking pieces of filter paper in a solution of the radionuclide. Each of these sources was used as an infinite plane source to small, shallow wells of ^7LiF thermoluminescent powder drilled in thin polystyrene plates. The wells were 13 mm in diameter, 0.18 mm deep, and symmetrically situated on opposite sides of the centres of the plates. There were two wells to each polystyrene plate. The wells in different plates, when stacked one above the other, did not overlap each other because they were rotationally shifted by multiples of 22.5° . Figure 2 shows how such a stack could be used to measure ratio D_R for a plane source of ^{32}P and for a plane polystyrene-aluminum interface.

^{32}P PLANE SOURCE : POLYSTYRENE/ALUMINUM INTERFACE



Max. Kinetic Energy of electrons at the interface
is in the range 1.68-1.70 MeV

Figure 2. Geometrical arrangement of dosimetry system used to measure the change in beta plane source dose distribution in polystyrene due to the presence of a plane polystyrene-aluminum interface.

III. RESULTS

1. Polystyrene-Aluminum Interface for a Point Source

With the point source of ^{32}P at the polystyrene-aluminum interface, beta doses at 0-31, 125-156, and 283-314 mg/cm^2 separations from the interface were increased by $(12 \pm 3)\%$, $(8 \pm 2)\%$, and $(3 \pm 2)\%$, respectively, compared with the doses in homogeneous polystyrene. Standard errors are quoted. A single exponential function can be fitted to the data as shown in Figure 3.

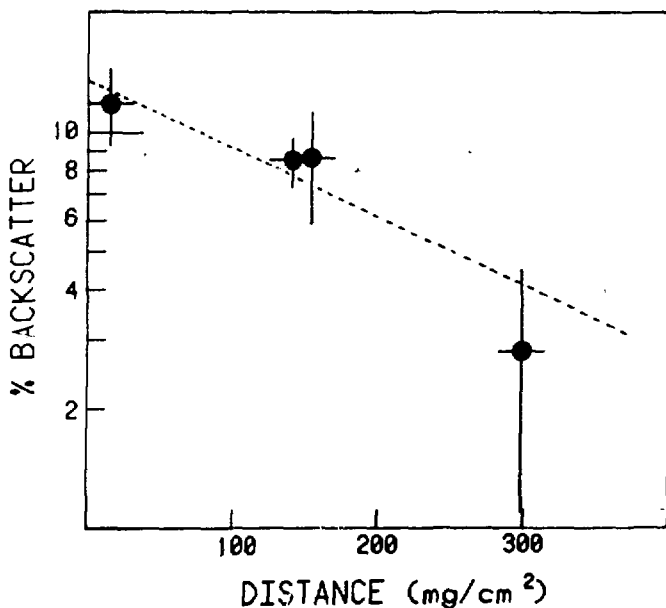


Figure 3. Variation of increase in backscattered dose from a plane polystyrene-aluminum interface with separation of dosimeters from the interface. The error bars correspond to 1 S.E. The dotted line represents the least-squares fit to the data points. A point source of ^{32}P was located at the interface.

When polystyrene plates of thicknesses 35.8, 149.2, and 278.3 mg/cm^2 were used to degrade the energies of the beta particles of ^{32}P incident on the polystyrene-aluminum interface, no significant difference in the increase of beta dose at 0-31 mg/cm^2 separation from the interface was observed. Table I gives the approximate average energies of the beta rays at the interface and the respective increases in beta dose at the interface. It remains to be determined if the same increase of $(12 \pm 3)\%$ in beta dose applies to lower average energy than 0.47 MeV at the interface.

Table 1. Increases in Backscattered Beta Dose at a Plane Polystyrene-Aluminum Interface for Three Different Average Energies of the Beta Particles of a Point Source of ^{32}P Incident on the Interface

Absorber thickness between source and interface (mg/cm^2)	Approximate average beta energy at interface (MeV)	$\frac{\text{PST-Aluminum dose rate}}{\text{PST-PST dose rate}}$
35.8	0.69	1.12 ± 0.026
149.2	0.57	1.14 ± 0.018
278.3	0.47	1.14 ± 0.036

2. Polystyrene-Air Interface for a Point Source

When the point source of ^{32}P was put at a plane polystyrene-air interface to simulate a soft tissue-air interface, beta doses at 0-31, 139-170, and 283-314 mg/cm^2 from the interface were decreased by $(25 \pm 4)\%$, $(11 \pm 7)\%$, and $(5 \pm 2)\%$, respectively. Standard errors are quoted. The rate of decrease with separation of the TLD dosimeter from the interface is exponential (see Figure 4).

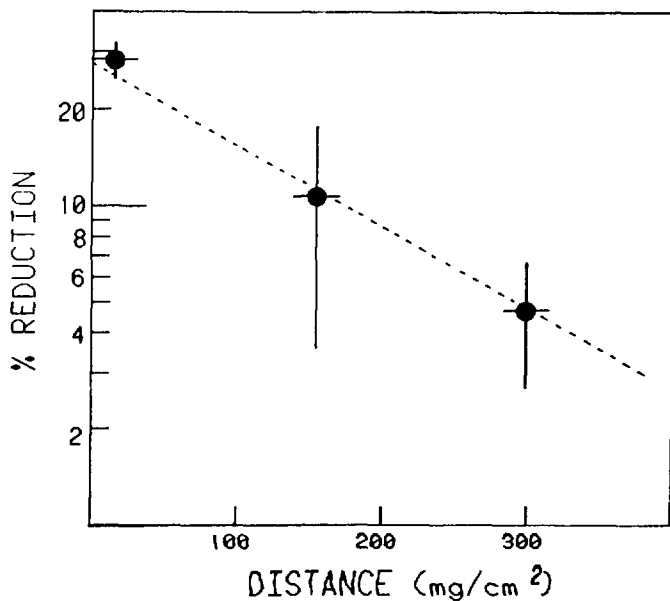


Figure 4. Variation of decrease in backscattered dose from a plane polystyrene-air interface with separation of dosimeters from the interface. See caption to Figure 3 for details.

3. Polystyrene-Aluminum Interface for a Plane Source

For the plane source configuration, the increases in beta dose were $(8 \pm 3)\%$, $(6 \pm 3)\%$, and $(5 \pm 5)\%$ for separations of 23-58, 150-184, and 277-311 mg/cm^2 , respectively, from the polystyrene-aluminum interface compared with the doses in homogeneous polystyrene. Standard errors of measurement are quoted. These increases in beta dose agree with those for the point source configuration (see section III.I) within the errors of measurement. As shown by the dotted line in Figure 5, a single exponential function fits the data well. In the same figure, the continuous curve represents the predicted variation of increase in backscattered dose with separation according to the "Two-Group" method of calculating beta doses in heterogeneous media proposed by Radzievsky and Komarov (20).

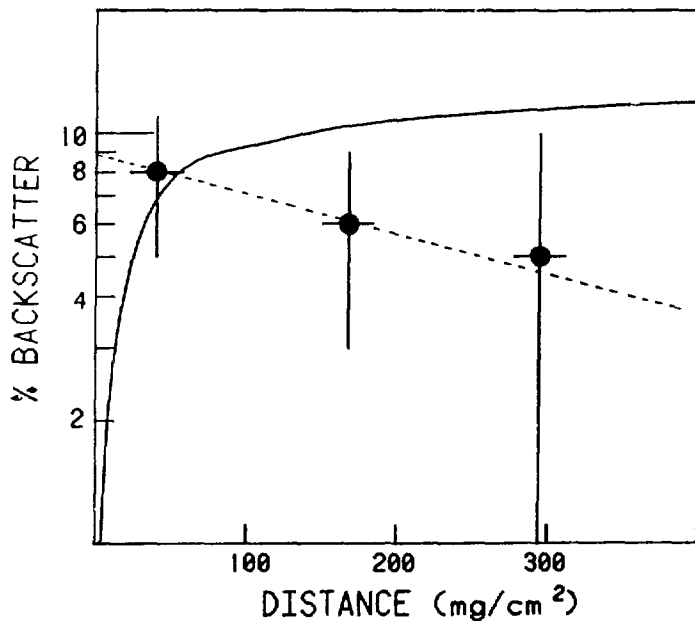


Figure 5. Variation of increase in backscattered dose from a plane polystyrene-aluminum interface with separation of dosimeters from the interface for a plane source of ^{32}P . The dotted line represents the least-square fit to the data points, shown as mean ± 1 standard error. The continuous curve is the prediction from the "Two Group" theory for a plane water-aluminum interface.

4. Monte Carlo Calculation Using the EGS Code

The Monte Carlo Code EGS has also been used to calculate the increase in backscattered dose at a polystyrene-aluminum interface due to an isotropic point source of monoenergetic electrons. The source was assumed to be at the interface. A small disc-like dosimeter having the same composition as water,

5 mm in diameter, and 31 mg/cm² in thickness was located just below the source in polystyrene. The dosimeter was used to score energy deposited by electrons from the source in a homogeneous medium of polystyrene or in the presence of a thick slab of aluminum on top of the source. The geometrical arrangement for this model calculation therefore was very close to that used experimentally in Figure 1.

The calculation result is shown in Table 2 for electron energies from 0.1 to 1.75 MeV. No increase in backscattered dose was observed below 0.2 MeV, but there was a rapid increase in backscattered dose to 6 ± 2 (S.E.)% at 0.5 MeV and 11 ± 2% at 1.0 MeV. By fitting a smooth curve to these data points by the least-square method and by integrating the dose increases with the beta spectrum of ³²P, an increase of 6 ± 2% would be predicted if a point source of ³²P were used in the model calculation.

Table 2. Monte Carlo Calculation Using EGS for an Isotropic Point Source of Monoenergetic Electrons Located at a Polystyrene (PST)-Aluminum (Al) Interface or a PST-PST Interface

Electron Energy (MeV)	0.1	0.2	0.5	0.75	1.00	1.25	1.5	1.75
Dose Ratio for PST-AL to PST-PST Interfaces	1.00	1.00	1.06	1.05	1.11	1.11	1.11	1.11

Standard error due to sampling = 2% of average value

IV. CONCLUSIONS

Due to a combination of several factors including the radiosensitivity of the red bone marrow and rapid entry of labelled antibody into bone marrow extracellular space, the red bone marrow and to less extent the endosteal cells of the bone are critical tissues to consider in using radiolabelled antibodies for systemic treatment of disseminated cancer. As the first step of a systematic approach to study the effect of bone on beta dose distribution in soft tissue, we have measured the increase in backscattered dose in polystyrene at several separations from a plane interface of polystyrene and aluminum due to a point source or a plane source of ³²P. We assumed that polystyrene is a good substitute for soft tissue and aluminum a good substitute for crystallised hard bone. Within the errors of measurement both the point source and the plane source give an exponential variation of dose increase with separation from the interface, the maximum increase being approximately 10 ± 3% at 0-31 mg/cm² from the interface. A main source of error was the inaccuracy of calibrating the thermoluminescent dosimeters.

When the average energy of the beta particles of ³²P incident on the polystyrene-aluminum interface was decreased from 0.69 MeV to 0.47 MeV, no significant difference in the increase of beta dose at 0-31 mg/cm² separation from the interface was observed. It appears therefore that the increase in backscattered dose from aluminum may not be a sensitive function of beta

energy provided that the energy is above a critical value. Experiments with beta emitters of lower end point energies, such as ^{204}Tl and ^{35}S , are required to prove this assumption.

Our set of backscattered dose increases for a plane source of ^{32}P at a polystyrene-aluminum interface can be compared and contrasted with the calculated values according to the "Two-Group" theory proposed by Radzievsky and Komarov (20) for the same plane source of ^{32}P at a water-aluminum interface. This has been done in Figure 5. The "Two-Group" theory predicts an initial rapid rise in the increased backscattered dose from 0% to 7% for separation from 0 to 50 mg/cm^2 approximately. This is followed by a much slower monotonic increase for larger separation. At 300 mg/cm^2 separation, for instance, the increase is about 11%. Our experimental results, however, show an exponential drop in the additional backscattered dose with separation from the interface. By the same experimental technique, we have also measured the increase in backscattered dose due to a plane polystyrene-cadmium interface at three distances. The results are shown in Figure 6. Cadmium results in higher backscattered dose than aluminum. An exponential function can be used to represent the variation of dose increase with separation. This again disagrees with the calculated values by the "Two-Group" theory, which are shown as a continuous curve in Figure 6. Reasons for the disagreement between our experimental results and the "Two-Group" theory are uncertain.

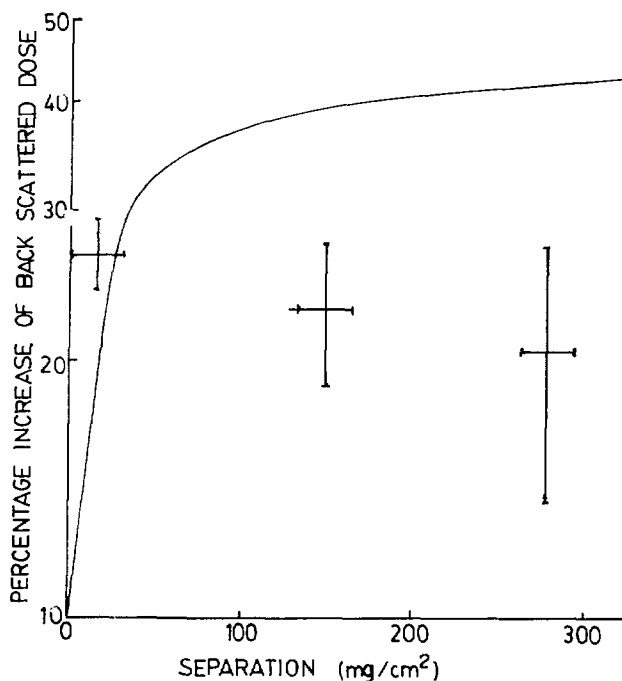


Figure 6. Variation of increase in backscattered dose from a plane polystyrene-cadmium interface with separation of dosimeters from the interface for a plane source of ^{32}P . The data points represent mean \pm standard error. The continuous curve is the prediction from the "Two-Group" theory for a plane water-cadmium interface.

Comparing the results in sections III.1 and III.4, it appears that the Monte Carlo EGS predicts a dose increase of $(6 \pm 2)\%$, different from our experimentally measured value of $(12 \pm 3)\%$ for a dosimeter located at $0\text{-}31$ mg/cm^2 from a plane polystyrene-aluminum interface. A point source of ^{32}P was assumed to be at the interface for both cases. We shall repeat the Monte Carlo calculation for a larger number of electron histories, especially for electron energies between 0.2 MeV and 1.0 MeV. If the accuracy of EGS is confirmed by experiments, it will be used to generate detailed dose distributions for point sources of beta emitters in the vicinity of realistic tissue boundaries.

The effect of air cavity on beta dose was investigated by the same experimental technique as for the effect of bone on beta dose. If the air cavity was assumed to be semi-infinite in dimension, a maximum decrease of $(25 \pm 4)\%$ in dose rate was obtained. It will be of practical importance, such as in the calculation of radiation dose for lung tumors, to extend our measurement to air cavities of smaller sizes and nuclides with lower end point energies than that of ^{32}P . A reliable Monte Carlo code will again be useful in generating detailed dose distributions for this type of interface.

Our objective is to develop an effective surface source concept which may explain quantitatively the perturbation of beta dose in heterogeneous media from their respective homogeneous media for different types of tissue boundary. Perturbations that result from anatomical configurations will be calculated with this concept, obviating the requirements for specific repetitive Monte Carlo calculations in clinical situations.

ACKNOWLEDGEMENT

This research work was supported by a National Science and Engineering Research Council operating grant and a Medical Research Council Research Grant in Canada.

REFERENCES

1. Order, S.E., J.L. Klein, D. Ettinger, P. Alderson, S. Siegelman, and P. Leichner. Phase I-II study of radiolabelled antibody integrated in the treatment of primary hepatic malignancies. *Int. J. Radiat. Oncol. Biol. Phys.* 6, 703-710, 1980.
2. Cole, W., S. DeNardo, C. Meares, G. DeNardo, and H. O'Brien. Development of copper-67 chelate conjugated monoclonal antibodies for radioimmuno-therapy. *J. Nucl. Med.* 24, P 30-31, 1983.
3. Fawwaz, R.A., T.S.T. Wang, S.C. Srivastava, J.M. Rosen, S. Ferrone, M.A. Hardy, and P.O. Alderson. Potential of palladium-109-labelled antimelanoma monoclonal antibody for tumor therapy. *J. Nucl. Med.* 25, 796-799, 1984.
4. Hnatowich, D.J., F. Virzi, and P.W. Doherty. DTPA-coupled antibodies labelled with yttrium-90. *J. Nucl. Med.* 26, 503-509, 1985.
5. Moshakis, V., R.A.J. McIlhinney, and A.M. Neville. Cellular distribution of monoclonal antibody in human tumors after i.v. administration. *Br. J. Cancer* 44, 663-669, 1981.

6. Buchegger, F., C.M. Haskell, M. Schreyer, B.R. Scazziga, S. Randin, S. Carrel, and J.P. Mach. Radiolabelled fragments of monoclonal antibodies against carcinoembryonic antigen for localization of human colon carcinoma grafted into nude mice. *J. Exp. Med.* 158, 413-427, 1983.
7. Loevinger, R., E.M. Japha, and G.L. Brownell. Discrete Radioisotope Sources in Radiation Dosimetry, ed. G.J. Hine and G.L. Brownell, Acad. Press, N.Y., 693-799, 1956.
8. Prestwich, W.V., L.B. Chan, C.S. Kwok, and B.C. Wilson. Dose point kernels for beta-emitting radioisotopes, in Proceedings of Fourth International Radiopharmaceutical Dosimetry Symposium, Oak Ridge, Tennessee, Nov. 5-8, 1985.
9. Cooley, J.W. and J.W. Tukey. An algorithm for the machine calculation of complex Fourier series. *Math. Comput.* 19, 297-301, 1965.
10. Singleton, R.C. An algorithm for computing the mixed Radix Fast Fourier Transform. *IEEE Trans. Audio Electroacoust.* AU-17, 93-103, 1969.
11. Kwok, C.S., W.V. Prestwich, and B.C. Wilson. Calculation of radiation doses for nonuniformly distributed β and γ radionuclides in soft tissue. *Med. Phys.* 12, 405-412, 1985.
12. Berger, M.J. Monte Carlo calculation of the penetration and diffusion of fast charged particles, in Methods in Computational Physics, ed. by B. Alder, S. Fernbach and M. Rotenberg, Academic Press, N.Y., pp 135-215, 1965.
13. Seltzer, S.M. and M.J. Berger. Transmission and reflection of electrons by foils. *Nucl. Inst. Method* 119, 157-179, 1974.
14. Ford, R.L. and W.R. Nelson. The EGS Code System, Stanford Linear Accelerator Center Report No. 210, Stanford, California, U.S.A., 1978.
15. Rogers, D.W.O. Low-energy electron transport with EGS. *Nucl. Inst. Meth.* A 227, 535-548, 1984.
16. Rohloff, F. A Monte Carlo program for the transport of beta particles through layers of different material in Proceedings of the International Beta Dosimetry Symposium, Washington, D.C., Feb. 15-18, 1983; U.S. Nuclear Regulatory Commission Pub. CP-0050, pp. 25-28.
17. O'Brien, K., S. Samson, R. Sanna, and J.E. McLaughlin. The application of "one-group" transport theory to β -ray dosimetry. *Nucl. Sci. Engin.* 18, 90-96, 1964.
18. Charlton, D.E. Energy dissipation near an interface: A more realistic approach to electron range and stopping power. *Radiat. Res.* 44, 575-593, 1970.
19. Unnikrishnan, K. Transport of energy by electrons across an interface. *Radiat. Res.* 70, 275-283, 1977.
20. Radzievsky, G.B. and N.A. Komarov. Dose distributions from β -radiation in heterogeneous media: "Two-Group" method of calculation. *Int. J. Appl. Radiat. Isot.* 33, 733-743, 1982.

DISCUSSION

WERNER: I did some work in this area in connection with external electron beam dosimetry. In fact, I have a paper which will appear in the November-December issue of Medical Physics¹ reporting on analytic calculations that show conclusions similar to those which you found. A year or two ago, Klevenhagen,^{2,3} in England, again looking at external electron beams found similar kinds of things that you're showing experimentally.

KWOK: As I recall, they used 3-MeV electron beams and above and recorded only about a 4% increase in dose rate. When we look at beta emitters with low energy, the increase in dose rates is higher.

WERNER: It's difficult to argue with Klevenhagen's work because most of his work is with lead, not aluminum, and most of it was with much higher energies. When he went down to low energies, he didn't believe his own measurements. He did talk about publications by other people, and he did indicate how things might vary with atomic numbers as you go down to lower atomic numbers. It's not very believable.

KWOK: I can add a little to that information. We did some experiments with a P-32 point source backscattered by lead, and we observed about 60% to 70% increase in the dose rate. In cadmium, as I recall, the increase was about 30%. As I understand it, if you have energy above 3 or 4 MeV, the backscattering was not as serious a problem as for low-energy electrons.

¹Werner, B.L. The perturbation of electron beam dose distributions at medium interfaces. *Medical Physics* 12(6), 754-763, 1985.

²Klevenhagen, S.C., G.D. Lambert, and A. Arbabi. Backscattering in electron beam therapy for energies between 3 and 35 MeV. *Phys. Med. Biol.*, 27(3): 363-375, 1982.

³Lambert, G.D. and S.C. Klevenhagen. Penetration of backscattered electrons in polystyrene for energies between 1 and 25 MeV. *Phys. Med. Biol.* 27(5): 721-725, 1982.

A PRELIMINARY MODEL OF THE CIRCULATING BLOOD FOR USE IN RADIATION DOSE CALCULATIONS

J. W. Poston, A. Aissi*, T. Y. Hui, and B. M. Jimba
Texas A&M University, College Station, TX 77843

3nd

*King Faisal Specialist Hospital, Riyadh, Saudi Arabia

ABSTRACT

Currently there is a need for a dosimetric model to describe the circulatory system in an adult human. This need exists because of the increasing number of radiopharmaceuticals used in nuclear medicine which are confined primarily to the blood, have short half-lives, and irradiate the body as they move through the circulatory system. A preliminary design of such a system has been completed based on a review of the literature. This model has been incorporated into the MIRD phantom and calculations have been completed for a number of exposure situations. The model will be discussed in detail and preliminary results of calculations using this model will be presented.

INTRODUCTION

Imaging procedures utilizing radiolabelled leukocytes, platelets, and erythrocytes have increased steadily over the last few years. Marcus et al (1) indicated recently that over 600 physician-sponsored Investigational New Drug Applications have been approved for the use of indium-111 labelled leukocytes. In addition, these authors estimated that perhaps tens of thousands of patients have undergone these procedures, utilizing this one radionuclide, for the imaging of infections and inflammatory foci. This rapid growth in the number of procedures and the number of radionuclides available for such studies emphasizes the need for estimates of the absorbed doses to tissues and organs of the body as well as the dose to the "blood", itself.

This is not a new problem, however. As early as 1974, estimates of the dose to blood from monoenergetic electron, beta radiation, and low energy photon sources distributed uniformly in the blood were reported (2). In this work⁺, blood levels were approximated by infinite right circular cylinders ranging in radius from 0.0004 cm (capillaries) to 1.75 cm (heart). Absorbed fractions for 20 beta-emitting radionuclides were calculated with values ranging from 1.0 for H-3 ($E_{max} = 0.0186$ MeV) to 0.70 for Y-90 ($E_{max} = 2.27$ MeV).

One interesting result of this work was the provision of data which showed the effect of assuming all nonpenetrating radiation is absorbed locally. In

⁺Editors' note: initial model was developed by Cloutier and Watson and reported on in 1970 at the first radiopharmaceutical dosimetry symposium (11).

other words, these data indicated the magnitude of the error associated with the assumption that none of the available radiation energy escaped the volume containing the radionuclide. Most dosimetry codes assume the radionuclide is distributed uniformly in the source region and, for non-penetrating radiation, consider only irradiation of the source region by itself. For high energy beta-emitting radionuclides, e.g., P-32, the absorbed dose to the blood was overestimated by about 50%.

DEVELOPMENT OF A MODEL OF THE CIRCULATING BLOOD

Currently, the MIRD Committee of The Society of Nuclear Medicine has a great need for a model to describe the circulatory system in an adult human (3) and a Task Group has been established to attack this problem. As stated previously, this need exists because of the large number of radionuclides used in nuclear medicine which have short half-lives and only irradiate the body as they are carried throughout the body in the circulatory system. In addition, no model is available at present which describes concentrations of radionuclides in regions, such as the "face", which are fed primarily from the blood pool.

An initial effort has been made toward the development of a very simple model of the circulating blood. The initial attempt was directed toward the development of a static model which incorporated the major features of the circulatory system and the most important organs or tissues. As the necessary data are accumulated more sophistication will be added to the model. This manuscript describes a preliminary model and presents the results of initial calculations of specific absorbed fractions for monoenergetic photon sources in the blood model, and describes plans for future activities.

DESCRIPTION OF THE BLOOD MODEL

Initial data, on which the model was based, were selected from the Report on Reference Man (4) and an evaluation of available data on blood volume and distribution in the circulatory system (5,6). Preliminary design of the model was developed by the MIRD Task Group. Data were available, from several sources (7,8), for a hypothetical male, weighing about 63 kg and having a total blood volume in the range 5000 to 5100 ml. A total blood volume of 5200 ml was selected as being appropriate for a 70 kg adult. This value was in agreement with the data selected for the Reference Man (4). Table 1 gives the distribution of the blood in the total body based on this blood volume. Table 2 shows a more extensive breakdown on the blood distribution in the adult. The total volume obtained from this table ranges between 5103 and 5437 ml and, therefore, the 5200 ml value selected for the model is in apparent agreement with these data.

The Report on Reference Man (4) also presented data on the total blood volume in most organs of the body. These data were used to select those organs which should be included explicitly in the model. In addition, these data provided important guidance on those organs or regions of the body which could be combined into a single region in the model. Organs included in the blood model were the brain, heart, kidneys, liver, lungs and the spleen. Special regions, created for use in the simplified model, included the extremities, face, intestines, aorta and vena cava, and the "remainder". Table 3 gives the total blood volume assumed to be in each organ or region of the model.

TABLE 1: Distribution of Blood in the Total Body (4)

Organ/Region/System	Blood Volume (ml)
Arterial system	1000
Venous system	3200
Pulmonary system	500
Heart cavities	500
TOTAL BLOOD VOLUME	5200

TABLE 2: Distribution of Blood in the Adult Human (4)

Organ/Region/System	Blood Volume (ml)
Arterial System	
Aorta	100 - 180
Arteries	420
Arterioles	70
Capillaries	280
TOTAL ARTERIAL SYSTEM:	800 - 950
Venous System	
Vena cava	300
Veins	2600
Venuoles	300
TOTAL VENOUS SYSTEM:	3200
Pulmonary System	
Arteries	200
Veins	230
Capillaries	100
TOTAL PULMONARY SYSTEM:	530
Heart	
Right atrium	100 - 185
Left atrium	100 - 130
Right ventricle	160 - 230
Left ventricle	143 - 212
TOTAL HEART:	500 - 757

Those organs named specifically in Table 3 are described mathematically by equations which were already part of the existing computer code. All other regions were designed especially for use in the model of the circulating blood. A short description of each of these regions is given below.

TABLE 3: Blood Model Parameters

Organ/Region/System	Blood Volume (ml)	Percentage of total
brain	260	5.0
heart	500	9.6
kidneys	70	1.3
liver	280	5.4
lungs	520	10.0
spleen	90	1.7
arms	520	10.0
legs	780	15.0
face	220	4.2
intestinal region	700	13.5
aorta and vena cava	410	7.9
remainder	850	16.3
TOTAL	5200	100.0

Extremities:

The extremities are right circular cylinders, 1 cm. in diameter, located just to the inside of the existing arm and leg bones. For example, cylinders representing the arm regions lie between the existing arm bone and the ribs and run parallel to the bone region. Each arm region had a length of 69 cm. while each leg region was 79.8 cm. in length. The arm regions were moved forward 2.5 cm. along the y-axis to eliminate overlapping with the ribs.

$$\text{Arm regions: } [x \pm (17.9 - 0.02029 z)]^2 + (y + 2.5)^2 \leq 0.5^2$$

$$0 \leq z \leq 69.$$

The + and - correspond to the right and left arm regions, respectively.

$$\text{Leg regions: } [x \pm (6 + 0.06892z)]^2 + y^2 \leq 0.5^2$$

$$-79.8 \leq z \leq 0.$$

Face region:

A region representing the "face" was added because of high blood flow through the region and data indicating that significant radioactivity was present in the region during some procedures. The face region was assumed to be a region on the lower two-thirds of the head (i.e., $70 < z < 85.5$). This region was formed by a plane which cut vertically through the elliptical cylinder of the head at $y = -7$. Care was taken in the definition of the face region to assure that there was no overlap between this region and the brain, another source organ.

$$-5 < x < 5$$

$$-7 \leq y \leq -10$$

$$70 \leq z \leq 85.5$$

$$\left(\frac{x}{7}\right)^2 + \left(\frac{y}{10}\right)^2 \leq 1$$

$$\left(\frac{x}{6}\right)^2 + \left(\frac{y}{9}\right)^2 + \left(\frac{z-86.5}{6.5}\right)^2 > 1$$

The last equation excludes the brain from the face region.

Intestinal Region:

The intestinal region was assumed to be located in the lower trunk constrained between $z = 0$ and $z = 27$. For simplicity, the region was assumed to be represented by an elliptical cylinder with essentially the same dimensions as the trunk. However, the skin was not included in this region. The semi-major axis of the elliptical cylinder was assumed to be 19.8 cm. and the semi-minor axis was 9.8 cm. The center of this region, a circular region with the same height and a radius of 2.5 cm., was removed to bring the volume in line with the design parameters. Care was also taken that the intestinal region did not overlap with the aorta and vena cava region.

$$x^2 + y^2 \geq 2.5^2$$

$$\left(\frac{x}{19.8}\right)^2 + \left(\frac{y}{9.8}\right)^2 \leq 1$$

$$0 \leq z \leq 27.$$

Aorta and Vena Cava:

This region was described by a right circular cylinder with a radius of 2.5 cm. located between $z = 8$ and $z = 44.8$. Care was taken to eliminate overlap with the liver and heart source organs.

$$x^2 + y^2 \leq (2.5)^2$$

$$\frac{x}{35} + \frac{y}{45} - \frac{z}{43} > - 1$$

$$8 \leq z \leq 44.7761$$

The second equation excludes the liver from the region whereas the last inequality excludes the heart.

Remainder:

The "remainder" was assumed to be the total body minus all other organs and regions mentioned above. This region was included to account for the essentially uniform distribution of a large fraction of the total blood volume in the body. A special source subroutine was prepared which allowed the selection of starting coordinates for photon histories uniformly throughout the phantom except in the organs and regions included explicitly in the model of the circulating blood.

CALCULATIONS OF ABSORBED FRACTIONS

Using the model described above, computer calculations of the absorbed fractions were performed for the 12 monoenergetic photon energies ranging from 0.01 to 4.0 MeV. In each calculation 60,000 photon histories were traced. Tables 4 through 6 present the absorbed fractions for the 12 monoenergetic photon sources uniformly distributed in the model of the circulating blood. Data on the specific absorbed fractions were also obtained from these calculations but tabulations have not been included in this manuscript.

It is difficult to draw significant conclusions from these initial results. One major reason for this is the influence of the source regions. In previous calculations, for example data given in MIRD Pamphlet No. 5 (9), a single source organ is selected and the specific absorbed fractions of energy are calculated for the source organ and all other organs of the MIRD phantom. In this calculation, there are eleven specific source organs or regions, as well as a region called the "remainder". The calculation scheme and the results obtained here are similar, but not directly analogous, to those of Fisher and Snyder (10) for Cs-137.

Trends in the data, however, can be divided into two general categories. These categories are those organs which serve as "significant" sources (i.e., those listed in Table 3) and those organs which comprise the remainder.

For the first category, the absorbed fraction of energy in the organ drops rapidly as the photon energy increases. Above 0.1 MeV, however, the absorbed

fraction becomes essentially constant for each individual organ. Table 7 presents a summary of the mean absorbed fraction for the six source organs named specifically. These data indicate that the absorbed fraction is constant (within about than 20%) for monoenergetic photon sources with energies between 0.1 and 4.0 MeV.

In contrast, the "remainder" organs serve primarily as targets. The remainder is assumed to contain more than 16% of the total blood volume but this amount of blood is distributed uniformly throughout the 70 kg mass of the phantom (with the exception of those source organs and regions named specifically). In this case, the absorbed fraction as a function of photon energy increases rapidly as the energy is increased. In the region 0.05 to 0.01 MeV, the distribution reaches a maximum and then declines rapidly as the photon energy is increased. Organs or regions which show this type of behavior include the red bone marrow and the stomach.

TABLE 4: ABSORBED FRACTIONS FOR MONOENERGETIC PHOTON EMITTERS IN
THE CIRCULATING BLOOD
60,000 PHOTON HISTORIES

TARGET ORGAN	0.01 MeV	0.015 MeV	0.02 MeV	0.03 MeV
	ABS. FRACT.	ABS. FRACT.	ABS. FRACT.	ABS. FRACT.
ADRENALS	0.17E-4 (100.0)*	0.15E-3 (31.8)	0.11E-3 (33.5)	0.17E-3 (19.5)
BLADDER	0.65E-3 (15.8)	0.44E-3 (17.6)	0.57E-3 (13.4)	0.60E-3 (10.5)
BRAIN	0.51E-1 (1.8)	0.47E-1 (1.8)	0.41E-1 (1.9)	0.28E-1 (2.2)
STOMACH	0.55E-3 (17.3)	0.56E-3 (16.2)	0.60E-3 (13.3)	0.12E-2 (7.3)
UL. INT.	0.32E-2 (7.1)	0.32E-2 (6.8)	0.29E-2 (6.4)	0.28E-2 (5.0)
LL. INT.	0.13E-2 (11.3)	0.12E-2 (11.3)	0.13E-2 (9.6)	0.13E-2 (7.4)
SM. INT.	0.29E-1 (2.4)	0.25E-1 (2.4)	0.26E-1 (2.4)	0.21E-1 (2.3)
HEART	0.93E-1 (1.3)	0.84E-1 (1.3)	0.72E-1 (1.4)	0.48E-1 (1.6)
KIDNEYS	0.12E-1 (3.8)	0.98E-2 (4.0)	0.82E-2 (4.2)	0.56E-2 (4.2)
LIVER	0.50E-1 (1.8)	0.49E-1 (1.8)	0.47E-1 (1.8)	0.40E-1 (1.7)
LUNGS	0.91E-1 (1.3)	0.75E-1 (1.4)	0.54E-1 (1.6)	0.32E-1 (1.7)
R. MARROW	0.74E-2 (3.0)	0.99E-2 (2.5)	0.14E-1 (1.9)	0.23E-1 (1.4)
Y. MARROW	0.72E-2 (2.3)	0.12E-1 (1.7)	0.18E-1 (1.3)	0.26E-1 (1.0)
OVARIES	0.66E-4 (50.0)	0.79E-4 (43.4)	0.12E-3 (31.2)	0.77E-4 (25.7)
PANCREAS	0.25E-2 (8.1)	0.32E-2 (6.9)	0.29E-2 (6.7)	0.20E-2 (6.4)
SKELETON	0.50E-1 (1.8)	0.79E-1 (1.4)	0.12E+0 (1.0)	0.17E+0 (0.8)
TOT. SKIN	0.13E-1 (3.4)	0.12E-1 (3.3)	0.13E-1 (2.8)	0.12E-1 (2.2)
SPLEEN	0.16E-1 (3.2)	0.12E-1 (3.4)	0.11E-1 (3.6)	0.69E-2 (4.0)
TESTES	0.17E-3 (31.3)	0.13E-3 (32.3)	0.81E-4 (38.0)	0.15E-3 (22.7)
THYMUS	0.13E-3 (35.2)	0.69E-4 (46.7)	0.13E-3 (27.5)	0.27E-3 (15.8)
THYROID	0.18E-2 (9.5)	0.14E-2 (10.4)	0.14E-2 (9.3)	0.72E-3 (10.3)
UTERUS	0.53E-2 (5.6)	0.53E-2 (5.4)	0.46E-2 (5.5)	0.29E-2 (5.7)
TOT. BODY	1.0 (0.02)	0.98 (0.05)	0.95 (0.08)	0.83 (0.2)

*Coefficient of variation.

TABLE 5: ABSORBED FRACTIONS FOR MONOENERGETIC PHOTON EMITTERS IN
THE CIRUCLATING BLOOD
60,000 PHOTON HISTORIES

	0.05 MeV	0.10 MeV	0.20 MeV	0.50 MeV
TARGET ORGAN	ABS. FRACT.	ABS. FRACT.	ABS. FRACT.	ABS. FRACT.
ADRENALS	0.13E-3 (14.9)*	0.11E-3 (15.1)	0.99E-4 (19.7)	0.86E-4 (26.8)
BLADDER	0.46E-3 (8.5)	0.31E-3 (9.4)	0.26E-4 (12.5)	0.22E-3 (16.6)
BRAIN	0.15E-1 (2.5)	0.89E-2 (2.8)	0.95E-2 (2.8)	0.95E-2 (3.1)
STOMACH	0.13E-2 (5.2)	0.98E-3 (5.7)	0.82E-3 (6.7)	0.89E-3 (8.2)
UL. INT.	0.22E-2 (4.1)	0.16E-2 (4.5)	0.15E-2 (5.4)	0.13E-2 (7.0)
LL. INT.	0.11E-2 (5.9)	0.90E-3 (5.8)	0.82E-3 (7.0)	0.69E-3 (9.1)
SM. INT.	0.14E-1 (2.3)	0.99E-2 (2.4)	0.94E-2 (2.5)	0.87E-2 (3.0)
HEART	0.24E-1 (1.8)	0.14E-1 (2.0)	0.14E-1 (2.1)	0.15E-1 (2.4)
KIDNEYS	0.34E-2 (3.9)	0.25E-2 (4.0)	0.23E-2 (4.7)	0.24E-2 (5.5)
LIVER	0.27E-1 (1.7)	0.18E-1 (1.8)	0.17E-1 (1.9)	0.17E-1 (2.2)
LUNGS	0.16E-1 (1.7)	0.10E-1 (1.9)	0.96E-2 (2.2)	0.97E-2 (2.7)
R. MARROW	0.24E-1 (1.2)	0.13E-1 (1.3)	0.88E-2 (1.5)	0.71E-2 (1.9)
Y. MARROW	0.24E-1 (0.9)	0.12E-1 (1.1)	0.77E-2 (1.3)	0.68E-2 (1.6)
OVARIES	0.71E-4 (20.1)	0.68E-4 (20.9)	0.84E-4 (20.8)	0.29E-4 (53.6)
PANCREAS	0.12E-2 (5.8)	0.85E-3 (6.3)	0.81E-3 (7.6)	0.64E-1 (10.4)
SKELETON	0.15E+0 (0.7)	0.81E-1 (0.9)	0.54E-1 (1.0)	0.46E-1 (1.2)
TOT. SKIN	0.87E-2 (1.9)	0.70E-2 (2.0)	0.75E-2 (2.3)	0.80E-2 (2.8)
SPLEEN	0.29E-2 (4.5)	0.21E-2 (4.6)	0.19E-2 (5.2)	0.21E-2 (6.2)
TESTES	0.12E-3 (16.2)	0.95E-4 (17.9)	0.73E-4 (21.8)	0.14E-3 (24.2)
THYMUS	0.19E-3 (13.3)	0.16E-3 (13.7)	0.17E-3 (15.8)	0.14E-3 (21.3)
THYROID	0.34E-3 (11.1)	0.15E-3 (14.0)	0.23E-3 (14.5)	0.25E-3 (16.9)
UTERUS	0.16E-2 (5.6)	0.10E-2 (6.2)	0.88E-3 (7.6)	0.88E-3 (9.3)
TOT. BODY	0.59 (0.3)	0.40 (0.4)	0.35 (0.4)	0.36 (0.4)

*Coefficient of variation.

TABLE 6: ABSORBED FRACTIONS FOR MONOENERGETIC PHOTON EMITTERS IN
THE CIRCULATING BLOOD
60,000 PHOTON HISTORIES

	1.0 MeV	1.5 MeV	2.0 MeV	4.0 MeV
TARGET ORGAN	ABS. FRACT.	ABS. FRACT.	ABS. FRACT.	ABS. FRACT.
ADRENALS	0.70E-4 (32.3)*	0.65E-4 (36.4)	0.88E-4 (32.0)	0.50E-4 (46.2)
BLADDER	0.23E-3 (18.8)	0.29E-3 (18.5)	0.25E-3 (19.6)	0.18E-3 (26.4)
BRAIN	0.87E-2 (3.5)	0.85E-2 (3.7)	0.77E-2 (3.9)	0.65E-2 (4.3)
STOMACH	0.75E-3 (10.3)	0.60E-3 (11.8)	0.70E-3 (12.0)	0.60E-3 (13.7)
UL. INT.	0.13E-2 (8.1)	0.13E-2 (8.5)	0.13E-2 (9.1)	0.10E-2 (10.5)
LL. INT.	0.84E-3 (10.2)	0.66E-3 (11.7)	0.71E-3 (11.7)	0.61E-3 (14.0)
SM. INT.	0.84E-2 (3.4)	0.74E-2 (3.7)	0.70E-2 (3.9)	0.57E-2 (4.6)
HEART	0.14E-1 (2.7)	0.12E-1 (3.1)	0.12E-1 (3.2)	0.94E-2 (3.6)
KIDNEYS	0.21E-2 (6.4)	0.21E-2 (6.9)	0.21E-2 (7.3)	0.15E-2 (8.7)
LIVER	0.17E-1 (2.5)	0.14E-1 (2.7)	0.13E-1 (2.9)	0.11E-1 (3.4)
LUNGS	0.86E-2 (3.3)	0.78E-2 (3.5)	0.75E-2 (3.8)	0.62E-2 (4.4)
R. MARROW	0.64E-2 (2.3)	0.62E-2 (2.5)	0.60E-2 (2.6)	0.48E-2 (3.0)
Y. MARROW	0.62E-2 (1.9)	0.60E-2 (2.0)	0.55E-2 (2.1)	0.46E-2 (2.5)
OVARIES	0.46E-4 (41.7)	0.57E-4 (41.4)	0.72E-5 (45.3)	0.39E-4 (55.6)
PANCREAS	0.74E-3 (10.8)	0.69E-3 (12.1)	0.63E-3 (12.9)	0.46E-3 (16.4)
SKELETON	0.42E-1 (1.4)	0.40E-1 (1.6)	0.38E-1 (1.6)	0.32E-1 (1.9)
TOT. SKIN	0.78E-2 (3.3)	0.81E-2 (3.4)	0.69E-2 (3.8)	0.62E-2 (4.3)
SPLEEN	0.20E-2 (6.9)	0.16E-2 (8.1)	0.16E-2 (8.3)	0.13E-2 (9.4)
TESTES	0.13E-3 (25.6)	0.11E-3 (31.8)	0.49E-4 (46.1)	0.84E-4 (37.6)
THYMUS	0.13E-3 (24.6)	0.66E-4 (32.0)	0.55E-4 (39.8)	0.11E-3 (31.7)
THYROID	0.23E-3 (20.5)	0.25E-3 (20.8)	0.12E-3 (29.6)	0.10E-3 (32.1)
UTERUS	0.59E-3 (11.7)	0.85E-3 (10.8)	0.66E-3 (12.8)	0.43E-3 (16.3)
TOT. BODY	0.34 (0.5)	0.31 (0.5)	0.29 (0.5)	0.25 (0.6)

*Coefficient of variation.

TABLE 7: Mean Absorbed Fraction of Energy for Organs Containing Blood

Source Organ	Percent Blood Volume	Mean Absorbed Fraction*	Standard Deviation	Percent Standard Deviation
Liver	5.4	0.015	0.003	20
Heart	9.6	0.013	0.002	15
Brain	5.0	0.0085	0.001	12
Lungs	10.0	0.0085	0.001	12
Kidneys	1.3	0.0021	0.0003	14
Spleen	1.7	0.0018	0.0003	17

*For photon energies between 0.1 and 4.0 MeV.

ON-GOING DEVELOPMENTS

It should be emphasized that these data are preliminary and results may change as modifications are made to the model. Several changes to the existing code are also in process which will provide more useful and more meaningful data.

First, the current code has no provision for calculating the absorbed fractions of energy for the "blood" itself nor for the specifically designed regions which comprise part of this model. Modifications to the code will be made to meet this need for those regions named specifically in the model. A plan of attack for the remainder region is being formulated but the exact approach is not clear at this point.

The source routine and other parts of the code are being modified with the goal of providing S-values for radionuclides in the circulating blood. This will require modification of the source routine to accept decay scheme information rather than simply specifying the photon energy. In addition, other parts of the code must be modified to allow the calculation of S rather than absorbed fractions and specific absorbed fractions.

Finally, once these modifications are complete, and the code has been checked carefully, the code will be used to calculate S-values for those radionuclides commonly used in imaging procedures involving the circulating blood. A preliminary list of the important radionuclides has been compiled by the MIRD Task Group. This list will serve as a starting point for use of the modified code and the blood model.

REFERENCES

1. Marcus C.S., M.G. Stabin, E.E. Watson, and J.H. Kuperus, "Contribution of contaminant indium - 114m/indium - 114 to indium - 111 oxine blood dosimetry," J. Nucl Med 26: 1091-1093, 1985.
2. McEwan A.C., "Dosimetry of radionuclides in blood", Brit. J. Radiology: 47 652-656, 1975.
3. Budinger T.F., Donner Laboratory, University of California, Berkeley, personal communication, 1983.
4. International Commission on Radiological Protection, Report of the Task Group on Reference Man, ICRP Publication 23, Pergamon Press, Oxford, 1975.
5. Cowles A.L., H.H. Bergstedt, and A.J. Gillies, "Tissue weights and rates of blood flow in man for the prediction of anesthetic uptake and distribution," Anesthesiology: 35, 523-526, 1971.
6. Albert S.N., Blood Volume, pp 28-30, Charles C. Thomas, Springfield, IL, 1963.
7. Bard P., Medical Physiology, 11th edition, p. 46, C.V. Mosby Co., St. Louis, 1961.
8. Burton A.C., Physiology and Biophysics of the Circulation; An Introductory Text, 2nd edition, Year Book Medical Publishers, Chicago, 1972.
9. Snyder W.S., M.R. Ford, and G.G. Warner, "Estimates of Specific Absorbed Fractions for Photon Sources Uniformly Distributed in Various Organs of a Heterogeneous Phantom," MIRD Pamphlet No. 5, Revised, Society of Nuclear Medicine, New York, 1978.
10. Fisher H.L., Jr. and W.S. Snyder, "Distribution of dose in the body for a source of gamma rays distributed uniformly in an organ," ORNL-4168, Union Carbide Corp., Nuclear Division, Oak Ridge National Laboratory, pp. 245-257, 1968.
11. Cloutier R.J. and E.E. Watson, "Radiation Dose from Radioisotopes in the Blood," in Medical-Radionuclides: Radiation Dose and Effects, eds. R.J. Cloutier, C.L. Edwards, and W.S. Snyder, pp. 325-346, Oak Ridge, Tennessee, 1970.

DISCUSSION

MITCHELL: I am not quite sure what problem you are solving. I don't think that it was clear in the presentation as to what the source organ is and what the target organ is. For example, are you talking about the blood within the small intestines as a source and the small intestines as a target, or what?

POSTON: Is your question pertaining to my comments about blood irradiating blood?

MITCHELL: You have 5200 ml of blood which is distributed throughout a 70-kg anthropomorphic phantom; you have the source within that blood; the activity within the blood emits penetrating and nonpenetrating radiations. Now, are you talking about the dose to an organ from the blood contained within the organ? If so, how does that differ from the dose to an organ from the activity within the organ?

POSTON: Well, the activity in the organ is only one component.

MITCHELL: But the blood is uniformly distributed throughout the organ or it is in those organs where it is not uniformly distributed throughout the organ. Are you taking that into consideration?

POSTON: That is taken into account in the remainder. Remember that the remainder has 16% of the blood. The source routine consists of naming those organs which contain the majority of the blood and making the assumptions that you just enumerated: Uniformly distributed activity emits both penetrating and nonpenetrating radiation. Now the remainder of the blood is assumed to be uniformly distributed throughout the entire 70-kg mass so that you have these defined regions in the phantom which have some amount of the activity and then there is another portion of the activity that is distributed uniformly in all tissues.

MITCHELL: Let's take something like the liver. Within the liver are vessels and sinuses of vastly different sizes and within those sinuses are areas where the dose to the blood itself is no different from the dose to the blood in the heart, or any other large pool. On the other hand, there are sections of the liver where the blood concentration per gram of tissue is not the same as it is in the sinuses or great vessels. Are you taking that into consideration?

POSTON: No, uniform distribution in the organ was one of our assumptions. At this point in the development of the model, we are working from a uniformly distributed source in the organ. We're not trying to model the detail of the kidneys or the liver or anything. Now, before I get a lot of questions requiring me to justify this, let me state I am a physicist and not a physician. I have to rely on some of my friends on the MIRD Committee to tell me what is important and what is not. So I may have to get one of them to help me.

RAO: You stated that the 16% of the blood you could not account for in the organs was assumed to be uniformly distributed throughout the 70-kg whole body. If that is the case, you will be overestimating the doses to organs. The unaccounted for blood should be distributed uniformly in the rest of the whole body not including the organs you mentioned.

POSTON: If that is what I said, that is incorrect. The "remainder" is the 70-kg mass of the phantom minus the organs which are identified specifically as source organs. Thank you for pointing that out.

SOUNDRY: You presented S values calculated for various target organs from blood distributed throughout the whole body. Have you compared those S values with values for the total body to those various organs already quoted in MIRD Pamphlet 11?

POSTON: No, we haven't at this time. We did some preliminary comparisons for cesium. Many years ago Fisher and Snyder published a paper¹ giving one of the first calculations using the phantom, where they had a cesium source uniformly distributed. The photon absorbed fraction curves from our calculations have shapes that are identical to their data. As I said, this is a preliminary model. We are still working out the details and we haven't made all the

comparisons that we should. But that's a good point and we certainly will do that.

¹H.L. Fisher, Jr. and Snyder, W.S. Variation of dose delivered by ¹³⁷Cs as a function of body size from infancy to adulthood. Health Physics Division Annual Progress Report, ORNL-4007, 1966, p. 221.

A SIMPLE DYNAMIC MODEL FOR CALCULATING
RADIATION ABSORBED DOSE TO THE BLADDER WALL

Chin-Tu Chen, Paul V. Harper, and Katherine A. Lathrop
The University of Chicago Medical Center
5841 South Maryland Avenue
Chicago, Illinois 60637

ABSTRACT

A simple model for estimating the radiation absorbed dose to the inner surface of the bladder wall has been developed. This model assumes a spherical bladder shape and takes into account the dynamic nature of the bladder filling and emptying processes. The model also allows for variable voiding schedules and a residual fraction after each voiding. Formulas for estimating the radiation absorbed dose to the bladder wall are derived analytically using classical dose calculation approaches. Two commonly used radiopharmaceuticals, F-18 labeled 2-[F-18]fluoro-2-deoxy-D-glucose (F-18-FDG) for positron imaging and Tc-99m labeled diethylenetriaminepentaacetic acid (Tc-99m-DTPA) for single-photon renal imaging, are employed to demonstrate the utility of this simple model in determining optimal strategies to achieve dose reduction. Computer simulation studies have been performed to investigate the effects of various initial bladder volumes, urine production rates, residual fractions, and voiding schedules. A general recommendation is a comfortably large initial bladder volume, a high urine production rate, and voiding after most of the activity has accumulated in the bladder, when possible. After the first few voidings at their strategically chosen times, more frequent voidings and smaller residual fractions sometimes can also reduce the radiation absorbed dose.

INTRODUCTION

The radiation absorbed dose to the surface of the bladder mucosa from the bladder content, especially for rapidly excreted radiopharmaceuticals such as F-18 labeled 2-[F-18]fluoro-2-deoxy-D-glucose (F-18-FDG) and Tc-99m labeled diethylenetriaminepentaacetic acid (Tc-99m-DTPA), is an important factor to consider in designing an optimal experimental procedure to reduce radiation hazard to the patient. Using the conventional MIRD approach (1), in which a constant bladder volume of 200 ml is assumed and the dynamic nature of bladder filling is ignored, one could be led to the questionable conclusion that earlier voiding would achieve a dose reduction in a direct linear proportion (2). More accurate estimations should involve the complex effect of variable bladder volume on the radiation absorbed dose rate calculation. Therefore, factors such as voiding schedule, urine production rate, and residual fraction, which have not been included in the current MIRD schema, can be the integral components of the formalism for calculating the radiation absorbed dose.

Several approaches have been previously proposed to incorporate the dynamic effect of variable bladder volume in the dose calculation (3-9). For

example, empirical functions describing the radiation absorbed dose to the bladder wall from the penetrating radiation (gamma ray) at various photon energies for an ellipsoidal bladder of various sizes were formulated based on Monte Carlo calculations by Snyder and Ford (5). They also used this mode to estimate the absorbed dose for I-131 iodine and Tc-99m pertechnetate from the non-penetrating radiation (beta ray and beta-like radiations such as Auger electrons, conversion electrons, low-energy fluorescent x-rays, etc.). Smith et al. later extended this approach to produce empirical formulas for describing the combined effect of both the penetrating and non-penetrating radiations (8). Numerical values of parameters used in these empirical formulas were listed for 31 radionuclides in the same paper. Spherical bladder models also have been used to derive the dose rate equations by Unnikrishnan for I-131 labeled hippuran (4), and by Diffey and Hilson for Tc-99m-DTPA (7). Recently, Dimitriou et al. employed the formula developed in (7) to calculate the absorbed dose to the bladder wall during direct radionuclide cystography using Tc-99m pertechnetate (9).

Alternatively, we propose a simple spherical dynamic model in which the radiation absorbed dose from both the penetrating and non-penetrating radiations can be calculated analytically in terms of variable bladder volumes using classical dose calculation approaches (10). Factors incorporated in the formulation include: the physical decay rate of the radionuclide, the biological disappearance rate for activity leaving the body to enter the bladder, the urine production rate, the initial bladder volume at administration time, the voiding schedule, and the residual fraction.

The analytical formulas derived from the present approach are both mathematically and conceptually simpler when compared with the ellipsoidal dynamic bladder model previously suggested (5,8). The new formulation is more concise when compared with those derived from other spherical models (4,7) and can be shown to be equivalent to their first order approximations. Non-uniform voiding schedules, variable residual fractions after each voiding, and an initial bladder volume are also incorporated in these new formulas.

THE DYNAMIC BLADDER MODEL

TIME-DEPENDENT BLADDER VOLUME

Assume the initial bladder volume is V_0 at administration time T_0 . If the instantaneous urine production rate at time t is $u(t)$, the bladder volume at any time after administration but before the first voiding can be written as

$$V(t) = V_0 + \int_{T_0}^t u(t)dt \quad (1)$$

for $T_0 \leq t < T_1$.

Suppose the first voiding takes place at time T_1 , the residual bladder volume, V_1 , after this voiding is

$$V_1 = f_1 V(T_1) \quad (2)$$

$$= f_1 \left(V_0 + \int_{T_0}^{T_1} u(t)dt \right) ,$$

where f_1 is the residual fraction of the first voiding. Therefore, the bladder volume at time t between T_1 and the second voiding time, T_2 , can be represented by

$$V(t) = V_1 + \int_{T_1}^t u(t)dt \quad (3)$$

for $T_1 \leq t < T_2$,

In general, the bladder volume at time t between the i^{th} voiding time T_i and the $(i+1)^{\text{th}}$ voiding time T_{i+1} is

$$V(t) = V_i + \int_{T_i}^t u(t)dt \quad (4)$$

for $T_i \leq t < T_{i+1}$,

where V_i is the residual volume after the i^{th} voiding. Summarizing the relationships of Equations (1) through (4), a generalized formulism for the bladder volume after n voidings can be written as

$$V(t) = \left(\prod_{i=1}^n f_i \right) V_0 + \sum_{i=1}^n \left(\prod_{j=i}^n f_j \right) \int_{T_{i-1}}^{T_i} u(t)dt \quad (5)$$

$$+ \int_{T_n}^t u(t)dt \quad \text{for } T_n \leq t < T_{n+1},$$

where f_i is the residual fraction of the i^{th} voiding.

Equation (5) represents a time-dependent bladder volume in which an initial volume, variable urine production rates and residual fractions, and non-uniform voiding schedule have all been considered.

TIME-DEPENDENT BLADDER ACTIVITY

If the body retention of the radioactivity can be described by an m -component exponential model, the activity in the bladder at any time after administration but before any voiding can be represented by

$$A(t) = A_0 e^{-\lambda_p(t-T_0)} \sum_{k=1}^m a_k \left[1 - e^{-\lambda_k(t-T_0)} \right] \quad (6)$$

for $T_0 \leq t < T_1$,

where A_0 is the administered activity; λ_p is the physical decay constant; a_k is the fraction of A_0 entering the bladder for the k^{th} component; and λ_k is the rate constant for the k^{th} component.

If the radioactivity is uniformly distributed in the urine, the residual activity after first voiding, A_1 , can be written as

$$A_1 = f_1 A(T_1) \quad (7)$$

$$= f_1 \left\{ A_0 e^{-\lambda_p (T_1 - T_0)} \sum_{k=1}^m a_k \left[1 - e^{-\lambda_k (T_1 - T_0)} \right] \right\} ;$$

and the amount of activity excreted in the first voiding is

$$E_1 = (1 - f_1) A(T_1) . \quad (8)$$

It is straightforward to derive that the activity in the bladder at time t between T_1 and T_2 is

$$\begin{aligned} A(t) &= A_0 e^{-\lambda_p (t - T_0)} \sum_{k=1}^m a_k \left[1 - e^{-\lambda_k (t - T_0)} \right] \\ &\quad - E_1 e^{-\lambda_p (t - T_1)} \\ &= A_0 e^{-\lambda_p (t - T_0)} \sum_{k=1}^m a_k \left[1 - e^{-\lambda_k (t - T_0)} \right] \\ &\quad - (1 - f_1) A(T_1) e^{-\lambda_p (t - T_1)} \\ &\quad \text{for } T_1 \leq t < T_2 . \end{aligned} \quad (9)$$

The generalization of Equation (9) to any time after n voidings gives

$$\begin{aligned} A(t) &= A_0 e^{-\lambda_p (t - T_0)} \sum_{k=1}^m a_k \left[1 - e^{-\lambda_k (t - T_0)} \right] \\ &\quad - \sum_{i=1}^n (1 - f_i) A(T_i) e^{-\lambda_p (t - T_i)} \\ &\quad \text{for } T_n \leq t < T_{n+1} \end{aligned} \quad (10)$$

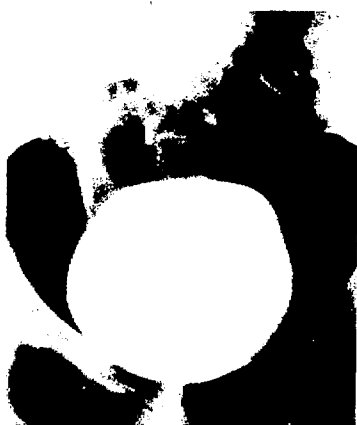
Although further derivation by recursively replacing the term $A(T_i)$ is possible, Equation (10) can depict the physical and biological factors more clearly. The first term represents the administered activity that has entered the bladder; the second term is the sum of administered activity previously voided. Each term includes an exponential function involving λ_p for the effect of physical decay.

THE SPHERICAL BLADDER MODEL

INTRODUCTION

The ellipsoidal model suggested by Snyder et al. to describe the shape of the bladder in the standard MIRD model (1) has been widely used in the radiation absorbed dose calculation (5,6,8). Using this ellipsoidal model, no theoretical formalism can be easily established to represent the radiation absorbed dose to the inner surface of the bladder wall. Their numerical values can be determined only by using the Monte Carlo method. Empirical equations can then be formulated based on the results from these Monte Carlo calculations (5,8). This simulation process is rather inconvenient, especially for those cases in which the bladder volume is varying.

Instead, a spherical model is employed in the present study to facilitate the analytical formulation of the absorbed dose calculation. The spherical model is a reasonably good approximation for relatively large bladder volumes. This has been validated by x-ray images of bladder filled with contrast material (Figure 1). At small volumes, however, the bladder shrinks to an irregular shape where both the spherical and ellipsoidal models fail. Nevertheless, the absorbed dose from the non-penetrating radiation, more or less independent of the actual shape of the bladder, can contribute a major fraction of the total radiation dose, especially when the volume is small. Therefore, the actual shape of the bladder becomes relatively unimportant for small bladder volumes. This will be illustrated later in the example of F-18-FDG and Tc-99m-DTPA.



(a) Spherical when volume is large.



(b) Irregular shape at small volumes, and both spherical and ellipsoidal models fail.

Figure 1. X-ray images of bladder filled with contrast material.

DOSE RATE FROM THE PENETRATING RADIATION

The classical formulation of the penetrating radiation dose rate (11) in units of rad/hr at a point x within a volume V containing a uniform distribution of radioactivity with concentration $C \mu\text{Ci/g}$ is

$$\dot{D}_{p,x} = 10^{-3} C \rho \Gamma \int_V \frac{e^{-\mu r}}{r^2} dV \quad (11)$$

where ρ is the density of the medium in g/cm^3 ; Γ is the gamma-ray dose rate constant in $\text{cm}^2\text{-rad/mCi-hr}$; μ is the effective linear absorption coefficient in $1/\text{cm}$; and dV is the volume element in cm^3 . It should be noted that, in a strict sense, Γ should be referred to as the exposure rate constant expressed in $\text{cm}^2\text{-R/mCi-hr}$. To convert the exposure rate constant to the gamma-ray dose rate constant, a conversion factor that depends on photon energy and medium composition must be applied. In soft tissue, however, this conversion factor is nearly equal to unity for a wide range of photon energies. Therefore, the conversion factor is ignored in subsequent derivations.

The integral term in Equation (11) is called the geometrical factor, g_x , (in cm^3) for point x , i.e.,

$$g_x = \int_V \frac{e^{-\mu r}}{r^2} dV \quad . \quad (12)$$

Substituting g_x as defined by Equation (12), Equation (11) can be rewritten as

$$\dot{D}_{p,x} = 10^{-3} C \rho \Gamma g_x \quad . \quad (13)$$

At the center of a sphere of radius R , the geometrical factor, g_c , can be determined as follows

$$\begin{aligned} g_c &= \int_0^R \frac{e^{-\mu r}}{r^2} 4\pi r^2 dr \\ &= \frac{4\pi}{\mu} (1 - e^{-\mu R}) \quad . \end{aligned} \quad (14)$$

Assuming $\mu R \ll 1$, the first order approximation yields

$$g_c = 4\pi R \quad . \quad (15)$$

One has to note that the value of μ is around 0.03 cm^{-1} for photon energies ranging from 100 keV to 2 MeV. Therefore, the assumption of $\mu R \ll 1$ stated earlier is a reasonable one for the photon energies normally considered in radionuclide imaging. The approximation that simplifies Equation (14) to Equation (15) produces an inaccuracy of less than 10% for a wide range of various bladder volumes (Figure 2).

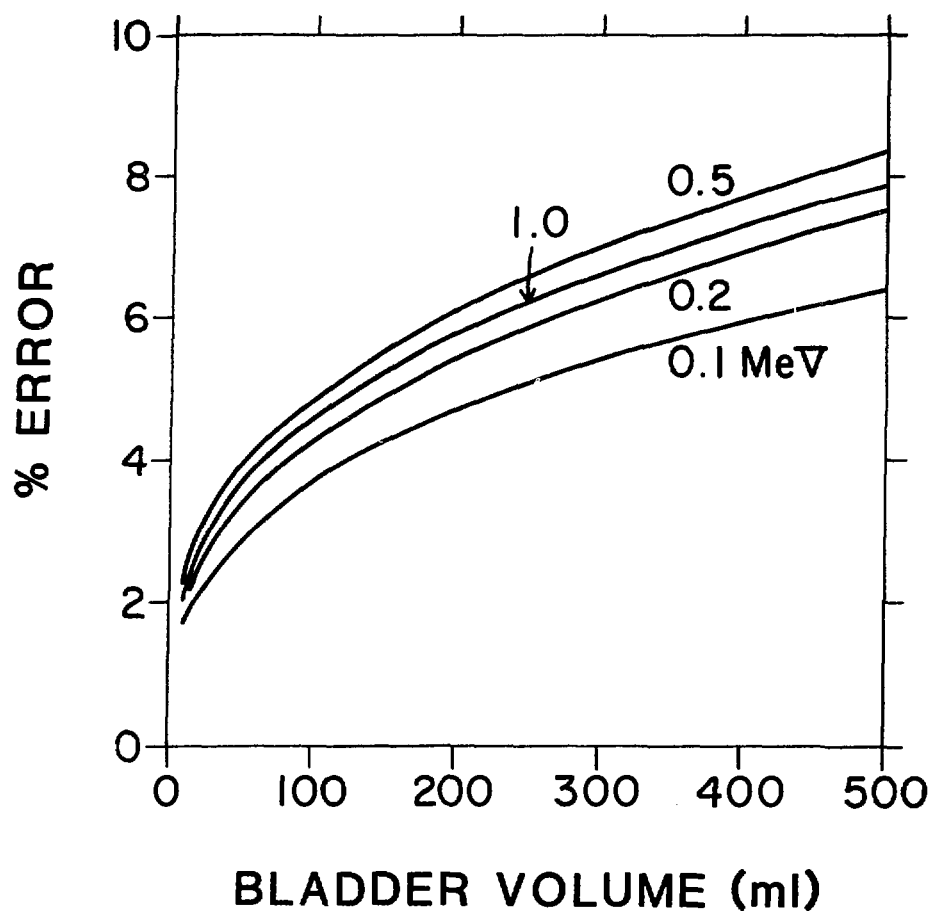


Figure 2: Resulting error when $\mu R \ll 1$ is used to simplify Equation (14) to Equation (15). For photon energies between 0.1 and 1.0 MeV, this inaccuracy is always less than 10% for various bladder volumes.

It has been demonstrated that the geometrical factor for a point at the surface of a sphere, g_s , is $1/2$ of that at the center of the same sphere (11). Hence, one has

$$g_s = 2\pi R . \quad (16)$$

Assuming the tissue density $\rho = 1 \text{ g/cm}^3$ and using Equation (16) and the following two equations

$$C(t) = \frac{A(t)}{V(t)} \quad (17)$$

$$R(t) = \left[\frac{3V(t)}{4\pi} \right]^{1/3} ,$$

the penetrating radiation dose rate at the surface of a sphere as a function of time can be represented by

$$\dot{D}_{p,S}(t) = 10^{-3} \Gamma A(t) \left[\frac{6\pi^2}{(V(t))^2} \right]^{1/3} \quad (18)$$

$$= \frac{3.9 \times 10^{-2} \Gamma A(t)}{[V(t)]^{2/3}}$$

If the radionuclide emits more than one type of penetrating radiation, the gamma-ray dose rate constant, Γ , in Equation (18) can be replaced by a weighted value of

$$\Gamma = \sum_i w_i \Gamma_i \quad , \quad (19)$$

where w_i is the relative abundance of i^{th} penetrating radiation.

Diffey and Hilson in their paper on absorbed dose to the bladder from Tc-99m-DTPA (7) used a different formula that was originally derived by Morgan and Emerson (12) for a point at the surface of a sphere. In essence, they employed a more elaborate geometrical factor that can be written as

$$g'_S = \frac{2\pi}{\mu} \left[1 - \frac{1 - e^{-2\mu R(t)}}{2\mu R(t)} \right] \quad . \quad (20)$$

If one assumes $2\mu R \ll 1$, it is easy to show that g'_S represented in Equation (16) is the first order approximation of g'_S in Equation (20). The ratios of g_S/g'_S for four photon energies are plotted as a function of bladder volume in Figure 3. The differences between g_S and g'_S are at most about 10%.

The penetrating radiation dose rate represented by Equation (18) can be readily converted to a function \bar{D}_{ph} specifying the average dose per photon by

$$\bar{D}_{ph}(V(t)) = \frac{\dot{D}_{p,S}(t)}{A(t)} \quad (21)$$

$$= 2.93 \times 10^{-11} \frac{\Gamma}{[V(t)]^{2/3}} \quad .$$

Based on the results from their Monte Carlo calculation using the ellipsoidal model, Snyder and Ford (5) formulated empirically a two-exponential equation for \bar{D}_{ph} as

$$\bar{D}'_{ph}(V) = a e^{-\alpha V} + b e^{-\beta V} \quad . \quad (22)$$

Comparisons of \bar{D}_{ph} and \bar{D}'_{ph} are illustrated in Figure 4 for various bladder volumes at four different photon energies. It can be noted that results from these two models differ little from each other except when the photon energy is relatively low.

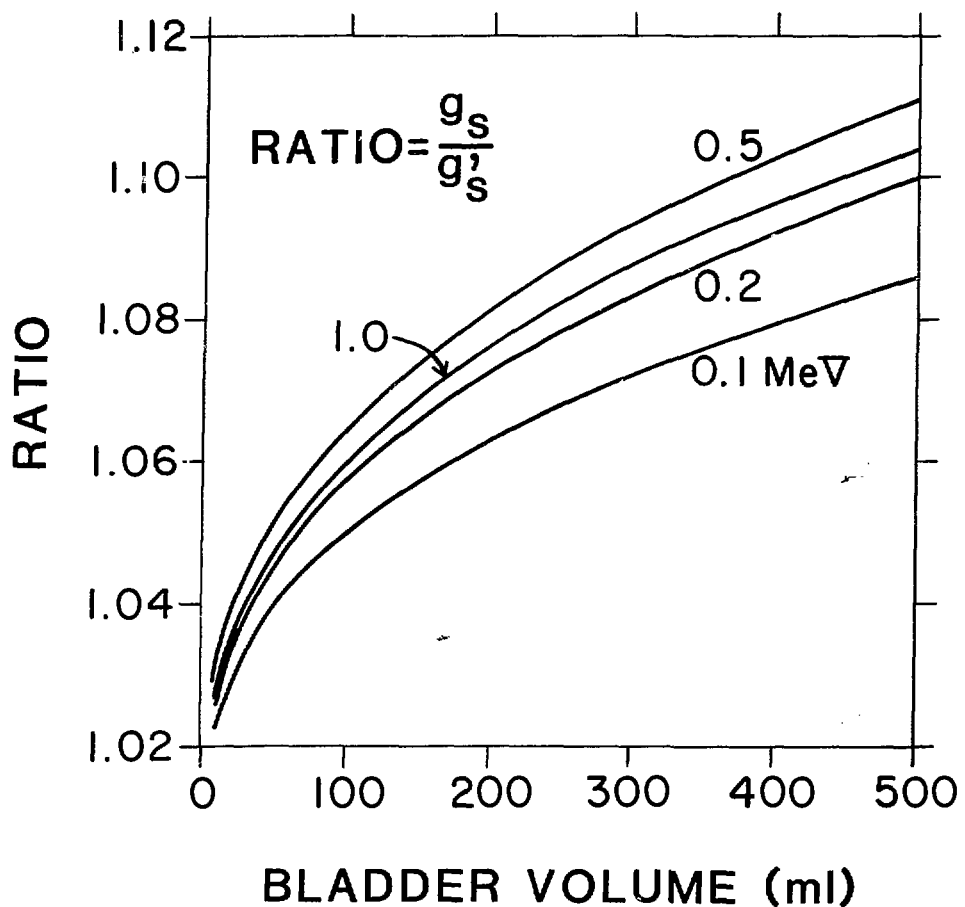


Figure 3: Ratio of geometrical factor using Equation (16) to that using Equation (20). For a wide range of bladder volumes, the differences are within 10% for photon energies between 0.1 and 1.0 MeV.

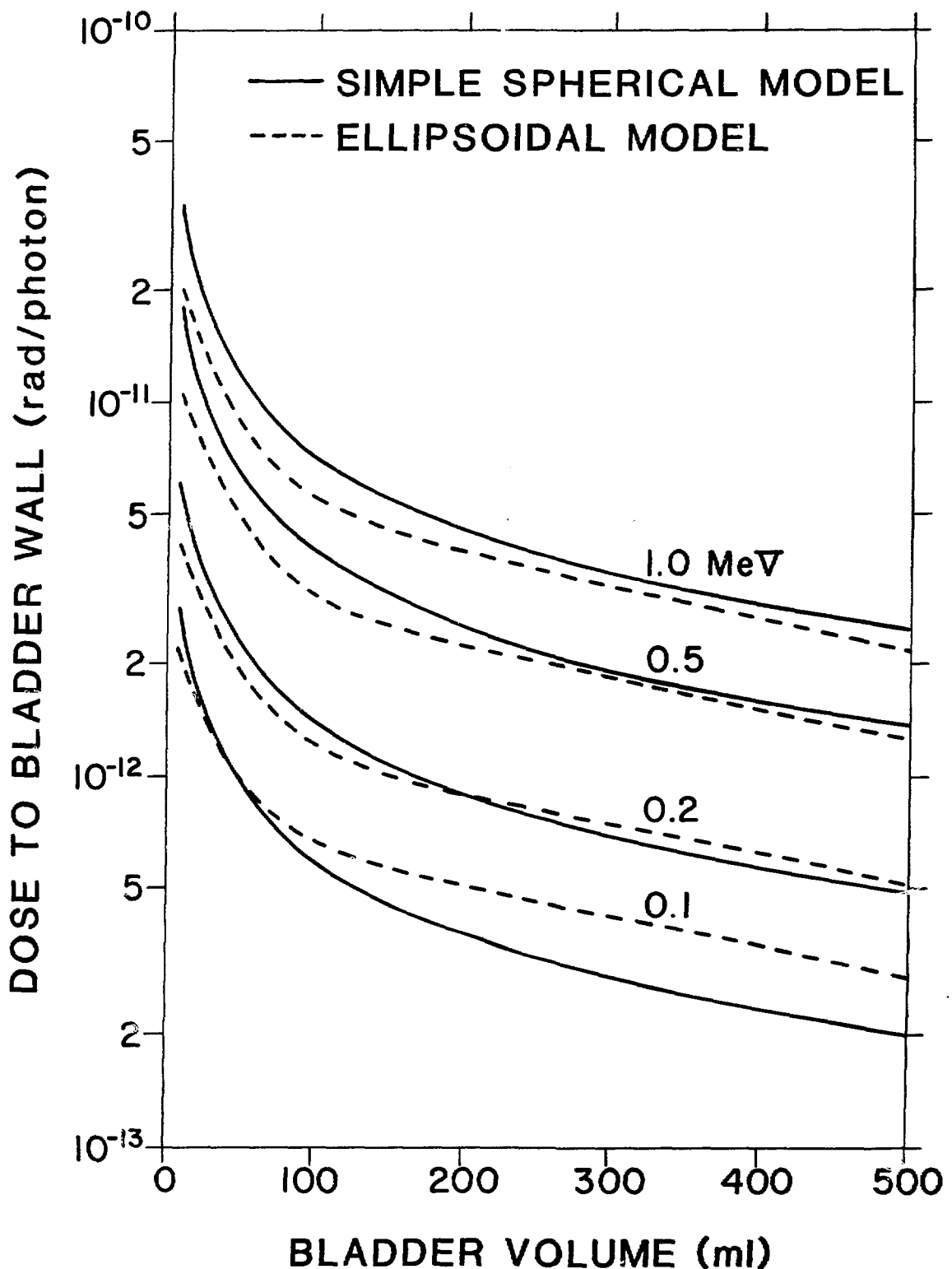


Figure 4: Comparison of the average absorbed dose per photon using the simple spherical model and the ellipsoidal model. Little difference occurs except when the photon energy is relatively low.

DOSE RATE FROM THE NON-PENETRATING RADIATION

The classical formalism for calculating the non-penetrating radiation dose rate at a point within a medium of reasonable size is

$$\dot{D}_{np} = 2.13 \frac{\bar{E}_\beta C}{\rho} \quad (23)$$

where \bar{E}_β is the average energy of beta or beta-like radiation per disintegration in MeV. If the radionuclide emits more than one type of non-penetrating radiation, the term \bar{E}_β in Equation (23) can be replaced by a weighted value of

$$\bar{E}_\beta = \sum_i n_i \bar{E}_{\beta i} \quad (24)$$

where n_i is the relative abundance of i^{th} type non-penetrating radiation. Defining an equilibrium dose constant by

$$\Delta_\beta = 2.13 \sum_i n_i \bar{E}_{\beta i}, \quad (25)$$

Equation (23) can be rewritten as

$$\dot{D}_{np} = \frac{\Delta_\beta C}{\rho}. \quad (26)$$

One can note that the non-penetrating radiation dose rate is linearly proportional to the activity concentration, C , distributed in the medium, rather than the total amount of activity.

Since the dose rate at the surface of a sphere is 1/2 of that within the medium, one has

$$\dot{D}_{np, S} = \frac{\Delta_\beta C}{2\rho}. \quad (27)$$

Using Equation (17) and assuming $\rho = 1 \text{ g/cm}^3$, the non-penetrating dose rate at the surface of a sphere as a function of time can be written as

$$\dot{D}_{np, S}(t) = \frac{\Delta_\beta A(t)}{2V(t)}. \quad (28)$$

Equation (28) generally holds for geometrical configurations other than spheres, as long as the range of non-penetrating radiation is small compared with the physical dimensions of the medium. Therefore, there is no difference in dose rate calculation for non-penetrating radiation between spherical and ellipsoidal models.

RADIATION ABSORBED DOSE CALCULATION

Using Equations (18) and (28), the total radiation absorbed dose to the inner surface of the bladder wall can now be represented by

$$D_{\text{Total}} = \int_{T_0}^{\infty} \left[\dot{D}_{p,S}(t) + \dot{D}_{np,S}(t) \right] dt \quad (29)$$

$$= \frac{1}{60} \int_{T_0}^{\infty} \left[\frac{3.9 \times 10^{-3} \Gamma A(t)}{[V(t)]^{2/3}} + \frac{\Delta \beta A(t)}{2V(t)} \right] dt$$

where $A(t)$ and $V(t)$ are represented by Equations (10) and (5), respectively; the factor 1/60 is inserted to allow dt to be expressed in minutes.

EXAMPLES: F-18-FDG AND Tc-99m-DTPA

INTRODUCTION

To demonstrate the utility of this simple spherical dynamic model in designing optimal strategies to reduce radiation absorbed dose to the patient, two commonly used radiopharmaceuticals, namely, F-18-FDG for positron imaging and Tc-99m-DTPA for single-photon renal imaging, are examined in this section. Values of parameters used in the calculations are extracted from the published literature, and are summarized in Table 1. Computer simulation studies have been performed to investigate the effects of various initial bladder volumes, urine production rates, residual fractions, voiding frequencies, and first voiding times. A comparison is also made of this spherical model with the ellipsoidal model developed by Snyder and Ford (5).

NON-PENETRATING RADIATION VERSUS PENETRATING RADIATION

Using Equations (18) and (28) with the values listed in Table 1, the ratio of the surface absorbed dose from the non-penetrating radiation to that from the penetrating radiation can be written as

$$\frac{\dot{D}_{np,S}}{\dot{D}_{p,S}} = \frac{11.03 V^{-1/3}}{5.91 V^{-1/3}} \quad \begin{aligned} &\text{for F-18} \\ &\text{for Tc-99m} \end{aligned} \quad (30)$$

Schematic illustration of Equation (30) is demonstrated as Figure 5. It is clear that, at small bladder volumes, the non-penetrating radiation constitutes the major part of the total absorbed dose. The non-penetrating radiation dose is normally independent of the geometrical configuration of a medium of reasonable size, i.e., the physical dimensions of the medium are large compared with the range of the non-penetrating radiation. Therefore, at small volumes, the choice of an exact model to describe the shape of the bladder becomes less important.

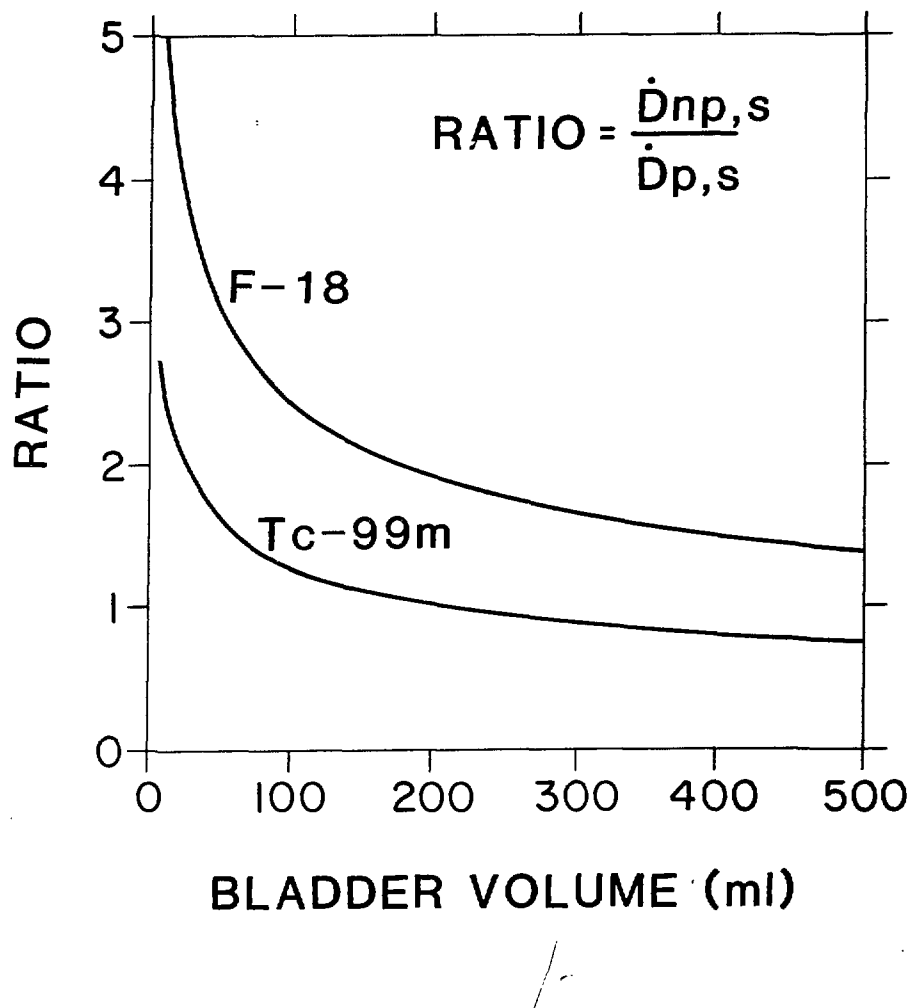


Figure 5. Ratio of non-penetrating radiation to penetrating radiation for F-18 and Tc-99m. At small bladder volumes, the non-penetrating radiation contributes the major fraction of the total radiation dose.

SIMPLE SPHERICAL MODEL VERSUS ELLIPSOIDAL MODEL

Figure 6 shows, in the cases of F-18 and Tc-99m, the ratio of the radiation absorbed dose calculated by using the simple spherical model to that estimated by employing the ellipsoidal model. For the penetrating radiation, Equation (18) is used for the simple spherical model and Equation (22) for the ellipsoidal model. For the non-penetrating radiation, Equation (28) is used for both models. Although differences are significant between these two models for penetrating radiation (dashed curves), the total absorbed doses (solid curves) are within 10% for a wide range of bladder volumes.

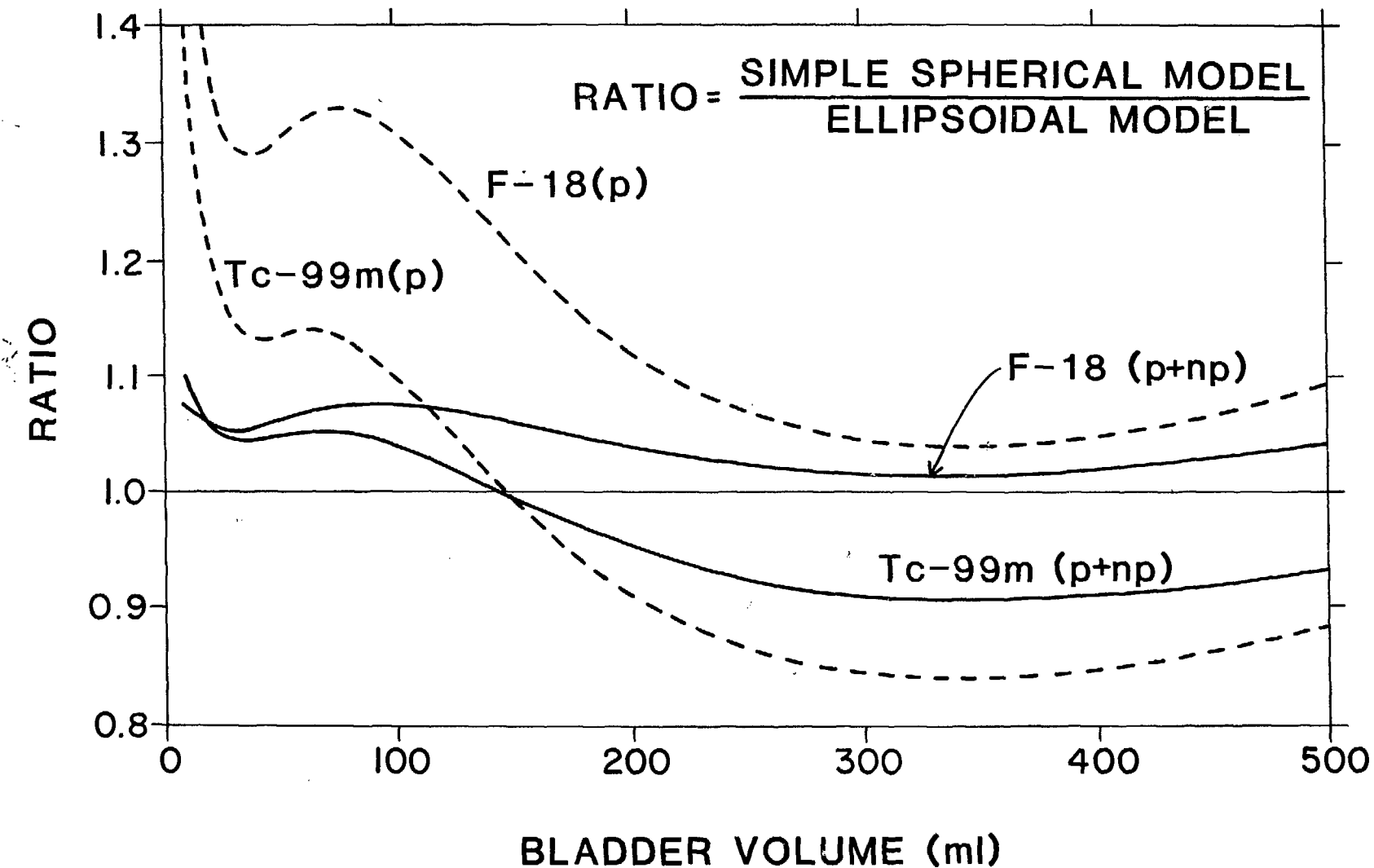


Figure 6: Comparison of the simple spherical model and the ellipsoidal model for F-18 and Tc-99m. Although differences are significant between these two models for penetrating radiation (dashed curves), the total absorbed doses (solid curves) are within 10% for a wide range of bladder volumes.

ACTIVITY IN THE BLADDER

Figure 7 gives an example of the time-activity curve of the bladder content in a typical F-18-FDG study. The curve that encompasses the shaded area represents the function $A(t)$ described by Equation (10) and is the result of the best fit of the urinary excretion data from Jones et al. (2). The urine production rate is assumed to be constant at 1.25 ml/min and the residual fraction is assumed to be 7% for each voiding. Although Figure 7 clearly demonstrates the time course of the activity entering the bladder, using this time-activity curve alone cannot determine the best voiding schedule for the purpose of dose reduction. One has to consider factors such as initial bladder volume, urine production rate, residual fraction, etc. in the analysis.

A similar time-activity curve of the bladder content for Tc-99m-DTPA can be constructed using data listed in Table 1.

Table 1. Values Used to Calculate the Absorbed Dose to the Bladder Wall

	F-18-FDG	Tc-99m-DTPA
λ_p (1/min)	0.00636*	0.00192 ⁺
λ_1 (1/min)	0.0385*	0.0115 ⁺
λ_2 (1/min)	0.00124*	0.00125 ⁺
a_1	0.19*	0.579 ⁺
a_2	0.06*	0.421 ⁺
Γ (cm ² -rad/mCi-hr)	6.0**	0.72**
Δ_β (g-rad/ μ Ci-hr)	0.516 ⁺⁺	0.0332 ⁺

*Estimated from data in reference (2).

⁺Reference (13).

**Reference (14).

⁺⁺Reference (15).

STRATEGIES FOR REDUCING THE ABSORBED DOSE

A computer code implementing Equation (29) for the calculation of the absorbed dose to the inner surface of the bladder wall has been developed. This program accepts various input values of λ_p , λ_k , a_k , Γ and Δ_β for specifying the physical and biological characteristics of the radioactive agent in use. It also has the flexibility to accommodate various initial bladder volumes, urine production rates, residual fractions, and non-uniform voiding schedules. This computer code has been used to explore possible strategies for achieving a dose reduction. Some of the examples, in the cases of F-18-FDG and Tc-99m-DTPA, are given as follows.

Figure 8 illustrates the effect of the initial bladder volume on the absorbed dose. In this case, the urine production rate is 1.25 ml/min; the

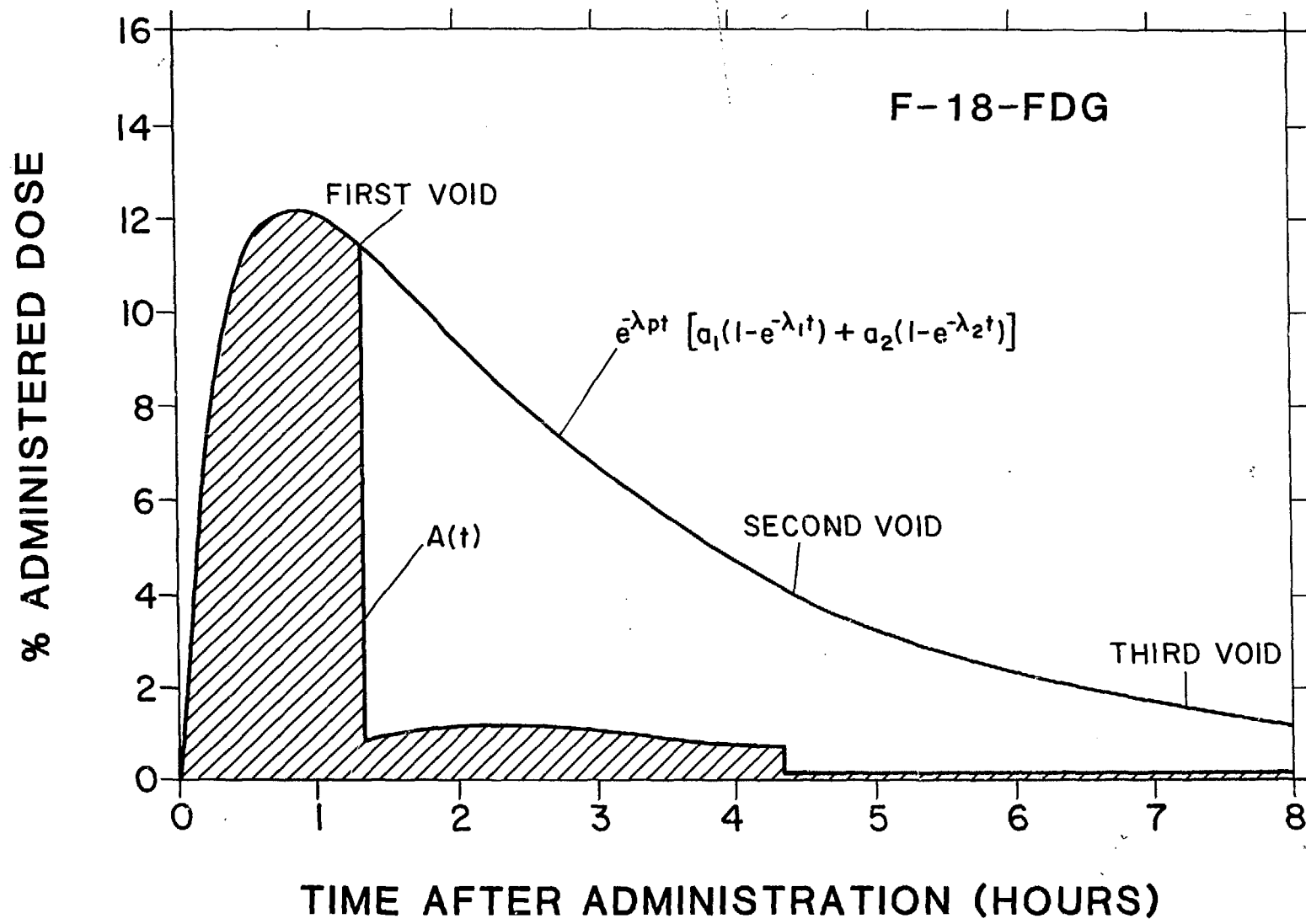


Figure 7: Time-activity curve of bladder content for F-18-FDG studies. This example is the best fit of the urinary excretion data in reference (2), i.e., $a_1 = 0.19$, $a_2 = 0.06$, $\lambda_1 = 0.0385 \text{ min}^{-1}$, $\lambda_2 = 0.00124 \text{ min}^{-1}$, $\lambda_p = 0.00636 \text{ min}^{-1}$. Also, $u(t) = \text{constant} = 1.25 \text{ ml/min}$, $f_i = 7\%$ for all i , $T_1 = 80 \text{ min}$, and the voiding intervals are every three hours after T_1 . The shaded area is the cumulated activity.

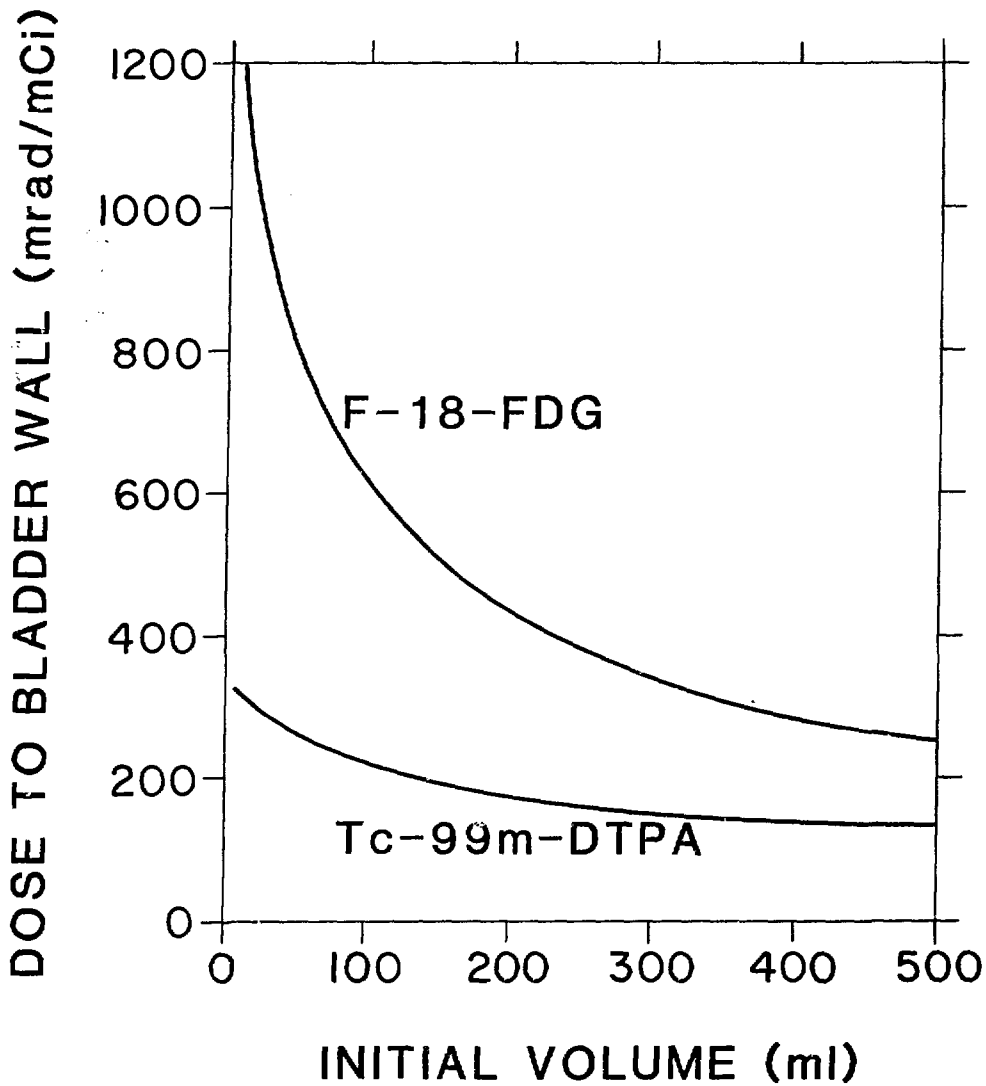


Figure 8: Effect of initial volume on absorbed dose. In these cases, $u(t) = \text{constant} = 1.25 \text{ ml/min}$, $f_i = 7\%$ for all i , and the voiding intervals are every three hours after T_0 .

residual fraction is 7% for each voiding; and voidings take place every three hours after administration. The radioactivity concentration decreases as the initial volume increases, resulting in relatively less absorbed dose. Therefore, the radiation absorbed dose can be reduced if one starts a study with a comfortably large bladder volume.

Figure 9 demonstrates that increasing the urine production rate can also achieve a dose reduction. Here, the initial volume is 200 ml; the residual volume is 7% for each voiding; and the bladder is emptied at three-hour intervals. Figures 8 and 9 suggest that the patient should be well hydrated both before and after administration in order to reduce the absorbed dose.

Examples of the effect of the residual fraction on the absorbed dose are given in Figures 10 and 11 for F-18-FDG and Tc-99m-DTPA, respectively. In these cases, the initial bladder volume is 200 ml; the urine production rate is 1.25 ml/min; and the voiding interval is three hours, after the first voiding at the indicated time. Results for various first voiding times are presented. These curves reveal that the actual effect of the residual fraction is very much dependent on when the first voiding takes place. For early first voiding times (for example, at 20 minutes after administration), larger residual fractions may sometimes reduce the absorbed dose. This is due to the fact that, before most of the activity has entered the bladder, it is desirable to maintain a relatively large bladder volume in order to keep the activity concentration low. For later first voiding times, however, larger residual fractions result in more activity retaining inside the bladder for a longer period of time, which in turn yields higher radiation absorbed doses. Therefore, if relatively late first voiding time is employed, one should urinate as completely as possible. Figures 10 and 11 also show that a preferred first voiding time can be chosen to reduce the absorbed dose. For the cases shown here, the preferred first voiding times are at about one hour after administration for F-18-FDG and at two hours for Tc-99m-DTPA.

The selection of the preferred first voiding time can be better demonstrated using Figures 12 and 13, in which the radiation absorbed dose is plotted as a function of the first voiding time for various initial bladder volumes. In these cases, the urine production rate is 1.25 ml/min; the residual fraction rate is 7%; and the voiding interval is three hours after the first voiding. For each initial bladder volume, a unique optimal first voiding time can be determined for the purpose of minimizing the absorbed dose. Before this strategically chosen time, the absorbed dose is increasingly higher as one goes to earlier first voiding time, contrary to what one would conclude from using the conventional MIRD approach (2). This is because early voiding results in a relatively high activity concentration distributed in a small bladder volume. Employing first voiding times later than this optimum results in a higher absorbed dose. The reason is that, after most of the activity has accumulated in the bladder, retaining the activity in the bladder longer results in a higher absorbed dose. The balance of these two competing factors, namely, a low activity concentration and a short retention time in the bladder, yields the optimal first voiding time. It can be noted that this optimal first voiding time occurs progressively later as the initial bladder volume increases. For an initial bladder of 200 ml, the optimal first voiding times are at about 70 minutes after administration for F-18-FDG and 140 minutes for Tc-99m-DTPA, similar to the times derived from Figures 10 and 11.

Once this optimal first voiding time is determined, employing shorter voiding intervals for later voidings can also reduce the absorbed dose. This is demonstrated in Figure 14. Here, the initial bladder volume is 200 ml, the urine production rate is 1.25 ml/min; the residual fraction is 7% for each

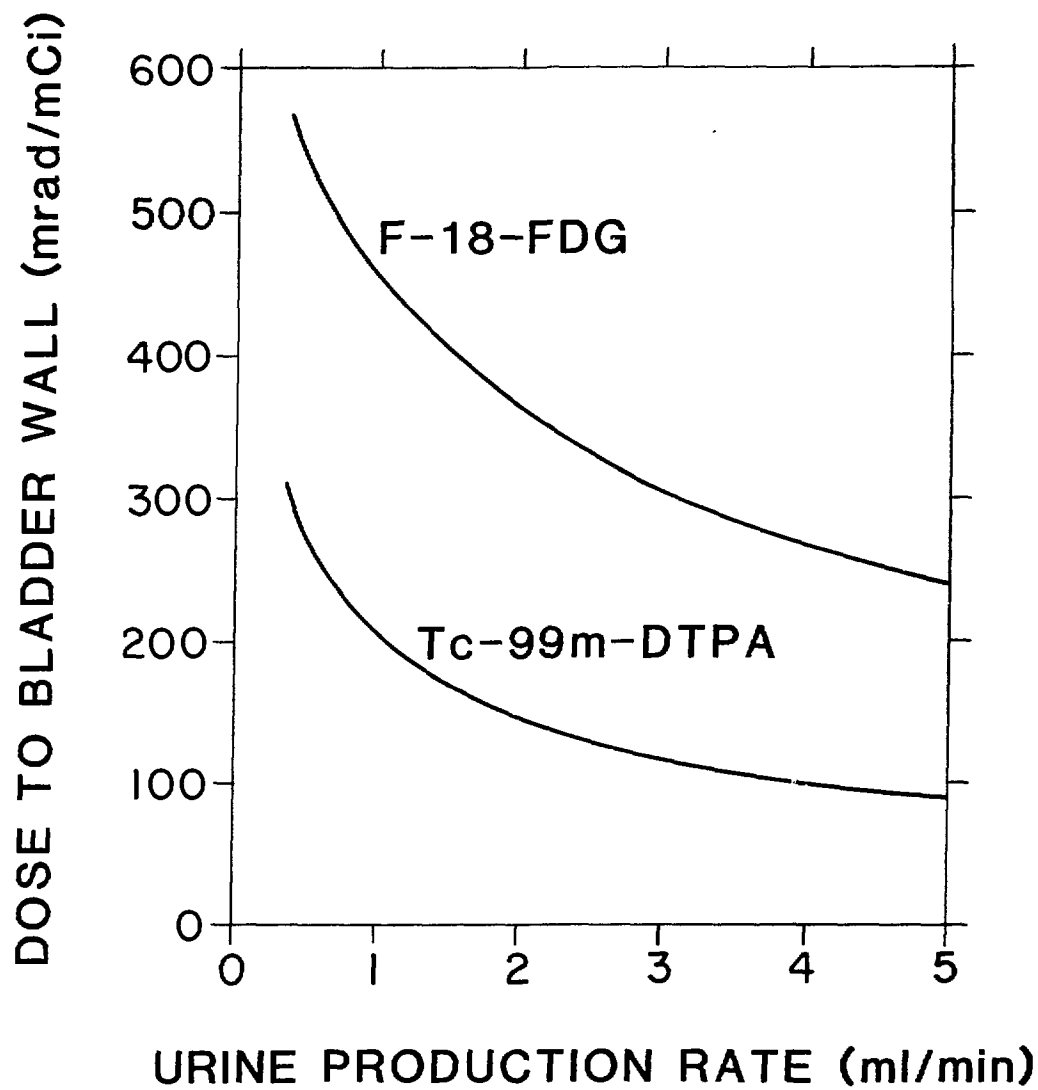


Figure 9: Effect of urine production rate on absorbed dose. Here, $V_0 = 200 \text{ ml}$, $f_i = 7\%$ for all i , and the bladder is emptied at three-hour intervals after administration.

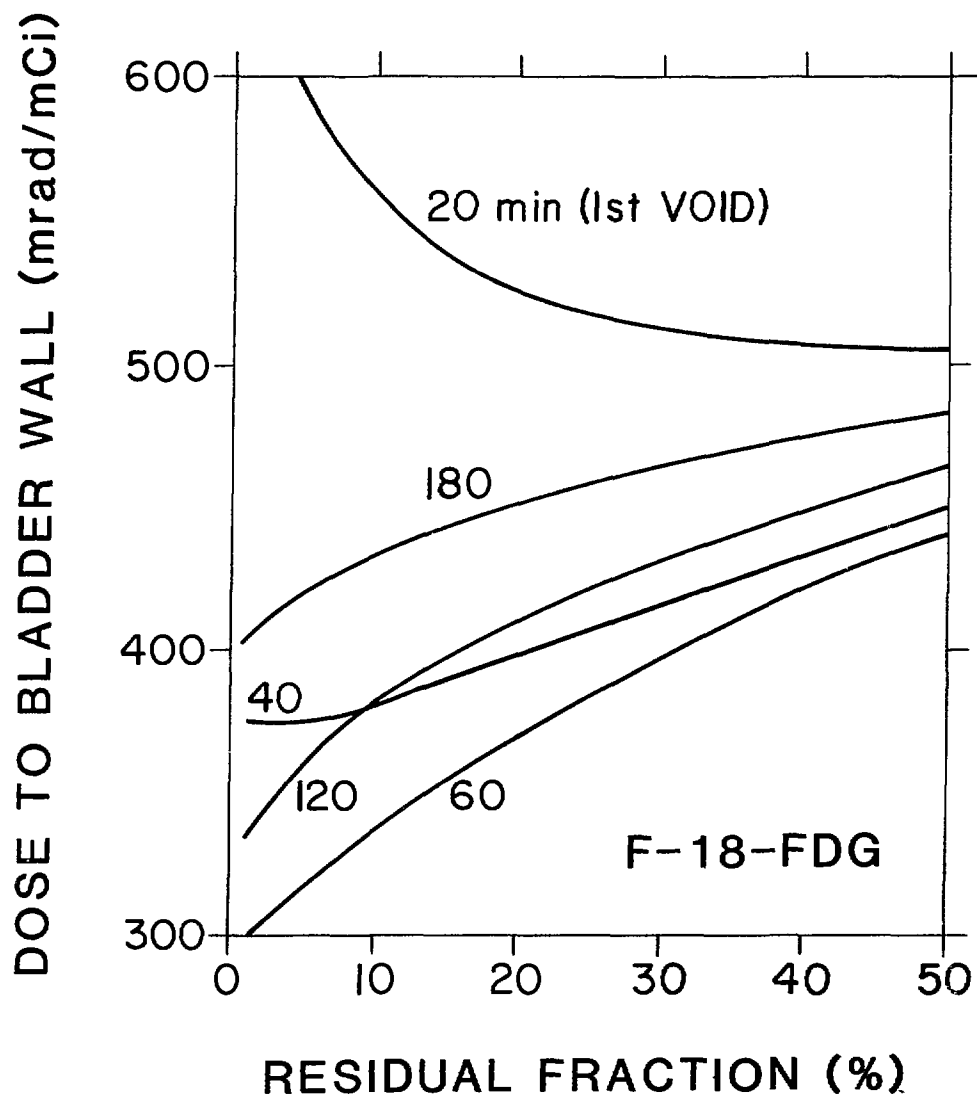


Figure 10: Effect of residual fraction on absorbed dose from F-18-FDG for various first voiding time (T_1). Parameters used are: $V_0 = 200 \text{ ml}$, $u(t) = \text{constant} = 1.25 \text{ ml/min}$, voiding intervals are every three hours after T_1 .

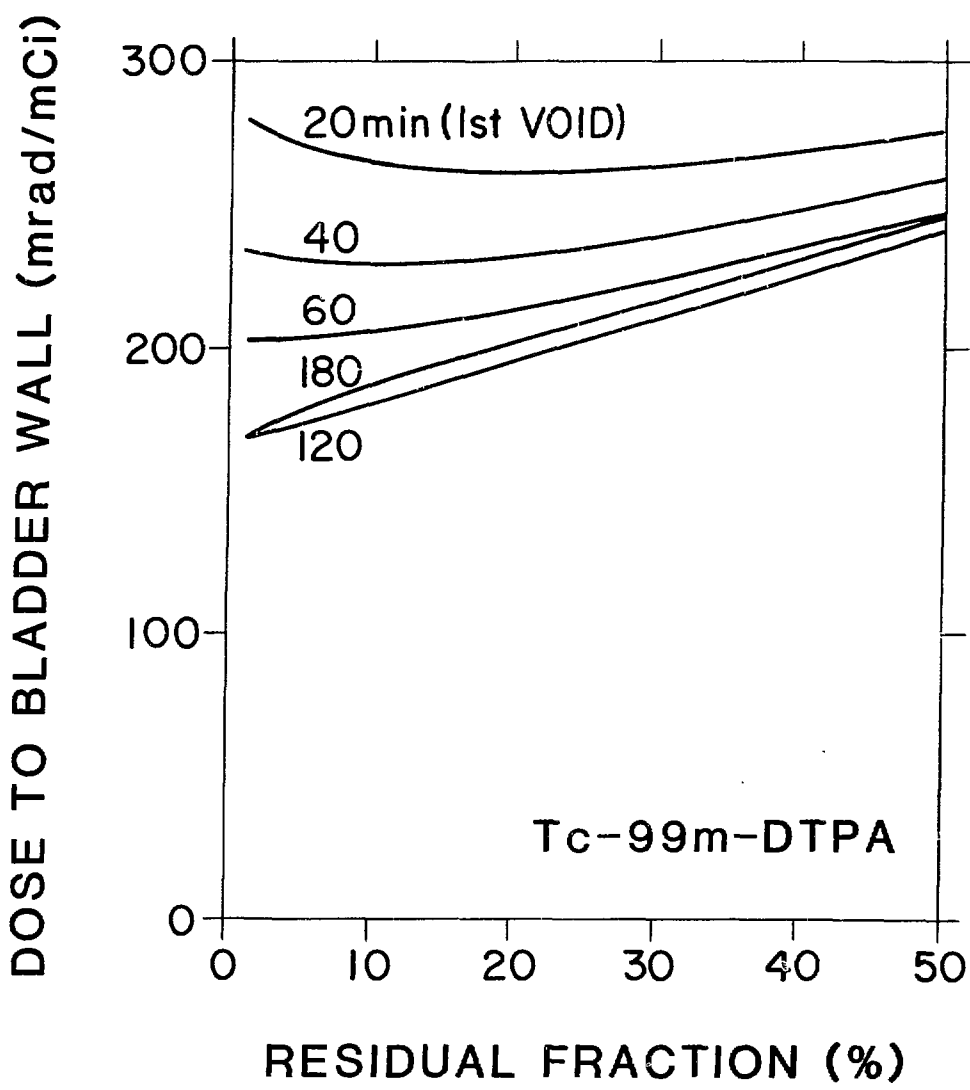


Figure 11: Effect of residual fraction on absorbed dose from Tc-99m-DTPA for various first voiding times (T_1). Parameters are the same as those listed in Figure 10.

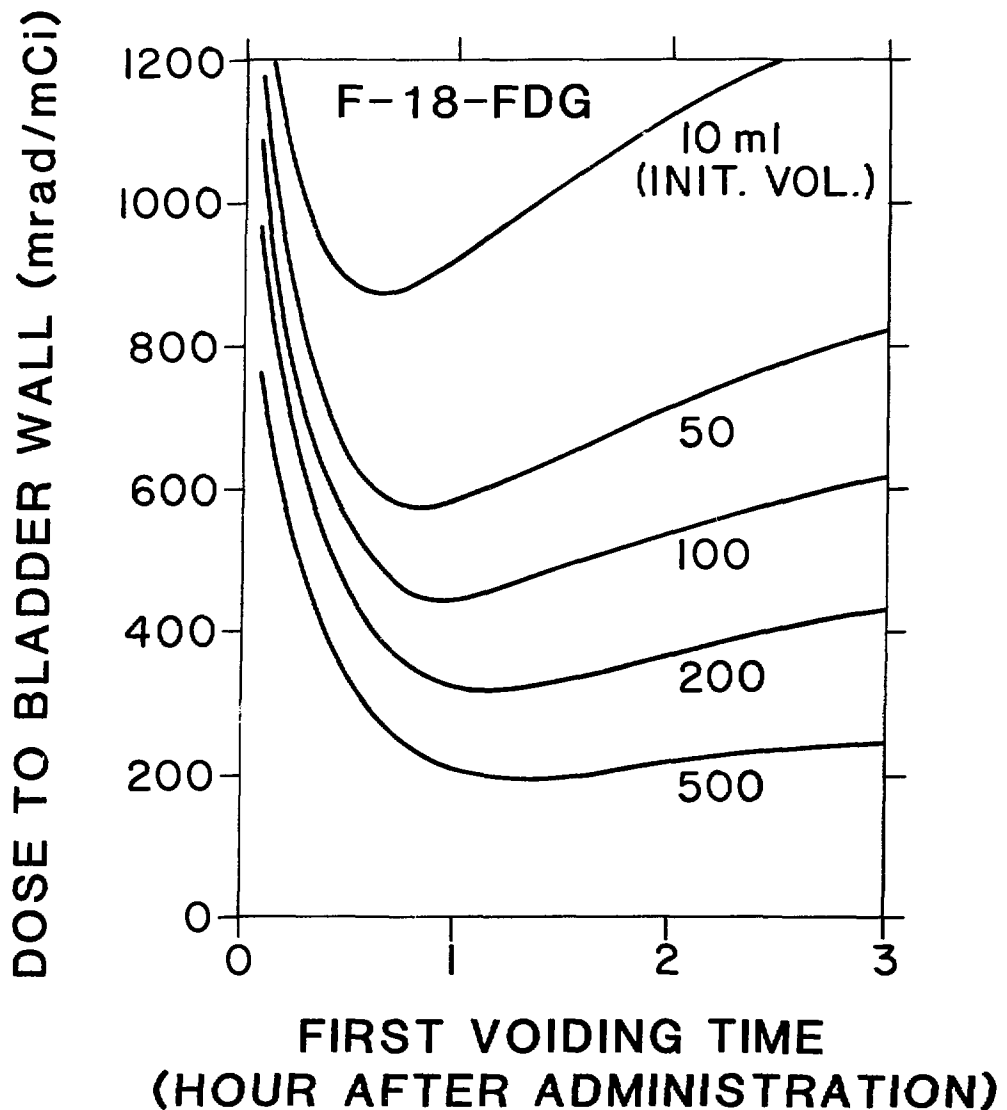


Figure 12: Effect of first voiding time on absorbed dose from F-18-FDG for various initial volumes (V_0). In these cases, $u(t) = \text{constant} = 1.25 \text{ ml/min}$, $f_i = 7\%$ for all i , the voiding intervals are every three hours after T_1 .

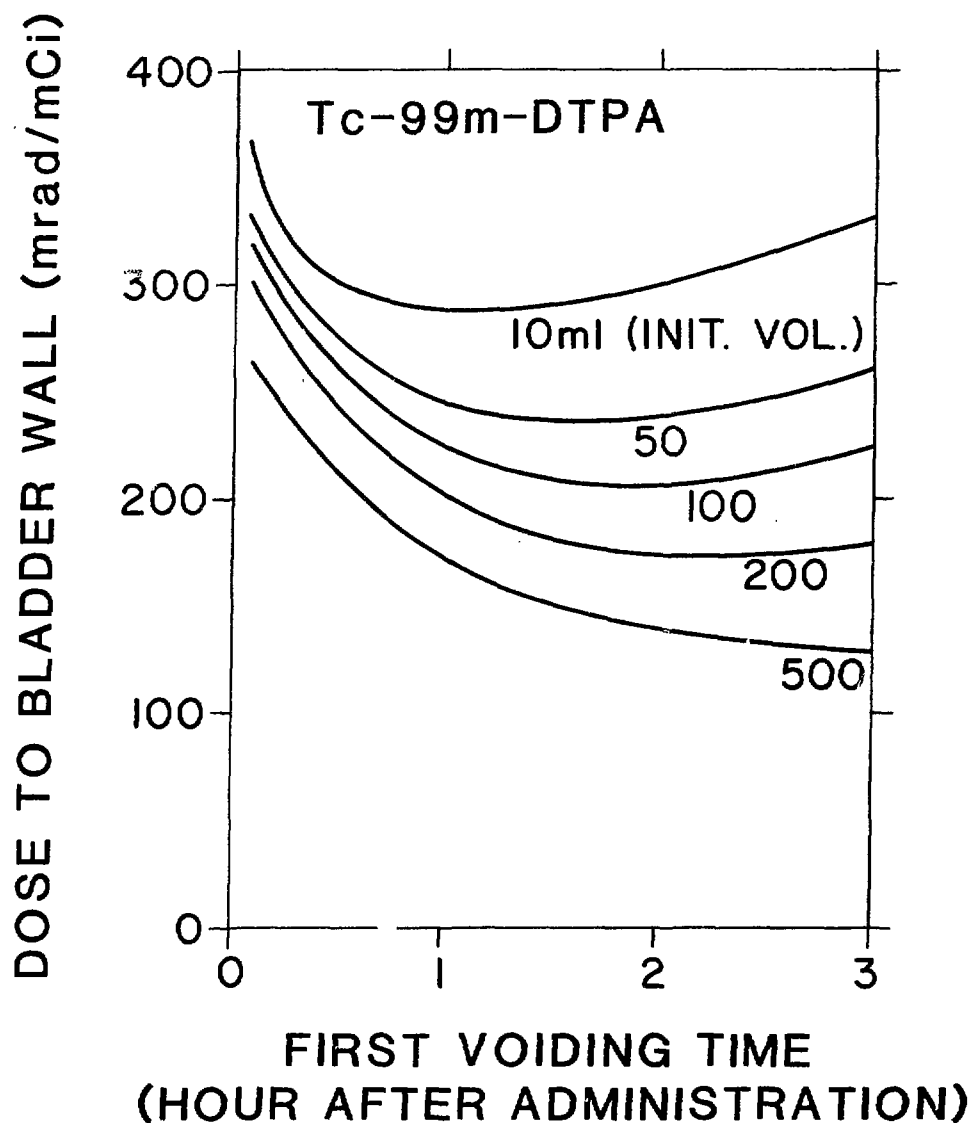


Figure 13: Effect of first voiding time on absorbed dose from Tc-99m-DTPA for various initial volumes (V_0). Parameters used are the same as those listed in Figure 12.

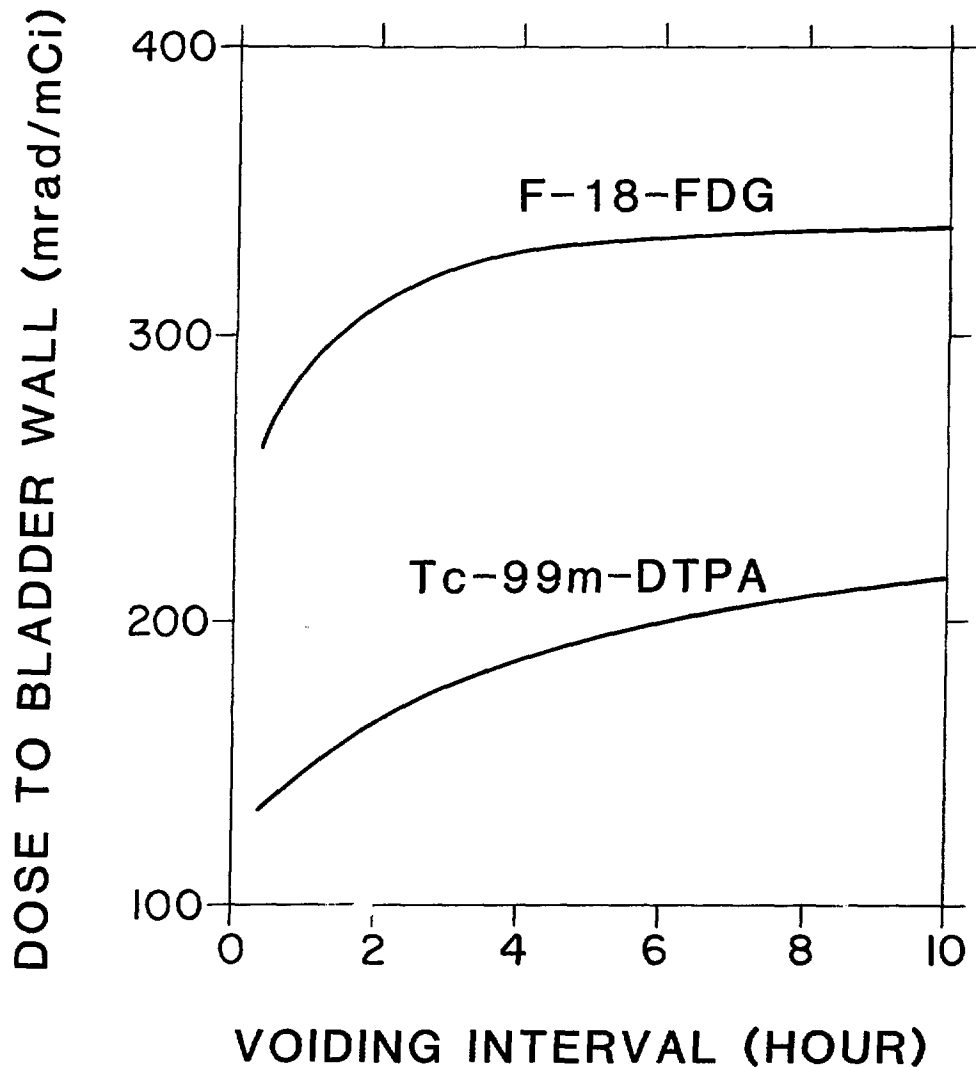


Figure 14: Effect of voiding interval on absorbed dose. Here, $V_0 = 200 \text{ ml}$, $u(t) = \text{constant} = 1.25 \text{ ml/min}$, $f_i = 7\%$ for all i , $T_1 = 70 \text{ min}$ for F-18-FDG and $T_1 = 140 \text{ min}$ for Tc-99m-DTPA.

voiding; the first voiding times are at 70 minutes and 140 minutes after administration for F-18-FDG and Tc-99m-DTPA, respectively.

A simulation study has been conducted to assess the radiation absorbed dose to the bladder under continuous drainage of urine by inserting a catheter directly into the bladder, a practice that had been often suggested for the purpose of dose reduction. The continuous drainage is simulated by employing a one-minute voiding interval with 7% residual fraction for each voiding commencing immediately after administration. For F-18-FDG, the resulting absorbed dose to the bladder wall is 611 mrad/mCi for an initial bladder volume of 10 ml and 589 mrad/mCi for 100 ml. Therefore, the continuous drainage approach is unfavorable for an F-18-FDG study when compared with most of the other possible strategies, for example, those displayed in Figure 12. For Tc-99m-DTPA, however, the absorbed dose by employing the continuous drainage method is from 160 to 165 mrad/mCi for a wide range of initial bladder volumes, comparable with the doses for the several strategies displayed in Figure 13.

SUMMARY

A simple spherical dynamic model has been developed for calculating the radiation absorbed dose to the inner surface of the bladder wall. A generalized formula that incorporates variable initial bladder volumes, urine production rates, residual fractions, and voiding schedules has been derived analytically. Results from computer simulation studies suggest the following strategies for achieving dose reductions for F-18-FDG and Tc-99m-DTPA: (1) a comfortably large initial bladder volume; (2) high urine production rates; (3) voiding after most of the activity has accumulated in the bladder; and (4) voiding more frequently and as completely as possible after the optimal first voiding time. The first voiding should take place at about one hour after administration for F-18-FDG and at two hours for Tc-99m-DTPA. This model is also applicable to other radiopharmaceuticals with excretion patterns deviating substantially from F-18-FDG and Tc-99m-DTPA. Dose reduction strategies for such cases can be designed using approaches similar to those presented in this paper.

REFERENCES

1. Snyder, W., M. Ford, and G. Warner. Estimates of specific absorbed fractions for photon sources uniformly distributed in various organs of a heterogeneous phantom, MIRD Pamphlet No. 5 (revised), Society of Nuclear Medicine, New York, 1978.
2. Jones, S.C., A. Alavi, D. Christman, I. Montanez, A.P. Wolf, and M. Reivich. The radiation dosimetry of 2-[F-18]fluoro-2-deoxy-D-glucose in man. J. Nucl. Med. 23, 613-617, 1982.
3. Cloutier, R.J., S.A. Smith, E.E. Watson, W.S. Snyder, and G.G. Warner. Dose to the fetus from radionuclides in the bladder. Health Phys. 25, 147-161, 1973.
4. Unnikrishnan, K. Dose to the urinary bladder from radionuclides in the urine. Phys. Med. Biol. 19(3). 329-340, 1974.
5. Snyder, W.S., and M.R. Ford. Estimation of dose to the urinary bladder and to the gonads, in Proceedings of Conference-Radiopharmaceutical Dosimetry Symposium, edited by R.J. Cloutier, J.L. Coffey, W.S. Snyder, and E.E. Watson, pp. 313-350, HEW Publication (FDA) 76-8044, 1976.

6. Smith, E.M., and G.G. Warner. Practical methods of dose reduction to the bladder wall, in Proceedings of Conference-Radiopharmaceutical Dosimetry Symposium, edited by R.J. Cloutier, J.L. Coffey, W.S. Snyder, and E.E. Watson, pp. 351-359, HEW Publication (FDA) 76-8044, 1976.
7. Diffey, B.L., and A.J.W. Hilson. Absorbed dose to the bladder from $^{99}\text{Tc}^{\text{m}}$ DTPA. Brit. J. Radiol. 49. 196-198, 1976.
8. Smith, T., N. Veall, and R. Wootton. Bladder wall dose from administered radiopharmaceuticals: The effects of variations in urine flow rate, voiding interval, and initial bladder content. Rad. Prot. Dosim. 2(3). 183-189, 1982.
9. Dimitriou, P., A. Fretzayas, P. Nicolaidou, F. Gritzali, A. Kasfiki, and T. Karpathios. Estimates of dose to the bladder during direct radio-nuclide cystography: Concise communication. J. Nucl. Med. 25. 792-795, 1984.
10. Chen, C.-T., P.V. Harper, and K.A. Lathrop. Radiation absorbed dose to the bladder from 2-FDG and other radiopharmaceuticals. J. Nucl. Med. 25(5). P92-93, 1984.
11. Loevinger, R., J.G. Holt, and G.J. Hine. Internally administered radio-isotopes, in Radiation Dosimetry, edited by G.J. Hine and G.L. Brownell, pp. 801-896, Academic Press, New York, 1956.
12. Morgan, K.Z., and L.C. Emerson. Dose from external sources of radiation, in Principles of Radiation Protection, edited by K.Z. Morgan and J.E. Turner, p. 285, John Wiley and Sons, New York, 1967.
13. Thomas, S.R., H.L. Atkins, J.G. McAfee, M.D. Blaufox, M. Fernandez, P.T. Kirchner, and R.C. Reba. Radiation absorbed dose from Tc-99m diethylenetriaminepentaacetic acid (DTPA), MIRD Dose Estimate Report No. 12. J. Nucl. Med. 25. 503-505, 1984.
14. Loevinger, R., E.M. Japha, and G.L. Brownell. Discrete radioisotope sources, in Radiation Dosimetry, edited by G.J. Hine and G.L. Brownell, pp. 693-789, Academic Press, New York, 1956.
15. Dillman, L.T. Radionuclide decay schemes and nuclear parameters for use in radiation-dose estimation. MIRD Pamphlet No. 4, Society of Nuclear Medicine, New York, 1969.

DISCUSSION

MITCHELL: Your geometric model is primarily concerned with penetrating radiation dose to the bladder wall. For nonpenetrating radiation does your model take into consideration that the bladder wall is thinning with increased bladder volume? The tissue at risk is proportional to the surface area of the bladder and the range of the nonpenetrating radiations. Are you concerned only with dose to the surface of the bladder?

CHEN: All our models are concerned only with the dose to the surface.

AN AGE- AND SEX-DEPENDENT MODEL FOR ESTIMATING
RADIOIODINE DOSE TO A NORMAL THYROID

George G. Killough and Keith F. Eckerman
Health and Safety Research Division
Oak Ridge National Laboratory
P.O. Box X
Oak Ridge, Tennessee 37831

ABSTRACT

This paper describes the derivation of an age- and sex-dependent model of radioiodine dosimetry in the thyroid and the application of the model to estimating the thyroid dose for each of 4215 patients who were exposed to ^{131}I in diagnostic and therapeutic procedures. In most cases, the available data consisted of the patient's age at the time of administration, the patient's sex, the quantity of activity administered, the clinically-determined uptake of radioiodine by the thyroid, and the time after administration at which the uptake was determined. The model was made to conform to these data requirements by the use of age-specific estimates of the biological half-time of iodine in the thyroid and an age- and sex-dependent representation of the mass of the thyroid. Also, it was assumed that the thyroid burden was maximum 24 hours after administration (the ^{131}I dose is not critically sensitive to this assumption). The metabolic model is of the form $A(t) = K[\exp(-\mu_1 t) - \exp(-\mu_2 t)]$ (μCi), where $\mu_i = \lambda_r + \lambda_i^b$ ($i = 1, 2$), λ_r is the radiological decay-rate coefficient, and λ_i^b are biological removal rate coefficients. The values of λ_i^b are determined by solving a nonlinear equation that depends on assumptions about the time of maximum uptake and the eventual biological loss rate (through which age dependence enters). The value of K may then be calculated from knowledge of the uptake at a particular time. The dosimetric S-factor ($\text{rad}/\mu\text{Ci-day}$) is based on specific absorbed fractions for photons of energy ranging from 0.01 to 4.0 MeV for thyroid masses from 1.29 to 19.6 g; the functional form of the S-factor also involves the thyroid mass explicitly, through which the dependence on age and sex enters. An analysis of sensitivity of the model to uncertainties in the thyroid mass and the biological removal rate for several age groups is reported. This model could prove useful in the dosimetry of very short-lived radioiodines. Tables of age- and sex-dependent coefficients are provided to enable readers to make their own calculations.

INTRODUCTION

This paper describes work performed at Oak Ridge National Laboratory (ORNL) for the National Center for Devices and Radiological Health (DRH) of the Food and Drug Administration (FDA) in support of the Diagnostic ^{131}I Study conducted by DRH. The task of ORNL was to examine a computer file consisting of records of the administration of ^{131}I to 4215 patients for completeness of data needed to estimate the radiation dose to the thyroid gland, and to compute the thyroid dose estimate for each administration for which the data were sufficient.

The dosimetric model was constructed specifically for the information contained in this file. As inputs, the model requires the patient's age and sex, the quantity of radioactivity administered, the fractional uptake of ^{131}I by the thyroid, and the time interval from the administration to the determination of fractional uptake.

This paper discusses details of the dosimetric model for radioiodines that was developed for the Diagnostic ^{131}I study. The model is described in the context of the ^{131}I administrations recorded in the FDA DRH computer file. Application of the model to other isotopes of iodine will be discussed in a forthcoming paper.

AN AGE- AND SEX-DEPENDENT MODEL FOR RADIOIODINE DOSIMETRY IN THE THYROID

The model that we have applied to the age, sex, and uptake data in the FDA DRH file estimates absorbed dose (rad) to the thyroid resulting from a known fractional uptake by the thyroid at a specified time after a clinical administration of ^{131}I . To an extent that we believe is consistent with observations, the model distinguishes age differences and, to a lesser degree, those related to sex. The model is based on data from euthyroid subjects; its elaboration to abnormal thyroid conditions has not been undertaken.

The model consists of two components, corresponding to the two factors in the right-hand side of the dose-rate equation

$$(1) \quad \dot{D}(t) = S(\text{thyroid} - \text{thyroid}) \cdot A(t),$$

where $\dot{D}(t)$ = absorbed dose rate (rad day^{-1}) to the thyroid at time t , $S(\text{thyroid} - \text{thyroid})$ = dosimetric "S-factor" ($\text{rad } (\mu\text{Ci-day})^{-1}$) for ^{131}I in the thyroid, and $A(t)$ = ^{131}I activity burden in the thyroid (μCi) at time t . In our model, S depends on age and sex, and $A(t)$ depends on age at the time of administration of the ^{131}I .

The ^{131}I activity in the thyroid, $A(t)$, is based on a metabolic model of iodine in the body. Several levels of detail have been incorporated into existing models. Multicompartment models aim at providing mechanistic representations of iodine kinetics [e.g., (1)], but the numerous parameters of such models are not readily expressed as functions of age. The International Commission on Radiological Protection (ICRP) has adapted a model of Riggs (2) for purposes of radiation protection for occupationally exposed adults (3). The Riggs/ICRP model (Fig. 1) consists of three compartments. The first is a "transfer compartment," into which the radioiodine is originally introduced and from which it is removed with biological half-time 0.25 days; 70% is excreted through the urine and the remaining 30% is taken up by the thyroid. Iodine is cleared from the thyroid compartment with a half-time of 80 days into an organic-iodine pool, which loses iodine through excretion and feedback to the transfer compartment.

The transfer compartment has proved useful in avoiding overestimates of dose to the thyroid by short-lived radioiodines, which decay significantly before reaching the thyroid, and we wished to retain this feature in the model implicitly. The feedback pathway, on the other hand, makes little contribution to the time integral of activity in the thyroid for ^{131}I . To support this assertion, we have performed calculations with the three-box model of Fig. 1 and a two-box counterpart that lacks the organic-iodine compartment (Fig. 2). When 1 μCi of ^{131}I is introduced into the transfer compartment at time $t = 0$, the two models agree in the following respects: (i) both model thyroids have their maximum activity between 1.2 and 1.3 days after administration; (ii) both

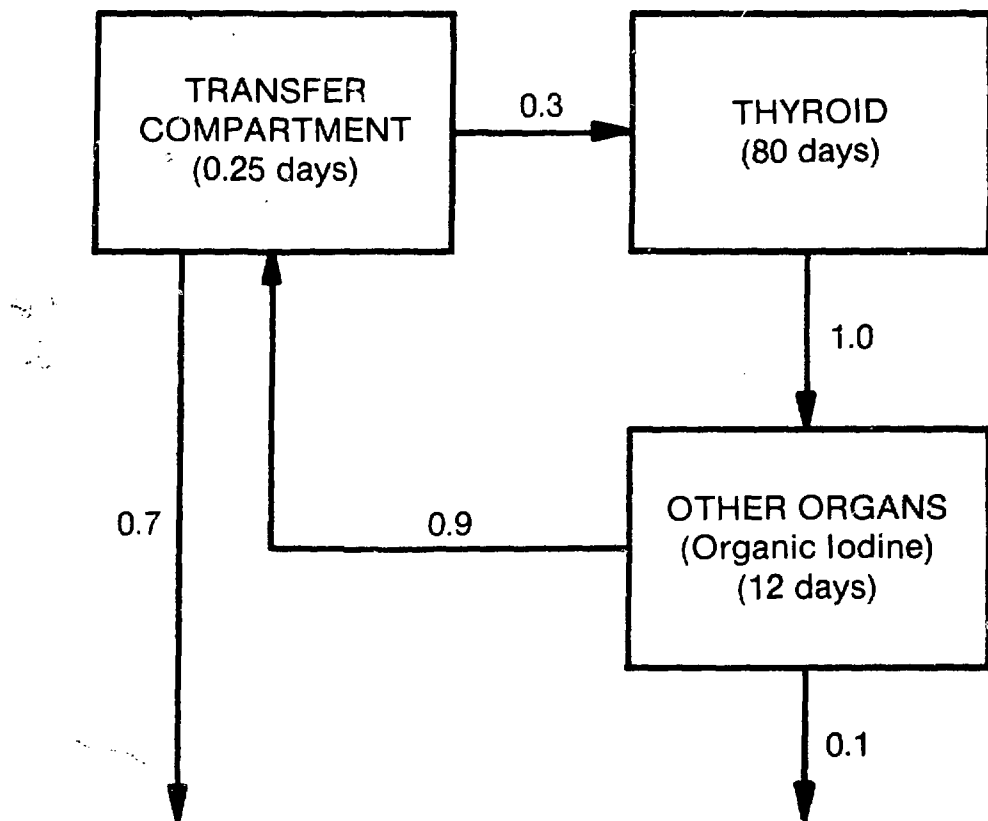


Figure 1. The Riggs/ICRP metabolic model for iodine. Times in the boxes are biological removal half-times. The connecting arrows are labeled with the corresponding pathway fractions.

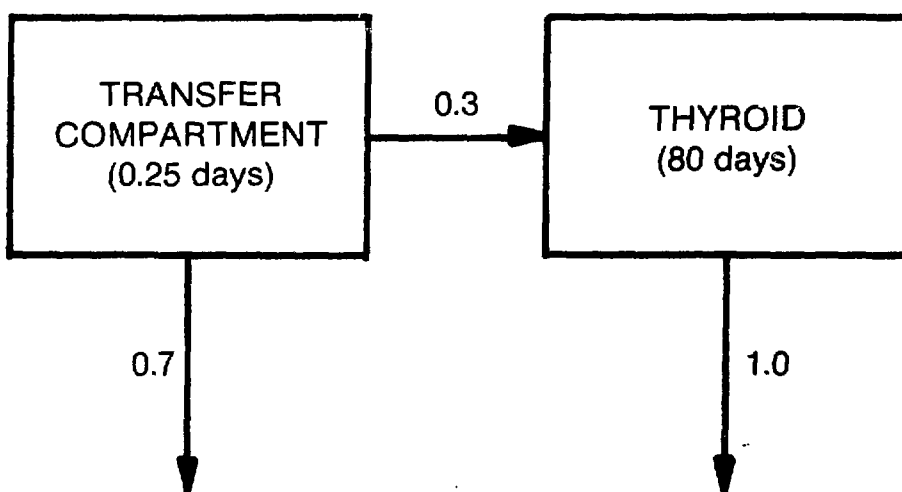


Figure 2. Two-box metabolic model for iodine, which predicts, for ^{131}I , the same time-integrated radioactivity in the thyroid as the three-box model of Fig. 1.

maximum uptakes by the thyroid are 26% of the administered activity; and (iii) the time integral of activity in the thyroid is $3.1 \mu\text{Ci}\text{-days per } \mu\text{Ci}$ taken into the body for both models. For our purposes, the model of Fig. 2 is essentially the functional equivalent of that of Fig. 1 and offers the advantage of fewer parameters.

But the formulation of the two-box model represented by Fig. 2 was not yet ideal for application to the FDA DRH computer file. We needed to be able to specify directly the fractional uptake by the thyroid of the administered isotope. The coefficient 0.3 (in the presence of the other parametric values) gives a maximum uptake of 26% and thus corresponds roughly to the maximum fractional uptake. But some patients' records contained measured uptakes only at times that were unlikely to correspond to the maximum. A model that accommodated such a pattern of data was needed. To construct one, we proceeded along the following lines of reasoning.

When the differential equations that describe the two-box model of Fig. 2 are solved explicitly, the representation of the thyroid compartment has the form

$$(2) \quad A(t) = K \cdot (e^{-\lambda_1 t} - e^{-\lambda_2 t}),$$

where $\mu_i = \lambda_i^b + \lambda_r$ ($i = 1, 2$) are effective decay-rate coefficients, $\lambda_i^b = \ln 2 / T_i^b$ are biological decay-rate coefficients (T_i^b are biological half lives), and λ_r is the radiological decay-rate coefficient for the radioiodine of interest. We assume throughout this discussion that $A(t)$ is normalized to the intake of $1 \mu\text{Ci}$ of radioactive iodine into the body; consequently, in applications, $A(t)$ must be multiplied by the actual number of μCi administered. Note that $A(0) = 0$, because the initial intake is not in the thyroid. We take K , λ_1 , and λ_2 as unknown parameters and impose three constraints to determine their values.

(i) $A(t)$ is required to have its maximum value at a specified time, $t = t_{\max}$. For this study we took $t_{\max} = 1$ day, corresponding to the clinical assumption that maximum uptake occurs in approximately 24 hours. For ^{131}I we tested the sensitivity of the time integral of $A(t)$ to the choice of t_{\max} by varying this parameter over a range from 0.5 to 2 days. The maximum deviation of the time integral of $A(t)$ from its reference value was 11%.

(ii) The function $y_b(t) = \exp(-\lambda_1 t) - \exp(-\lambda_2 t)$ is required to have a specified "apparent" biological half-time, T^* , with respect to a given interval, $t_1 \leq t \leq t_2$ ($t_1 \leq t_{\max}$). We used $t_1 = t_{\max}$ and $t_2 = 15$ days, corresponding to common experimental practice of reporting a single clearance-rate parameter based on the first 15 days' observations. We express this requirement by the equation

$$(3) \quad \frac{y_b(t_2)}{y_b(t_1)} = \exp\left(-\frac{\ln 2}{T^*}(t_2 - t_1)\right).$$

(iii) Finally, we require that at a specified time, T , the fractional uptake, u , of iodine to the thyroid can be assigned: $A(T) = u$. The time T at which the fractional uptake is actually determined often does not coincide with t_{\max} ; for example, the data file contained a number of observations at $T = 6$ hours.

Within the parametric range of interest in this work, the requirements (i)-(iii) given above determine the parameters K , λ_1 , and λ_2 as functions of t_{\max} , t_1 , t_2 , T^* , T , and u . The numerical calculation of K , λ_1 , and λ_2 in a given case involves solving a nonlinear equation. We give details of the procedure in Appendix A.

Table 1 displays the rate coefficients μ_1 and μ_2 of Eq. 2 vs age. The tabulation is based on the parameter values $t_{\max} = 1$ day, $t_1 = 1$ day, and $t_2 = 15$ days. The following example illustrates how the retention function corresponding to a particular uptake observation is determined. Suppose that 25 μCi of ^{131}I is administered to a ten year old male, and after 6 hours it is determined that the thyroid has taken up 9%. Let us calculate the fractional retention function. From Table 1 we have the effective rate coefficients $\mu_1 = 0.1032$, $\mu_2 = 3.6759 \text{ day}^{-1}$, and we are given that for $t = 6 \text{ hours} = 0.25 \text{ day}$,

$$K \cdot [\exp(-0.1032 \times 0.25) - \exp(-3.6759 \times 0.25)] = 0.09$$

so that $K = 0.09/0.5756 = 0.1564$. Since the maximum value occurs at $t_{\max} = 1$ day, we may compute it as follows:

$$u_{\max} = 0.1564 \times [\exp(-0.1032 \times 1) - \exp(-3.6759 \times 1)] = 0.1371$$

or 13.7% (3.4 μCi).

For some combinations of input parameters, however, the formulation just described and illustrated gives misleading answers. Such an occurrence results from an estimate of the fractional uptake u at time T that predicts a maximum uptake $u_{\max} = A(t_{\max})$ that exceeds any amount that the thyroid could possibly take up by time t_{\max} , given the structural assumptions of the model and the values of the remaining input parameters. A necessary constraint may be expressed by the inequality

$$(4) \quad A(t_{\max}) < \exp(-\lambda_r t_{\max}),$$

because the value $\exp(-\lambda_r t_{\max})$ is an upper bound for the fraction of the administered radioactivity that survives radioactive decay and is available for uptake by the thyroid at time t_{\max} . This upper bound is conservative, because some of the radioiodine would also be removed from the body by biological processes during the interval $[0, t_{\max}]$. But the constraint of Eq. 4 is not built into the model as we have formulated it above. Our remedy for physically impossible cases is to replace the retention function $A(t)$ by $A^*(t)$, which is computed in the same way, but with $T = t_{\max}$ and $u = u_{\max} = \exp(-\lambda_r t_{\max})$. This use of the conservative upper bound for u_{\max} insures that A^* will not underestimate the uptake, given the model's structure and the other parameter values. But the use of A^* also has the advantage of avoiding dose estimates that are greatly in excess of what is physically possible. The choice, of course, is not consistent with the original input value of u .

We illustrate the handling of such exceptions with the case of a six year old who was given 20 μCi of ^{131}I and observed to have taken up 41.4% after 2 hours

Table 1. Age-dependent retention parameters for ^{131}I in the thyroid

Age (years)	Rate coefficients (day^{-1})		Age (years)	Rate coefficients (day^{-1})	
	μ_1	μ_2		μ_1	μ_2
0	0.1324	3.369	10	0.1032	3.676
1	0.1403	3.298	11	0.1020	3.690
2	0.1328	3.365	12	0.1010	3.702
3	0.1241	3.449	13	0.0997	3.719
4	0.1182	3.509	14	0.0988	3.730
5	0.1140	3.554	15	0.0980	3.740
6	0.1108	3.589	16	0.0973	3.748
7	0.1083	3.617	17	0.0967	3.756
8	0.1062	3.640	≥ 18	0.0962	3.763
9	0.1046	3.660			

= 0.083 day. For age six years, $\mu_1 = 0.1107$ and $\mu_2 = 3.5891 \text{ day}^{-1}$, and we are given

$$K \cdot [\exp(-0.1107 \times 0.083) - \exp(-3.5891 \times 0.083)] = 0.414$$

so that $K = 0.414/0.2485 = 1.666$. This retention function predicts a maximum fractional uptake, at $t_{\max} = 1 \text{ day}$, of

$$u_{\max} = 1.666 \times [\exp(-0.1107 \times 1) - \exp(-3.5891 \times 1)] = 1.45$$

or 145%, which is impossible. We must conclude that the observation was taken, recorded, or transcribed incorrectly, or that the patient's uptake of the radioiodine was approaching its maximum somewhat earlier than the assumed 24 hours. Having no further information about the patient or the procedure, we discard the observation of 41.4% after 2 hours and instead assume that $u = u_{\max} = \exp(-\lambda_r t)$ at $t = t_{\max} = 1 \text{ day}$. This gives $u_{\max} = 0.917$ and

$$K \cdot [\exp(-0.1107 \times 1) - \exp(-3.5891 \times 1)] = 0.917$$

so that $K = 0.917/0.8676 = 1.057$. As we noted earlier, the recomputed retention function A^* cannot be consistent with the observed 41.4% at 2 hours; instead, the value after 2 hours is

$$\begin{aligned} u = A^*(0.084) &= 1.057 \times [\exp(-0.1107 \times 0.083) - \exp(-3.5891 \times 0.083)] \\ &= 0.263 \end{aligned}$$

or 26.3%. The interpretation of this default retention function is that during the first 24 hours, radioiodine is lost from the body only by radioactive decay, whereas after 24 hours it is removed by a combination of radioactive decay and biological processes. Thus, the default represents an upper bound for retention curves having their maximum values at $t = 1 \text{ day}$ and having the same values for the parameters t_1 , t_2 , and T^* .

The biological half-time, T^* , of iodine in the thyroid has been estimated in numerous studies with different age groups and is one of the parameters considered by Dunning and Schwarz in a review of literature for euthyroid patients (4). They estimated distributions of T^* for each of several age groups ranging from newborn to adult. Their mean value of 85 days for the adult is similar to the 80-day value used by ICRP (3). We will use a function that interpolates the mean values given by Dunning and Schwarz (4) as an age-dependent representation of T^* (Fig. 3).

Thus, Eq. 2, together with constraints (i)-(iii) described above, defines an age-dependent metabolic model of iodine retention in the thyroid. The model can be tied directly to population data through its biological half-time parameter T^* and to specific individual clinical data through the uptake parameters T and u , and it depends only marginally on a parameter (t_{\max}) to which we have less direct access.

The remaining factor in the dose-rate equation (Eq. 1) is the S-factor, which depends on the mass of the thyroid, which in turn depends strongly on age and to a much lesser extent on sex. We outline the considerations used in obtaining the S-factors for the model.

We express the S-factor, which represents absorbed dose rate to (target) organ Y per unit radioactivity of the radionuclide of interest in (source) organ X, in the form

$$(5) \quad S(Y \leftarrow X) = k \sum_i n_i E_i \Phi_i(Y \leftarrow X)$$

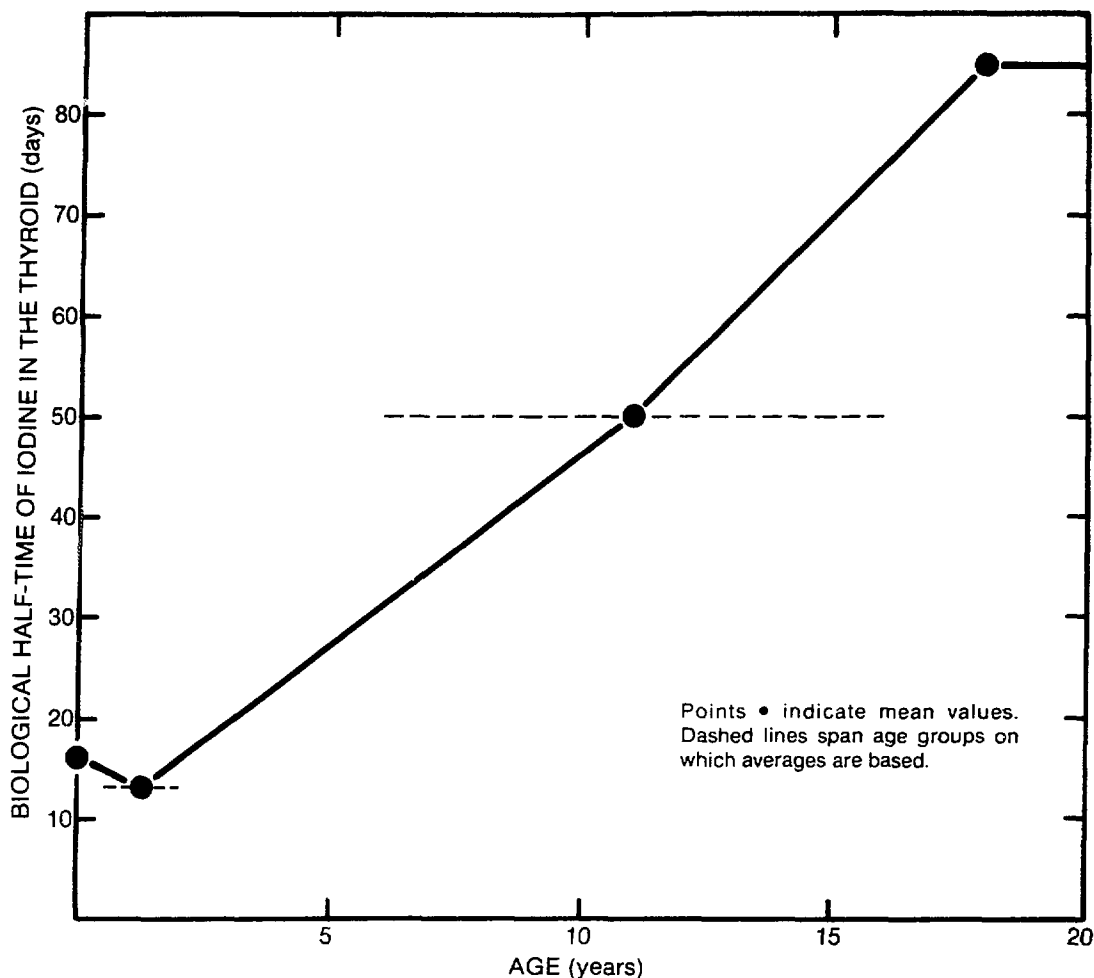


Figure 3. Biological half-time of iodine in the thyroid as a function of age, based on estimates of Dunning and Schwarz (Ref. 4).

where

n_i = mean number of radiations of type i per nuclear transformation

E_i = mean energy per radiation of type i (MeV)

$\Phi_i(Y \leftarrow X)$ = specific absorbed fraction for radiation type i (g^{-1})

$k = 2.13 \text{ (rad-g)} / (\mu\text{Ci} \cdot \text{hr} \cdot \text{MeV})$.

In the present context, $X = Y = \text{thyroid}$. The absorbed dose rate from non-penetrating radiation as a function of thyroid mass M_{th} is

$$S_{np}(\text{thyroid} \leftarrow \text{thyroid}) = \frac{2.13 \sum n_i E_i}{M_{th}},$$

because $\Phi = 1/M_{th}$ for such radiations. For ^{131}I , 0.191 MeV of non-penetrating radiation is emitted per nuclear transformation (5). Thus,

$$S_{np}(\text{thyroid} \leftarrow \text{thyroid}) = \frac{2.13 \times 0.191}{M_{th}} = \frac{0.406}{M_{th}} \text{ rad}/(\mu\text{Ci} \cdot \text{hr}).$$

Monte Carlo calculations of the specific absorbed fraction for photons of energy ranging from 0.01 to 4.0 MeV have been performed for thyroid mass values from 1.29 to 19.6 g (Table 2). An S-factor for the penetrating radiations of ^{131}I was calculated for several thyroid masses in this range (Table 3) and fitted to a power function of thyroid mass. The resulting expression is

$$S_p(\text{thyroid} \leftarrow \text{thyroid}) = 1.014 \times 10^{-2} M_{\text{th}}^{-0.666}.$$

This function fits the data with reasonable accuracy. The total S-factor is the sum of the components for non-penetrating and penetrating radiations:

$$(6) \quad S(\text{thyroid} \leftarrow \text{thyroid}) = \frac{0.406}{M_{\text{th}}} + 1.014 \times 10^{-2} M_{\text{th}}^{-0.666}.$$

It remains for us to express the thyroid mass, M_{th} , as a function of age and sex. Kay and coworkers (6) analyzed the masses at autopsy of thyroids of 537 subjects of both sexes and ages ranging from prenatal to 19 years (all but eight were under 15 years of age). These data were fitted by the regression line

$$(7) \quad M_{\text{th}} = 1.48 + 0.648a \pm 1.94 \text{ g},$$

where a = age in years and 1.94 g is the residual standard error. Over the range of ages considered, the difference in thyroid mass between sexes was not found to be significant. To construct our function, we used the regression line of Eq. 7 for both sexes and ages ranging from newborn to 15 years. For adults, we adopted the average values 17.5 ± 6.8 g (male) and 14.9 ± 6.7 g (female) from a study of New York City cases (7, 8). The articulation was accomplished by interpolating linearly, for each sex, between the value of M_{th} given by Eq. 6 for $a = 15$ years and the appropriate adult value at $a = 25$ years. After 25 years, the functions are considered to be constant (Fig. 4). This scheme furnishes, for each age and sex, a value of M_{th} , which is substituted into Eq. 6 to obtain the S-factor.

Table 4 shows S-factors for males and females and for ages newborn to 25 years. We illustrate the dose computation procedure by referring to an earlier example of a ten year old male who was given $25 \mu\text{Ci}$ of ^{131}I and found to have taken up 9% to the thyroid after 6 hours. The fractional retention function was found to be

$$A(t) = 0.1564 \times [\exp(-0.1032t) - \exp(-3.6759t)].$$

Integration gives

Table 2. Photon specific absorbed fraction for the thyroid as a function of thyroid mass

Photon energy (keV)	Mass (g) →	$\Phi(\text{thyroid} \leftarrow \text{thyroid}) (\text{kg}^{-1})$					
		1.29	1.78	3.45	7.93	12.4	19.6
10	533.	390.	215.	100.	66.4	42.9	
15	280.	209.	123.	62.7	43.5	29.3	
20	145.	110.	67.6	36.4	26.0	18.1	
30	49.0	37.0	23.9	13.7	10.2	7.41	
50	15.4	11.7	7.68	4.45	3.43	2.42	
100	8.73	6.90	4.58	2.62	2.03	1.44	
200	9.42	7.72	5.09	2.88	2.20	1.55	
500	10.2	8.70	5.71	3.22	2.43	1.66	
1000	9.89	8.18	5.45	3.02	2.29	1.54	
2000	8.26	6.86	4.57	2.56	1.90	1.31	
4000	6.83	5.46	3.38	2.04	1.49	1.05	

Table 3. Iodine-131 S-factor as a function of thyroid mass

Thyroid mass (g)	S (rad/ μ Ci-hr)		
	Non-penetrating	Penetrating	Total
1.29	0.314	8.32×10^{-3}	0.323
1.78	0.228	6.95×10^{-3}	0.235
3.45	0.118	4.56×10^{-3}	0.122
7.93	0.0512	2.57×10^{-3}	0.0538
12.4	0.0327	1.95×10^{-3}	0.0347
19.6	0.0207	1.35×10^{-3}	0.0221

$$\bar{A} = \int_0^{+\infty} A(t) dt = \frac{0.1564}{0.1032} - \frac{0.1564}{3.6759} = 1.473 \text{ } \mu\text{Ci-days per } \mu\text{Ci intake.}$$

(The infinite limit of integration, in the case of ^{131}I , gives the same result as an integration time of 50, 70, or 100 years.) The S-factors in Table 4 are in units of rad/ μ Ci-day. Hence the dose to this patient's thyroid is estimated to be

$$D = 25 \text{ } \mu\text{Ci} \times 1.285 \text{ rad}/\mu\text{Ci-day} \times 1.473 \text{ } \mu\text{Ci-day}/\mu\text{Ci}$$

$$= 47.3 \text{ rad to the thyroid.}$$

Table 5 shows the results of a calculation performed with the composite dosimetric model. Dose (rad/ μ Ci) is tabulated by age and sex. For this tabulation, the fractional maximum uptake was based on the age-specific mean values from the review of Dunning and Schwarz (4). For comparison, corresponding estimates of ^{131}I dose to the thyroid by Dunning and Schwarz (4), ICRP (9), Medical Internal Radiation Dosimetry (MIRD) Committee (10), and the U.K. National Radiological Protection Board (NRPB) (11) are shown alongside. In general, the agreement is good.

SENSITIVITY OF THE DOSE MODEL TO UNCERTAINTIES IN ITS PARAMETERS

For the case of ^{131}I we have tested the sensitivity of the dose estimate to uncertainties in two of the model parameters by replacing those parameters with probability distributions and estimating the corresponding distribution of the dose. The parameters are the biological half-time of iodine in the thyroid and the mass of the thyroid. The calculations, which were performed by pseudorandom sampling from the input probability distributions, were carried out for each of the four age groups considered by Dunning and Schwarz (4) (newborn; children 0.5-2 years; adolescents 6-16 years; and adults ≥ 18 years). For each age group, the corresponding Dunning and Schwarz estimate of the mean value of fractional uptake by the thyroid was used. Substitution of different values of fractional uptake – such as clinically determined uptakes – would, of course, lead to different distributions of dose, but the distributions we have computed should give a reasonable impression of variability in the dose estimates for fixed fractional uptake.

Other fixed parameters and their values that were used in the simulations were t_{\max} (1 day), t_1 (1 day), t_2 (15 days), and T (1 day).

The biological half-time of iodine in the thyroid, T^* , and the mass of the thyroid, M_{th} , were treated, for each age group, as independent random variables. (In the present context, this assumption was taken as an extreme case.) The distribution of T^* was assumed to be lognormal with values of the logarithmic mean and standard deviation, μ and σ , taken from Dunning and Schwarz (4). For nonadult age groups, M_{th} was assumed lognormally distributed with mean lying on

Table 4. Sex- and age-dependent S-factors for ^{131}I in the thyroid

Age (years)	S-factors (rad/ μCi -day)		Age (years)	S-factors (rad/ μCi -day)	
	Male	Female		Male	Female
0	6.771	6.771	13	1.037	1.037
1	4.726	4.726	14	0.9740	0.9740
2	3.633	3.633	15	0.9187	0.9187
3	2.953	2.953	16	0.8706	0.8898
4	2.488	2.488	17	0.8273	0.8627
5	2.151	2.151	18	0.7882	0.8372
6	1.895	1.895	19	0.7527	0.8132
7	1.693	1.693	20	0.7203	0.7906
8	1.531	1.531	21	0.6906	0.7692
9	1.397	1.397	22	0.6632	0.7490
10	1.285	1.285	23	0.6380	0.7298
11	1.190	1.190	24	0.6146	0.7115
12	1.108	1.108	≥ 25	0.5929	0.6942

Table 5. Iodine-131 dose to the thyroid by age and sex (rad/ μCi)

Age	Present model		Dunning and Schwarz (1981)	ICRP methodology ^b	MIRD (1975)	NRPB ^d (1983)
	Male	Female	Both sexes	Both sexes	Both sexes	Both sexes
0	27.4	27.4	25.3			
1	15.7	15.7				13.7
2	12.4	12.4				
3	10.9	10.9				
4	9.8	9.8				
5	8.9	8.9				
6	8.2	8.2				
7	7.6	7.6				
8	7.1	7.1				
9	6.7	6.7				
10	6.4	6.4				4.4
11	6.1	6.1	8.5			
12	5.2	5.2				
13	4.5	4.5				
14	3.8	3.8				
15	3.2	3.2				
16	2.7	2.7				
17	2.2	2.3				
18	1.7	1.8	1.4	1.8	1.3 ^c	1.6
19	1.6	1.8				
20	1.6	1.7				
21	1.5	1.7				
22	1.4	1.6				
23	1.4	1.6				
24	1.3	1.5				
25	1.3	1.5				

^a0.5-2 years.^bRef. 9.^cBased on maximum uptake to the thyroid of 25% and thyroid mass 20 g.^dRef. 11.

the age regression line given by Kay et al. (6) (Eq. 7). We used the residual standard deviation (1.94 g), together with the predicted mean, α , to compute the logarithmic parameters μ and σ . If a denotes the age (years), the equations are

$$\alpha = 1.48 + 0.65 a \text{ g}$$

$$\beta = 1.94 \text{ g}$$

$$\mu = \ln [\alpha / \sqrt{1 + \beta^2 / \alpha^2}]$$

$$\sigma^2 = \ln (1 + \beta^2 / \alpha^2)$$

where the equations for μ and σ^2 were obtained by solving the inverse equations given by Aitchison and Brown (12). The lognormal distribution was then shifted upward to make its median coincide with the regression line. Substitution of the median for the mean serves to eliminate a bias in the dose distribution. For adults, the normal distribution was used, with parameters adopted directly from the Reference Man report (8). The values are

	μ	σ
male	17.5	6.8
female	14.9	6.7

We carried out the pseudorandom simulations by sampling independently from the distributions of T^* and M_{th} . Each nonadult age group was represented by its midrange age. Each sample pair was substituted into the dose-rate formula (Eqs. 1, 2, 6, and 7), and a dose D was computed by integration. The resulting values of D were assembled into an empirical distribution, the form of which is approximately lognormal, and which we therefore characterize by giving the logarithmic parameters μ and σ . For the pseudorandom sampling, we used the sample size $N = 1000$. Figure 5 shows these distributions of dose, together with the parameters that define the underlying lognormal distributions of T^* and M_{th} .

ORNL-DWG 85-13115

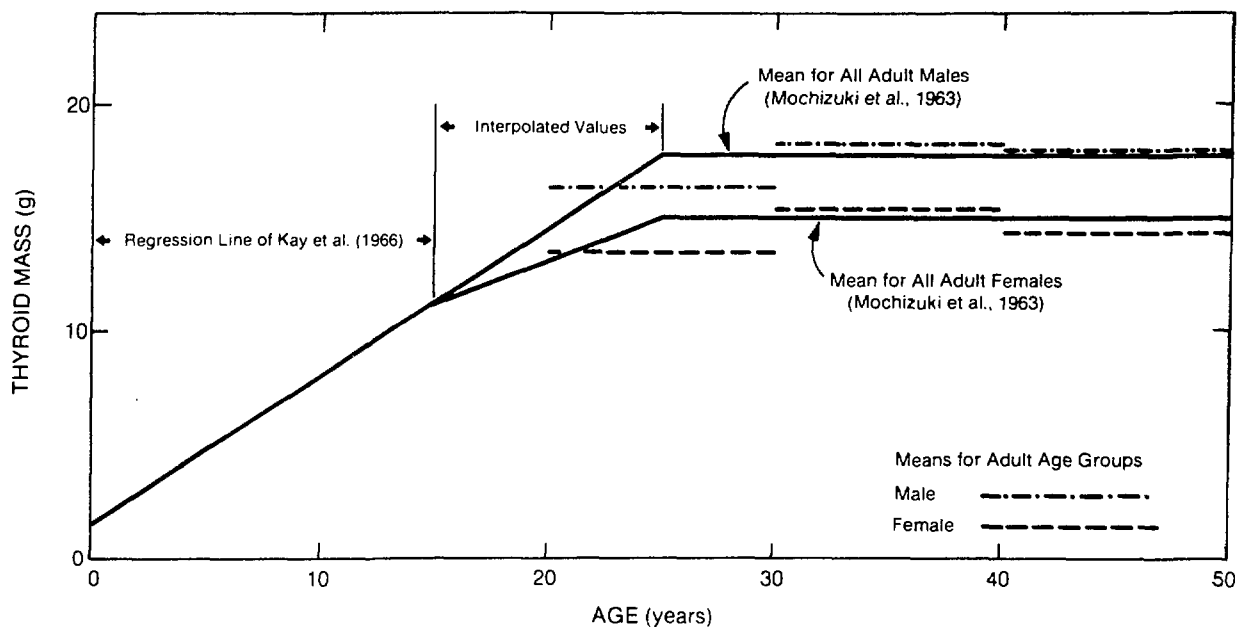


Figure 4. Mass of the thyroid as a function of age.

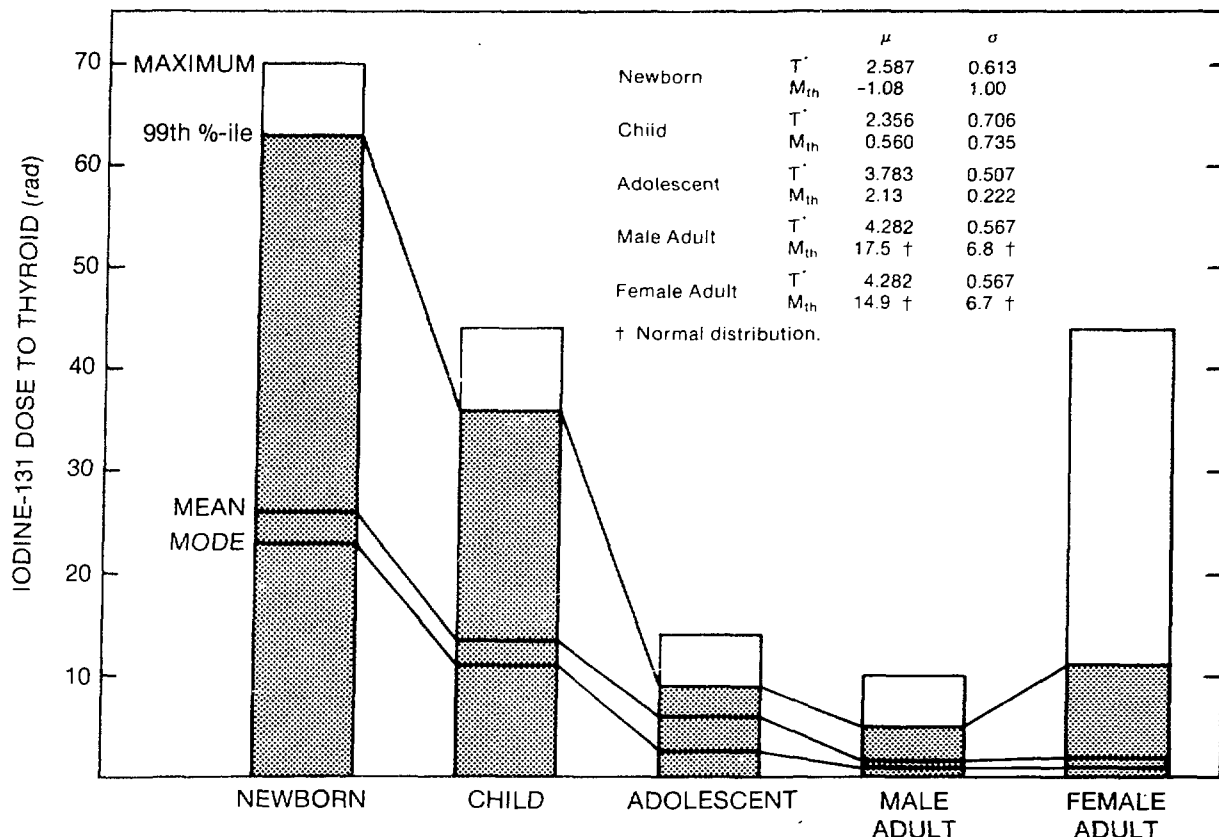


Figure 5. Distributions of thyroid dose corresponding to uncertainties in biological half-time T^* and mass M_{th} .

In absolute terms, the variability shown in Fig. 5 is large for the newborn and children's groups (99th percentiles = 63 and 36 rad, respectively) and progressively smaller with increasing age. But in relative terms, the 99th percentile as a multiple of the mean is larger for the two adult groups than for newborns (4.1 and 6.1 for males and females, respectively, vs. 2.4 for newborns). We caution that the 99th percentile statistic is itself highly variable, and consequently, so are these ratios.

Finally, we note that the arithmetic means of the dose distributions are in good agreement with the dose estimates in Table 5. This agreement would not have been achieved without substitution of the median thyroid mass for the mean in each age group, as we described above.

SUMMARY AND CONCLUSIONS

We have described the derivation and application of an age- and sex-specific model of ^{131}I dosimetry for the thyroid. The model was specially formulated for the data base that will support the Diagnostic ^{131}I Study conducted by DRH; in particular, the model accommodates values of fractional uptake to the thyroid that were determined at various times after administration, including but not restricted to the time of maximum thyroid burden. The model has been applied to all records of the data file for which the uptake and retention data are complete or can be estimated from other records for the same patient, and each computed thyroid dose has been incorporated into the appropriate record.

Tests of sensitivity of the model's predictions to uncertainties in the biological half-time of iodine in the thyroid and the mass of the organ were performed. These tests showed large absolute variability in the dose for newborns and children, but relative measures of dispersion (e.g., the 99th percentile as a multiple of the mean) differed less dramatically among the age groups. Inasmuch as there was clinical determination neither of thyroid mass nor of biological half-time of iodine in the thyroid for the patients in this study, our estimates of variability in dose due to uncertainty about these variables could be of interest to the investigators in the study and also to those who make generic applications of the model.

ACKNOWLEDGMENT

The research reported in this paper was sponsored by the U.S. Food and Drug Administration under Interagency Agreement FDA 224-84-6014 under Martin Marietta Energy Systems, Inc., contract DE-AC05-84OR21400 with the U.S. Department of Energy.

REFERENCES

1. Berman, M. Iodine kinetics, Chapter 11 in: The Thyroid and Biogenic Amines (J.E. Rall and I.J. Kopin, editors), Vol. I of Methods in Investigative Endocrinology (S.A. Berson, series editor). North-Holland Publishing Company, 1972.
2. Riggs, D.S. Quantitative aspects of iodine metabolism in man. Pharmacol. Rev. 4. 284-370, 1952.
3. International Commission on Radiological Protection. Limits for intakes of radionuclides by workers, ICRP Publication 30 Part 1. Ann. ICRP 2(3/4). 88-93, 1979.
4. Dunning, D.E., Jr., and G. Schwarz. Variability of human thyroid characteristics and estimates of dose from ingested ^{131}I . Health Phys. 40(5), 661-675, 1981.
5. International Commission on Radiological Protection. Radionuclide Transformations - Energy and Intensity of Emissions, ICRP Publication 38. Pergamon Press. Oxford, 1983.
6. Kay, C., S. Abrahams, and P. McClain. The weight of normal thyroid glands in children. Arch. Path. 82. 349-352, 1966.
7. Mochizuki, Y., R. Mowafy, and B. Pasternack. Weights of human thyroids in New York City. Health Phys. 9. 1299-1301, 1963.
8. International Commission on Radiological Protection. Report of the Task Group on Reference Man, ICRP Publication 23, p 198. Pergamon Press. Oxford, 1975.
9. Eckerman, K.F., M.R. Ford, and S.B. Watson. Internal Dosimetry Data and Methods of ICRP - Part 2, Vol. 1: Committed Dose Equivalent and Secondary Limits. NUREG/CR-1962 Volume 1, ORNL/NUREG/TM-433/VI. 1981.
10. Medical Internal Radiation Dosimetry (MIRD) Committee. Summary of Current radiation dose estimates to humans from ^{123}I , ^{124}I , ^{126}I , ^{130}I , ^{131}I , and ^{132}I as sodium iodide, Dose Estimate Report No. 5. J. Nucl. Med. 16(9). 857-860, 1975.

11. Stather, J.W., J.R. Greenhalgh, and N. Adams. The Metabolism of Iodine in Children and Adults. NRPB Radiol. Prot. Bull. No. 54 (ISSN 0308-4272). 1983.
12. Aitchison, J., and J.A.C. Brown. The Lognormal Distribution, p 8. Cambridge University Press, 1969.

APPENDIX

COMPUTATIONAL PROCEDURE FOR THE THYROID UPTAKE AND RETENTION FUNCTION

This appendix gives details of the determination of the fractional uptake and retention function given by Eq. 2 for radioactive iodine in the thyroid. The basis for the determination of the parameters μ_1 , μ_2 , and K is three constraints, which we recapitulate:

FIRST CONSTRAINT

The fraction $A(t)$ of Eq. 2 must take its maximum value at a specified time $t = t_{\max}$:

$$dA/dt = -K(\mu_1 e^{-\mu_1 t_{\max}} - \mu_2 e^{-\mu_2 t_{\max}}) = 0,$$

from which we obtain

$$(A1) \quad \mu_1/\mu_2 = e^{(\mu_1 - \mu_2)t_{\max}}.$$

We introduce the following transformation of $(\mu_1, \mu_2) \rightarrow (r, s)$:

$$(A2) \quad r = \mu_1/\mu_2, \quad s = \mu_2 - \mu_1$$

$(0 \leq \mu_1 < \mu_2)$ with inverse

$$(A3) \quad \mu_1 = rs/(1-r), \quad \mu_2 = s/(1-r)$$

$(0 \leq r < 1, s > 0)$. Using Eq. A1, we may express s explicitly in terms of r :

$$(A4) \quad s = -t_{\max}^{-1} \ln r.$$

This relationship will be useful in simplifying a system of nonlinear equations to be derived below.

SECOND CONSTRAINT

The biological retention function

$$(A5) \quad q(t) = K^{-1} e^{\lambda_r t} A(t) = e^{-\lambda_1 t} - e^{-\lambda_2 t}$$

is to have a specified biological half-time, T^* , with respect to a given interval $t_1 \leq t \leq t_2$, where $t_1 \geq t_{\max}$, in the sense that the equation

$$(A6) \quad q(t_2)/q(t_1) = \exp\left(-\frac{\ln 2}{T^*}(t_2 - t_1)\right)$$

must be satisfied.

The function $q(t)$, through λ_1 and λ_2 and the transformation (A2), depends on the parameters r and s ; the latter parameter can be eliminated by Eq. A4, leaving q as a function of t with parameter r . The explicit dependence can be shown to be

$$(A7) \quad q(t; r) = r^{[r/(1-r)](t/t_{\max})} e^{\lambda_r t} (1 - r^{t/t_{\max}}).$$

When Eq. A7 is substituted into Eq. A6, the result is a nonlinear equation in the variable r , which can be solved numerically to obtain the solution $r = r^*$. Then from Eqs. A3 and A4, we may compute

$$s^* = -t_{\max}^{-1} \ln r^*$$

$$(A8) \quad \lambda_1 = \mu_1 - \lambda_r = r^* s^* / (1 - r^*) - \lambda_r$$

$$\lambda_2 = \mu_2 - \lambda_r = s^* / (1 - r^*) - \lambda_r,$$

and thus $q(t)$ (Eq. A5) is determined.

THIRD CONSTRAINT

For a specified time T and fractional uptake u by the thyroid, we must have

$$(A9) \quad A(T) = u \quad \text{if} \quad A(t_{\max}) \leq \exp(-\lambda_r t_{\max}).$$

In the event that $A(t_{\max}) > \exp(-\lambda_r t_{\max})$, we substitute the function $A^*(t)$, which is computed by the requirement

$$(A10) \quad A^*(t_{\max}) = \exp(-\lambda_r t_{\max}).$$

In case of the condition of Eq. A9, the determination of the constant K is as follows:

$$(A11) \quad K = u / (e^{-\mu_1 T} - e^{-\mu_2 T}).$$

Otherwise

$$(A12) \quad K = e^{-\lambda_r t_{\max}} / (e^{-\mu_1 t_{\max}} - e^{-\mu_2 t_{\max}}).$$

SUMMARY OF THE COMPUTATIONAL PROCEDURE

Substitute Eq. A7 into Eq. A6 and solve for $r = r^*$. Then use Eq. A8 to calculate μ_1 and μ_2 . Finally, obtain K from Eq. A11 or Eq. A12, according to whether

$$u \cdot (e^{-\mu_1 t_{\max}} - e^{-\mu_2 t_{\max}}) / (e^{-\mu_1 T} - e^{-\mu_2 T}) \leq e^{-\lambda_r t_{\max}}$$

or not.

DISCUSSION

WATSON: (Question directed to Cristy following Killough's paper.) Did you assume all of the beta radiation from I-131 would be absorbed in the small thyroids (from 1-3 g)?

CRISTY: We haven't looked at that, Evelyn. We probably should, because that's getting fairly small.

THYROID CANCER IN THE MARSHALLESE: RELATIVE
RISK OF SHORT-LIVED INTERNAL EMITTERS
AND EXTERNAL RADIATION EXPOSURE

Lessard, E.T.,^a Brill, A.B.,^b and Adams, W.H.^b
Brookhaven National Laboratory
^aSafety & Environmental Protection Division
^bMedical Department
Upton, NY 11973

ABSTRACT

In a study of the comparative effects of internal versus external irradiation of the thyroid in young people, we determined that the dose from internal irradiation of the thyroid with short-lived internal emitters produced several times less thyroid cancer than did the same dose of radiation given externally. We determined this finding for a group of 85 Marshall Islands children, who were less than 10 years of age at the time of exposure and who were accidentally exposed to internal and external thyroid radiation at an average level of 1400 rad. The assumed risk coefficient for children, from external radiation alone, was derived from 1) values in The Effects on Populations of Exposure to Low Levels of Ionizing Radiation: 1980, National Academy Press, 2) values in Report of the Ad Hoc Working Group to Develop Radioepidemiological Tables, National Institutes of Health, and 3) values in Induction of Thyroid Cancer by Ionizing Radiation, National Council on Radiation Protection, Report 80. The risk from internal irradiation was computed from dose, health effect results which were reported in a recent BNL study, and an estimate of the external risk coefficient based on other studies. The external risk coefficient ranged between 2.5 and 4.9 cancers per million person-rad-years at risk, and thus, from our computations, the internal risk coefficient for the Marshallese children was estimated to range between 1.0 and 1.4 cancers per million person-rad-years at risk.

In contrast, for individuals more than 10 years of age at the time of exposure, the dose from internal irradiation of the thyroid with short-lived internal emitters produced several times more thyroid cancer than did the same dose of radiation given externally. The external risk coefficients for the older age groups were reported in the above literature to be in the range of 1.0 to 3.3 cancers per million person-rad-years-at risk. We computed internal risk coefficients of 3.3 to 8.1 cancers per million person-rad-years at risk for adolescent and adult groups. This higher sensitivity to cancer induction in the exposed adolescents and adults, is different from that seen in other exposed groups. The small number of cancers (9) in the exposed population and the influence of increased levels of TSH, nonuniform irradiation of the thyroid, and thyroid cell killing at high dose make it difficult to draw firm conclusions from these studies.

INTRODUCTION

The long-term health effects of external thyroid irradiation are known to include excess hypothyroidism, thyroid nodules, and thyroid cancer, and in this study we attempt to quantitate the relative risk of internal irradiation of the thyroid, for induction of thyroid cancer. The effects of external irradiation of child thyroids have been summarized in BEIR III (1) and by the NCRP (2). Internal irradiation of the thyroid from a mixture of radionuclides has occurred in children as a result of accidental exposure to fallout from nuclear weapons testing. Larger numbers of persons have received diagnostic and therapeutic doses from ^{131}I used in medical applications. Apart from the Marshallese, studies of internally irradiated human populations have not revealed an increased risk of thyroid malignancy (1,2). For example, studies of a group of children exposed to 90,000 person-rad in Utah have not revealed any excess thyroid cancer. The fallout in Utah contained ^{131}I and was reported to deliver up to several hundred rad of absorbed dose to thyroids of children who were less than 10 years of age (1,2). There are several studies which report no carcinogenic effect from large doses of ^{131}I (2). For example, Holm reported that persons irradiated with ^{131}I , with doses ranging between 6000 and 10,000 rad, exhibited no statistically significant increase in thyroid cancer (2). Studies of the children in the Marshall Islands conducted since 1954, on the other hand, do show a statistically significant increase in thyroid cancer in these irradiated subjects. Since the Marshall Islands' children were exposed simultaneously to external and internal irradiation, we have analyzed the data in an attempt to relate each type of exposure, internal versus external radiation, to the observed thyroid health effects. The mixture of radionuclides, contributing to internal dose in the Marshallese, included mostly short-lived ^{133}I and ^{135}I , and only 10-20% of the thyroid dose came from ^{131}I , thus the radiobiological considerations differ greatly in these various exposure circumstances.

Estimates of thyroid-absorbed dose were recently reassessed for people exposed to fallout in the Marshall Islands (3). The accidental exposure of people on March 1, 1954, occurred as a result of nuclear weapons testing. Over the years, several estimates of thyroid-absorbed dose were made (4,5). The earliest estimate of thyroid dose was reported by Cronkite (4) who indicated a population-averaged thyroid dose. A 1962 study by James (5) listed the most probable thyroid dose to girls who were 3 to 4 years old at the time of exposure. However, the James dose estimate was flawed by the incorrect association of ^{133}I and ^{135}I dose relative to the dose from ^{131}I . The most recent assessment of dose provided detailed information on the type of nuclides in fallout, the mode of intake, and the contributions from internal and external sources. The study of Lessard et al. (3) established greater absorbed dose to people based upon greater intake of the shorter-lived radio-iodines. The thyroid dose ranged from several hundred to five thousand rad, and the highest doses were assigned to young people. The revised dose estimates accounted for the radioactivity from all iodine isotopes.

Uncertainties with the dose estimates are associated with the amount of radioactivity measured in the urine of the exposed people, the intake of the short-lived radiotellurium and radioiodine isotopes and percent of thyroid uptake as determined from a physiologic model, errors in estimating the exact amount of each radioiodine isotope, the dose rate and pattern of energy distribution from this radioiodine mixture, and the shape and thickness of the thyroid.

Adams et al. (6) reported the medical status of the Marshallese accidentally exposed to fallout. Through March 1985 there were 35 adenomatous nodules, 5 adenomas, 9 papillary carcinomas, 1 atypical adenoma or follicular carcinoma, and 2 occult papillary carcinomas. A comparison group of equal

size exhibited 3 adenomatous nodules, 1 adenoma, 2 carcinomas, and 2 occult papillary carcinomas, one of which may have been a follicular carcinoma. Uncertainty was associated with diagnosis of follicular carcinoma, one in the exposed group and one in the comparison group, because of equally divided opinion among consulting pathologists. However, it was reasoned that both follicular carcinomas could be excluded from a risk coefficient estimate without seriously biasing the results. Diagnoses on five other individuals are pending. All five are from Utirik Atoll; three are in the <10-year old age group, and two are in the 10- to 18-year-old age group.

METHODS

Adams et al. (6) classified thyroid abnormalities following a scheme similar to that used by the World Health Organization and a committee of pathologists who had special expertise in diseases of the thyroid (7). The following nomenclature was used:

Adenomatous nodule: a focal proliferative lesion consisting of changes typical of adenomatous goiter; the lesions do not fulfill criteria of true neoplasms.

Adenoma: an encapsulated proliferative lesion with a uniform internal growth pattern and benign clinical course.

Occult papillary carcinoma: a small nonencapsulated sclerosing carcinoma, considered to be clinically benign even with positive regional lymph nodes.

Papillary carcinoma: larger, infiltrating carcinoma, usually containing both papillary and follicular components. The smallest lesion diagnosed as a papillary carcinoma, by the consultant pathologists, was 0.8 cm in diameter.

The recent computation of thyroid absorbed dose was performed for inhabitants of Rongelap, Utirik, and Ailingnae Atolls who were exposed to fallout on March 1, 1954. The amount of fallout activity taken into the body was estimated from the value of ^{131}I excreted in urine obtained from 64 persons who were at Rongelap. The other components of fallout taken into the body, particularly ^{133}I and ^{135}I , had to be inferred from studies on fallout composition. The authors of the reassessment study made dose estimates on the basis of actual BRAVO fallout composition. The intake pathway and the time post-detonation at which intake was likely to have occurred were obtained from interviews with the exposed people, and historical records and were factored into the new dose estimates. A detailed development of the dose reassessment was reported by Lessard et al. (3).

The radioepidemiological tables assembled by the Working Group (8) represented the best scientific judgment for the assignment of cancer risk from external radiation; thus we obtained one estimate of external exposure risk coefficient from this source. For persons less than 20 years of age, the Working Group adopted an average risk coefficient of 3.3 excess cancers per million person-rad-years at risk, and for persons 20 years or older they chose a value of 1.0 excess cancer per million person-rad-years at risk. A 10-year minimum latent period was chosen for thyroid cancer. The Working Group calculated thyroid cancer risk based on a linear dose-response function and maintained that the estimates of risk applied to external x and gamma irradiation, but not to the intake of radioisotopes of iodine.

The BEIR III (1) risk coefficients were based, in large part, on external

exposure of children less than 10 years of age, and upon data available through 1979. A central value of 4.0 cancers per million person-rad-years at risk was reported, but after review of their report, we modified the estimate to 4.9 cancers per million person-rad-years at risk. Our result, based on this modification, is discussed in the text and is noted in Table 7. The adjustment was based on weighting the risk coefficient from each study according to the number of excess cancers observed; that is, we gave more weight to cancer risk coefficients developed from studies reporting the greatest number of cancers. The BEIR risk coefficient was based on a minimum latent period of 10 years and on studies involving only external irradiation of the thyroid.

Risk coefficients for external and internal radiation were given in NCRP Report 80 (2), and these coefficients were estimated for a five-year latent period. Report 80 indicated the external risk coefficient applied to ^{135}I and ^{131}I intake, but not for ^{131}I exposure. The two short-lived isotopes of iodine were assumed to have the same effectiveness as x rays, because of the fairly uniform distribution of dose, and because of the comparatively higher dose rates (2). In our analyses, we used risk coefficients for external exposure computed for 5- and 10-year latent periods derived from the following reports. We used external risk coefficients from NCRP Report 80 because they were based on a five-year latent period, and these appear in the results section along with the coefficients developed by the Working Group, which were based on a ten-year latent period.

Risk coefficient estimates, made here, were based on the total external and internal thyroid dose, the total number of cancers, the risk value published for external irradiation of the thyroid, and the partitioning of external and internal dose as follows

$$A B + C D = (A + C)E, \quad (1)$$

where

A = the person-rad to all thyroids from radioisotopes of iodine,

B = the risk coefficient for internal exposure of the thyroid from radioisotopes of iodine, cancers per person-rad-years at risk,

C = the person-rad to all thyroids from external gamma radiation,

D = the risk coefficient from external exposure of the thyroid, for example, 1.0×10^{-6} cancers per person-rad-years at risk for adults, or in the case of children <10 years of age, 4.9×10^{-6} cancers per person-rad-years at risk, and

E = the risk coefficient determined from the observed health effects, the total thyroid dose, and the spontaneous rates of thyroid disease in the Marshall Islands subjects. The value of E was computed from Eq. (2-1) given in NCRP Report 80 (2).

Computations of B and E were for latent periods of both 5 and 10 years, since the length of latent period affects the years at risk and the risk coefficient. Years at risk are the period from the end of the latent period to the time cancer is observed in a subject. The value for years at risk strongly affected the computation of risk coefficients.

RESULTS

The data in the Appendix are the result of 31 years of medical and

radiological follow-up and, in the case of cancer diagnosis, of consensus opinion of pathologists. The Appendix is provided to allow others to perform different analyses of the data, recognizing that the data base is incomplete. Verifying the data over the last seven years has resulted in changes in age, identification number, assigned dose, and diagnosis. Several independent groups reported age at exposure, and the Adams et al. (6) version was used here. Different ages at exposure influences the age distribution of cancers, which in turn impacts strongly on the risk coefficient for a given age group.

The external thyroid dose was due to gamma exposure from the fallout cloud and fallout on the ground, and was taken as equal to the external whole-body dose reported by Lessard et al. (3), i.e., 190 rad at Rongelap, 110 rad at Ailingnae, and 11 rad at Utirik.

These external doses were estimated for a point which was 1 meter above the ground, thus some variation in external thyroid dose with a person's height may have occurred. To a first approximation external thyroid dose is inversely proportional to height above the ground. We derived this proportionality by neglecting photon attenuation and buildup, and by limiting the height above ground to between 0.5 and 1.5 meters. The impact on the risk coefficient estimates, relative to assuming that external thyroid dose was height dependent, was minimal, since the person-rad from external exposure was much less than the person-rad from internal exposure.

The data for the unexposed comparison groups are indicated in Table 1. In the age- and sex-matched comparison group used for this study, two papillary carcinomas have been observed. The summary is completed through 1983. To apply the data for risk coefficient determination, we modified the matched group results by the ratio of 31/29, which corrects for the difference in the number of reported observation years. The larger, less defined comparison population studied by Conard et al. (7) is shown in the first half of Table 1 to show that spontaneous cancer risk is not a strong function of group age for the Marshallese people. The comparison data indicated a spontaneous rate of 3×10^{-4} cancers per person-rad-years at risk. A lower spontaneous rate has been reported for the U.S. population, 1×10^{-4} per person per year (2). The Marshallese comparison data were used in the risk coefficient computations made here.

A summary of data in the Appendix appears in Tables 2 through 4. Note that out of 9 papillary cancers listed in the Appendix, only 2 were observed in males. This male to female ratio is similar to that reported in other studies (1,2,8). Tables 2 through 4 contain the input data which we used with Eq. (1). The data were grouped in the same manner as in other reports dealing with cancer and radiation exposure of the thyroid. The age groups were the same as that used by Conard et al. (7) and Adams et al. (6). To determine the average years post-exposure to onset of carcinoma, we set onset of carcinoma as the time of clinical observation of a thyroid nodule; thus, a latent period was assumed, but a period of several years could have elapsed before a nodule became large enough for detection by routine palpation by the physician. Therefore, the true latent period could be shorter than that assumed here. Tables 2 through 4 include the expected carcinomas, computed from the age- and sex-matched comparison group, and a summary of the total person-rad from man-made internal and external sources.

Table 1

Summary of Thyroid Abnormalities in the
Marshallese Unexposed Comparison Groups 1954-1983

<u>Group</u> <u>Age 1954</u>	<u>Number</u>	<u>Total Nodules</u>	<u>Carcinoma</u>	<u>Hypofunction</u>
<10	229	6	2	--
10-18	79	6	1	1
>18	292	25	2	1
Total	600	37	5	2

Age- and Sex-	{	227	5	2	--
Matched Group					
Followed					
Since 1954					

Table 2

Age Group <10 Data Summary

Number of Persons.....	85
Internal Exposure, Person-Rad.....	120,000
External Exposure, Person-Rad.....	5400
Number of Observed Carcinomas.....	3
Average Years Post-Exposure to Onset of Carcinoma.....	22
Assumed Latent Period, Years.....	5 and 10
Number of Expected Spontaneous Carcinomas.....	0.80

Table 3

Age Group 10 to 18 Data Summary

Number of Persons.....	32
Internal Exposure, Person-Rad.....	18,000
External Exposure, Person-Rad.....	2500
Number of Observed Carcinomas.....	3
Average Years Post-Exposure to Onset of Carcinoma.....	28
Assumed Latent Period, Years.....	5 and 10
Number of Expected Spontaneous Carcinomas.....	0.30

Table 4

Age Group >18 Data Summary

Number of Persons.....	120
Internal Exposure, Person-Rad.....	48,000
External Exposure, Person-Rad.....	8,000
Number of Observed Carcinomas.....	3
Average Years Post-Exposure to Onset of Carcinoma.....	16
Assumed Latent Period, Years.....	5 and 10
Number of Expected Spontaneous Carcinomas.....	1.1

Table 5

Risk Coefficients^a for Marshall Islanders, 10-Year Latent Period

Group <u>Age 1954</u>	Number	Excess		Years	
		Thyroid <u>Cancers</u>	Total <u>Person-Rad</u>	at <u>Risk</u>	Risk <u>Coefficient</u>
<10	85	2.2	120,000	12.2	1.5×10^{-6}
10-18	32	2.7	21,000	17.7	7.4×10^{-6}
>18	120	1.9	56,000	6.2	5.4×10^{-6}
Total	237	6.8	200,000	11.3	3.0×10^{-6}

^aThyroid cancers per person-rad-years at risk, based on thyroid dose from internal plus external sources.

Table 6

Risk Coefficients^a for Marshall Islanders, 5-Year Latent Period

Group	Age 1954	Number	Excess		Years	
			Thyroid Cancers	Total Person-Rad	at Risk	Risk Coefficient
<10		85	2.2	120,000	17.2	1.1×10^{-6}
10-18		32	2.7	21,000	22.7	5.8×10^{-6}
>18		120	1.9	56,000	11.2	3.0×10^{-6}
Total		237	6.8	200,000	14.9	2.3×10^{-6}

^aThyroid cancers per person-rad-years at risk, based on thyroid dose from internal plus external sources.

Table 7

Estimated Risk Coefficient^a for Internal and External Exposure

Group	Age 1954	Number	10-Year Latent Period		5-Year Latent Period	
			External	Internal	External	Internal
			Risk	Risk	Risk	Risk
<10		85	3.3×10^{-6}	1.4×10^{-6} (b)	2.5×10^{-6}	1.0×10^{-6}
10-18		32	3.3×10^{-6}	8.0×10^{-6}	2.5×10^{-6}	6.3×10^{-6}
>18		120	1.0×10^{-6}	6.1×10^{-6}	1.3×10^{-6}	3.3×10^{-6}
Total		237	2.1×10^{-6}	4.7×10^{-6}	1.9×10^{-6}	2.9×10^{-6}

^aThyroid cancers per person-rad-years at risk.

bA value of 1.3×10^{-6} results when 4.9×10^{-6} is used for the external risk coefficient.

The risk coefficient, E, for different age groups, computed from total dose resulting from internal plus external exposure for Marshall Islanders, ranged from 1.5×10^{-6} to 7.4×10^{-6} per person-rad-years at risk, assuming a 10-year latent period, and 1.1×10^{-6} to 5.8×10^{-6} , assuming a 5-year latent period. These data are indicated in Tables 5 and 6, respectively. The total risk coefficient, E, was used in Eq. (1) to determine the internal risk coefficient, B. For external risk coefficients and 10-year latent period, we chose 3.3×10^{-6} for age <20 and 1.0×10^{-6} for age >20 based on the Working Group study (8); for 5-year latent period we chose 2.5×10^{-6} for age <18 and 1.3×10^{-6} for age >18, based on NCRP Report 80 (2). The results for internal risk coefficients are in Table 7. Finally, as we explained in the Methods, we chose a special value for the <10-year age group, since it was based on a large group of children exposed to x rays (1). This value was 4.9×10^{-6} cancers per person-rad-years at risk, and the estimate for the internal risk coefficient was 1.3×10^{-6} , virtually the same as the value given in Table 7 for the 10-year latent period.

A tabulation of risk coefficient versus internal thyroid dose is given in Table 8. These internal dose groupings resulted in little variation in external dose as a function of age. These groupings were made to examine the effect of dose on the value for internal risk coefficient.

Table 8

Average Dose Versus Internal and
External Risk Coefficients, 10-Year Latent Period

Group	Average		Average			Total
	Internal Thyroid Dose, rad	Internal Risk Coefficient ^a	External Thyroid Dose, rad	External Risk Coefficient ^b	Total Risk Coefficient ^a	
Age 1954						
<10	1400	1.4×10^{-6}	63	3.3×10^{-6}	1.5×10^{-6}	
10-18	560	8.0×10^{-6}	78	3.3×10^{-6}	7.4×10^{-6}	
>18	400	6.1×10^{-6}	66	1.0×10^{-6}	5.4×10^{-6}	

^aThis study.

^bReference 8.

A sensitivity analysis, of the parameters in Eq. (1), shows that the value for the total risk coefficient, E, impacts greatly on the estimate of the internal risk coefficient, B, in this specific Marshall Islands study. This is because of the wide difference between internal thyroid dose, A, and external thyroid dose, C. Thus, our estimate of internal risk coefficient depends largely on the observed incidence of thyroid cancer because the total risk coefficient, E, is very sensitive to the small number of spontaneous and excess thyroid cancers observed.

DISCUSSION/CONCLUSION

Interest in the relative risk of ^{131}I taken internally and external radiation dose to the thyroid relates to radiation protection and medical care issues. Unfortunately for those interested in obtaining information on this important issue, the complex mixture of radionuclides taken up by the Marshallese precludes such an analysis. The results obtained for these studies are specific to the case where the thyroid dose was due to a mixture of short-lived radioisotopes of iodine, some of which were produced by the decay of tellurium within the body. Current information on animal and human data was summarized recently in NCRP Report 80 (2). The Committee concluded that ^{131}I was less than one third as effective for thyroid cancer induction as external radiation. This can not be compared directly to the results of the present study because of the small amount of ^{131}I in the Marshallese exposures. In most animal studies, which used rodents, high TSH levels were found to be necessary co-factors for thyroid cancer induction. Thus, goitrogen plus ^{131}I exposures were needed to induce thyroid cancer, except in several studies using Long-Evans rats which behaved differently from all other strains studied. Results of ^{131}I treatment of children for hyperthyroidism were reported in two large studies. In reviewing results of treatment of nine children, Sheline et al. (9) found that all of them subsequently developed thyroid nodules and one was diagnosed as having of thyroid cancer, about which there was disagreement regarding pathology. None of those children received thyroid replacement therapy after ^{131}I treatment, and all presumably developed high endogenous TSH levels. In Los Angeles, at a later date, 73 children were treated with approximately the same ^{131}I dose, all were placed on thyroid replacement, and none developed thyroid nodules (10). Thus the relative risk of thyroid dose from internal emitters compared to external radiation for Marshall Islanders may be influenced by a high TSH co-factor, since thyroid replacement therapy began 11 years after exposure. Replacement therapy was recommended only for the high-dose group which, at that time, was thought to be the people at Rongelap.

Also no increased incidence of thyroid cancer was seen in large numbers of human subjects exposed to similar or higher doses of ^{131}I in the treatment of thyrotoxicosis (11), or in children given ^{131}I in lower diagnostic doses (12).

Hypothyroidism is a nonstochastic effect of ionizing radiation exposure, with estimated threshold for induction of 2000 rad to the thyroid (1). In the Marshallese children, whose thyroids were exposed to doses in the several thousand rad range, hypothyroidism and increased TSH levels certainly existed in the early years following exposure. In later years, uneven acceptance of thyroid supplementation by children may have led to persistent increased TSH levels. The combination of high TSH and high internal and external radiation doses may account for the unusually high incidence of nodules in this population, and in the unusual age distribution of sensitivity.

The numbers of individuals in the study are small, and statistical segregation of the interacting factors is not possible. Thus, it will be difficult to draw precise conclusions from this study with respect to apportionment of risk between internal and external doses. Further, the differences between the radiological characteristics of ^{131}I , ^{133}I , and ^{135}I and the larger doses from ^{133}I and ^{135}I make it difficult to assess the relative risk of ^{131}I and external radiation in this circumstance. A simple statistical model was used (3) to indicate the one sigma confidence interval. This confidence interval is indicated in the following paragraph in parentheses. The standard deviation of the risk estimate, E, was 1.5 times the average value for the risk estimate, and development of this standard deviation was given by Lessard et al. (3).

The results support the notion that external risk coefficients are different from internal risk coefficients following exposure to a mixed radiation field. The total risk coefficients [3.0×10^{-6} ($\pm 4.5 \times 10^{-6}$) cancers per person-rad-year at risk, 10-year latent period, and 2.3×10^{-6} ($\pm 3.5 \times 10^{-6}$) cancers per person-rad-year at risk, 5-year latent period] are similar to the literature values (1,2) for this age distribution and for external exposure. The literature values are 2.1×10^{-6} for a 10-year latent period and 1.9×10^{-6} for a 5-year latent period. However, if the risk is examined as a function of age or as a function of dose, differences are encountered. For example, the ratio of the risk coefficient for external exposure to the risk coefficient for internal exposure, in the <10 year age group, is 2.5 (0.38 to 4.6). In the 10- to 18-year age group, this risk coefficient ratio is 0.40 (0.22 to 2.6).

Small group size, in this study, and the uncertainties reported in studies on medical and fallout exposures make it difficult to establish relative risks of thyroid cancer from internal and external radiation doses to the thyroid. The possible synergistic effect of internal and external exposures and the modifying factors such as high TSH levels and nonuniform irradiation of thyroid cells complicate the biological interpretation of the risk. In this study, different age groups correspond to different dose levels, and very high dose to the thyroid may be a significant modifying factor. Because of the high interest in evaluating human sensitivity to ^{131}I , continued efforts are needed to obtain data and to conduct analyses that will establish better estimates of risk coefficients than are now available. It is not likely that data for the Marshallese exposures will contribute to the answer to that important question.

ACKNOWLEDGMENT

The authors fully appreciate the efforts of John Baum, Associate Head for Research in the Safety and Environmental Protection Division, for his review of this manuscript.

This work was performed by members of Brookhaven National Laboratory, Associated Universities, Incorporated, under contract No. DE-AC02-76CH00016 with the United States Department of Energy, and under contract No. Y01-CP-40503 with the National Cancer Institute.

REFERENCES

1. Committee on the Biological Effects of Ionizing Radiation, The Effects on Populations of Exposure to Low Levels of Ionizing Radiation: 1980, National Research Council Report, National Academy Press, Washington, DC, 1980.
2. Recommendations of the National Council on Radiation Protection and Measurements, Induction of Thyroid Cancer by Ionizing Radiation, NCRP Report No.80, Bethesda, MD, 1985.
3. Lessard, E.T., R.P. Miltenberger, R.A. Conard, S.V. Musolino, J.R. Naidu, A. Moorthy, and C.J. Schopfer, Thyroid Absorbed Dose for People at Rongelap, Utirik and Sifo on March 1, 1954, Brookhaven National Laboratory Report, Upton, NY, BNL 51882, 1985.

4. Cronkite, E.P., V.P. Bond, and C.L. Dunham, A Report on the Marshallese and Americans Accidentally Exposed to Radiation from Fallout and a Discussion of Radiation Injury in the Human Being, in: Some Effects of Ionizing Radiation on Human Beings, U.S. Atomic Energy Commission, Washington, DC, USAEC-TID 5358, 1956.
5. James, R.A., Estimate of Radiation Dose to Thyroids of Rongelap Children Following the BRAVO Event, Lawrence Radiation Laboratory Report, Livermore, CA, UCRL-12273, 1964.
6. Adams, W.H., J.A. Harper, R.S. Rittmaster, P.M. Heotis, and W.A. Scott, Medical Status of the Marshallese Accidentally Exposed to BRAVO Fallout Radiation: January 1980 Through December 1982, Brookhaven National Laboratory Report, Upton, NY, BNL 51761, 1982.
7. Conard, R.A. et al. (9 co-authors), Review of Medical Findings in a Marshallese Population Twenty-Six Years After Accidental Exposure to Radioactive Fallout, Brookhaven National Laboratory Report, Upton, NY, BNL 51261, 1980.
8. Ad Hoc Working Group to Develop Radioepidemiological Tables, Report of the National Institutes of Health, January 4, 1985. Office of the Director, NIH Publication No. 85-2748. U.S. Dept. HHS, PHS, NIH.
9. Sheline, G.E. et al., "Thyroid Nodules Occurring Late After Treatment of Thyrotoxicosis with Radioiodine," J. Clin Endoc. & Metab. 22, 8, 1962.
10. Starr, P., "Later Results of I-131 Treatment of Hypothyroidism in 73 Children and Adolescents: 1967 Follow-up," J. Nucl. Med. 10, 586-590, 1969.
11. Dobyns, B.M. et al., "Malignant and Benign Neoplasms of the Thyroid in Patients Treated for Hypothyroidism: A Report of the Cooperative Thyro-toxicosis Follow-up Study," J. Clin, End. & Metab. 38, 976-998, 1974.
12. Holm, L.E. et al., "Incidence of Malignant Thyroid Tumors in Humans After Exposure to Diagnostic Doses of I-131," J. National Cancer Institute, 64, 1055-1059, 1980.
13. Prentice, R.L. et at., Radiation Exposure and Thyroid Cancer Incidence among Hiroshima and Nagasaki Residents, National Cancer Institute Monograph 62, 207-212, 1982.
14. Ishimary, T. et al., Incidence of Thyroid Cancer Among Atomic Bomb Survivors and Controls Hiroshima and Nagasaki, 1958-79: Relationship to Radiation Absorbed Dose in the Thyroid, RERF Technical Report 1984.

DISCUSSION

MITCHELL: A few years ago Dale Sandler, a graduate student at Hopkins, did her thesis on radiation effects of adenoidal radiation for patients who had been treated with radium. The thyroid doses were quite small, but she found an increase in both hypo-and hyperthyroidism. Although doses in the thyroid were extremely small, the pituitary doses were quite high. I was wondering whether you looked at the pituitary dose in this population; and, if so, whether some of the effects, particularly those in the Marshallese individuals, might not be also modified by the pituitary irradiation?

BRILL: In studies on the Marshallese, high levels of TSH were found and those led to the institution of replacement therapy with thyroid hormone. If these medical recommendations had been adhered to, there would possibly have been fewer nodules and thyroid cancer in the Marshallese than have been experienced. In any case, decreased pituitary function has not been observed. I don't know what dose the pituitary receives from treatment of adenoidal hyperplasia with Ra-226 or was received from the exposures to the Marshallese, but I'll attempt to obtain calculations for the latter group and include a statement on those doses in future publications.

CLOUTIER: The number of person-years at risk in the Marshall Islanders is quite small and the number of person-years at risk for the Utah children is quite large. How does the Marshall Island data compare with the Utah data?

BRILL: The number of exposed children in the South Utah study was 1378, the follow-up averaged 14 years, and the mean thyroid dose estimated by Rallison was 18 rads. This computes to 3.5×10^5 person-rad-years, in contrast to the 2.3×10^6 person-rad-years represented in the 237 exposed Marshallese.

FUEGER: Would you happen to know the incidences of nodules and/or cancer of the thyroid gland in an iodine deficient population? The data presented by you are reminiscent of thyroid degeneration in areas of endemic goiter, suggesting that perhaps the internal radiation absorbed dose from the iodine radionuclides in fallout caused a diffuse diminution of thyroid cells. The residual thyroid tissue might be subjected to increased metabolic burden similar to the situation in an iodine deficient population.

BRILL: That is an interesting observation and may be quite appropriate. In the peripheral regions, for example in the Kyushu populations, where they have a large quantity of fish in their diets, the same kind of observation has been made and recorded in the literature. The incidence of thyroid nodules and thyroid cancer is higher in iodine-deficient than in iodine-sufficient areas. This is believed to be due to the high levels of TSH stimulating the thyroid glands in the iodine deficient individuals. In many strains of rats, thyroid cancer can not be induced by I-131 alone, but the addition of antithyroid agents (goitrogens) which increase TSH levels results in significantly increased thyroid cancer rates. The presence of elevated TSH levels has been demonstrated in exposed Marshallese not receiving thyroid replacement therapy, and this may contribute to their high thyroid cancer rates. It should be reiterated that the Marshallese received less than 15% of their internal dose from I-131. Hence, the carcinogenicity of I-131 versus the other high-energy short-lived nuclides responsible for the major part of the dose commitment can not be established from risk studies.

MARCUSE: Was inhomogeneous uptake of radioiodine in the thyroid gland taken into account when you looked into the expected radiation effects? During a period of one physical half-life of I-131 less than one third of the thyroid

tissue may function. Autoradiographic studies have shown that after one intake the dose rate will be in clusters where the dose may be three times the average over the whole gland.

BRILL: No, the calculation of dose for the hot spot as opposed to the average dose is very difficult. That's one of the uncertainties in population dosimetry. Another is that the radiological hazard of a mixed radiation field is not entirely clear. I know that Eric Pochin and his colleagues have speculated for many years on the leukemias that resulted from treatment of thyroid cancer with curie doses of iodine. The question they have entertained is whether other materials in the radioactive iodine they were using were more carcinogenic than the iodine itself. That kind of question would remain open in a population like this that has such a diverse kind of exposure.

APPENDIX

Tabulation of Thyroid Dose
and Thyroid Health Effects

Rongelap and Ailingnae Population

ID Number	Sex	Age in 1954	Comment	Diagnosis	Internal Thyroid Dose, Rad	Years Post Exposure
*1	F	52	Died 1985		290	
2	M	1		Adenomatous Nodule	5000	11
3	M	1		Myxedema	5000	
4	M	36			1000	
5	M	1		Myxedema	5000	
*6	M	1			1300	
7	M	34			1000	
*8	F	5		Adenomatous Nodule	740	18.5
9	M	20			1000	
10	M	22			1000	
11	M	48			1000	
12	F	16			1200	
13	F	59	Died 1966		1100	
14	F	3			3500	
15	F	5	Surgery(2x)	Adenomatous Nodule	2800	22;32
*16	M	37			280	
17	F	1		Adenomatous Nodule	5000	10.5
18	F	19		Papillary Carcinoma	1100	15.5
19	M	3		Adenomatous Nodule	3500	14.5
20	M	5		Adenomatous Nodule	2800	11
21	F	1		Adenomatous Nodule	5000	10.5
22	F	15			1300	
23	M	2		Adenomatous Nodule	4000	14.5
24	F	11			1700	
25	M	44	Died 1956		1000	
26	M	13	Died 1962		1500	
27	M	33			1000	
*28	F	69	Died 1965		290	
*29	M	65	Died 1966		280	
30	F	52	Died 1962		1100	
*31	M	31	Died 1958		280	
32	M	2			4000	
33	F	1		Adenomatous Nodule	5000	12
34	F	43			1100	
35	M	11			1700	
36	M	5		Adenomatous Nodule	2800	15.5
37	M	18			1000	
38	M	75	Died 1957		1000	
39	F	13			1500	
40	M	31			1000	
*41	M	42			280	
42	F	1		Adenomatous Nodule	5000	12
*43	F	67	Died 1964		290	

**Tabulation of Thyroid Dose
and Thyroid Health Effects
(Continued)**

Rongelap and Ailingnae Population

ID Number	Sex	Age in 1954	Comment	Diagnosis	Internal Thyroid Dose, Rad	Years Post Exposure
*44	M	2				
*45	F	30				
46	M	76	Died 1962	Adenomatous Nodule	290	19
47	M	6			1000	
*48	F	4			2400	
49	F	13			820	
*50	M	34	Died 1971		1500	
*51	F	23	Died 1982	Follicular Adenoma	280	20
52	F	46	Died 1963		290	
*53	F	5		Adenomatous Nodule with Occult Papillary Carcinoma	1100	27
54	M	1	Died 1972	Adenomatous Nodule	740	
55	M	76	Died 1968		5000	14.5
56	F	67	Died 1962		1000	
57	F	98	Died 1963		1100	
58	F	59	Died 1977		1100	
*59	F	44	Died 1968	Adenomatous Nodule	1100	12
60	F	56	Died 1972		290	
61	F	6		Adenomatous Nodule	1100	
62	F	55	Died 1959		2400	12
63	F	34			1100	
64	F	28		Papillary Carcinoma	1100	11
65	F	1		Adenomatous Nodule	5000	
66	F	29		Adenomatous Nodule	1100	12
67	F	12		Papillary Carcinoma	1100	25.5
68	M	44	Died 1974		1600	
69	F	2		Adenomatous Nodule	1000	31
*70	F	5			4000	10.5
71	F	26			740	
72	M	5		Papillary Carcinoma	1100	
73	M	16			2800	15.5
74	F	14		Papillary Carcinoma	1200	
75	F	10		Adenomatous Nodule	1400	22
				with Follicular Adenoma	1800	18.5
76	M	9			2000	
77	M	24			1000	
78	F	35			1100	
79	M	37			1000	
80	M	44	Died 1983		1000	
*81	F	6			640	
82	M	49	Died 1980		1000	
83	M	In Utero		Adenomatous Nodule		20
*84	M	In Utero				

Tabulation of Thyroid Dose
and Thyroid Health Effects
(Continued)

Rongelap and Ailingnae Population

ID Number	Sex	Age in 1954	Comment	Diagnosis	Internal Thyroid Dose, Rad	Years Post Exposure
-----------	-----	-------------	---------	-----------	----------------------------	---------------------

85	M	In Utero		Adenomatous Nodule		25.5
86	F	In Utero				

*Ailingnae Exposed

Utirik Population

2101	M	48	Died 1968		150	
2102	M	3			480	
2103	M	43			150	
2104	F	22			160	
2105	M	45			150	
2106	M	4			430	
2107	F	25			160	
2108	M	11			250	
2109	F	45	Died 1978		160	
2110	M	47			150	
2111	F	6			340	
2112	M	53	Died 1968		150	
2113	F	3			480	
2114	M	40			150	
2115	M	1			670	
2116	F	21	Died 1960		160	
2117	F	24			160	
2119	F	18			160	
2120	M	4	Died 1982		430	
2121	M	57	Died 1965		150	
2122	M	82	Died 1959		150	
2123	M	15			200	
2124	M	2			550	
2125	M	37			150	
2126	F	5			390	
2127	M	68	Died 1959		150	
2128	F	8	Died 1985		310	
2129	F	17			160	
2130	F	3			480	
2131	F	29	Died		160	
2132	F	1		Adenomatous Nodule	670	27
2134	F	1			670	
2135	M	31	Died 1977		150	

Tabulation of Thyroid Dose
and Thyroid Health Effects
(Continued)

Utirik Population

ID Number	Sex	Age in 1954	Comment	Diagnosis	Internal Thyroid Dose, Rad	Years Post Exposure
2136	M	3			480	
2137	M	14			220	
2138	F	4			430	
2139	F	44			160	
2140	F	45			160	
2141	F	53	Died 1968		160	
2142	M	5			390	
2143	M	3			480	
2144	M	7			330	
2145	M	34			150	
2146	F	36	Died 1980		160	
2147	F	5		Adenomatous Nodule	390	25.5
2148	M	44			150	
2149	F	9		Diagnosis Pending	300	30
2150	M	10			270	
2150	M	12		Follicular Adenoma	240	22
2151	F	4			430	
2152	M	17		Papillary Carcinoma	150	30
2153	M	1			670	
2154	F	40	Died 1965		160	
2155	M	1			670	
2156	M	8			310	
2157	M	26	Died 1984		150	
2158	F	28			160	
2159	F	3			480	
2160	F	4		Papillary Carcinoma	430	21
2161	F	29	Died 1981		160	
2162	F	32			160	
2163	M	65	Died 1964-65?		150	
2164	F	7	Died 1984		330	
2165	M	11			250	
2166	M	38			150	
2167	M	14			220	
2168	M	18	Died 1984	Diagnosis Pending	150	30
2169	M	62	Died 1978		150	
2170	M	41	Died 1959		150	
2171	F	2		Papillary Carcinoma	550	30
2172	F	12		Diagnosis Pending	240	30
2174	M	1			670	
2175	M	57	Died 1970		150	
2176	M	10			270	
2177	M	5	Died 1961		390	
2178	M	19	Died 1972		150	
2179	M	2			550	
2180	M	70	Died 1960		150	

Tabulation of Thyroid Dose
and Thyroid Health Effects
(Continued)

Utirik Population

ID Number	Sex	Age in 1954	Comment	Diagnosis	Internal Thyroid Dose, Rad	Years Post Exposure
2181	M	65	Died 1967		150	
2182	F	52			160	
2183	M	56	Died 1965		150	
2184	M	60	Died 1961		150	
2185	M	32	Died 1984		150	
2187	F	56	Died 1959		160	
2188	M	3			480	
2189	F	26			160	
2190	F	75	Died 1964-65?		160	
2191	F	75	Died 1969		160	
2192	F	74	Died 1964-65?		160	
2193	F	31		Adenomatous Nodule	160	25
2194	F	35	Died 1984	Papillary Carcinoma	160	22
2195	F	24		Adenomatous Nodule	160	25
2196	F	38		Adenomatous Nodule	160	26.5
2197	F	3		Diagnosis Pending	480	31
2198	F	58	Died 1979		160	
2199	F	42	Died 1961		160	
2200	F	43			160	
2201	F	50	Died 1974		160	
2202	F	59	Died 1967		160	
2203	F	62	Died 1963		160	
2204	F	60	Died 1965		160	
2205	M	29			150	
2206	M	32			150	
2207	M	5			390	
2208	F	37		Adenomatous Nodule	160	19
2209	F	5			390	
2210	F	1			670	
2212	F	34		Adenomatous Nodules	160	19
2213	F	1			670	
2214	M	65	Died 1969		150	
2215	M	1		Adenomatous Nodule with Occult Papillary Carcinoma	670	25.5
2216	F	33			160	
2217	F	22			160	
2218	F	1			670	
2219	F	54	Died 1957		160	
2220	F	25			160	
2221	F	52		Adenomatous Nodules	160	19
2222	F	60	Died 1957		160	
2223	F	66	Died 1967		160	
2224	F	31			160	
2225	F	6		Diagnosis Pending	340	30

Tabulation of Thyroid Dose
and Thyroid Health Effects
(Continued)

Utirik Population

ID Number	Sex	Age in 1954	Comment	Diagnosis	Internal Thyroid Dose, Rad	Years Post Exposure
2226	F	1			670	
2227	F	4			430	
2228	F	8			310	
2229	F	18		Follicular Carcinoma Possible Atypical Adenoma	160	15.5
2230	F	13			230	
2231	F	1			670	
2232	M	1			670	
2234	M	12			240	
2235	M	7			330	
2236	M	11		Follicular Adenoma	260	24
2237	M	7			330	
2238	F	54	Died 1965		160	
2239	F	3		Adenomatous Nodule	480	27
2240	M	33	Died 1977		150	
2241	F	28	Died 1981		150	
2242	M	1			670	
2243	M	46	Died 1958		150	
2245	M	1			670	
2246	F	8	Died 1971		160	
2247	F	8			310	
2248	F	15		Occult Papillary Carcinoma	200	29
2249	F	15			200	
2250	M	10			270	
2251	F	4			430	
2252	M	39	Died 1972		150	
2253	M	45	Died 1965		150	
2254	F	5			390	
2255	F	1			670	
2256	F	5			390	
2257	M	7			330	
2258	M	47	Died 1971		150	
2259	F	21	Died 1968		160	
2260	F	1			670	
2261	M	26			150	
2268	M	In Utero				
2269	M	In Utero				
2271	M	In Utero				
2273	M	In Utero				
2274	M	In Utero				
2276	M	In Utero				
2277	F	In Utero				
2548	M	In Utero				

RADIOLABELED BLOOD CELLS: RADIATION DOSIMETRY AND SIGNIFICANCE

Mathew L. Thakur, Ph.D.
Thomas Jefferson University
Department of Radiation Therapy
and Nuclear Medicine
11th and Walnut Streets
Philadelphia, Pennsylvania 19107

ABSTRACT

Over the past few years blood cells labeled with In-111 have become increasingly useful in clinical diagnosis and biomedical research. Indium-111 by the virtue of its physical characteristics and ability to bind to cell cytoplasmic components, provides an excellent cell tracer and thereby, allows investigators to monitor *in vivo* cell distribution by external imaging and help determine a course of regimen in treating life threatening diseases.

Due to natural phenomena such as margination, blood pool, and reticuloendothelial cell activity, in the normal state, depending upon the cell type and the quality of cell preparations, 30%-50% of the administered radioactivity is immediately distributed in the liver, spleen and bone marrow.

Over a period of time the radioactivity in these organs slightly increases and decays with a physical half-life of In-111. The resulting radiation dose to these organs ranges between 1-25 rads/mCi In-111 administered. Radiation dose is minimized by the high quality of preparations and administering no more than 500 μ Ci In-111 to a patient weighing 70 kg or more. Generally, the benefits outweigh the potential risk involved.

Indium-111 also emits Auger electrons ranging in energy 0.6 to 25.4 keV and having a short tissue penetration range between 0.025 to 12.55 μ m. One mCi of In-111 contains 1.3×10^{13} atoms. Radiation dose resulting from a complete decay of a single In-111 atom to a human neutrophil or lymphocyte is 0.135 rad and to those of platelets is 14.5 rad. Although 10^8 neutrophils labeled with 500 μ Ci of In-111 have shown no adverse effect of In-111 radiation, chromosomal aberrations in labeled lymphocytes have been observed, and overdevelopment of open canalicular spaces and aggregated dense granules have been reported in 10^8 platelets labeled with 200 μ Ci of In-111.

We have developed a new In-111 labeling technique which preserves platelet ultrastructure and shown that human lymphocytes labeled with In-111 in mixed leukocytes preparations a) are only 0.003% of the total-body lymphocytes population and b) are killed. The consequence if any may be considered insignificant, particularly because 5.6% metaphases from normal men and 6.5% metaphases from normal women in the United States have at least one chromosome aberration. Calculations have shown that the risk of fatal hematological malignancy, over a 30 year period, in recipients of 100 million lymphocytes labeled with 100 μ Ci In-111 is 1/million patients studied. This risk is less than 0.025% of the 1981 spontaneous cancer patient rate in the country.

INTRODUCTION

Blood cells labeled with Tc-99m or In-111 have become increasingly popular for use in clinical diagnosis and experimental medicine. Technetium-99m has been long used in such applications. Indium-111 is a relatively new tracer for blood cells and has been a subject of extensive investigations and discussions in order to assess the potential risk and derived benefits to the recipient. In a normal situation blood cells are not eliminated through excretion, generally circulate in the body for a long period of time, and are eventually destroyed largely in organs rich in reticuloendothelial cells. Although the fate of In-111 following cell destruction is not fully understood, measurements for a limited period of time have shown that the radioactivity does not wash out from these organs and is eliminated predominantly by decay with the physical half-life of In-111.

The dosimetry of In-111 becomes complex by several factors. The radioactivity in labeled cells binds to cytoplasmic components of cells and thereby remains in association with the cells and does not elute from them.

Indium-111 has a half-life of 67 hrs. and decays with the emission of two gamma rays (173 keV, 84% and 247 keV, 94%), conversion electrons, cadmium x-rays, and Auger electrons.

In-111 solutions used for labeling blood cells also contain In-114m as an impurity. This arises from the production of In-114m + In-114 by the photon bombardment of cadmium [^{114}Cd (p,n)]. The quantity of In-114m varies with respect to the quantity of In-111 produced [^{112}Cd (p,2n)] and depends upon the length of bombardment as well as the time elapsed between the production and the use of In-111. Indium-114m has a half-life of 50 days and decays by isomeric transition (96.5%) and electron capture (3.5%).

The gamma, beta and x-rays will highly contribute to the radiation dose to the total body and to the critical organs such as the liver and spleen in which a higher proportion of cells are accumulated. Since these radiations have path ranges longer than the blood cell diameter, the radiation will not affect individual blood cells circulating in the blood stream. However, labeled cells will receive radiation dose from short range Auger electrons originating from the decay of the In-111 atoms situated within the cell. Depending upon the diameter and the volume of the cell, the radiation dose received by the different cell types will be different for the same number of In-111 atoms incorporated into each cell. Furthermore, one type of cell will be more susceptible to the radiation damage than another.

Since each type of blood cell has different in vivo distribution and survival time, the radiation dose to the whole body and to the critical organs will vary for the types of cells used. In this article we will focus on In-111 labeled blood cells, discuss radiation dose to a recipient from different cells, and estimate radiation dose to the cells and highlight its significance.

INDIUM-111 DOSIMETRY (ORGAN)

LEUKOCYTES

The most useful routine clinical application of In-111 labeled leukocytes has been in the detection of inflammatory diseases by scintillation scanning.

In this application, a mixed population of white cells, leukocytes, labeled with 500 μ Ci In-111 are most commonly used. The radiation dosimetry will depend upon the in vivo distribution of the cells, which will be governed by many factors such as a) the type of cell preparations; in that damaged leukocytes will be largely taken up by the liver (1). Damaged and agglutinated cells are sequestered by the lungs in larger quantities and are retained for a longer period of time than normal. b) The in vivo cell distribution is also expected to be different in health and disease and c) the accuracy of in vivo quantification which may be affected by attenuation of In-111 gamma rays.

Distribution of In-111 leukocytes in patients with normal and abnormal scans and two splenectomized human subjects was studied by Thakur et al and Goodwin et al respectively (1,2). These results together with the estimated absorbed radiation dose to the critical organs are tabulated in Table 1.

Table-1

Tissue Distribution 24 Hours Following I.V. Administration of In-111 Leukocyte and Estimated Absorbed Radiation Dose

Organ	Normal Scan ^a % rad/500 μ Ci		Abnormal Scan ^{a,b} % rad/500 μ Ci		Spln.Patient ^a % rad/500 μ Ci	
Liver	19 <u>±</u> 5	1.32	18 <u>±</u> 5	1.26	26 <u>±</u> 2	1.74
			21 <u>±</u> 3	2.5 ^b		
Spleen	19 <u>±</u> 6	8.51	21 <u>±</u> 10	9.38	0.7 <u>±</u> .05	0
			13 <u>±</u> 5 ^b	9 ^b		
Whole Body	62	2.3	61	2.3	78.3	2.7
				0.25 ^b		

a - Ref (2)

b - Ref (1)

The table indicates that the target organs are the liver and the spleen and that in splenectomized patients, the liver and whole-body dose is increased.

PLATELETS

Relatively fewer numbers of human studies determining in vivo platelet distribution have been performed. There are, however, some fundamental differences between platelet and leukocyte distribution; in that i) platelets have a high blood concentration due to the fact that they have 8-10 days life span compared to that of 8-10 hr. $t_{1/2}$ for neutrophils; ii) Unlike leukocytes, platelets are accumulated in much higher proportion in the spleen than in the liver (Table 2); and iii) the bone marrow uptake of platelets in a normal patient is much less than that of leukocytes. In patients with idiopathic thrombocytopenic purpura (ITP), platelets may be taken up by the spleen in much higher quantities and may have shorter survival period than in normals. Similarly, in patients with

splenomegaly, an increased quantity of platelets will be accumulated in the spleen. All such abnormalities will alter the radiation dosimetry. In hematologically normal patients, Goodwin et al (3) have reported the following distribution of platelets and estimated the radiation dose as given in Table-2.

Table 2

Distribution of In-111 Platelets in Normal Adult Humans at 24 Hour Post Injection

	% Radioactivity	rad/500 μ Ci
Liver	8.5 + 0.05	3.15
Spleen	23.5 + 4.5	8.6
Whole Body	68 + 4	0.32

LYMPHOCYTES

Lymphocytes are most heterogeneous. Their life span varies from days to years. Given intravenously, cells enter the lymphatic system and appear again in circulation. In patients with Hodgkin's disease much higher percentages of lymphocytes are accumulated in the spleen than those in normal volunteers. These parameters complicate the dosimetric calculations. In Table 3 are tabulated the percentages of In-111 lymphocytes distributed in the liver and spleen of normal volunteers and in 3 patients with Hodgkin's disease.

Table-3

Distribution of In-111 Lymphocytes at 24 hr. post administration in Normal Human Volunteers In Patients With Normal Scans and With Hodgkin's Disease

Organ	Normal Volunteers*		Hodgkin's Disease*		Normal Scan**	
	%	rad/500 μ Ci	%	rad/500 μ Ci	%	rad/500 μ Ci
Liver	11	0.5	16.6 + 6.3	0.8	11 + 2	0.76
Spleen	22	4	31 + 7.5	10	15 + 3	6.7
Whole Body	63	0.3	55.5 + 2.8	0.4	74 + 12	1.4

* Ref. (4)

** Ref. (2)

INDIUM-114/IN-114m

As discussed earlier, In-111 solutions contain In-114m as a radionuclidian

impurity. Using eleven decayed In-111-oxine samples obtained from one manufacturer, Marcus et al (5) determined that the In-114m amounted to 0.05% of the In-111 present at the time of calibration. Since the half-life of In-114m is much longer than the half-life of In-111, this proportion will continue to increase as the quantity of In-111 will decrease by decay.

Taking the estimated in vivo distribution of In-111 labeled leukocytes, platelets, or erythrocytes and following the standard MIRD schema (6) and ORNL-5000 S values (7), Marcus et al (5) calculated the radiation dose absorbed in various organs in patients receiving labeled blood cells. For every 500 μCi In-111 injected, the estimated radiation doses due to In-114m/In-114 are given in Table 4.

Table-4

Contribution of In-114m/In-114 to Radiation Dose (rad) From 500 μCi In-111-oxine Labeled Blood Cells

<u>Organ</u>	<u>Leukocytes</u>	<u>Platelets</u>	<u>Erythrocytes</u>
Liver	0.09	0.015	0.06
Spleen	0.9	0.22	0.5
Red Marrow	0.2	0.003	0.025
Ovaries	0.0016	0.0004	0.005
Testes	0.0012	0.00038	0.005
Whole body	0.012	0.0014	0.008

EXCRETION OF IN-111 WBC RADIOACTIVITY IN BREAST MILK AND RADIATION DOSE TO AN INFANT

Mountford and Coakley (8) in England injected autologous leukocytes labeled with 700 μCi In-111, to a 26 year old female suspected to have an abscess in the Pouch of Douglas, 10 days after delivery. Breast feeding to the infant was interrupted and milk was collected for up to 48 hr. post injection for the determination of In-111 radioactivity in the milk. The time of collection, radioactivity/ml milk and estimated whole-body radiation dose that might have been received by the infant after drinking 100 ml milk are given in Table 5.

Table-5

In-111 WBC Radioactivity in Breast Milk and Radiation Dose Equivalent To An Infant

Post Injection Time in hours	nCi/ml	Total-body dose (mrem) Equivalent/100 ml
2.2	0.089	0.108
7.2	0.174	0.211
12.7	0.204	0.247
18.2	0.165	0.200
22.2	0.171	0.207
28.0	0.147	0.178
32.2	0.149	0.180
45.2	0.137	0.165
47.4	0.148	0.179

How does the In-111-blood cell dosimetry compare with that of more frequently administered radionuclides such as Ga-67 and how can the possible consequences of such diffuse radiation dose be assessed?

Although in most nuclear medicine centers, 3 mCi Ga-67 are used for abscess or tumor localization studies, in many as high as 6 mCi or 10 mCi are used. In Table 6 is given the absorbed radiation dose from one mCi and six mCi of Ga-67 as estimated by the MIRD Committee in 1975. (9)

Table-6
Dosimetry of Ga-67 Citrate

<u>Organ</u>	<u>rad /mCi</u>	<u>rad/6mCi</u>
GI Tract		
stomach	0.3	1.8
small intestine	0.39	2.34
large intestine	1.39	8.34
Gonads		
Ovaries	0.3	1.8
Testes	0.25	1.5
Kidneys	0.5	3.0
Liver	0.63	3.78
Marrow	1.8	10.8
Bone	0.35	2.1
Spleen	0.7	4.2
Total body	0.26	1.56

In an attempt to assess the consequences of such radiation, long-term followup studies of radioiodine therapy in hyperthyroid patients may be recalled (10). In 802 patients treated, the marrow dose averaged 13 rad and the blood dose 16.6 rad. Several followup studies of such patients have not observed an increased incidence of leukemia. Pochin (11) found for example, 18 cases of leukemia compared to an expected incidence of 12-28 in 59,200 patients.

RADIATION DOSE TO LABELED CELLS

This concerns the absorbed radiation dose to labeled cells rather than to the organs in which labeled cells are deposited. We have found (12,13) and others have obtained (14-17) corroborating data that when cells are labeled with a lipid soluble complex of In-111, the radioactivity binds irreversibly to cell cytoplasmic components of different molecular weight and is not spontaneously eluted from the labeled cell. In a clinical preparation, approximately 1×10^{10} platelets and 10^8 leukocytes are normally used.

One mCi In-111 is equivalent to 1.3×10^{13} In-111 atoms (i.e. 65×10^{11} atoms for 500 μ Ci). Assuming uniform labeling in a typical clinical preparation, the number of In-111 atoms each cell will receive are shown in Table 7.

Table-7

In Typical 500 μCi Clinical Preparation Estimated Number of In-111 Atoms Received By Each Cell

Cell Type	No. of Cells	In-111 atoms/cell
Platelets	10^{10}	6.5×10^2
Leukocytes		
(Neutrophils)	$7-8 \times 10^7$	6.5×10^4
(Lymphocytes)	$2-3 \times 10^7$	6.5×10^4

While calculating the radiation received by each labeled blood cell, (although platelets and erythrocytes are not cells in strict sense, since they have no nuclei) Silvester and Waters (18) have considered that once in the blood stream labeled blood cells will be virtually unaffected by the radiation from other labeled cells. Each cell will, however be affected by short range radiation resulting from the decay of each In-111 atom located within the cell. For dosimetric calculations, therefore, Silvester and Waters (18) have considered only Auger electrons or occasionally, conversion electrons of very low energy having a range shorter than or comparable to the cell diameter. The cell diameter, the particle energy and their ranges are given in Table 8 and 9.

Table-8

Some Parameters of Blood Cell Components*

Cell Type	Diameter (μm)	Mass (g)	No./ cm^3 blood
Platelets	2	4.2×10^{-12}	3×10^8
Neutrophils	10 (Mean)	5.2×10^{-10}	$5-10 \times 10^6$
Lymphocytes	10 (Mean)	5.2×10^{-10}	$1-3 \times 10^6$
Erythrocytes	4.6 (Mean)	5.2×10^{-11}	5×10^9
Monocytes	15	1.8×10^{-9}	$1-6 \times 10^5$

* Ref. (18)

Table-9

Indium-111-Auger Electrons*

Radiation (Auger Electrons)	Mean No. per Disinteg. (n)	Mean Energy Particle (E) (MeV)	nE (MeV)	Range (r) μm	p**
KLL	0.1103	0.0192	0.0021	8	0.24
KLX	0.0441	0.0223	0.0009	10	0.12
KXY	0.0067	0.0254	0.0002	12.55	0.06
LMM	0.9867	0.0024	0.0024	0.230	1.0
MXY	2.2886	0.0006	0.0014	0.025	1.0
		Total	0.0070		

(MeV/disinteg.)

* Ref. (18)

** p = Vol. of cell/vol. of sphere of radius r

Electrons with a range $r < 1 \mu\text{m}$ are assumed to be totally absorbed within the cell, whereas those with a range $r > 1 \mu\text{m}$ are assumed to deposit a fraction equivalent to the ratio of cell volume to the volume of the sphere of radius $r(P)$. Taking these into consideration the total energy deposited in each neutrophil or lymphocyte from the decay of a single In-111 atom is 4.38 keV. This is equivalent to $4.38 \times 1.6 \times 10^{-9} / 5.2 \times 10^{10}$ erg/g or 0.135 rad. In a typical 500 μCi In-111 clinical preparation, therefore (Table 7) each neutrophil or lymphocyte will receive 8750 rad (19).

Each labeled platelet, from the complete decay of a single In-111 atom will receive 14.5 rad., making it, in a clinical preparation, a total absorbed radiation dose per platelet of $(14.5 \times 6.5 \times 10^2) = 9425$ rad (18).

Previous studies have shown that neutrophils and platelets in plasma are remarkably resistant to the damaging effect of ionizing radiation (20,21). External radiation of up to 75,000 rad did not induce any apparent ultrastructural changes in human neutrophils. Similarly, our recent studies demonstrated that In-111 labeled human platelets receiving 36,700-110,000 rad had intact and undisturbed alpha granules, canalicular system and particulate glycogen. It is possible, therefore, the radiation dose received by human neutrophils or platelets in a normal clinical In-111 labeled preparation does not cause detrimental effect to these cells.

Contrary to this, lymphocytes are more susceptible to radiation damage than any other cells in circulation. Lymphocytes, although unique in morphology, are heterogeneous and have been separated functionally into a spectrum of sub-populations with a life span of a few days to years; lymphocytes play many major roles in immune system and sometimes carry immunologic memory for many years. Upon interaction with specific antigens, lymphocytes undergo transformation or blastogenesis (22) dividing into more cells with the same specific function including replication of DNA.

SIGNIFICANCE

It is because of these characteristics of lymphocytes, that much attention has been drawn to the possible consequences of radiation dose to lymphocytes. ten Berge et al (23) observed that lymphocytes, from two human donors, labeled with In-111-oxine had increased chromatid and chromosomal aberrations. Per 10^8 lymphocytes labeled with 30 μCi In-111, 54% cells were abnormal. The percentage of abnormal cells increased to 90-92% and to 100% when the cells were labeled with 80-90 μCi and 100 μCi respectively. In unlabeled cells, 3-14% were abnormal. Although these results have not prevented the use of In-111-oxine labeled lymphocytes clinically (24) the significance of such damage has been seriously considered (23). In an attempt to assess the risk involved, Thakur and McAfee (19) have put together some pertinent facts about the chromosomal aberrations and oncogenic potential of irradiated human lymphocytes. Some of these facts are discussed here.

Each human lymphocyte has 46 chromosomes in 23 pairs. Each chromosome contains approximately 100,000 genes and each gene about 1000 nucleotides (25). Chromosome structure can be altered by many physical and chemical interactions. Such interactions result in chromosomal breakage and change in chromosome number. Both such changes cause genetic disturbances in the cell.

"Spontaneous" chromosome aberrations in normal population have been, however noted. The incidence varies with age, geographic location, smoking habits, and the extent of exposure to chemicals (26). Spontaneous chromosome aberration in

normal adult males and females has been studied by many investigators. Lubs and Samuelson (27) studied 3,720 lymphocyte metaphases from 10 normal volunteers and found 1-20% of the cells with one or more breaks. In four of eleven control cultures Nichols et al (28) noted 10% to 20% chromosome breaks. Littlefield and Goh (29) analysed 11,950 lymphocyte metaphases from 122 cultures from 10 normal men and 17,759 lymphocyte metaphases from 183 cultures from 21 normal women, and found that 5.6% metaphases from men and 6.5% metaphases from women had at least one chromosome aberration.

Chromosome breaks are produced by many industrial chemicals such as food additives, pesticides, plastics, suspensions, and aerosols. The industrial toxicants have entered into our ecological system through air, water supply, beverages, and food products. Fossil fuels consumed for home heating, energy generation, motor vehicles and airplanes, as well as pollutants from manufacturing, mining, smelting and refining contribute to air toxicants. Increasing concentrations of air toxicants such as sulfur oxides, nitrogen oxide, hydrocarbons and depletion of ozone in small quantities have been found to be the contributing factors for chromosomal aberration (30).

Total body lymphocytes are numbered to be approximately 10^{12} . At 5%, the total number of lymphocytes with at least one chromosome break would be 5×10^{10} . The total number of lymphocytes that need to be labeled with In-111 for clinical study are normally 10^8 or less. These amount to be 0.01% of the total body lymphocyte population and 0.2% of lymphocytes that exist in the body with at least one chromosome aberration.

From the ten Berge data (23) 90 μCi In-111 incorporated into 10^8 lymphocytes produced chromosomal damage with the same frequency as 200 rad x-radiation which is about 90% abnormal cells. With 200 rad whole-body radiation, the risk of hematological malignancy during a 30-yr life time would be 9600 per 10^6 population(19). In keeping with the hypothesis that the somatic mutation is the initial step in radiation induced malignant transformation, 10^8 lymphocytes with chromosomal damage would increase the risk of hematological malignancy over 30 yr. in $0.01\% \times 9600/10^6$ or about one per 10^6 population subjected to the In-111 lymphocyte study. This risk is less than 0.025% of the 1981 spontaneous cancer patient rate in the country.

As discussed previously, when 10^8 mixed leukocytes are labeled with 500 μCi for abscess localization studies, each of the estimated 30×10^6 lymphocytes receives greater than 8000 rad. There is evidence that lymph node cells receiving approximately 6000 rad die immediately (31) and about half of the human lymphocytes irradiated outside the body with 300-400 rad fail to undergo mitosis in culture (32). These results suggest that lymphocytes labeled with In-111 in mixed population of leukocytes are killed by radiation and may pose no long term risk.

Keeping the basic assumptions that the radioactivity is distributed evenly and is predominantly inside the cell and that the short ranged Auger electrons are absorbed within the cell, Silvester and Waters (18) have calculated radiation dose to leukocytes or lymphocytes when labeled with some other potential alternative radionuclides to In-111. The data are given in Table 10.

Table 10

Estimated Radiation Dose to Leukocytes or Lymphocytes Labeled With Some Alternative Radionuclides To In-111

Radionuclide	Half-life	dose from decay of a single atom (rad)*	mCi/ 10^8 cells	Estimated dose (rad)	Ratio to In-111
In-111	2.83 d	0.135	0.5	8775	1
Cr-51	27.7 d	0.113	0.5	7175	0.8
Ga-67	3.26 d	0.202	1.5	45566	5.2
Ga-68	68 min.	0.016	15	523	0.06
Ru-97	2.88 d	0.155	0.5	10296	1.17
Tc-99m	6.02 h	0.077	20	17820	2
In-113m	99.5 min.	0.038	20	2422	0.27

* Ref. (18)

Although Cr-51, Ga-67 and In-113m chosen in these examples (Table 10) may not be useful abscess imaging agents, Ga-67, Ru-97 and Tc-99m have been considered as possible alternative radionuclides to In-111 for labeling leukocytes. All of these deliver higher radiation doses to the cells than In-111.

In an attempt to minimize the radiation dose, cell surface labeling has been considered. The use of cell specific monoclonal antibodies labeled with In-111 provides an excellent possibility for surface cell labeling. However, the possibility of internalization of labeled antibodies has not yet been ruled out. Nevertheless, numerous studies are underway that will fully explore the potential of radiolabeled antibodies as agent for labeling blood cells which might reduce radiation dose to labeled blood cells.

From the foregoing discussion it appears that:

- i) The radiation dose received by the liver and spleen from a 500 μ Ci In-111 blood cell preparations is acceptable.
- ii) Chromosome damage does result from radiolabeling of lymphocytes.
- iii) The increased burden of chromosomal aberration is relatively small compared to that induced by other environmental causes.
- iv) Lymphocytes incidentally labeled with In-111 in clinical leukocyte preparation are killed by radiation and pose no long term risk and,
- v) Based on the estimated cell radiation dose resulting from a clinical preparation, In-111 appears to be the most acceptable radioactive tracer for labeling blood cells.

REFERENCES

1. Thakur, M.L, J.P. Lavender, R.N. Arnot and D. J. Silverster. Indium-111-labeled autologous leukocytes in Man. J. Nucl. Med. 18, 509-514, 1977.

2. Goodwin, D. A., C. F. Mears. Indium-111 labeled cells. New approaches and radiation dosimetry. In radiolabeled cellular blood elements: Pathophysiology techniques and scintigraphic applications. Ed. Thakur, M.L., Plenum Publishing Co., New York, 1985.
3. Goodwin, D. A., J. T. Bushberg and P.W. Doherty. Indium-111 labeled autologous platelets for localization of vascular thrombi in humans. *J. Nucl. Med.* 19, 626-634, 1978.
4. Lavender, J. P., M.L. Thakur, J.M. Goldman and R.N. Arnot. Kinetics of Indium-111 labeled lymphocytes in normal subjects and patients with Hodgkin's disease. *Br. Med. J.* 2, 797-799, 1977.
5. Marcus, C.S., M. G. Stabin, E.E. Watson, and J. H. Kuperus. Contribution of contaminant Indium 114m/In-114 to In-111 oxine blood dosimetry. *J. Nucl. Med.* 26, 1091-1093, 1985.
6. Loevinger, R., M. A. Berman. A revised schema for calculating the absorbed dose from biologically distributed radionuclides. MIRD Pamphlet No. 1 revised, The Soc. Nucl. Med. New York, 1976.
7. Snyder, W., M. Ford, and G. Warner. A tabulation of dose equivalent per microcurie - day for source and target organs of an adult for various radionuclides. ORNL-5000, National Technical Information Service, Springfield, VA., 1974.
8. Mountford, P.J., A.J. Coakley. Excretion of radioactivity in breast milk after an In-111 leukocyte scan. *J. Nucl. Med.* 26, 1096-1097, 1985.
9. Snyder, W.S., M.R. Ford, and G.G. Warner "S" absorbed dose per unit canulated activity in selected radionuclides and organs. *J. Nucl. Med.* MIRD Pamphlet, No.11, 1975.
10. Green, M., M. Fisher, and H. Miller. Blood radiation dose after ^{131}I therapy of thyrotoxicosis. Calculations with reference to leukemia. *Br. Med. J.* 2, 210-215, 1961.
11. Pochin, J.E. Leukemia following radioiodine treatment of thyrotoxicosis, *Br. Med. J.* 2, 1545-1550, 1961.
12. Thakur, M.L, A. W. Segal, L. Louis, M.J. Welsh, J. Hopkins and T. J. Peters. Indium-111-labeled cellular blood components. Mechanism of labeling and intracellular location in human neutrophils. *JNM*, 18 (10), 1022-1026, 1977.
13. Thakur, M.L, S. M. McKennney. Indium-111-Mercaptopyridine-N-Oxide (Merc) labeled human leukocytes and platelets. Mechanism of labeling and intracellular location of In-111 and Merc. *J. Lab. Clin. Med.* (in press).
14. Baker, J.R.J., K. D. Butler, M.N. Eakins, G. F. Pay and M.A. White. Subcellular localization of In-111 in human and rabbit platelets. *Blood*. 59, 351-359, 1982.
15. Hudson, E.M., R.B. Ramsey and B.L. Evatt. Subcellular localization of indium-111 in indium-111-labeled platelets. *J. Lab. Clin. Med.* 58, 164-170, 1981.
16. Joist, J.H., R. K. Baker and M.J. Welsh. Methodologic and basic aspects of In-111-platelets. *Thromb. and Hemos.* 9, 86-99, 1983.

17. Mathias, C.J. and M.J. Welch. Labeling mechanism and localization of In-111 in human platelets. *J. Nucl. Med.* 20, 659, 1979.
18. Silvester, D.J., and S.L. Walters. Dosimetry of radiolabeled blood cells. *Int. J. Nucl. Med. Biol.* 10, 141-144, 1983.
19. Thakur, M.L., J.A. McAfee. The significance of chromosomal aberrations in In-111 labeled lymphocytes. *J. Nucl. Med.* 25, 922-927, 1984.
20. Zakhireh, B., M. L. Thakur, H.L., Malech, M.S. Cohen, A. Gottschalk and R.R. Root. Indium-111 labeled human polymorphonuclear leukocytes. Viability random migration, chemotaxis, Bacterial capacity and ultrastructure. *J. Nucl. Med.* 20, 741-747, 1979.
21. Thakur, M.L., A.W. Sedar. Ultrastructure of human platelets following In-111 labeling in plasma. Submitted *J. Nucl. Med.* 1985.
22. William, W. L., E. Butler, A.J. Erslev, Ed. *Hematology 2nd Edition*, p.71 and p.845, McGraw Hill Book Co, New York, 1977.
23. ten Berge, R.J.M., A.T. Natarajan, M.R. Hardeman. Labeling with Indium-111 has detrimental effects on human lymphocytes. concise communication. *J. Nucl. Med.* 24, 615-620, 1983.
24. Wagstaff, J., C. Gibson, N. Thatcher. Human lymphocyte traffic assessed by Indium-111 oxine labeling; clinical observations. *Clin Exp. Immunol.* 43, 443-449, 1981.
25. Valentine, G.H. The Chromosome Disorder. An introduction for clinicians. Third edition, J.B. Lippincott Co, Philadelphia, Chap.1. 26. Bauchinger, M. Chromosome aberrations in human as a quantitative indication of radiation exposure. In *Mutagen-Induced Chromosome Damage in Man*. Evans, H.J., Lloyd, D.C. eds. New Haven, Yale University Press, 9, 267, Chap. 9, 1978.
27. Lubs, H.A., J. Samuelson. Chromosome abnormalities in lymphocytes from normal human subjects. *Cytogenetics* 6, 402-411, 1967.
28. Nichols, W.W., A. Levan, B.A. Kihlman. Chromosome breakage associated with viruses and DNA inhibitors. In *Cytogenetics of Cells in Culture*. R.J.C. Harris, ed. Academic Press, New York pp 255-271, 1964.
29. Littlefield, G.L, K.O. Goh. Cytogenetic studies in control men and women: I. Variations in aberration frequencies in 29,709 metaphases from 305 cultures obtained over a three year period. *Cytogenet Cell Cenet* 12, 17-34, 1973.
30. Fishbein, L. Principles and methods for their detection. In *Chemical Mutagens*, Hollaender A, ed, New York, Plenum, Vol.4, Chapter 42, 1976.
31. Anderson, R.E., N.L. Warner. Ionizing radiation and the immune response. *Adv Immunol.* 24, 215-335, 1976.
32. Field, E.O, H.B.A. Sharpe, K.B. Dawson. Turnover rate of normal blood lymphocytes and exchangeable pool size in man, calculated from analysis of chromosomal aberrations sustained during extracorporeal irradiation of the blood. *Blood* 39, 39-56, 1972.

DISCUSSION

BIGLER: Are any of the data used to develop bone marrow radiation dose estimations based upon human bone marrow aspiration biopsies that have been corrected for bleeding?

THAKUR: The strict answer to that question is, "No." Of course, you are not going to aspire bone marrow from a human. I have attempted it in a dog but it is not easy to aspire all the bone marrow from the whole animal. You can only estimate. In one case when I was at Hammersmith working with Rosemary Arnot, we estimated bone marrow in the pelvic area of a patient. From that estimate we estimated the whole-body bone marrow; then, we calculated a figure that I did not quote because it was so approximate. But aspiration as such, no.

BRILL: As a follow-up to Dr. Bigler's question, which may have been misunderstood, let me note that a bone marrow aspiration may consist of up to 95% peripheral blood. This can be established and corrected without taking out all of the marrow. The traditional way is to inject a red cell label before bone marrow sampling and then correct the marrow activity for the fractional contamination by labeled blood obtained in the bone marrow aspiration.

THAKUR: Yes, I agree with that. It has not been done though, unfortunately.

AN ASSESSMENT OF THE RISK TO PATIENTS FROM THE
LABELLING OF LEUCOCYTES WITH INDIUM-111

Alan A. Edwards and David C. Lloyd

National Radiological Protection Board
Chilton, Didcot, Oxon, OX11 ORQ, UK

ABSTRACT

Indium-111 oxine is used in diagnostic nuclear medicine to label leucocytes. A typical procedure might be to label white cells in 50 ml of blood with about 500 μCi ($\sim 20 \text{ MBq}$) of indium-111 and return them to the body.

Both theoretical and experimental information from measurements of chromosome aberrations in lymphocytes show that the labelled cells receive doses of some tens of grays, mostly delivered within one to two weeks. Much of the dose is due to short range Auger electrons. The doses to organs of the body due to circulating labelled cells are much lower. The risk to the patient thus has two components, due to the low dose irradiation of body organs and the localised high dose to the labelled cells. The former is estimated using the concept of effective dose equivalent as recommended by ICRP. An effective dose equivalent of $2 \times 10^{-2} \text{ Sv} \cdot \text{mCi}^{-1}$ for the above procedure was calculated making use of recent data on the distribution of the label within the body. The resulting risk of inducing a fatal cancer is calculated as about $3 \times 10^{-4} \text{ mCi}^{-1}$.

Attempts to evaluate the risk of leukaemia and lymphatic cancer due to direct irradiation of labelled leucocytes are more difficult. Nevertheless an attempt has been made using stated assumptions. If cellular doses are as high as 50 Gy, cell killing can be used to argue that the risk is much lower than the whole-body risk. For lower cellular doses an argument based on the fraction of cells irradiated is used and the risk due to the labelled cells appears to be two orders of magnitude lower than the whole-body risk.

We conclude that the dominant risk is that due to effective dose equivalent and that for typical activities used, the risk lies in the range accepted for other radiopharmaceutical diagnostic procedures.

INTRODUCTION

The technique of labelling white blood cells with indium oxine was introduced by McAfee and Thakur (1). The clinical applications include the identification and localisation of abscesses using a scanning gamma camera following the injection of indium-111 labelled autologous white cells. Although for more specific tasks it is possible to label sub-populations of white cells and platelets, the normal procedure is to label a mixed white cell population. The advantages of this technique are claimed to be the favourable half-life, the stability of the label and the normal behaviour of the labelled cells within the body (2).

Ten Berge et al (3) questioned some of these claims. They found in vitro that about 50% of the label was lost from lymphocytes after 48 hours. At a labelling level of $20 \mu\text{Ci}/10^7$ cells they verified that cell viability was better than 90% but their proliferative capacity was seriously impaired although some cells survived. In addition there were large numbers of chromosome aberrations in the lymphocytes implying doses to the labelled cells in excess of 2 Gy at a labelling level of $9 \mu\text{Ci}/10^7$ cells. The authors envisaged that the main risk of the technique comes from returning to the body highly irradiated cells of which some may contain potentially malignant lesions. In particular they stressed cancers of the lymphatic system arising from damaged lymphocytes.

The purpose of this paper is to make an assessment of the risk of malignant disease arising from this diagnostic procedure. Radiologically there are two components to the risk represented respectively by the doses to body organs from label within them and in adjacent organs and the higher dose received specifically by the labelled cells. These components will be assessed separately.

CALCULATION OF DOSES

THE DECAY OF INDIUM-111

Both assessments require a knowledge of the decay of indium-111. Indium-111 has a half-life of 2.83 days and decays by electron capture. The nucleus captures an orbital electron leaving the resulting nucleus of cadmium-111 in an excited state and a vacancy in one of the orbital electron shells. This vacancy is filled by an electron from another shell and the energy lost is either emitted as an X-ray or is transferred to another orbital electron which escapes from the atom and is called an Auger electron. Thus either one or two vacancies appear in the electron shells and these are filled by the same process. The excited nucleus decays to its ground state either by emitting two γ -rays or by transferring the energy to orbital electrons which escape leaving vacancies. If the latter process, called internal conversion, takes place the vacancy initiates another X-ray/Auger electron cascade. Thus an indium-111 decay may result in solely X and γ radiations or solely electrons or more commonly a mixture of the two. Table 1, which was extracted from the decay scheme (4), shows in a simplified form the radiations, their energy and the average energy emitted per disintegration of indium-111. The groups of electrons were chosen so that the ranges were very much greater, of the same order and very much smaller than the cell diameter. Their approximate ranges (5) are also shown in Table 1.

TABLE 1

Radiations produced by the decay of indium-111

Radiation	Energy keV	Energy per disintegration keV	Range μm
γ_2	245	231	-
γ_1	171	155	-
X	23-26	19	-
e(I.C.)	150-250	27.3	280-640
e Auger	19-25	3.1	8-13
e Auger	< 3.6	3.8	< 1

CALCULATION OF THE EFFECTIVE DOSE EQUIVALENT

The concept which underpins this calculation is that the risk to an individual is the sum of the risks to the various organs within the body (6). This makes it possible to take into account the differing sensitivities to radiation of the various organs. This concept is used in radiological protection to calculate limits for taking radioactive substances into the body in the working environment. Weighting factors are ascribed to each organ such that the sum of the factors is unity. The effective dose equivalent is the sum of the organ doses times their weighting factors and is considered to relate directly to risk. To calculate the effective dose equivalent the following information is required.

- 1) The distribution of label in the organs
- 2) The dose to each organ due to label in the same and all other organs
- 3) The weighting factors

Label Distribution

The distribution of label within the body seems to depend upon whether neutrophils or lymphocytes or mixed populations of leucocytes are labelled. Wagstaff et al (7) using labelled lymphocytes showed that the organ distribution of indium-111 varied with time after injection and between patients. They detected activity in the spleen and the liver with a higher count coming from the spleen. Although they measured count rates at the surface of the body no attempt was made to convert these to activity in the organ. These authors also stated that there was evidence that some indium-111 labelled cells had migrated to the bone marrow.

Lavender et al (8) also using labelled lymphocytes found indium-111 in the spleen and liver in percentage concentrations which varied little with time but much more from patient to patient. The average values were 25% and 15% in the spleen and liver respectively.

Thakur et al (2) using labelled leucocytes also found very little variation of indium-111 concentration with time after the first 20 minutes

but a large individual variation. These authors reported on average about 20% in the liver and about 15% in the spleen with a smaller amount in the bone marrow.

Goodwin et al (9) also using labelled leucocytes found 20% in each of the liver and spleen, about 50% in the bone marrow and the remainder generally distributed in all other body tissues. For labelled lymphocytes they found 11% in the liver, 15% in the spleen and the remainder principally in the bone marrow. In view of the variations among authors and among patients it is difficult to select representative values. Nevertheless an attempt has been made and these values are shown in Table 2. They are intended to represent time averaged values and purposes of this assessment are regarded as time independent.

TABLE 2

The distribution of indium-111 amongst organs

Organ	Fraction of total-body activity
Spleen	.2
Liver	.2
Red bone marrow	.2
Blood	.2
Rest of body	.2

Organ Doses and Weighting Factors

The procedures outlined in the standard MIRD schema (10) were followed to estimate doses to organs of interest. Doses from 1 mCi of indium-111 oxine labelled mixed white blood cells are given in Table 3. Also shown in Table 3 are the weighting factors and the organ components of effective dose equivalent. The gonad dose was taken as an average of the doses to the ovaries and the testes. This is an example of following the ICRP philosophy of average male and female risks. In this example the ovary dose is about 2.5 times that to the testes. It makes very little difference to the effective dose equivalent however the gonad doses are treated. Breast tissue was assumed to be the same as other tissue (muscle). When blood was the target organ, it was assumed to be the same as muscle except when the blood was also the source organ. In this case the dose to blood was estimated assuming all the electron energy was completely absorbed in the blood. The dose due to the X-and γ -ray components was estimated from tables for the total body (11). The total effective dose equivalent of 0.0182 Sv/mCi (Table 3) may be compared with a figure of 0.024 Sv/mCi derived by Johansson et al (12). In view of the uncertainties in the distribution of label and approximations made in deriving organ dose we decided to use a figure of 0.02 Sv/mCi for the effective dose equivalent.

TABLE 3

Organ weighting factors and
dose for 1 mCi labelling

Organ	Weighting factor	Dose 10^{-2} Sv	Weighting factor \times dose 10^{-2} Sv
Gonad	.25	.31	.08
Lung	.12	.53	.06
Breast	.15	.53	.08
Red bone marrow	.12	1.8	.22
Thyroid	.03	.23	.01
Bone	.03	.48	.01
Remainder Liver	.06	2.8	.17
Spleen	.06	18.0	1.08
Blood	.06	0.75	.05
Another	.06	.53	.03
Another	.06	.53	.03
		Total	1.82

CALCULATION OF THE DOSE TO LABELLED CELLS

In this section an attempt is made to calculate the dose to the labelled cells for an injected activity of 1 mCi. The assumptions made are listed below.

- 1) 50 ml of blood is taken from the patient. The haematological picture is normal so that there are $\sim 350 \times 10^6$ white cells of total mass ~ 0.2 gm. The 350×10^6 white cells consist of approximately 200×10^6 neutrophils, 120×10^6 lymphocytes and the remainder comprise small numbers of monocytes, eosinophils, basophils (13) and some circulating stem cells. These last are ~ 5000 CFU_c (colony forming units, which are granulocyte precursors), and ~ 25000 BFU_e (burst forming units, which are erythrocyte precursors) (14).
- 2) The white cells are labelled intracellularly with 1 mCi of indium-111 and it remains associated with those cells even after they are returned to the body.
- 3) All electrons of range $< 1 \mu\text{m}$ deposit all of their energy in the cell in which the decay occurs. All electrons of range about $10 \mu\text{m}$ deposit half of their energy in the cell. Electrons of range about $400 \mu\text{m}$ deposit only about 1% of their energy in the cell and X- and γ -rays deposit no energy at all.
- 4) Compared with the internal dose to the cell, the dose caused by decays in neighbouring cells can be ignored. This applies both during the preparation of the labelled cells and after their return to the body.

On these assumptions the average energy per decay deposited in a cell is $3.8 + \frac{1}{2} (3.1) + 1/100 (27.3) = 5.7$ keV and converting this to dose for

1 mCi in 0.2 g gives about 0.6 Gy h⁻¹. Integrating over all time and allowing for radioactive decay gives a total dose of about 60 Gy.

ten Berge et al (3) labelled lymphocytes with various concentrations of indium-111 oxine cultured the cells to metaphase, and scored chromosome aberrations. At a concentration of 15 µCi/10⁷ cells (about 500 µCi/3.5 x 10⁸ cells) they observed an aberration yield (dicentrics plus rings) of about 0.7 per cell which was the average from two donors. This value can be used to estimate an absorbed dose to the labelled lymphocytes using X-ray calibration curves published by Lloyd et al (15,16). These curves are for dicentrics per cell but as rings occur with a frequency of < 10% of dicentrics the curves may be used with little error. The calibration curves (15,16), reproduced in Fig 1, show that not only is there a dependence of the yield on radiation quality but also a dependence on dose rate or more correctly the time of irradiation. As well as chromosome type aberrations, ten Berge et al (3) observed much chromatid damage. This is to be expected as the nuclide was present during the whole culture period. Chromosome type damage (dicentrics and rings) are only produced in the G₀, G₁ and early S phases and we estimate that this period is about 24 hours which is half of the culture period. This is a chronic irradiation so that we would convert the observed dicentric yield to a dose of about 4 Gy in 24 hours. Converting this to allow for full decay and a dose of 1 mCi/3.5 x 10⁸ cells gives a dose of about 30 Gy which is only a factor of 2 lower than the dose calculated above.

Strictly these cytogenetically determined doses should be compared with calculated doses to the nucleus of the lymphocyte which requires detailed knowledge concerning the exact distribution of indium-111 within the cell and a knowledge of the nuclear and cell diameters. An approximate calculation for the small lymphocyte (cell diameter 7.2 µm, nuclear diameter ~ 6 µm) shows that the nuclear dose could be 5 to 10 times higher if the activity were in the nucleus than if it were bound to cytoplasmic components. Thakur et al (17) have investigated the intracellular location of In-111 in human neutrophils labelled with the oxine. They indicated that most of the In-111 remains in the cytoplasm but some of the activity had a distribution similar to that of DNA. The cytogenetic results (3) support the idea that indium binds more to cytoplasmic rather than nuclear components. For the purposes of risk assessment we shall assume that the dose to cells containing label is 50 Gy but bearing in mind the uncertainties attached to this estimate.

THE ESTIMATION OF RISK

RISK DUE TO EFFECTIVE DOSE EQUIVALENT

We have calculated that labelling with 1 mCi produces an effective dose equivalent of 0.02 Sv. ICRP (6) recommends a risk coefficient of 165 x 10⁻⁴ Sv⁻¹ which gives an overall risk of 3.3 x 10⁻⁴. It should be remembered that this risk coefficient is for fatal cancers plus hereditary effects in the first two generations. It is intended to apply to an adult working population and represents an average for male and female. If it is felt that hereditary effects are not important in the context of this paper then the component due to gonad irradiation may be ignored which would reduce the risk by about 5%. Overall the fatal cancer risk is in the region of 3 x 10⁻⁴ mCi⁻¹.

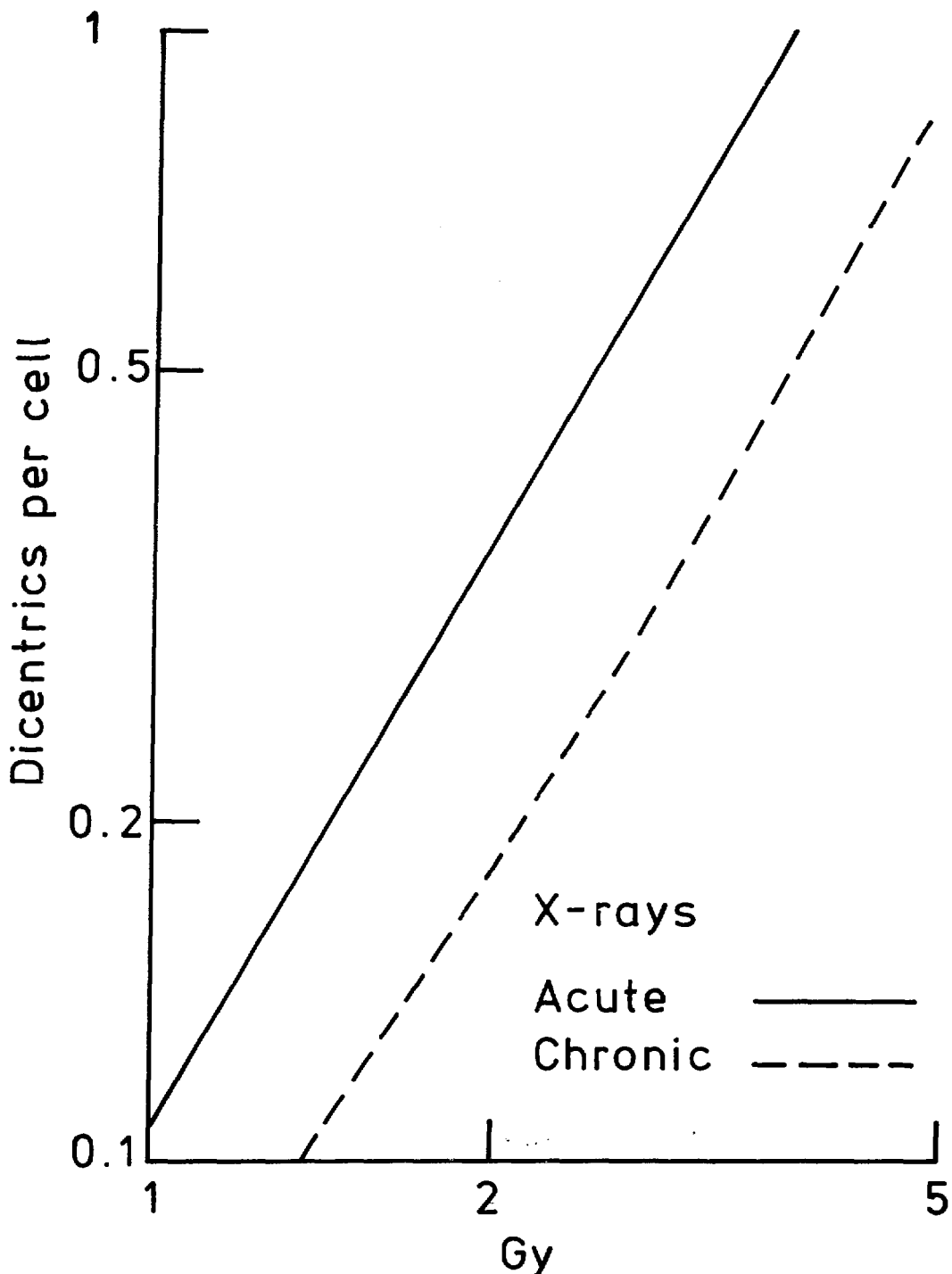


Figure 1 Calibration curves for the conversion of dicentric yield in human lymphocytes to absorbed dose

RISK DUE TO THE HIGHLY DOSED WHITE CELLS

We have estimated an internal dose of about 50 Gy at which the dominant effect is cell killing. Many experiments have been performed to measure the shape of the survival curve. It is generally agreed that at high doses the survival fraction $\frac{S}{S_0}$ can be described by equation (1) where D is the observed dose, D_0 a dose characteristic of the sensitivity and n is a number called the extrapolation number which usually lies in the range 1 to 10.

$$\frac{S}{S_0} = n e^{-D/D_0} \quad \dots \dots (1)$$

Values for D_0 and n of 1.0 Gy and 1.0 respectively have recently been determined for lymphocytes irradiated with cobalt-60 gamma-rays (18) and this value is probably representative of other white cells. Values of D_0 for human CFU_c and BFU_e cells of 1.5 Gy and 1.0 Gy respectively have been determined (19). These D_0 values were obtained with acute irradiation and there are no appropriate data for blood cells after protracted in vitro exposure. However based on data from cultured cell lines (20) we shall double the acute D_0 for the purpose of this assessment. Another factor is that the dose is principally due to electrons of energy less than 3 keV and Cox et al (21) have shown that aluminium X-rays which produce electrons of energy 1.5 keV have an RBE for cell killing in human fibroblasts of about 2 with respect to 250 kVp X-rays. Thus it might be appropriate to reduce the value of D_0 by a factor of 1.5 or 2. However for this assessment we shall adopt a worst case attitude and ignore this correction. We thus consider D_0 values of 2 Gy for lymphocytes, other leucocytes and BFU_e cells and 3 Gy for CFU_c cells to be high and thus will overestimate the survivors. If the cellular dose is 50 Gy the probability that one labelled leucocyte will survive from a population of 3.5×10^8 cells is about 5×10^{-3} . These values are about a factor 10^4 lower for BFU_e cells but a factor 20 lower for CFU_c cells.

Mature white cells do not normally divide in vivo and thus it could be assumed that their potential for oncogenesis is small. The BFU_e and CFU_c are stem cells which probably return to the bone marrow and are more likely to attempt division. With these assumptions the probability of a stem cell surviving is no more than 3×10^{-4} . Even if all of these had the capacity to become malignant the chance of a malignancy would not exceed 3×10^{-4} , a risk identical to the whole-body risk calculated earlier. In the steps leading to the estimate of risk due to intra-cellular indium-111 we have consistently made pessimistic assumptions so that it is permissible to conclude that if the internal dose exceeds 50 Gy the carcinogenic effect can be ignored on cell killing grounds.

We have argued that the 50 Gy dose estimate upon which this conclusion is based may be high. Also some physicians tend to use lower activities of In-111, in the range 200-500 μCi , so that the cellular dose is lower and therefore the effect of cell killing is not so great. We shall therefore consider a worst case situation in which the dose to the cells is 5 Gy. This dose is representative of doses at which the maximum mutation or cancer yield would occur (22).

Approximate whole-body doses up to ~ 5.0 Gy have been experienced by some people including some A-bomb survivors and it is from subsequent cancers in these people that ICRP (6) has estimated a risk coefficient of $125 \times 10^{-4} \text{ Sv}^{-1}$ assuming linearity and no threshold for the induction of all

fatal cancers. Of these ~ 20% are cancers of the blood forming and lymphatic systems which one might expect to be the cancers of concern arising from labelled leucocytes. These values apply at low doses and low dose rates. In the present situation when the dose to the labelled cells is high and delivered at a fairly high rate a risk coefficient of $5 \times 10^{-4} \text{ Sv}^{-1}$ may be appropriate (23). This risk applies when all cells in the body have been irradiated to a dose equivalent of 1 Sv which for the purposes of radiations considered here is 1 Gy. It follows from the linear hypothesis that one has to consider the number of labelled cells returned to the body as a proportion of the total number of such cells in the body.

At any given moment ~ 1% of the body's lymphocytes are in the circulating blood (24). Circulating stem cells also comprise a small percentage of those in the whole body as the vast majority are contained in the hematopoietic tissue, especially the bone marrow (25). 1% of CFU_c and BFU_e in the blood at any moment is probably an overestimate. Thus assuming a 5 Gy dose to the labelled fraction which itself comprises ~ 1% (50 ml) of the total blood volume (26), the risk of cancer arising from the lymphocytes, CFU_c and BFU_e is

$$\sim \frac{50 \times 10^{-4}}{100} \times 5 = 2.5 \times 10^{-6}$$

The remaining leucocytes comprise mostly neutrophils of which approximately 50% are in the vascular pool (25).

For the neutrophils the calculation is

$$\frac{50 \times 10^{-4}}{100} \times \frac{5}{2} = 1.3 \times 10^{-6}$$

It should be stressed that these two estimates are mutually exclusive, because the former assumes that radiation induced leukaemia can only be caused by irradiation of either lymphocytes or CFU or BFU cells while the latter assumes that it is caused only by irradiating mature neutrophils. There is no evidence that the irradiation of mature white cells in vivo can cause leukaemia so that a risk value approaching $2 \times 10^{-6} \text{ Gy}^{-1}$ is more likely because this applies to the stem cell fraction of the blood.

DISCUSSION

We have calculated a life-time risk of $3 \times 10^{-4}/\text{mCi}$ from an effective dose equivalent of about $0.02 \text{ Sv}/\text{mCi}$. The risk of $165 \times 10^{-4} \text{ Sv}^{-1}$ is a risk for fatal cancers but includes a component for hereditary factors, that is risk to future generations. It is not clear therefore that the gonad dose and its weighting factor should be included in the calculation for assessing cancer risk from diagnostic radiopharmaceuticals. However since the gonad dose makes only a small contribution to the effective dose equivalent it makes no difference to the assessment whether hereditary effects are considered or not. The major contribution to the effective dose equivalent is that due to the spleen and it is doubtful whether such a large weight should be given to an organ for which there is no evidence of cancers linked to radiation. The recommendation to represent the remainder organs by the five most irradiated organs is just an approximation suggested to help computation. If the average dose to all the remainder organs were used instead the effective dose equivalent would reduce to about $6 \times 10^{-3} \text{ Sv}$. Because of the uncertainty due to whether the spleen dose should be included

or not, it must be remembered that the calculation of effective dose provides no more than a general guide to risk and therefore should not be used as a precise tool.

The calculation of risk due to the high dose to a small fraction of white cells involves assumptions of more doubtful validity. One of the assumptions is that the irradiation of mature fully differentiated cells within the blood has a negligible chance of causing a cancer. This is based on the fact that in order to divide the cells need to dedifferentiate into a blast form and this is an unlikely event. Another more important assumption is that the risk is directly proportional to the number of cells irradiated. To our knowledge there is no experimental evidence to support or to reject the assumption. Nevertheless with these assumptions we have assessed that the risk due to high doses to a few white cells is more than a factor of 100 lower than the risk due to whole-body irradiation using 1 mCi of indium-111. Even if we halve the administered activity to 500 μ Ci which is the normal patient dose, the real risks would still differ by a factor 50. Consequently our basic assumptions on the risk for high dose to cells would have to be in error by at least an order of magnitude for the two risks to be equivalent. This suggests that experimental evidence is required to show that doses of about 5.0 Gy to a small fraction of blood cells produces negligible risk. This could be done using animals by irradiating the blood in vitro with X- or γ -rays or by giving indium-111 oxine in the usual way, returning the blood to the animals and comparing the incidence of induced cancer with that of an equivalent dose of X-rays to the whole body.

The studies of ten Berge (3) indicate that some of the label dissociates from the cells and presumably would be available for redistribution throughout the body. As it is no longer in the oxine form it may not attach so readily to leucocytes. The indium may bind to serum transferrin and could be deposited in the red bone marrow. For considerations of effective dose equivalent this component is covered by the assumed 20% in Table 2 leading to an organ dose of 0.018 Sv, Table 3.

However Touya et al (27) indicate that the transferrin/indium complex in marrow selectively binds to erythroblastic stem cells. These comprise approximately 100 gm in a 70 kg man (11). If all the bone marrow activity went specifically to this subset of cells their dose would be approximately 0.04 Gy of which about 60% is contributed by the Auger electrons. The associated risk would presumably be primarily a "red cell leukaemia", e.g. erythraemic myelosis. There is no evidence from studies such as the A-bomb survivors that such a leukaemia is radiation linked. Moreover Goodwin (28) has shown that indium is unlikely to go to the marrow via the transferrin route. At physiological pH the released metal ions are more likely to form insoluble hydroxide colloidal particles that concentrate in the reticuloendothelial system. On balance we feel that the possibility of indium going selectively to bone marrow stem cells does not contribute greatly to overall risk.

CONCLUSIONS

The dose to other body tissues from the X- and γ -rays emitted from the labelled leucocytes would seem to be the major contributor to risk. The high level of risk which ten Berge et al (3) proposed due to the injection of highly labelled cells is, in our opinion, invalid. Making pessimistic assumptions the associated risk of a cancer arising from one of these cells is no greater than that from the whole-body exposure and in reality, we

believe, considerably lower. If the ICRP recommended scheme for deriving effective dose equivalent is followed, the lifetime dose to the patient appears to fall within the range although towards the higher end, of dose equivalents which have been calculated for diagnostic uses of other radiopharmaceuticals (29).

Another way to view the doses is to consider how they compare with the limits set for human volunteer experiments. Using 500 mCi the indium labelling procedure would appear to fall within the limit for category III type experiments as defined by the World Health Organisation (30).

REFERENCES

1. McAfee J G and M L Thakur. Survey of radioactive agents for in vitro labeling of phagocytic leukocytes. 1. Soluble agents. *J. Nucl. Med.* 17, 480-487, (1976).
2. Thakur M L, J P Lavender, R N Anot, D J Silvester and A W Segal. Indium-111 labeled autologous leukocytes in man. *J. Nucl. Med.* 18, 1014-1021, (1977).
3. ten Berge R J M, A T Natarajan, M R Aardeman, E A van Royen and P Th A Schellekens. Labeling with indium-111 has detrimental effects on human lymphocytes: concise communication. *J. Nucl. Med.* 24, 615-620, (1983).
4. Annals of the ICRP. Publication 38 Radionuclide transformations Energy and intensity of emissions Pergamon Press. Oxford-New York-Frankfurt. pp 344, (1983).
5. ICRU Report 37 Stopping powers for electrons and positrons, (1984).
6. Annals of the ICRP 1 (3) ICRP Publication 26 Recommendations of the International Commission on Radiological Protection, (1977).
7. Wagstaff J, C Gibson, N Thatcher, W L Ford, H Sherma and D Crowther Human lymphocyte traffic assessed by indium-111 oxine labelling: clinical observations. *Clin. Exp. Immunol.* 43, 443-449, (1981).
8. Lavender J P, J M Goldman, R N Arnot and M L Thakur. Kinetics of indium-111 labelled lymphocytes in normal subjects and patients with Hodgkin's disease. *British Medical Journal* 2, 797-799, (1977).
9. Goodwin D A, R A Finston and S I Smith. The distribution and dosimetry of In-111 labeled leukocytes and platelets in humans. Proceedings of the Third International Radiopharmaceutical Dosimetry Symposium FDA81-8166, 88-101, (1980).
10. Snyder W S, M R Ford, G G Warner and Watson S B. NM/MIRD Pamphlet No 11 "S" Absorbed dose per unit cumulated activity for selected radionuclides and organs pp 164, (1975).
11. ICRP Publication 23, Report of the task group on Reference Man, (1974).
12. Johansson L, S Mattsson and B Nosslin. Effective dose equivalent from radiopharmaceuticals *Eur. J. Nucl. Med.* 9, 485-489, (1984).
13. Dacie J V and S M Lewis. Practical Haematology. Fifth Edition published Churchill Livingstone pp 13, (1975).
14. Grilli G, F Carbonell and T M Fliedner. Variations in erythroid and myeloid progenitor cell numbers in normal human peripheral blood. *Brit. J. Haematol.* 44, 679-681, (1980).
15. Lloyd D C, R J Purrott, Dolphin G N, Bolton D, Edwards A A and Corp M J. The relationship between chromosome aberrations and low LET radiation dose to human lymphocytes. *Int. J. Radiat. Biol.* 28, 75-90, (1975).
16. Edwards A A and Lloyd D C. On the prediction of dose rate effects for dicentric production in human lymphocytes by X- and γ -rays. *Int. J. Radiat. Biol.* 37, 89-92, (1980).

17. Thakur M L, A W Segal, L Louis, M J Welch, John Hopkins and T J Peters. Indium-111 - Labelled cellular blood components: Mechanism of labelling and intracellular location in human neutrophils. *J. Nucl. Med.* 18, 1022-1026, (1977).
18. James S E, C F Arlett, M L H Green and B A Bridges. Radiosensitivity of human T-lymphocytes proliferating in long term culture *Int. J. Radiat. Biol.* 44, 417-422, (1983).
19. Grilli G, W Northdurft and T M Fliedner. Radiation sensitivity of human erythropoietic and granulopoietic cells in the blood and in the bone marrow *Int. J. Radiat. Biol.* 41, 685-687, (1982).
20. Bedford J S and E J Hall. Survival of HeLa cells cultured in vitro and exposed to protracted gamma-irradiation. *Int. J. Radiat. Biol.* 7, 377-383, (1963).
21. Cox R, J Thacker and D T Goodhead. Inactivation and mutation of cultured mammalian cells by aluminium characteristic ultrasoft X-rays II Dose responses of Chinese hamster and human diploid cells to aluminium X-rays and radiations of different LET. *Int. J. Radiat. Biol.* 31, 561-576, (1977).
22. Hall E J. Radiobiology for the Radiologist. 2nd edn pub Harper and Row pp 361, (1978).
23. NRPB Report P/2(Rev). Sizewell B Inquiry. The biological bases of the assumptions made by NRPB in the calculation of health effects (1983).
24. Sharpe H B A, G W Dolphin, K B Dawson and E O Field. Methods for computing lymphocyte kinetics in man by analysis of chromosomal aberrations sustained during extracorporeal irradiation of blood. *Cell Tissue Kinetics* 1, 263-271, (1980).
25. Quesenberry P and L Levitt. Haematopoietic stem cells. *New England J. Medicine* 301, 755-761, (1979).
26. Wintrobe M M, G R Lee, D R Boggs, T C Bithell, J W Athens and J Forester. *Clinical Haematology* 7th edn pub Lea & Febiger, Philadelphia (1974).
27. Touya J J, O E Anselmi, R F Riley and L R Bennet. Metabolism of indium-111 - transferrin as a measure of bone marrow activity in Dynamic Studies with Radioisotopes in Medicine 1974. Proceedings of a Symposium, Knoxville 15-19 July 1974, IAEA, (1975).
28. Goodwin, D A. Recent advances in radiopharmaceuticals: Indium-111 and gallium-67 radiopharmaceuticals. *Nuclear Medicine and Biology* 2, 1199-1200, (1982).
29. UNSCEAR. Report to the General Assembly. Ionising radiation: sources and biological effects pp 358, (1982).
30. WHO. Use of ionising radiation and radionuclides on human being for medical research, training and non-medical purposes. Tech. Report Series 611, (1977).

DISCUSSION

MOUNTFORD: I should like to make two comments concerning the risk to a patient after re-injection of In-111 leukocytes. Firstly, one of the aims of the leukocyte-labeling procedure is to minimize the platelet contamination of the final cell suspension. This is achieved by low speed centrifugation which also has the effect of losing many of the lymphocytes because of their smaller size compared to leukocytes. The overall recovery of lymphocytes in the labeling procedure is much less than the overall recovery of leukocytes; therefore, the risk to the patient from irradiated lymphocytes is even less than that given in these papers. Secondly, in evaluating the overall risk, it should also be taken into account that an In-111 leukocyte scan in many cases is a life-saving investigation.

VARIATIONS IN ABSORBED DOSES FROM ^{51}Cr IN INVESTIGATIONS WITH LABELLED ERYTHROCYTES

P. Roth, E. Werner, K. Henrichs

Gesellschaft für Strahlen- und Umweltforschung

Paul-Ehrlich-Str. 20

D-6000 Frankfurt am Main, FRG

U. Elsasser, A. Kaul

Bundesgesundheitsamt, Institut für Strahlenhygiene

Ingolstädter Landstr. 1

D-8042 Neuherberg, FRG

ABSTRACT

In nuclear medicine ^{51}Cr labelled red blood cells are used to determine erythrocyte volume, red cell survival, or the site of red cell destruction. We examined the variations in absorbed doses from ^{51}Cr in 77 patients with various diseases in whom erythrokinetic investigations were performed for diagnostic purposes. Autologous erythrocytes were incubated with Na_2CrO_4 (37 kBq (1.0 μCi) $^{51}\text{Cr}/\text{kg}$ body weight) and injected intravenously. ^{51}Cr activity in blood was then followed for 10 weeks. ^{51}Cr activity over liver, spleen, and sacrum and whole-body retention of ^{51}Cr were measured for the same period. A compartmental model was assumed to describe the kinetics of ^{51}Cr tagged to red blood cells. It is a noncirculating linear model with the compartments represented by organs (spleen, liver, bone, residual body) rather than physiological compartments. The computer program SAAM-25 was used to provide the kinetic parameters and the organ retention functions. From the cumulated activities of the source regions, organ doses and effective dose equivalents were calculated according to the MIRD concept. The highest organ doses were found for spleen, liver, and red marrow. The bone marrow doses were comparable in all diseases studied; the mean values ranging from 2.6 nSv/Bq (iron deficiency) to 3.9 nSv/Bq (haemolytic anaemias). Similar doses were found for the spleen, with the exception of haemolytic anaemias (mean value 16.8 nSv/Bq; range 11.0 - 20.2 nSv/Bq). The liver doses are about half that of corresponding spleen doses (haemolytic anaemias about one fifth) but otherwise show a similar distribution (mean values between 1.2 and 2.2 nSv/Bq). The doses to the kidneys and the lungs are comparable to those for the liver but with smaller variations within and between the groups of patients. Lower doses were found for the gonads and the bones (mean values between 0.3 and 0.5 nSv/Bq; individual values ranging from 0.1 to 0.7 nSv/Bq). Mean values for the effective dose equivalent D_E are uniform (1.0 to 1.2 nSv/Bq) with the exception of haemolytic anaemias, where it was 2.2 nSv/Bq. Individual D_E values range from 2.0 to 2.7 nSv/Bq in haemolytic anaemias and 0.6 to 1.7 nSv/Bq in the other diseases. The calculated dose values for ^{51}Cr found in this study confirm only partly the values reported in ICRP Publication 17, but are higher up to a factor of 9 for some organs.

INTRODUCTION

^{51}Cr labelled red blood cells are widely used to determine erythrocyte and blood volume (1), red cell survival (2), or the site of red cell destruction (3). In clinical use the latter is mostly performed to decide whether splenectomy would be of benefit. Differences in the effective half-life of ^{51}Cr in the blood and different distribution and retention patterns in pathological conditions may significantly affect the radiation doses to the patients. We examined the variations in absorbed doses from ^{51}Cr in patients with different diseases in whom ^{51}Cr labelled red blood cells were administered for diagnostic purposes.

PATIENTS

A total of 77 patients was investigated. The distribution of the patients according to diagnosis is shown in Table 1.

Table 1. Distribution of patients investigated according to diagnosis

DIAGNOSIS	NUMBER OF PATIENTS
HYPOLASITC ANAEMIA	12
DYSERYTHROPOIETIC ANAEMIA	8
HAEMOLYTIC ANAEMIA	4
RENAL FAILURE WITHOUT DIALYSIS	28
RENAL FAILURE HAEMODIALYSIS	9
RENAL FAILURE PERITONEAL DIALYSIS	12
IRON DEFICIENCY	4
TOTAL	77

EXPERIMENTAL PROCEDURE

The labelling of the erythrocytes with radiochromium was performed according to the recommendations of the ICSH (2). A sample of autologous red cells was incubated with Na_2CrO_4 (37 kBq $^{51}\text{Cr}/\text{kg}$ of body weight) for 20 minutes at 37° C. After stopping the uptake process with 50 mg of ascorbic acid, the suspension was re-injected intravenously. During the following hour three blood samples were drawn to determine the blood volume. For the purpose of this study the ^{51}Cr activity concentration in the blood was measured for 10 - 12 weeks, in contrast to routine red cell survival studies, in which investigation periods of 2 - 4 weeks are sufficient, to determine the "apparent half-time" of ^{51}Cr in the blood. Sequential in vivo organ measurements over liver, spleen, and sacrum with a special organ counting device (4) were performed also for 3 - 4 months. For medical purposes, surface counting data are interpreted only qualitatively. In clinical use only the ratio of gross counts obtained over spleen and liver (spleen/liver ratio) or the excess counts with respect to the initial values are used as an index of red cell sequestration in the respective organs. For the dose calculations, however, it was necessary

to determine absolute values of ^{51}Cr activity in the organs. This required extensive calibration measurements for the counting device used. Whole-body retention of ^{51}Cr was measured for the same period by means of a human body counter (5).

^{51}Cr KINETICS

A compartmental model was assumed to describe the kinetics of ^{51}Cr tagged to red blood cells. The model, shown in Figure 1, is based on several assumptions.

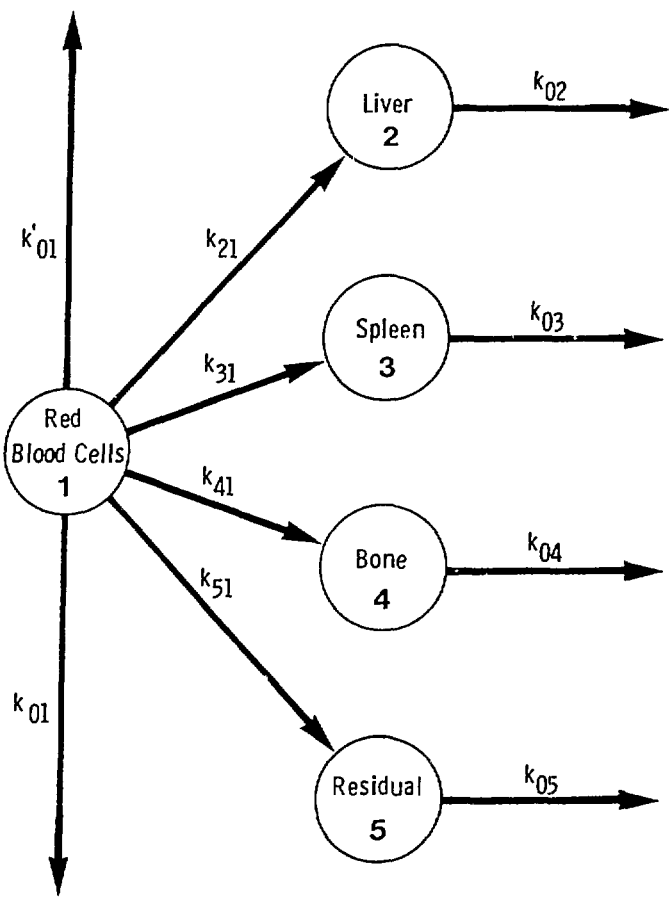


Fig. 1 Compartmental model used to describe ^{51}Cr kinetics in man. k_{01} = elution rate from red blood cells = 0.0094/day (8), k'_{01} = excretion rate due to blood loss, k_{ij} = fractional uptake rates, k_{0i} = fractional excretion rates.

It is a non-circulating model with all ^{51}Cr in red blood cells (compartment 1) at zero time. On the basis of present data it is reasonable to assume that ^{51}Cr eluted from labelled red cells in the circulation is quickly cleared from the body and not deposited elsewhere (6). Since there are no accurate data for ^{51}Cr elution in disease states (7), we assumed the elution rate k_{01} to be constant with a mean value of 0.0094/day (8). A direct excretion of ^{51}Cr from the red cell compartment occurs in patients with occult blood losses. In the present study, these excretion rates k'_{01} were determined individually by blood loss measurements with ^{59}Fe (9), performed over the whole period of investigation. All other loss of ^{51}Cr from the circulation is assumed to be due to destruction of red blood cells. The parameters k_{21} to k_{51} are the rate constants associated with red cell sequestration by the liver, the spleen or other tissues. It is further assumed that the ^{51}Cr is excreted directly from the organ of deposition(at the rates k_{02} to k_{05}) without redistribution. Uptake and clearance rates are assumed to be proportional to the amount of ^{51}Cr in the compartment (first order processes). Consequently ^{51}Cr kinetics is described by a set of linear first order differential equations with constant coefficients:

a) blood compartment:

$$\frac{d}{dt} Q_1(t) = -k \cdot Q_1(t) \quad (I)$$

where $k = k_{01} + k'_{01} + k_{21} + k_{31} + k_{41} + k_{51}$ is the disappearance of ^{51}Cr from the circulating red blood cells (compartment Q_1), and

b) tissue compartments:

$$\frac{d}{dt} Q_i(t) = k_{ij} \cdot Q_1(t) - k_{oi} \cdot Q_i(t) \quad (i=2,3,4,5) \quad (II)$$

where $Q_i(t)$ is the ^{51}Cr activity in the tissue compartment i , k_{ij} is the fractional uptake rate, and k_{oi} is the excretion rate.

From the blood data, the external organ measurements and the whole body retention of ^{51}Cr , the transfer rate constants were determined for each subject by use of the computer program SAAM25 (Simulation Analysis And Modelling) (10). The program determines iteratively a set of parameter values by a non-linear least square fitting procedure that provides a best fit of the model to the experimental data. The quantitative analysis of the external organ measurements requires a careful calibration of the counting device to correct for different dimensions of the organs, different depths of tissue and count rate contribution from other organs (4). The measurements over the sacrum provided indirect but strong evidence for a significant chromium accumulation in the skeleton. (The counts obtained over the sacrum provide only a relative estimate of the ^{51}Cr and can not be converted into absolute activity units). The contributions of spleen and liver to the total tissue ^{51}Cr (whole body retention minus blood activity) were remarkably low in most patients. After 2 - 3 months, spleen ^{51}Cr was usually $\leq 20\%$ and liver $^{51}\text{Cr} \leq 30\%$ of the total tissue ^{51}Cr at that time. The ^{51}Cr not found in spleen, liver or circulating red cells was attributed to the compartments 4 (bone) and 5 (residual) in a 1:1 ratio.

DOSE CALCULATIONS

The calculations of absorbed doses were based on the method described in MIRD Pamphlet No. 1, revised (11). The mean absorbed dose $\bar{D}(r_k)$ in any target region r_k is given by:

$$\bar{D}(r_k) = \sum_h \tilde{A}_h \cdot S(r_k \leftarrow r_h) \quad (III)$$

where \tilde{A}_h is the cumulated activity in source region r_h , $S(r_k \leftarrow r_h)$ is the absorbed dose in r_k per unit cumulated activity in r_h , and h is the number of source regions. The source regions for ^{51}Cr were liver, spleen, bone, lung, kidneys and residual body.

From the organ doses, the effective dose equivalent D_E was calculated by:

$$D_E = \sum_k w_k \cdot \bar{D}(r_k) \quad (IV)$$

where w_k are the risk weighting factors as described in ICRP Publication No.26 (12).

The required 'S' values were taken partly from MIRD Pamphlet No. 11 (13). For those organs, for which individual organ masses were available (liver, spleen, whole body), S values corrected for these masses were used (14). Liver and spleen masses were determined sonographically at the beginning of

the investigation.

The contributions of the compartments to the activities in the source organs are shown in Table 2.

Table 2. Fractional distribution of the compartments to the activities in source organs.

SOURCE ORGANS	COMPARTMENTS				
	RED BLOOD CELLS (1)	LIVER (2)	SPLEEN (3)	BONE (4)	RESIDUAL (5)
LIVER (a)	$S_{a1} \cdot \tilde{\alpha}_1$	$1.0 \cdot \tilde{\alpha}_2$	-	-	-
LUNG (b)	$S_{b1} \cdot \tilde{\alpha}_1$	-	-	-	-
SPLEEN (c)	$S_{c1} \cdot \tilde{\alpha}_1$	-	$1.0 \cdot \tilde{\alpha}_3$	-	-
KIDNEYS (d)	$S_{d1} \cdot \tilde{\alpha}_1$	-	-	-	-
BONE (e)	$S_{e1} \cdot \tilde{\alpha}_1$	-	-	$1.0 \cdot \tilde{\alpha}_4$	-
RESIDUAL (f)	$(1 - \sum_i S_{i1}) \cdot \tilde{\alpha}_1$	-	-	-	$1.0 \cdot \tilde{\alpha}_5$

The fractions of the red blood cell compartment were taken from ICRP Publication 23 (15) corrected for the organ masses.

RESULTS AND DISCUSSION

The results of the dose calculations for ^{51}Cr are summarized in Table 3. The table shows the mean values and ranges for the most relevant organ doses and the effective dose equivalents for the different groups of patients. The highest organ doses were found for spleen, liver and bone marrow. The bone marrow doses were similar in all diseases studied, the mean values ranging from 2.6 nSv/Bq in iron deficiency to 3.9 nSv/Bq in haemolytic anaemias. Similar doses as for the bone marrow were found for the spleen, with one exception. As it was to be expected, the spleen doses were significantly higher in the patients with haemolytic anaemias. The mean value for this group was 16.8 nSv/Bq, whereas it ranged from 2.8 nSv/Bq to 3.8 nSv/Bq in the other diseases. The liver doses are lower but otherwise show a similar pattern with the highest values for the patients with haemolysis (mean 3.4 nSv/Bq) and lower and more uniform values for the other patients (mean values between 1.2 and 2.2 nSv/Bq). The doses to the kidneys and the lungs are comparable with those for the liver but with smaller variations within and between the groups of patients. The doses to the gonads and the bones are nearly the same for all groups of patients (mean values from 0.3 to 0.5 nSv/Bq, individual values ranging from 0.1 to 0.7 nSv/Bq). The mean values of the effective dose equivalent D_E are very uniform (1.0 to 1.2 nSv/Bq) with the exception of the patients with haemolytic anaemias where a mean value of 2.2 nSv/Bq was found. The individual D_E values range from 2.0 to 2.7 nSv/Bq in haemolytic anaemias and from 0.6 to 1.7 nSv/Bq in other diseases.

The present model used to interpret the ^{51}Cr data is undoubtedly an oversimplification of the actual processes. The ^{51}Cr eluted from the circulating

Table 3. Organ doses and effective dose equivalent (D_E) to patients undergoing erythrokinetic investigations with ^{51}Cr . Mean Values and ranges (nSv/Bq).

DIAGNOSIS	ORGAN DOSE (nSv/Bq)						D_E (nSv/Bq)	
	BONE MARROW	LIVER	SPLEEN	GONADS	KIDNEYS	BONE	LUNG	
HYPOPLASTIC ANAEMIA	3.2 (.8-4.8)	1.2 (.6-2.3)	3.8 (1.6-6.8)	.4 (.1-.5)	1.1 (.9-1.3)	.4 (.1-.5)	1.0 (.8-1.3)	1.1 (.6-1.5)
DYSERYTHROPOIETIC ANAEMIA	3.2 (.2-5.7)	1.8 (1.0-3.4)	2.9 (1.3-4.2)	.4 (.2-.7)	1.2 (1.0-1.5)	.4 (.2-.6)	1.1 (.8-1.2)	1.1 (.6-1.7)
HAEMOLYTIC ANAEMIA	3.9 (3.1-5.0)	3.4 (1.2-5.5)	16.8 (11.0-20.2)	.5 (.4-.6)	1.5 (1.3-1.7)	.5 (.4-.7)	1.1 (1.0-1.2)	2.2 (2.0-2.7)
RENAL FAILURE WITHOUT DIALYSIS	2.8 (1.3-4.5)	1.7 (.9-3.4)	2.9 (1.8-5.1)	.3 (.2-.5)	1.3 (1.2-1.5)	.4 (.2-.5)	1.2 (1.1-1.4)	1.1 (.7-1.4)
RENAL FAILURE HAEMODIALYSIS	3.5 (2.8-5.3)	1.8 (1.3-2.2)	3.3 (1.3-4.9)	.4 (.3-.6)	1.3 (1.1-1.4)	.4 (.4-.6)	1.2 (1.1-1.4)	1.2 (1.0-1.4)
RENAL FAILURE PERITONEAL DIALYSIS	2.6 (2.0-3.7)	2.2 (1.1-4.1)	3.5 (2.0-5.2)	.3 (.2-.4)	1.4 (1.2-1.5)	.3 (.3-.4)	1.3 (1.1-1.4)	1.1 (.9-1.4)
IRON DEFICIENCY	2.6 (2.3-3.0)	1.7 (1.3-2.0)	2.8 (2.2-3.6)	.3 (.3-.4)	1.4 (1.2-1.4)	.3 (.3-.4)	1.3 (1.2-1.3)	1.0 (.9-1.0)

red blood cells as well as the ^{51}Cr leaving the sites of the red cell destruction may to some extent be subsequently redistributed. The attribution of the tissue ^{51}Cr , not found in liver or spleen, to bones and residual body in a 1:1 ratio may be questionable. However, these errors seem to be of minor importance. Changing the bone to residual ratio to 2:1 did not significantly change the dose values.

The present study provides detailed results on absorbed doses from ^{51}Cr labelled red blood cells in different diseases. The dose values reported here confirm only in part previous estimates referenced in ICRP Publication 17 (16). The spleen doses given there (5.4 and 18.9 nSv/Bq) show a similar range of variation as our results. However, the ratio of organ doses from the present study to the ICRP values is about a factor of 3 for the liver, a factor of 7 for the gonads, and a factor of 6 for the total body. It is concluded from these comparisons that the ICRP values may underestimate significantly doses from ^{51}Cr , administered in clinical investigations.

The authors gratefully acknowledge the skillful technical assistance of Ms. H. Hahn, Ms. U. Tacke, and Mrs. B. Moock.

This work was supported in part by grant St. Sch. 757i, Bundesminister des Inneren.

REFERENCES

1. Standard techniques for the measurement of red-cell and plasma volume. A report by the International Committee for Standardization in Haematology (ICSH): Panel on diagnostic applications of radioisotopes in haematology. *Br. J. Haemat.* 25. 801 - 814, 1973.
2. Recommended methods for radioisotope red-cell survival studies. A report by the ICSH Panel on diagnostic applications of radioisotopes in haematology. *Br. J. Haemat.* 21. 241 - 250, 1971.
3. Recommended methods for surface counting to determine sites of red-cell destruction. A report by the Panel on diagnostic applications of radioisotopes in haematology of the International Committee for Standardization in Haematology (ICSH). *Br. J. Haemat.* 30. 249 - 254, 1975.
4. Roth, P. and E. Werner. Einsatz von Teilkörperzählern für Organmessungen bei Ferrokinetikuntersuchungen, in *Medizinische Physik '81*, edited by E. Bunde, pp. 737 - 741, A. Hüthig Verlag, Heidelberg, 1981.
5. Werner, E., S. M. Morsy, W. Stahlhofen, and W. Pohlitz. A whole-body counter with invariant response, in *Diagnosis and Treatment of Incorporated Radionuclides*, pp. 231, International Atomic Energy Agency, Vienna, 1976.
6. Owen, C. A., jr., A. L. Orvis, and J. M. Kiely. Sequestration of erythrocytes by rat spleen. *Am. J. Physiol.* 211. 273 - 280, 1966.
7. Cline, M. J. and N. I. Berlin. The red cell chromium elution rate in patients with some haematological disorders. *Blood.* 21. 63 - 69, 1963.
8. Szymanski, I. O. and C. R. Valeri. Factors influencing chromium elution from labelled red cells in vivo and the effect of elution on red-cell survival measurements. *Br. J. Haemat.* 19. 397 - 409, 1970.

9. Werner, E., J. P. Kaltwasser and H. W. Wahner. Occult blood loss: assessment and clinical relevance, in Nuclear Medicine: Quantitative Procedures, edited by H. W. Wahner, pp. 267 - 291, Little, Brown & Co, Boston, 1983.
10. Foster, D. M. and R. C. Boston. The use of computers in compartmental analysis: The SAAM and CONSAM programs, in Compartmental Distribution of Radiotracers, edited by J. S. Robertson, pp. 73 - 142, CRC Press, Boca Raton, Florida, 1983.
11. Loevinger, R. and M. Berman. A revised schema for calculation the absorbed dose from biologically distributed radionuclides. MIRD Pamphlet No. 1, revised, New York, Society of Nuclear Medicine, 1976.
12. Recommendations of the International Commission of Radiation Protection. ICRP Publication 26, Pergamon Press, Oxford, 1976.
13. Snyder, W. S., M. R. Ford, G. G. Warner and S. B. Watson. "S", Absorbed dose per unit cumulated activity for selected radionuclides and organs. MIRD Pamphlet No. 11, New York, Society of Nuclear Medicine, 1975.
14. Roedler, H. D. and A. Kaul. Dose to target organs from remaining body activity: results of the formally exact and approximate solution. In Radio-pharmaceutical Dosimetry Symp., HEW Publ. (FDA) 76 - 8044. pp 155 - 163, 1976.
15. Snyder, W. S. (Chairman). Report of the Task Group on Reference Man. ICRP Publications 23, Pergamon Press, New York, 1975.
16. Protection of the Patient in Radionuclide Investigations. ICRP Publication 17, Pergamon Press, Oxford, 1971.

DISCUSSION

MARCUS: Indium-111-oxine red blood cells are now used to assess red blood cell mass, half-life, and splenic sequestration at lower absorbed doses than studies with Cr-51. Red blood cell mass determination requires 15 μ Ci; half-life and splenic sequestration studies require approximately 500 μ Ci if imaging of the patient is used for the splenic sequestration.

ROEDLER: May I comment on that. As you know, collection of biokinetic data in patients always takes a long time and actually if I recall correctly, this research project was started half a decade ago. At that time indium labeling, at least in Germany, was not as common as it would now be here.

RADIOBIOLOGICAL HALF-LIVES FOR CARBON-14 AND HYDROGEN-3 LEUCINE IN MAN

Kelly L. Classic, W. Frederick Schwenk, and Morey W. Haymond.
Radiation Safety Office and Department of Pediatrics, Mayo Clinic and
Foundation, Rochester, MN, 55905.

ABSTRACT

In vivo estimates of protein metabolism in man are often made by oral or intravenous administration of leucine or its α -ketoacid, α -ketoisocaproate, labeled with ^{14}C or ^3H . Previous estimates of radiation dose from such tracers have been based on the measurement of $^{14}\text{CO}_2$ in breath. Using measurements of the decay of ^3H or ^{14}C leucine from plasma proteins, longer biological half-lives for these compounds were obtained. The estimated total-body radiation absorbed dose is 0.97 mrad/ μCi for [$1-^{14}\text{C}$]KIC (or [$1-^{14}\text{C}$]leucine) and 0.11 mrad/ μCi for [$4,5-^3\text{H}$]leucine (or [^3H]KIC). Assuming administered doses of 100 μCi each, the total-body radiation absorbed dose is still well within the limits set by the FDA for Radioactive Drug Research Committees.

INTRODUCTION

In vivo studies of protein metabolism in man frequently involve the administration of a ^3H or ^{14}C radiolabeled amino acid as tracer (1-3). One of the most frequently used compounds in such studies is the amino acid leucine or its α -ketoacid, α -ketoisocaproate (KIC). Leucine is chosen as a tracer because in man it is an essential amino acid, so that in the fasting individual estimates of its rate of appearance into the plasma may provide an estimate of protein breakdown.

When labeled leucine is administered to a human, the label enters the intracellular space where some of the tracer is rapidly converted to labeled KIC which reenters the plasma space (2, Figure 1). Similarly, labeled leucine rapidly appears in the plasma space following administration of labeled KIC (2). Recent studies in man suggest that, at least in the overnight fasted individual, intracellular transamination is not rate determining and leads to a rapidly equilibrating intracellular pool of leucine and KIC (1,3).

Once in the intracellular space, leucine can be incorporated into protein or irreversibly oxidized to CO_2 and isovaleryl coenzyme A. Previous estimates of the total-body radiation absorbed dose from the use of labeled leucine have been based on the measurement of $^{14}\text{CO}_2$ in breath following administration of [$1-^{14}\text{C}$]leucine (4). Because this technique may be associated with a large coefficient of variation at the terminal portion of the decay curve, the present studies were undertaken to obtain similar estimates of the total-body radiation absorbed dose using the decay of both ^3H and ^{14}C from plasma proteins.

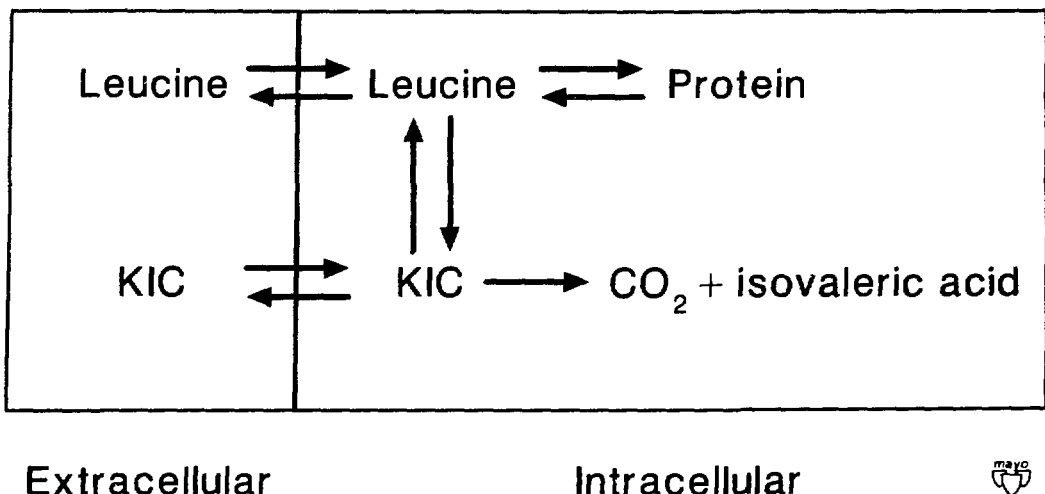


Figure 1. Intracellular interconversion of leucine and its α -ketoacid, α -ketoisocaproate (KIC). Intracellular leucine/KIC can be incorporated into protein or irreversibly oxidized.

MATERIALS AND METHODS

L-[4,5-³H]leucine (131 Ci/mmol) and L-[1-¹⁴C]leucine (>55 mCi/mmol) were obtained from Amersham (Arlington Heights, IL). α -[1-¹⁴C]KIC was enzymatically prepared from the [1-¹⁴C]leucine (5) and purified by HPLC as previously described (6), except that a 10% ethanol:90% 0.02M phosphate buffer (vol:vol), pH 7.0, was used as the liquid phase. Radioisotopic purity was determined by HPLC (6) and was > 98%. Isotopes were diluted in sterile saline, passed through a 0.2 μ m filter, and demonstrated to be sterile and pyrogen free.

ANALYSIS

To determine the ³H and ¹⁴C radioactivity in plasma, 50 μ l of plasma was placed in a 20-ml glass liquid scintillation vial (Research Products International, Corp., Mt. Prospect, IL), and 1 ml of deionized water, and 7 ml of Safety Solve^R (Research Products International Corp., Mt. Prospect, IL) were added. Radioactivity was determined in triplicate samples (Beckman LS9800 Liquid Scintillation Counter, Beckman Instruments, Inc., Irvine, CA) using the dual counting mode for 10 minutes, which corrects the radioactivity for both quench and spillover of ¹⁴C radioactivity into the ³H energy spectrum. Counting coefficient of variation was < 5%. The subject's plasma prior to the administration of radioactivity was used as a blank.

EXPERIMENTAL DESIGN

Following written informed consent, 7 normal volunteers (5 female, 2 male; aged 24 \pm 1 years, weight 64 \pm 4 kg, height 168 \pm 4 cm, mean \pm SEM) were studied in the postabsorptive state after fasting overnight. Each subject received a 4-h simultaneous infusion of [³H]leucine (207.8 \pm 4.7 μ Ci per 4 h) and [¹⁴C]KIC (70.5 \pm 5.5 μ Ci per 4 h) through a forearm vein beginning at 0800 h on the day of study. The infusions were discontinued

after 4 h (0 time). Blood samples were obtained at -1, 0, +1 and +2 h [arterialized venous blood from a superficial hand vein using the "hot hand" technique (7)] and +6 h (venous blood from antecubital fossa).

Additional blood samples were obtained by venipuncture between 0700 and 0900 on days 1, 2, 3, 6, 10, 14, 29 and 90. All blood samples were placed in tubes containing sodium EDTA, the tubes placed on ice and then centrifuged at 4°C. The plasma was stored at -70°C until assayed. In addition, during the last hour of the isotope infusion (-60, -45, -30, -15, and 0 min), expired air was collected over 1-min periods in 50-1 latex bags to determine the rate of expired $^{14}\text{CO}_2$ (2).

CALCULATIONS

The ^3H and ^{14}C radioactivity in plasma (dpm/50 μl) for each patient at each time point was divided by the maximum ^3H and ^{14}C plasma radioactivity, (respectively) obtained for that patient. Data for each isotope was then averaged at each time point to obtain the final decay curves. Curve stripping using nonlinear regression analysis was done to break each decay curve into its components (8).

Radiobiological half-lives were then determined for each component by using the radioactivity decay law. Radiation absorbed dose was calculated using these half-lives and the MIRD table of "S" factors (9). The values of "S" for ^3H and ^{14}C ($S = 1.7 \times 10^{-7}$ rad/ $\mu\text{Ci} \cdot \text{h}$ and $S = 1.5 \times 10^{-6}$ rad/ $\mu\text{Ci} \cdot \text{h}$, respectively) with total body as both source and target organ were used since the radioisotopes were considered to be distributed throughout the entire body.

All data are expressed as mean \pm SEM. Statistics were carried out using a student's t-test and standard nonlinear regression analysis.

RESULTS

Following termination of the isotope infusions, free plasma [^3H]- and [^{14}C]leucine and -KIC specific activities decreased (Figure 2) and were below the lower limits of our assay (0.25 dpm/nmol) by 6 h after the infusion. In contrast, total ^3H and ^{14}C counts in plasma continued to rise following termination of the isotope infusions and did not peak until 6 h after the isotope infusions were stopped (Table 1, Figure 3). Ninety days following termination of the isotope infusions, $10.7 \pm 0.8\%$ and $10.6 \pm 0.8\%$ of the maximal ^3H and ^{14}C plasma radioactivity, respectively, were still present (Table 1, Figure 3). Over this time period, plasma ^3H radioactivity decreased from 667 ± 40 to 73 ± 5 dpm/50 μl , while plasma ^{14}C radioactivity fell from 202 ± 9 to 21 ± 3 dpm/50 μl (Table 1).

Over the last hour of the infusion of [$1-^{14}\text{C}$]KIC [$(9.1 \pm 0.50) \times 10^3$ dpm $\cdot\text{kg}^{-1}\cdot\text{min}^{-1}$], the expired $^{14}\text{CO}_2$ was $(1.4 \pm 0.2) \times 10^3$ dpm $\cdot\text{kg}^{-1}\cdot\text{min}^{-1}$. Therefore, over this time period, $15.4 \pm 1\%$ of the infused [$1-^{14}\text{C}$]KIC appeared as $^{14}\text{CO}_2$ in breath.

Between 1 and 6 days, the ^3H radioactivity decayed ($p < 0.01$) more slowly than the ^{14}C radioactivity (Figure 3). When the decay curves were analyzed by component, each of the curves could be easily broken down into 2 components (Table 2). The breakpoint between component I and component II for ^3H and ^{14}C occurred with 58.3% and 50.3% of the maximum activity remaining, respectively. From the decay data in Table 2, the radiation

absorbed dose was calculated using MIRD tables (9) to be 0.97 mrad/ μ Ci for [$1-^{14}\text{C}$]KIC (or [$1-^{14}\text{C}$]leucine) and 0.11 mrad/ μ Ci for [$4-5-^{3}\text{H}$]leucine (or [^{3}H]KIC).

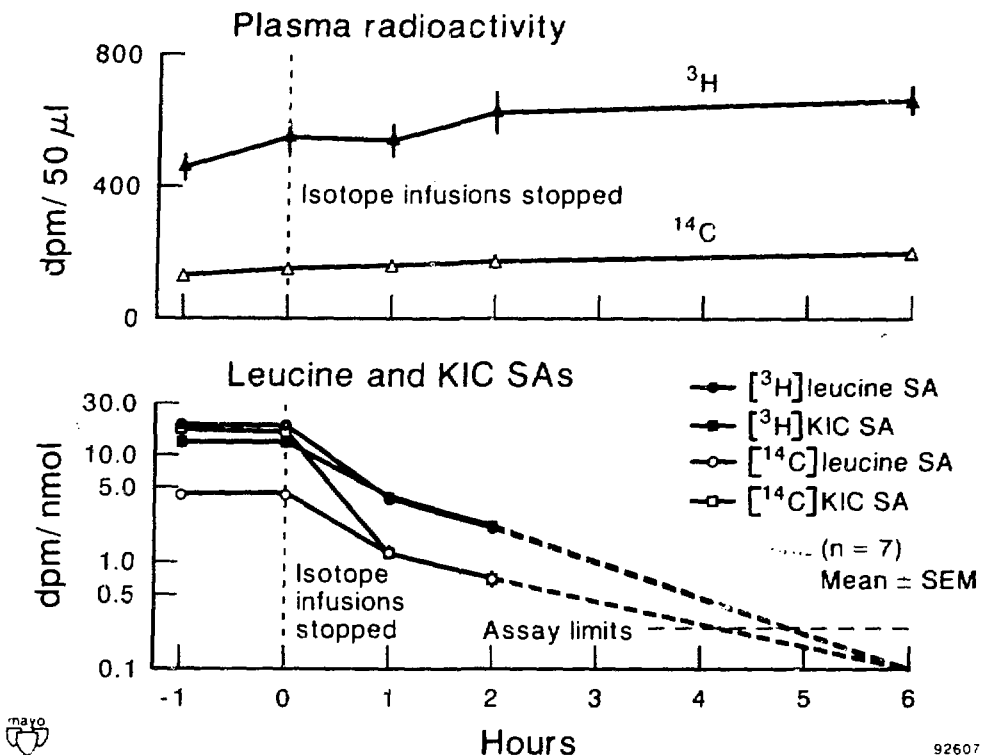


Figure 2. Decay of plasma $[{}^3\text{H}]$ - and $[{}^{14}\text{C}]$ leucine and KIC specific activities (SAs) and rise in total plasma ${}^3\text{H}$ and ${}^{14}\text{C}$ radioactivity per 50 μ l following termination of 4-hr intravenous infusions of $[4,5-{}^3\text{H}]$ leucine and $[1-{}^{14}\text{C}]$ KIC.

Table 1. ${}^3\text{H}$ and ${}^{14}\text{C}$ radioactivity in plasma expressed as dpm/50 μ l and % maximal radioactivity for 7 normal human subjects who received 4-h, i.v. infusions of $[4,5-{}^3\text{H}]$ leucine ($207.8 \pm 4.7 \mu\text{Ci}$) and $[1-{}^{14}\text{C}]$ KIC ($70.5 \pm 5.5 \mu\text{Ci}$). Isotopes were discontinued at time 0.

Time	${}^3\text{H}$ Radioactivity		${}^{14}\text{C}$ Radioactivity	
	dpm/50 μ l	% maximum	dpm/50 μ l	% maximum
-1h	458 \pm 39	66.9 \pm 2.8	130 \pm 9	63.3 \pm 3.3
0	551 \pm 45	80.0 \pm 2.3	152 \pm 11	74.6 \pm 4.5
+1h	542 \pm 48	79.7 \pm 5.3	162 \pm 15	78.9 \pm 6.2
2h	628 \pm 61	90.7 \pm 3.7	175 \pm 18	84.1 \pm 6.1
6h	667 \pm 40	97.4 \pm 1.4	202 \pm 9	98.1 \pm 3.7
1d	598 \pm 43	87.1 \pm 1.5	171 \pm 10	85.2 \pm 2.1
2d	520 \pm 42	75.4 \pm 1.7	143 \pm 9	68.9 \pm 2.2
3d	481 \pm 35	70.1 \pm 2.1	127 \pm 7	61.9 \pm 2.3
6d	398 \pm 35	57.9 \pm 1.9	100 \pm 6	51.0 \pm 1.7
10d	357 \pm 35	51.6 \pm 2.3	94 \pm 6	45.4 \pm 2.1
14d	348 \pm 23	44.9 \pm 1.2	80 \pm 4	39.8 \pm 1.6
29d	207 \pm 15	30.6 \pm 1.3	61 \pm 3	29.9 \pm 2.0
90d	73 \pm 5	10.7 \pm 0.8	21 \pm 3	10.6 \pm 0.8

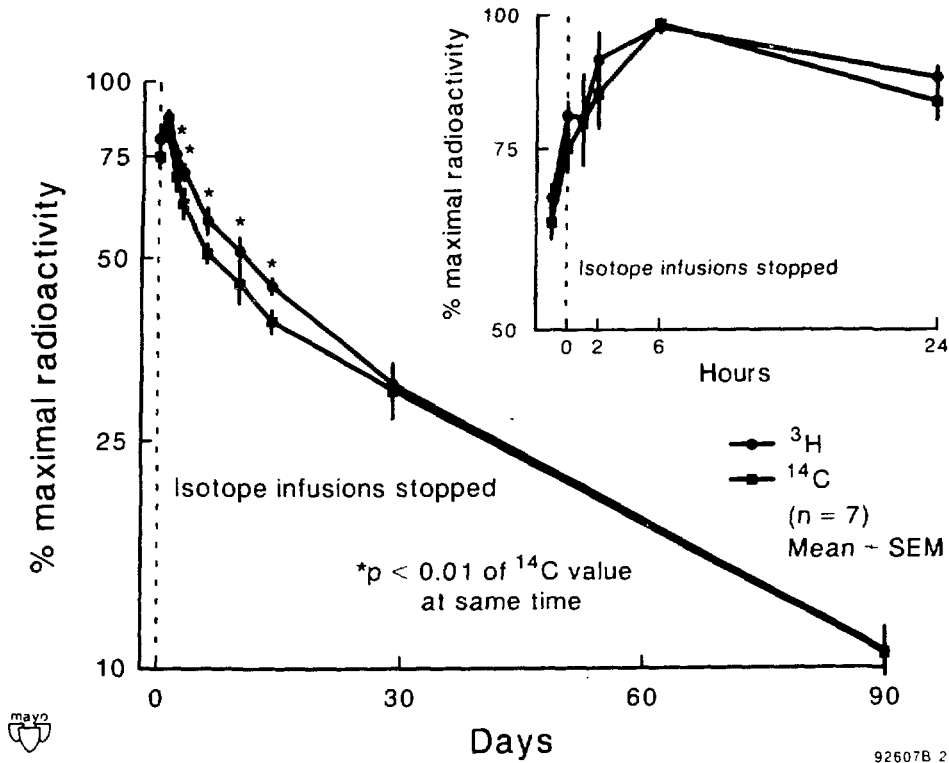


Figure 3. Decay of ^3H and ^{14}C radioactivity from plasma expressed as % maximum following 4-hr infusions of [$4,5-^3\text{H}$]leucine and [$1-^{14}\text{C}$]KIC in 7 normal human subjects. Insert shows decay during first 24 hours.

Table 2. Half-life components I and II for the decay of ^3H and ^{14}C radioactivity from plasma when administered as $[^3\text{H}]$ leucine and $[^{14}\text{C}]$ KIC over 4 hrs in 7 normal human subjects.

	Component I	Component II
[^3H] Radioactivity	8.3 ± 1.2 days*	26.6 ± 3.4 days
[^{14}C] Radioactivity	6.2 ± 1.5 days*	30.8 ± 4.7 days

* Values different by $p < 0.01$

° Values different by $p < 0.05$

To determine the amount of nonvolatile radioactivity, plasma was dried under nitrogen and the ^3H and ^{14}C radioactivity was determined in a single subject. After nitrogen drying there was 89%, 78%, and 79% of the ^3H radioactivity left and 100%, 100%, and 98% of the ^{14}C radioactivity at 6 h, 6 d, and 28 d, respectively. Since free plasma $[^3\text{H}]$ - and $[^{14}\text{C}]$ leucine and -KIC radioactivity was essentially below limits of detectability, the nonvolatile radioactivity in these plasma samples most likely represents incorporation of label into plasma proteins. The volatile ^3H radioactivity is most likely attributable to $^3\text{H}_2\text{O}$ removed in the drying process.

DISCUSSION

The present data verifies that infused traces of leucine are incorporated into plasma proteins and suggests that previous estimates of the radiation absorbed doses for [^3H]leucine (or [^3H]KIC) and [^{14}C]leucine (or [^{14}C]KIC) have been too low. In particular, the component II half-life for ^{14}C in our study was nearly 1.5 times longer than previous estimates derived from expired $^{14}\text{CO}_2$ measurements (4) and 3 times longer than the effective half-life reported in ICRP 2 (10). The difference between our results and those obtained using expired $^{14}\text{CO}_2$ can be explained by the large coefficient of variation for the latter method at the terminal points in the decay curve.

When the half-lives for [^{14}C]KIC and [^3H]leucine determined in this study are used to calculate radiation absorbed doses, assuming 15.4% of the administered KIC dose has already left the body as $^{14}\text{CO}_2$ during the isotope infusion, the ^3H and ^{14}C values obtained are 35.5% and 46.4% higher, respectively, than the estimates obtained using MIRD tables and 30.9% and 43.3% higher than the radiation absorbed doses for [^3H] and [^{14}C]leucine, respectively, obtained using ICRP 2 (Table 3).

Table 3. Comparison of estimated radiation absorbed doses in man for [$4,5-^3\text{H}$]leucine (or [$4,5-^3\text{H}$]KIC) and [$1-^{14}\text{C}$]KIC (or [$1-^{14}\text{C}$]leucine)

Study	Determination of $T_{\frac{1}{2}}$	Radiation Absorbed Doses (mrad/ μCi)	
		^3H	^{14}C
Present Study	Decay of radioactivity from plasma proteins	0.11	0.97
Bothe, et al.	Decay of $^{14}\text{CO}_2$ in breath	--	0.80
ICRP 2	Total body (10)	0.076	0.55
MIRD	(Using ICRP 2 half-lives)	0.071	0.52

The half-lives for both ^3H and ^{14}C plasma radioactivity are longer than the plasma half-lives of albumin and immunoglobulin G, the major proteins in plasma [$T_{\frac{1}{2}} = 19$ days and 21 days, respectively (11)]. Since only plasma was sampled in the present study, and since incorporation of labeled leucine into other body proteins with even longer half-lives may occur, our calculations may still be underestimates of the radiation absorbed dose. For an administered dose of 100 μCi of [$1-^{14}\text{C}$]leucine (or [$1-^{14}\text{C}$]KIC) and 200 μCi of [$4,5-^3\text{H}$]leucine (or [$4,5-^3\text{H}$]KIC), the total-body radiation absorbed dose is still well within the limits set by the FDA for Radioactive Drug Research Committees (12).

ACKNOWLEDGMENTS

The authors wish to thank Carol Van Huysen, Collette Schmidt, and Edith Rubanyi for their technical assistance, and Marylee Campion for her secretarial help. This work was supported by Public Health Service Grants AM-26989 and RR585 and by the Mayo Foundation. Dr. Schwenk was supported by Public Health Service Grant AM-07352.

REFERENCES

1. Schwenk, W.F., E. Tsalikian, B. Beaufrere, and M.W. Haymond. Recycling of an amino acid label with prolonged isotope infusion: implications for kinetic studies. *Am. J. Physiol.* 248:E482-E487, 1985.
2. Tessari, P., E. Tsalikian, W.F. Schwenk, S.L. Nissen, and M.W. Haymond. Effects of [¹⁵N]leucine infused at low rates on leucine metabolism in humans. *Am. J. Physiol.* 249:E121-E130, 1985.
3. Schwenk, W.F., B. Beaufrere, and M.W. Haymond. Use of reciprocal pool specific activities to model leucine metabolism in man. *Am. J. Physiol.* In press.
4. Bothe, A., L.L. Moldawer, B.R. Bistrian, and G.L. Blackburn. Radiation hazard of L-[1-¹⁴C]leucine in studies of protein metabolism. *Clin. Res.* 28:386A, 1980.
5. Rudiger, H.W., U. Langerbeck, and H.W. Goedde. A simplified method for the preparation of [¹⁴C]labeled branched chain beta-oxoacids. *Biochem. J.* 126:445-446, 1972.
6. Nissen, S.L., C. Van Huysen, and M.W. Haymond. Measurement of branched chain amino acids and branched chain α -ketoacids in plasma by high performance liquid chromatography. *J. Chromat.* 232:170-175, 1982.
7. Abumrad, N.N., D. Rabin, M.P. Diamond, and W.W. Lacy. Use of a heated superficial hand vein as an attractive site for measurements of amino acid concentrations and for the study of glucose and alanine kinetics in man. *Metabolism.* 30:936-940, 1981.
8. Steel, R.G.D., J.H. Torrie. *Principles and procedures of statistics*, 1st Edition, p 161-181, McGraw-Hill Book Co., New York, 1960.
9. Snyder, W.S., M.R. Ford, G.G. Warner, and S.B. Watson. "S," absorbed dose per unit cumulated activity for selected radionuclides and organs, in MIRD pamphlet No. 11, p 12-13, 18-19, Society of Nuclear Medicine, New York, NY, 1975.
10. Recommendations of the ICRP. Report of committee II on permissible dose for internal radiation, ICRP Publication 2, p 154-156, Pergamon Press, Oxford, 1959.
11. Rapaport, F.I. *Physiological basis of medical practice*. p 337, J.B. West ed. Williams & Wilkins. Baltimore, MD, 1985.
12. Code of Federal Regulations. Prescription drugs for human use generally recognized as safe and effective and not misbranded: drugs used in research. U.S. Food and Drug Administration 21CFR361.1, p 161-162, 1981.

SYMPOSIUM SUMMARY BY ROGER CLOUTIER

This symposium was sponsored by the Department of Energy and the Food and Drug Administration, as were the preceding symposia held in 1969, 1976, and 1980. Once again the symposium has accomplished its goal of information exchange and of creating new ideas that will be useful in the solution of complex internal dosimetry problems. The credit for this success not only belongs to the program committee and the speakers but to the audience which has also contributed a great deal. The audience, however, doesn't consist of only the 150 of us at the meeting but includes the larger audience that will read and use the proceedings of this meeting. In fact, several dosimetrists have told me that the work they presented at this meeting resulted from information or ideas generated at a previous symposium. At each symposium, speakers have presented results that immediately led to new ideas which led to more results and yet more ideas.

We are all striving to get a better estimate of the radiation absorbed dose. The dosimetrist's real goal is the clarification of the relationships between interactions of radiation with matter and the biological effects by which we generally mean detrimental effects. Dosimetrists are searching for ways to describe the risks. If we were absolutely sure there are no risks associated with radiation, we wouldn't need to hold this meeting. We know there are risks even if it is tough to quantify them. We also know that without good dosimetry the risk can not be properly evaluated.

Dr. Wagner introduced this meeting by talking about the benefits and risks of nuclear medicine. He explained that measurements of risk - that is, the dose and the effects - are difficult but the measurements of benefits are also very difficult. The introduction of new radionuclides, radiopharmaceuticals, and instrumentation has changed the questions that we now ask and the results that we seek. In the past the nuclear medicine community was usually content to consider only macrodosimetry questions. Dr. Adelstein showed that when you use an intracellular agent such as thallium-201 the observed biological effects may be different from those of an extracellular agent even though the same "gross" or average organ dose is given. The difference appears to be related to the effect of Auger and Coster-Kronig electrons, types of electrons that were only beginning to be considered at the 1980 symposium. Several papers that followed Dr. Adelstein's paper dealt with microdosimetry, obviously becoming an important topic. I was impressed with how Monte Carlo calculations can tell us so much about dosimetry on the microscale as they do on the macroscale. Obviously a great deal of study will be needed before we learn to properly use microdosimetry as a measure of risk. On the microdosimetry scale, doses may be in the thousands of rads. Just how should we handle this information?

Since our last symposium, the positron camera and SPECT systems have come into their own. These two instrumentation technologies have helped to provide quantitative distribution and retention data. Not too many years ago, we had to make lots of assumptions about the activity in the body. Development of these instruments can help us do our job much better. Several of the speakers presented the type of information we need, but we still lack a great deal of data on distribution and retention. A concerted effort needs to be undertaken to collect such data now that we have the tools. I believe that centers for data collections will need to be established.

Dr. Gilday gave us his thoughts about using radiopharmaceuticals in children. At the time he was talking, I was examining the cover of our program which has an inverted pyramid supported by the fetus and the child. The dosimetry of radiopharmaceuticals in pregnant women and children needs to have high priority. The delayed effects of radiation and the long life expectancy of the fetus or child now causes us to use great caution when administering radionuclides or even to choose not to use radionuclides at all. These decisions could result in a missed diagnosis and thus lead to a shortened life expectancy.

Because the radiation dose is frequently the key as to whether or not a test is done, it behooves us to be careful with our dosimetry. Several groups are working on this problem including the groups in West Germany reported on by Dr. Roedler, in the United Kingdom reported on by Dr. Mountford, and in the Netherlands reported on by Dr. Marcuse. We are making progress, but the problems will be with us for a long time.

Someone reminded me that the use of short-lived nuclide generators was once considered by knowledgeable experts to be unfeasible. Several papers at this meeting described the use of generators for producing ultrashort-lived radionuclides eluted off the generator and immediately infused into the patient. These ultrashort-lived radionuclides allow many new studies to be performed but are not without risks. We heard about a new dosimetry problem, the high dose at the point of entry. We heard about the multiple studies which now become much easier to do because the short-lived nuclide disappears quickly, but multiple studies can add up to a large dose. We also heard about the problem of contaminants on the total dose. Evelyn Watson's paper showed the influence contaminants have on the dose.

Several excellent papers were presented on what I shall call biochemistry. Because the future of nuclear medicine may well deal with the metabolism of unique biochemicals, the field of radiopharmaceutical dosimetry will have to follow. The idea of doing dosimetry for neuronal synapses is extremely challenging.

Commander Abel told us that FDA's role is to safeguard the public, a really difficult role, but one that all of us recognize as necessary. When Dr. Marcus told us about the dosimetry consideration in patients with renal pathology, she also told us that she did not agree with how some radiopharmaceuticals were being used. Her concern should be our concern. We need to use the right product for the right purpose. Dr. Croft showed us dosimetry results that indicated different types of large particle preparations give different radiation doses.

Dr. Shani showed us that drugs can alter the distribution of radionuclides and that the radiopharmacist is not just a supplier of radiopharmaceuticals. The radiopharmacist can help explain why certain results occur. Dr. Goodwin showed how improved images can be obtained by using a chelate chase. His paper and several others dealt with monoclonal antibodies which may provide an extremely high tumor-to-normal tissue ratio. While the microdosimetry problem associated with monoclonal antibodies will test us severely, conventional dosimetry cannot be overlooked. Drs. Eckerman, Bigler, Kwok, Poston, Chen, and many others offered improvement in the anthropomorphic model, our calculational techniques, and the kinetic models used for absorbed dose calculation. Each improvement moves us closer to the right answer. A model, however, gives us only the dose to the model and suggests only the possible dose to the patient.

Not too many years ago, speakers at meetings like this would exclaim "Look what my computer did!" Today the computer is just another tool to help us do our work. I should mention another change that has occurred: the switch from

conventional to SI units. We used both types of units at this meeting and also talked about rads and effective rads as well as sieverts and the effective dose equivalent in sieverts. Trying to keep track of all these units is difficult, but because the transition is occurring and there is little we can do about it, we had better move with it. The National Council on Radiation Protection and Measurement (NCRP) recently issued Report No. 82, in which they recommended that the United States switch to SI units by 1989. That's approximately the time of our next meeting, so at our next meeting be prepared to talk in becquerels, grays, and sieverts.

I also want to make a comment about the number of significant figures. Sometimes I may question the validity of one significant figure, but I don't know how to get by with less than one. Two significant figures give me no real trouble; but when I see four and five significant figures, I start to feel anxious. I am not really worried that somebody might misunderstand the results and read more into them than they deserve, but I believe that, if we as dosimetrists understand the significance of the significant figures, we will use greater care in reporting our results.

Although I can't mention all of the papers and the authors, we owe them a sincere thanks. We also thank the questioners for they also stimulated ideas. I want to close by mentioning Dr. Brill's paper on the thyroid cancer in the Marshall Islanders. Although the thyroid exposure was not the result of a nuclear medicine procedure, the exposure does appear to be responsible for an increased risk of thyroid cancer. This symposium started by discussing the risk of radiation. The Marshall Islanders represent a very small group that may have experienced such a risk. The number of nuclear medicine patients however, is a much larger group and it's our job as clinicians, researchers and dosimetrists to do our best to understand the dose the patient will receive so that the risk may be properly evaluated before administering the radioactive material.

Panel Discussion

CLOUTIER: We'll end this meeting with a panel discussion primarily to give people an opportunity to hear some experts discuss their thoughts about dosimetry now and in the future. But we also want to give the audience an opportunity to express their opinions. The panel consists of Lloyd Struttman, Mallinckrodt; Jim Robertson, Department of Energy; Norman McElroy, Nuclear Regulatory Commission; Carol Marcus, Harbor-University of California Medical Center; and Neil Abel, Food and Drug Administration.

MARCUS: Thank you very much, Roger. I was asked to speak for about five minutes, talking about problems in dosimetry from the physician's point of view, but Roger already mentioned just about everything on my list. Obviously we're both on the same wavelength, so I assume we both understand exactly what's important. I certainly share his concerns about what the dosimetry means, the numbers, and especially microdosimetry.

One thing I would like to see supported is research to look at what is happening to the DNA. Those of you who follow molecular biology may know that there are fragile sites on DNA, the breakage of which expose oncogenes. I would really like to know a little more about the molecular radiobiology and what the microdosimetry means.

As a physician, it would also help me a lot if additional dosimetry information were available to me either in the package inserts or in some easily accessible source. I think Lloyd Struttman is going to talk more about this. Roger already talked about the need for accurate dosimetry. I won't dwell on it, but we certainly do need more of it.

I think I'll let Lloyd speak now because I would be repeating what Roger said.

STRUTTMAN: When I receive a request for dosimetry information for one of our radiopharmaceutical products, it is almost always for information that is not in the product package insert. I am then left with two choices: tell the person that I do not have it or that I will search for it. "Search for it" means call Mike Stabin at the ORAU Radiopharmaceutical Internal Dose Information Center.

I would offer the following method for improving this situation. For each radiopharmaceutical currently marketed under an approved NDA, complete bio-distribution and biokinetic data should be collected for the normal human model, for altered distribution and kinetics produced by diseases, medication, lactation, age, sex difference, blocking agents, and for any other factors of consequence. These data should be used to calculate absorbed dose estimates for the fetus throughout term, the child - newborn to adult - and the adult. Absorbed dose estimates should be made for all organs, including the lens of the eye and, in those instances where there is a question of pregnancy after the administration of a radiopharmaceutical, the uterus. Dose values should be presented as ranges, reflecting the variances inherent in the distribution and kinetic data. All distribution and kinetic data should be tabulated, and all assumptions made in developing the dose estimates should be stated. To make this dosimetry information readily available to the clinical user, this

information should be compiled into a monograph or similar single reference format that would lend itself to updating. Finally, as new radiopharmaceuticals are developed and become available for routine clinical use, they should be the subject of an estimated absorbed radiation dose monograph. Thank you.

ROBERTSON: Before this session, the panel members were discussing what the panel should talk about in our introductory presentations. One question that arose was, "Why do we do dosimetry?" This is a question that would never occur to me because I think the subject is interesting in its own right, but there are certain audiences for whom it might need to be defended. One justification that comes to mind is that in diagnostic procedures dosimetry is the basis for the upper limit of the amount of activity that can be given. Sometimes there is confusion as to which organ should be used to set the upper limit. Sometimes the radiopharmaceutical is given to study one organ or structure, but the activity actually concentrates somewhere else. For example, it can affect the kidney and the bladder system or the bone marrow. This is easily overlooked by somebody that's interested in something else. In some nuclear medicine procedures, the absorbed doses do tend to creep up. It was mentioned at this meeting that as much as 10 millicuries of gallium-67 are given at some places. This becomes somewhat alarming when you realize the dose to the bone marrow that can result.

For treatment planning, the dosimetry is even more essential. The absorbed dose in the target that you are trying to treat can only be determined through dosimetry. With the new agents like monoclonal antibodies that are being developed, we are entering into unknown territory so far as the actual relationship between radiation dose and the biological effect in terms of whether it kills the tumor cells or not. At the same time that we are treating the tumor, we need to worry about what goes on in the rest of the body. This depends on the specificity of the agent.

I see dosimetry switching from what the MIRD Committee has been doing. A lot of the MIRD Committee activities have concentrated on the average dose to an organ. For many situations this is rather gross dosimetry. I think we will probably want to move toward the range of the beta or alpha particle dose; that is, at the centimeter or millimeter level. There isn't a good name for this; it isn't what people usually mean by microdosimetry, so I'll just call it small-scale dosimetry or millidosimetry.

Now, switching hats to the role of the Department of Energy in all this. One of the main things that my section of the department does is promote the development of new instrumentation that will give higher spatial and temporal resolution. Another is promote the development of new radiopharmaceuticals. I see dosimetry as being at the heart of the utilization of the new procedures that will result from these developments.

McELROY: The NRC is in a curious position here. Our charter from Congress directs us to assure public health and safety. We don't regulate the practice of medicine, but there is a very fine line we dance around. It's hard for us laymen to understand the practice of medicine, but, to protect the public, sometimes we must cross over that fine line. I recall a physician in Washington who had a radium source for treating dermatitis. When he was asked what the radiation dose he gave to his patients was, he said, "About two minutes." In spite of this type of practice, no matter what the NRC does as far as the application of radiation in medicine is concerned they don't seem to do it quite right, but they keep plugging away.

The topics that were presented here seem to me to be essential scientific information that will aid in developing radiopharmaceuticals that we will see

in the clinics in the next 10 to 20 years. Of course, the dosimetry is an integral part of this development of radiopharmaceuticals, but NRC defers to the FDA's judgment on the efficacy and safety of radiopharmaceuticals. Still, I don't want to jump up and walk away on that note. The NRC requires that physicians use radiopharmaceuticals for the clinical procedures listed on the package inserts which to some extent is regarded as regulating the practice of medicine. We have now modified this requirement to allow physicians to use the material for other indications if they follow the administration route and the chemical and physical form listed in the package insert. This alternative was provided to allow new uses even though the dosimetry for other indications has not been done.

This leads into a little commercial for great new things that the NRC has done recently. Those of you who read your Federal Register on Friday, July 26, 1985, know we published about 40 pages of material dealing with a revision of 10 CFR Part 35 on medical uses of radiation. We retained, in this proposed revision, the policy of requiring physicians to use materials as described in the package insert. We also retained several other policies that have been around for quite a long time. Those of you who are interested in the clinical use of material, and I think probably all of you are, should take some time to look at the revision and let us know where we went astray and where we did something right. I certainly would appreciate it. If you can get your hands on it, the material will be open for comment for another three or four weeks.

I see the NRC's place as standing on the sidelines making sure the developmental work is done safely, but as a health physicist and medical consumer, I encourage all of you to continue with this very important work of developing radiopharmaceuticals. Of course a lot of the work that you are doing is also going to apply to NRC's handling of the radiation dose to the worker.

If I can be allowed a postscript, although it's probably not my place to make it, the toughest job that I see in the next few years is for Carol Marcus to explain why she used to administer a thousandth of a curie but now is administering millions of becquerels. I wish her good luck.

ABEL: It's always fun to be the last person on a panel and get to say all the good things and all the bad things. As I stated in my earlier talk, the Food and Drug Administration is concerned with the safety and the efficacy of drugs. Because most radiopharmaceuticals we deal with don't exhibit any pharmacological effect, the safety evaluation for these products is primarily concerned with the radiation dose. Therefore, it is imperative, I believe, that the sponsor of an IND - the manufacturer, physician or whoever is involved in the dose estimate - list all the ways the patient can receive a dose, including the dose from radioactive contaminants, from other procedures utilized in the study, and, of course, from the principal radionuclide. Carol Marcus mentioned in her talk that the dose from repeat injections is very important, but few people include these in their estimates. Only after we have considered the total radiation dose, can I in my position or the physician in his position, or any of us for that matter, come up with the risk the patient will be subjected to and be able to do any kind of risk-benefit analysis. Therefore, I find that dosimetry is not just wanted, it's essential.

The panel was also asked to talk a little bit about the package insert. I would be interested, and I know the FDA would be interested, in comments on what new things to include, and what's wrong with the package insert. We have regulations that prescribe the way we write the package insert, but these can be changed. When we put out a package insert, we're not always aware of everything that the nuclear medicine community wants. The FDA works for the American people, and I would certainly like the user to tell me how to improve

the package insert.

We were also asked to briefly address the kind of information that should be included in articles published on radiopharmaceuticals. Personally I find it very discouraging to read an article that does not give me all the information I need to understand how the authors came to their results. I would ask publishers to tell authors that they should at least allow the reader to understand how they went from A to Z.

At this stage in a meeting, we usually look to the future. I think whatever the future brings, whether it's better programs for our computers, better models, better understanding, or new dosimetry methods, such as microdosimetry, the point is we will have a more accurate method of predicting the absorbed radiation dose from a radioactive pharmaceutical to a particular patient. In this way, the FDA and the physician will be better able to judge the benefit-risk situation. Moreover, the real winner in this whole thing is the patient. By bringing more accuracy or better predictions to a somewhat inexact situation, we can give the patient the best possible care and treatment.

In conclusion, I want to impress something upon you that has been very apparent to me for the past few years, and that's the importance of cooperation and communication. To me, each of us is like a spoke on a wheel with a patient as a hub. Without a rim on those spokes, we tend to move, but we're very rocky, we're very disjointed. That rim is our avenue of communication. That rim can be a very broad, strong rim or a very thin, weak rim. Only with conferences such as these and other educational forms can our progress be ascertained.

CLOUTIER: Does the audience have questions or comments?

WATSON: I want to address what Lloyd Struttman said about monographs, because I think something on that order is a very good idea. The Radiopharmaceutical Internal Dose Center, and Mike Stabin in particular, has many requests for the kind of information that Lloyd wants to see in one particular location. Because we answer these questions, I know how hard it is to pull the information together. You certainly don't find it in any one single place. Being on the MIRD Committee, I know how difficult it is to analyze the data and put it into a form that should be released to the public and be "in stone" as Kelly Classic said. Once information is in print, people think it is true. The mechanism for updating has to be very carefully considered in advance. Our center would be very glad to undertake this project, but it would be time-consuming and expensive.

MARCUS: It might be better, Evelyn, to put it in a computer data base because all you have to do is delete it. Nobody really believes a computer printout. It's the printed word, but you know that it's not the same, so maybe it would be easier and cheaper and surely more accessible, and easily upgradeable as well.

CLOUTIER: I want to follow up on what Neil said about publishing in journals. I understand that, when data for calculating radiation dose is in a paper submitted to a journal and the editor asks the authors to shorten the manuscript, they often elect to delete the dosimetry. I would urge the authors to keep the dosimetry and find something else to delete.

FUEGER: I want to address Mr. Cloutier's remark that in using Standard Man we're calculating the absorbed dose to a model rather than to the patient. I think most of us in nuclear medicine are absolutely aware of this fact, but a little note of historical development seems in order. The first major book on

dosimetry was published by Jerry Hine thirty years ago, in the early 50's. If you look up the rules in those days, you find that you started with an estimation of total body and gonadal dose of about 0.2 rad, and then you worked your way backward to find a limiting amount of activity to be administered. It is not happenstance that we are using 10 microcuries of iron-59, or did use it, and no more than 50 microcuries of chromium-51 when we used it, because these doses had been calculated or guessed at rather intelligently.

The rules of the game haven't really changed. At that time we considered the critical organ, and the concept was already there. For example, in the rose bengal studies, you had to think of delayed elimination such as biliary atresia, and we knew that certain organs would of necessity receive a relatively large dose.

Dr. Marcus's talk about the kidney reminds me that once upon a time it was necessary to use mercury-203 chlormerodrin for kidney imaging. This gave a slightly grilling dose to the kidney. It's been 20 years since then, and I haven't heard of any awkward or unpleasant follow-up in this matter. The basic point I want to make is that it might not be bad to remind ourselves about the historical development and add a historical note to our considerations of benefits and risks.

BRODSKY: I reminded myself occasionally in the midst of listening to all these interesting papers that my main responsibility at the NRC is worker protection. Roger Cloutier may recall that he submitted a very nice proposal to us a few years ago to study worker exposure. One of our administrators thought it wasn't necessary, so the last real study of worker exposure in hospitals where radionuclides are administered, so far as I can remember, is what the AAPM published about 10 years ago. I've not heard very much about the worker's exposure from the new radiopharmaceuticals at this meeting. Occasionally at coffee breaks, people have indicated that the use of higher quantities in terms of activity for agents with short half-lives brings up the question of the workers including the technicians and, perhaps, the attending nurse, who is frequently close to the patient or even to many patients. If we use many procedures and the same people attend the injections of the patients, these people are close to large quantities of activity because, on the average, many millicuries are administered. Is anybody keeping an eye on these workers' exposures? Also can ordinary syringes block out enough of the radiation? These are all questions I can't answer, even though I'm supposed to be specialized in worker protection. I'd also like to ask Mr. Abel if the FDA is examining the exposure to the workers in approving these radiopharmaceuticals?

MARCUS: Dr. Brodsky, you have brought up an excellent point not only for short-lived nuclides or ultrashort-lived nuclides from generators. I review the monthly badges at my institution just to make sure that nobody is getting a high exposure. One month I really had a fit when I noticed that my partner won the prize for the biggest exposure of the month. He was doing most of the research with the gold-195m generator which, as you know, has a lot of mercury in the column.

Certainly, the exposures to workers with these newer short-lived nuclides can be a real problem, but I don't know anyone that's looked into it scientifically. It's just a personal observation. For this reason I think people should consider this problem.

One point I should have made in my introductory statement was that we don't have a good way to know how much activity we are administering with some of these short-lived nuclides that are generator-produced. I would like to see an on-line detector on the generator so you can know how much daughter and how much parent contaminant is present before you infuse it.

ABEL: Dr. Brodsky, you brought up a point about which the FDA is currently concerned. The situation is really no different from using chemotherapy agent and worrying about what chemotherapy agents the person preparing the dose or administering the dose ingests, inhales, or accidentally gets injected with. That doesn't answer your question. Your organization and mine should make a concerted effort to place these values either in a pamphlet, in the package insert, or someplace where the workers can get an idea of what their exposures are going to be.

MOUNTFORD: I have a comment on Dr. Brodsky's question about dose to nursing staff. There's a paper in Nuclear Medicine Communications by Harding from Birmingham in the United Kingdom dealing with this matter.

McELROY: May I respond to the syringe shield question that Dr. Brodsky raised. There was a paper in Health Physics about four years ago that I wrote about syringe shields. When I was working on the paper, I found that a lot of syringe shield manufacturers weren't considering where the radioactive volume was and where the technician's fingers were; therefore, the shielding was in the wrong place. If you act on Dr. Brodsky's comments when you get back to the lab, please keep that in mind.

MCLEOD: With respect to operation of a PET center cyclotron we do not see anything out of the ordinary with the monthly film badge for the extremity exposure of the technicians. What is out of the ordinary is the exposure to the chemists preparing these radionuclides, such as F-18 deoxyglucose.

DAVIS: As we begin to consider these radiopharmaceuticals that deliver a significant fraction of their dose through Auger electrons and may have a very short half-life, are we finding out anything useful with traditional TLD badging and bioassay? If not, what kind of monitoring might we use?

BIGLER: Perhaps an additional urine and blood level analysis at very low levels of activity will handle the problem in conjunction with film badges or TLD.

SASTRY: As Roger Cloutier pointed out, the dosimetry considered at the Symposium four years ago was mostly macroscopic. At this Symposium, we are recognizing the need for cellular dosimetry and microdosimetry, especially in the case of Auger-electron-emitting radionuclides. We may expect to see more work along these lines at our next Symposium. I would like to draw the attention of our colleagues to the lack of information on the distribution of these Auger electron emitters - whether they are extracellular, localized in the cytoplasm or the cell nucleus, or bound to the DNA. The biological effects and dosimetry depend on this information. Dr. Marcus has urged that dosimetry be pursued at these levels in the future. I would like to emphasize the need for the distribution studies in this regard. Such studies provide interesting and valuable new research. An understanding of the dosimetry at the more microscopic levels also has important implications for therapy.

FISHER: I have a simple comment on microdosimetry. It pleases me to see this topic becoming more and more important in the dosimetry of radiopharmaceuticals. Keep in mind one basic principle: At the cellular level or at the mini-level, the dose is a highly variable number. It's important then to know a little about the variability in the average dose. Often we find that the average is very atypical of the actual value. Knowing a little about the distribution of the dose can provide a lot of information critical to the radiobiology. For example, if we know the fraction of targets, or cells or cell nuclei that are missed, this can tell us a lot about the probability of the radiation dose causing an effect. Once again, microdosimetry is really an

important topic, but the key to understanding microdosimetry is in understanding that doses to individual cells are highly variable. We need to know how to characterize this variability or the frequency distribution or the histogram or whatever you would like to call it at the microscopic level. We don't yet know how to correlate these distributions with biological effect, but that will come as we do more and more experimentation.

MITCHELL: I have two questions that are somewhat related. First, Mr. Abel mentioned that risk estimates are made at the FDA on the basis of dosimetry provided by the investigator, and I would like to know whether you could tell us about the source of the dose effect data on which your risk projections are made. Do you use the new NIH tables on probability of causation or do you have some other source you refer to?

ABEL: When we examine a proposal for a study, we look at the total risk to the population in which the drug is going to be utilized. Many variables come into play: what the investigator is trying to do, what is currently available. It is not an easy black and white situation nor is it meant to be a black and white situation. I can't give you the answer you want. You would have to present me with the situation before I could really do that.

MITCHELL: My second question relates to dose rate effects. There is a great deal of interest in total dose to the liver. About 30 years ago, it was thought that both genetic and carcinogenic effects of radiation were additive regardless of when the radiation was received. Today we know that is not the case. There is recovery from radiation effects. No one who mentioned the dose here took into consideration the dose rate effects. If you look at the data on which many risk estimates are made, they are based on radiation which is delivered in a short period of time, such as the A bomb in terms of instantaneous exposure or x-ray exposure when the dose is given over a very short period of time.

This morning I did a very quick calculation on one of the estimates. Let's say we have 15 microcuries in 10^7 cells which comes out to roughly one disintegration per cell every 20 seconds. From Dr. Wright's paper about the biophysical and the biochemical aspects of radiation, that's really a long period of time between irradiations. I wonder if we really shouldn't give some thought to the fact that radioactive materials do deliver the dose over a relatively long period of time. Because of the diminished effect with protraction or fractionation, perhaps we should crank in the dose rate effect. These doses may not be as bad as they sound on the basis of a single number.

EDWARDS: When the ICRP set their risk estimates, it was meant to be low dose, low dose-rate estimates. One or two rads is low dose, and that is already taken into account to the best of our knowledge at the moment.

CLOUTIER: Since no one is at the mike, let me return to a topic that we touched on briefly. At this meeting, people have talked about the effective dose equivalent, and the banquet speaker talked about probability of causation. I have been worried about what appears to be happening. The effective dose equivalent is an attempt to predict the risk that somebody is going to get cancer. Let's imagine I am in the nuclear medicine practice and I have a patient that just came in who has cancer. Now someone wants me to worry about predicting whether he is going to get cancer from a treatment or diagnostic study. I am not quite sure how I use probability of causation because he's already got cancer, and so I'm troubled a little bit about using weighted dose equivalents to calculate the dose to a patient who already has cancer. Did I complicate it enough? I hope so because it strikes me that making this transition is rather complicated.

EDWARDS: I agree with you. If the patient has cancer, you are going to treat him, and it would seem to me that whatever dose you are going to give that patient is quite permissible. If he has cancer, you are going to treat him even if the charts show 50% probability you will give him a cancer. That is weighing risks and benefits. At the moment his risk of dying if he is not treated is one, but if you treat him, you've got a chance of saving him. You can use effective dose equivalent to calculate your risk of giving him the treatment, but it doesn't matter what you come up with, you are going to treat him.

BRILL: I'm not sure that when you compute effective dose equivalent you are considering the number of cancers you are going to cause. In my estimation, in a nuclear medicine practice you are looking at the available alternatives. You are trying to find out something about the patient and looking for the tracer that is most likely to give you the best benefit and will have the least integrated risk when you consider the total biodistributional information and the way in which risk is partitioned. I don't know that one uses it properly for anything more than that in the practice of nuclear medicine.

FUEGER: I don't think dosimetry is only an assessment to weigh possible risks. I think it is also what the word says, measurement of dose. If you want to treat the patient, you want to know the absorbed energy. I don't think we want to know weighted averages. That is one point that I think should be made, and I wanted to know what your opinion was. The other point is that I want to get back to this idea of dose rate. When radium was first used, there was an enormous fight about ultrafractionation and protraction. One group thought you should insert the radium needle for maybe as long as 24 hours, and another school of thought was that the dose had to be delivered in a very short period of time. Now I understand that on the basis of radiobiological experiments radiotherapy is back to a very gentle form of fractionation, delivering perhaps two treatments a day over a six week period. Now with the delivery of radioactive material from a ultrashort-lived generator, it seems to me that we're delivering a very small dose in rads, but the dose rate seems to be quite high.

BRODSKY: Roger brought up the subject of the probability of causation. In connection with this, I would like to address the possibility of litigation. I have testified on both sides in cases where people are trying to prove cancers were caused by exposure to radiation, and I have been impressed with how unruly the legal system can get in this area. When you get up to talk about dosimetry in front of a jury, you must have all the detailed information and knowledge you can get on what the radiation doses were to the various parts of the body. At least you should be able to show that you made your best effort to understand the risk and benefits to the patient at the time the decision was being made.

I hope that the medical profession will not be beleaguered by any more unnecessary trauma from unreasonable cases; but looking at what has been happening, I think the pharmaceutical companies, as well as the medical profession as a whole, would be well advised to form this data bank we have been talking about and come up with data that have been honed by elegant and august bodies recommended by ICRP and NCRP and anybody else you can find to give the dose ranges. Then you will be able to speak with the best knowledge about the radiation dose received by the patient, as well as discuss whether the procedure was warranted when benefit versus risk is considered. The patient who, as Dr. Wagner pointed out, has refused a life-saving procedure, has made a tragic mistake; on the other hand, the patient who receives the procedure that may not have been entirely necessary may have a lawyer who would suggest she sue if she later gets cancer.

I think the probability of causation approach can be defeated if it is unreasonably used because we can all point to many other sources of cancer. This has been done successfully on many occasions when the jury was convinced that the dose was reasonably small for the purpose of the procedure. Every medical diagnosis depends on more than a single procedure. Am I right? I may be entirely wrong, but I understand that usually when you diagnose a disease, you have many factors to consider. It's like a detective story. If somebody who gets a procedure later gets cancer and learns from somebody else that the diagnosis could have been made by palpation, I can see the possibility for a suit. Am I off base on that?

MARCUS: Not very much, Dr. Brodsky. It's just that it gets you either way. It used to be that you could make a diagnosis of a liver tumor by feeling a rock-hard mass over the liver and that was all you had to do. Today, you can be sued for not having done an extensive workup to make absolutely sure that what you think is true is really true, so the patient may get a CT scan and a liver scan and an ultrasound or whatever. These days a jury loves a picture. I think they are into imaging sciences more than anybody. It doesn't always take a lot of tests to make a diagnosis, but to cover yourself, you have to run lots of tests.

LATHROP: I think I heard Roger suggest in his summarizing statement that it might be well to establish several centers for acquiring the quantitative data that are needed, particularly for the estimation of dose. This set me off thinking about what would go into such a laboratory and how it would be funded. I would like to hear some discussion on this.

CLOUTIER: I can't let it die right there, Katherine. Who's that man that gives out money in the newspapers? You write to him and he jumps up and says he will send your grandmother who is 200 years old a wheelchair. I was hoping he was here and would jump up.

The fact of the matter is, as you well know, we have tried a number of different ways to try to collect the data systematically and it never happens. I think we have reached a point where some concerted effort has to be made to collect the data. In the past, the instrumentation wasn't really available. It is available today and, therefore, someone needs to start thinking about it. All of us should be trying to plant seeds in the minds of those people who do have the funds or might possibly get the funds or might know somebody who might have some funds.

LATHROP: Well, that's the reason I asked that question. I think it's an excellent idea. If we can just start with one laboratory that would be a very good beginning. Do you have the address of this man that gives out money?

MARCUSE: The ICRP is in some way financially related to the United Nations. Possibly there may be some amount of money there. I imagine that it would not be so high compared to the total budget.

BIGLER: One possible source might be pharmaceutical companies. They have large analytical and pharmacology divisions in place and are currently looking at the possibility of adding PET facilities and SPECT facilities. I think they are elegantly set up to stimulate and to support that kind of research.

STABIN: On the issue about the need to acquire biokinetic data, I think one area where this is acutely needed is in the pediatric population. I would suggest that, rather than establishing several institutes to collect the data, it might be less expensive to organize a group that understands the needs of dosimetry and the methods for quantitating the data which would work with people who are already acquiring these data. I believe a lot of data are being

acquired but people don't realize that we need it. This group could work with various groups around the country that are acquiring data, and teach them what is needed for dosimetry. This might require another 10% of effort on top of what they are already doing instead of a 100% effort of starting up a new organization to study this.

BRILL: One of the pleas that I've heard is for people to collect data and make it available so others can calculate the radiation dose. One of the best ways to get interested in dosimetry is to get involved in dosimetry computations and become intellectually interested in it. When you do, you become aware of the pitfalls and problems and the way in which data have to be collected if they are to be analyzable.

One minor suggestion that perhaps I could make is that many of us who have worked in this area have become familiar with particular computer software that are useful, some of which are in our own laboratories, some of which are more general, and some of which are available through the national laboratories themselves. A listing of the various dose calculation programs that are available and where you can get information about them would be useful to many people and might help to stimulate some interest.

CLOUTIER: That is a good suggestion - if any of you will send us information we will see what we can compile from your input and from our own resources.

If no one else has any comments, I now want to thank the panel for stimulating this discussion. The members represent a wide range of interests: the manufacturers of radiopharmaceuticals; the Department of Energy that wants to fund the sort of research we would like to have done; the Nuclear Regulatory Commission that is interested in the workers; clinicians who have the patients' interests at heart; and the FDA that is out there to help all of us.

I would also like to thank the program committee for putting together an excellent program, and the speakers because they really composed the program, especially the foreign speakers because they contributed things that we don't always hear about.

A number of other people should be recognized for their help in putting on this symposium. Jo Tipton and her staff, Myra Perry and Terrie Cox, who helped with the administrative details; Bonnie Branch, Judy Mattina, and Fanny Smith, who worked at the registration desk; the projection and recording crew - Howard McCloud, Dale Anderson, and Maynard Ludwig; Elbert Carlton and Mike Momeni who helped with the question cards. Evelyn Watson and her staff have worked very hard. Fanny Smith has done all of the secretarial work connected with the preparation for this meeting. We thank all of these people for their efforts.

We wish all of you well in your travels and hope to see you at the Fifth Radiopharmaceutical Dosimetry Symposium. Y'all come back!

FOURTH INTERNATIONAL RADIOPHARMACEUTICAL DOSIMETRY SYMPOSIUM
PARTICIPANT LIST
November 5-8, 1985

NEIL M. ABEL
Food and Drug Administration
Office of Drug Research and Review
Center for Drugs & Biologics
Div. of Oncology & Radio-
pharmaceutical Drug Products
5600 Fishers Lane (HFN-150)
Rockville, MD 20857

S. JAMES ADELSTEIN
Harvard Medical School
25 Shattuck St., Bldg. A
Boston, MA 02115

ELIZABETH ALGER
Univ. of Medicine & Dentistry
of New Jersey
New Jersey Medical School
100 Bergen St.
Newark, NJ 07103

E. GIFFORD AMMERMANN
Salem V.A. Hospital
5323 North Lakes Dr., N.W.
Roanoke, VA 24019

PHILLIP C. BERRY
Brooke Army Medical Center
Box 145
Ft. Sam Houston, TX 78234-6200

RODNEY E. BIGLER
New York Hospital - Cornell Med. Ctr.
525 E. 68th St.
New York, NY 10021

WILLIAM R. BOYLE
Oak Ridge Associated Universities
MERT Division
P.O. Box 117
Oak Ridge, TN 37831-0117

A.B. BRILL
Brookhaven National Laboratory
Medical Department
Upton, NY 11973

ALLEN BRODSKY
Nuclear Regulatory Commission
16412 Kipling Road
Derwood, MD 20855

DONALD BUCHSBAUM
Univ. of Michigan Medical Ctr.
Dept. of Radiation Therapy
Room X3003 Main, Box 056
1405 East Ann Street
Ann Arbor, MI 48109

WILLIAM F. BUTLER
Hybritech, Inc.
P.O. Box 269006
San Diego, CA 92126

BILL L. BYRD*
Oak Ridge Associated Universities
Medical and Health Sciences Div.
P.O. Box 117
Oak Ridge, TN 37831

EDMUND F. BYRNE
Medi-Physics, Inc.
5855 Christie Avenue
Emeryville, CA 94608

J. ELBERT CARLTON
Oak Ridge Associated Universities
MERT Division
P.O. Box 117
Oak Ridge, TN 37831-0117

RANDALL W. CARTER
Emory University
Office of Allied Health
Atlanta, GA 30322

CHIN-TU CHEN
The Univ. of Chicago Medical Ctr.
IB-6, Box 433
5841 S. Maryland Avenue
Chicago, IL 60637

KELLY CLASSIC
Mayo Clinic
Radiation Safety Office
Rochester, MN 55905

ROGER CLOUTIER
Oak Ridge Associated Universities
MERT Division
Oak Ridge, TN 37831-0117

MARK CRISTY
Oak Ridge National Laboratory
Health & Safety Research Division
Bldg. 7509, P.O. Box X
Oak Ridge, TN 37831

BARBARA Y. CROFT
University of Virginia
Department of Radiology
P.O. Box 170
Charlottesville, VA 22908

JAMES E. CROOK
Oak Ridge Associated Universities
Medical & Health Sciences Division
P.O. Box 117
Oak Ridge, TN 37831-0117

JOEL L. DAVIS
Oak Ridge National Laboratory
Health & Safety Research Div.
P.O. Box X
Oak Ridge, TN 37830

PAUL W. DOHERTY
Univ. of Massachusetts Med. School
Dept. of Nuclear Medicine
55 Lake Avenue North
Worcester, MA 01605

KEITH F. ECKERMAN
Oak Ridge National Laboratory
Health & Safety Research Div.
P.O. Box X
Oak Ridge, TN 37831

ALAN A. EDWARDS
National Radiological Protection Bd.
Chilton, Didcot, Oxon OX11 ORQ, U.K.

BRADLEY EICHORST
Food & Drug Administration
1010 W. Peachtree St.
Atlanta, GA 30309

N.A. FARID
Eli Lilly and Company
Lilly Laboratory
for Clinical Research
Wishard Memorial Hospital
1001 West 10th Street
Indianapolis, IN 46202

WILLIAM E. FELLING
Oak Ridge Associated Universities
P.O. Box 117
Oak Ridge, TN 37831-0117

DARRELL R. FISHER
Battelle, Pacific Northwest Labs.
P.O. Box 999
Richland, WA 99352

JOHN FRAZIER
Oak Ridge Associated Universities
MERT Division
P.O. Box 117
Oak Ridge, TN 37831-0117

ALAN FRITZBERG
NeoRx Corp.
410 West Harrison
Seattle, WA 98119

GERHARD FUEGER
University of Graz Hospital
Department of Radiology
A-8036 Graz-Landeskrankenhaus
Austria

DAVID L. GILDAY
The Hospital for Sick Children
Division of Nuclear Medicine
555 University Avenue
Toronto M5G 1X8
Ontario, Canada

MARK GOODMAN
Oak Ridge National Laboratory
Nuclear Medicine Technology Group
Health & Safety Research Div.
P.O. Box X
Oak Ridge, TN 37831

DAVID A. GOODWIN
V.A. Medical Center
Nuclear Medicine Service (115)
3801 Miranda Avenue
Palo Alto, CA 94304

EDGAR D. GRADY
Medical Research Foundation, Inc.
181-A Upper Riverdale Rd.
Riverdale, GA 30274

PETER GROËR
Oak Ridge Associated Universities
Ctr. for Epidemiological Research
P.O. Box 117
Oak Ridge, TN 37831-0117

DAVID E. HANNA
2025 Huron Parkway
Ann Arbor, MI 48109

PAUL V. HARPER
Univ. of Chicago Medical Ctr.
Box 433
5841 S. Maryland Avenue
Chicago, IL 60637

CRAIG HARRIS
Duke Univ. Medical Center
Dept. of Radiology
Box 3949
Durham, NC 27710

CHRISTOPHER HAYDOCK
Mayo Clinic & Foundation
Dept. of Pharmacology
Rochester, MN 55905

L.C. HENLEY
I.T./Radiological Science Lab.
P.O. Box 549
Oak Ridge, TN 37830

PETER HERSCOVITCH
Washington Univ. School of Med.
Radiation Sciences
Box 8131
510 South Kingshighway
St. Louis, MO 63110

HORACE HINES
ADAC Laboratory
4747 Hellyer Ave.
San Jose, CA 95138

EDWARD J. HOFFMAN
UCLA School of Medicine
Ctr. for Health Sciences Room B2-128
Div. of Nuclear Medicine
& Radiological Sciences
Los Angeles, CA 90024

ROGER W. HOWELL
University of Massachusetts
Dept. of Physics & Astronomy
GRC Tower B, 4th Floor
Amherst, MA 01003

KARL HUBNER
Univ. of Tennessee Memorial
Hospital & Research Ctr.
Department of Radiology
1924 Alcoa Highway, S.W.
Knoxville, TN 37920

RENE HUISKAMP
The Netherlands Cancer Institute
121 Plesmanlaan, 1066 CX Amsterdam
The Netherlands

NOBUYA IGARASHI*
Teijin America, Inc.
10 Rockefeller Plaza, Suite 1001
New York, NY 10020

M.F. JAHNS
M.D. Anderson Hospital
& Tumor Institute
Univ. of Texas Cancer System
6723 Bertner Avenue
Houston, TX 77030

RONALD JASCZCAK
Duke Univ. Medical Center
2307 Honeysuckle Road
Chapel Hill, NC 27154

LENNART JOHANSSON
National Defence
Research Institute
FOA 451
S-901 82 Umeå, Sweden

DONALD A. KAPLAN
The Dow Chemical Company
CR-Biotechnology Lab, 1701 Bldg.
Midland, MI 48674

HENRY C. KARP
Emory University
Office of Radiation Safety
Atlanta, GA 30322

MICHAEL KAVULA
Mercer Univ. School of Pharmacy
345 Boulevard, N.E.
Atlanta, GA 30312

LINDA KETCHUM
The Society of Nuclear Medicine
SNM Newsline
136 Madison Avenue, 8th Floor
New York, NY 10016

GEORGE G. KILLOUGH
Oak Ridge National Laboratory
Health & Safety Research Div.
P.O. Box X
Oak Ridge, TN 37831

F.F. KNAPP, JR.
Oak Ridge National Laboratory
Nuclear Medicine Tech. Group
Health & Safety Research Div.
Oak Ridge, TN 37831

CONRAD KNIGHT
Duke University Medical Ctr.
P.O. Box 3155
Durham, NC 27710

BERNICE KOSLA
The Johns Hopkins School
of Hygiene & Public Health
615 North Wolfe Street
Baltimore, MD 21205

JOHN KOVACH
Mayo Clinic
Oncology Dept.
200 First St., SW
Rochester, MN 55905

PADMAKER V. KULKARNI
Univ. of Texas Health
Science Center at Dallas
Dept. of Radiology
E 6.238
5323 Harry Hines Blvd.
Dallas, TX 75235

C.S. KWOK
Hamilton Regional Cancer Centre, OCF
711 Concession Street
Hamilton, Ontario, Canada L8V 1C3

KATHERINE LATHROP
Univ. of Chicago Medical Ctr.
P.O. Box 433 (I-B-9)
950 East 59th Street
Chicago, IL 60637

JAMES L. LEAR
V.A. Medical Center
Nuclear Medicine (115)
3801 Miranda Avenue
Palo Alto, CA 94304

RICHARD LEGGETT
Oak Ridge National Laboratory
Health & Safety Research Div.
P.O. Box X
Oak Ridge, TN 37830

PETER K. LEICHNER
The Johns Hopkins Hospital
Radiation Oncology
600 North Wolfe Street
Baltimore, MD 21205

CATHERINE LUCCIONI
Laboratoire de Biophysique Appliquée
IPSN/DPS/SEAPS
CEA Fontenay aux Roses BP6
92260 France

PETE MANSPEAKER
DuPont NEN Medical Products
331 Treble Cove Rd.
N. Billerica, MA 01862

CAROL S. MARCUS
UCLA School of Medicine
Nuclear Medicine Outpatient Clinic
Harbor-UCLA Medical Center
Bldg A-13
1000 Carson Street
Torrance, CA 90509

H.R. MARCUSE
The Netherlands Cancer Institute
Department for Nuclear Medicine
Plesmanlaan 121, 1066 CX Amsterdam
The Netherlands

SØREN MATTSSON
Sahlgren Hospital
Department of Radiation Physics
S-41345 Göteborg
Sweden

NORMAN MCELROY
Nuclear Regulatory Commission
Material Licensing Branch, SS-396
Washington, D.C. 20555

THOMAS MCLEOD
Mt. Sinai Medical Center
Health Physics Dept.
4300 Alton Road
Miami Beach, FL 33140

THOMAS G. MITCHELL
The Johns Hopkins University School
of Hygiene & Public Health
615 North Wolfe Street
Baltimore, MD 21205

MICHAEL MOMENI
Oak Ridge Associated Universities
MERT Division
P.O. Box 117
Oak Ridge, TN 37831-0117

P.J. MOUNTFORD
Kent & Canterbury Hospital
Department of Nuclear Medicine
Ethelbert Road
Canterbury, Kent CT13NG, U.K.

M.J. MYERS
Royal Postgraduate Medical School
Hammersmith Hospital, Ducane Road
London W12 OHS, England

WILLIAM P. NEACY
E.I. duPont de Nemours, Co., Inc.
NEN Medical Products
Immunopharmaceutical R & D
Bldg. 500-1, 331 Treble Cove Road
North Billerica, MA 01862

MICHAEL P. NUNNO
Albert Einstein Medical Center
Dept. of Radiology
5501 Old York Rd.
Philadelphia, PA 19141

NEIL A. PETRY
University of Michigan
Box 021 W5628
Main Hospital 1405 E. Ann St.
Ann Arbor, MI 48109

MARY SUE PHILP
Medi-Physics, Inc.
5855 Christie Ave.
Emeryville, CA 94608

JOHN W. POSTON
Texas A & M University
Dept. of Nuclear Engineering
College Station, TX 77843

D.V. RAO
Univ. of Medicine & Dentistry
of New Jersey
Department of Radiology
100 Bergen St.
Newark, NJ 07103

SIMON J. RIGGS
Charing Cross Hospital
Cancer Research Campaign Laboratories
Department of Medical Oncology
Fulham Palace Road
London W6 8RF, U.K.

JAMES S. ROBERTSON
Department of Energy
Human Health and Assessments Division
ER-73, GTN
Washington, DC 20545

HANS D. ROEDLER
Bundesgesundheitsamt
Ingolstädter Landstrasse 1
8042 Neuherberg, F.R. Germany

KAREN ROSENSPIRE
Sloan-Kettering
Memorial Cancer Ctr.
Biophysics Laboratory
1275 York Avenue
New York, NY 10021

PAUL ROTH
Institut fur Biologie
Abt. f. Biophysikal Strahlenforschung
Ges. f. Strahlen- und Umweltforschung
Paul-Ehrlich-Str. 20
D-6000 Frankfurt/M, FRG

JAMES RYAN
Univ. of Chicago Medical Center
Nuclear Medicine Building
Box 429
950 E. 59th St.
Chicago, IL 60637

EUGENE SAENGER
Cincinnati General Hospital
Radioisotope Laboratory
Cincinnati, OH 45267

GOPAL B. SAHA
Cleveland Clinic Foundation
Department of Nuclear Medicine
Cleveland, OH 44106

KANDULA S.R. SASTRY
University of Massachusetts
Department of Physics & Astronomy
GRC Tower B 4th Floor
Amherst, MA 01003

SATYA SASTRY
Cooley Dickinson Hospital, Inc.
Nuclear Medicine Department
30 Locust Street
Northampton, MA 01060

AUDREY T. SCHLAFKE-STELSON
Oak Ridge Associated Universities
MERT Division
P.O. Box 117
Oak Ridge, TN 37831-0117

TUVIA SCHLESINGER
Soreq Nuclear Research Center
Yavne, Israel 20600

BERNARD SCHMALL
14 Alling Street
Hicksville, NY 11801

JASHOVAM SHANI
U.S.C. School of Pharmacy
1985 Zonal Avenue
Los Angeles, CA 90033

DOUGLAS R. SHEARER
Rhode Island Hospital
Medical Physics Dept.
593 Eddy Street
Providence, RI 02902

SHIAO-WEI SHEN
University of Michigan Medical
Center
2242 Stellar St.
Ann Arbor, MI 48105

ROBERT EDMOND SIMPSON
Food and Drug Administration
Ctr. for Devices
& Radiological Health
Rockville, MD 20857

TERRY SMITH
Clinical Research Centre
Radioisotopes Division
Watford Road
Harrow, Middlesex HA1 3UJ
England

R.G. SOUNDY
Amersham International Plc.
Amersham Laboratories
White Lion Road
Amersham, Buckinghamshire
HP7 9LL England

P.C. SRIVASTAVA
Oak Ridge National Laboratory
Nuclear Medicine Technology Group
Health & Safety Research Division
Oak Ridge, TN 37831

SURESH C. SRIVASTAVA
Brookhaven National Laboratory
Medical Department, Bldg. 801
Upton, NY 11973

MICHAEL G. STABIN
Oak Ridge Associated Universities
MERT Division
P.O. Box 117
Oak Ridge, TN 37831-0117

H. WILLIAM STRAUSS
Massachusetts General Hospital
Division of Nuclear Medicine
32 Fruit Street
Boston, MA 02114

LLOYD G. STRUTTMAN
Mallinckrodt, Inc.
675 McDonnell Blvd.
St. Louis, MO 63134

RANDALL TENHAKEN
Univ. of Michigan Medical Ctr.
Department of Radiation Therapy
Rm X3003 Main, Box 056
1405 E. Ann Street
Ann Arbor, MI 48109

MATTHEW L. THAKUR
Thomas Jefferson University
10th & Walnut St.
Philadelphia, PA 19107

J.W. THIESSEN
U.S. Department of Energy (GTN)
ER-70
Washington, DC 20545

MARIE ANNETTE VAUGHAN
The Johns Hopkins University School
of Hygiene & Public Health
Div. of Radiation Health Sciences
615 North Wolfe Street
Baltimore, MD 21205

ROBERT VESSELLA
V.A. Medical Center
Research Building 31
Minneapolis, MN 55417

WYNN A. VOLKERT
University of Missouri
Health Sciences Center
Department of Radiology
Columbia, MO 65212

HENRY N. WAGNER, JR.
Johns Hopkins Medical Institutions
Department of Radiological Sciences
615 N. Wolfe Street, Room 2001
Baltimore, MD 21205-2179

LEE C. WASHBURN
Oak Ridge Associated Universities
Medical and Health Sciences Div.
P.O. Box 117
Oak Ridge, TN 37831-0117

EVELYN E. WATSON
Oak Ridge Associated Universities
MERT Division
P.O. Box 117
Oak Ridge, TN 37831-0117

BARRY WERNER
University of Minn. Hospitals
Dept. of Therapeutic Radiology
Box 494
420 Delaware St., S.E.
Minneapolis, MN 55455

PARRY W. WESSELS
George Washington Univ. Med. Ctr.
Radiation Oncology
& Biophysics Div.
Washington, DC 20037

JAMES S. WIKE
Oak Ridge National Laboratory
Isotope Operations Division
P.O. Box X
Oak Ridge, TN 37831

DEAN F. WONG
Johns Hopkins Medical Institutions
615 N. Wolfe Street
Baltimore, MD 21205-2179

HARVEL WRIGHT
Oak Ridge National Laboratory
Health & Safety Research Division
P.O. Box X
Oak Ridge, TN 37830

PAT B. ZANZONICO
New York Hospital - Cornell Med. Ctr.
Dept. of Radiology
525 E. 68th St.
New York, NY 10021

*Registered but did not attend the meeting.

INDEX

A

Absorbed dose. See Dose, radiation.
Absorbed fractions
alpha particle, 75, 76
beta ray, 57
for blood, 579-583
for bone, 520-524, 525, 526
electron, 57, 61, 74, 76, 81
for embryo/fetus, 157-158
microdosimetric calculation of, 61, 71-76
MIRD basis for calculation of, 155-158
photon, 57, 579-583
Actinides. See alpha emitters.
Actinomycin D, radiopharmaceutical uptake altered by, 298
Acute tubular necrosis, 276, 279
Adenoma, thyroid, 630
Adipose tissue, radioxenon uptake by, 303
Administration, radiotracer continuous, 195-200
mode dependence, 56, 220, 225-238, 296-297
subcutaneous monoclonal, 488
tumor volume effect on, 458
Adrenal cortex imaging, 303-304
Adrenal medulla
imaging of, 304
iodine-131-MIBG kinetic data and absorbed dose in, 389, 393, 394, 395, 396
hyperplasia 389, 393, 394, 395
Adrenocorticotrophic hormone (ACTH)
in adrenal imaging, 303
affecting I-123-IMP uptake in brain, 294
radioiodine uptake altered by, 301-302
Adriamycin, increased radiopharmaceutical deposition with, 292
Ailingnae inhabitants
thyroid absorbed dose from fallout, 630, 642-644
Alcohol,
interaction with Tc-99m-HIDA, 297
Alderson phantom, 465, 466, 469
Algorithms
for particle path calculation, 78-80
reconstruction, 96
SPECT attenuation compensation, 85
Alpha emitters
bismuth-212, 30-34, 36
cytoidal potential, 27-28, 36
delta functions, 30, 31

in labeled monoclonal antibodies, 2
microdosimetry, 27
model for distribution, 30-33
path through cell, 68-73, 74, 76
range, 27-29, 36, 418
specific energy densities, 30-34
track structure, 27-28, 30, 39
tumor treatment with, 27, 33-34, 35-36
Aluminum, altering uptake of Tc-99m compounds, 295
Aluminum-polystyrene interface, backscattered beta dose at, 566, 568-569
Amino acids, See also specific listings.
biodistribution, 218-221
C-11-labeled, 239-242, 244
C-14-labeled, 681-686
decarboxylation of labeled, 244
H-3-labeled, 681-686
metabolic fate, 221
radiolabeled for cell killing, 14, 15, 52-66
Se-75-labeled, 14, 15, 52-66
S-35-labeled, 52-66
tumor uptake, 218, 220-221, 225-237
 α -Aminobutyric acid, 218, 219, 231
Amiodarone, 301
Ammonia, nitrogen-13-labeled, 218-219, 220-221, 225, 232, 233, 236, 238
Amphetamine, adrenal response to, 304
Anemia
chromium-51 doses to organs in patients with, 678
iron-59 doses to organs in patients with, 311, 314, 315
Anesthetics
use in pediatric studies, 151
Aneurysm, glucocorticoid-induced, 292
Angiography, 293, 294
Anti-AFP, hepatoma treatment with, 458
Antibodies. See also Monoclonal antibodies, radiolabeled.
antitumor, 427-441, 461, 462, 537-538, 544
cancer cure rate with, 462-463
localization in bone marrow, 537, 538, 544
medical uses, 3
model for, 427-441
organ distribution, 470-473
Y-90-labeled, 460, 462
Antigen
antibody interaction with, 429-432
radiolabeled monoclonal antibody

for, 26, 27, 30-31
 sites of, 36, 429-432
 stem cell expression of, 537
Antimyosin, 381
Antitussives, radioiodide competition with, 301
Aorta, blood volume of, 576, 577, 579
Arms, blood volume of, 577
Arterial circulation, 260-261
Astatine-211, 27, 33, 418
Atomic decay process, 496-504, 512
Atropine, gallbladder response to, 297
Auger electron emitters
 cellular concentration of, 14, 15, 61, 64
 decay of, 53, 498-501, 502, 512
Auger electrons
 average spectrum of, 56
 in bismuth-212 decay, 30
 cascade, 512
 conventional dosimetry for, 53
 cytoidal effects of, 13, 14, 18-21, 53, 59-60, 494-495
 dosimetric model for, 53, 54
 in indium-111 decay, 654
 nuclear dose rate enhancement factor for, 60-64
 in radioplatinum decay, 495-501
 range of, 418, 649
Autoradiography
 carbon-14, 110, 113
 digital analysis for, 111-114, 116-117
 fluorine-18, 110
 hydrogen-3, 113
 iodine-123, 110, 113
 method, 105-106, 107
 quantitative optimization, 106-111
 thallium-201, 110, 113
Average dose. See also Dose, radiation.
 Auger electrons in calculation of, 53
 conventional calculation of, 58
 in microdosimetry, 34
 to patient's family, 184, 185
 use of weighting factors in, 38

B

Background activity
 beta, 568-570
 reducing by chelate chase, 486-489
BEIR risk coefficients, 630-631
Benactyzine, 301
Benefit vs. risk assessment
 education about, 8-9
 for ionizing radiation, 1-3, 6
 for new drugs, 267, 270, 273

in pediatric medicine, 149, 152-154
 public perception of, 4-6
Benzodiazepine receptor complex, drugs affecting, 294
Beta emitters
 absorbed dose from, 16, 545-546
 biological effects of, 54-60
 dose point kernel for, 547-551, 552-559, 560
 in homogeneous tissues, 563
 mutations from, i3
 nuclear dose rate enhancement factors for, 62-64
 point source function for, 195, 196-198, 202-206
 radiolabeled monoclonal antibodies, 26, 27
 sulfur-35, 57, 59
 therapeutic use of, 27
Betadine, 301
Bethanechol, gallbladder response to, 296
Bethe-Bacher approximation, 551
Bicarbonate, elevated radiopharmaceutical uptake with, 292
Bile release inhibitors, 296
Biokinetics. See kinetics
Biological distribution. See Distribution.
Biological effects, radiation
 of alpha emitters, 27, 30, 33-34
 of Auger emitters, 53, 418, 494
 of charged particle interactions, 39-40, 47-49
 in children, 148-154, 289
 DNA damage, 19, 20, 21, 38, 44-49, 72-73, 494
 in infants from breast milk, 168-174
 of iodine-125, 19-20
 lymphoblast mutations, 21
 on normal tissue, 27
 PET reduction of, 101
 of radioplatinum, 494
 of radiohalogens, 19, 21, 33
 specific energy density related to, 33
 of tritium, 20, 21, 23-24
 on tumor cells, 33-34, 35-36
 time scale for, 40-41, 43, 44

Bismuth-212
 decay, 27, 30
 half-life, 30, 36
 microdosimetry, 30-33
 radiolabeled monoclonal antibodies, 26-36

Bismuth-212 + polonium-212
 microdosimetry, 33-34

Bladder
 absorbed doses from myocardial

- imaging agents, 373-380
 biokinetic data and absorbed doses from isotopes of I-131, 141, 144, 146
C-11-NMSP dose to, 250, 252-256
 continuous drainage of, 611
 copper-64 dose to, 378-379
 dosimetric model for, 120, 121, 587-598, 612
 dynamic spherical model, 587-598 612
F-18-FDG dose to, 372, 373
I-123-triphosphonium iodide dose to, 372, 373
 iodine-131-MIBG dose to, 396
 PET scans of, 99-100
 protection from radiation dose, 137
 radiolabeled fatty acid dose to, 373, 374, 375
 rubidium-82 dose to, 377-378
Tc-99m-DEPE dose to, 132
Tc-99m-porphyrin (TPPS) dose to, 127
Tc-99m-PYP dose to, 380
 voiding schedule for, 588-590, 601-611
 volume of, 587-589, 591, 595, 596, 601-604, 612
Bleeding, chronic, 311, 314, 315, 316
Bleomycin, 299, 303
Blocking, thyroid, 169, 177, 390, 393, 394, 432.
Blood
 absorbed fractions for photon emitters in, 579-583
 activity in, 120, 137, 140, 214, 219-220, 225-235, 241, 311-314, 361, 390, 395, 436-438, 449, 537-540, 682-686
 distribution in body, 576-579, 585
 dose limit for radiotherapy, 536
 dosimetric model for, 575-580
 drugs affecting myocardial flow, 292
 iodine-131-MIBG activity in, 395
 renal flow, 354
 tumor supply of, 261
Blood-brain barrier, 293-294
Blood cells, radiolabeled
 absorbed dose in, 657
 clinical uses, 674
 compartmental model for, 674-676, 677
CR-51-RBC dose estimates for disease states, 673-679
 dose to cells from alternative radionuclides, 657
In-111-labeled, absorbed dose estimates, 173, 175, 650-652, 657, 665-666
 indium-111 dosimetry for, 648-657, 662-666
Tc-99m-RBC dose to infant from breastmilk, 170
Bone
 absorbed fractions for electrons, 520-524, 525, 526
 calcium uptake by, 297
 cancer of, 516
 chord-length energy distribution in, 517-520, 521
 dose estimates, 514-515, 529
 dosimetric model for beta particles, 564-571
 imaging, 149, 176, 177
 phosphate uptake by, 297-298
 structure, 516-517, 534
 types, 516, 534
Bone marrow
 absorbed dose calculations for *I-131-anti-CEA monoclonal antibody*, 535-542, 544
 absorbed dose estimates from isotopes of *I-labeled ortho-iodohippurate*, 146
 absorbed dose ratios for *In-111* and contaminants, 341
 absorbed fraction calculations 520-524, 525, 526
 alterations in distribution of, 296
 antibody localization in, 537, 544
 chord-length energy distribution in, 517-521
 cumulated activities in, 538-539, 541
 descriptive parameters for, 527
 dose after chelate chase, 482-485
 dosimetry aspects of, 514-532
 iron-59 dose to, 314, 315
 microdosimetry for beta source in, 562-571
 myocardial radiotracer dose to, 373-380
 radiotherapy, toxicity in, 536-537, 541-542
 rubidium-82 dose estimates for, 352, 353, 355, 356
 technetium-99m-DEPE dose estimate for, 132, 134
 technetium-99m-TPPS (Porphyrin) dose estimate for, 127, 134
Bragg curve, 28
Brain
 blood-brain barrier penetration altered in, 293-294
 blood volume, 577
 carbon-11-N-methylspiperone distribution in, 250-252

- caudate, 247-248, 251-252
 CT scan dose, 255, 256-257, 259
 drug effects on imaging, 252, 257, 293-294
 F-18-FDG dose estimate, 377-378
 neurotransmitter localization in, 247, 248, 249
 pertechnetate imaging, 293-294
 PET scans, 2, 99-100, 102
 putamen, 247-248, 251-252
 radiolabeled amino acids, 218
 tumors of, 2-3
- Breakthrough**
- in faulty generators, 329, 331, 342-344
 - of parent radionuclide, 186-187, 188, 189, 193
 - radiopharmaceutical contamination with, 319-329, 330
 - of strontium-82, 355-356
- Breast**, absorbed dose at breast surface from Tc-99m studies, 176
 Tc-99m porphyrin uptake in, 127
- Breast milk**, radionuclides in, 167-174, 176-178, 180, 652
- Breathing study**, tracheal dose measurements, 200-207, 208-211
- Bromine-77**, 27, 298
 cell energy deposition, 20-21, 27
- Bromine-77-IUDR**, 21
- Bromine-77-spiperone**,
 absorbed dose estimates and kinetics, 122-125
- Bücherer-Strecker synthesis**, 239
- C**
- Cadmium-polystyrene interface**, 570, 573
- Calcium**
- bone uptake, 297
 - myocardial levels of, 292
- Calcium sulfate: dysprosium thermoluminescent dosimeters**, 447, 450-451, 452-455
- Calibration**, SPECT system, 90-91
- Cancer**
- alpha emission for treatment of, 33-34, 35-36
 - amino acids in diagnosis of, 239
 - antigen sites of, 36
 - bone marrow toxicity in treatment of, 536-537, 541-542
 - cavity radiotherapy for, 416-417
 - colon, 436-441, 537, 540-542
 - compensation for, 406
 - Cu-64 for tumor imaging, 212-216
 - drugs altering radionuclide uptake in, 294, 302
- iodine-131-MIBG in assessment of**, 389, 395
- lymphatic**, 662
- pancreatic**, 239
- radiogenic**, 4, 38, 403-406, 666, 668-670
- radiolabeled antibodies for**, 3, 26-27, 31, 34-36, 409-420, 436-441, 443, 454-456, 458-465, 493-495, 505-509, 535, 537-542, 562-563
- Thorotrast-induced**, 405
- thyroid**, 410, 542, 629, 630, 632-635, 642-647
- Captopril**, 302
- Carbamazole**, 301
- Carbon-11**
- amino acid labeling with, 218, 239-242, 244
 - half-life, 6, 381, 382
- Carbon-11-3N-methylspiperone (NMSP)**
- absorbed doses from, 250-252, 255-258
 - bio kinetics, 250-255, 257-258
 - haloperidol effect on brain uptake, 245, 247, 250-251, 252, 257, 294
 - ligand competition, 247, 248
- Carbon-11-D- and -L-tryptophan**
- absorbed dose estimates and kinetics, 240-242
- Carbon-11-D- and -L-valine**
- absorbed dose estimates and kinetics, 240-242
- Carbon-11-palmitate**
- absorbed dose estimates, 385
 - effective half-time in heart, 382
 - as myocardial imaging agent, 376
- Carbon-11-suriclonine, receptor binding of**, 294
- Carbon-14**
- beta dose point kernel, 552, 554, 555
 - in human body, 3-4
- Carbon-14-glucose**, 110
- Carbon-14-iodoantipyrine**, 110, 111, 114
- Carbon-14-KIC**
- absorbed dose estimates, 681, 686
 - kinetics, 681-686
- Carbon-14-leucine**
- absorbed dose estimates, 681, 686
 - kinetics, 681-686
- Carcinoembryonic antigen (CEA)**
- compartmental model, 429, 436-441
 - radiolabeled monoclonal antibodies directed against, 537, 540-542
- Cardiac output**, 264-265
- Cardiovascular disease**, 212, 216
- Carotid artery, radionuclide study of**, 263, 264
- Catheter placement**, 260

Caudate, brain
absorbed dose in, 247-248, 251-252

Causality, 403, 406

Causation, probability of, 403-405, 406

Cavity therapy, 416-417

Cell(s)
antigen sites on, 36
Auger-electron emission in, 13, 14, 15, 53, 56, 418, 494
bone, 516, 536
concentration of radionuclides by, 14-18, 53
Coster-Kronig emission in, 14, 56, 418
killing by alpha emitters, 27, 30-34, 35-36, 418
killing of tumor, 33-34, 35-36, 417, 418, 494
membrane, 23
myocardial, 291, 292
radiation path through, 68-76, 649
radiosensitivity of, 13, 649
radioimmunotherapy for, 26, 494, 505-507. See also Monoclonal antibodies, radiolabeled.
sterilization, 19-20

Cerebral blood flow
unaffected by drugs, 294

Ceruleotide, 296

Cesium-129, in myocardial imaging, 371

CHA255 antibody
chelate chase of, 479, 480-485
uptake of, 479

Charged-coupled device, autoradiographic, 113-117

Charged-particle equilibrium, 514-515

Charged-particle radiation
alpha, 47, 49
DNA interaction with, 47-49
energy loss of, 38-39, 42-45, 51, 514-515
interaction times for, 38, 40, 43, 44-46
ionizing energy from, 38-39, 42-45
models for reactions of, 39, 41-42
path through cell, 68-76, 649
track produced by, 38, 39, 41-49
in water, 39, 41

Chelate chase
dose reduction following, 480-485
indium-benzyl EDTA transferrin, 488-489

Chemo-Auger therapy, 494-495, 505-509

Chemotherapy
fluorine-18 uptake altered by, 298
gallium-67 uptake altered by, 297-300
monitoring, 3
radioplatinum in, 494-495, 505-507

Children, nuclear medicine for, 148-154

Cholecystokinin, 296

Cholesterol, steroid suppression of adrenal uptake, 303

Chloral hydrate, 151

Chord length. See Path, radiation.

Chromium-51
blood cell labeling with, 657
clinical use of, 674
concentration by cells, 53
kinetics, 674-676
model for labeled cells, 674-676, 677

Chromium-51-EDTA
absorbed dose to infant from breast milk, 173

Chromium-51-leukocytes or lymphocytes
absorbed dose to cells, 657

Chromium-51-RBC,
absorbed dose estimates and kinetics, 673-680

Chromium-51-sodium chromate,
cell concentration, 14, 15
mean lethal dose, 15

Chromosomal aberrations, 655-657, 666-667

Cimetidine, 300

Circulatory system. Also see Blood.
model for radiation dose calculation, 575-580

Cisplatin, 302. Also see Platinum.

Clearance, radionuclide. See kinetics

Clofibrate, xenon retention by, 303

Cocaine, 304

Coherence, 401

Collimator, high-resolution, 84, 86, 96

Colloid, liver uptake, 475, 476

Colon cancer, 436-441, 537, 540-542

Committed effective dose equivalent
See effective dose equivalent

Compensation, disease, 406

Compartmental analysis
determination of cumulated activities with, 424-427
for radioiodinated antitumor antibody, 427-441
rate constants in, 444

Compton scattering, 83, 471

Congestive heart failure, fluid infusion in, 191-192

Conjugate counting technique
for uptake measurements, 137, 142-146, 348-350, 354

Contaminants, radionuclide
in approved radiopharmaceuticals, 271
in copper-64, 216
generator-produced, 329, 331, 342-344
half-lives of, 331, 332-333
in indium-111, 276, 335, 341, 649, 651-652

- in iodine-123, 275-276, 290,
 335-338, 359, 369
 kinetic model for molydenum-99,
 319-329
 radiation dose altered by, 330,
 331, 332, 345
 in rubidium-82, 355-356, 377, 383
 temporal variations in, 333,
 334-335
 in thallium-201, 335, 339-340
Continuous administration,
 absorbed dose from, 195-200
Continuous breathing administration,
 200-207, 208-211
Copper-64
 possible label for therapy, 27
 contaminants in, 216
Copper-64-citrate
 absorbed dose estimates, 213,
 215, 216, 379, 384, 385
 committed effective whole-body
 dose equivalent, 384
 effective half-time in heart, 382
 as myocardial imaging agent,
 378-379
 tumor uptake of, 212-216, 382
Copper-67, possible label for anti-
 body therapy, 27, 563
Coronary artery disease, 3
Cortical bone, 516-517, 527, 534
Cosmic radiation, dose from, 3
Coster-Kronig electron emitters
 average spectrum of, 56
 cellular concentration of, 15
 cytoidal effects of, 14
 electron range of, 418
 platinum-193m, 498-501
 platinum-195m, 502
CT scan, dose to brain from, 255,
 256-257, 259
 in tumor volumetrics, 459, 461
Cumulated activities
 for absorbed dose calculations,
 120, 145, 146, 360-368
 in bone marrow, 538-539
 calculation of, 423-427
 for chelate-antibody complex, 479
 compartmental model for, 434-436,
 440, 444-445
 for iodine-131 in embryo/fetus,
 163
 for iodohippurate, 135, 145, 146
 of radiolabeled antibodies in
 bone marrow, 537, 541
Cyclophosphamide, pulmonary
 interstitial fibrosis after
 administration of, 303
 radiopharmaceutical uptake
 altered by, 298, 299
Cyclosporin A
 in kidney scans, 302
 toxicity of, 276
Cytoplasm, radiolabeled amino acid
 concentration in, 60
- D**
- Daunorubicin**, 292
De-iodination of antibody, 431-432
Decapeptide, 296
Delta function, 30, 31, 33
Delta rays, 28, 39, 45-47
Densitometer
 dynamic range in, 112
 limitations of, 111, 112, 113
Deoxyglucose, brain tumor evaluation
 with, 2
Deoxyribonucleic acid (DNA)
 Auger emission effect on, 54
 charged particle interactions
 with, 47-49
 chemical damage to, 655-656
 copper associated with, 216
 diameter of, 40, 42
 enzymatic repair of, 38
 HIED damage to, 494, 501
 iodine-125 decay and, 19, 494
 platinum binding to, 494
 radiation damage to, 19, 21, 38
 tritium-labeled precursors for,
 21, 23-24
Desferoxamine, reduced radiation
 dose with, 299
Dexamethasone, radiopharmaceutical
 uptake altered by, 294, 303
Dextrose, radiopharmaceutical uptake
 altered by, 295
Dextrose/krypton-81m solution, 187
Diabetic gastroenteropathy, 300
Diagnostic tests
 glucose metabolism, 2, 3
 in pediatric patients, 148-149
Dialysis, iron-59 uptake in, 311,
 315
cis-Dichlorodiamine platinum II, 494
Dielectric response function, 41
Diethylstilbestrol therapy,
 affecting Tc-99m-PYP uptake, 298
Digitized density maps, autoradio-
 graphic, 111-117
Digoxin, 293, 295
Dilantin, 293
Dihydrotachysterol, 297
1,25-Dihydroxy-vitamin D, 297
Diphenylhydantoin, 293
Dipyridamole, 292
Disappearance. See kinetics

Disease
radiogenic, 4, 38, 403-406, 666, 668-670
Disopyramide, myocardial treatment with, 293
Disposal sites, radiopharmaceutical, 7-8
Distribution. Also see specific radiopharmaceutical administration mode influence on, 56, 220, 225-238, 296-297 of alpha emitters, 27, 28-33, 36 aluminum-induced changes in, 295 of amino acids, 218, 219, 224, 225-238, 241 autoradiographic measurement of, 106-117 blood, 576-579, 585 chemotherapeutic agents affecting, 296 conjugate counting in determining, 137, 142-146, 348-352 contamination affecting, 136-137, 140 gamma camera determination, 119, 138, 141, 411-412 mineral-altered, 297 PET measurement of, 98-101, 216 of positron emitters, 198, 214, 220-221, 240-241, 250-254, 352 quantitative (definition), 136 of radiolabeled antibodies, 427, 431, 464 sedative influence on, 151 in small target sites, 30-33 SPECT imaging of, 83, 84-91 tissue inhomogeneity and, 564-571 uniformity of, 67, 70, 88, 410, 417 vitamin-altered, 297
Diuretic radionuclide urography, 302
Diuretics, 292
Dobutamine, 293
Dose, radiation. See specific radionuclide or organ absorbed (definition), 28 absorbed dose per unit photon fluence in bone, 524, 529 absorbed dose rates at breast surface for Tc-99m radiopharmaceuticals, 176 absorbed dose ratios of contaminants vs. primary radionuclides, 336-344 absorbed dose ratios for I-131-monoclonal antibodies, 452-454 from alpha particles 27, 30-34, 195, 418 assumptions affecting, 83, 415-416, 467, 473 from Auger electrons, 14-16, 18-21, 53 average, 34, 38, 53, 67 background, 358 backscattered, 568-570 from beta particles, 16, 545-559 from breast feeding, 167-174, 177-178, 180 in cavity therapy, 417 cellular, 14-18, 24-25, 58 after chelate chase, 299, 481-485, 488 in children, 289, 290 contaminant contribution to, 325-329, 330, 331-345, 369, 374 in continuous administration, 195-200 from CT brain scan, 255-257, 259 directly verified, 447, 450-455 for embryo/fetus, 155-165 exposure time in calculation of, 198, 199-200 fluctuations in, 28-30 from gamma rays, 195 ICRP system for calculating, 67-68 for infant, 176 information required by regulatory agencies, 119, 120-132, 268-269, 272 from inhaled radionuclides, 195, 200-207, 208-211 from intra-arterially injected particles, 261, 262, 263, 264, 265 in intravenous administration, 195-200 localized deposition of, 501-504, 512 from low-energy electrons, 60-64 from lung scanning, 24, 200 mean, 15-16, 67, 360 microscopic distribution of, 13, 14, 31, 34, 38 MIRD assumptions for, 67-68 nasopharyngeal, 206-207 path-length in calculation of, 39, 68-76 in pediatric medicine, 149-150, 153, 176, 182-185 from radiolabeled amino acids, 240, 242 from radiolabeled antiferritin, 458-459, 462 from radiolabeled blood cells, 170, 173, 175, 284-287, 648-660, 665-666, 673, 676-679 from radiolabeled monoclonal antibodies, 409-417, 422, 435-436, 440, 441, 458-460, 541-542 in radium-dial painters, 5 for renal patients, 275, 277-281, 284-287

S-factors, 67-68, 155, 157-159, 621
 from secondary electrons, 515, 524
 from short-range radiation, 418
 to small target sites, 28-30, 31
 target size in, 28-30, 31, 38, 84, 418
 from technetium-99m-labeled compounds, 262-265, 380
 to thyroid from radioiodine, 619-621, 622
 tracheal, 206-207, 208-211
 from tryptophan enantiomers, 242
 from ultrashort-lived radio-nuclides, 186-192
 from valine enantiomers, 242
 from x-ray CT, 256-257, 259
Dose point kernels
 for beta particles, 547-551, 552-559
 for carbon-14, 554, 555
 for iodine-131, 552, 557, 558, 559
 for mercury-203, 552, 556
 for monoenergetic electrons, 546-547, 548-550, 551
 Monte Carlo method for calculation of, 546, 552, 559
 parameters for, 547, 560-561
 for phosphorus-32, 552, 553, 558, 559
 for sulfur-35, 552, 554, 556
Dose rate enhancement factors, 60-64, 201
Dosimeter, thermoluminescent, implanted, 447, 450-451, 452-455
Doxorubicin, 292, 298
Drug addicts, lung scans in, 303
Drug Master File, 271
Dynamic range, in video camera and densitometers, 112
Dynamic spherical bladder model, 588-598

iodine-131-MIBG, 396
iron-59-transferrin, 314, 315, 316
 medical use of, 134
technetium-99m-DEPE, 128
technetium-99m-porphyrin, 128
technetium-99m-PYP, 384
technetium-99m-RBC, 128
thallium-201-chloride, 384
Ejection fractions, 191
Electron capture
 decay by, 494, 662
 in radiolabeled antibodies, 26
 tissue irradiation by, 13, 14, 53
Electrons
 cellular dosimetry of, 505-506
 path of, 68-70
Ellipsoidal bladder model, 588, 591, 596, 599-600
Embryo, radiation dose to, 158-165
Endotoxin, *E. coli*, 295
Energy deposition. See **Dose**, radiation.
Enflurane, 296
Epilepsy, 3
Epinephrine
 splenic response to, 296
 for ulcers, 301
Erythrocytes, 170, 654, 673-679
 See also **Blood cells** and **Dose**, radiation
Estrogen supplementation, 298
Ethacrynic acid, 292
Europium-254 as contaminant in Cu-64, 216
Exposure
 in autoradiography, 106
 external beam irradiation prior to radioimmunotherapy, 460
External probe
 bladder activity measurements with, 253-254
External radiation exposure
 risk coefficients for, 628-640
 thyroid cancer from, 628-647

E

Edge detection, 216
Effective dose equivalents
 bromine-77-p-spiperone, 122
 chromium-51-RBC, 678
 contaminant contribution to, 345
 copper-64-citrate, 384
 fluorine-18-FDG, 384
 indium-111-WBC, 663-665, 666
 iodine-123-BMIPP, 384
 iodine-123-DMIPP, 384
 iodine-123-IPPA, 384
 iodine-123-triphenylphosphonium iodide, 384

F
Fab fragments. See **specific radio-nuclide or antibody**
Face, blood volume of, 577, 578
Fallout
 dose estimations for, 631, 632
 gamma irradiation from, 630
 thyroid absorbed dose from, 629, 630
False carrier effect in gallium uptake, 299
Fatty acids, radiolabeled
 effective half-times for, 382

in myocardial imaging, 373-376, 382
in myocardial metabolism, 3, 359, 368-369
Fetus, absorbed dose estimates in, 163, 164
maternal radiation source, 158-165
Film darkening, autoradiographic, 106
Fluorine-18
absorbed dose level for, 195
bone imaging with, 298
compartmental model, 298
half-life, 381
Fluorine-18-fluorodeoxyglucose
absorbed dose estimates for, 373, 383, 384, 385
in autoradiography, 110
availability of, 384, 385
committed effective whole-body dose equivalent, 384
compartmental kinetic model, 298
dose to bladder wall, 587-611
effective half-time in heart, 382
in myocardial imaging, 372-373, 382, 384, 385
5-Fluorodeoxyuridine, 297
Food and Drug Administration.
dosimetry requirements by, 267-273
guidelines for pediatric medicine, 152-153
Food, Drug, and Cosmetic Act, 267
Furosemide, 292

G

Gallbladder
drugs affecting visualization of, 296-297
technetium-99m-DEPE in, 129-132
Gallium-66
contaminant in Ga-67, 333-335
Gallium-67
cell concentration, 14
contaminants in, 333, 335
drugs altering uptake of, 292, 296, 299-300, 302
imaging, 26, 96, 149
for SPECT scans, 96
stable gallium competition with, 299
Gallium-67-citrate
absorbed dose estimates, 653
absorbed dose estimates in renal patients, 284-287
absorbed dose to infant from breast milk, 172, 173,
tumor uptake of, 215
Gallium-67-leukocytes or lymphocytes
absorbed dose to cells, 675

Gallium-68
blood cells labeled with, 657
monoclonal antibodies labeled with, 420
Gallium-68-leukocytes or -lymphocytes
absorbed dose to cells, 657
Gamma camera
for biodistribution data, 119, 127, 138, 347, 412
spatial resolution, 412
in SPECT imaging, 84, 85, 86, 87
for ultrashort-lived radionuclides, 190, 349
Gamma irradiation, 195, 630
Gastrointestinal tract
dosimetry model, 120
imaging of, 300-301
radionuclide distribution in, 122-127, 129-132
Genetic damage, zero-threshold hypothesis for, 5
Geometric linearity, 111, 112
Germanium-68/gallium-68 generator system, 350-351, 354
Glucagon, 301
Glucocorticoids, 292, 294, 303
Glucose metabolism, 2, 3
Glutamate, N-13 labeled, 218, 219, 226
Glutaminase, tumor sensitivity to, 218, 224
Glutamine, dosimetric measurements with, 218, 219, 220-221, 224, 227, 234, 238
Gold-195/Gold-195m
absorbed dose ratios, 344
Gold-195m
contaminants in, 344
dose limit for infusion, 187
generator production, 186, 187
half-life of, 189, 192
medical application of, 189
radiation dose, 187
Gray (definition), 28
Gray scale resolution, 112
Grisorixin, 293
Growth hormone, 303

H

Haldol. See haloperidol
Half-life, physical
bismuth-212, 30
carbon-11, 6
effect on exposure time in autoradiography, 106
fluorine-18, 38
gold-195m, 189, 192

hydrogen-3, 57
indium-114m, 649
iodine isotopes, 145-147
iridium-191m, 188, 192
krypton-81m, 187, 188
mercury-195m, 342
osmium-191, 342
oxygen-15, 195
parent vs. daughter nuclide, 186
platinum-195m, 507
rubidium-81, 186, 342
rubidium-82, 189, 192, 195, 346
safety and, 6
selenium-75, 57
strontium-82, 342
sulfur-35, 57

Half-times

- age-dependence, 163
- antichelate antibody influence on, 480-481, 489
- antiferritin, 459
- carbon-14-KIC, 685, 686
- cis-platinum-195m, 508
- in compartmental analysis, 427-428
- hydrogen-3-leucine, 685, 686
- hydrogen-3-methionine, 56-57
- of intra-arterially injected particles, 261
- iodine in fetal thyroid, 158, 163
- iodine-131-MIBG, 390
- iodine in thyroid, 618-619
- iron-59 in fetal liver, 164
- of radionuclide contaminants, 336-341
- of radiopharmaceuticals in breast milk, 169, 170
- Se-75-selenomethionine, 56-57
- sulfur-35-methionine, 57
- thallium-201 in myocardium, 371

Haloperidol

- decreased C-11-NMSP uptake with, 245, 247, 250-251, 252, 257, 294
- ligand competition, 247, 248

Halothane, 296

Headroom, 112

Health care costs, 7

Heart. See also **Myocardial infarction**.

- amino acids in study of, 218
- blood volume of, 576, 577
- carbon-11-palmitate as imaging agent, 376
- comparison of absorbed doses, half-times and uptake fractions for imaging agents, 371-385
- copper in health of, 212, 216
- copper-64-citrate as imaging agent, 378-379
- drug and radiopharmaceutical interactions in treatment of, 291-293

fatty acid metabolism in, 362-369, 373-376

fluorine-18-FDG localization in, 372

gold-195m for imaging, 189

intra-arterially injected particles, 260

iodine-123-labeled free fatty acids as imaging agents, 373-376

iodine-123-triphosphonium iodide as perfusion agent, 376-377

iridium-191m for imaging, 188-189

krypton-81m for imaging, 187-188

PET scans of, 99-100, 102

rubidium-82 dose to, 189-190, 352, 355, 356, 378

technetium-99m dose to, 124, 126, 127, 129-132, 262-263, 379-380

thallium-201 compared to other imaging agents, 383-385

ultrashort-lived radionuclides for imaging, 186-190, 191-192

Hemochromatosis, 297

Hematopoietic stem cells, 516, 536-537

Heparin, 294-295

Hepatobiliary imaging

- drugs affecting, 296-297

Hepatoma

- radioimmunotherapy for, 458-460

Heroin addicts, lungs scans of, 303

High-performance liquid chromatography, (HPLC)

- amino acid resolution with, 239-240

Highly localized energy density, HILED

- DNA damage by, 14, 15
- at radionuclide decay site, 494, 501-504

Human serum albumin microspheres, 261, 262-264

Hybrid scanner, 169

Hybridoma cell lines, 478, 490

Hydralazine, 295

Hydrochlorothiazide, 293

Hydrocortisone, 292

Hydrogen-3

- beta emission of, 57
- biological effects of, 19-21
- nuclear dose rate enhancement factor for, 61-63
- RBE, 59-60, 64

Hydrogen-3-KIC

- absorbed dose estimates, 681, 686
- kinetics, 681-686

Hydrogen-3-leucine

- absorbed dose estimates, 681, 686
- kinetics, 681-686

Hydrogen-3-methionine

- kinetics, 54-64
- radiation dose to testis, 58

Hydrogen-3-thymidine
biological effects in cells,
19-21
Hyperthyroidism, 2, 24
Hypothalamus-pituitary axis, 303
Hypothyroidism, 2, 629, 637

I

Imaging
adrenal, 303-304
anterior and posterior combined,
465
bone, 296, 297-298
with chelate chase, 486-489
contaminants altering, 331, 344
gastrointestinal, 300-301
heart, 187-190, 191-192, 291-293,
371-384
iron-sorbitol-citrate, 299
liver, 296-297, 475
lung, 302-303
monoclonal antibody-chelate,
479-480
neuroreceptor, 247, 248, 249
nuclear magnetic, 12, 148, 411,
414
pancreatic, 303
PET system, 98-101, 104, 200, 208,
209, 414
planar, 83, 465, 466, 467,
468-469
quality of, 84, 331, 344, 381-382
of radiolabeled antibodies, 26-27,
413, 414, 419-420, 458-459,
464-473, 477-480, 486, 489
scatter in, 89-90, 412, 465-466
sedatives for, 151
SPECT, 82-91, 413, 464-473
total-body, 119, 137-138, 151,
411-413, 459, 466, 479-480
IND, requirements for, 267, 268-270,
272-273
Indium 3+ benzyl EDTA
as chelate chase for antibody
complex, 479-490
Indium 3+ benzyl EDTA-transferrin
as chelate chase for antibody
complex, 479-480
Indium-111
Auger electron emission of, 654,
655, 663
binding to serum transferrin, 488,
670
blood cells labeled with, 276,
284-287, 648-660, 661-672, 673-687
in breast milk, 173, 174, 177, 652
chelate labeled radiopharma-
ceuticals, 477-492

contaminant affecting dose of, 140,
146, 275-281, 333, 335, 341, 649,
652
decay of, 649, 662-663
dose from close contact, 174-175,
184-185
effective dose equivalent of,
182-185, 663-665, 666
inaccuracies in data acquisition
of, 412
monoclonal antibodies labeled with,
26, 413, 416, 458-460, 462,
464-473, 477-490
S-factors for embryo or fetus, 159
Indium-111-antiferritin IgG
biokinetics, 459
whole-body imaging with, 458
Indium-111-antimyosin
uptake in infarcted myocardial
tissue, 381
Indium-111-benzyl EDTA
biokinetics, 477-482, 486-487
Indium-111-benzyl EDTA-CHA255 complex
absorbed dose estimates, 482
biokinetics, 477-482, 486-490
dose reduction following chelate
chase, 482
Indium-111-BLEDTA II
biokinetics, 477-482, 490
Indium-111-BLEDTA II-CHA255 complex
absorbed dose estimates, 483
biokinetics, 477-482, 487-490
dose reduction following chelate
chase, 483
Indium-111-BLEDTA IV
biokinetics, 477-482, 490
Indium-111-BLEDTA IV-CHA255 complex
biokinetics, 480
Indium-111-BLEDTA IV-CHA255 complex
absorbed dose estimates, 483
biokinetics, 477-482, 485-490
dose reduction following chelate
chase, 483
Indium-111-DTPA, contaminants in, 333,
335
effects of morphine on gastric
emptying of, 300
Indium-111-F(ab')2 of 19-9
antibodies
absorbed dose estimates, 471
biokinetics, 464-465, 466-473,
475
Indium-111-F(ab')2 of OC-125
antibodies
absorbed dose estimates, 471
biokinetics, 464-465, 466-473, 475
Indium-111-H17E2 (monoclonal antibody
to placental alkaline phosphatase)
biokinetics, 413, 416
Indium-111-IgG Fab

biokinetics, 487-490
distribution data, 484
Indium-111-IgG Fab-CHA255 complex
absorbed dose estimates, 485
biokinetics, 480-481, 483-485,
487-490
Indium-111-leukocytes
absorbed dose estimates, 173, 175,
650, 652, 657, 665-666
absorbed dose to infant from
breast milk, 173-174, 177, 652
contaminant affecting dose of, 652
distribution, 663-664
effective dose equivalent for,
128, 663-665, 666, 669
risk assessment, 661-671
Indium-111-lymphocytes
distribution, 651, 663-664
dose to cells, 648, 655, 665-666
radiation effects, 648,
655-657, 666-671
risk assessment for, 661-671
Indium-111-MAA
absorbed dose to heart wall, 263
Indium-111-monoclonal antibodies. See
specific antibody or monoclonal
antibodies.
Indium-111-neutrophils
dose to cells, 648, 655, 665-666
radiation effects, 648, 655
risk assessment for, 669
Indium-111-oxine. Also see specific
blood cell
contaminants affecting dose, 335
labeled blood cells, 276, 284-287,
652, 655-656, 666, 670, 680
sperm cell killing by, 53
Indium-111-platelets
absorbed dose estimates, 651
absorbed dose estimates in renal
pathology, 276, 284-287
distribution data, 651
dose to cells, 648, 655
radiation effects, 648, 655
Indium-111-transferrin, 488
Indium-113m-DTPA, effect of
metoclopramide on gastric emptying,
300
Indium-113m-HAM
dose to leg after intra-arterial
injection, 264
Indium-113m-leukocytes or lymphocytes
dose to cells, 657
Indium-113m-MAA
absorbed dose to heart wall, 263
Indium-114m and Indium-114
as contaminants in In-111, 333,
335, 341, 649
contribution to blood cell dose,
651-652
decay of, 649
**/Indium-111 absorbed dose ratios for
red marrow**, 341
Inflammatory disease, 649-650
Information density, 151-152
Inhalation, radiation exposure from,
0-15-CO₂, 194, 200-207
Injection site
radioactivity distribution at, 220,
297-298
Interior radiator randomness
(I-randomness), 68-71
Internal conversion
radiation emission by, 494, 496-497,
498-501
selenium-75 decay by, 57
tissue irradiation by, 13, 14, 53
**International Commission on
Radiological Protection (ICRP)**,
2, 4, 67-68, 121, 122, 134, 316,
383, 671
**International X-Ray and Radium
Protection Committee**, 2
Intestinal region, blood volume of,
577, 578
Intra-arterially injected particles,
260-265
Intracellular concentration factor,
53, 61, 64
Intraperitoneal administration,
radionuclide distribution affected
by, 55, 220
Iodine
internal and external exposure from
fallout, 628-647
radiation dose to thyroid from
fallout, 628-647
radioiodine mixture in fallout,
629-638
thyroid cancer risk coefficients,
634-638
Iodine-121/Te-121
contaminant in I-123, 335
Iodine-123
half-life, 381
radioiodide contamination affecting
distribution, 137
S-values for embryo or fetus, 159
in SPECT, 82, 96
**Iodine-123-BMIPP (15-(p-iodophenyl)-
-3-R,S-methylpentadecanoic acid)**
absorbed dose estimates, 374
committed effective whole-body
dose equivalent, 384
effective half-time in heart, 382
as myocardial imaging agent,
373-374
**Iodine-123-DMIPP (15-(p-iodophenyl)-
-3-3-dimethylpentadecanoic acid)**
absorbed dose estimates, 375

- committed effective whole-body dose equivalent, 384
 effective half-time in heart, 382
 as myocardial imaging agent, 374-375
- Iodine-123-FLA** (*N*-(1-ethyl-2-pyro-lidinylmethyl)-2-hydroxy-6-methoxy benzamide hydrochloride), 125
- Iodine-123-IMP** (isopropyl iodoamphetamine), in autoradiography, 110, 113
- drugs affecting biodistribution, 294
- Iodine-123-IPPA** (phenylpentadecanoic acid)
- absorbed dose estimates, 369, 376
 committed effective whole-body dose equivalent, 383, 384
 dose calculations and biokinetics, 359-369
 effective half-time in heart, 382
 as myocardial imaging agent, 375
- Iodine-123-IUDR** (iododeoxyuridine)
 electron yield, energy deposition and cell survival, 21
- Iodine-123-OIH** (orthoiodohippurate or hippuran)
- absorbed dose estimates, 146
 absorbed dose estimates in renal pathology, 278, 280, 284-287
 biokinetics, 139, 141-146
 conjugate counting uptake quantitation, 138
 contaminant affecting dose, 278, 281
 pediatric dose estimates, 281
 renal imaging with, 276-277
- Iodine-123-triphosphonium iodide**
- absorbed dose estimates, 377
 committed effective whole-body dose equivalent, 384
 effective half-time in heart, 382
 as myocardial imaging agent, 376-377
- Iodine-124**
- contaminant in I-123, 277-281, 333, 335, 338, 374-377, 383
 /Iodine-123 absorbed dose ratios for thyroid, 338
- Iodine-124-OIH**
- absorbed dose estimates, 146
 biokinetic data, 146
- Iodine-125**
- contaminant in I-123, 278, 335, 336-337, 359, 369
 cytotoxic effects of, 19, 21, 494
 energy deposition of, 18-21, 24-25
 HILED at decay sites, 494
 /Iodine-123 absorbed dose ratios for total body, 336
- Iodine-125-Concanavalin A**, 23
- Iodine-125-fibrinogen**
- absorbed dose to infant from breast milk, 169, 180
- Iodine-125-HSA**
- absorbed dose to infant from breast milk, 169
- Iodine-125-16-iodohexadecanoic acid**
- drug altered uptake of, 293
- I-125-IPPA**
- biokinetic data, 361
- I-125-IUDR**
- electron yield, energy deposition and cell survival, 21
- Iodine-125-OIH (Hippuran)**
- absorbed dose estimates, 146
 absorbed dose to infant from breast milk, 169
 biokinetic data, 146
- Iodine-125-MIBG**
- drugs altering biodistribution, 304
- Iodine-125-sodium iodide**
- hyperthyroidism therapy, 24-25
- Iodine-126-, -130-, -132-OIH**
- absorbed dose estimates, 146
 biokinetic data, 146
- Iodine-131**
- absorbed dose to fetus, 155-163
 absorbed doses to thyroid, 163, 622
 age-dependent retention of, 163
 age- and sex-dependent model for thyroid dosimetry, 613-627
 beta dose point kernel, 552, 557, 558, 559
 biokinetic maternal/fetal data, 158-163
 biological effects from, 19-20, 24, 536, 537, 542, 631-634
 bone marrow depression from, 536, 537, 542
 contaminant in Xe-133, 335
 internal and external thyroidal exposures, 628-647
 as label for antibody radiotherapy, 415, 563
 problems in data acquisition of, 411-412
 radiation dose from fallout, 628-647
 risk estimates for thyroid cancer, 630-631
- S-factors for embryo/fetus, 159
- S-factors for thyroid, 622
- TLDs(mini) calibrated for, 447
- Iodine-131-anti-CEA antibody**
- absorbed dose estimates, 440, 541, 542
- biokinetics, 432-441, 540-541
- bone marrow dosimetry, 535-544
- bone marrow toxicity, 542
- compartmental model for dosimetry, 427-441, 443-445
- Iodine-131-anti-p97 Fab**
- bone marrow depression, 537, 542
- tumor absorbed dose, 537

- Iodine-131-antiferritin IgG**
 absorbed dose estimates in therapy, 458
 response to therapy, 461
- 19-Iodine-131-cholesterol**
 drugs affecting biodistribution, 303-304
- Iodine-131-IgG melanoma antibody**
 biokinetics, 450, 453
- Iodine-131-IgG-p96.5 melanoma antibody**
 biokinetics, 449-450
 dose ratios, 453
 TLD absorbed dose measurements, 452
- Iodine-131-MAA**
 absorbed dose to heart wall, 263
 absorbed dose to infant from breast milk, 169
- Iodine-131-MIBG**
 absorbed dose estimates, 396
 biokinetic data, 389-396, 398
 drugs affecting biodistribution, 304
 effective dose equivalents, 184, 185, 396
 effective half-times, 392-393
 radiation exposure from radiotherapy patients, 181-185
 radiotherapy, 181-185, 390
- Iodine-131-monoclonal antibody**
 absorbed doses in intracavitary therapy, 417
 absorbed doses in therapy, 415
- Iodine-131-NP59**
 drugs affecting biodistribution, 303-304
- Iodine-131-OIH (Hippuran)**
 absorbed dose estimates, 146
 absorbed dose to infant from breast milk, 169
 absorbed dose in renal pathology, 278, 284-287
 drugs altering uptake in thyroid, 301-302
 for renal imaging, 275, 289, 302
- Iodine-131-p96.5 F(ab')₂ fragments of melanoma antibody**
 biokinetics, 452
 dose ratios, 453
- Iodine-131-p96.5 melanoma antibody**
 biokinetics, 448-449, 454
 TLD absorbed dose measurements, 451
- Iodine-131-sodium iodide.**
 absorbed dose to infant from breast milk, 169
 bone marrow depression, 536, 542
 radiotherapy for hyperthyroidism, 24
 radiotherapy for thyroid cancer, 536, 542
- Iodine-131-ZME melanoma antibody**
 biokinetics, 448-449
 dose rate analyses, 454-455
- Iodine-133 and -135**
 internal and external thyroid exposures, 628-647
 radiation dose from fallout, 628-647
 risk estimates for thyroid cancer, 630-631
- Iodipamide**, 301
- Iodobenzoate**, 137
- Iodohippurates**, absorbed dose from, 146, 277-281, 284-287, 289
- Iodophenyl pentadecanoic acid.** See **Iodine-123**.
- Ionizing radiation**
 alpha emission, 27-28, 30
 biological effects of, 2, 41, 42-44
 charged-particle interactions, 38-39
 cosmic, 3
 dose equivalent from naturally occurring, 1
 factors affecting absorption of, 83
 late effects of, 403-404
 in pediatric medicine, 148, 152-153
 plasmon decay, 39
 public fear of, 4-9
 risk-benefit of, 2-4
 safe dose of, 4-5
- Iridium-191m**
 absorbed dose estimates, 343
 contaminants in, 343
 generator production, 188-189
 for heart imaging, 187, 188-189
 radiation burden, 188
- Iridium-192**
 contaminant in Iridium-191m, 343
 absorbed dose estimates, 343
- Iron deficiency**, 311-312, 678
- Iron-dextran**, 297-298, 299
- Iron-55**, cytocidal effects of, 16, 53, 56, 58, 494
- Iron-59**
 absorbed dose to fetal liver, 164-165
 calculation methods, 156-157
 fetal/maternal biokinetics, 162-163
 S-factors for embryo/fetus, 159
 sperm killing by, 16, 53, 56
- Iron-59-transferrin**
 absorbed dose estimates for disease states, 315
 biokinetics, 310-316
 effective dose equivalents in disease states, 315
- Iron-sorbitol-citrate**, 299
- Isolation, patient**, 181-185

Isopropyl-p-iodo-amphetamine, 110, 113, 114, 294
Isoproterenol, 292
Isosorbide dinitrate, 292
Isotropic field, 73-76, 79-80

K

α -Ketoisocaproate. See also C-14- or H-3-KIC
in protein metabolism, 681-686

Kidney

absorbed doses from isotopes of I-labeled iodohippurate, 146
absorbed dose from myocardial imaging agents, 373-380
absorbed dose from Tl-201-chloride and contaminants, 340
blood volume of, 577
chemotherapy affect on, 298
chromium-51 in disease of, 678
cumulated activities for radio- iodine in, 146, 365, 368
dose in children, 153-154
dose reduction after chelate chase, 482-485
drug-altered function, 302
flow studies, 275, 277, 279, 288, 289
iodine labeled orthiodohippurate studies of, see specific radionuclide
iodine-123-PPA dose estimates for, 369, 376
iron-59 absorbed dose in disease states, 315
long-term effects of irradiation, 289
PET scan of, 99-100
phosphate uptake in, 298
platinum damage to, 494
radiopharmaceuticals for studies of, 275-288, 289-290
rubidium-82 kinetics and absorbed dose in, 346, 351-356
technetium-99m-DEPE absorbed dose in, 127
transplants, 279-288
Kidney-bladder model, 120
Kinetic models. See Models.
Kinetics. See also specific radionuclide or radiopharmaceutical acquisition of human data, 82-96, 97-102, 105-118, 135-147, 347-356, 411-415, 459, 465-473, 537-539
arterial infusion of labeled microspheres and macroaggregated particles, 260-265

beta emitters in homogeneous tissues, 562-571
bladder, 120-121, 587-612
blood, 574-586
blood cells, 648-660, 661-672, 673-680
bone and marrow, 298, 514-534, 535-544
cell, 13-25, 26-36, 52-66, 67-81, 493-513, 514-534, 535-544
drugs that alter, 291-318
fetal, 158-164
iron, 163-164, 297-299, 311-313, 316
myocardial imaging agents, 371-388
neuroreceptor binding radioligands, 245-260
pathology affecting, 264, 275-279, 291-309, 311-316, 398
positron emitters, 98-101, 194-211, 212-216, 217-238, 239-244, 245-260, 350-356, 372, 376-379, 382, 598-611
radiolabeled amino acids, 55-57, 172-173, 217-238, 239-244, 681-687
radiolabeled monoclonal antibodies, 26-36, 409-420, 421-445, 446-457, 458-463, 464-476, 477-492, 493-513
radiopharmaceuticals in breast milk, 167-178
thyroid, 613-627, 637
Krypton-81m
in blood pool imaging, 187
generator production of, 187-188
in lung imaging, 192
Krypton-85
contaminant in Xe-133, 333, 335

L

Lead-201
as contaminant in Tl-201, 335
absorbed doses from, 340
Lead-203
as contaminant in Tl-201, 335
absorbed doses from, 340
LIB thermoluminescent dosimeter, 174
Lactoferrin, gallium binding to, 172
Legs, blood volume of, 577
Leucine
absorbed dose estimates and kinetics for C-14- and H-3-labeled, 681-686
resolution of C-11-DL-labeled, 239-240
uptake of N-13-labeled, 219, 229
Leukocytes. See also indium-111
alternative labeling of, 657

assessment of cancer risk from radiolabeled, 661-671
physical parameters for, 654, 669

Lidocaine, 295

Ligand competition, 247, 249

Line source array calculations, 197-198, 202-206

Linear Energy Transfer (LET), 20, 39, 494

Lipiodol, 301

Liver
absorbed dose from Cr-51-RBC in disease states, 678
absorbed dose in fetal, 163-165
absorbed dose from Mo-99 contaminated radiopharmaceuticals, 326-328
absorbed dose from myocardial imaging agents, 373-379
absorbed dose from P-32- and Y-90-MoAb, 416
absorbed dose from Tl-201-chloride and contaminants, 340
antitumor antibody in, 429, 432
blood volume of, 577
bromine-77-spiperone kinetics and absorbed dose, 122-124
CT tumor volumetrics in, 460, 461
cumulated activities for iodine isotopes in, 364, 368
dose reduction after chelate chase, 482-485, 490
imaging of, 99-100, 153, 261-262, 473, 475
iodine-123-PPA dose estimates for, 369, 376
iodine-131-MIBG kinetics & absorbed dose in, 390, 391-392, 395-396
iron-59 uptake and absorbed dose in, 164, 314, 315
kinetics of Mo-99 in, 324-328
over-dose in radioimmunotherapy, 416
PET scans of, 99-100
radiolabeled amino acids uptake in, 225-235
radiolabeled antibody absorbed dose and kinetics in, 416, 438, 440, 449, 454, 458-460, 471-473, 475, 482-485, 488, 537-542
radiolabeled blood cell kinetic data & dose to, 649, 650, 651, 657, 664
rubidium-82 kinetic data & dose estimates for, 352, 355, 356
technetium-99m-DEPE kinetics and absorbed dose in, 128-132

technetium-99m-TPPS kinetics & absorbed dose in, 124-127
tumor treatment, 261-262, 458-463

Lugol's solution, as radioiodide competitor, 301

Lungs
absorbed dose from myocardial imaging agents, 373-379
blood volume of, 577
bromine-77-p-bromospiperone kinetics and absorbed dose in, 122, 123
cumulated activities for radioiodine in, 364, 368
dose reduction after chelate chase, 482-485
imaging, 24, 176, 177, 302-303
iodine-123-PPA dose estimates for, 369, 376
iodine-131-MIBG uptake and absorbed dose in, 395, 396
rubidium-82 kinetic data & dose estimates for, 352-353, 355, 356
Tc-99m-DEPE kinetics & absorbed dose in, 131-132
Tc-99m-TPPS kinetics & absorbed dose in, 126-127

Lymphoblasts, mutations induced by I-125-IUDR, 21

Lymphocytes. See also In-111-labeled alternative labeling of, 657
assessment of cancer risk from radiolabeled, 666-669
cancer of, 666, 668-669
physical parameters for, 654, 656, 669
radiosensitivity of, 655-656, 662, 666, 668-669

Lymphomatous disease, 212

M

Macroaggregated albumin particles, 170, 171, 175, 261, 262-264

Macrodosimetry, 13, 14

Mannitol, 302

Marrow. See **Bone marrow**.

Marshallese
radioiodine dose to, 629, 632, 634
thyroid cancer in, 629-630, 632-635

Mass
in calculation of dose, 28, 29, 30, 31, 362, 370
in compartmental analysis, 427-428
uptake of radionuclide altered by, 394, 395

Mass-normalized exchange rates, 427-428

Mean absorbed dose, 67-76, 360
Mean-free-path (μ) randomness,
68-71, 73
Mean lethal dose, 15
Mechlorethamine, 300
Meckel's diverticulum, 301
**Medical Internal Radiation Dose
(MIRD)**
 blood model, 574-586
 calculations compared with TLD
 measurements, 45
 data for betas per disintegration,
 198
 dosimetry schema, 67-68, 156,
 422-423, 563
 inadequacy of calculations for
 microdosimetry, 15-18, 52, 53, 563
 iron-59 dose report, 316, 318
Medicines Regulations of 1978, 118
Melphalan, 298
Menkes' kinky-hair syndrome, 212
Mental diseases, nuclear medicine
 tests for, 2
Meperidine, 297
Meprobamate, 301
Mercury-195/gold-195m generator, 186,
 187
Mercury-195m
 contaminant in Au-195m, 342
Mercury-203, beta dose point kernel
 for, 552, 555, 556
Methionine,
 cellular concentration of, 63-64
 H-3-labeled, 52-64
 N-13-labeled, 218, 219, 228
 S-35-labeled, 52-64
 Se-75-selenomethione, 52-64
 spermatagonial killing by, 54,
 58-59
Methotrexate, 296, 299, 300
Methoxyfluorane, 296
Methyldopa, 294, 295
Methylprednisolone, 292
Metoclopramide, 300
Metyrapone
 adrenal response to, 303
 radiopharmaceutical uptake with, 294
Microdosimetry
 absorbed fractions in cell for
 alpha particles & electrons
 71-76, 81
 alpha particles, 26-36, 418
 beta emitters, 52-64, 563-571
 Bi-212-MoAB, 30-33
 Bi-212 + Po-212, 33-34
 bone marrow absorbed fractions for,
 514-534
 Br-77-UdR, 21
 charged particle track structures
 in, 37-51
 compared to organ dosimetry, 13-25,
 53, 56-64, 411, 418
 compartmental model incorporating
 microscopic source regions, 440
 Cr-51-sodium chromate, 15
 H-3-methionine, 52-64
 H-3-UdR, 21
 I-123-IUdR, 21
 I-125-IUdR, 21
 K-43, 18
 P-32 source in inhomogeneous
 tissue, 563-571
 cis-Pt-193m, 493-513
 cis-Pt-195m, 493-513
 Po-212, 33-34
 in radioimmunotherapy, 418
 Rb-86, 18
 S-35-methionine, 52-64
 Se-75-selenomethione, 15, 52-64
 Tl-201-chloride, 15, 16, 18, 27
 Tl-204-chloride, 16
Milk. See breast
Minerals, thyroidal blocking by, 301
Mitochondria, copper use by, 216
Models
 adult anatomical, 68
 animal, 53, 54, 98-101, 212-215,
 217-238, 239-242, 249-250,
 446-456, 467-469, 477-490, 507-508
 assumptions affecting, 415-416,
 419
 for beta dose calculations in
 inhomogeneous tissue, 564-571
 for bladder wall absorbed dose,
 587-612
 for blood, circulating, 575-580
 brain phantom, 255-256
 compartmental, 120-121, 123, 127,
 132, 298, 319-323, 370, 421-445,
 613-627, 674-677
 for dosimetry of radiopharma-
 ceuticals contaminated with Mo-99,
 319-323
 embryo/fetus phantom, 155-156
 for F-18 kinetics in bone, 298
 for I-131 kinetics in thyroid,
 613-627
 for iron kinetics in man, 311-313,
 316
 for kidney uptake, 142-143
 mathematical, for bone and marrow
 dosimetry, 514-534
 mathematical, for calculating
 specific energy densities for
 alpha particles, 30-33
 mathematical, for charged-particle
 passage in liquid water, 39,
 41-42, 51
 mathematical, for decay processes,
 496-501

mathematical, for transversal of radiation in cells, 67-71, 77-80
for radiolabeled monoclonal antibodies, 415, 421-445, 464-470, 477-490
Riggs/ICRP iodine, 614-616
Tc-99m-diphosphonate kinetics in bone, 298
tracheal phantom, 201-206
Modulation transfer function, 112
Molybdenum-99, contamination in Tc-99m radiopharmaceuticals, 319-342
Monoclonal antibodies, radiolabeled absorbed fraction data for, 73 alpha-labeled, 27-29, 30-34 anti-CEA antibody, see I-131 antiferritin IgG, see In-111 and Y-90 as beta emitting carriers, 563 biodistribution of, 449, 464 bone marrow localization of, 537, 538, 544 CHA235 complex, see In-111 CHA255 complex, see In-111 chelate chase of, 479, 480-485 direct measurements of dose, 447-453, 455 dosimetry problems in therapy, 409-415, 418 Fab CHA255 complex, see In-111 F(ab)₂ of 19-9 antibodies, see In-111 F(ab)₂ of OC-125 antibodies, see In-111 H17E2, see In-111 IgG-p96.5 melanoma antibody, see I-131 imaging of, 26-27, 413, 414, 419-420, 486-489 models for, 415-416, 419, 427-441 protein catabolism effect, 431-432 radionuclides for labeling, 26-27, 409-410, 415, 418, 420, 563 requirements for effective therapy with, 26-27, 409-411, 414-415, 422, 441 specificity of, 409 subcutaneous injection of, 488 tumor treatment with, 26, 33-36, 427-441, 462-463, 478 useless radiation exposure from, 478 ZME-018 melanoma antibody, see Y-90
Monocytes, physical parameters for, 654
Monoenergetic dose point kernel, 546-547, 548-550, 551
Monte Carlo calculations
absorbed fraction estimation, 71, 156, 164 charged particle in water, 28, 29, 39, 41-42, 51 dose point kernel, 546, 552, 559 isotope radiation simulations, 494, 495, 496-501 particulate radiation distribution, 77-80 photon transport, 515 for SPECT scatter estimation, 90
Morphine, 297
Mortality, from radiation exposure, 4
MPAA (minimum practical administered activity), 267
MUMPI system, 84
Myocardial imaging
adrenal tumor competition with, 398 F-18-fluorodeoxyglucose for, 3, 372-373 quality of, 318-382 radiolabeled fatty acids in, 3, 359, 373-376 rubidium-82 in, 346, 377-378 technetium-99m-labeled agents for, 379-381 thallium-201 for, 371
Myocardial infarction
agents that localize in, 3, 380-381 drugs affecting radiopharmaceutical uptake in, 291-293

N

Narcotic addicts, lung scans in, 303
Nasopharyngeal radiation dose, 206-207
National Council on Radiation Protection (NCRP), 4
National Institutes of Health
probability and causality report 400, 405
Natural radiation, 3-5
Nembutal
gastrointestinal response to, 309 radiopharmaceutical distribution unaffected by, 151
Neoplastic diseases. See **Cancer or Tumor**
Neuroblastoma
iodine-131-MIBG concentration in, 389 radiation exposure from radiotherapy patient, 182-185
Neuroreceptors
density of, 248 distribution studies of, 246-247

- imaging, 247, 248, 249
- ligand binding to, 249
- properties of, 246
- types of, 246
- Neutrophils**
 - physical parameters for, 650, 654, 665, 669
 - radiosensitivity of, 655
- New Drug Application (NDA),** 267
- Nicotinic acid**
 - false positive scans from, 297
 - radiopharmaceutical uptake altered by, 369
- Nitrates,** 292
- Nitrogen-13**
 - absorbed dose levels of, 195
 - amino acids labeled with, 218-238
 - in myocardial imaging, 102, 371
- Nitrogen-13-O-aminobutyric acid**
 - biokinetics and metabolism, 217-224, 231
- Nitrogen-13-ammonia**
 - biokinetics and metabolism, 217-224, 225, 232, 233, 234, 236, 238
 - PET imaging of heart, 101, 102, 371
- Nitrogen-13-cis-platinum**
 - distribution of, 512
- Nitrogen-13-glutamate**
 - biokinetics and metabolism, 217-224, 226
- Nitrogen-13-glutamine**
 - biokinetics and metabolism, 217-224, 227, 235, 237, 238
- Nitrogen-13-leucine**
 - biokinetics & metabolism, 217-224, 229
- Nitrogen-13-methionine**
 - biokinetics & metabolism, 217-224, 228
- Nitrogen-13-urea,** 218
- Nitrogen-13-valine,**
 - biokinetics and metabolism, 217-224, 230
- Nitroglycerin,** 292, 293
- Notice of Claimed Investigational Exemption for a New Drug (IND),** 267
- Novel drugs,** dose calculation for, 121-132
- Nuclear dose rate enhancement factor,** 61-63
- Nuclear energy,** fear of, 4, 8, 9
- Nuclear medicine**
 - future of, 11
 - multiple procedures in renal patients, 275-290
 - radiation protection methods for, 181-182
 - regulations restricting, 6-8
- sedatives used in,** 151
- Nuclear magnetic imaging,** 12, 148
- Nuclear power,** opposition to, 4
- Nuclear Regulatory Commission (NRC),** 8
- Nuclear war,** 4, 5
- Nuclear waste,** disposal of, 7-8
- Nucleus, cell**
 - dose rate enhancement factor for, 60-64
 - electron energies for penetration of, 81
 - radiation path through, 72-73
- Nursing infant,**
 - absorbed dose from close contact with mother, 174-176
 - absorbed dose from radiopharmaceuticals in breast milk, 169, 170, 173
 - dose equivalent from In-111-WBC activity in breast milk, 652
- O**
- Obstruction, renal,** 275, 277-279, 288, 289
- Occult papillary carcinoma,** 630
- Optical density,** 106, 107-111
- Orphan Drug Act (Public Law 97-414),** 399
- Osmium-191**
 - absorbed dose estimates, 342, 343
 - contaminant in Ir-191m, 342, 343
- Osmium-191/iridium-191m generator system,** 186, 187, 188, 191-192, 343
- Osteocytes**
 - number of alpha particles needed to kill a cell, 36
- Osteogenic cells,** radiation risks for, 516-517, 536
- Osteomyelitis,** tests for, 149
- Ouabain,** 16, 17, 293
- Ovaries**
 - absorbed doses from isotopes of I-labeled iodohippurate, 146
 - absorbed doses from myocardial imaging agents, 373-380
 - absorbed dose from Tl-201-chloride and contaminants, 340
 - C-11-NMSP dose estimate for, 250
 - cavity therapy for cancer of, 417
 - iodine-123-PPA dose estimate for, 369, 376
 - iodine-131-MIBG dose estimate for, 396
 - rubidium-82 dose estimate for, 352, 353, 355, 356
- Oxygen, myocardial requirements for,** 292

Oxygen-15, absorbed dose level, 195
absorbed dose in vein wall, 195-200
Oxygen-15-CO₂
absorbed dose in trachea, 200-208,
210-211

P

Palladium-109, as possible label
for antibody radiotherapy, 563
Palmitate
C-11-labeled, 376
splenic response to, 296
Pancreas
absorbed dose from myocardial
imaging agents, 373, 378
drug-altered scans of, 303
radiolabeled amino acids uptake
in, 225-235
Papillary carcinoma, thyroid, 630
Parathyroid hormone, 297
Particle tracks, 517-521
Path, radiation
calculation of, 77-80
in microdosimetry calculations,
68-76
in radiolabeled blood cells, 649
Pediatric nuclear medicine, 148-154
dose estimation in, 149-150, 151,
153, 289
parent contamination from radio-
therapy, 182-185
risks of, 152-154
sedative use in, 151
ultrashort-lived radionuclides for,
188
Pentagastrin, 301
Pentobarbital anesthesia, altered
radiopharmaceutical uptake with,
293
Perchlorate ions, iodide competition
with, 301
Pertechnetate. See also Tc-99m
aluminum affecting imaging with,
295
thyroidal iodine uptake and, 301
Phantoms. See also Models.
Alderson, 465, 469
anthropomorphic conceptual, 259
brain, 255, 256
for fetal dose estimates, 155
organ, 466, 467, 470
for short-lived radionuclide
dosimetry, 192
tracheal, 201-206
Phase I studies, new drug, 267,
270-271
Phenobarbital
gastrointestinal response to, 309

in hepatobiliary scans, 296
radionuclide uptake altered by, 299
Phenoxybenzamine, 304
Phenylbutazone, 301
Phenylephrine, 304
Pheochromocytoma
iodine-131-MIBG uptake in, 393,
394, 395, 398
scintigraphic localization of, 389
Phosphate, 292
Phosphorus-32
backscattered dose from, 568-570
beta dose point kernel for, 545-560
imaging with antibodies, 414
as label for antibody radiotherapy,
27, 415
microdosimetry for beta source in
bone marrow, 562-571
TLDs (mini) calibrated for, 447
P-32-chromic chloride
intracavitary therapy with, 407
Photometric linearity, 112
Photometric uniformity, 112
Photon emitters
calculation of bone dose from, 515,
524-532
external imaging with, 26-27
in planar imaging, 83
in SPECT imaging, 87
Pitressin, 301
Planar imaging, 465-471
quantitative properties compared to
SPECT, 464-471
Plasma radioactivity, 120
Plasmon, 39
Platelets. See also In-111-labeled
physical parameters for, 654
radiosensitivity of, 648, 655
cis-Platinum, cancer therapy with,
494, 507, 508-509, 512
Platinum-193m
in cancer therapy, 494-495
decay of, 496-501
dose rates, 506, 512
electron spectra for, 494, 495, 496
localized energy deposition by,
501-504
microdosimetry, 493-513
radioimmunotherapy with, 505-509
specific activity for, 504, 505
Platinum-195m
in cancer therapy, 302, 494
decay of, 496-501, 502, 508
microdosimetry, 493-513
radioimmunotherapy with, 507
specific acitivity for, 505
Point source function, 195, 196-198,
202-206
Polonium-212
microdosimetry for, 33

Positron Camera System, 200, 208, 209
Positron Emission Tomography (PET) in amino acid imaging, 239, 414, 419-420
attenuation correction, 99
brain imaging with, 2, 98, 99, 100, 245-259
copper-64 tumor imaging with, 213, 216
expense of, 11-12
with fluorine-18, 98
instrumentation, 97-98
neuroreceptor imaging with C-11-NMSP, 245-259
partial volume effect, 257
in pediatric medicine, 152
quantitation of bladder activity, 253
quantitation of data for dosimetry, 97-102, 257-258
of receptor ligand competition, 247, 248
rectilinear scanning and, 97, 99-100
resolution, 97-98, 100, 104, 257, 414
with rubidium-82, 98, 189-190
time-of-flight in, 104
Positron emitters. See specific radionuclide
helicity of, 244
Potassium-43 cellular concentration of, 16, 17
in myocardial imaging, 3, 371
Potassium iodide, 390, 393, 394
Practical threshold for low-level radiation, 5
Prazosin, 295
Prednisone, 299
Probability average, 406
of causation, 403-406
coherence constraints on, 401
historical background for, 399-402
of exchangeable events, 401
radiogenic cancer, 403, 404-406
of unique events, 401, 402
Probability density function, 30, 31-33, 71, 73, 79
Probenecid, 302
Procainamide, 293
Procarbazine, 299
Propanolol, 292, 293, 294
Propylthiouracil, 301, 303
Prostaglandins, 303
Protein catabolism, 431-432
Protein metabolism, radiolabeled amino acids for, 681, 682-683
Pseudoephedrine, 304

Public Law 97-414, (Orphan Drug Act), 399
Pulmonary interstitial fibrosis, 303
Putamen, brain absorbed dose in, 247-248, 251-252

Q

Quality factor, 38
Q-density, 32
Quinidine, 293, 295

R

Rad, definition of, 28
Radiation benefit-risk assessment of, 1-3
cancer from, 1, 273, 403-405, 629-633, 655-657, 661-671
cosmic, 3
dose. See Dose, radiation
natural, 3-4
safety standards for, 2, 4-5, 181-182
zero threshold hypothesis for, 4-5
Radioactive drugs, requirements for testing new, 268-273
Radioactive materials disposal of, 7-8
transportation of, 6-7
Radioactive Substance Advisory Committee (ARSAC), 118
Radiogenic cancer, 1, 273, 403-405, 629-633
Radiographic contrast agents, 294
Radiohalogens, biological effects of, 19, 21, 33
Radioimmunotherapy. See also Monoclonal antibodies, radio-labeled
bone marrow toxicity from, 536-537, 541-542
dosimetry considerations in, 409-420
for hepatoma, 458-460, 461
for metastatic colon cancer, 537, 540-542
with platinum isotopes, 493, 495, 505-509
radionuclide path determination for, 68-76, 77-80
TLD quantitation of response in tumor model, 446-456
Radiolabeled antibodies. See Monoclonal antibodies, radiolabeled
Radioligands, 247-251, 258
Radionuclides. See specific radioisotope

Radiopharmaceuticals. See also specific listings.
aluminum-altered distribution of, 295
autoradiographic determination of distribution, 105-111
breast milk contamination with, 167-174, 176-178, 180, 652
calibration and expiry time, 333-335
disposal and safety of, 6-9
drug-altered kinetics of, 291-308
FDA guidelines for, 152-153, 268-273
PET measurements of, 97-102, 104, 253, 257-258
receptor study with, 245-259
in renal studies, 275, 277, 279, 284-287
requirements for new, 119, 120, 267-273, 359
reversibly bound, 489
SPECT measurements of, 82-84, 91, 413, 414, 464
transportation of, 6-7, 9

Radium-dial painters, 5

Radius, charged-particle track, 39

Receptors. See Neuroreceptors

Reconstruction algorithm, 96

Red blood cells, radiolabeling of, 294-295

Reference Man, 427-429, 432-436

Rejection, kidney transplant, 276

Regulations, nuclear medicine, 6-8

Relative biological effectiveness (RBE)
of Auger emitters, 59-60
in average dose calculations, 38, 63-64
of beta emitters, 59-60
radionuclide localization altering, 60

Renal disease. See Kidney

Renographin, 294

Replacement therapy, thyroid, 637

Reserpine, 304

Resolution
autoradiographic, 111, 112
Gray scale, 112
PET system, 97-98, 101, 104, 257, 412-414
SPECT system, 86

RES stimulants, 295

Restraints, pediatric, 150

Reticuloendothelial system
antibody exchange in, 429
radionuclide uptake in, 475-476

Retro-orbital administration, 220

Reversible radiolabeling, 488-489

Rhenium-186
TLDs (mini) calibrated for, 447

Riggs/ICRP metabolic model for iodine, 614-616

Risks, radiation, 1, 3-4
of cancer, 4, 38, 403-406, 655, 666, 668-670
practical threshold of, 5
public perception of, 4-9, 12
zero threshold hypothesis for, 4-5

Ro-151788, 294

Rongelap inhabitants, fallout doses for, 630, 637, 642-644

Rubidium-81, 188
absorbed dose contribution as contaminant in Kr-81m, 342
physical half-life for, 186, 342

Rubidium-81/krypton-81m generator system, 186, 187, 188-189, 193, 342

Rubidium-82
absorbed dose estimates, 198-200, 346, 348-350, 352, 378, 384, 385
calculation of dose to vein wall, 195-200
committed effective whole-body dose equivalent, 383, 384
contaminants in, 189, 191, 342, 355-356, 377-378, 383
effective half-time in myocardium, 378
generator production of, 189-190, 346-347, 377
kinetic data, 346-356, 377-378, 385
for myocardial imaging, 189-191, 377-378, 385
physical half-life, 185, 192, 377

Rubidium-85
in cyclotron production of Sr-82, 189
physical half-life, 189

Rubidium-86
distribution, 377
radiotoxicity in cells, 16-17

Rubidomycin, 292

Ruthenium-97, leukocytes or lymphocytes, absorbed dose to WBC, 657

S

Safety

new drug, 267-272
public perception of, 4-6
radiation, 2

Salivary glands, I-131-MIBG uptake in, 392-393, 395-396

Sapirstein tracer, 189

- Scaled dose point kernel**, 546, 547, 548-550, 560
Scandium-47, candidate for labeling, monoclonal antibodies, 27
Scanning time, autoradiographic, 112-113
Scatter, in imaging techniques, 89-90, 465-466, 470
Scavengers, biochemical, 44, 49
Secondary electron energy transport, 514-515, 524
Sedatives, radiopharmaceutical uptake altered by, 151
Self-dose calculation, 157, 348, 350, 352, 355
Selenium-75-selenomethionine
 absorbed dose to infant from breast milk, 172-173
 cellular concentration, 14, 15, 59-60, 63-64
 diagnosis of pancreatic tumors, 239
 dose rate to cells, 18
 kinetics, 54-64
 mean lethal dose in cells, 15
 microdosimetry, 18, 52
 radiotoxicity of, 59, 64
 RBE, 59-60, 64
Signal-to-noise ratio, in autoradiography, 112
Simulation, Analysis, and Modeling (SAAM) computer code, 313, 432, 444
Sincalide, 296
Single exponential model, 319-329
Single photon emission computed tomography (SPECT)
 attenuation compensation, 87-88, 465-466
 comparison with planar imaging, 465-473
 development of, 82
 factors affecting, 86-91, 96
 instrumentation for, 83-85, 86-87
 liver scan with, 472-475
 reconstruction, 87-91, 96, 466
 scatter compensation, 89-90
 spatial resolution, 88-89, 413
 system calibration, 90-91
 uptake quantitation with, 82-84, 91, 413, 414, 464
Skeleton. See also Bone.
 absorbed fractions for, 520-524, 525, 526
 descriptive parameters for human, 527
 dose estimates for, 529
 dosimetry considerations for, 514-532
Sodium-24
 as contaminant in I-123, 335
Sodium chromate, 14, 15
Sodium nitroprusside, 292
Somatostatin, 296, 300
Spatial resolution, in autoradiography, 112
Specific absorbed fractions,
 for embryo or fetus, 156-157, 164
 for thyroid, 620
Specific energy density, 28-34
 biological effects related to, 33, 34
Spermatogenesis, radiosensitivity of, 53, 54, 56, 58-59, 66
Spherical dynamic bladder model, 587-611, 612
Spleen
 absorbed dose from indium-labeled blood cells, 649-651, 657, 664
 absorbed dose from myocardial imaging agents, 373-379
 blood volume of, 577
 cumulated activities for iodine in, 365, 368
 dose reduction after chelate chase, 482-485, 490
 enlarged, 296
 iodine-131-MIBG kinetics and absorbed dose in, 391-392, 394-396
 iron-59 kinetics and absorbed dose in, 314, 315
S-randomness, 68-71
 for calculation of absorbed fractions, 72-73
 for probability density function, 71
Stability
 image analysis, autoradiographic, 112
 radiopharmaceutical, 271
Stem cells, 536
 radiotherapy risks to, 516, 536-537
Stereoselectivity, 244
Steroids
 iodine uptake altered by, 301-302
 radiopharmaceutical uptake altered by, 295, 303
 splenic response to, 296
Stomach, cumulated activities of iodine in, 366, 368
Strontium-82
 contaminant in Rb-82, 191, 342, 355, 377-378
 production of, 189
 radiation burden from, 189
Strontium-82/Rubidium-82 generator, 189, 191, 346, 347, 377
 breakthrough, 191, 355
Strontium-85
 contaminant in Rb-82, 191, 355, 377

Subcutaneous injection, monoclonal antibodies, 488
Sulfur-35
 beta emission, 54, 57
Sulfur-35-methionine
 cellular concentration, 59-60, 63-64
 dose point kernel, 552, 554, 556
 kinetics, 54-64
 microdosimetry, 52
 radiotoxicity of, 59, 64
 RBE, 59-60, 64
Surface radiator randomness
 (S-randomness), 68-71
 in absorbed fraction calculations, 72-73
 for probability density function, 71
S-values
 age- and sex-dependent for I-131
 in thyroid, 618-620, 622
 correction method for remaining body activity, 353
 errors in published for bladder, 252-253
 in MIRD and ICRP dosimetry schema, 67-68
 for pediatric absorbed dose estimates, 276
 for self-irradiation of embryo or fetus, 157-159
 source for absorbed dose calculations, 121-122, 276, 313, 348, 362, 368

T

Technetium-99m
 aluminum effect on radiopharmaceutical distribution, 295
 blood cells labeled with, 294, 649, 657
 in blood pool imaging, 294-295
 cellular concentration of, 15
 labeled cations for myocardial imaging, 379-380
 Mo-99 contamination in, 319, 324-329, 330, 342, 345
 replacement for iodinated hippuran, 290
 S-values for embryo or fetus, 159
 in SPECT imaging, 82, 87, 96
Tc-99m-albumin microspheres
 drugs affecting lung perfusion images, 303
Tc-99m-DEPE
 absorbed dose estimates, 132
 biokinetic data, 128-132

Tc-99m-DIARS Complexes
 as potential myocardial imaging agents, 379
Tc-99m-diphosphonate
 aluminum effect on biodistribution, 295
 drugs affecting biodistribution, 298, 303
Tc-99m-DISIDA
 kinetics and absorbed dose to liver from Mo-99 contamination in, 325-327
Tc-99m-DMPE complexes
 as myocardial imaging agents, 379
Tc-99m-DMSA
 drugs affecting kidney uptake, 302
Tc-99m-DTPA
 absorbed dose to infant from breast milk, 170
 absorbed dose rate at breast surface, 176
 absorbed dose in renal studies, 284, 285, 286, 287
 breast milk excretion of, 170, 171
 drugs affecting kidney images, 302
 kinetics and absorbed dose to bladder, 587, 598-611
 kinetics and absorbed dose to liver from Mo-99 contamination in, 325-328
 kinetics in vein, 195-196
 for renal studies, 274, 276, 282, 289
Tc-99m-DTPA aerosol
 absorbed dose to infant from close contact with mother, 175
 absorbed dose rates at breast surface, 176
 breast milk excretion of, 171
 drugs affecting lung images, 302
Tc-99m-EDTA
 absorbed dose to infant from breast milk, 170
 breast milk excretion of, 170, 171
Tc-99m-EHDP, 298
Tc-99m-gluconate, 297
 absorbed dose to infant from close contact with mother, 175
 absorbed dose rate at breast surface, 176
Tc-99m-HAM
 absorbed dose estimates, 264-266
 kinetics for intra-arterial injection of, 260-265
Tc-99m-HEDP
 drugs affecting biodistribution, 277
Tc-99m-Heparin, 294

- Tc-99m-HIDA**
 drugs affecting biodistribution, 296-297, 309
- Tc-99m-HSA**
 drugs affecting biodistribution, 293
- Tc-99m-leukocytes or lymphocytes**
 absorbed dose to cells, 657
- Tc-99m-MAA**
 absorbed dose estimates, 262, 263
 absorbed dose to infant from breast milk, 170
 absorbed dose to infant from close contact with mother, 175
 absorbed dose rate at breast surface, 176
 breast milk excretion of, 170, 171
 kinetics for intra-arterial injection of, 260-265
- Tc-99m-MDP (Medronate)**
 absorbed dose to infant from breast milk, 170
 absorbed dose to infant from close contact with mother, 175
 absorbed dose rate at breast surface, 176
 breast milk excretion of, 170
 kinetics and absorbed dose to bone and liver from Mo-99 contaminant in, 325-329
- Tc-99m-Pertechnetate**
 absorbed dose to infant from breast milk, 170
 absorbed dose rate at breast surface, 176
 aluminum affecting biodistribution, 295
 breast milk excretion of, 170
 drugs affecting biodistribution, 293, 294, 300, 301
 kinetics and absorbed dose to liver from Mo-99 contamination in, 325-327
- Tc-99m-PYP altering biodistribution**, 293
- Tc-99m-PIPIDA**
 drugs affecting biodistribution, 296-297
- Tc-99m-Plasmin**
 absorbed dose to infant from breast milk, 170
 breast milk excretion of, 170
- Tc-99m-PM-Tetracycline**
 effect of isoproterenol on distribution, 292
- Tc-99m-(POM-POM)₃**
 as potential myocardial imaging agent, 379-380
- Tc-99m-Porphyrin (TPPS)**
 absorbed dose estimates, 127
- biokinetic data, 124-127
- Tc-99m-PYP (Pyrophosphate)**
 committed effective whole-body dose equivalent, 384
 drugs affecting distribution, 292, 297-298
 effect on Tc-99m-pertechnetate brain scan, 293
 kinetic data and absorbed dose estimates, 371, 380, 382, 383
- Tc-99m-RBC**
 absorbed dose to infant from breast milk, 170
 breast milk excretion of, 170
 drugs affecting biodistribution, 293
 drugs altering labeling efficiency, 294-295
- Tc-99m-SC**
 absorbed dose rate at breast surface, 176
 aluminum effect on distribution, 295
 CT for liver study, 461
 drugs affecting biodistribution, 295-296, 300-301
 kinetics and absorbed dose to liver from Mo-99 in, 325-329
- Tc-99m-SC-DTPA CCL**
 drugs affecting biodistribution, 300
- Tc-99m-(TBIN)₆**
 as potential myocardial imaging agent, 380
- Tc-99m-(TMP)₆**, as potential myocardial imaging agent, 379
- Testes**
 absorbed doses from isotopes of I-labeled orthoiodohippurate, 146
 absorbed doses from myocardial imaging agents, 373-379
 biokinetics and biological effects of Auger electrons and beta emitters in, 52-64
 intratesticular administration, 55
 iodine-123-PPA dose estimate for, 369, 376
 iodine-131-MIBG dose estimate for, 396
 microdosimetry, 56-64
 radiosensitivity of, 53, 54
 rubidium-82 dose estimate for, 352, 354, 355, 356
 spermatogenesis, 52
 thallium-201 dose estimate for, 356
- Thallium-200**
 absorbed doses from, 340
 as contaminant in Tl-201, 334, 335, 339-340

/Tl-201 absorbed dose ratios for heart wall, 339

Thallium-201

- contaminants in, 331, 333-334, 335, 339, 340
- electron range in water, 15
- S-values for embryo or fetus, 159

Thallium-201-chloride

- absorbed dose estimates, 340, 356
- absorbed dose in renal transplant patients, 284-287
- cellular concentration, 14, 15
- cellular dose rates, 17-18
- committed effective whole-body dose equivalent, 384
- compared to other agents for myocardial imaging, 385
- cytotoxicity, 16, 18, 53, 59
- dose characteristics for, 384
- drugs affecting biodistribution, 292, 293
- lack of data for breast milk milk excretion, 178
- mean lethal dose, 15
- microdosimetry vs. simulated tissue geometry, 18
- for myocardial perfusion studies, 262, 385

Thallium-201-diethyldithiocarbamate

- autoradiographic studies with, 110, 113

Thallium-202

- absorbed doses from, 340
- as contaminant in Tl-201, 334, 335, 339, 340

/Tl-201 absorbed dose ratios for heart wall, 340

Thallium-204-chloride

- cytotoxicity of, 16, 52, 53

Thermoluminescent dosimeters (mini)

- 447-455

Thiocyanate ions, iodide competition with, 301

Thorotrast, cancer risk from, 405

Three Mile Island accident, 4, 8

Threshold levels, radioactivity, 7-8

Thrombocytopenia, 536

Thyroid

- absorbed doses from myocardial imaging agents, 374-379
- blocking agents for, 181, 301
- blocking of, 169, 177, 181, 390, 393, 394, 432
- cancer of, 410, 542, 630, 632-635, 637, 642-647
- cumulated activities of iodine in, 366, 368
- drugs affecting uptake, 301-302
- fallout dose to, 628-641
- fetal, 158-162, 165

fetal absorbed dose from I-131, 165

fetal/maternal I-131 concentrations in, 160-161

hormones affecting radiopharmaceutical uptake, 295, 301

infant, kinetics and doses from I- and Tc-99m radiopharmaceuticals in breast milk, 169, 170, 177, 180

I-123-PPA dose estimates for, 369

I-131-MIBG kinetic data and dose estimates, 390, 393, 395, 396

mass of, 158, 160-161, 620, 621, 623, 627

maternal, 158-162, 165

models, age- and sex-dependent for I-131 dose to normal, 614-625, 626-627

nodules in, 629, 630, 637

risk from internal and external iodine exposure, 628-641

S-factors for I-131, 621, 622

specific absorbed fractions for, 620

technetium-99m prophyrin in, 127

uptake of I-123-OIH, 137, 142, 145

Thyrotoxicosis, 301, 637

Time-of-flight in PET, 104

Time

- calibration and expiry, 333-335
- for charged particle events, 38, 40-41, 43, 44-46
- scanning, autoradiographic, 112-113
- scavenge, 44, 49

Tissue inhomogeneity

- effect on beta dose calculation, 562-571

Toluene, brain uptake of, 294

Trabecular bone, 515, 517, 527, 534

Tracer principle, 2-3

Tracheal phantom, 201-206

Track, charged particle, 39

- alpha, 47, 49
- chemical events in, 42-47
- DNA reaction with, 47-49
- energy levels influencing, 39
- energy loss along, 38-39, 42-45, 51
- models for, 39, 41-42, 51
- radii of, 39, 49
- times for events in, 38, 40-41, 43, 44-46

Tranquilizers, 301

Transmittance, 106, 107-111

Transparenchymal plasma flow, 536-537, 538

Transplant patients, renal

- dose estimates for, 275, 277-281, 284-287
- nuclear medicine procedures in, 276, 283, 288

pediatric, 277, 280-281, 289-290
Transportation of radioactive materials, 6-9
Triage, pediatric medicine, 148
Triccatecholamide, 299
Triglycerides, 295
Tritium. See **Hydrogen-3**
Tryptophan
 dosimetry and kinetics for C-11-labeled, 240-242
 resolution of enantiomers of, 239-240
Tumor
 antibody concentration in, 461, 462, 478, 479, 481-482
 antiferritin treatment of, 458-460
 brain, 2-3
 chemo-Auger therapy for, 494-495, 505-509
 copper kinetics in, 212-215
 deoxyglucose test for, 2-3
 direct verification of dose to, 447, 449
 gallium-67 uptake in, 299-300
 glutaminase sensitivity of, 217, 218
 iodine-131-MIBG uptake in, 389, 395
 kinetics of In-111-EDTA-MoAb in, 477-490
 monoclonal antibody therapy for, 409-410, 411, 412, 436-441, 443
 pancreatic, 239
 perfusion of, 260, 261, 262
 platinum therapy for, 494, 507, 508-509, 512
 radiation dose for eradication of, 33-36, 417, 418
 radiogenic, 4, 38, 403-406, 666, 668-670
 radioimmunotherapy, results of, 462-463
 radiolabeled amino acid uptake by, 218, 220-221, 224, 225-237, 239
 thyroid, 410, 542, 629, 630, 632-635, 642-647
 vascularity, 460
 volumetrics, 458, 459, 460, 461
Two-compartment dosimetry model, 326, 327

U

Ulcer, gastrointestinal, 300-301
Uniformly distributed radiation, 68, 69, 70
Unique events, probabilities for, 401, 402

Uptake. See also **specific organs and radiopharmaceuticals**.
 calculation for inhalation, 206-207
 conjugate counting for, 137, 142-146, 348-354
 drug-altered, 291-304, 309
 increased antibody by irradiated tumor, 462
 maternal vs. fetal, 160-161
 of radiolabeled amino acids, 60, 219-220, 224, 225-238, 241
 renal, 279, 284-287, 289
Uterus, specific absorbed fractions for, 156-158
Utirik inhabitants, fallout dose to 630, 645-647

V

Valine
 biodistribution of γ -14-labeled, 241
 dosimetry for C-11 labeled enantiomers of, 240, 242
 resolution of enantiomers of, 239-240
 uptake of N-13 labeled, 219, 230
Vasopressin, 301
Vein wall, dose from intravenous administration, 195-200, 211
Vena cava, blood volume of, 576, 579
Ventricular aneurysms, 292
Vincristine, 298, 299, 300
Vioform, 301
Vitamins
 altering radiopharmaceutical uptake, 295, 297, 301

W

Water
 charged-particle passage in, 39, 41-50
 dielectric response function for, 41
Weighting factors
 for effective dose equivalent, 122, 664, 665
Whole body
 committed effective dose equivalent for heart agents, 384
 compartmental model, 427
 counting, 120, 137, 471
 scanning, 390

self dose from Rb-82, 353
Wilson's disease, 212

X

Xenon-131m
as contaminant in Xe-133, 333, 335
Xenon-133
contaminants in, 333, 335
drugs altering lung scans,
302-303
and fat content in liver, 303
Xenon-133m
as contaminant in Xe-133, 333, 335
X-ray exposure, 15, 21, 256, 498

Y

Yttrium-90
TLDs (mini) calibrated for, 447
Yttrium-90-antiferritin IgG
biokinetics and absorbed dose
estimates, 458-463
radioimmunotherapy for hepatoma,
458-463
Yttrium-90-monoclonal antibodies
absorbed dose estimates, 416
gamma camera imaging, 414
potential for radioimmunotherapy,
27, 414, 415, 416, 460-463

Z

Zero threshold hypothesis, 4-5, 6, 7
Zinc-65
as contaminant in Ga-67 and
In-111-DTPA, 333, 335
Zirconium-89, as candidate for
labeling monoclonal antibodies,
27

AUTHOR INDEX

Abel, N.M.	267	Greer, K.L.	82
Adams, W.H.	628	Griffith, M.H.	446
Adelstein, S.J.	13	Groér, P.G.	399
Aissi, A.	574	Hamm, R.N.	37
Alger, E.	421, 535	Harper, P.V.	135, 194, 346, 587
Bartlett, R.	135	Haymond, M.W.	681
Beck, T.	245	Henrichs, K.	155, 310, 673
Bice, A.	245	Hill, H.Z.	493
Bigler, R.E.	421, 535	Hoefnagel, C.A.	181
Bradley, E.W.	446	Hoffman, E.J.	97
Brennan, K.	421, 535	Hooker, G.R.	409
Brill, A.B.	628	Howell, R.W.	52, 493
Byrd, B.L.	239	Hubner, K.F.	239
Callahan, R.	186	Hui, T.Y.	574
Carlton, J.E.	212	Irfan, M.	562
Chan, L.B.	545	Jacobsson, L.	389
Chatterjee, A.	37	Jaszczak, R.J.	82
Chen, C.-T.	135, 194, 587	Jimba, B.M.	574
Chou, J.-S.	135	Johansson, L.	389
Clark, G.	359	Kassis, A.I.	13
Classic, K.L.	681	Kaul, A.	155, 310, 673
Coakley, A.J.	167	Kerr, G.D.	67
Coffey, J.L.	239	Killough, G.G.	613
Coleman, R.E.	82	King, M.	464
Corbett, J.R.	359	Klein, J.L.	458
Cosma, M.	535	Knapp, F.F., Jr.	371
Crawley, J.C.W.	118	Koyle, M.A.	274
Croft, B.Y.	260	Kulkarni, P.V.	359
Crook, J.E.	212, 239	Kwok, C.S.	545, 562
Dannals, R.F.	245	Lathrop, K.A.	135, 194, 346, 587
David, G.S.	477	Lear, J.	105
DeJager, R.	421, 535	Leichner, P.K.	458
Doherty, P.	464	Leonard, R.	535
Eckerman, K.F.	67, 514, 613	Lessard, E.T.	628
Edwards, A.A.	661	Lindberg, S.	389
Elmaleh, D.	186	Links, J.M.	245
Elsasser, U.	155, 310, 673	Lloyd, D.C.	661
Epenetos, A.A.	409	Maessen, H.J.M.	181
Faulhaber, P.	135	Magee, J.L.	37
Finston, R.	477	Marcus, C.S.	274
Fisher, D.R.	26	Marcuse, H.R.	181
Fjälling, M.	389	Mattsson, S.	389
Ford, E.	421, 535	McTigue, M.	477
Gelbard, A.S.	217	Meares, C.F.	477
Gilday, D.L.	148	Mido, K.	105
Gill, J.	186	Miller, D.D.	186
Gionet, M.	464	Mountford, P.J.	167
Goldenberg, D.M.	421, 535	Muth, R.	105
Goodman, M.M.	371	Myers, M.J.	409
Goodwin, D.A.	477	Order, S.E.	458
Govelitz, G.F.	52	Parkey, R.W.	359

Peterson, E.	346
Pezzullo, J.	319
Plotnick, J.	105
Poston, J.W.	574
Powell, G.	194
Prestwich, W.V.	545,562
Primis, F.J.	421,535
Rao, D.V.	52,493
Reddy, A.R.	155
Reft, C.S.	194
Roedler, H.D.	155
Rosenspire, K.C.	217
Roth, P.	310,673
Ryan, J.	346
Ryman, J.C.	67
Sastry, K.S.R.	13,52,493
Schwenk, W.F.	681
Schwinger, R.	464
Shani, J.	291
Shearer, D.R.	319
Skibinski, B.	446
Smith, S.I.	477
Smith, T.	118
Srivastava, P.C.	371
Stabin, M.G.	212,331,371
Stark, V.	135,346
Stowe, S.	421,535
Strauss, H.W.	186
Sun, T.T.	239
Taner, A.C.	67
Thakur, M.	648
Turner, J.E.	37
van der Steen, J.	181
Voûte, P.A.	181
Wagner, H.N., Jr.	1,245
Washburn, L.C.	239
Watson, E.E.	212,239,331,371
Werner, E.	310,673
Wessels, B.W.	446
Willerson, J.T.	359
Wilson, B.	545
Wong, D.F.	245
Woo, M.K.	562
Wright, H.A.	37
Zanelli, G.D.	118
Zanzonico, P.B.	421,535